

**Fragment-based development of inhibitors
of New Delhi metallo- β -lactamase-1
(NDM-1) and validation of their mode-of-
action against multiresistant bacteria**

Inaugural-Dissertation

to obtain the academic degree

Doctor rerum naturalium (Dr. rer. nat.)

submitted to the Department of Biology, Chemistry, Pharmacy
of Freie Universität Berlin

by

YUWEN JIA

2022

The doctoral project was conducted from October 2016 till March 2022 under the supervision of Prof. Dr. Jörg Rademann at the Institute of Pharmacy of Freie Universität Berlin.

1st Reviewer: Prof. Dr. Jörg Rademann

2nd Reviewer: Prof. Dr. Gerhard Wolber

Date of defense: 15.09.2022

Declaration

I hereby declare that this dissertation was written and prepared by me independently. Furthermore, no sources and aids other than those indicated have been used. Intellectual property of other authors has been marked accordingly. I also declare that I have not applied for an examination procedure at any other institution and that I have not submitted the dissertation in this or any other form to any other faculty as a dissertation.

Yuwen Jia

Acknowledgements

I would like to gratefully appreciate the financial supporting from Chinese Scholarship Council (CSC).

I would like to express my sincere acknowledgement to Prof. Dr. Jörg Rademann who offered me the interesting doctoral project and thanks for his guidance. His patience, encouragement, trust and help have made me more and more confident and constantly improve myself step by step. Thanks to Prof. Dr. Gerhard Wolber for accepting to be the second reviewer of this dissertation, and kindly supporting me to conduct some docking studies in his lab.

I would like to thank all the cooperators and people who have kindly helped me about my doctoral work, especially Dr. Christoph Arkona, Dr. Yvonne Pfeifer, Dr. Lihua Deng, Dr. Benno Kuroпка, Dr. Christopher Fröhlich, Dr. Kenichi Ataka, Dr. Christoph Weise and Bernhard Wuest.

I acknowledge all the group members of AG Rademann. Ms. Allner always knows the smartest way to order the best reagents and keeps everything organized. Our talented technical team always support us efficiently. Silke Bergemann gave me a lot of help about protein expression and cell assays. Eleonore Christmann often surprised me by nice mass data. Thomas Rudolf can amazingly make every broken thing work again. Mike Jaegle, Ee Lin Wong, Eric Nawrotzky, and so on, with your company, I have gone through a nice long journey in the pharmacy institute. Thanks to our machine responsible people and the MATE drink suppliers, especially Jan-Niklas Dürig and Umer Bin Abdul Aziz. Thanks to my Chinese speaking colleagues and friends Xinning Wang, Wei Song and Jan-Niklas Dürig who have always been sought out and stand my tendency to keep talking in Chinese. Thanks to Lukas Lassak, a Chinese beginner, for making me feel like a language teacher. Especially thanks for my lab-mates, Marc Roeger, Markus Tiemann and Xinting Zhang, the homelike lab was a warm stage for us working flexibly, cooking with diverse chemical reagents, sharing strange smells from each other's unbelievable creations, taking care of the glassware babies which were always getting less and less and never enough, playing hide-and-seek with naughty products, and praying for everything. Thanks for the 'Good luck' given by the night lab companion, the most hard-working person Saan Voss every day during the final period.

I also thank other group members in the pharmacy institute for their help, especially, Sijie Liu, Dr. Wenyan Xie and Yan Dyck.

I thank all my friends who enriched my life and gave me a lot of professional and technical supporting, especially Lihua Deng, Huan Lan and Hongqiang Wang.

Finally, I would like to express my deepest gratitude to my parents and relatives who normally disagree with me but allow me to do whatever I want.

This is a colourful experience about science and life, thanks all.

Abstract

New Delhi metallo- β -lactamase-1 (NDM-1) was first reported in 2009 from a patient who had traveled to India from Sweden and has been rapidly spread worldwide until today. Resistance by NDM-1 is commonly identified in strains of *Enterobacteriaceae*, *Pseudomonas aeruginosa*, *Acinetobacter baumannii*, and some other Gram-negative strains. *Enterobacteriaceae* are the largest family of clinically important bacteria, infections caused by them related to many diseases, e.g., gastroenteritis, hemorrhagic colitis, bacteremia, neonatal meningitis, urinary tract infections, intraabdominal infections, and pneumonia. With a broad substrate spectrum and improved stability for zinc ion starvation conditions compared with other B1 metallo- β -lactamases (MBLs), NDM-1 is currently one of the most challenging resistance factors threatening the efficacy of carbapenems, the last resort of β -lactam antibiotics. Synergistic usages of inhibitors for β -lactamases with β -lactam antibiotics have become a promising way for keeping the efficacy of carbapenems as well as other essential β -lactam antibiotics. However, until now no effective inhibitors for NDM-1-expressing pathogens are available for clinical treatment, thus there is an urgent requirement for the development of inhibitors targeting NDM-1.

In this work, derivatives of DPA (dipicolinic acid or pyridine-2,6-dicarboxylic acid) and quinoline scaffold derivatives were developed as inhibitors for NDM-1 based on the initial fragment screening and supported by docking studies. The modified derivatives had improved inhibitory activity and binding affinity relative to the fragment hits, especially the substituted 8-sulfonamide derivatives such as compounds **94(YJh182)**, **95(YJh196)** and **83(YJh174)** with IC_{50} values ranging from 0.2 μ M to 0.3 μ M.

The interaction modes of the top active and some other representative compounds with NDM-1 were studied by bio-layer interferometry (BLI), isothermal titration calorimetry (ITC), native protein mass spectrometry, thermal shift assay (TSA), circular dichroism (CD) and zinc restoration assays. The top active compounds **94(YJh182)** and **95(YJh196)** with the 4- or 5-phenyl groups were more specific for the active pocket of NDM-1 compared with compound **83(YJh174)** according to docking studies and interacted with NDM-1 mainly by forming stable binding complexes of holo-NDM-1 with the inhibitors which was identified by native protein mass spectrometry. Compounds **94(YJh182)**, **95(YJh196)** and **83(YJh174)** all bound the protein reversibly under the BLI assay conditions, and the trend of the K_d values obtained from BLI assays correlated with the trend of the inhibitory activity of the inhibitors. The ITC assays showed binding of ligands to protein and binding of zinc ions to ligands. No or less significant changes for the secondary structures of NDM-1 treated with low excess of the inhibitors were detected by CD measurements, and some changes of the CD signals for NDM-1 treated with high excess of the inhibitors especially compounds **95(YJh196)** and **83(YJh174)** might be contributed by ligand binding. The inhibition by compounds **94(YJh182)**, **95(YJh196)** and **83(YJh174)** for NDM-1 can be partially restored by zinc ions, the different entropic changes observed in the ITC measurements could be contributed by conformational changes at the active site about the amino acid residues and the coordinated Zn(II) ions, and binding with the inhibitors reduced the thermal stability of NDM-1 which was identified via TSA studies.

Furthermore, the activity of some representative compounds was also tested toward other clinically relevant B1 MBLs including IMP-1, VIM-2 and GIM-1, and all the tested compounds were potent inhibitors, which suggested that the developed inhibitors are broad-spectrum candidates for B1 MBLs. Activity tests by other metalloenzymes such as hCAII, HDAC-1 and MMP-2 showed that the tested inhibitors all had high selectivity for NDM-1 and had no inhibitory activity for hCAII and HDAC-1 at all. The selected substituted 8-sulfonamide inhibitors all could significantly reduce the MICs of meropenem

for the bacteria recombinantly expressing *bla*_{NDM-1} and clinical resistant isolates co-expressing *bla*_{NDM-1} to susceptible levels with lower combined concentrations and had no or little effects on the proliferation and viability of HEK293 cells, which demonstrated that the substituted 8-sulfonamide inhibitors developed in this work are potent and non-toxic or weakly toxic Zn(II)-binding inhibitors targeting NDM-1 restoring the carbapenem susceptibility of multidrug-resistant clinical isolates.

Above all, the best active inhibitors developed in this work for NDM-1 had improved specificity and inhibitory activity especially at the cell-level compared to most previously published Zn(II)-chelating or Zn(II)-binding inhibitors such as the AMA-type inhibitors, DPA derivatives and thiol-based structures. The interaction mode of forming protein-inhibitor complexes and reducing the thermal stability of NDM-1 is a more promising mode of action for drug-like candidates than other more toxic mechanisms such as the Zn(II) ion depriving function of EDTA or AMA-type inhibitors and the covalent binding mechanism which is generally limited to the cysteine or lysine residues at the active site.

Abstrakt

Die Neu-Delhi-Metallo- β -Lactamase-1 (NDM-1) wurde erstmals 2009 von einem Patienten gemeldet, der von Schweden nach Indien gereist war, und hat sich bis heute schnell weltweit verbreitet. Antibiotika-Resistenz durch NDM-1 wird häufig in Stämmen von *Enterobacteriaceae*, *Pseudomonas aeruginosa*, *Acinetobacter baumannii* und einigen anderen Gram-negativen Stämmen identifiziert. *Enterobacteriaceae* sind die größte Familie von klinisch wichtigen Bakterien, durch sie verursachte Infektionen sind mit vielen Krankheiten verbunden, z. B. Gastroenteritis, hämorrhagische Colitis, Bakteriämie, neonatale Meningitis, Harnwegsinfektionen, intraabdominale Infektionen und Lungenentzündung. Mit einem breiten Substratspektrum und verbesserter Stabilität bei Zinkionenmangel im Vergleich zu anderen B1-Metallo- β -Lactamasen (MBLs) ist NDM-1 derzeit einer der herausforderndsten Resistenzfaktoren, der die Wirksamkeit von Carbapenemen, den letzten β -Lactam-Reserve-Antibiotika. Synergistische Verwendungen von Inhibitoren für β -Lactamasen mit β -Lactam-Antibiotika sind zu einem vielversprechenden Weg geworden, um die Wirksamkeit von Carbapenemen sowie von anderen essentiellen β -Lactam-Antibiotika aufrechtzuerhalten. Bis jetzt sind jedoch keine wirksamen Inhibitoren für NDM-1-exprimierende Pathogene für die klinische Behandlung verfügbar, daher besteht ein dringender Bedarf für die Entwicklung von Inhibitoren, die auf NDM-1 abzielen.

In dieser Arbeit wurden Derivate von DPA (Dipicolinsäure oder Pyridin-2,6-dicarbonsäure) und Chinolin-Gerüstderivate als Inhibitoren für NDM-1 entwickelt, basierend auf einem anfänglichen Fragment-Screening und unterstützt durch Docking-Studien. Die modifizierten Derivate hatten eine verbesserte inhibitorische Aktivität und Bindungsaffinität im Vergleich zu den Fragment-Hits, insbesondere die substituierten 8-Sulfonamid-Derivate wie die Verbindungen **94(YJh182)**, **95(YJh196)** und **83(YJh174)** mit IC_{50} -Werten im Bereich von 0,2 μ M bis 0,3 μ M.

Die Wechselwirkungsmodi des besten Wirkstoffs und einiger anderer repräsentativer Verbindungen mit NDM-1 wurden durch Biolayer-Interferometrie (BLI), isothermale Titrationskalorimetrie (ITC), native Protein-Massenspektrometrie, Thermo-Shift-Assays (TSA), Zirkulardichroismus (CD) und Zink-Wiederherstellungsassays untersucht. Die besten Wirkstoffe **94(YJh182)** und **95(YJh196)** mit den 4- bzw. 5-Phenylgruppen waren laut Docking-Studien spezifischer für die aktive Tasche von NDM-1 im Vergleich zu Verbindung **83(YJh174)** und interagierten mit NDM-1 hauptsächlich durch Bildung stabiler Bindungskomplexe von Holo-NDM-1 mit den Inhibitoren, die durch native Protein-Massenspektrometrie identifiziert wurden. Die Verbindungen **94(YJh182)**, **95(YJh196)** und **83(YJh174)** bindeten alle unter den BLI-Testbedingungen reversibel an das Protein, und der Trend der aus BLI-Tests erhaltenen K_d -Werte korrelierte mit dem Trend der inhibitorischen Aktivitäten der Inhibitoren, obwohl die Werte durch die zusätzlichen Zinkionen im Testpuffer verschoben wurden. Die Ergebnisse der ITC-Assays spiegelten das Gleichgewicht für die Wechselwirkungen des gesamten Titrationssystems einschließlich des Proteins und der Liganden sowie der möglicherweise freigesetzten Zinkionen wider. Keine oder wenig signifikante Veränderungen der Sekundärstrukturen von NDM-1 wurden bei geringem Überschuss an Inhibitoren durch CD-Messungen nachgewiesen. Veränderungen der CD-Signale von NDM-1 könnten bei hohem Überschuss der Verbindungen **95(YJh196)** und **83(YJh174)** durch Ligandenbindung bewirkt sein. Die Hemmung von NDM-1 durch die Verbindungen **94(YJh182)**, **95(YJh196)** und **83(YJh174)** wurde teilweise durch zusätzliche Zinkionen aufgehoben. Es könnte zu Konformationsänderungen am aktiven Zentrum um die Aminosäurereste und die koordinierten Zn(II)-Ionen kommen, die in den ITC-Messungen beobachteten entropischen Änderungen beeinflussen

könnten, und die Bindung der Inhibitoren verringerte die thermische Stabilität von NDM-1, wie durch TSA-Studien gezeigt wurde.

Darüber hinaus wurde die Aktivität einiger repräsentativer Verbindungen auch gegenüber anderen klinisch relevanten B1-MBLs getestet, darunter IMP-1, VIM-2 und GIM-1, und alle getesteten Verbindungen waren starke Inhibitoren, was darauf hindeutet, dass die entwickelten Inhibitoren ein breites Wirkungsspektrum gegenüber B1 MBLs aufweisen. Aktivitätstests von anderen Metalloenzymen wie hCAII, HDAC-1 und MMP-2 zeigten, dass die getesteten Inhibitoren alle eine hohe Selektivität für NDM-1 und überhaupt keine inhibitorische Aktivität gegenüber hCAII und HDAC 1 aufwiesen. Alle ausgewählten substituierten 8-Sulfonamid-Inhibitoren reduzierten die MICs von Meropenem für Bakterien, die rekombinant blaNDM-1 exprimieren, und klinisch resistente Isolate, die blaNDM-1 koexprimieren, auf niedrige kombinierte Konzentrationen und hatten keine oder geringere Auswirkungen auf die Proliferation und Lebensfähigkeit von HEK293-Zellen. Dies zeigte, dass die in dieser Arbeit entwickelten substituierten 8-Sulfonamid-Chinolinsäuren vielversprechende, potente und nicht bzw. schwach toxische Zn(II)-bindende Inhibitoren darstellen, die auf NDM-1 abzielen und die Carbapenem-Empfindlichkeit von Multidrug-resistenten klinischen Isolaten wiederherstellen.

Vor allem zeigten die in dieser Arbeit für NDM-1 entwickelten Inhibitoren hatten eine verbesserte Spezifität und inhibitorische Aktivität, insbesondere auf Zellebene, als die bislang veröffentlichten Zn(II)-chelatbildenden oder Zn(II)-bindenden Inhibitoren wie dem AMA-Typ Inhibitoren, DPA-Derivate und Thiol-basierte Strukturen. Der Interaktionsmodus der Bildung von Protein-Inhibitor-Komplexen und der Verringerung der thermischen Stabilität von NDM-1 ist ein vielversprechenderer Wirkungsmodus für wirkstoffähnliche Kandidaten als andere toxischere Mechanismen wie die Zn(II)-Ionen-entziehende Funktion von EDTA oder AMA- Typ-Inhibitoren und der kovalente Bindungsmechanismus, der im Allgemeinen auf die Cystein- oder Lysinreste an der aktiven Tasche beschränkt ist.

List of abbreviations

A

ACE	angiotensin-converting enzyme
7-ACA	7-aminocephalosporonic acid
AIM	Adelaide imipenemase
AMA	Aspergillomarasmine A
AMB	Aspergillomarasmine B
ATP	adenosine triphosphate (ATP)
ABC	adenosine triphosphate (ATP)-binding cassette (ABC) superfamily
<i>A. baumannii</i>	<i>Acinetobacter baumannii</i>
6-APA	6-aminopenicillanic acid
AZA	acetazolamide

B

BLs	β -lactamases
BLIs	β -lactamase inhibitors
BLI	bio-layer interferometry
3BP	3-bromopyruvate
BSA	bovine serum albumin
BSI	bloodstream infections
BTZ	bisthiazolidine

C

CAs	Carbonic Anhydrases
CBS	colloidal bismuth subcitrate
CoA	coenzyme A
CD	circular dichroism
CLSI	Clinical Laboratory Standards Institute
cIAI	complicated intra-abdominal infections
cUTI	complicated urinary tract infections
cDNA	complementary DNA
CRE	carbapenem-resistant Enterobacterales
p-CMB	<i>p</i> -chloromecuribenzoate

D

DEME	Dulbecco's modified Eagle medium
DIM	Dutch imipenemase
Da	dalton
DMSO	dimethyl sulfoxide
DMF	dimethylformamide
DPA	dipicolinic acid or pyridine-2,6-dicarboxylic acid
DSF	differential scanning fluorimetry

E

EDC	1-ethyl-3-(3-dimethylaminopropyl)carbodiimide
EDDS	ethylenediamine- <i>N,N'</i> -disuccinic acid

EUCAST	European Committee on Antimicrobial Susceptibility Testing
ESBLs	extended-spectrum β -lactamases
ESI-MS	electrospray ionization mass spectrometry
EDTA	ethylenediaminetetraacetic acid
<i>E. coli</i>	<i>Escherichia coli</i>
EPIs	efflux pump inhibitors
F	
FBDD	fragment-based drug discovery
FDA	the United States Food and Drug Administration
G	
ΔG	change of Gibbs free energy
ΔG_u	the Gibbs free energy of unfolding
GlcNAc (NAG, G)	<i>N</i> -acetylglucosamine
GIM	German imipenemase
GNB	Gram-negative bacteria
H	
ΔH	enthalpic change
hCAII	human carbonic anhydrase II
HDAC-1	histone deacetylase-1
HDACis	HDAC inhibitors
HEPES	4-(2-hydroxyethyl)-1-piperazineethanesulfonic acid
HL	Hodgkin lymphoma
8-HQA	8-hydroxyquinoline-2-carboxylic acid
HTS	high-throughput screening
I	
IBTs	isatin- β -thiosemicarbazones
IC ₅₀	half maximal inhibitory concentration
IDA	iminodiacetic acid
IMP	Imipenemase
IPTG	isopropyl β -D-1-thiogalactopyranoside
ITC	isothermal titration calorimetry
K	
K_a	association constant,
K_d	dissociation constant
K_m	the value of the Michaelis constant
<i>K. pneumoniae</i>	<i>Klebsiella pneumoniae</i>
L	
LPS	lipopolysaccharide
M	
MATE	multidrug and toxic compound extrusion
MBL	metallo- β -lactamase
MBLs	metallo- β -lactamases
MBP	metal-binding pharmacophore
MDR-GNB	multidrug-resistant Gram-negative bacteria

MEM	meropenem
MFS	major facilitator superfamily
MIC	minimum inhibitory concentration
MMP-2	matrix metalloproteinase-2
MMTZs	2-mercaptomethyl-thiazolidines
MRE	mean residual ellipticity
MRSA	methicillin-resistant <i>Staphylococcus aureus</i>
8-MSQA	8-(methylsulfonamido)quinoline-2-carboxylic acid
MurNAc (NAM, M)	<i>N</i> -acetylmuramic acid
N	
NAD+	nicotinamide adenine dinucleotide
NDM-1	New Delhi metallo- β -lactamase-1
Ni-NTA	nickel - nitrilotriacetic acid
NMR	nuclear magnetic resonance
NP	nosocomial pneumonia
pNPA	<i>p</i> -nitrophenyl acetate
NRMSD	normalized root mean square deviation
S-NSA	<i>N</i> -([1,1'-biphenyl]-4-ylsulfonyl)-L-phenylalanine
R-NSA	<i>N</i> -([1,1'-biphenyl]-4-ylsulfonyl)-D-phenylalanine
NSPCs	<i>N</i> -sulfamoylpyrrole-2-carboxylates
O	
OMVs	outer membrane vesicles
P	
PBPs	penicillin-binding proteins
<i>P. aeruginosa</i>	<i>Pseudomonas aeruginosa</i>
PCR	polymerase chain reaction
PDB	Protein Data Bank
PEM	photoelastic modulator
PMSF	phenylmethylsulfonyl fluoride
POIs	protein of interests
PROTACs	proteolysis-targeting chimeras
Q	
qPCR	quantitative polymerase chain reaction
Q-TOF	Quadrupole time-of-flight
R	
RND superfamily	resistance-nodulation-cell division (RND) superfamily
S	
ΔS	entropic change
SAHA	suberoylanilide hydroxamic acid
SAR	structure-activity relationship
SBLs	serine β -lactamases
SDS-PAGE	sodium dodecyl sulphate–polyacrylamide gel electrophoresis
SIT	spiro-indoline-thiadiazole
SMB	<i>Serratia</i> metallo- β -lactamase

SMR family	small multidrug resistance (SMR) family
SPM	Sao Paulo metallo- β -lactamase
SPR	surface plasmon resonance
SSA biosensor	Super Streptavidin biosensor
ST11	sequence type 11
<i>S. pneumoniae</i>	<i>Streptococcus pneumoniae</i>
T	
T_m	melting point
ΔT_m	change of the melting point
TSA	thermal shift assay
V	
VIM	Verona integron-encoded metallo- β -lactamase
Z	
ZBG	zinc binding group

Table of Contents

Acknowledgements	v
Abstract	vii
List of abbreviations	xi
1 Introduction	1
1.1 Bacterial resistance	1
1.2 β -Lactam antibiotics	2
1.2.1 Cell wall of Gram-positive and Gram-negative bacteria	2
1.2.2 Classification of β -lactam antibiotics	5
1.3 β -Lactamases	8
1.3.1 Classification of β -lactamases	8
1.3.2 Metallo- β -lactamases.....	10
1.3.3 Mechanisms of β -lactamases	15
1.4 New Delhi metallo- β -lactamase (NDM-1).....	16
1.4.1 Structure characteristic and hydrolysis mechanism of NDM-1	17
1.4.2 Inhibitors of NDM-1	20
1.4.2.1 Thiol-based inhibitors	20
1.4.2.2 Bicyclic boronate inhibitors.....	22
1.4.2.3 Metal ion chelating or binding inhibitors	23
1.4.2.4 Covalent binding inhibitors and others	27
1.4.3 Methods for discovery of the leading compounds	29
2 Project aim and design.....	31
3 Results and discussion	33
3.1 Fragment screening.....	34
3.1.1 Forming of screening assays.....	34
3.1.2 Screening of the carboxylic acid and amine libraries.....	36
3.1.3 Screening of the prepared analogues	39
3.1.3.1 Preparation of analogues	39
3.1.3.2 Measuring of the prepared analogues.....	39
3.2 Compound synthesis and their enzyme-based <i>in vitro</i> activity	44
3.2.1 DPA derivatives	44
3.2.1.1 Compound design and synthesis of DPA derivatives	44
3.2.1.2 Enzyme-based <i>in vitro</i> activity of DPA derivatives	48

3.2.2 8-HQA derivatives	51
3.2.2.1 Compound design and synthesis of 8-HQA derivatives	51
3.2.2.2 Enzyme-based <i>in vitro</i> activity of 8-HQA derivatives.....	55
3.2.3 8-MSQA derivatives	58
3.2.3.1 Compound design and synthesis of 8-MSQA derivatives	58
3.2.3.2 Enzyme-based <i>in vitro</i> activity of 8-MSQA derivatives	62
3.2.4 Summary of the developed inhibitors	71
3.3 Mode of action	75
3.3.1 Bio-layer interferometry (BLI) assays.....	75
3.3.2 Isothermal titration calorimetry (ITC) assays.....	79
3.3.3 Native mass spectrometry studies.....	86
3.3.4 Thermal shift assay (TSA)	92
3.3.5 Solution NMR assays.	95
3.3.6 Circular dichroism (CD)	96
3.3.7 Zinc ion restoration assays	101
3.3.8 Summary of mode-of-action studies.....	105
3.4 Specificity studies of DPA, 8-HQA and 8-MSQA derivatives	108
3.4.1 Other clinically relevant B1 MBLs	108
3.4.2 Other Zn(II) metalloenzymes	114
3.4.2.1 General structural characters and relevant diseases	114
3.4.2.2 Activity tests by <i>in vitro</i> assays	116
3.5 Microbiological susceptibility tests.....	121
3.6 Alamar blue assays	125
4 Conclusion and outlook.....	127
5 Experiment part.....	131
5.1 Biological evaluation methods	132
5.1.1 Protein expression and purification	132
5.1.2 IC ₅₀ determinations	133
5.1.3 Bio-layer Interferometry (BLI) assays.....	133
5.1.4 Isothermal titration calorimetry (ITC) assays.....	134
5.1.5 Interaction studies by native mass spectrometry.....	135
5.1.6 Thermal shift assays	136
5.1.7 Circular dichroism.....	136
5.1.8 Zinc ion restoration assays	136

5.1.9 Enzyme-based <i>in vitro</i> activity assays for several other metalloenzymes	137
5.1.9.1 MMP-2 assays	137
5.1.9.2 HDAC-1 assays	137
5.1.9.3 hCAII assays	138
5.1.10 Microbiological susceptibility tests.....	138
5.1.11 Alamar blue assays.....	139
5.2 Molecule docking.....	139
5.3 Synthesis	140
5.3.1 Materials and methods	140
5.3.2 Synthetic routes	141
5.3.3 Synthesis procedures	148
6 Appendices	226
6.1 Tables and figures	226
6.2 NMR spectra.....	267
7 References	419

1 Introduction

1.1 Bacterial resistance

Antibiotics were one of the major discoveries of the 20th century, especially for severe wound infections or fatal diseases caused by bacterial pathogens. The discovery of penicillin opened the golden age of antibiotic research. However, the widespread use of antibiotics has promoted the production of resistant bacteria including multi-drug resistant strains, which has been a long-term problem worldwide.^{1,2} Bacterial resistance involves many factors and mechanisms, such as increased active effluxes and permeability barriers, emergence of resistance genes coding enzymes degrading antibiotics, and mutations of antibiotic binding targets. In addition, the rapid spreading of bacterial resistance genes made the occasions even worse especially in hospitals, and the nosocomial antibiotic resistance continued spreading to surrounding communities.^{3,4} The synergism has resulted in intrinsic or acquired high-level resistance in many clinical Gram-negative pathogens, which has brought great difficulties to the treatment and prevention of related bacteria-caused diseases.^{5,6}

In general, bacterial drug efflux transporters are divided into five categories: the major facilitator superfamily (MFS), the adenosine triphosphate (ATP)-binding cassette (ABC) superfamily, the small multidrug resistance (SMR) family, the resistance-nodulation-cell division (RND) superfamily, and the multidrug and toxic compound extrusion (MATE) family. Compared with other efflux pumps, RND pumps play the major role in the resistance of Gram-negative bacteria. One important property of RND pumps is their broad spectrum of substrates, including β -lactams, polymyxin, macrolides, aminoglycosides, etc. For overcoming the resistance caused by efflux pumps, there were developed efflux pump inhibitors (EPIs), e.g., 2,8-dimethyl-4-(2'-pyrrolidinoethyl)-oxyquinolone, inhibiting efflux pumps of *Klebsiella pneumoniae*, phenylalanyl-arginyl- β -naphthylamide (MC-207,110), a broad spectrum RND pump inhibitor. The combination usages of these inhibitors with antibiotics potentiated the activity of relevant antibiotics against efflux pump-related resistance pathogens.^{7,8}

Porins on the outer membrane of Gram-negative bacteria play important roles for the penetrating of many hydrophilic antibiotics such as fluoroquinolones, chloramphenicol and β -lactams, e.g., the resistance for β -lactams of *K. pneumoniae* is always caused by the loss of porins together with the expressions of β -lactamases. In addition, lipopolysaccharide (LPS) is responsible for blocking the hydrophobic antibiotics and detergents, which has been identified by the hypersensitivities of LPS mutation isolates to antibiotics. For overcoming the permeability related resistance, permeabilizers were developed, like polycationic compounds particularly for LPS.⁸⁻¹⁰

Compared with non-specific resistant factors such as the increased efflux pumps and permeability barriers of the outer membrane for Gram-negative bacteria, the resistance genes coding for enzymes are more selective for substrates or antibiotics. The degrading mechanisms of antibiotics by enzymes can be mainly classified as follows: (1) Antibiotics are degraded by enzymes via hydrolysis, e.g., β -lactamases, macrolide esterases and epoxidases which only need water as a co-substrate. Some of the enzymes are excreted by the resistant bacteria, thus the relevant antibiotics can be degraded even without entering the bacteria. (2) Antibiotics are degraded by enzymes via group transfer. Group transferases, the largest group of resistance enzymes, with co-substrates including acetyl-CoA, NAD⁺, ATP, glutathione or UDP glucose, impair the antibiotics in the cytosol by O-acylation, N-acylation, O-phosphorylation, O-nucleotidylation, etc. (3) Antibiotics are degraded by enzymes via other mechanisms. Such as the flavin-dependent monooxygenase TetX inactivates tetracycline by

hydroxylating its position 11a, and type B streptogramins can be inactivated by the Vgb lyase (virginiamicin family B component lyase). To overcome the enzymatic resistances, diverse antibiotics have been developed and inhibitors targeting the resistance enzymes have been used together with antibiotics, e.g., the combination use of β -lactams with clavulanic acid for overcoming resistant isolates expressing serine β -lactamases (SBLs). However, the updating speed of new antibiotics or inhibitors usually is too slow to meet the rapid evolutions of the resistance genes.¹¹

Table 1.1 Enzymatic Mechanisms for Antibiotic Inactivation¹¹

Mechanism	Type	Antibiotics
Hydrolysis		β -Lactams
		Macrolides
Group transfer	Acyl	Aminoglycoside
		Chloramphenicol
		Type A streptogramin
	Phosphoryl	Aminoglycoside
		Macrolide
		Rifamycin
		Peptide
	Thiol	Fosfomycin
	Nucleotidyl	Aminoglycoside
		Lincosamide
	ADP-ribosyl	
	Glycosyl	Rifamycin
		Macrolide
		Rifamycin
Other	Redox	Tetracycline
		Rifamycin
		Lyase
		Type B streptogramin

^a The table is reproduced from Ref.11.

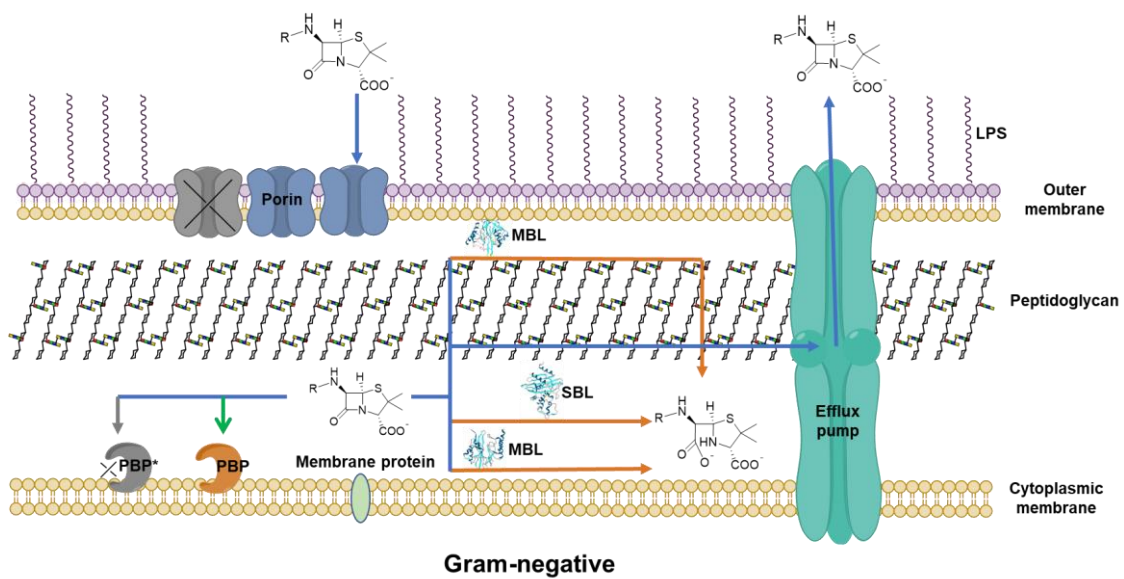
The modifications of the antibiotic binding targets have also been discovered in some isolates, such as the expressions of PBP 2a in *Staphylococcus aureus* and PBP 2x in *Streptococcus pneumoniae*, ribosomal modification, etc.¹²

1.2 β -Lactam antibiotics

1.2.1 Cell wall of Gram-positive and Gram-negative bacteria

Cell walls play important roles in keeping the shape of bacteria or to adapt them to the changeable osmotic environment and involve bacterial replication. Most prokaryotes are covered with peptidoglycan layers outside their cytoplasmic membranes, except *Archaea* organisms and mycoplasmas.^{13, 14} The structures, components, and functions of the cell wall might be different for different kinds of bacteria. For Gram-positive bacteria, the main component of the cell wall, the peptidoglycan layer, is thick (150

to 500 Å), mesh-like and cross-linked by short peptide chains. In addition to the peptidoglycan layer, the cell wall of Gram-positive bacteria also includes other components such as virulence proteins, teichoic acids, and lipoteichoic acids which are essential for bacterial virulence, adherence, and cell viability.^{13, 14} The cell wall of Gram-negative bacteria is quite different from Gram-positive bacteria and is more complex. Outside of the thin peptidoglycan layer, there is an outer membrane which is unique for Gram-negative bacteria.^{13, 14} The peptidoglycan layer of Gram-negative bacteria is covalently linked with lipoproteins which are anchored in the outer membrane. The periplasmic space between the outer surface of cytoplasmic membrane and the inner side of outer membrane contains transport systems, enzymes for metabolism, and virulence factors for pathogenic species (collagenases, hyaluronidases, proteases, and β -lactamases). In general, the asymmetric bilayer of the outer membrane is composed of phospholipids for the inner leaflet and lipopolysaccharides for the outer leaflet, and the phosphates of the lipopolysaccharide (LPS) molecules are also linked by cations (e.g., Mg^{2+} and Ca^{2+}).^{13, 14} As a result, the outer membrane is essential to maintaining the structure of Gram-negative bacteria and acting as a permeability barrier for large molecules (e.g., lysozyme) and hydrophobic molecules (e.g., some antibiotics). In addition, the porins, a group of transmembrane proteins is important for the diffusion of size limited hydrophobic molecules including many antibiotics (e.g., β -lactam antibiotics).¹³⁻¹⁶



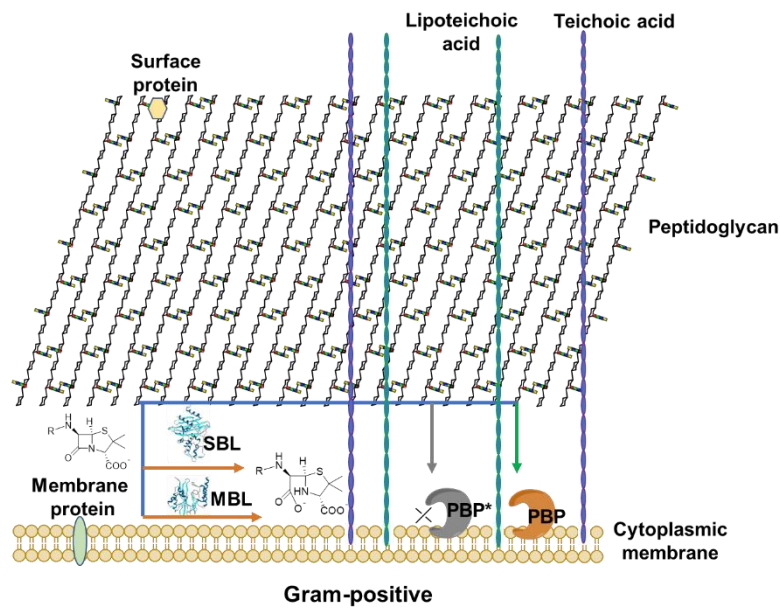


Figure 1.1 Schematic diagrams for Gram-positive and Gram-negative bacterial cell membranes and related resistance factors for β -lactam antibiotics.

The peptidoglycan is made up of linear polysaccharide chains which are cross-linked by peptides.¹⁴ The polysaccharide chains consist of repeating disaccharides of *N*-acetylglucosamine (G, NAG, GlcNAc) and *N*-acetylmuramic acid (M, NAM, MurNAc). The first two amino acids of the tetrapeptide attached to MurNAc might be various for different bacteria, but the third amino acid should belong to diamino amino acids (e.g., lysine) and the fourth amino acid is *D*-alanine. The free amine of the diamino amino acid could be linked with the *D*-alanine of another tetrapeptide by a peptide bridge (e.g., a glycine₅ peptide). The precursor of the peptide linked to MurNAc has another *D*-alanine attached to the fourth *D*-alanine which is removed during the transpeptidation reaction. The transpeptidation reaction is catalyzed by transpeptidases and limited by *D*-carboxypeptidases, both of which are the targets for β -lactam antibiotics and called penicillin-binding proteins (PBPs).^{14, 17, 18}

The β -lactam antibiotics are mimics of the transition state of the *D*-alanine-*D*-alanine structure binding with PBPs, which can interrupt the cell wall construction by competitively binding with PBPs and inactivate PBPs by forming the stable and irreversible complexes.¹⁸

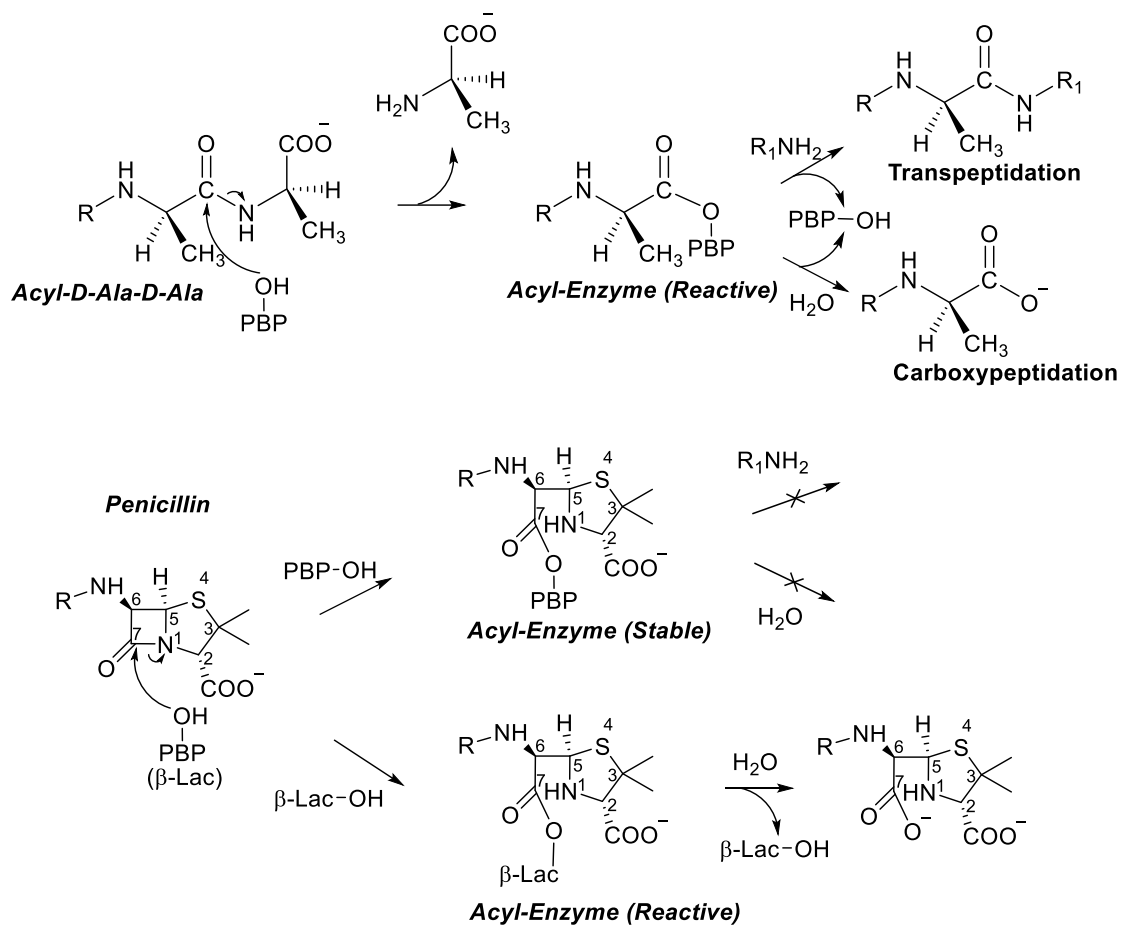


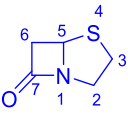
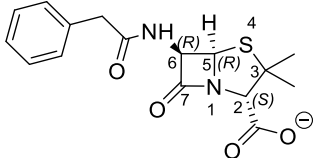
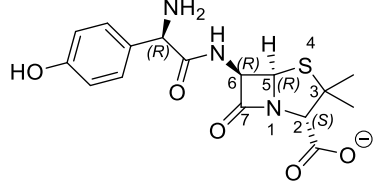
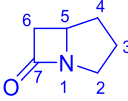
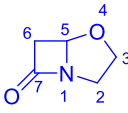
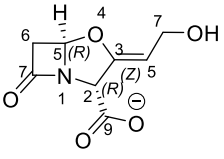
Figure 1.2 Mechanism of β -lactam antibiotics.¹⁸ (The picture is reproduced from Ref.18.)

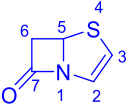
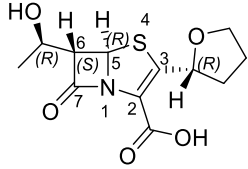
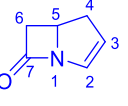
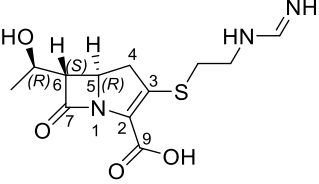
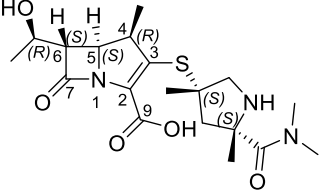
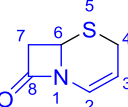
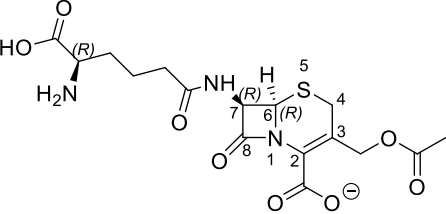
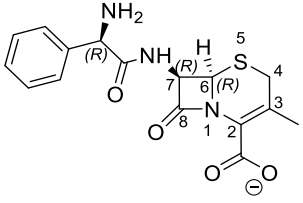
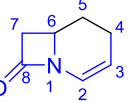
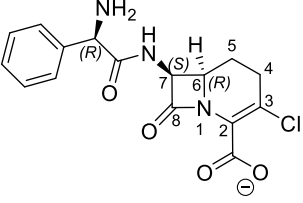
1.2.2 Classification of β -lactam antibiotics

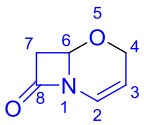
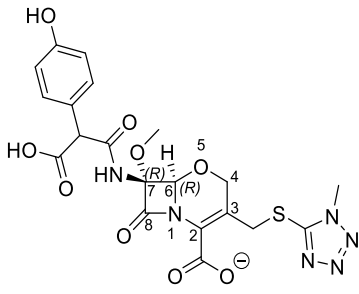
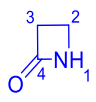
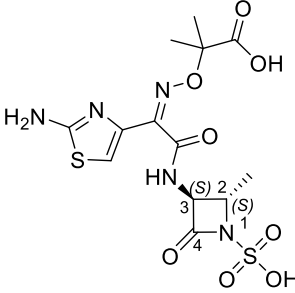
β -Lactam antibiotics have been the most widely used antibacterial agents for the treatment of bacterial infections for decades of years and remain as the cornerstone in antibacterial area at present due to their high effectiveness and few side effects.¹⁴ As mimics of the acyl-*D*-Ala-*D*-Ala C-terminus, β -lactam antibiotics interfere with the construction of the bacterial cell wall by forming a covalent bond with the serine residue of PBPs.¹⁴ Penicillin was first described by Alexander Fleming in 1929, further research on its function as an antibiotic and industrial-scale production were realized in the 1940s.^{19, 20} In 1945, cephalosporin C was discovered by Giuseppe Brotzu. Afterwards, the realization of synthesizing 6-aminopenicillanic acid (6-APA) and 7-aminocephalosporonic acid (7-ACA) in large scale enabled the development of different kinds of β -lactam antibiotics.^{21, 22} Except the core functional β -lactam ring and the acid group, based on the characters of the second rings which are fused to the β -lactam ring, β -lactam antibiotics can be mainly classified to penicillins, cephalosporins including carbacephems like loracarbef, monobactams, penems and carbapenems (**Table.1**).²² Compared with penicillins, the stability of cephalosporins was obviously improved since the less ring tension scaffold.²² The fifth generation of cephalosporins, including ceftaroline and ceftibiprole, retained broad antibacterial activity against Gram-negative bacteria especially methicillin-resistant *Staphylococcus aureus* (MRSA), and were mainly used for the treatment of community-acquired bacterial pneumonia and

bacterial skin infections.²³ The combined usage of amoxicillin and clavulanic acid was the first-line treatment for many kinds of infections, such as urinary infections, pyelonephritis, sinus infections. Aztreonam, unlike most bicyclic β -lactam antibiotics, the nitrogen of the 2S,3S monobactam ring bonds with a sulfonic acid moiety, which had less activity toward Gram-positive bacteria but broad antibacterial spectra for Gram-negative aerobes (e.g., *Pseudomonas aeruginosa*).²² Monobactams were the only class which could overcome the resistance of metallo- β -lactamases (MBLs), but could be hydrolyzed by serine- β -lactamases.²⁴ Carbapenems were the most effective antibiotics among β -lactam antibiotics and were considered to be the most reliable last resort for the treatment of severe infections, since they had highly effectivity against both Gram-positive and Gram-negative bacteria and were much safer compared with polymyxin.²⁵

Table 1.2 Classification of β -Lactam Antibiotics²²

No.	Characterization of the fused rings	Core scaffold	Examples
1	Saturated five-membered	 <p>Penam</p>	 <p>Benzylpenicillin</p>  <p>Amoxicillin</p>
		 <p>Carbapenam</p>	Biosynthetic intermediates of carbapenems
		 <p>Clavam or Oxapenam</p>	<p>This type β-lactams was divided into inhibitors of β-lactameases as most of them had no useful antibiotic functions by themselves, such as clavulanic acid.</p>  <p>Clavulanic acid</p>

2	Unsaturated five-membered	 <p>Penem</p>	 <p>Faropenem</p>
		 <p>Carbapenem</p>	 <p>Imipenem</p>  <p>Meropenem</p>
3	Unsaturated six-membered	 <p>Cephem</p>	 <p>Cephalosporin C</p>  <p>Cefalexin</p>
		 <p>Carbacephem</p>	 <p>Loracarbef</p>

		 <p>Oxacephem</p>	 <p>Latamoxef</p>
4	No fused ring	 <p>Monobactam</p>	 <p>Aztreonam</p>

1.3 β -Lactamases

1.3.1 Classification of β -lactamases

As β -lactams are the most widely utilized class antibiotics, resistance against them compromises the therapeutic choices for clinical treatment and has been a major concern threatening public health.²⁶ The most challenging resistance factors are β -lactamases (BLs).^{27, 28} The progressions of β -lactamases in *Enterobacteriaceae* family and *Pseudomonas aeruginosa* (*P. aeruginosa*) pathogens have raised global concerns in the treatment of infectious diseases.²⁷ The genes of β -lactamases are located on both chromosomes and mobile genetic elements (e.g., integrons, plasmids and transposons), and the mobile genetic elements speed up the spreading among the same or different categories.²⁸⁻³⁰ There are two kinds of nomenclatures of β -lactamases commonly used by researchers, the Ambler molecular classification using the amino acid sequences of the enzymes for classification and the Bush–Jacoby–Medeiros functional classification which is based on substrates and responses to different inhibitors.²⁷⁻³¹ 7137 β -lactamases have been discovered and documented (updated: 7th April 2021), according to the Ambler molecular classification which is used more often, and the β -lactamases have been classified into four groups, class A (1631), C (3519), D (1046) are serine β -lactamases (SBLs), whereas class B (758) are metallo- β -lactamases (MBLs).^{31, 32}

Ambler class A β -lactamases include the initial penicillinases, extended-spectrum β -lactamases (ESBLs) and some serine carbapenemases.³¹ The initial penicillinases and ESBLs are broad-spectrum enzymes mainly hydrolyzing penicillins and cephalosporins.³³ TEM-1 (the initial ampicillin resistance in *Escherichia coli* and penicillin resistance in *Neisseria gonorrhoeae*) and SHV-1 (the initial ampicillin resistance in *Klebsiella pneumoniae*) are the primary penicillinases commonly found in *Enterobacteriaceae*.^{30, 33} With the amino acid substitutions, the spectrum profiles were expanded which resulted in more variants of TEM-type and SHV-type ESBLs.³⁴ At present, CTX-M types are the most

prevalent ESBLs detected in Enterobacteriaceae, others are less common such as BES, BEL, most of GES, PER, SFO, TLA, VEB, etc.³⁵⁻⁴⁰ With mutations, TEM-type and SHV-type β -lactamases have been getting difficult to be inhibited by the previous β -lactamase inhibitors (BLIs) such as clavulanic acid and sulbactam, but most of them and the reported ESBLs are susceptible to the FDA approved inhibitors, such as tazobactam, avibactam, relebactam and vaborbactam.³¹ KPC, IMI, NMC-A, SME and some variants of GES (GES-2, GES-4, GES-11 and GES-14) are the serine carbapenemases included in class A β -lactamases.^{31, 33} KPC types are commonly found in *K. pneumoniae* and many other species of Enterobacteriaceae, especially KPC-2 and KPC-3 have been the most prevalent serine carbapenemases worldwide.³⁶ KPC types could be inhibited by avibactam and vaborbactam but not clavulanate and tazobactam.^{31, 36}

Ambler class B comprised MBLs with at least one Zn(II) ion in the active site. These lactamases hydrolyze most β -lactam antibiotics including carbapenems except for monobactams.³¹ Without approved inhibitors until now, MBLs pose severe threats to human health, especially the plasmid-encoded resistance genes which rapidly disseminated.⁴¹ The most widespread clinically related MBLs are currently IMP, VIM and NDM variants which were identified in many Gram-negative clinical isolates.^{41, 42} In 1988, IMP-1 was first detected from a strain of *P. aeruginosa* in Japan, VIM-1 was first mentioned in 1999 and identified from an isolate of *P. aeruginosa* in Verona, and NDM-1 was first identified in a *K. pneumoniae* isolate from a patient who was in India during 2007 and transferred to Sweden later. Other MBLs are less prevalent, like GIM and SPM, which were restricted to Germany and Brazil, respectively.^{41, 42}

Ambler class C are AmpC-type β -lactamases which mainly hydrolyze cephalosporins, and to a lesser extent penicillins and some monobactams.³¹ The genes of AmpC-type β -lactamases are located on chromosomes or plasmids.^{45, 46} The plasmid-encoded types like CMY, MIR, ACT and DHA are widely disseminated at present, e.g., some porin loss clinical *K. pneumoniae* and *Salmonella enterica* isolates expressing the plasmid-encoded AmpC-type β -lactamases.⁴⁵⁻⁴⁹ The plasmid-borne CMY-10 from *Enterobacter aerogenes* and the chromosomal ADC-68 from *A. baumannii* were reported exhibiting carbapenem resistance.⁴⁷

Ambler class D are constituted by oxacillin-hydrolyzing β -lactamases which have less amino acid sequence identities with class A and class C.³¹ OXA types hydrolyze most members of penicillins, and some of them could hydrolyze cephalosporins and carbapenems such as OXA-23, 24/40, 51, 58 and OXA-48 which were particularly concerned.^{50, 51} OXA-48, OXA-162, OXA-163, OXA-181 and QXA-232 were carbapenemases which have been widely spread in European and Mediterranean at present.³¹ Some enzymes of this class are inhibited by tazobactam and avibactam and most of them could be weakly inhibited by clavulanate.^{31, 50, 51}

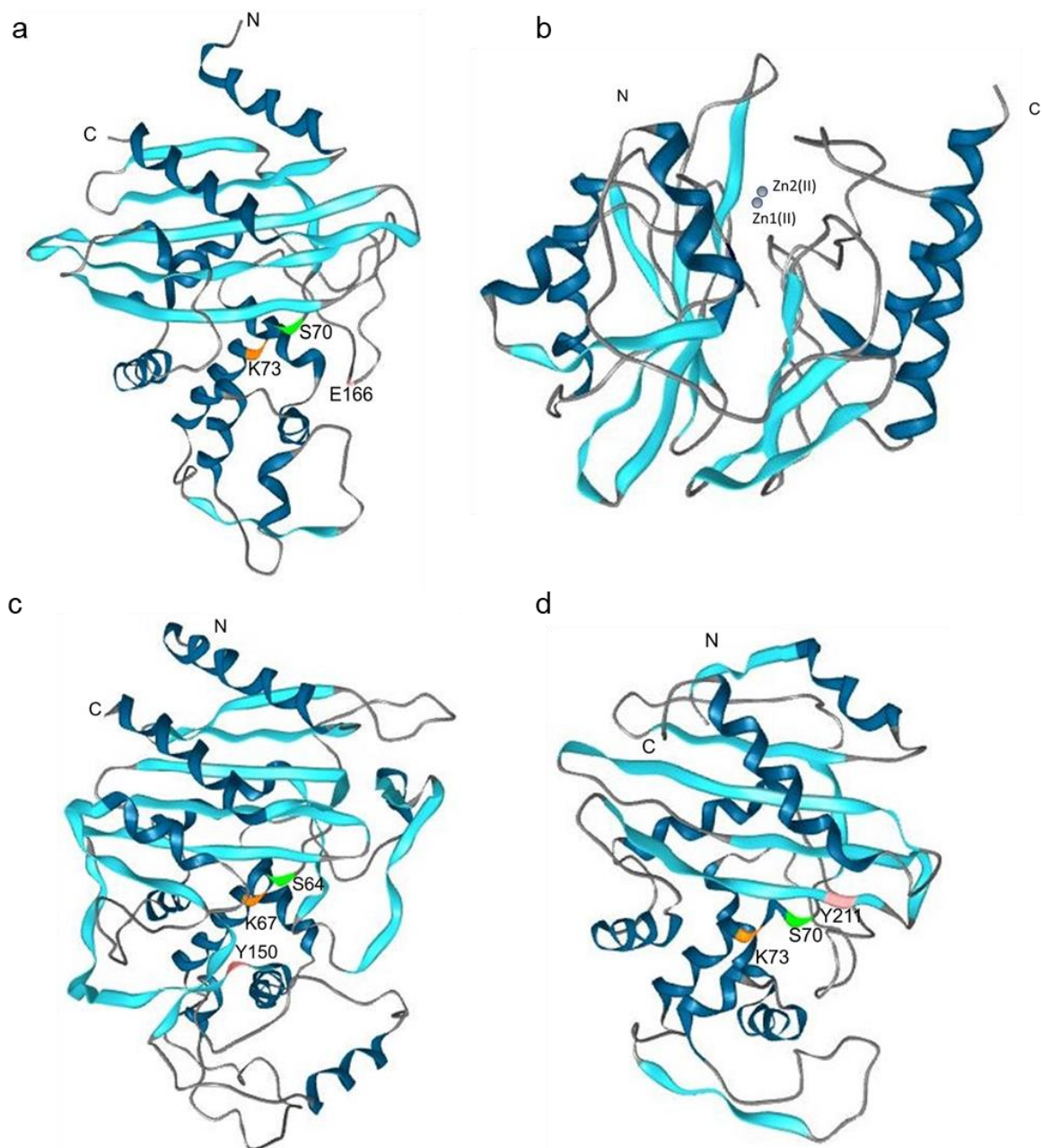


Figure 1.3 Crystal structures of BLs. a. KPC-2 (PDB ID: 5MGI); b. VIM-2 (PDB ID: 4BZ3); c. AmpC from *E. coli* (PDB ID: 6T7L); d. OXA-48 (PDB ID: 6P98). The pictures were generated by LigandScout 4.2.

1.3.2 Metallo- β -lactamases

Metallo- β -lactamases (MBLs) belong to carbapenemases and there have been no effective inhibitors against them for clinical treatments until now.^{31, 41} Instead of possessing a serine residue degrading β -lactam antibiotics through acylation and deacylation, MBLs require one or two Zn(II) ions at the active site for catalyzing the hydrolysis of the β -lactam bond.⁵² It was considered that MBLs evolved from different origins than PBPs and SBLs.^{41, 53} The first MBL was found in the Gram-positive bacterium of

Bacillus cereus in 1966.⁵⁵ The sequence similarities of MBLs are low, but their conformations are conserved. The β -sheet core enveloped by five α -helices has been described as a $\alpha\beta/\beta\alpha$ sandwich folding which is comprised by two domains, N-terminal domain ($\beta_1\beta_2\beta_3\beta_4\beta_5\alpha_1\beta_6\alpha_2\beta_7\alpha_3$) and C-terminal domain ($\beta_8\beta_9\beta_{10}\beta_{11}\alpha_4\beta_{12}\alpha_5$).^{27, 29, 53} The active site is located at the shallow grooves formed by the β -sheets, and the amino acid residues from different loops, α -helices or β -sheets coordinate one or two Zn(II) ions together, linking the two $\alpha\beta$ domains²⁷ (Figure 1.4).

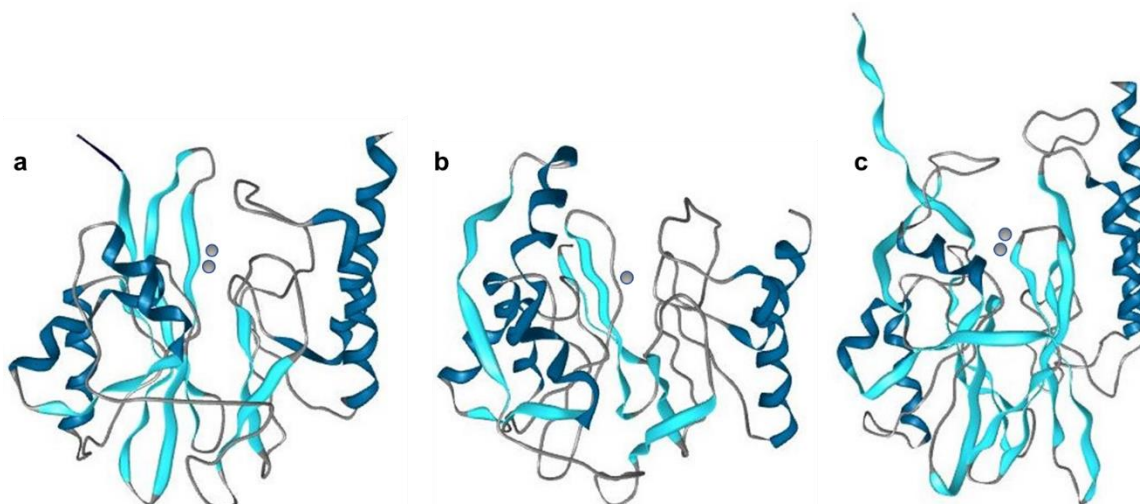


Figure 1.4 Crystal structures of MBLs. a. IMP-1 (PDB ID: 5EV6); b. CphA (PDB ID: 1X8G); c. L1 (PDB ID: 5EVK). The pictures were generated by LigandScout 4.2.

The Amble class B β -lactamases are further grouped to three subclasses B1 (522), B2 (23) and B3 (213) based on the sequence homology at the active site, zinc stoichiometry and ligands, as well as folding architectures (updated: 7th April 2021).³² The structure alignment shows that the similarity of B1 MBLs is more than 23%.²⁷ Most MBLs of subclasses B2 and B3 are chromosomal MBLs, while the genes of B1 subclass are located on chromosomes or mobile genetic elements.^{41, 53, 27}

The B1 MBLs with broad substrate spectra including penicillins, cephalosporins and carbapenems except monobactams are the largest group of MBLs and are considered to be clinically important resistance factors due to their mobile genetic characteristics, especially the most worldwide disseminated acquired MBLs including IMP, VIM and NDM types.²⁷ Generally, IMP and VIM are encoded within integrons which might be embedded with transposons allowing to be inserted to both bacterial chromosomes and plasmids.⁴¹ The genes of NDM types are different from IMP and VIM as they are not integron-related and located on the narrow-host-range plasmids belonging to IncF. Thus, *bla*_{NDM} has been frequently found in the hosts with the IncF group plasmids, e.g., *K. pneumoniae* and *E. coli*, especially the sequence type 11 (ST11), ST14, ST15, ST147 for *K. pneumoniae* and the ST167, ST410, ST617 for *E. coli*.^{41, 56} In addition, *bla*_{NDM} is generally embedded within the composite transposon Tn125 between two copies of a strong promoter ISAb₁₂₅ in *A. Baumannii*.^{57, 58} *K. pneumoniae* and *A. Baumannii* strains containing the *bla*_{NDM} gene are potentially more dangerous pathogens than the prevalent *K. pneumoniae* ST258 variants with KPC expression and *A. Baumannii* with OXA carbapenemases.^{56, 57, 58} The B1 subclass has two Zn(II) ions at the active site, however, for some IMP-types the metal ions have been different, one was zinc ion and the other has been iron ion.⁵⁹ According

to the crystallographic studies of B1 MBLs, the Zn1(II) ion binds a hydroxide anion and is surrounded by three histidine residues His116, His118, and His196 (3H site), resulting in a tetrahedral complexation.²⁷ The Zn2(II) ion binds with the same hydroxide anion, an additional water molecule and three other amino acid residues, Asp120, Cys221 and His263 (DCH site), resulting in a trigonal bipyramidal coordination.²⁷ For the hydrolytic reaction, the Zn1(II) ion polarizes the carbonyl group of the β -lactam ring, and the Zn2(II) ion prepared to link with the nitrogen atom of the β -lactam ring, as a result, the cooperation of the two zinc ions put the β -lactam bond in a proper pose for nucleophilic attack, and some studies described the substrate pose of β -lactam antibiotics as **S** and the inhibiting pose as **I**.^{27, 48, 59} The Zn1(II) ion had higher affinity with the active site than the Zn2(II) ion, however there were synergistic effects of the linkages for the two Zn(II) ions with the active site.^{48, 59}

The B2 group is the smallest category of MBLs which only had one zinc ion in the active site such as CphA and exclusively hydrolyzes carbapenems.^{27, 28, 53} Most B2 MBLs carriers are environmental bacteria and not the primary human pathogens, however an increase of CphA producing clinical isolates has been reported.⁵³ The Zn1(II) ion is lost which should link with Asn116, His118 and His196, while the Zn2(II) ion bound with Asp120, Cys221 and His263 was kept and with a higher binding affinity.⁵³ B2 MBLs apply a different hydrolyzing mechanism compared to B1 and B3 MBLs, a water molecule attacks the carbonyl carbon of the β -lactam bond with the help of Asp120 and the Zn(II) ion stabilizes the anionic nitrogen atom of the intermediate.²⁷ An extended α -helix in the active site limits the side chains of the substrates which attributes at least in part for the narrow substrate spectrum.⁵³

The B3 MBLs have less sequence similarity among their members compared with other subclasses. Similar to B1 subclass, B3 MBLs also possess a broad substrate spectrum generally, which can hydrolyze penicillins, cephalosporins, and carbapenems. However, there are some exceptions, e.g., CAR-1 nearly has no hydrolytic activity for carbapenems, SPR-1 degrades penicillins efficiently but with poor hydrolytic activity for cephalosporins and carbapenems. There are some clinically related B3 MBLs although which are less prevalent than the B1 MBLs, e.g., L1 identified only second to BcII is one of the main resistance factors for *Stenotrophomonas maltophilia*, GOB enzymes are possessed by the opportunistic pathogen *Elizabethkingia meningoseptica*.⁵³ Except for the chromosomally encoded members, some plasmid-borne B3 MBLs have been reported recently such as LMB-1, in addition, AIM-1 and SMB-1 reported to be located in chromosome were found associated to mobile genetic elements which allowed horizontal gene transfer.⁵³ The B3 MBLs contain two Zn(II) ions at the active site, for most B3 MBLs, like L1 family, the Zn1(II) ion is surrounded by His116, His118 and His196, and the Zn2(II) ion is bound with Asp120, His121 and His263, the cysteine residue which is conserved for B1 and B2 groups is absent and replaced by a histidine residue. For GOB types, the Zn1(II) ion is surrounded by Gln116, His118 and His196, while more substitutions at the Zn(II) binding locations were found for SPR-1, the HRH/DQK (H118R, H121Q, and H263K) motif was observed in SPR-1.^{27, 48, 53}

The MBLs of different subclasses can be generally distinguished by the conserved amino acid motifs at the active site, the 3H (His116, His118 and His196) and DCH (Asp120, Cys221 and His263) sites, the NHH (Asn116, His118 and His196) and DCH (Asp120, Cys221 and His263) sites, and the 3H/Q2H (His/Gln116, His118 and His196) and DHH (Asp120, His121 and His263) sites, were special for B1, B2 and B3 MBLs, respectively.^{27, 48, 53, 60, 61}

Table 1.3 Examples of Chromosomal and Plasmid Associated MBLs⁴¹

Subclass	Conventional active site		Gene types	Enzymes and species	
B1	Zn1(II), Zn2(II)	3H, DCH	Chromosomal	BclI	<i>Bacillus cereus</i>
				IND	<i>Chryseobacterium indologenes</i>
				BlaB	<i>Elizabethkingia meningoseptica</i>
				MUS and MYO	<i>Myroides odoratimimus</i>
				CfiA/CcrA	<i>Bacteroides fragilis</i>
			Plasmid associated	Verona integron-encoded metallo-β-lactamase (VIM)	
				New Delhi metallo-β-lactamase (NDM)	
				Imipenemase (IMP)	
				Sao Paulo metallo-β-lactamase (SPM)	
				German imipenemase (GIM)	
				KHM	
Dutch imipenemase (DIM)					
B2	Zn2(II)	NHH, DCH	Chromosomal (most)	CphA	<i>Aeromonas spp.</i>
				PFM	<i>Pseudomonas spp.</i>
B3	Zn1(II), Zn2(II)	3H/Q2H, DHH (most)	Chromosomal	L1	<i>Stenotrophomonas maltophilia</i>
				GOB	<i>Elizabethkingia meningoseptica</i>
			Plasmid associated	<i>Serratia</i> metallo-β-lactamase (SMB)	
				Adelaide imipenemase (AIM)	

Currently, options of clinical treatment for MBL-producing pathogens are narrow, besides most Enterobacterales with acquired MBLs co-produce resistances for fluoroquinolones and aminoglycosides.⁶³ The severe side effects of the limited choices should be highly concerned.

Polymyxins largely abandoned for clinical use as the high nephrotoxicity and neurotoxicity previously are reconsidered for treatment of multidrug-resistant Gram-negative bacteria (MDR-GNB) infections.⁶³ Colistin (Polymyxin E) is utilized as the last-resort treatment for infections caused by MBL-producing pathogens, e.g., most MBL-producing Enterobacterales and *P. aeruginosa*.⁶⁴ Colistin has high affinity with LPS and kills Gram-negative bacteria (GNB) mainly by interrupting the outer membrane and other related membrane systems, however, the resistance strains for colistin have appeared more along with the recovered usages, and some strains with intrinsic polymyxin resistance such as *Serratia marcescens* and *Neisseria spp.* are not sensitive to colistin.⁶⁴

The tetracyclines such as tigecycline, omadacycline and eravacycline showed strong activity against MBL producers except *Proteaeae* and *P. aeruginosa in vitro*.⁶³⁻⁶⁶ But there were less clinical experiences for monotherapy used for patients and the mortalities were increased by monotherapy.⁶³⁻⁶⁶ The difference of the susceptibility breakpoints for tigecycline obtained by the European Committee on Antimicrobial Susceptibility Testing (EUCAST) ($\leq 0.5 \mu\text{g/mL}$) and FDA ($\leq 2 \mu\text{g/mL}$) also made

uncertainties.^{63, 66} Given the limitations and uncertainties, combination treatments have been recommended.^{63, 65}

Aztreonam belonging to monobactams is stable to MBLs but cannot inhibit ESBLs or AmpC enzymes which are prevalently coproduced in MBL-producing *Enterobacterales*.⁶⁷ Although there were records of successful cases for the combinational usage of Aztreonam with ceftazidime-avibactam against infections of *K. pneumoniae* expressing NDM-1 and other serine carbapenemases, the safety and efficacy should be estimated.^{67, 68}

Fosfomycin might be a therapeutic option for the treatment of infections caused by MBL producers, however same as tetracyclines, the combinational usage is recommended, and more explorations are still needed.^{69, 70}

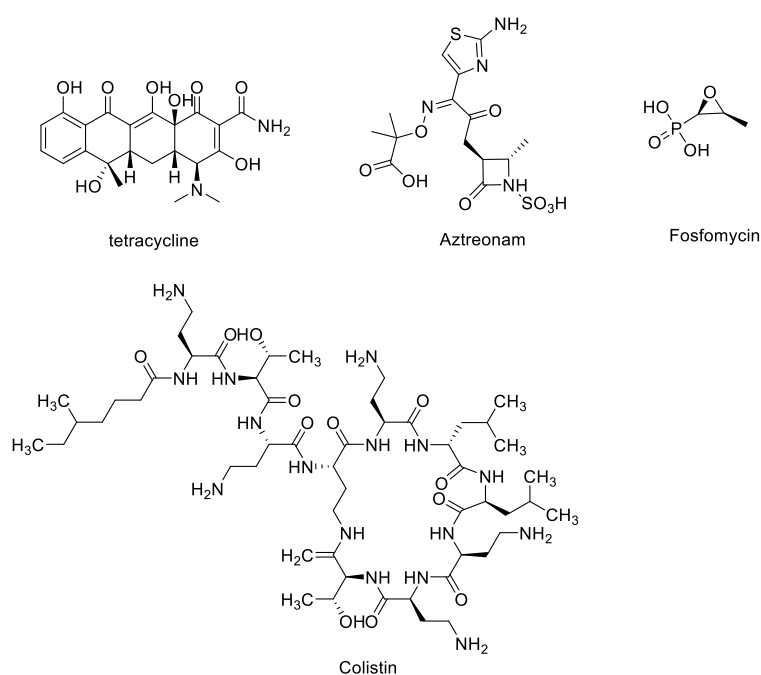


Figure 1.5 Current limited antibiotics for MBL-producing pathogens.

With less choices and limitations of monotherapies, combinational therapies have become one of the main strategies for clinical treatments and preclinical research.⁶² As for the development pipeline, the combination of Aztreonam and avibactam was at the stage of phase 3 study for infectious diseases due to MBL-producing Gram-negative bacteria, e.g., complicated intra-abdominal infections (cIAI), nosocomial pneumonia (NP), complicated urinary tract infections (cUTI) and bloodstream infections (BSI).^{68, 71} Cefiderocol (s-649266), an MBL-stable β -lactam was approved for treatment of infections due to aerobic Gram-negative pathogens with limited treatment options for adults in European Union and United Kingdom as well as for the treatment of cUTI in the United States, while there were little published cases for MBL producers, full efficacy analysis is still needed to be evaluated.⁷² BOS-228 is also a monobactam and stable to MBLs as well as most SBLs which was at the phase II development for the treatment of cUTI and cIAI.⁴¹ For Cephalosporins or carbapenems combined with DBOs, e.g., Cefepime-zidebactam was in phase 1 trial.⁷³ Cyclic boronates, VNRX-5133 (taniborbactam) and QPX7228 were inhibitors targeting at both MBLs and SBLs with additional inhibitory activities for some

PBPs.⁶³ For the more advanced taniborbactam which could inhibit classes A, C, D SBLs as well as NDM and VIM MBLs but not IMP types, the combination with cefepime was at phase III trial.⁷³ The thiol containing inhibitors against most MBLs, e.g., L/D-captopril, bisthiazolidines, ANT2681 (the lead compounds from thiazole carboxylate derivatives) and chelating agents, e.g., EDTA, Aspergillomarasmine A (AMA) were all at preclinical stages.⁶³

1.3.3 Mechanisms of β -lactamases

Although there were differences of the amino acid sequences for class A, C and D SBLs, the hydrolyzing mechanisms of them all can be concluded as acylation-deacylation mechanism. Like other serine proteases, the relevant serine residue in the active site was activated by a base and attacked the carbonyl carbon of the β -lactam bond, which generated the tetrahedral oxyanion transition state and then formed the acylenzyme intermediate. A water molecular joined the deacylation process by indirectly or directly hydrolyzing the acylenzyme, liberating the degraded substrate (**Figure 1.6**). The exact base residue for activating the serine residue was under debate for class A SBLs, both amino residues Lys73 and Glu166 were supported by relevant experimental data. The mechanism for class C SBLs remained more doubts, based on the comparison with trypsin, a conserved residue Tyr150 in the deprotonated form could serve as the general base for both the acylation and deacylation processes. An alternative hypothesis considered that the Lys67 acted as the general base for the acylation, but for the diacylation, the cooperation of the Lys67, Tyr150 and the deacylating water or substrate assisting mechanism was involving. For class D OXA enzymes, as reported, the carboxylated lysine in the active site was the general base for both acylation and deacylation process.^{48, 74}

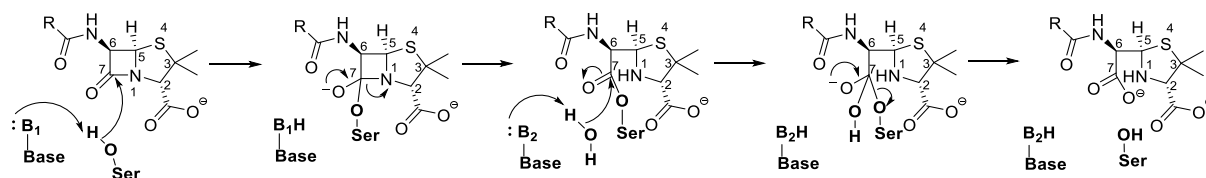


Figure 1.6 Hydrolysis of penicillin substrates by SBLs.

For MBLs, the hydrolysis was catalyzed by the two or one Zn (II) ions in the active site. As for bi-Zn(II)-MBLs, Zn1(II) ion was bound with three histidine residues and a hydroxide anion to form a tetrahedral configuration, Zn2(II) ion was linked with the hydroxide anion, an additional water molecule and three other amino acid residues, aspartic acid, cysteine and histidine to form a trigonal bipyramid configuration. The deprotonated 2-carboxyl group and the nitrogen of the β -lactam bond tended to bind with Zn2(II) ion which released the bridged hydroxide anion. Zn1(II) ion polarized the carbonyl group of the β -lactam bond, and the linked hydroxide anion attacked the carbonyl carbon forming a tetrahedral intermediate. Afterwards, the β -lactam bond was broken, the electron pair were given to the nitrogen atom which forming the anionic intermediate. For carbapenem substrates, the electron pair of the anionic intermediate was delocalized among the nitrogen and the adjacent double bond, as a result, there were two forms of the degraded substrate, one was protonated at the nitrogen and the other was protonated at the carbon atom adjacent to the sulphur atom. For mono-Zn(II)-MBLs, the carbonyl group

of the β -lactam bond was attacked by a water molecular linked with the histidine and aspartic acid residues (**Figure 1.7**).^{55, 60-62, 75}

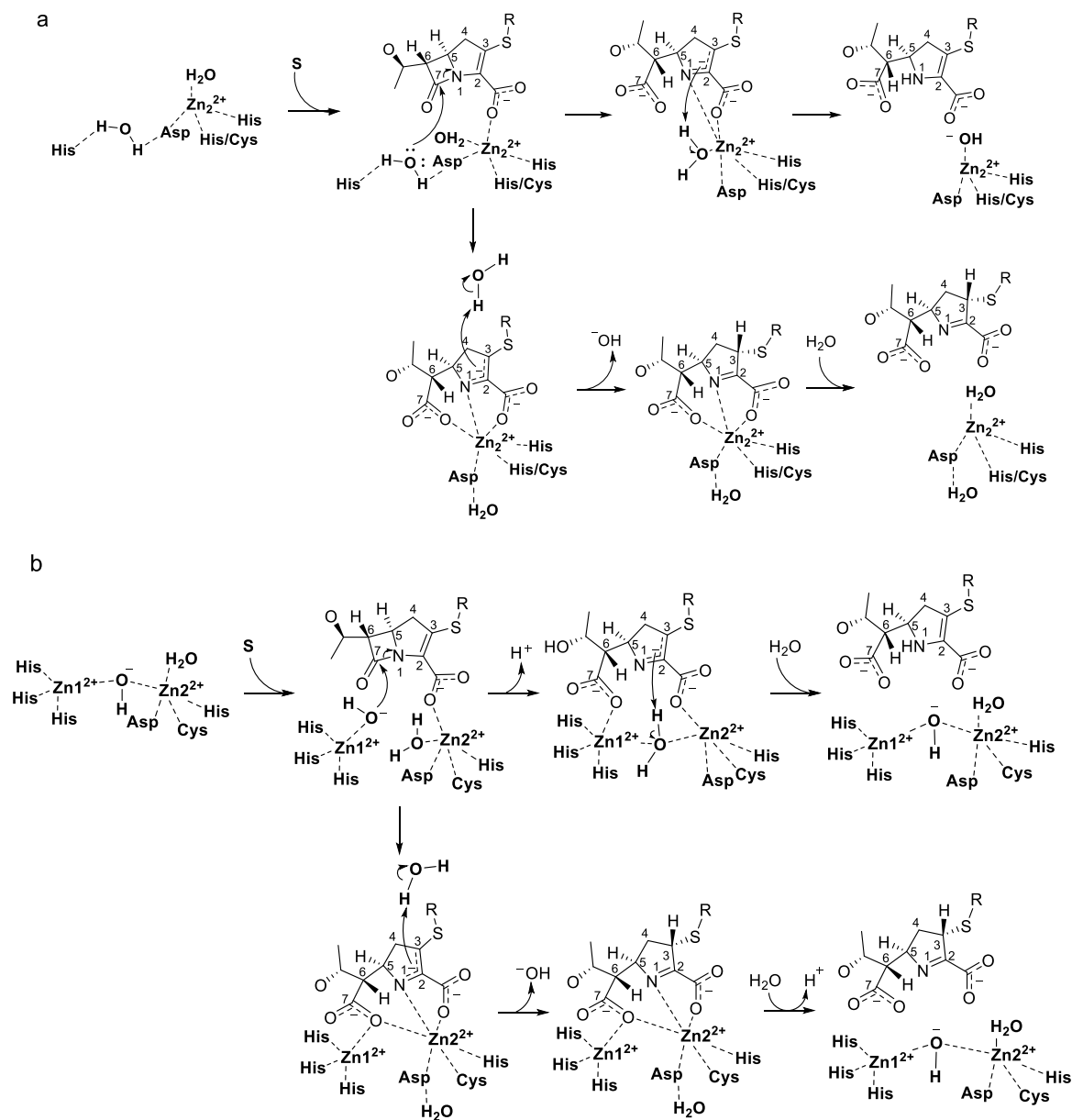


Figure 1.7 Hydrolysis of carbapenems by MBLs. a. Mechanism for mono-Zn(II)-MBLs; b. Mechanism for bi-Zn(II)-MBLs.

1.4 New Delhi metallo- β -lactamase (NDM-1)

NDM-1 was first reported by Yong et al. (2009) and has been fast disseminated and spread worldwide.⁷⁶⁻⁷⁸ Resistance by NDM-1 is commonly identified in strains of *Enterobacteriaceae*, *Pseudomonas aeruginosa*, *Acinetobacter baumannii* and other Gram-negative strains.⁷⁹⁻⁸¹ *Enterobacteriaceae* are the largest family of the clinically important bacteria, which are related to many diseases, e.g., gastroenteritis, hemorrhagic colitis, bacteremia, neonatal meningitis, urinary tract

infections, intraabdominal infections, and inflammation of lungs.¹⁴ *Klebsiella* strains are one of the major clinical challenges at present, which resist all β -lactam antibiotics and most antibiotics of other classes. *Pseudomonas aeruginosa* is related to diseases such as infections of respiratory tract, urinary tract, ears, eyes, skin and soft tissues, endocarditis, and bacteremia. *Acinetobacter baumannii* is related to nosocomial wound and pulmonary infections.^{14, 81} With a broad substrate spectrum, NDM-1 hydrolyzes nearly all the β -lactam antibiotics except for monobactams, but which can be hydrolyzed by many coproduced SBLs and aztreonam hydrolyzed by NDM-1 was even reported.^{82, 83} Compared with other B1 MBLs, the membrane located NDM-1 was more stable for zinc ion starvation conditions and had more transfer mechanisms.⁸⁴⁻⁸⁸ In addition, plasmids containing *ndm-1* always co-expressed other resistance genes against quinolones, aminoglycosides, macrolides, chloramphenicol, and rifampicin.⁸⁹ As a result, diseases and infections caused by NDM-1 producing pathogens have less treatment choices, there has been an urgent need for inhibitors targeting NDM-1.⁷⁹

1.4.1 Structure characteristic and hydrolysis mechanism of NDM-1

NDM-1 belongs to the most clinically relevant B1 MBLs, like other B1 MBLs, NDM-1 has the ' $\alpha\beta/\beta\alpha$ sandwich' conserved architecture and two catalytic Zn(II) ions in the active site. It was reported, the functional unit of NDM-1 was monomer in solution, comprising of 269 amino acid residues and with a molecular weight of 27.5 kDa. For the N-terminal subdomain, there are seven anti-parallel β -sheets surrounded by three α -helices, and for the C-terminal subdomain, there are another five anti-parallel β -sheets surrounded by two α -helices, the two subdomains are connected by additional residues from Phe163 to Asn166 locating at the loop region. The active site of NDM-1 is shallow and surround by several loops, the two Zn(II) ions in the active site are enclosed by loop 3 and loop 10, loop 3 containing important hydrophobic amino acid residues (Leu65, Met67, Phe70 and Val73) for substrate recognition, loop 10 containing Asn220 and Lys211 which joined the hydrolysis process of the substrate as well as Cys208 which bound with Zn2(II) ion. Zn1(II) ion was coordinated by three histidine residues (His120, His122 and His189) and a hydroxide showing a tetrahedral conformation, Zn2(II) ion bound with Cys208, Asp124 and His250 residues, one water molecular and the same hydroxide bridged with Zn1(II) ion forming the trigonal pyramidal architecture. Except the amino acid residues of loop 3, the Trp93 and Ile35 were also joining the formation of the hydrophobic surface for interacting with the R group of β -lactam antibiotics, on the contra, Trp93, Gln123, Asp124 and His250 formed the hydrophilic surface for substrate binding. Gln123 and Asp124 could form H-bond interactions with substrates. Except the amino acid residues for the hydrolyzing activity of NDM-1, there were other important amino acid residues for keeping the stability of the active site or the protein, Tyr229 stabilized loop 10 by both hydrophilic and hydrophobic interactions, Lys125 stabilized loop 6 through H-bond interactions and restricted residues coordinating Zn1(II) ion. Phe70 favored the flexibility of loop 3 for interacting with substrates. The two Zn(II) ions played important roles for both the activity and stability of NDM-1. Compared with other B1 MBLs, the relatively larger active pocket of NDM-1 offered it a broader substrate spectrum.^{82-86, 90}

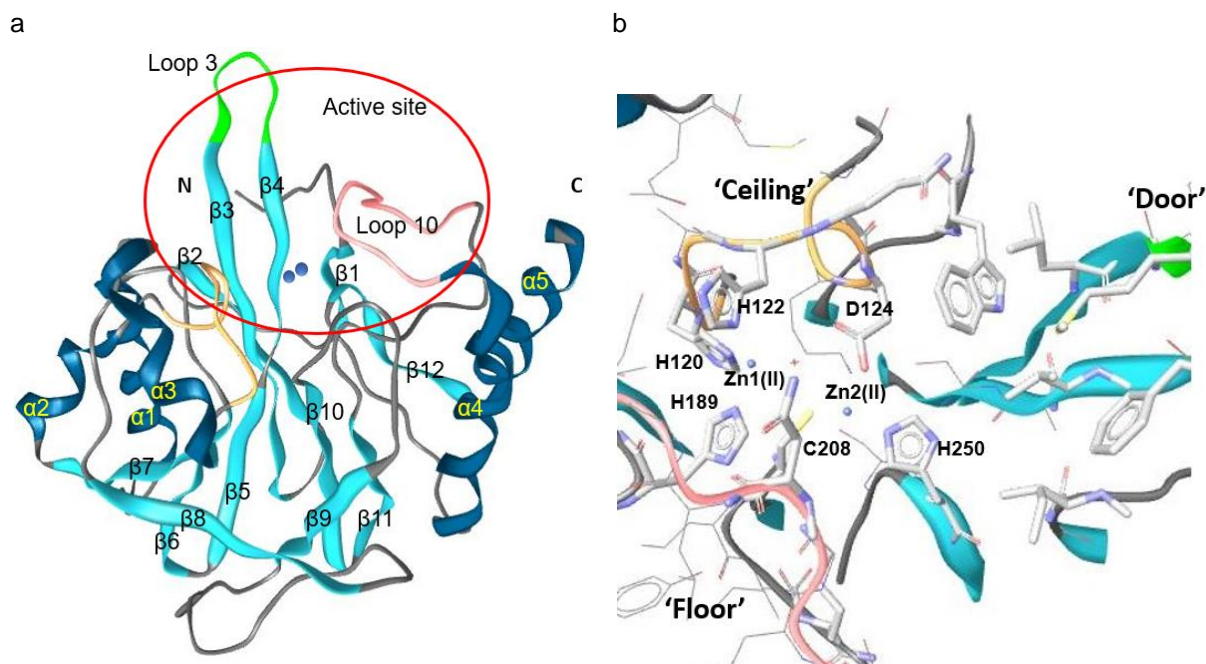


Figure 1.8 Crystal structure of NDM-1 (PDB ID: 5ZGR). a. The structure of NDM-1; b. The active site of NDM-1. The pictures were generated by LigandScout 4.2. The loop region from Met67 to Gly71 acting as the 'Door' was colored in green, the loop region from Thr119 to Met126 acting as the 'Ceiling' was colored in orange and the loop region from Ser217 to Asp225 acting as the 'Floor' was colored in pink.

For the hydrolysis mechanism of NDM-1, the general two key steps, anionic intermediate formation and the followed protonation process were most accepted.^{48, 83, 91-103} Zn₂(II) ion released the bridged hydroxide anion and bound with the deprotonated 2-carboxyl group and the nitrogen of the β -lactam bond. Zn₁(II) ion orientated the carbonyl group of the β -lactam bond, and the linked nucleophilic hydroxide attacked the carbonyl carbon forming the tetrahedral transition state.⁹¹⁻⁹³ After the β -lactam bond was broken, the anionic intermediate was formed.⁹¹⁻⁹³ The following rate limiting protonation step was under debated especially for carbapenem substrates, the two main points were the water source for protonation and the possible protonated positions caused by the delocalized electron pairs between the nitrogen atom and the adjacent double bond.^{52, 95-103} The proposed mechanisms of cephalosporin and carbapenem substrates hydrolyzed by NDM-1 are shown in **Figure 1.9**.^{52, 93-103}

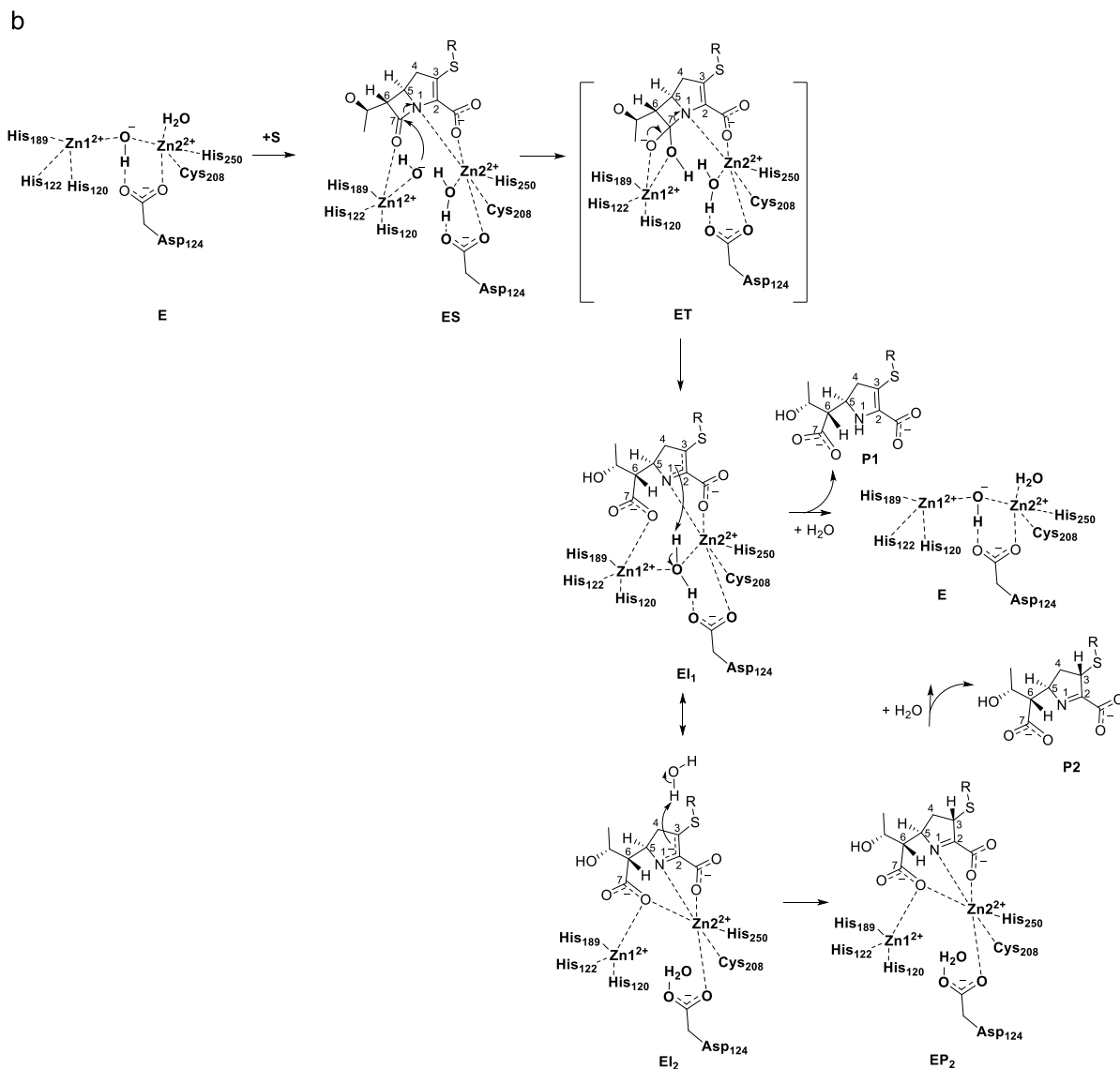
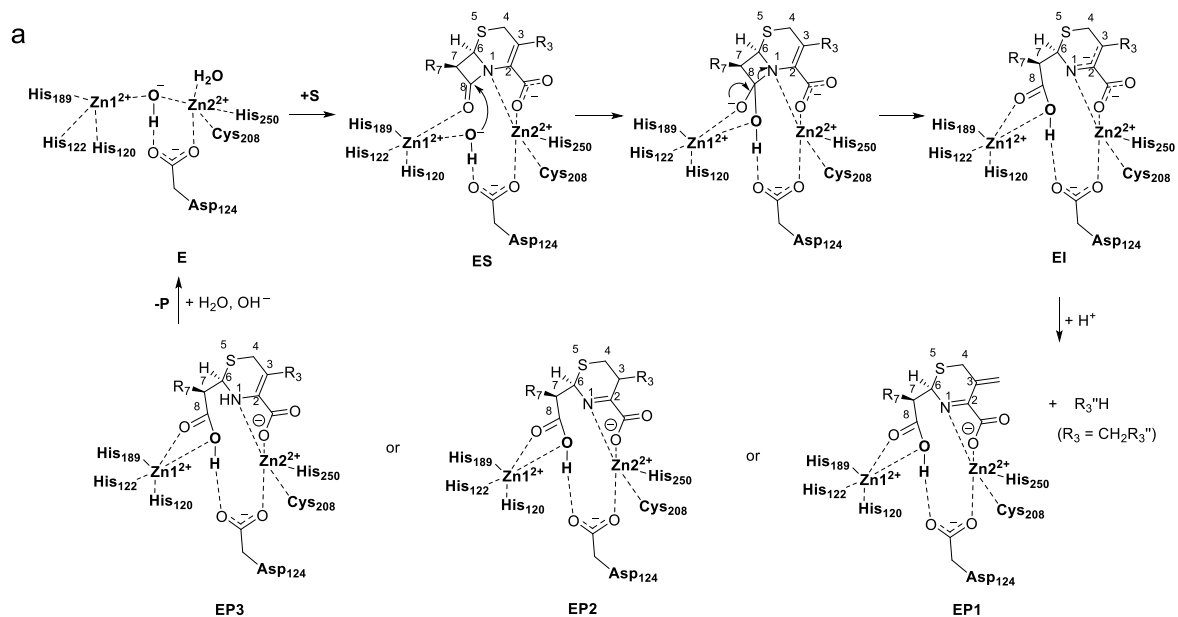


Figure 1.9 Proposed mechanisms of cephalosporin and carbapenem substrates hydrolyzed by NDM-1. a. Cephalosporins hydrolyzed by NDM-1; b. Carbapenems hydrolyzed by NDM-1.

For Gram-negative bacteria, the precursors of MBLs had N-terminal signal sequences, which guided them to the secretion machinery for the translocation to the periplasmic space.^{89, 91, 104-107} Different from other MBLs, such as VIM, IMP and SPM, which were soluble periplasmic proteins, NDM-like proteins were lipoproteins and anchored at the inner side of the outer membranes for Gram-negative bacteria. The metal ions not only played key roles for the activities of MBLs, but also their stabilities.¹⁰⁶ Under Zn(II) ion starvation conditions, soluble apo MBLs were easily to be degraded, but the existing form of NDM-1 and its variants favored their improved stabilities to Zn(II) ion deprivation.^{87, 88} The unique localization of NDM-1 as well as its variants also favored the secretion of outer membrane vesicles (OMVs), which was another communication strategy among bacteria.^{87, 88} On the one hand, the OMVs of NDM proteins protected the nearby carbapenem-susceptible bacteria by hydrolyzing the antibiotics in the environment directly or transferring the protein or relevant resistant genes, on the other hand, the OMVs helped to relieve the pressure of outer membrane and periplasmic space reducing the degradation of the overexpressed protein, which improved the efficiency of protein expression.^{87, 88}

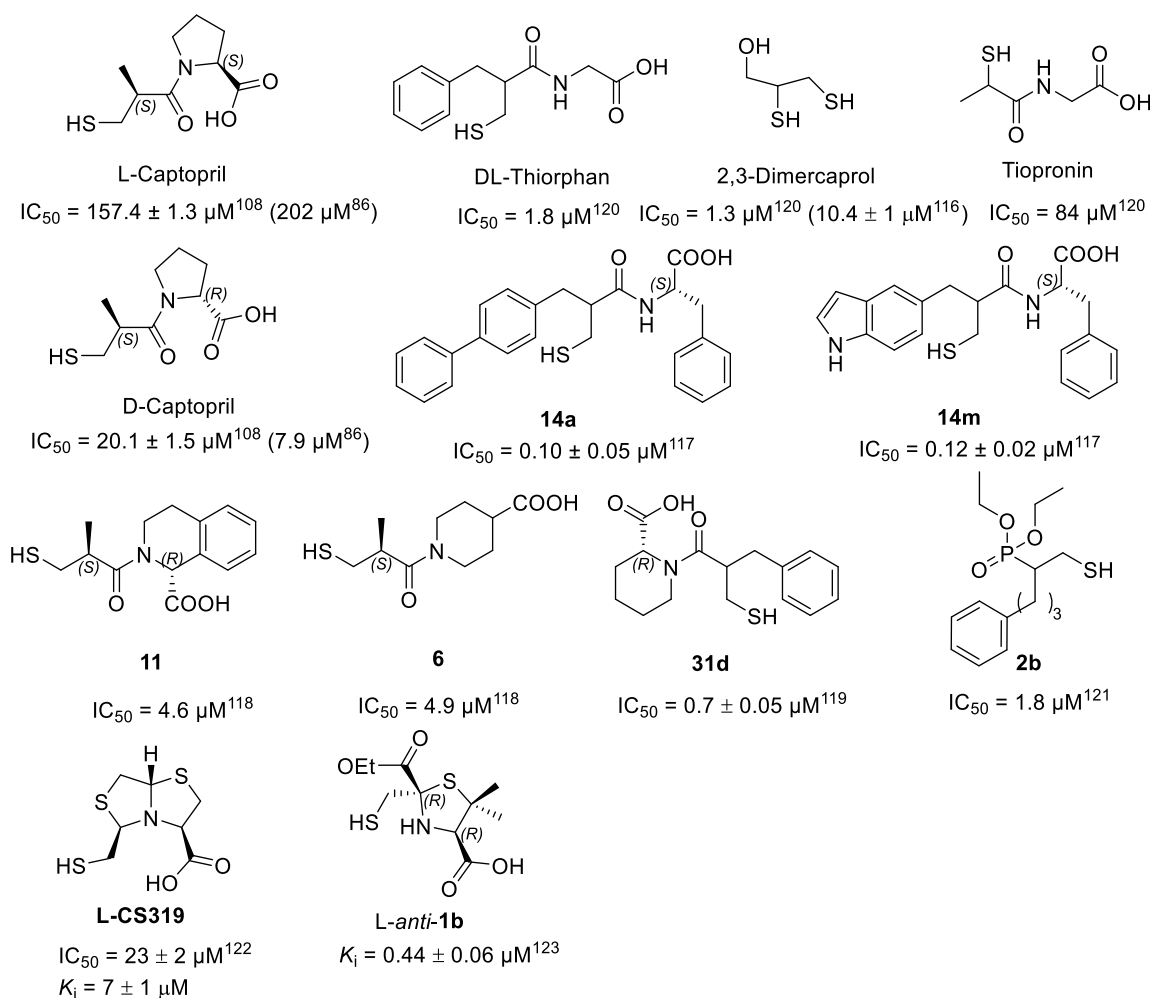
30 variants of NDM-type MBLs were reported after the first identification of NDM-1, which were even more stable to Zn(II) ion starvation conditions than NDM-1, however there have been no effective inhibitors of NDM-1 producing pathogens for clinical treatment until now.^{85,89} The rapid spreading and evolution speed of NDM-1, limited and toxic alternations of the last line antibiotics and even the resistance emergence of the alternative antibiotics have increased the nervous situation.^{79,89}

1.4.2 Inhibitors of NDM-1

1.4.2.1 Thiol-based inhibitors

L-Captopril targeting human angiotensin-converting enzyme (ACE) had been used for treating hypertension for decades of years and gradually replaced by other optimized types. Both L-captopril and D-captopril were inhibitors for NDM-1 as well as some other MBLs, and it was reported that D-captopril was more active than L-captopril for NDM-1.^{86, 108-111} The general mechanism for thiol containing inhibitors was binding with the Zn(II) ions in the active site of relevant MBLs via their thiol groups.¹¹²⁻¹²³ According to crystallographic studies as well as some docking studies of NDM-1 with L- or D-captopril, the interactions of the thiol groups with the Zn(II) ions and the amino acid residues in the active site were similar, both L- and D-captopril could bind with the two Zn(II) ions and form H-bond interactions with His189 and His250, and L-captopril also had H-bond interactions with Asp124.¹⁰⁸ In addition, it was reported that the thiol group might replace the nucleophilic hydroxide or water molecular coordinated with the two Zn(II) ions. The methyl groups of both L- and D-captopril showed hydrophobic interactions with Trp93, while the construction of D-captopril enabled its more hydrophobic interactions, such as interactions with Met67, and its deprotonated carboxyl group of the proline part had the H-bond interaction with Asn220 and the negative ionizable interaction with Lys211. L-captopril had no interaction with Lys211, as for Asn220, except for the interaction with the deprotonated carboxyl group of the proline part, the carbonyl group of the amide bond showed the H-bond interaction with Asn220.^{108, 109} These differences might contribute a better IC₅₀ value of D-captopril than L-captopril for NDM-1. There were developed inhibitors for NDM-1 derived from D-captopril which were optimized via different

strategies, e.g., increasing the five-membered ring of the proline to six-membered ring and adding or replacing the ring by a phenyl or other groups to increase the hydrophobic interactions, changing the position of the carboxyl group to strengthen the interactions with relevant amino acid residues.¹¹⁶⁻¹¹⁹ Except for D/L-captopril, Klingler et al. (2015) discovered other approved thiol containing drugs had inhibitory activities for NDM-1, VIM-1 or IMP-7, e.g., D/L-Thiorphan (an enkephalinase inhibitor), *N*-Acetylcysteine (a medication used for treating paracetamol overdose or loosening thick mucus for patients with chronic bronchopulmonary disorders and only against IMP-7), 2,3-Dimercaprol (a medication used for treating acute poisoning of metalloids or heavy metals), and Tiopronin (an orphan drug used for treating with cystinuria).¹²⁰ Skagseth et al. (2017) developed NDM-1 inhibitors by bioisosteric replacement substituting the carboxyl group of mercaptocarboxylic acids by phosphonic acid or phosphonate groups.¹²¹ There were many other thiol containing inhibitors for NDM-1, e.g., Gonzalez et al. (2015) developed substrate-like structures based on the bithiazolidine (BTZ) scaffold, the represented inhibitor was L-CS319 ($IC_{50} = 23 \mu M$);¹²² according to the studies of BTZs and L/D-captopril, Rossi, M. A. developed a series of 2-mercaptomethyl-thiazolidines (MMTZs), the representative compound is shown in **Figure 1.10**, L-*anti*-**1b** ($K_i = 0.44 \pm 0.06 \mu M$).¹²³



^a The IC_{50} or K_i values were tested via different substrates or assay conditions.

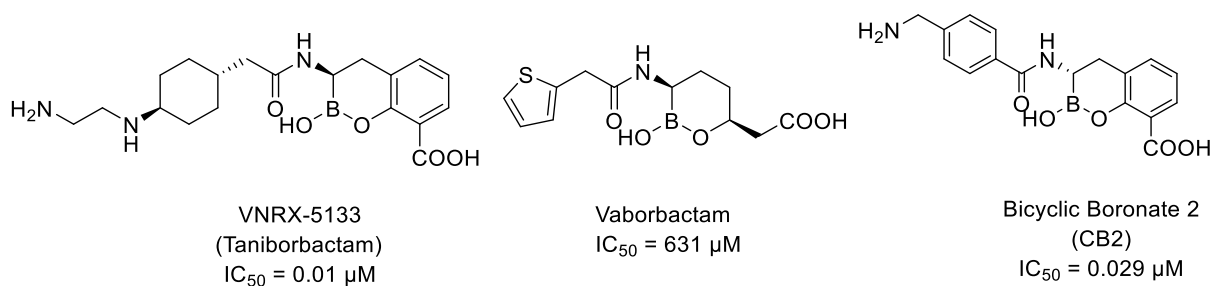
Figure 1.10 Thiol containing inhibitors of NDM-1.^{86,108, 116-123}

Although thiols with high affinity to Zn(II) ions, their instabilities and undesirable smells limited the further development. In addition, most of the reported thiol containing inhibitors were not broad-spectrum inhibitors or did not test and some promising inhibitors failed at or without the evaluations of re-sensitizing clinical isolates. Furthermore, a larger number of the thiol containing inhibitors were developed based on the approved drugs targeting human enzymes, the selectivity, side effects and possible reduced *in vivo* efficacy should be considered and most of them did not address the potential problems. Above all, there is still a far way for the thiol containing inhibitors to arrive to the clinical treatment.

1.4.2.2 Bicyclic boronate inhibitors

Most inhibitors of NDM-1 were under preclinical research stages, the bicyclic boronate VNRX-5133 (taniborbactam) with an IC_{50} value of 0.01 μM against NDM-1 (using cephalosporin probe FC5 as the substrate for the *in vitro* activity test) which was also inhibiting SBLs and some other B1 MBLs including VIM-1/2 but with less activity for IMP-1. According to the crystallographic studies, VNRX-5133 inhibited both SBLs and MBLs via tetrahedral boron moieties binding with the active site of the BLs.¹²⁴⁻¹²⁶ The interchange of the hybridization forms sp^2 and sp^3 of the boron atom was enable VNRX-5133 to be the mimics of the β -lactam substrates during the hydrolysis especially the transition state from the intact carbonyl of the β -lactam bond to the tetrahedral intermediate.¹²⁴ Compared with the previous generations of boron inhibitors, VNRX-5133 had a broader inhibitory spectrum, e.g., vaborbactam mainly against SBLs, CB2 with the less broad inhibitory spectrum. The bicyclic boronate ring was necessary for the inhibitory activity and the modifications of the amino side chain played important roles for broadening the inhibitory spectra.^{124, 125} However, there were less proved drugs containing boronic acid moiety, the acceptance of boronic acid moiety for drug development is little, and the oxidative cleavage of C-B bond is one of the concerns.

a



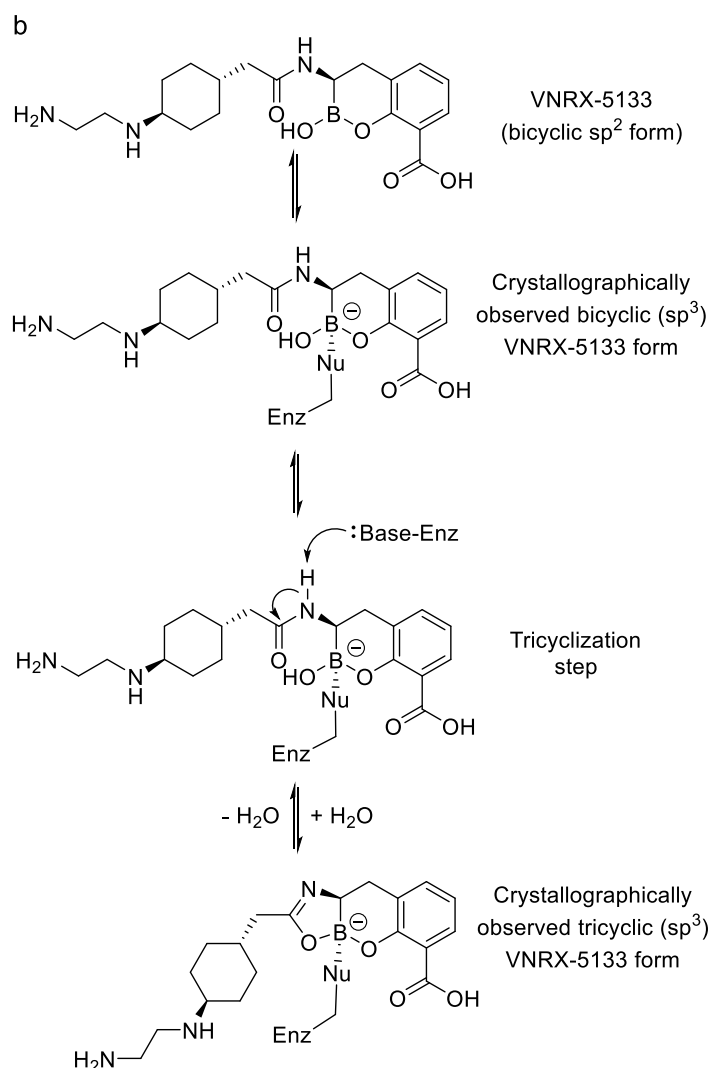


Figure 1.11 a. Boron inhibitors for β -lactamases; b. Proposed mechanism of VNRX-5133. (The picture is reproduced from Ref.124.)^{124, 125}

1.4.2.3 Metal ion chelating or binding inhibitors

The commonly used metal chelator ethylenediaminetetraacetic acid (EDTA) inhibited NDM-1 and other relevant MBLs via depriving the Zn(II) ions in the active site of the protein.⁸⁶ Discovered by King et al. (2014), Aspergillomarasmine A (AMA), a fungal extract from *Aspergillus versicolor* against NDM-1 and other relevant MBLs with a similar mechanism as EDTA, could re-sensitized the resistant strains expressing NDM-1 and VIM-2 but not IMP-1, animal tests indicated that AMA could restore the capacity of meropenem for the mice infected with NDM-1-expressing *Klebsiella pneumoniae*.¹²⁷⁻¹³⁰ Albu et al. (2016) synthesized the analogues of AMA, e.g. Aspergillomarasmine B (AMB) and Lycomarasmine, the *in vitro* inhibitory activities of the analogues for NDM-1 were remained, but the abilities for restoring the capacity of meropenem for the tested resistant isolates were reduced.¹²⁸ Via chemoenzymatically catalyzing method, Tehrani et al. (2020) developed NDM-1 inhibitors based on AMA and ethylenediamine-*N,N'*-disuccinic acid (EDDS), highlighting the important roles played by the aliphatic spacers.¹³¹ The unselective metal ion sequestering mechanism and the initial complex synthesizing

routes of AMA or its analogues hindered their further development. Based on the published works about AMA, EDTA, DPA and the hydrolyzed structures of penicillins, Chen et al. (2020) concluded the iminodiacetic acid (IDA) metal-binding pharmacophore (MBP) of the chelating inhibitors which played key roles for inhibiting NDM-1 and other relevant MBLs.¹³² The representing IDA derivatives, e.g., **1** ($IC_{50} = 25 \mu M$) and **23f** ($IC_{50} = 8.6 \mu M$) could form ternary binding complexes with NDM-1 protein including the Zn(II) ions, and opposite to EDTA, the IDA derivatives stabilized NDM-1 protein for the thermal shift assays, while the ΔT_m values did not consistent with the IC_{50} values of the tested inhibitors.¹³² 2,6-Dipicolinic acid (DPA) is a relative weaker chelator than EDTA, Chen et al. (2017) developed DPA derivatives with improved selectivity and activity, the representing compound **36** ($IC_{50} = 0.08 \mu M$) was included in **Figure 1.12**.¹³³

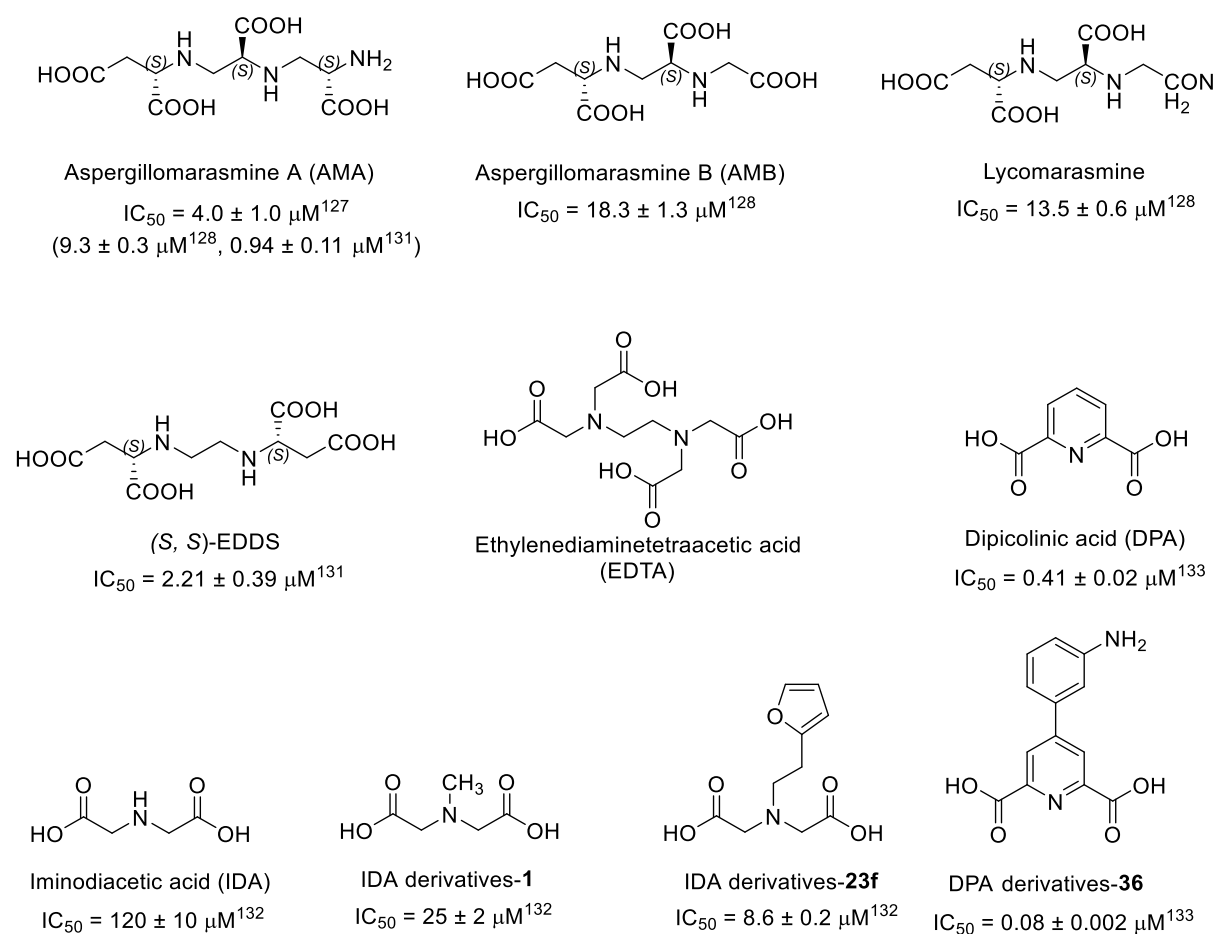


Figure 1.12 Metal ion chelating or binding inhibitors of NDM-1.^{127, 128, 131-133}

Although the less selectivity of most initial chelators hindered their further development for clinical treatment of infections or diseases caused by isolates expressing MBLs, their highly efficacy for inhibiting MBLs and improved specificity via rational modifications and designs supported the therapeutic potential of metal binding pharmacophore containing analogues for overcoming the MBLs. Except the analogues of EDTA and DPA mentioned above, there were some other scaffolds. Falconer et al. (2015) improved the specificity of spiro-indoline-thiadiazole chelators for Zn(II) ions via adding aromatic substituents at both the nitrogen of the indoline ring and the carbon of the thiadiazole ring,

e.g., **SIT-Z5** ($IC_{50} = 6.6 \mu\text{M}$), which effectively re-sensitized the NDM-1 producers to meropenem.¹³⁴ Zhai et al. (2016) designed and synthesized triazolylthioacetamide inhibitors targeting NDM-1, according to docking studies, the triazole played important roles for bridging the two Zn(II) ions, and the amide part interacted with Lys211.¹³⁵ Based on an old antiviral drug methisazone, Song et al. (2017) synthesized a series of isatin- β -thiosemicarbazones (IBTs), improving the IC_{50} value of 297.60 μM of methisazone to 2.72 μM of the most active compound **14**.¹³⁶ According to docking studies, the sulfur atom of the IBT scaffold was responsible for coordinating with the two Zn(II) ions and forming H-bond interactions with His189, the other part of the scaffold also formed multi interactions with the amino acid residues (e.g., Thr34, Val73, Trp93, Gly219, Asn220, Gly222 and Gly69) in the active pocket of NDM-1.¹³⁶ The natural product embelin was isolated from *Embelia ribes*, which had been reported with anti-tumour effects before, and recently the inhibiting activity of embelin against NDM-1 was discovered and tested by Ning et al. (2018).¹³⁷ The IC_{50} value of embelin for NDM-1 was 2.1 μM using meropenem as the substrate. According to docking studies, embelin coordinated with one of the Zn(II) ions via a hydroxyl group, the H-bond interactions with Cys208 and Asp124 as well as the hydrophobic interactions with Asn220, His122 and His189 were important for the specificity of embelin binding with NDM-1.¹³⁷ Magnolol, a natural product isolated from the bark of magnolia trees was first found inhibiting NDM-1 with an IC_{50} value of 6.47 $\mu\text{g/mL}$ (24.3 μM , nitrocefin as the substrate) by Liu et al. (2018).¹³⁸ Shi et al. (2019) found five potential inhibitors for NDM-1 via virtual screening of a natural product library, the most active compound was hesperidin ($IC_{50} = 3.348 \pm 1.35 \mu\text{M}$).¹³⁹ Ge et al. (2019) synthesized a series of dithiocarbamate analogues, **DC1**, **DC8** and **DC10** had broad inhibitory spectra inhibiting MBLs including NDM-1, IMP-1, VIM-2, ImiS, and L1.¹⁴⁰ According to the performed docking studies for **DC1** and **DC8**, the carbonyl group played important roles for coordinating the Zn(II) ions and the sulfur atoms had H-bond interactions with Lys211 and Asn220. As for **DC1**, the hydroxyl group of the benzene ring also coordinated with the two Zn(II) ions.¹⁴⁰ Farley et al. (2021) reported that *N*-sulfamoylpyrrole-2-carboxylates (NSPCs) analogues were potent inhibitors for B1 MBLs including NDM-1, according to the crystallographic studies of compound **6a** in the active pocket of VIM-1, the sulfamoyl group replaced the water molecule bridging the two Zn(II) ions. The carboxyl group interacted with both Zn(II) ions and was closer to Zn2(II) ion, the fluoro-substituted benzene ring and pyrrole ring contributed the hydrophobic interactions with Trp67 and Trp87. There were also H-bond interactions of the ligand with His179, His114, Asp118 and Asn210.¹⁴¹ Jackson et al. (2021) developed analogues of the bacterial natural product UK-1, compound **9** against NDM-1 with an IC_{50} of 0.38 μM and recovered the meropenem susceptibility for strains expressing NDM-1 at 25 μM . According to their mechanism and docking studies, compound **9** could forming the complex with NDM-1 including the Zn(II) ions and mainly interacted with Zn2(II) ion.¹⁴² Rhodanines had been used for inhibitor studies for PBPs,¹⁴³ SBLs (P99 and TEM-1),¹⁴⁴ and MBLs (VIM-2 and IMP-1) before,¹⁴⁵ Xiang et al. (2018) synthesized analogues of Rhodanines for developing broad spectrum inhibitors, the diaryl-substituted rhodanines showed broad inhibitory activities against NDM-1, VIM-2, ImiS, and L1, and the representing compound **21** ($IC_{50} = 1.31 \mu\text{M}$) is listed in **Figure 1.13**.¹⁴⁶ Their works suggested that rhodanines might be a promising scaffold for broad-spectrum inhibitor development, but there were contradicting modifications against MBLs and SBLs, which should be considered.

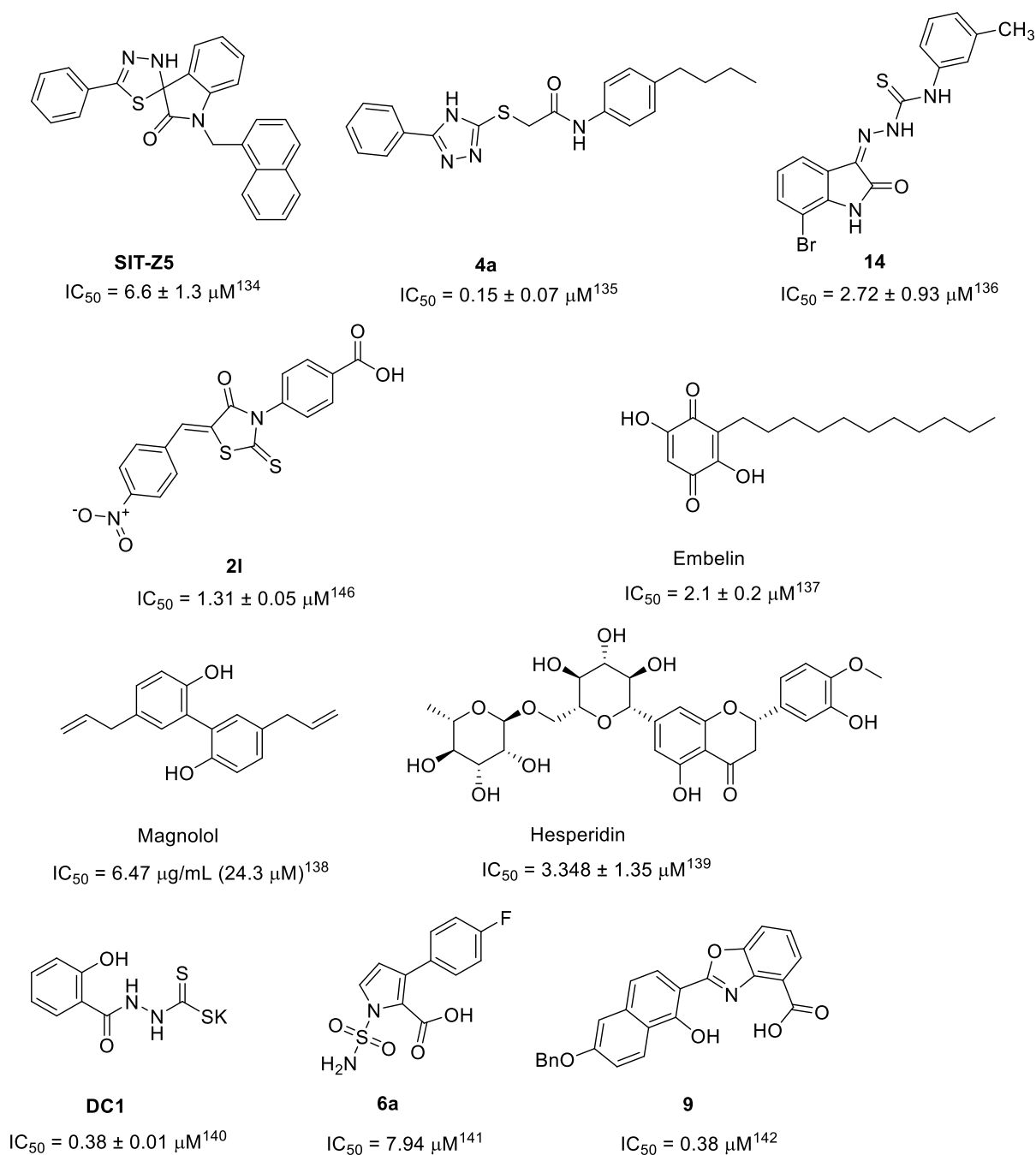


Figure 1.13 Metal binding pharmacophore containing analogues for overcoming NDM-1.^{134-142, 146}

The Zn(II) ions in the active site played essential roles for the hydrolyzing activity and stability of NDM-1, all the reported inhibitors relied on their direct or indirect interactions with the Zn(II) ions. The metal ion chelating or binding inhibitors could efficiently inhibit NDM-1, but the zinc depriving mechanism was not preferred by drug development considering the less selectivity. Currently, most of the developed metal ion chelating or binding inhibitors such as EDTA, AMA and their derivatives have been hindered for further studies, as their inhibiting mechanism depends on the depriving metal ions of the protein instead of specifically binding with the active pockets, which might influence other metalloproteins and disturbs the metal ion metabolism. In addition, the polyanionic structures also have

poor permeability for the membrane which might influence the cell-level activity. Most of the structures in **Figure 1.13** were multi-target structures, their specificity and binding affinity still have a much bigger space to improve. Above all, it is necessary to optimize the ligands improving the binding affinity to excel the advantages of zinc ion binding inhibitors and speed up the process for inhibitor development. Compared with the initial metal chelators such as EDTA and AMA, the metal binding pharmacophore containing analogues with both improved activity and selectivity for NDM-1 via reasonable modifications is a promising strategy for inhibitor development of NDM-1.

1.4.2.4 Covalent binding inhibitors and others

Except the zinc ion binding inhibitors, the amino acid residue Cys208 coordinating with Zn2(II) ion at the active site of NDM-1 offered the clue for the development of covalent inhibitors. Chiou et al. (2015) discovered the inhibitory activity of ebselen for NDM-1 via cell-based screenings.¹⁴⁷ Ebselen inhibited NDM-1 by forming covalent bond with Cys208, which disturbed the coordination of the protein and Zn2(II) ion, as a result, the protein covalently bound with ebselen and lost Zn2(II) ion.¹⁴⁷ Based on the previous work, Jin et al. (2018) developed a series analogues of ebselen by substituting the *N*-phenyl by other groups, a representative molecule **11_a38** ($IC_{50} = 13 \mu M$) showed highly synergistic activity with meropenem against clinical strains expressing NDM-1.¹⁴⁸ Su et al. (2019) developed inhibitors based on the ebsulfur scaffold which was substituted the selenium atom of ebselen by sulfur, the most active compound **1g** ($IC_{50} = 0.16 \mu M$) is shown in **Figure 1.14**.¹⁴⁹ Chen et al. (2019) developed derivatives of ebselen, most of them were inhibitors for B1 and B2 MBLs, and compound **5b** which was linked ebselen with a cephalosporin also showed competitively inhibitory activity for L1. Their work suggested a way for broadening the inhibitory spectra of ebselen analogues.¹⁵⁰ Kang et al. (2019) reported that 3-bromopyruvate (3BP) inhibited NDM-1 by both enzyme-based and cell-based assays, and the inhibitory mechanism might be related to the forming of a reversible covalent bond with Cys208 in the active site of NDM-1.¹⁵¹ Disulfiram used for treating alcohol dependence was found inhibiting NDM-1 by Chen et al. (2020). Not only forming S-S covalent bond with Cys208 by disulfiram itself, but also the *in vivo* metabolite Cu(DTC)₂ could inhibit NDM-1 via a oxidation mechanism.¹⁵²

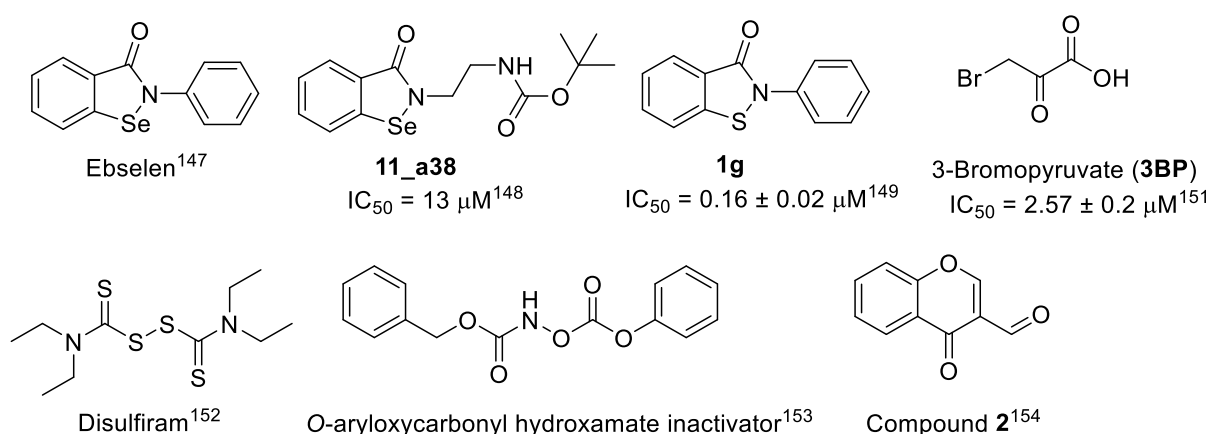


Figure 1.14 Inhibitors of NDM-1 by forming covalent bond with Cys208 or Lys211.^{147-149, 151-154}

Except the amino acid residue Cys208 coordinated Zn₂(II) ion at the active center of NDM-1, the Lys211 was playing important roles for substrate recognition of the protein, which was another potential binding position for covalent inhibitors. The *O*-aryloxy carbonyl hydroxamate inactivators were special covalent inhibitors for P99 one of class C SBLs, which covalently bound with both the serine and lysine residues in the active site of P99.¹⁵³ The commonly existing of a lysine residue for most B1 MBLs offered possibilities for developing broad spectrum inhibitors.¹⁵³ Thomas et al. (2019) identified that the *O*-aryloxy carbonyl hydroxamate inhibited NDM-1 by the possible reversible covalent binding mechanism.¹⁵³ However, the weak stability of the *O*-aryloxy carbonyl hydroxamate had to be considered for the inhibitor development of both SBLs and MBLs.¹⁵³ Based on the previous screenings, Christopheit et al. (2016) optimized the active inhibitor 3-cyanochromone to 3-formylchromone which could form a reversible covalent bond with the lysine at the active site of NDM-1.¹⁵⁴ Thomas et al. (2014) identified cephalothin, moxalactam, and cefaclor could form covalent bond with Lys211 at supratherapeutic doses. However, except for the covalent mechanism, their inhibitory activities also involved in other non-covalent binding mechanisms which brought difficulties for the interaction studies.¹⁵⁵

Above all, covalent binding inhibitors of NDM-1 depend on the cysteine or lysine residues in the active site of the protein, which limits the inhibitory spectrum of this type inhibitors, such as B3 MBLs do not have the cysteine residue at the active site, and the relatively low selectivity leads to more side effects, which hinder their further preclinical or clinical studies. Improving specificity and reducing relevant toxicity of the covalent binding inhibitors are still thorny issues.

Some metal ion containing inhibitors for NDM-1 were reported, the metal ions could tightly bind with Cys208, and most of them were irreversible.¹⁵⁶⁻¹⁵⁸ Wang et al. (2018) reported that colloidal bismuth subcitrate (CBS), an anti-*Helicobacter pylori* drug inhibited NDM-1 by both *in vitro* and *in vivo* studies and the special irreversible mechanism was identified, the Bi(III) ion could replace both two Zn(II) ions in the active site and tightly bound with Cys208. Given the less toxicity, special mechanism and high irreversible effectivity against NDM-1 as well as some other B1 MBLs, CBS and related Bi(III) compounds might be another promising type of inhibitors for B1 and B2 MBLs.¹⁵⁶ Chen et al. (2020) identified that cisplatin and Pd(II) complexes irreversibly inhibited NDM-1 via tightly binding with Cys208 replacing Zn₂(II) ion in the active site of NDM-1.¹⁵⁷ Thomas et al. (2013) found *p*-chloromecuribenzoate (*p*-CMB) and nitroprusside inhibiting NDM-1 via high-throughput screening (HTS). *p*-CMB inhibited NDM-1 by a time-dependent irreversible mechanism forming covalent bond with Cys208 at the active site of NDM-1.¹⁵⁸

As the inhibitory mechanism of the metal complexes generally based on the higher affinity of the metal ions for Cys208 compared with the Zn(II) ions of NDM-1, this kind of inhibitors might be promising candidates for B1 and B2 MBLs, but for B3 MBLs which did not containing the cysteine residue at the active site, their inhibitory activity might be lost. In addition, the toxicity of the metal complexes has to be concerned.

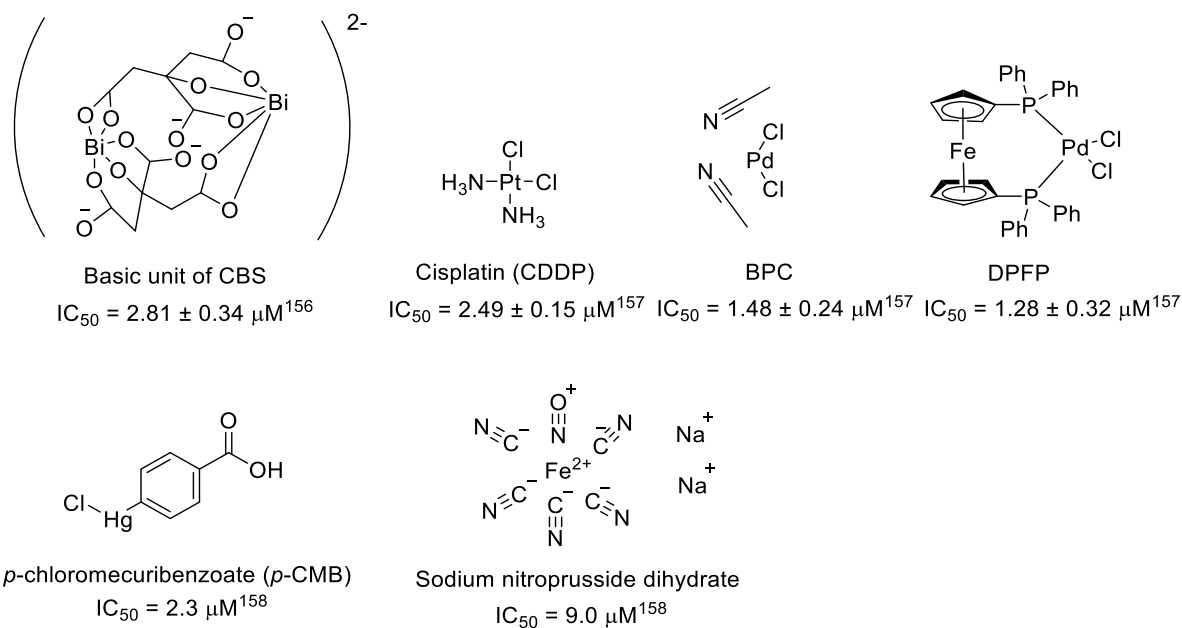


Figure 1.15 Metal ion containing Inhibitors of NDM-1.¹⁵⁶⁻¹⁵⁸

Above all, different types of inhibitors targeting NDM-1 were developed, most of them were discovered via high-throughput or fragment-based screenings and chemical syntheses. Besides, natural products provided new active structures, virtual screening approaches had gradually improved accuracy, and the developed biological technologies offered more reliable evaluation methods, which all supported the discovery of potent drug candidates. However, most of the developed inhibitors for NDM-1 are still at preclinical studies, there are no approved inhibitors for clinical treatment at present. In addition, the limitation and toxicity of the last line antibiotics as well as the emergence of relevant resistances allow less choices for clinical treatment, thus there are urgent need for developing inhibitors targeting NDM-1.

1.4.3 Methods for discovery of the leading compounds

There are several approaches for the discovery of the chemical leads for the target proteins. Developing chemical leads from an existing lead or drug is an efficient direction for drug development, which is successful for generating improved and optimised structures. However, the similarity limits the diversity of the leads, as a result, the emergence of resistance or loss of effects will strengthen the nervous situations, especially for the targets with fast evolution speeds such as β -lactamases and disease-related target proteins of virus. Discovering chemical leads from a natural product, the natural ligands or substrates is a historically successful method, which is a time-consuming approach although improved by new technologies. High-throughput screening (HTS) is one of the main methods applied in pharmaceutical industry. Recently, the idea of HTS has been moved from the number games to the screening of "drug-like" or "lead-like" compounds, and gradually fragment-based drug discovery (FBDD) has become the more preferred alternative approach than HTS.¹⁵⁹⁻¹⁶³

In general, around 1000 fragments with molecular weights less than 300 Da are screened by biophysical methods for FBDD, the binding affinity of the fragments are relatively lower even at millimole

range. Compared with HTS, fewer structures were screened and the starting hits from FBDD normally have lower molecular weights with sufficient affinities for the target proteins. The smaller hits with efficient atoms from FBDD have more advantages for optimization than the molecules from HTS with relative higher affinity but higher molecular weights and more uncertain atoms. There is a bigger molecular weight window for optimizing other properties for the hits from FBDD. The hit with smaller size has relatively simple interactions with the target, during the optimization process, the high-quality interactions are easier to be identified which are the basis for the potent drugs and the key part for optimization. Generally, the main binding mode can be kept from the fragments to the leads. The efficient fragments can be used for fragment ligation reactions which are more available for generating drug-like molecules.¹⁶⁰⁻¹⁶³

Zelboraf (vemurafenib, PLX4032) developed based on FBDD method was approved by FDA in 2011 for the treatment of BRAF-mutant cancer, and there are other promising leads discovered by FBDD targeting different proteins related to different diseases which have been progressed to clinical trials or at preclinical studies.¹⁶¹ FBDD has become a more efficient method for drug discovery applied in both academic research and pharmaceutical industry. Considering the successful applications of the method, FBDD has been applied to the discovery of inhibitors for NDM-1 in this work.

2 Project aim and design

β -Lactam antibiotics take more than half of the antibiotics used for clinical treatment, while the emergence of BLs has been the main resistance factor threatening their efficacy especially carbapenemases.²⁶⁻²⁸ Compared with colistin, tetracyclines, fosfomycin and fluoroquinolones, carbapenems, the last resort of β -lactam antibiotics, were less toxic and had broad antibacterial spectra.^{25, 31, 33, 36, 41, 47, 50, 51} The synergistic treatments combining BLs with β -lactam antibiotics has been the efficient strategies for keeping the efficacy of carbapenems as well as other essential β -lactam antibiotics.^{41, 62, 63, 68, 71, 73} The commonly mentioned carbapenemases included some of the KPC (e.g., KPC-2 and -3) and OXA (e.g., OXA-48) types, and all the MBLs (especially the most clinically relevant B1 MBLs).^{31, 33, 36, 41, 47, 50, 51} Most of the KPC and OXA types could be inhibited by the approved SBL inhibitors, e.g., the KPC types were inhibited by avibactam and vaborbactam, while the OXA types were inhibited by tazobactam and avibactam, and some of them were weakly inhibited by clavulanate.^{31, 36, 50, 51} However, there are no approved inhibitors of MBLs for clinical treatment at present, the bicyclic boronate VNRX-5133 (taniborbactam) was in phase 3, and other classes inhibitors were all at preclinical or discovery and development stages.^{62, 124-126} Aspergillomarasmine A (AMA) was reported inhibiting NDM-1 and some other MBLs with a similar mechanism as EDTA removing Zn(II) ions at the active site of the protein, however the side effects especially the less selectivity and the complicated synthesis route hindered its further clinical studies.^{63, 86, 127-131} Most of the thiols like L/D-captopril inhibited NDM-1 via bridging the two zinc ions at the active site by their thiol groups. Whereas a larger number of the thiols were developed based on the approved drugs targeting human enzymes, the potential side effects, less selectivity, and reduced efficacy *in vivo* should be concerned.^{63, 84, 108-123} The covalent inhibitors such as ebselen inhibited NDM-1 by covalently binding with Cys208, which resulted in the loss of Zn₂(II) ion of the protein.¹⁴⁷⁻¹⁵² However, the relevant high toxicity associated with the covalent inhibitors has been a concern.¹⁴⁷⁻¹⁵⁵ Other inhibitors such as metal-based inhibitors colloidal bismuth subcitrate (CBS), most of them were in preclinical or discovery and development stages.¹⁵⁶⁻¹⁵⁸ Compared with other B1 MBLs, the membrane anchored NDM-1 had improved stability for zinc ion starvation conditions and more kinds of mechanisms for dissemination and resistance, e.g., the secretion of outer membrane vesicles (OMVs).⁸⁴⁻⁸⁸ In addition, the relative larger active pocket of NDM-1 offered it a broad substrate spectrum, and aztreonam hydrolyzing by NDM-1 was even reported.^{82, 83} Therefore, development of inhibitors targeting NDM-1 is urgently required.⁷⁹

There were various strategies and approaches for the inhibitor development of MBLs. The published inhibitors could be mainly divided into Zn(II)-binding inhibitors, non-Zn(II)-binding inhibitors and some other natural products or structures. The Zn(II)-binding inhibitors included metal ion stripping compounds such as EDTA and AMA, and metal ion binding compounds such as the thiol containing inhibitors as well as the boronates. The applications of different screening approaches such as high-throughput screening (HTS), computer-based virtual screening and fragment-based drug discovery (FBDD) improved the efficiency for drug discovery.^{127, 139, 159, 160} FBDD method is a more preferred alternative approach compared with HTS, screening of relative smaller amount of fragments (e.g., around 1000) with lower molecular weight (less than 300 Da), and leaving a sufficient optimizing window for the bioactive fragments with efficient atoms to arrive to drug-like compounds.

The two Zn(II) ions in the active pocket of NDM-1 were essential for the hydrolysis of β -lactam substrates and played important roles for the stability of the protein.^{82-86, 90} Most of the published inhibitors contained one or more carboxyl groups responsible for zinc binding or interacting with the

amino acid residues in the active site of NDM-1, moreover, the 2-carboxyl group of the β -lactam substrate was essential for the substrate recognition.^{48, 82-158} Thus, the carboxyl groups or the isosteric groups of the inhibitors should favor their inhibitory activity and might contribute for the specific binding with the active pocket.

Above all, considering the important roles played by the Zn(II) ions and the shortcomings of the current inhibitors for NDM-1, e.g., potential side effects and relatively low activity of the thiols, the less acceptance of the boronates as their reactive property, the toxicity and limitation of the covalent inhibitors, as well as the less selectivity and poor cell-level activity of current Zn(II)-binding inhibitors, the focus of this work is developing potent and less toxic Zn(II)-binding inhibitors as promising drug-like candidates for NDM-1. The first aim of this work is to discovery Zn(II)-binding inhibitors with high specificity and inhibitory activity especially at the cell-level; the second aim is to study the interaction modes of the top active as well as some other representative inhibitors with the protein; the third aim is to discovery the inhibitors with potential broad inhibitory spectrum toward other MBLs as well as evaluate their selectivity using several other human metalloenzymes. To achieve these goals, the fragment screening, modification of the initial hits, mode-of-action studies, microbiological susceptibility tests as well as other activity measurements were planned as follows:

First, protein expression systems of NDM-1 should be constructed which could be used to produce the protein for the fragment screening, *in vitro* activity tests as well as other biological evaluation assays.

Second, form proper *in vitro* activity assays for the fragment screening.

Third, perform the fragment screenings of the carboxylic acid and amine libraries as well as other designed structures.

Fourth, design and synthesize structures according to the screening results. IC₅₀ determinations and docking studies should be performed at the same time to support reasonable modifications.

Fifth, study the interaction modes of the top active as well as other representative compounds via different biological assays, e.g., isothermal calorimetry (ITC) which is a standard method to evaluate binding interactions of biomolecules, bio-layer interferometry (BLI) monitoring the real time association and dissociation curves of the ligands with the protein, protein native mass specifying the binding complexes of the target protein and the ligands, solution NMR which can be used to detect the conformational changes of the important amino acid residues of the protein, thermal shift assay (TSA) testing the effects of the inhibitors on the thermal stability of the target protein, circular dichroism (CD) which is a convenient method to investigate the possible changes of the secondary structures of the protein, zinc ion restoration assays testing the reversibility of the inhibition.

Sixth, evaluate the inhibitory activity of the developed inhibitors toward several other B1 MBLs to find the potential broad-spectrum inhibitors and test the selectivity by several human metalloenzymes.

Seventh, test the synergistic functions of the compounds with meropenem via broth microdilution assays using both the NDM-1-producing *E. coli* transconjugants and the clinical strains co-expressing NDM-1 and evaluate the effects on the proliferation and viability of human cells via Alamar blue assays.

3 Results and discussion

3.1 Fragment screening

3.1.1 Forming of screening assays

Screening methods, e.g., high-throughput screening (HTS), fragment-based drug discovery (FBDD) and virtual screening approaches were commonly utilized in pharmaceutical industry which could efficiently generate original hits for disease related targets and highly speed up the time-consuming drug development processes.¹⁶¹⁻¹⁶⁵ Both enzyme-based and cell-based *in vitro* activity screening methods have been used for the inhibitor development of NDM-1 in published works.¹²⁷ For the cell-based screenings, the minimum inhibitory concentrations (MICs) or other relevant activities of the β -lactam antibiotics with or without the screening fragments for the bacterial strains producing NDM-1 were determined.¹²⁷ As the last resort of β -lactam antibiotics, carbapenems such as meropenem and imipenem were often chosen as the combined β -lactams.¹²⁷ For enzyme-based screenings, there were detectable shifts of ultraviolet absorption for the hydrolyzed products compared with the intact β -lactams, thus chromogenic substrates (e.g., nitrocefin and imipenem) were the most used substrates for the *in vitro* enzyme-based assays. Nitrocefin discovered by O'Callaghan et al. (1972) with a visible shift from yellow (around 380 nm) of the intact structure to red (around 500 nm) of the hydrolyzed product (**Figure 3.1**), brought great improvements on the detection and inhibitor development of BLs.¹⁶⁶⁻¹⁶⁸ Fluorogenic substrates have also been used recently (e.g., FC-3 to FC-5), and some of them offered better IC₅₀ values than chromogenic substrates. However, most of the fluorogenic substrates were self-synthesized with different structures, which was not conveniently for comparison of similar works.¹⁶⁹

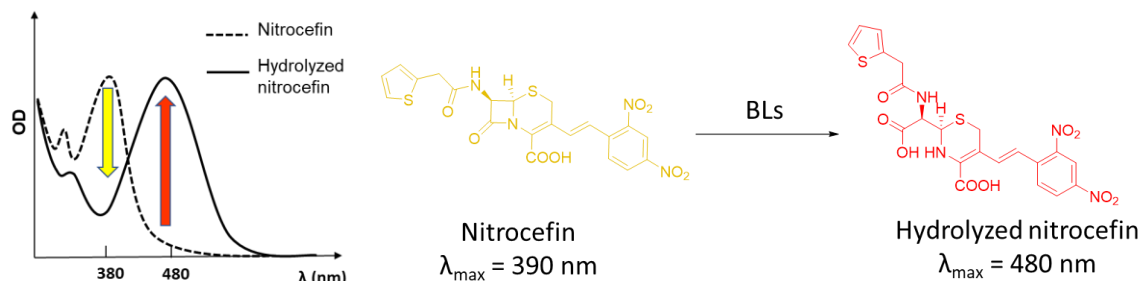


Figure 3.1 Diagram of the absorbance shifts for nitrocefin hydrolyzed by BLs.¹⁶⁸

According to the published methods and available fragment libraries in the laboratory, both enzyme-based and cell-based assays were established for the fragment screenings to discover the initial active hits.

At first, NDM-1 producing systems were constructed.^{f1} The cDNA of NDM-1 was inserted into two different positions of the pET-11a vector, i.e., the regular multiple cloning site or the backbone replacing the cDNA of the dependent serine β -lactamase. The former allowed for IPTG inducible NDM-1 expression while the second drove constitutive expression, both systems were designed and constructed for the cell-based screening. For enzyme-based screening and further activity studies, another two expression systems were constructed. The gene of the full-length NDM-1 with 6xHis tag at

^{f1} The cloning work was done by Dr. Christoph Arkona.

C-terminal was inserted into pET-22(+) vector between sites 5'NdeI and 3'HindIII, and the gene of the truncated NDM-1 (residues 36 to 270) with 6xHis tag at C-terminal was inserted into pET-30 vector. The constructed vectors were transformed into chemically competent *E. coli* BL21 (DE3) cells, respectively, which were sufficient for the expression and purification of NDM-1 protein.^{76, 91} The signal peptide at N-terminal did not participate the main functional part of NDM-1, and did not influence the enzymatic activity of the protein, thus the truncated NDM-1 which was available for productive expression and had better stability in assay conditions was commonly used for biological studies.^{88, 91, 104-107} The truncated NDM-1 was mainly used for ITC, BLI, native protein mass spectrometry and CD studies in this work.

L-captopril was used as a positive control for both cell-based and enzyme-based assays. For cell-based method, the MICs of meropenem with or without the testing inhibitors for the two bacterial strains expressing NDM-1 (without 6xHis tag) were determined (**Table 3.1**). Reductions of the MICs were observed using L-captopril at both 10 µg/ml and 25 µg/ml for the strain expressing NDM-1 induced by IPTG but not for the other strain expressing NDM-1 constitutively.

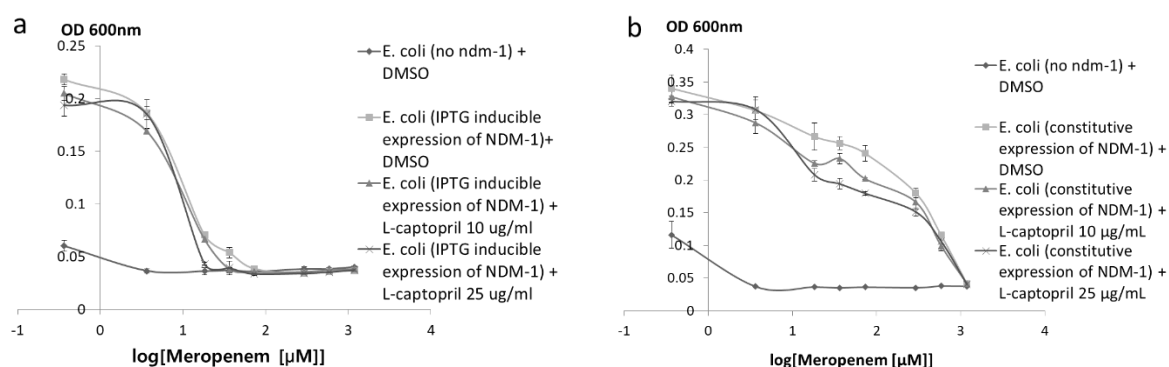


Figure 3.2 *In vitro* cell-based assays. a. Bacterial strain expressing NDM-1 induced by IPTG; b. Bacterial strain expressing NDM-1 constitutively.

Table 3.1 Potentiation of Meropenem Activity against the Recombinant NDM-1 Producing *E. coli* by L-captopril

Bacterial Strain	Genotype	MIC (mg/L)		
		MEM	MEM + L-captopril (10 mg/L) (46 µM)	MEM + L-captopril (25 mg/L) (115 µM)
<i>E. coli</i> BL21 (DE3)	Empty expression control	1.6	-	-
<i>E. coli</i> BL21 (DE3)	IPTG inducible expression of NDM-1	32	16	8
<i>E. coli</i> BL21 (DE3)	Constitutive expression of NDM-1	521	521	521

^a '-' means 'did not test'; 'MEM' means meropenem.

Enzyme-based assays using nitrocefin or imipenem as the substrate were formed. At first, the tested compound was preincubated with NDM-1 (5.4 nM) in the assay buffer (50 mM HEPES-NaOH pH 7.5, 2 mg/100 mL BSA, 0.02% Tween-20) at room temperature for 15 min, then the substrate with the final concentration of 13 μM for nitrocefin or 100 μM for imipenem was added. The absorbance was monitored at 490 nm for nitrocefin or 300 nm for imipenem for 30 min with an interval of 60 s. The IC_{50} values of L-captopril determined using nitrocefin or imipenem as substrates were 169.15 μM and 20.72 μM , respectively, which were compatible with the reported values.^{108, 170-174} Considering the reproducibility, quantities of compounds required, and time consumed, enzyme-based assays were more convenient and efficient for the initial screenings. In addition, absorptions at 300 nm might be easily influenced by relative tested compounds, therefore nitrocefin was used as the substrate finally.

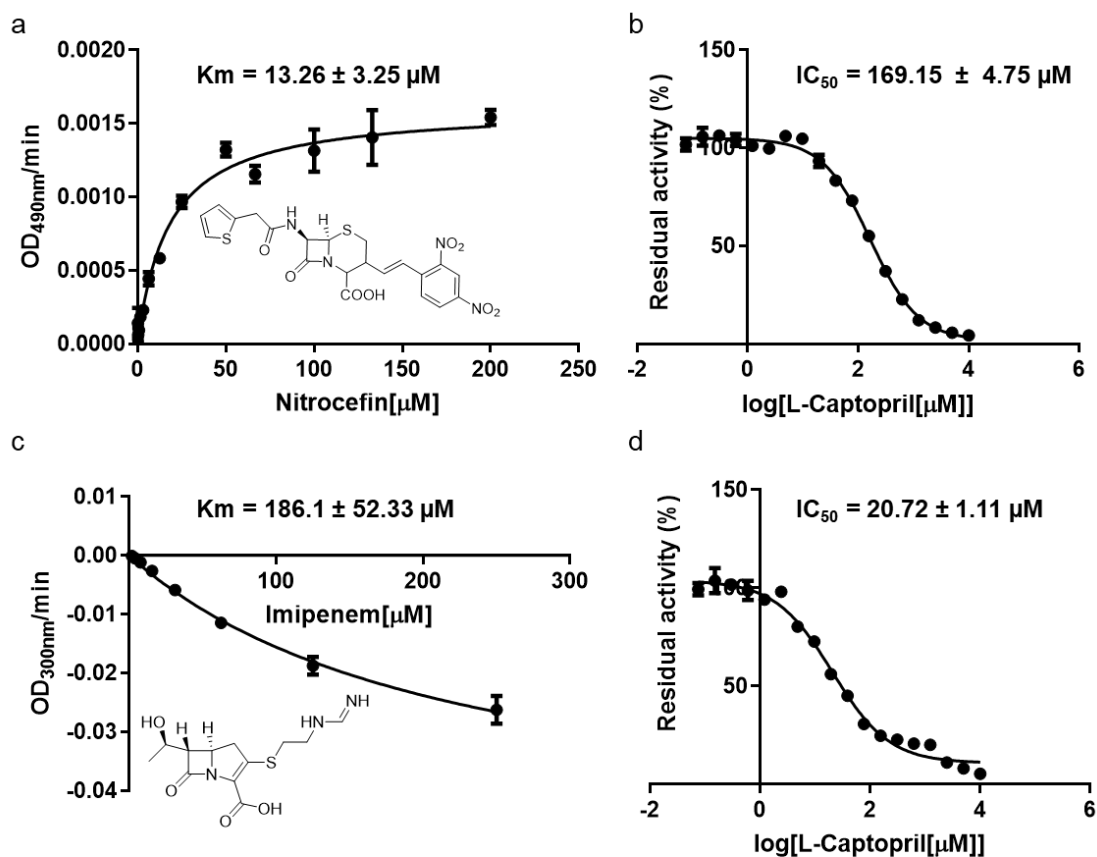


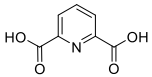
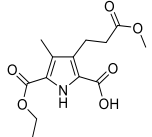
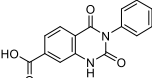
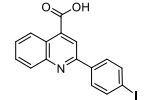
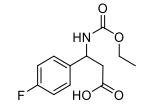
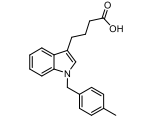
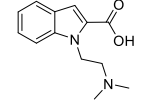
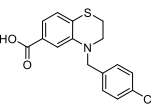
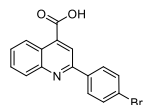
Figure 3.3 *In vitro* enzyme-based assays. a. The K_m of nitrocefin for NDM-1 (This K_m was obtained with 10 μM zinc ions in the assay buffer at the beginning and used for calculation in this dissertation, without zinc ions the K_m value was around 4.24 μM , the data was supplied in the appendices.); b. The IC_{50} of L-captopril for NDM-1 measured using nitrocefin as the substrate with a final concentration of 13 μM ; c. The K_m of imipenem for NDM-1; d. The IC_{50} of L-captopril for NDM-1 measured using imipenem as substrate with a final concentration of 100 μM .

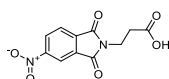
3.1.2 Screening of the carboxylic acid and amine libraries

Most of the reported inhibitors of NDM-1 containing one or more carboxyl groups which played important roles for the inhibitory activity. In addition, the carboxyl group at the 2-position of the β -lactam

antibiotics was essential for the substrate recognition by NDM-1, therefore 1615 fragments of the carboxylic acid library were screened by the *in vitro* enzyme-based assays. Given the good nucleophilic property of amines and potential fragments for ligation reactions with the active hits of the carboxylic acid library, 781 fragments of the amine library were screened as well. Most of the fragments were less than 300 Da, and their stock solutions with a concentration of 20 mM in DMSO were stored in 384-well plates. To find more potential fragments, a relative higher concentration of the fragments was used for the screening. The final concentrations of the substrate and fragments were 13 μ M and 400 μ M, respectively. Around 30 fragments were identified with residual activity less than 60%, and the relevant structures are listed in **Table 3.2** and **Table 3.3**.

Table 3.2 Fragment Screening of the Carboxylic Acid Library

Compound	Structure	Residual activity
C1		5%
C2		22%
C3		40%
C4		45%
C5		48%
C6		50%
C7		51%
C8		51%
C9		52%



C10

53%

^a Residual activity of L-captopril at 400 μM was around 40%; The assay buffer for the screening of the carboxylic acid library contained 10 μM ZnSO_4 .

Table 3.3 Fragment Screening of the Amine Library

Compound	Structure	Residual activity
A1		23.86%
A2		38.67%
A3		46.78%
A4		54.87%
A5		57.09%
A6		57.48%
A7		57.48%
A8		58.90%
A9		60.05%

^a The residual activity of L-captopril at 400 μM was around 40%; the solution of fragment **A2** had a dark color which might interfere with its activity determination.

The most active hit was DPA (dipicolinic acid or pyridine-2,6-dicarboxylic acid) with an IC_{50} value of 7.02 μM , and another active hit **C2** was also measured with an IC_{50} value of 123.75 μM (**Figure 3.4**). DPA had strong zinc ion binding ability as its metal ion chelating functions which was relatively weaker

than EDTA. The inhibitory activities of DPA for MBLs such as IMP and VIM type had been reported before, and DPA derivatives inhibiting NDM-1 were synthesized by Chen et al. (2017).^{133, 175} According to the published works, most of the optimized derivatives of DPA had improved IC₅₀ values but still low cell level activities. Therefore, improving the binding affinity with the active pocket of NDM-1 and the activity at cell level were key issues that must be solved for DPA type inhibitors.

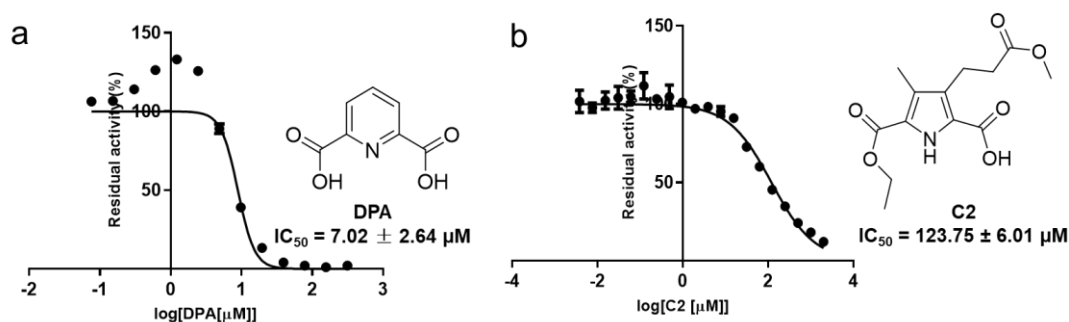


Figure 3.4 IC₅₀ determination of the active hits. a. DPA; b. C2.

3.1.3 Screening of the prepared analogues

3.1.3.1 Preparation of analogues

The compounds in Table 3.4 and Table 3.5 were commercially available or self-synthesized. Compound 6(YJh1) was synthesized by methyl esterification of DPA and compound 7(YJh4) was synthesized by hydrolyzing one of the methyl ester groups of compound 6(YJh1).^{176, 133} Compound 22(YJh38) and 19(YJh145) was synthesized via Doebner–Miller reaction.¹⁷⁷⁻¹⁸² Compounds 29(YJh67) and 20(YJh149) were synthesized via oxidation of compounds 22(YJh38) and 19(YJh145) by selenium dioxide, respectively.^{183, 184} Compounds 37(YJh31) and 26(YJh33) were synthesized by reacting corresponding 8-hydroxylquinoline structures with iodomethane in DMF under base condition (K₂CO₃).¹⁸⁵ Compound 34(YJh32) was synthesized by deprotecting the methyl ester of compound 37(YJh31) under base condition.^{176, 133} Compound 25(YJh118) was synthesized by coupling compound 22(YJh38) with benzenesulfonamide.¹⁸⁶ Compound 24(YJh80) was synthesized via hydrogenation of 2-methyl-8-nitroquinoline.¹⁸⁷ The synthesis of compounds 30(YJh36), 38(YJh89), 36(YJh63) and 33(YJh65) were depicted in the synthesis section of the 8-(methylsulfonamido)quinoline-2-carboxylic acid (8-MSQA) derivatives.

3.1.3.2 Measuring of the prepared analogues

Based on the initial screening, DPA was chosen as the starting hit. To obtain a preliminary structure-activity relationship (SAR), a panel of designed DPA analogues were tested, and their IC₅₀ values are listed in Table 3.4. Without the nitrogen atom of the pyridine ring, compounds 2 to 4 did not show any activity. The methyl ester 7(YJh4) nearly killed all the activity of DPA, which demonstrated the importance of the carboxyl group. For further investigation, compounds 8 to 13 were tested, which contained different numbers of carboxyl groups and were substituted at different positions. At least one

of the carboxyl groups at the 2- or 6-positions for the pyridine ring was necessary for keeping the inhibitory activity for NDM-1, while more substitutions at other positions did not contribute to the improvement of the inhibitory activity, which could be explained by **Figure 3.5**. For compound **13**, the similar moiety like DPA would be the active moiety for inhibiting NDM-1, while other moieties like compounds **2** or **3** might reduce its inhibitory activity. According to this relationship, a molecule like 1,3,5-triazine-2,4,6-tricarboxylic acid should be active which has not been tested considering the less optimizing space and possible stronger zinc ion chelating property. For compounds **14** to **20**, their carboxyl groups and related parts were replaced by other different groups (e.g., aromatic hydroxyl, amino, thiol, sulfonamide, pyridine ring, etc). It was found that compound **14** (8-hydroxyquinoline-2-carboxylic acid, **8-HQA**) with an IC_{50} value of 9.8 μ M had the similar inhibitory activity as DPA. Compound **15** ($IC_{50} = 323.1 \mu$ M) was a derivative of **8-HQA** with a hydroxyl group at the 4-position, and the reduce of the inhibitory activity might come from the ketone interconversion of the aromatic hydroxyl group at the 4-position which might be proved by changing the 4-hydroxyl to 4-methoxyl. The 4-position methoxy-substituted compound has not been synthesized at present. Different from the inactive compound **19**(**YJh145**), compound **20**(**YJh149**) containing the picolinic acid moieties with an IC_{50} value of 32.74 μ M was active but less than DPA.

Table 3.4 DPA Derivatives Used to Obtain a Rudimentary SAR

Compound	Structure	IC_{50} (μ M)
1 (DPA)		7.02 ± 2.64
2 (Isophthalic acid)		>1000
3 (Phthalic acid)		>1000
4 (2-Bromoisophthalic acid)		>1000
5 (Pyridine-2,6-dicarboxamide) ^{f2}		>1000
6 (YJh1)		>1000
7 (YJh4)		>1000/1852
8 (Picolinic acid)		303.3 ± 26.4
9 (Nicotinic acid)		>1000

^{f2} Compound **5** was synthesized by Péter Varga.

10	(Isonicotinic acid)		>1000
11	(Pyridine-2,4-dicarboxylic acid)		>400
12	(Pyridine-2,3-dicarboxylic acid)		>400
13	(TR276) ^{f3}		243.5 ± 21.33
14	(8-HQA)		9.05 ± 0.14
15	(Xanthurenic acid)		323.1
16	(Pyridin-2-amine)		>1000
17	(Pyridine-2-sulfonamide)		>1000
18	(Pyridine-2-thiol)		>1000
19	(YJh145)		>1000
20	(YJh149)		32.74 ± 3.38

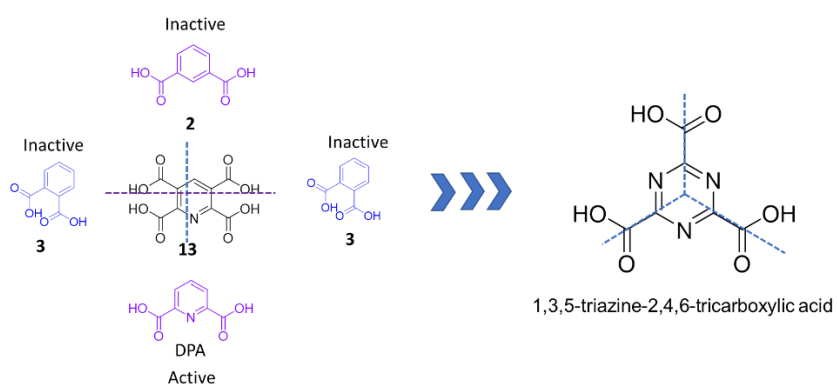
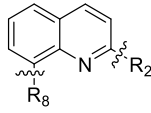

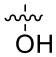

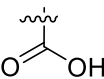

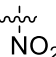


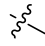

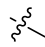
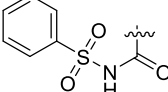
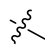
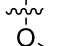
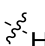
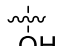
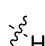

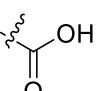
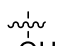
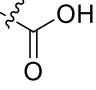
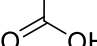
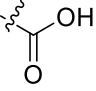

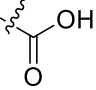

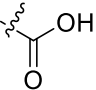
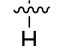
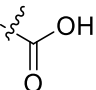
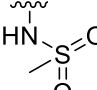
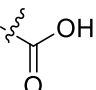
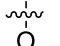
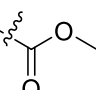
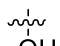
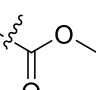
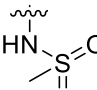
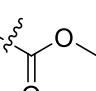
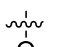
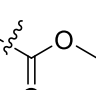
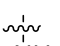
Figure 3.5 Diagram of the activity analysis for compound **13**.

^{f3} Compound **13** was synthesized by Thomas Rudolf.

According to the above tests, the nitrogen atom of the pyridine ring and at least one of the carboxyl groups attached to the adjacent carbons were essential for the inhibitory activity, as demonstrated by compound **8**, picolinic acid ($IC_{50} = 303.3 \mu M$), although DPA with two carboxyl groups was almost 40 times more potent ($7.02 \mu M$). In addition, the pyridine ring could be developed into a quinoline ring by replacing one of the carboxyl groups to an aromatic hydroxyl group at the 8-position of the quinoline ring, **8-HQA** ($IC_{50} = 9.05 \mu M$). A panel of quinoline derivatives at the 8- and 2-positions were prepared to investigate more possible isosteric substitution groups (**Table 3.5**). For compounds **21** to **26**, their 2-positions were all substituted by methyl groups, the 8-positions were substituted by hydroxyl, carboxyl, nitro, amino, sulfonyl carboxamide, and methoxy groups, respectively. Among them, compound **21** had an IC_{50} of $273.5 \mu M$ which demonstrated that the 8-hydroxyl quinoline might have a similar activity as compound **8** (picolinic acid). For compounds **27** and **28** with a hydrogen at the 2-position, compound **27** ($IC_{50} = 133.5 \mu M$) also highlighted the active moiety 8-hydroxyl quinoline. With carboxyl group at the 2-position, **8-HQA** was much more active than compounds **21** or **27**, but compound **32** with a hydrogen at the 8-position was inactive, which emphasized the important relationship between the 2-position and the 8-position. In case possible active substituents for the 8-position were missed, compounds **29**(**YJh67**) to **31**, **33**(**YJh65**), and **34**(**YJh32**) with their 2-positions substituted by carboxyl groups were tested. Compared with the inactive compound **22**(**YJh38**) with a methyl group at the 2-position, the inhibitory activity of compound **29**(**YJh67**) ($IC_{50} = 7.66 \mu M$) was recovered by a carboxyl group at the 2-position. It might be the same case for compound **25**(**YJh118**), which have not been tested at present. Nitro group was important for Zn(II)-binding which was reported by Xiang et al. (2017), while both nitro-containing compounds **30**(**YJh36**) and **23** were inactive, thus the activity of the nitro group should be related to the scaffolds.¹⁴⁶ Like compounds **24** and **28**, compound **31** with an amino group at the 8-position was still not active. In addition, compounds **26**(**YJh33**), **34**(**YJh32**) and **37**(**YJh31**) all with a methoxy at the 8-position were inactive, which suggested that a relatively more acidic substituent was required for the 8-position. To increase the acidity of the 8-amino group, compound **33** (**YJh65**, 8-(methylsulfonamido)quinoline-2-carboxylic acid, **8-MSQA**) was synthesized and tested. Surprisingly, **8-MSQA** ($IC_{50} = 1.64 \mu M$) was even more active than **8-HQA** and DPA. To verify the active substituent methyl-substituted 8-sulfonamide group, compounds **35**(**YJh209**), **36**(**YJh63**) and **38**(**YJh89**) were tested, compound **38**(**YJh89**) was still inactive, while compound **36**(**YJh63**) ($IC_{50} = 17.61 \mu M$) was more active than compound **35**(**YJh209**) ($IC_{50} = 156.25 \mu M$).

Table 3.5 Quinoline Derivatives at the 8-Position and the 2-Position

				
Compound		R ₂	R ₈	IC ₅₀ (μM)
21				273.5 ± 15.65
22	(YJh38)			>1000
23				>1000

24	(YJh80)			>1000
25	(YJh118)			>1000
26	(YJh33)			>1000
27				133.5 ± 16.28
28				>1000
	(8-HQA)			9.05 ± 0.14
29	(YJh67)			7.66
30	(YJh36)			>1000
31				>1000
32				>1000
33	(YJh65 or 8-MSQA)			1.64 ± 0.31
34	(YJh32)			>1000
35	(YJh209)			156.25 ± 16.9
36	(YJh63)			17.61 ± 2.24
37	(YJh31)			>1000
38	(YJh89)			>1000

Above all, the substituent at the 8-position of the quinoline ring played essential roles for the activity. The 8-position of the quinoline substituted by a hydroxyl or a substituted-sulfonamide group could keep the inhibitory activities even with a methyl or a methyl ester group at the 2-position such as compounds **21** ($IC_{50} = 273.5 \mu\text{M}$) and compound **36(YJh63)** ($IC_{50} = 17.61 \mu\text{M}$), furthermore, the inhibitory activity was obviously improved with the 2-position substituted by a carboxyl group, such as **8-HQA** and **8-MSQA**. With the 2-position substituted by a carboxyl group, compound **29(YJh67)** containing a carboxyl group at the 8-position was active, but with a methyl group at the 2-position compound **22(YJh38)** lost the inhibitory activity. Compared the activity of the quinoline derivatives, the 2- and 8-positions tightly cooperated with each other and significantly influenced the inhibitory activity. Based on the initial screening and the general SAR, DPA, **8-HQA** and **8-MSQA** derivatives were developed and docking studies were applied for reasonable modifications. The screenings and the modifications were carried out at the same time, **DPA** and **8-HQA** were discovered earlier than **8-MSQA**, the specific modification processes for derivatives of each type were described in the following chapters.

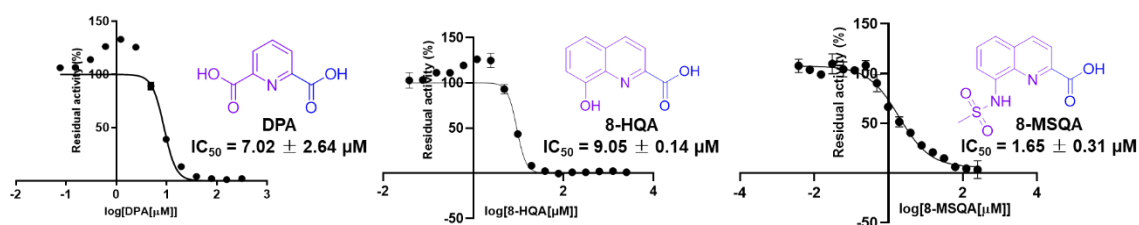


Figure 3.6 *In vitro* activity tests of DPA, **8-HQA** and **8-MSQA**.

3.2 Compound synthesis and their enzyme-based *in vitro* activity

The synthesis routes, detailed procedures, and identification information of the **DPA**, **8-HQA** and **8-MSQA** derivatives were described in the experiment part, their structure activity relationships (SARs) and relevant docking studies were mainly discussed in this chapter.

3.2.1 DPA derivatives

3.2.1.1 Compound design and synthesis of DPA derivatives

Based on the initial screening of the DPA analogues (Table 3.4), the importance of at least one of the carboxyl groups at the 2- or 6-positions and the nitrogen of DPA were realized. The preliminary SAR is listed in Figure 3.7.

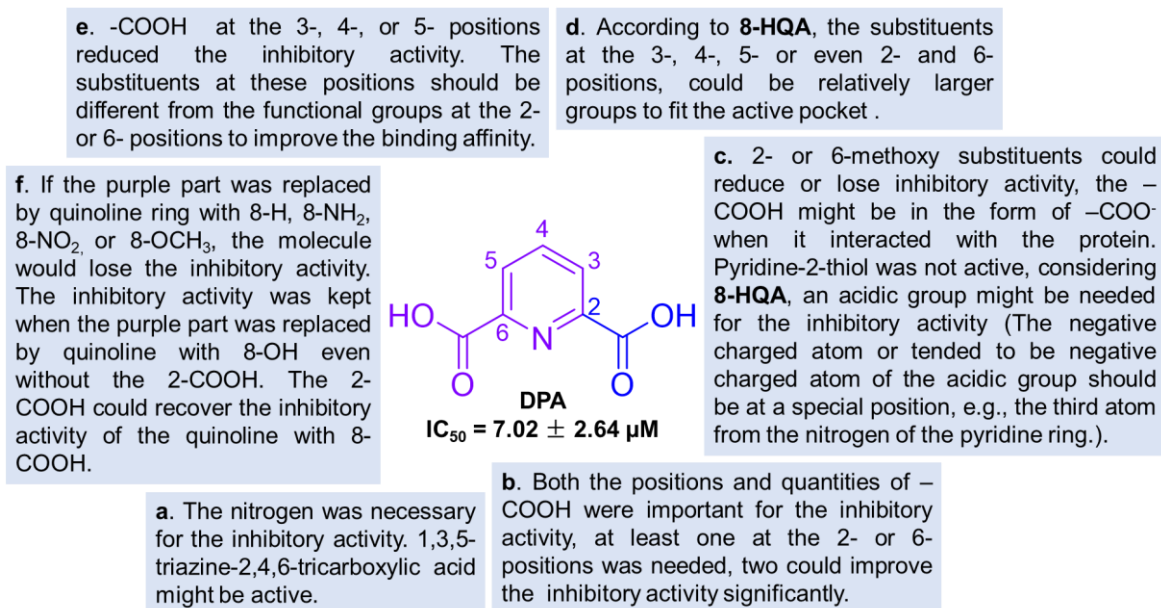


Figure 3.7 Preliminary SAR for DPA derivatives.

To investigate the interactions of the ligands with the active pocket and optimize the active hits with reasonable modifications, docking studies were performed. The crystal structure of NDM-1 (PDB ID: 5ZGR) was utilized, as its buffer conditions (50 mM HEPES, pH 7.3) was closer to the assay conditions of most biological evaluation methods in this work. The hydrolyzed ampicillin was re-docked in the active site to test the docking method, and its proposed binding pose overlapped well with the original ligand of the crystal structure.

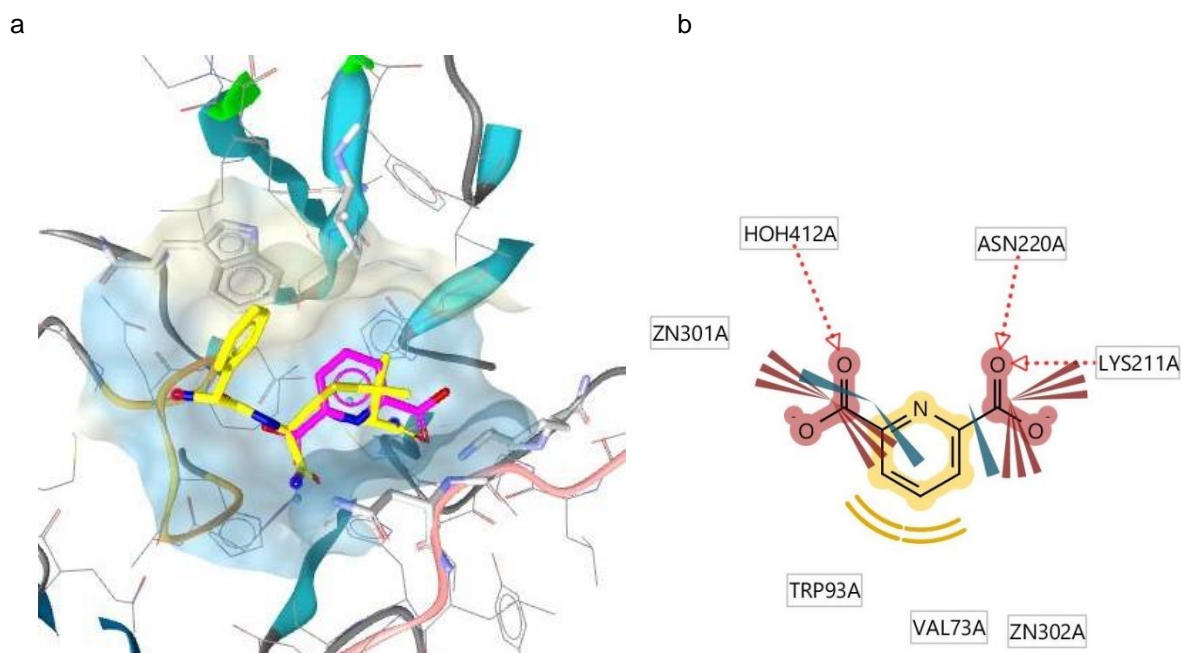


Figure 3.8 Proposed binding pose of DPA in the active site of NDM-1 (PDB ID: 5ZGR). The docking studies were performed by Gold 5.8.1 and the results were analyzed by LigandScout 4.2. The loop

region from Met67 to Gly71 acting as the 'Door' was colored in green, the loop region from Thr119 to Met126 acting as the 'Ceiling' was colored in orange, and the loop region from Ser217 to Asp225 acting as the 'Floor' was colored in pink. a. Proposed binding pose of DPA in the active site (The hydrolyzed ampicillin was colored in yellow and the DPA molecule was colored in magenta.); b. 2D depiction for the interactions of the proposed binding pose of DPA with the active site (The yellow lines indicated lipophilic contacts, red arrows indicated hydrogen bond acceptor functionalities, blue wedges indicated zinc binding locations, and the red wedges indicated negative ionizable interactions.).

For most predicted binding poses of DPA, at least one of the -COO^- groups interacted with the Zn(II) ions, and the closer Zn(II) ion would be tightly bound. When the -COO^- group overlapped well with the original the -COO^- group of the ampicillin, Zn2(II) ion was tightly bound, and there were H-bond or ionizable interactions of DPA with Lys211 for most cases. When the -COO^- group overlapped well with the -COO^- from the hydrolyzed β -lactam bond, Zn1(II) ion was tightly bound. The favorable proposed binding pose of DPA is shown in **Figure 3.8**, one of the binding moieties formed by the nitrogen and the -COO^- groups functionalized as zinc binding locations for both Zn(II) ions, while the other worked as the zinc binding location only for Zn2(II) ion. Except the strong zinc ion binding interactions, the -COO^- groups had negative ionizable interactions with Zn(II) ions and Lys211. In addition, there were three H-bond interactions: the H-bond of the deprotonated carboxyl group with the structural water molecule (The existing of the water molecule was still under debate.); the H-bond of the deprotonated carboxyl group with Lys211; the H-bond of the deprotonated carboxyl group with Asn220. Asn220 and Lys211 were essential residues for the substrate recognition of NDM-1. There were hydrophobic interactions of the pyridine ring with residues Val73 and Trp93, which belonged to the important loop called 'door' of the active pocket. Above all, the proposed binding pose in **Figure 3.8** showed strong interactions with both Zn(II) ions, especially Zn2(II), which suggested DPA could interact with both Zn(II) ions and the interactions with Zn(II) ions were essential for the inhibitory activity of DPA.

DPA overlapped well with the hydrolyzed β -lactam ring of the substrate (**Figure 3.8a**), which suggested that DPA might also work as a mimic of the intact or hydrolyzed β -lactam substrate instead of only stripping Zn(II) ions in the active site of NDM-1 like EDTA. Nevertheless, the relatively less hydrophobic interactions and strong zinc ion stripping function of DPA (although weaker than EDTA) limited its further application for inhibiting NDM-1. Considering more hydrophobic interactions in the active pocket could improve the selectivity, increase the binding affinity with the active pocket and optimize the permeability for cell level assays, in addition, the active pocket was much bigger than the DPA ligand (**Figure 3.8a**), hydrophobic substituents were recommended and at least one of the carboxyl groups could be changed to larger groups with similar properties. The modifications should obey the preliminary SAR in **Figure 3.7**.

Hydroxamates or hydroxamic acids were prevalently applied to inhibitors for metalloenzymes,¹⁸⁸⁻¹⁹² thus compounds **44(YJh6)** and **39** (*N*-hydroxypicolinamide) were synthesized at first. However, these two inactive compounds demonstrated that the commonly used zinc binding group (ZBG) hydroxamic acid might be not strong enough to competitively bind with the Zn(II) ions at the active site of NDM-1 by itself, and the pyridine ring might also influenced its binding modes or affinity. In addition, the zinc ions played different roles for different proteins, most of the inhibitors containing hydroxamates or hydroxamic acids were targeting mono-zinc proteins.¹⁸⁸⁻¹⁹⁰ Nevertheless, the hydroxamic acid cannot cooperate with the nitrogen of the pyridine ring as the carboxyl group to inhibit NDM-1. Reconsidering the property of the hydroxamic acids, the -OH was more acidic than the -NH- of compound **44(YJh6)**,

the negative charged or tending to be negative charged part was the oxygen of the terminal hydroxyl group instead of the amido nitrogen, so the terminal hydroxyl group would be the first choice for the acidic cooperating group. According to the primary SAR, the atom of the substituents at the 2- or 6-positions playing important roles for zinc binding not only needed to be acidic groups (might be negative charged or tend to be negative charged), but the position was also limited, which should be the third atom away from the nitrogen of the pyridine ring (**Figure 3.9**). To verify this thinking, compounds with the terminal hydroxyl groups substituted by methoxy or benzyloxy groups of the hydroxamic acid or hydroxamate parts were synthesized, e.g., compounds **40(YJh8)** to **42(YJh10)** and **45(YJh2)** to **48(YJh207)**. The acidity of the terminal hydroxyl group was reduced (the oxygen could not be negatively charged or tend to be negatively charged), then the chance for the -NH- of the amide to be the cooperating acidic group which might be negatively charged or tend to be negatively charged when interacted with the active site could be increased. Compound **43 (YJh13)** was synthesized to investigate whether the conjugation from the phenyl group could change the activity of compound **5** (pyridine-2,6-dicarboxamide) and the potential zinc binding ability of nitro group reported by some other groups.¹⁴⁶

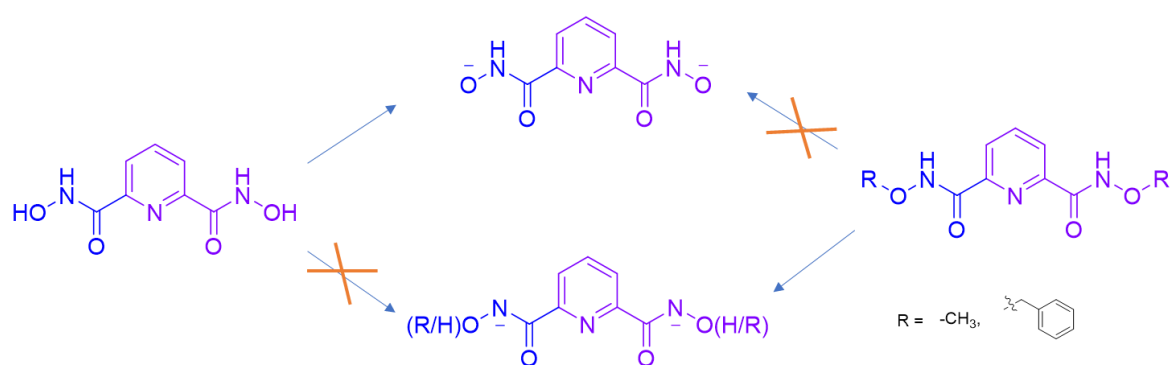


Figure 3.9 One of the predicted inactive mechanisms for compound **44(YJh6)**. (The ionized forms were used to show the more acidic parts of the molecules.)

Besides, the Zn1(II) ion was coordinated by three histidine residues and Zn2(II) ion interacted with Cys208, His250 and Asp124 at the active site of NDM-1, considering the zinc binding ability of histidine, compound **49(YJh12)** and the methyl deprotected compound **50(YJh15)** were synthesized which might play as competitors mimicking the binding conditions of the histidine residues in the active pocket for the Zn(II) ions. In addition, it was reported that compound **49(YJh12)** had strong binding affinity with copper(II) ions which could form pentadentate copper(II) complexes and a similar structure with a mono histidine showed strong binding affinity with palladium(II) ion.^{193, 194}

Compounds **40(YJh8)**, **41(YJh9)**, **42(YJh10)**, **43(YJh13)**, **45(YJh2)** and **46(YJh11)** were synthesized by the general procedure of amide coupling, and the corresponding acids were activated by EDC.¹⁹⁵ Compound **44(YJh6)** was synthesized by removing the benzyl group of compound **45(YJh2)** via palladium-catalyzed hydrogenation.¹⁹⁶ Compound **44(YJh6)** was purified by HPLC, since the less differences of the retention times for the side products and **44(YJh6)**, the reaction should be monitored by TLC frequently and stopped at around 25 min (**Figure 3.10**). Since the steric strains or lower reactivity of the amine, compound **49(YJh12)** was synthesized by the relevant acid chloride.¹⁹⁴ The detailed synthesis routes and procedures of DPA derivates are shown in the experiment part (**Scheme S1**).

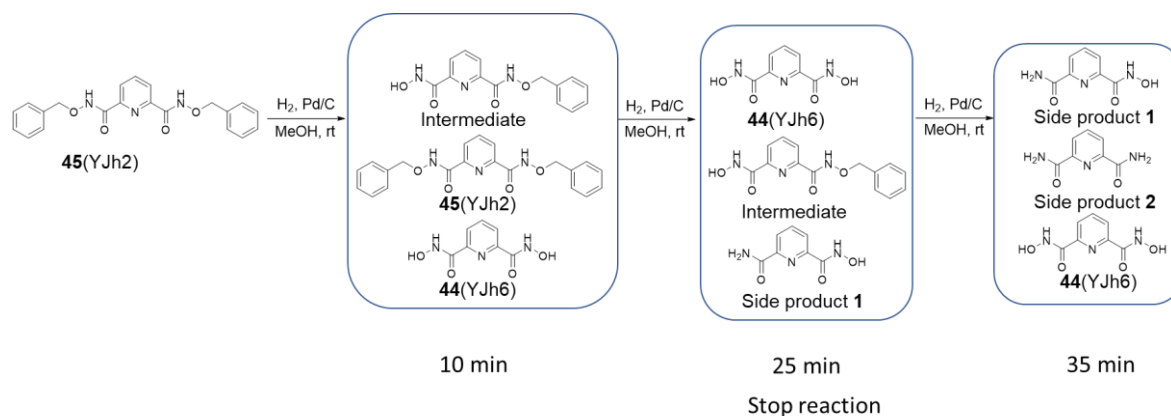


Figure 3.10 Synthesis procedure for compound **44(YJh6)**. (The main components of different stages are listed.)

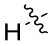
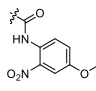
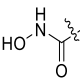
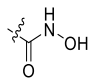
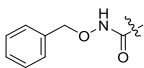
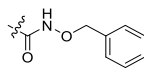
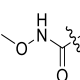
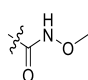
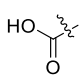
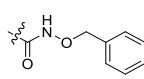
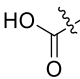
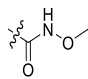
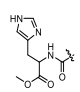
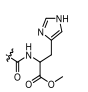
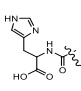
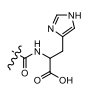
3.2.1.2 Enzyme-based *in vitro* activity of DPA derivatives

The activity of the DPA derivatives at the 2- and 6-positions were measured by enzyme-based *in vitro* assays and the IC_{50} values are listed in **Table 3.6**. The hydroxamic acid containing compounds **44(YJh6)** and **39** were inactive for NDM-1 and the reasons might come from the different characters of the active sites for different metalloenzymes and the binding affinity of the functional groups of the ligands. Most of the metalloenzymes targeted by hydroxamates or hydroxamic acids were mono-zinc proteins such as MMP family, HDAC family and hCAII. In addition, zinc ions played important roles for NDM-1 influencing both its activity and stability. The distances and angles for the nitrogen of the pyridine ring and the oxygens of the carboxyl groups were essential for the zinc binding affinity of DPA. The acidic group, the terminal hydroxyl group of the hydroxamic acid was not suitable for cooperating with the nitrogen of the pyridine ring (**Figure 3.9**).

Table 3.6 DPA Derivatives at the 2- and 6-Positions

Compound	R_2	R_6	IC_{50} (μM)
39 ^{f4}			>1000
40 (YJh8)			530.75 ± 9.97
41 (YJh9)			>2000
42 (YJh10)			1236.33 ± 26.58

^{f4} Compound **39** was synthesized by Alexander Langhans.

43 (YJh13)			>400
44 (YJh6)			>1000
45 (YJh2)			7.16 ± 0.56
46 (YJh11)			84.29 ± 14
47 (YJh20)			22.68 ± 5.16
48 (YJh207)			27.76 ± 1.91
49 (YJh12)			>1000
50 (YJh15)			>1000

^a Compounds **45**(YJh2) and **46**(YJh11) did not have good solubility in buffer.

As expected, the inhibitory activity of all the compounds with the terminal hydroxyl groups of the hydroxamic acid parts substituted by methoxy or benzyloxy groups were recovered. Compounds **40**(YJh8) ($IC_{50} = 530.75 \mu\text{M}$) and **42**(YJh10) ($IC_{50} = 1236.33 \mu\text{M}$) kept the inhibitory activity for NDM-1 although were less active than compound **8**(picolinic acid) ($IC_{50} = 303.3 \mu\text{M}$), which suggested that the *N*-(methoxy)amide or *N*-(benzyloxy)amide groups could be used for replacing the carboxyl group of picolinic acid or DPA, and *N*-(benzyloxy)amide was more active than *N*-(methoxy)amide. The same as DPA and compound **8**(picolinic acid), compounds with both 2- and 6-positions substituted by *N*-(methoxy)amide or *N*-(benzyloxy)amide groups such as compounds **45**(YJh2) ($IC_{50} = 7.16 \mu\text{M}$) and **46**(YJh11) ($IC_{50} = 84.29 \mu\text{M}$) were more active than the corresponding monosubstituted compounds **40**(YJh8) and **42**(YJh10), respectively, and compound **45**(YJh2) with two *N*-(benzyloxy)amide groups was more active than compound **46**(YJh11) with two *N*-(methoxy)amides. Although the di-substituted compounds had better IC_{50} values, their solubility in the buffer was reduced especially compound **45**(YJh2), which influenced their activity studies. Considering the permeability and solubility, compounds with one carboxyl and one *N*-(benzyloxy)amide or *N*-(methoxy)amide groups such as compounds **47**(YJh20) and **48**(YJh207) were tested, and their IC_{50} values were 22.68 μM and 27.76 μM , respectively. Compared with di-substituted compounds **45**(YJh2) and **46**(YJh11), as well as mono substituted compounds **40**(YJh8) and **42**(YJh10), the activity difference between the mixed substituted compounds **47**(YJh20) and **48**(YJh207) was less, which implied the higher activity of the carboxyl substituent (Figure 3.11).

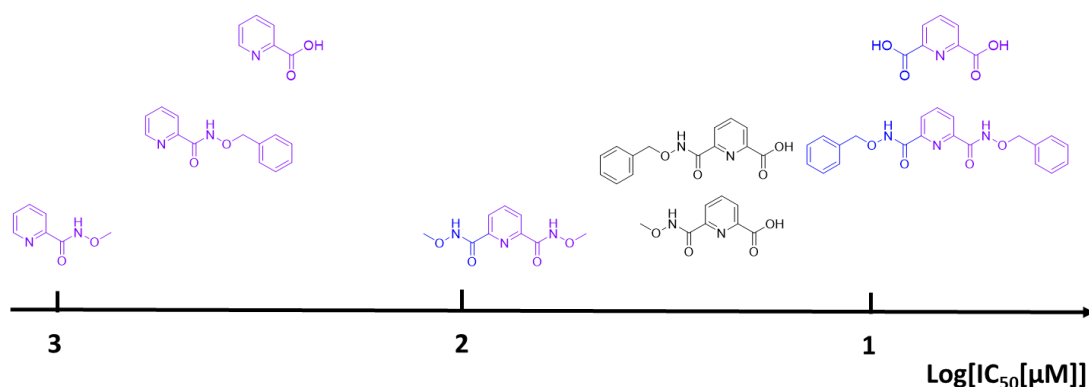


Figure 3.11 Inhibitory activity of DPA derivatives for NDM-1.

In addition, both the mimics of the histidine residues binding with the zinc ions in the active site of NDM-1, compounds **49(YJh12)** and **50(YJh15)** were inactive, the similar binding conditions of the ligands might not have advantages to competing with the histidine residues of the protein. Compound **43(YJh13)** was inactive, which might be due to the insufficient acidity of the amide or the steric hindrance of the phenyl group.

According to the proposed binding pose of compound **45(YJh2)** in **Figure 3.12**, compound **45(YJh2)** was more fit for the active pocket of NDM-1 compared with DPA. Except for the most interactions of DPA in **Figure 3.8**, the benzyloxy contributed more hydrophobic interactions, e.g., interactions with Met154 and Ile35. The benzyloxy interacting with Met154 in **Figure 3.12** was flexible, when it was rotated to a lower position, it would have the aromatic interaction with the residue His122 which played an important role for holding Zn1(II) ion of NDM-1.

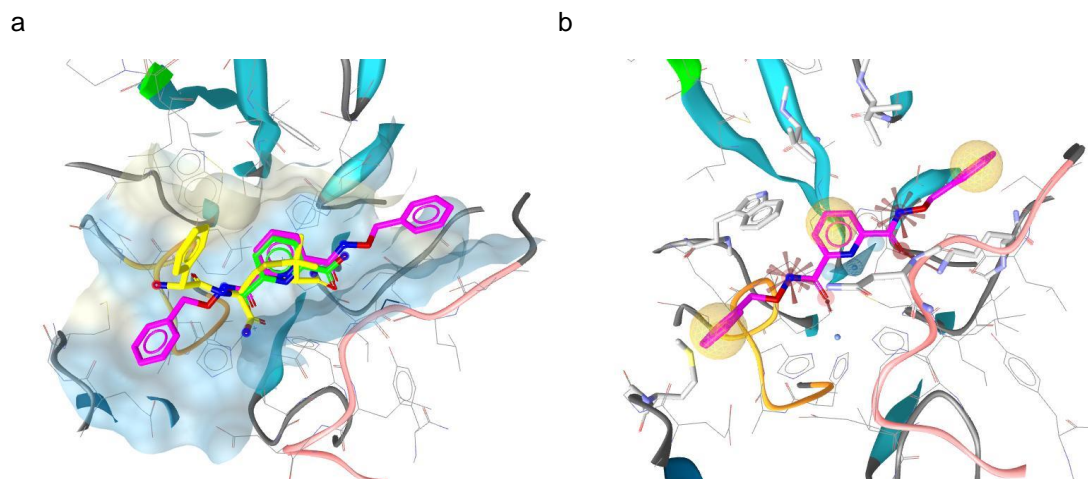


Figure 3.12 Proposed binding pose of compound **45(YJh2)** in the active site of NDM-1 (PDB ID: 5ZGR). The docking studies were performed by Gold 5.8.1 and the results were analyzed by LigandScout 4.2. The loop region from Met67 to Gly71 acting as the 'Door' was colored in green, the loop region from Thr119 to Met126 acting as the 'Ceiling' was colored in orange and the loop region from Ser217 to Asp225 acting as the 'Floor' was colored in pink. a. Proposed binding pose of compound **45(YJh2)** in the binding pocket (The hydrolyzed ampicillin was colored in yellow, the DPA molecule was colored in green, and compound **45(YJh2)** was colored in magenta); b. 3D depiction for the interactions of

compound **45(YJh2)** with the active site (The yellow spheres indicated lipophilic contacts, red arrows indicated hydrogen bond acceptor functionalities, blue wedges indicated zinc binding locations, and the red wedges indicated negative ionizable interactions.)

Above all, the substituents *N*-(benzyloxy)amide or *N*-(methoxy)amide at the 2- and 6-positions of DPA derivatives offered more choices for further modifications to change the polarities of the inhibitors for proper permeability and solubility. The methyl or benzyl groups of the substituents could be optimized to different structures even aromatic groups, e.g., change the alkoxy to phenolic group. According to the published work about *O*-aryloxycarbonyl hydroxamate inactivators for both NDM-1 and SBLs by Thomas, P. W. in 2019, combining the covalent binding strategy with the *N*-(alkoxy)amides might expand the inhibiting spectra to SBLs as well.¹⁵³ On the one hand, the optimization of the *N*-(alkoxy)amides might improve the acidity of the amide which might increase the zinc ion binding affinity of the ligand, on the other hand, proper modifications could increase the H-bond or hydrophobic as well as other kinds of interactions with the active site to improve the binding affinity and selectivity of the ligands to the target protein.

Based on the development process from compound **44(YJh6)** to compound **45(YJh2)**, compound **17**(pyridine-2-sulfonamide) was reconsidered (**Figure 3.13**). Substitution of the hydrogen of the sulfonamide, especially by aromatic groups or strong electron withdrawing groups, e.g., carbonyl, sulfonyl, phosphoryl, etc., which might revive the activity of pyridine-2-sulfonamide structure. As for the more promising quinoline derivatives, this direction was not tried until the development of compound **83(YJh174)**, the *N*-phenylpyridine-2-sulfonamide (**YJh210**) and *N*-(benzyloxy)pyridine-2-sulfonamide (**YJh211**) were synthesized and tested, while both were inactive.

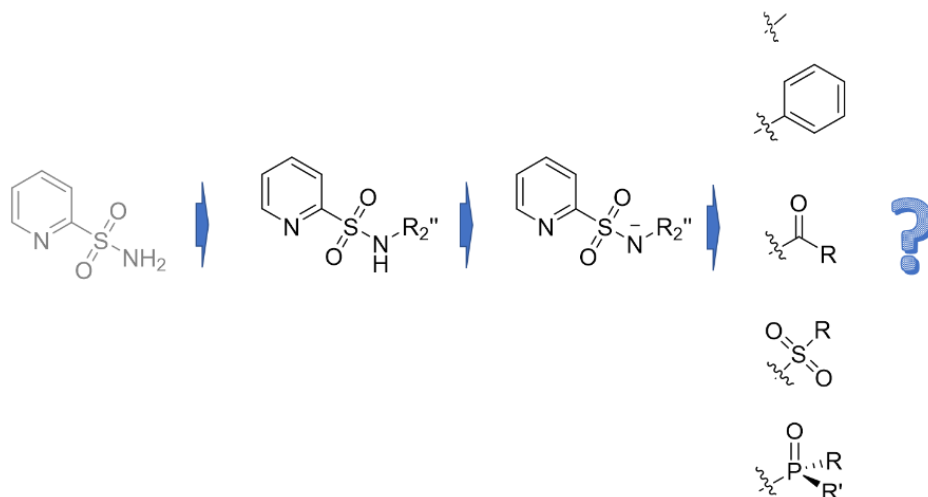


Figure 3.13 Possible modification strategies for pyridine-2-sulfonamide.

3.2.2 8-HQA derivatives

3.2.2.1 Compound design and synthesis of 8-HQA derivatives

8-HQA was deduced from DPA, the isosteric replacement of one of the carboxyl groups in DPA by a aromatic hydroxyl group furnished **8-HQA** with an IC₅₀ value of 9.05 μM. Compound **21**(8-hydroxy-2-

methyl-quinoline) and compound **27** (8-hydroxyquinoline) with IC_{50} values of 273.5 μ M and 133.5 μ M, respectively, implied that the 8-hydroxyquinoline moiety might be more active than picolinic acid ($IC_{50} = 303.3 \mu$ M). Given the reduction of carboxyl groups might improve the permeability for cell level assays and the relative larger quinoline ring could enhance the hydrophobic interactions with the active pocket, **8-HQA** derivatives were developed. The initial SAR based on the screenings of the compounds in **Table 3.4** and **Table 3.5** before the discovery of **8-MSQA** is listed in **Figure 3.14**.

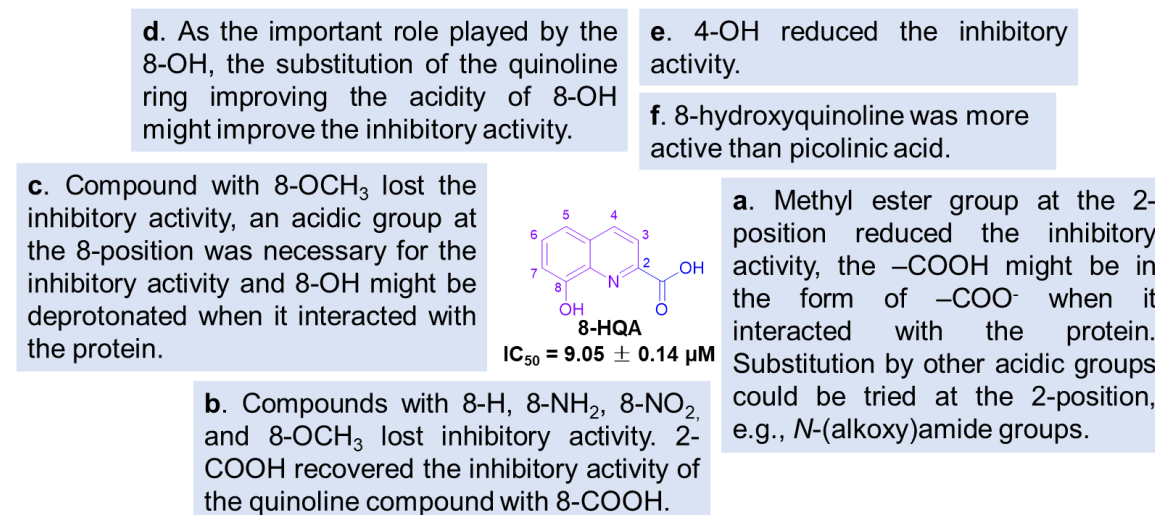


Figure 3.14 Initial SAR for the development of **8-HQA** derivatives.

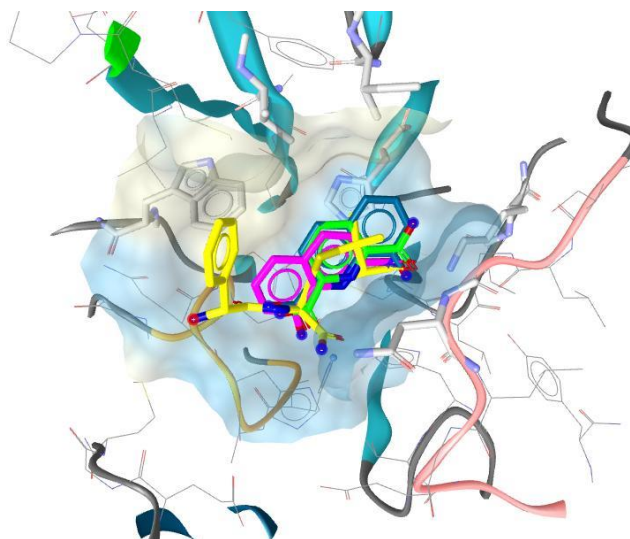


Figure 3.15 Proposed binding poses of **8-HQA** in the active site of NDM-1. The docking studies were performed by Gold 5.8.1 and the results were analyzed by LigandScout 4.2. The loop region from Met67 to Gly71 acting as the 'Door' was colored in green, the loop region from Thr119 to Met126 acting as the 'Ceiling' was colored in orange and the loop region from Ser217 to Asp225 acting as the 'Floor' was colored in pink. For ligands, the hydrolyzed ampicillin was colored in yellow, DPA molecule was colored in green, and **8-HQA** molecules were colored in magenta and blue, respectively.

According to docking studies, **8-HQA** kept the most interactions of DPA with the active site, e.g., zinc binding location functionalities, negative ionizable interactions with both Zn(II) ions, both the H-bond and negative ionizable interactions with Lys211 and Asn220, and hydrophobic interactions with important amino acid residues of loop 3. As **8-HQA** containing two different zinc ion binding moieties, two main proposed binding poses are shown in **Figure 3.15** for **8-HQA**, and both overlapped well with the hydrolyzed β -lactam part of the substrate or the proposed binding pose of DPA. For the first binding pose of **8-HQA** colored in magenta, the 8-hydroxyl group and its related moiety played as zinc binding locations for both Zn(II) ions, the 2-COO⁻ and its related moiety played as zinc binding location for Zn2(II) ion. For the other binding pose of **8-HQA** colored in blue, the two zinc ion binding moieties exchanged their roles. The fitness score of the first binding pose was higher than the other. Compared with DPA colored in green, the relative larger quinoline ring of **8-HQA** offered more hydrophobic interactions with Trp93, Val73 and Ile35 of the binding pocket. Besides, larger substituents at the 4-, 5- or 6-positions of the quinoline ring could increase the hydrophobic interactions with the amino acid residues of loop 3 acting as 'door' of the active pocket and the different properties of the substituents might influence the binding affinity with the Zn(II) ions. Above all, docking studies supported the modification strategies from the primary SAR.

Based on the initial studies, the effects of halogen substituents were investigated considering the contribution for additional hydrophobic interactions and the acidity of the 8-hydroxyl group which could improve the binding affinity of the ligands for the active pocket. The *N*-(alkoxy)amide groups applied for DPA derivatives might also work for **8-HQA** derivatives..

For the synthesis of **8-HQA** derivatives, compounds **59(YJh22)**, **58(YJh34)** and **61(YJh59)** were tried to be synthesized by reacting **8-HQA** with *N*-iodosuccinimide, *N*-bromosuccinimide and *N*-chlorosuccinimide, respectively (**Figure 3.16**). However, only compound **59(YJh22)** was synthesized by *N*-bromosuccinimide and the purification was done in small quantities and many times by HPLC as its poor solubility in acetonitrile and water.^{197, 198} Through the same method, the relatively mono 5-position halogen-substituted by-products were always mixed with products **61(YJh59)** and **58(YJh34)**, respectively. In addition, the similar polarity of the compounds and other side products made the purification by silica gel chromatograph difficult. Besides, HPLC purification was also difficult to be performed due to the less solubility of the compounds in acetonitrile and water. In this case, compounds **58(YJh34)**, **61(YJh59)** and **60(YJh66)** were synthesized by oxidizing the di-halogen-substituted 2-methylquinoline-8-ol or 8-(benzyloxy)-2-methylquinoline via selenium dioxide.¹⁸³ Due to the corresponding di-halogen-substituted 2-methylquinoline-8-ols for synthesizing compounds **61(YJh59)** and **60(YJh66)** were iodo-substituted at their 7-positions, the iodo group at the 7-positions would be lost under the oxidation condition.^{199, 200} Therefore, the 8-hydroxyl groups of the di-halogen-substituted 2-methylquinoline-8-ols with the 7-positions iodo-substituted were protected before the oxidation by selenium dioxide, and the protecting benzyl groups were removed by boron trichloride after oxidation.²⁰⁰ For compound **60(YJh66)**, the material 5-chloro-7-iodo-2-methylquinolin-8-ol was synthesized by two steps, the 5-chloro-2-methylquinolin-8-ol was synthesized by Doebner–Miller reaction and then reacted with *N*-iodosuccinimide.^{177, 179, 180, 185}

Some other modifications for **8-HQA** derivatives have also been tried. The substitution at the 5-position by phenyl or substituted phenyl groups was possible by Suzuki reaction since the halogen-substituted analogues had already been synthesized. Furthermore, the 5- and 7-positions substituted by different halogens had different reactivity to the Suzuki reaction, thus selective modification could be realized.^{201, 202} Doebner–Miller reactions allowed more freedom for the modifications of the quinoline

ring by starting with different aniline and α,β -unsaturated carbonyl compounds, such as starting with 3-aminonaphthalen-2-ol could add one more aromatic benzene ring adjacent to the quinoline ring which would increase the hydrophobic interactions of the ligand with the active pocket, the compound is listed as **YJh68** in the synthesis route of **8-HQA** derivatives. There were reported inhibitors which were designed by isosteric replacement substituting one of the 2- or 6-carboxyl groups of **DPA** with a phosphonomethyl or related group.^{203, 204} The same strategy has been tried for **8-HQA** derivatives in this work, 8-methoxy-2-methylquinoline was used to react with LDA and (EtO)₂POCl reagents, instead of the planned **YJh35** (diethyl ((8-methoxyquinolin-2-yl)methyl)phosphonate), a side product with diethyl methyl phosphate at the 2-position was synthesized.²⁰⁵ For optimization, the method by using 2-(bromomethyl)-8-methoxyquinoline reacted with P(OEt)₃ could be tried in the future.^{203, 204} The synthesis route for **8-HQA** derivatives with 5-phenyl group was formed, however, considering the better cell-based activity results of **8-MSQA** derivatives, this direction was not continued which might be developed in the future as well as the branches by changing the starting materials of Doebner–Miller reaction and the phosphonates (or phosphonic acids).^{177, 179, 180, 206} The isosteric replacement of the 2-carboxyl by *N*-(benzyloxy)amide or *N*-(methoxy)amide groups at the 2-position for **8-HQA** derivatives was applied and the compounds were synthesized by the same coupling condition used for **DPA** derivatives.¹⁹⁵ Compound **56(YJh83)** with the 5- and 7-positions nitro-substituted was synthesized by stirring quinolin-8-ol in a 7/3 mixed solution of the concentrated HNO₃ and H₂SO₄.²⁰⁷ However, compound **56(YJh83)** had deep yellow color which might influence the activity measurement. The 8-hydroxyquinolines halogen-substituted at the 5- and 7-positions were commercially available. The detailed synthesis routes and procedures are shown in **Scheme S2** of the experiment part.

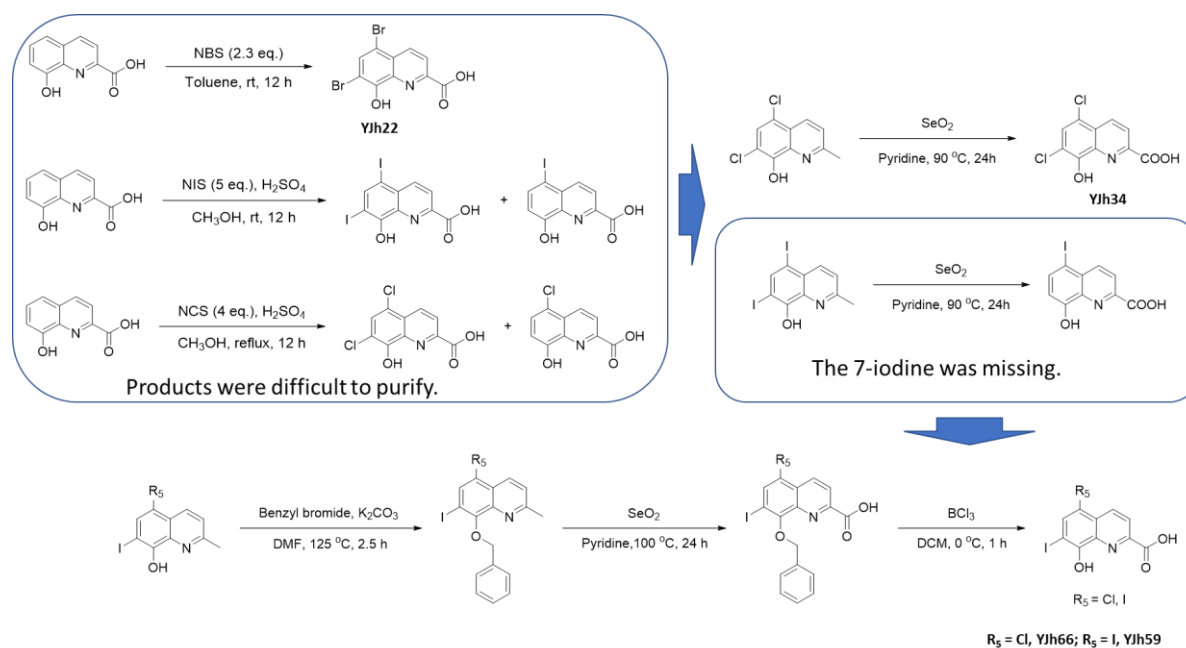


Figure 3.16 Synthesis of 5,7-di-halogen-substituted **8-HQA** derivatives.

3.2.2.2 Enzyme-based *in vitro* activity of 8-HQA derivatives

The activity of 8-HQA derivatives were measured by *in vitro* enzyme-based assays and the IC₅₀ values are listed in Table 3.7.

Table 3.7 8-HQA Derivatives

The image shows the chemical structure of a 8-HQA derivative. It consists of a benzene ring fused to a pyridine ring. The benzene ring has a hydroxyl group (-OH) at the 8-position. The pyridine ring has a nitrogen atom at the 1-position. Substituents are indicated at the 2, 5, and 7 positions: R₂ at the 2-position, R₅ at the 5-position, and R₇ at the 7-position.

Compound	R ₂	R ₅	R ₇	IC ₅₀ (μM)
27		H	H	133.5 ± 1.13
51		Cl	H	28.14 ± 1.06
52 Chloroxine		Cl	Cl	4.9
53		Br	Br	4.22 ± 0.8
54 Clioquinol		Cl	I	2.98 ± 1.09
55		I	I	2.49 ± 1.08
56 (YJh83)		NO ₂	O ₂ N	20.03 ± 2.06 ^a
57		H	H	>1000
HQA		H	H	9.05 ± 0.14
58 (YJh34)		Cl	Cl	0.54 ± 0.09
59 (YJh22)		Br	Br	0.46 ± 0.07
60 (YJh66)		Cl	I	0.48 ± 0.02
61 (YJh59)		I	I	0.3 ± 0.08
62 (YJh18)		H	H	13.72 ± 1.09
63 (YJh14)		H	H	11.19 ± 1.06
64 (YJh27)		Br	Br	1.47 ± 0.15

^a When the concentration of compound **56(YJh83)** was higher than 3.9 μM , the buffer would be yellow, therefore its IC_{50} value might be influenced.

Compounds **51** to **54** were measured at first, compared with compound **27**(quinoline-8-ol) ($\text{IC}_{50} = 133.5 \mu\text{M}$), the inhibitory activity of compound **51** ($\text{IC}_{50} = 28.14 \mu\text{M}$) with the 5-position chloro-substituted was improved nearly 4 times, which suggested that the halogen-substitution at the 5-position was efficient for improving the inhibitory activity of the molecules. The activity of compound **52** ($\text{IC}_{50} = 4.9 \mu\text{M}$) with both the 5- and 7-positions chloro-substituted was 5 times higher than compound **51** with only the 5-position chloro-substituted, which meant that both the 5- and 7-positions halogen-substituted could improve the activity of the molecules. Compound **53**(5, 7-dibromoquinolin-8-ol), **54**(5-chloro-7-iodoquinoline-8-ol), and **55**(5, 7-diiodoquinolin-8-ol) were tested, the IC_{50} values were 4.22 μM , 2.98 μM , 2.49 μM , respectively. For both the 5- and 7-position halogen-substituted compounds, the activity improved gradually according to the order of the substituents from chloro, bromo, to iodo. Compound **56(YJh83)** with the 5- and 7-positions nitro-substituted was tested, but the deep yellow color of the compound might have an influence on the measurement. Apparently, the modification strategies were successful, the halogen-substituted quinoline ring could have additional hydrophobic interactions with the active pocket and increase the acidity of the 8-hydroxyl group which was able to improve the zinc ion binding affinity of the moiety interacting with the Zn(II) ions. When switching from the quinoline-8-ol to **8-HQA** by adding the 2-carboxyl group and keeping the halogen-substitution at the 5- and 7-positions, like in compounds **58(YJh34)**, **59(YJh22)**, **60(YJh66)** and **61(YJh59)**, the IC_{50} values were improved 10 times relative to the respective compounds with a hydrogen at the 2-position, namely to submicromolar IC_{50} values of 0.3-0.54 μM . This observation also highlighted the cooperative effect of the 8- and 2-positions of the quinoline structures.

In addition, compound **57** with 2-phenyl substituent was not active which might be due to the steric hindrance. As expected, *N*-(benzyloxy)amide or *N*-(methoxy)amide groups were also worked for **8-HQA** derivatives, compounds **62(YJh18)**, **63(YJh14)** and **64(YJh27)** were all active and had IC_{50} values of 13.72 μM , 11.19 μM and 1.47 μM , respectively, although the activity was a little lower than the relative 2-carboxyl compounds.

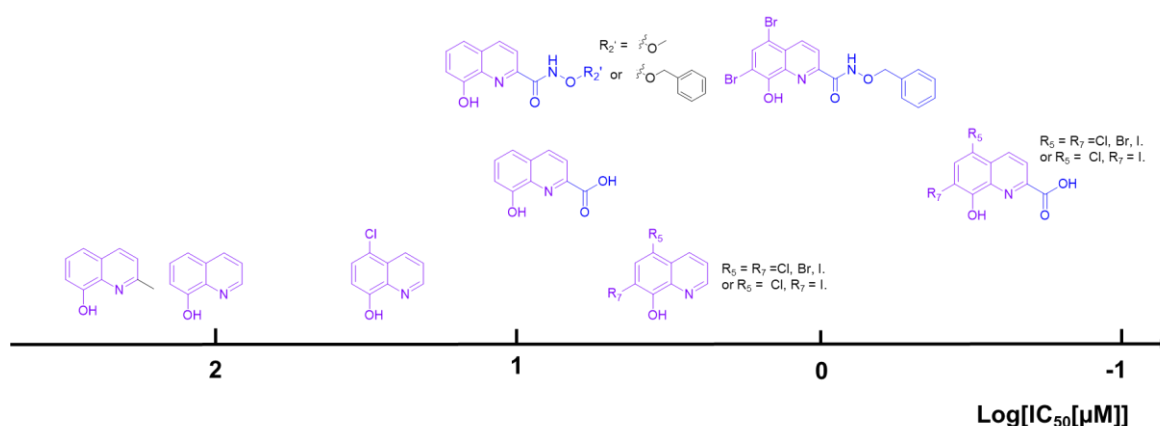


Figure 3.17 Inhibitory activity of **8-HQA** derivatives.

Docking studies also supported the high activity of compounds with the 5- and 7-positions halogen-substituted. Compared with **8-HQA**, compounds **58(YJh34)**, **59(YJh22)**, **60(YJh66)** and **61(YJh59)** with

the halogen-substitution at the 5- and 7-positions bound with the active site of the protein by the similar proposed poses, especially the two main proposed binding poses with high fitness scores (**Figure 3.15**), however, the preferred binding pose was more apparent. On the one hand, the different preference of the binding poses might come from the increased size of the halogen-substituted parts of the quinoline ring which need take more space, on the other hand, the redistributed electron density influenced by the halogen substituents which made the hydroxyl group at the 8-position and its related moiety with a stronger Zn(II) ion binding affinity than the carboxyl group at the 2-position and its related moiety. The preferred binding pose is shown in **Figure 3.18**, the hydroxyl group at the 8-position and its related moiety had zinc binding location functionalities with both Zn(II) ions, the carboxyl group at the 2-position and its related moiety showed zinc binding location functionalities with Zn₂(II) ion. The deprotonated hydroxyl group at the 8-position had negative ionizable interactions with both Zn(II) ions, and the deprotonated carboxyl group at the 2-position had negative ionizable interactions with Lys211 and Zn₂(II) ion. There were four H-bond interactions: the deprotonated carboxyl group at the 2-position with Asn220 and Lys211, the structural water molecule with the nitrogen of the pyridine ring and the deprotonated hydroxyl group at the 8-position. The interactions of the ligand with Asn220, Lys211 and the structural water molecule were similar as the interactions described for the proposed recognition and hydrolysis mechanism of β -lactam substrates in the active site of NDM-1. The moiety including the pyridine ring especially its nitrogen atom and the 2-carboxyl group (or other replaceable functional groups) might play as the mimics of the intact or hydrolyzed β -lactam antibiotics. Except the hydrophobic interactions of the quinoline ring with Trp93, the halogen substituent at the 5-position had hydrophobic interactions with Leu65, Met67 and Val73, and the halogen substituent at the 7-position had hydrophobic interactions with Met154. The increased hydrophobic interactions contributed for the selectivity, binding affinity, and improved inhibitory activity of the ligands for NDM-1.

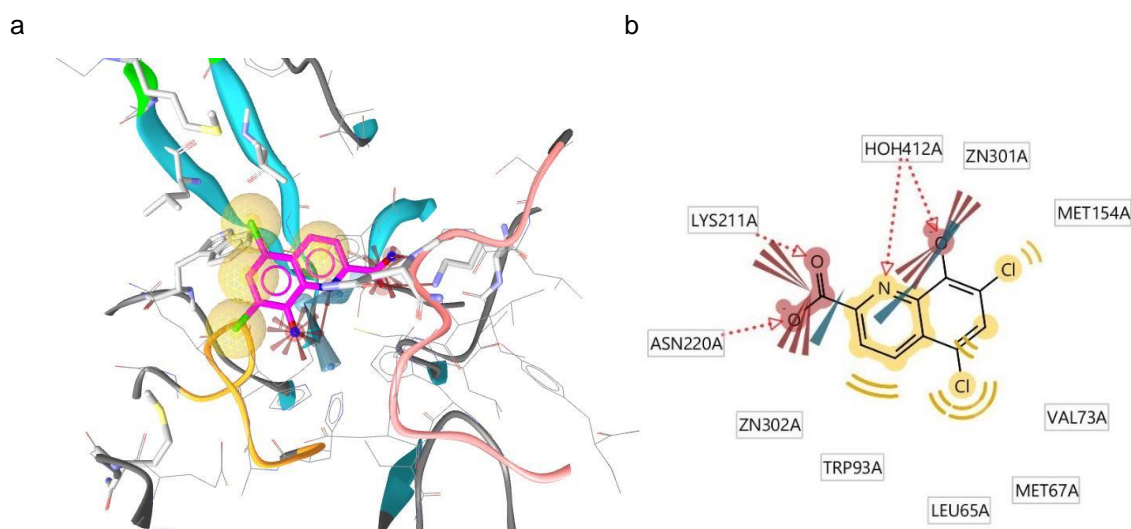


Figure 3.18 Proposed binding pose of compound **58(YJh34)** in the active site of NDM-1 (PDB ID: 5ZGR). The docking studies were performed by Gold 5.8.1 and the results were analyzed by LigandScout 4.2. The loop region from Met67 to Gly71 acting as the 'Door' was colored in green, the loop region from Thr119 to Met126 acting as the 'Ceiling' was colored in orange and the loop region from Ser217 to Asp225 acting as the 'Floor' was colored in pink. Compound **58(YJh34)** was colored in magenta. a. 3D depiction for interactions of compound **58(YJh34)** with the active site (The yellow

spheres indicated lipophilic contacts, red arrows indicated hydrogen bond acceptor functionalities, blue wedges indicated zinc binding locations, and the red wedges indicated negative ionizable interactions.); b. 2D depiction for interactions of compound **58(YJh34)** with the active site (The yellow lines indicated lipophilic contacts, red arrows indicated hydrogen bond acceptor functionalities, blue wedges indicated zinc binding locations, and the red wedges indicated negative ionizable interactions.).

Above all, the halogen substitution at the 5- and 7-positions brought the derivatives to sub-micromolar IC_{50} values of 0.3-0.54 μ M. The halogen substituents at the 5- and 7-positions of **8-HQA** derivatives contributed more hydrophobic interactions of the ligands with the active site and the acidity of the hydroxyl group at the 8-position was strengthened by the halogen substitutions. Docking studies also supported the intact or hydrolyzed β -lactam mimic theories of the developed inhibitors. In addition, both compounds **52** (chloroxine) and **54** (clioquinol) are approved drugs which have bacteriostatic, fungistatic or antiprotozoal activities,²⁰⁸ the inhibitory activity for NDM-1 might expand their applications in the future. For further development of **8-HQA** derivatives, 5-position substituted by a phenyl group was considered to offer more hydrophobic interactions with the active site and contribute to the preferred binding mode, the synthesis route was formed and tried (in **Scheme 2**). As the inhibitory activity of **8-MSQA**, a derivative deduced from **8-HQA** was discovered which was a more promising hit, the 5-position phenyl-substituted was applied for **8-MSQA** derivatives.

3.2.3 8-MSQA derivatives

3.2.3.1 Compound design and synthesis of 8-MSQA derivatives

DPA was discovered by the initial fragment screening, and **8-HQA** was deduced by isosteric replacement. The zinc ion binding moieties picolinic acid and 8-hydroxyl quinoline were identified by the screenings of the DPA analogues in **Table 3.4** and a prepared quinoline-based scaffolds with different substituents at the 2- and 8-positions in **Table 3.5**. Based on the modification and development of both DPA and **8-HQA** derivatives, the importance of the acidity or the tendency to offer negative charged atom for binding with Zn(II) ions of the substituent at the 8-position for quinoline derivatives was realized. The inactive 8-aminoquinoline containing structures in **Table 3.5** were reconsidered, as increasing the acidity of the 8-amino group might change the inhibitory activity of relative molecules. Imide was considered at first, while compound **25(YJh118)** in **Table 3.5** was tested but inactive, the one more atom or the carbonyl between the nitrogen of the imido group and the quinoline ring might influence the collaboration of the acidic group at the 8-position with the nitrogen atom of the quinoline ring. The inactive compounds **22(YJh38)** and **44(YJh6)** should have the similar reason. In this case, the amino group at the 8-position was chosen to be an amide group such as a carbonamide group, a sulfonamide group, or a phosphoramidate group. Comparing the pKa of relative acids, the organic sulfonic acids with the lowest pKa values in **Figure 3.19**, which offered a clue, the sulfonamides would be more acidic than carbonamides and phosphoramidates, thus sulfonamide groups were used for the inhibitor development.

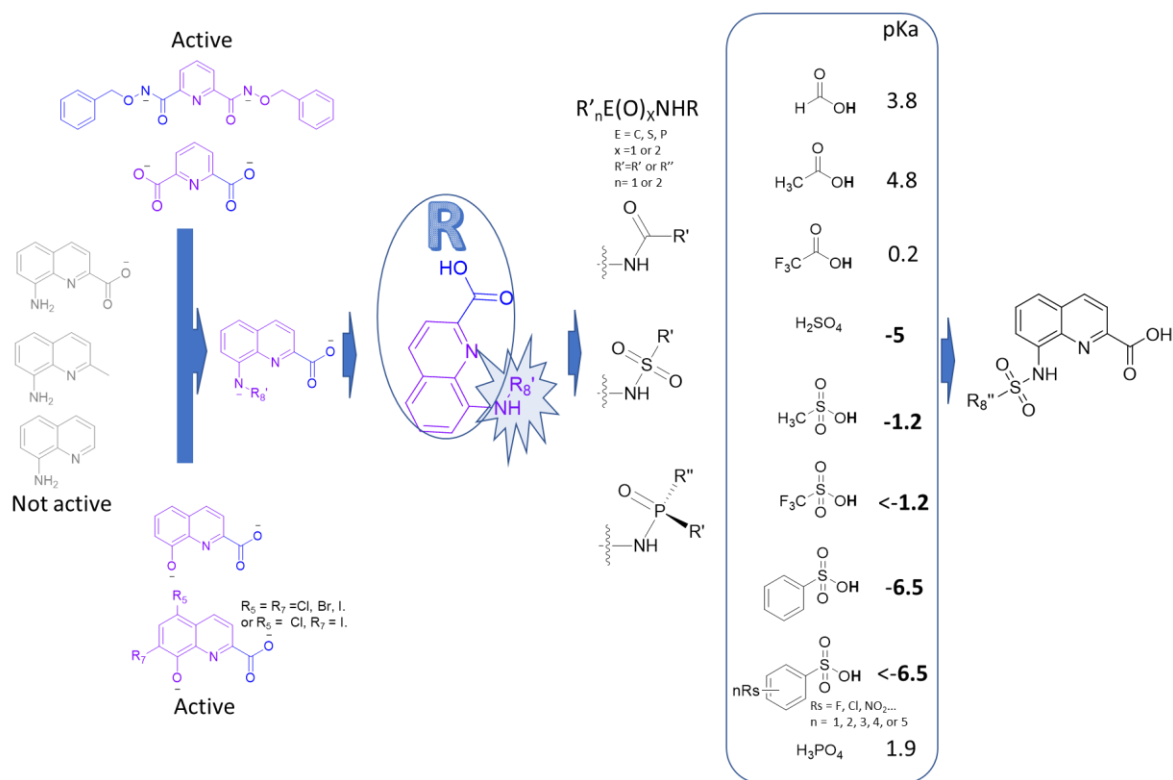


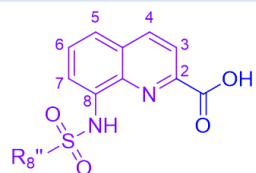
Figure 3.19 Development of **8-MSQA** inhibitors. (The negative charged atoms were used to highlight the acidic groups.)

Surprisingly, 8-methylsulfonamido-quinoline-2-carboxylate (**8-MSQA**) with an IC_{50} value of $1.64 \mu\text{M}$ was a more potent inhibitor than **8-HQA** ($\text{IC}_{50} = 9.05 \mu\text{M}$). To investigate whether the 8-methylsulfonamide group could replace the 8-hydroxyl group of the quinoline ring for the inhibitory activity and the collaboration of the 2- and 8-positions, several **8-MSQA** derivatives were synthesized and tested at first (**Table 3.8**). Compounds **65(YJh82)** ($\text{IC}_{50} = 1.6 \mu\text{M}$), **66(YJh85)** ($\text{IC}_{50} = 1.4 \mu\text{M}$) and **67(YJh208)** ($\text{IC}_{50} = 6.24 \mu\text{M}$) were active even without the 2-carboxyl group which demonstrated that the 8-sulfonamidoquinoline moiety was essential for **8-MSQA** derivatives playing the similar role as 8-hydroxyquinoline for **8-HQA** derivatives and picolinic acid for **DPA**, and the activity was higher. Comparing the IC_{50} values of **8-MSQA** and compound **36(YJh63)**, or compound **68(YJh93)** and **69(YJh90)**, **66(YJh85)**, **67(YJh208)**, the 2-carboxyl group still contributed to the improvement of the inhibitory activity. Compound **66(YJh85)** was more active than compound **65(YJh82)**, and compound **68(YJh93)** was more active than **8-MSQA** which suggested that different aryl substituents of the substituted-sulfonamide groups could change its acidity and aryl substituents was better than alkyl substituents. The relative stronger electron withdrawing ability or the larger size of the aryl substituents contributed to the binding poses with higher activity. Furthermore, there were less differences of the activity for compounds **68(YJh93)** and **69(YJh90)** or **66(YJh85)** compared with **8-HQA** ($\text{IC}_{50} = 9.05 \mu\text{M}$) and compounds **21** ($\text{IC}_{50} = 273.5 \mu\text{M}$) or **35(YJh209)** ($\text{IC}_{50} = 156.25 \mu\text{M}$). On the one hand, the less difference implied the substituted-sulfonamide group played more important roles than the 2-carboxyl group, on the other hand, **8-MSQA** derivatives might bind with the active site of NDM-1 with more selectivity.

Table 3.8 Primary Activity Tests of a Panel of 8-MSQA Derivatives

Compound	R ₂	R _{8''}	IC ₅₀ (μM)
8-MSQA (YJh65)			1.64 ± 0.31
36 (YJh63)			17.61 ± 2.24
65 (YJh82)			1.6 ± 0.24
66 (YJh85)			1.4 ± 0.3
67 (YJh208)			6.24 ± 0.94
68 (YJh93)			0.68 ± 0.06
69 (YJh90)			1.74

For the 2-, 3-, 4-, 5-, and 6-positions, substitution might influence binding poses. Halogen substitution at the 5-, 6-, and 7-positions could influence the acidity of the sulfonamide group at the 8-position.



2-COOH could improve inhibitory activity. *N*-(alkoxy)amide groups might be possible substituents as **8-HQA** derivatives.

For R_{8''}, aryl was more active than alkyl, strong electron withdrawing groups were preferred.

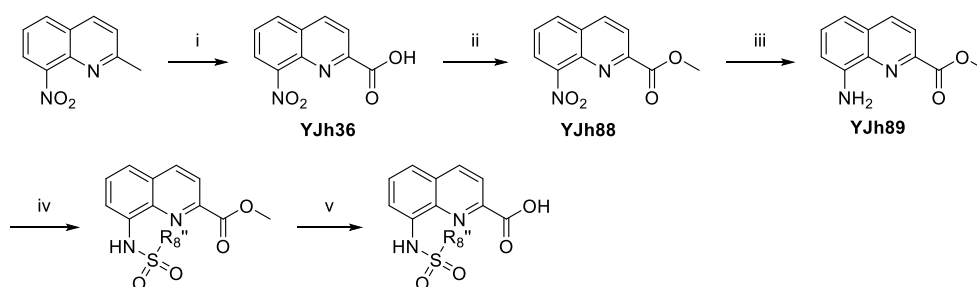
Figure 3.20 Primary SAR for the development of **8-MSQA** inhibitors.

According to the primary SAR, a series **8-MSQA** derivatives at the 8-position were developed at first and their inhibitory activities are shown in **Table 3.9** and **Table 3.10**. The compounds in **Table 3.9** were synthesized by a general five step route shown in **Scheme 3.1**. The starting material 2-methyl-8-nitroquinoline was commercially available and the 2-methyl group was oxidized to 2-carboxyl group by selenium dioxide to obtain compound **30(YJh36)**.¹⁸³ The 2-carboxyl group of compound **30(YJh36)** was changed to a methyl ester group (**YJh88**) by refluxing in methanol with a catalytic amount of concentrated sulfuric acid to make the subsequent compounds be easier purified by silica gel chromatograph.¹⁷⁶ The nitro group of **YJh88** was hydrogenated to amine catalyzed by palladium on carbon to get compound **38(YJh89)**.¹⁸⁷ Compound **38(YJh89)** was reacted with corresponding sulfonyl chlorides under the general sulfonamide coupling condition and the methyl ester group of the products was hydrolyzed by 1 or 2 M NaOH solution/MeOH to arrive to the final compounds.^{176, 133, 209} The sulfonamide coupling condition above was not suitable for compound **70(YJh103)**, as the trifluoromethanesulfonyl chloride was quite reactive, trifluoromethanesulfonic anhydride was tried and the sodium bicarbonate or TEA was used as the base which offered a better yield of the compound.^{209, 210} The final compound **70(YJh103)** was estimated with a 90% purity according to the ¹H NMR spectrum which might be influenced by the different protonated forms of the compound or there were some other side products that could not be separated by silica gel chromatograph, which needed to be further investigated, and the inhibitory activity of compound **70(YJh103)** was tested with the product obtained.

There were mainly two routes for the synthesis of the halogen-substituted compounds. For most 5-, 6-, or 7-position mono halogen-substituted or 5- and 6-position di-halogen-substituted compounds, the corresponding halogen-substituted 2-methyl-8-nitroquinolines were synthesized by Doebner–Miller reaction, then the similar route as **8-MSQA** derivatives at the 8-position was used.^{177, 179, 180, 209} For the 4-position chloro-substituted compound, methyl 4-hydroxy-8-nitroquinoline-2-carboxylate (**YJh124**) was synthesized at first according to the published procedure and the 4-position was halogen-substituted by POCl₃ to get **YJh128**.²¹¹⁻²¹⁵ The 8-nitro group of **YJh128** was reduced to 8-amine (**YJh139** or **YJh152**), and the final products were obtained by the general two steps sulfonamide coupling and hydrolysis of the methyl ester.^{176, 133, 209, 217} For the 5- and 7-position di-halogen-substituted compounds, the materials such as methyl 8-amino-5,7-diiodoquinoline-2-carboxylate (**YJh94**) and methyl 8-amino-5,7-dichloroquinoline-2-carboxylate (**YJh133**) were synthesized via the methods reported by Ashoka Sahadevan et al. (2018) and the followed sulfonamide coupling steps need longer reaction time since the lower reactivity of the 8-amine influenced by the di-halogen-substitution.^{209, 216, 217} The 5-position iodo-substituted compound **86(YJh113)** was synthesized by reacting compound **36(YJh63)** with *N*-Iodosuccinimide and then the methyl ester was hydrolyzed under base condition.^{133, 176, 197, 198} For the 4- or 5-position phenyl or substituted-phenyl containing compounds, the phenyl (or substituted-phenyl) substitution steps were realized by Suzuki reaction and some functional groups needed to be protected at first, such as the amino group of the substituted boronic acids was protect by Boc group and the Boc group was remove by heating at acid condition later.^{218, 219} The detailed synthesis procedures for **8-MSQA** derivatives are shown in the experiment part (**Scheme S3**).

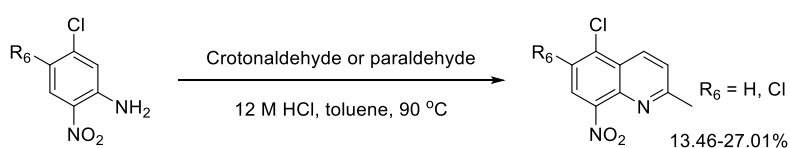
Scheme 3.1 General synthetic route for **8-MSQA** derivatives.

a) Synthetic route for **8-MSQA** derivatives at the 8-position.^{133, 176, 183, 187, 209}

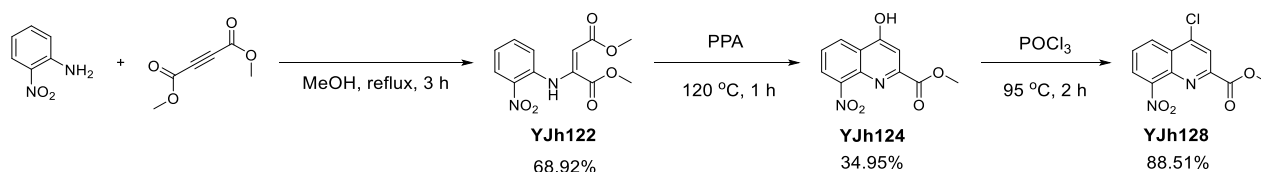


i. SeO_2 , pyridine, 90 °C, overnight, 60-81.5%;¹⁸³ ii. H_2SO_4 , MeOH, reflux, overnight, 92.61-94.96%;¹⁷⁶ iii. Pd/C, H_2 , rt, overnight, 73.98-80.7% or Fe, 1 : 3 AcOH/MeOH, reflux, 2 h, 61.32% or SnCl_2 , MeOH, reflux, 24 h, 48.63-86.48%;¹⁸⁷ iv. RSO_2Cl , 1: 2 pyridine/DCM, rt, 12 h to 3 d, 60-95%;²⁰⁹ v. 2 : 1 2 M NaOH/MeOH, rt, 4 - 24 h, > 90%.^{176, 133}

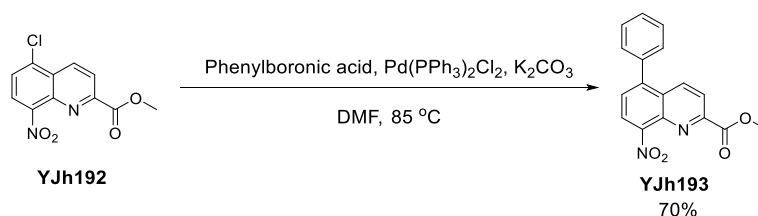
b) Doebner–Miller reaction^{177, 179, 180}



c) Synthetic route for 4-chloro derivatives of **8-MSQA**.²¹¹⁻²¹⁵



d) Synthesizing **YJh193** by Suzuki reaction²¹⁸

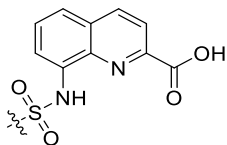


3.2.3.2 Enzyme-based *in vitro* activity of **8-MSQA** derivatives

The activity of **8-MSQA** derivatives at the 8-position was measured by enzyme-based assay and the IC_{50} values are listed in **Table 3.9**. As expected, compound with phenyl substituent of the 8-sulfonamide moiety was more active than the one with methyl substituent, the inhibitory activity of compound **71**(**YJh84**) ($\text{IC}_{50} = 0.71 \mu\text{M}$) was higher than **8-MSQA** ($\text{IC}_{50} = 1.64 \mu\text{M}$) as well as compound **80**(**YJh104**) ($\text{IC}_{50} = 1.28 \mu\text{M}$) with the benzyl substituent. For compounds with the hydrogens of the phenyl groups substituted by one or more strong electron withdrawing groups, their IC_{50} values were even better. For mono chloro-substituted phenyl substituents, the ortho- or para-position substituted compounds were more active than the meta-position substituted compound, the IC_{50} values of compounds **76**(**YJh171**), **77**(**YJh112**) and **78**(**YJh172**) were $0.44 \mu\text{M}$, $0.5 \mu\text{M}$ and $0.45 \mu\text{M}$, respectively. In addition, compound **77**(**YJh112**) was more active than compound **68**(**YJh93**) ($\text{IC}_{50} = 0.68 \mu\text{M}$), thus the chloro-substituted phenyl group was better than the fluoro-substituted phenyl group. The strong electron withdrawing function of the substituent for the 8-sulfonamide group improved the acidity of the amide, which

increased the binding affinity with the Zn(II) ions. The IC₅₀ values for compounds **75**(YJh110) (0.37 μM) and **83**(YJh174) (0.29 μM) were improved half compared with compound **71**(YJh84).

Table 3.9 8-MSQA Derivatives at the 8-Position



Compound	Structure	IC ₅₀ (μM)
8-MSQA (YJh65)		1.64 ± 0.31
70 (YJh103)		0.9 ± 0.03
71 (YJh84)		0.71 ± 0.04
72 (YJh101)		0.75 ± 0.09
73 (YJh100)		1.41 ± 0.21
74 (YJh119)		0.83 ± 0.06
75 (YJh110)		0.37 ± 0.06
76 (YJh171)		0.44 ± 0.09
77 (YJh112)		0.5 ± 0.04
78 (YJh172)		0.45 ± 0.08
79 (YJh121)		0.44 ± 0.05
68 (YJh93)		0.68 ± 0.06
80 (YJh104)		1.28 ± 0.02
81 (YJh111)		0.56 ± 0.11
82 (YJh156)		0.47 ± 0.04
83 (YJh174)		0.29 ± 0.02

Compound **75**(YJh110) was more active as the strong electron withdrawing ability of the nitro group, while considering the *in vivo* toxicity of nitro groups,²²⁰ the substituent in 8-sulfonamide of compound

75(YJh110) was replaced by a pyridine ring as the similar property of the nitrogen, thus compound **83(YJh174)** was designed. Given compound **83(YJh174)** was not only a derivative for **8-MSQA**, but also the pyridine-2-sulfonamide which was discussed at the end of DPA derivatives (**Figure 3.21**), *N*-phenylpyridine-2-sulfonamide (**YJh211**) and *N*-(benzyloxy)pyridine-2-sulfonamide (**YJh211**) were synthesized and tested which were all inactive. Thus, the inhibitory activity of compound **83(YJh174)** should still mainly come from the general mechanisms of **8-MSQA** derivatives.

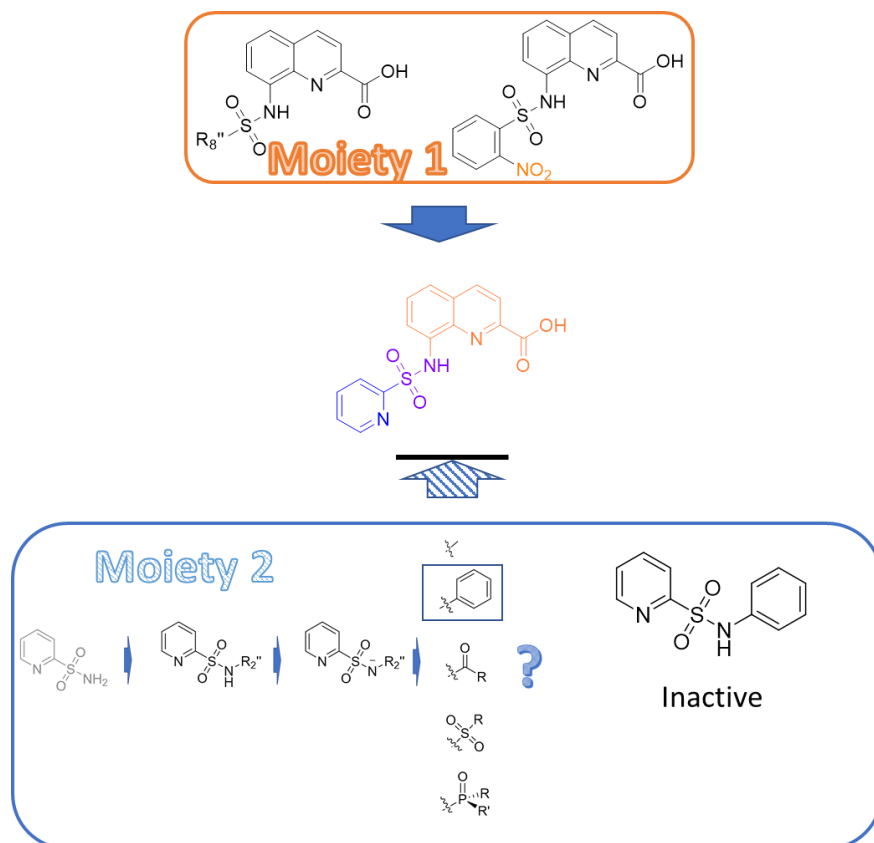
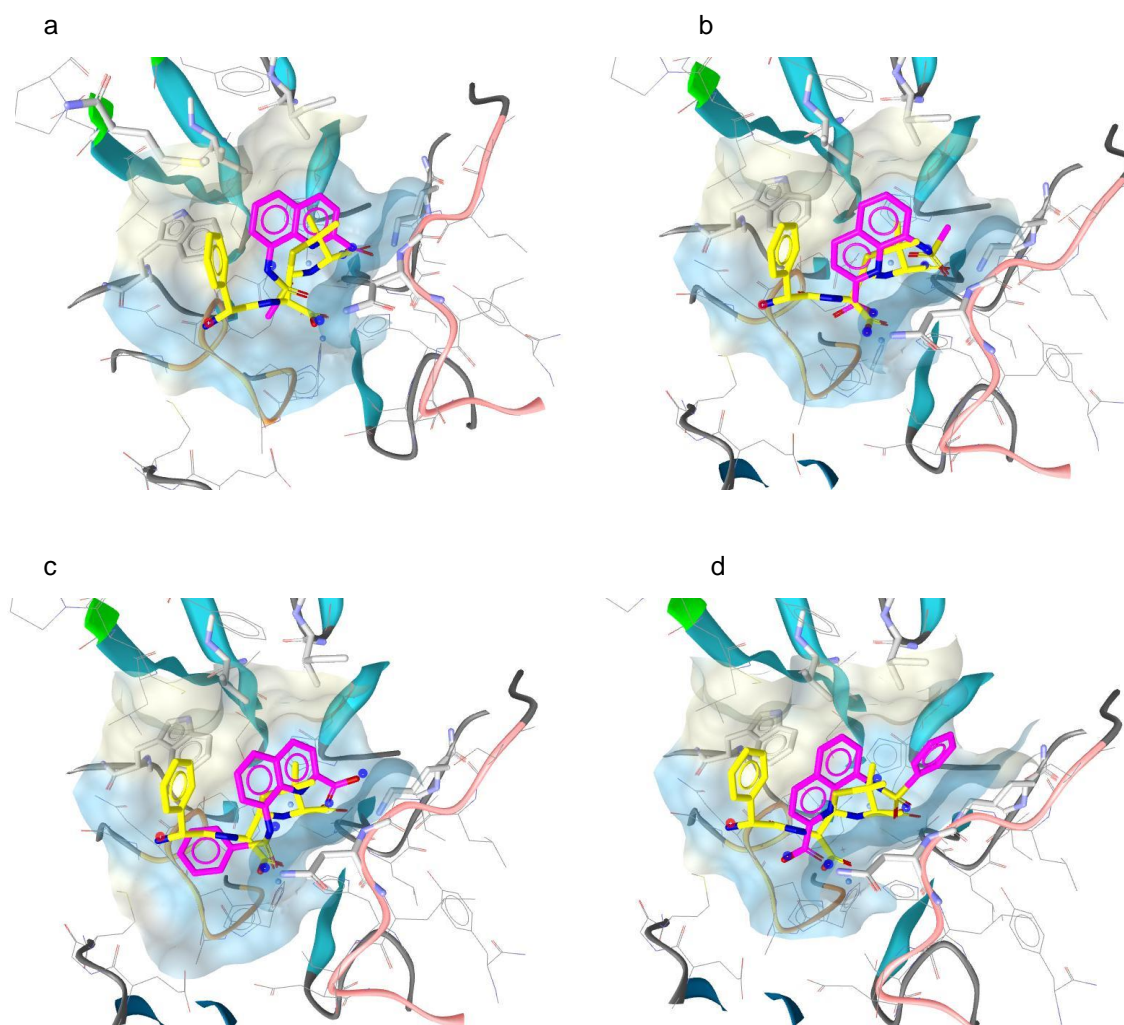


Figure 3.21 Development of compound **83(YJh174)**.

In general, the proposed docking poses of **8-MSQA** or compound **71(YJh84)** were similar as **8-HQA**, except the Zn(II) ions either interacted with the 2-carboxyl group and its related moiety or the substituted 8-sulfonamide and its related moiety. There were two main proposed binding poses similar as **8-HQA**, in addition, the alkyl- or aryl-substituted groups of the 8-sulfonamide groups showed more hydrophobic interactions with the active pocket. For **8-MSQA** derivatives, the expected zinc ion binding groups were slightly farther away from the Zn(II) ions at the active site compared with **8-HQA** derivatives, which might influence the binding affinity with the Zn(II) ions and increase the relevant hydrophobic interactions as the upper moved quinoline ring was closer to the loop 3. The substituted 8-sulfonamide group of the **8-MSQA** derivative was relatively larger than the hydroxyl group at the 8-position of the **8-HQA** derivative, which need more space to avoid the repelling interactions. However, little farther distance with the Zn(II) ions and improved hydrophobic interactions with the active pocket of **8-MSQA** derivatives could improve the selectivity of the inhibitor and reduce the off-target or the metal ion stripping effects as EDTA.

As for compound **83(YJh174)**, except the similar proposed binding poses as other **8-MSQA** derivatives at the 8-position, the binding pose in **Figure 3.22g** with a high fitness score was special which might be contributed by the pyridine-2-sulfonamide derivatives in **Figure 3.22h**. Although *N*-phenylpyridine-2-sulfonamide (**YJh211**) was inactive, considering there were more interactions of the compound **83(YJh174)**, this proposed binding pose was kept. The special binding pose might offer compound **83(YJh174)** different or multi-interaction modes and influence the inhibitory activity. The nitrogen of the pyridine ring acted as the zinc binding location for Zn2(II) ion, the nitrogen of the sulfonamide showed negative ionizable interactions with both Zn(II) ions. There were H-bond interactions of the oxygens of the sulfonamide with Asn220 and the structural water molecule. The pyridine ring showed hydrophobic interactions with Val73 and Ile35, the quinoline ring showed hydrophobic interaction with Trp93 and aromatic interaction with His122 which was one of the essential amino acids of the active pocket for binding with Zn1(II) ion.

Although the quinoline ring of **8-MSQA** showed stronger hydrophobic interactions than the pyridine ring of DPA, there was still larger space in the active pocket could be occupied to improve the specificity of the ligands. Like **8-HQA** derivatives, larger substituents at 4-, 5- or 6-positions of the quinoline ring could increase the hydrophobic interactions with the active pocket. In addition, the different substituted groups of the 8-sulfonamide groups influenced the binding affinity with the Zn(II) ions, and the different size of the alkyl or aryl substituents would cause different steric strains which might change the main binding modes.



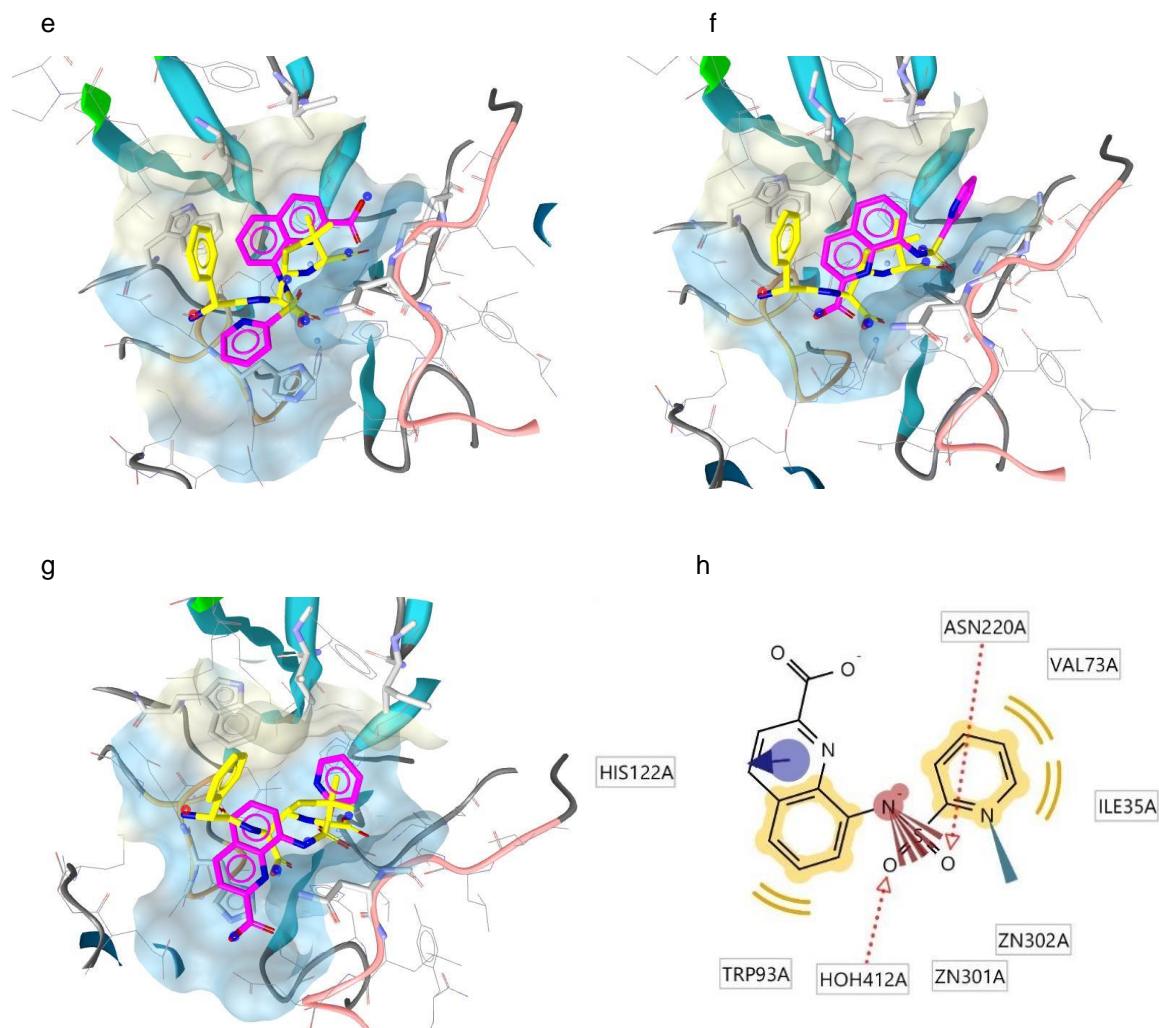
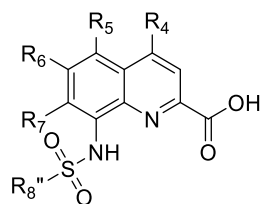


Figure 3.22 Proposed binding poses of **8-MSQA** derivatives in the active site of NDM-1(PDB ID: 5ZGR). The docking studies were performed by Gold 5.8.1 and the results were analyzed by LigandScout 4.2. The loop region from Met67 to Gly71 acting as the 'Door' was colored in green, the loop region from Thr119 to Met126 acting as the 'Ceiling' was colored in orange and the loop region from Ser217 to Asp225 acting as the 'Floor' was colored in pink. The original hydrolyzed ampicillin was colored in yellow, and the inhibitors were colored in magenta. a. b. Proposed binding poses of **8-MSQA** in the active site; c. d. Proposed binding poses of compound **71(YJh84)** in the binding pocket; e. f. g. Proposed binding poses of compound **83(YJh174)** in the active site; h. 2D depiction for the interactions of the proposed binding pose of compound **83(YJh174)** with the active site in g.

Above all, to improve the selectivity of the molecules and increase more interactions with the active pocket, a set of **8-MSQA** derivatives at the 4-, 5-, 6- and 7-positions were synthesized and the IC₅₀ values are listed in **Table 3.10**.

Table 3.10 8-MSQA Derivatives at the 4-, 5-, 6- and 7-Positions

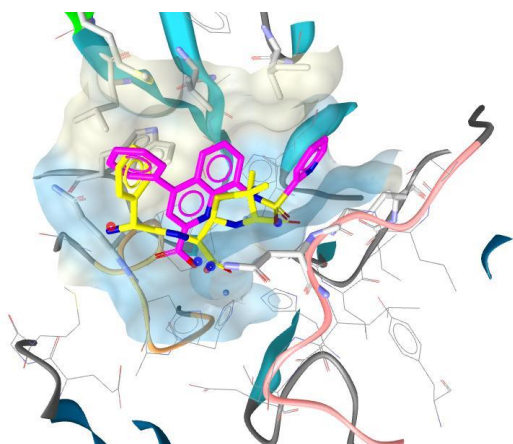


Compound	R _{8''}	R ₄	R ₅	R ₆	R ₇	IC ₅₀ (μM)
84 (YJh97)		H	I	H	I	>1000
85 (YJh141)		H	Cl	H	Cl	>1000
86 (YJh113)		H	I	H	H	1.36 ± 0.21
87 (YJh169)		H	Cl	Cl	H	0.95 ± 0.04
88 (YJh159)		Cl	H	H	H	1.01 ± 0.01
89 (YJh125)		H		H	H	2.14 ± 0.21
90 (YJh144)			H	H	H	0.71 ± 0.04
91 (YJh205)		H	Cl	H	H	0.29 ± 0.03
92 (YJh183)		H	Cl	Cl	H	0.52 ± 0.02
93 (YJh214)		Cl	H	H	H	0.28 ± 0.07
94 (YJh182)			H	H	H	0.23 ± 0.01
95 (YJh196)		H		H	H	0.21 ± 0.02
96 (YJh212)			H	H	H	0.37 ± 0.03
97 (YJh215)			H	H	H	0.25 ± 0.05
98 (YJh184)						0.41 ± 0.04

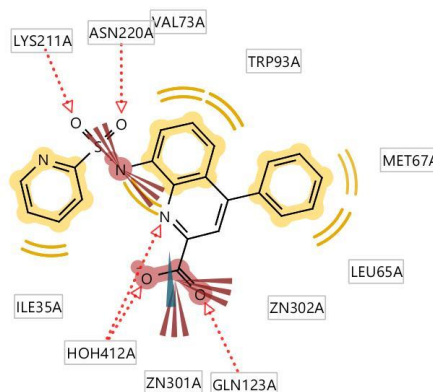
Based on the successful halogen modification used for **8-HQA** derivatives, the 5- and 7-position di-halogen-substituted compounds **84**(YJh97) and **85**(YJh141) were synthesized and tested. Which were quite different from **8-HQA** derivatives, both two compounds were inactive, The huge difference might come from the repelling interaction of the 7-iodo or chloro substituents with the substituted 8-sulfonamide groups, which influenced the molecules to form proper binding poses or bind with the Zn(II) ions. The inactive 5- and 7-position di-halogen-substituted **8-MSQA** derivatives demonstrated

that the substituted 8-sulfonamide group and its related moiety played essential roles for the inhibitory activity of NDM-1, and for the active binding poses, the substituted sulfonyl group need take the space the same or near to the substituent at the 7-position of the quinoline ring. This information was important for evaluating the effective binding poses from docking studies. To verify and investigate the relationships, compounds **86(YJh113)** ($IC_{50} = 1.36 \mu\text{M}$), **87(YJh169)** ($IC_{50} = 0.95 \mu\text{M}$), **92(YJh183)** ($IC_{50} = 0.52 \mu\text{M}$) and **91(YJh205)** ($IC_{50} = 0.29 \mu\text{M}$) were developed which were all active molecules. The substituent of the 8-sulfonamide group for compound **98(YJh184)** was linked with the 7-position of the quinoline ring directly, as a result, compound **98(YJh184)** ($IC_{50} = 0.41 \mu\text{M}$) was more active than compound **72(YJh101)** ($IC_{50} = 0.75 \mu\text{M}$). Compound **98(YJh184)** offered new method for improving the inhibitory activity by linking the substituent of the 8-sulfonamide group with the quinoline ring, the linking methods and positions as well as the substituents of the 8-sulfonamide groups could be further investigated such as the pyridinyl of compounds **83(YJh174)**, **94(YJh182)** and **95(YJh196)**. Above all, the 7-position of **8-MSQA** derivatives cannot be substituted by larger groups, which need to be prepared for the substituted sulfonyl group. The 5- and 6-positions could be halogen-substituted, although the improvement of the activity did not as much as **8-HQA** derivatives, the IC_{50} value of compound **91(YJh205)** was improved less than $0.01 \mu\text{M}$. The IC_{50} value of compound **92(YJh183)** was $0.52 \mu\text{M}$ which was less active than compound **83(YJh174)**, as the 5- and 6-position di-halogen-substituted compounds **87(YJh169)** and **92(YJh183)** did not have a good solubility in DMSO, the effect of the substituent at the 6-position need to be further investigated by mono substituted compounds. The 4-position chloro-substituted compound **88(YJh159)** was synthesized and tested which had an improved IC_{50} value of $1.01 \mu\text{M}$, and the IC_{50} value of compound **93(YJh214)** was $0.28 \mu\text{M}$. Based on the activity of the halogen-substituted compounds, the 4- and 5-positions were chosen for further optimizations. Compound **90(YJh144)** ($IC_{50} = 0.74 \mu\text{M}$) was more active than compound **89(YJh125)** ($IC_{50} = 2.14 \mu\text{M}$), which suggested that the 4-position might be more suitable to be substituted by larger groups. However, the inhibitory activity of compounds **94(YJh182)** and **95(YJh196)** showed a different trend, and their IC_{50} values were $0.23 \mu\text{M}$ and $0.21 \mu\text{M}$, respectively, which might be influenced by the substituent of the 8-sulfonamide group. Compounds **97(YJh215)** and **96(YJh212)** with substituted-phenyl groups at their 4-positions had IC_{50} values of $0.25 \mu\text{M}$ and $0.37 \mu\text{M}$, respectively, which suggested that the different substituents of the phenyl group at the 4-position might have different effects on the inhibitory activity, compound **96(YJh212)** with fluoro-substituted phenyl group at the 4-position even had a lower inhibitory activity than compound **83(YJh174)**. The activity of the compounds with substituted-phenyl group at the 4-position should be further investigated.

a



b



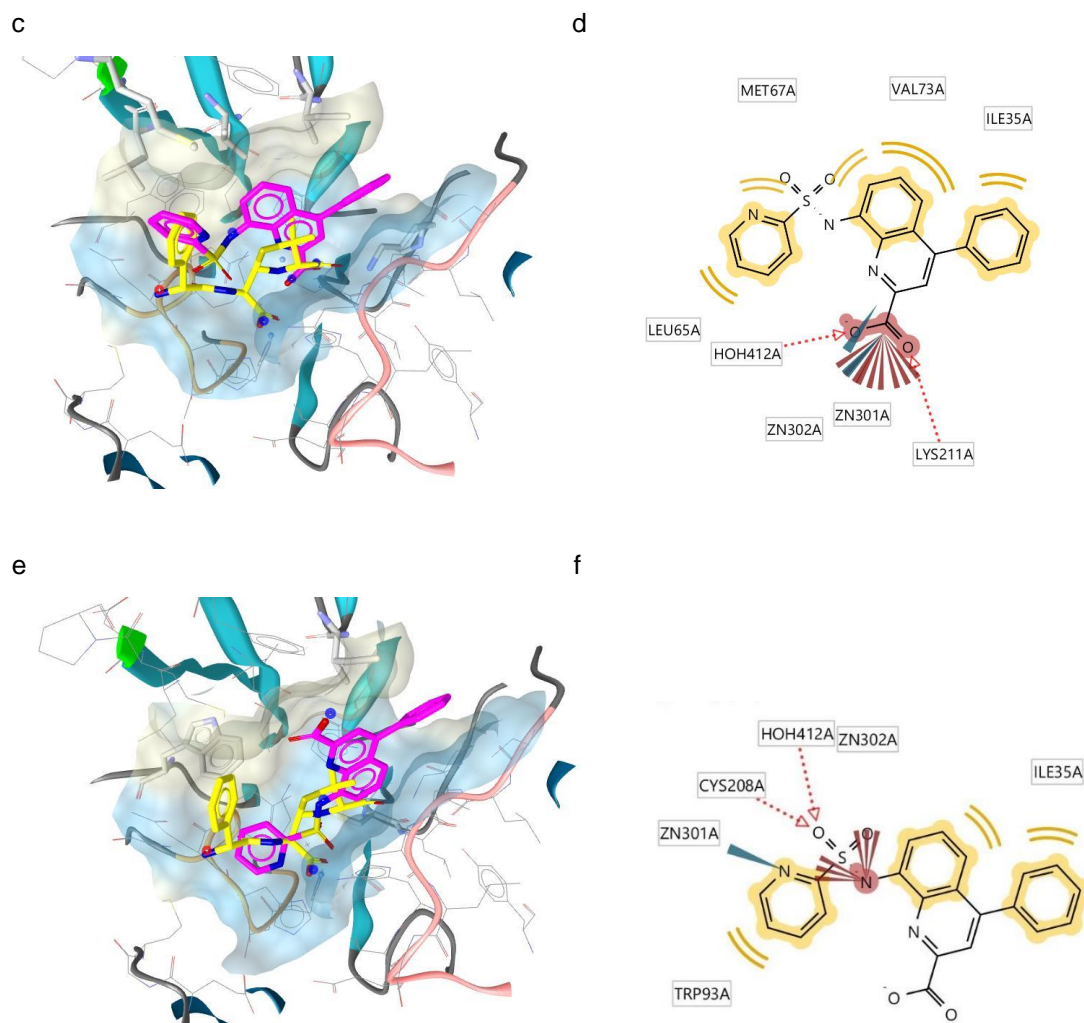


Figure 3.23 Proposed binding poses of compound **94(YJh182)** in the active site of NDM-1(PDB ID: 5ZGR). The docking studies were performed by Gold 5.8.1 and the results were analyzed by LigandScout 4.2. The loop region from Met67 to Gly71 acting as the 'Door' was colored in green, the loop region from Thr119 to Met126 acting as the 'Ceiling' was colored in orange and the loop region from Ser217 to Asp225 acting as the 'Floor' was colored in pink. The original hydrolyzed ampicillin was colored in yellow, and compound **94(YJh182)** was colored in magenta. a, c, e. The proposed binding poses of compound **94(YJh182)** in the active site; b, d, f. 2D depictions for the interactions of the proposed binding poses of compound **94(YJh182)** with the active site in a, c, e, respectively (The yellow lines indicated lipophilic contacts, red arrows indicated hydrogen bond acceptor functionalities, blue wedges indicated zinc binding locations, and the red wedges indicated negative ionizable interactions.).

For **8-MSQA** derivatives, the substitution at the 4- or 5-positions by halogen, phenyl or substituted-phenyl groups not only improved the inhibitory activity but also increased the hydrophobic interactions with the active pocket which improved the binding affinity of the ligands with the active pocket according to docking studies. For example, the proposed binding pose of compound **94(YJh182)** in **Figure 3.23a**, the phenyl group at the 4-position had hydrophobic interactions with Met67 and Leu65, the quinoline ring had hydrophobic interactions with Val73 and Trp93, and the pyridine ring of the substituted 8-sulfonamide group had hydrophobic interactions with Ile35. There were H-bond interactions for the

oxygen atoms of the 8-sulfonamide group with Lys211 and Asn220. The 2-carboxyl group and its related moiety acted as the zinc binding location for Zn1(II) ion. The deprotonated carboxyl group also showed negative ionizable interactions with both Zn(II) ions. The nitrogen of the substituted 8-sulfonamide group showed negative ionizable interactions with Zn2(II) ion and Lys211. Compared with **8-MSQA**, compound **94(YJh182)** was more fit to the active pocket. As reported, Zn2(II) ion was not as stable as Zn1(II) ion at the active site of NDM-1, a reduced binding affinity with Zn2(II) ion, remained strong binding affinity with Zn1(II) ion and increased hydrophobic interactions with the active site of NDM-1 for compound **94(YJh182)** supported its higher binding affinity with the active pocket. There was another binding pose of compound **94(YJh182)** in **Figure 3.23c**. The 2-carboxyl group and its related moiety showed strong binding affinity with Zn2(II) ion. And the deprotonated carboxyl group itself also showed strong binding affinity with Zn2(II) and negative ionizable interactions with both Zn(II) ions and Lys211. There were H-bond interactions of the two oxygen atoms of the deprotonated carboxyl group with Lys211 and the structural water molecule at the active site. The pyridine ring of the substituted 8-sulfonamide group had hydrophobic interactions with Leu65 and Met67, the quinoline ring had hydrophobic interactions with Ile35, Met67 and Val73, and the phenyl group at the 4-position had hydrophobic interactions with Ile35. Another proposed binding pose in **Figure 3.23e** with low fitness score should be contributed by the pyridine-2-sulfonamide moiety which was not suitable for compound **94(YJh182)** compared with compound **83(YJh174)**, as the 4-phenyl substituent of compound **94(YJh182)** preferred the binding pose in **Figure 3.23a**. Compound **95(YJh196)** showed similar inhibitory activity as compound **94(YJh182)**, but its proposed binding poses were more tended to the pose of compound **94(YJh182)** in **Figure 3.23c** and even in **Figure 3.23e**. The main binding poses of the compound should contribute the most to the inhibitory activity and other different binding poses should also influence the final activity of the ligand.

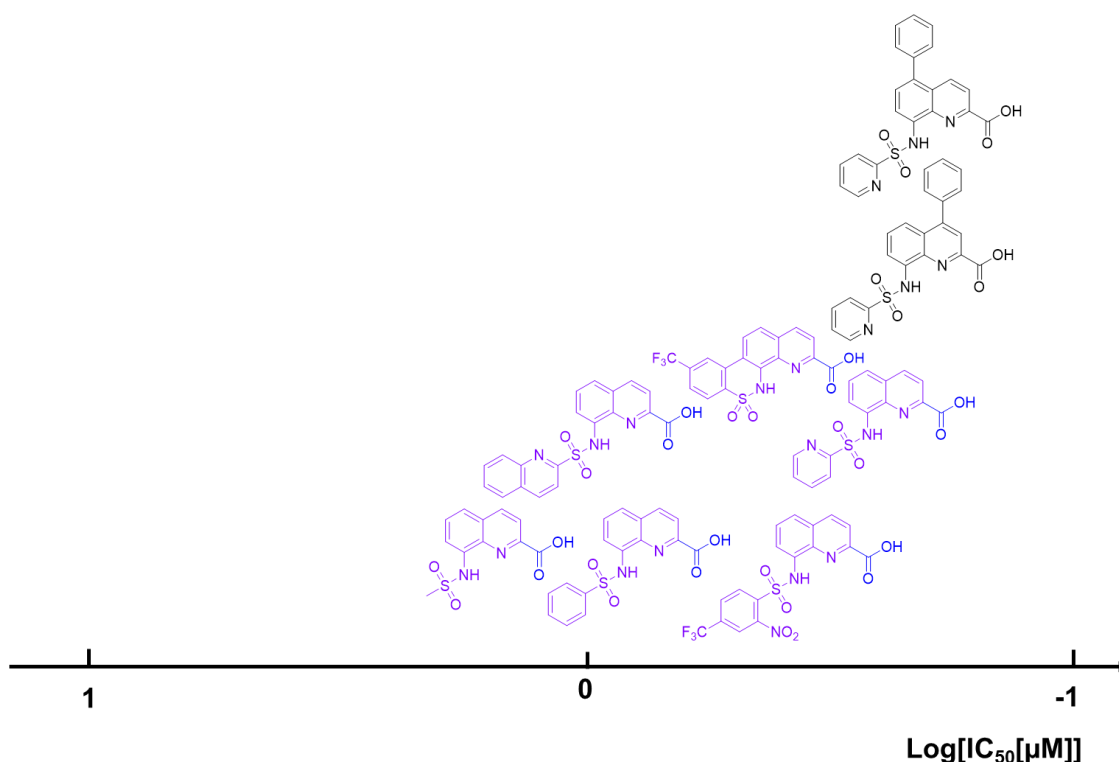


Figure 3.24 Inhibitory activity of **8-MSQA** derivatives.

Above all, according to the *in vitro* enzyme-based activity tests, compounds **94(YJh182)** and **95(YJh196)** have been the most active inhibitors developed from the representative compound **83(YJh174)** of this work at present. Compared with the starting **8-MSQA** or **8-HQA** and **DPA**, the top active compounds had more interactions with the active pocket, especially the hydrophobic interactions which improved the binding affinity with the active site of NDM-1. The interaction modes of the top active compounds as well as some other representative compounds were further studied by different assays which were discussed in the following chapters.

Compound **98(YJh184)** might offer another strategy linking the substituent of the 8-sulfonamide group with the quinoline ring to improve the inhibitory activity of the molecules for NDM-1, the linking methods and positions could be diverse, and the substituents of the 8-sulfonamide groups could be investigated such as the pyridinyl of compounds **83(YJh174)**, **94(YJh182)** and **95(YJh196)**. The different substituents of the 8-sulfonamide groups especially the quinolyl of compound **74(YJh119)** and the pyridinyl of compounds **83(YJh174)**, **94(YJh182)** and **95(YJh196)**, the linking strategy of compound **98(YJh184)** as well as the substituents at 4- or 5-positions of the quinoline ring played important roles for the selectivity of the inhibitors, which was discussed in **Figure 3.45** of the chapter for the specificity studies by testing the activity of other human metalloenzymes.

3.2.4 Summary of the developed inhibitors

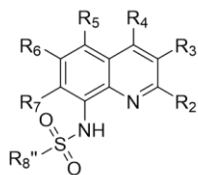
At first, **DPA** was discovered by fragment screening with an IC_{50} value of 7.05 μ M. Based on the initial SAR, **8-HQA** with a hydroxyl group at the 8-position and compound **45(YJh2)** with *N*-(benzyloxy)amide group at the 2- and 6-positions were developed by isosteric replacement, and their IC_{50} values were 9.05 μ M and 7.16 μ M, respectively. The 5- and 7-position di-halogen-substituted **8-HQA** derivatives, not only improved the acidity of the 8-hydroxyl group but also increased the hydrophobic interactions with the active pocket of NDM-1. The 2- and 6-carboxyl groups of **DPA**, the *N*-(benzyloxy)amide groups at the 2- and 6-positions of compound **45(YJh2)**, as well as the 2-carboxyl and the 8-hydroxyl groups of **8-HQA** derivatives were all acidic groups, and most likely negatively charged or tending to be negatively charged when they were interacting with the active site of NDM-1. In addition, the different acidity of the functional groups influenced the activity differently. According to the inhibitor developing processes of **DPA** and **8-HQA** derivatives, the more active **8-MSQA** derivatives were deduced from the inactive 8-amino quinoline structures by changing the acidity of the -NH- at the 8-position of the quinoline ring, and the IC_{50} values of the representatively top active compounds **94(YJh182)**, **95(YJh196)** and **83(YJh174)** were improved to a sub-micromolar level ranging from 0.2 μ M to 0.3 μ M.

In addition, different substituents of the 8-sulfonamide groups especially the quinolyl of compound **74(YJh119)** and the pyridinyl of compounds **83(YJh174)**, **94(YJh182)** and **95(YJh196)**, the linking strategy of compound **98(YJh184)** as well as the substituents at 4- or 5-positions of the quinoline ring played important roles for the inhibitory activity and selectivity of the inhibitors for NDM-1, which was discussed in the chapter for the specificity studies.

R₆: halogen-substituted compounds were still active.

R₇: halogen-substitution would lose activity.

R₅, R₄: generally, both halogen and phenyl substitutions improved the inhibitory activity, while the effects of the substituted-phenyl groups should be further investigated.



R₂: -COOH could improve inhibitory activity. -CH₃, -COOCH₃, or -H substitutions were still active. *N*-(alkoxy)amide or *N*-(benzyloxy)amide groups might be active substituents as **8-HQA** derivatives.

R₈: aryl was more active than alkyl, strong electron withdrawing substituents were preferred for the inhibitory activity. Linking the substituent with the 7-position of the quinoline ring might improve the inhibitory activity. The substituents played important roles for the selectivity of the inhibitors.

Figure 3.25 The SAR of **8-MSQA** derivatives.

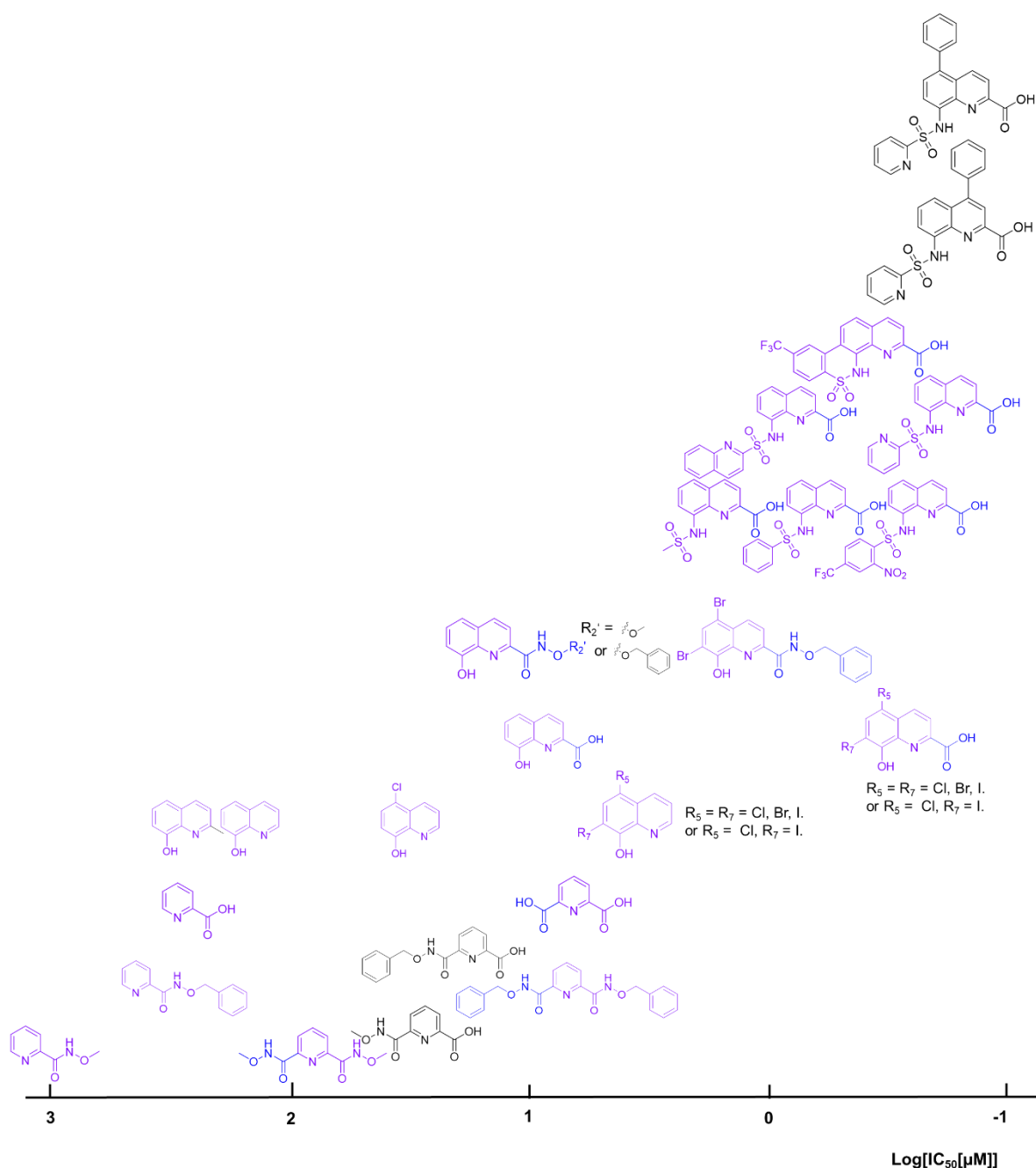
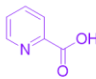
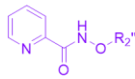
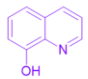
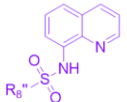
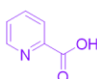
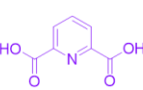
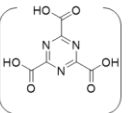
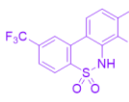
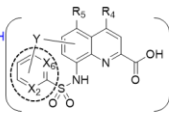
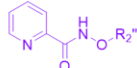
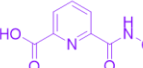
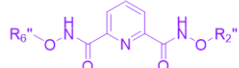
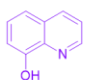
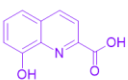
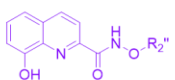
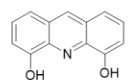
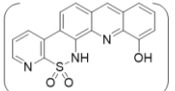
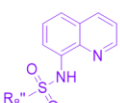
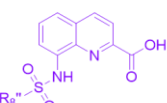
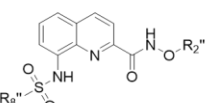
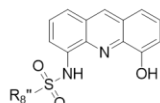
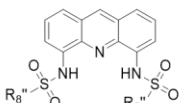


Figure 3.26 Representative inhibitors of DPA, **8-HQA** and **8-MSQA** derivatives for NDM-1.

Based on the developed inhibitors, four independent active moieties were discovered, picolinic acid, pyridine with a *N*-(alkoxy)amide group at the 2-position, quinoline-8-ol, quinoline with a substituted 8-sulfonamide group. One of the moieties was necessary for the inhibitory activity and the carboxyl group at the 2-position (2- or 6-positions for DPA) could highly improve the inhibitory activity and the solubility of the molecules in buffer. Linking the substituent of the 8-sulfonamide group with the quinoline ring could improve the inhibitory activity of the molecules for NDM-1, diverse linking methods and the substituents of the 8-sulfonamide groups could be investigated. According to the regularity, the potential structures were designed and concluded in **Table 3.11**, and the inhibitory activity should be further investigated.

Table 3.11 Inhibitor Development for NDM-1

Basic moieties				
				
				
				
				

According to the docking studies, the developed inhibitors overlapped well with the hydrolyzed ampicillin and kept the important interactions of both hydrolyzed and unhydrolyzed β -lactam substrates with the active pocket of NDM-1, such as the binding and negative ionizable interactions with Zn(II) ions, the H-bond and negative ionizable interactions with Lys211 and Asn220, and the hydrophobic interactions with the active site. The mimic interactions contributed for the binding affinity of the inhibitors with the active pocket.

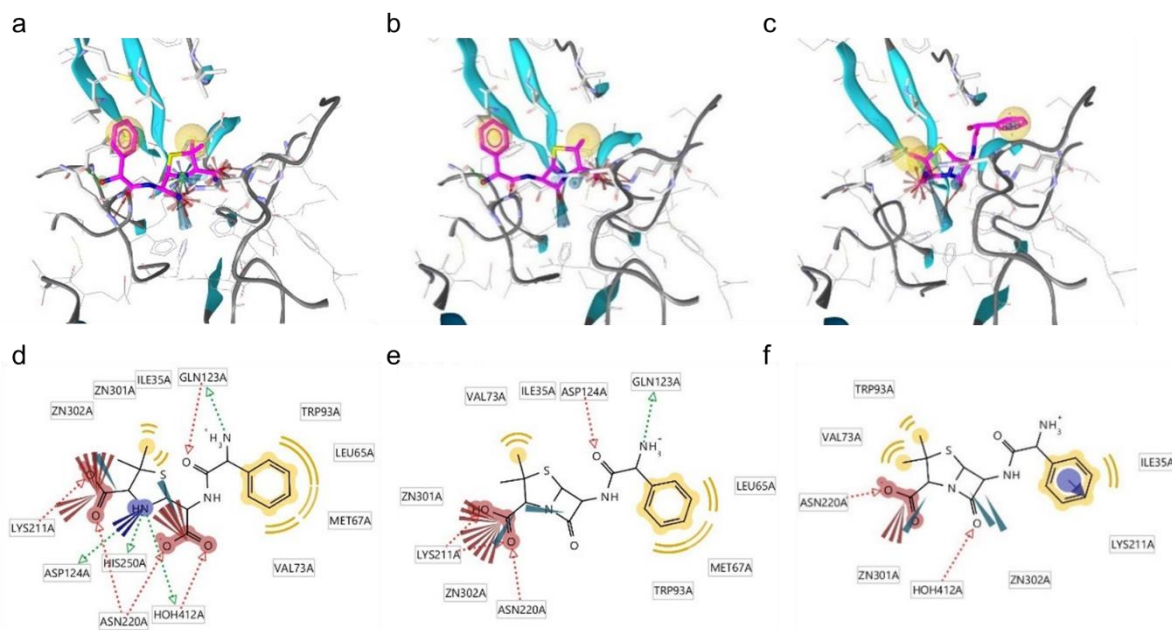


Figure 3.27 Proposed binding poses of hydrolyzed and unhydrolyzed ampicillin molecules in the active site of NDM-1 (PDB ID: 5ZGR). The docking studies were performed by Gold 5.8.1 and the results were analyzed by LigandScout 4.2. a. 3D depiction for the interactions of the hydrolyzed ampicillin with the active site of NDM-1; b. 3D depiction for the interactions of ampicillin acting as **S** (substrate) with the active site of NDM-1; c. 3D depiction for the interactions of ampicillin acting as **I** (inhibitor) with the active site of NDM-1; d, e, f. 2D depictions for the interactions of the hydrolyzed and unhydrolyzed ampicillins with the active site in a, b, c, respectively (The yellow lines indicated lipophilic contacts, red or green arrows indicated hydrogen bond interactions, blue wedges indicated zinc binding locations, and the red wedges indicated negative ionizable interactions.).

3.3 Mode of action

The optimized inhibitors especially the substituted 8-sulfonamide compounds had improved inhibitory activity than the initial hit DPA based on the IC_{50} values obtained via *in vitro* enzyme-based tests, and according to docking studies, the top active compounds **94(YJh182)** and **95(YJh196)**, as well as some other representative compounds had more interactions with the active pocket of NDM-1 such as the hydrophobic interactions which contributed for the specificity of the ligands and the binding affinity for the target protein. To further investigate the mode of action and inhibitory mechanisms of the top active as well as some other representative compounds, different assays were utilized. Bio-layer interferometry (BLI) assays was used to detect the real time association and dissociation between the target protein and ligands with different concentrations. Isothermal titration calorimetry (ITC) assays offered the total enthalpic changes and entropic changes caused by the interactions of the molecules during the titration process. Affinity binding parameters can be obtained from both BLI and ITC assays, differences might be caused by different assay conditions. Compared with BLI and ITC assays which offered the general binding information, native protein mass spectrometry studies showed the fine details about the binding complexes, which helped to explain the main actions of the ligands and other different influences on the target protein. Thermal shift assay (TSA) has been frequently used to estimate the stability of the protein influenced by ligands binding which can be performed to evaluate the binding effects of the developed Zn(II)-binding inhibitors on NDM-1. The tested inhibitors influenced the stability and the catalytic activity of the target protein, and there might be constitution or structural changes about the cofactors, partial conformation of the active site or secondary structures of the protein, the cofactor or the Zn(II) ion binding conditions could be reflected by the native protein mass spectrometry assays, the partial conformational changes of the amino acids at the active site could be detected by solution NMR assays, and the influence on the secondary structures of the protein was measured by circular dichroism (CD) assays. The reversible or irreversible changes were evaluated by the zinc ion restoration assays which also reflected the specificity of the different tested inhibitors. As different evaluation methods were performed under different assay conditions, the mode of action or main interactions discussed in the following chapters should be related to the utilized assay conditions.

3.3.1 Bio-layer interferometry (BLI) assays

BLI is a label-free optical analytic method which monitors the real time association and dissociation of ligands via optical shifts caused by interactions of the ligands with the immobilized biomolecules on the tips of the biosensors (**Figure 3.28**).²²¹ The interference patterns for the reflected beams of the white light from the surface of the immobilized biomolecules and the surface of the internal reference are monitored. The thickness changes of the immobilized biomolecular layer result in the shifts of the interference patterns. The raw kinetic curves can be obtained by monitoring the shifts in nanometer of the association or dissociation steps as well as other steps which have different influences on the thickness of the immobilized biomolecular layer, and the association steps with different concentrations of the analyte and the corresponding dissociation steps are always chosen for the calculation of the kinetic parameters.^{221, 222} Various interactions can be studied via BLI assays such as the interactions of bacteria or virus with relevant analytes, antibody with antigen, DNA with protein, antibody with peptide, protein with small molecules, etc.²²¹ Generally, the molecular weights of the analytes are ranging from 150 Da to more than 1,000,000 Da, and the relevant shifts are related to the molecular weights of the

analytes.²²¹ There are different types of the sensors which offer more choices for the immobilization of the biomolecules.²²¹

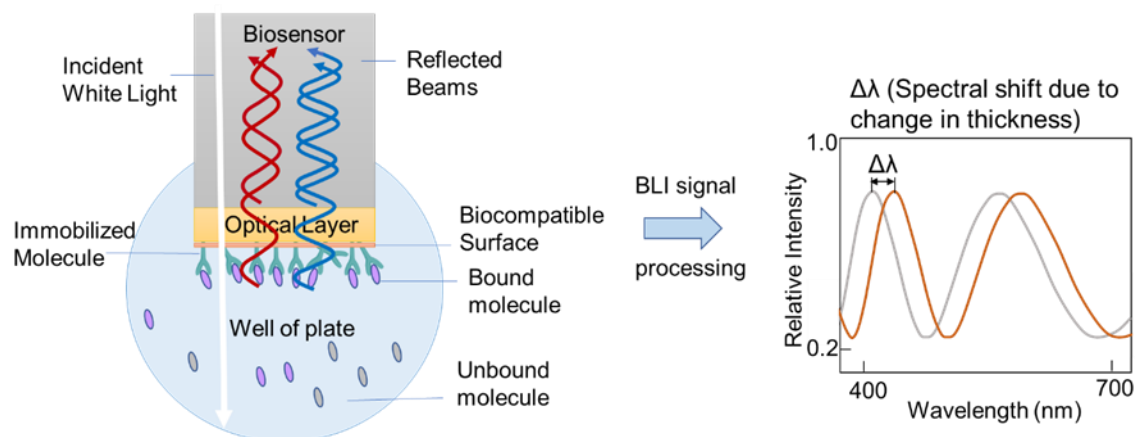


Figure 3.28 The principle of BLI assays.²²¹

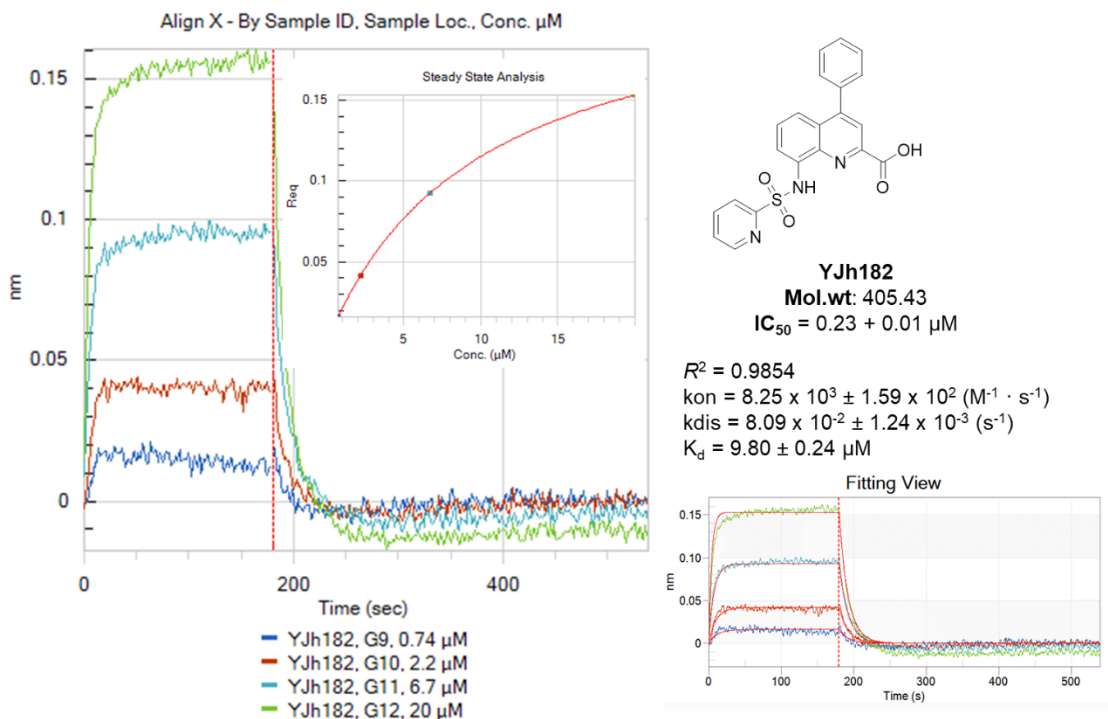
Super streptavidin (SSA) biosensors were used in this work, which is a kind of streptavidin-coated biosensors specially designed for investigating the interactions of protein with small molecules.^{220, 221} The protein was labelled by biotin for immobilization on the SSA biosensors, and the activity of the labelled protein was tested by the *in vitro* enzyme-based assays both before and after the BLI assays. The experiments were performed at 25 °C with the Octet K2 (ForteBio) instrument. Both wild-type NDM-1 and truncated NDM-1 were tested without significant difference, and the data using truncated NDM-1 are shown in **Figure 3.29**. The detailed procedures are described in the experiment part.

This is the first time that the interactions of NDM-1 and inhibitors have been studied by BLI assay, and the assay conditions have been optimized according to the surface plasmon resonance (SPR) method reported by Christopheit et al. (2015).²²³ The kinetic curves of both compounds **94(YJh182)** and **95(YJh196)** obtained from BLI assays were fitted to the 1 to 1 binding model, and the effects of nonspecific binding of the compounds with the biotin-blocked streptavidin sensors and system artifacts were subtracted. The K_d value of compound **94(YJh182)** was $9.80 \pm 0.24 \mu\text{M}$, and the k_{on} and k_{dis} were $8.25 \times 10^3 \pm 1.59 \times 10^2 \text{ (M}^{-1} \cdot \text{s}^{-1}\text{)}$, $8.09 \times 10^{-2} \pm 1.24 \times 10^{-3} \text{ (s}^{-1}\text{)}$, respectively. The K_d value of compound **95(YJh196)** was $7.88 \pm 0.29 \mu\text{M}$, the k_{on} and k_{dis} were $1.10 \times 10^4 \pm 3.07 \times 10^2 \text{ (M}^{-1} \cdot \text{s}^{-1}\text{)}$, $8.66 \times 10^{-2} \pm 1.99 \times 10^{-3} \text{ (s}^{-1}\text{)}$, respectively. All the experiments were repeated three times, and the values were at the same ranges. The association responses were getting higher as the concentrations of the compounds increased, and the dissociation curves could get back to the baselines at the end, which indicated that the binding of compounds **94(YJh182)** and **95(YJh196)** to NDM-1 was reversible under the BLI assay conditions. The K_d values were remarkably higher from BLI assays than the K_i values $0.12 \mu\text{M}$ for compound **94(YJh182)** and $0.11 \mu\text{M}$ for compound **95(YJh196)** calculated from their IC_{50} values by the *in vitro* enzyme-based activity tests. One reason for this observation might be that the free zinc ions at the concentration of $25 \mu\text{M}$ in the assay buffer used for BLI assays which helped to stabilize the immobilized protein on the sensor bound to the inhibitor molecules as well thereby competing with the protein for ligands.

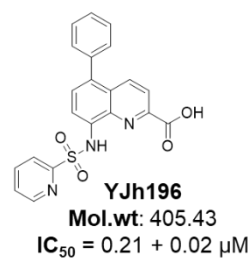
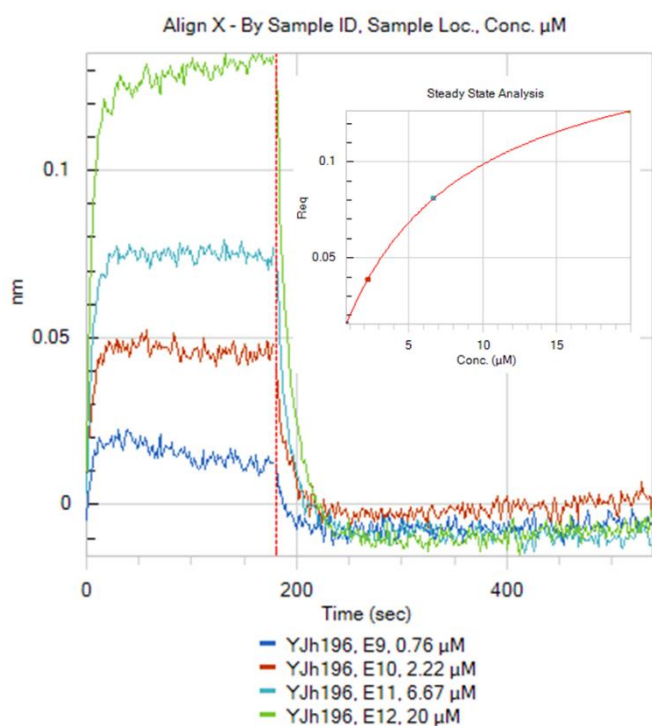
The kinetic curves of compound **83(YJh174)** were not as typical as those recorded for compounds **94(YJh182)** and **95(YJh196)** under the same assay conditions. On the one hand, although compounds

94(YJh182), **95(YJh196)** and **83(YJh174)** all have strong binding affinities with Zn(II) ions, compounds **94(YJh182)** and **95(YJh196)** with the 4- or 5-position substituted by phenyl group fitted better to the active pocket of the protein, which can lead to higher affinity. The binding of compound **83(YJh174)** with the protein might be not as stable as compounds **94(YJh182)** and **95(YJh196)**, thus the nonspecific binding might have more influences on compound **83(YJh174)**. In this case, the free zinc ions in the buffer would influence compound **83(YJh174)** more than compounds **94(YJh182)** and **95(YJh196)** which was proved by the zinc ion restoration assays. On the other hand, compound **83(YJh174)** might inhibit NDM-1 through different or multi-mechanisms, as its structure was more flexible and supported diverse binding modes according to docking studies. However, a lower molecule weight also influenced the responses of the BLI assay. The conditions without blocking the sensors by biotin after the protein loading step were also tried and the K_d value of $14.1 \pm 0.37 \mu\text{M}$ was obtained for compound **83(YJh174)**. L-captopril was used as a positive control, and its K_d , k_{on} and k_{dis} values were $435 \pm 12.5 \mu\text{M}$, $70.9 \pm 1.86 \text{ M}^{-1} \cdot \text{s}^{-1}$ and $3.09 \times 10^{-2} \pm 3.62 \times 10^{-4} \text{ s}^{-1}$, respectively. Above all, there were always interactions of the protein, inhibitors and Zn(II) ions, considering the native mass analysis and results of the ITC assays, compounds **94(YJh182)**, **95(YJh196)** and **83(YJh174)** all have strong binding affinity with NDM-1, and the binding was reversible under the BLI assay conditions. Although the absolute K_d -values were shifted, possibly due to the free zinc ions in the assay buffer, the BLI method has given relative binding affinities which correlate well with the enzyme inhibition assays. There might be difference for the main interactions of the measured inhibitors with NDM-1 which were further investigated by other assays.

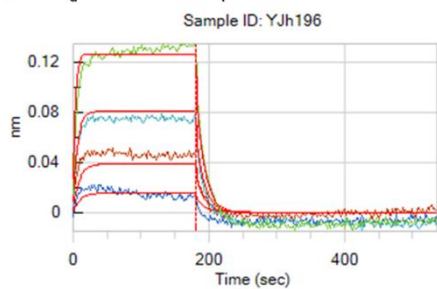
a



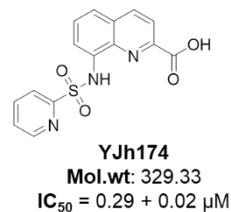
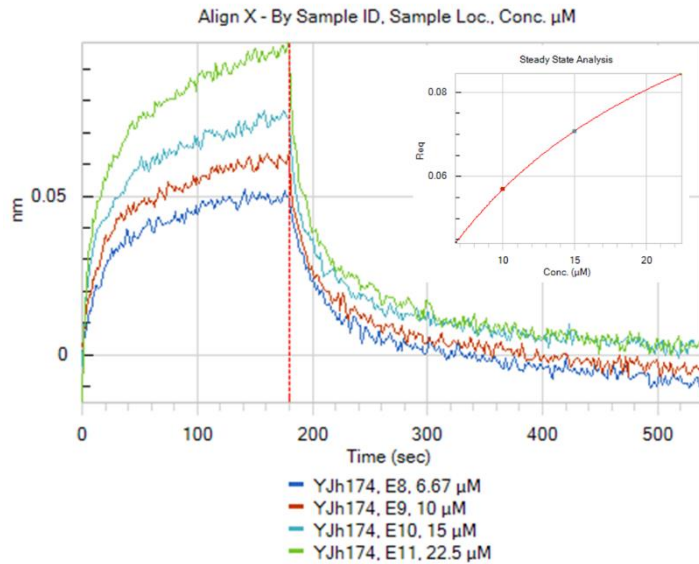
b



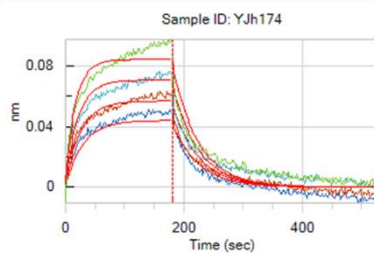
$R^2 = 0.9709$
 $k_{on} = 1.10 \times 10^4 \pm 3.07 \times 10^2 \text{ (M}^{-1} \cdot \text{s}^{-1}\text{)}$
 $k_{dis} = 8.66 \times 10^{-2} \pm 1.99 \times 10^{-3} \text{ (s}^{-1}\text{)}$
 $K_d = 7.88 \pm 0.29 \mu\text{M}$



c



$R^2 = 0.9668$
 $k_{on} = 1.63 \times 10^3 \pm 38.6 \text{ (M}^{-1} \cdot \text{s}^{-1}\text{)}$
 $k_{dis} = 2.30 \times 10^{-2} \pm 2.47 \times 10^{-4} \text{ (s}^{-1}\text{)}$
 $K_d = 14.1 \pm 0.37 \mu\text{M}$



immobilization steps are needed, offers rich information including all binding and thermodynamic parameters in a single experiment.²²⁴⁻²²⁶

$$\Delta G^\circ = RT \ln K_d \quad (1)$$

$$\Delta G^\circ = \Delta H^\circ - T\Delta S^\circ \quad (2)$$

The thermodynamic parameters can be determined via ITC and van't Hoff analysis. ΔG° is the standard Gibbs free energy change, the free energy of binding, R is the gas constant, T is the absolute temperature, K_d is the equilibrium dissociation constant. ΔH° is the standard enthalpic change obtained by a series correction of ΔH . ΔS° can be calculated via equation (1) and (2).²²⁴⁻²²⁶

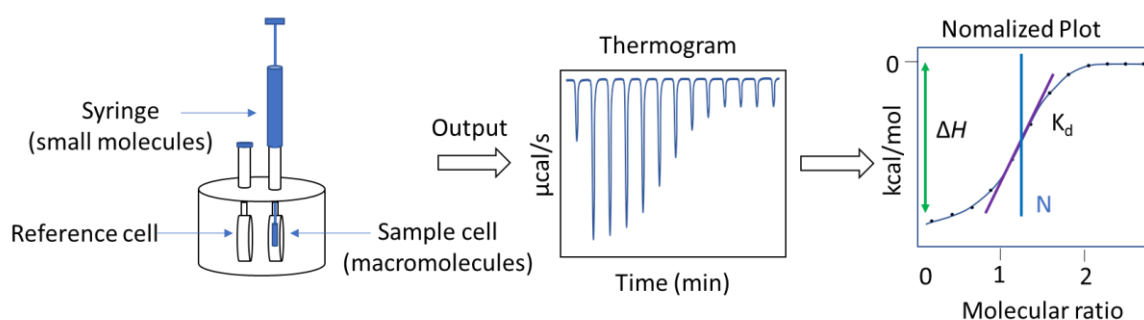


Figure 3.30 Basic working principles of ITC instruments.²²⁶

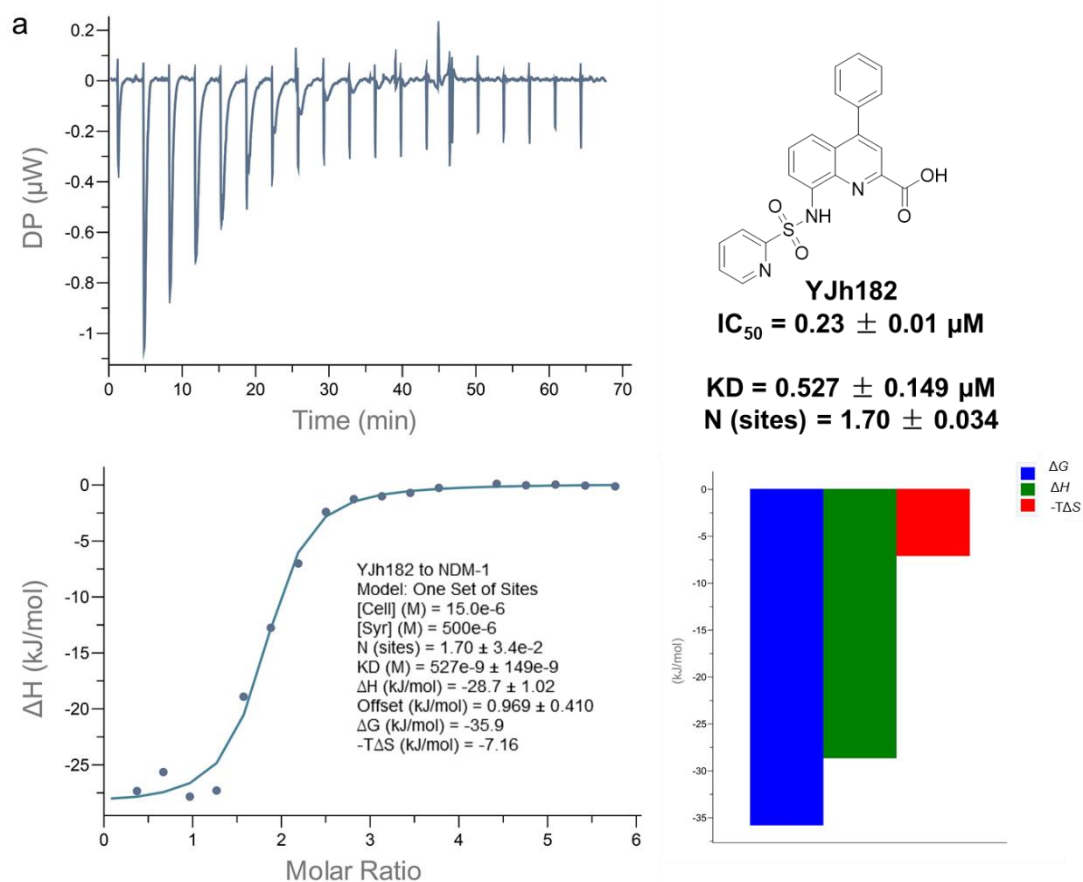
The thermograms for compounds **94(YJh182)**, **95(YJh196)**, and **83(YJh174)** were fitted to the mode of one set binding sites, and the binding sites n were 1.70 ± 0.034 , 1.81 ± 0.035 and 1.98 ± 0.015 , respectively. The binding sites n obtained from ITC experiments is identical to the expected binding stoichiometry only when the concentrations used for the fitting are correct and 100% active, in other words, it reflects the binding stoichiometry of the real active ligands and active macromolecules. The binding sites n for compounds **94(YJh182)**, **95(YJh196)** and **83(YJh174)** were all around 2, there were several reasons. First, the active concentration of NDM-1 protein was not accurate and the released free Zn(II) ions can influence the values. The active concentration of the protein with low stability was lower than the prepared concentration, as there might be aggregates or precipitations of the protein which might cause a lower binding sites, while the influence of the released free Zn(II) ions from the degraded protein should be higher than the influence of the reduced active concentration of the protein since one molecule protein can release two Zn(II) ions and the free Zn(II) ions can bind with the ligands with a relative higher stoichiometry according to the ITC assays using free zinc ions titrating relevant ligands. Thus, the obtained binding sites could be bigger than the expected values. Second, the active concentration of the ligands in the syringe might be lower than the prepared concentration, as the high concentration could also influence the freedom of the ligands, there could be aggregates. Third, it is possible that there might be more binding sites of the protein for the ligands, the mode of sequential binding sites was tried, while the fitting curves by using the sequential binding mode were not used for the data analysis at the end, since the fitting was not as good as that by using the mode of one set binding sites. In addition, although compounds **94(YJh182)**, **95(YJh196)** and **83(YJh174)** all can bind with NDM-1 according to the BLI assays, the stability of the protein-inhibitor binding complexes was

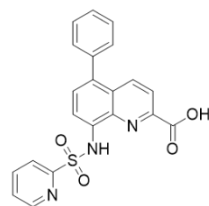
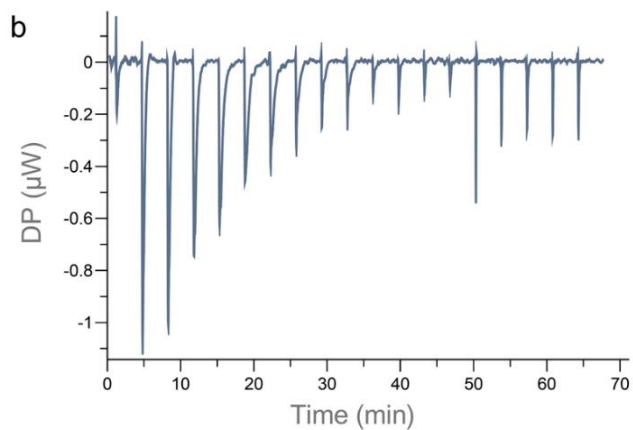
different which was related to both the binding affinity of the ligands with the protein and the destabilizing ability of the ligand binding for the target protein. Binding with the compounds could reduce the stability of the protein and the effects were different according to the results of TSA studies. The main binding complexes of compounds **94(YJh182)**, **95(YJh196)** or **83(YJh174)** with NDM-1 were formed by one molecule of NDM-1 with two Zn(II) ions and one molecule of relative compound, but there were some other diverse complexes or forms, e.g., one molecule of apo-NDM-1 with one Zn(II) ion and one molecule of the ligand, apo-NDM-1 with one Zn(II) ion, and apo-NDM-1 without any Zn(II) ions. Therefore, the binding sites *n* of the ITC assays reflected the total effects of the active ligands and protein, and the exact binding stoichiometry needed to be further investigated relating to different conditions such as the dose of the ligands. In addition, as for the thermodynamic parameters, the binding of compounds **94(YJh182)**, **95(YJh196)** and **83(YJh174)** with the protein was exothermic which was common for the binding of ligands and proteins, but their entropic changes were different, and the entropic changes contributed less to the binding compared with the enthalpic changes. For compound **83(YJh174)**, the binding was both enthalpy and entropy favoured. The negative enthalpic change is the direct result of all binding interactions, such as the interactions of the ligand with the Zn(II) ions, the H-bond interactions of the ligand with Asn220, Lys211 and the structure water molecule according to the docking studies. For the positive entropic changes, ligands took the positions of the water molecules in the active pocket by binding, the releasing of water molecules caused positive entropic changes, and binding of the ligand and protein enriched the types of complexes which increased the freedom of the system. For compound **94(YJh182)**, the negative enthalpic change contributed the most for the binding, the phenyl group at the 4-position made compound **94(YJh182)** fit the active pocket better which could lead to more proper binding poses increasing or strengthening the relevant interactions. However, compound **94(YJh182)** with 4-phenyl group had less freedom for interacting with the protein compared with compound **83(YJh174)**, in addition, there might be conformational changes for the protein or the ligands which caused the less favored entropic change for compound **94(YJh182)**. Compound **95(YJh196)** had the relative less enthalpic change than compounds **94(YJh182)** and **83(YJh174)**, and the similar entropic change as compound **83(YJh174)**. The Zn(II)-binding inhibitors might cause conformational changes of the amino acid residues in the active site which was supported by some published works, such as the ¹H NMR spectroscopy studies performed by Chen et al. (2017), the solution NMR study of ¹⁵N-labeled NDM-1 by Guo et al. (2020), and crystallographic studies of apo- and monometalated forms of NDM-1 by Kim et al. (2011).^{84, 110, 133, 227, 228} According to the protein native mass studies, binding with compound **83(YJh174)** led more apo-NDM-1 than binding with compounds **94(YJh182)** and **95(YJh196)** for the protein, and the apo-NDM-1 was less stable compared with native NDM-1, which might influence the conformations of the protein and even cause precipitation of the protein, the relative influence might contribute negative entropic changes, while the entropic change obtained from the ITC instrument was the sum of the total entropic change.

The trend of the K_d values of compounds **94(YJh182)** ($0.527 \pm 0.149 \mu\text{M}$), **95(YJh196)** ($0.532 \pm 0.149 \mu\text{M}$), and **83(YJh174)** ($0.105 \pm 0.028 \mu\text{M}$) did not correlate with the trend of the K_d values obtained from BLI assays or their IC_{50} values ($0.23 \mu\text{M}$, $0.21 \mu\text{M}$ and $0.29 \mu\text{M}$, respectively). Both the mechanisms of the methods and the different assay conditions should be considered. The ITC method measured the thermodynamic parameters, and the results of the ITC assays reflected the equilibrium of the whole titrating system such as the binding of NDM-1 with the ligand and the binding of the possible released Zn(II) ions with the ligand, while the results of the BLI assays mainly showed the binding of the ligand and the protein. The trend of the inhibitory activity correlated to the trend of the K_d values obtained from

the BLI assays, which highlighted that forming of the binding complexes of holo-NDM-1 with the inhibitor was the main interaction mode and contributing the most for the inhibitory activity for the tested inhibitors. In addition, different interactions such as the binding with the Zn(II) ions, H-bond and hydrophobic interactions with the active pocket contributed differently for the thermodynamic parameters measured by ITC assays and the IC₅₀ tests (or the inhibition for the target protein). The assay conditions were different, e.g., the free zinc ions in the buffer for the BLI assays helped to stabilize the protein, and the buffer conditions were softer and the concentration of the protein was much lower for the IC₅₀ measurements which might reduce the destabilizing function of the ligand binding although the temperature for the IC₅₀ measurements was higher than ITC assays.

Above all, the tested compounds **94(YJh182)**, **95(YJh196)** and **83(YJh174)** all could bind with NDM-1 protein, the K_d values obtained from the ITC assays were smaller than the values from the BLI assays as there were no additional zinc ions added in the assay buffer of the ITC assays, while the trends of the K_d values for compounds **94(YJh182)**, **95(YJh196)** and **83(YJh174)** did not correlate with their IC₅₀ values, which might be influenced by both the mechanism of the method and the different assay conditions. The results using truncated NDM-1 are shown in **Figure 3.31**, compounds **94(YJh182)**, **95(YJh196)** and **83(YJh174)** were also tested by using full-length NDM-1, the values might be a little different as the different stability of the truncated and full-length protein, but the trends were the same. The results using full-length NDM-1 are shown in the appendices (**Figure S9**).



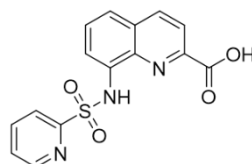
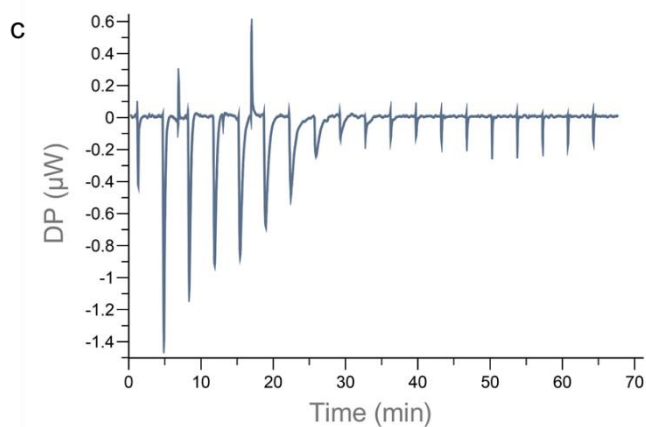
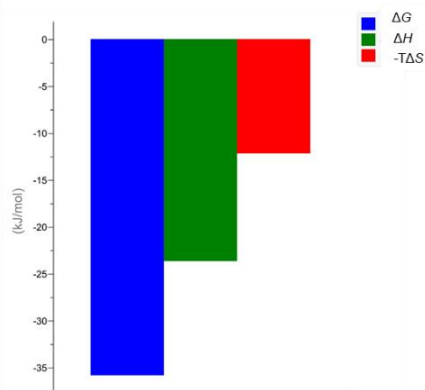
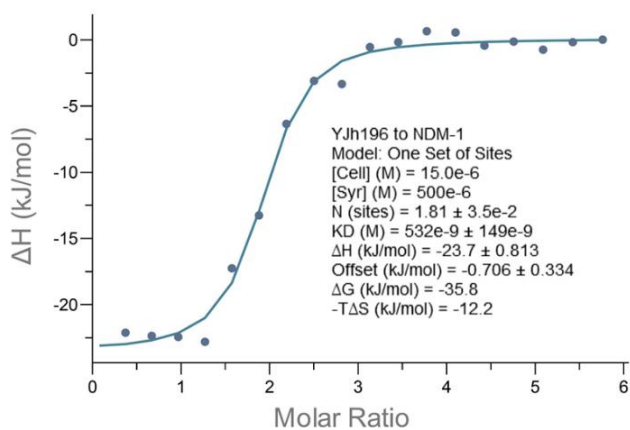


YJh196

$\text{IC}_{50} = 0.21 \pm 0.02 \mu\text{M}$

$\text{KD} = 0.532 \pm 0.149 \mu\text{M}$

$\text{N (sites)} = 1.81 \pm 0.035$



YJh174

$\text{IC}_{50} = 0.29 \pm 0.02 \mu\text{M}$

$\text{KD} = 0.105 \pm 0.028 \mu\text{M}$

$\text{N (sites)} = 1.98 \pm 0.015$

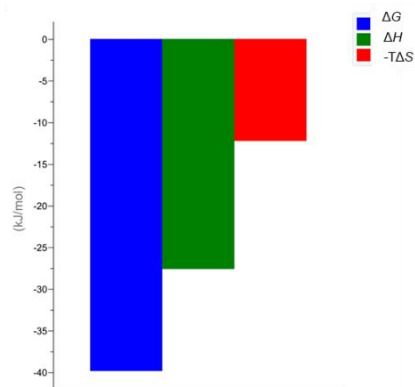
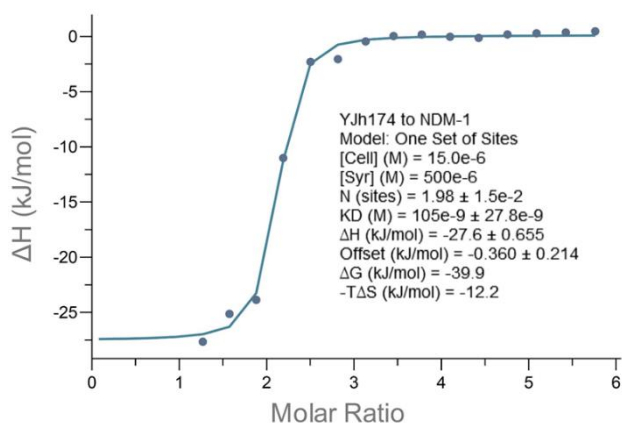
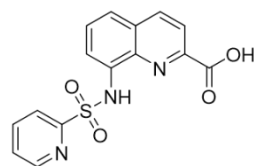
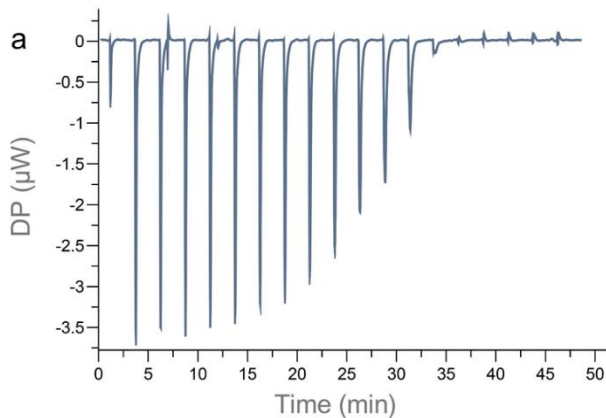
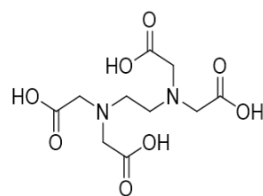
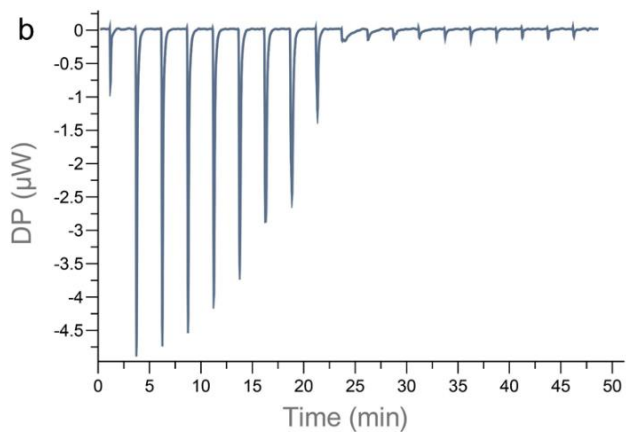
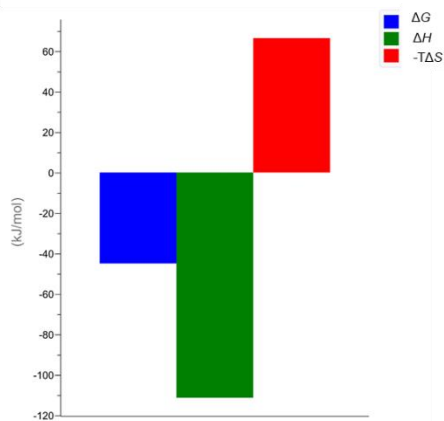
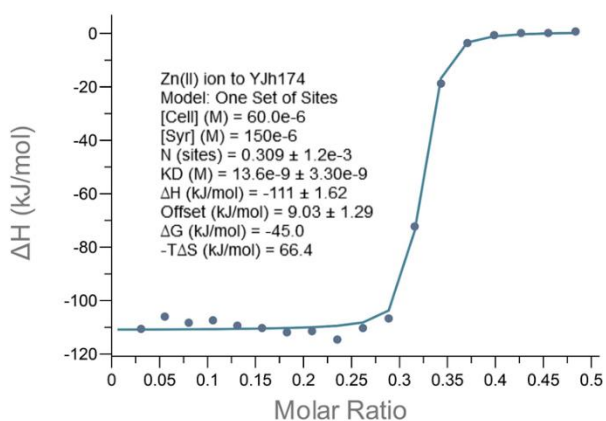


Figure 3.31 Thermograms of ITC assays. (The corresponding controls were subtracted during data analysis, and the thermograms of the controls are listed in **Figure S8** in the appendices.) a. Compound **94(YJh182)** to NDM-1; b. Compound **95(YJh196)** to NDM-1; c. Compound **83(YJh174)** to NDM-1.

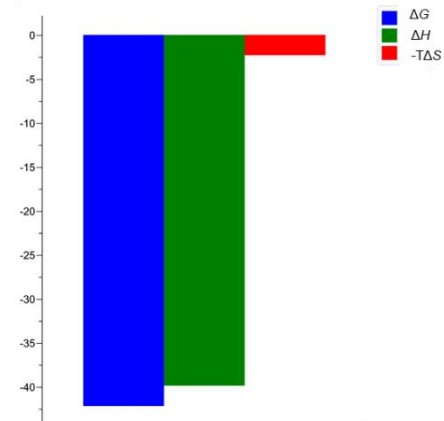
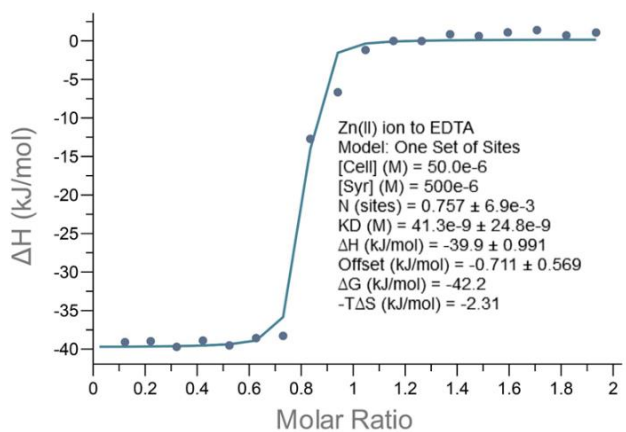
According to the published works, direct or indirect interactions with the Zn(II) ions were essential for the inhibitory activity of the inhibitors for NDM-1, as the two Zn(II) ions at the active site played important roles for both the hydrolysis activity and stability of the protein. The zinc ion binding ability of the developed inhibitors was necessary for their activity, which was supported by the structure development process and relative docking studies. For investigating their zinc ion binding ability, the ITC assays titrating the assay buffer containing free zinc ions to compound containing buffer were performed (**Figure 3.32**). The results showed that the substituted-8-sulfonamide compound **83(YJh174)** ($K_d = 13.6 \pm 3.30$ nM) could bind with the free zinc ion, and EDTA ($K_d = 41.3 \pm 24.8$ nM) as well as DPA ($K_d = 7.71 \pm 1.63$ μ M) were also tested. Their binding sites were different, on average, 0.309, 0.757 and 0.466 zinc ions need bind with one molecule **83(YJh174)**, EDTA and DPA, respectively. However, the binding sites were measured from the real active concentrations of the free zinc ions and compounds. In addition, the entropic change was quite different for compound **83(YJh174)**, binding with free zinc ions might cause some conformational changes of the molecules, this phenomenon might be also existed for binding with the protein. For the negative enthalpic change favoured the binding most, compound **83(YJh174)** was nearly 3 times of EDTA and 5 times of DPA, which could be related to both the different stoichiometries and the binding affinity. The different thermodynamic parameters, binding affinity and binding sites of the compounds should contribute differently for their inhibitory activity for NDM-1. Related to the docking studies, the stronger zinc ion binding ability of the **8-MSQA** derivatives allowed them to keeping interactions with the Zn(II) ions in the active site of NDM-1 with a little further distance as well as more and stronger hydrophobic interactions with other important amino acid residues as the relative closer distances with essential loops of the active site. The binding affinity and enthalpic or entropic changes were similar among the substituted-8-sulfonamide compounds, while the binding affinity of the di-halogen-substituted **8-HQA** derivatives **58(YJh34)** and **61(YJh59)** was improved nearly ten times compared with the binding affinity of **8-HQA**, the results are supplied in the appendices part (**Figure S11**). Furthermore, the zinc ion binding ability of different moieties such as picolinic acid, *N*-(alkoxyl)amide derivatives, quinoline-8-ol, 8-sulfonamide derivatives, etc. could be compared which would be helpful for the mechanism studies of relative inhibitors.



YJh174
 $K_d = 13.6 \pm 3.30 \text{ nM}$
 $N (\text{sites}) = 0.309 \pm 0.001$



EDTA
 $K_d = 41.3 \pm 24.8 \text{ nM}$
 $N (\text{sites}) = 0.757 \pm 0.007$



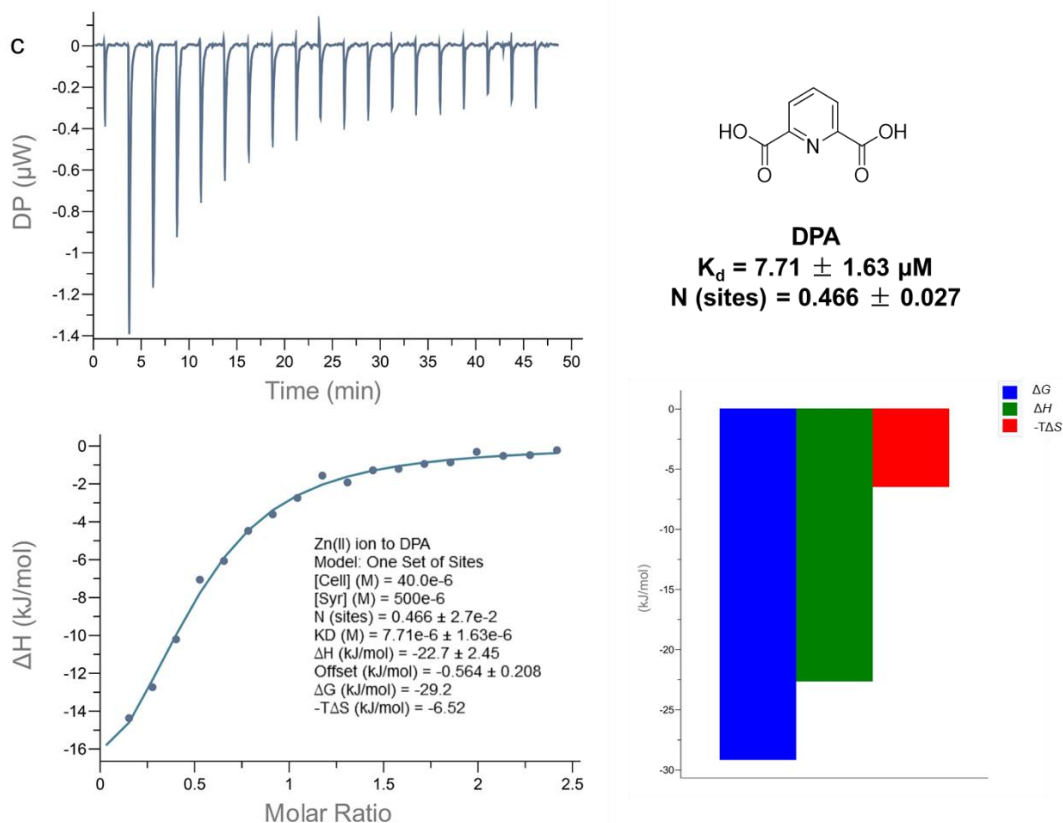


Figure 3.32 Thermograms of ITC assays. (The corresponding controls were subtracted during data analysis and the thermograms of the controls are listed in **Figure S12** in the appendices.) a. Zinc ions to compound **83(YJh174)**; b. Zinc ions to EDTA; c. Zinc ions to DPA.

3.3.3 Native mass spectrometry studies

Mass spectrometry is a powerful method for determining the mass of biomolecules with high efficiency, accuracy, and sensitivity.^{229, 230} Especially the native mass analysis with gentle ionization and volatile buffer system, intact assemblies can be detected with the preserved noncovalent interactions under native conditions, and the noncovalent interactions play vital roles for protein and binding partners, e.g., metal ions, cofactors, chaperones, etc.²²⁹ As for protein-ligand interactions via noncovalent binding, native mass spectrometry offered the rapid determination of the composition and relative abundance of different complexes formed by ligand binding, and the binding stoichiometry as well as binding affinity could be also obtained.²²⁹⁻²³¹ Combined with other technologies, it was possible to characterize the binding site.^{229, 230} For the two soft ionization sources electrospray ionization (ESI), and matrix-assisted laser desorption/ionization (MALDI) commonly used for biological mass studies, ESI has been preferred for native mass.^{229, 230} In addition, the measuring samples for native mass should be buffer exchanged to volatile buffers such as ammonium acetate and ethylenediammonium diacetate. Various complexes can be measured, and no labeling requirements of the protein or ligands are needed.^{86, 132, 229-233} Native mass studies have been successfully applied to the development for both covalent and noncovalent inhibitors for NDM-1 as well as other MBLs, e.g., Chiou et al. (2015) reported that Ebselen inhibited NDM-1 by covalent binding and the binding complex was detected by

native mass spectrometry, Chen et al. (2020) developed NDM-1 inhibitors from derivatives of iminodiacetic acid (IDA) and the most active compound **23f** formed complex with NDM-1 which was investigated by native mass method.^{86, 147, 132, 232, 233}

The two Zn(II) ions at the active site of NDM-1 held by the 3H region (His120, His122 and His189) and DCH (Asp124, Cys208 and His250) region, respectively, via noncovalent interactions play important roles for the catalytic activity and stability of the protein. Truncated NDM-1 was used for native mass spectrometry studies and measured under both denaturing and native conditions (**Figure 3.33**). Compared with the denaturing mass spectrum, the native mass spectrum was less charged as the soft condition allowed the protein to be folded and charged at the surface of the architecture, in addition, the two Zn(II) ions were kept by native mass spectrometry, which offered conditions for studying Zn(II)-binding inhibitors.

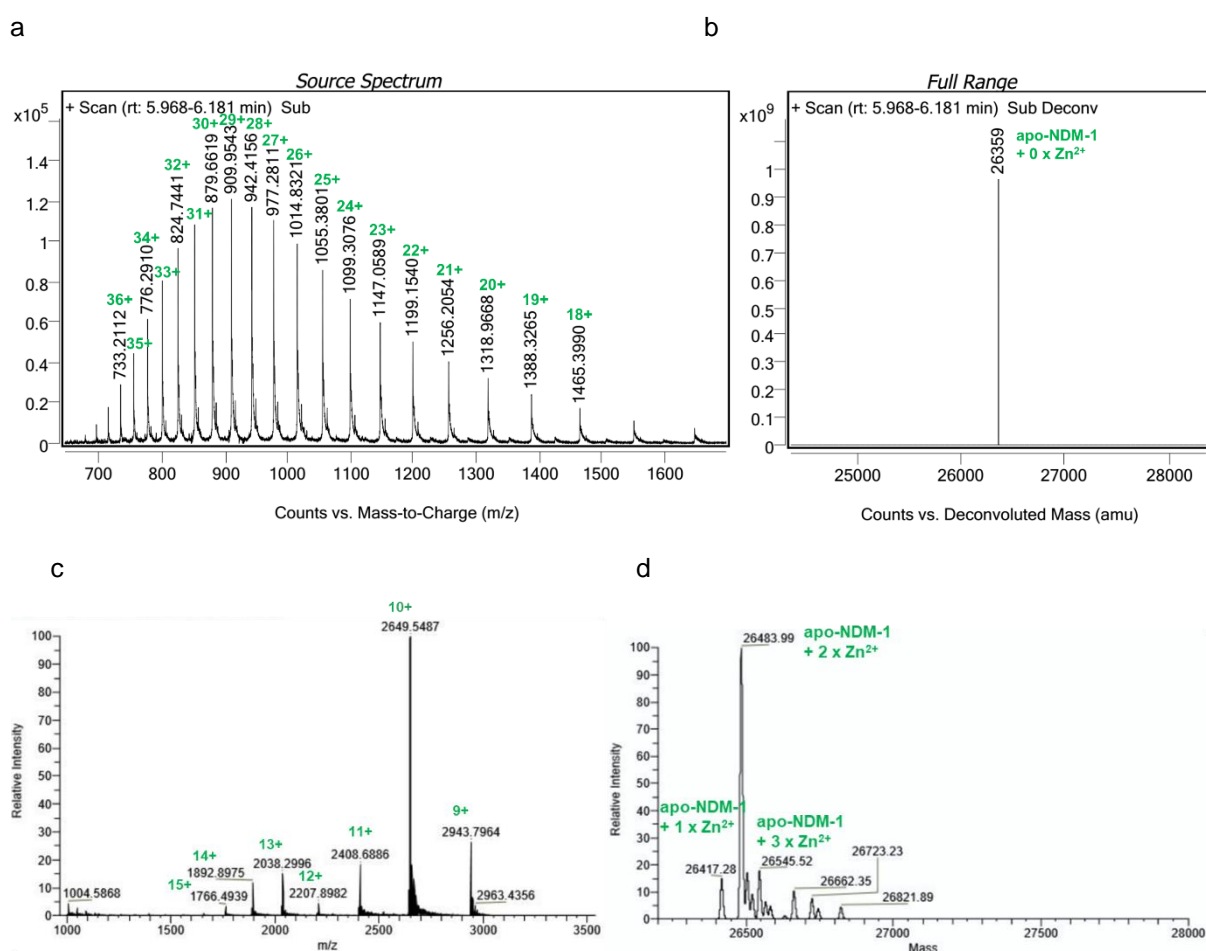


Figure 3.33 Mass spectra of NDM-1 obtained under different conditions. a. Source spectrum of NDM-1 obtained under denaturing condition; b. Deconvoluted spectrum of a; c. Source spectrum of NDM-1 obtained under native condition; d. Deconvoluted spectrum of c.

The main peak of the obtained native spectrum for NDM-1 was the holo-protein which offered the basic conditions for interaction studies of the developed inhibitors with the protein. As the stock solutions of the selected inhibitors were prepared using DMSO, proper content of DMSO need be decided, which should be the same for all the measuring samples. NDM-1 without DMSO and with 0.01%, 0.02% and

0.05% DMSO were measured under the native mass condition, respectively (**Figure 3.34**). According to the measurements, the gradually increased content of DMSO did not influence the stability of NDM-1, which only changed the main charged states of the protein from +10 to +9, thus all the measurements were performed with 0.05% DMSO.^{f5}

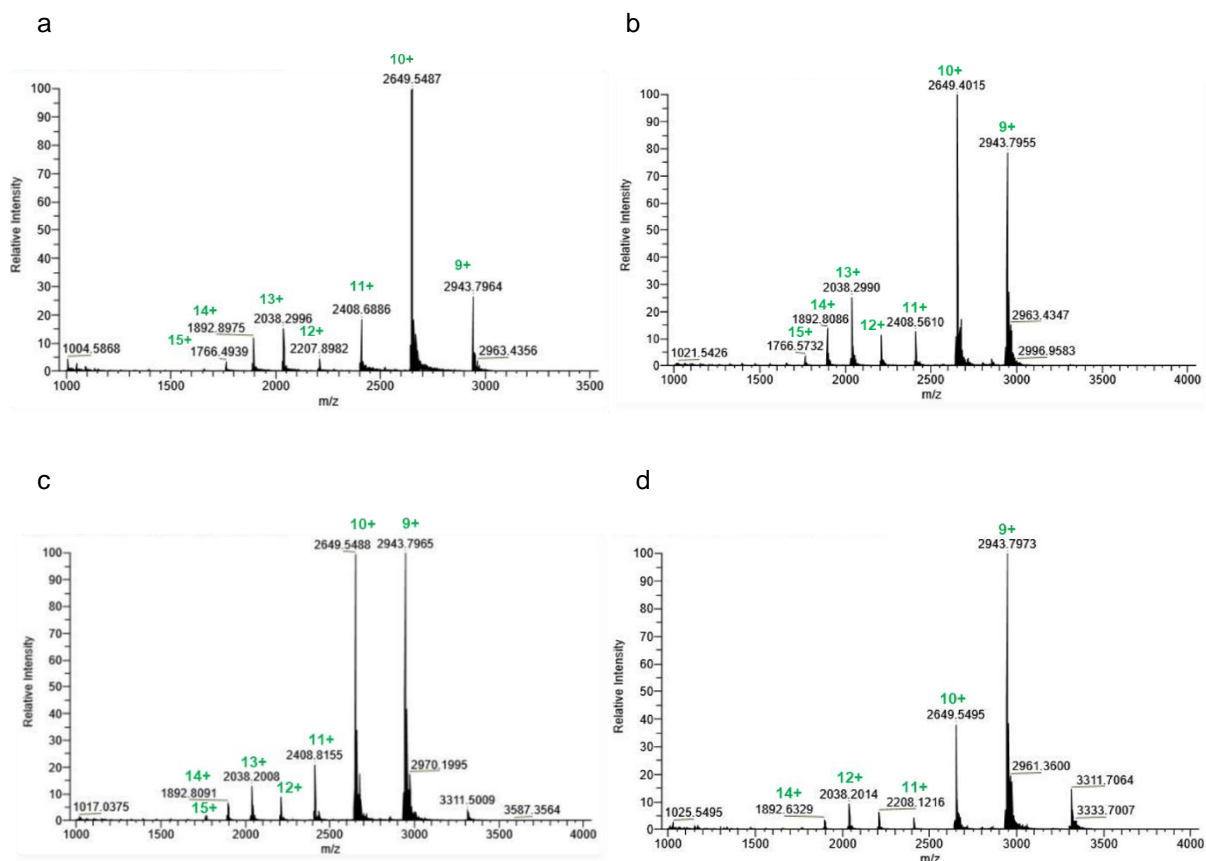


Figure 3.34 Source spectra for NDM-1 with different content of DMSO obtained under native condition. a. NDM-1 without DMSO; b. NDM-1 with 0.01% DMSO; c. NDM-1 with 0.02% DMSO; d. NDM-1 with 0.05% DMSO.

The inhibitors developed in this work were Zn(II)-binding inhibitors, and according to the results of BLI assays, the tested compounds **94**(YJh182), **95**(YJh196) and **83**(YJh174) all could bind with NDM-1 protein. The protein native mass spectrometry allowed rapid determination and clear analysis of the complexes formed from protein, Zn(II) ions and inhibitors. Comparing their native mass spectra with the spectra of EDTA, DPA and L-captopril helped to explain the interactions of the protein with the inhibitors. L-Captopril could bind with the protein without removing any Zn(II) ions, a two-fold excess of L-captopril (20 μ M) to NDM-1 (10 μ M) resulted in a strong peak at 26700.60 Da (ca. 60% relative intensity) of the complex formed by one molecule of NDM-1 with two Zn(II) ions and one molecule of L-captopril in **Figure 3.35b**, on the contrary, an equal excess of EDTA, apo-NDM-1 without any Zn(II) ions at 26356.37 Da was the dominant product (100% relative intensity) (**Figure 3.35c**), indicating the complete

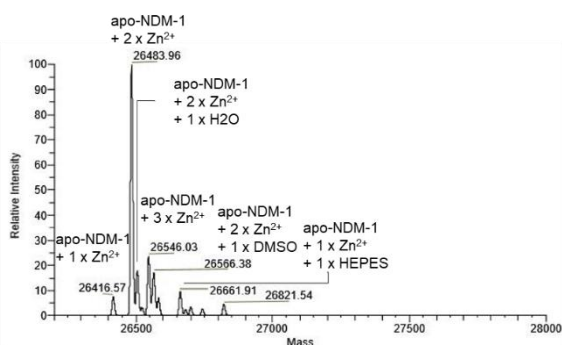
^{f5} Dr. Benno Kuroпка helped to measure the prepared samples for the native mass spectra and Eleonore Christmann helped to measure the prepared samples for the denaturing protein mass spectra.

removal of Zn(II) ions from the protein and no formation of protein-inhibitor complex. The main peak of the two-fold excess of DPA (20 μ M) to NDM-1 (10 μ M) was still the native NDM-1 protein at 26484.26 Da (100% relative intensity), and there were a peak at 26419.14 Da (ca. 30% relative intensity) of NDM-1 protein losing one Zn(II) ion and another peak at 26355.57 Da (less than 5% relative intensity) of the apo-NDM-1 without any Zn(II) ions (**Figure 3.35d**), while with a five-fold excess of DPA (50 μ M) to NDM-1(10 μ M), except for the obvious increases of the apo-NDM-1 with one Zn(II) ion (ca. 42% relative intensity) and the apo-NDM-1 without any Zn(II) ions (ca. 52% relative intensity), weaker peaks of the binding complexes formed by one molecule of apo-NDM-1 with one or two Zn(II) ions and one molecule of DPA were discovered with around 30% and 20% relative intensity, respectively (**Figure 3.35e**), which indicated a weaker metal-stripping function of DPA compared with EDTA and the binding complex of NDM-1 and DPA might could be formed but with a lower stability. For other measured inhibitors with a two-fold excess (20 μ M) to NDM-1 (10 μ M), the peaks of the binding complexes all could be found under the measuring conditions, and the results are shown in **Figure 3.35**. For the spectrum of compound **58(YJh34)** to NDM-1 (**Figure 3.35f**), the peak of the native NDM-1 at 26484.34 Da was still the highest, while apo-NDM-1 with one Zn(II) ion was also existed (ca. 35% relative intensity). Complexes of one molecule of apo-NDM-1 with one or two Zn(II) ions and one molecule of **58(YJh34)** had the relative intensity of around 30% and 20%, respectively. Compared with DPA, compound **58(YJh34)** can form more stable binding complex with NDM-1. The complexes of one molecule of apo-NDM-1 with one Zn(II) ion and one molecule **58(YJh34)** suggested that the ligand could interacted with both Zn(II) ions and binding with compound **58(YJh34)** might could let the protein lose one Zn(II) ion easily. The destabilizing function of the tested compounds to NDM-1 was proved by TSA studies, the loss of Zn(II) ions of the protein might be also caused by the high temperature of the measuring process since the protein was less stable when bound with the ligand, which was also applied to the following tested compounds **8-MSQA(YJh65)**, **94(YJh182)**, **95(YJh196)** and **83(YJh174)**. For the spectrum of compound **8-MSQA(YJh65)** to NDM-1 (**Figure 3.35g**), the highest peak was still the native NDM-1, apo-NDM-1 with one Zn(II) ion or without any Zn(II) ions had the relative intensity of around 25% and 40%, complexes of one molecule of apo-NDM-1 with one or two Zn(II) ions and one molecule of **8-MSQA(YJh65)** had a similar relative intensity around 15%. **8-MSQA(YJh65)** can form more stable protein-inhibitor complexes with NDM-1 than DPA. For the spectrum of compound **83(YJh174)** to NDM-1 (**Figure 3.35h**), the highest peak was still the native NDM-1, apo-NDM-1 with one Zn(II) or without any Zn(II) ions had the relative intensity of around 40% and 60%, complexes of one molecule of apo-NDM-1 with one or two Zn(II) ions and one molecule of **83(YJh174)** had the relative intensity of around 35% and 50%, respectively. Compared with **8-MSQA(YJh65)**, compound **83(YJh174)** had an obviously improvement for forming stable binding complexes with NDM-1. For the spectrum of compound **94(YJh182)** to NDM-1 (**Figure 3.35i**), most of the NDM-1 protein formed complexes with the inhibitor. The main peaks were native NDM-1 (100% relative intensity), the complex of one molecule of NDM-1 with two Zn(II) ions and one molecule of **94(YJh182)** (ca. 93% relative intensity), and the complex of one molecule of NDM-1 with two Zn(II) ions and two molecules of **94(YJh182)** (ca. 87% relative intensity), even the complex of one molecule of NDM-1 with one or three Zn(II) ions and one molecule of **94(YJh182)** had the relative intensity of around 31% and 64%, respectively. The apo-NDM-1 with one Zn(II) ion or without any Zn(II) ions had the relative intensity of around 21% and 25%, respectively. Compound **94(YJh182)** can form more stable complexes with NDM-1 compared with compound **83(YJh174)**, and one molecule of NDM-1 might could bind with one or two molecules of compound **94(YJh182)** which needed to be further investigated in the future. For

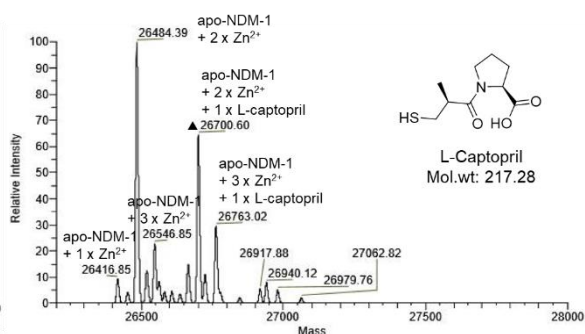
the spectrum of compound **95(YJh196)** to NDM-1 (**Figure 3.35j**), complex of one molecule of NDM-1 with two Zn(II) ions and one molecule of **95(YJh196)** was the main form (100% relative intensity). Compared with other tested compounds, **95(YJh196)** can form the most stable complex with NDM-1 of one molecule of NDM-1 with two Zn(II) ions and one molecule of the compound.

The formation of the protein-inhibitor complexes depended on the different kinds of interactions of the ligands and the target protein, a stronger binding affinity of the ligand with the target protein favored the formation of the binding complexes, while the destabilizing function of the ligand binding might let NDM-1 lose one or two Zn(II) ions which influenced the stability of the protein-inhibitor complexes. According to the native mass spectra, the selected compounds interacted with NDM-1 differently from both EDTA and L-captopril. All the selected derivatives of **8-HQA** and **8-MSQA** could bind with the protein, and the binding complexes were less stable compared with the holo-protein or complex of NDM-1 with L-captopril, which might be influenced by the stronger Zn(II)-binding interactions of the ligands with the protein, and Zn(II) ions might be lost during the interacting processes, especially the unstable Zn₂(II) ion. The **8-MSQA** derivatives **94(YJh182)**, **95(YJh196)** and **83(YJh174)** all can form more stable protein-inhibitor binding complexes than **8-HQA** derivative **58(YJh34)**. For the **8-MSQA** derivatives, the binding with the protein of **83(YJh174)** was highly improved compared with the starting **8-MSQA(YJh65)**. Compared with **83(YJh174)**, the modification at the 4-position of **94(YJh182)** and the 5-position of **95(YJh196)** contributed for more stable binding with the protein significantly, which was compatible with the BLI assays. The complexes of one molecule of NDM-1 with two Zn(II) ions and one or two molecules of the corresponding ligand for compound **94(YJh182)** were the main formations. For compounds **83(YJh174)** and **95(YJh196)**, the main binding complexes were in the formation of one molecule of NDM-1 with two Zn(II) ions and one molecule of the corresponding ligand, and other relatively weaker diverse binding forms might be nonspecific binding or the effects that the compounds influenced the stability of the protein. The peaks of apo-NDM-1 for compounds **83(YJh174)** and **95(YJh196)** were a little stronger than that for compound **94(YJh182)**, which might be contributed by different binding modes or their different destabilizing abilities. This difference influenced the conformational stability of the protein which might interfere the entropic change of the ITC assays. Above all, compared with the starting DPA, the derivatives developed have improved both the inhibitory activity and binding with the active pocket of NDM-1, which formed the binding complexes with the protein, especially compounds **94(YJh182)** and **95(YJh196)**. The results of the native mass spectrometry supported the analysis of docking and other studies.

a



b



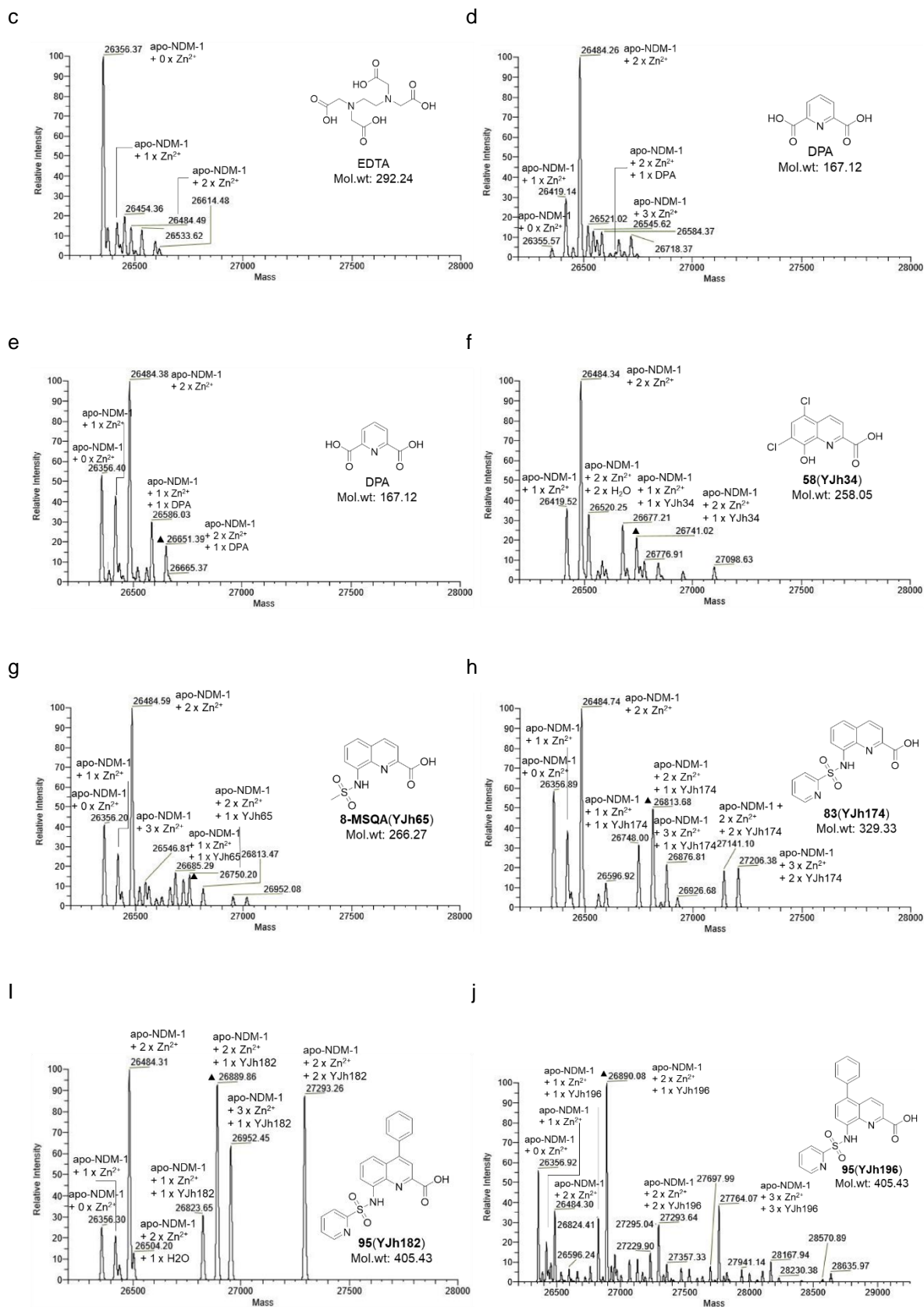


Figure 3.35 Interaction studies of the selected inhibitors with NDM-1 by protein native mass spectrometry. A. NDM-1 (10 μ M) treated with 0.05% DMSO; b. NDM-1 (10 μ M) treated with L-captopril

(20 μM); c. NDM-1 (10 μM) treated with EDTA (20 μM); d. NDM-1 (10 μM) treated with DPA (20 μM); e. NDM-1 (10 μM) treated with DPA (50 μM); f. NDM-1 (10 μM) treated with **58**(YJh34) (20 μM); g. NDM-1 (10 μM) treated with **8-MSQA** (YJh65) (20 μM); h. NDM-1 (10 μM) treated with **83**(YJh174) (20 μM); i. NDM-1 (10 μM) treated with **94**(YJh182) (20 μM); j. NDM-1 (10 μM) treated with **95**(YJh196) (20 μM).

3.3.4 Thermal shift assay (TSA)

Binding with ligands can impact on the stability of the target proteins.²³⁴⁻²³⁶ Most of the drug-like binding increases the stability of the target proteins, however the important roles of the destabilizers playing in physiological activities have been getting more concerns in recent years, e.g., the hot topics proteolysis-targeting chimeras (PROTACs) and molecular glues aiming at protein of interests (POIs) degradation, and numerous cases observed that binding with ligand can decrease the thermal stability of the protein.^{234, 237-239} The stability of a protein is related to the Gibbs free energy of unfolding (ΔG_u) which is temperature dependent. The stability of most proteins decreases with the increasing of the temperature. At a certain temperature, the concentrations of the folded and unfolded proteins are equal, and the ΔG_u is zero, the temperature of this equilibrium is called the melting point of the protein.^{234, 236} The change of the melting point (ΔT_m) for a protein can be used to reflect the influence of the ligand binding on the stability of the protein, and the relevant measuring methods have been used for drug-like candidate screenings.^{234, 236} Differential scanning fluorimetry (DSF) is the commonly used thermal shift assay (TSA) for detecting the T_m values of proteins.^{234, 236} For the assay, a fluorescence dye is used which displays high fluorescence in non-polar environment, such as the hydrophobic sites of the unfolded protein and the fluorescence intensity is monitored by a real-time PCR instrument.^{234, 236} SYPRO orange can nonspecifically bind with the hydrophobic surface of the protein, and its fluorescence is highly quenched by water. As the high signal-to-noise ratio and the relative high wavelength for excitation (nearly 500 nm), SYPRO orange is the most favorable dye used at present. The general principle of the DSF assays by using SYPRO orange is shown in **Figure 3.36**.^{234, 236} The folded protein exposes fewer hydrophobic sites, thus the intensity is at the baseline. As the temperature increases, more hydrophobic sites are exposed for the unfolded protein resulting in non-specific binding with the SYPRO orange molecules, the fluorescence intensity is increased. Following the high peak, the intensity is reduced gradually, which can be explained by many reasons such as the unfolded protein is easily aggregated or precipitated, and some dye molecules dissociate from the aggregates.^{234,}

²³⁶

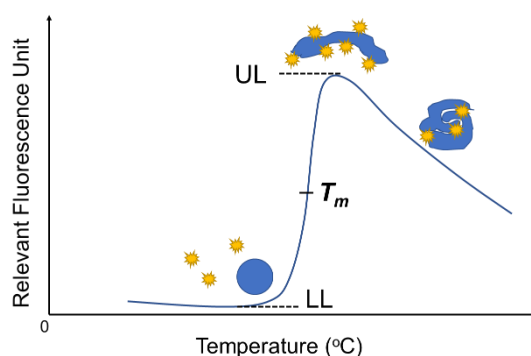


Figure 3.36 The principle of DSF assays using SYPRO orange.²³⁴

$$y = LL + \frac{UL - LL}{1 + e^{\frac{T_m - x}{a}}} \quad (3)$$

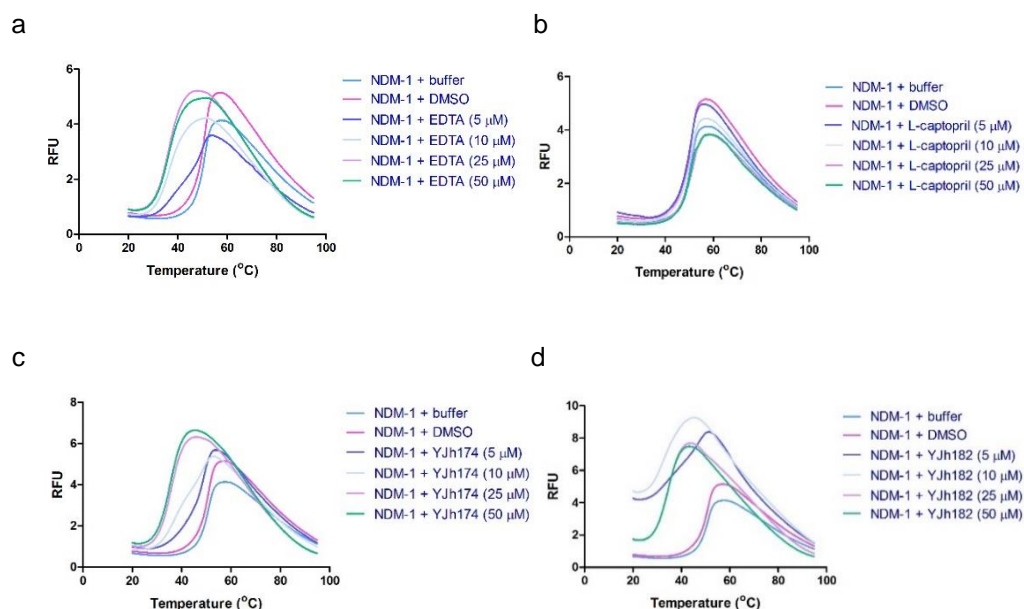
The T_m can be calculated according to the Boltzmann equation. The UL and LL are the minimum and maximum intensity, respectively, which are labeled in **Figure 3.36** and a is the slope of the curve within T_m . Most of the software packages coupled with the PCR instruments can offer the maximum of the first derivative, which is convenient for obtaining the T_m values.²³⁴

The two Zn(II) ions at the active site play important roles for keeping the native structure of NDM-1, and addition of zinc ions to the buffer improves the stability of NDM-1.^{171, 240, 241} Thus except for the essential roles played for hydrolyzing the β -lactam antibiotics for NDM-1, the two Zn(II) ions also act as stabilizers for the protein.^{106, 171, 240, 241}

Truncated NDM-1 at the concentration of 5 μ M was treated with compounds **83(YJh174)**, **94(YJh182)**, **95(YJh196)**, EDTA and L-captopril at the concentrations of 5 μ M, 10 μ M, 25 μ M and 50 μ M, respectively. The T_m of NDM-1 protein was 51.12 ± 0.29 °C under the measuring condition (5 μ M protein in 50 mM HEPES buffer, pH 7.5) which was similar to the published values.^{119, 120, 132, 242} The melting curves are shown in **Figure 3.37**, and the ΔT_m values are listed in **Table 3.12**. As the strong Zn(II) ion stripping function instead of binding with the protein, a negative ΔT_m for NDM-1 was obtained for EDTA (**Figure 3.37a**), which illustrated the stabilizer roles of the two Zn(II) ions for NDM-1. On the contra, L-captopril induced a smaller positive ΔT_m for NDM-1 (**Figure 3.37b**) as the conventional drug-like compounds, which correlated to its proposed mechanism that the thiol group of L-captopril replaced the structural water molecule linked the two Zn(II) ions. The binding of the thiol group with the two Zn(II) ions was stronger than the original water molecule which stabilized the Zn(II) ions at the active site, thus the stability of the binding complex was improved. Negative ΔT_m values were obtained for NDM-1 interacting with compounds **83(YJh174)**, **94(YJh182)** or **95(YJh196)** (**Figure 3.37c, d and e**). While the destabilizing functions of compound **94(YJh182)** and **95(YJh196)** were a little different from compound **83(YJh174)**, especially at the ratio 1 to 1 and 1 to 2 (P/L). High background at low temperature might be caused by conformational changes or aggregations of the protein. For compounds **94(YJh182)** or **95(YJh196)** at the ratio of 1 to 1 and 1 to 2 (P/L), the baselines were higher than the controls, it seemed that the binding complexes of compound **94(YJh182)** or **95(YJh196)** with the protein were at high energy states which reduced the Gibbs free energy of unfolding (ΔG_u). There were two T_m values for compound **83(YJh174)** at the ratio 1 to 2 (P/L) as well as compounds **94(YJh182)**, **95(YJh196)** and EDTA at the ratio 1 to 1 (P/L), one T_m was near to the native T_m of the protein, and the other was at a lower temperature. The multiple transitions appearing might be caused by different domains, the increasing aggregation as the heating process, or ligands that destabilized or stabilized a portion of the protein sample. Apo-NDM-1 without any Zn(II) ions was less stable than holo-NDM-1. According to native mass studies, the different binding complexes might contribute to the two T_m values, especially the protein-inhibitor complexes with two Zn(II) ions, and the protein-inhibitor complexes with one Zn(II) ion or apo-NDM-1 without any Zn(II) ions. While at high concentrations of the ligands, the curves of compounds **94(YJh182)**, **95(YJh196)** and **83(YJh174)** were similar, which suggested the ligands, especially compounds **94(YJh182)** and **95(YJh196)** might have different inhibitory mechanisms under different concentrations. Other compounds **75(YJh110)**, **58(YJh34)** and **71(YJh84)** were helped tested by Barbara Schroeder using the ¹⁵N-labeled full-length NDM-1, which all had negative ΔT_m .

Above all, according to the results of the TSA studies, the interactions of compounds **94(YJh182)**, **95(YJh196)** and **83(YJh174)** with NDM-1 can reduce the thermal stability of the protein, and the

destabilizing effects were stronger with the increased doses of the inhibitors. The destabilizing function of compound **94(YJh182)** was a little higher than (or similar to) compound **95(YJh196)**, and both compounds **94(YJh182)** and **95(YJh196)** had higher destabilizing function for NDM-1 than compound **83(YJh174)**. Given the native mass analysis, the tested inhibitors mainly formed complexes with NDM-1 protein, therefore compounds **94(YJh182)**, **95(YJh196)** and **83(YJh174)** destabilized NDM-1 through forming the binding complexes instead of stripping the Zn(II) ions out of the active pocket of the protein directly which were essentially different from EDTA. The inhibitors had strong Zn(II) ion binding affinity and the interactions with the Zn(II) ions in the active pocket played important roles for the inhibitory activity. As the key roles played by the Zn(II) ions on both the hydrolysis of β -lactams and stabilizers for keeping the conformation of NDM-1 protein, the compounds were also inhibiting NDM-1 by different mechanisms, not only the substrate mimics occupying and binding with the active pocket but also a special anti-stabilizer-like mechanism for inhibiting NDM-1. In addition, the stabilization or destabilization phenomena could be also explained by the energy states of the complexes formed by the ligands with the protein. If the binding complexes lowered the energy state of the native protein, increased the energy state of the transition form, or improved the energy state of the denatured protein, there would be an increased thermal stability. On the contra, if the binding complexes improved the energy state of the native protein, decreased the energy state of the transition form, or decreased the energy state of the denatured protein, there would be a decreased thermal stability. The destabilization phenomena caused by the tested compounds suggested the complexes of the inhibitors with the Zn(II) ions and the apo-NDM-1 protein should have a less energy threshold arriving to the denatured protein. The different anti-stabilizer-like abilities of the differ inhibitors could result in different kinds of binding complexes for the native mass spectra and influence the entropic and enthalpic changes in ITC assays. The complexes of the inhibitors with one Zn(II) ion and the apo-NDM-1 protein in the native mass spectra, which also supported the destabilization functions from TSA analysis.



e

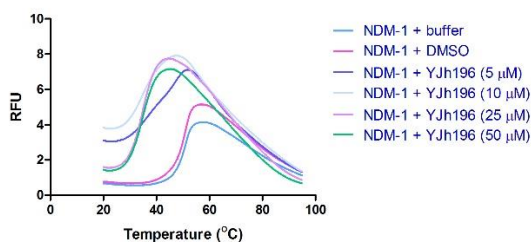


Figure 3.37 Melting curves of NDM-1. a. NDM-1 with EDTA; b. NDM-1 with L-captopril; c. NDM-1 with **83**(YJh174); d. NDM-1 with **94**(YJh182); e. NDM-1 with **95**(YJh196). (Each measurement was in quadruplicate, and the curves were averaged.)

Table 3.12 Thermal Shift of NDM-1 with the Selected Compounds at Different Concentrations

Compound	ΔT_m (°C) ^{a1}			
	5 μ M	10 μ M	25 μ M	50 μ M
EDTA	-0.88 \pm 0.34/-12.73 \pm 0.34 ^{a2}	-14.39 \pm 0.34	-14.54 \pm 0.29	-14.69
L-Captopril	0.15 \pm 0.29	0.59	1.17	1.32 \pm 1.00
83 (YJh174)	-1.76	-2.20 \pm 0.29/-12.92 ^{a2}	-15.13 \pm 0.29	-15.13 \pm 0.29
94 (YJh182)	-3.52 \pm 0.83/-16.89 \pm 0.74 ^{a2}	-17.92 \pm 0.34	-15.86	-15.86
95 (YJh196)	-3.39 \pm 0.29/-13.51 \pm 0.48 ^{a2}	-15.72 \pm 0.29	-15.86	-15.86

^{a1} Values were averaged from four replicates. The T_m values of NDM-1 with buffer and with buffer containing 0.05% DMSO were 51.12 \pm 0.29 °C and 50.67 °C, respectively.

^{a2} The first derivative curves for these samples generated from the qPCR instrument had two peaks, the data was shown in the form of ' T_{m1}/T_{m2} ', T_{m1} was calculated from the relatively higher peak.

3.3.5 Solution NMR assays.

Solution NMR is an essential method to investigate the protein conformational changes and dynamics. Barbara Schroeder expressed the ¹⁵N-labeled full length NDM-1 and the ¹H-¹⁵N HSQC spectrum of the di-Zn-NDM-1 was obtained at the concentration of around 150 μ M in the buffer of 50 mM HEPES pH 7.5 according to the published procedure (Yao et al., 2017), furthermore, she helped to test compounds **83**(YJh174), **75**(YJh110), **71**(YJh84) and **58**(YJh34) by solution NMR assays. However, precipitations of the protein were formed after the addition of compound **83**(YJh174), in this case, the spectra of the protein treated with the inhibitors were not obtained.^{226, 243, 244}

On the one hand, the full-length NDM-1 was more sensitive to the high concentration or harsh conditions which hindered the proceeding of some biological assays.^{89, 91, 104-106, 245} The assay conditions could be optimized by using the truncated NDM-1, lowering concentrations of both protein and inhibitors, testing samples of the protein and ligands with different ratios, or trying other inhibitors as the different main inhibitory mechanisms. On the other hand, the precipitation phenomenon also highlighted the destabilizer function of the inhibitors for the protein, which might be obvious at the high concentration required for the assays, however the stability of the membrane protein decreased at high concentrations should also be considered.²⁴⁴ In addition, for structural studies required high concentrations and long-

time stability, only 20% nonmembrane proteins can be the candidates, solving the solubility and stability problems are essential.²⁴⁵ Removing the relevant signal sequence was the method applied in this doctoral work which improved the production of protein expression and stability of the protein in different assay conditions. As the successful examples of using truncated NDM-1 in BLI, ITC, native mass spectrometry, TSA and CD studies, truncated NDM-1 can also be tried in solution NMR assays. Except for changing the sequence of the protein (e.g., expressing only the catalytic domain, adding hydrophilic sequences such as polyhistidine tag, site-directed mutagenesis including hydrophobic to hydrophilic mutations on the protein surface or replacement of amino acid residues with similar property), there were other ways for improving the conditions, such as adding free zinc ions in the buffer to improve the stability of MBLs, adding charged amino acids Arg and Glu in the assay buffers reported by Golovanov et al. (2004), prescreening the suitable buffer as well as other conditions by the thermofluor-based high-throughput methods reported by Ericsson et al. (2006).²⁴⁵⁻²⁴⁹

3.3.6 Circular dichroism (CD)

Circular dichroism (CD) is the differential absorbance of left- and right-handed circular polarized light. A CD active molecule must be structurally asymmetric and has absorbance. Generally, chromophores inherently chiral and non-chiral chromophores covalently attached to a chiral molecule or located in asymmetrical environment have CD signals. Proteins are CD active molecules, the peptide bond (amide chromophore) is the main contributor for the far-UV range of the CD spectrum (178-260 nm), and the aromatic amino acid side chains as well as the disulfide bond and cofactor or ligand binding mainly contribute for the near-UV range of the CD spectrum (255-340 nm) and visible CD spectrum. The Far-UV CD spectra are commonly used to study the secondary structures of proteins, which have been widely used for estimating folding of the expressed protein, mutation influence on the conformation or stability of the protein, ligand binding effects, etc. The near-UV CD signals can provide fingerprints of the tertiary structures of proteins, and visible CD also offers some binding information such as cofactor or ligand binding, while the CD spectra of the near-UV and visible region for proteins have been relatively less used due to their complication for analysis and limited technologies at present. CD spectroscopy is a convenient method for determining the conformations adopted by proteins and needs relatively small amount of material (e.g., around 2 mL protein solution at the concentration of 0.1 mg/mL in a cuvette with the pathlength of 1 mm for NDM-1) in physiological buffers. However, CD spectra cannot provide detailed information about amino acid residues which can be obtained from X-ray crystallography studies or solution NMR. The basic principle of CD spectrometers is similar, the linearly polarized light with the defined wavelength and bandwidth is selected by the monochromator from the white unpolarized light and converted to the left- and right-handed circular polarized light by the photoelastic modulator (PEM), the differential absorbance for the left- and right-handed circular polarized light of the tested sample is detected. At a given wavelength, the CD can be reported in different forms, such as the difference of absorbance ΔA ($\Delta A = A_L - A_R$, where A_L and A_R are the absorbance of the left- and right-handed circular polarized light, respectively), molar circular dichroism $\Delta \epsilon$ ($\Delta \epsilon = \epsilon_L - \epsilon_R$, where ϵ_L and ϵ_R are the extinction coefficient of the left- and right-handed circular polarized light, respectively). The unit of $\Delta \epsilon$ is $M^{-1} \cdot cm^{-1}$. ϵ_L and ϵ_R can be calculated according to the Beer-Lambert law, $A = \epsilon cl$, where A is the absorbance, c and l are the molar concentration and pathlength in cm of the sample, respectively), ellipticity in degrees θ ($\theta = \tan^{-1}(b/a)$, where b and a are the minor and major axes of the resultant ellipse, respectively). The left- and right-handed circular

polarized light with same amplitude can generate plane polarized light after being combined, while the two components with different magnitude due to the different absorbance of the measured sample generate elliptically polarized light. θ and ΔA are numerically interconvertible by the relationship, which is $\theta = 32.98 \Delta A$, and the molar ellipticity $[\theta]$ in $\text{deg}\cdot\text{cm}^2\cdot\text{dmol}^{-1}$ ($[\theta] = 100\theta/c$, where c and l are the molar concentration and pathlength in cm, respectively). $[\theta]$ and $\Delta\epsilon$ were also interconvertible, $[\theta] = 3298 \Delta\epsilon$.²⁵⁰⁻²⁵²

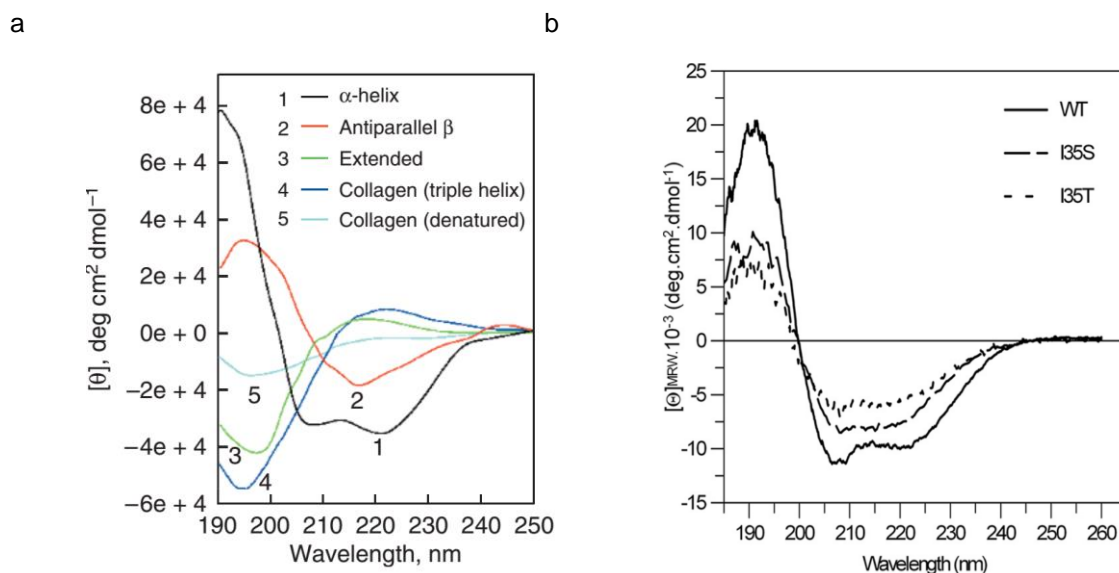


Figure 3.38 a. CD spectra for representative secondary structures;²⁵⁰ b. CD spectra of wild-type NDM-1 and NDM-1 mutants.²⁵¹ (The two pictures were reproduced from the references.)

Different secondary structures of polypeptides or proteins have different characteristic CD signals (**Figure 3.38a**). α -helices contribute typical negative bands at around 222 nm and 208 nm and a positive band at about 193 nm, while β -sheets have negative bands at around 218 nm and 195 nm. The characteristic bands of α -helices and β -sheets are commonly used for specifying the secondary structures of proteins. There are overlapped parts of the typical bands for different secondary structures, thus the CD spectra for proteins offer the integrated signals. The CD signal at 222 nm can be used for estimating the content of α -helices for protein. The mean residual ellipticity (MRE or $[\theta]_{\text{MRW}}$, the MRW is the mean residue weight calculated by using the molecular weight of the protein dividing $N-1$, where N is the number of the amino acids.) and α -helical content can be calculated according to the equation (4) and (5), respectively.^{250, 253-255}

$$\text{MRE} = \frac{\theta_{\text{obs}}}{10ncl} \quad (4)$$

$$\% \alpha - \text{helix} = \left[\frac{\text{MRE}_{222\text{nm}} - 2340}{30300} \right] \times 100 \quad (5)$$

θ_{obs} is the measured ellipticity in millidegrees, n is the number of the backbone amides (or the number of the amino acids minus one if the protein is not acetylated,²⁵⁰ while in some published works n is defined as the number of the amino acids,²⁵³⁻²⁵⁵ and the other such as the references relating to the

DICHROWEB server n is defined as the number of the amino acids minus one²⁵⁶⁻²⁶³), c is the concentration of the protein in mole, and l is the pathlength of the cuvette in centimeter and α -helical content can be calculated from the values of MRE at 222 nm wavelength MRE_{222nm} .^{250, 253-255}

The secondary structures of most proteins include more than one structural element, and the CD signals are the sum of all the contributions of each element as well as some noise terms. There are some commonly used sources of the analysis software to estimate the secondary structures more accurately such as CDPro, Circular Dichroism at UMDNJ, CONTIN, DICROPROT, DICHROWEB, K2D, and SOMCD. DICHROWEB is an online analysis server by which different programs can be chosen for data analysis such as CONTINLL, VARSLC, K2d, CDSSTR and SELCON3, providing various algorithms and reference sets, and the normalized root mean square deviation (NRMSD) is the standard goodness-of-fit parameter used to evaluate the correspondence of the calculated secondary-structure data and the experimental CD data.²⁵⁰⁻²⁶³

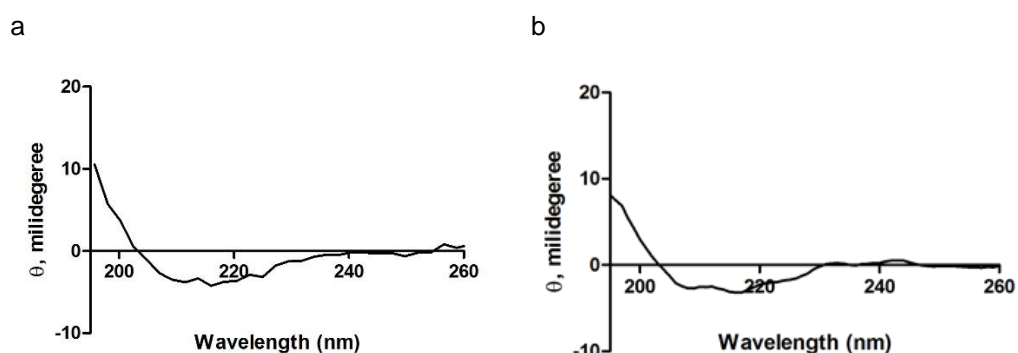


Figure 3.39 CD spectra for NDM-1. a. CD spectrum of the wild-type NDM-1 (obtained at 20°C using PBS buffer, with a concentration of ca. 0.06 to 1 mg/mL)^{f6}; b. CD spectrum of the truncated NDM-1 (obtained at 20°C using 20 mM sodium phosphate buffer pH 7.0, with a concentration of ca. 0.06 to 0.1 mg/mL).

The CD spectra were obtained for both the wild-type and truncated NDM-1, and the ellipticities in millidegrees were compared directly (**Figure 3.39**). There were typical negative band from around 205 nm to 230 nm and positive band from around 195 nm to 200 nm for the α -helices and β -sheets, thus both proteins were folded well. As the low yield of the wild-type, truncated NDM-1 was used for the measurements to investigate the conformational changes of the protein by ligand binding. The CD spectra were recorded with the Olis CD spectrometer, and secondary structures were analyzed using CDSSTR algorithm and reference set 4 with the DICHROWEB online server. The normalized root mean square deviation (NRMSD) was used to evaluate the accuracy of the analysis, and the NRMSD values of all the samples were below 0.08, which indicated a good correspondence between the original and reconstructed spectra. The reconstructed spectra are presented in mean residual ellipticity (MRE or $[\theta]_{MRW}$) in **Figure 3.40**, and the analysis of the secondary structures are listed in **Table 3.13**.

^{f6} Dr. Kenichi Ataka helped to measure one of the prepared samples for the wild-type NDM-1 in **Figure 3.39a**.

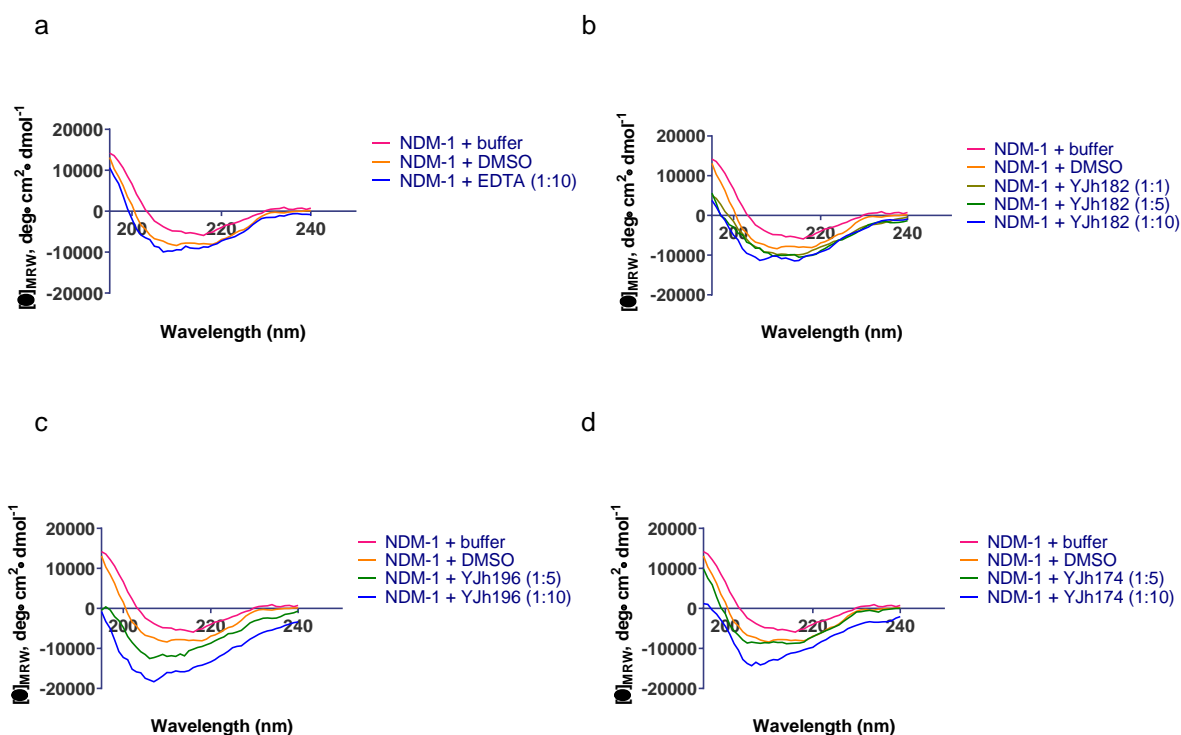


Figure 3.40 CD spectra of NDM-1 incubated with inhibitors at different mole ratios. a. NDM-1 incubated with EDTA; b. NDM-1 incubated with **94(YJh182)**; c. NDM-1 incubated with **95(YJh196)**; d. NDM-1 incubated with **83(YJh174)**. The data were obtained at 20°C using 20 mM sodium phosphate buffer pH 7.0, and the concentration of the protein was ca. 0.06 to 0.1 mg/mL (ca. 2.28 to 3.8 μ M).

Table 3.13 Calculated Secondary Structure Fractions

Protein samples	Helices (%)	Strands (%)	Turns (%)	Unordered (%)
NDM-1 + buffer	9	44	18	28
NDM-1 + DMSO	12	35	21	30
NDM-1 + YJh182 (1:1)	10	36	23	31
NDM-1 + YJh182 (1:5)	7	37	24	33
NDM-1 + YJh196 (1:5)	12	33	22	32
NDM-1 + YJh174 (1:5)	12	38	21	30
NDM-1 + YJh182 (1:10)	11	34	22	33
NDM-1 + YJh196 (1:10)	19	23	28	30
NDM-1 + YJh174 (1:10)	20	27	29	24
NDM-1 + EDTA (1:10)	15	32	24	30

The CD spectra of NDM-1 at ca. 0.06 to 0.1 mg/mL (ca. 2.28 to 3.8 μ M) with inhibitors or without inhibitors were obtained using 20 mM phosphate sodium buffer pH 7.0 at 20 °C. The α -helix content of NDM-1 with assay buffer and NDM-1 with 0.038% DMSO was 9% and 12%, respectively, and the β -sheet content was 44% and 35%, respectively. The DMSO content might have some effects on the obtained CD signals, thus all the other measured samples were kept the same content of DMSO (0.038%). The typical bands were similar for the spectra of NDM-1 incubated with EDTA at the (P/L)

ratio of 1 to 10 and NDM-1 with 0.038% DMSO (**Figure 3.40a**), and the differences of the content for each secondary-structure element were less or equal to 3%. According to the native mass studies, a two-fold excess EDTA removed all the Zn(II) ions of NDM-1, the protein existed as apo-NDM-1 without any Zn(II) ions and did not bind with EDTA, thus under the CD assay condition with a ten-fold excess EDTA, the existing form of the protein should be the same. Therefore, the CD spectra of holo-NDM-1 and apo-NDM-1 were almost the same or less different, which suggested that the holo-NDM-1 and apo-NDM-1 had similar secondary structures and the loss of two Zn(II) ions had little or no effect on the far-UV spectra of NDM-1. EDTA did not bind with the protein, thus there should be no effect from ligand binding.

For CD spectra of NDM-1 incubated with different ratio of compounds **94(YJh182)** and **83(YJh174)**, the spectra of the (P/L) ratio 1 to 1 or 1 to 5 had the similar bands as the spectrum of NDM-1 with 0.038% DMSO, while the spectra of the (P/L) ratio 1 to 10 had obvious difference for compounds **95(YJh196)** and **83(YJh174)**, especially the negative bands from around 205 nm to 215 nm were increased (**Figure 3.40b, c and d**). For CD spectra of NDM-1 incubated with different ratio of compound **95(YJh196)**, the negative bands from around 200 nm to 230 nm were more different from that of the spectrum for NDM-1 with 0.038% DMSO, and there is a dose related increase of the band at 205 nm to 215 nm (**Figure 3.40b**). The calculated helical content of the spectra of NDM-1 with compound **94(YJh182)** at the (P/L) ratio 1 to 5 was 7%, which was around 5% lower than the value for NDM-1 with 0.038% DMSO, and the calculated helical content of the spectra of NDM-1 with compounds **95(YJh196)** and **83(YJh174)** at the (P/L) ratio 1 to 10 was 19% and 20%, respectively, which was around 8% higher than the value for NDM-1 with 0.038% DMSO.

At first, the results supported that the interactions of compound **94(YJh182)**, **95(YJh196)** and **83(YJh174)** with NDM-1 were different from that of EDTA. According to native mass studies, **94(YJh182)**, **95(YJh196)** and **83(YJh174)** all could bind with NDM-1 forming the protein-inhibitor complexes of one molecule NDM-1 with two Zn(II) ions and one molecule inhibitor, and compounds **94(YJh182)** and **95(YJh196)** can form more stable protein-inhibitor complexes than compound **83(YJh174)**. Thus, the change of the CD signals of the spectra for compounds **94(YJh182)**, **95(YJh196)** and **83(YJh174)** should be caused by the protein-inhibitor binding complexes. The increased chromophores in the asymmetric environment might increase the negative bands. Compound **95(YJh196)** could form the most stable complex of one molecule NDM-1 containing two Zn(II) ions and one molecule of compound, which might have more stronger influence on the CD signals compared with compounds **94(YJh182)** and **83(YJh174)**.

Above all, the results were compatible with the protein native mass spectrometry studies. On the one hand, there were no or less significant changes of the secondary structures for NDM-1 of all the measured compounds at the (P/L) ratio of 1 to 5, which suggested that the protein was still folded well after binding with the inhibitors under the measuring assay conditions. The relevant changes should be caused by ligand binding, which were obvious at a high ligand ratio such as 1 to 10 (P/L), especially for compounds **95(YJh196)** and **83(YJh174)**. On the other hand, all the measured ligands had destabilizing functions for the protein, and the functions were dose-related according to the TSA studies, thus the conformations of the proteins might be changed under a high concentration of ligands. In addition, there was more non-specific binding at the high ratio of compounds which might influence the results, and the measurements were sensitive to buffer conditions such as pH, the contents of DMSO or salts, although the controls of each sample only containing relevant inhibitors in the same buffer without

protein were subtracted. The CD measurements provided a qualitative recognition for the binding of the protein and ligands, and different factors needed to be considered for the relevant band changes.

3.3.7 Zinc ion restoration assays

The hydrolysis activity of NDM-1 inhibited by Zn(II)-chelating inhibitors such as AMA could be restored by the addition of excessive zinc ions.¹²⁷ Restoration of the activity of NDM-1 by zinc ions can principally happen by several mechanism. First, for Zn(II)-chelating inhibitors such as EDTA and AMA, most of the protein losing one or two Zn(II) ions but still well folded, rebinding with zinc ions can restore the hydrolysis activity. Second, for Zn(II)-binding inhibitors which can form protein-inhibitor complexes, the additional zinc ions can competitively bind with the inhibitors resulting in the free protein, the hydrolysis activity of the free protein is recovered, however, the possible loss of Zn(II) ions of the protein can be amended by the excess zinc ions. Third, for some denatured protein, incubation with Zn(II) ions might could induce the active folding again which always need longer incubation time and the efficiency is low. Above all, zinc ion restoration assays can be used to investigate the reversibility of the inhibition, and the stability of the protein-inhibitor complexes for Zn(II)-binding inhibitors (or comparison the binding affinity of different inhibitors with NDM-1). In addition, the β -lactam substrates also can bind with free zinc ions, the influence of the real active concentration of the substrates needs to be considered.

According to the results of ITC assays (zinc ion containing buffer titrating inhibitor containing buffers), the tested inhibitors had strong Zn(II)-binding affinity, which was important for their inhibitory activity for NDM-1. Negative enthalpic changes were obtained for compounds **94(YJh182)**, **95(YJh196)** and **83(YJh174)** of the ITC assays with inhibitor containing buffer titrating protein buffer, the entropic changes for compounds **83(YJh174)** and **95(YJh196)** were more favored for binding than compound **94(YJh182)**. Normally the conformational changes and the reduction of freedom contribute to negative entropic change. Compound **94(YJh182)** might cause more conformational changes than compounds **95(YJh196)** and **83(YJh174)** for binding with NDM-1. The conformational changes might be mainly happened at the active binding pocket especially the important amino acid residues and the coordinated Zn(II) ions. For BLI assays, there were free zinc ions in the assay buffer, compounds **94(YJh182)** and **95(YJh196)** had stronger binding affinity with the protein than compound **83(YJh174)**, while for ITC assays without the addition of free zinc ions in the assay buffer, compound **83(YJh174)** had stronger binding affinity with the protein than **94(YJh182)** and **95(YJh196)**. The stability of the complexes formed of the protein and the inhibitors of native mass studies were different, and binding with compounds **94(YJh182)**, **95(YJh196)** and **83(YJh174)** reduced the thermal stability of NDM-1. Above all, zinc ions played important roles for the stability of the protein and the inhibitory activity of the inhibitors. Zinc ion restoration assays can be used to investigate the reversibility of inhibition for NDM-1 by the representative compounds, and the assays were performed at different temperatures and with different concentrations of the inhibitors.

At first, compounds **83(YJh174)** (20 μ M) and **94(YJh182)** (20 μ M) were incubated with NDM-1 (10 nM), respectively, at room temperature for 15 min, then incubated with zinc ions of different concentrations, respectively, for 15 min, a same volume of the substrate (nitrocefin) buffer (26 μ M) was added, the absorption was monitored at 37 °C under the wavelength of 490 nm (**Figure 3.41a**). According to the control groups (NDM-1 with DMSO), it seemed that zinc ions at high concentrations reduced the hydrolyzing activity of the protein. The phenomenon should come from the β -lactam

substrate which had zinc ion binding ability, the additional zinc ions in the buffer competed with NDM-1 protein to bind with the substrate, thus less substrate bound with NDM-1 to be hydrolyzed. With the gradually increased concentration of the zinc ions, more substrate molecules were occupied by the free zinc ions in the buffer, the substrate molecules hydrolyzed by NDM-1 were gradually reduced (**Figure 3.41a**). For protein treated with compounds **83(YJh174)** and **94(YJh182)**, the trend of curves for the residual activity can be divided into three parts (**Figure 3.41a**). For the final concentration of the zinc ions was less than around 1 μM , the residual activity was nearly zero; for the final concentration of the zinc ions ranged from around 1 μM to 5 μM , the residual activity was relatively fast increased with the gradually increased concentration of zinc ions; for the final concentration of the zinc ions was more than around 5 μM , the residual activity was relatively slowly reduced with the gradually increased concentrations of zinc ions. At the first stage (the plateau part), there were more free inhibitor molecules in the buffer, the less zinc ions would mainly been bound with the free inhibitor molecules (or in other word, quenched by the excess inhibitor molecules in the buffer), and had no chance to interact with other molecules. At the second stage (the part with an upward trend), with increased concentration of the zinc ions, there were less free inhibitor molecules in the buffer, the zinc ions would also interact with others. On the one hand, the excess zinc ions can bind with the apo-NDM-1 with one Zn(II) ion or without any Zn(II) ions which might be caused during the interacting process with the inhibitors. On the other hand, the excess zinc ions would compete with NDM-1 proteins to bind with the inhibitors, which could release the protein from the binding complexes. Thus, the hydrolysis activity of some protein molecules was recovered. At the third stage (the part with a downward trend), the increased zinc ions would mainly bind with the substrate, the amount of the substrate could be hydrolyzed for the recovered NDM-1 protein were reduced. The difference of the residual activity for NDM-1 treated with compounds **83(YJh174)** and **94(YJh182)** was obvious when the final concentration of the zinc ions was 5 μM . With 5 μM zinc ions, the residual activities of NDM-1 with DMSO, **83(YJh174)** and **94(YJh182)** were around 75%, 54% and 26%, respectively (**Figure 3.41b**), the residual activity of NDM-1 treated with compound **83(YJh174)** was nearly 20% lower than the control but two times of the protein treated with compound **94(YJh182)**. There were several possible reasons for the difference of compounds **83(YJh174)** and **94(YJh182)**. First, compound **94(YJh182)** with the 4-phenyl substituent was more suitable for the active site of NDM-1 according to docking studies, which was less influenced by the free zinc ions in the buffer. According to native mass studies, compound **94(YJh182)** can form more stable complex of NDM-1 with two Zn(II) ions and the inhibitor than compound **83(YJh174)**. In addition, there were some apo-NDM-1 with one Zn(II) ion or without any Zn(II) ions for native mass spectra of NDM-1 with compounds **94(YJh182)** and **83(YJh174)**, and the percentage for NDM-1 with compound **83(YJh174)** was more than NDM-1 with compound **94(YJh182)**. Therefore, for the second stage, it was more difficult for the zinc ions to compete with NDM-1 to binding with compound **94(YJh182)** than compound **83(YJh174)**, and there were more apo-NDM-1 with one Zn(II) ions or without any Zn(II) ions to be recovered by rebinding with the excess zinc ions for NDM-1 inhibited by compound **83(YJh174)** than inhibited by **94(YJh182)**. Another reason could be that under the measuring conditions, irreversible conformational changes might happen for some of the protein molecules, and the destabilizing function for NDM-1 of compound **94(YJh182)** was stronger. According to the TSA studies, the T_m values of NDM-1 (5 μM) incubated with compounds **94(YJh182)** (50 μM) and **83(YJh174)** (50 μM) were 15.13 $^{\circ}\text{C}$ and 15.86 $^{\circ}\text{C}$ lower than the T_m value of NDM-1 (5 μM) incubated with 0.05% DMSO (50.67 $^{\circ}\text{C}$), respectively. However, the assay conditions were different for the TSA and zinc restoration assays, especially the low protein concentration and soft buffer conditions of the zinc restoration assays which helped to

stabilize the protein, thus the destabilizer effects of the inhibitors might be relatively reduced. The assay was also monitored at 28 °C (**Figure 3.41b**), the same trend was kept for compounds **83(YJh174)** and **94(YJh182)**, and the residual activity of NDM-1 with DMSO, compounds **83(YJh174)** and **94(YJh182)** with 5 μM were around 69%, 34% and 15%, respectively. The curve for NDM-1 inhibited by compound **95(YJh196)** was similar as NDM-1 inhibited by compound **94(YJh182)**, which correlated to their similar results from native mass and TSA studies. Compounds **58(YJh34)** and **61(YJh59)** were also measured, the activity of NDM-1 inhibited by compound **58(YJh34)** was between the effects of compounds **83(YJh174)** and **94(YJh182)** or **95(YJh196)**. According to the native mass studies, compound **58(YJh34)** caused less apo-NDM-1 with one Zn(II) ion but also formed less protein-inhibitor complexes than compound **83(YJh174)**, and the destabilizer function of compound **58(YJh34)** was stronger than compound **83(YJh174)**. Therefore, the result of the restoration assays should be the collaborated effects of compound **58(YJh34)** for NDM-1. The activity of NDM-1 inhibited by compound **61(YJh59)** was the most difficult one to be recovered compared with others. Compound **61(YJh59)** had higher inhibitory activity for NDM-1 than compound **58(YJh34)**, which was supported the low recovered activity of NDM-1 inhibited by compound **61(YJh59)**, and the mechanism need be further investigated. The lower concentration (1 μM) of inhibitors was also tested (**Figure 3.41c**), as there were less inhibitors in the buffer, the first plateau stages were almost disappeared, and the differences of different inhibitors were decreased. Generally, the recovered activity of NDM-1 inhibited by all the tested inhibitors with a final concentration of 1 μM was higher compared to respective samples with the final concentration of 10 μM for the inhibitors and the peak of the residual activity was moved to around 0.6 μM of zinc ions. It suggested that the restoration was related to the dose of the inhibitors, the hydrolysis activity would be recovered more with less inhibitors.

Above all, the hydrolysis activity of NDM-1 inhibited by the tested compounds could be partially recovered by the additional zinc ions. The hydrolysis activity of the apo-NDM-1 with one Zn(II) ion or without any Zn(II) ions can be recovered via rebinding with the additional zinc ions. With increased zinc ions competing with NDM-1 for the inhibitors, some NDM-1 molecules can be released from the protein-inhibitor complexes. The destabilizer function of the tested inhibitors might lead some irreversible conformational changes. The recovered activities of NDM-1 inhibited by different tested inhibitors were different, which was related to the different main inhibitory mechanisms of the inhibitors, and correlated with the results of docking, native mass, and TSA studies. The 4- or 5-position phenyl-substituted compounds **94(YJh182)** and **95(YJh196)** were more fitted for the active pocket of NDM-1, formed more stable protein-inhibitor complexes and less apo-NDM-1 with one Zn(II) ions or without any Zn(II) ions, and had stronger destabilizing function for NDM-1 than compound **83(YJh174)**, which resulted in the less recovered hydrolysis activity for NDM-1 inhibited by compounds **94(YJh182)** and **95(YJh196)** than NDM-1 inhibited by compound **83(YJh174)**.

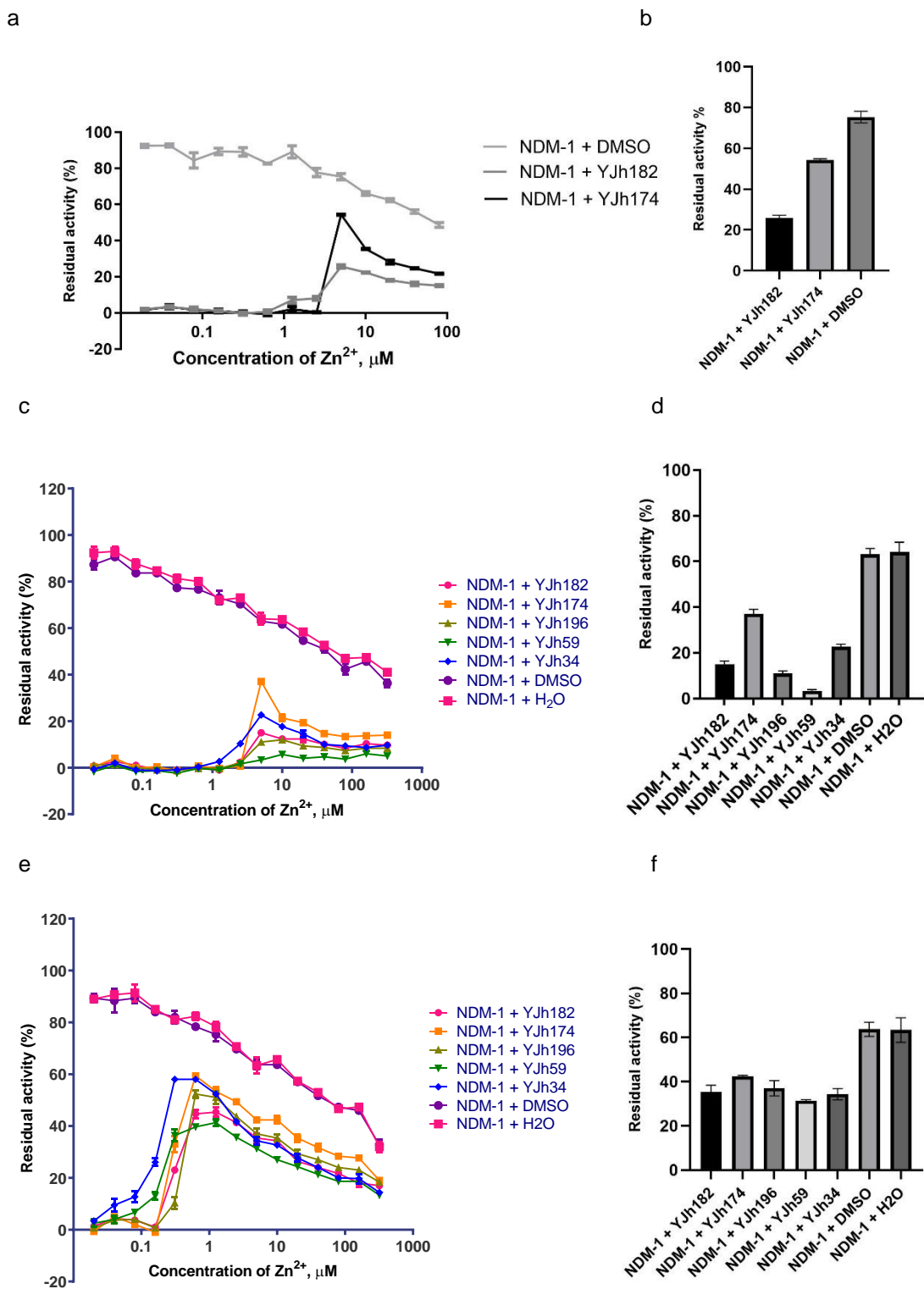


Figure 3.41 Addition of excess zinc ions to restore the activity for NDM-1 inhibited by the selected inhibitors. a. Zinc ions restoration assay monitored at 37 °C, 10 μM inhibitors; b. Zinc ions restoration assay monitored at 37 °C with 5 μM zinc ions, 10 μM inhibitors; c. Zinc ions restoration assay monitored at 28 °C, 10 μM inhibitors; d. Zinc ions restoration assay monitored at 28 °C with 5 μM zinc ions, 10 μM inhibitors; e. Zinc ions restoration assay monitored at 28 °C, 1 μM inhibitors; f. Zinc ions restoration

assay monitored at 28 °C with 5 μ M zinc ions, 1 μ M inhibitors. (The concentrations were final concentrations.)

3.3.8 Summary of mode-of-action studies

The interaction modes of the top active inhibitors as well as some other representative compounds with NDM-1 were studied by different assays. The main results for compounds **94(YJh182)**, **95(YJh196)** and **83(YJh174)** with NDM-1 are listed in **Table 3.14**. The general relationship of the different evaluation assays for the interaction studies of the representative inhibitors are shown in **Figure 3.42**.

Compounds **94(YJh182)**, **95(YJh196)** and **83(YJh174)** all can reversibly bind with NDM-1 under the BLI assay conditions, compounds **94(YJh182)** and **95(YJh196)** had higher binding affinity for NDM-1 than compound **83(YJh174)**. Compounds **94(YJh182)**, **95(YJh196)** and **83(YJh174)** had similar binding affinity for free zinc ions which was identified by ITC assays titrating inhibitors with zinc ions. Given the free zinc ions in the assay buffer of BLI assays which might shift the K_d values of the inhibitors, ITC assays were performed using inhibitors titrating the protein without additional zinc ions in the assay buffer. Better K_d values were obtained for ITC assays, but the trend did not correlate with the IC_{50} values, compound **83(YJh174)** showed higher binding affinity than compounds **94(YJh182)** and **95(YJh196)**, which might be due to the different mechanisms and assay conditions of the methods. ITC method measures the thermodynamic parameters, the results of the ITC assays reflected the equilibrium of the whole titrating system including interactions such as the binding of NDM-1 with ligands and the binding of the released Zn(II) ions with ligands, while the results of the BLI assays mainly reflected the binding complexes of the ligand and protein. The trend of the inhibitory activity correlated to the trend of the K_d values obtained from the BLI assays, which highlighted that forming of the complexes of holo-NDM-1 with the inhibitors was the main interaction mode and contributing the most for the inhibitory activity for the tested inhibitors. According to native mass spectrometry studies, compounds **94(YJh182)** and **95(YJh196)** with the 4- or 5-phenyl groups could form more stable protein-inhibitor binding complexes with holo-NDM-1 than compound **83(YJh174)**, which was supported by docking studies, BLI assays, and zinc ion restoration assays. The inhibitors can reduce the thermal stability of NDM-1 according to the TSA studies, which also correlated to the different types of the complexes in the native mass spectra, especially the complexes of apo-NDM-1 with one Zn(II) ion and one molecule of the inhibitor. In addition, the different types of the complexes of the native mass spectra and the destabilizing function identified from TSA studies helped to explain the partial recovered hydrolysis activity of the zinc ion restoration assays. According to the results of the CD spectrometry studies, at a lower concentration of the inhibitors, there were less changes about the CD signals of the protein, but for a higher concentration of the compounds, there were significant changes of the CD signals for the protein, especially for protein incubated with compounds **95(YJh196)** and **83(YJh174)**. There might be conformational changes for the ligands or the protein of the binding complexes, and the detailed conformational changes at the active site especially the important amino acid residues can be investigated by solution NMR method. While compound **83(YJh174)** caused precipitate of the full-length NDM-1 for the solution NMR assay, the assay conditions can be optimized by using the truncated NDM-1.

Above all, the developed Zn(II)-binding inhibitors, especially the top active inhibitors **94(YJh182)** and **95(YJh196)** of the **8-MSQA** derivatives with 4- or 5-phenyl groups had improved specificity and binding affinity for the active pocket of NDM-1, and the Zn(II) ion binding ability played important roles. The inhibitors interacted with NDM-1 mainly by forming protein-inhibitor binding complexes with the holo

protein, on the one hand, they competitively bound with the catalytic active site, on the other hand, their binding can reduce the stability of the protein. There might be conformational changes about the protein or relevant ligands which needed to be further investigated. The different binding effects on the protein of the inhibitors depended on the assay conditions. Interacting with target protein by mainly forming protein-inhibitor complexes and effecting the thermal stability of the protein is a more promising mode of action for the Zn(II)-binding inhibitors compared with other more toxic mechanisms. Interaction with target protein by specific binding instead of depriving Zn(II) ions from the active site of metalloenzymes such as EDTA or AMA type inhibitors has improved the selectivity of the inhibitors. Compared with the covalent binding mechanism, on the one hand, the interaction modes of the top active inhibitors as well as some other compounds have broadened their potential inhibiting spectra of MBLs, which will not be limited to the cysteine residue containing active sites, e.g., the B3 subclass MBLs did not have the cysteine residue at the active site, on the other hand, the mechanism of forming binding complexes of the Zn(II)-binding inhibitors with target protein has been less toxic than the covalent binding mechanism.

Table 3.14 Mode of Action Studies for Compounds 94(YJh182), 95(YJh196) and 83(YJh174)

Methods	Main results and conclusions		
	94(YJh182)	95(YJh196)	83(YJh174)
<i>In vitro</i> inhibitory activity test	IC ₅₀ = 0.23 ± 0.01 μM	IC ₅₀ = 0.21 ± 0.02 μM	IC ₅₀ = 0.29 ± 0.02 μM
Docking studies	Zinc binding locations: Zn(II) ions Negative ionizable interactions: Zn(II) ions, Asn220, Lys211; H-bond interactions: Asn220, Lys211; Hydrophobic interactions: Trp93, Val73, Ile35, Met67, Leu65	Zinc binding locations: Zn(II) ions Negative ionizable interactions: Zn(II) ions, Asn220, Lys211; H-bond interactions: Asn220, Lys211; Hydrophobic interactions: Trp93, Val73, Ile35, Met67, Leu65	Zinc binding locations: Zn(II) ions Negative ionizable interactions: Zn(II) ions, Asn220, Lys211; H-bond interactions: Asn220, Lys211; Hydrophobic interactions: Trp93, Val73, Ile35
	The favored proposed binding poses were different, the general interactions were concluded from their several main binding poses.		
BLI	K _d = 9.80 ± 0.24 μM	K _d = 7.88 ± 0.29 μM	K _d = 14.1 ± 0.37 μM
	The K _d values might be shifted as the additional zinc ions in the assay buffer, but the trend correlated well with the IC ₅₀ values.		
ITC (Compound titrating NDM-1)	K _d = 0.527 ± 0.149 μM N (sites) = 1.70 ± 0.034 ΔH(kJ/mol) = -28.7 ± 1.02 ΔG(kJ/mol) = -35.9 -TΔS(kJ/mol) = -7.16	K _d = 0.532 ± 0.149 μM N (sites) = 1.81 ± 0.035 ΔH(kJ/mol) = -23.7 ± 0.81 ΔG(kJ/mol) = -35.8 -TΔS(kJ/mol) = -12.2	K _d = 0.105 ± 0.028 μM N (sites) = 1.98 ± 0.015 ΔH(kJ/mol) = -27.6 ± 0.66 ΔG(kJ/mol) = -39.9 -TΔS(kJ/mol) = -12.2

	The K_d values obtained were smaller than the values from BLI assays as there were no additional zinc ions added in the assay buffer of ITC assays, but the trend did not correlate with the IC_{50} values, which might be influenced by both the mechanism of the method and the different assay conditions. The different entropic change of 94(YJh182) might be caused by conformational changes of the protein and the ligand.		
ITC (Zinc ions titrating compound)	They all can bind with free zinc ions with a similar binding affinity.		
Native mass spectrometry	The complex of one molecule of NDM-1 with two Zn(II) ions and one molecule of compound 94(YJh182) (ca. 93% relative intensity), and the complex of one molecule of NDM-1 with two Zn(II) ions and two molecules of 94(YJh182) (ca. 87% relative intensity) were the main binding complexes.	Complex of one molecule of NDM-1 with two Zn(II) ions and one molecule of compound 95(YJh196) was the main form (100% relative intensity).	Complexes of one molecule of apo-NDM-1 with one or two Zn(II) ions and one molecule of compound 83(YJh174) had the relative intensity of around 35% and 50%, respectively.
TSA	Dose-related, negative ΔT_m The destabilizing function of the ligands for NDM-1(from the highest to the lowest) : 94(YJh182), 95(YJh196), 83(YJh174)		
Solution NMR	-	-	Cause precipitation (using full-length NDM-1)
	The assay can be optimized using truncated NDM-1.		
CD	There were less changes about the far-UV CD spectrum of the protein, and some changes about the far-UV CD spectrum of the protein with high concentration of the compound especially compounds 95(YJh196) and 83(YJh174) might be caused by ligand binding.		
Zinc ion restoration assays	The inhibition was partially reversible. Around 20%, 20% and 50% hydrolysis activity can be recovered for NDM-1 inhibited by compounds 94(YJh182) , 95(YJh196) and 83(YJh174) , respectively (at 28 °C, with 10 μ M corresponding inhibitor and 5 μ M zinc ions).		

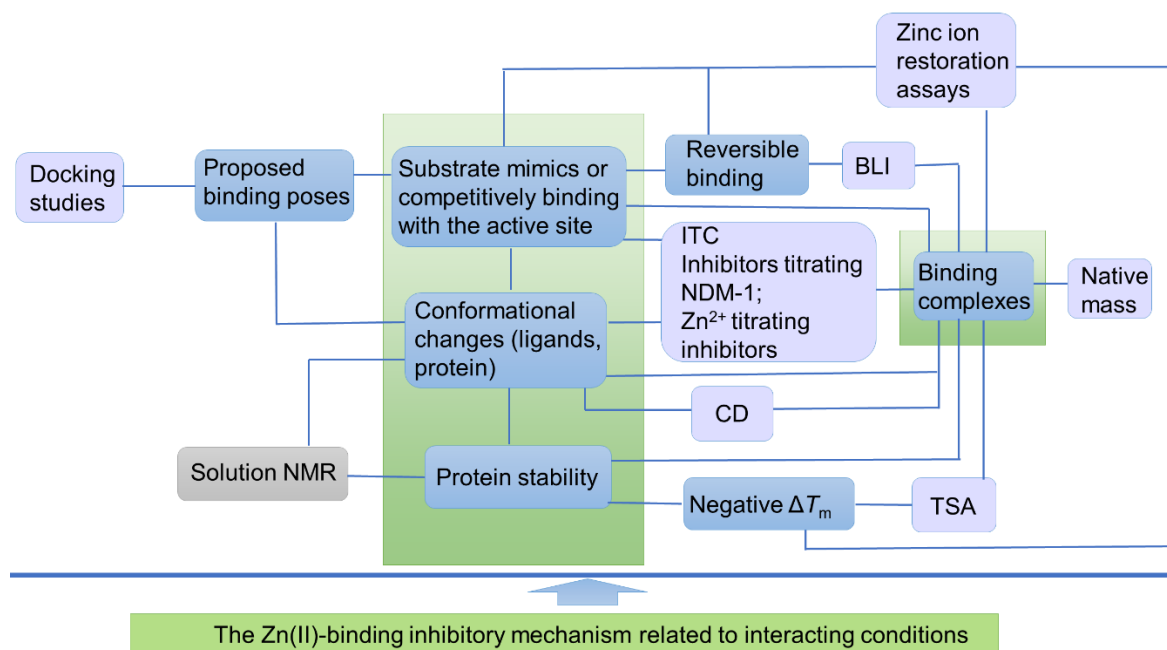


Figure 3.42 The relationship of the different evaluation assays for the interaction studies of the selected inhibitors with NDM-1.

3.4 Specificity studies of DPA, 8-HQA and 8-MSQA derivatives

3.4.1 Other clinically relevant B1 MBLs

The activities of some selected inhibitors were also tested by several other clinically relevant B1 MBLs including Imipenemase-1 (IMP-1), Verona-Integron-Encoded MBL-2 (VIM-2) and German imipenemase-1 (GIM-1) via *in vitro* enzyme-based assays, and nitrocefin was used as the substrate. The IC_{50} values are listed in **Table 3.15**^{f7} and the detailed procedures are depicted in the experiment part. All the selected compounds were potent inhibitors for the utilized B1 MBLs. Compared with **8-HQA** and **8-MSQA(YJh65)**, the developed derivatives of **8-HQA** and **8-MSQA** had improved inhibitory activities for IMP-1, VIM-2 and GIM-1, and the trends were similar as that for NDM-1. The differences of the IC_{50} values for NDM-1, IMP-1, VIM-2 and GIM-1 might be influenced by the assay conditions as well as the characters of each protein. **8-MSQA(YJh65)** and some of its derivatives had better inhibitory activities for NDM-1 and VIM-2 than IMP-1 and GIM-1. According to the docking studies, **8-MSQA** and its derivatives occupied more spaces for binding with the active sites of the proteins than DPA or **8-HQA**, the size as well as other characters of the active sites influenced the proposed binding poses of the ligands.

^{f7} The IC_{50} values of the selected compounds for VIM-2 and GIM-1 were tested by Dr. Christopher Fröhlich via *in vitro* enzyme-based assays.

Table 3.15 IC₅₀ Values of the Selected Compounds for the MBLs

Compound	IC ₅₀ (μM)			
	NDM-1	IMP-1	VIM-2	GIM-1
DPA	7.02 ± 2.64	9.75 ± 0.43	0.45 ± 0.16	15.61 ± 5.6
8-HQA	9.05 ± 0.14	10.32 ± 0.92	0.61 ± 0.24	7.38 ± 3.7
58 (YJh34)	0.54 ± 0.09	0.48 ± 0.03	0.16 ± 0.02	1.26 ± 0.15
8-MSQA (YJh65)	1.64 ± 0.31	7.27 ± 1.14	0.79 ± 0.23	50.06 ± 20
63 (YJh14)	11.19 ± 1.06	25.16 ± 2.75	-	-
45 (YJh2)	7.16 ± 0.56	101.64 ± 4.33	-	-
71 (YJh84)	0.71 ± 0.04	1.22 ± 0.05	0.43 ± 0.21	3.07 ± 0.88
83 (YJh174)	0.29 ± 0.02	0.37 ± 0.08	0.24 ± 0.14	0.65 ± 0.12
75 (YJh110)	0.37 ± 0.06	0.24 ± 0.09	0.38 ± 0.26	1.50 ± 0.21
88 (YJh159)	1.01 ± 0.01	8.11 ± 1.03	0.47 ± 0.16	21.09 ± 14
87 (YJh169)	0.95 ± 0.04	5.23 ± 1.12	0.47 ± 0.18	11.21 ± 4.6
94 (YJh182)	0.23 ± 0.01	0.25 ± 0.02	0.61 ± 0.23	0.49 ± 0.10
87 (YJh196)	0.21 ± 0.02	0.69 ± 0.12	0.40 ± 0.10	0.65 ± 0.20

^aCompounds **63**(YJh14) and **45**(YJh2) did not have good solubilities at high concentrations in the assay buffers, **87**(YJh169) precipitated in DMSO at high concentrations, so their IC₅₀ values might be influenced.

'-' means 'did not test'.

NDM-1, IMP-1, VIM-2 and GIM-1 all belong to B1 MBLs occupying the typical αβ/βα architecture of MBLs, the alignment of their crystal structures is shown in **Figure 3.43**. As for the active sites, the main differences were from loop 3, loop 10, and the distances of the two Zn(II) ions. Compared with NDM-1, the loop 3 of GIM-1 was a little further away from the Zn(II) ions, and its loop 10 was closer to the Zn(II) ions. Both loop 3 and loop 10 were closer to the Zn(II) ions for IMP-1 and VIM-2 than for NDM-1, and for IMP-1 they were more closer. Thus, IMP-1 and VIM-2 had relatively smaller active pockets than NDM-1. For the Zn(II) ions, the distance between the two Zn(II) ions of NDM-1 was farther than others.

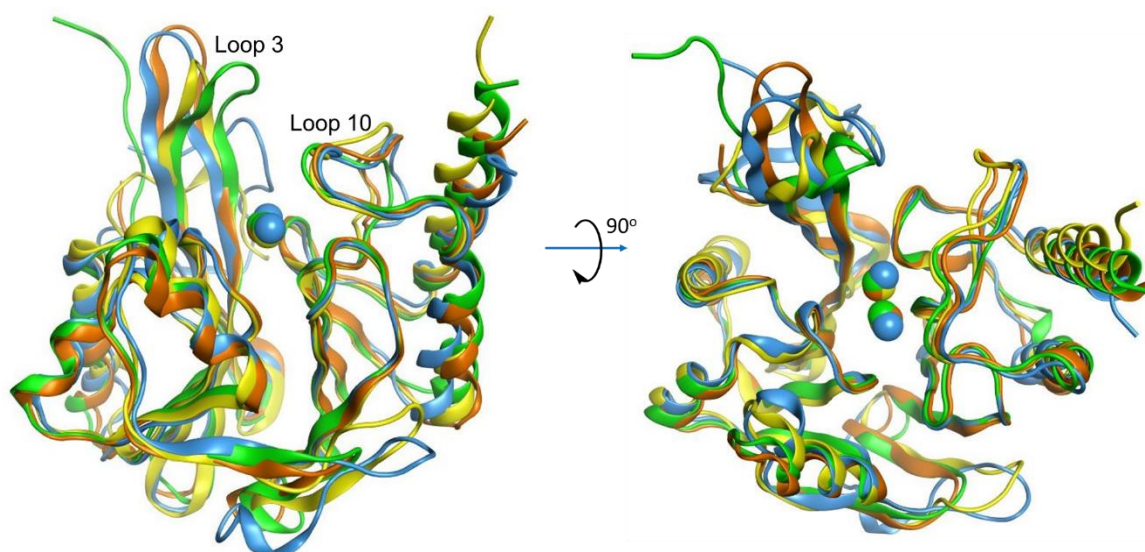


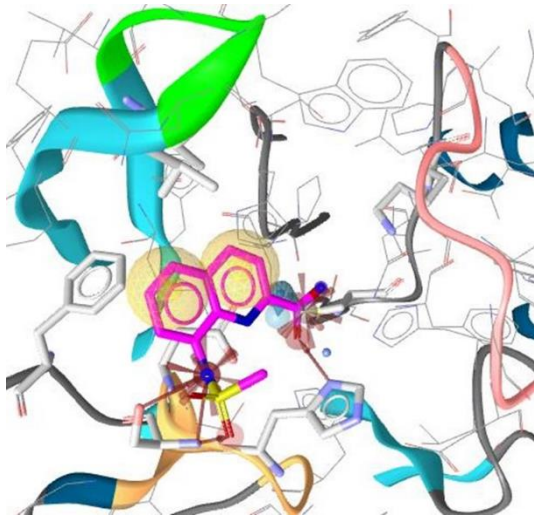
Figure 3.43 Alignment of relevant B1 MBLs. The crystal structures of the proteins were downloaded from the PDB database. The alignment was generated by Molecular Operating Environment (MOE) version 2020.09.01. NDM-1 (5ZGR) was colored in marine blue, IMP-1 (5EV6) was colored in green, VIM-2 (4BZ3) was colored in yellow, and GIM-1 (2YNW) was colored in orange.

Docking studies about the selected compounds with IMP-1, VIM-2 and GIM-1 were also performed. The representative proposed binding poses of **8-MSQA** in the active sites of IMP-1, VIM-2 and GIM-1 are listed in **Figure 3.44**. In general, the fitness scores of the proposed binding poses of **8-MSQA** for NDM-1, IMP-1 and VIM-2 were higher than that for GIM-1. For NDM-1, the hydrophobic interactions of **8-MSQA** with loop 3 played important roles. For IMP-1 and VIM-2, the hydrophobic interactions with both loop 3 and loop 10 were essential for the binding poses of **8-MSQA** in the active site, as the smaller binding pockets contributed by the closer distances with Zn(II) ions of their loop 3 and loop 10. For **GIM-1**, as its loop 3 was further away from the Zn(II) ions, the hydrophobic interactions as well as other H-bond or ionizable interactions were mainly from other loops, especially the closer loop 10. The closer loop 10 of IMP-1, VIM-1, and GIM-1 contributed more interactions with the ligands, but also limited the binding poses, especially for the relatively larger substituted 8-sulfonamide groups, coupled with the closer distances between the two Zn(II) ions, the Zn(II) ions preferred to bind with only one of the Zn(II) ion binding moieties, either the 2-carboxyl group related moiety or the substituted 8-sulfonamide related moiety.

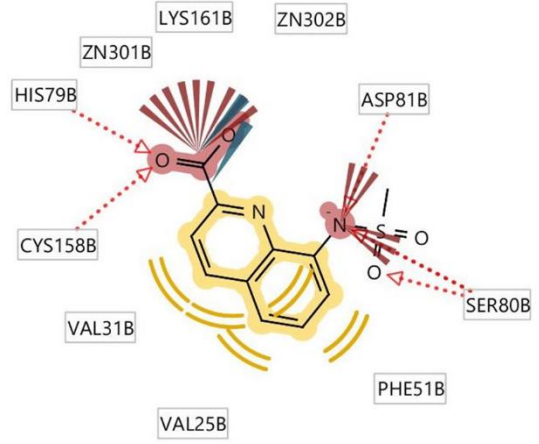
The proposed binding poses of **8-MSQA(YJh65)** in the active site of IMP-1 are shown in **Figure 3.44 a** and **c**. For the proposed binding pose in **Figure 3.44a**, the deprotonated carboxyl group at the 2-position had negative ionizable interactions with the two Zn(II) ions, Lys161, Asn167. The negatively charged nitrogen of the methyl-substituted 8-sulfonamide had negative ionizable interactions with Lys161, Gly166 and His197. There were three H-bond interactions: the oxygens of the deprotonated carboxyl group at the 2-position with Lys161, Asn167 and the structural water molecule, respectively. The quinoline ring had hydrophobic interactions with Val25, Trp28 and Val31. For another proposed binding poses in **Figure 3.44c**, the carboxyl group at the 2-position and its related moiety acted as the zinc binding location for Zn(II) ion, the deprotonated carboxyl group itself also acted as the zinc binding location for Zn(II) ion and had negative ionizable interactions with the two Zn(II) ions and Lys161. The negatively charged nitrogen of the methyl-substituted 8-sulfonamide had negative ionizable interactions with Ser80 and Asp81. There were five H-bond interactions: one of the oxygens of the deprotonated carboxyl group at the 2-position with His79 and Cys158, one of the oxygens of the methyl-substituted 8-sulfonamide and the negatively charged nitrogen of the methyl-substituted 8-sulfonamide with Ser80. The quinoline ring had hydrophobic interactions with Val25, Val31 and Phe51. The amino acid residues of loop 3 (e.g., Trp28, Val25 and Val31) and loop 10 (e.g., Gly166 and Asn167) played important roles for the interactions with the ligand.

The proposed binding poses of **8-MSQA(YJh65)** in the active site of VIM-2 are shown in **Figure 3.44 e** and **g**. For the proposed binding pose in **Figure 3.44e**, the carboxyl group at the 2-position and its related moiety acted as the zinc binding location for Zn(II) ion. The deprotonated carboxyl group at the 2-position had negative ionizable interactions with the two Zn(II) ions and Asn210. The negatively charged nitrogen of the methyl-substituted 8-sulfonamide had negative ionizable interactions with the two Zn(II) ions and Asp118. There were five H-bond interactions: the oxygens of the deprotonated carboxyl group at the 2-position, the nitrogen of the quinoline ring, the negatively charged nitrogen and one of the oxygens of the methyl-substituted 8-sulfonamide with the structural water molecule, and one

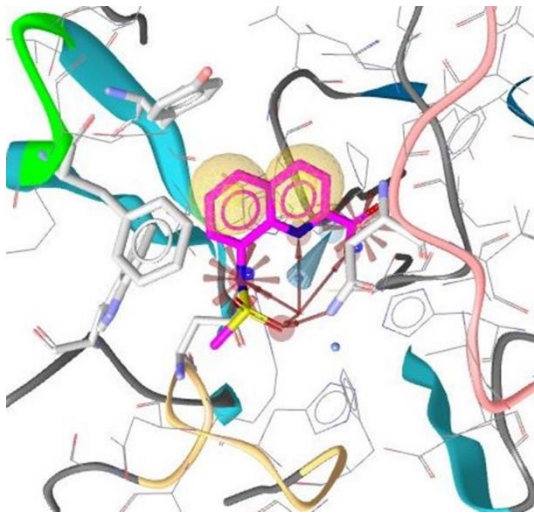
c



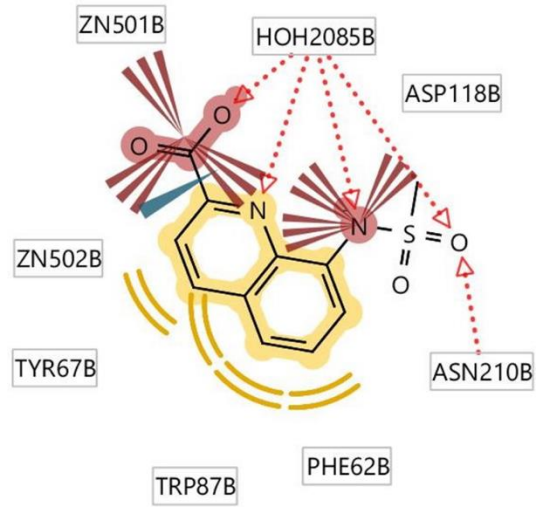
d



e



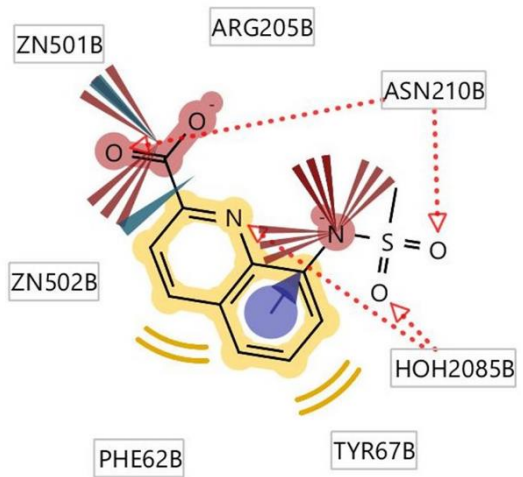
f



g



h



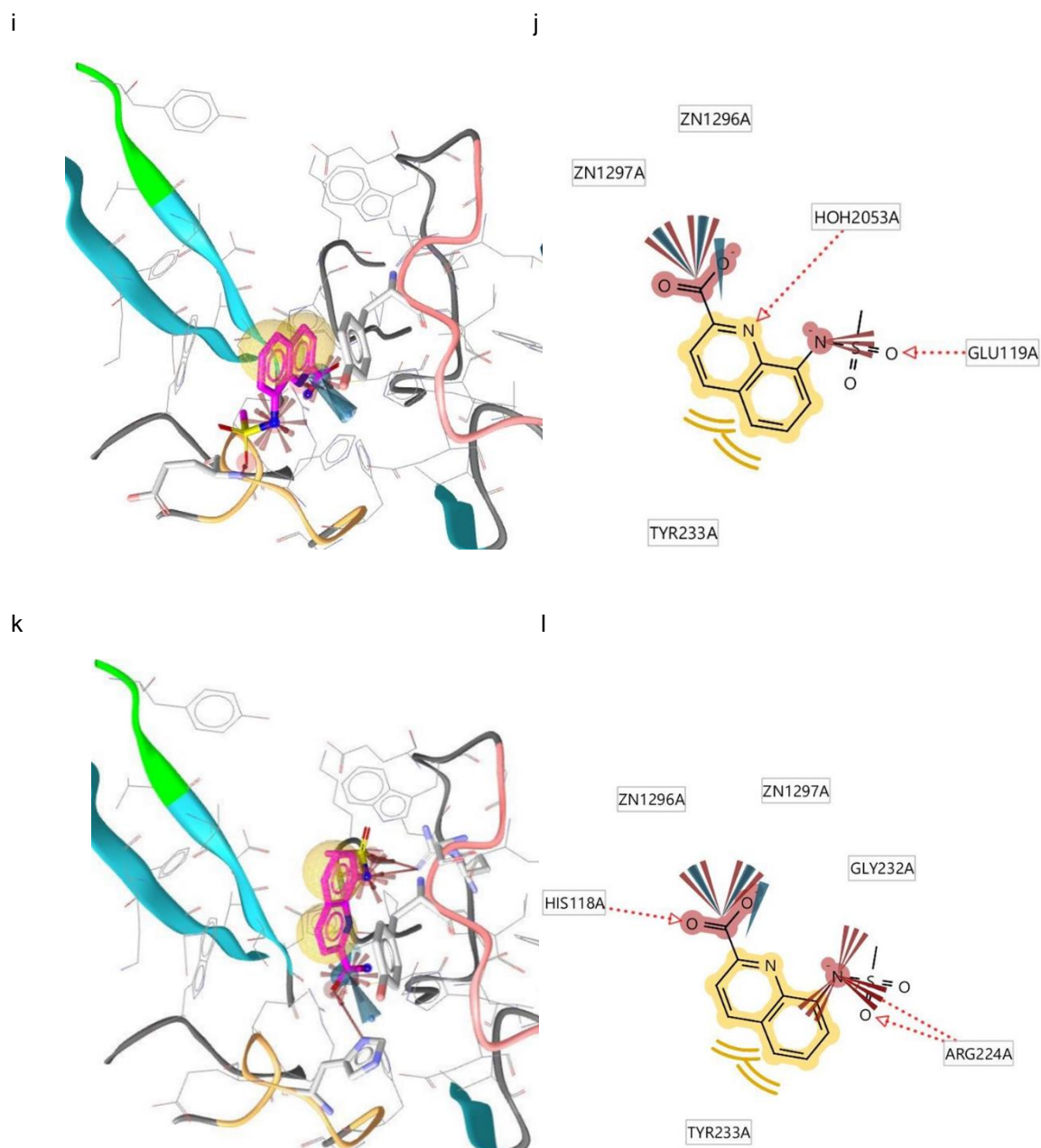


Figure 3.44 Interactions of the proposed binding poses of **8-MSQA** with the active sites of IMP-1 (PDB ID: 5EV6), VIM-2 (PDB ID: 4BZ3), and GIM-1 (PDB ID: 2YNW). The docking studies were performed by Gold 5.8.1 and the results were analyzed by LigandScout 4.2. The loop regions at a similar position as the 'Door' (Met67 to Gly71) of NDM-1 were colored in green, the loop regions at a similar position as the 'Ceiling' (Thr119 to Met126) of NDM-1 were colored in orange and the loop regions at a similar position as the 'Floor' (Ser217 to Asp225) of NDM-1 were colored in pink. The ligands were colored in magenta. The yellow spheres indicated lipophilic contacts, red arrows indicated hydrogen bond acceptor functionalities, blue wedges indicated zinc binding locations, purple rings indicated aromatic interactions, and the red wedges indicated negative ionizable interactions. a. 3D depiction of the interactions for the proposed binding pose of **8-MSQA** with the active site of IMP-1; b. 2D depiction of a; c. 3D depiction of the interactions for the proposed binding pose of **8-MSQA** with the active site of IMP-1; d. 2D depiction of c; e. 3D depiction of the interactions for the proposed binding pose of **8-MSQA**

with the active site of VIM-2; f. 2D depiction of e; g. 3D depiction of the interactions for the proposed binding pose of **8-MSQA** with the active site of VIM-2; h. 2D depiction of g; i. 3D depiction of the interactions for the proposed binding pose of **8-MSQA** with the active site of GIM-1; j. 2D depiction of i; k. 3D depiction of the interactions for the proposed binding pose of **8-MSQA** with the active site of GIM-1; l. 2D depiction of k.

Above all, all the selected inhibitors were identified with strong inhibitory activities for the main clinically relevant B1 MBLs, combined with the results of the microbiological susceptibility tests, especially the clinical bacterial strains which co-expressed many resistance genes including NDM-5, NDM-7, VIM-1, etc., the developed inhibitors might be potential broad-spectrum inhibitors for B1 MBLs.

3.4.2 Other Zn(II) metalloenzymes

3.4.2.1 General structural characters and relevant diseases

The representative compounds were also tested by several commonly disease-related human Zn(II) metalloenzymes including matrix metalloproteinase-2 (MMP-2), histone deacetylase-1 (HDAC-1) and human carbonic anhydrase II (hCAII).²⁶⁴ MMP-2 (or gelatinase A) belonging to MMP family is a zinc-dependent peptidase involved in the degradation of extracellular matrix (ECM) and has played important roles for many pathological processes particularly in cancer, such as tumor growth, angiogenesis, and metastasis.^{264, 265} The full-length pro-MMP-2 (PDB ID: 1CK7) contains 551 residues, two Zn(II) ions and three Ca(II) ions. Except the signal peptide and the propeptide at the amino-terminal domains, the active protein is constituted by the catalytic domain, the hemopexin-like domain, three fibronectin-type domains which are inserted into the sequence of the catalytic domain, and a linker region (connecting the catalytic and hemopexin-like domains). A Cysteine residue of the conserved sequence in the propeptide (Pro100 to Asp106) coordinated the catalytic Zn(II) ion of the catalytic domain by its thiol group, and the interaction needed to be removed to realize the matrix degradation function of MMP-2.²⁶⁴ The Zn(II) ion in the active site of the catalytic domain was bound with His403, His407, and His413 residues, and cooperated with a glutamic acid residue and a water molecular to cleave the relevant peptide substrates.²⁶⁴⁻²⁶⁶ There were another zinc ion and two or three calcium ions for the structure of the catalytic domain.²⁶⁴⁻²⁶⁶ The hydrophobic S1' pocket of MMP-2 was important for its substrate recognition and inhibitor development, and the hydroxamate moiety has been extensively used as a zinc binding group (ZBG) for its inhibitors.^{264, 265, 267}

Histone deacetylases (HDACs) are acted as acyl-lysine “erasers” which are often dysregulated in tumorigenesis, and have been divided into four classes (I, II, III and IV) including 18 HDACs according to their homology with relevant yeast proteins, subcellular locations and enzymatic activities.²⁶⁸⁻²⁷⁰ Class I, II, and IV are zinc-dependent deacetylases, while the catalytic activity of class III (or sirtuins) is nicotinamide adenine dinucleotide-(NAD⁺)-dependent and cannot be inhibited by the conventional HDAC inhibitors (HDACis).^{268, 269} HDACis targeting class I, II, and IV have been used for the development of antitumor agents such as the approved drugs vorinostat (suberoylanilide hydroxamic acid, SAHA) and romidepsin.²⁶⁸ HDAC-1 belongs to class I HDACs, which has been commonly overexpressed in cancers of gastric, breast, colorectal, lung, liver, and Hodgkin lymphoma (HL). The substrates of HDAC-1 include histone substrates as well as nonhistone substrates such as transcription factors p53 and STAT 1/3.²⁶⁸ In general, the acetylation of histones associates with elevated

transcription, while the deacetylation of histones is related to gene repression.²⁶⁸ The knockdown of HDAC-1 resulted in growth arrest, increased apoptosis, decreased viability for some cancer cell lines, but there were also studies supporting the possible tumor suppressor roles of HDAC-1, -2 and -3.²⁶⁸ The impact of class I HDACs should be evaluated at each step of tumorigenesis as their paradoxical roles.²⁶⁸ HDAC-1 formed by around 483 amino acid residues is ubiquitously expressed and localized in the nucleus.²⁶⁹ Eight stranded parallel and one antiparallel β -sheets together with six or three α -helices on either face forms the α/β core of HDAC-1 (PDB ID: 4BKX or 5ICN). Another mainly six to nine α -helices clustering on one side of the α/β core and about seven larger loops together extend the structure of HDAC-1 beyond the α/β core, which results in the deep, narrow tube-like binding pocket and an internal cavity adjacent to the bottom of the pocket.^{269, 271-273} The catalytic Zn(II) ion is at the bottom of the active pocket and has formed a tetrahedral architecture by cooperating with Asp264, Asp176, His 178 and a water molecule.^{269, 271} The water molecule was also linked with His141 which was interacted with Asp174.^{269, 271} There are two potassium ions, one of them is located at site1 near to the Zn(II) ion with a distance of around 7.2 Å which is hexacoordinated with the backbone carbonyl oxygens of Asp174, Asp176, His178, and Phe198, the carboxylate group of Asp174, and the hydroxyl group of Ser197, and the other is located at site2 with a distance of around 19.6 Å to the Zn(II) ion which is tricoordinated with the backbone carbonyl oxygens of Phe187, Val193 and Tyr222.^{269, 272} The two potassium ions were supposed to be structural ions, and absence one of the ions might increase the volume of the tube-like pocket.^{269, 272} The K⁺ at site1 was considered to stabilize the loops and the active pocket, as well as connect with the Zn(II) ion, while the absence of the K⁺ at site2 can cause conformational changes of the protein which might influence the catalytic activity.^{269, 272} The concentration of the K⁺ in the buffer influenced the activity of the protein for *in vitro* assays, and the low concentration of K⁺ supported high activity.^{269, 272} The deacetylation mechanism of HDAC-1 combined the mechanisms for normal metallo and serine proteases.^{271, 272} The water molecule linked by the Zn(II) ion and His141, attacked the carbonyl carbon, which released the acetyl group from the acetylated lysine residue of the substrate.^{271, 272} A tetrahedral transition state of the substrate might be formed by the interactions with the Zn(II) ion and Tyr303.^{271, 272} The His141 connected with the water molecule was acting as the base which was similar as the catalytic process for serine proteases.^{271, 272} The typical non-natural inhibitors for HDAC-1 or some other HDAC isomers such as SAHA have occupied a ZBG to bind with the catalytic Zn(II) ion, a cap region to interact with the entrance of the pocket or relevant adjacent parts, and a linker between the ZBG and the cap region to deliver the ZBG through the tunnel pocket to the Zn(II) ion as well as interact with the wall of the tube-like pocket by hydrophobic interactions. Hydroxamate has been the commonly used ZBG for the inhibitors of HDACs, which might not only bind with the Zn(II) ion but also interacted with the nearby His140 and His141.^{269, 274, 275} There were also some other inhibitors with larger structures and did not have ZBGs which could inhibit the protein by other mechanisms.^{271, 272, 275}

Carbonic Anhydrases (CAs) are ubiquitously expressed in organisms including Archaea, prokaryotes and eukaryotes, which have been divided into different classes (e.g., α -CAs, β -CAs, γ -CAs, etc.) according to the independently distinct gene families, and the CAs in vertebrates are α -CAs based on the reports at present.²⁷⁶⁻²⁸⁰ Human carbonic anhydrase II (hCAII) has been the most studied enzyme of the human CA family, which are zinc-dependent enzymes catalyzing the reversible hydration of CO₂ to yield HCO₃⁻ and H⁺.²⁷⁶ hCAII exists in almost all human cells playing important roles for diverse physiological functions related to respiration and CO₂/HCO₃⁻ transport such as pH regulation, ion transport, secretion of gastric, bone resorption, cerebrospinal fluid secretion, etc.²⁷⁶⁻²⁷⁸ The

dysregulation of CAs has been involved in many pathological processes such as glaucoma, epilepsy, congestive heart failure, gastric and duodenal ulcers, neurological disorders, osteoporosis, and obesity.²⁷⁶ Thus, hCAII as well as other CAs have been the drug targets for treating relevant diseases for a long time, especially glaucoma, obesity, and cancer, and there are approved inhibitors targeting hCAII used for treating relevant diseases, e.g., Acetazolamide, a sulfonamide inhibitor used for the treatment of glaucoma, benign intracranial hypertension, and altitude sickness; Methazolamide with a longer elimination half-life than Acetazolamide and less unfavorable effects related to kidney; Dorzolamide used for the treatment of ocular hypertension or open-angle glaucoma. For the inhibitors targeting hCAII, sulfonamide was the commonly used moiety, which was interacted with the active site by the general ionized form RSO_2NH^- .^{276, 277, 280} hCAII (PDB ID: 3K34, 2VVA or 2VVB) consists of around 260 residues and has the highly conserved polyhedral structure as other CAs.²⁷⁶ A larger twisted architecture constituted by eight antiparallel β -sheets in the central as well as several other β -sheets or turns form the skeleton of the protein, six to eight α -helices are located on the surface of the larger twisted architecture, the catalytic Zn(II) ion is cooperated with His94, His96 and His119 from the middle β -sheets as well as a hydroxide ion or water molecule as the fourth ligand, and most of the larger loops are clustered on the side with the Zn(II) ion. The twisted β -sheets together with two or three short α -helices and several loops form the deep cone-type active pocket, and the Zn(II) ion is located at the bottom. The active pocket could be divided into the hydrophobic and the hydrophilic parts, which has facilitated the conversion of CO_2 to HCO_3^- . The hydration of CO_2 involved the nucleophilic attack by the enzyme-Zn(II)-OH⁻.^{276, 278} At first, the enzyme-Zn(II)-OH⁻ attacked the carbon of the CO_2 forming enzyme-Zn(II)- HCO_3^- . Second, another water molecular attacked the Zn(II) ion with the interactions of the nearby amino acid residues, and the HCO_3^- and H^+ were released.^{276, 278} The second step was the rate-limiting step.^{276, 278} The hydroxide ion or water molecule linked with the Zn(II) ion had H-bond interactions with Thr199, and the later had H-bond interactions with Glu106, which were stabilized the enzyme-Zn(II)-OH⁻. The Thr199 also played important roles for the orientation and polarization of the CO_2 , and the complicated H-bond net formed by the residues of the active pocket also made the active pocket more selective for the CO_2 substrate. The histidine cluster formed by His3, 10, 15, and 17 facilitated the proton transfer, and the flexible protonated-His64 side chain worked as the proton shuttle could rotate maximumly to the exterior surface to release the proton. Except the treatment targets for relevant diseases, the catalytic mechanism of CAs has been also used for relevant catalytic development for chemical reactions, application for carbon capture, etc.^{276, 281} Except the developed inhibitors, such as the sulfonamide compounds, CAs were also inhibited by the metal complexing inorganic anions (e.g., azide, cyanate, thiocyanate etc.). CA activators has also been investigated recently which could be used for the treatment of CA deficiency syndromes, and most of them activated the enzyme by facilitating the proton transfer step.^{276, 277}

3.4.2.2 Activity tests by *in vitro* assays

The assays were performed according to the relevant published literatures. The activity of MMP-2 was monitored via a kinetic assay which measured the increase of the fluorescence intensity upon cleavage of a peptide substrate (OmniMMP).^{133, 282, 283} HDAC-1 can deacetylate the substrate BOC-lys-(ac)-AMC releasing the BOC-lys-AMC. After incubating the protein with the substrate (with or without tested compound) for an appropriate time, a stop solution containing excessive suberoylanilide hydroxamic acid (SAHA) and trypsin was added, then the activity of the HDAC-1 protein was quenched

by the excessive SAHA, and trypsin could selectively cut the deacetylated substrate BOC-lys-AMC releasing the fluorescent AMC moiety. Thus, stronger inhibition by the tested ligands would lead to less deacetylation and less fluorescence intensity.^{133, 282, 284, 285} *p*-Nitrophenyl acetate (pNPA) has high absorbance at 348 nm and can be hydrolyzed to *p*-nitrophenol or *p*-nitrophenolate by hCAII. Therefore, the activity of hCAII could be monitored via the decreased absorbance at 348 nm by using pNPA as the substrate.^{133, 282, 286-294} The IC₅₀ values of the positive controls *N*-([1,1'-biphenyl]-4-ylsulfonyl)-*L*-phenylalanine (*S*-NSA) and *N*-([1,1'-biphenyl]-4-ylsulfonyl)-*D*-phenylalanine (*R*-NSA) for MMP-2, SAHA for HDAC-1, and acetazolamide (AZA) for hCAII were 265.9 nM, 66.07 nM, 70.65 nM, and 46.88 nM, respectively, which were compatible with the relative published literatures.^{282, 284, 286-289, 291} The detailed procedures were depicted in the experiment part and the test results of the selected compounds are listed in **Table 3.16a** and **b**.

Table 3.16a Percent Inhibition of DPA, 8-HQA and 8-MSQA Derivatives (at 10 μ M) against Other Zn(II) Metalloenzymes

Compound	MMP-2	HDAC-1	hCAII
DPA	N	N	N
8-HQA	N	N	N
8-MSQA (YJh65)	93	N	N
29 (YJh67)	N	N	N
45 (YJh2)	N	N	N
58 (YJh34)	N	N	N
61 (YJh59)	20	N	N
63 (YJh14)	5	N	N
71 (YJh84)	97	N	N
75 (YJh110)	97	N	N
83 (YJh174)	78	N	N
86 (YJh113)	94	N	N
87 (YJh169)	91	N	N
88 (YJh159)	90	N	N
89 (YJh125)	95	N	N
94 (YJh182)	70	N	N
95 (YJh196)	76	N	N
98 (YJh184)	34	N	N
L-Captopril	N	N	N
EDTA-Na	23	N	N

^a 'N': no inhibition.

Table 3.16b Comparison of the Activity of the Selected Compounds against MMP-2 and NDM-1

Compound	Structure	K_i or IC_{50} (MMP-2) (μM)	K_i (NDM-1) (μM)	K_i (MMP-2) / K_i (NDM-1)
33 (YJh65 or 8-MSQA)		4.08 ± 0.37	0.82 ± 0.16	4.98
71 (YJh84)		2.12 ± 0.14	0.36 ± 0.02	5.97
72 (YJh101)		2.27 ± 0.31	0.38 ± 0.05	6.05
75 (YJh110)		0.6 ± 0.04	0.19 ± 0.03	3.24
74 (YJh119)		20.73 ± 2.9	0.42 ± 0.03	49.95
83 (YJh174)		5.78 ± 1.19	0.15 ± 0.01	39.86
94 (YJh182)		6.92 ± 1.59	0.12 ± 0.01	60.17
95 (YJh196)		7.75 ± 0.86	0.11 ± 0.01	73.81
98 (YJh184)		27.63 ± 3.94	0.21 ± 0.02	134.78

^a The final concentration of the substrate used for MMP-2 assays was $4 \mu\text{M}$, which was much less than the K_m value (ca. $57.22 \mu\text{M}$), according to the Cheng-Prusoff equation, the K_i and IC_{50} values were quite similar, thus the obtained IC_{50} values were used for MMP-2 assays to represent the K_i values. The K_i values of NDM-1 were calculated from the relative IC_{50} values by using the equation $K_i = IC_{50}/(1 + [S]/K_m)$.

All the tested compounds did not show any inhibitory activity for HDAC-1 and hCAII at the concentration of $10 \mu\text{M}$, while at this concentration the activity of NDM-1 was completely inhibited by most of the selected compounds, even for **DPA** and **8-HQA**, more than 50% activity of NDM-1 was inhibited. For **8-HQA** derivatives, there was no significant inhibition, especially compounds **58**(YJh34) and **29**(YJh67) did not show any inhibitory activity for each of the tested protein, compound **61**(YJh59)

showed 20% inhibition against MMP-2 but considering its high activity for NDM-1, there should be no significant off-target effect. Some **8-MSQA** derivatives showed inhibitory activity for MMP-2, thus the K_i values were further compared (**Table 3.16b**) and the results correlated with docking studies. According to the proposed binding poses of the positive controls *S*-NSA or *R*-NSA as well as other tested **8-MSQA** derivatives in the active site of MMP-2 (**Figure S14** in the appendices), the substituted-sulfonamide groups might have interactions with the hydrophobic S1' pocket of MMP-2. The size and polarity of the substituent of the sulfonamide moiety influenced the interacting conformations of the ligand, which contributed differently for the interactions with the S1' pocket. For the positive controls *S*-NSA or *R*-NSA (**Figure S14 a** and **b** in the appendices), their biphenyl groups could go inside the S1' pocket and have more hydrophobic interactions with the S1' pocket, the configuration advantages of *R*-NSA allowed it to have more H-bond interactions with nearby loops, and the activity tests also showed that *R*-NSA ($IC_{50} = 66.07$ nM) was more active than *S*-NSA ($IC_{50} = 265.9$ nM). The proposed binding poses of **MSQA** derivatives had significantly reduced interactions with the S1' pocket (**Figure S14 c** and **d** in the appendices), the polar groups such as the 2-carboxyl and the substituted-sulfonamide groups might influence the interactions, as a result, their activities for MMP-2 were drastically reduced compared with the positive controls. The inhibitory activity of **8-MSQA** for NDM-1 ($K_i = 0.82$ μ M) was around 5 times that of MMP-2 ($K_i =$ ca. 4.08 μ M). The K_i values of the phenyl-substituted compound **71(YJh84)** and compound **72(YJh101)** with substituted-phenyl group for NDM-1 were 0.36 μ M and 0.38 μ M, respectively, and around 2.12 μ M and 2.27 μ M for MMP-2, respectively, the ratios of their K_i values for NDM-1 and MMP-2 were 5.97 and 6.05 , respectively, which were improved a little compared with **8-MSQA**. While for compound **75(YJh110)**, its K_i values for NDM-1 and MMP-2 were 0.19 μ M and 0.6 μ M, respectively, and the ratio was reduced to 3.24 . Surprisingly, the pyridyl-substituted compound **83(YJh174)** had highly improved inhibitory activity for NDM-1 ($K_i = 0.15$ μ M) but reduced inhibitory activity for MMP-2 ($K_i =$ ca. 5.78 μ M), thus the ratio of the K_i values for NDM-1 and MMP-2 were increased to 39.86 . Compounds **94(YJh182)** and **95(YJh196)** with phenyl group at the 4- or 5-positions had even better selectivity for NDM-1 than compound **83(YJh174)**, which had K_i values of 0.12 μ M and 0.11 μ M, respectively, for NDM-1, and around 6.92 μ M and 7.75 μ M, respectively, for MMP-2, and their ratios of the K_i values for NDM-1 and MMP-2 were increased to 60.17 and 73.81 . According to docking studies (**Figure S14 e** in the appendices), except the two main type binding poses as **8-MSQA**, compound **83(YJh174)** had another type binding poses, which the pyridine-2-sulfonamide acted as the Zn(II) binding moiety for MMP-2. The different Zn(II) binding moieties might have different effects on the inhibitory activity. For compounds **94(YJh182)** and **95(YJh196)** (**Figure S14 f** and **g** in the appendices), the binding poses which the pyridine-2-sulfonamide acted as the Zn(II) binding moiety had even higher fitness scores. Considering the substituent with larger size of the substituted-sulfonamide part could bring more hindrance for binding with the S1' pocket of MMP-2 and more hydrophobic interactions with the active site of NDM-1, compound **74(YJh119)** was synthesized and tested, the inhibitory activity was improved for NDM-1 ($K_i = 0.42$ μ M) compared with **8-MSQA** but highly reduced for MMP-2 ($K_i = 20.73$ μ M), and the ratio of the K_i values for NDM-1 and MMP-2 were increased to 49.95 . The quinolyl-substituted strategy used for compound **74(YJh119)** offered more choices for the inhibitor development of NDM-1 with high selectivity. Inspired by compound **74(YJh119)**, compound **98(YJh184)** was also tested. Compared with compound **72(YJh101)**, compound **98(YJh184)** arranged the substituted-sulfonamide moiety into a more active conformation for binding with the active site of NDM-1 by linking the substituted-phenyl group of the sulfonamide moiety to the 7-position of the quinoline ring, but the fixed substituted-phenyl group could not bind with the S1' pocket of MMP-2

anymore. The K_i values of compound **98(YJh184)** for NDM-1 and MMP-2 was 0.21 μM and ca. 27.63 μM , respectively, and the ratio of the K_i values for NDM-1 and MMP-2 were 134.78. The docking studies also showed that the fixed substituent or the larger substituent of the substituted-sulfonamide groups had less or no interactions with the S1' pocket for compounds **74(YJh119)** and **98(YJh184)** (Figure S14 h and i in the appendices). According to the activity for MMP-2 of the tested **8-MSQA** inhibitors, the size, polarity, flexibility, and the adjacent positions of the substituent of the sulfonamide moiety played the key roles for the selectivity, and the substituents at 4- and 5-positions might also influence the selectivity. The strategies used for compound **98(YJh184)**, **74(YJh119)** and the top active compounds such as compounds **83(YJh174)**, **94(YJh182)** and **95(YJh196)** could be combined to develop other diverse inhibitors with high activity and selectivity for NDM-1 (Figure 3.45).

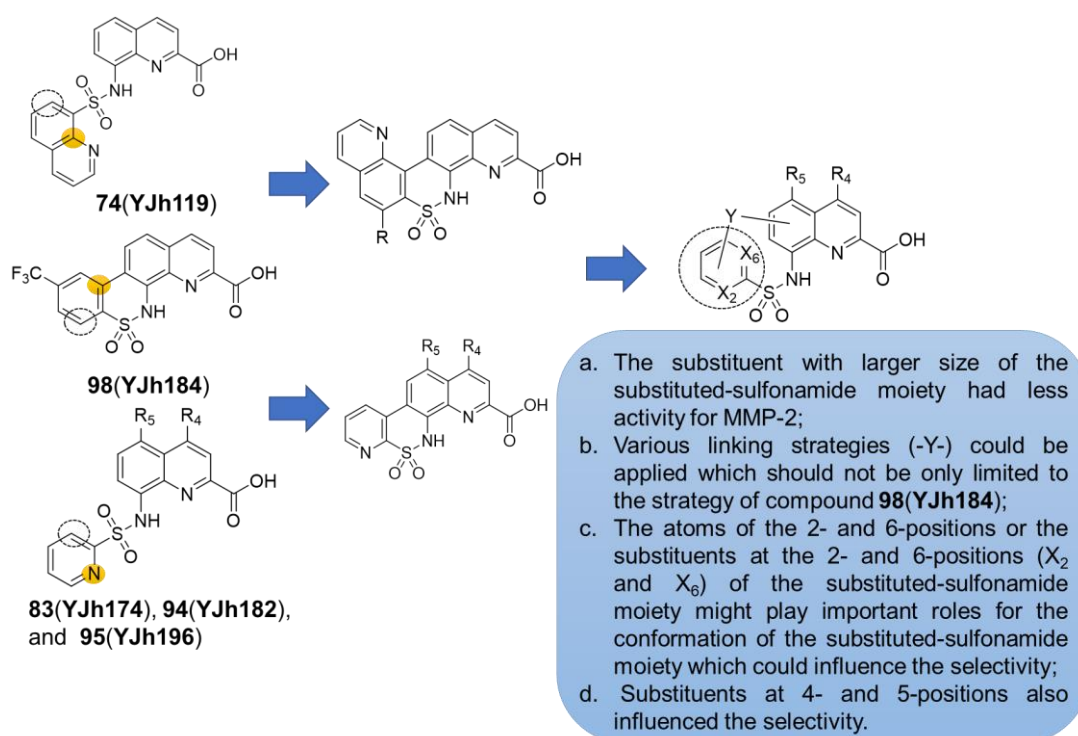


Figure 3.45 Structure and selectivity relationship of the inhibitors for NDM-1 and MMP-2.

Above all, all the tested inhibitors had higher selectivity for NDM-1 than the tested metalloenzymes. The deep, narrow, and tube-like active pocket of HDAC-1 was naturally designed for its substrate acyl-lysine residue, which limited the entrance of the DPA and quinoline derivatives with relative larger size than the typical HDAC inhibitors such as SAHA. Besides, the catalytic Zn(II) ion was located at the bottom of the pocket, slim ZBGs such as hydroxamic acid and linkers with proper length were preferred for the inhibitors of HDAC-1. For hCAII, the catalytic Zn(II) ion was located at the bottom of the cone-type active pocket, the gradually smaller volume from the entrance to the Zn(II) ion hindered the DPA or quinoline derivatives which need excel the binding affinity with the Zn(II) ion by the binding moieties including at least the nitrogen of the aromatic ring and 2- or 6-COOH of DPA (2-COOH, 8-OH or the substituted-sulfonamide of the quinoline derivatives). In addition, the complicated H-bond net, as well as the specifically divided hydrophobic and hydrophilic parts of the active pocket for hCAII facilitated the CO_2 binding but avoided the tested DPA and quinoline derivatives. The active pocket of MMP-2 was

broader which was sufficient for its larger substrates *in vivo* as well as other larger molecules. Except for the catalytic Zn(II) ion, the catalytic domain of MMP-2 also occupied another structural Zn(II) ion, which also could be the possible binding sites for Zn(II)-binding inhibitors. In addition, the MMP-2 protein used for the *in vitro* activity test was not the intact protein, which did not contain the hemopexin-like domains. The *in vivo* natural substrates should have higher binding affinity with the intact protein as full interactions with the whole protein would be involved, which might be stronger than the partial interactions of the smaller inhibitors. Thus, there were more factors which need be considered. Although most of the tested **8-MSQA** derivatives showed more or less inhibitory activity for MMP-2, they all had stronger binding affinity with NDM-1, especially the top active compounds **94(YJh182)** and **95(YJh196)**, the ratios of the K_i values for NDM-1 and MMP-2 were more than 60 or 70. In addition, compound **74(YJh119)** with quinolyl-substituted sulfonamide moiety had obviously reduced activity for MMP-2, which offered more choices for the development of inhibitors for NDM-1. More significantly, the ratio of the K_i values of compound **98(YJh184)** for NDM-1 and MMP-2 were more than 130. The key functions of the size, flexibility, and the adjacent positions of the substituent of the sulfonamide moiety were highlighted as well as the substituents at the 4- and 5-positions of the quinoline ring, the strategy of linking the substituted group of the sulfonamide part with the quinoline ring such as compound **98(YJh184)** could be applied by combining with the top active compounds such as **83(YJh174)**, **94(YJh182)** and **95(YJh196)** as well as compound **74(YJh119)** or other inhibitors for NDM-1 in the future.

3.5 Microbiological susceptibility tests

To investigate the inhibitory activity of the inhibitors at cell level, four transconjugants and eight clinical isolates from the strain collection of the Robert Koch Institute were used for the broth microdilution assays. The transconjugants were NDM-1 producing *E. coli* strains. The clinical isolates including five *Klebsiella pneumoniae* strains, two *Escherichia coli* strains and one *Acinetobacter baumannii* strains produced carbapenemases NDM-1 (n=4), NDM-1+OXA-48 (n=1), NDM-5 (n=1), NDM-7 (n=1) and VIM-1 (n=1). All clinical isolates and two transconjugants harboured further beta-lactamase genes, e.g., *bla*_{OXA-1, -2, -9, -10, and -64}, *bla*_{TEM-1}, *bla*_{SHV-1, -11, and -28}, *bla*_{CTX-M-14 and -15} and *bla*_{CMY-4, -2, and -2like}. The effects of the selected compounds were tested both alone and combined with meropenem for all the strains.^{f8} The synergistic activities of **8-MSQA(YJh65)** with meropenem for resistant isolates were significant and there were no growth influences by the inhibitor alone for both the NDM-1-producing *E. coli* clones and the clinical resistant bacterial strains at the tested concentrations (10.65 mg/L and 21.3 mg/L) (**Table. 3.17**). For compounds **94(YJh182)**, **95(YJh196)** and **83(YJh174)**, the tested concentrations were 12 mg/L and 21.3 mg/L. Obvious reductions of the MICs of meropenem were found for all the tested strains (**Table. 3.17**), the MICs of meropenem were brought back to susceptible range (MIC < 8 mg/L) for most bacterial isolates (even the strain *K. pneumoniae*-ST23 213/19 which contained *bla*_{OXA-48}, a resistance gene of serine carbapenemases, the MICs were back to 16 mg/L.). Compared the MICs determined with the selected compounds at different concentrations, there were dose-related increases of the susceptibility.

^{f8} Dr. Pfeifer Yvonne helped to test the activity of the selected compounds by the broth microdilution assays.

Chloroxine (compound **52**, 5,7-dichloroquinolin-8-ol), has bacteriostatic (e.g., *Streptococcus*, *Staphylococcus*), fungistatic and antiprotozoal activities and is an approved drug which is mainly used for the treatment of seborrheic dermatitis, dandruff, disorder of intestinal microflora, infectious diarrhea, inflammatory bowel disease and giardiasis.²⁰⁸ Chloroxine showed high inhibitory activity for NDM-1 by enzyme-based *in vitro* activity test, its inhibitory activity was also tested by the antimicrobial susceptibility assays. Chloroxine had growth influences for all the NDM-1-producing *E. coli* clones. For clinical bacterial isolates, either chloroxine had bacteriostatic activities by itself or highly reduced the MICs of meropenem by synergistic effects and the growth influences for the controls should come from the antibacterial activity of chloroxine itself. Except strains *K. pneumoniae*-ST14 93/10, *K. pneumoniae*-ST23 213/19 and the strains showed growth influences by using chloroxine alone, the MICs of meropenem were reduced to susceptible range (MIC < 8 mg/L) for other tested strains with the synergistic use of chloroxine at the concentrations of 5.03 mg/L and 10.06 mg/L, and there were also dose-related increases of the susceptibility.

In addition, the clinical bacterial strains co-expressed many other resistance genes, such as genes for NDM-5, NDM-7, VIM-1, etc., which suggested that the **8-MSQA** derivatives might be potential broad-spectrum inhibitors. Compared with NDM-1, other NDM variants had the similar hydrolyzing activity but with improved stability for the zinc scarcity conditions.^{85, 89} Their T_m values were significantly higher than the T_m value of NDM-1, such as NDM-5 and NDM-7 with the T_m values nearly 8 °C and 7 °C higher than NDM-1, respectively.^{85, 89} Thus, except the ability of competitively binding with the active pocket, the destabilizing functions of the **8-MSQA** derivatives provided their advantages to efficiently overcome the other NDM variants. As for strain *K. pneumoniae*-ST23 213/19 which contained *bla*_{OXA-48}, the MIC was also reduced but not as much as other strains. Whether the developed inhibitors had inhibitory activity for serine carbapenemases such as OXA-48 was not sure, which could be investigated in the future.

Above all, the selected inhibitors of **8-MSQA** derivatives significantly reduced the MICs of meropenem for both the NDM-1-producing *E. coli* transconjugants and the clinical strains co-expressing NDM-1 at lower concentrations compared with most reported inhibitors, which realized the initial aims of the project not only improving the inhibitory activity and specificity of the DPA type inhibitors for the target protein but also their activity at the cell level assays. The inhibitory activity for bacterial strains of chloroxine as well as **8-MSQA** derivatives without 2-COOH could be further investigated which might offer new clues for antibiotic development. Given the co-expressed other resistance genes of the clinical bacterial strains and the *in vitro* activity test for other MBLs, the developed inhibitors might be potential broad-spectrum inhibitors for MBLs. Compared the high effects at both enzyme-based and cell-based assays and less toxicity, the developed inhibitors were a potent type of Zn(II)-binding inhibitors targeting NDM-1.

Table 3.17a Potentiation of Meropenem Activity against NDM-1-producing *E. coli* Transconjugants by the Selected Compounds

Bacterial Strain	Genotype (β -lactamase)	MIC (mg/L)					
		MEM	MEM + YJh65 (10.65/21.3 mg/L) (40/80 μ M)	MEM + YJh182 (12/24 mg/L) (29.60/59.20 μ M)	MEM + YJh196 (12/24 mg/L) (29.60/59.20 μ M)	MEM + YJh174 (12/24 mg/L) (36.44/72.88 μ M)	MEM + chloroxine (5.03/10.06 mg/L) (23.5/47 μ M)
<i>E. coli</i> K12 J53 – ST10 684/18	<i>bla</i> _{NDM-1} ; <i>bla</i> _{CMY-2} ; <i>bla</i> _{OXA-10}	64	$\leq 0.125/\leq 0.125$	0.25/ ≤ 0.125	0.5/ ≤ 0.125	$\leq 0.125/\leq 0.125^a$	$\leq 0.125^a/\leq 0.125^a$
<i>E. coli</i> K12 J53 – ST10 696/17	<i>bla</i> _{NDM-1} ; <i>bla</i> _{CMY-4}	16	$\leq 0.125/\leq 0.125$	$\leq 0.125^a/\leq 0.125$	0.25/ ≤ 0.125	$\leq 0.125/\leq 0.125^a$	$\leq 0.125^a/\leq 0.125^a$
<i>E. coli</i> K12 J53 – ST10 618/15	<i>bla</i> _{NDM-1}	32	$\leq 0.125/\leq 0.125$	$\leq 0.125^a/\leq 0.125$	$\leq 0.125^a/\leq 0.125$	$\leq 0.125/\leq 0.125^a$	$\leq 0.125^a/\leq 0.125^a$
<i>E. coli</i> K12 J53 – ST10 699/15	<i>bla</i> _{NDM-1}	32	$\leq 0.125/\leq 0.125$	1/ ≤ 0.125	1/ ≤ 0.125	0.5/ $\leq 0.125^a$	$\leq 0.125^a/\leq 0.125^a$

^a There were growth influences by using the inhibitors alone.

Table 3.17b Potentiation of Meropenem Activity against MBL-producing Clinical Strains by the Selected Compounds

Bacterial Strain	Genotype (β -lactamase)	MIC (mg/L)					
		MEM	MEM + YJh65 (10.65/21.3 mg/L) (40/80 μ M)	MEM + YJh182 (12/24 mg/L) (29.60/59.20 μ M)	MEM + YJh196 (12/24 mg/L) (29.60/59.20 μ M)	MEM + YJh174 (12/24 mg/L) (36.44/72.88 μ M)	MEM + chloroxine (5.03/10.06 mg/L) (23.5/47 μ M)
<i>A. baumannii</i> -IC6 19/09	<i>bla</i> _{NDM-1} ; <i>bla</i> _{OXA-64}	>128	4 (8)/2	8 (16) /1 (2)	16/1	4/1	$\leq 0.125^a/\leq 0.125^a$
<i>E. coli</i> -ST101 2/10	<i>bla</i> _{NDM-1} ; <i>bla</i> _{TEM-1} ; <i>bla</i> _{CTX-M-15} ; <i>bla</i> _{OXA-1} ; <i>bla</i> _{OXA-2}	128	$\leq 0.125/\leq 0.125$	1/ $\leq 0.125^a$	0.5/ ≤ 0.125	$\leq 0.125/\leq 0.125^a$	$\leq 0.125^a/\leq 0.125^a$
<i>K. pneumoniae</i> - ST14 93/10	<i>bla</i> _{NDM-1} ; <i>bla</i> _{CMY-2like} ; <i>bla</i> _{TEM-1} ; <i>bla</i> _{CTX-M-15} ; <i>bla</i> _{SHV-28} ; <i>bla</i> _{OXA-1} ; <i>bla</i> _{OXA-9}	128	4/2	4 (8) /1 (2)	4/1	2/1	128/16
<i>K. pneumoniae</i> 50/11	<i>bla</i> _{NDM-1} ; <i>bla</i> _{TEM-1} ; <i>bla</i> _{SHV-28} ; <i>bla</i> _{CTX-M-15} ; <i>bla</i> _{OXA-1}	64	$\leq 0.125/\leq 0.125$	0.5/ $\leq 0.125^a$	0.5/0.25	$\leq 0.125/\leq 0.125^a$	4/ $\leq 0.125^a$
<i>K. pneumoniae</i> 50/20	<i>bla</i> _{NDM-5} ; <i>bla</i> _{TEM-1} ; <i>bla</i> _{SHV-1}	64	$\leq 0.125/\leq 0.125$	2/ $\leq 0.125^a$	2/ ≤ 0.125	0.5/ ≤ 0.125	4/ $\leq 0.125^a$
<i>E. coli</i> 371/12	<i>bla</i> _{NDM-7} ; <i>bla</i> _{CTX-M-15} ; <i>bla</i> _{OXA-1}	128	2/0.25	32/ $\leq 0.125^a$	32/ ≤ 0.125	8/ ≤ 0.125	$\leq 0.125^a/\leq 0.125^a$
<i>K. pneumoniae</i> - ST23 213/19	<i>bla</i> _{NDM-1} ; <i>bla</i> _{OXA-48} ; <i>bla</i> _{SHV-11} ; <i>bla</i> _{CTX-M-15} ; <i>bla</i> _{OXA-1}	>128	16/16	32/16	16/16	16/16	128/16
<i>K. pneumoniae</i> 62/07	<i>bla</i> _{VIM-1} ; <i>bla</i> _{SHV-1} ; <i>bla</i> _{CTX-M-14} ; <i>bla</i> _{CMY-4}	128	1/0.5	8/0.5	8/0.25	2/0.25	8/ $\leq 0.125^a$

^a There were growth influences by using the inhibitors alone.

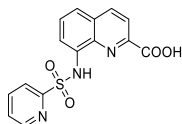
3.6 Alamar blue assays

The effects on the proliferation or viability for human cells of the representative compounds were determined by Alamar Blue assays, by which the generation of reducing equivalents such as NADH was quantified in cells as a measurement for the activity of cellular metabolism and proliferation. HEK293 cells were used for the assays.^{295, 296} Compared with chloroxine (compound **52**, the 5,7-Dichloro quinolin-8-ol), an approved drug for the treatment of seborrheic dermatitis, dandruff, disorder of intestinal microflora, infectious diarrhea, inflammatory bowel disease and giardiasis,²⁰⁸ all the selected compounds had less effects on the proliferation or viability of HEK293 cells. In addition, the high activity of the microbiological susceptibility testing for the **8-MSQA** derivatives demonstrated that the **8-MSQA** derivatives were potent inhibitors for NDM-1 with less influence on the proliferation or viability of HEK293 cells.

Table 3.18 Effects of Representative Inhibitors on the Proliferation and Viability of HEK293 Cells

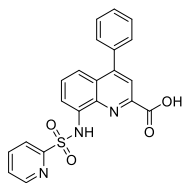
Compound	Structure	EC ₅₀ (μM) 12h/24h
DPA		>400 (ca. 4000)/>400 (ca. 4000)
45(YJh2)		336.9 ± 118.6 /340.9 ± 125.6
8-HQA		>400 (ca. 1190)/>400 (ca. 1176)
61(YJh59)		801.5 ± 187.6/622.6 ± 80.05
52(Chloroxine)		238.1 ± 48.9/49.14 ± 4.37
8-MSQA(YJh65)		900.5 ± 144.9/1151 ± 249.9

83(YJh174)



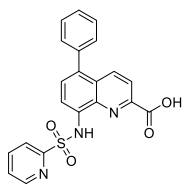
2903 ± 1164/1274 ± 263.85

94(YJh182)



696.2 ± 110.45/344.3 ± 43.73

95(YJh196)



>800/559.1 ± 84.6

^a For DPA and **8-HQA**, there were nearly no effects on the proliferation and viability of the cells at 400 μ M. For compounds **83(YJh174)** and **95(YJh196)**, there were less or no effects on the proliferation and viability of the cells at 1000 μ M and 800 μ M, respectively, when the incubating time was 12 h.

4 Conclusion and outlook

Fragment-based drug discovery (FBDD) strategy was applied to find the initial hit DPA, with reasonable modifications according to the gradually obtained SAR and docking studies, DPA, **8-HQA**, and **8-MSQA** derivatives were developed. The top active compounds **94(YJh182)** and **95(YJh196)** with the 4- or 5-phenyl groups had improved inhibitory activity and binding affinity for NDM-1, which interacted with the target protein by forming stable protein-inhibitor complexes. Both the top active inhibitors and some other representative compounds can reduce the thermal stability of NDM-1, and their highly inhibitory activities for several other clinically relevant B1 MBLs were also identified. The tested inhibitors from **8-MSQA** derivatives all can obviously reduce the MICs of meropenem for both the NDM-1-producing *E. coli* transconjugants and the clinical resistant bacterial strains co-expressing NDM-1. The selectivity of the representative inhibitors was also tested by several other Zn(II) metalloenzymes and there were no or little effects on the proliferation or viability for HEK293 cells of the representative inhibitors. The general results and achievements were concluded as follows.

At first, both the cell-based and enzyme-based screening assays were formed according to published works. Through the enzyme-based screenings for both the carboxylic acid and amine libraries, the initial hit DPA with an IC_{50} value of 7 μ M was discovered. The **8-HQA** scaffold was identified by testing a panel of designed DPA analogues. With a further screening of the developed quinoline analogues, an initial structure activity relationship was obtained about the important roles played by the nitrogen atom and carboxyl groups of the pyridine ring as well as the 2- and 8-positions of the quinoline scaffold. Through the screenings and the optimizing processes for both DPA and **8-HQA** derivatives, the necessity of an acidic group at the 8-position was realized (the acidic groups might be negatively charged when they were interacting with the active site of the protein), **8-MSQA** was deduced by increasing the acidity of the 8-NH₂ of the inactive 8-amino quinoline containing structures.

Second, based on the results of the fragment screenings and the primary SAR supported by docking studies, DPA, **8-HQA** and **8-MSQA** derivatives were designed and synthesized with reasonable modifications. The *N*-(alkoxy)amide groups could replace the carboxyl groups of DPA, the halogen-substitution at the 5- and 7-positions improved the inhibitory activity for 8-quinolin-ol derivatives, substituents such as aromatic rings with high electronic withdrawing groups of the substituted 8-sulfonamide moiety increased the binding affinity of the **8-MSQA** derivatives with the protein. Both the 2- and 8-positions were important for the activity of the quinoline based inhibitors. The substitution by halogen, phenyl, or some substituted-phenyl groups at the 4- or 5-positions of the **8-MSQA** derivatives, improved the specificities of the inhibitors for the active pocket of NDM-1, which was supported by both docking studies and subsequent evaluation assays.

Third, the interaction modes were studied by different assays for the top active inhibitors as well as some other representative compounds. Under the assay conditions of the BLI assays, compounds **94(YJh182)**, **95(YJh196)** and **83(YJh174)** could bind with NDM-1 reversibly, and the K_d values for compounds **94(YJh182)**, **95(YJh196)** and **83(YJh174)** were $9.80 \pm 0.24 \mu$ M, $7.88 \pm 0.29 \mu$ M and $14.1 \pm 0.37 \mu$ M, respectively. While for ITC assays, the K_d values had a different trend, which were $0.527 \pm 0.149 \mu$ M, $0.532 \pm 0.149 \mu$ M and $0.105 \pm 0.028 \mu$ M for compounds **94(YJh182)**, **95(YJh196)** and **83(YJh174)**, respectively. The differences of the K_d values obtained from BLI and ITC assays were due to the constrains of the different assay conditions and mechanisms applied for different assays. For BLI assays, there were additional zinc ions in the assay buffer, which might shift the K_d to larger values of the tested compounds, and the ligands more specific for the active site of NDM-1 would be less

influenced by the free zinc ions in the buffer. For ITC assays, there were no additional zinc ions added in the assay buffer, thus the K_d values obtained were better than the values obtained from BLI assays. In addition, ITC method measures the thermodynamic parameters, the released Zn(II) ions of the protein can also binding with the ligands or the protein. Thus, the results of the ITC assays reflected the equilibrium of the whole titrating system, such as the binding of NDM-1 with ligands and the binding of the released Zn(II) ions with ligands or the protein. Therefore, the results of the BLI assays mainly reflected the binding complexes of the protein and ligands, and the results of ITC assays reflected the titrating equilibrium for all binding interactions of the protein, ligands and the possible released Zn(II) ions. The trend of the inhibitory activity correlated to the trend of the K_d values obtained from the BLI assays, which highlighted that forming of the complexes of holo-NDM-1 with the inhibitors was the main interaction mode and contributed the most for the inhibitory activities of the tested inhibitors. The Zn(II)-binding abilities of the inhibitors played important roles for their interactions with the target protein. Given the Zn(II) ions at the active site of NDM-1 were essential for both its hydrolyzing activity and stability, the interactions of the developed Zn(II)-binding inhibitors can influence both the function and structure of the protein. The binding of the inhibitors with the protein was mainly driven by the negative enthalpic changes, and the less entropic change obtained of the measurement for compound **94(YJh182)** might be contributed by the conformational changes of both the ligand and the protein. CD spectrometry was mainly used to detect the conformational changes of the secondary structures for the protein, there were no or less significant differences of the secondary structures for the protein interacting with the compounds at relative low concentrations, while some changes of the CD signals were detected for the protein interacting with compounds at the high concentration especially for compounds **95(YJh196)** and **83(YJh174)**, which might be contributed by ligand binding. The possible conformational changes for the amino acid residues at the active site could be studied by solution NMR. Compound **83(YJh174)** caused precipitation of the protein for the solution NMR measurements, which might be due to the less stable full-length protein at high concentrations, as well as the destabilizer functions of the ligand for the protein. The assay conditions can be optimized for the solution NMR, such as using the truncated NDM-1, lowering the concentrations of both the protein and inhibitors, and trying more inhibitors. Binding with the developed inhibitors reduced the thermal stability of NDM-1 which was determined by DSF assays. On the one hand, instead of stripping the metal ions from the active pocket, they mainly formed the binding complexes with the protein together with the Zn(II) ions. On the other hand, although the selected inhibitors bound with the protein, instead of improving the thermal stability of the protein as L-captopril or the traditional drug-like molecules, binding with the inhibitors destabilized the protein. Stable active conformations were the foundation of the activity for the protein, the destabilizing effects of the inhibitors on the target protein were fitted the idea of inducing protein degradation in essence, which were related to assay conditions. Protein native mass spectrometry studies directly indicated that the inhibitors can interacted with the protein by forming binding complexes. Especially compounds **94(YJh182)** and **95(YJh196)**, the main binding complexes were formed by the holo-NDM-1 with one or two molecules of the ligands, and there were other types of the binding complexes with less amount which might be caused by the destabilizing function of the ligands. The results of the native mass studies perfectly explained and related with other binding assays which supported the different effects under different assay conditions of the Zn(II)-binding inhibitors. In addition, according to the docking studies, the developed inhibitors competitively occupying the active pocket of NDM-1 hindered the hydrolysis of β -lactam antibiotics. Above all, the developed top active inhibitors with Zn(II)-binding ability interacted with NDM-1 by mainly forming binding complexes of holo-NDM-1 with inhibitors, which not only bound

with the active site for hydrolyzing β -lactam substrates competitively, but also could destabilize the protein through binding.

Fourth, the selected representative compounds also exhibited good inhibitory activities for other clinically relevant B1 MBLs including IMP-1, VIM-2, and GIM-1, which demonstrated that the inhibitors might be potential broad-spectrum inhibitors for B1 MBLs. And the selected inhibitors did not show any inhibitory activities to human metalloenzymes such hCAII, HDAC-1 at the tested concentrations. Although some **8-MSQA** derivatives showed inhibitory activities for MMP-2, they all had stronger binding affinity with NDM-1, especially the top active inhibitors such as compounds **94(YJh182)**, **95(YJh196)** and **83(YJh174)**. Compounds **74(YJh119)** with larger substituent of its sulfonamide moiety and compound **98(YJh184)** with its substituent of the sulfonamide moiety linked with the 7-position of the quinoline ring significantly improved the selectivity for NDM-1 offered other diverse strategies for the optimization of the inhibitors, and the SAR could be further investigated.

Fifth, compounds **8-MSQA(YJh65)**, **94(YJh182)**, **95(YJh196)**, **83(YJh174)** and chloroxine all can significantly reduce the MICs of meropenem for the transconjugants or the clinical resistant isolates expressing or co-expressing NDM-1 to susceptible levels with lower synergistic concentrations compared with the published inhibitors. Other resistance factors co-expressed by the clinical bacterial strains such as NDM-5, NDM-7 and VIM-1 also suggested that the **8-MSQA** derivatives might be potential broad-spectrum inhibitors for MBLs. In addition, chloroxine was an approved drug with bactericidal ability by itself,²⁰⁸ its inhibitory activity for the NDM-1 producing strains alone or synergistically with meropenem might expand its applications in the future. Clioquinol (5-chloro-7-iodo-8-quinolinol), an antifungal and antiprotozoal drug,²⁰⁸ showed inhibitory activity ($IC_{50} = 2.98 \mu\text{M}$) for NDM-1 via *in vitro* enzyme-based assays (**Table 3.7**) which can also be investigated by the cell-level assays.

Finally, the developed inhibitors had no or little effects on the proliferation or viability of HEK293 cells compared with chloroxine, which was evaluated by Alamar blue assays. Given the obvious reductions of the MICs by the synergistic use of the tested **8-MSQA** derivatives at lower concentrations, the selectivity index (SI) of the tested **8-MSQA** derivatives should be ≥ 10 .

Above all, the top active inhibitors represent a promising type of Zn(II)-binding inhibitors for NDM-1 as well as other B1 MBLs such as IMP-1, VIM-2 and GIM-1 with potent inhibitory activity and less toxicity, which effectively re-sensitize the multi-drug resistant bacteria expressing NDM-1 as well as other resistance factors for carbapenems. The developed potent Zn(II)-binding inhibitors with improved inhibitory activity especially the cell-level activity which is a significant achievement compared with most of the published Zn(II)-chelating or Zn(II)-binding inhibitors. Interacting with NDM-1 by mainly forming protein-inhibitor complexes and effecting the thermal stability of the protein is a more promising mode of action for drug-like candidates compared with other more toxic mechanisms such as the Zn(II) ion depriving function of EDTA or AMA type inhibitors and the covalent binding mechanism which generally has been limited to the cysteine or lysine residue containing active site.

For further development of the inhibitors, the modifications at the 6- and 3-positions of the quinoline structures, as well as comparison of the rigid substituents at the 4- or 5-positions with flexible substituents will enrich the SAR obtained at present. Other interesting modification directions discussed in the results and discussion part can be tried such as the strategies for improving selectivity. Template reactions are promising strategies for the development of pocket fitted inhibitors, which can be applied but need proper conditions. Addition of protein in small amounts and multiple times might be needed for Zn(II)-dependent inhibitors in template reactions as the Zn(II) ions played important roles for both

the activity and stability of the protein. To increase the stability of the protein, excessive zinc ions or other stabilizing reagents might be needed. In addition, adding covalent binding functional groups to the initial inhibitors will help to locate the initial fragments tightly at the active site as their relative less affinity at the beginning as well as the relative shallow binding pocket of NDM-1, which can improve the guided function of the protein to ligate with other suitable fragments.

For activity test, developing of new expressing systems such as the truncated NDM-1 protein (starting at the Gly29) with or without His₆ tag and other mutants may offer more chances for the activity studies. Broad BLs inhibitory spectra of the inhibitors are their advantages, as the pathogens always co-expressed many resistance factors. The representative inhibitors in this work can inhibit the most clinically relevant B1 MBLs, and their activity to SBLs can be tested or developed such as adding covalent binding groups for SBLs. At this point, multifunctional inhibitors can be developed by synthesis or template reactions.

For mechanism studies, the solution NMR studies were hindered by the less stable full-length NDM-1 with high concentrations at the earlier stage, and truncated NDM-1 in the following studies was applied which could offer the conformational changes about the amino acid residues and information about the active site of the protein interacting with the inhibitors. X-ray crystallography studies can be applied for identify the exact binding mode of the inhibitors with the active pocket.

There were published works about the animal tests for the activity studies of NDM-1 inhibitors using mice infected by multi-resistant bacteria,¹²⁷ which can be applied for the developed inhibitors in this work.

5 Experiment part

5.1 Biological evaluation methods

5.1.1 Protein expression and purification

The gene of the full-length ndm-1 with 6xHis tag at C-terminal was transferred into the pET-22(+) vector via sites 5'NdeI and 3'HindIII. The constructed vectors were transformed into chemically competent *Escherichia coli* BL21 (DE3) cells. *Escherichia coli* BL21 (DE3) cells containing the recombinant plasmids were grown in 3 mL LB media containing 100 mg/L ampicillin at 37 °C overnight. 600 μ L of the cell media was transferred into 400 mL LB media containing 100 mg/L ampicillin and cultured at 37 °C until the optical density at 600 nm (OD_{600}) arrived to 0.6 to 0.8 (around 4 h). Afterwards, the media was cooled to 18 - 20 °C, both isopropyl- β -D-1-thiogalactopyranoside (IPTG) and $ZnSO_4$ were added into the media with a final concentration of 0.5 mM. The protein expression was induced at 18 - 20 °C for 20 h, then the media was removed by centrifugation with the speed of 4500 rpm at 4 °C for 30 min. The collected bacterial pellet was resuspended in around 15 mL lysis buffer (25 mM Tris-HCl, 50 mM NaCl at pH 7.5 with 1% Triton*100 and 10% Glycine), and phenylmethylsulfonyl fluoride (PMSF) was added with the final concentration of 0.5 mM. The resuspended bacterial cells were lysed by sonication on ice with the BANDELIN SONOPULS HD 2070 homogenizer (8 x 20 s, 70% power, and interval of 1 min). The bacterial debris was removed by centrifugation with the speed of 16000 rpm at 4 °C for 30 min, and the supernatant was adjusted to contain 20 mM Imidazole by addition of the buffer B (50mM Tris-HCl, 500mM NaCl at pH 8.0 with 500 mM Imidazole) and centrifuged with the speed of 16000 rpm at 4 °C for 30 min to remove the bacterial debris again. The protein was purified via affinity chromatograph (Ni-NTA agarose), eluting with a gradient of 20 mM to 500 mM imidazole-containing buffers. The imidazole-containing buffers were prepared by mixing of the buffer A (50mM Tris-HCl, 500mM NaCl at pH 8.0) and the buffer B by different ratios. The target protein was starting to come out at 250 mM imidazole and the eluate was collected according to the quantification by Nanoquant reagent. Imidazole of the collected eluate was removed by Ultrafiltration or dialysis. Furthermore, the protein was purified via size-exclusion chromatograph (Superdex 75 HL16/600) with the eluting buffer (25 mM HEPES, 50 mM NaCl, at pH 7.5), and the purity of the protein was evaluated by SDS-PAGE and Q-Tof mass. The gene of the truncated ndm-1 was transferred to pET-30 vector, and the procedure of the expression and purification was similar as the wild-type NDM-1, except ampicillin (final concentration of 100 mg/L) was replaced by kanamycin (final concentration of 50 mg/L) for the culture of the bacteria. The amino acid sequence of the full length or the truncated NDM-1 are listed in **Table S1** in appendices, and the SDS-PAGE and Q-Tof mass data are shown in **Figure S1** to **S4** in appendices.

The constructed imp-1-containing pET-47b vector was given by Gottfried Otting's group of Australia National University. The procedure for the expression and purification was similar as the truncated NDM-1, except a cation exchange column (CM Sepharose) eluting by a gradient of 50 mM to 1000 mM NaCl-containing buffer (20 mM Tris-HCl pH 8.0) was used for purification instead of the affinity chromatograph (Ni-NTA agarose) eluting by imidazole containing buffer. The amino acid sequence is listed in **Table S1**, and the SDS-PAGE and Q-Tof mass data are shown in **Figure S5** and **S6**, respectively.

5.1.2 IC₅₀ determinations

The IC₅₀ values of the compounds for NDM-1 and the selected compounds for IMP-1, VIM-2 and GIM-1 were determined by using colorimetric substrate nitrocefin. The assays were carried out in 384-well plates (Greiner Bio-One, Item No.: 781101) with a volume of 50 μ L per well. The Steady-state rate parameters of NDM-1 and IMP-1 were determined in the assay buffer (50 mM HEPES, 2 mg/100mL BSA, 0.02% Tween-20, at pH 7.5) with 2% DMSO: NDM-1 ($K_m = 13.26 \pm 2.82 \mu\text{M}$, $V_{\text{max}} = 0.0011 \pm 0.0007 \text{ OD}_{490 \text{ nm}}/\text{min}$, $k_{\text{cat}} = 0.237 \pm 0.052 \text{ OD}_{490 \text{ nm}} \cdot \mu\text{M}^{-1} \cdot \text{min}^{-1}$); IMP-1 ($K_m = 29.96 \pm 3.59 \mu\text{M}$, $V_{\text{max}} = 0.0075 \pm 0.0013 \text{ OD}_{490 \text{ nm}}/\text{min}$, $k_{\text{cat}} = 163.3 \pm 15.18 \text{ OD}_{490 \text{ nm}} \cdot \mu\text{M}^{-1} \cdot \text{min}^{-1}$). The final concentrations of the enzymes used for the assays were as following: 5.4 nM NDM-1, 0.052 nM IMP-1, 0.25 nM VIM-2 and 0.7 nM GIM-1. The assays for NDM-1 and IMP-1 were performed in assay buffer (50 mM HEPES, 2 mg/100 mL BSA, 0.02% Tween-20, at pH 7.5) with 2% DMSO at final. For VIM-2 and GIM-1, the assay buffer was 50 mM HEPES, pH 7.5 supplemented with 1 μM ZnSO₄ and 2 mg/L BSA. Most of the compounds were dissolved in DMSO and serially diluted to the concentrations ranging from 100 mM to 0.19 μM . The enzymes were incubated with the dilutions of approximately 20 different concentrations for each compound at room temperature for 15 min. Afterwards, the substrate was added and the changes of the absorbance at 490 nm were monitored at 30 - 37 $^{\circ}\text{C}$ (25 $^{\circ}\text{C}$ for VIM-2 and GIM-1) for 30 min by the Tecan Safire 2 Microplate Reader. The concentrations of the substrate used were as followings: 13 μM for NDM-1, 30 μM for IMP-1, VIM-2 and GIM-1. The IC₅₀ values were analyzed by GraphPad Prism. The assays were performed in triplicate or quadruplicate.

5.1.3 Bio-layer Interferometry (BLI) assays

The experiments were performed at 25 $^{\circ}\text{C}$ with the Octet K2 (ForteBio) instrument using super streptavidin (SSA) sensors (ForteBio). The SSA biosensors were prewetted in PBS for 40 min in a 96-well plate (SARSTEDT, Order No.: 82.1581) at room temperature, and the instrument was pre-warmed for 30 min before using.

Preparation of the biotinylated protein. The stock solution of NDM-1 (26.5 kDa) protein was buffer exchanged from 50 mM HEPES (pH 7.5) to PBS and concentrated to 1.5 mg/mL by membrane ultrafiltration (Vivaspin® 500, 10 kDa MWCO, PES). The concentrated protein solution was incubated with 5 equivalent biotin reagent (biotin-PEO4-NHS, Pierce, Cat. No. 21329) at room temperature for 30 min, then the excessive biotin reagent was removed by membrane ultrafiltration (Vivaspin® 500, 10 kDa MWCO, PES). The biotinylated NDM-1 protein was stored at 4 $^{\circ}\text{C}$ with the concentration of 2 mg/mL for using. The activity of the biotinylated protein was evaluated by *in vitro* enzyme-based activity test (nitrocefin as the substrate).

Preparation of the compound solutions and others. The stock solutions of the compounds **94(YJh182)**, **95(YJh196)**, **83(YJh174)** and L-captopril (100 mM in DMSO) were serially diluted to 4 different concentrations by buffer (50 mM HEPES, pH 7.5, 0.005% Tween 20 and 25 μM ZnSO₄), e.g., 0.76 μM , 2.22 μM , 6.67 μM and 20 μM for compounds **94(YJh182)** and **95(YJh196)**, 6.67 μM , 10 μM , 15 μM and 20 μM for compound **83(YJh174)**, 300 μM , 450 μM , 600 μM and 900 μM for L-captopril, and the DMSO content of the diluted solutions was all adjusted to 1%. The biocytin blocking solution was diluted from 2 mg/mL in Milli-Q H₂O to 10 $\mu\text{g}/\text{mL}$ in PBS. The assay buffer was 50 mM HEPES, pH 7.5, 0.005% Tween 20 and 25 μM ZnSO₄ with 1% DMSO.

Preparation of the plates and setting the assay parameters. The Double Reference method was recommended by the standard procedures of BLI assays for K_d determination of small molecules, which was applied. An example of the layouts for the sensor plate and sample plate as well as the program settings for the Double Reference method are shown in **Figure S13a** in appendices. The sample solutions including PBS buffer, biotinylated protein buffer, blocking solution, assay buffer, compound solutions were pipetted in the defined wells of the black 96-well plates (Thermo Scientific™, Cat. No. 137101) with the volume of 0.24 mL for each well. The flow rate for each step was set to be 500 rpm. The pre-wetted SSA biosensors were initially equilibrated in PBS buffer for 10 min via the baseline step and followed by loading of the biotinylated NDM-1 protein (100 $\mu\text{g/mL}$ in PBS) for 10 min. Afterwards, the biosensors were blocked by the biocytin solution (10 $\mu\text{g/mL}$ in PBS) for 60 s and then washed in the assay buffer for 15 min to remove the excessive biocytin. After a further baseline step for 240 s in the assay buffer, the steps of baseline 60 s, association 180 s and dissociation 360 s were performed subsequently. The association steps were performed in the wells of the compound samples from the lowest concentration to the highest concentration. The corresponding baseline and dissociation steps were performed in a same well for each association step to minimize the inter-step drifts. The compound solutions were replaced by the assay buffer of the reference wells for the double reference subtraction of data analysis, which was used for most of the experiments, and the protein solutions were replaced by PBS for the reference sensors.

Data analysis. The kinetic data were analyzed by the software ForteBio Data Analysis 9.0. The parameters of the data analysis were set as follows: the Double Reference was chosen for subtraction of most experiments; the last 10 s of the baseline step was used for aligning Y axis; the inter-step correction was aligning to dissociation or baseline; the Savitzky-Golay Filtering was processed for most assays; the 1 to 1 model was chosen for the association and dissociation curves and the K_d values were generated by global (full) mode grouped by colour with Rmax unlinked by sensor; R equilibrium was set for the steady state analysis. All the measurements were repeated 3 times.

For compound **83(YJh174)** and L-captopril, the biocytin quenching step and the Double Reference method were not suitable, thus the program without the biocytin quenching step and the Reference Wells method were used, an example of the layouts of the sensor plate and sample plate as well as the program settings are shown in **Figure S13b** in appendices. In addition, for compounds **94(YJh182)** and **95(YJh196)**, the results were no significant difference by using both methods.

5.1.4 Isothermal titration calorimetry (ITC) assays

Interaction studies of NDM-1 protein and ligands by ITC assays. The experiments were carried out using the MicroCal PEAQ-ITC instrument (Malvern). The ITC cell was filled with 300 μL NDM-1-protein solution (15 μM), and the protein solution was titrated by compound solution (500 μM). The titration mode was set to be 19 injections with the volume of 1.8 μL each time (except for 0.4 μL for the first injection) and an interval of 210 s. All the experiments were performed at 25 $^{\circ}\text{C}$ with the reference power set at 10 $\mu\text{cal/s}$ and 500 rpm for the stirring speed. The stock solutions of the compounds (100 mM in DMSO) and truncated NDM-1 (4.5 mg/mL in 50 mM HEPES buffer, pH 7.5) were diluted by the assay buffer (50 mM HEPES, pH 7.5), and the DMSO content for all the measuring samples was adjusted to 0.5%. Protein samples were degassed by centrifugation at 8000 rpm for 10 min and other samples were degassed by sonication for 10 min. Controls such as the assay buffer titrating the assay buffer, the assay buffer titrating the protein solution and relative compound solution titrating the assay

buffer were subtracted for each compound during the data analyzing process. The data were analyzed by the supplied software of the MicroCal PEAQ-ITC instrument. The results of compounds **94(YJh182)**, **95(YJh196)** and **83(YJh174)** are shown in **Figure 3.31**. EDTA and L-captopril were also tested, while no typical binding curves for EDTA were obtained and the concentration of the protein solution needed to be increased for L-captopril.

Compounds **94(YJh182)**, **95(YJh196)** and **83(YJh174)** have also been tested by the full-length NDM-1 for ITC assays with the assay buffer (50 mM HEPES, pH 7.5, 0.005% Tween-20), and the results are shown in **Figure S9** in appendices.

Interaction studies of zinc ions and compounds by ITC assays. The experiments were performed using the MicroCal PEAQ-ITC instrument (Malvern). The ZnSO₄ solution (500 μM) was titrated into the compound solution (50 μM, 300 μL) in 19 × 2 μL aliquots (except for the first 0.4 μL) with an interval of 150 s. The titrations were performed at 25 °C, the reference power was set to 10 μcal/s, and the stirring speed was 750 rpm. The stock solutions of the compounds (100 mM in DMSO) and ZnSO₄ (0.5 M in Milli-Q H₂O) were diluted by Tris-HCl buffer (100 mM, pH 7.0). The DMSO content for all the measuring samples was adjusted to 0.5%. All the measuring samples were degassed by sonication for 10 min. Controls such as the assay buffer titrating the assay buffer, the assay buffer titrating the relative compound solution and the ZnSO₄ solution titrating the assay buffer were subtracted for each compound during the data analyzing process. The data were analyzed by the supplied software of the MicroCal PEAQ-ITC instrument. Compounds **94(YJh182)**, **95(YJh196)**, **83(YJh174)**, **8-MSQA(YJh65)**, **58(YJh34)**, **61(YJh59)**, **8-HQA**, EDTA and DPA have been tested, and the results are shown in **Figure 3.32** and **Figure S11**.

5.1.5 Interaction studies by native mass spectrometry

Truncated NDM-1 was utilized for the native mass spectrometry studies. The protein was buffer exchanged from 50 mM HEPES (pH 7.5) to 10 mM ammonium acetate (pH 6.8) by dialysis at the concentration of 1 mg/mL. The stock solutions of all selected compounds (100 mM in DMSO, except for EDTA, 10 mM in assay buffer 10 mM ammonium acetate) and the protein were diluted by the assay buffer (10 mM ammonium acetate pH 6.8), and the content of DMSO for each sample was adjusted to 0.05% except for one of the controls. The samples of the protein (10 μM) with assay buffer, assay buffer containing 0.05% DMSO and compounds in 10 μM, 20 μM or 50 μM were measured, and all samples were incubated at room temperature for 5 min before the measurement.

The assays were performed with the Orbitrap Q Exactive HF mass spectrometer (Thermo Scientific). The measurement of each sample was operated with the direct injection by offline nano-ESI. The positive full scan mass spectra were recorded in profile mode with the scan range from 1000 to 4000 m/z. Data analysis and deconvolution were processed by FreeStyle 1.6 and BioPharmaFinder 3.2.

The major parameters of the instrument were set as follows: intact protein mode(on), HMR mode(off), Trapping gas pressure setting (0.2), Spectrum data type(profile), C-trap Charge Detector Support(on). The scan parameter settings of the instrument control were as follows: scan type (full MS), scan range (1000 to 4000 m/z), fragmentation(none), resolution (15000), polarity(positive), microscans (5), lock mass(off), AGC target(3e6), Maximum inject time (200). The NSI source settings of the instrument control were as follows: Sheath gas flow rate (0), Aux gas rate (0), Sweep gas flow rate (0), Spay voltage (2.20 kV), Spray current (0), Capillary temperature(175°C), S-lens RF level (60.0).

5.1.6 Thermal-shift assays

Truncated NDM-1 was utilized for the thermal shift assays. The assays were performed with the working volume of 20 μL per well in the 96-well 0.2 mL optical plates (BIO-RAD, E607159). The stock solutions of the protein, compounds and SYPRO Orange (Sigma, cat. S5692) were all diluted by assay buffer (50 mM HEPES pH 7.5). 10 μL of each compound dilution and 5 μL of NDM-1 solution (20 μM) were added to each well. The plate was sealed and incubated at room temperature for 15 min before the addition of 5 μL SYPRO Orange solution (20x) to each well. The plate was sealed and incubated by another 15 min before measurement. The prepared plate was heated from 20 $^{\circ}\text{C}$ to 95 $^{\circ}\text{C}$ with the speed of 1 $^{\circ}\text{C}$ /min using the real-time PCR setup (LightCycler, Roche Diagnostics, Mannheim, Germany) and the fluorescence intensity was monitored with an interval of 0.3 s. The samples of protein (5 μM) with compounds at 5 μM , 10 μM , 25 μM and 50 μM were tested. The measurement was performed in quadruplicate and the content of DMSO was 0.05% (except for one of the controls). The data were analyzed by GraphPad Prism 5 software.

5.1.7 Circular dichroism

Truncated NDM-1 was utilized for CD spectrometry studies. NDM-1 protein was buffer-exchanged from 50 mM HEPES (pH 7.5) to 20 mM sodium phosphate (pH 7.0) by dialysis at the concentration of 1 mg/mL. The stock solutions of all selected compounds were 100 mM in DMSO (except EDTA, 10 mM in assay buffer 20 mM sodium phosphate pH 7.0). The final concentration of the protein was ca. 0.06 - 1 mg/mL (ca. 2.28 - 3.8 μM), and the final concentrations of the inhibitors were 3.8 μM , 19 μM and 38 μM . The samples of the mixed protein and compounds in 20 mM sodium phosphate (pH7.0) containing 0.038% DMSO were incubated at room temperature for 15 min before measurement. The 1-mm-path-length quartz cuvette (Starna, type 31/CD) was used, and the CD spectra were recorded with the interval of 1 nm from 180 to 270 nm at around 20 $^{\circ}\text{C}$ with the integration time of 1 s by the Olis CD spectrometer. Data were averaged for each sample from four scans. Relevant baselines buffer with DMSO or buffer with each compound were subtracted during the measurement, and the results were analyzed by using the online server DICHROWEB and GraphPad Prism 5 software.

5.1.8 Zinc ion restoration assays

NDM-1(10 nM) in assay buffer (50 mM HEPES, 2 mg/100mL BSA, 0.02% Tween-20, at pH 7.5) was incubated with inhibitors at 20 μM and 2 μM , respectively, for 15 min, then incubated with zinc ions at the concentrations ranging from 4 nM to 640 μM for 30 min in 384- well plates, a same volume (24.5 μL) of the substrate buffer (26 μM) was added to each well. The plates were measured at 37 $^{\circ}\text{C}$ and 28 $^{\circ}\text{C}$, respectively, under the wavelength of 490 nm. The data were analyzed by GraphPad Prism 5 software.

5.1.9 Enzyme-based *in vitro* activity assays for several other metalloenzymes

5.1.9.1 MMP-2 assays

Matrix metalloproteinase-2 (MMP-2) was purchased from Enzo Life Sciences (cat. BML-SE237-0010), and the stock solution at 1 mg/mL in the buffer of 50 mM Tris-HCl, pH 7.5, containing 300 mM NaCl, 5 mM CaCl₂, 20 μM ZnCl₂, 0.05% Brij-35 and 20% glycerol was stored at -80 °C. The OMNIMMP® fluorogenic substrate (cat. BML-P126-0001) was diluted to 10 mM by DMSO and stored in -80 °C. The selected compounds were dissolved in DMSO and diluted to 0.5 mM. The assays were carried out in the black 384-well plates (cat. CLS3658). MMP-2 and the dilutions of the selected compounds were incubated in the assay buffer (50 mM HEPES, 10 mM CaCl₂, 0.05% Brij-35, pH 7.5) at 37 °C for 30 min prior to the addition of the substrate. The total volume of each well was 50 μL and the final concentrations of the protein, compounds and substrate were 10 nM, 10 μM and 4 μM, respectively. The DMSO content of each sample was 2% except for one of the controls. The changes of the fluorescence intensity were monitored at the excitation wavelength of 320 nm and emission wavelength of 400 nm for 20 min. The wells of protein incubated with DMSO instead of compounds were negative controls, and the average change was set to be 100% activity. For positive control wells, the compound dilutions were replaced by 200 μM *N*-([1,1'-biphenyl]-4-ylsulfonyl)-*L*-phenylalanine (NSA) solutions. The activities of the wells containing the selected compounds were defined by the ratios of the fluorescence changes relative to the negative control wells. The IC₅₀ of NSA was 265.9 nM under this assay conditions. The assays were performed in triplicate and the data were analyzed by GraphPad Prism 5 software.

5.1.9.2 HDAC-1 assays

Histone Deacetylase-1 (HDAC-1) was purchased from BPS Bioscience (cat. 50051) and the stock solution of HDAC-1 (0.84 mg/mL, 14.74 μM) was stored in separate packs at -80 °C. The assays were carried out in the black 384-well plates (cat. CLS3658) with the assay buffer of 25 mM Tris-HCl, 2.7 mM KCl, 1 mM MgCl₂, 137 mM NaCl, 0.1 mg/mL BSA, pH 8.0. The selected compounds were dissolved in DMSO and diluted to 0.5 mM. The stock solution of HDAC-1 (56kD) was diluted to 16.37 nM by the assay buffer for using. Boc-lys-(ac)-AMC was used as the substrate and diluted to 54 μM by the assay buffer. A stop solution was prepared using the assay buffer containing 7.36 mg/mL trypsin and 245.78 μM suberoylanilide hydroxamic acid (SAHA). Each well contained 15 μL HDAC-1 diluted solutions and 1 μL dilutions of the selected compounds, and the plates were incubated at room temperature for 10 min prior to the addition of 15 μL substrate solutions. The DMSO content of each sample was 2% except for one of the controls. Afterwards, the plates were incubated at 37 °C for 1 h in dark, followed by addition of 15 μL stop solution for each well and continuedly incubated at 37 °C for 30 min in dark. The fluorescence intensity was monitored at the excitation wavelength of 390 nm and emission wavelength of 460 nm. The dilutions of the selected compounds for the negative control wells were replaced by DMSO and set as 100% activity. For positive control wells, the compound dilutions were replaced by 200 μM SAHA solutions. The activities of the wells containing the selected compounds were defined by the ratios of the fluorescence intensity relative to the negative control wells. The IC₅₀ of SAHA was

70.65 ± 8.51 nM under this assay conditions. The assays were performed in triplicate and the data were analyzed by GraphPad Prism 5 software.

5.1.9.3 hCAII assays

Human carbonic anhydrase II (hCAII) was purchased from Sigma (cat. C6165) and the stock solution at 0.5 mg/mL in assay buffer (50 mM HEPES at pH = 8.0) was stored at -80 °C. The selected compounds were dissolved in DMSO and diluted to 0.5 mM. The substrate *para* nitrophenol acetate (pNPA) was dissolved in DMSO at a stock concentration of 3 M. Assays were performed in the 384-well plates (Greiner Bio-One, Item No.: 781101) with a volume of 50 µL per well. hCAII (36.9 nM) was incubated with the dilutions of the selected compounds (10 µM) for 15 min at room temperature prior to the addition of the substrate (500 µM). The DMSO content of each sample was 2% except for one of the controls. The absorbance at 405 nm was monitored at 30 - 37 °C for 30 min by the Tecan Safire 2 Microplate Reader. The wells of the protein incubated without compounds were negative controls, and the average absorbance change was set to be 100% activity. The wells of protein incubated with 50 µM acetazolamide (AZA) were positive controls. The activities of the selected compounds were defined by the ratios of their absorbance changes compared with the average change of the negative controls. The IC₅₀ of AZA was 46.88 ± 3.60 nM under this assay conditions. The assays were performed in triplicate and the data were analyzed by GraphPad Prism 5 software.

5.1.10 Microbiological susceptibility tests

Bacterial strains. To investigate the inhibitory effect of the selected compounds, eight clinical isolates and four transconjugants from the strain collection of the Robert Koch Institute were used for the Broth microdilution tests. The species of the clinical isolates, *Klebsiella pneumoniae* (n=5), *Escherichia coli* (n=2) and *Acinetobacter baumannii* (n=1), were sent from different hospitals in Germany (2007-2020) and produced carbapenemases NDM-1 (n=4), NDM-1+OXA-48 (n=1), NDM-5 (n=1), NDM-7 (n=1) and VIM-1 (n=1). The transconjugants were obtained by broth mating using four NDM-1 producing clinical isolates and the sodium azide-resistant recipient strain *E. coli* K12J53 Azi^r. All clinical isolates and one transconjugant harboured further β-lactamase genes, e.g., encoding broad-spectrum beta-lactamases, extended-spectrum beta-lactamases (ESBL) or AmpC beta-lactamases. Species identification was performed by VITEK 2 GN card (bioMérieux, Nuertingen, Germany). Antimicrobial susceptibility testing was performed by broth microdilution and VITEK 2 card AST N248 with interpretation of results according to EUCAST criteria (EUCAST v10.0). The presence of different carbapenemase and other beta-lactamase genes (*bla*_{NDM-like}, *bla*_{VIM-like}, *bla*_{OXA-48-like}, *bla*_{KPC-like}, *bla*_{OXA1-2-9-10-group}, *bla*_{TEM-like}, *bla*_{SHV-like}, *bla*_{CTX-M-1-2-9-group}, *bla*_{CMY-like}) was investigated by PCR and sequencing. Bacterial strain typing was done by multilocus sequence typing (MLST) for *Klebsiella pneumoniae* (<https://bigsd.b.pasteur.fr/klebsiella/klebsiella.html>), and *Escherichia coli* (https://pubmlst.org/bigsd?db=pubmlst_ecoli_achtman_seqdef) using PCR and Sanger sequencing. Furthermore, the plasmid sizes were determined for several isolates via S1-nuclease restriction and subsequent pulsed field gel electrophoresis (PFGE).

Broth microdilution assays. Antimicrobial susceptibilities of meropenem with or without selected compounds were identified by broth microdilution assays and carried out in 96-well microplates. The MICs were determined according to Clinical and Laboratory Standards Institute (CLSI) methods. The

2-fold dilution series of meropenem were diluted to a final concentration ranging from 128 mg/L to 0.125 mg/L by the cation adjusted Mueller-Hinton (MH) broth or the MH broths containing the selected compounds with fixed concentrations. Each bacterial strain was incubated in 4 mL broth at 37 °C for around 2 h and used until the Mc Farland Standard equal to 0.5. The bacterial isolates (ca. 5×10^5 cells/mL) were incubated with the serial dilutions (100 μ L/well) at 37 °C for 20 h. Growth controls were incubated at the same conditions without meropenem. Following the incubation, the growth for each plate was checked. Reference isolate *E. coli* ATCC25922 was used as quality control. All tests were performed in triplicate. (For the selected compounds, **94(YJh182)** and **95(YJh196)** were tested at fixed concentrations of 24 mg/L and 12 mg/L, **83(YJh174)** was tested at concentrations of 4.775 mg/L, 2.388 mg/L, 0.955 mg/L, 0.478 mg/L, 0.096 mg/L, 24 mg/L and 12 mg/L. **8-MSQA(YJh65)** was tested at concentrations of 21.3 mg/L, 10.65 mg/L, 4.26 mg/L, 2.13 mg/L, and 0.43 mg/L. 5,7-dichloro-quinolin-8-ol was tested at concentrations of 50.3 mg/L, 25.15 mg/L, 10.06 mg/L, 5.03 mg/L and 1.006 mg/L.)

5.1.11 Alamar blue assays

HEK293 cells were seeded (20000 cells/well) in 96-well plates (SARSTEDT, Order No.: 83.3924) by 100 μ L per well and incubated for 24 h. The stock solutions of the selected compounds were diluted to serial concentrations by DMEM media supplied with 10% fetal calf serum (FCS) and 1% Na-Pyruvate (11 g/L). 100 μ L of each dilution was pipetted to the relevant wells of the prepared plates. The final volume of each well was 200 μ L and the DMSO content is 1% except for relevant control wells. The plates were incubated at 37 °C, 5% CO₂ for 12 h or 24 h. Afterwards, Alamar Blue reagent was added (20 μ L/well) and the plates were incubated at 37 °C, 5% CO₂ for another 5 h. The fluorescence intensity was monitored with the excitation wavelength of 560 nm and the emission wavelength of 590 nm. The assays were performed in quadruplicate. The data were analyzed by GraphPad Prism 5 software.

5.2 Molecule docking

Preparation of protein structures and the ligand data base were performed in Molecular Operating Environment (MOE) version 2020.09.01. The crystal structures were download from the Protein Data Bank (PDB) as follows: NDM-1 (PDB ID: 5ZGR), IMP-1 (PDB ID: 5EV6), VIM-2 (PDB ID: 4BZ3) and GIM-1 (PDB ID: 2YNW), catalytic domain of MMP-2 (PDB ID: 1QIB). The unnecessary water molecules and buffer components of the proteins were removed. The proteins were further prepared by the Structure Preparation application in MOE. The smiles strings of the ligands were saved in a '.txt' file prior to input to the data base. The ligand data base was prepared by following steps: database washing, correction of bonding patters, protonation, setting of proper tautomeric states and atomic partial charges and energy minimization. Protein-ligand docking was performed by GOLD v 5.8.1 and the docking process involved: loading of the prepared protein structure, addition of protons, extraction of water molecules and ligands, defining the binding site using a radius of 10 Å around the center between the two Zn(II) ions (a radius of 10 Å around the catalytic Zn(II) ion for MMP-2), loading the ligand database, changing necessary default parameters, saving results as '.sdf' files and running the docking process. The docking results were analyzed by LigandScout 4.2. The docking poses of the ligands were inserted into corresponding prepared protein structures, docking scores could be checked directly and 2D interaction patterns of each docking pose were generated automatically after forming the fitted pharmacophores.

5.3 Synthesis

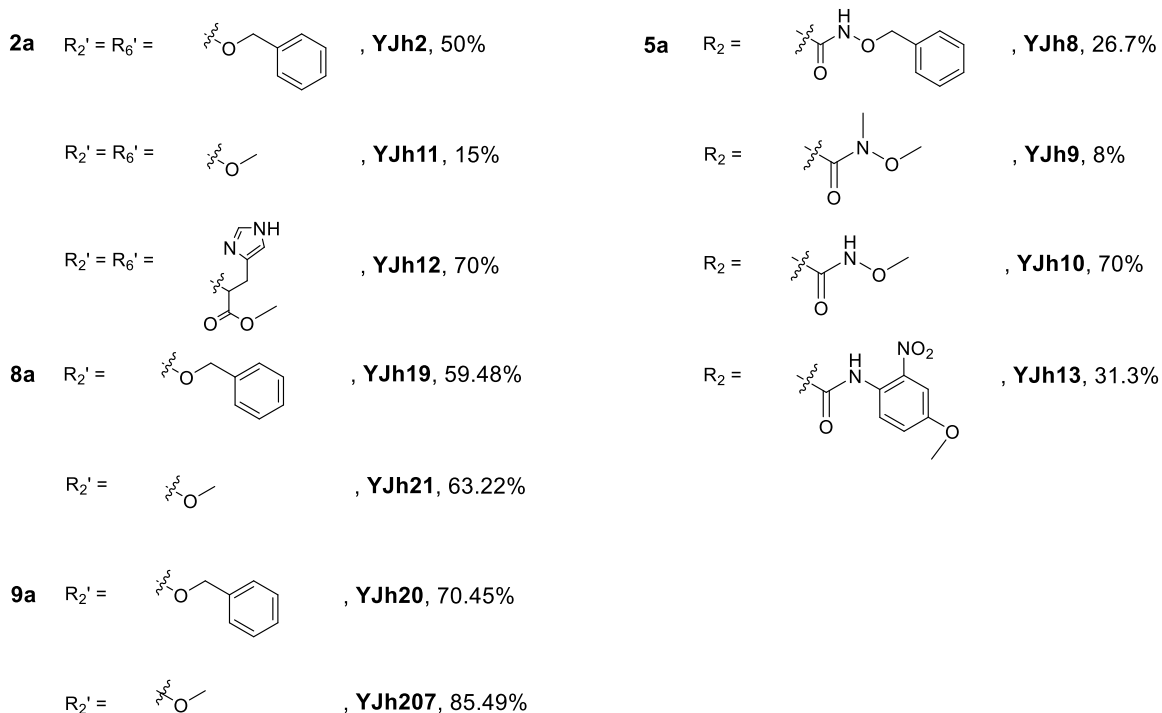
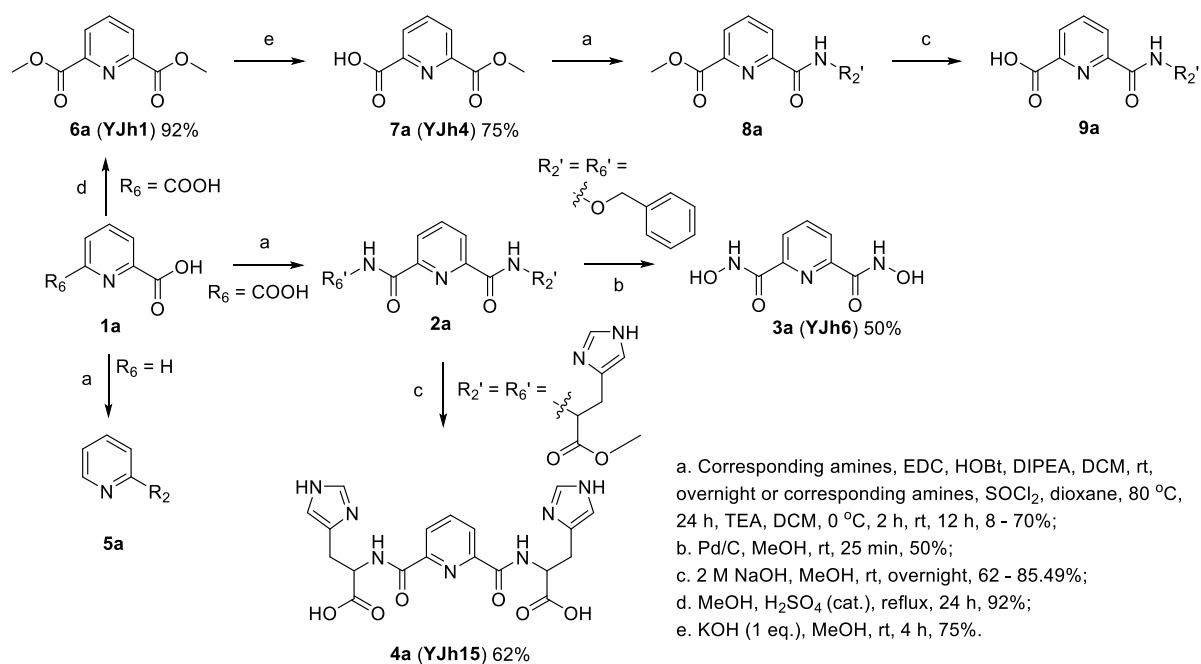
5.3.1 Materials and methods

All chemical reagents and solvents used for synthesizing corresponding compounds were commercially available and used without further purification. Preparative HPLC was performed on an Agilent 1260 Infinity series system with the C18 column (Macherey Nagel, VP Nucleodur C18 HTec, 5 μm , 32x150 mm) and the eluents were mixtures of water and acetonitrile (with 0.1% trifluoroacetic acid). The analytic LCMS was performed with the Agilent 1100 series system coupled with electrospray ionization (ESI) mass spectrometer and the column was Luna C18 (Phenomenex, 3 μm , 4.6x100 mm). Eluents were gradient mixtures of water and acetonitrile (with 0.1% formic acid). High resolution mass spectra were measured by an ESI-QTOF iFunnel Model 6550 spectrometer coupled with the HPLC system of Series Infinity II 1290. The $^1\text{H-NMR}$ or $^{13}\text{C-NMR}$ spectra were mainly measured on the ECP500 (Jeol, Akishima, Japan) or the AVANCE III 700 (Bruker, Billerica, MA, USA), and analyzed by the software MestReNova. The chemical shift δ was reported in ppm. The purity of relevant compounds was determined by the area under the peak from the LCMS data recorded for 254 nm.

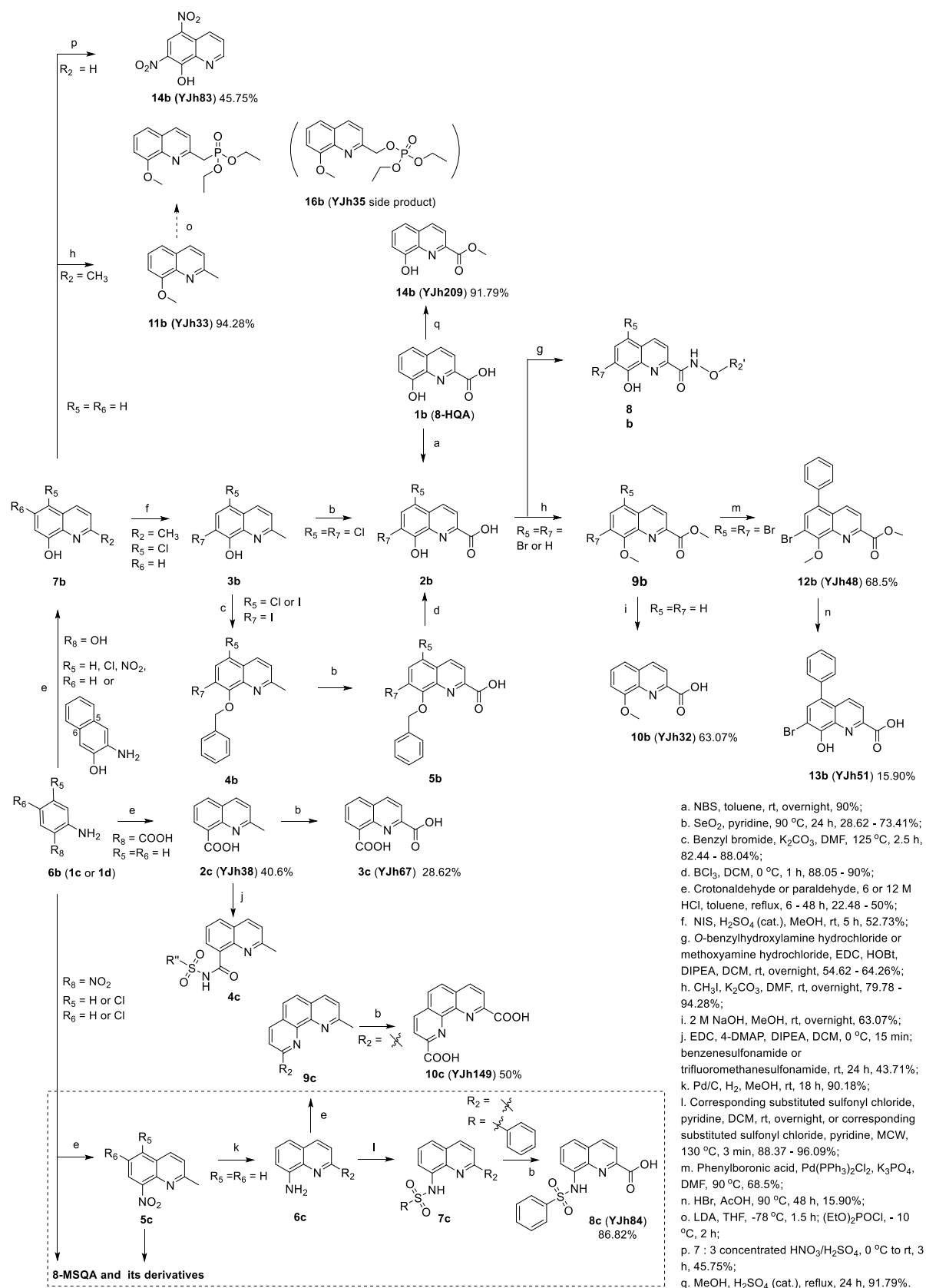
All the compounds synthesized by the author had a notebook name starting with the abbreviation 'YJ', the 'h' was the compound series, other series such as 'a', 'd' and 'g' for the di-glycine, di-*D*-alanine and captopril derivatives did not list in the experiment part.

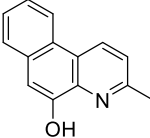
5.3.2 Synthetic routes

Scheme S1. Synthetic route for DPA derivatives.

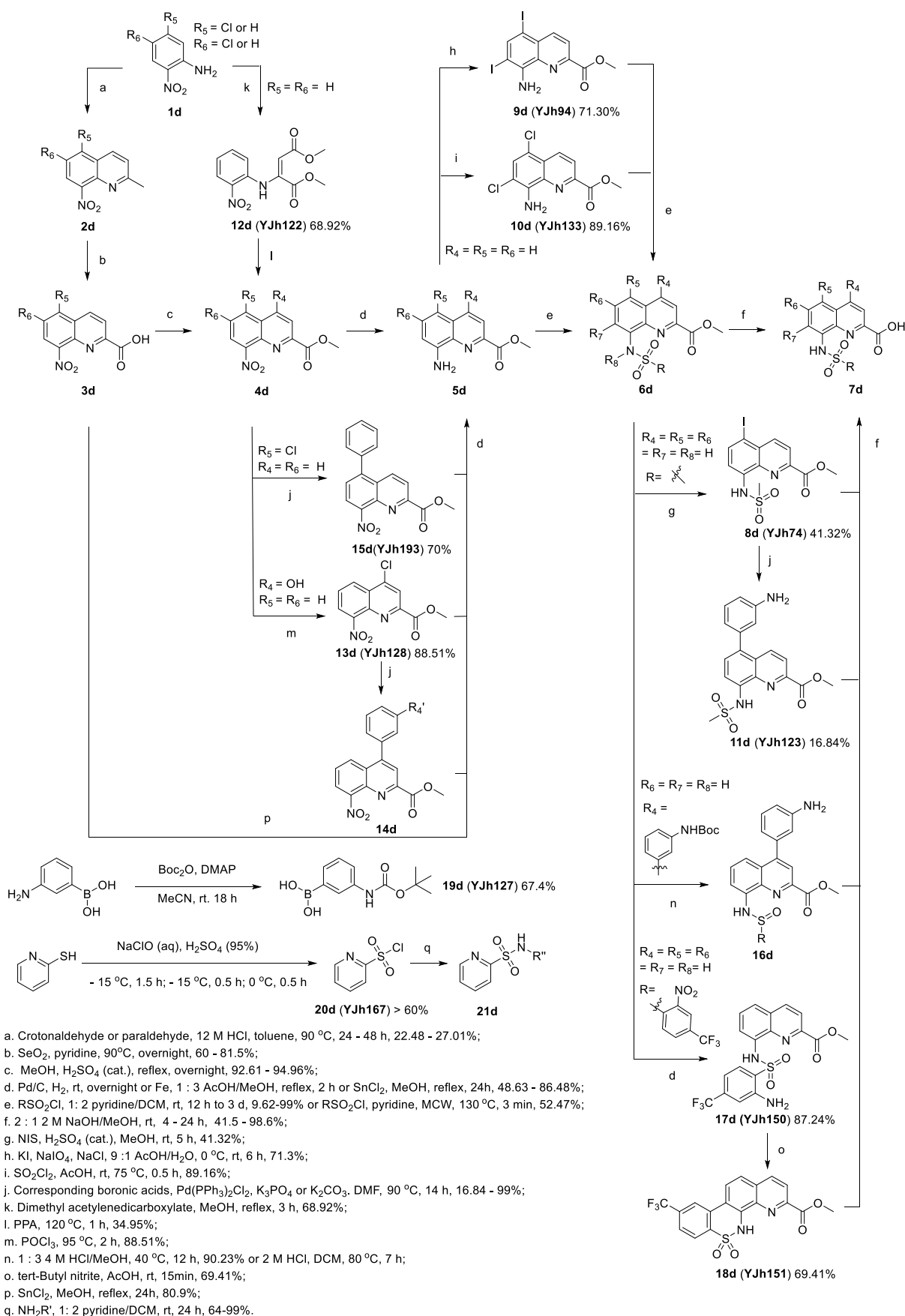


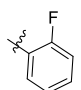
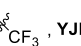
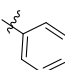
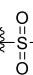
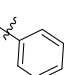
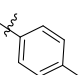
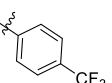
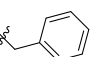
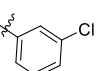
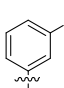
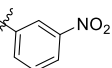
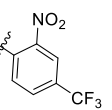
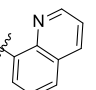
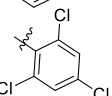
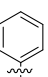
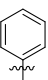
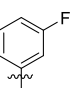
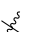
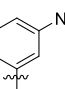


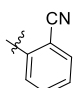
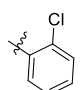
Scheme S2. Synthetic route for quinolin-8-ol derivatives.

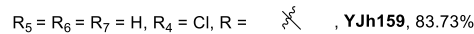
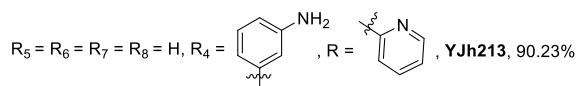
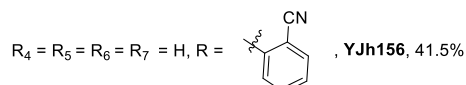
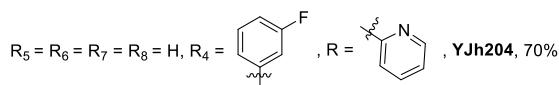
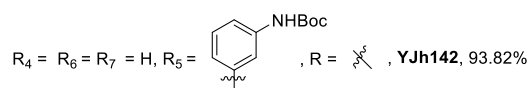
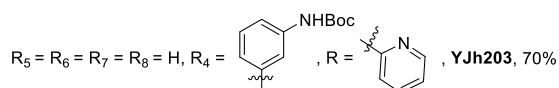
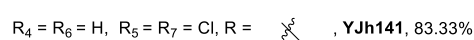
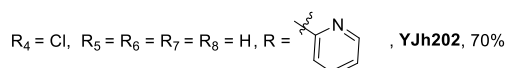
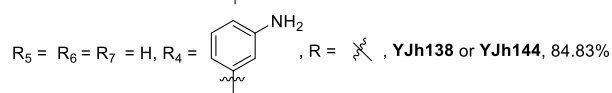
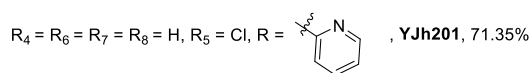
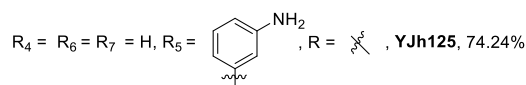
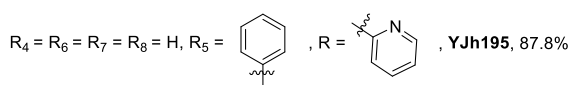
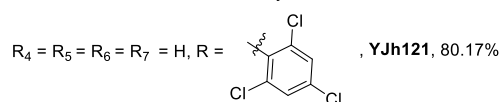
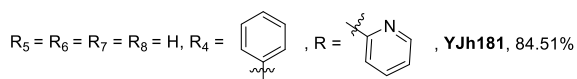
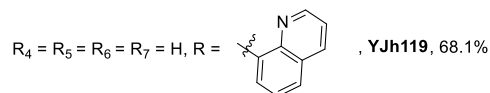
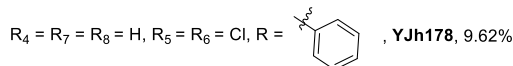
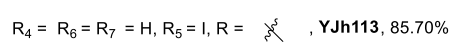
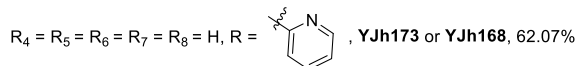
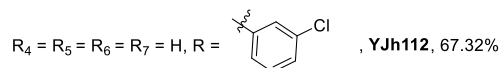
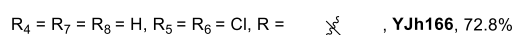
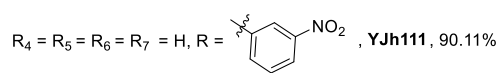
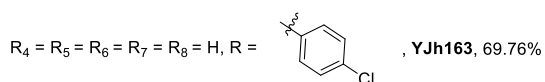


- 2b** $R_5 = R_7 = H$, **8-HQA**
 $R_5 = R_7 = Br$, **YJh22**, 90%
 $R_5 = R_7 = Cl$, **YJh34**, 47%
 $R_5 = R_7 = I$, **YJh59**, 90%
 $R_5 = Cl$, $R_7 = I$, **YJh66**, 88.05%
- 3b** $R_5 = Cl$, $R_7 = I$, **YJh52**, 52.73%
 $R_5 = R_7 = Cl$, 5,7-dichloro-2-methylquinolin-8-ol
- 4b** $R_5 = R_7 = I$, **YJh53**, 88.04%
 $R_5 = Cl$, $R_7 = I$, **YJh62**, 82.44%
- 5b** $R_5 = R_7 = I$, **YJh54**, 52.08%
 $R_5 = Cl$, $R_7 = I$, **YJh64**, 73.41%
- 6b** $R_5 = Cl$, $R_6 = H$, $R_8 = OH$, 2-amino-4-chlorophenol
 $R_5 = NO_2$, $R_6 = H$, $R_8 = OH$, 2-amino-4-nitrophenol
3-aminonaphthalen-2-ol
 $R_5 = R_6 = H$, $R_8 = COOH$, 2-aminobenzoic acid
 $R_5 = R_6 = H$, $R_8 = NO_2$, 2-nitroaniline
 $R_5 = Cl$, $R_6 = H$, $R_8 = NO_2$, 5-chloro-2-nitroaniline
 $R_5 = R_6 = Cl$, $R_8 = NO_2$, 4,5-dichloro-2-nitroaniline
 $R_5 = H$, $R_6 = Cl$, $R_8 = NO_2$, 4-chloro-2-nitroaniline
- 7b** $R_5 = R_6 = R_2 = H$, quinolin-8-ol
 $R_5 = R_6 = H$, $R_2 = \text{Me}$, 2-methylquinolin-8-ol
 $R_5 = Cl$, $R_6 = H$, $R_2 = \text{Me}$, **YJh37**, 50%
 $R_5 = NO_2$, $R_6 = H$, $R_2 = \text{Me}$, **YJh41** (no NMR data)
-  **YJh68** (no NMR data)
- 8b** $R_5 = R_7 = H$, $R_2' = \text{Me}$, **YJh18**, 54.62%
 $R_5 = R_7 = H$, $R_2' = \text{Ph}$, **YJh14**, 57.8%
 $R_5 = R_7 = Br$, $R_2' = \text{Ph}$, **YJh27**, 64.26%
- 9b** $R_5 = R_7 = H$, **YJh31**, 93.73%
 $R_5 = R_7 = Br$, **YJh47**, 79.78%
- 4c** $R'' = \text{CF}_3$, **YJh116** (no NMR data)
 $R'' = \text{Ph}$, **YJh118**, 43.71%
- 5c** $R_5 = R_6 = H$, 2-methylquinolin-8-amine
 $R_5 = Cl$, $R_6 = H$, **YJh170**, 22.48%
 $R_5 = Cl$, $R_6 = Cl$, **YJh153** or **YJh155**, 27.01%
 $R_5 = H$, $R_6 = Cl$, **YJh198** (no NMR data)
- 6c** $R_2 = H$, 8-aminoquinoline
 $R_2 = \text{Me}$, **YJh80**, 90.18%
- 7c** $R_2 = \text{Me}$, $R = \text{Ph}$, **YJh82**, 88.58%
 $R_2 = \text{Me}$, $R = \text{3-F-Ph}$, **YJh85**, 88.37%
 $R_2 = H$, $R = \text{3-F-Ph}$, **YJh208**, 96.09%
- 9c** $R_2 = H$, **YJh157** (no NMR data)
 $R_2 = \text{Me}$, **YJh145**, 35%

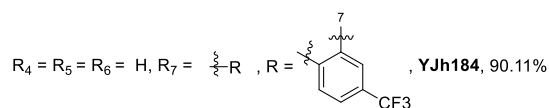
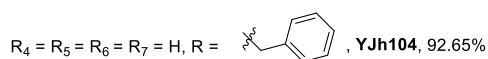
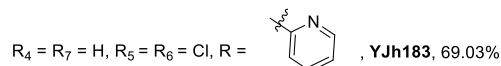
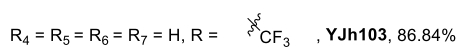
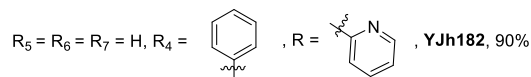
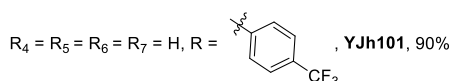
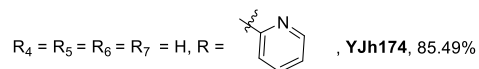
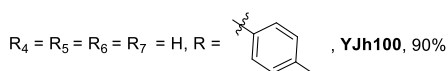
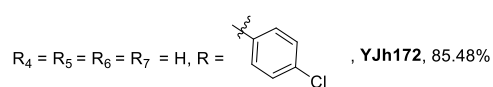
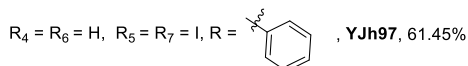
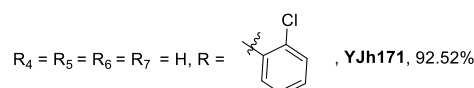
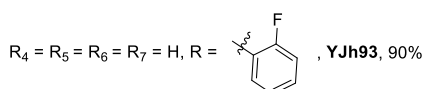
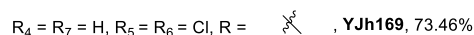
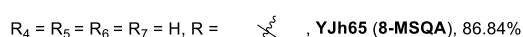
Scheme S3. Synthetic route for 8-MSQA derivatives.

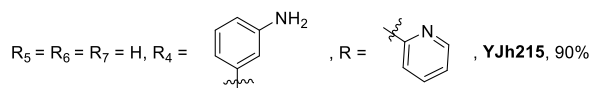
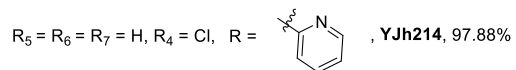
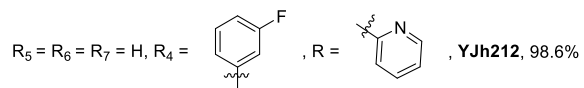
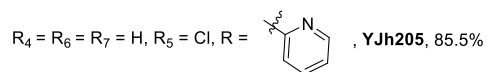
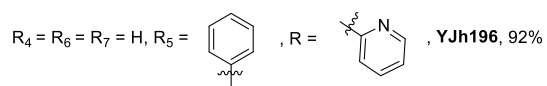


1dR₅ = R₆ = H, 2-nitroanilineR₅ = Cl, R₆ = H, 5-chloro-2-nitroanilineR₅ = R₆ = Cl, 4,5-dichloro-2-nitroanilineR₄ = R₅ = R₆ = R₇ = R₈ = H, R = , **YJh90**, 88.37%R₄ = R₅ = R₆ = R₇ = R₈ = H, R = , **YJh92** or **YJh107**, 55.6%**2d**R₅ = R₆ = H, 2-methyl-8-nitroquinolineR₅ = R₆ = Cl, **YJh153** or **YJh155**, 27.01%R₅ = Cl, R₆ = H, **YJh170**, 22.48%R₅ = H, R₆ = Cl, **YJh198** (no NMR data)R₄ = R₆ = R₈ = H, R₅ = R₇ = I, R = , **YJh95**, 50.43%R₄ = R₆ = H, R₅ = R₇ = I, R₈ = -R, R = , **YJh96**, 60%**3d**R₅ = R₆ = H, **YJh36**, 71.25%R₅ = R₆ = Cl, **YJh158**, 81.5%R₅ = Cl, R₆ = H, **YJh191**, 60%R₄ = R₅ = R₆ = R₇ = R₈ = H, R = , **YJh98**, 65.25%R₄ = R₅ = R₆ = R₇ = R₈ = H, R = , **YJh99**, 94.12%**4d**R₄ = R₅ = R₆ = H, **YJh88**, 94.96%R₄ = R₆ = H, R₅ = Cl, **YJh192**, 92.61%R₄ = OH, R₅ = R₆ = H, **YJh124**, 34.95%R₄ = R₅ = R₆ = R₇ = R₈ = H, R = , **YJh102**, 76.64%R₄ = R₅ = R₆ = R₇ = R₈ = H, R = , **YJh105**, 82.05%**5d**R₄ = R₅ = R₆ = H, **YJh61** or **YJh89**, 81.09%R₅ = R₆ = H, R₄ = , **YJh135**, 70.6%R₄ = Cl, R₅ = R₆ = H, **YJh139** or **YJh152**, 48.63 - 61.32%R₄ = H, R₅ = R₆ = Cl, **YJh160**, 80.9%R₄ = R₅ = R₆ = R₇ = R₈ = H, R = , **YJh106**, 78.82%R₄ = R₅ = R₆ = R₇ = R₈ = H, R = , **YJh109**, 95.61%R₄ = R₅ = R₆ = R₇ = R₈ = H, R = , **YJh117**, 94.16%R₄ = R₅ = R₆ = R₇ = R₈ = H, R = , **YJh120**, 56.3%R₅ = R₆ = H, R₄ = , **YJh179**, 76.69%R₄ = R₆ = H, R₅ = , **YJh194**, 73.98%R₄ = R₆ = H, R₅ = Cl, **YJh197**, 86.48%R₅ = R₆ = H, R₄ = , **YJh200**, 86.48%R₄ = R₆ = R₈ = H, R₅ = R₇ = Cl, R = , **YJh136**, 26.06%R₅ = R₆ = R₇ = R₈ = H, R₄ = , R = , **YJh137**, 35.85%R₅ = R₆ = R₇ = R₈ = H, R₄ = Cl, R = , **YJh140**, 52.5%**6d**R₄ = R₅ = R₆ = R₇ = R₈ = H, R = , **YJh63**, 99%R₄ = R₅ = R₆ = R₇ = R₈ = H, R = , **YJh154**, 75.96%R₄ = R₅ = R₆ = R₇ = R₈ = H, R = , **YJh162**, 88.87%

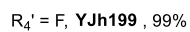
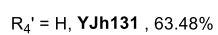
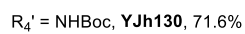


7d

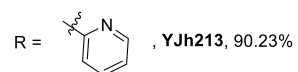
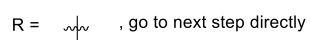




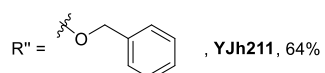
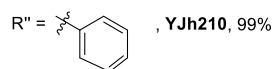
14d



16d



21d



5.3.3 Synthesis procedures

General procedure for amide coupling. Relative carboxylic acid (1 eq.), EDC·HCl (1.2 eq.), HOBT (1.2 eq.) and DIPEA (3.6 eq.) were added to a proper amount of dichloromethane (ca. 2-10 mL) and stirred for 15 min with ice bath protect before the addition of the corresponding amine (1.2 eq.). The reaction mixture was stirred at room temperature overnight and quenched by brine (ca. twice of the reaction volume). The mixture was extracted 3 times with ethyl acetate. The collected organic phase was washed by brine and dried over anhydrous Na₂SO₄, then the solvent was evaporated via reduced pressure. The resulting residue was purified via hexane and ethyl acetate silica gel chromatograph.

General procedure for reduction reaction.

(a) Hydrogenation reduction. Palladium on carbon (ca. 10% of the weight of the object to be reduced) was added to the corresponding 8-nitroquinoline containing structure in a proper amount of methanol under nitrogen. The mixture was stirred at room temperature under hydrogen for 8 h. The reaction solution was filtered and evaporated via reduced pressure. The resulting residue was purified via hexane and ethyl acetate silica gel chromatograph.

(b) Reduction of aromatic nitro compounds to amines by tin (II) chloride. Tin (II) chloride (6 eq.) and catalytic amount of concentrated hydrochloric acid were added to the aromatic nitro compound (1eq.) in a proper amount of methanol. The reaction mixture was stirred at 65 °C for 24 h. The solvent was evaporated to a small volume via reduced pressure. The reaction was quenched by sodium bicarbonate saturated solution and extracted 5 times with ethyl acetate. The collected organic phase was washed by brine and dried over anhydrous Na₂SO₄. The solvent was evaporated via reduced pressure. The resulting residue was purified via hexane and ethyl acetate silica gel chromatograph.

General procedure for hydrolysis of methyl esters catalyzed by hydroxide ion. 2 M NaOH (2 to 10 mL) was added to the corresponding methyl ester (around 0.3 mmol) in methanol (a smaller or same volume as the 2 M NaOH). The reaction was stirred at room temperature overnight. Afterwards, the pH of the mixture was adjusted to 2 by 2 M HCl and extracted 3 times with dichloromethane. The collected organic phase was washed with water and dried over anhydrous Na₂SO₄, then the solvent was evaporated via reduced pressure. The resulting residue was purified via silica gel chromatograph.

General procedure for methyl esterification of carboxylic acids. Catalytic amount of concentrated H₂SO₄ (0.5 mL) was added dropwise to the relevant carboxylic acid (around 6 mmol) in methanol (100 mL). The mixture was stirred at 70 °C for 24 h and monitored by TLC. After the reaction was completed, the solvent was evaporated via reduced pressure. The residue was purified via hexane and ethyl acetate silica gel chromatograph (15% ethyl acetate).

General procedure for synthesis of 2-methyl quinoline analogues. Crotonaldehyde (5.83 mmol) in toluene (5.4 mL) was added dropwise in corresponding substituted aniline (2.92 mmol) in 6 M HCl (35.4 mL) and stirred at 75 °C overnight. The organic layer was removed. The pH of the water phase was adjusted to 3 with concentrated ammonia solution and extracted 3 times with ethyl acetate. The collected organic phase was washed by brine and dried over anhydrous Na₂SO₄. The solvent was evaporated via reduced pressure. The resulting residue was purified via hexane and ethyl acetate silica gel chromatograph. The quantity of each reactant and the volumes of relevant solutions for a specific reaction could be changed according to the above equivalent.

General procedure for oxidation of 2-methyl quinoline analogues by selenium dioxide. Selenium dioxide (1.5 eq.) was added to corresponding 2-methyl quinoline structure (1eq.) in a proper amount of pyridine and stirred at 100 °C for 16 h. Then the reaction mixture was filtered immediately to

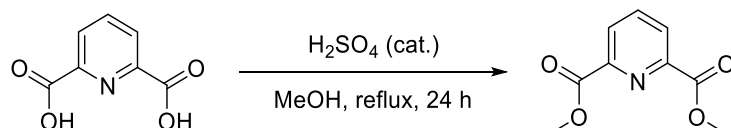
remove the precipitate. The filtrate was evaporated via reduced pressure. The residue was treated with a proper amount of 1 M NaOH and washed with ethyl acetate 3 times. The pH of the water phase (together with the formed precipitate) was adjusted to 2 by 2 M HCl and extracted 3 times with ethyl acetate. The collected organic phase was dried over anhydrous Na₂SO₄ and evaporated via reduced pressure. The resulting residue was purified via silica gel chromatograph (ethyl acetate, MeOH and H₂O, the ratio was 8 to 1.5 to 1).

General procedure for sulfonamide coupling. The corresponding sulfonyl chloride (1.5 eq.) was added to the relevant 8-aminoquinoline containing structure (1 eq.) in pyridine/ dichloromethane (1/2) and stirred at room temperature overnight. The reaction was quenched by sodium bicarbonate saturated solution and extracted 3 times with ethyl acetate. The collected organic phase was washed by brine and dried over anhydrous Na₂SO₄. The solvent was evaporated under reduced pressure. The resulting residue was purified via hexane and ethyl acetate silica gel chromatograph.

General procedure for Suzuki reaction. Bis(triphenylphosphine)palladium(II) dichloride (194.8 mg, 0.278 mmol) was added to a mixture of methyl 4- (or 5-) chloro-8-nitroquinoline-2-carboxylate (370 mg, 1.39 mmol), corresponding boronic acid (1.80 mmol) and K₂CO₃ (383.54 mg, 2.78 mmol) in DMF (6 mL) under nitrogen. The reaction was stirred at 90 °C for 14 h and then quenched by 10 mL brine solution. The mixture was extracted 3 times with ethyl acetate. The collected organic phase was washed by brine and dried over anhydrous Na₂SO₄. The solvent was evaporated via reduced pressure. The resulting residue was purified via hexane and ethyl acetate silica gel chromatograph.

Synthesis procedures

Dimethyl pyridine-2,6-dicarboxylate (YJh1)



The synthesis was according to the general procedure for methyl esterification of carboxylic acids. The corresponding carboxylic acid was pyridine-2, 6-dicarboxylic acid (1 g, 5.98 mmol). The product was obtained as white solid.

Yield: 1.07 g (92%).

¹H NMR (500 MHz, Chloroform-*d*) δ 8.29 (d, *J* = 7.8 Hz, 2H), 8.01 (t, *J* = 7.8 Hz, 1H), 4.00 (s, 3H).

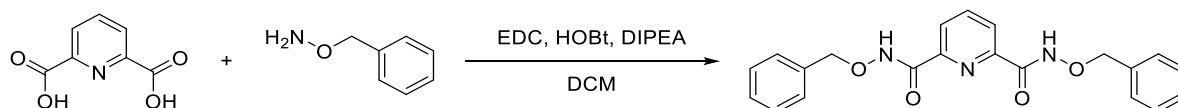
¹³C NMR (126 MHz, Chloroform-*d*) δ 165.16, 148.35, 138.48, 128.14, 53.29.

ESI-HRMS calc. for [C₉H₉NO₄ + H]⁺ *m/z* 196.0604, found *m/z* 196.0612 [M + H]⁺.

Melting point: 123 °C

Purity: 97.97%

*N*²,*N*⁶-Bis(benzyloxy)pyridine-2,6-dicarboxamide (YJh2)



The synthesis was according to the general procedure for amide coupling and the equivalents of the reagents was as follows. Pyridine-2,6-dicarboxylic acid (0.5 g, 2.99 mmol), EDC·HCl (1.26 g, 6.58 mmol), HOBT (0.89 g, 6.58 mmol) and DIPEA (3.44 mL, 19.75 mmol) were added to 10 mL

dichloromethane. The corresponding amine was *O*-benzylhydroxylamine hydrochloride (1.05 g, 6.58 mmol). The resulting residue was purified via hexane and ethyl acetate silica gel chromatograph (60% ethyl acetate). The product was obtained as white solid.

Yield: 564.56 mg (50%).

¹H NMR (400 MHz, Chloroform-*d*) δ 10.16 (s, 2H), 8.30 (d, *J* = 7.8 Hz, 2H), 8.01 (t, *J* = 7.8 Hz, 1H), 7.39 – 7.29 (m, 10H), 4.99 (s, 4H).

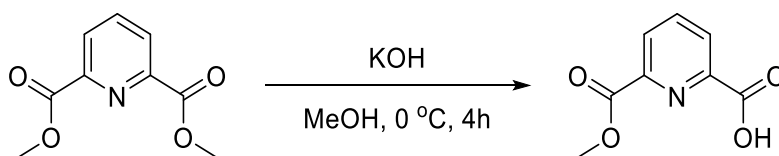
¹³C NMR (126 MHz, Chloroform-*d*) δ 161.50, 148.03, 139.29, 134.99, 129.23, 128.87, 128.58, 125.61, 78.65.

ESI-HRMS calc. for [C₂₁H₁₉N₃O₄ + H]⁺ *m/z* 378.1448, found *m/z* 378.1449 [M + H]⁺.

Melting point: 159 °C

Purity: 95.76%

6-(Methoxycarbonyl)picolinic acid (YJh4)



Potassium hydroxide pellets (287.67g, 5.13mmol) in 20 mL methanol was added to dimethyl pyridine-2,6-dicarboxylate (**YJh1**) (1g, 5.13mmol) in 40 mL methanol with ice bath protect. The reaction mixture was stirred at 0 °C for 4 h. The methanol was evaporated to a smaller volume via reduced pressure. The residue was dissolved in a proper amount of water and washed by ethyl acetate 5 times to remove the starting material. The pH of the water phase was adjusted to 2 by 2 M HCl and extracted 3 times with dichloromethane. The collected organic phase was dried over anhydrous Na₂SO₄ and the solvent was removed via reduced pressure. The product was obtained as white solid.

Yield: 0.697 g (75%).

¹H NMR (500 MHz, Chloroform-*d*) δ 10.25 (s, 1H), 8.40 (dd, *J* = 7.8, 1.1 Hz, 1H), 8.35 (dd, *J* = 7.9, 1.1 Hz, 1H), 8.12 (t, *J* = 7.8 Hz, 1H), 4.02 (s, 3H).

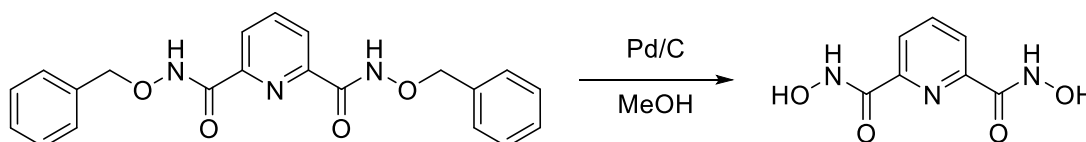
¹³C NMR (126 MHz, Chloroform-*d*) δ 164.31, 163.86, 147.00, 146.55, 139.74, 128.92, 127.02, 53.30.

ESI-HRMS calc. for [C₈H₇NO₄ + H]⁺ *m/z* 182.0448, found *m/z* 182.0454 [M + H]⁺.

Melting point: 149.8 °C

Purity: 95.22%

*N*²,*N*⁶-Dihydroxypyridine-2,6-dicarboxamide (YJh6)



10 mg Pd/C was added to *N*²,*N*⁶-bis(benzyloxy)pyridine-2,6-dicarboxamide **YJh2** (100 mg, 0.26 mmol) in 5 mL methanol. The mixture was stirred under hydrogen at room temperature for 25 min and monitored by TLC. Once the reaction was nearly completed, the mixture was filtrated by filter paper and the filtrate was evaporated via reduced pressure. The product was purified by HPLC and obtained as white solid after lyophilization.

Yield: 52.24 mg (50%).

¹H NMR (400 MHz, DMSO-*d*₆) δ 11.84 (s, 2H), 9.29 (s, 2H), 8.45 – 7.79 (m, 3H).

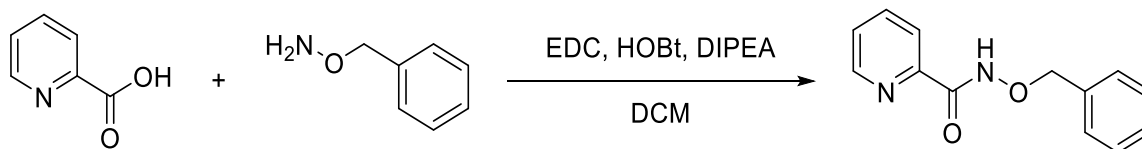
¹³C NMR (101 MHz, DMSO-*d*₆) δ 160.52, 148.82, 140.07, 124.30.

ESI-HRMS calc. for [C₇H₇N₃O₄ - H]⁻ m/z 196.0364, found m/z 196.03637 [M - H]⁻.

Melting point: 223 °C

Purity: 100%

***N*-(Benzyloxy)picolinamide (YJh8)**



The synthesis was according to the general procedure for amide coupling. The corresponding carboxylic acid was picolinic acid (200 mg, 1.62 mmol), and the amine was *O*-benzyloxylamine hydrochloride (311.16 mg, 1.95 mmol). The product was purified via silica gel chromatography eluting by hexane and ethyl acetate (30% ethyl acetate). The compound was obtained as white solid after lyophilization.

Yield: 99.01 mg (26.7%).

¹H NMR (500 MHz, Chloroform-*d*) δ 10.23 (s, 1H), 8.46 (s, 1H), 8.17 (d, *J* = 9.8 Hz, 1H), 7.96 – 7.77 (m, 1H), 7.53 – 7.31 (m, 6H), 5.06 (s, 2H).

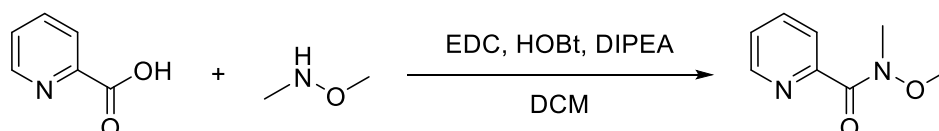
¹³C NMR (126 MHz, Chloroform-*d*) δ 162.06, 149.18, 148.33, 137.53, 135.39, 129.33, 128.86, 128.72, 126.79, 122.47, 78.70.

ESI-HRMS calc. for [C₁₃H₁₂N₂O₂ + H]⁺ m/z 229.0972 Da, found m/z 229.0977 Da [M + H]⁺.

Melting point: 96.4 °C

Purity: 97.98%

***N*-methoxy-*N*-methylpicolinamide (YJh9)**



The synthesis was according to the general procedure for amide coupling. The corresponding carboxylic acid was picolinic acid (200 mg, 1.62 mmol), and the amine was *N*,*O*-dimethylhydroxylamine hydrochloride (119.07 mg, 1.95 mmol). The product was purified via silica gel chromatography eluting by hexane and ethyl acetate (50% ethyl acetate). The compound was obtained as colorless oil after lyophilization.

Yield: 23 mg (8%).

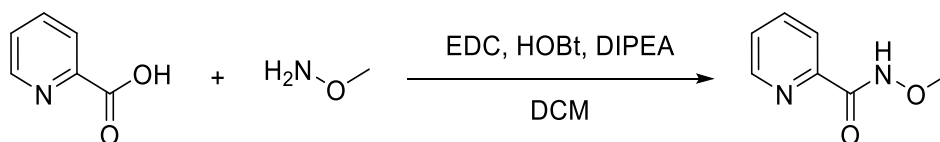
¹H NMR (400 MHz, Chloroform-*d*) δ 8.60 (d, *J* = 4.6 Hz, 1H), 7.95 – 7.70 (m, 1H), 7.64 (s, 1H), 7.35 (dd, *J* = 7.9, 4.5 Hz, 1H), 3.73 (s, 3H), 3.38 (s, 3H).

¹³C NMR (126 MHz, CHLOROFORM-*D*) δ 163.49, 153.17, 148.65, 136.87, 125.02, 123.34, 61.56, 32.82.

ESI-HRMS calc. for [C₈H₁₀N₂O₂ + H]⁺ m/z 167.0815, found m/z 167.0821 [M + H]⁺.

Purity: 98.01%

***N*-Methoxypicolinamide (YJh10)**



The synthesis was according to the general procedure for amide coupling. The corresponding carboxylic acid was picolinic acid (200 mg, 1.62 mmol), the amine was methoxyamine hydrochloride (162.82 mg, 1.95 mmol). The product was purified via silica gel chromatography eluting by hexane and ethyl acetate (60% ethyl acetate). The compound was obtained as colorless oil after lyophilization.

Yield: 173.02 mg (70%).

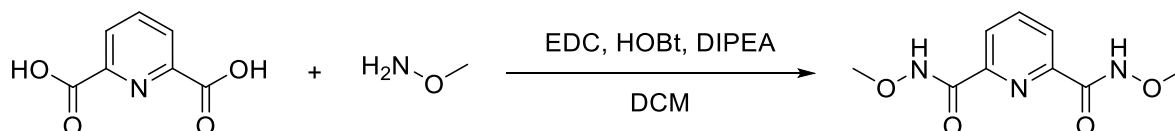
¹H NMR (500 MHz, Chloroform-*d*) δ 10.47 (s, 1H), 8.46 (s, 1H), 8.12 (d, *J* = 7.8 Hz, 1H), 7.81 (t, *J* = 7.8 Hz, 1H), 7.41 (d, *J* = 6.4 Hz, 1H), 3.85 (s, 3H).

¹³C NMR (126 MHz, Chloroform-*d*) δ 161.95, 149.05, 148.23, 137.49, 126.75, 122.43, 64.60.

ESI-HRMS calc. for [C₇H₈N₂O₂ + H]⁺ *m/z* 153.0659, found *m/z* 153.0668 [M + H]⁺.

Purity: 98.85%

N²,N⁶-Dimethoxypyridine-2,6-dicarboxamide (YJh11)



The synthesis was according to the general procedure for amide coupling. The equivalents of the reagents were as follows. Pyridine-2,6-dicarboxylic acid (200 mg, 1.20 mmol), EDC·HCl (504.72 mg, 2.63 mmol), HOBT (355.78 mg, 2.63 mmol) and DIPEA (1.38 mL, 7.90 mmol) were added to 5 mL dichloromethane. The corresponding amine was methoxyamine hydrochloride (219.89 mg, 2.63 mmol). The product was purified via silica gel chromatography eluting by dichloromethane and methanol (4% methanol) and the final compound was obtained as white solid.

Yield: 67.7 mg (15%).

¹H NMR (500 MHz, Chloroform-*d*) δ 11.79 (s, 2H), 8.36 (d, *J* = 8.3 Hz, 1H), 8.07 (t, *J* = 7.7 Hz, 1H), 3.78 (s, 3H).

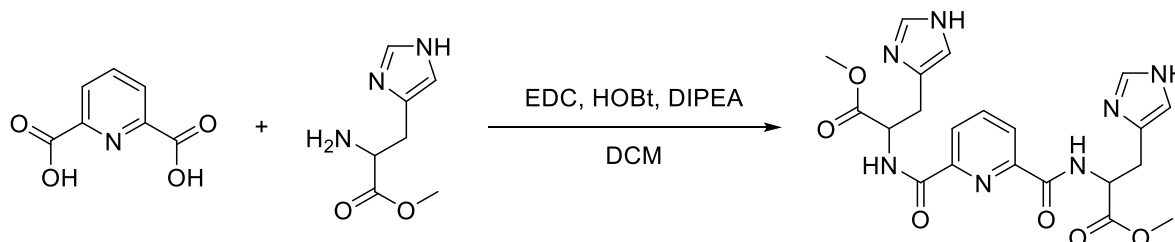
¹³C NMR (126 MHz, Chloroform-*d*) δ 161.60, 148.11, 139.31, 125.53, 64.48.

ESI-HRMS calc. for [C₉H₁₁N₃O₄ + H]⁺ *m/z* 226.0822, found *m/z* 226.0829 [M + H]⁺.

Melting point: 93 °C

Purity: 93.87%

Dimethyl 2,2'-((pyridine-2,6-dicarbonyl)bis(azanediyl))bis(3-(1*H*-imidazol-4-yl)propanoate) (YJh12 method 1)

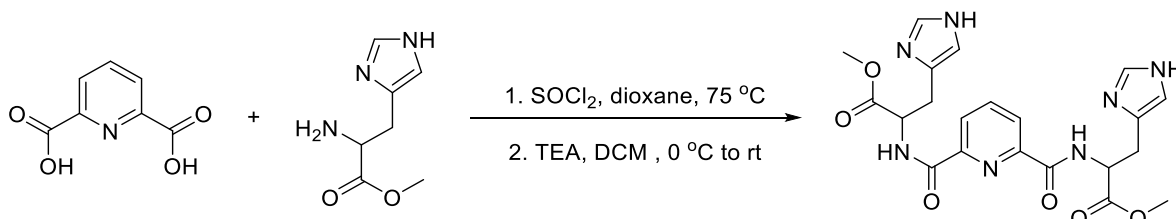


The synthesis was according to the general procedure for amide coupling. Pyridine-2,6-dicarboxylic acid (200 mg, 1.20 mmol), EDC·HCl (504.72 mg, 2.63 mmol), HOBT (355.78 mg, 2.63 mmol) and DIPEA

(1.38 mL, 7.90 mmol) were added to 5 mL dichloromethane. The reaction was stirring for 15 min with ice bath protect before the addition of histidyl methyl ester dihydrochloride (637.41 mg, 2.63 mmol). The reaction was stirred at room temperature overnight. The product was purified via silica gel chromatography eluting by hexane and ethyl acetate containing 0.4% TEA (50% ethyl acetate). The compound was obtained as white solid.

Yield: 28.09 mg (5%).

Dimethyl 2,2'-((pyridine-2,6-dicarbonyl)bis(azanediyl))bis(3-(1*H*-imidazol-4-yl)propanoate) (YJh12 method 2)



Thionyl chloride (868.08 μL , 11.97 mmol) was added dropwise into 2,6-pyridinedicarboxylic acid (400 mg, 2.39 mmol) in 1,4-dioxane (5 mL). The reaction mixture was stirred at 80 $^{\circ}\text{C}$ for 24 h. Thionyl chloride and 1,4-dioxane were removed via reduced pressure to afford the acid chloride as white solid. The acid chloride was dissolved in dichloromethane (30 mL) and slowly added into a solution of histidyl methyl ester dihydrochloride (1.16 g, 4.79 mmol) and triethylamine (4.01 mL, 28.72 mmol) in dichloromethane (30 mL). The reaction mixture was stirred at 0 $^{\circ}\text{C}$ for 2 h and room temperature for 12 h. The final mixture was diluted by dichloromethane and washed by saturated NaHCO_3 solution and brine. The organic phase was dried over anhydrous Na_2SO_4 and concentrated via reduced pressure. The resulting residue was purified via flash chromatography eluting by hexane and ethyl acetate containing 0.4% TEA (50% ethyl acetate). The compound was obtained as white solid.

Yield: 786.55 mg (70%).

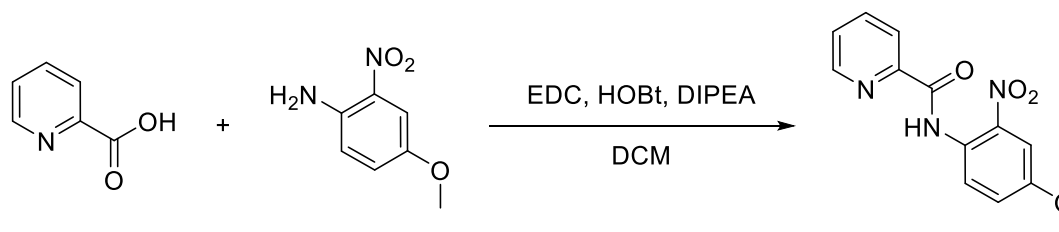
$^1\text{H NMR}$ (600 MHz, Methanol- d_4) δ 8.24 (d, $J = 7.7$ Hz, 2H), 8.13 (dd, $J = 8.2, 7.3$ Hz, 1H), 7.58 (d, $J = 1.2$ Hz, 2H), 6.94 (d, $J = 1.2$ Hz, 2H), 4.94 (dd, $J = 9.0, 5.1$ Hz, 2H), 3.77 (s, 6H), 3.37 – 3.20 (m, 4H).

$^{13}\text{C NMR}$ (151 MHz, Methanol- d_4) δ 173.30, 165.71, 149.90, 140.50, 136.53, 135.18, 126.27, 117.68, 54.48, 52.95, 30.09.

ESI-HRMS calc. for $[\text{C}_{21}\text{H}_{23}\text{N}_7\text{O}_6 + \text{H}]^+$ m/z 470.1783, $[\text{C}_{21}\text{H}_{23}\text{N}_7\text{O}_6 + 2\text{H}]^{2+}$ m/z 235.5928, found m/z 470.1781 $[\text{M} + \text{H}]^+$, 235.5936 $[\text{M} + 2\text{H}]^{2+}$.

Purity: 99.57%

***N*-(4-methoxy-2-nitrophenyl)picolinamide (YJh13)**



The synthesis was according to the general procedure for amide coupling. The corresponding carboxylic acid was picolinic acid (200 mg, 1.62 mmol), and the amine was 4-methoxy-2-nitroaniline

(327.80 mg, 1.95 mmol). The product was purified via silica gel chromatography eluting by hexane and ethyl acetate (15% ethyl acetate) and the final compound was obtained as yellow solid.

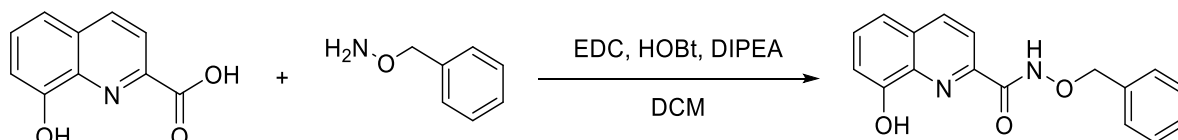
Yield: 138.94 mg (31.3%).

¹H NMR (500 MHz, Chloroform-*d*) δ 12.53 (s, 1H), 8.93 (d, *J* = 9.2 Hz, 1H), 8.73 (s, 1H), 8.28 (d, *J* = 7.8 Hz, 1H), 7.92 (t, *J* = 8.0 Hz, 1H), 7.74 (s, 1H), 7.51 (dd, *J* = 7.7, 4.9 Hz, 1H), 7.29 (d, *J* = 10.2 Hz, 1H), 3.88 (s, 3H).

¹³C NMR (126 MHz, Chloroform-*d*) δ 163.31, 155.25, 149.67, 148.74, 137.81, 137.74, 128.38, 126.96, 123.74, 123.23, 122.76, 109.08, 56.06.

ESI-HRMS calc. for [C₁₃H₁₁N₃O₄ + H]⁺ *m/z* 274.0822, found *m/z* 274.0826 [M + H]⁺.

***N*-(benzyloxy)-8-hydroxyquinoline-2-carboxamide (YJh14)**



The synthesis was according to the general procedure for amide coupling. 8-hydroxyquinoline-2-carboxylic acid (200 mg, 1.06 mmol), EDC·HCl (243.21 mg, 1.27 mmol), HOBT (171.44 g, 1.27 mmol) and DIPEA (662.99 μ L, 3.81 mmol) were added to dichloromethane (5 mL) and stirred for 15 min with ice bath protect, then *O*-benzylhydroxylamine hydrochloride (202.50 mg, 1.27 mmol) was added. The product was purified via hexane and ethyl acetate silica gel chromatograph (50% ethyl acetate) and the final compound was obtained as white solid.

Yield: 179.85 mg (57.8%).

¹H NMR (500 MHz, Chloroform-*d*) δ 8.22 (s, 2H), 7.51 (t, *J* = 7.9 Hz, 1H), 7.37 – 7.28 (m, 3H), 7.26 – 7.17 (m, 4H), 5.02 (s, 2H).

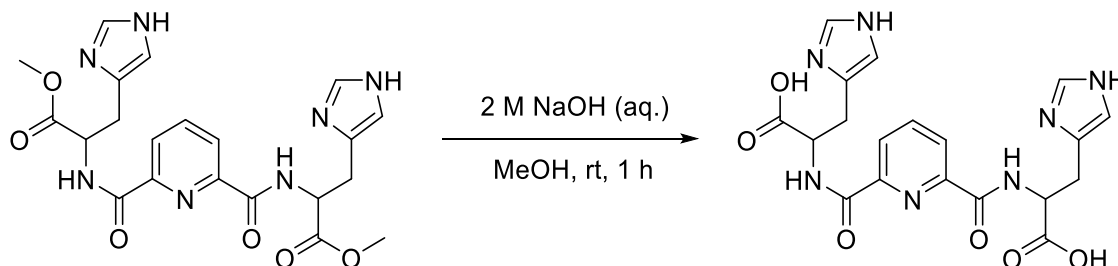
¹³C NMR (126 MHz, Chloroform-*d*) δ 162.70, 152.52, 146.44, 138.06, 136.73, 134.82, 130.11, 129.95, 129.48, 129.00, 128.65, 119.69, 118.40, 111.79, 78.95.

ESI-HRMS calc. for [C₁₇H₁₄N₂O₃ + H]⁺ *m/z* 295.1077, [C₁₇H₁₄N₂O₃ + 2H]²⁺ *m/z* 148.0575, found *m/z* 295.1080 [M + H]⁺, 148.0599 [M + 2H]²⁺.

Melting point: 88.5 °C

Purity: 97.65%

2,2'-((Pyridine-2,6-dicarbonyl)bis(azanediyl))bis(3-(1*H*-imidazol-4-yl)propanoic acid) (YJh15)



The synthesis was according to the general procedure for hydrolysis of methyl esters catalyzed by hydroxide ion. 2 M NaOH (3 mL) was added into dimethyl 2, 2'-((pyridine-2,6 dicarbonyl)bis(azanediyl))bis(3-(1*H*-imidazol-4-yl)propanoate) (YJh12) (50 mg, 0.107 mmol) in methanol (1 mL). The compound was purified via HPLC. The final product was obtained as white solid after lyophilization.

Yield: 29 mg (62%).

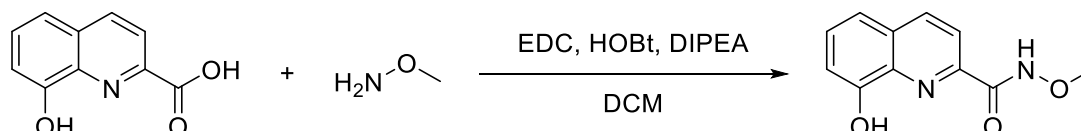
¹H NMR (500 MHz, Deuterium Oxide) δ 8.58 (d, J = 1.4 Hz, 2H), 8.23 – 8.04 (m, 3H), 7.31 (d, J = 1.4 Hz, 2H), 5.06 (dd, J = 9.4, 5.0 Hz, 2H), 3.54 (dd, J = 15.4, 4.9 Hz, 3H), 3.37 (dd, J = 15.5, 9.4 Hz, 2H).

¹³C NMR (126 MHz, Deuterium Oxide) δ 173.97, 165.93, 140.31, 147.80, 133.63, 129.25, 125.95, 117.45, 52.41, 26.62.

ESI-HRMS calc. for [C₁₉H₁₉N₇O₆ + H]⁺ m/z 442.1470, found m/z 442.1489 [M + H]⁺.

Purity: 98.19%

8-hydroxy-N-methoxyquinoline-2-carboxamide (YJh18)



The synthesis was according to the general procedure for amide coupling. 8-Hydroxyquinoline-2-carboxylic acid (200 mg, 1.06 mmol), EDC-HCl (243.21 mg, 1.27 mmol), HOBT (171.44 g, 1.27 mmol) and DIPEA (662.99 mL, 3.81 mmol) were added to dichloromethane (5 mL) and stirred for 15min with ice bath protect before addition of methoxyamine hydrochloride (105.96 mg, 1.27 mmol). The reaction was stirred at room temperature overnight. The compound was purified via chloromethane and methanol silica gel chromatograph (2% methanol). The final product was obtained as white solid.

Yield: 126.01 mg (54.62%).

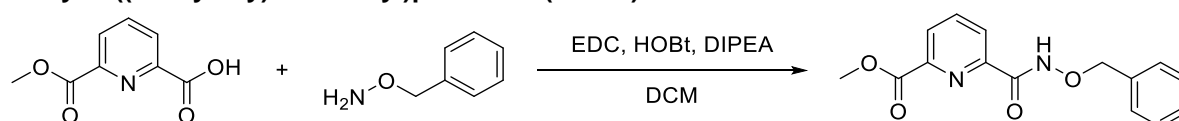
¹H NMR (500 MHz, Methanol-*d*₄) δ 8.40 (d, J = 8.5 Hz, 1H), 8.13 (d, J = 8.5 Hz, 1H), 7.54 (dd, J = 8.3, 7.6 Hz, 1H), 7.42 (dd, J = 8.3, 1.2 Hz, 1H), 7.16 (dd, J = 7.6, 1.2 Hz, 1H), 3.90 (s, 3H). **¹³C NMR** (126 MHz, Methanol-*d*₄) δ 163.74, 154.93, 147.74, 138.94, 138.31, 131.54, 130.85, 119.82, 119.01, 112.77, 64.66.

ESI-HRMS calc. for [C₁₁H₁₀N₂O₃ + H]⁺ m/z 219.0764, found m/z 219.0770 [M + H]⁺.

Melting point: 213.7 °C

Purity: 98.96%

Methyl 6-((benzyloxy)carbamoyl)picolinate (YJh19)



The synthesis was according to the general procedure for amide coupling. 6-(methoxycarbonyl)picolinic acid (**YJh4**) (200 mg, 1.10 mmol), EDC-HCl (253.98 mg, 1.32 mmol), HOBT (179.03 g, 1.32 mmol) and DIPEA (692.34 μ L, 3.97 mmol) were added to 5 mL dichloromethane. The corresponding amine was O-benzylhydroxylamine hydrochloride (211.46 mg, 1.32 mmol). The reaction was stirred at room temperature overnight. The compound was purified via hexane and ethyl acetate silica gel chromatograph (33% ethyl acetate). The final product was obtained as white solid.

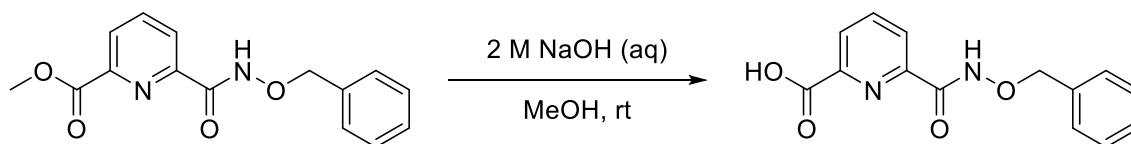
Yield: 188 mg (59.48%).

¹H NMR (500 MHz, Chloroform-*d*) δ 10.80 (s, 1H), 8.36 (dd, J = 7.8, 1.1 Hz, 1H), 8.21 (dd, J = 7.8, 1.1 Hz, 1H), 8.01 (t, J = 7.8 Hz, 1H), 7.50 – 7.44 (m, 2H), 7.40 – 7.34 (m, 3H), 5.07 (s, 2H), 3.97 (s, 3H).

¹³C NMR (126 MHz, Chloroform-*d*) δ 164.98, 161.23, 149.65, 146.58, 138.77, 135.34, 129.43, 128.88, 128.68, 127.75, 125.70, 78.77, 53.10.

ESI-MS calc. for $[C_{15}H_{14}N_2O_4 + H]^+$ m/z 287.1, $[C_{15}H_{14}N_2O_4 + Na]^+$ m/z 309.1, found m/z 287.3 $[M + H]^+$, 309.3 $[M + Na]^+$.

6-((Benzyloxy)carbamoyl)picolinic acid (YJh20)



The synthesis was according to the general procedure for hydrolysis of methyl esters catalyzed by hydroxide ion. The corresponding methyl ester was methyl 6-((benzyloxy)carbamoyl)picolinate (**YJh19**) (80 mg, 0.279 mmol). The final product was obtained as white solid.

Yield: 53.60 mg (70.45%).

¹H NMR (500 MHz, DMSO-*d*₆) δ 12.91 (s, 1H), 12.32 (s, 1H), 8.29 – 8.21 (m, 3H), 7.52 – 7.45 (m, 2H), 7.43 – 7.35 (m, 3H), 5.00 (s, 2H).

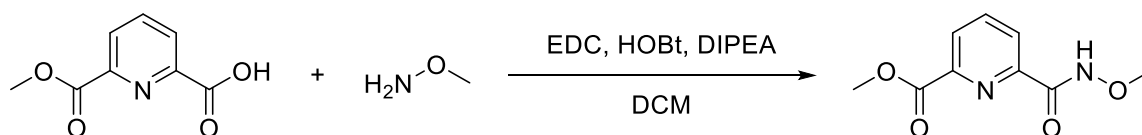
¹³C NMR (126 MHz, DMSO-*d*₆) δ 164.62, 160.40, 148.51, 145.98, 140.08, 135.66, 129.03, 128.49, 128.42, 126.83, 125.44, 77.42.

ESI-HRMS calc. for $[C_{14}H_{12}N_2O_4 + H]^+$ m/z 273.0870, found m/z 273.0874 $[M + H]^+$.

Melting point: 157.9 °C

Purity: 99.73%

Methyl 6-(methoxycarbamoyl)picolinate (YJh21)



The synthesis was according to the general procedure for amide coupling. 6-(Methoxycarbonyl)picolinic acid (**YJh4**) (200 mg, 1.10 mmol), EDC·HCl (253.98 mg, 1.32 mmol) and HOBt (179.03 g, 1.32 mmol) were added to 5 mL dichloromethane with DIPEA (692.34 μ L, 3.97 mmol) and stirred for 15 min with ice bath protect before the addition of methoxyamine hydrochloride (110.65 mg, 1.32 mmol). The compound was purified via hexane and ethyl acetate silica gel chromatograph (60% ethyl acetate). The final product was obtained as white solid.

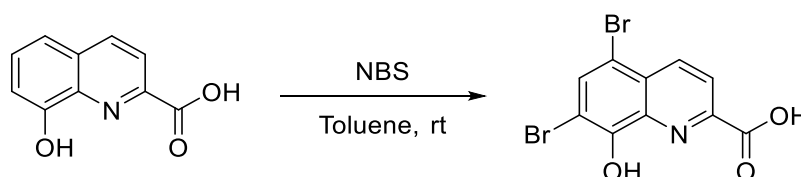
Yield: 146.71 mg (63.22%).

¹H NMR (500 MHz, Chloroform-*d*) δ 10.95 (s, 1H), 8.34 (dd, $J = 7.8, 1.1$ Hz, 1H), 8.20 (dd, $J = 7.8, 1.2$ Hz, 1H), 8.00 (t, $J = 7.8$ Hz, 1H), 3.98 (s, 3H), 3.89 (s, 3H).

¹³C NMR (126 MHz, Chloroform-*d*) δ 164.97, 161.00, 149.58, 146.49, 138.77, 127.72, 125.69, 64.64 (q, $J = 2.2$ Hz), 53.11 (q, $J = 2.2$ Hz).

ESI-MS calc. for $[C_9H_{10}N_2O_4 + H]^+$ m/z 211.1, $[C_{15}H_{14}N_2O_4 + Na]^+$ m/z 233.1, found m/z 211.0 $[M + H]^+$, 233.0 $[M + Na]^+$.

5,7-Dibromo-8-hydroxyquinoline-2-carboxylic acid (YJh22 or YJh23)



N-bromosuccinimide (207 mg, 1.16 mmol) was added to 8-hydroxyquinoline-2-carboxylic acid (100 mg, 0.529 mmol) in toluene (20 ml) and stirred overnight. The reaction was quenched by 1 M HCl and extracted 3 times with ethyl acetate. The collected organic phase was washed by brine and dried over anhydrous Na₂SO₄. The solvent was evaporated via reduced pressure. The resulting residue was purified via HPLC or silica gel chromatograph (ethyl acetate, methanol and H₂O, the ratio was 20 to 1.5 to 1). The final product was obtained as yellow solid.

Yield: 165.07 mg (90%).

¹H NMR (500 MHz, DMSO-*d*₆) δ 12.98 (s, 1H), 11.13 (s, 1H), 8.59 (d, *J* = 8.7 Hz, 1H), 8.28 (d, *J* = 8.7 Hz, 1H), 8.19 (s, 1H).

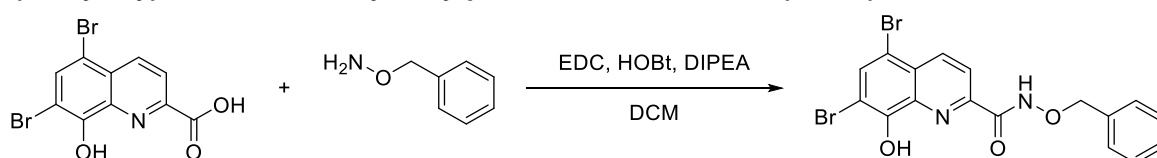
¹³C NMR (126 MHz, DMSO-*d*₆) δ 164.38, 151.38, 145.82, 137.93, 137.01, 135.67, 127.71, 121.84, 108.88, 105.65.

ESI-HRMS calc. for [C₁₀H₅Br₂NO₃ + H]⁺ *m/z* 345.8709 (51.4%), 347.8688 (100.0%), 349.8668 (48.6%), found *m/z* 345.87101 (46.4%), 347.8686 (100%), 349.86687 (44.3%) [M + H]⁺.

Melting point: 263 °C

Purity: 100%

***N*-(benzyloxy)-5,7-dibromo-8-hydroxyquinoline-2-carboxamide (YJh27)**



The synthesis was according to the general procedure for amide coupling. 5,7-Dibromo-8-hydroxyquinoline-2-carboxylic acid (**YJh22**) (150 mg, 0.432 mmol), EDC·HCl (99.45 mg, 0.519 mmol), HOBT (70.10 mg, 0.519 mmol) and DIPEA (271.12 μL, 1.56 mmol) were added to dichloromethane (5 mL) and stirred for 15min with ice bath protect before the addition of *O*-benzylhydroxylamine hydrochloride (82.80 mg, 0.519 mmol). The compound was purified via hexane and ethyl acetate silica gel chromatograph (30% ethyl acetate). The final product was obtained as brown solid.

Yield: 125.60 mg (64.26%).

¹H NMR (700 MHz, Methanol-*d*₄) δ 8.64 (d, *J* = 8.7 Hz, 1H), 8.28 (d, *J* = 8.7 Hz, 1H), 8.02 (s, 1H), 7.54 – 7.47 (m, 2H), 7.42 – 7.34 (m, 3H), 5.07 (s, 2H).

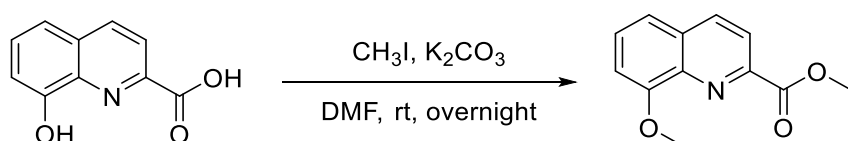
¹³C NMR (151 MHz, Methanol-*d*₄) δ 163.00, 152.74, 149.29, 138.86, 136.80, 133.63, 130.50, 129.83, 129.57, 129.28, 121.30, 110.17, 106.67, 102.23, 79.55.

ESI-HRMS calc. for [C₁₇H₁₂Br₂N₂O₃ + H]⁺ *m/z* 450.9287 (51.4%), 452.9267 (100.0%), 454.9247 (48.6%), found *m/z* 450.9283, 452.9265, 454.9246 [M + H]⁺.

Melting point: 194.6 °C

Purity: 97.88%

Methyl 8-methoxyquinoline-2-carboxylate (YJh31)



Iodomethane (263.40 μL, 4.23 mmol) was added to 8-hydroxy-2-quinoline carboxylic acid (200 mg, 1.06 mmol) and K₂CO₃ (730.56 mg, 5.29 mmol) in DMF (8 mL) with ice bath protect. The mixture was stirred

at room temperature overnight. Then 10 mL brine solution was poured into the reaction mixture and extracted 3 times with ethyl acetate. The collected organic phase was washed by brine and dried over anhydrous Na_2SO_4 . The solvent was evaporated via reduced pressure. The residue was washed with Et_2O . The insoluble material was collected and dried in vacuo to offer the product. The compound was further purified via hexane and ethyl acetate silica gel chromatograph (3% ethyl acetate). The final product was obtained as white (a little yellow) solid.

Yield: 215.26 mg (93.73%).

^1H NMR (500 MHz, Chloroform-*d*) δ 8.26 (d, $J = 8.4$ Hz, 1H), 8.21 (d, $J = 8.5$ Hz, 1H), 7.55 (t, $J = 8.0$ Hz, 2H), 7.41 (d, $J = 8.5$ Hz, 1H), 7.07 (d, $J = 7.9$ Hz, 1H), 4.07 (s, 5H), 4.03 (s, 5H).

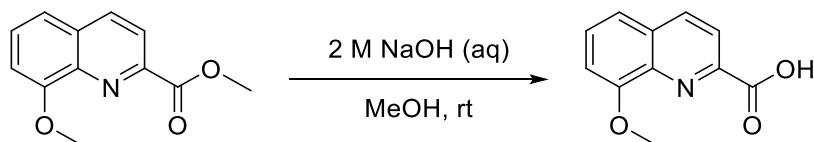
^{13}C NMR (126 MHz, Chloroform-*d*) δ 166.11, 156.07, 146.70, 139.56, 137.27, 130.64, 129.28, 121.67, 119.21, 108.15, 56.18, 53.12.

ESI-HRMS calc. for $[\text{C}_{12}\text{H}_{11}\text{NO}_3 + \text{H}]^+$ m/z 218.0812, found m/z 218.0818 $[\text{M} + \text{H}]^+$.

Melting point: 121 °C

Purity: 97.21%

8-Methoxyquinoline-2-carboxylic acid (YJh32)



The synthesis was according to the general procedure for hydrolysis of methyl esters catalyzed by hydroxide ion. 2 M NaOH (3 mL) was added into methyl 8-methoxyquinoline-2-carboxylate (**YJh31**) (100 mg, 0.460 mmol) in methanol (3 mL). The final product was obtained as white (a little yellow) solid. Yield: 59 mg (63.07%).

^1H NMR (500 MHz, Chloroform-*d*) δ 10.07 (s, 1H), 8.33 (d, $J = 8.4$ Hz, 1H), 8.25 (d, $J = 8.4$ Hz, 1H), 7.61 (t, $J = 8.0$ Hz, 1H), 7.47 (dd, $J = 8.4, 1.2$ Hz, 1H), 7.13 (dd, $J = 7.8, 1.1$ Hz, 1H), 4.07 (s, 3H).

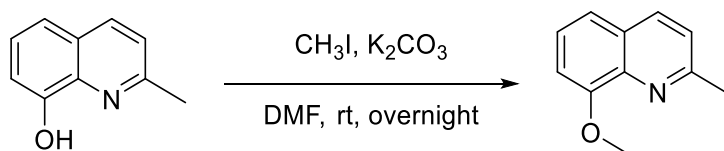
^{13}C NMR (126 MHz, Chloroform-*d*) δ 164.67, 155.53, 144.72, 138.65, 137.98, 131.21, 129.79, 119.85, 119.50, 109.13, 56.14.

ESI-HRMS calc. for $[\text{C}_{11}\text{H}_9\text{NO}_3 + \text{H}]^+$ m/z 204.0655, found m/z 204.0662 $[\text{M} + \text{H}]^+$.

Melting point: 160 °C

Purity: 98.78%

8-Methoxy-2-methylquinoline (YJh33)



Iodomethane (626.01 μL , 10.05 mmol) was added into 2-methylquinolin-8-ol (800 mg, 5.03 mmol) and K_2CO_3 (2.08 g, 15.08 mmol) in DMF (5 mL) with ice bath protect. The mixture was stirred at room temperature overnight. Then 10 mL brine solution was poured into the reaction mixture and extracted 3 times with ethyl acetate. The collected organic phase was washed with water and dried over anhydrous Na_2SO_4 . The solvent was evaporated via reduced pressure. The resulting residue was purified via hexane and ethyl acetate silica gel chromatograph (30% ethyl acetate). The final product was obtained as white solid.

Yield: 820.71 mg (94.28%).

¹H NMR (500 MHz, Chloroform-*d*) δ 7.98 (d, *J* = 8.4 Hz, 1H), 7.37 (t, *J* = 8.1 Hz, 1H), 7.32 (dd, *J* = 8.2, 1.4 Hz, 1H), 7.28 (d, *J* = 8.4 Hz, 1H), 7.01 (dd, *J* = 7.6, 1.3 Hz, 1H), 4.05 (s, 3H), 2.78 (s, 3H).

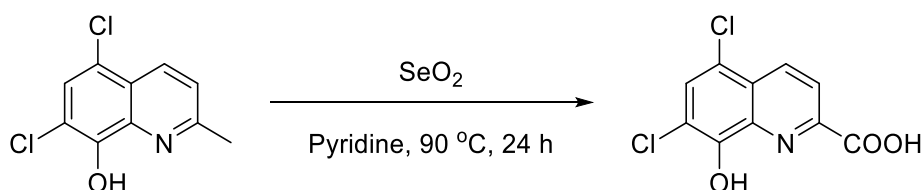
¹³C NMR (126 MHz, Chloroform-*d*) δ 158.21, 154.88, 139.77, 136.19, 127.63, 125.76, 122.67, 119.49, 107.66, 56.05, 25.80.

ESI-HRMS calc. for [C₁₁H₁₁NO + H]⁺ *m/z* 174.0913, found *m/z* 174.0919 [M + H]⁺.

Melting point: 125.3 °C

Purity: 99.02%

5, 7-Dichloro-8-hydroxyquinoline-2-carboxylic acid (YJh34)



The synthesis was according to the general procedure for oxidation of 2-methyl quinoline analogues by selenium dioxide. Selenium dioxide (146 mg, 1.32 mmol) was added into 5,7-dichloro-2-methylquinolin-8-ol (200 mg, 0.88 mmol) in pyridine (4 mL). The compound was purified via silica gel chromatograph (ethyl acetate, MeOH and H₂O, the ratio was 8 to 1.5 to 1). The final product was obtained as yellow solid after lyophilization.

Yield: 106.36 mg (47%).

¹H NMR (500 MHz, DMSO-*d*₆) δ 13.01 (s, 1H), 10.99 (s, 1H), 8.61 (d, *J* = 8.7 Hz, 1H), 8.23 (d, *J* = 8.7 Hz, 1H), 7.91 (s, 1H).

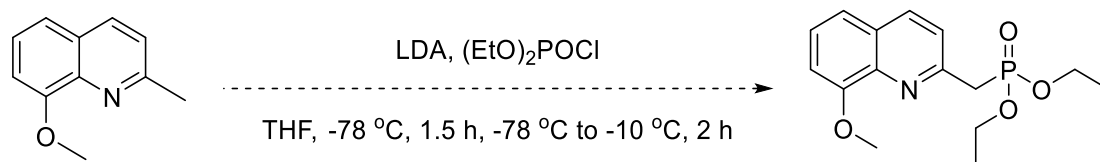
¹³C NMR (126 MHz, DMSO-*d*₆) δ 164.42, 149.44, 145.83, 136.96, 135.36, 130.18, 125.92, 121.30, 119.14, 116.14.

ESI-HRMS calc. for [C₁₀H₅Cl₂NO₃ + H]⁺ *m/z* 257.9719 (100.0%), 259.9690 (63.9%), 261.9660 (10.2%), found *m/z* 257.97199 (100%), 259.96857 (65.6%), 261.96523 (9.5%) [M + H]⁺.

Melting point: 246.6 °C

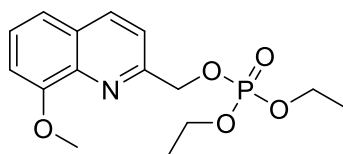
Purity: 99.59%

Diethyl ((8-methoxyquinolin-2-yl)methyl)phosphonate (YJh35)



LDA (1.27 mL, 2.53 mmol) was added dropwise to 8-methoxy-2-methylquinoline (**YJh33**) (350 mg, 2.02 mmol) in THF (3 mL) at -78 °C. The reaction was stirred at -78 °C for 1.5 h. After diethyl chlorophosphate (321.20 μ l, 2.22 mmol) was added dropwise to the reaction flask at -78 °C, the reaction system was allowed to warm to -10 °C over 2 h. Then the reaction mixture was poured on 10 mL saturated aqueous ammonium chloride solution and extracted 3 times with ethyl acetate. The collected organic phase was washed with water and dried over anhydrous Na₂SO₄. The solvent was evaporated via reduced pressure. The resulting residue was purified via chloromethane and methanol silica gel chromatograph (3% methanol).

This reaction did not get the aimed product, but a side product (brown solid) as follows.



Diethyl ((8-methoxyquinolin-2-yl)methyl) phosphate (YJh35 side product)

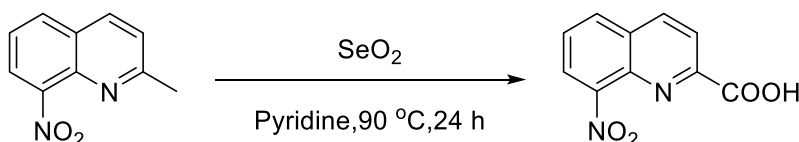
¹H NMR (400 MHz, Chloroform-*d*) δ 8.17 (d, *J* = 8.5 Hz, 1H), 7.69 (d, *J* = 8.5 Hz, 1H), 7.44 (dd, *J* = 8.2, 7.6 Hz, 1H), 7.38 (dd, *J* = 8.3, 1.4 Hz, 1H), 7.05 (dd, *J* = 7.6, 1.3 Hz, 1H), 5.39 (d, *J* = 7.5 Hz, 2H), 4.20 – 4.12 (m, 4H), 4.06 (s, 3H), 1.32 (td, *J* = 7.1, 1.0 Hz, 6H).

¹³C NMR (101 MHz, Chloroform-*d*) δ 155.67 (d, *J* = 9.1 Hz), 155.14, 139.29, 137.16, 128.83, 126.92, 119.66, 119.52 (d, *J* = 1.0 Hz), 108.14, 70.08 (d, *J* = 5.7 Hz), 64.19, 56.18, 16.21 (d, *J* = 6.7 Hz).

³¹P NMR (162 MHz, Chloroform-*d*) δ -0.53.

ESI-MS calc. for [C₁₅H₂₀NO₅P + H]⁺ *m/z* 326.1, found *m/z* 326.0 [M + H]⁺.

8-Nitroquinoline-2-carboxylic acid (YJh36)



The synthesis was according to the general procedure for oxidation of 2-methyl quinoline analogues by selenium dioxide. Selenium dioxide (176.89 mg, 1.59 mmol) was added to 2-methyl-8-nitroquinoline (200 mg, 1.06 mmol) in pyridine (4 mL). The reaction mixture was stirred at 100 °C for 16 h. The compound was purified via silica gel chromatograph (ethyl acetate, MeOH and H₂O, the ratio was 8 to 1.5 to 1). The final product was obtained as white solid after lyophilization.

Yield: 165.20 mg (71.25%).

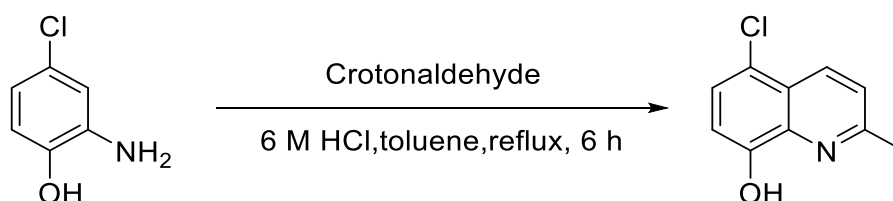
¹H NMR (500 MHz, DMSO-*d*₆) δ 13.74 (s, 1H), 8.75 (d, *J* = 8.6 Hz, 1H), 8.37 (td, *J* = 7.7, 1.3 Hz, 2H), 8.26 (d, *J* = 8.5 Hz, 1H), 7.87 (dd, *J* = 8.3, 7.5 Hz, 1H).

¹³C NMR (126 MHz, DMSO-*d*₆) δ 165.69, 150.76, 148.26, 138.32, 137.71, 131.97, 129.28, 127.69, 124.22, 122.66.

ESI-HRMS calc. for [C₁₀H₆N₂O₄ + H]⁺ *m/z* 219.0400, [C₁₀H₆N₂O₄ + 2H]²⁺ *m/z* 110.0237, found *m/z* 219.0407 [M + H]⁺, 110.0201 [M + 2H]²⁺.

Melting point: 174.6 °C

5-Chloro-2-methylquinolin-8-ol (YJh37)



The synthesis was according to the general procedure for synthesis of 2-methyl quinoline analogues. Crotonaldehyde (1.15 mL, 0.976 mmol) was diluted in toluene (13.54 mL) and added dropwise to 2-amino-4-chlorophenol (1 g, 6.97 mmol) in 6 M HCl (88.75 mL). The reaction was stirred under 75 °C for

5 h. The compound was purified via hexane and ethyl acetate silica gel chromatograph (2%, 15%, and 95% ethyl acetate). The final product was obtained as yellow solid.

Yield: 674.34 mg (50%).

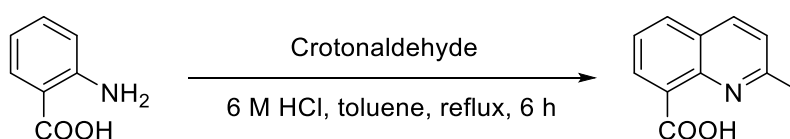
¹H NMR (500 MHz, Chloroform-*d*) δ 8.37 (d, *J* = 8.6 Hz, 1H), 7.42 (d, *J* = 8.2 Hz, 1H), 7.40 (d, *J* = 8.6 Hz, 1H), 7.06 (d, *J* = 8.2 Hz, 1H), 2.74 (s, 3H).

¹³C NMR (126 MHz, Chloroform-*d*) δ 157.80, 150.96, 138.23, 133.54, 126.52, 124.64, 123.63, 120.42, 109.94, 24.93.

ESI-HRMS calc. for [C₁₀H₈CINO + H]⁺ *m/z* 194.0367 (100.0%), 196.0338 (32.0%), found *m/z* 194.0373, 196.0344 [M + H]⁺.

Purity: 98.54%

2-Methylquinoline-8-carboxylic acid (YJh38)



The synthesis was according to the general procedure for synthesis of 2-methyl quinoline analogues. Crotonaldehyde (483.29 μL, 5.83 mmol) in toluene (5.4 mL) was added dropwise in 2-aminobenzoic acid (400 mg, 2.92 mmol) in 6 M HCl (35.4 mL). The reaction was stirred at 75 °C overnight. The compound was purified via hexane and ethyl acetate silica gel chromatograph (30% ethyl acetate). The final product was obtained as white solid.

Yield: 221.68 mg (40.6%).

¹H NMR (500 MHz, Chloroform-*d*) δ 8.71 (dd, *J* = 7.3, 1.5 Hz, 1H), 8.26 (d, *J* = 8.5 Hz, 1H), 8.02 (dd, *J* = 8.1, 1.5 Hz, 1H), 7.65 (t, *J* = 7.7 Hz, 1H), 7.45 (d, *J* = 8.5 Hz, 1H), 2.81 (s, 3H).

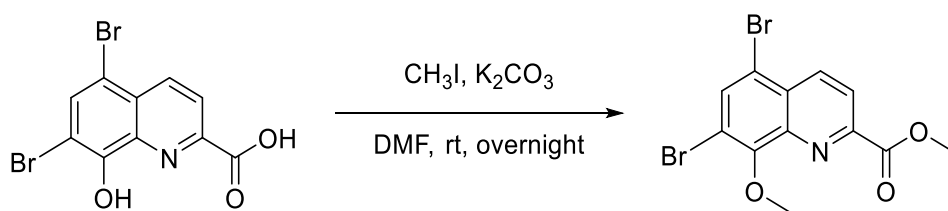
¹³C NMR (126 MHz, Chloroform-*d*) δ 167.64, 158.81, 145.00, 138.71, 135.11, 132.82, 126.53, 126.49, 124.10, 122.86, 24.89.

ESI-HRMS calc. for [C₁₁H₉NO₂ + H]⁺ *m/z* 188.0706, found *m/z* 188.0713 [M + H]⁺.

Melting point: 153.8 °C

Purity: 97.55%

Methyl 5,7-dibromo-8-methoxyquinoline-2-carboxylate (YJh47)



Iodomethane (198.2 μL, 3.18 mmol) was added to 5,7-dibromo-8-hydroxyquinoline-2-carboxylic acid (YJh22) (138 mg, 0.40 mmol) and K₂CO₃ (274.84 mg, 1.99 mmol) in DMF (8 mL) with ice bath protect. The mixture was stirred at room temperature overnight. Then the reaction mixture was poured on 10 mL brine solution and extracted 3 times with ethyl acetate. The collected organic phase was washed by brine and dried over anhydrous Na₂SO₄. The solvent was evaporated via reduced pressure. The residue was washed with Et₂O. The insoluble material was collected and dried in vacuo. The compound

was further purified via hexane and ethyl acetate silica gel chromatograph (3% ethyl acetate). The final product was obtained as white solid.

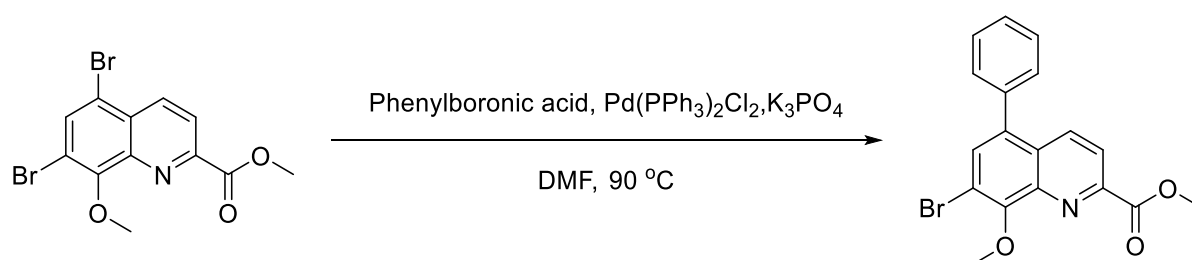
Yield: 119 mg (79.78%).

¹H NMR (500 MHz, Chloroform-*d*) δ 8.61 (d, *J* = 8.8 Hz, 1H), 8.27 (d, *J* = 8.8 Hz, 1H), 8.08 (s, 1H), 4.30 (s, 3H), 4.07 (s, 3H).

¹³C NMR (151 MHz, Chloroform-*d*) δ 165.46, 154.42, 148.13, 142.94, 137.72, 135.73, 129.21, 122.38, 116.84, 115.70, 63.05, 53.33.

ESI-HRMS calc. for [C₁₂H₉Br₂NO₃ + H]⁺ *m/z* 375.9 (100.0%), 373.9 (51.4%), 377.9 (48.6%), [C₁₂H₉Br₂NO₃ + Na]⁺ *m/z* 397.8821 (100.0%), 395.8841 (51.4%), 399.8800 (48.6%), found *m/z* 375.9005, 373.9025, 377.8986 [M + H]⁺, 397.8822, 395.8840, 399.8803 [M + Na]⁺.

Methyl 7-bromo-8-methoxy-5-phenylquinoline-2-carboxylate (YJh48)



Bis(triphenylphosphine)palladium(II) dichloride (2.81 mg, 0.004 mmol) was added to a mixture of methyl 5,7-dibromo-8-methoxyquinoline-2-carboxylate (YJh47) (50 mg, 0.133 mmol), phenylboronic acid (48.77 mg, 0.400 mmol) and K₂PO₃ (84.90 mg, 0.400 mmol) in DMF (4 mL) under nitrogen. The reaction was stirred at 90 °C for 14 h then quenched by 10 mL brine solution and extracted 3 times with ethyl acetate. The collected organic phase was washed by brine and dried over anhydrous Na₂SO₄. The solvent was evaporated via reduced pressure. The resulting residue was purified via hexane and ethyl acetate silica gel chromatograph (3% ethyl acetate). The final product was obtained as yellow solid.

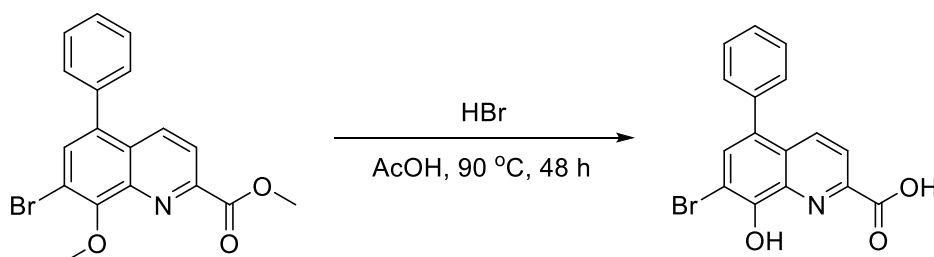
Yield: 34 mg (68.5%).

¹H NMR (500 MHz, Chloroform-*d*) δ 8.32 (d, *J* = 8.8 Hz, 1H), 8.12 (d, *J* = 8.8 Hz, 1H), 7.75 (s, 1H), 7.54 – 7.45 (m, 4H), 7.44 – 7.40 (m, 2H), 4.34 (s, 3H), 4.06 (s, 3H).

¹³C NMR (126 MHz, Chloroform-*d*) δ 165.92, 153.73, 147.39, 142.77, 137.67, 136.54, 136.43, 133.24, 130.06, 128.88, 128.59, 128.35, 121.26, 116.70, 62.82, 53.16.

ESI-HRMS calc. for [C₁₈H₁₄BrNO₃ + H]⁺ *m/z* 372.0230 (100.0%), 374.0209 (97.3%), [C₁₈H₁₄BrNO₃ + Na]⁺ *m/z* 394.0049 (100.0%), 396.0029 (97.3%), found *m/z* 372.0233, 374.0214 [M + H]⁺, 394.0053, 396.0035 [M + Na]⁺

7-Bromo-8-methoxy-5-phenylquinoline-2-carboxylic acid (YJh51)



Hydrobromic acid (5 mL) was added to methyl 7-bromo-8-methoxy-5-phenylquinoline-2-carboxylate (**YJh48**) (34 mg, 0.091 mmol) in glacial acid (5 mL). The mixture was stirred at 90 °C for 48 h. The pH was adjusted to 11 by saturated sodium bicarbonate solution, and the mixture was washed by ethyl acetate 3 times. The pH of the water phase was adjusted to 2 by 1 M HCl and extracted by ethyl acetate 3 times. The collected organic phase was washed by brine and dried over anhydrous Na₂SO₄. The solvent was evaporated via reduced pressure. The final product was obtained as brown solid.

Yield: 5 mg. (15.90%).

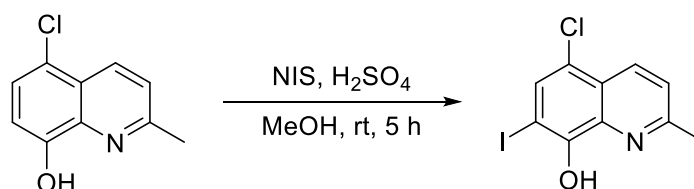
¹H NMR (700 MHz, DMSO-*d*₆) δ 8.41 (d, *J* = 8.7 Hz, 1H), 8.19 (d, *J* = 8.7 Hz, 1H), 7.79 (s, 1H), 7.64 – 7.60 (m, 1H), 7.58 – 7.53 (m, 2H), 7.50 (d, *J* = 7.2 Hz, 2H).

¹³C NMR (176 MHz, DMSO-*d*₆) δ 174.46, 164.78, 150.63, 145.28, 137.04, 136.89, 136.76, 133.21, 129.90, 128.78, 127.91, 126.98, 120.78, 105.34.

ESI-HRMS calc. for [C₁₆H₁₀BrNO₃ + H]⁺ *m/z* 343.9917 (100.0%), 345.9896 (97.3%), [C₁₆H₁₀BrNO₃ + Na]⁺ *m/z* 365.9736 (100.0%), 367.9716 (97.3%), found *m/z* 343.9914, 345.9893 [M + H]⁺.

ESI-MS calc. for [C₁₆H₁₀BrNO₃ + H]⁺ *m/z* 343.9917 (100.0%), 345.9896 (97.3%), found *m/z* 345.0, 343.0 [M + H]⁺.

5-Chloro-7-iodo-2-methylquinolin-8-ol (**YJh52**)



N-Iodosuccinimide (1.12 g, 2.07 mmol) and concentrated sulphuric acid (661.6 μL) were added to 5-chloro-2-methylquinolin-8-ol (**YJh37**) (400 mg, 2.07 mmol) in methanol (32 mL) with ice bath protect and stirred at 0 °C for 15 min and room temperature for 5 h. Then the reaction mixture was poured on ice and decolorized by addition of Na₂SO₃ (around 1.2 g). The pH of the mixture was adjusted to 3 by 1 M HCl and extracted 3 times with ethyl acetate. The collected organic phase was washed by brine and dried over anhydrous Na₂SO₄. The solvent was evaporated via reduced pressure. The resulting residue was purified via hexane and ethyl acetate silica gel chromatograph (0, 5% ethyl acetate). The final product was obtained as white (a little yellow) solid.

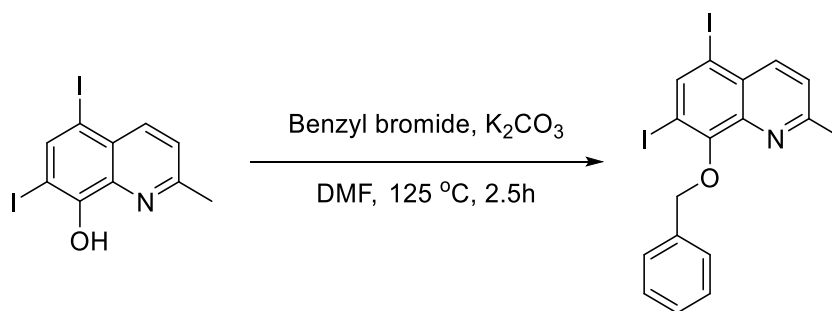
Yield: 348.06 mg (52.73%).

¹H NMR (500 MHz, Chloroform-*d*) δ 8.31 (d, *J* = 8.6 Hz, 1H), 7.76 (s, 1H), 7.40 (d, *J* = 8.6 Hz, 1H), 2.74 (s, 3H).

¹³C NMR (126 MHz, Chloroform-*d*) δ 158.78, 151.91, 136.91, 134.22, 133.75, 124.30, 123.92, 121.28, 75.02, 24.94.

ESI-HRMS calc. for [C₁₀H₇ClINO + H]⁺ *m/z* 319.9334 (100.0%), 321.9304 (32.0%), found *m/z* 319.9336, 321.9307 [M + H]⁺.

8-(Benzyloxy)-5,7-diiodo-2-methylquinoline (**YJh53**)



Benzyl bromide (138.91 μL , 1.17 mmol) was added to 5, 7-diiodo-8-hydroxy-2-methylquinoline (400 mg, 0.973 mmol) and K_2CO_3 (269.02 mg, 1.95 mmol) in 4mL DMF (4 mL). The mixture was stirred at 125 $^\circ\text{C}$ for 2.5 h. The reaction was cooled to room temperature and poured on 10 mL brine and extracted 3 times with ethyl acetate. The collected organic phase was washed with brine and dried over anhydrous Na_2SO_4 . The solvent was evaporated under reduced pressure. The resulting residue was purified via hexane and ethyl acetate silica gel chromatograph (3% ethyl acetate). The final product was obtained as white (a little yellow) solid.

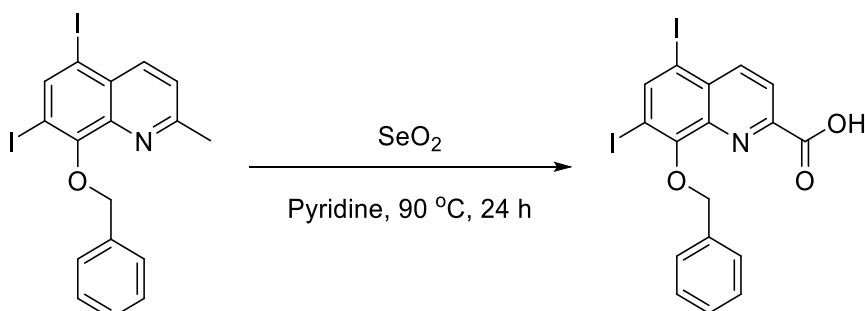
Yield: 429.39 mg (88.04%).

^1H NMR (500 MHz, Chloroform-*d*) δ 8.36 (s, 1H), 8.18 (d, J = 8.6 Hz, 1H), 7.73 – 7.62 (m, 2H), 7.46 – 7.32 (m, 4H), 5.46 (s, 2H), 2.80 (s, 3H).

^{13}C NMR (126 MHz, Chloroform-*d*) δ 159.72, 156.00, 144.23, 142.35, 140.79, 137.35, 129.85, 129.04, 128.43, 128.27, 124.12, 92.35, 92.27, 76.55, 25.36.

ESI-HRMS calc. for $[\text{C}_{17}\text{H}_{13}\text{I}_2\text{NO} + \text{H}]^+$ m/z 501.9159, found m/z 501.9167 $[\text{M} + \text{H}]^+$.

8-(Benzyloxy)-5,7-diiodoquinoline-2-carboxylic acid (YJh54)



The synthesis was according to the general procedure for oxidation of 2-methyl quinoline analogues by selenium dioxide. Selenium dioxide (66.43 mg, 0.599 mmol) was added into 8-(benzyloxy)-5,7-diiodo-2-methylquinoline (**YJh53**) (200 mg, 0.399 mmol) in pyridine (4 mL). The compound was purified via silica gel chromatograph eluting by a mixed solution of dichloromethane and methanol (4% methanol). The final product was obtained as white (a little yellow) solid.

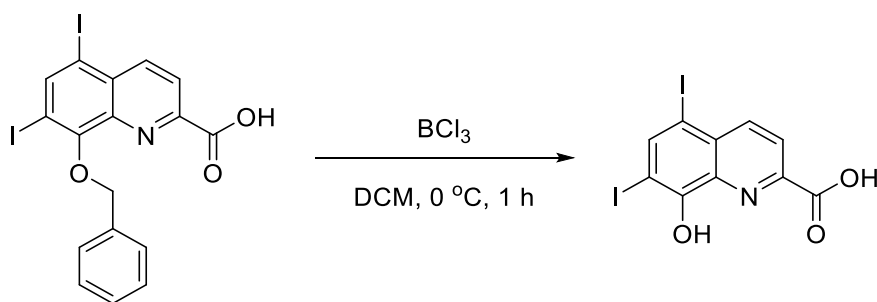
Yield: 110.39 mg (52.08%).

^1H NMR (500 MHz, DMSO-*d*₆) δ 13.65 (s, 1H), 8.58 (s, 1H), 8.49 (d, J = 8.8 Hz, 1H), 8.24 (d, J = 8.7 Hz, 1H), 7.69 – 7.65 (m, 2H), 7.40 – 7.32 (m, 3H), 5.55 (s, 2H).

^{13}C NMR (126 MHz, DMSO-*d*₆) δ 165.63, 156.10, 148.53, 146.21, 142.10, 141.09, 136.90, 131.64, 128.93, 128.20, 123.15, 94.15, 92.99, 76.06.

ESI-HRMS calc. for $[\text{C}_{17}\text{H}_{11}\text{I}_2\text{NO}_3 + \text{H}]^+$ m/z 531.8901, found m/z 531.8907 $[\text{M} + \text{H}]^+$.

8-Hydroxy-5, 7-diiodoquinoline-2-carboxylic acid (YJh59)



Boron trichloride (1 M in DCM) (1.32 mL, 1.32 mmol) was added to 8-(benzyloxy)-5,7-diiodoquinoline-2-carboxylic acid (**YJh54**) (70 mg, 0.132 mmol) in anhydrous dichloromethane (10 mL) at 0 °C under nitrogen. The mixture was stirred for 1 h. Then the reaction was diluted by 15 mL dichloromethane and quenched by ice water (20 mL). The mixture was extracted 3 times with ethyl acetate. The collected organic phase was washed by water and dried over anhydrous Na₂SO₄. The solvent was evaporated via reduced pressure. The resulting residue was purified via silica gel chromatograph (ethyl acetate, MeOH and H₂O, the ratio was 8 to 1.5 to 1). The final product was obtained as yellow solid after lyophilization.

Yield: 52.31 mg (90%).

¹H NMR (400 MHz, DMSO-*d*₆) δ 13.02 (s, 1H), 11.14 (s, 1H), 8.50 – 8.39 (m, 2H), 8.23 (d, *J* = 8.6 Hz, 1H).

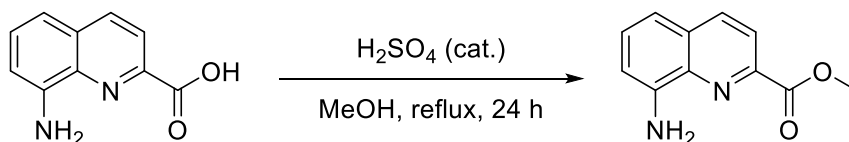
¹³C NMR (101 MHz, DMSO-*d*₆) δ 164.28, 155.17, 146.94, 145.51, 142.39, 135.86, 130.86, 122.25, 85.13, 81.67.

ESI-HRMS calc. for [C₁₀H₅I₂NO₃ + H]⁺ *m/z* 441.8432, found *m/z* 441.84229 [M + H]⁺.

Melting point: 200.7 °C

Purity: 98.24%

Methyl 8-aminoquinoline-2-carboxylate (**YJh61**)



Concentrated H₂SO₄ (50 μL) was added dropwise to 8-aminoquinoline-2-carboxylic acid (100 mg, 0.531 mmol) in methanol (10 mL). The mixture was stirred at 70 °C for 24 h and monitored by TLC. After the reaction was completed, the solvent was evaporated via reduced pressure. The residue was neutralized and extracted 3 times with ethyl acetate. The collected organic phase was washed by brine and dried over anhydrous Na₂SO₄. The solvent was evaporated via reduced pressure. The resulting residue was purified via hexane and ethyl acetate silica gel chromatograph (15% ethyl acetate). The final product was obtained as yellow solid after lyophilization.

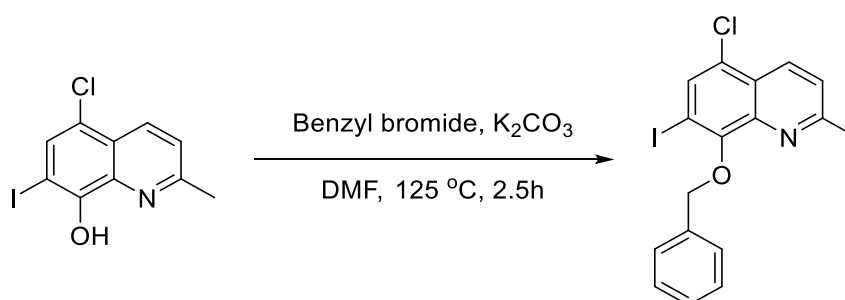
Yield: 86.74 mg (80.73%).

¹H NMR (500 MHz, Chloroform-*d*) δ 8.14 (d, *J* = 8.6 Hz, 1H), 8.09 (d, *J* = 8.5 Hz, 1H), 7.39 (dd, *J* = 8.1, 7.6 Hz, 1H), 7.13 (dd, *J* = 8.2, 1.2 Hz, 1H), 6.92 (dd, *J* = 7.6, 1.2 Hz, 1H), 5.23 (s, 2H), 4.02 (s, 3H).

¹³C NMR (126 MHz, Chloroform-*d*) δ 166.08, 145.24, 144.73, 137.59, 136.97, 130.14, 129.99, 121.24, 115.28, 110.32, 52.79.

ESI-HRMS calc. for [C₁₁H₁₀N₂O₂ + H]⁺ *m/z* 203.0815, found *m/z* 203.0822 [M + H]⁺.

8-(Benzyloxy)-5-chloro-7-iodo-2-methylquinoline (YJh62)



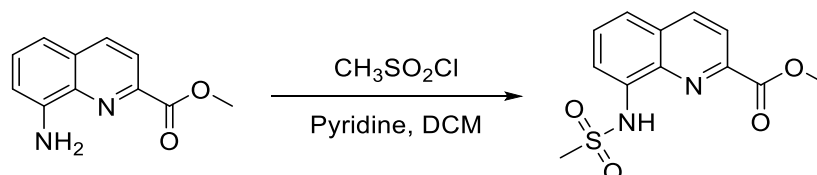
5-Chloro-7-iodo-2-methylquinolin-8-ol (YJh52) (400 mg, 1.25 mmol), K₂CO₃ (346.01 mg, 2.50 mmol) and benzyl bromide (178.67 μ L, 1.44 mmol), were added to DMF (4 mL) and stirred at 125 °C for 2.5 h. The reaction was cooled to room temperature and poured on 10 mL brine and extracted 3 times with ethyl acetate. The collected organic phase was washed with brine and dried over anhydrous Na₂SO₄. The solvent was evaporated via reduced pressure. The resulting residue was purified via hexane and ethyl acetate silica gel chromatograph (3% ethyl acetate). The final product was obtained as white solid. Yield: 422.77 mg (82.44%).

¹H NMR (500 MHz, Chloroform-*d*) δ 8.38 (d, *J* = 8.7 Hz, 1H), 7.88 (s, 1H), 7.75 – 7.66 (m, 2H), 7.44 – 7.31 (m, 4H), 5.45 (s, 2H), 2.80 (s, 3H).

¹³C NMR (126 MHz, Chloroform-*d*) δ 159.67, 154.39, 142.14, 137.36, 134.21, 133.63, 129.06, 128.43, 128.27, 126.63, 125.90, 123.25, 90.67, 76.55, 25.67.

ESI-HRMS calc. for [C₁₇H₁₃ClINO + H]⁺ *m/z* 409.9803 (100.0%), 411.9774 (32.0%), 410.9837 (18.4%), found *m/z* 409.9804, 411.9782 [M + H]⁺.

Methyl 8-(methylsulfonamido)quinoline-2-carboxylate (YJh63)



The synthesis was according to the general procedure for sulfonamide coupling. Methanesulfonyl chloride (57.41 μ L, 0.74 mmol) was added to methyl 8-aminoquinoline-2-carboxylate (YJh61 or YJh89) (100 mg, 0.495 mmol) in pyridine / dichloromethane (1 mL/2 mL). The compound was purified via hexane and ethyl acetate silica gel chromatograph (45% ethyl acetate). The final product was obtained as white solid after lyophilization.

Yield: 137.23 mg (99%).

¹H NMR (500 MHz, Chloroform-*d*) δ 8.97 (s, 1H), 8.32 (d, *J* = 8.5 Hz, 1H), 8.23 (d, *J* = 8.5 Hz, 1H), 7.91 (dd, *J* = 7.1, 1.8 Hz, 1H), 7.71 – 7.53 (m, 2H), 4.06 (s, 3H), 3.09 (s, 3H).

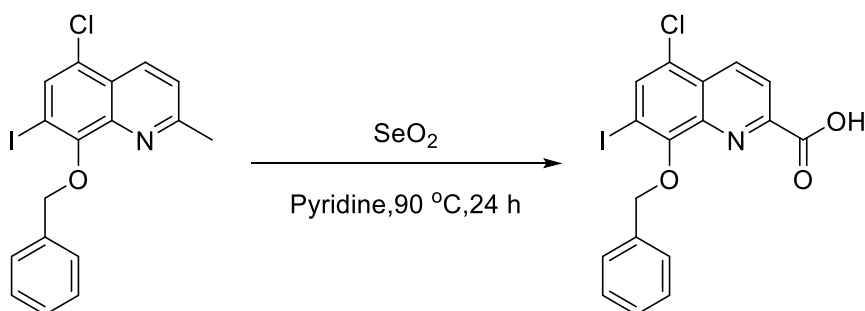
¹³C NMR (126 MHz, Chloroform-*d*) δ 165.50, 146.66, 137.94, 137.74, 135.20, 129.72, 129.42, 122.21, 122.14, 115.54, 53.12, 39.60.

ESI-HRMS calc. for [C₁₂H₁₂N₂O₄S + H]⁺ *m/z* 281.0591, [C₁₂H₁₂N₂O₄S + 2H]²⁺ *m/z* 141.0332, found *m/z* 281.0594 [M + H]⁺, 141.0281 [M + 2H]²⁺.

Melting point: 141 °C

Purity: 99.34%

8-(Benzyloxy)-5-chloro-7-iodoquinoline-2-carboxylic acid (YJh64)



The synthesis was according to the general procedure for oxidation of 2-methyl quinoline analogues by selenium dioxide. Selenium dioxide (81.26 mg, 0.732 mmol) was added into 8-(benzyloxy)-5-chloro-7-iodo-2-methylquinoline (**YJh62**) (200 mg, 0.488 mmol) in pyridine (4 mL). The compound was purified via silica gel chromatograph eluting by a mixed solution of dichloromethane and methanol (5% methanol). The final product was obtained as white solid.

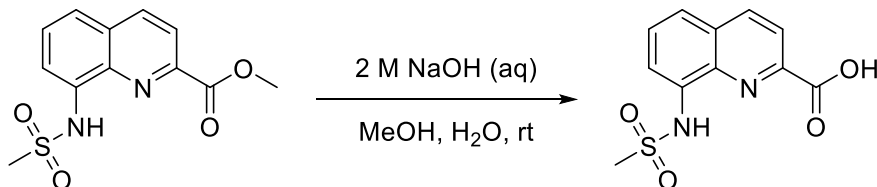
Yield: 157.56 mg (73.41%).

¹H NMR (500 MHz, DMSO-*d*₆) δ 13.77 (s, 1H), 8.69 (d, *J* = 8.7 Hz, 1H), 8.29 (d, *J* = 8.7 Hz, 1H), 8.23 (s, 1H), 7.72 – 7.64 (m, 2H), 7.42 – 7.32 (m, 3H), 5.54 (s, 2H).

¹³C NMR (126 MHz, DMSO-*d*₆) δ 165.78, 154.88, 148.62, 140.81, 136.87, 136.48, 134.96, 128.94, 128.21, 127.52, 125.19, 122.43, 92.43, 76.11.

ESI-HRMS calc. for [C₁₇H₁₁ClINO₃ + H]⁺ *m/z* 439.9545 (100%), 441.9515 (32%), found *m/z* 439.9555 (100%), 441.9527 (31.62%) [M + H]⁺.

8-(Methylsulfonamido)quinoline-2-carboxylic acid (YJh65)



The synthesis was according to the general procedure for hydrolysis of methyl esters catalyzed by hydroxide ion. 2 M NaOH solution (10 mL) was added to methyl 8-(methylsulfonamido)quinoline-2-carboxylate (**YJh63**) (100 mg, 0.357 mmol) in methanol (2 mL). The reaction mixture was stirred at room temperature for 3 h. The compound was purified via silica gel chromatograph (ethyl acetate, MeOH and H₂O, the ratio was 8 to 1.5 to 1). The final product was obtained as white (a little yellow) solid after lyophilization.

Yield: 82.49 mg (86.84%).

¹H NMR (500 MHz, DMSO-*d*₆) δ 13.44 (s, 1H), 10.46 (s, 1H), 8.62 (d, *J* = 8.5 Hz, 1H), 8.22 (d, *J* = 8.5 Hz, 1H), 7.87 (dd, *J* = 7.6, 1.3 Hz, 1H), 7.80 (dd, *J* = 8.3, 1.3 Hz, 1H), 7.74 (dd, *J* = 8.2, 7.6 Hz, 1H), 3.16 (s, 3H).

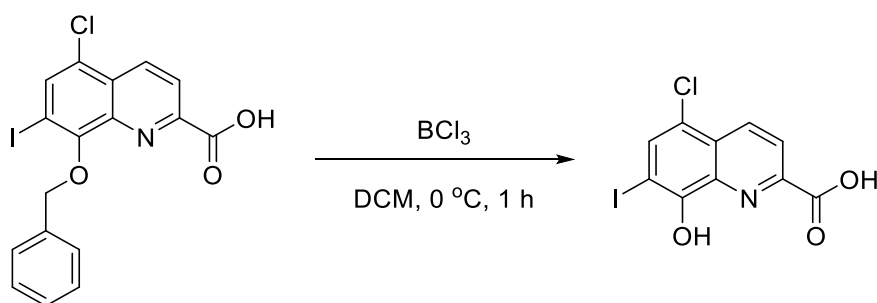
¹³C NMR (126 MHz, DMSO-*d*₆) δ 165.19, 145.64, 138.79, 137.02, 135.52, 129.67, 129.51, 122.07, 120.78, 116.44, 39.62.

ESI-HRMS calc. for [C₁₁H₁₀N₂O₄S + H]⁺ *m/z* 267.0434, found *m/z* 267.04377 [M + H]⁺.

Melting point: 246.7 °C

Purity: 99.2%

5-Chloro-8-hydroxy-7-iodoquinoline-2-carboxylic acid (YJh66)



Boron trichloride (1 M in DCM) (1.14 mL, 1.14 mmol) was added to 8-(benzyloxy)-5-chloro-7-iodoquinoline-2-carboxylic acid (YJh64) (50 mg, 0.114 mmol) in anhydrous dichloromethane (10 mL) at $0\text{ }^\circ\text{C}$ under nitrogen. The mixture was stirred for 1 h. Then the reaction was diluted by 15 mL dichloromethane and quenched by ice water (20 mL). The mixture was extracted 3 times with ethyl acetate. The collected organic phase was washed by water and dried over anhydrous Na_2SO_4 . The solvent was evaporated via reduced pressure. The resulting residue was purified via silica gel chromatograph (ethyl acetate, MeOH and H_2O , the ratio was 8 to 1.5 to 1). The final product was obtained as yellow solid after lyophilization.

Yield: 35 mg (88.05%).

$^1\text{H NMR}$ (400 MHz, $\text{DMSO-}d_6$) δ 13.01 (s, 1H), 11.09 (s, 1H), 8.60 (d, $J = 8.6$ Hz, 1H), 8.25 (d, $J = 8.6$ Hz, 1H), 8.09 (s, 1H).

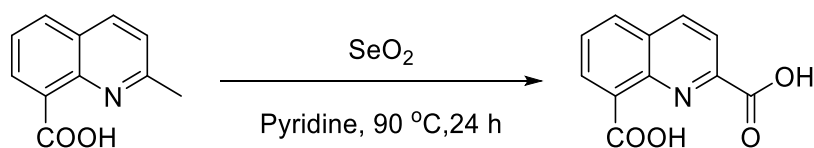
$^{13}\text{C NMR}$ (101 MHz, $\text{DMSO-}d_6$) δ 164.43, 153.93, 145.53, 137.39, 135.46, 135.41, 126.79, 121.50, 119.52, 79.68.

ESI-HRMS calc. for $[\text{C}_{10}\text{H}_5\text{ClINO}_3 + \text{H}]^+$ m/z 349.9075 (100.0%), 351.9046 (32.0%), found m/z 349.90715 (100%), 351.90477 (33.4%) $[\text{M} + \text{H}]^+$.

Melting point: $215.5\text{ }^\circ\text{C}$

Purity: 100%

Quinoline-2,8-dicarboxylic acid (YJh67)



The synthesis was according to the general procedure for oxidation of 2-methyl quinoline analogues by selenium dioxide. Selenium dioxide (88.91 mg, 0.801 mmol) was added into 2-methylquinoline-8-carboxylic acid (YJh38) (100 mg, 0.534 mmol) in pyridine (4 mL). The reaction mixture was stirred at $100\text{ }^\circ\text{C}$ for 16 h. The final compound was obtained as brown solid after lyophilization.

Yield: 33.20 mg (28.62%).

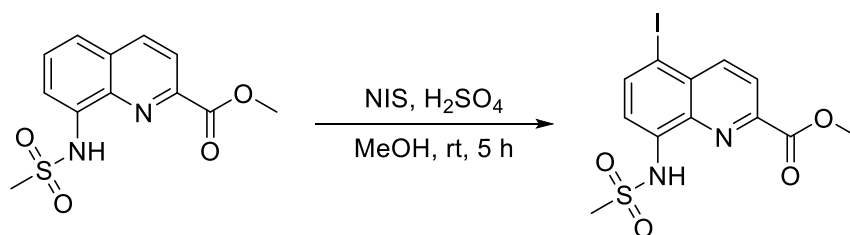
$^1\text{H NMR}$ (500 MHz, $\text{DMSO-}d_6$) δ 16.18 (s, 1H), 14.21 (s, 1H), 8.87 (d, $J = 8.6$ Hz, 1H), 8.63 (dd, $J = 7.2$, 1.4 Hz, 1H), 8.43 (dd, $J = 8.2$, 1.5 Hz, 1H), 8.29 (d, $J = 8.5$ Hz, 1H), 7.93 (t, $J = 7.7$ Hz, 1H).

$^{13}\text{C NMR}$ (126 MHz, $\text{DMSO-}d_6$) δ 165.85, 164.41, 146.91, 143.60, 140.74, 135.29, 133.46, 129.11, 128.93, 124.73, 121.55.

ESI-HRMS calc. for $[\text{C}_{11}\text{H}_7\text{NO}_4 + \text{H}]^+$ m/z 218.0448, $[\text{C}_{11}\text{H}_7\text{NO}_4 + 2\text{H}]^{2+}$ m/z 109.5260, found m/z 218.0454 $[\text{M} + \text{H}]^+$, 109.5230 $[\text{M} + 2\text{H}]^{2+}$.

Melting point: $235.6\text{ }^\circ\text{C}$

Methyl 5-iodo-8-(methylsulfonamido)quinoline-2-carboxylate (YJh74)



N-Iodosuccinimide (321.06 mg, 1.43 mmol) was added to methyl 8-(methylsulfonamido)quinoline-2-carboxylate (**YJh63**) (80 mg, 0.285 mmol) and concentrated sulphuric acid (22.8 μ L) in methanol (2 mL) at 0 °C. The reaction was stirred at 0 °C for 15 min and room temperature for 5 h. Then the reaction mixture was poured onto ice and decolorized by addition of Na₂SO₃ (around 0.8 g). The pH was adjusted to 3 by 1 M HCl and extracted 3 times with ethyl acetate. The collected organic phase was washed by brine and dried over anhydrous Na₂SO₄. The solvent was evaporated via reduced pressure. The resulting residue was purified via hexane and ethyl acetate silica gel chromatograph (50% ethyl acetate). The final product was obtained as yellow solid.

Yield: 47.90 mg (41.32%).

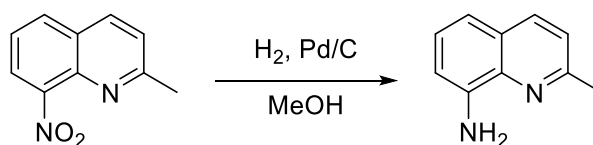
¹H NMR (500 MHz, Chloroform-*d*) δ 8.98 (s, 1H), 8.50 (d, *J* = 8.7 Hz, 1H), 8.27 (d, *J* = 8.7 Hz, 1H), 8.15 (d, *J* = 8.2 Hz, 1H), 7.68 (d, *J* = 8.2 Hz, 1H), 4.07 (s, 3H), 3.10 (s, 3H).

¹³C NMR (126 MHz, Chloroform-*d*) δ 164.87, 147.24, 142.32, 139.96, 138.29, 136.11, 131.41, 123.68, 116.58, 89.71, 53.29, 39.79.

ESI-HRMS calc. for [C₁₂H₁₁IN₂O₄S + H]⁺ *m/z* 406.9557, found *m/z* 406.9563 [M + H]⁺.

Purity: 96.64%

2-Methylquinolin-8-amine (YJh80)



The synthesis was according to the general procedure for reduction reaction: (a) hydrogenation reduction. Palladium on carbon (80 mg) was added to 2-methyl-8-nitroquinoline (800 mg, 4.25 mmol) in methanol (100 mL) under nitrogen. The mixture was stirred at room temperature under hydrogen for 18 h. The reaction solution was filtered and evaporated via reduced pressure. The resulting residue was purified via hexane and ethyl acetate silica gel chromatograph (6% ethyl acetate). The final product was obtained as white solid.

Yield: 606.47 mg (90.18%).

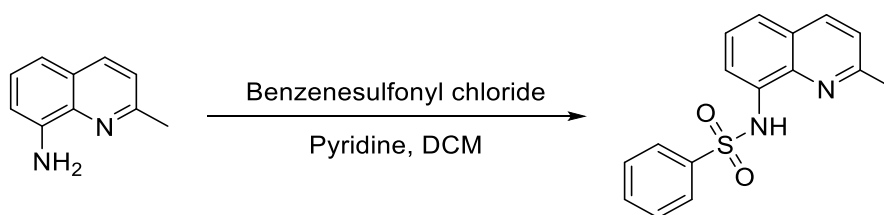
¹H NMR (500 MHz, Chloroform-*d*) δ 7.95 (d, *J* = 8.4 Hz, 1H), 7.27 (dd, *J* = 8.1, 7.5 Hz, 1H), 7.24 (d, *J* = 8.4 Hz, 1H), 7.12 (dd, *J* = 8.1, 1.3 Hz, 1H), 6.91 (dd, *J* = 7.5, 1.3 Hz, 1H), 4.98 (s, 2H), 2.72 (s, 3H).

¹³C NMR (126 MHz, Chloroform-*d*) δ 156.24, 143.49, 137.94, 136.17, 126.98, 126.41, 122.23, 115.98, 110.22, 25.31.

ESI-HRMS calc. for [C₁₀H₁₀N₂ + H]⁺ *m/z* 159.0917, found *m/z* 159.0921 [M + H]⁺.

Purity: 99.57%

N-(2-methylquinolin-8-yl)benzenesulfonamide (YJh82)



The synthesis was according to the general procedure for sulfonamide coupling. Benzenesulfonyl chloride (243.09 μL , 1.90 mmol) was added to 2-methylquinolin-8-amine (**YJh80**) (200 mg, 1.26 mmol) in pyridine/dichloromethane (3 mL/6 mL). The compound was purified via hexane and ethyl acetate silica gel chromatograph (33% ethyl acetate). The final product was obtained as white solid.

Yield: 334.12 mg (88.58%).

^1H NMR (500 MHz, Chloroform-*d*) δ 9.30 (s, 1H), 7.94 (d, J = 8.4 Hz, 1H), 7.95 – 7.87 (m, 2H), 7.76 (dd, J = 7.5, 1.4 Hz, 1H), 7.45 – 7.40 (m, 1H), 7.39 (dd, J = 8.2, 1.4 Hz, 1H), 7.37 – 7.31 (m, 3H), 7.25 (d, J = 8.4 Hz, 1H), 2.68 (s, 3H).

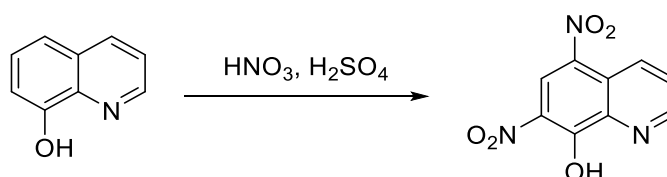
^{13}C NMR (126 MHz, Chloroform-*d*) δ 158.00, 139.57, 138.02, 136.37, 133.16, 132.93, 128.94, 127.31, 126.41, 125.87, 122.94, 122.07, 115.19, 25.23.

ESI-HRMS calc. for $[\text{C}_{16}\text{H}_{14}\text{N}_2\text{O}_2\text{S} + \text{H}]^+$ m/z 299.0849, found m/z 299.0865 $[\text{M} + \text{H}]^+$.

Melting point: 161.9 $^\circ\text{C}$

Purity: 99.75%

5, 7-Dinitroquinolin-8-ol (**YJh83**)



Quinolin-8-ol (145.16 mg, 1 mmol) was added portionwise to a 7/3 mixed solution of concentrated HNO_3 and H_2SO_4 (10 mL) at 0 $^\circ\text{C}$. The reaction was stirred at room temperature for 3 h. The reaction mixture was poured onto ice water. The precipitate was filtered and purified by dichloromethane and methanol silica gel chromatograph (10% methanol). The final product was obtained as yellow solid.

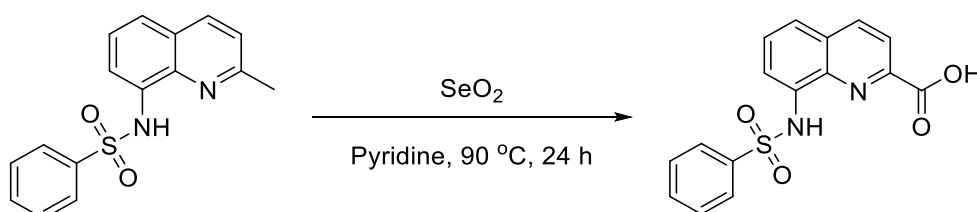
Yield: 107.59 mg (45.75%).

^1H NMR (500 MHz, DMSO-*d*₆) δ 9.82 (d, J = 8.7 Hz, 1H), 9.26 (s, 1H), 8.94 (s, 1H), 8.27 (s, 1H).

^{13}C NMR (126 MHz, DMSO-*d*₆) δ 161.76, 142.09, 141.64, 137.56, 130.51, 129.84 (d, J = 16.0 Hz), 127.60 (d, J = 17.2 Hz), 127.00, 122.56.

ESI-HRMS calc. for $[\text{C}_9\text{H}_5\text{N}_3\text{O}_5 + \text{H}]^+$ m/z 236.0302, found m/z 236.0306 $[\text{M} + \text{H}]^+$.

8-(Phenylsulfonamido)quinoline-2-carboxylic acid (**YJh84**)



The synthesis was according to the general procedure for oxidation of 2-methyl quinoline analogues by selenium dioxide. Selenium dioxide (111.57 mg, 1.01 mmol) was added to N-(2-methylquinolin-8-yl)benzenesulfonamide (**YJh82**) (200 mg, 0.670 mmol) in pyridine (4 mL). The compound was purified via silica gel chromatograph (ethyl acetate, MeOH and H₂O, the ratio was 8 to 1.5 to 1). The final compound was obtained as white (a little yellow) solid after lyophilization.

Yield: 191.09 mg (86.82%).

¹H NMR (500 MHz, DMSO-*d*₆) δ 13.40 (s, 1H), 11.04 (s, 1H), 8.53 (d, *J* = 8.5 Hz, 1H), 8.16 (d, *J* = 8.5 Hz, 1H), 7.93 – 7.85 (m, 2H), 7.86 (dd, *J* = 7.7, 1.3 Hz, 1H), 7.72 (dd, *J* = 8.3, 1.3 Hz, 1H), 7.65 (t, *J* = 7.8 Hz, 1H), 7.58 – 7.48 (m, 1H), 7.47 (ddt, *J* = 8.3, 6.7, 1.4 Hz, 2H).

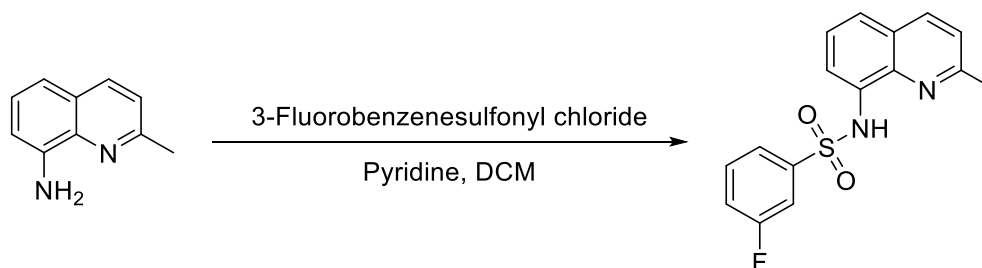
¹³C NMR (126 MHz, DMSO-*d*₆) δ 164.98, 145.45, 139.12, 138.81, 136.95, 134.65, 133.25, 129.49, 129.28, 126.73, 122.54, 120.63, 116.98.

ESI-HRMS calc. for [C₁₆H₁₂N₂O₄S + H]⁺ *m/z* 329.0591, found *m/z* 329.05907 [M + H]⁺.

Melting point: 239.7 °C

Purity: 99.47%

3-Fluoro-N-(2-methylquinolin-8-yl)benzenesulfonamide (**YJh85**)



The synthesis was according to the general procedure for sulfonamide coupling. 3-Fluorobenzenesulfonyl chloride (252.25 μL, 1.90 mmol) was added to 2-methylquinolin-8-amine (**YJh80**) (200 mg, 1.26 mmol) in pyridine/dichloromethane (2 mL/4 mL) and stirred at room temperature overnight. The product was purified via hexane and ethyl acetate silica gel chromatograph (30% ethyl acetate). The final product was obtained as white solid after lyophilization.

Yield: 353.42 mg (88.37%).

¹H NMR (500 MHz, Chloroform-*d*) δ 9.29 (s, 1H), 7.96 (d, *J* = 8.4 Hz, 1H), 7.77 (dd, *J* = 7.5, 1.3 Hz, 1H), 7.68 (ddd, *J* = 7.9, 1.7, 1.0 Hz, 1H), 7.63 – 7.59 (m, 1H), 7.43 (dd, *J* = 8.3, 1.3 Hz, 1H), 7.37 (dd, *J* = 8.3, 7.6 Hz, 1H), 7.34 – 7.30 (m, 1H), 7.28 (d, *J* = 8.4 Hz, 1H), 7.12 (tdd, *J* = 8.3, 2.6, 1.0 Hz, 1H), 2.69 (s, 3H).

¹³C NMR (126 MHz, Chloroform-*d*) δ 162.31 (d, *J* = 251.5 Hz), 158.23, 141.53 (d, *J* = 7.2 Hz), 138.09, 136.44, 132.77, 130.69 (d, *J* = 7.8 Hz), 126.47, 125.89, 123.13 (d, *J* = 3.6 Hz), 123.07, 122.52, 120.18 (d, *J* = 21.4 Hz), 115.61, 114.77 (d, *J* = 24.4 Hz), 25.23.

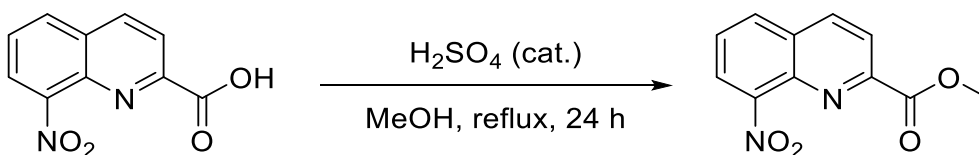
¹⁹F NMR (471 MHz, Chloroform-*d*) δ -109.82 (td, *J* = 8.6, 5.6 Hz).

ESI-HRMS calc. for [C₁₆H₁₃FN₂O₂S + H]⁺ *m/z* 317.0755, found *m/z* 317.0758 [M + H]⁺.

Melting point: 153.8 °C

Purity: 98.87%

Methyl 8-nitroquinoline-2-carboxylate (**YJh88**)



The synthesis was according to the general procedure for methyl esterification of carboxylic acids. Concentrated H₂SO₄ (0.25 mL) was added dropwise to 8-nitroquinoline-2-carboxylic acid (**YJh36**) (600 mg, 2.75 mmol) in methanol (10 mL). The compound was purified via hexane and ethyl acetate silica gel chromatograph (17%-50% ethyl acetate). The final product was obtained as white solid.

Yield: 606.4 mg (94.96%).

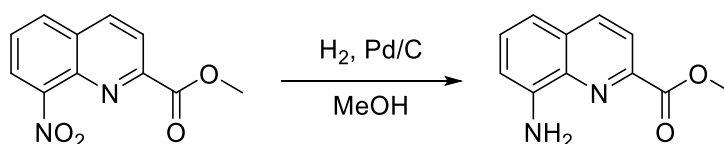
¹H NMR (500 MHz, Chloroform-*d*) δ 8.42 (d, *J* = 8.6 Hz, 1H), 8.31 (d, *J* = 8.5 Hz, 1H), 8.14 (dd, *J* = 7.5, 1.4 Hz, 1H), 8.11 (dd, *J* = 8.3, 1.4 Hz, 1H), 7.73 (dd, *J* = 8.3, 7.5 Hz, 1H), 4.04 (s, 3H).

¹³C NMR (126 MHz, Chloroform-*d*) δ 165.35, 150.20, 148.67, 139.03, 137.63, 132.01, 129.91, 127.39, 124.97, 122.82, 53.43 (q, *J* = 2.2 Hz).

ESI-HRMS calc. for [C₁₁H₈N₂O₄ + H]⁺ *m/z* 233.0557, found *m/z* 233.0563 [M + H]⁺.

Purity: 98.01%.

Methyl 8-aminoquinoline-2-carboxylate (**YJh89**)



The synthesis was according to the general procedure for reduction reaction: (a) hydrogenation reduction. Palladium on carbon (80 mg) was added to methyl 8-nitroquinoline-2-carboxylate (**YJh88**) (800 mg, 3.45 mmol) in methanol (100 mL) under nitrogen. The mixture was stirred at room temperature under hydrogen overnight. The reaction solution was filtered and evaporated via reduced pressure. The resulting residue was purified via hexane and ethyl acetate silica gel chromatograph (17% ethyl acetate). The final product was obtained as yellow solid after lyophilization.

Yield: 564.93 mg (81.09%).

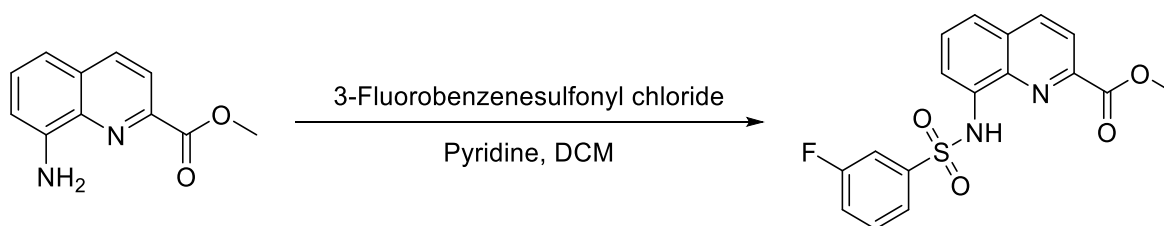
¹H NMR (500 MHz, Chloroform-*d*) δ 8.16 (d, *J* = 8.5 Hz, 1H), 8.10 (d, *J* = 8.5 Hz, 1H), 7.41 (dd, *J* = 8.1, 7.6 Hz, 1H), 7.15 (dd, *J* = 8.2, 1.2 Hz, 1H), 6.94 (dd, *J* = 7.6, 1.2 Hz, 1H), 5.25 – 5.14 (m, 2H), 4.03 (s, 3H).

¹³C NMR (126 MHz, Chloroform-*d*) δ 166.13, 145.28, 144.81, 137.63, 137.01, 130.19, 130.03, 121.30, 115.34, 110.30, 52.83.

ESI-HRMS calc. for [C₁₁H₁₀N₂O₂ + H]⁺ *m/z* 203.0815, found *m/z* 203.0822 [M + H]⁺.

Purity: 98.03%.

Methyl 8-((3-fluorophenyl)sulfonamido)quinoline-2-carboxylate (**YJh90**)



The synthesis was according to the general procedure for sulfonamide coupling. 3-Fluorobenzenesulfonyl chloride (98.68 μL , 0.742 mmol) was added to methyl 8-aminoquinoline-2-carboxylate (**YJh89**) (200 mg, 1.26 mmol) in pyridine/dichloromethane (2 mL/4 mL). The compound was purified via hexane and ethyl acetate silica gel chromatograph (30%-40% ethyl acetate). The final product was obtained as white solid.

Yield: 353.42 mg (88.37%).

^1H NMR (500 MHz, Chloroform-*d*) δ 9.55 (s, 1H), 8.23 (d, J = 8.5 Hz, 1H), 8.15 (d, J = 8.5 Hz, 1H), 7.88 (dd, J = 6.8, 2.0 Hz, 1H), 7.71 (ddd, J = 7.9, 1.7, 0.9 Hz, 1H), 7.67 (ddd, J = 8.2, 2.6, 1.7 Hz, 1H), 7.58 – 7.51 (m, 2H), 7.32 (td, J = 8.1, 5.3 Hz, 1H), 7.12 (tdd, J = 8.3, 2.6, 1.0 Hz, 1H), 4.07 (s, 3H).

^{13}C NMR (126 MHz, Chloroform-*d*) δ 165.47, 162.29 (d, J = 251.7 Hz), 146.40, 141.37 (d, J = 7.2 Hz), 138.21, 137.65, 134.51, 130.74 (d, J = 7.7 Hz), 129.52, 129.21, 123.16 (d, J = 3.2 Hz), 122.46, 121.96, 120.30 (d, J = 21.3 Hz), 116.76, 114.88 (d, J = 24.5 Hz), 53.15.

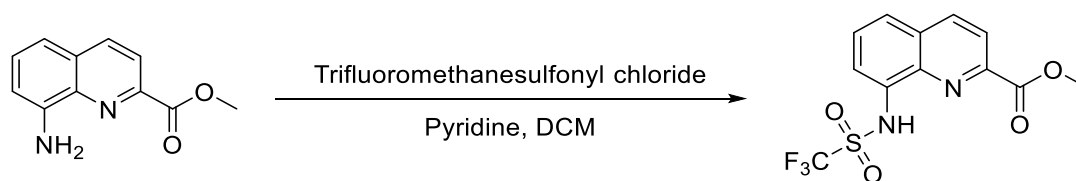
^{19}F NMR (471 MHz, Chloroform-*d*) δ -109.63 (td, J = 8.1, 5.1 Hz).

ESI-HRMS calc. for $[\text{C}_{17}\text{H}_{13}\text{FN}_2\text{O}_4\text{S} + \text{H}]^+$ m/z 361.0653, found m/z 361.0658 $[\text{M} + \text{H}]^+$.

Melting point: 122 °C

Purity: 99.76%.

Methyl 8-((trifluoromethyl)sulfonamido)quinoline-2-carboxylate (**YJh92** or **YJh107**)



Method 1 The synthesis was according to the general procedure for sulfonamide coupling. Trifluoromethanesulfonyl chloride (123.20 μL , 0.593 mmol) was added to methyl 8-aminoquinoline-2-carboxylate (**YJh89**) (100 mg, 0.495 mmol) in pyridine /dichloromethane (2 mL/4 mL) with ice bath protect. The compound was purified via hexane and ethyl acetate silica gel chromatograph (45% ethyl acetate). The final product was obtained as yellow solid.

Yield: 5 mg (3%).

Method 2 Trifluoromethanesulfonic anhydride (206 μL , 0.99 mmol) was added to methyl 8-aminoquinoline-2-carboxylate (**YJh89**) (100 mg, 0.495 mmol), NaHCO_3 (83.09 mg, 0.989 mmol) and TEA (103.2 μL , 0.742 mmol) in dichloromethane (4 mL) with ice bath protect. The mixture was stirred at room temperature overnight. The reaction was quenched by sodium bicarbonate saturated solution and extracted 3 times with ethyl acetate. The collected organic phase was washed by brine and dried over anhydrous Na_2SO_4 . The solvent was evaporated under reduced pressure. The compound was purified via hexane and ethyl acetate silica gel chromatograph (45% ethyl acetate). The final product was obtained as yellow solid.

Yield: 91.91 mg (55.6%).

Method 3 Trifluoromethanesulfonic anhydride (308 μL , 1.484 mmol) was added to methyl 8-aminoquinoline-2-carboxylate (**YJh89**) (150 mg, 0.741 mmol) in pyridine (6 mL) with ice bath protect. The mixture was warmed to room temperature and heated at 80 °C for 8 h. The reaction was diluted by water and extracted 3 times with ethyl acetate. The collected organic phase was washed by saturated NaHCO_3 solution and dried over anhydrous Na_2SO_4 . The solvent was evaporated under reduced

pressure. The compound was purified via hexane and ethyl acetate silica gel chromatograph (45% ethyl acetate). The final product was obtained as yellow solid.

Yield: 122.5 mg (49.4%).

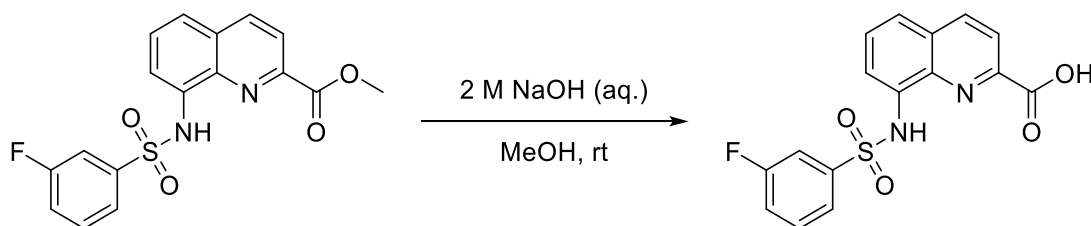
¹H NMR (500 MHz, Chloroform-*d*) δ 8.36 (d, *J* = 8.5 Hz, 1H), 8.25 (d, *J* = 8.5 Hz, 1H), 7.97 (dd, *J* = 7.6, 1.3 Hz, 1H), 7.70 (dd, *J* = 8.3, 1.3 Hz, 1H), 7.64 (dd, *J* = 8.4, 7.6 Hz, 1H), 4.08 (s, 3H).

¹³C NMR (126 MHz, Chloroform-*d*) δ 165.34, 146.90, 138.02, 137.94, 133.06, 129.56, 129.19, 123.66, 122.35, 120.02 (q, *J* = 322.8 Hz), 116.91, 53.28.

¹⁹F NMR (471 MHz, Chloroform-*d*) δ -75.80.

ESI-HRMS calc. for [C₁₂H₉F₃N₂O₄S + H]⁺ m/z 335.0308 (100.0%), 336.0341 (13.0%), 337.0266 (4.5%), found m/z 335.0309 [M + H]⁺.

8-((3-Fluorophenyl)sulfonamido)quinoline-2-carboxylic acid (YJh93)



The synthesis was according to the general procedure for hydrolysis of methyl esters catalyzed by hydroxide ion. 2 M NaOH solution (10 mL) was added to methyl 8-((3-fluorophenyl)sulfonamido)quinoline-2-carboxylate (**YJh90**) (60 mg, 0.167 mmol) in methanol (2 mL). The reaction mixture was stirred at room temperature for 3 h. The compound was purified via silica gel chromatograph (ethyl acetate, methanol and H₂O, the ratio was 8 to 1.5 to 1). The final product was obtained as white (a little yellow) solid after lyophilization.

Yield: 51.90 mg (90%).

¹H NMR (500 MHz, DMSO-*d*₆) δ 13.34 (s, 1H), 11.07 (s, 1H), 8.55 (d, *J* = 8.5 Hz, 1H), 8.16 (d, *J* = 8.5 Hz, 1H), 7.89 (dd, *J* = 7.7, 1.2 Hz, 1H), 7.77 (dd, *J* = 8.3, 1.3 Hz, 1H), 7.71 – 7.66 (m, 3H), 7.51 (td, *J* = 8.2, 5.5 Hz, 1H), 7.40 (tdd, *J* = 8.5, 2.6, 1.0 Hz, 1H).

¹³C NMR (126 MHz, DMSO-*d*₆) δ 164.95, 161.50 (d, *J* = 249.1 Hz), 145.57, 141.10 (d, *J* = 6.9 Hz), 138.89, 137.19, 134.22, 131.72 (d, *J* = 7.9 Hz), 129.51, 129.32, 123.12, 122.99 (d, *J* = 3.1 Hz), 120.67, 120.47 (d, *J* = 21.2 Hz), 117.97, 113.89 (d, *J* = 24.5 Hz).

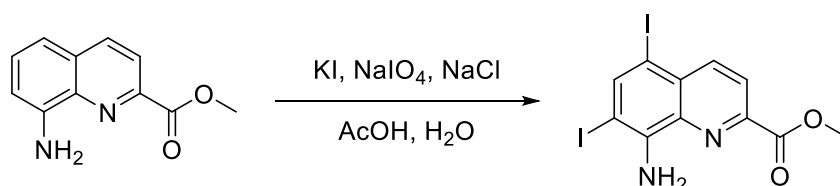
¹⁹F NMR (471 MHz, DMSO-*d*₆) δ -110.04 (td, *J* = 8.6, 5.2 Hz).

ESI-HRMS calc. for [C₁₆H₁₁FN₂O₄S + H]⁺ m/z 347.0496, found m/z 347.05131 [M + H]⁺.

Melting point: 235.6 °C

Purity: 99.79%

Methyl 8-amino-5,7-diiodoquinoline-2-carboxylate (YJh94)



Potassium iodide (1.31 g, 7.91 mmol) was added slowly to methyl 8-aminoquinoline-2-carboxylate (**YJh89**) (400 mg, 1.98 mmol), sodium metaperiodate (1.69 g, 7.91 mmol) and sodium chloride (924.82

mg, 15.83 mmol) in a 9/1 mixed solution of acetic acid and water (32 mL). The mixture was stirred at room temperature for 5 h. The reaction was quenched by 50 mL water and extracted 3 times with ethyl acetate. The collected organic phase was washed by brine and dried over anhydrous Na₂SO₄. The solvent was evaporated under reduced pressure. The resulting residue was purified via hexane and ethyl acetate silica gel chromatograph (10% ethyl acetate). The final product was obtained as yellow solid.

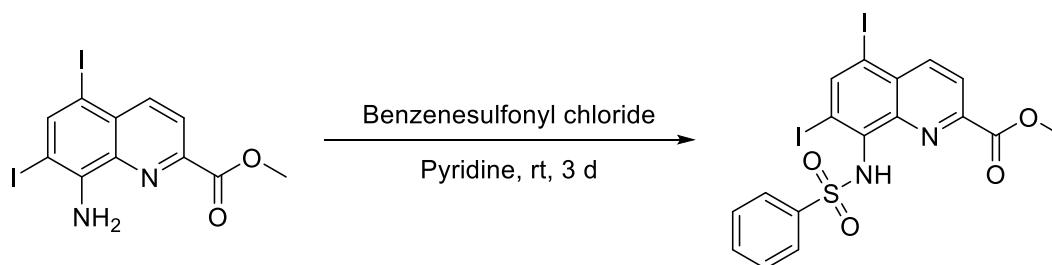
Yield: 640.34 mg (71.30%).

¹H NMR (500 MHz, Chloroform-*d*) δ 8.32 (d, *J* = 8.7 Hz, 1H), 8.24 (s, 1H), 8.15 (d, *J* = 8.7 Hz, 1H), 5.73 (s, 2H), 4.05 (s, 3H).

¹³C NMR (126 MHz, Chloroform-*d*) δ 165.14, 147.25, 147.15, 145.82, 141.54, 136.61, 131.08, 123.20, 79.91, 78.03, 53.09.

ESI-HRMS calc. for [C₁₁H₈I₂N₂O₂ + H]⁺ *m/z* 454.8748, 477.8601 (11.9%), found *m/z* 454.8753 [M + H]⁺.

Methyl 5,7-diiodo-8-(phenylsulfonamido)quinoline-2-carboxylate (YJh95)



The synthesis was according to the general procedure for sulfonamide coupling. Benzenesulfonyl chloride (63.53 μL, 0.496 mmol) was added to methyl 8-amino-5,7-diiodoquinoline-2-carboxylate (**YJh94**) (150 mg, 0.330 mmol) in pyridine (3 mL). The mixture was stirred at room temperature for 3 days. The compound was purified via hexane and ethyl acetate silica gel chromatograph (5%, 15%, 20%, 30% ethyl acetate). The final product was obtained as white (a little yellow) solid.

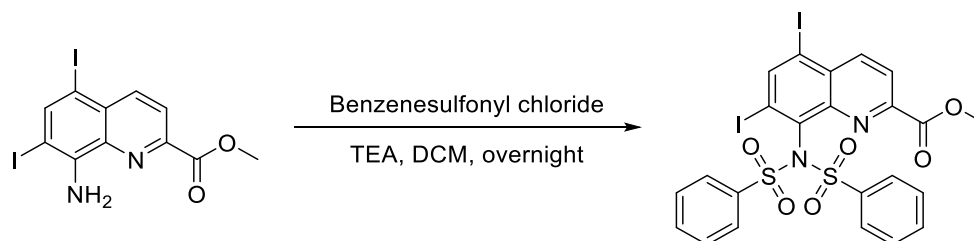
Yield: 99 mg (50.43%).

¹H NMR (500 MHz, Chloroform-*d*) δ 8.71 (s, 1H), 8.31 (d, *J* = 8.6 Hz, 1H), 8.12 (s, 1H), 7.98 (d, *J* = 8.8 Hz, 1H), 7.58 – 7.52 (m, 2H), 7.32 – 7.28 (m, 1H), 7.15 – 7.11 (m, 2H), 3.98 (s, 3H).

¹³C NMR (126 MHz, Chloroform-*d*) δ 164.28, 149.28, 147.82, 142.14, 142.09, 138.90, 138.69, 132.82, 131.04, 128.27, 127.95, 123.02, 99.97, 96.42, 53.07.

ESI-HRMS calc. for [C₁₇H₁₂I₂N₂O₄S + H]⁺ *m/z* 594.8680, found *m/z* 594.8688 [M + H]⁺.

Methyl 5,7-diiodo-8-(*N*-(phenylsulfonyl)phenylsulfonamido)quinoline-2-carboxylate (YJh96)



Benzenesulfonyl chloride (141.18 μL, 1.10 mmol) was added to methyl 8-amino-5,7-diiodoquinoline-2-carboxylate (**YJh94**) (200 mg, 0.440 mmol) in a mixed solution of triethylamine (100 μL) and dichloromethane (3 mL). The mixture was stirred at room temperature overnight. The reaction was quenched by sodium bicarbonate saturated solution and extracted 3 times with ethyl acetate. The

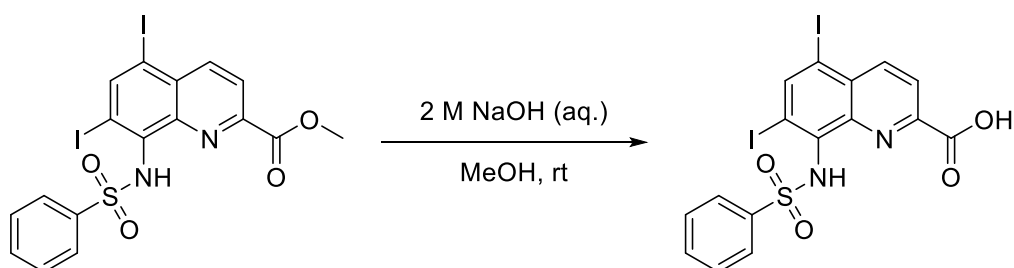
collected organic phase was washed by brine and dried over anhydrous Na_2SO_4 . The solvent was evaporated via reduced pressure. The resulting residue was purified via hexane and ethyl acetate silica gel chromatograph (5%, 15%, 20%, 30% ethyl acetate). The final product was obtained as white solid. Yield: 194.09 mg (60%).

$^1\text{H NMR}$ (500 MHz, Chloroform-*d*) δ 8.76 (s, 1H), 8.40 (d, $J = 8.7$ Hz, 1H), 8.07 (d, $J = 8.7$ Hz, 1H), 7.98 – 7.91 (m, 4H), 7.67 – 7.52 (m, 2H), 7.51 – 7.35 (m, 4H), 3.76 (s, 3H).

$^{13}\text{C NMR}$ (126 MHz, Chloroform-*d*) δ 164.91, 149.15, 149.08, 145.77, 141.89, 140.22, 139.26, 133.82, 131.85, 130.32, 128.44, 123.42, 108.21, 101.79, 52.95.

ESI-HRMS calc. for $[\text{C}_{23}\text{H}_{16}\text{I}_2\text{N}_2\text{O}_6\text{S}_2 + \text{H}]^+$ m/z 734.8612 (100.0%), 735.8645 (24.9%), found m/z 734.8620, 735.8647 $[\text{M} + \text{H}]^+$.

5,7-Diiodo-8-(phenylsulfonamido)quinoline-2-carboxylic acid (YJh97)



The synthesis was according to the general procedure for hydrolysis of methyl esters catalyzed by hydroxide ion. 2 M NaOH solution (2 mL) was added to methyl 5,7-diiodo-8-(phenylsulfonamido)quinoline-2-carboxylate (**YJh95**) (40 mg, 0.067 mmol) in methanol (2 mL). The reaction mixture was stirred at room temperature for 3 h. The compound was purified via silica gel chromatograph (ethyl acetate, MeOH and H_2O , the ratio was 8 to 1.5 to 1). The final product was obtained as white solid after lyophilization.

Yield: 24 mg (61.45%).

$^1\text{H NMR}$ (500 MHz, DMSO-*d*₆) δ 12.47 (s, 1H), 10.28 (s, 1H), 8.80 (s, 1H), 8.42 (d, $J = 8.6$ Hz, 1H), 7.98 (d, $J = 8.7$ Hz, 1H), 7.41 – 7.34 (m, 3H), 7.22 – 7.17 (m, 2H).

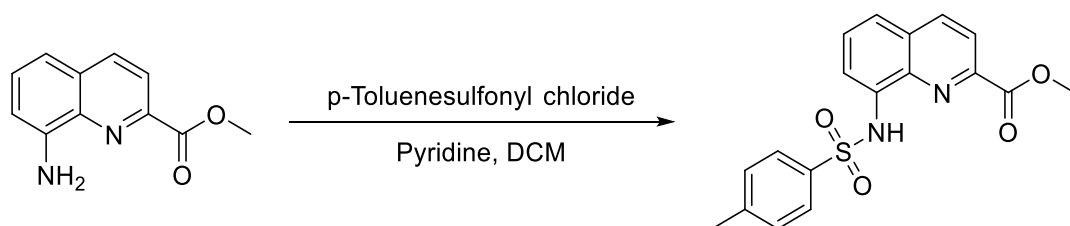
$^{13}\text{C NMR}$ (126 MHz, DMSO-*d*₆) δ 164.04, 148.25, 146.92, 142.46, 141.51, 138.95, 138.13, 132.43, 130.77, 128.43, 127.04, 121.87, 104.02, 98.44.

ESI-HRMS calc. for $[\text{C}_{16}\text{H}_{10}\text{I}_2\text{N}_2\text{O}_4\text{S} + \text{H}]^+$ m/z 580.8523, found m/z 580.85406 $[\text{M} + \text{H}]^+$.

Melting point: 205.4 °C

Purity: 95.98%

Methyl 8-((4-methylphenyl)sulfonamido)quinoline-2-carboxylate (YJh98)



The synthesis was according to the general procedure for sulfonamide coupling. *p*-Toluenesulfonyl chloride (141.42 mg, 0.742 mmol) was added to methyl 8-aminoquinoline-2-carboxylate (**YJh89**) (100 mg, 0.495 mmol) in pyridine/dichloromethane (1.5 mL/3 mL). The compound was purified via hexane

and ethyl acetate silica gel chromatograph (60% ethyl acetate). The final product was obtained as white (a little yellow) solid.

Yield: 115 mg (65.25%).

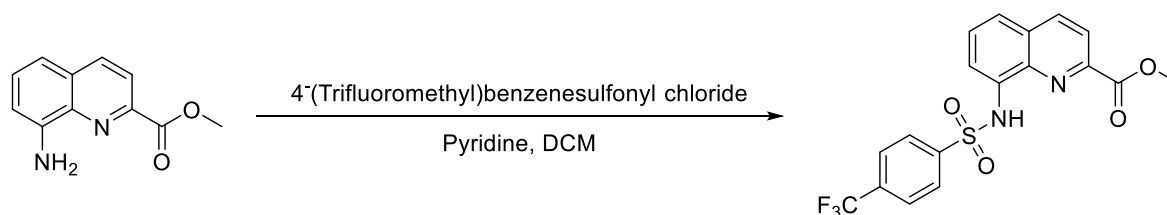
¹H NMR (500 MHz, Chloroform-*d*) δ 9.32 (s, 1H), 8.21 (d, *J* = 8.5 Hz, 1H), 8.14 (d, *J* = 8.5 Hz, 1H), 7.52 (dd, *J* = 8.2, 7.4 Hz, 1H), 7.48 (dd, *J* = 8.3, 1.5 Hz, 1H), 7.19 – 7.11 (m, 2H), 4.07 (s, 2H), 2.29 (s, 3H).

¹³C NMR (126 MHz, Chloroform-*d*) δ 165.58, 146.38, 144.03, 137.95, 137.54, 136.45, 134.94, 129.68, 129.49, 129.22, 127.46, 121.93, 121.79, 115.75, 53.10, 21.58.

ESI-HRMS calc. for [C₁₈H₁₆N₂O₄S + H]⁺ *m/z* 357.0904 (100.0%), found *m/z* 357.0908 [M + H]⁺.

Purity: 97.04%

Methyl 8-((4-(trifluoromethyl)phenyl)sulfonamido)quinoline-2-carboxylate (YJh99)



The synthesis was according to the general procedure for sulfonamide coupling. 4-(Trifluoromethyl)benzenesulfonyl chloride (181.46 mg, 0.742 mmol) was added to methyl 8-aminoquinoline-2-carboxylate (**YJh89**) (100 mg, 0.495 mmol) in pyridine/dichloromethane (1.5 mL/3 mL). The compound was purified via hexane and ethyl acetate silica gel chromatograph (60% ethyl acetate). The final product was obtained as yellow solid.

Yield: 191.01 mg (94.12%).

¹H NMR (500 MHz, Chloroform-*d*) δ 9.33 (s, 1H), 8.24 (d, *J* = 8.5 Hz, 1H), 8.16 (d, *J* = 8.5 Hz, 1H), 8.06 (d, *J* = 8.2 Hz, 2H), 7.90 (dd, *J* = 5.4, 3.5 Hz, 1H), 7.62 (d, *J* = 8.5 Hz, 2H), 7.57 – 7.55 (m, 2H), 4.07 (s, 3H).

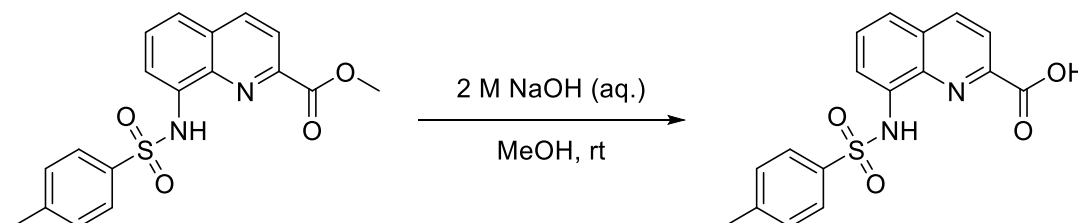
¹³C NMR (176 MHz, Chloroform-*d*) δ 165.36, 146.59, 142.94, 138.16, 137.74, 134.72 (q, *J* = 32.9 Hz), 134.29, 129.57, 129.20, 127.94, 126.21 (q, *J* = 3.6 Hz), 123.18 (q, *J* = 271.9 Hz), 122.69, 122.11, 116.72, 53.19.

¹⁹F NMR (376 MHz, Chloroform-*d*) δ -63.16.

ESI-HRMS calc. for [C₁₈H₁₃F₃N₂O₄S + H]⁺ *m/z* 411.0621, found *m/z* 411.0626 [M + H]⁺.

Purity: 99.05%

8-((4-Methylphenyl)sulfonamido)quinoline-2-carboxylic acid (YJh100)



The synthesis was according to the general procedure for hydrolysis of methyl esters catalyzed by hydroxide ion. 2 M NaOH (10 mL) was added to methyl 8-((4-methylphenyl)sulfonamido)quinoline-2-carboxylate (**YJh98**) (90 mg, 0.321 mmol) in methanol (2 mL) and stirred at room temperature for 3 h.

The compound was purified via silica gel chromatograph (ethyl acetate, MeOH and H₂O, the ratio was 8 to 1.5 to 1). The final product was obtained as yellow solid after lyophilization.

Yield: 98.94 mg (90%).

¹H NMR (500 MHz, DMSO-*d*₆) δ 13.43 (s, 1H), 11.00 (s, 1H), 8.54 (d, *J* = 8.5 Hz, 1H), 8.17 (d, *J* = 8.5 Hz, 1H), 7.84 (dd, *J* = 7.7, 1.3 Hz, 1H), 7.80 – 7.74 (m, 2H), 7.71 (dd, *J* = 8.3, 1.3 Hz, 1H), 7.64 (t, *J* = 8.0 Hz, 1H), 7.37 – 7.22 (m, 2H), 2.24 (s, 3H).

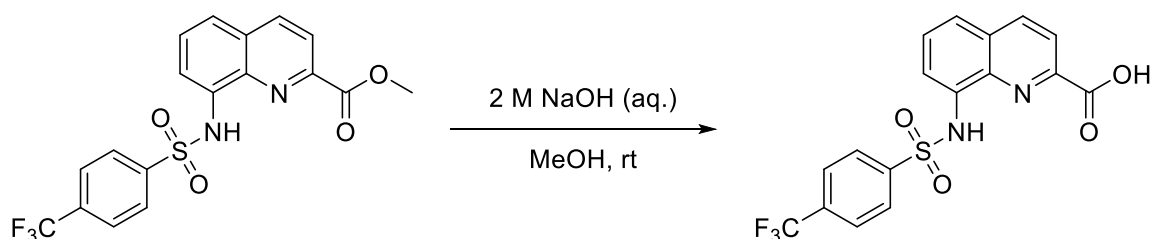
¹³C NMR (126 MHz, DMSO-*d*₆) δ 165.01, 145.44, 143.73, 138.82, 136.85, 136.28, 134.78, 129.74, 129.51, 129.32, 126.79, 122.31, 120.65, 116.56, 20.86.

ESI-HRMS calc. for [C₁₇H₁₄N₂O₄S + H]⁺ *m/z* 343.0747, found *m/z* 343.07722 [M + H]⁺.

Melting point: 220.3 °C

Purity: 98.62%

8-((4-(Trifluoromethyl)phenyl)sulfonamido)quinoline-2-carboxylic acid (YJh101)



The synthesis was according to the general procedure for hydrolysis of methyl esters catalyzed by hydroxide ion. 2 M NaOH (10 mL) was added to methyl 8-((4-(trifluoromethyl)phenyl)sulfonamido)quinoline-2-carboxylate (YJh99) (110 mg, 0.268 mmol) in methanol (2 mL). The reaction mixture was stirred at room temperature for 3 h. The compound was purified via silica gel chromatograph (ethyl acetate, MeOH and H₂O, the ratio was 8 to 1.5 to 1). The final product was obtained as yellow solid after lyophilization.

Yield: 95.62 mg (90%).

¹H NMR (500 MHz, DMSO-*d*₆) δ 13.31 (s, 1H), 11.17 (s, 1H), 8.56 (d, *J* = 8.5 Hz, 1H), 8.16 (d, *J* = 8.5 Hz, 1H), 8.07 (d, *J* = 8.2 Hz, 2H), 7.88 (dd, *J* = 7.7, 1.2 Hz, 1H), 7.85 (d, *J* = 8.4 Hz, 2H), 7.78 (dd, *J* = 8.3, 1.3 Hz, 1H), 7.68 (t, *J* = 8.0 Hz, 1H).

¹³C NMR (176 MHz, DMSO-*d*₆) δ 164.93, 145.64, 142.98, 138.92, 137.19, 134.14, 132.84 (q, *J* = 32.7 Hz), 129.56, 129.32, 127.75, 126.56 (q, *J* = 3.7, 3.3 Hz), 123.24, 123.20 (q, *J* = 272.7 Hz), 120.71, 117.89.

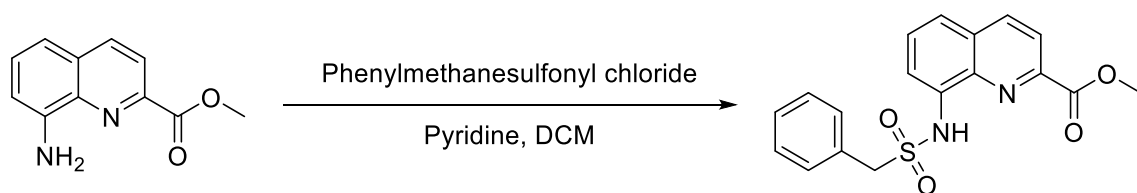
¹⁹F NMR (376 MHz, DMSO-*d*₆) δ -61.78.

ESI-HRMS calc. for [C₁₇H₁₁F₃N₂O₄S + H]⁺ *m/z* 397.0464, found *m/z* 397.04902 [M + H]⁺.

Melting point: 222 °C

Purity: 97.41%

Methyl 8-((phenylmethyl)sulfonamido)quinoline-2-carboxylate (YJh102)



The synthesis was according to the general procedure for sulfonamide coupling. Phenylmethanesulfonyl chloride (134.45 mg, 0.705 mmol) was added to methyl 8-aminoquinoline-2-carboxylate (**YJh89**) (95 mg, 0.470 mmol) in pyridine/dichloromethane (1.5 mL/3 mL). The compound was purified via hexane and ethyl acetate silica gel chromatograph (33% ethyl acetate). The final product was obtained as solid.

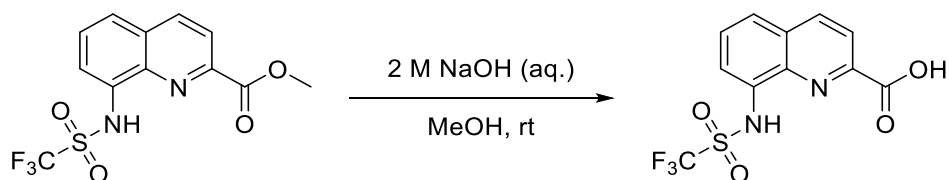
Yield: 128.33 mg (76.64%).

¹H NMR (500 MHz, Chloroform-*d*) δ 8.87 (s, 1H), 8.30 (d, *J* = 8.5 Hz, 1H), 8.20 (d, *J* = 8.5 Hz, 1H), 7.83 (dd, *J* = 6.6, 2.3 Hz, 1H), 7.61 – 7.52 (m, 2H), 7.22 (ddd, *J* = 6.2, 5.5, 2.8 Hz, 1H), 7.17 – 7.07 (m, 4H), 4.42 (s, 2H), 4.01 (s, 3H).

¹³C NMR (126 MHz, Chloroform-*d*) δ 165.51, 146.44, 137.59, 137.57, 135.38, 130.81, 129.53, 129.35, 128.81, 128.74, 128.19, 122.03, 121.93, 115.47, 58.36, 52.96.

ESI-HRMS calc. for [C₁₈H₁₆N₂O₄S + H]⁺ *m/z* 357.0904, found *m/z* 357.0907 [M + H]⁺.

8-((Trifluoromethyl)sulfonamido)quinoline-2-carboxylic acid (**YJh103**)



The synthesis was according to the general procedure for hydrolysis of methyl esters catalyzed by hydroxide ion. 2 M NaOH (10 mL) was added to methyl 8-((trifluoromethyl)sulfonamido)quinoline-2-carboxylate (**YJh92**) (100 mg, 0.299 mmol) in methanol (2 mL). The reaction mixture was stirred at room temperature for 3 h. The compound was purified via silica gel chromatograph (ethyl acetate, MeOH and H₂O, the ratio was 8 to 1.5 to 1). The final product was obtained as yellow solid after lyophilization.

Yield: 83.19 mg (86.84%).

¹H NMR (500 MHz, DMSO-*d*₆) δ 8.70 (d, *J* = 8.5 Hz, 1H), 8.26 (d, *J* = 8.5 Hz, 1H), 8.02 (dd, *J* = 8.3, 1.2 Hz, 1H), 7.94 (dd, *J* = 7.7, 1.2 Hz, 1H), 7.80 (t, *J* = 8.0 Hz, 1H).

¹³C NMR (126 MHz, DMSO-*d*₆) δ 165.03, 146.53, 139.07, 138.43, 132.37, 129.60, 129.11, 125.61, 121.15, 121.02, 119.56 (q, *J* = 390.0 Hz).

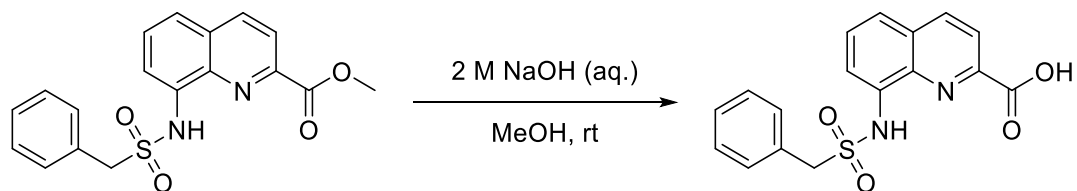
¹⁹F NMR (565 MHz, DMSO-*d*₆) δ -75.66.

ESI-HRMS calc. for [C₁₁H₇F₃N₂O₄S + H]⁺ *m/z* 321.0151, found *m/z* 321.01676 [M + H]⁺.

Melting point: 173.7 °C

Purity: 95.14%

8-((Phenylmethyl)sulfonamido)quinoline-2-carboxylic acid (**YJh104**)



The synthesis was according to the general procedure for hydrolysis of methyl esters catalyzed by hydroxide ion. 2 M NaOH (10 mL) was added to methyl 8-((phenylmethyl)sulfonamido)quinoline-2-carboxylate (**YJh102**) (100 mg, 0.281 mmol) in methanol (6 mL). The reaction mixture was stirred at

room temperature for 3 h. The compound was purified via silica gel chromatograph (ethyl acetate, MeOH and H₂O, the ratio was 8 to 1.5 to 1). The final product was obtained as yellow solid after lyophilization.

Yield: 89 mg (92.65%).

¹H NMR (500 MHz, DMSO-*d*₆) δ 13.35 (s, 1H), 10.45 (s, 1H), 8.62 (d, *J* = 8.5 Hz, 1H), 8.23 (d, *J* = 8.5 Hz, 1H), 7.86 (dd, *J* = 7.7, 1.2 Hz, 1H), 7.78 (dd, *J* = 8.3, 1.3 Hz, 1H), 7.69 (t, *J* = 8.0 Hz, 1H), 7.26 – 7.20 (m, 1H), 7.19 – 7.12 (m, 4H), 4.65 (s, 2H).

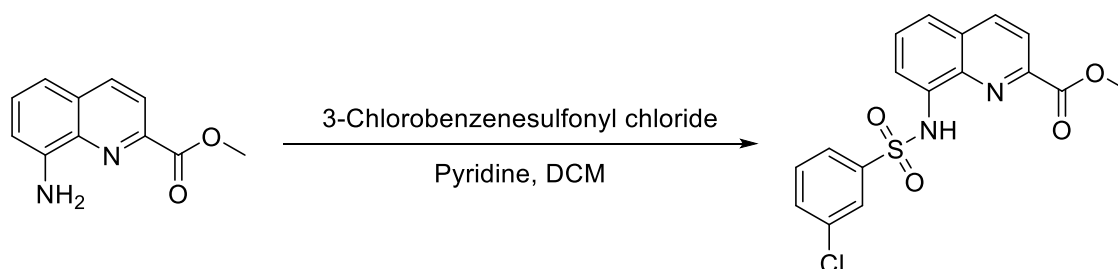
¹³C NMR (126 MHz, DMSO-*d*₆) δ 165.15, 145.39, 138.71, 136.83, 135.64, 130.85, 129.59, 129.42, 129.00, 128.19, 128.14, 122.00, 120.66, 116.43, 57.37.

ESI-HRMS calc. for [C₁₇H₁₄N₂O₄S + H]⁺ *m/z* 343.0747, found *m/z* 343.07651 [M + H]⁺.

Melting point: 212.0 °C

Purity: 99.46%

Methyl 8-((3-chlorophenyl)sulfonamido)quinoline-2-carboxylate (YJh105)



The synthesis was according to the general procedure for sulfonamide coupling. 3-chlorobenzenesulfonyl chloride (104.45 μL, 0.742 mmol) was added to methyl 8-aminoquinoline-2-carboxylate (**YJh89**) (100 mg, 0.495 mmol) in pyridine/dichloromethane (1.5 mL/3 mL). The compound was purified via hexane and ethyl acetate silica gel chromatograph (33% ethyl acetate). The final product was obtained as white solid after lyophilization.

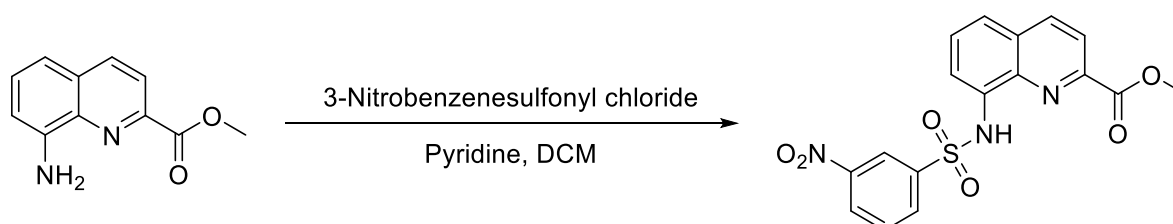
Yield: 152.9 mg (82.05%).

¹H NMR (500 MHz, Chloroform-*d*) δ 9.30 (s, 1H), 8.24 (d, *J* = 8.5 Hz, 1H), 8.16 (d, *J* = 8.5 Hz, 1H), 7.95 (t, *J* = 1.9 Hz, 1H), 7.87 (dd, *J* = 6.6, 2.3 Hz, 1H), 7.77 (ddd, *J* = 7.9, 1.8, 1.0 Hz, 1H), 7.61 – 7.52 (m, 2H), 7.38 (ddd, *J* = 8.0, 2.1, 1.0 Hz, 1H), 7.27 (t, *J* = 8.0 Hz, 1H), 4.08 (s, 3H).

¹³C NMR (126 MHz, Chloroform-*d*) δ 165.44, 146.60, 141.03, 138.18, 137.66, 135.22, 134.34, 133.25, 130.24, 129.51, 129.20, 127.58, 125.48, 122.65, 122.06, 116.96, 53.16.

ESI-HRMS calc. for [C₁₇H₁₃ClN₂O₄S + H]⁺ *m/z* 377.0357 (100.0%), 379.0328 (32.0%), found *m/z* 377.0361, 379.0337 [M + H]⁺.

Methyl 8-((3-nitrophenyl)sulfonamido)quinoline-2-carboxylate (YJh106)



The synthesis was according to the general procedure for sulfonamide coupling. 3-nitrobenzenesulfonyl chloride (164.40, 0.742 mmol) was added to methyl 8-aminoquinoline-2-carboxylate (**YJh89**) (100 mg,

0.495 mmol) in pyridine/dichloromethane (1.5 mL/3 mL). The compound was purified via hexane and ethyl acetate silica gel chromatograph (33% ethyl acetate). The final product was obtained as white solid.

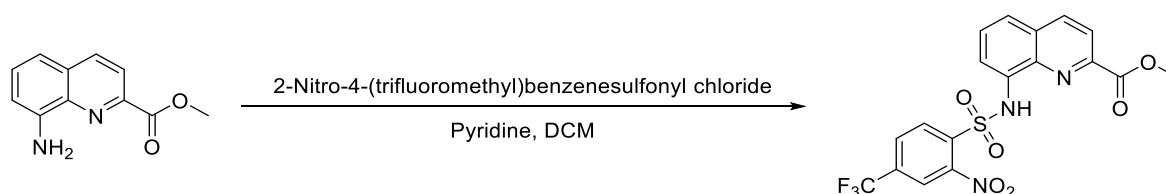
Yield: 151 mg (78.82%).

¹H NMR (500 MHz, Chloroform-*d*) δ 9.43 (s, 1H), 8.77 (t, *J* = 2.0 Hz, 1H), 8.25 (ddd, *J* = 8.2, 2.2, 1.0 Hz, 1H), 8.24 (d, *J* = 8.5 Hz, 1H), 8.20 (ddd, *J* = 7.9, 1.8, 1.1 Hz, 1H), 8.15 (d, *J* = 8.5 Hz, 1H), 7.95 (dd, *J* = 5.8, 3.1 Hz, 1H), 7.62 – 7.57 (m, 2H), 7.54 (t, *J* = 8.0 Hz, 1H), 4.08 (s, 3H).

¹³C NMR (126 MHz, Chloroform-*d*) δ 165.31, 148.21, 146.80, 141.42, 138.37, 137.79, 133.90, 132.82, 130.34, 129.55, 129.21, 127.51, 123.32, 122.73, 122.15, 117.95, 53.23.

ESI-HRMS calc. for [C₁₇H₁₃N₃O₆S + H]⁺ *m/z* 388.0598, found *m/z* 388.0602 [M + H]⁺.

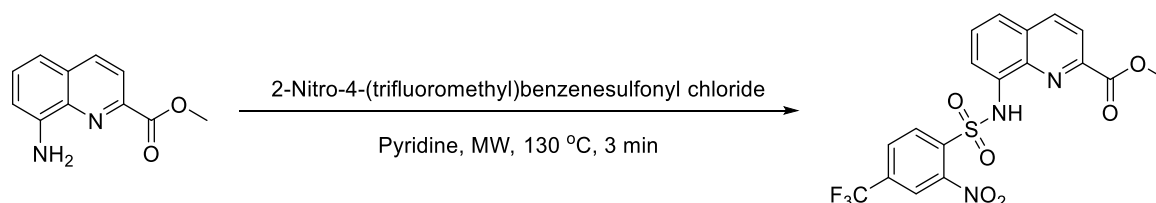
Methyl 8-((2-nitro-4-(trifluoromethyl)phenyl)sulfonamido)quinoline-2-carboxylate (YJh109) method 1



The synthesis was according to the general procedure for sulfonamide coupling. 2-Nitro-4-(trifluoromethyl)benzenesulfonyl chloride (214.84 mg, 0.742 mmol) was added to methyl 8-aminoquinoline-2-carboxylate (YJh89) (100 mg, 0.495 mmol) in pyridine/dichloromethane (1.5 mL/3 mL). The compound was purified via hexane and ethyl acetate silica gel chromatograph (60% ethyl acetate). The final product was obtained as yellow solid.

Yield: 215.31 mg (95.61%).

Methyl 8-((2-nitro-4-(trifluoromethyl)phenyl)sulfonamido)quinoline-2-carboxylate (YJh109) method 2



2-Nitro-4-(trifluoromethyl)benzenesulfonyl chloride (214.84 mg, 0.742 mmol) and methyl 8-aminoquinoline-2-carboxylate (YJh89) (100 mg, 0.495 mmol) were added to pyridine (2 mL) and heated by microwave reactor at 130 °C for 3 min. The solution was poured into sodium bicarbonate saturated solution (10 mL) and extracted 3 times with ethyl acetate. The collected organic phase was washed by brine and dried over anhydrous Na₂SO₄. The solvent was evaporated under reduced pressure. The resulting residue was purified via hexane and ethyl acetate silica gel chromatograph (20%-50% ethyl acetate). The final product was obtained as yellow solid.

Yield: 118.16 mg (52.47%).

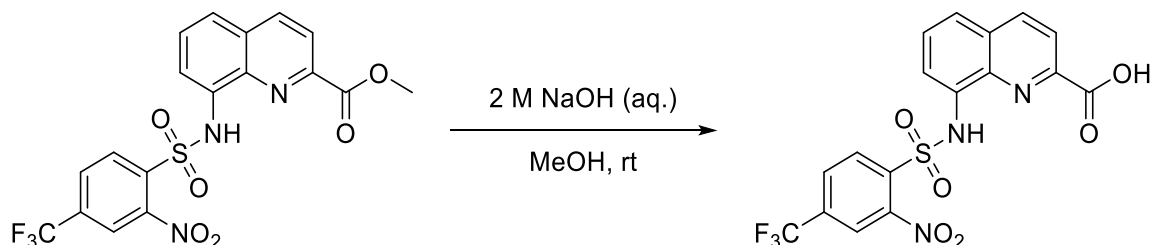
¹H NMR (500 MHz, Chloroform-*d*) δ 10.05 (s, 1H), 8.26 (d, *J* = 8.5 Hz, 1H), 8.17 – 8.12 (m, 2H), 8.11 (d, *J* = 1.8 Hz, 1H), 8.07 (dd, *J* = 5.9, 2.9 Hz, 1H), 7.76 (ddd, *J* = 8.2, 1.9, 0.8 Hz, 1H), 7.69 – 7.61 (m, 2H), 4.05 (s, 3H).

¹³C NMR (176 MHz, Chloroform-*d*) δ 165.32, 148.33, 146.97, 138.99, 137.68, 136.55, 135.77 (q, *J* = 34.8 Hz), 133.89, 131.90, 129.58, 129.28 (q, *J* = 3.2 Hz), 129.19, 123.81, 123.29 (q, *J* = 3.5 Hz), 122.10, 122.02 (q, *J* = 273.8 Hz), 119.10, 53.18.

¹⁹F NMR (471 MHz, Chloroform-*d*) δ -63.28.

ESI-HRMS calc. for [C₁₈H₁₂F₃N₃O₆S + H]⁺ *m/z* 456.0472, found *m/z* 456.0480 [M + H]⁺.

8-((2-Nitro-4-(trifluoromethyl)phenyl)sulfonamido)quinoline-2-carboxylic acid (YJh110)



The synthesis was according to the general procedure for hydrolysis of methyl esters catalyzed by hydroxide ion. 2 M NaOH (10 mL) was added to methyl 8-((2-nitro-4-(trifluoromethyl)phenyl)sulfonamido)quinoline-2-carboxylate (**YJh109**) (60 mg, 0.132 mmol) in methanol (6 mL). The reaction mixture was stirred at room temperature for 3 h. The compound was purified via silica gel chromatograph (ethyl acetate, MeOH and H₂O, the ratio was 8 to 1.5 to 1). The final product was obtained as yellow solid after lyophilization.

Yield: 52.40 mg (90.11%).

¹H NMR (500 MHz, DMSO-*d*₆) δ 13.37 (s, 1H), 11.46 (s, 1H), 8.61 (d, *J* = 8.5 Hz, 1H), 8.49 (d, *J* = 1.8 Hz, 1H), 8.35 (d, *J* = 8.3 Hz, 1H), 8.20 (d, *J* = 8.5 Hz, 1H), 8.15 (dd, *J* = 8.4, 1.8 Hz, 1H), 7.86 (dd, *J* = 8.2, 1.3 Hz, 1H), 7.77 (dd, *J* = 7.7, 1.2 Hz, 1H), 7.70 (t, *J* = 8.0 Hz, 1H).

¹³C NMR (176 MHz, DMSO-*d*₆) δ 165.14, 148.09, 146.18, 138.94, 137.64, 134.86, 134.12 (q, *J* = 34.0 Hz), 133.27, 131.30, 129.76 (q, *J* = 3.5 Hz), 129.65, 129.27, 124.19, 122.47 (q, *J* = 3.8 Hz), 122.13 (q, *J* = 274.1 Hz), 121.01, 119.12.

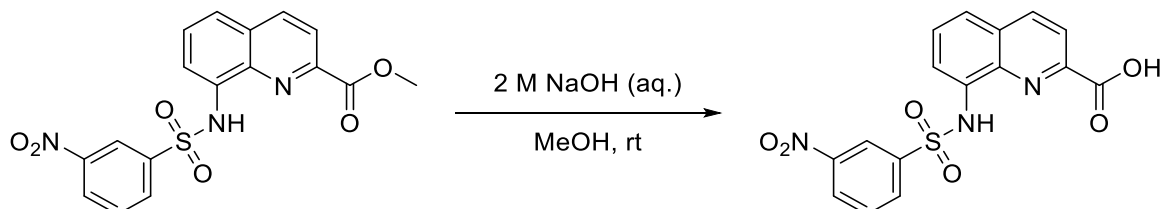
¹⁹F NMR (565 MHz, DMSO-*d*₆) δ -61.88.

ESI-HRMS calc. for [C₁₇H₁₀F₃N₃O₆S + H]⁺ *m/z* 442.0315, found *m/z* 442.03327 [M + H]⁺.

Melting point: 233.4 °C

Purity: 99.76%

8-((3-Nitrophenyl)sulfonamido)quinoline-2-carboxylic acid (YJh111)



The synthesis was according to the general procedure for hydrolysis of methyl esters catalyzed by hydroxide ion. 2 M NaOH solution (6 mL) was added to methyl 8-((3-nitrophenyl)sulfonamido)quinoline-2-carboxylate (**YJh106**) (150 mg, 0.387 mmol) in methanol (6 mL). The reaction mixture was stirred at room temperature for 3 h. The compound was purified via silica gel chromatograph (ethyl acetate, MeOH and H₂O, the ratio was 8 to 1.5 to 1). The final product was obtained as yellow solid after lyophilization.

Yield: 100 mg (69.17%).

¹H NMR (500 MHz, DMSO-*d*₆) δ 13.26 (s, 1H), 11.15 (s, 1H), 8.62 (t, *J* = 2.0 Hz, 1H), 8.55 (d, *J* = 8.5 Hz, 1H), 8.32 (ddd, *J* = 8.3, 2.3, 1.0 Hz, 1H), 8.17 (ddd, *J* = 7.9, 1.8, 1.0 Hz, 1H), 8.13 (d, *J* = 8.5 Hz, 1H), 7.93 (dd, *J* = 7.7, 1.2 Hz, 1H), 7.81 (dd, *J* = 8.3, 1.3 Hz, 1H), 7.71 (td, *J* = 8.0, 2.5 Hz, 2H).

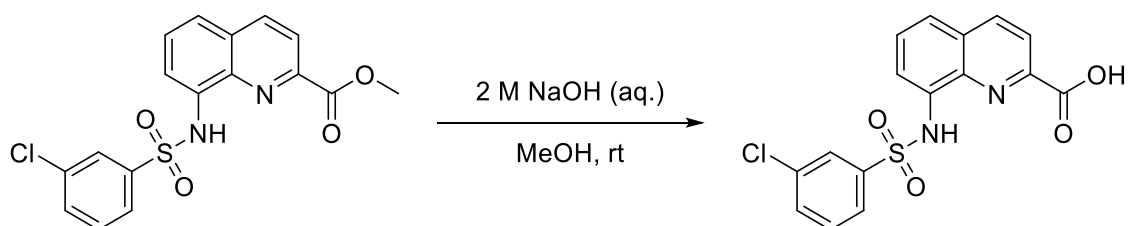
¹³C NMR (126 MHz, DMSO-*d*₆) δ 164.86, 147.76, 145.73, 140.60, 138.92, 137.56, 133.80, 132.47, 131.25, 129.53, 129.29, 127.73, 123.86, 121.59, 120.66, 119.47.

ESI-HRMS calc. for [C₁₆H₁₁N₃O₆S + H]⁺ *m/z* 374.0441, found *m/z* 374.04573 [M + H]⁺.

Melting point: 211.1 °C

Purity: 99.39%

8-((3-Chlorophenyl)sulfonamido)quinoline-2-carboxylic acid (YJh112)



The synthesis was according to the general procedure for hydrolysis of methyl esters catalyzed by hydroxide ion. 2 M NaOH (10 mL) was added to methyl 8-((3-chlorophenyl)sulfonamido)quinoline-2-carboxylate (**YJh105**) (152.9 mg, 0.406 mmol) in methanol (10 mL). The reaction mixture was stirred at room temperature for 3 h. The compound was purified via silica gel chromatograph (ethyl acetate, MeOH and H₂O, the ratio was 8 to 1.5 to 1). The final product was obtained as yellow solid after lyophilization.

Yield: 99.10 mg (67.32%).

¹H NMR (500 MHz, DMSO-*d*₆) δ 13.32 (s, 1H), 11.06 (s, 1H), 8.56 (d, *J* = 8.5 Hz, 1H), 8.16 (d, *J* = 8.5 Hz, 1H), 7.94 – 7.86 (m, 2H), 7.81 – 7.75 (m, 2H), 7.69 (t, *J* = 8.0 Hz, 1H), 7.59 (ddd, *J* = 8.0, 2.1, 1.0 Hz, 1H), 7.47 (t, *J* = 8.0 Hz, 1H).

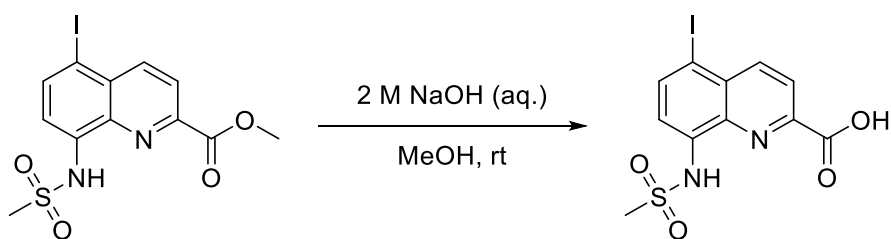
¹³C NMR (126 MHz, DMSO-*d*₆) δ 164.91, 145.60, 140.91, 138.91, 137.29, 134.11, 133.78, 133.17, 131.27, 129.51, 129.30, 126.37, 125.37, 123.34, 120.65, 118.45.

ESI-HRMS calc. for [C₁₆H₁₁ClN₂O₄S + H]⁺ *m/z* 363.0201 (100.0%), 365.0171 (32.0%), found *m/z* 363.02217 (100%), 365.01893 (32.7%) [M + H]⁺.

Melting point: 212.6 °C

Purity: 99.34%

5-Iodo-8-(methylsulfonamido)quinoline-2-carboxylic acid (YJh113)



The synthesis was according to the general procedure for hydrolysis of methyl esters catalyzed by hydroxide ion. 2 M NaOH (5 mL) was added to methyl 5-iodo-8-(methylsulfonamido)quinoline-2-carboxylate (**YJh74**) (48 mg, 0.118 mmol) in methanol (5 mL). The reaction mixture was stirred at room

temperature for 3 h. The compound was purified via silica gel chromatograph (ethyl acetate, MeOH and H₂O, the ratio was 8 to 1.5 to 1). The final product was obtained as white (a little yellow) solid after lyophilization.

Yield: 39.72 mg (85.70%).

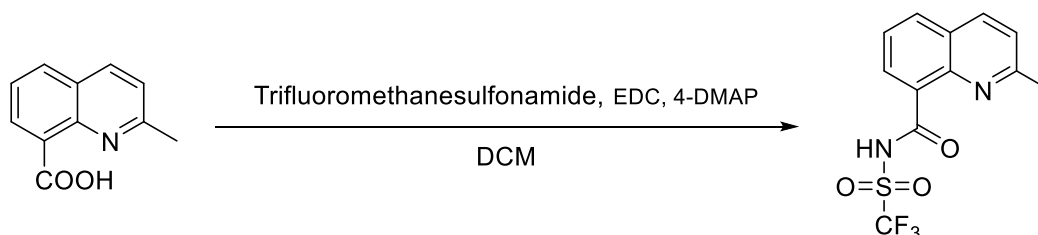
¹H NMR (500 MHz, DMSO-*d*₆) δ 13.55 (s, 1H), 10.53 (s, 1H), 8.57 (d, *J* = 8.7 Hz, 1H), 8.31 (d, *J* = 8.7 Hz, 1H), 8.30 (d, *J* = 8.2 Hz, 1H), 7.67 (d, *J* = 8.3 Hz, 1H), 3.18 (s, 3H).

¹³C NMR (126 MHz, DMSO-*d*₆) δ 164.60, 146.28, 142.48, 139.99, 137.65, 136.50, 130.93, 122.74, 117.71, 90.16, 39.19.

ESI-HRMS calc. for [C₁₁H₉N₂O₄S + H]⁺ *m/z* 392.9400, found *m/z* 392.94133 [M + H]⁺.

Melting point: 210.9 °C

2-Methyl-N-((trifluoromethyl)sulfonyl)quinoline-8-carboxamide (YJh116)

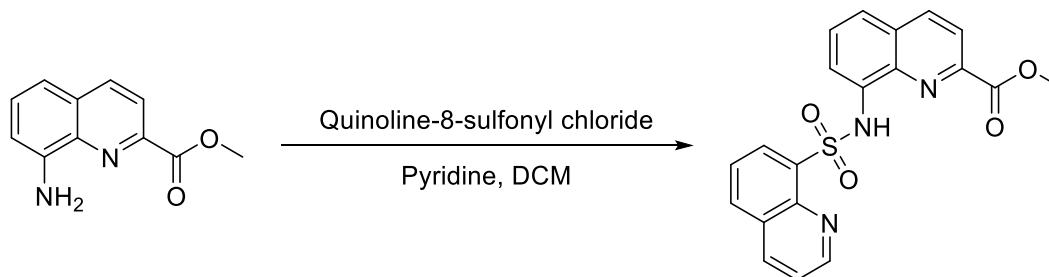


2-Methylquinoline-8-carboxylic acid (**YJh38**) (50 mg, 0.267 mmol), EDC·HCl (66.56 mg, 0.347 mmol) and 4-DMAP (48.95 mg, 0.401 mmol) were added to 4 mL dichloromethane. The reaction was stirring for 15min with ice bath protect. Trifluoromethanesulfonamide (47.79 mg, 0.321 mmol) was added. The reaction was stirred at room temperature overnight. Then the reaction mixture was poured on 10 mL brine solution and extracted 3 times by ethyl acetate. The collected organic phase was washed by brine and dried over anhydrous Na₂SO₄. The solvent was evaporated via reduced pressure. The resulting residue was purified via silica gel chromatograph. The final product was obtained as brown solid.

Yield: >16 mg.

ESI-MS calc. for [C₁₂H₉F₃N₂O₃S + H]⁺ *m/z* 319.0359, [C₁₂H₉F₃N₂O₃S + Na]⁺ *m/z* 341.0178, found *m/z* 319.0 [M + H]⁺, 341.0 [M + Na]⁺.

Methyl 8-(quinoline-8-sulfonamido)quinoline-2-carboxylate (YJh117)



The synthesis was according to the general procedure for sulfonamide coupling. Quinoline-8-sulfonyl chloride (168.89 mg, 0.742 mmol) was added to methyl 8-aminoquinoline-2-carboxylate (**YJh89**) (100 mg, 0.495 mmol) in pyridine/dichloromethane (1.5 mL/3 mL). The product was purified via hexane and ethyl acetate silica gel chromatograph (60% ethyl acetate). The final product was obtained as yellow solid.

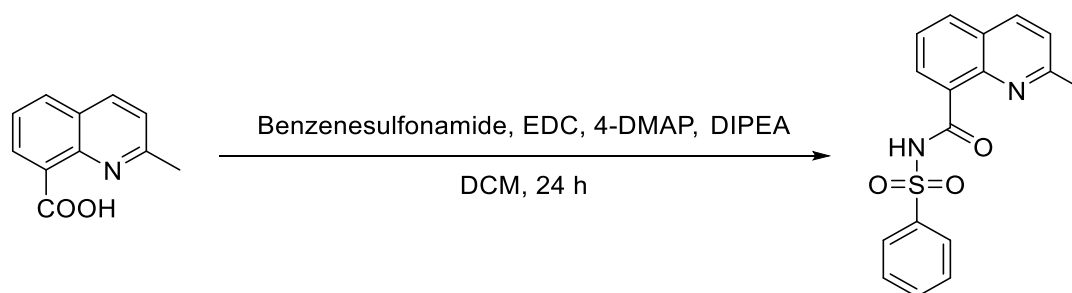
Yield: 183.20 mg (94.16%).

¹H NMR (500 MHz, Chloroform-*d*) δ 10.68 (s, 1H), 9.13 (dd, *J* = 4.3, 1.8 Hz, 1H), 8.50 (dd, *J* = 7.3, 1.4 Hz, 1H), 8.09 (d, *J* = 8.5 Hz, 1H), 8.12 – 8.06 (m, 2H), 8.04 (d, *J* = 8.4 Hz, 1H), 7.91 (dd, *J* = 8.3, 1.4 Hz, 1H), 7.54 (dd, *J* = 8.2, 7.3 Hz, 1H), 7.45 (t, *J* = 8.0 Hz, 1H), 7.41 (dd, *J* = 8.3, 4.3 Hz, 1H), 7.36 (dd, *J* = 8.2, 1.2 Hz, 1H), 4.15 (s, 3H).

¹³C NMR (126 MHz, Chloroform-*d*) δ 165.78, 151.67, 146.14, 143.45, 138.10, 137.13, 136.36, 135.99, 135.71, 133.73, 131.66, 129.43, 129.26, 128.74, 125.24, 122.28, 121.67, 121.36, 115.22, 53.01.

ESI-MS calc. for [C₂₀H₁₅N₃O₄S + H]⁺ *m/z* 394.0856 (100.0%), 395.0890 (21.6%), [C₂₀H₁₅N₃O₄S + Na]⁺ *m/z* 416.0675 (100.0%), 417.0709 (21.6%), found *m/z* 393.8, 394.8 [M + H]⁺, 415.8 [M + Na]⁺.

2-Methyl-N-(phenylsulfonyl)quinoline-8-carboxamide (YJh118)



2-Methylquinoline-8-carboxylic acid (**YJh38**) (100 mg, 0.534 mmol), EDC·HCl (133.13 mg, 0.694 mmol) and 4-DMAP (97.89 mg, 0.801 mmol) were added to 9 mL dichloromethane. The reaction was stirring for 15 min with ice bath protect then followed by addition of benzenesulfonamide (100.76 mg, 0.641 mmol) and DIPEA (325.68 μL, 1.87 mmol). The reaction mixture was stirred at room temperature overnight then quenched by 10 mL brine solution and extracted 3 times with ethyl acetate. The collected organic phase was washed by brine and dried over anhydrous Na₂SO₄. The solvent was evaporated via reduced pressure. The resulting residue was purified via silica gel chromatograph (33% ethyl acetate). The final product was obtained as white solid.

Yield: 76.21 mg (43.71%).

¹H NMR (500 MHz, Chloroform-*d*) δ 8.65 (dd, *J* = 7.4, 1.6 Hz, 1H), 8.27 – 8.22 (m, 2H), 8.21 (d, *J* = 8.5 Hz, 1H), 7.99 (dd, *J* = 8.1, 1.6 Hz, 1H), 7.66 – 7.50 (m, 4H), 7.44 (d, *J* = 8.5 Hz, 1H), 2.89 (s, 3H).

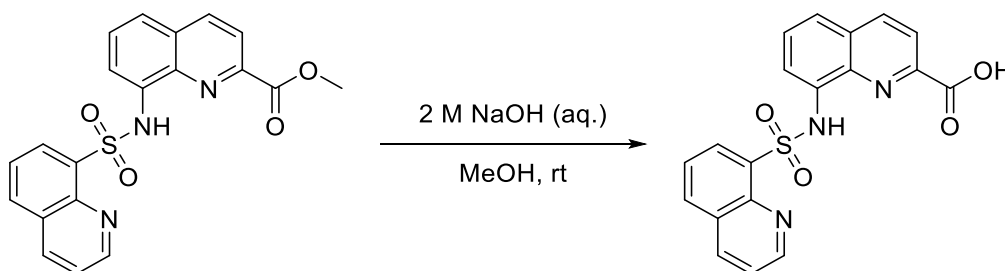
¹³C NMR (126 MHz, Chloroform-*d*) δ 163.59, 159.44, 144.48, 139.95, 138.50, 134.49, 133.66, 133.47, 128.87, 128.50, 126.83, 125.95, 125.24, 122.61, 25.31.

ESI-HRMS calc. for [C₁₇H₁₄N₂O₃S + H]⁺ *m/z* 327.0798, found *m/z* 327.0800 [M + H]⁺.

Melting point: 196.2 °C

Purity: 97.91%

8-(Quinoline-8-sulfonamido)quinoline-2-carboxylic acid (YJh119)



The synthesis was according to the general procedure for hydrolysis of methyl esters catalyzed by hydroxide ion. 2 M NaOH (9 mL) was added to methyl 8-(quinoline-8-sulfonamido)quinoline-2-carboxylate (**YJh117**) (137.2 mg, 0.349 mmol) in methanol (9 mL). The reaction mixture was stirred at room temperature for 3 h. The compound was purified via silica gel chromatograph (ethyl acetate, MeOH and H₂O, the ratio was 8 to 1.5 to 1). The final product was obtained as yellow solid after lyophilization.

Yield: 90.1 mg (68.1%).

¹H NMR (600 MHz, DMSO-*d*₆) δ 13.81 (s, 1H), 11.03 (s, 1H), 8.97 (dd, *J* = 4.3, 1.8 Hz, 1H), 8.50 (dd, *J* = 7.4, 1.4 Hz, 1H), 8.39 (d, *J* = 8.5 Hz, 1H), 8.36 (dd, *J* = 8.4, 1.8 Hz, 1H), 8.19 (dd, *J* = 8.3, 1.4 Hz, 1H), 8.07 (d, *J* = 8.5 Hz, 1H), 7.85 (dd, *J* = 7.4, 1.6 Hz, 1H), 7.71 (dd, *J* = 8.2, 7.4 Hz, 1H), 7.59 – 7.50 (m, 3H).

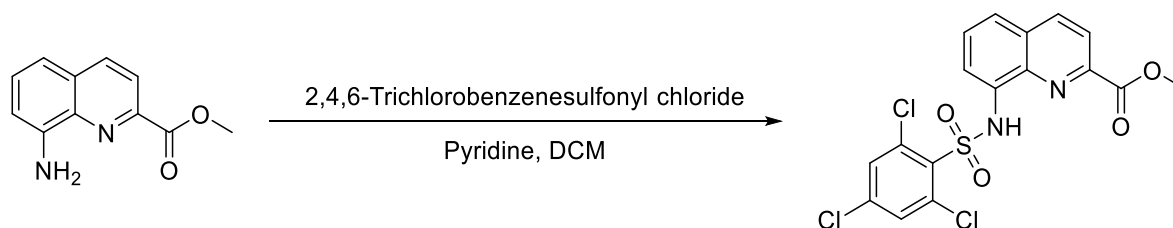
¹³C NMR (151 MHz, DMSO-*d*₆) δ 165.56, 151.32, 146.08, 142.43, 138.19, 136.84, 136.76, 135.01, 134.63, 134.52, 132.13, 129.14, 129.05, 128.31, 125.58, 122.65, 121.74, 121.07, 114.83.

ESI-HRMS calc. for [C₁₉H₁₃N₃O₄S + H]⁺ *m/z* 380.0700, found *m/z* 380.07202 [M + H]⁺.

Melting point: 252.6 °C

Purity: 99.38%

Methyl 8-((2,4,6-trichlorophenyl)sulfonamido)quinoline-2-carboxylate (**YJh120**)



The synthesis was according to the general procedure for sulfonamide coupling. 2,4,6-Trichlorobenzenesulfonyl chloride (207.68 mg, 0.742 mmol) was added to methyl 8-aminoquinoline-2-carboxylate (**YJh89**) (100 mg, 0.495 mmol) in pyridine/dichloromethane (3 mL/6 mL). The compound was purified via hexane and ethyl acetate silica gel chromatograph (20% ethyl acetate). The final product was obtained as white solid after lyophilization.

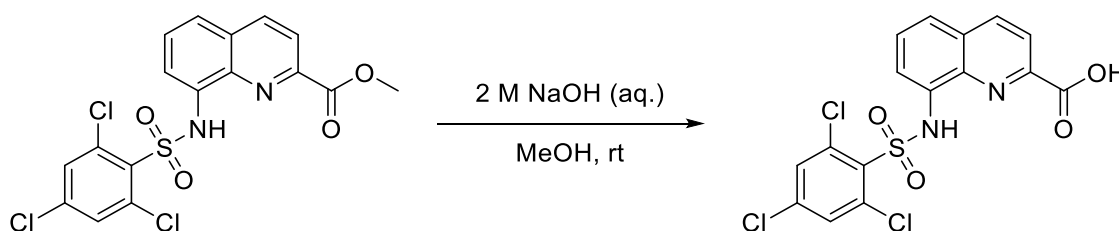
Yield: 124.09 mg (56.3%).

¹H NMR (500 MHz, Chloroform-*d*) δ 10.06 (s, 1H), 8.26 (d, *J* = 8.5 Hz, 1H), 8.20 (d, *J* = 8.5 Hz, 1H), 7.94 (t, *J* = 4.5 Hz, 1H), 7.54 (dd, *J* = 4.4, 0.6 Hz, 2H), 7.35 (s, 2H), 4.06 (s, 3H).

¹³C NMR (126 MHz, Chloroform-*d*) δ 165.44, 146.52, 138.62, 137.70, 137.56, 136.68, 134.07, 133.27, 131.28, 129.61, 129.31, 122.35, 122.17, 115.04, 53.10.

ESI-HRMS calc. for [C₁₇H₁₁Cl₃N₂O₄S + H]⁺ *m/z* 444.9578 (100.0%), 446.9548 (95.9%), 448.9519 (30.6%), found *m/z* 444.9581, 446.9554, 448.9527 [M + H]⁺.

8-((2,4,6-Trichlorophenyl)sulfonamido)quinoline-2-carboxylic acid (**YJh121**)



The synthesis was according to the general procedure for hydrolysis of methyl esters catalyzed by hydroxide ion. 2 M NaOH (10 mL) was added to methyl 8-(quinoline-8-sulfonamido)quinoline-2-carboxylate (**YJh120**) (68 mg, 0.153 mmol) in methanol (8 mL). The reaction mixture was stirred at room temperature for 3 h. The compound was purified via silica gel chromatograph (ethyl acetate, MeOH and H₂O, the ratio was 8 to 1.5 to 1). The final product was obtained as white (a little yellow) solid after lyophilization.

Yield: 52.80 mg (80.17%).

¹H NMR (500 MHz, DMSO-*d*₆) δ 13.49 (s, 1H), 11.52 (s, 1H), 8.62 – 8.54 (m, 1H), 8.22 (d, *J* = 8.5 Hz, 1H), 7.80 (s, 2H), 7.74 (dd, *J* = 6.4, 3.1 Hz, 1H), 7.66 – 7.60 (m, 2H).

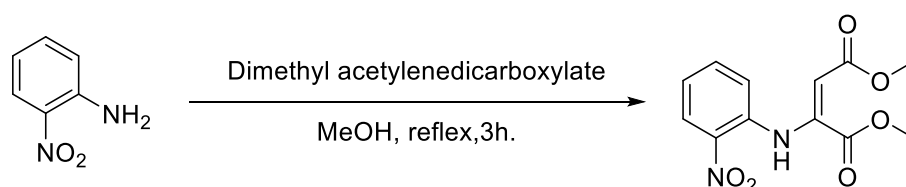
¹³C NMR (126 MHz, DMSO-*d*₆) δ 165.05, 145.75, 138.81, 138.22, 136.51, 135.67, 133.95, 132.46, 131.46, 129.62, 129.15, 122.64, 121.01, 114.81.

ESI-HRMS calc. for [C₁₆H₉Cl₃N₂O₄S + H]⁺ *m/z* 430.9421 (100.0%), 432.9392 (95.9%), 434.9362 (30.6%), 436.9333 (3.3%), found *m/z* 430.9413, 432.9397 [M + H]⁺.

Melting point: 176.8 °C

Purity: 99.76%

Dimethyl 2-((2-nitrophenyl)amino)maleate (**YJh122**)



Dimethyl acetylenedicarboxylate (13.35 mL, 108.59 mmol) was added to 2-nitroaniline (10 g, 72.39 mmol) in methanol (100 mL) and stirred at 65 °C for 24 h. The reaction solution was cooled to room temperature and concentrated to a volume of around 15 mL. The flask was stored at -20 °C overnight. The yellow precipitate was filtered and washed by cold methanol (80 mL at -20 °C). The yellow crystal was collected and dried under vacuum.

Yield: 13.98 g (68.92%).

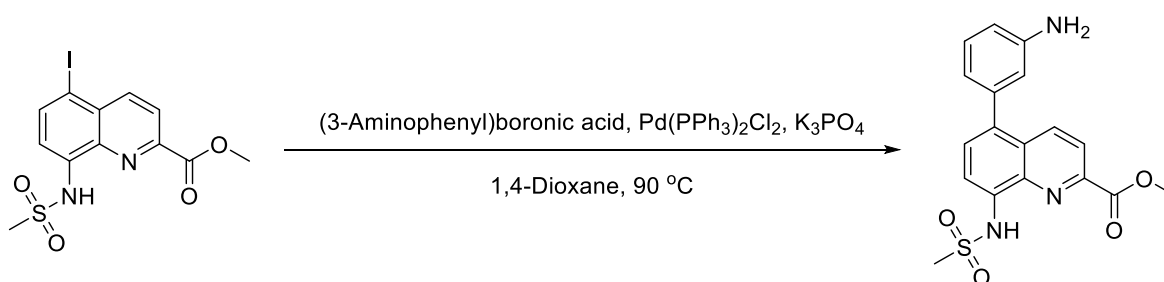
¹H NMR (500 MHz, Chloroform-*d*) δ 11.11 (s, 1H), 8.13 (dd, *J* = 8.4, 1.6 Hz, 1H), 7.46 (dddt, *J* = 8.3, 7.3, 1.6, 0.5 Hz, 1H), 7.08 (ddd, *J* = 8.4, 7.2, 1.2 Hz, 1H), 6.76 (dd, *J* = 8.4, 0.8 Hz, 1H), 5.83 (s, 1H), 3.80 (s, 3H), 3.74 (s, 3H).

¹³C NMR (126 MHz, Chloroform-*d*) δ 168.12, 164.48, 143.63, 138.23, 137.02, 134.35, 126.34, 122.21, 120.54, 103.11, 53.19, 51.96.

ESI-HRMS calc. for [C₁₂H₁₂N₂O₆ + H]⁺ *m/z* 281.0768, found *m/z* 281.0775 [M + H]⁺.

Purity: 97.27%

Methyl 5-(3-aminophenyl)-8-(methylsulfonamido)quinoline-2-carboxylate (**YJh123**)



Bis(triphenylphosphine)palladium(II) dichloride (34.56 mg, 0.049 mmol) was added to a mixture of methyl 5-iodo-8-(methylsulfonamido)quinoline-2-carboxylate (**YJh74**) (100 mg, 0.246 mmol), (3-aminophenyl)boronic acid (50.57 mg, 0.369 mmol) and K_2PO_3 (104.52 mg, 0.492 mmol) in 1,4-dioxane (5 mL) under nitrogen. The reaction was stirred at 90 °C for 14 h and then quenched by 10 mL brine solution and extracted 3 times with ethyl acetate. The collected organic phase was washed by brine and dried over anhydrous Na_2SO_4 . The solvent was evaporated under reduced pressure. The resulting residue was purified via hexane and ethyl acetate silica gel chromatograph (30%-100% ethyl acetate). The final product was obtained as yellow solid.

Yield: 15.4 mg (16.84%).

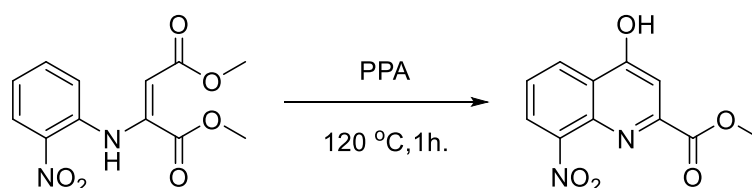
1H NMR (500 MHz, Chloroform-*d*) δ 8.48 (d, J = 8.8 Hz, 1H), 8.15 (d, J = 8.7 Hz, 1H), 7.94 (d, J = 7.9 Hz, 1H), 7.57 (d, J = 7.9 Hz, 1H), 7.30 (t, J = 7.7 Hz, 1H), 6.74 (d, J = 24.5 Hz, 3H), 4.06 (s, 3H), 3.11 (s, 3H).

^{13}C NMR (176 MHz, Chloroform-*d*) δ 165.52, 146.81, 146.35, 139.41, 138.08, 136.65, 135.51, 134.30, 129.70, 129.39, 128.21, 121.92, 120.48, 116.66, 115.31, 114.83, 53.13, 39.67.

ESI-HRMS calc. for $[C_{18}H_{17}N_3O_4S + H]^+$ m/z 372.1013 (100.0%), 373.1046 (19.5%), found m/z 372.1016 $[M + H]^+$.

Purity: 97.25%

Methyl 4-hydroxy-8-nitroquinoline-2-carboxylate (**YJh124**)



Dimethyl 2-((2-nitrophenyl)amino)maleate (**YJh122**) (5.8 g, 20.7 mmol) was added to polyphosphoric acid (35 g) and stirred at 120 °C for 1h. The reaction solution was cooled to room temperature and quenched by saturated sodium bicarbonate solution. The precipitate was collected by filtration and purified via recrystallization from ethanol. The final product was obtained as yellow solid.

Yield: 1.795 g (34.95%).

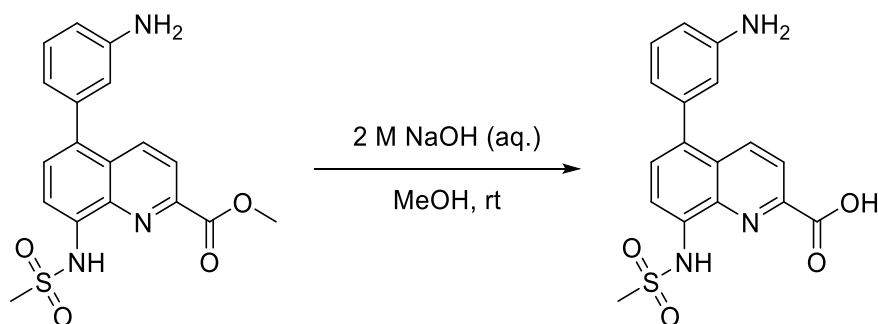
1H NMR (500 MHz, Chloroform-*d*) δ 11.76 (s, 1H), 8.72 (ddd, J = 8.1, 5.7, 1.6 Hz, 2H), 7.48 (t, J = 8.0 Hz, 1H), 7.05 (d, J = 1.5 Hz, 1H), 4.08 (s, 3H).

^{13}C NMR (126 MHz, Chloroform-*d*) δ 178.04, 162.40, 137.47, 136.07, 135.31, 134.35, 131.28, 128.38, 122.91, 113.60, 54.27.

ESI-HRMS calc. for $[C_{11}H_8N_2O_5 + H]^+$ m/z 249.0506, found m/z 249.0512 $[M + H]^+$.

Purity: 100%.

5-(3-Aminophenyl)-8-(methylsulfonamido)quinoline-2-carboxylic acid (**YJh125**)



The synthesis was according to the general procedure for hydrolysis of methyl esters catalyzed by hydroxide ion. 2 M NaOH (4 mL) was added to methyl 5-(3-aminophenyl)-8-(methylsulfonamido)quinoline-2-carboxylate (**YJh123**) (14 mg, 0.038 mmol) in methanol (4 mL). The compound was purified via silica gel chromatograph (ethyl acetate, MeOH and H₂O, the ratio was 8 to 1.5 to 1). The final product was obtained as yellow solid after lyophilization.

Yield: 10 mg (74.24%).

¹H NMR (600 MHz, DMSO-*d*₆) δ 13.45 (s, 1H), 10.49 (s, 1H), 8.53 (d, *J* = 8.8 Hz, 1H), 8.23 (d, *J* = 8.7 Hz, 1H), 7.92 (d, *J* = 8.0 Hz, 1H), 7.65 (d, *J* = 8.0 Hz, 1H), 7.18 (t, *J* = 7.7 Hz, 1H), 6.70 – 6.62 (m, 2H), 6.58 (d, *J* = 7.4 Hz, 1H), 3.19 (s, 3H).

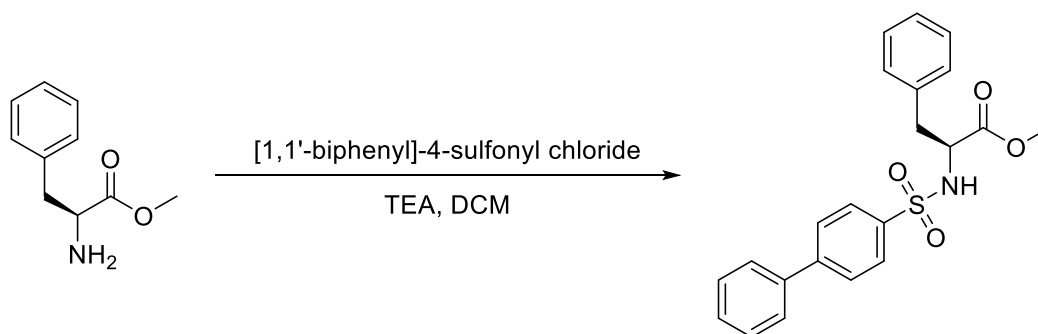
¹³C NMR (151 MHz, DMSO-*d*₆) δ 165.13, 148.91, 145.39, 138.55, 137.24, 136.92, 135.03, 134.59, 129.28, 129.18, 127.65, 120.86, 117.31, 116.21, 115.15, 113.35, 40.06.

ESI-HRMS calc. for [C₁₇H₁₅N₃O₄S + H]⁺ *m/z* 358.0856, found *m/z* 358.0857 [M + H]⁺.

Melting point: 203.8 °C

Purity: 96.53%

Methyl ([1,1'-biphenyl]-4-ylsulfonyl)-L-phenylalaninate (**YJh126**)



4-Biphenyl sulfonyl chloride (758.13 mg, 3 mmol) was added to L-phenylalanine methyl ester hydrochloride (431.36 mg, 2 mmol) and triethylamine (831.70 μL, 6.01 mmol) in dichloromethane (50 mL) and stirred at room temperature overnight. The reaction was quenched by sodium bicarbonate saturated solution and extracted 3 times with ethyl acetate. The collected organic phase was washed by brine and dried over anhydrous Na₂SO₄. The solvent was evaporated via reduced pressure. The resulting residue was purified via dichloromethane and methanol silica gel chromatograph (100% dichloromethane). The final product was obtained as white powder after lyophilization.

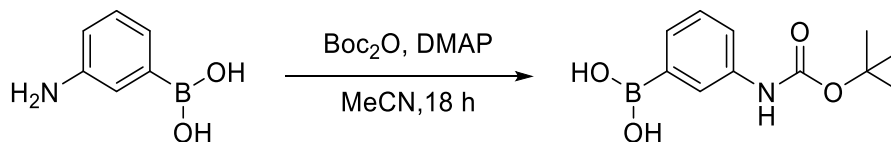
Yield: 502 mg (63.5%).

¹H NMR (500 MHz, Chloroform-*d*) δ 7.82 – 7.78 (m, 2H), 7.66 – 7.63 (m, 2H), 7.60 – 7.57 (m, 2H), 7.51 – 7.46 (m, 2H), 7.45 – 7.40 (m, 1H), 7.27 – 7.21 (m, 3H), 7.10 – 7.07 (m, 2H), 5.19 (d, *J* = 9.2 Hz, 1H), 4.26 (dt, *J* = 9.2, 6.1 Hz, 1H), 3.51 (s, 3H), 3.06 (qd, *J* = 13.8, 6.1 Hz, 2H).

¹³C NMR (126 MHz, Chloroform-*d*) δ 171.41, 145.78, 139.35, 138.28, 135.08, 129.53, 129.21, 128.74, 128.68, 127.81, 127.70, 127.41, 127.40, 56.88, 52.54, 39.51.

ESI-MS calc. for [C₂₂H₂₁NO₄S + H]⁺ m/z 396.1264 (100.0%), 397.1298 (23.8%), [C₂₂H₂₁NO₄S + Na]⁺ m/z 418.1083 (100.0%), 419.1117 (23.8%), found m/z 396.0, 397.0 [M + H]⁺, 417.8, 418.8 [M + Na]⁺.

(3-((Tert-butoxycarbonyl)amino)phenyl)boronic acid (YJh127)



Di-*tert*-butyl dicarbonate (1.75 g, 8.03 mmol) was added to (3-aminophenyl)boronic acid (1 g, 7.30 mmol) and DMAP (14.27 mg, 0.117 mmol) in anhydrous acetonitrile (70 mL) under argon. The reaction was stirred at room temperature for 18 h. The reaction solvent was removed in vacuo, and ethyl acetate (50 mL) and saturated ammonium chloride solution (20 mL) were added. The organic phase was washed with 1 M HCl solution and brine then dried over anhydrous Na₂SO₄. The solvent was evaporated via reduced pressure. The white solid was used directly in the next step without further purification.

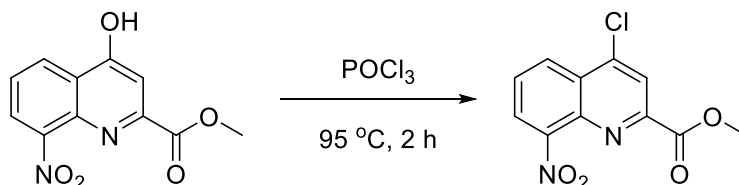
Yield: 1.166 g (67.4%)

¹H NMR (500 MHz, Chloroform-*d*) δ 8.05 – 7.73 (m, 3H), 7.42 (t, *J* = 7.8 Hz, 1H), 6.72 (s, 1H), 1.56 (s, 9H).

¹³C NMR (126 MHz, Chloroform-*d*) δ 153.07, 146.91, 138.28, 130.47, 128.95, 125.59, 123.36, 80.74, 27.55.

ESI-HRMS calc. for [C₁₁H₁₆BN₂O₄ + H]⁺ m/z 238.1245, found m/z 238.0893 [M + H]⁺.

Methyl 4-chloro-8-nitroquinoline-2-carboxylate (YJh128)



Phosphoryl chloride (6 mL) was added to methyl 4-hydroxy-8-nitroquinoline-2-carboxylate (YJh124) (550 mg, 2.22 mmol) and stirred at 95 °C for 2 h. The reaction was allowed to cool to room temperature and quenched by saturated bicarbonate sodium solution at 0 °C. The resulted mixture was extracted 3 times with dichloromethane. The collected organic phase was washed by brine and dried over anhydrous Na₂SO₄. The solvent was evaporated via reduced pressure. The resulting residue was purified via hexane and dichloromethane silica gel chromatograph (50% dichloromethane). The final product was obtained as yellow solid.

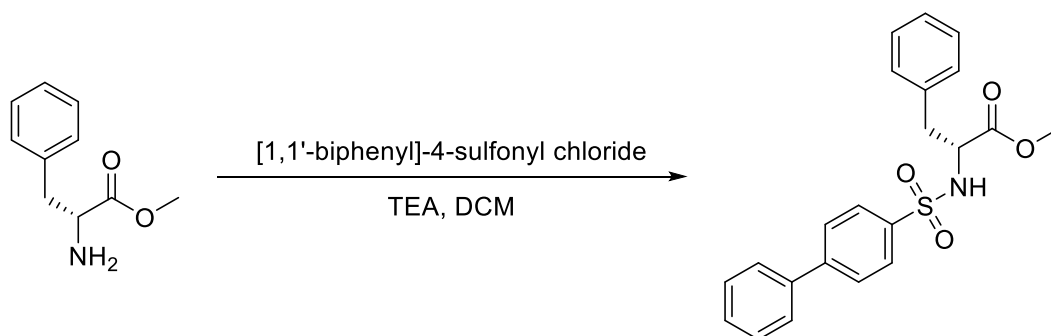
Yield: 522.99 mg (88.51%).

¹H NMR (500 MHz, Chloroform-*d*) δ 8.51 (dd, *J* = 8.6, 1.3 Hz, 1H), 8.39 (s, 1H), 8.16 (dd, *J* = 7.5, 1.3 Hz, 1H), 7.84 (dd, *J* = 8.6, 7.5 Hz, 1H), 4.05 (s, 3H).

¹³C NMR (126 MHz, Chloroform-*d*) δ 164.50, 149.88, 149.06, 144.56, 139.87, 128.42, 128.24, 128.22, 125.41, 123.02, 53.67.

ESI-HRMS calc. for [C₁₁H₇ClN₂O₄ + H]⁺ m/z 267.0167, found m/z 267.0172 [M + H]⁺.

Methyl ([1,1'-biphenyl]-4-ylsulfonyl)-D-phenylalaninate (YJh129)



4-Biphenyl sulfonyl chloride (456.96 mg, 1.81 mmol) was added to D-phenylalanine methyl ester hydrochloride (300 mg, 1.39 mmol) and triethylamine (578.43 μ L, 4.17 mmol) and dichloromethane (20 mL). The mixture was stirred at room temperature overnight. The reaction was quenched by sodium bicarbonate saturated solution and extracted 3 times with ethyl acetate. The collected organic phase was washed by brine and dried over anhydrous Na_2SO_4 . The solvent was evaporated via reduced pressure. The resulting residue was purified via dichloromethane and methanol silica gel chromatograph (100% dichloromethane). The final product was obtained as white solid.

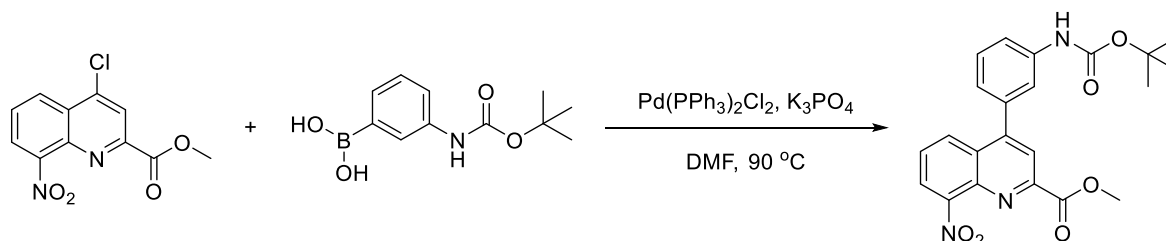
Yield: 304.58 mg (55.37%).

^1H NMR (500 MHz, Chloroform-*d*) δ 7.86 – 7.77 (m, 2H), 7.67 – 7.62 (m, 2H), 7.62 – 7.57 (m, 2H), 7.51 – 7.45 (m, 2H), 7.42 (dq, J = 8.5, 3.1, 2.7, 1.6 Hz, 1H), 7.29 – 7.20 (m, 3H), 7.12 – 7.06 (m, 2H), 5.20 (d, J = 9.1 Hz, 1H), 4.30 – 4.21 (m, 1H), 3.50 (s, 3H), 3.12 – 3.01 (m, 2H).

^{13}C NMR (126 MHz, Chloroform-*d*) δ 171.42, 145.79, 139.35, 138.30, 135.09, 129.52, 129.21, 128.74, 128.67, 127.81, 127.70, 127.41, 127.40, 56.88, 52.54, 39.51.

ESI-HRMS calc. for $[\text{C}_{22}\text{H}_{21}\text{NO}_4\text{S} + \text{H}]^+$ m/z 396.1264, found m/z 396.1267 $[\text{M} + \text{H}]^+$.

Methyl 4-(3-((tert-butoxycarbonyl)amino)phenyl)-8-nitroquinoline-2-carboxylate (YJh130)



Bis(triphenylphosphine)palladium(II) dichloride (105.30 mg, 0.15 mmol) was added to a mixture of methyl 4-chloro-8-nitroquinoline-2-carboxylate (**YJh128**) (200 mg, 0.75 mmol), (3-((Tert-butoxycarbonyl)amino)phenyl)boronic acid (**YJh127**) (231.16 mg, 0.975 mmol) and K_2PO_3 (318.44 mg, 1.50 mmol) in DMF (4 mL) under nitrogen and stirred at 90 °C for 14 h. The reaction was quenched by 10 mL brine solution and extracted 3 times with ethyl acetate. The collected organic phase was washed by brine and dried over anhydrous Na_2SO_4 . The solvent was evaporated via reduced pressure. The resulting residue was purified via hexane and ethyl acetate silica gel chromatograph (20% ethyl acetate). The final product was obtained as white (a little yellow) solid.

Yield: 227 mg (71.6%).

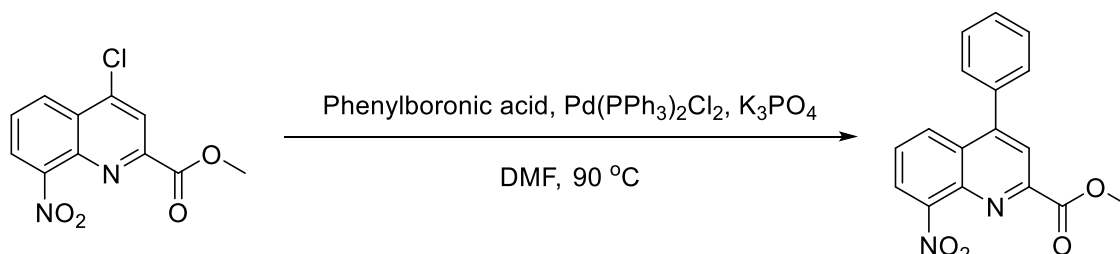
^1H NMR (500 MHz, Chloroform-*d*) δ 8.23 (s, 1H), 8.20 (dd, J = 8.6, 1.3 Hz, 1H), 8.09 (dd, J = 7.4, 1.3 Hz, 1H), 7.67 – 7.62 (m, 2H), 7.49 – 7.45 (m, 2H), 7.13 (ddd, J = 5.4, 2.8, 1.6 Hz, 1H), 6.75 (s, 1H), 4.04 (s, 3H), 1.50 (s, 9H).

^{13}C NMR (126 MHz, Chloroform-*d*) δ 165.43, 152.76, 150.29, 149.51, 149.22, 139.66, 139.29, 137.30, 130.21, 129.69, 128.65, 127.22, 124.44, 124.18, 122.80, 119.52, 119.34, 81.16, 53.41, 28.42.

ESI-HRMS calc. for $[\text{C}_{22}\text{H}_{21}\text{N}_3\text{O}_6 + \text{H}]^+$ m/z 424.1503, found m/z 424.1508 $[\text{M} + \text{H}]^+$.

Purity: 97.42%.

Methyl 8-nitro-4-phenylquinoline-2-carboxylate (YJh131)



Bis(triphenylphosphine)palladium(II) dichloride (105.30 mg, 0.15 mmol) was added to a mixture of methyl 4-chloro-8-nitroquinoline-2-carboxylate (YJh128) (200 mg, 0.75 mmol), phenylboronic acid (118.90 mg, 0.975 mmol) and K₂PO₃ (318.44 mg, 1.50 mmol) in DMF (4 mL) with under nitrogen. The reaction was stirred at 90 °C for 14 h and then quenched by 10 mL brine solution and extracted 3 times with ethyl acetate. The collected organic phase was washed by brine and dried over anhydrous Na₂SO₄. The solvent was evaporated via reduced pressure. The resulting residue was purified via hexane and ethyl acetate silica gel chromatograph (36% ethyl acetate). The final product was obtained as white solid.

Yield: 146.79 mg (63.48%).

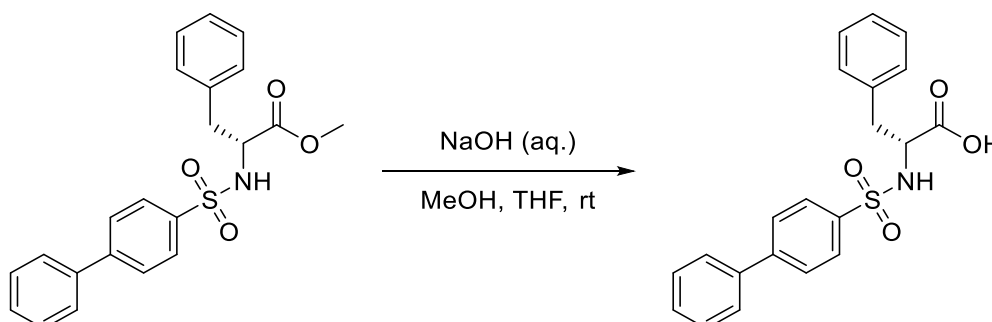
^1H NMR (500 MHz, Chloroform-*d*) δ 8.26 (s, 1H), 8.19 (dd, J = 8.6, 1.3 Hz, 1H), 8.10 (dd, J = 7.4, 1.4 Hz, 1H), 7.67 (dd, J = 8.6, 7.4 Hz, 1H), 7.61 – 7.53 (m, 3H), 7.52 – 7.48 (m, 2H), 4.05 (s, 3H).

^{13}C NMR (126 MHz, Chloroform-*d*) δ 165.49, 150.53, 149.56, 149.29, 139.72, 136.49, 130.12, 129.68, 129.52, 129.12, 128.69, 127.19, 124.39, 122.90, 53.44.

ESI-HRMS calc. for $[\text{C}_{17}\text{H}_{12}\text{N}_2\text{O}_4 + \text{H}]^+$ m/z 309.0870, found m/z 309.0876 $[\text{M} + \text{H}]^+$.

Purity: 100%

([1,1'-biphenyl]-4-ylsulfonyl)-*D*-phenylalanine (YJh132)



Sodium hydroxide solution (NaOH 0.682 g in 5.42 mL H₂O) was added to methyl ([1,1'-biphenyl]-4-ylsulfonyl)-*D*-phenylalaninate (YJh129) (189 mg, 0.478 mmol) in a mixed solvent of methanol (8.2 mL) and tetrahydrofuran (8.2 mL), and stirred at room temperature for 4 h. The pH of the reaction mixture was adjusted to 2 by 2 M HCl solution and extracted 3 times with dichloromethane. The collected organic phase was washed by brine and dried over anhydrous Na₂SO₄. The solvent was evaporated

via reduced pressure. The resulting residue was purified via dichloromethane and methanol silica gel chromatograph (4%-10% methanol). The final product was obtained as white solid after lyophilization. Yield: 164.07 mg (90%).

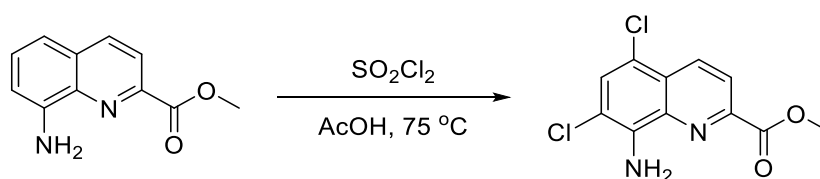
¹H NMR (500 MHz, DMSO-*d*₆) δ 7.72 (s, 4H), 7.70 – 7.67 (m, 2H), 7.52 – 7.47 (m, 2H), 7.44 – 7.41 (m, 1H), 7.17 – 7.10 (m, 5H), 3.66 (t, *J* = 5.9 Hz, 1H), 2.98 (dd, *J* = 14.0, 5.8 Hz, 2H), 2.91 (dd, *J* = 13.5, 6.4 Hz, 1H).

¹³C NMR (126 MHz, DMSO-*d*₆) δ 172.30, 143.55, 139.53, 138.66, 138.08, 129.74, 129.13, 128.40, 127.74, 127.18, 127.11, 127.02, 125.88, 58.31, 38.27.

ESI-HRMS calc. for [C₂₁H₁₉NO₄S + H]⁺ *m/z* 382.1108 (100.0%), 383.1141 (22.7%), [C₂₁H₁₉NO₄S + Na]⁺ *m/z* 404.0927 (100.0%), 405.0961 (22.7%), found *m/z* 382.1109, 383.1139 [M + H]⁺.

Purity: 95.91%

Methyl 8-amino-5,7-dichloroquinoline-2-carboxylate (YJh133)



A solution of sulfuryl chloride (240.53 μL, 2.97 mmol) in glacial acetic acid (2 mL) was added to methyl 8-aminoquinoline-2-carboxylate (**YJh89**) (300 mg, 1.484 mmol) in glacial acetic acid (1.5 mL). The mixture was stirred at 75 °C for 30 min. The reaction was quenched by sodium acetate solution (sodium acetate 7.2 g in 54 mL H₂O) and extracted 3 times with ethyl acetate. The collected organic phase was washed by brine and dried over anhydrous Na₂SO₄. The solvent was evaporated under reduced pressure. The resulting residue was purified via hexane and ethyl acetate silica gel chromatograph (20%-60% ethyl acetate). The final product was obtained as yellow solid.

Yield: 358.61 mg (89.16%).

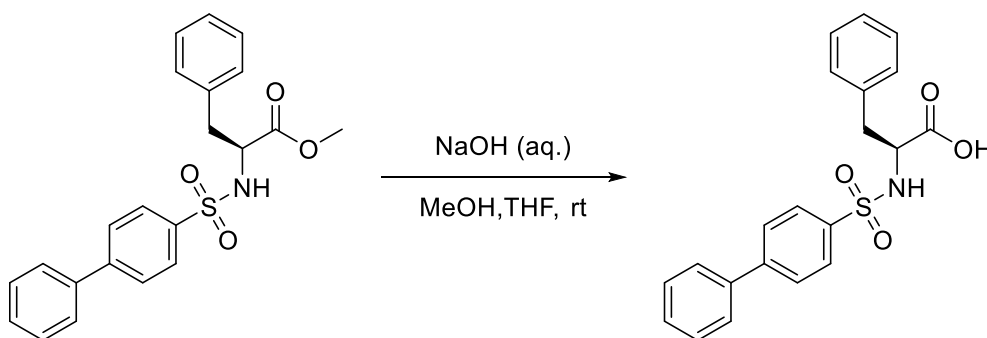
¹H NMR (500 MHz, Chloroform-*d*) δ 8.50 (d, *J* = 8.7 Hz, 1H), 8.18 (d, *J* = 8.7 Hz, 1H), 7.55 (s, 1H), 5.20 (s, 2H), 4.05 (s, 3H).

¹³C NMR (126 MHz, Chloroform-*d*) δ 165.40, 146.05, 141.12, 137.59, 134.41, 129.78, 126.47, 121.98, 117.23, 113.82, 53.07.

ESI-HRMS calc. for [C₁₁H₈Cl₂N₂O₂ + H]⁺ *m/z* 271.0036 (100.0%), 273.0006 (63.9%), found *m/z* 271.0040, 273.0013 [M + H]⁺.

Purity: 98.34%

[(1,1'-biphenyl)-4-ylsulfonyl]-L-phenylalanine (YJh134)



Sodium hydroxide solution (NaOH 0.682 g in 5.42 mL H₂O) was added to methyl ([1,1'-biphenyl]-4-ylsulfonyl)-L-phenylalaninate (**YJh126**) (189 mg, 0.478 mmol) in a mixed solvent of methanol (8.2 mL) and tetrahydrofuran (8.2 mL) and stirred at room temperature for 4 h. The pH of the reaction mixture was adjusted to 2 by 2 M HCl solution and extracted 3 times with dichloromethane. The collected organic phase was washed by brine and dried over anhydrous Na₂SO₄. The solvent was evaporated under reduced pressure. The resulting residue was purified via dichloromethane and methanol silica gel chromatograph (5%-10% methanol). The final product was obtained as white solid after lyophilization.

Yield: 167.3 mg (91.77%).

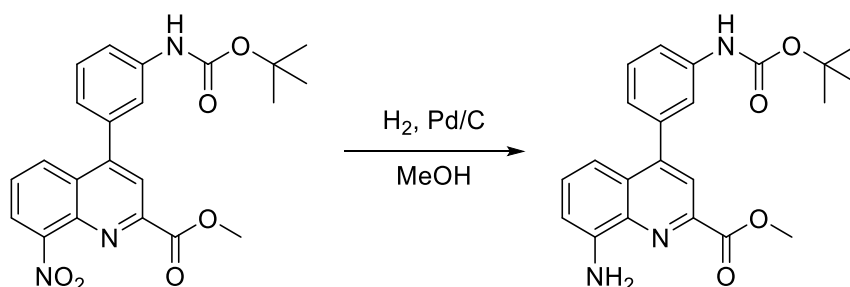
¹H NMR (500 MHz, DMSO-*d*₆) δ 8.09 (s, 1H), 7.73 – 7.66 (m, 4H), 7.66 – 7.62 (m, 2H), 7.53 – 7.48 (m, 2H), 7.45 – 7.41 (m, 1H), 7.19 – 7.11 (m, 5H), 3.85 (dd, *J* = 8.5, 5.6 Hz, 1H), 2.96 (dd, *J* = 13.7, 5.4 Hz, 1H), 2.78 (dd, *J* = 13.7, 8.5 Hz, 1H).

¹³C NMR (126 MHz, DMSO-*d*₆) δ 172.21, 143.50, 139.76, 138.64, 137.10, 129.30, 129.10, 128.38, 128.00, 126.99, 126.93, 126.26, 57.67, 37.89.

ESI-HRMS calc. for [C₂₁H₁₉NO₄S + H]⁺ *m/z* 382.1108 (100.0%), 383.1141 (22.7%), [C₂₁H₁₉NO₄S + Na]⁺ *m/z* 404.0927 (100.0%), 405.0961 (22.7%), found *m/z* 382.1112, 383.1141 [M + H]⁺.

Purity: 99.02%

Methyl 8-amino-4-(3-((tert-butoxycarbonyl)amino)phenyl)quinoline-2-carboxylate (**YJh135**)



The synthesis was according to the general procedure of hydrogenation reduction. Palladium on carbon (20 mg) was added to methyl 4-(3-((tert-butoxycarbonyl)amino)phenyl)-8-nitroquinoline-2-carboxylate (**YJh130**) (200 mg, 0.472 mmol) in methanol (20 mL) under nitrogen. The mixture was stirred at room temperature under hydrogen overnight. The reaction solution was filtered and evaporated in vacuo. The resulting residue was purified via hexane and ethyl acetate silica gel chromatograph (25% ethyl acetate). The final product was obtained as yellow solid.

Yield: 131.2 mg (70.6%).

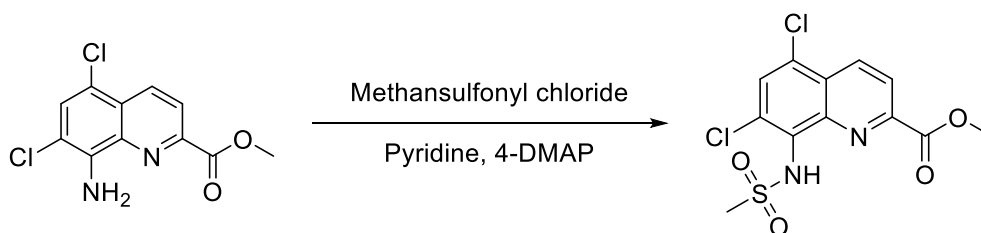
¹H NMR (500 MHz, Chloroform-*d*) δ 8.04 (s, 1H), 7.55 – 7.46 (m, 2H), 7.42 (td, *J* = 7.6, 1.0 Hz, 1H), 7.35 (dd, *J* = 8.4, 7.5 Hz, 1H), 7.22 (dd, *J* = 8.4, 1.2 Hz, 1H), 7.16 (dt, *J* = 7.5, 1.2 Hz, 1H), 6.96 (dd, *J* = 7.5, 1.2 Hz, 1H), 6.70 (s, 1H), 4.03 (s, 3H), 1.51 (s, 9H).

¹³C NMR (126 MHz, Chloroform-*d*) δ 166.15, 152.83, 149.24, 145.30, 144.27, 139.04, 138.83, 138.21, 129.96, 129.26, 128.65, 124.31, 121.58, 119.60, 118.65, 113.88, 110.42, 80.91, 52.85, 28.45.

ESI-HRMS calc. for [C₂₂H₂₃N₃O₄ + H]⁺ *m/z* 394.1761, found *m/z* 394.1767 [M + H]⁺.

Purity: 99.49%

Methyl 5,7-dichloro-8-(methylsulfonamido)quinoline-2-carboxylate (**YJh136**)



Methanesulfonyl chloride (47.96 μL , 0.62 mmol) was added to methyl 8-amino-5,7-dichloroquinoline-2-carboxylate (**YJh133**) (140 mg, 0.516 mmol) and 4-DMAP (6 mg) in pyridine (2 mL). The reaction mixture was stirred at room temperature for 3 d. The reaction was quenched by sodium bicarbonate saturated solution and extracted 3 times with ethyl acetate. The collected organic phase was washed by brine and dried over anhydrous Na_2SO_4 . The solvent was evaporated via reduced pressure. The resulting residue was purified via hexane and ethyl acetate silica gel chromatograph (5%-30% ethyl acetate). The final product was obtained as white solid.

Yield: 47 mg (26.06%).

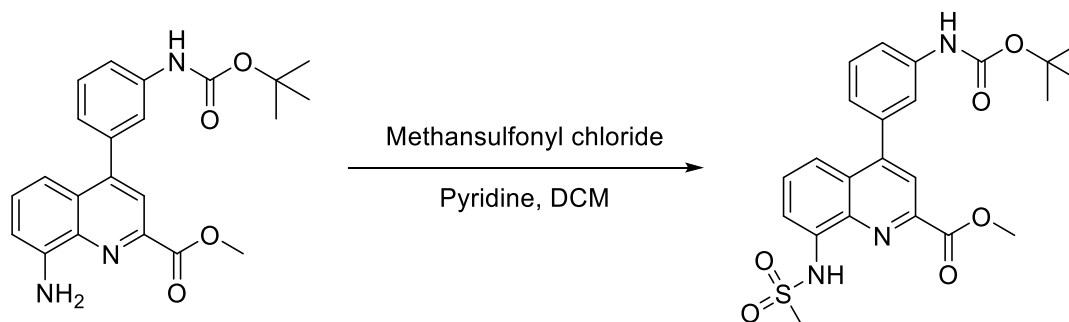
$^1\text{H NMR}$ (500 MHz, Chloroform-*d*) δ 8.68 (dd, $J = 8.8, 0.6$ Hz, 1H), 8.29 (dd, $J = 8.8, 0.6$ Hz, 1H), 7.80 (d, $J = 0.6$ Hz, 1H), 7.36 (s, 1H), 4.06 (s, 3H), 3.72 (s, 3H).

$^{13}\text{C NMR}$ (126 MHz, Chloroform-*d*) δ 164.84, 148.60, 143.17, 135.35, 132.56, 130.46, 129.86, 129.28, 126.96, 122.57, 53.28, 43.20.

ESI-HRMS calc. for $[\text{C}_{12}\text{H}_{10}\text{Cl}_2\text{N}_2\text{O}_4\text{S} + \text{H}]^+$ m/z 348.9811 (100.0%), 350.9782 (63.9%), found m/z 348.9814, 350.9787 $[\text{M} + \text{H}]^+$.

Purity: 96.47%

Methyl 4-(3-((*tert*-butoxycarbonyl)amino)phenyl)-8-(methanesulfonamido)quinoline-2-carboxylate (**YJh137**)



The synthesis was according to the general procedure for sulfonamide coupling. Methanesulfonyl chloride (29.51 μL , 0.38 mmol) was added to methyl 8-amino-4-(3-((*tert*-butoxycarbonyl)amino)phenyl)quinoline-2-carboxylate (**YJh135**) (100 mg, 0.254 mmol) in pyridine/dichloromethane (1 mL/2 mL). The compound was purified via hexane and ethyl acetate silica gel chromatograph (33%-50% ethyl acetate). The final compound was obtained as white solid.

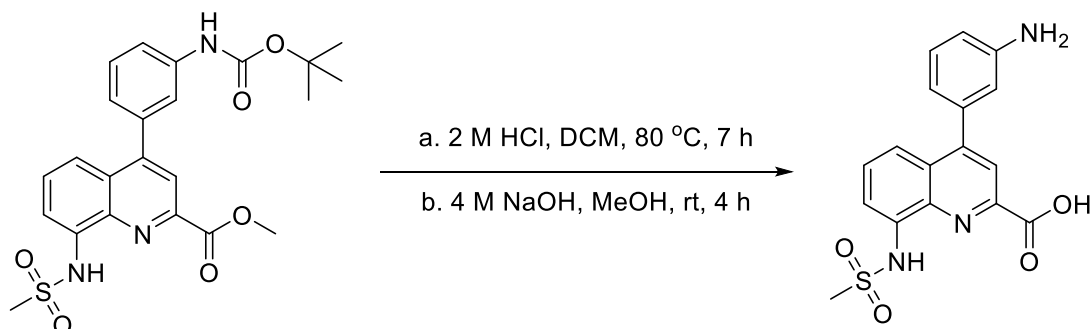
Yield: 42.97 mg (35.85%).

$^1\text{H NMR}$ (500 MHz, Chloroform-*d*) δ 9.11 (s, 1H), 8.16 (s, 1H), 7.92 (dd, $J = 7.7, 1.2$ Hz, 1H), 7.69 (d, $J = 8.4$ Hz, 1H), 7.62 (s, 1H), 7.57 (dd, $J = 8.6, 7.6$ Hz, 1H), 7.48 – 7.41 (m, 2H), 7.15 (td, $J = 4.1, 1.6$ Hz, 1H), 6.73 (s, 1H), 4.05 (s, 3H), 3.09 (s, 3H), 1.51 (s, 9H).

$^{13}\text{C NMR}$ (126 MHz, Chloroform-*d*) δ 165.54, 152.79, 150.38, 146.03, 139.10, 138.62, 138.02, 135.40, 129.49, 129.29, 128.29, 124.15, 122.34, 120.64, 119.50, 119.03, 115.67, 81.07, 53.12, 39.55, 28.44.

ESI-HRMS calc. for $[\text{C}_{23}\text{H}_{25}\text{N}_3\text{O}_6\text{S} + \text{H}]^+$ m/z 472.1537, found m/z 472.1545 $[\text{M} + \text{H}]^+$.

4-(3-Aminophenyl)-8-(methylsulfonamido)quinoline-2-carboxylic acid (YJh138 or YJh144)



2 M HCl solution (1.5 mL) was added to methyl 4-(3-((*tert*-butoxycarbonyl)amino)phenyl)-8-(methylsulfonamido)quinoline-2-carboxylate (**YJh137**) (28 mg, 0.059 mmol) in dichloromethane (2 mL). The mixture was stirred at 80 °C for 7 h and then cooled to room temperature. 4 M NaOH (3 mL) and methanol (3 mL) were added to the reaction mixture and stirred at room temperature for 4 h. The pH of the reaction mixture was adjusted to 2 by 2 M HCl and extracted 3 times with ethyl acetate. The collected organic phase was washed by brine and dried over anhydrous Na₂SO₄. The solvent was evaporated under reduced pressure. The resulting residue was purified via silica gel chromatograph (ethyl acetate, MeOH and H₂O, the ratio was 8 to 1.5 to 1). The final product was obtained as yellow product after lyophilization.

Yield: 18 mg (84.83%).

¹H NMR (700 MHz, DMSO-*d*₆) δ 10.51 (s, 1H), 8.06 (s, 1H), 7.92 (dd, *J* = 7.7, 1.2 Hz, 1H), 7.75 (dd, *J* = 8.5, 7.7 Hz, 1H), 7.67 (dd, *J* = 8.5, 1.2 Hz, 1H), 7.48 (s, 1H), 7.16 (s, 3H), 3.19 (s, 3H).

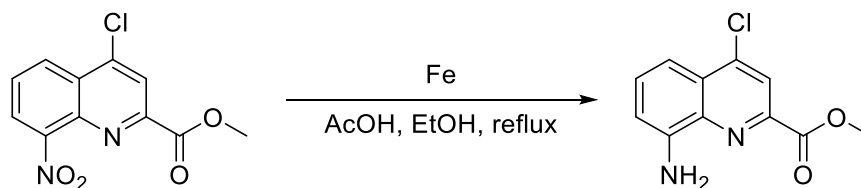
¹³C NMR (176 MHz, DMSO-*d*₆) δ 165.27, 151.12, 149.12, 145.29, 137.78, 137.38, 135.88, 129.41, 129.39, 127.80, 120.26, 119.95, 116.69, 116.40, 114.46, 114.44, 40.01.

ESI-HRMS calc. for [C₁₇H₁₅N₃O₄S + H]⁺ *m/z* 358.0856, found *m/z* 358.08693 [M + H]⁺.

Melting point: ca. 120 °C (< 150 °C)

Purity: 97.76%

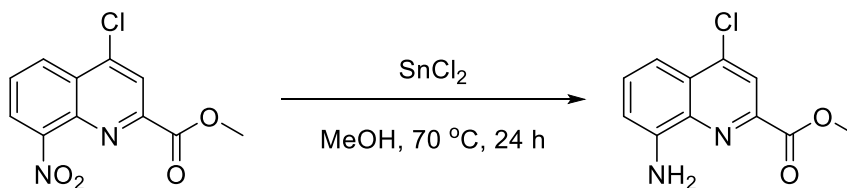
Methyl 8-amino-4-chloroquinoline-2-carboxylate (YJh139 or YJh152) method 1



Iron powder (100.54 mg, 1.8 mmol) and glacial acetic acid (1.5 mL) were added to methyl 4-chloro-8-nitroquinoline-2-carboxylate (**YJh128**) (120 mg, 0.45 mmol) in ethanol (4.5 mL). The reaction mixture was heated to reflux at approximately 65 °C and stirred for 3 h. The reaction was quenched by sodium bicarbonate saturated solution and extracted 3 times with ethyl acetate. The collected organic phase was washed by brine and dried over anhydrous Na₂SO₄. The solvent was evaporated via reduced pressure. The resulting residue was purified via hexane and ethyl acetate silica gel chromatograph (15% ethyl acetate). The final product was obtained as yellow or orange solid.

Yield: 65.31 mg (61.32%).

Methyl 8-amino-4-chloroquinoline-2-carboxylate (YJh139 or YJh152) method 2



The synthesis was according to the general procedure for reduction of aromatic nitro compounds to amines by tin (II) chloride. Tin (II) chloride (1.442 g, 7.61 mmol) and concentrated hydrochloric acid (500 μ L) were added to methyl 4-chloro-8-nitroquinoline-2-carboxylate (**YJh128**) (338 mg, 1.268 mmol) in MeOH (10 mL). The resulting residue was purified via hexane and ethyl acetate silica gel chromatograph (15% ethyl acetate). The final product was obtained as yellow solid.

Yield: 145.89 mg (48.63%).

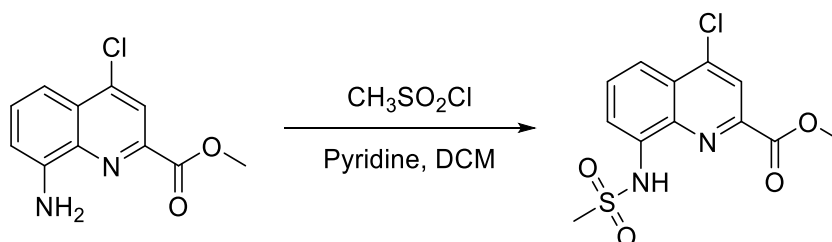
¹H NMR (500 MHz, Chloroform-*d*) δ 8.19 (s, 1H), 7.53 – 7.46 (m, 2H), 7.02 – 6.96 (m, 1H), 5.02 (s, 2H), 4.03 (s, 3H).

¹³C NMR (126 MHz, Chloroform-*d*) δ 165.24, 145.61, 144.22, 143.51, 138.12, 131.08, 128.39, 121.59, 111.81, 111.27, 53.05.

ESI-HRMS calc. for [C₁₁H₉ClN₂O₂ + H]⁺ *m/z* 237.0425, found *m/z* 237.0431 [M + H]⁺.

Purity: 99.58%

Methyl 4-chloro-8-(methylsulfonamido)quinoline-2-carboxylate (**YJh140**)



The synthesis was according to the general procedure for sulfonamide coupling. Methanesulfonyl chloride (58.87 μ L, 0.761 mmol) was added to methyl 8-amino-4-chloroquinoline-2-carboxylate (**YJh139**) (120 mg, 0.507 mmol) in pyridine/dichloromethane (1 mL/2 mL). The compound was purified via hexane and ethyl acetate silica gel chromatograph (33% ethyl acetate). The final product was obtained as white solid.

Yield: 83.79 mg (52.5%).

¹H NMR (500 MHz, Chloroform-*d*) δ 8.96 (s, 1H), 8.30 (s, 1H), 7.97 (dd, *J* = 7.6, 1.2 Hz, 1H), 7.96 (dd, *J* = 8.6, 1.2 Hz, 1H), 7.72 (dd, *J* = 8.6, 7.7 Hz, 1H), 4.06 (s, 3H), 3.10 (s, 3H).

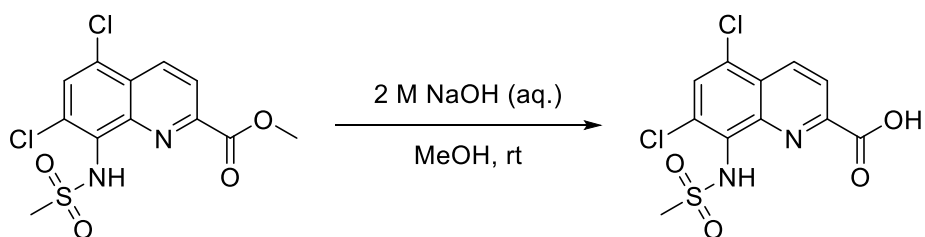
¹³C NMR (126 MHz, Chloroform-*d*) δ 164.61, 146.25, 144.58, 138.61, 135.68, 130.43, 128.05, 122.46, 118.57, 116.23, 53.36, 39.76.

ESI-MS calc. for [C₁₂H₁₁ClN₂O₄S + H]⁺ *m/z* 315.0201 (100.0%), 317.0171 (32.0%), found *m/z* 315.0, 317.0 [M + H]⁺.

ESI-HRMS calc. for [C₁₂H₁₁ClN₂O₄S + H]⁺ *m/z* 315.0201 (100.0%), 317.0171 (32.0%), found *m/z* 315.0210 (100%), 317.0178 (37.06%) [M + H]⁺.

Purity: 99.15%

5,7-Dichloro-8-(methylsulfonamido)quinoline-2-carboxylic acid (**YJh141**)



The synthesis was according to general procedure for hydrolysis of methyl esters catalyzed by hydroxide ion. 2 M NaOH solution (10 mL) was added to methyl 5,7-dichloro-8-(methylsulfonamido)quinoline-2-carboxylate (**YJh136**) (30 mg, 0.086 mmol) in methanol (3 mL). The reaction mixture was stirred at room temperature for 3 h. The compound was purified via silica gel chromatograph (ethyl acetate, MeOH and H₂O, the ratio was 8 to 1.5 to 1). The final product was obtained as white solid.

Yield: 24 mg (83.33%).

¹H NMR (500 MHz, DMSO-*d*₆) δ 8.75 (d, *J* = 8.6 Hz, 1H), 8.31 (d, *J* = 8.7 Hz, 1H), 8.17 (s, 1H), 3.45 (s, 3H).

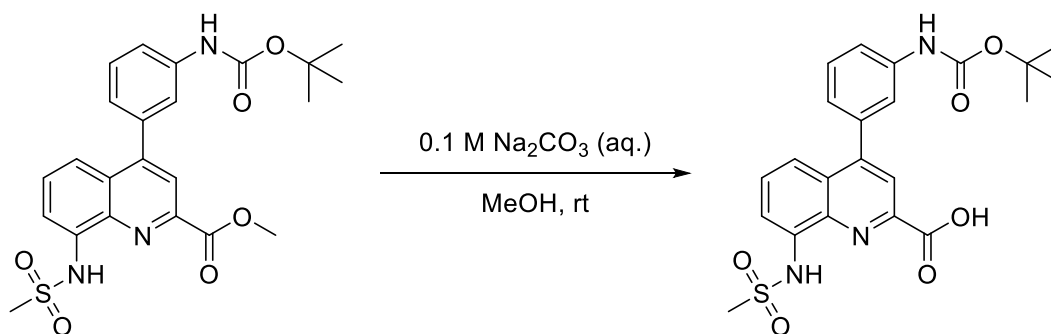
¹³C NMR (126 MHz, DMSO-*d*₆) δ 165.58, 149.91, 144.17, 135.11, 133.46, 132.55, 129.42, 128.93, 126.09, 122.45, 42.68.

ESI-HRMS calc. for [C₁₁H₈Cl₂N₂O₄S + H]⁺ *m/z* 334.9655 (100.0%), 336.9625 (63.9%), 338.9596 (10.2%), found *m/z* 334.9671 (100%), 336.96405 (63.9%), 338.96049 (8%) [M + H]⁺.

Melting point: 178.1 °C

Purity: 98.4%

4-(3-((*tert*-Butoxycarbonyl)amino)phenyl)-8-(methylsulfonamido)quinoline-2-carboxylic acid (**YJh142**)



0.1 M Na₂CO₃ solution (3 mL) was added to methyl 4-(3-((*tert*-butoxycarbonyl)amino)phenyl)-8-(methylsulfonamido)quinoline-2-carboxylate (**YJh137**) (23.4 mg, 0.050 mmol) in methanol (3 mL). The reaction mixture was stirred at room temperature for 5 h. The pH of the reaction mixture was adjusted to 2 by 2 M HCl solution and extracted 3 times with ethyl acetate. The collected organic phase was washed by brine and dried over anhydrous Na₂SO₄. The solvent was evaporated under reduced pressure. The resulting residue was purified via silica gel chromatograph (ethyl acetate, MeOH and H₂O, the ratio was 8 to 1.5 to 1). The final product was obtained as yellow solid after lyophilization.

Yield: 21.3 mg (93.82%).

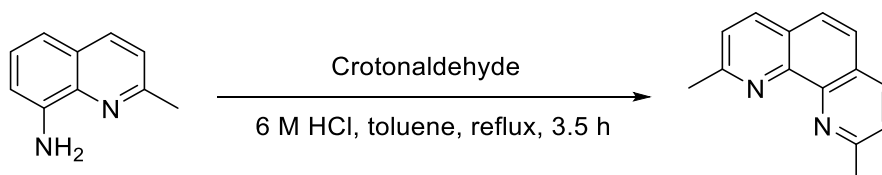
¹H NMR (500 MHz, DMSO-*d*₆) δ 13.54 (s, 1H), 10.51 (s, 1H), 9.59 (s, 1H), 8.05 (s, 1H), 7.91 (dd, *J* = 7.7, 1.2 Hz, 1H), 7.76 – 7.71 (m, 2H), 7.65 (dd, *J* = 8.6, 1.2 Hz, 1H), 7.61 (d, *J* = 8.2 Hz, 1H), 7.48 (t, *J* = 7.9 Hz, 1H), 7.17 (ddd, *J* = 7.6, 1.8, 1.0 Hz, 1H), 3.18 (s, 3H), 1.47 (s, 9H).

¹³C NMR (126 MHz, DMSO-*d*₆) δ 165.17, 152.83, 150.23, 145.15, 140.02, 137.79, 137.13, 136.00, 129.78, 129.30, 127.72, 123.04, 120.52, 119.70, 118.74, 118.64, 116.59, 79.36, 39.65, 28.09.

ESI-HRMS calc. for [C₂₂H₂₃N₃O₆S + H]⁺ m/z 458.1380, found m/z 458.1385 [M + H]⁺.

Purity: 95.09%

2,9-Dimethyl-1,10-phenanthroline (YJh145)



The synthesis was according to general procedure for synthesis of 2-methyl quinoline analogues. Crotonaldehyde (209.48 μL, 2.53 mmol) in toluene (2.7 mL) was added dropwise to 2-methylquinolin-8-amine (**YJh80**) (200 mg, 1.26 mmol) in 6 M HCl (17.7 mL). The reaction was stirred at 75 °C for 3.5 h. The compound was purified via hexane and ethyl acetate silica gel chromatograph (60%-100% ethyl acetate). The final product was obtained as white solid.

Yield: 92.15 mg (35%).

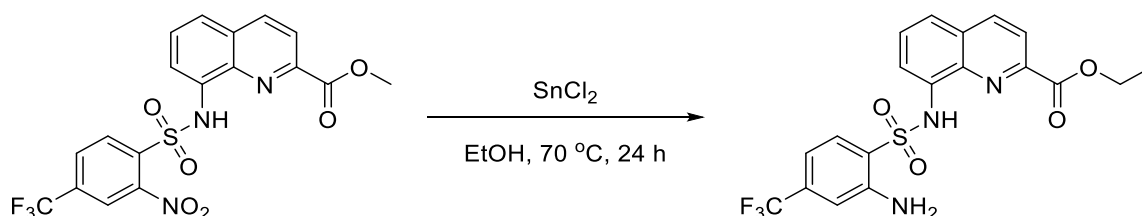
¹H NMR (500 MHz, Chloroform-*d*) δ 8.10 (d, *J* = 8.2 Hz, 2H), 7.67 (s, 2H), 7.47 (d, *J* = 8.2 Hz, 2H), 2.93 (s, 6H).

¹³C NMR (126 MHz, Chloroform-*d*) δ 159.46, 145.38, 136.35, 126.89, 125.52, 123.58, 25.99.

ESI-HRMS calc. for [C₁₄H₁₂N₂ + H]⁺ m/z 209.1073, found m/z 209.1079 [M + H]⁺.

Purity: 98.04%

Ethyl 8-((2-amino-4-(trifluoromethyl)phenyl)sulfonamido)quinoline-2-carboxylate (YJh147)



Tin (II) chloride (124.93 mg, 0.659 mmol) was added to methyl 8-((2-nitro-4-(trifluoromethyl)phenyl)sulfonamido)quinoline-2-carboxylate (**YJh109**) (50 mg, 0.110 mmol) in ethanol (4 mL). The reaction mixture was stirred at 75 °C for 24 h. The solvent was evaporated to a little amount via reduced pressure. The reaction was quenched by sodium bicarbonate saturated solution and extracted 5 times with ethyl acetate. The collected organic phase was washed by brine and dried over anhydrous Na₂SO₄. The solvent was evaporated via reduced pressure. The resulting residue was purified via hexane and ethyl acetate silica gel chromatograph (30% ethyl acetate). The final product was obtained as white solid.

Yield: 37.8 mg (78.34%).

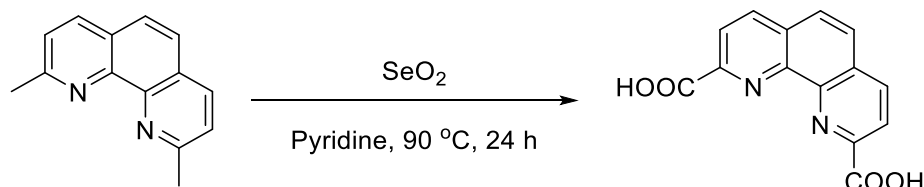
¹H NMR (500 MHz, Chloroform-*d* and Methanol-*d*₄ 3 to 1) δ 8.24 (d, *J* = 8.5 Hz, 1H), 8.10 (d, *J* = 8.4 Hz, 1H), 7.85 (d, *J* = 8.4 Hz, 1H), 7.76 (dd, *J* = 5.6, 3.3 Hz, 1H), 7.63 – 7.45 (m, 2H), 6.82 (s, 1H), 6.73 (d, *J* = 8.4 Hz, 1H), 4.52 (q, *J* = 7.1 Hz, 2H), 1.46 (t, *J* = 7.1 Hz, 3H).

¹³C NMR (126 MHz, Chloroform-*d* and Methanol-*d*₄ 3 to 1) δ 165.93, 146.63, 145.92, 138.85, 138.11, 135.47, 134.82 (q, *J* = 32.9 Hz), 131.48, 130.12, 129.58, 123.57 (q, *J* = 272.6 Hz), 122.08, 121.92, 121.79, 116.14, 114.40 (q, *J* = 4.5 Hz), 111.86 (q, *J* = 4.0 Hz), 63.00, 14.30.

¹⁹F NMR (565 MHz, Chloroform-*d*) δ -60.29.

ESI-HRMS calc. for [C₁₉H₁₆F₃N₃O₄S + H]⁺ *m/z* 440.0886, found *m/z* 440.0890 [M + H]⁺.

1,10-Phenanthroline-2,9-dicarboxylic acid (YJh149)



The synthesis was according to the general procedure for oxidation of 2-methyl quinoline analogues by selenium dioxide. Selenium dioxide (35.96 mg, 0.324 mmol) was added to 2,9-dimethyl-1,10-phenanthroline (**YJh145**) (45 mg, 0.216 mmol) in pyridine (4 mL). The final product was obtained as white solid after lyophilization.

Yield: 29 mg (50%).

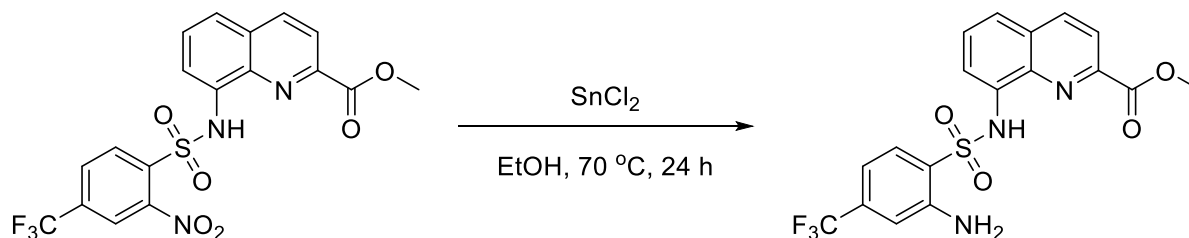
¹H NMR (500 MHz, DMSO-*d*₆) δ 8.73 (d, *J* = 8.2 Hz, 2H), 8.41 (d, *J* = 8.1 Hz, 2H), 8.21 (s, 2H).

¹³C NMR (126 MHz, DMSO-*d*₆) δ 166.24, 148.29, 144.74, 138.12, 130.46, 128.38, 123.39.

ESI-HRMS calc. for [C₁₄H₈N₂O₄ + H]⁺ *m/z* 269.0557, [C₁₄H₈N₂O₄ + 2H]²⁺ *m/z* 135.0315, found *m/z* 269.0583 [M + H]⁺, 135.0262 [M + 2H]²⁺.

Purity: 98.12%

Methyl 8-((2-amino-4-(trifluoromethyl)phenyl)sulfonamido)quinoline-2-carboxylate (YJh150)



The synthesis was according to the general procedure for reduction of aromatic nitro compounds to amines by tin (II) chloride. Tin (II) chloride (599.64 mg, 3.162 mmol) and concentrated hydrochloric acid (50 μL) were added to methyl 8-((2-nitro-4-(trifluoromethyl)phenyl)sulfonamido)quinoline-2-carboxylate (**YJh109**) (240 mg, 0.527 mmol) in methanol (20 mL). The reaction mixture was stirred at 75 °C for 24 h. The resulting residue was purified via hexane and ethyl acetate silica gel chromatograph (30% ethyl acetate). The final product was obtained as white solid.

Yield: 195.59 mg (87.24%).

¹H NMR (500 MHz, DMSO-*d*₆) δ 10.31 (s, 1H), 8.54 (d, *J* = 8.6 Hz, 1H), 8.12 (d, *J* = 8.5 Hz, 1H), 7.87 (d, *J* = 8.4 Hz, 1H), 7.75 (dd, *J* = 8.3, 1.3 Hz, 1H), 7.62 (dd, *J* = 8.2, 7.7 Hz, 1H), 7.52 (dd, *J* = 7.7, 1.3 Hz, 1H), 7.10 (d, *J* = 1.8 Hz, 1H), 6.81 (dd, *J* = 8.5, 1.7 Hz, 1H), 6.66 (s, 2H), 4.00 (s, 3H).

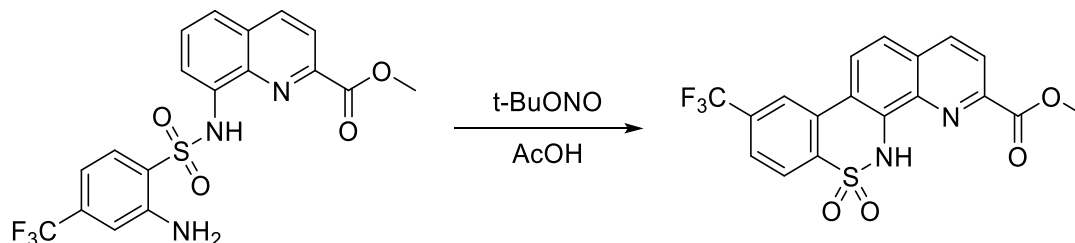
¹³C NMR (176 MHz, DMSO-*d*₆) δ 165.13, 146.99, 146.56, 138.50, 138.23, 134.40, 133.91 (q, *J* = 31.7 Hz), 131.17, 129.33, 128.91, 123.48 (q, *J* = 274.2 Hz), 122.98, 121.71, 121.55, 117.64, 113.70 (d, *J* = 3.7 Hz), 110.33 (d, *J* = 3.6 Hz), 52.92.

¹⁹F NMR (471 MHz, DMSO-*d*₆) δ -62.43.

ESI-HRMS calc. for $[C_{18}H_{14}F_3N_3O_4S + H]^+$ m/z 426.0730, found m/z 426.0734 $[M + H]^+$.

Purity: 99%.

Methyl 9-(trifluoromethyl)-5H-benzo[5,6][1,2]thiazino[4,3-h]quinoline-3-carboxylate 6,6-dioxide (YJh151)



tert-Butyl nitrite (36.95 μ L, 0.311 mmol) was added to methyl 8-((2-amino-4-(trifluoromethyl)phenyl)sulfonamido)quinoline-2-carboxylate (**YJh150**) (88.1 mg, 0.207 mmol) in acetic acid (0.7 ml). The reaction mixture was stirred at room temperature for 10 min then quenched by water. The mixture was extracted 5 times with ethyl acetate. The collected organic phase was washed by brine and dried over anhydrous Na_2SO_4 . The solvent was evaporated via reduced pressure. The resulting residue was purified via hexane and ethyl acetate (30%, 60% ethyl acetate) as well as dichloromethane and methanol (7% methanol) silica gel chromatograph. The product was obtained as yellow or orange solid.

Yield: 58.7 mg (69.41%).

1H NMR (600 MHz, $DMSO-d_6$) δ 8.53 – 8.40 (m, 3H), 8.12 (dd, $J = 8.7, 3.8$ Hz, 1H), 8.03 (dd, $J = 8.3, 3.6$ Hz, 1H), 7.86 – 7.81 (m, 1H), 7.39 (d, $J = 6.1$ Hz, 1H), 4.00 (s, 3H).

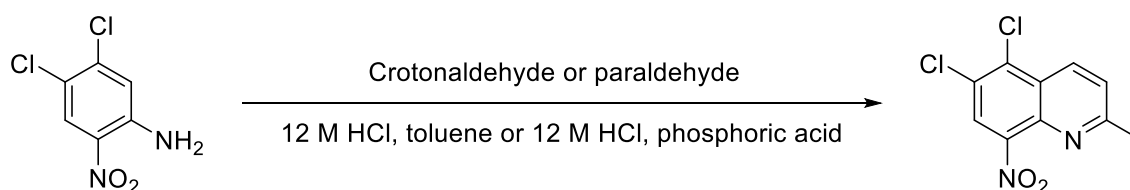
^{13}C NMR (176 MHz, $DMSO-d_6$) δ 165.99, 147.00, 141.08, 138.19, 136.74, 133.42, 132.05, 130.57, 129.90, 125.94, 125.23, 124.21 (q, $J = 272.7$ Hz), 123.52, 123.15, 122.64, 120.66, 119.25, 53.34.

^{19}F NMR (565 MHz, $DMSO-d_6$) δ -60.96.

ESI-HRMS calc. for $[C_{18}H_{11}F_3N_2O_4S + H]^+$ m/z 409.0464, found m/z 409.0467 $[M + H]^+$.

Purity: 97.3%.

5,6-Dichloro-2-methyl-8-nitroquinoline (YJh153 or YJh155)



The synthesis was according to the general procedure for synthesis of 2-methyl quinoline analogues.

Method 1 Crotonaldehyde (1.60 mL, 19.32 mmol) was diluted in toluene (14 mL) and added dropwise to a solution of 4,5-dichloro-2-nitroaniline (2 g, 9.66 mmol) in 12 M HCl (40 mL). The reaction was stirred at 75 $^{\circ}C$ for 48 h. The resulting residue was purified via hexane and ethyl acetate silica gel chromatograph (5% ethyl acetate). The final product was obtained as yellow solid.

Yield: 670.83 mg (27.01%).

Method 2 Paraldehyde (1.93 mL, 14.49 mmol) was added dropwise to a solution of 4,5-dichloro-2-nitroaniline (2 g, 9.66 mmol) in 12 M HCl (40 mL). The reaction was stirred at 0 $^{\circ}C$ for 15 min and 75 $^{\circ}C$ for 24 h. Without removing the organic phase, other purification steps were similar as method 1. The final product was obtained as yellow solid.

Yield: 496.73 mg (20%).

Method 3 Crotonaldehyde (600.32 μ L, 7.246 mmol) was gradually added to a solution of 4,5-dichloro-2-nitroaniline (1 g, 4.83 mmol) in 12 M HCl (5.85 mL) and phosphoric acid (2.20 mL) at 80 °C for 30 min. Then the reaction was allowed to be heated to 95 °C and stirred for 3 h. Without removing the organic phase, other purification steps were similar as method 1. The final product was obtained as yellow solid.

Yield: 167.15 mg (13.46%).

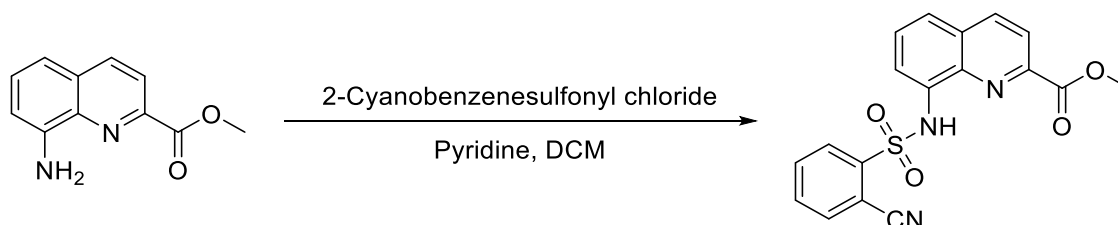
¹H NMR (500 MHz, Chloroform-*d*) δ 8.49 (d, *J* = 8.8 Hz, 1H), 8.02 (s, 1H), 7.53 (d, *J* = 8.8 Hz, 1H), 2.77 (s, 3H).

¹³C NMR (126 MHz, Chloroform-*d*) δ 162.84, 146.74, 138.21, 133.17, 133.07, 128.84, 126.47, 125.36, 124.50, 25.63.

ESI-HRMS calc. for [C₁₀H₆Cl₂N₂O₂ + H]⁺ *m/z* 256.9879 (100.0%), 258.9850 (63.9%), found *m/z* 256.9886, 258.9858 [M + H]⁺.

Purity: 98.28%

Methyl 8-((2-cyanophenyl)sulfonamido)quinoline-2-carboxylate (YJh154)



The synthesis was according to the general procedure for sulfonamide coupling. 2-Cyanobenzenesulfonyl chloride (224.35 mg, 1.113 mmol) was added to methyl 8-aminoquinoline-2-carboxylate (**YJh89**) (150 mg, 0.742 mmol) in pyridine/dichloromethane (1.5 mL/3 mL). The compound was purified via hexane and ethyl acetate silica gel chromatograph (60% ethyl acetate). The final product was obtained as white (a little yellow) solid.

Yield: 207.01 mg (75.96%).

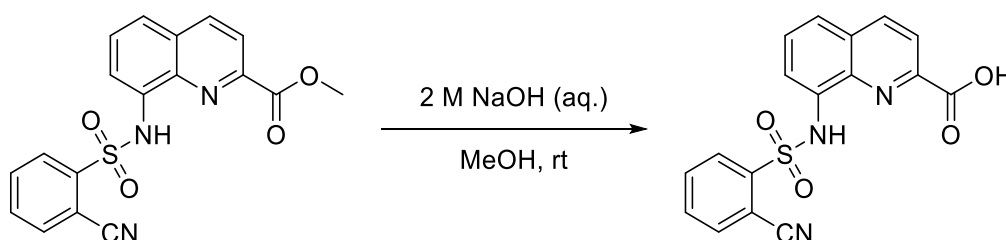
¹H NMR (500 MHz, Chloroform-*d*) δ 9.59 (s, 1H), 8.24 (d, *J* = 8.5 Hz, 1H), 8.16 (d, *J* = 8.5 Hz, 1H), 8.13 (dd, *J* = 7.9, 1.3 Hz, 1H), 7.87 (dd, *J* = 6.8, 2.1 Hz, 1H), 7.71 (dd, *J* = 7.6, 1.4 Hz, 1H), 7.61 (td, *J* = 7.7, 1.5 Hz, 1H), 7.59 – 7.52 (m, 3H), 4.07 (s, 3H).

¹³C NMR (126 MHz, Chloroform-*d*) δ 165.55, 146.92, 141.62, 138.10, 137.55, 135.37, 133.75, 133.06, 132.71, 130.10, 129.44, 129.05, 122.91, 122.09, 116.91, 115.64, 111.02, 53.07.

ESI-HRMS calc. for [C₁₈H₁₃N₃O₄S + H]⁺ *m/z* 368.0700, found *m/z* 368.0702 [M + H]⁺.

Purity: 99.4%

8-((2-Cyanophenyl)sulfonamido)quinoline-2-carboxylic acid (YJh156)



The synthesis was according to the general procedure for hydrolysis of methyl esters catalyzed by hydroxide ion. 2 M NaOH (20 mL) was added to methyl 8-((2-cyanophenyl)sulfonamido)quinoline-2-carboxylate (**YJh154**) (120 mg, 0.327 mmol) in methanol (20 mL). The reaction mixture was stirred at room temperature for 3 h. The compound was purified via silica gel chromatograph (ethyl acetate, MeOH and H₂O, the ratio was 8 to 1.5 to 1). The final product was obtained as white (a little yellow) solid after lyophilization.

Yield: 47.90 mg (41.5%).

¹H NMR (500 MHz, DMSO-*d*₆) δ 13.29 (s, 1H), 11.31 (s, 1H), 8.59 (d, *J* = 8.5 Hz, 1H), 8.17 (d, *J* = 8.5 Hz, 1H), 8.13 (dd, *J* = 8.0, 1.2 Hz, 1H), 7.96 (dd, *J* = 7.7, 1.3 Hz, 1H), 7.85 – 7.76 (m, 3H), 7.73 (td, *J* = 7.6, 1.2 Hz, 1H), 7.67 (t, *J* = 7.9 Hz, 1H).

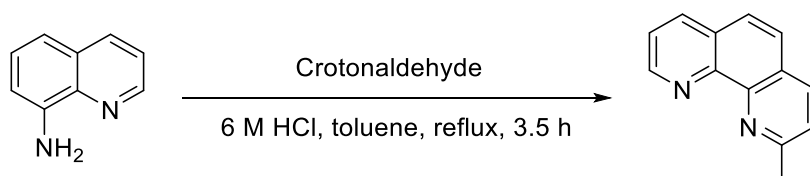
¹³C NMR (126 MHz, DMSO-*d*₆) δ 164.97, 145.74, 140.60, 138.87, 137.31, 135.98, 133.88, 133.83, 133.68, 129.52, 129.46, 129.24, 123.52, 120.70, 118.52, 115.49, 109.22.

ESI-HRMS calc. for [C₁₇H₁₁N₃O₄S + H]⁺ *m/z* 354.0543, found *m/z* 354.05598 [M + H]⁺.

Melting point: 205 °C

Purity: 98.99%

2-Methyl-1,10-phenanthroline (**YJh157**)

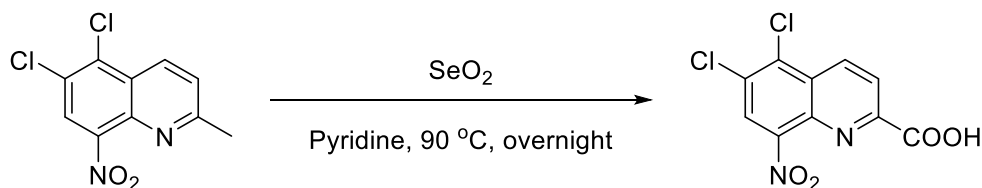


The synthesis was according to the general procedure for synthesis of 2-methyl quinoline analogues. Crotonaldehyde (919.46 μL, 11.098 mmol) was diluted in toluene (12 mL) and added dropwise to a solution of 5-Aminoquinoline (800 mg, 5.55 mmol) in 6 M HCl (78 mL). The reaction was stirred at 75 °C for 3.5 h. The resulting residue was purified via silica gel chromatograph.

ESI-MS calc. for [C₁₃H₁₀N₂ + H]⁺ *m/z* 195.0917, found *m/z* 195.0 [M + H]⁺.

Purity: 97.47%

5,6-Dichloro-8-nitroquinoline-2-carboxylic acid (**YJh158**)



The synthesis was according to the general procedure for oxidation of 2-methyl quinoline analogues by selenium dioxide. Selenium dioxide (253.15 mg, 2.28 mmol) was added to 5,6-dichloro-2-methyl-8-nitroquinoline (**YJh155** or **YJh153**) (391 mg, 1.52 mmol) in pyridine (8 mL). The reaction mixture was stirred at 100 °C for 16 h. The compound was purified via silica gel chromatograph (ethyl acetate, MeOH and H₂O, the ratio was 8 to 1.5 to 1). The final product was obtained as yellow solid.

Yield: 355.8mg (81.5%).

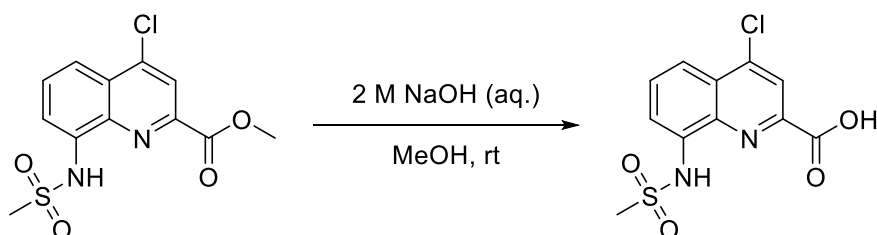
¹H NMR (500 MHz, DMSO-*d*₆) δ 13.97 (s, 1H), 8.88 (d, *J* = 8.9 Hz, 1H), 8.83 (s, 1H), 8.39 (d, *J* = 8.9 Hz, 1H).

¹³C NMR (126 MHz, DMSO-*d*₆) δ 165.01, 151.19, 147.20, 137.02, 135.29, 131.85, 130.85, 127.94, 125.25, 124.47.

ESI-HRMS calc. for [C₁₀H₄Cl₂N₂O₄ + H]⁺ m/z 286.9621 (100.0%), 288.9591 (63.9%), found m/z , 286.9624 (100%), 288.9596 (68.19%) [M + H]⁺.

ESI-MS calc. for [C₁₀H₄Cl₂N₂O₄ + H]⁺ m/z 286.9621 (100.0%), 288.9591 (63.9%), [C₁₀H₄Cl₂N₂O₄ + Na]⁺ m/z 308.9440 (100.0%), 310.9411 (63.9%), found m/z 286.8, 288.8 [M + H]⁺, 308.8, 310.8 [M + Na]⁺.

4-Chloro-8-(methylsulfonamido)quinoline-2-carboxylic acid (YJh159)



The synthesis was according to the general procedure for hydrolysis of methyl esters catalyzed by hydroxide ion. 2 M NaOH solution (4 mL) was added to methyl 4-chloro-8-(methylsulfonamido)quinoline-2-carboxylate (**YJh140**) (50 mg, 0.159 mmol) in methanol (4 mL). The reaction mixture was stirred at room temperature for 3 h. The compound was purified via silica gel chromatograph (ethyl acetate, MeOH and H₂O, the ratio was 8 to 1.5 to 1). The final product was obtained as white (a little green) solid after lyophilization.

Yield: 40 mg (83.73%).

¹H NMR (500 MHz, DMSO-*d*₆) δ 13.51 (s, 1H), 10.43 (s, 1H), 8.27 (s, 1H), 7.96 – 7.90 (m, 2H), 7.86 (t, *J* = 8.2 Hz, 1H), 3.20 (s, 3H).

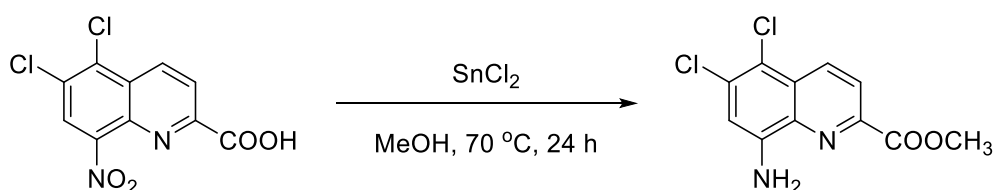
¹³C NMR (126 MHz, DMSO-*d*₆) δ 164.36, 145.95, 143.46, 137.79, 136.21, 130.94, 127.21, 120.97, 117.62, 117.35, 39.78.

ESI-HRMS calc. for [C₁₁H₉ClN₂O₄S + H]⁺ m/z 301.0044 (100.0%), 303.0015 (32.0%), found m/z 301.00636 (100%), 303.00282 (29.5%) [M + H]⁺.

Melting point: 241.6 °C

Purity: 99.42%

Methyl 8-amino-5, 6-dichloroquinoline-2-carboxylate (YJh160)



The synthesis was according to the general procedure for reduction of aromatic nitro compounds to amines by tin (II) chloride. Tin (II) chloride (1.19 g, 6.27 mmol) and concentrated hydrochloric acid (500 μL) were added to 5, 6-dichloro-8-nitroquinoline-2-carboxylic acid (**YJh158**) (300 mg, 1.05 mmol) in methanol (100 mL). The reaction mixture was stirred at 65 °C for 24 h. The product was purified via hexane and ethyl acetate silica gel chromatograph (20% ethyl acetate). The final product was obtained as yellow solid.

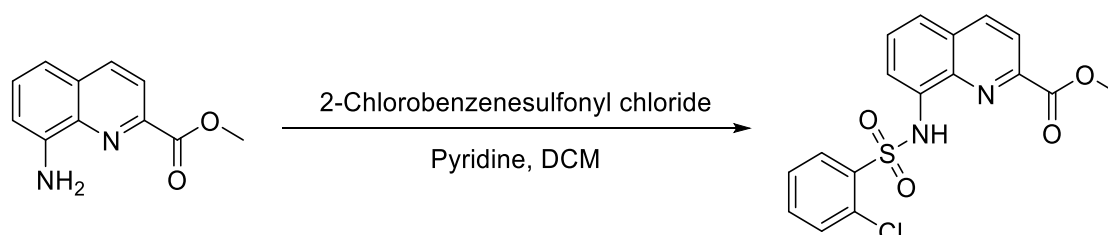
Yield: 229.07 mg (80.9%).

¹H NMR (500 MHz, DMSO-*d*₆) δ 8.53 (dd, *J* = 8.8, 1.3 Hz, 1H), 8.20 (dd, *J* = 8.8, 1.0 Hz, 1H), 7.04 (s, 1H), 6.53 (s, 2H), 3.96 (s, 3H).

¹³C NMR (126 MHz, DMSO-*d*₆) δ 164.66, 146.55, 144.53, 135.64, 133.98, 133.49, 127.81, 123.05, 111.17, 108.88, 52.71.

ESI-HRMS calc. for [C₁₁H₈Cl₂N₂O₂ + H]⁺ *m/z* 271.0036 (100.0%), 273.0006 (63.9%), found *m/z* 271.0037, 273.0009 [M + H]⁺.

Methyl 8-((2-chlorophenyl)sulfonamido)quinoline-2-carboxylate (YJh162)



The synthesis was according to the general procedure for sulfonamide coupling. 2-Chlorobenzenesulfonyl chloride (156.57 mg, 0.742 mmol) was added to methyl 8-aminoquinoline-2-carboxylate (YJh89) (100 mg, 0.495 mmol) in pyridine/dichloromethane (1.5 mL/3 mL). The compound was purified via hexane and ethyl acetate silica gel chromatograph (50% ethyl acetate). The final product was obtained as white solid.

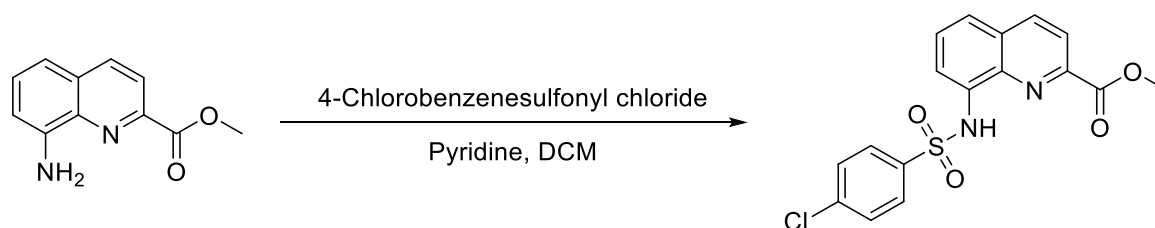
Yield: 165.61 mg (88.87%).

¹H NMR (500 MHz, Chloroform-*d*) δ 9.83 (s, 1H), 8.25 – 8.15 (m, 3H), 7.85 – 7.79 (m, 1H), 7.52 – 7.43 (m, 2H), 7.41 – 7.32 (m, 3H), 4.07 (s, 3H).

¹³C NMR (126 MHz, Chloroform-*d*) δ 165.62, 146.47, 137.79, 137.42, 136.49, 134.43, 134.15, 132.29, 131.98, 129.51, 129.16, 126.90, 122.05, 121.89, 114.90, 53.07.

ESI-HRMS calc. for [C₁₇H₁₃ClN₂O₄S + H]⁺ *m/z* 377.0357 (100.0%), 379.0328 (32.0%), found *m/z* 377.0362, 379.0336 [M + H]⁺.

Methyl 8-((4-chlorophenyl)sulfonamido)quinoline-2-carboxylate (YJh163)



The synthesis was according to the general procedure for sulfonamide coupling. 4-Chlorobenzenesulfonyl chloride (156.57 mg, 0.742 mmol) was added to methyl 8-aminoquinoline-2-carboxylate (YJh89) (100 mg, 0.495 mmol) in pyridine/dichloromethane (1.5 mL/3 mL). The compound was purified via hexane and ethyl acetate silica gel chromatograph (40% ethyl acetate). The final product was obtained as white (a little yellow) solid.

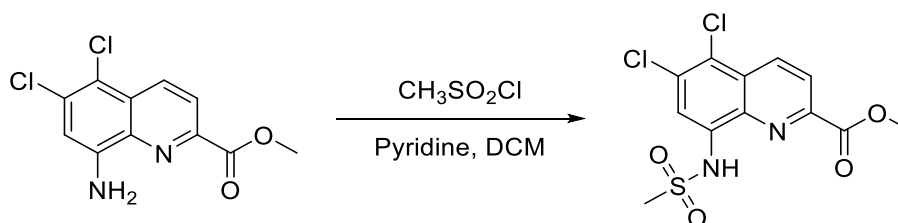
Yield: 130 mg (69.76%).

¹H NMR (500 MHz, Chloroform-*d*) δ 9.31 (s, 1H), 8.24 (d, *J* = 8.5 Hz, 1H), 8.16 (d, *J* = 8.5 Hz, 1H), 7.91 – 7.82 (m, 3H), 7.57 – 7.50 (m, 2H), 7.37 – 7.27 (m, 2H), 4.07 (s, 3H).

¹³C NMR (126 MHz, Chloroform-*d*) δ 165.43, 146.57, 139.68, 138.08, 137.86, 137.68, 134.48, 129.53, 129.36, 129.18, 128.88, 122.41, 122.08, 116.43, 53.15.

ESI-HRMS calc. for $[C_{17}H_{13}ClN_2O_4S + H]^+$ m/z 377.0357 (100.0%), 379.0328 (32.0%), found m/z 377.0362, 379.0337 $[M + H]^+$.

Methyl 5,6-dichloro-8-(methylsulfonamido)quinoline-2-carboxylate (YJh166)



The synthesis was according to the general procedure for sulfonamide coupling. Methanesulfonyl chloride (52.67 μ L, 0.68 mmol) was added to methyl 8-amino-5,6-dichloroquinoline-2-carboxylate (**YJh160**) (123 mg, 0.45 mmol) in pyridine/dichloromethane (6 mL/12 mL). The reaction mixture was stirred at room temperature for 48 h. The compound was purified via hexane and ethyl acetate silica gel chromatograph (50% ethyl acetate). The final product was obtained as white solid.

Yield: 115 mg (72.8%).

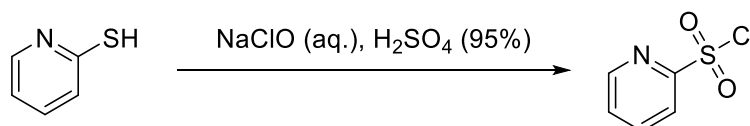
1H NMR (500 MHz, Chloroform-*d*) δ 8.97 (s, 1H), 8.70 (d, J = 8.8 Hz, 1H), 8.34 (d, J = 8.8 Hz, 1H), 7.99 (s, 1H), 4.07 (s, 3H), 3.15 (s, 3H).

^{13}C NMR (126 MHz, Chloroform-*d*) δ 164.83, 146.94, 136.95, 135.27, 134.76, 134.25, 128.48, 123.81, 123.08, 116.41, 53.35, 40.09.

ESI-HRMS calc. for $[C_{12}H_{10}Cl_2N_2O_4S + H]^+$ m/z 348.9811 (100.0%), 350.9782 (63.9%), found m/z 348.9815 (100%), 350.9787 (67.45%) $[M + H]^+$.

ESI-MS calc. for $[C_{12}H_{10}Cl_2N_2O_4S + H]^+$ m/z 348.9811 (100.0%), 350.9782 (63.9%), 352.9752 (10.2%), $[C_{12}H_{10}Cl_2N_2O_4S + Na]^+$ m/z 370.9631 (100.0%), 372.9601 (63.9%), 371.9664 (13.0%), 374.9572 (10.2%), found m/z 349.0, 350.8, 352.8 $[M + H]^+$, 370.8, 372.8, 374.8 $[M + Na]^+$.

Pyridine-2-sulfonyl chloride (YJh167)

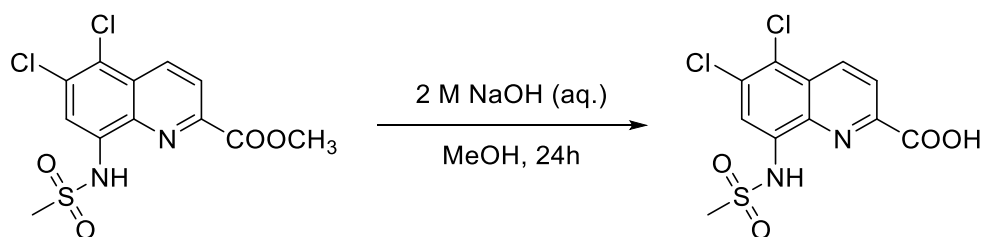


Sodium hypochlorite solution (chlorine content 5%) (32 mL) was added dropwise to 2-mercaptopyridine (500 mg, 4.498 mmol) in sulfuric acid (12.5 mL) at -15 $^{\circ}C$ for 1.5 h. The mixture was further stirred at -15 $^{\circ}C$ for 30 min and 0 $^{\circ}C$ for 30 min then quenched by 25 mL water. The aqueous was extracted 3 times with dichloromethane. The collected organic phase was washed by brine and dried over anhydrous Na_2SO_4 . The solvent was evaporated via reduced pressure. The colorless oil residue was used directly for next step without further purification.

Yield: > 60%

ESI-MS calc. for $[C_5H_4ClNO_2S + H]^+$ m/z 177.9724 (100.0%), 179.9695 (32.0%), $[C_5H_4ClNO_2S + Na]^+$ m/z 199.9543 (100.0%), 201.9514 (32.0%), found m/z 178.0, 179.8 $[M + H]^+$.

5,6-Dichloro-8-(methylsulfonamido)quinoline-2-carboxylic acid (YJh169)



The synthesis was according to the general procedure for hydrolysis of methyl esters catalyzed by hydroxide ion. 2 M NaOH (20 mL) was added to methyl 5,6-dichloro-8-(methylsulfonamido)quinoline-2-carboxylate (**YJh166**) (80 mg, 0.229 mmol) in methanol (20 mL). The reaction mixture was stirred at room temperature for 24 h. The compound was purified via silica gel chromatograph (ethyl acetate, MeOH and H₂O, the ratio was 8 to 1.5 to 1). The final product was obtained as white (a little green) solid after lyophilization.

Yield: 56.41 mg (73.46%).

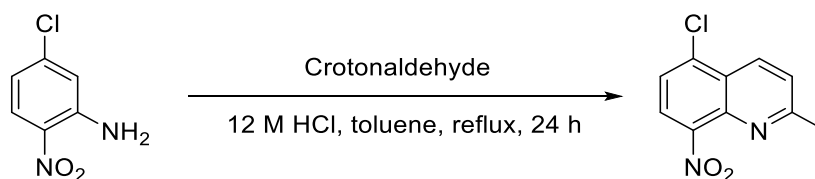
¹H NMR (500 MHz, MeOD, CD₃Cl) δ 8.77 (d, *J* = 8.8 Hz, 1H), 8.38 (d, *J* = 8.8 Hz, 1H), 8.05 (s, 1H), 3.12 (s, 3H).

ESI-HRMS calc. for [C₁₁H₈Cl₂N₂O₄S + H]⁺ *m/z* 334.9655 (100.0%), 336.9625 (63.9%), 338.9596 (10.2%), found *m/z* 334.96663 (100%), 336.96362 (65.1%), 338.9601 (10.7%) [M + H]⁺.

Melting point: 261.7 °C

Purity: 98.11%

5-Chloro-2-methyl-8-nitroquinoline (**YJh170**)



The synthesis was according to the general procedure for synthesis of 2-methyl quinoline analogues. Crotonaldehyde (960.18 μL, 11.59 mmol) was diluted in toluene (17.02 mL) and added dropwise to 5-chloro-2-nitroaniline (1000 mg, 5.79 mmol) in 6 M HCl (111.57 mL). The reaction was stirred at 75 °C for 24 h. The compound was purified via hexane and dichloromethane silica gel chromatograph (50% dichloromethane). The product was obtained as brown solid.

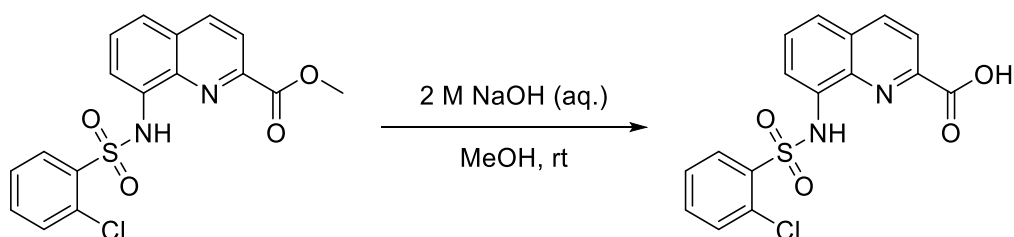
Yield: 290.01 mg (22.48%).

¹H NMR (500 MHz, Chloroform-*d*) δ 8.48 (d, *J* = 8.8 Hz, 1H), 7.88 (d, *J* = 8.1 Hz, 1H), 7.60 (d, *J* = 8.2 Hz, 1H), 7.50 (d, *J* = 8.7 Hz, 1H), 2.78 (s, 3H).

¹³C NMR (126 MHz, Chloroform-*d*) δ 163.02, 147.05, 139.88, 135.30, 133.02, 125.55, 124.68, 124.48, 123.22, 25.74.

ESI-HRMS calc. for [C₁₀H₇ClN₂O₂ + H]⁺ *m/z* 223.0269 (100.0%), 225.0239 (32.0%), found *m/z* 223.0278 (100%), 225.0249 (31.25%) [M + H]⁺.

8-((2-Chlorophenyl)sulfonamido)quinoline-2-carboxylic acid (**YJh171**)



The synthesis was according to the general procedure for hydrolysis of methyl esters catalyzed by hydroxide ion. 2 M NaOH (10 mL) was added to methyl 8-((2-chlorophenyl)sulfonamido)quinoline-2-carboxylate (**YJh162**) (140 mg, 0.372 mmol) in methanol (6 mL). The reaction mixture was stirred at room temperature for 3 h. The compound was purified via silica gel chromatograph (ethyl acetate, MeOH and H₂O, the ratio was 8 to 1.5 to 1). The final product was obtained as white (a little yellow) solid after lyophilization.

Yield: 124.71 mg (92.52%).

¹H NMR (500 MHz, DMSO-*d*₆) δ 13.52 (s, 1H), 11.28 (s, 1H), 8.56 (d, *J* = 8.5 Hz, 1H), 8.25 – 8.15 (m, 2H), 7.70 (dd, *J* = 8.1, 1.3 Hz, 1H), 7.65 (dd, *J* = 7.7, 1.2 Hz, 1H), 7.61 – 7.56 (m, 2H), 7.53 (dd, *J* = 8.7, 7.2 Hz, 2H).

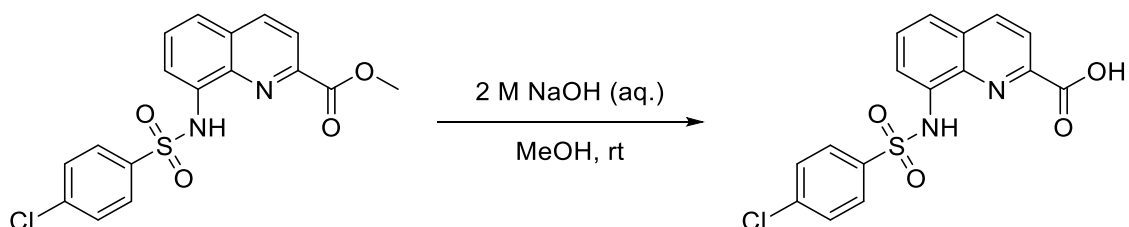
¹³C NMR (126 MHz, DMSO-*d*₆) δ 165.12, 145.67, 138.76, 136.57, 135.84, 134.99, 134.25, 132.08, 131.87, 130.84, 129.53, 129.16, 127.76, 122.23, 120.89, 115.28.

ESI-HRMS calc. for [C₁₆H₁₁ClN₂O₄S + H]⁺ *m/z* 363.0201 (100.0%), 365.0171 (32.0%), found *m/z* 363.02189 (100%), 365.01884 (31.7%) [M + H]⁺.

Melting point: 232.7 °C

Purity: 99.56%

8-((4-Chlorophenyl)sulfonamido)quinoline-2-carboxylic acid (**YJh172**)



The synthesis was according to the general procedure for hydrolysis of methyl esters catalyzed by hydroxide ion. 2 M NaOH (8 mL) was added to methyl 8-((4-chlorophenyl)sulfonamido)quinoline-2-carboxylate (**YJh163**) (100 mg, 0.265 mmol) in methanol (6 mL). The reaction mixture was stirred at room temperature for 3 h. The compound was purified via silica gel chromatograph (ethyl acetate, MeOH and H₂O, the ratio was 8 to 1.5 to 1). The final product was obtained as white (a little yellow) solid after lyophilization.

Yield: 82.3 mg (85.48%).

¹H NMR (500 MHz, DMSO-*d*₆) δ 13.33 (s, 1H), 10.92 (s, 1H), 8.56 (d, *J* = 8.5 Hz, 1H), 8.17 (d, *J* = 8.4 Hz, 1H), 7.90 – 7.83 (m, 3H), 7.75 (dd, *J* = 8.3, 1.2 Hz, 1H), 7.66 (t, *J* = 8.0 Hz, 1H), 7.58 – 7.51 (m, 2H).

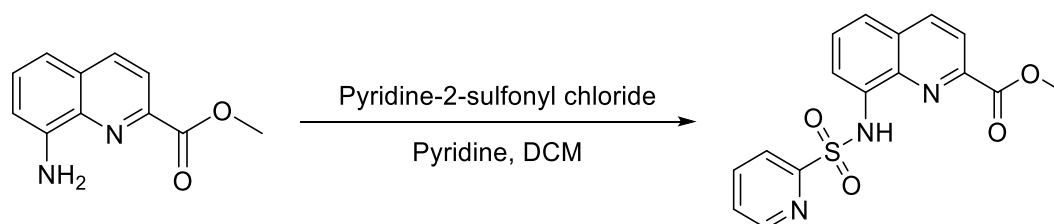
¹³C NMR (126 MHz, DMSO-*d*₆) δ 164.98, 145.66, 138.85, 138.16, 137.97, 137.04, 134.37, 129.51, 129.46, 129.27, 128.67, 122.84, 120.71, 117.32.

ESI-HRMS calc. for [C₁₆H₁₁ClN₂O₄S + H]⁺ *m/z* 363.0201 (100.0%), 365.0171 (32.0%), found *m/z* 363.02154 (100%), 365.01837 (29.3%) [M + H]⁺.

Melting point: 205.8 °C

Purity: 97.59%

Methyl 8-(pyridine-2-sulfonamido)quinoline-2-carboxylate (YJh173 or YJh168)



The synthesis was according to the general procedure for sulfonamide coupling. Pyridine-2-sulfonyl chloride (**YJh167**) (88.54 μL , 0.742 mmol) was added to methyl 8-aminoquinoline-2-carboxylate (**YJh89**) (100 mg, 0.495 mmol) in pyridine/dichloromethane (1.5 mL/3 mL). The compound was purified via hexane and ethyl acetate silica gel chromatograph (80% ethyl acetate). The final product was obtained as yellow solid.

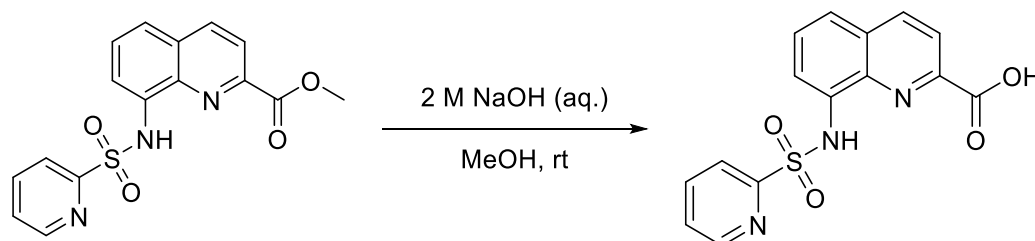
Yield: 105.4 mg (62.07%).

^1H NMR (500 MHz, Chloroform-*d*) δ 9.46 (s, 1H), 8.58 (ddd, $J = 4.7, 1.8, 0.9$ Hz, 1H), 8.23 (d, $J = 8.5$ Hz, 1H), 8.16 (d, $J = 8.5$ Hz, 1H), 8.13 (dt, $J = 7.8, 1.0$ Hz, 1H), 7.96 (dd, $J = 7.2, 1.7$ Hz, 1H), 7.86 (td, $J = 7.8, 1.7$ Hz, 1H), 7.55 – 7.47 (m, 2H), 7.40 (ddd, $J = 7.7, 4.7, 1.1$ Hz, 1H), 4.05 (s, 3H).

^{13}C NMR (126 MHz, Chloroform-*d*) δ 165.61, 156.74, 150.37, 146.46, 138.01, 137.68, 137.50, 134.78, 129.43, 129.19, 127.16, 122.84, 121.98, 121.74, 115.25, 53.07.

ESI-HRMS calc. for $[\text{C}_{16}\text{H}_{13}\text{N}_3\text{O}_4\text{S} + \text{H}]^+$ m/z 344.0700, found m/z 344.0703 $[\text{M} + \text{H}]^+$.

8-(Pyridine-2-sulfonamido)quinoline-2-carboxylic acid (YJh174)



The synthesis was according to the general procedure for hydrolysis of methyl esters catalyzed by hydroxide ion. 2 M NaOH solution (2 mL) was added to methyl 8-(pyridine-2-sulfonamido)quinoline-2-carboxylate (**YJh173**) (80 mg, 0.0.233 mmol) in methanol (2 mL). The compound was purified via silica gel chromatograph (ethyl acetate, MeOH and H_2O , the ratio was 8 to 1.5 to 1). The final product was obtained as white solid.

Yield: 65.6 mg (85.49%).

^1H NMR (500 MHz, DMSO-*d*₆) δ 13.45 (s, 1H), 11.15 (s, 1H), 8.60 (dt, $J = 4.5, 1.3$ Hz, 1H), 8.57 (d, $J = 8.5$ Hz, 1H), 8.18 (t, $J = 8.5$ Hz, 2H), 8.08 (td, $J = 7.8, 1.7$ Hz, 1H), 7.84 (dd, $J = 7.7, 1.2$ Hz, 1H), 7.72 (dd, $J = 8.3, 1.3$ Hz, 1H), 7.66 – 7.59 (m, 2H).

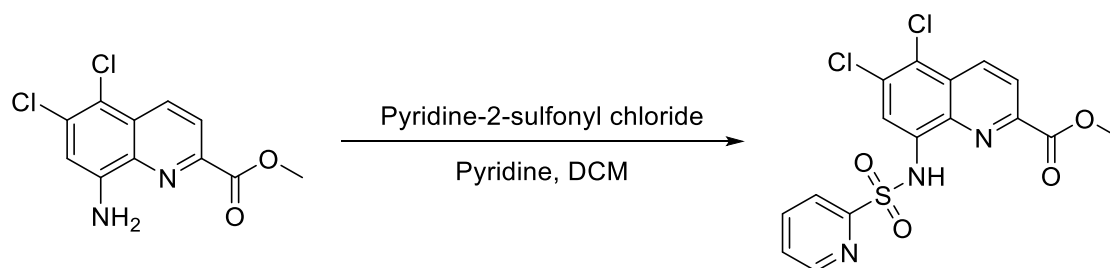
^{13}C NMR (126 MHz, DMSO-*d*₆) δ 165.06, 156.05, 150.27, 145.43, 138.93, 138.77, 136.61, 134.91, 129.48, 129.24, 127.76, 122.65, 122.06, 120.68, 115.90.

ESI-HRMS calc. for $[\text{C}_{15}\text{H}_{11}\text{N}_3\text{O}_4\text{S} + \text{H}]^+$ m/z 330.0543, found m/z 330.05588 $[\text{M} + \text{H}]^+$.

Melting point: 240.2 °C

Purity: 100%

Methyl 5,6-dichloro-8-(pyridine-2-sulfonamido)quinoline-2-carboxylate (YJh178)



The synthesis was according to the general procedure for sulfonamide coupling. Pyridine-2-sulfonyl chloride (YJh167) (54.15 μ L, 0.454 mmol) was added to methyl 8-amino-5,6-dichloroquinoline-2-carboxylate (YJh160) (82 mg, 0.302 mmol) in pyridine (2.5 mL). The mixture was stirred at room temperature for 48 h. The compound was purified via hexane and ethyl acetate silica gel chromatograph (60% ethyl acetate). The final product was obtained as yellow solid.

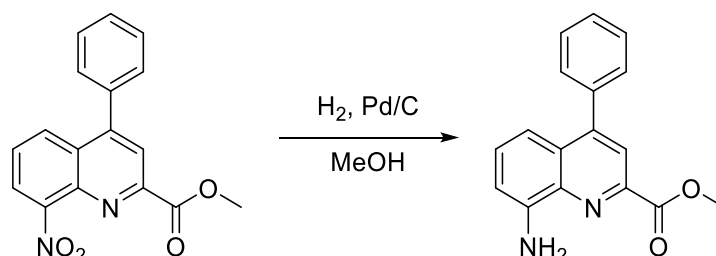
Yield: 12 mg (9.62%).

$^1\text{H NMR}$ (500 MHz, Chloroform-*d*) δ 9.67 (s, 1H), 8.63 (d, J = 8.8 Hz, 1H), 8.60 (ddd, J = 4.7, 1.7, 0.9 Hz, 1H), 8.28 (d, J = 8.7 Hz, 1H), 8.15 (dt, J = 7.9, 1.0 Hz, 1H), 8.11 (s, 1H), 7.91 (td, J = 7.8, 1.7 Hz, 1H), 7.45 (ddd, J = 7.7, 4.7, 1.1 Hz, 1H), 4.07 (s, 3H).

$^{13}\text{C NMR}$ (126 MHz, Chloroform-*d*) δ 165.02, 156.54, 150.49, 146.63, 138.26, 137.00, 135.05, 134.67, 134.07, 128.19, 127.48, 123.48, 122.79, 122.73, 116.91, 53.36.

ESI-HRMS calc. for $[\text{C}_{16}\text{H}_{11}\text{Cl}_2\text{N}_3\text{O}_4\text{S} + \text{H}]^+$ m/z 411.9920 (100.0%), 413.9891 (63.9%), found m/z 411.9921, 413.9893 $[\text{M} + \text{H}]^+$.

Methyl 8-amino-4-phenylquinoline-2-carboxylate (YJh179)



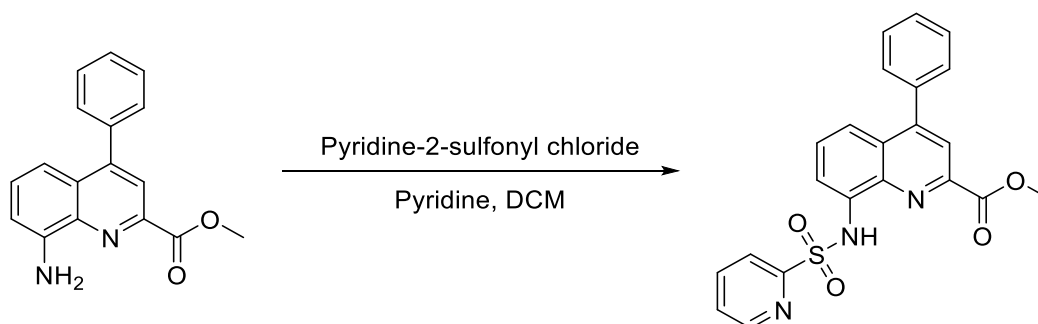
The synthesis was according to the general procedure for hydrogenation reduction. Palladium on carbon (26 mg) was added to methyl 8-nitro-4-phenylquinoline-2-carboxylate (YJh131) (260 mg, 0.843 mmol) in methanol (30 mL) under nitrogen. The mixture was stirred at room temperature under hydrogen overnight. The reaction solution was filtered and evaporated via reduced pressure. The resulting residue was purified via hexane and ethyl acetate silica gel chromatograph (15% ethyl acetate). Yield: 180 mg (76.69%).

$^1\text{H NMR}$ (500 MHz, Chloroform-*d*) δ 8.07 (s, 1H), 7.55 – 7.47 (m, 5H), 7.37 (dd, J = 8.5, 7.5 Hz, 1H), 7.23 (dd, J = 8.4, 1.2 Hz, 1H), 6.97 (dd, J = 7.5, 1.2 Hz, 1H), 4.04 (s, 3H).

$^{13}\text{C NMR}$ (126 MHz, Chloroform-*d*) δ 166.21, 149.56, 145.41, 144.32, 138.24, 129.93, 129.64, 128.72, 128.64, 128.61, 121.67, 113.80, 110.34, 52.86.

ESI-HRMS calc. for $[\text{C}_{17}\text{H}_{14}\text{N}_2\text{O}_2 + \text{H}]^+$ m/z 279.1128, found m/z 279.1133 $[\text{M} + \text{H}]^+$.

Methyl 4-phenyl-8-(pyridine-2-sulfonamido)quinoline-2-carboxylate (YJh181)



The synthesis was according to the general procedure for sulfonamide coupling. Pyridine-2-sulfonyl chloride (**YJh167**) (61.11 μL , 0.512 mmol) was added to methyl 8-amino-4-phenylquinoline-2-carboxylate (**YJh179**) (95 mg, 0.341 mmol) in pyridine/dichloromethane (1.5 mL/3 mL). The mixture was stirred at room temperature for 24 h. The compound was purified via hexane and ethyl acetate silica gel chromatograph (87% ethyl acetate). The final product was obtained as yellow solid.

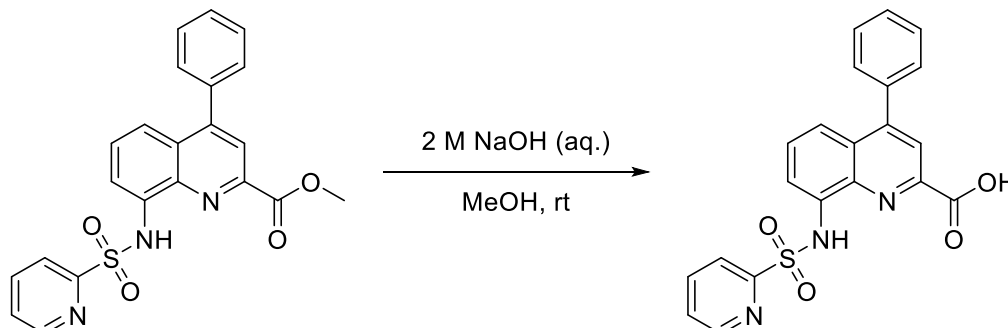
Yield: 121 mg (84.51%).

$^1\text{H NMR}$ (500 MHz, Chloroform-*d*) δ 9.72 – 9.51 (m, 1H), 8.61 (ddd, $J = 4.7, 1.7, 0.9$ Hz, 1H), 8.16 (dt, $J = 8.0, 1.0$ Hz, 1H), 8.12 (s, 1H), 7.98 (dd, $J = 7.7, 1.2$ Hz, 1H), 7.88 (td, $J = 7.8, 1.8$ Hz, 1H), 7.58 (dd, $J = 8.6, 1.2$ Hz, 1H), 7.55 – 7.44 (m, 6H), 7.42 (ddd, $J = 7.7, 4.7, 1.1$ Hz, 1H), 4.07 (s, 3H).

$^{13}\text{C NMR}$ (126 MHz, Chloroform-*d*) δ 165.71, 156.84, 150.40, 150.35, 145.86, 138.29, 138.03, 137.25, 135.04, 129.60, 129.06, 129.04, 128.84, 128.02, 127.15, 122.87, 122.23, 120.05, 115.08, 53.11.

ESI-HRMS calc. for $[\text{C}_{22}\text{H}_{17}\text{N}_3\text{O}_4\text{S} + \text{H}]^+$ m/z 420.1013, found m/z 420.1016 $[\text{M} + \text{H}]^+$.

4-Phenyl-8-(pyridine-2-sulfonamido)quinoline-2-carboxylic acid (**YJh182**)



The synthesis was according to the general procedure for hydrolysis of methyl esters catalyzed by hydroxide ion. 2 M NaOH solution (3 mL) was added to methyl 4-phenyl-8-(pyridine-2-sulfonamido)quinoline-2-carboxylate (**YJh181**) (87.8 mg, 0.209 mmol) in methanol (3 mL). The reaction mixture was stirred at room temperature for 3 h. The pH of the reaction mixture was adjusted to 2 by 2 M HCl solution and extracted 3 times with ethyl acetate. The collected organic phase was washed by brine and dried over anhydrous Na_2SO_4 . The solvent was evaporated via reduced pressure. The resulting residue was purified via silica gel chromatograph (ethyl acetate, MeOH and H_2O , the ratio was 8 to 1.5 to 1). The final product was obtained as yellow solid after lyophilization.

Yield: 76.37 mg (90%).

$^1\text{H NMR}$ (500 MHz, DMSO-*d*₆) δ 13.59 (s, 1H), 11.21 (s, 1H), 8.63 (ddd, $J = 4.8, 1.8, 0.9$ Hz, 1H), 8.20 (dt, $J = 8.0, 1.0$ Hz, 1H), 8.10 (td, $J = 7.8, 1.7$ Hz, 1H), 8.03 (s, 1H), 7.88 (dd, $J = 7.8, 1.2$ Hz, 1H), 7.65 – 7.51 (m, 8H).

¹³C NMR (126 MHz, DMSO-*d*₆) δ 165.10, 156.06, 150.34, 150.13, 145.02, 138.98, 137.26, 136.63, 135.41, 129.52, 129.41, 129.09, 128.86, 127.82, 127.61, 122.73, 120.69, 119.53, 115.68.

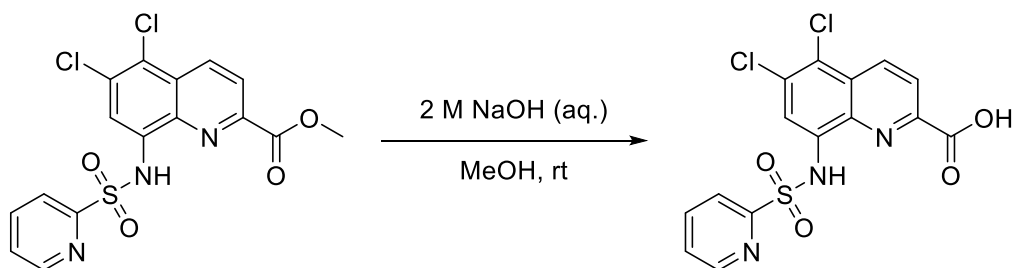
¹³C NMR (126 MHz, DMSO-*d*₆) δ 165.10, 156.06, 150.34, 150.13, 145.02, 138.98, 137.26, 136.63, 135.41, 129.52, 129.41, 129.09, 128.86, 127.82, 127.61, 122.73, 120.69, 119.53, 115.68.

ESI-HRMS calc. for [C₂₁H₁₅N₃O₄S + H]⁺ m/z 406.0856, found m/z 406.0857 [M + H]⁺.

Melting point: 213.8 °C

Purity: 96.98%

5,6-Dichloro-8-(pyridine-2-sulfonamido)quinoline-2-carboxylic acid (YJh183)



The synthesis was according to the general procedure for hydrolysis of methyl esters catalyzed by hydroxide ion. 2 M NaOH (2 mL) was added to methyl 5,6-dichloro-8-(pyridine-2-sulfonamido)quinoline-2-carboxylate (**YJh178**) (12 mg, 0.029 mmol) in methanol (2 mL). The reaction mixture was stirred at room temperature for 3 h. The compound was purified via silica gel chromatograph (ethyl acetate, MeOH and H₂O, the ratio was 8 to 1.5 to 1). The final product was obtained as yellow solid after lyophilization.

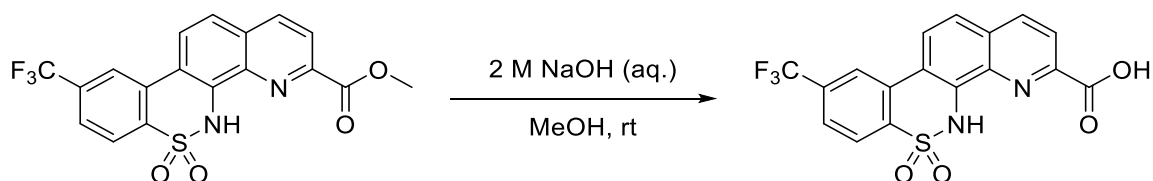
Yield: 8 mg (69.03%).

¹H NMR (600 MHz, Methanol-*d*₄ and Chloroform-*d*) δ 8.69 (d, *J* = 8.7 Hz, 1H), 8.54 (d, *J* = 4.6 Hz, 1H), 8.32 (d, *J* = 8.8 Hz, 1H), 8.13 (t, *J* = 7.7 Hz, 2H), 7.96 (t, *J* = 7.6 Hz, 1H), 7.50 – 7.48 (m, 1H).

ESI-HRMS calc. for [C₁₅H₉Cl₂N₃O₄S + H]⁺ m/z 397.9764 (100.0%), 399.9734 (63.9%), 401.9705 (10.2%), found m/z 397.97738 (100%), 399.97473 (64.5%), 401.97133 (9.6%) [M + H]⁺.

Melting point: 238.1 °C

9-(Trifluoromethyl)-5H-benzo[5,6][1,2]thiazino[4,3-h]quinoline-3-carboxylic acid 6,6-dioxide (YJh184)



The synthesis was according to the general procedure for hydrolysis of methyl esters catalyzed by hydroxide ion. 2 M NaOH (10 mL) was added to methyl 9-(trifluoromethyl)-5H-benzo[5,6][1,2]thiazino[4,3-h]quinoline-3-carboxylate 6,6-dioxide (**YJh151**) (20 mg, 0.049 mmol) in methanol (3 mL). The reaction mixture was stirred at room temperature for 3 h. The compound was purified via silica gel chromatograph (ethyl acetate, MeOH and H₂O, the ratio was 8 to 1.5 to 1). The final product was obtained as brown solid after lyophilization.

Yield: 17.4 mg (90.11%).

¹H NMR (600 MHz, DMSO-*d*₆) δ 8.83 – 8.67 (m, 3H), 8.31 (t, *J* = 8.3 Hz, 2H), 8.12 (d, *J* = 8.2 Hz, 1H), 7.96 (d, *J* = 8.7 Hz, 1H).

¹³C NMR (151 MHz, DMSO-*d*₆) δ 165.20, 146.17, 138.97, 137.49, 136.48, 135.59, 132.91 (q, *J* = 34.1, 32.2 Hz), 132.67, 130.26, 125.94, 125.85, 123.66 (q, *J* = 273.5 Hz), 123.40, 123.37, 122.00, 121.62, 118.21.

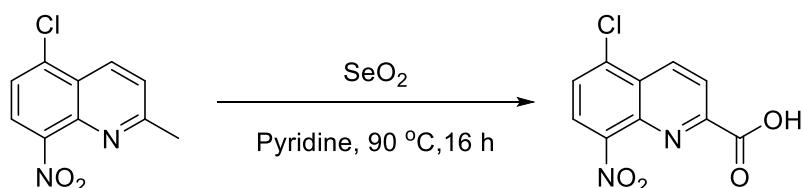
¹⁹F NMR (565 MHz, DMSO-*d*₆) δ -61.14.

ESI-HRMS calc. for [C₁₇H₉F₃N₂O₄S + H]⁺ *m/z* 395.0308, found *m/z* 395.0305 [M + H]⁺.

Melting point: 252.8 °C

Purity: 97.65%

5-Chloro-8-nitroquinoline-2-carboxylic acid (YJh191)



The synthesis was according to the general procedure for oxidation of 2-methyl quinoline analogues by selenium dioxide. Selenium dioxide (696.77 mg, 6.28 mmol) was added to 5-chloro-2-methyl-8-nitroquinoline (**YJh170**) (932 mg, 4.19 mmol) in pyridine (5 mL). The compound was purified via silica gel chromatograph (ethyl acetate, MeOH and H₂O, the ratio was 8 to 1.5 to 1). The final product was obtained as orange solid after lyophilization.

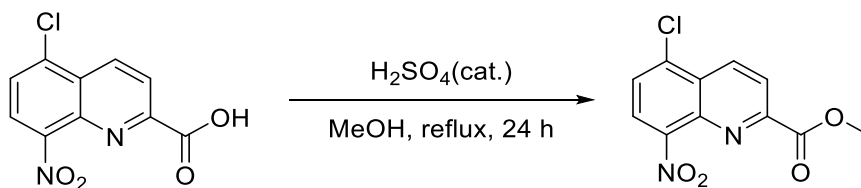
Yield: 634.5 mg (60%).

¹H NMR (500 MHz, DMSO-*d*₆) δ 14.01 (s, 1H), 8.86 (d, *J* = 8.8 Hz, 1H), 8.40 (d, *J* = 8.1 Hz, 1H), 8.36 (d, *J* = 8.8 Hz, 1H), 8.08 (d, *J* = 8.1 Hz, 1H).

¹³C NMR (126 MHz, DMSO-*d*₆) δ 165.25, 151.40, 147.38, 138.49, 135.00, 133.82, 127.86, 126.97, 124.47, 123.84.

ESI-HRMS calc. for [C₁₀H₅ClN₂O₄ + H]⁺ *m/z* 253.0011 (100.0%), 254.9981 (32.0%), found *m/z* 253.0017, 254.9989 [M + H]⁺.

Methyl 5-chloro-8-nitroquinoline-2-carboxylate (YJh192)



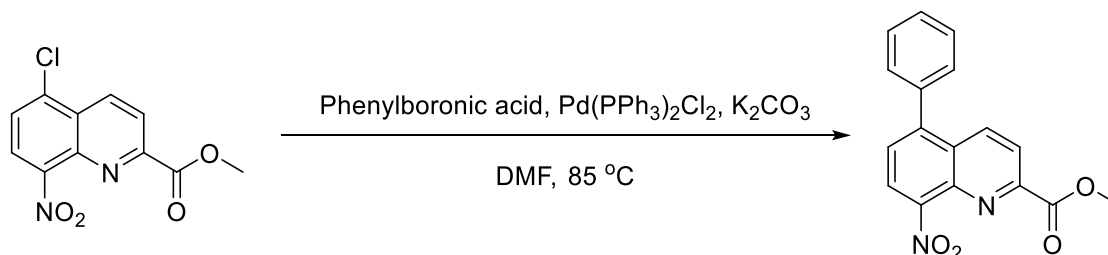
The synthesis was according to the general procedure for methyl esterification of carboxylic acids. Concentrated H₂SO₄ (0.25 mL) was added dropwise to 5-chloro-8-nitroquinoline-2-carboxylic acid (**YJh191**) (400 mg, 1.58 mmol) in methanol (40 mL). The compound was purified via hexane and ethyl acetate silica gel chromatograph (15% ethyl acetate). The final product was obtained as orange solid. Yield: 391.01 mg (92.61%).

¹H NMR (500 MHz, Chloroform-*d*) δ 8.80 (d, *J* = 8.8 Hz, 1H), 8.40 (d, *J* = 8.8 Hz, 1H), 8.09 (d, *J* = 8.1 Hz, 1H), 7.81 (d, *J* = 8.1 Hz, 1H), 4.06 (d, *J* = 0.8 Hz, 3H).

¹³C NMR (126 MHz, Chloroform-*d*) δ 164.98, 150.74, 147.51, 139.67, 135.81, 134.97, 127.97, 127.28, 124.81, 123.53, 53.59.

ESI-HRMS calc. for $[C_{11}H_7ClN_2O_4 + H]^+$ m/z 267.0167 (100.0%), 269.0138 (32.0%), found m/z 267.0173, 269.0147 $[M + H]^+$.

Methyl 8-nitro-5-phenylquinoline-2-carboxylate (YJh193)



Bis(triphenylphosphine)palladium(II) dichloride (194.8 mg, 0.278 mmol) was added to a mixture of methyl 5-chloro-8-nitroquinoline-2-carboxylate (YJh192) (370 mg, 1.39 mmol), phenylboronic acid (219.95 mg, 1.80 mmol) and K₂CO₃ (383.54 mg, 2.78 mmol) in DMF (6 mL) under nitrogen. The reaction was stirred at 90 °C for 14 h and then quenched by 10 mL brine solution and extracted 3 times with ethyl acetate. The collected organic phase was washed by brine and dried over anhydrous Na₂SO₄. The solvent was evaporated via reduced pressure. The resulting residue was purified via hexane and ethyl acetate silica gel chromatograph (15% ethyl acetate). The final compound was obtained as yellow (or orange) solid.

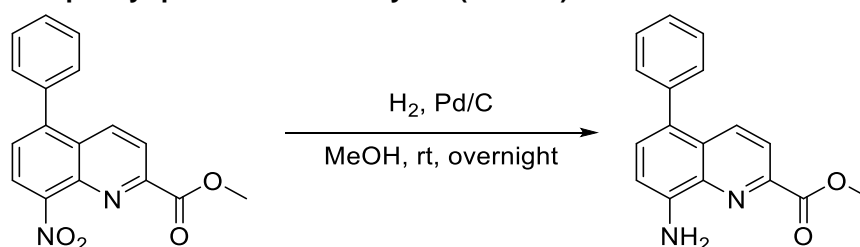
Yield: 299.46 mg (70%).

¹H NMR (500 MHz, Chloroform-*d*) δ 8.44 (d, J = 8.8 Hz, 1H), 8.24 (d, J = 8.8 Hz, 1H), 8.18 (d, J = 7.7 Hz, 1H), 7.67 (d, J = 7.7 Hz, 1H), 7.59 – 7.52 (m, 3H), 7.48 – 7.43 (m, 2H), 4.05 (s, 3H).

¹³C NMR (126 MHz, Chloroform-*d*) δ 165.41, 149.81, 147.84, 145.15, 139.47, 137.37, 136.38, 129.89, 129.09, 128.52, 127.68, 124.40, 122.61, 53.44.

ESI-HRMS calc. for $[C_{17}H_{12}N_2O_4 + H]^+$ m/z 309.0870, found m/z 309.0874 $[M + H]^+$.

Methyl 8-amino-5-phenylquinoline-2-carboxylate (YJh194)



The synthesis was according to the general procedure for hydrogenation reduction. Palladium on carbon (40.9 mg) was added to methyl 8-nitro-5-phenylquinoline-2-carboxylate (YJh193) (409.1 mg, 1.327 mmol) in methanol (100 mL) under nitrogen. The mixture was stirred at room temperature under hydrogen overnight. The reaction solution was filtered and evaporated via reduced pressure. The resulting residue was purified via hexane and ethyl acetate silica gel chromatograph (20% ethyl acetate). The final product was obtained as yellow solid.

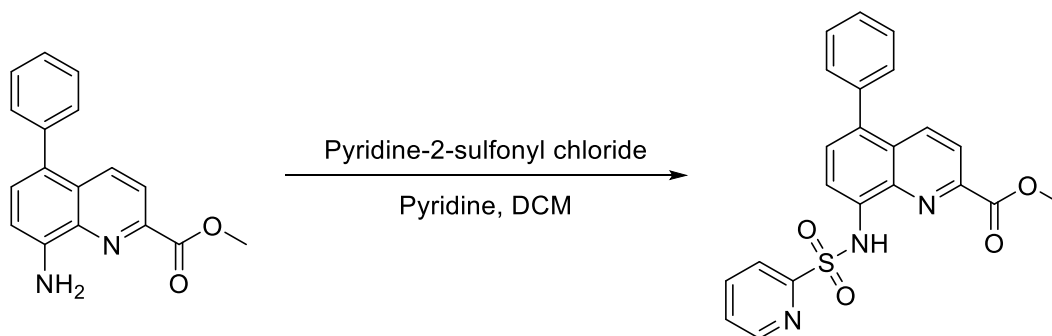
Yield: 273.22 mg (73.98%).

¹H NMR (500 MHz, Chloroform-*d*) δ 8.33 (d, J = 8.8 Hz, 1H), 8.06 (d, J = 8.8 Hz, 1H), 7.54 – 7.36 (m, 6H), 7.00 (d, J = 7.8 Hz, 1H), 4.04 (s, 3H).

¹³C NMR (126 MHz, Chloroform-*d*) δ 166.08, 144.70, 144.62, 139.73, 137.54, 135.36, 130.68, 130.24, 128.62, 128.29, 128.26, 127.14, 121.23, 109.84, 52.85.

ESI-HRMS calc. for $[C_{17}H_{14}N_2O_2 + H]^+$ m/z 279.1128, found m/z 279.1133 $[M + H]^+$.

Methyl 5-phenyl-8-(pyridine-2-sulfonamido)quinoline-2-carboxylate (YJh195)



The synthesis was according to the general procedure for sulfonamide coupling. Pyridine-2-sulfonyl chloride (**YJh167**) (64.33 μ L, 0.539 mmol) was added to methyl 8-amino-5-phenylquinoline-2-carboxylate (**YJh194**) (100 mg, 0.359 mmol) in pyridine/dichloromethane (1.5 mL/3 mL). The compound was purified via hexane and ethyl acetate silica gel chromatograph (86% ethyl acetate). The final product was obtained as yellow solid.

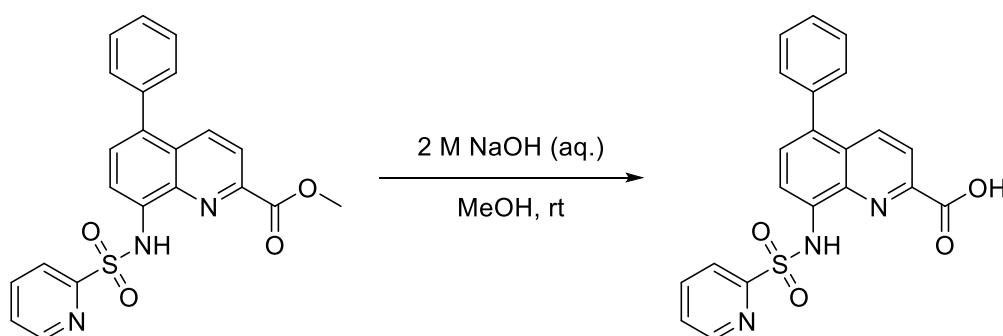
Yield: 173.4 mg (87.8%).

$^1\text{H NMR}$ (500 MHz, Chloroform-*d*) δ 9.60 (s, 1H), 8.62 (ddd, $J = 4.7, 1.7, 0.9$ Hz, 1H), 8.34 (d, $J = 8.8$ Hz, 1H), 8.18 (dt, $J = 7.9, 1.1$ Hz, 1H), 8.11 (d, $J = 8.8$ Hz, 1H), 8.03 (d, $J = 8.0$ Hz, 1H), 7.89 (td, $J = 7.8, 1.7$ Hz, 1H), 7.54 – 7.33 (m, 7H), 4.06 (s, 3H).

$^{13}\text{C NMR}$ (126 MHz, Chloroform-*d*) δ 165.60, 156.86, 150.39, 146.13, 138.46, 138.08, 137.81, 136.11, 134.68, 134.07, 130.05, 129.59, 128.79, 127.97, 127.89, 127.18, 122.86, 121.82, 114.90, 53.11.

ESI-HRMS calc. for $[C_{22}H_{17}N_3O_4S + H]^+$ m/z 420.1013, found m/z 420.1017 $[M + H]^+$.

5-Phenyl-8-(pyridine-2-sulfonamido)quinoline-2-carboxylic acid (YJh196)



The synthesis was according to the general procedure for hydrolysis of methyl esters catalyzed by hydroxide ion. 2 M NaOH (10 mL) was added to methyl 5-phenyl-8-(pyridine-2-sulfonamido)quinoline-2-carboxylate (**YJh195**) (100 mg, 0.238 mmol) in methanol (3 mL). The reaction mixture was stirred at room temperature for 3 h. The compound was purified via silica gel chromatograph (ethyl acetate, MeOH and H_2O , the ratio was 8 to 1.5 to 1). The final product was obtained as white (a little green) solid after lyophilization.

Yield: 40 mg (92%).

$^1\text{H NMR}$ (500 MHz, DMSO-*d*₆) δ 13.57 (s, 1H), 11.27 (s, 1H), 8.64 (ddd, $J = 4.7, 1.7, 0.9$ Hz, 1H), 8.39 (d, $J = 8.8$ Hz, 1H), 8.22 (d, $J = 7.9$ Hz, 1H), 8.20 (d, $J = 8.8$ Hz, 1H), 8.12 (td, $J = 7.8, 1.7$ Hz, 1H), 7.91

(d, $J = 8.1$ Hz, 1H), 7.65 (ddd, $J = 7.7, 4.7, 1.1$ Hz, 1H), 7.60 (d, $J = 8.0$ Hz, 1H), 7.54 – 7.49 (m, 2H), 7.48 – 7.41 (m, 3H).

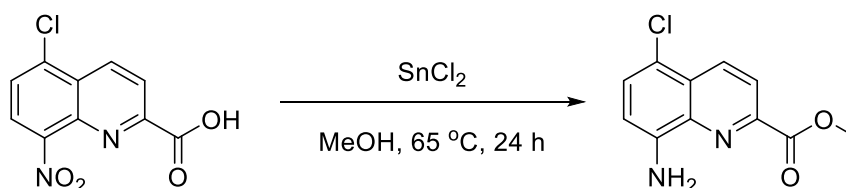
^{13}C NMR (126 MHz, DMSO- d_6) δ 165.05, 156.17, 150.39, 145.36, 139.08, 137.83, 136.81, 136.66, 134.43, 133.91, 129.88, 129.70, 128.77, 127.88, 127.45, 122.69, 121.14, 115.42.

ESI-HRMS calc. for $[\text{C}_{21}\text{H}_{15}\text{N}_3\text{O}_4\text{S} + \text{H}]^+$ m/z 406.0856, found m/z 406.0863 $[\text{M} + \text{H}]^+$.

Melting point: 252.1 °C

Purity: 99.41%

Methyl 8-amino-5-chloroquinoline-2-carboxylate (YJh197)



The synthesis was according to the general procedure for reduction of aromatic nitro compounds to amines by tin (II) chloride. Tin (II) chloride (974.78 mg, 5.13 mmol) and concentrated hydrochloric acid (100 μL) were added to 5-chloro-8-nitroquinoline-2-carboxylic acid (**YJh191**) (216 mg, 0.855 mmol) in methanol (40 mL). The compound was purified via hexane and ethyl acetate silica gel chromatograph (15% ethyl acetate). The final product was obtained as orange solid.

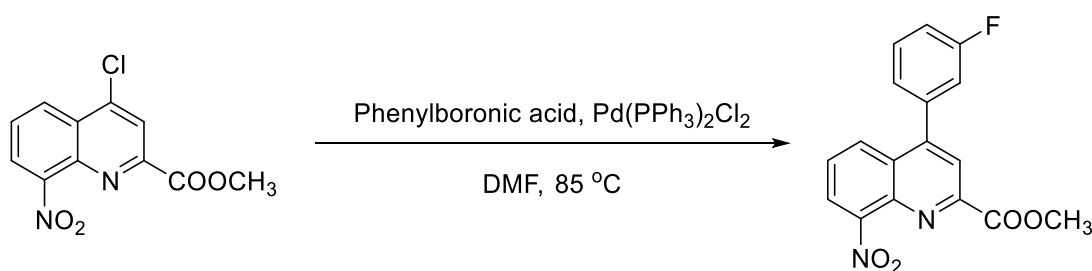
Yield: 175 mg (86.48%).

^1H NMR (500 MHz, Chloroform- d) δ 8.55 (d, $J = 8.8$ Hz, 1H), 8.19 (d, $J = 8.8$ Hz, 1H), 7.46 (d, $J = 8.2$ Hz, 1H), 6.84 (d, $J = 8.2$ Hz, 1H), 5.23 (s, 2H), 4.04 (s, 3H).

^{13}C NMR (126 MHz, Chloroform- d) δ 165.73, 145.21, 144.56, 137.91, 134.21, 129.80, 127.79, 122.03, 117.59, 109.82, 52.98.

ESI-HRMS calc. for $[\text{C}_{11}\text{H}_9\text{ClN}_2\text{O}_2 + \text{H}]^+$ m/z 237.0425 (100.0%), 239.0396 (32.0%), found m/z 237.0431, 239.0404 $[\text{M} + \text{H}]^+$.

Methyl 4-(3-fluorophenyl)-8-nitroquinoline-2-carboxylate (YJh199)



Bis(triphenylphosphine)palladium(II) dichloride (194.8 mg, 0.278 mmol) was added to a mixture of methyl 4-chloro-8-nitroquinoline-2-carboxylate (**YJh128**) (370 mg, 1.39 mmol), 3-fluorophenylboronic acid (252.41 mg, 1.80 mmol) and K_2CO_3 (383.54 mg, 2.78 mmol) in DMF (6 mL) under the nitrogen. The reaction was stirred at 90 °C for 14 h and then quenched by 10 mL brine solution and extracted 3 times with ethyl acetate. The collected organic phase was washed by brine and dried over anhydrous Na_2SO_4 . The solvent was evaporated under reduced pressure. The resulting residue was purified via hexane and dichloromethane silica gel chromatograph (60% dichloromethane). The final product was obtained as white solid.

Yield: 448.23 mg (99%).

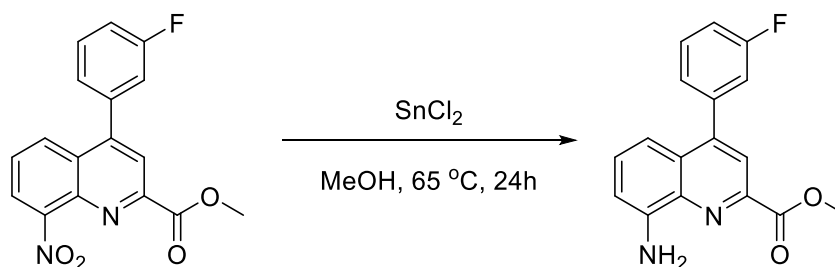
¹H NMR (600 MHz, Chloroform-*d*) δ 8.25 (s, 1H), 8.16 (dd, *J* = 8.6, 1.3 Hz, 1H), 8.12 (dd, *J* = 7.4, 1.3 Hz, 1H), 7.70 (dd, *J* = 8.6, 7.4 Hz, 1H), 7.56 (ddd, *J* = 8.5, 7.6, 5.7 Hz, 1H), 7.30 (ddd, *J* = 7.6, 1.6, 1.0 Hz, 1H), 7.28 – 7.25 (m, 1H), 7.23 (ddd, *J* = 9.1, 2.5, 1.6 Hz, 1H), 4.06 (s, 3H).

¹³C NMR (151 MHz, Chloroform-*d*) δ 165.35, 162.97 (d, *J* = 248.9 Hz), 149.62, 149.35, 149.02 (d, *J* = 2.1 Hz), 139.71, 138.49 (d, *J* = 7.9 Hz), 130.92 (d, *J* = 8.6 Hz), 129.71, 128.36, 127.56, 125.50 (d, *J* = 3.0 Hz), 124.55, 122.86, 116.83 (d, *J* = 22.6 Hz), 116.58 (d, *J* = 21.0 Hz), 53.54.

¹⁹F NMR (565 MHz, Chloroform-*d*) δ -111.31 (q, *J* = 8.2 Hz).

ESI-HRMS calc. for [C₁₇H₁₁FN₂O₄ + H]⁺ *m/z* 327.0776, found *m/z* 327.0780 [M + H]⁺.

Methyl 8-amino-4-(3-fluorophenyl)quinoline-2-carboxylate (YJh200)



The synthesis was according to the general procedure for reduction of aromatic nitro compounds to amines by tin (II) chloride. Tin (II) chloride (1.12 g, 5.88 mmol) and concentrated hydrochloric acid (100 μL) were added to methyl 4-(3-fluorophenyl)-8-nitroquinoline-2-carboxylate (**YJh199**) (320 mg, 0.981 mmol) in methanol (40 mL). The reaction mixture was stirred at 65 °C overnight. The product was purified via hexane and ethyl acetate silica gel chromatograph (15% ethyl acetate). The final product was obtained as yellow or brown solid.

Yield: 251.31 mg (86.48%).

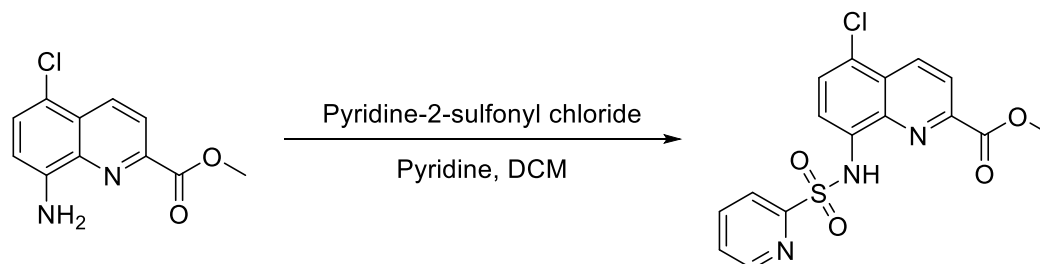
¹H NMR (600 MHz, Chloroform-*d*) δ 8.05 (s, 1H), 7.48 (ddd, *J* = 8.4, 7.6, 5.8 Hz, 1H), 7.39 (dd, *J* = 8.4, 7.5 Hz, 1H), 7.30 (ddd, *J* = 7.6, 1.6, 1.0 Hz, 1H), 7.24 (ddd, *J* = 9.4, 2.6, 1.6 Hz, 1H), 7.22 – 7.15 (m, 2H), 6.97 (dd, *J* = 7.6, 1.2 Hz, 1H), 4.04 (s, 3H).

¹³C NMR (126 MHz, Chloroform-*d*) δ 166.07, 162.81 (d, *J* = 247.9 Hz), 148.08, 145.68, 144.25, 140.34 (d, *J* = 8.3 Hz), 138.14, 130.34, 130.29, 128.42, 125.44, 121.58, 116.73 (d, *J* = 22.1 Hz), 115.57 (d, *J* = 21.0 Hz), 113.25, 110.33, 52.93.

¹⁹F NMR (565 MHz, Chloroform-*d*) δ -100.69 – -147.25 (m).

ESI-HRMS calc. for [C₁₇H₁₃FN₂O₂ + H]⁺ *m/z* 297.1034, found *m/z* 297.1038 [M + H]⁺.

Methyl 5-chloro-8-(pyridine-2-sulfonamido)quinoline-2-carboxylate (YJh201)



The synthesis was according to the general procedure for sulfonamide coupling. Pyridine-2-sulfonyl chloride (**YJh167**) (76 μL, 0.634 mmol) was added to methyl 8-amino-5-chloroquinoline-2-carboxylate (**YJh197**) (100 mg, 0.423 mmol) in pyridine/dichloromethane (1.5 mL/3 mL) and stirred at room

temperature for 24 h. The product was purified via hexane and ethyl acetate silica gel chromatograph (80% ethyl acetate). The final product was obtained as yellow solid.

Yield: 113.9 mg (71.35%).

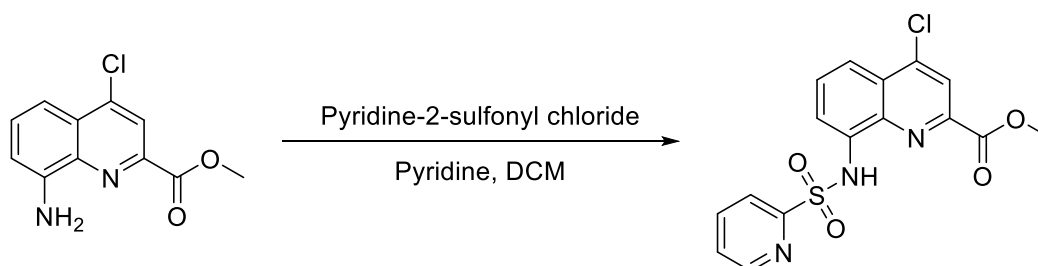
¹H NMR (500 MHz, Chloroform-*d*) δ 9.40 (s, 1H), 8.62 (d, *J* = 8.7 Hz, 1H), 8.57 (ddd, *J* = 4.7, 1.8, 0.9 Hz, 1H), 8.26 (d, *J* = 8.7 Hz, 1H), 8.12 (dt, *J* = 7.9, 1.0 Hz, 1H), 7.94 (d, *J* = 8.4 Hz, 1H), 7.88 (td, *J* = 7.8, 1.7 Hz, 1H), 7.59 (d, *J* = 8.3 Hz, 1H), 7.42 (ddd, *J* = 7.7, 4.7, 1.1 Hz, 1H), 4.07 (s, 3H).

¹³C NMR (126 MHz, Chloroform-*d*) δ 165.20, 156.64, 150.41, 147.00, 138.22, 138.10, 134.89, 134.07, 128.92, 127.42, 127.30, 124.99, 122.79, 122.68, 115.33, 53.24.

ESI-HRMS calc. for [C₁₆H₁₂ClN₃O₄S + H]⁺ *m/z* 378.0310 (100%), 380.0280 (32.0%), found *m/z* 378.0332 (100%), 380.0294 (45.6%) [M + H]⁺.

ESI-MS calc. for [C₁₆H₁₂ClN₃O₄S + H]⁺ *m/z* 378.0310 (100.0%), 380.0280 (32.0%), [C₁₆H₁₂ClN₃O₄S + Na]⁺ *m/z* 400.0129 (100.0%), 402.0100 (32.0%), found *m/z* 378.0, 379.8 [M + H]⁺, 399.8, 401.8 [M + Na]⁺.

Methyl 4-chloro-8-(pyridine-2-sulfonamido)quinoline-2-carboxylate (YJh202)



The synthesis was according to the general procedure for sulfonamide coupling. Pyridine-2-sulfonyl chloride (**YJh167**) (45 μL, 0.38 mmol) was added to methyl 8-amino-4-chloroquinoline-2-carboxylate (**YJh139**) (60 mg, 0.254 mmol) in pyridine/dichloromethane (1.5 mL/3 mL) and stirred at room temperature for 24 h. The product was purified via hexane and ethyl acetate silica gel chromatograph (20%-35% ethyl acetate). The final product was obtained as yellow solid.

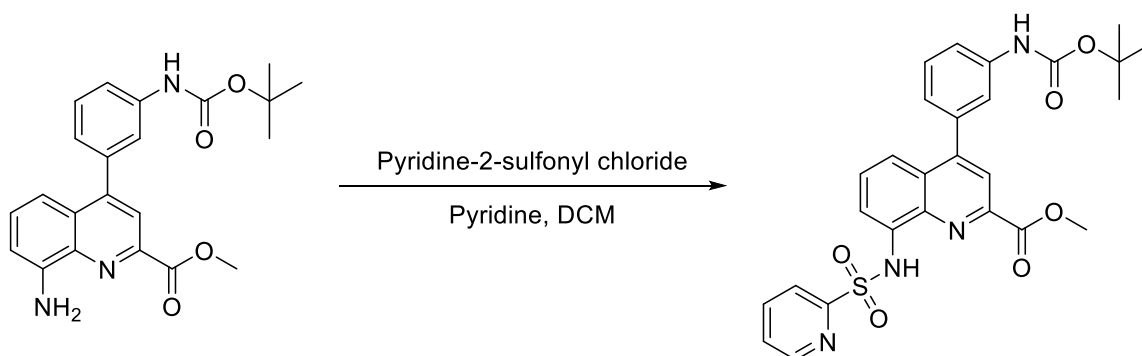
Yield: 67 mg (70%).

¹H NMR (600 MHz, Chloroform-*d*) δ 9.44 (s, 1H), 8.58 (ddd, *J* = 4.7, 1.7, 0.9 Hz, 1H), 8.25 (s, 1H), 8.14 (dt, *J* = 7.9, 1.0 Hz, 1H), 8.04 (dd, *J* = 7.8, 1.1 Hz, 1H), 7.88 (td, *J* = 7.8, 1.7 Hz, 1H), 7.86 (dd, *J* = 8.5, 1.2 Hz, 1H), 7.62 (dd, *J* = 8.5, 7.8 Hz, 1H), 7.42 (ddd, *J* = 7.7, 4.7, 1.1 Hz, 1H), 4.06 (s, 3H).

¹³C NMR (151 MHz, Chloroform-*d*) δ 164.73, 156.63, 150.43, 146.07, 144.32, 138.36, 138.09, 135.28, 130.21, 127.75, 127.28, 122.85, 122.23, 118.21, 116.07, 53.34.

ESI-HRMS calc. for [C₁₆H₁₂ClN₃O₄S + H]⁺ *m/z* 378.0310, found *m/z* 378.0314 [M + H]⁺.

Methyl 4-(3-((tert-butoxycarbonyl)amino)phenyl)-8-(pyridine-2-sulfonamido)quinoline-2-carboxylate (YJh203)



The synthesis was according to the general procedure for sulfonamide coupling. Pyridine-2-sulfonyl chloride (**YJh167**) (59 μL , 0.496 mmol) was added to methyl 8-amino-4-(3-((tert-butoxycarbonyl)amino)phenyl)quinoline-2-carboxylate (**YJh135**) (130 mg, 0.33 mmol) in pyridine/dichloromethane (1.5 mL/3 mL) and stirred at room temperature for 24 h. The product was purified via hexane and ethyl acetate silica gel chromatograph (60%-100% ethyl acetate). The final product was obtained as white solid.

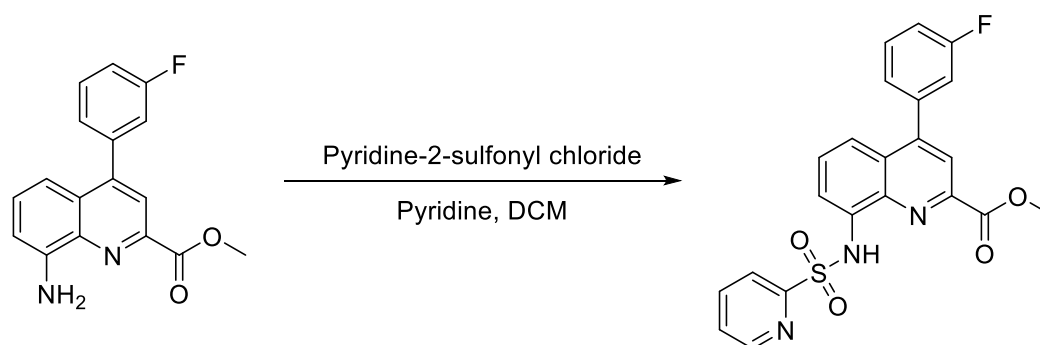
Yield: 124 mg (70%).

$^1\text{H NMR}$ (600 MHz, Chloroform-*d*) δ 9.60 (s, 1H), 8.60 (ddd, $J = 5.2, 1.5, 0.7$ Hz, 1H), 8.13 (dd, $J = 7.9, 1.1$ Hz, 1H), 8.09 (s, 1H), 7.97 (dd, $J = 7.67, 1.2$ Hz, 1H), 7.86 (td, $J = 7.8, 1.7$ Hz, 1H), 7.57 (dd, $J = 8.6, 1.2$ Hz, 1H), 7.56 (s, 1H), 7.48 – 7.44 (m, 1H), 7.43 – 7.38 (m, 3H), 7.09 (dt, $J = 5.5, 1.8$ Hz, 1H), 6.67 (s, 1H), 4.05 (s, 3H), 1.49 (s, 9H).

$^{13}\text{C NMR}$ (151 MHz, Chloroform-*d*) δ 165.65, 156.71, 152.76, 150.42, 150.04, 145.81, 138.96, 138.22, 138.07, 138.01, 134.92, 129.42, 129.06, 127.97, 127.17, 124.15, 122.86, 122.14, 120.15, 119.44, 118.89, 115.16, 81.03, 53.09, 28.42.

ESI-MS calc. for $[\text{C}_{27}\text{H}_{26}\text{N}_4\text{O}_6\text{S} + \text{H}]^+$ m/z 535.1646 (100.0%), 536.1679 (29.2%), 537.1604 (4.5%), $[\text{C}_{27}\text{H}_{26}\text{N}_4\text{O}_6\text{S} + \text{Na}]^+$ m/z 557.1465 (100.0%), 558.1499 (29.2%), found m/z 535.0, 536.0, 537.0 $[\text{M} + \text{H}]^+$, 557.0, 558.0 $[\text{M} + \text{Na}]^+$.

Methyl 4-(3-fluorophenyl)-8-(pyridine-2-sulfonamido)quinoline-2-carboxylate (**YJh204**)



The synthesis was according to the general procedure for sulfonamide coupling. Pyridine-2-sulfonyl chloride (**YJh167**) (24.4 μL , 0.192 mmol) was added to methyl 8-amino-4-(3-fluorophenyl)quinoline-2-carboxylate (**YJh200**) (38 mg, 0.128 mmol) in pyridine/dichloromethane (1.5 mL/3 mL) and stirred at room temperature for 24 h. The product was purified via hexane and ethyl acetate silica gel chromatograph (30%-100% ethyl acetate). The final product was obtained as yellow solid.

Yield: 39.3 mg (70%).

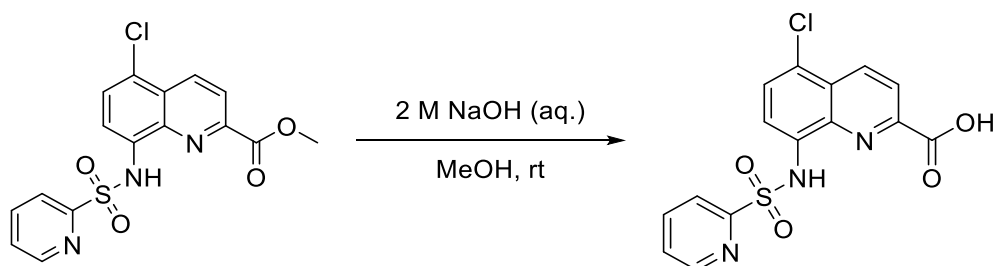
¹H NMR (600 MHz, Chloroform-*d*) δ 9.61 (s, 1H), 8.61 (ddd, *J* = 4.7, 1.7, 0.9 Hz, 1H), 8.11 (s, 1H), 8.00 (dd, *J* = 7.5, 1.3 Hz, 1H), 7.88 (td, *J* = 7.8, 1.7 Hz, 1H), 7.55 (dd, *J* = 8.6, 1.3 Hz, 1H), 7.52 – 7.47 (m, 2H), 7.43 (ddd, *J* = 7.7, 4.7, 1.1 Hz, 1H), 7.25 (ddd, *J* = 7.6, 1.6, 0.9 Hz, 1H), 7.23 – 7.15 (m, 2H), 4.07 (s, 3H).

¹³C NMR (151 MHz, Chloroform-*d*) δ 165.58, 162.85 (d, *J* = 247.9 Hz), 156.80, 150.44, 148.84 (d, *J* = 2.1 Hz), 145.89, 139.30 (d, *J* = 7.5 Hz), 138.23, 138.06, 135.18, 130.58 (d, *J* = 8.3 Hz), 129.40, 127.72, 127.20, 125.41 (d, *J* = 2.9 Hz), 122.90, 122.17, 119.62, 116.72 (d, *J* = 22.6 Hz), 116.07 (d, *J* = 21.0 Hz), 115.16, 53.19.

¹⁹F NMR (565 MHz, Chloroform-*d*) δ -111.87 – -111.99 (m).

ESI-HRMS calc. for [C₂₂H₁₆FN₃O₄S + H]⁺ *m/z* 438.0918, found *m/z* 438.0924 [M + H]⁺.

5-Chloro-8-(pyridine-2-sulfonamido)quinoline-2-carboxylic acid (YJh205 or YJh206)



The synthesis was according to the general procedure for hydrolysis of methyl esters catalyzed by hydroxide ion. 2 M NaOH solution (10 mL) was added to methyl 5-chloro-8-(pyridine-2-sulfonamido)quinoline-2-carboxylate (**YJh201**) (36 mg, 0.095 mmol) in methanol (3 mL). The product was purified via silica gel chromatograph (ethyl acetate, MeOH and H₂O, the ratio was 8 to 1.5 to 1). The final product was obtained as yellow solid after lyophilization.

Yield: 30 mg (85.5%).

¹H NMR (500 MHz, DMSO-*d*₆) δ 13.55 (s, 1H), 11.20 (s, 1H), 8.66 (d, *J* = 8.7 Hz, 1H), 8.60 (ddd, *J* = 4.7, 1.7, 0.9 Hz, 1H), 8.30 (d, *J* = 8.7 Hz, 1H), 8.17 (dt, *J* = 7.9, 1.0 Hz, 1H), 8.10 (td, *J* = 7.8, 1.7 Hz, 1H), 7.84 (d, *J* = 8.5 Hz, 1H), 7.81 (d, *J* = 8.6 Hz, 1H), 7.63 (ddd, *J* = 7.6, 4.7, 1.2 Hz, 1H).

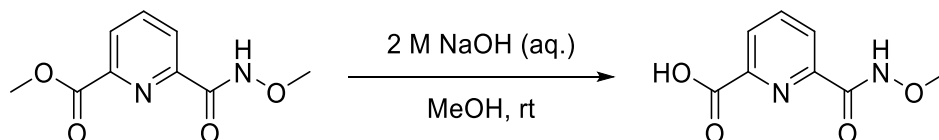
¹³C NMR (126 MHz, DMSO-*d*₆) δ 164.64, 155.93, 150.30, 146.18, 139.02, 137.33, 135.27, 134.62, 129.20, 127.88, 126.85, 123.66, 122.60, 121.98, 116.10.

ESI-HRMS calc. for [C₁₅H₁₀ClN₃O₄S + H]⁺ *m/z* 364.0153 (100.0%), 366.0124 (32.0%), found *m/z* 364.0155, 366.0125 [M + H]⁺.

Melting point: 246.3 °C

Purity: 99.4%

6-(Methoxycarbamoyl)picolinic acid (YJh207)



The synthesis was according to the general procedure for hydrolysis of methyl esters catalyzed by hydroxide ion. The corresponding methyl ester was methyl 6-(methoxycarbamoyl)picolinate (**YJh21**) (60 mg, 0.285 mmol). The final product was obtained as white solid.

Yield: 47.88 mg (85.49%).

¹H NMR (500 MHz, Methanol-*d*₄) δ 8.30 (td, *J* = 7.7, 1.1 Hz, 2H), 8.18 (t, *J* = 7.8 Hz, 1H), 3.86 (s, 3H).

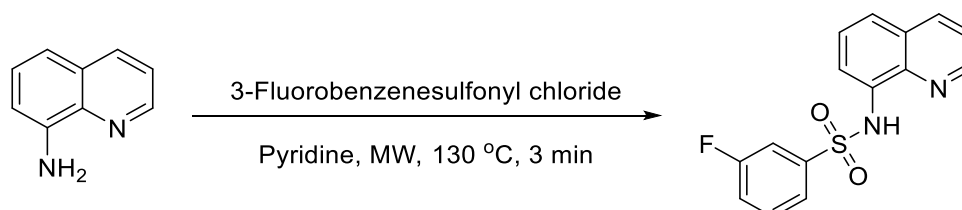
¹³C NMR (126 MHz, Methanol-*d*₄) δ 167.32, 162.76, 150.37, 148.01, 140.68, 128.71, 126.63, 64.58.

ESI-HRMS calc. for [C₈H₈N₂O₄ + H]⁺ *m/z* 197.0557, found *m/z* 197.0563 [M + H]⁺.

Melting point: 172.1 °C

Purity: 100%.

3-Fluoro-*N*-(quinolin-8-yl)benzenesulfonamide (YJh208)



3-Fluorobenzenesulfonyl chloride (138.4 μL, 1.04 mmol) and 8-aminoquinoline (100 mg, 0.694 mmol) were added to pyridine (2 mL) and heated by microwave reactor at 130 °C for 3 min. The solution was poured into sodium bicarbonate saturated solution (10 mL) and extracted 3 times with ethyl acetate. The collected organic phase was washed by brine and dried over anhydrous Na₂SO₄. The solvent was evaporated under reduced pressure. The resulting residue was purified via hexane and ethyl acetate silica gel chromatograph (10%-15% ethyl acetate). The final product was obtained as white solid.

Yield: 201.5 mg (96.09%).

¹H NMR (500 MHz, Chloroform-*d*) δ 9.25 (s, 1H), 8.76 (dd, *J* = 4.2, 1.6 Hz, 1H), 8.11 (dd, *J* = 8.3, 1.7 Hz, 1H), 7.84 (dd, *J* = 7.3, 1.6 Hz, 1H), 7.69 (ddd, *J* = 7.8, 1.7, 0.9 Hz, 1H), 7.61 (ddd, *J* = 8.2, 2.6, 1.7 Hz, 1H), 7.49 (dd, *J* = 8.3, 1.6 Hz, 1H), 7.47 – 7.41 (m, 2H), 7.34 (td, *J* = 8.1, 5.3 Hz, 1H), 7.13 (tdd, *J* = 8.3, 2.6, 0.9 Hz, 1H).

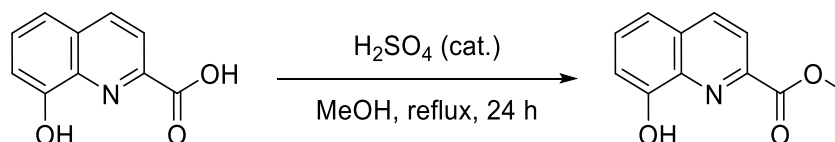
¹³C NMR (126 MHz, Chloroform-*d*) δ 162.32 (d, *J* = 251.7 Hz), 149.01, 141.47 (d, *J* = 6.6 Hz), 138.68, 136.44, 133.48, 130.79 (d, *J* = 7.8 Hz), 128.35, 126.97, 123.12 (d, *J* = 3.6 Hz), 122.73, 122.22, 120.28 (d, *J* = 21.3 Hz), 115.51, 114.78 (d, *J* = 24.9 Hz).

¹⁹F NMR (565 MHz, Chloroform-*d*) δ -109.72 (td, *J* = 7.9, 5.5 Hz).

ESI-HRMS calc. for [C₁₅H₁₁FN₂O₂S + H]⁺ *m/z* 303.0598, found *m/z* 303.0600 [M + H]⁺.

Melting point: 75.7 °C

Methyl 8-hydroxyquinoline-2-carboxylate (YJh209)



The synthesis was according to the general procedure for methyl esterification of carboxylic acids. The corresponding carboxylic acid was 8-hydroxyquinoline-2-carboxylic acid (100 mg, 0.529 mmol). The resulting residue was purified via hexane and ethyl acetate silica gel chromatograph (10%-14% ethyl acetate). The product was obtained as white (a little orange) solid.

Yield: 98.6 mg (91.79%).

¹H NMR (500 MHz, Chloroform-*d*) δ 8.59 (s, 1H), 8.27 (d, *J* = 8.4 Hz, 1H), 8.15 (d, *J* = 8.5 Hz, 1H), 7.56 (dd, *J* = 8.3, 7.6 Hz, 1H), 7.37 (dd, *J* = 8.3, 1.2 Hz, 1H), 7.23 (dd, *J* = 7.7, 1.2 Hz, 1H), 4.05 (s, 3H).

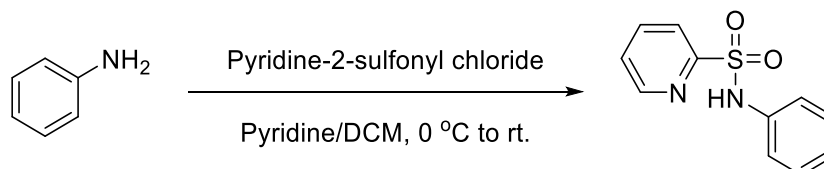
¹³C NMR (126 MHz, Chloroform-*d*) δ 165.65, 153.47, 145.42, 137.91, 137.37, 130.40, 129.88, 121.68, 117.75, 111.28, 53.05.

ESI-HRMS calc. for [C₁₁H₉NO₃ + H]⁺ m/z 204.0655, found m/z 204.0659 [M + H]⁺.

Melting point: 103.8 °C

Purity: 99.26%

N-phenylpyridine-2-sulfonamide (YJh210)



The synthesis was according to the general procedure for sulfonamide coupling. Pyridine-2-sulfonyl chloride (**YJh167**) (97 μL, 0.805 mmol) was added to aniline (50 mg, 0.537 mmol) in pyridine/dichloromethane (1 mL/2 mL) and stirred at room temperature for 24 h. The product was purified via hexane and ethyl acetate silica gel chromatograph (30%-60% ethyl acetate). The final product was obtained as white solid.

Yield: 124.53 mg (99%).

¹H NMR (500 MHz, DMSO-*d*₆) δ 10.55 (s, 1H), 8.71 (ddd, *J* = 4.7, 1.8, 0.9 Hz, 1H), 8.04 (td, *J* = 7.7, 1.7 Hz, 1H), 7.96 (dt, *J* = 7.9, 1.1 Hz, 1H), 7.63 (ddd, *J* = 7.6, 4.7, 1.2 Hz, 1H), 7.26 – 7.17 (m, 2H), 7.15 – 7.09 (m, 2H), 6.99 (tt, *J* = 7.2, 1.2 Hz, 1H).

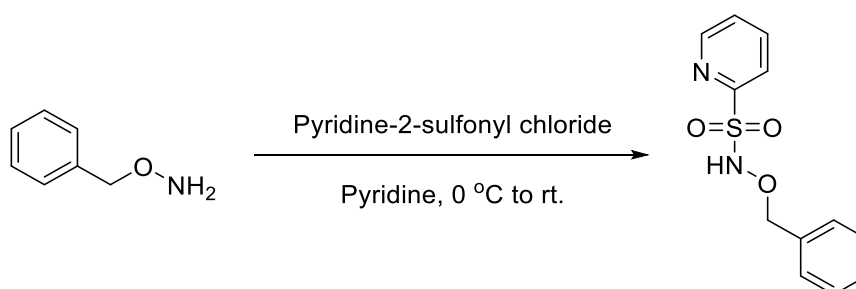
¹³C NMR (126 MHz, DMSO-*d*₆) δ 156.43, 150.17, 138.74, 137.58, 129.03, 127.39, 123.92, 122.48, 120.04.

ESI-HRMS calc. for [C₁₁H₁₀N₂O₂S + H]⁺ m/z 235.0536, found m/z 235.0541 [M + H]⁺.

Melting point: 173.7 °C

Purity: 100%

N-(benzyloxy)pyridine-2-sulfonamide (YJh211)



The synthesis was according to the general procedure for sulfonamide coupling. Pyridine-2-sulfonyl chloride (**YJh167**) (90 μL, 0.752 mmol) was added to *O*-benzylhydroxylamine hydrochloride (80 mg, 0.501 mmol) in pyridine/dichloromethane (1 mL/2 mL) and stirred at room temperature for 24 h. The product was purified via hexane and ethyl acetate silica gel chromatograph (20% ethyl acetate). The final product was obtained as white solid.

Yield: 85 mg (64%).

¹H NMR (600 MHz, Chloroform-*d*) δ 8.75 – 8.55 (m, 1H), 8.15 (s, 1H), 8.12 (dt, *J* = 7.8, 1.0 Hz, 1H), 7.94 (td, *J* = 7.8, 1.7 Hz, 1H), 7.50 (ddd, *J* = 7.8, 4.7, 1.1 Hz, 1H), 7.32 (s, 5H), 4.99 (s, 2H).

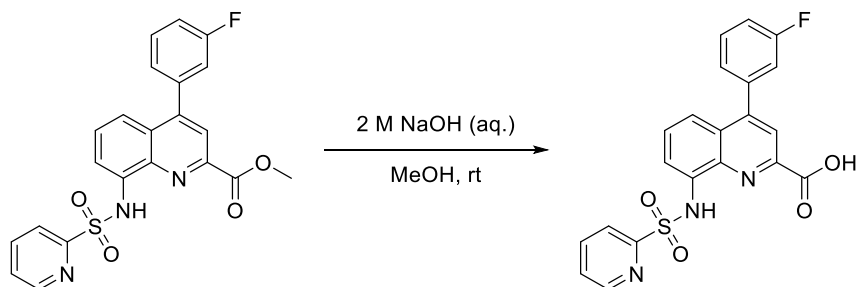
¹³C NMR (151 MHz, Chloroform-*d*) δ 154.86, 150.50, 138.17, 135.24, 129.53, 128.81, 128.59, 127.55, 124.27, 79.51.

ESI-HRMS calc. for [C₁₂H₁₂N₂O₃S + H]⁺ m/z 265.0641, found m/z 265.0643 [M + H]⁺.

Melting point: 122.4 °C

Purity: 98%

4-(3-fluorophenyl)-8-(pyridine-2-sulfonamido)quinoline-2-carboxylic acid (YJh212)



The synthesis was according to the general procedure for hydrolysis of methyl esters catalyzed by hydroxide ion. 2 M NaOH solution (10 mL) was added to methyl 4-(3-fluorophenyl)-8-(pyridine-2-sulfonamido)quinoline-2-carboxylate (**YJh204**) (22 mg, 0.05 mmol) in methanol (2 mL). The product was purified via silica gel chromatograph (ethyl acetate, MeOH and H₂O, the ratio was 8 to 1.5 to 1). The final product was obtained as white (a little green) solid after lyophilization.

Yield: 21 mg (98.6%).

¹H NMR (600 MHz, DMSO-*d*₆) δ 13.61 (s, 1H), 11.22 (s, 1H), 8.63 (d, *J* = 4.1 Hz, 1H), 8.20 (d, *J* = 7.8 Hz, 1H), 8.11 (td, *J* = 7.7, 1.7 Hz, 1H), 8.06 (s, 1H), 7.88 (dd, *J* = 7.7, 1.1 Hz, 1H), 7.68 – 7.58 (m, 3H), 7.51 (dd, *J* = 8.6, 1.1 Hz, 1H), 7.46 (ddd, *J* = 9.7, 2.6, 1.5 Hz, 1H), 7.45 – 7.35 (m, 2H).

¹³C NMR (151 MHz, DMSO-*d*₆) δ 164.98, 162.11 (d, *J* = 245.0 Hz), 156.00, 150.36, 148.67, 144.99, 138.99, 138.85 (d, *J* = 7.9 Hz), 137.16, 135.43, 130.94 (d, *J* = 8.4 Hz), 129.77, 127.84, 127.44, 125.71 (d, *J* = 2.9 Hz), 122.75, 120.81, 119.36, 116.42 (d, *J* = 22.8 Hz), 115.96 (d, *J* = 20.9 Hz), 115.73.

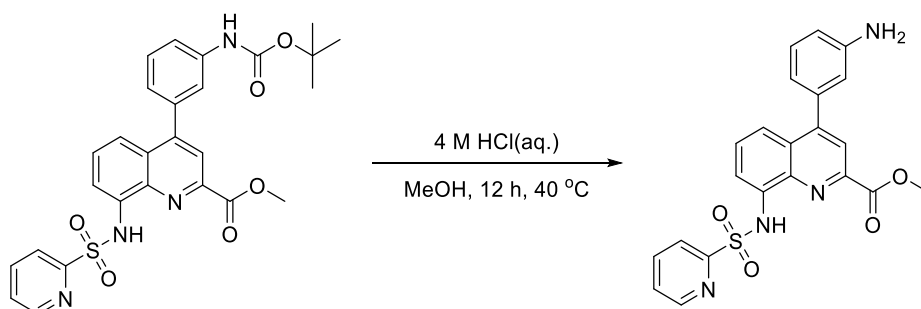
¹⁹F NMR (565 MHz, DMSO-*d*₆) δ -112.23 – -112.29 (m).

ESI-HRMS calc. for [C₂₁H₁₄FN₃O₄S + H]⁺ m/z 424.0762, found m/z 424.0767 [M + H]⁺.

Melting point: 234.1 °C

Purity: 99.5%

Methyl 4-(3-aminophenyl)-8-(pyridine-2-sulfonamido)quinoline-2-carboxylate (YJh213)



4 M HCl solution (10 mL) was added to methyl 4-(3-((tert-butoxycarbonyl)amino)phenyl)-8-(pyridine-2-sulfonamido)quinoline-2-carboxylate (**YJh203**) (60 mg, 0.112 mmol) in methanol (30 mL). The mixture was stirred at 40 °C for 12 h and then cooled to room temperature. The reaction mixture was neutralized

by saturated bicarbonate sodium solution and extracted 3 times with ethyl acetate. The collected organic phase was washed by brine and dried over anhydrous Na₂SO₄. The solvent was evaporated under reduced pressure. The resulting residue was purified via hexane and ethyl acetate silica gel chromatograph (60%-100% ethyl acetate). The final product was obtained as yellow solid after lyophilization.

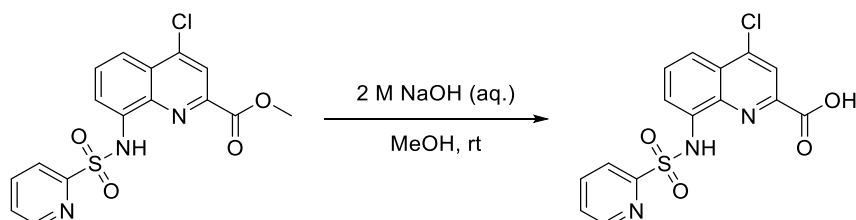
Yield: 44 mg (90.23%).

¹H NMR (600 MHz, Methanol-*d*₄ and Chloroform-*d*) δ 8.45 (d, *J* = 4.7 Hz, 1H), 8.03 (d, *J* = 7.9 Hz, 1H), 7.94 (s, 1H), 7.89 (d, *J* = 7.7 Hz, 1H), 7.77 (t, *J* = 7.8 Hz, 1H), 7.54 (d, *J* = 8.5 Hz, 1H), 7.36 (t, *J* = 8.2 Hz, 1H), 7.32 (dd, *J* = 7.6, 4.8 Hz, 1H), 7.16 (t, *J* = 7.8 Hz, 1H), 6.72 (d, *J* = 8.0 Hz, 1H), 6.69 (d, *J* = 7.6 Hz, 1H), 6.66 (s, 1H), 3.95 (s, 3H).

¹³C NMR (151 MHz, Methanol-*d*₄ and Chloroform-*d*) δ 165.97, 156.64, 150.80, 149.86, 146.64, 144.99, 138.75, 138.13, 138.04, 135.11, 129.50, 128.89, 128.15, 127.05, 122.68, 121.57, 120.45, 119.72, 116.17, 116.00, 115.73, 53.08.

ESI-HRMS calc. for [C₂₂H₁₈N₄O₄S + H]⁺ *m/z* 435.1122, found *m/z* 435.1120 [M + H]⁺.

4-Chloro-8-(pyridine-2-sulfonamido)quinoline-2-carboxylic acid (YJh214)



The synthesis was according to the general procedure for hydrolysis of methyl esters catalyzed by hydroxide ion. 2 M NaOH solution (10 mL) was added to methyl 4-chloro-8-(pyridine-2-sulfonamido)quinoline-2-carboxylate (**YJh202**) (33 mg, 0.087 mmol) in methanol (2 mL). The product was purified via silica gel chromatograph (ethyl acetate, MeOH and H₂O, the ratio was 8 to 1.5 to 1). The final product was obtained as yellow solid after lyophilization.

Yield: 31.1 mg (97.88%).

¹H NMR (600 MHz, DMSO-*d*₆) δ 13.62 (s, 1H), 11.15 (s, 1H), 8.61 (d, *J* = 4.3 Hz, 1H), 8.27 (s, 1H), 8.18 (d, *J* = 7.9 Hz, 1H), 8.10 (td, *J* = 7.8, 1.7 Hz, 1H), 7.94 (dd, *J* = 7.8, 1.2 Hz, 1H), 7.87 (dd, *J* = 8.5, 1.2 Hz, 1H), 7.78 (t, *J* = 8.1 Hz, 1H), 7.64 (ddd, *J* = 7.7, 4.7, 1.1 Hz, 1H).

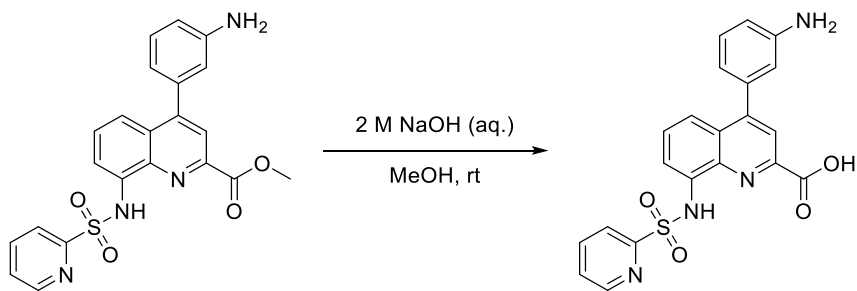
¹³C NMR (151 MHz, DMSO-*d*₆) δ 164.18, 155.89, 150.35, 145.52, 143.57, 139.04, 137.32, 135.67, 130.81, 127.90, 127.14, 122.70, 120.92, 117.68, 116.80.

ESI-HRMS calc. for [C₁₅H₁₀ClN₃O₄S + H]⁺ *m/z* 364.0153, found *m/z* 364.0157 [M + H]⁺.

Melting point: 233.3 °C

Purity: 99.71%

4-(3-Aminophenyl)-8-(pyridine-2-sulfonamido)quinoline-2-carboxylic acid (YJh215)



The synthesis was according to the general procedure for hydrolysis of methyl esters catalyzed by hydroxide ion. 2 M NaOH solution (10 mL) was added to methyl 4-(3-aminophenyl)-8-(pyridine-2-sulfonamido)quinoline-2-carboxylate (**YJh213**) (31.1 mg, 0.072 mmol) in methanol (2 mL). The product was purified via silica gel chromatograph (ethyl acetate, MeOH and H₂O, the ratio was 8 to 1.5 to 1). The final product was obtained as yellow solid after lyophilization.

Yield: 27 mg (90%).

¹H NMR (600 MHz, DMSO-*d*₆) δ 13.53 (s, 1H), 11.17 (s, 1H), 8.63 (dt, *J* = 4.6, 1.2 Hz, 1H), 8.19 (dd, *J* = 8.0, 1.1 Hz, 1H), 8.10 (td, *J* = 7.8, 1.8 Hz, 1H), 7.99 (s, 1H), 7.86 (dd, *J* = 7.5, 1.4 Hz, 1H), 7.71 – 7.54 (m, 3H), 7.20 (t, *J* = 7.7 Hz, 1H), 6.76 – 6.66 (m, 2H), 6.63 (dt, *J* = 7.6, 1.3 Hz, 1H).

¹³C NMR (151 MHz, DMSO-*d*₆) δ 165.14, 156.04, 151.11, 150.33, 149.10, 144.96, 138.97, 137.28, 137.26, 135.30, 129.36, 129.20, 127.80, 127.64, 122.72, 120.16, 119.86, 116.66, 115.63, 114.46, 114.43.

ESI-HRMS calc. for [C₂₁H₁₆N₄O₄S + H]⁺ *m/z* 421.0965, found *m/z* 421.0969 [M + H]⁺.

Melting point: 129.3 °C

Purity: 96.63%

6 Appendices

6.1 Tables and figures

List of tables		Page
Table 1.1	Enzymatic Mechanisms for Antibiotic Inactivation ¹¹	2
Table 1.2	Classification of β -Lactam Antibiotics ²²	6
Table 1.3	Examples of Chromosomal and Plasmid Associated MBLs ⁴¹	13
Table 3.1	Potential of Meropenem Activity against the Recombinant NDM-1 Producing <i>E. coli</i> by L-captopril	35
Table 3.2	Fragment Screening of the Carboxylic Acid Library	37
Table 3.3	Fragment Screening of the Amine Library	38
Table 3.4	DPA Derivatives Used to Obtain a Rudimentary SAR	40
Table 3.5	Quinoline Derivatives at the 8-Position and the 2-Position	42
Table 3.6	DPA Derivatives at the 2- and 6-Positions	48
Table 3.7	8-HQA Derivatives	55
Table 3.8	Primary Activity Tests of a Panel of 8-MSQA Derivatives.	60
Table 3.9	8-MSQA Derivatives at the 8-Position	63
Table 3.10	8-MSQA Derivatives at the 4-, 5-, 6- and 7-Positions	67
Table 3.11	Inhibitor Development for NDM-1	73
Table 3.12	Thermal Shift of NDM-1 with the Selected Compounds at Different Concentrations	95
Table 3.13	Calculated Secondary Structure Fractions	99
Table 3.14	Mode of Action Studies for Compounds 94(YJh182), 95(YJh196) and 83(YJh174)	106
Table 3.15	IC ₅₀ Values of the Selected Compounds for the MBLs	109
Table 3.16a	Percent Inhibition of DPA, 8-HQA and 8-MSQA Derivatives (at 10 μ M) against Other Zn(II) Metalloenzymes	117
Table 3.16b	Comparison of the Activity of the Selected Compounds against MMP-2 and NDM-1	118
Table 3.17a	Potential of Meropenem Activity against NDM-1-producing <i>E. coli</i> Transconjugants by the Selected Compounds	123
Table 3.17b	Potential of Meropenem Activity against MBL-producing Clinical Strains by the Selected Compounds	124
Table 3.18	Effects of Representative Inhibitors on the Proliferation and Viability of HEK293 Cells	125
Table S1	Protein Information	230
Table S2a	IC ₅₀ Curves of the Developed Inhibitors for NDM-1	235
Table S2b	IC ₅₀ Curves of the Selected Inhibitors for IMP-1	244
Table S2c	IC ₅₀ Curves of the Selected Inhibitors for MMP-2	246
Table S3	Alamar Blue Assays (HEK293 cell)	260
Table S4	Fractional Abundance of Native MS Analysis at Ratio (P/L) 1 to 2 (%)	264
Table S5	Some Other Structures	266

List of Figures

Figure 1.1	Schematic diagrams for Gram-positive and Gram-negative bacterial cell membranes and related resistance factors for β -lactam antibiotics.	3
Figure 1.2	Mechanism of β -lactam antibiotics. ¹⁸ (The picture is reproduced from Ref.18.)	5
Figure 1.3	Crystal structures of BLs.	10
Figure 1.4	Crystal structures of MBLs.	11
Figure 1.5	Current limited antibiotics for MBL-producing pathogens.	14
Figure 1.6	Hydrolysis of penicillin substrates by SBLs.	15
Figure 1.7	Hydrolysis of carbapenems by MBLs.	16
Figure 1.8	Crystal structure of NDM-1 (PDB ID: 5ZGR). a. The structure of NDM-1; b. the active site of NDM-1.	18
Figure 1.9	Proposed mechanisms of cephalosporin and carbapenem substrates hydrolyzed by NDM-1.	19
Figure 1.10	Thiol containing inhibitors of NDM-1. ^{86,108, 116-123}	21
Figure 1.11	a. Boron inhibitors for β -lactamases; b. Proposed mechanism of VNRX-5133. (The picture is reproduced from Ref.124.) ^{124, 125}	22
Figure 1.12	Metal ion chelating or binding inhibitors of NDM-1. ^{127, 128, 131-133}	24
Figure 1.13	Metal binding pharmacophore containing analogues for overcoming NDM-1. ^{134-142, 146}	26
Figure 1.14	Inhibitors of NDM-1 by forming covalent bond with Cys208 or Lys211. ^{147-149, 151-154}	27
Figure 1.15	Metal ion containing Inhibitors of NDM-1. ¹⁵⁶⁻¹⁵⁸	29
Figure 3.1	Diagram of the absorbance shifts for nitrocefin hydrolyzed by BLs. ¹⁶⁸	34
Figure 3.2	<i>In vitro</i> cell-based assays. a. Bacterial strain expressing NDM-1 induced by IPTG; b. Bacterial strain expressing NDM-1 constitutively.	35
Figure 3.3	<i>In vitro</i> enzyme-based assays.	36
Figure 3.4	IC ₅₀ determination of the active hits. a. DPA; b. C2 .	39
Figure 3.5	Diagram of the activity analysis for compound 13 .	41
Figure 3.6	<i>In vitro</i> activity tests of DPA, 8-HQA and 8-MSQA .	44
Figure 3.7	Preliminary SAR for DPA derivatives.	45
Figure 3.8	Proposed binding pose of DPA in the active site of NDM-1 (PDB ID: 5ZGR).	45
Figure 3.9	One of the predicted inactive mechanisms for compound 44(YJh6) .	47
Figure 3.10	Synthesis procedure for compound 44(YJh6) .	48
Figure 3.11	Inhibitory activity of DPA derivatives for NDM-1.	50
Figure 3.12	Proposed binding pose of compound 45(YJh2) in the active site of NDM-1 (PDB ID: 5ZGR).	50
Figure 3.13	Possible modification strategies for pyridine-2-sulfonamide.	51
Figure 3.14	Initial SAR for the development of 8-HQA derivatives.	52
Figure 3.15	Proposed binding poses of 8-HQA in the active site of NDM-1.	52
Figure 3.16	Synthesis of 5,7-di-halogen-substituted 8-HQA derivatives.	54
Figure 3.17	Inhibitory activity of 8-HQA derivatives.	56

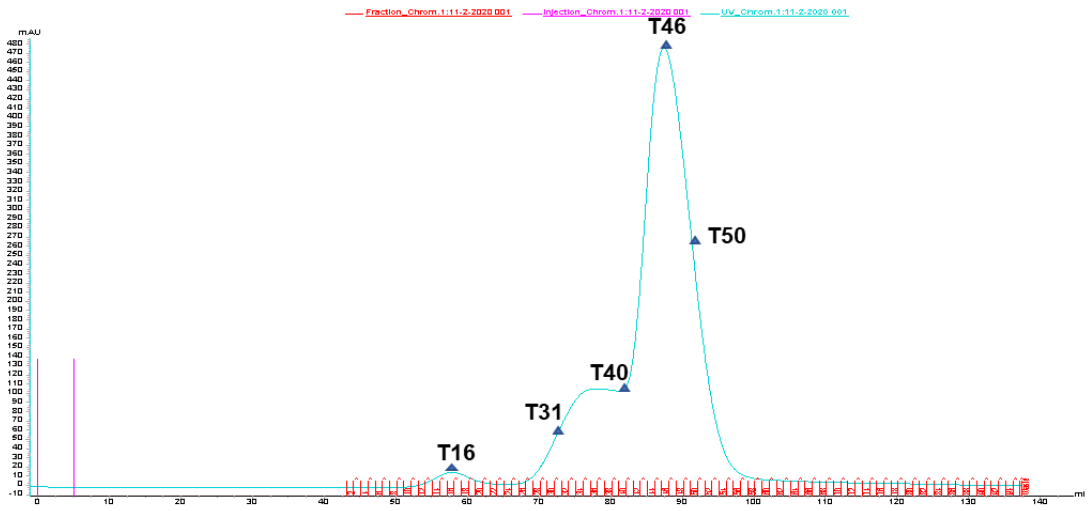
Figure 3.18	Proposed binding pose of compound 58(YJh34) in the active site of NDM-1. (PDB ID: 5ZGR).	57
Figure 3.19	Development of 8-MSQA inhibitors.	59
Figure 3.20	Primary SAR for the development of 8-MSQA inhibitors.	60
Figure 3.21	Development of compound 83(YJh174) .	64
Figure 3.22	Proposed binding poses of 8-MSQA derivatives in the active site of NDM-1(PDB ID: 5ZGR).	65
Figure 3.23	Proposed binding poses of compound 94(YJh182) in the active site of NDM-1(PDB ID: 5ZGR).	68
Figure 3.24	Inhibitory activity of 8-MSQA derivatives.	70
Figure 3.25	The SAR of 8-MSQA derivatives.	72
Figure 3.26	Representative inhibitors of DPA, 8-HQA and 8-MSQA derivatives for NDM-1.	72
Figure 3.27	Proposed binding poses of hydrolyzed and unhydrolyzed ampicillin molecules in the active site of NDM-1 (PDB ID: 5ZGR).	74
Figure 3.28	The principle of BLI assays. ²²¹	76
Figure 3.29	Kinetic curves for the interaction studies of NDM-1 with the inhibitors by BLI assays. a. 94(YJh182) ; b. 95(YJh196) ; c. 83(YJh174) ; d. L-Captopril.	77
Figure 3.30	Basic working principles of ITC instruments. ²²⁶	80
Figure 3.31	Thermograms of ITC assays. a. Compound 94(YJh182) to NDM-1; b. Compound 95(YJh196) to NDM-1; c. Compound 83(YJh174) to NDM-1.	82
Figure 3.32	Thermograms of ITC assays. a. Zinc ions to compound 83(YJh174) ; b. Zinc ions to EDTA; c. Zinc ions to DPA.	85
Figure 3.33	Mass spectra of NDM-1 obtained under different conditions.	87
Figure 3.34	Source spectra for NDM-1 with different content of DMSO obtained under native condition.	88
Figure 3.35	Interaction studies of the selected inhibitors with NDM-1 by protein native mass spectrometry.	90
Figure 3.36	The principle of DSF assays using SYPRO orange. ²³⁴	92
Figure 3.37	Melting curves of NDM-1. a. NDM-1 with EDTA; b. NDM-1 with L-captopril; c. NDM-1 with 83(YJh174) ; d. NDM-1 with 94(YJh182) ; e. NDM-1 with 95(YJh196) .	94
Figure 3.38	a. CD spectra for representative secondary structures; ²⁵⁰ b. CD spectra of wild-type NDM-1 and NDM-1 mutants. ²⁵¹ (The two pictures were reproduced from the references.)	97
Figure 3.39	CD spectra for NDM-1.	98
Figure 3.40	CD spectra of NDM-1 incubated with inhibitors at different mole ratios.	99
Figure 3.41	Addition of excess zinc ions to restore the activity for NDM-1 inhibited by the selected inhibitors.	104
Figure 3.42	The relationship of the different evaluation assays for the interaction studies of the selected inhibitors with NDM-1.	108
Figure 3.43	Alignment of relevant B1 MBLs.	109

Figure 3.44	Interactions of the proposed binding poses of 8-MSQA with the active sites of IMP-1 (PDB ID: 5EV6), VIM-2 (PDB ID: 4BZ3), and GIM-1 (PDB ID: 2YNW).	111
Figure 3.45	Structure and selectivity relationship of the inhibitors for NDM-1 and MMP-2.	120
Figure S1	a, b. Absorption curves of the truncated NDM-1 purified by size exclusion chromatography; c, d, e, f. SDS-PAGE of the truncated NDM-1.	231
Figure S2	Mass spectrum for truncated NDM-1 obtained under conventional condition.	232
Figure S3	a. Absorption curves of wild-type NDM-1 purified by size-exclusion chromatograph; b. SDS-PAGE of wild-type NDM-1.	233
Figure S4	Mass spectra for wild-type NDM-1 obtained under conventional condition.	234
Figure S5	SDS-PAGE of IMP-1.	234
Figure S6	Mass spectrum for wild-type IMP-1 obtained under denaturing condition.	235
Figure S7	<i>In vitro</i> enzyme-based assays of the selected metalloenzymes.	247
Figure S8	Thermograms of ITC assays for relevant control groups (Inhibitor titrating NDM-1 using truncated NDM-1).	248
Figure S9	Thermograms of ITC assays (Inhibitor titrating NDM-1 using full-length NDM-1).	250
Figure S10	Thermograms of ITC assays for relevant control groups (Inhibitor titrating NDM-1 using full length NDM-1).	252
Figure S11	Thermograms of ITC assays (zinc ions titrating compounds).	253
Figure S12	Thermograms of ITC assays for relevant control groups (zinc ion titrating compounds).	257
Figure S13	Description of the layouts for the plates and program settings of the BLI assays.	262
Figure S14	Proposed binding poses of S-NSA and R-NSA as well as some selected 8-MSQA derivatives in the active site of the catalytic domain of MMP-2 (PDB ID: 1QIB).	265
List of schemes		
Scheme 3.1	General synthetic route for 8-MSQA derivatives.	61
Scheme S1	Synthetic route for DPA derivatives.	141
Scheme S2	Synthetic route for quinolin-8-ol derivatives.	142
Scheme S3	Synthetic route for 8- MSQA derivatives.	144

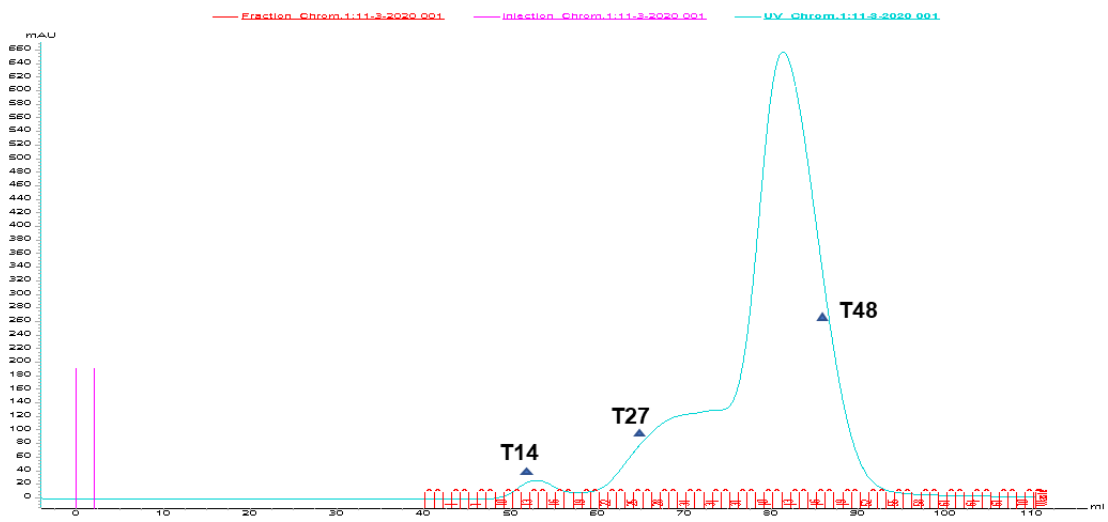
Table S1 Protein Information

Protein	Molecular weight (kDa)	Sequence
Full length NDM-1	30.01915 (Without zinc ions, calculated by https://web.expasy.org/protparam/)	<i>M</i> ELPNIMHPVAKLSTALAAALMLSGCMPGEIRPTIG QQMETGDQRFGDLVFRQLAPNVWQHTSYLDMPG FGAVASNGLIVRDGGRVLVVDTAWTDDQTAQILN WIKQEINLPVALAVVTHAHQDKMGGMDALHAAGI ATYANALSNQLAPQEGMVAAQHSLTFAANGWVE PATAPNFGPLKVFYPPGPGHTSDNITVGIDGTDIAF GGCLIKDSKAKSLGNLGDADTEHYAASARAFGAA FPKASMIVMSHSAPDSRAAITHTARMADKLR <i>KL</i> <i>AAALE HHHHHH</i>
Wild-type NDM-1	28.271 (Without zinc ions, obtained by measurement)	Not clear.
Truncated NDM-1	26.359 (Without zinc ions, obtained by measurement)	GQQMETGDQRFGDLVFRQLAPNVWQHTSYLDM PGFGAVASNGLIVRDGGRVLVVDTAWTDDQTAQI LNWIKQEINLPVALAVVTHAHQDKMGGMDALHAA GIATYANALSNQLAPQEGMVAAQHSLTFAANGW VEPATAPNFGPLKVFYPPGPGHTSDNITVGIDGTDI AFGGCLIKDSKAKSLGNLGDADTEHYAASARAFG AAFPKASMIVMSHSAPDSRAAITHTARMADKLR KLAAALE HHHHHH.
IMP-1	25.174 (Without zinc ions, obtained by measurement)	MESLPDLKIEKLDEGVYVHTSFEEVNGWGVVPHGLVVLVNAEAYLID TPFTAKDTEKLVTFVVERGYKIKGSISSHFSDSTGGIEWLNSRSIPTY ASELTNELLKKGDKVQATNSFSGVNYWLVKNKIEVFYPPGPGHTPDNV VVWLPERKILFGGCFIKPYGLGNLGDANIEAWPKSAKLLKSKYGKAKL VVP SHSEVGDASLLKLTLEQAVKGLNESKKPSKPSN
MMP-2	40	Enzo Life Sciences (cat. BML-SE237-0010)
HDAC-1	56	BPS Bioscience (cat. 50051)
hCAII	30	Sigma (cat. C6165)

a



b



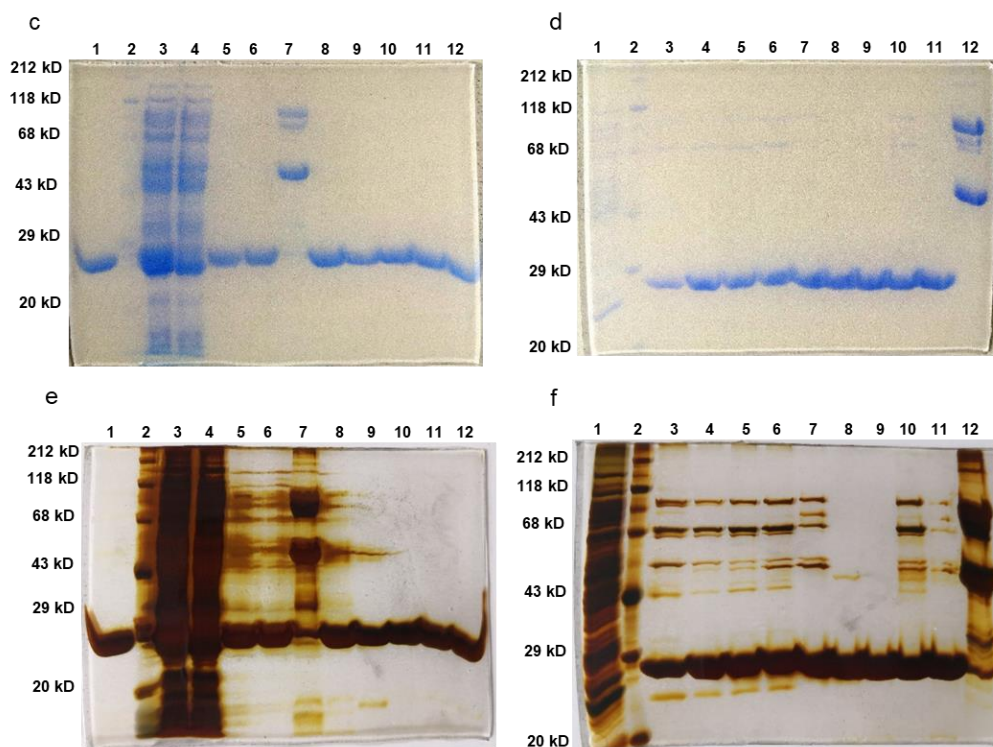


Figure S1 a, b. Absorption curves of the truncated NDM-1 purified by size exclusion chromatography (The protein sample purified by Ni-NTA column was divided into two parts for the size exclusion chromatography. a. Eluate of 150 mM to 250 mM imidazole; b. Eluate of 75 mM to 100 mM imidazole.); c, d, e, f. SDS-PAGE of the truncated NDM-1. c: 1. truncated NDM-1 (previously purified protein); 2. protein marker; 3. supernatant before Ni-NTA; 4. filtrate after Ni-NTA loading; 5. eluate of 75 mM to 100 mM imidazole; 6. eluate of 150 mM to 250 mM imidazole; 7. T16 in a; 8. T31 in a; 9. T40 in a; 10. T46 in a; 11. T50 in a; 12. T48 in b. d: 1. eluate without imidazole; 2. protein marker; 3. eluate of 20 mM imidazole; 4. eluate of 25 mM imidazole; 5. eluate of 50 mM imidazole A; 6. eluate of 50 mM imidazole B; 7. eluate of 75 mM to 100 mM imidazole; 8. T48 to T61 in a; 9. T48 in b; 10. T27 in b; 11. truncated NDM-1 (previously purified protein); 12. T14 in b; e, f. silver stain of c and d, respectively.

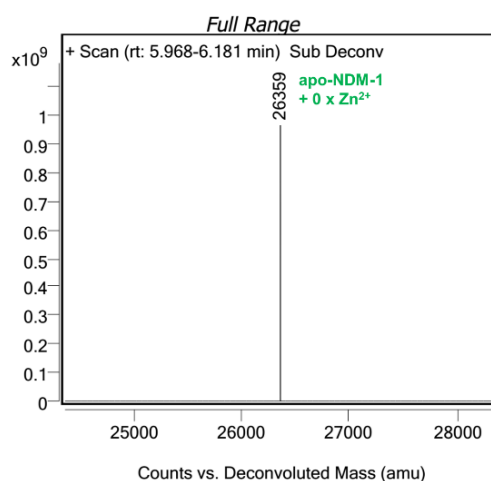
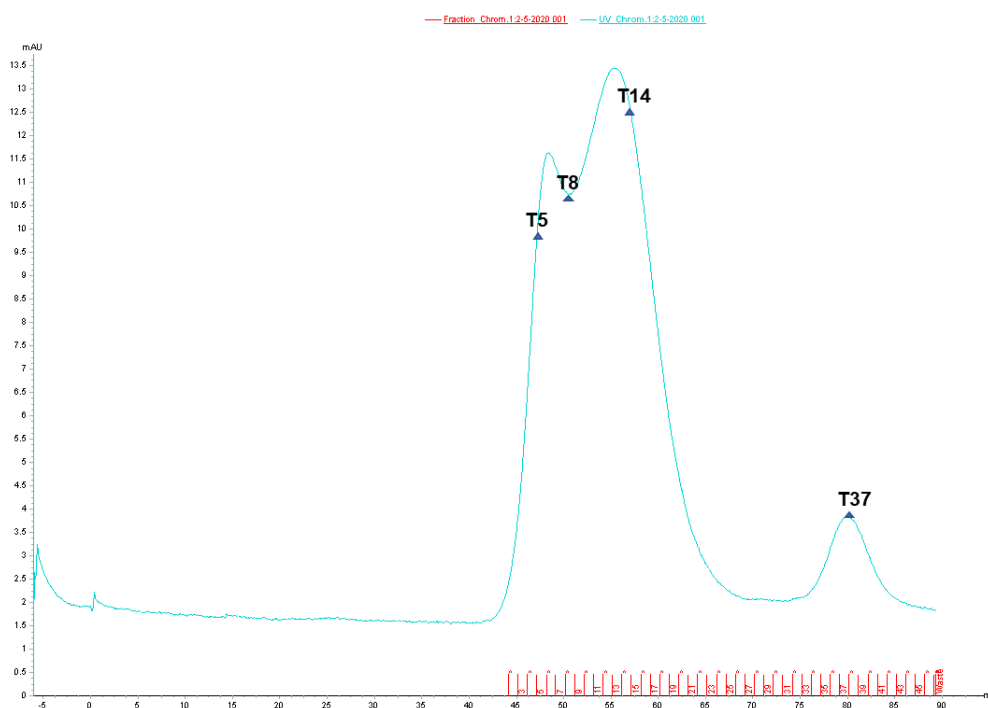


Figure S2 Mass spectrum for truncated NDM-1 obtained under conventional condition

a



b

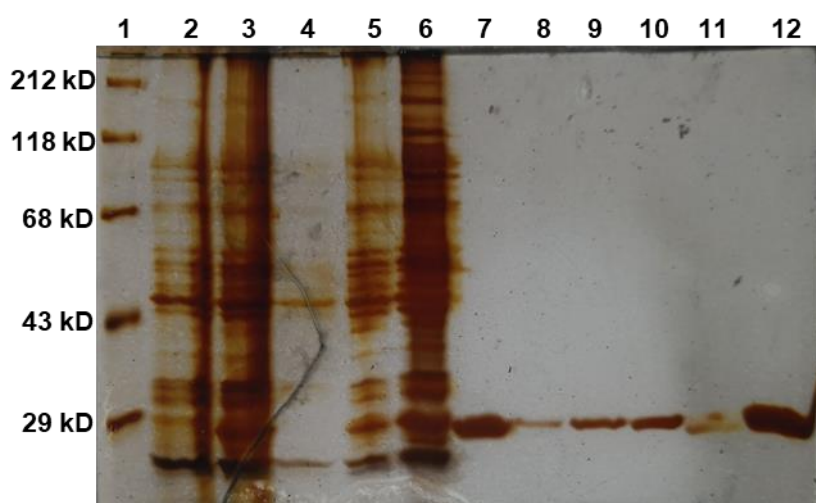


Figure S3 a. Absorption curves of wild-type NDM-1 purified by size-exclusion chromatograph; b. SDS-PAGE of wild-type NDM-1. b: 1. protein maker; 2. bacterial pellet (LB media); 3. bacterial pellet (LB media containing 0.5 mM IPTG); 4. bacterial pellet (LB media containing 0.5 mM ZnSO₄); 5. bacterial pellet (LB media containing 0.5 mM IPTG and 0.5 mM ZnSO₄); 6. supernatant before Ni-NTA; 7. eluate of 300 to 500 mM imidazole; 8. T5 in a; 9. T8 in a; 10. T14 in a; 11. T37 in a; 12. wild-type NDM-1(purified protein from last time)^{f9}

^{f9} The SDS-gel of the wild-type NDM-1 was prepared under the guidance of Silke Bergemann.

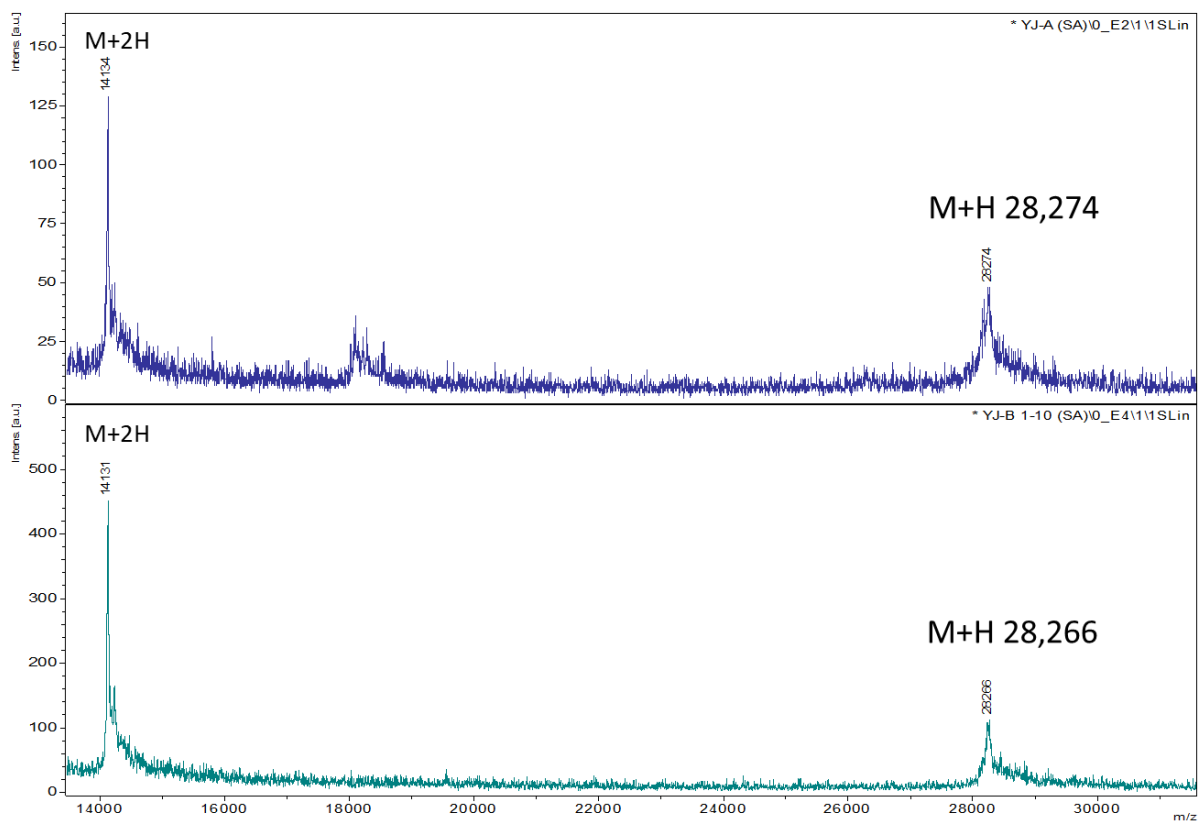


Figure S4 Mass spectra for wild-type NDM-1 obtained under conventional condition (The deep blue spectrum was for the soluble wild-type NDM-1 sample; the green spectrum was for a precipitated wild-type NDM-1 sample)^{f10}

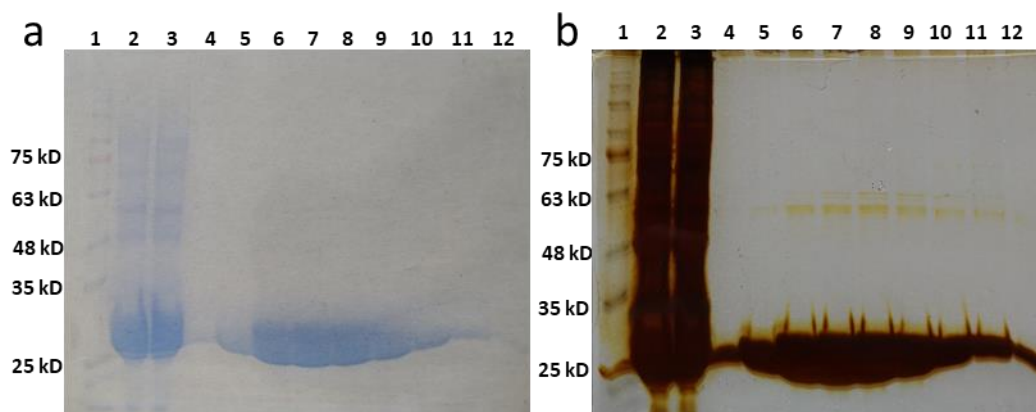


Figure S5 SDS-PAGE of IMP-1. a: 1. protein marker; 2. supernatant before CM-Sepharose column; 3. filtrate after CM-Sepharose column; 4. eluate with 100 mM NaCl; 5. eluate with 150 mM NaCl; 6. eluate with 200 mM NaCl (A); 7. eluate with 200 mM NaCl (B); 8. eluate with 250 mM NaCl (A); 9. eluate with 250 mM NaCl (B); 10. eluate with 300 mM NaCl (A); 11. eluate with 300 mM NaCl (B); 12. eluate with 500 mM NaCl. b. silver stain of a.

^{f10} Dr. Christoph Weise, Bernhard Wuest and Eleonore Christmann helped to measure the mass spectra of the prepared protein samples for the wild-type NDM-1.

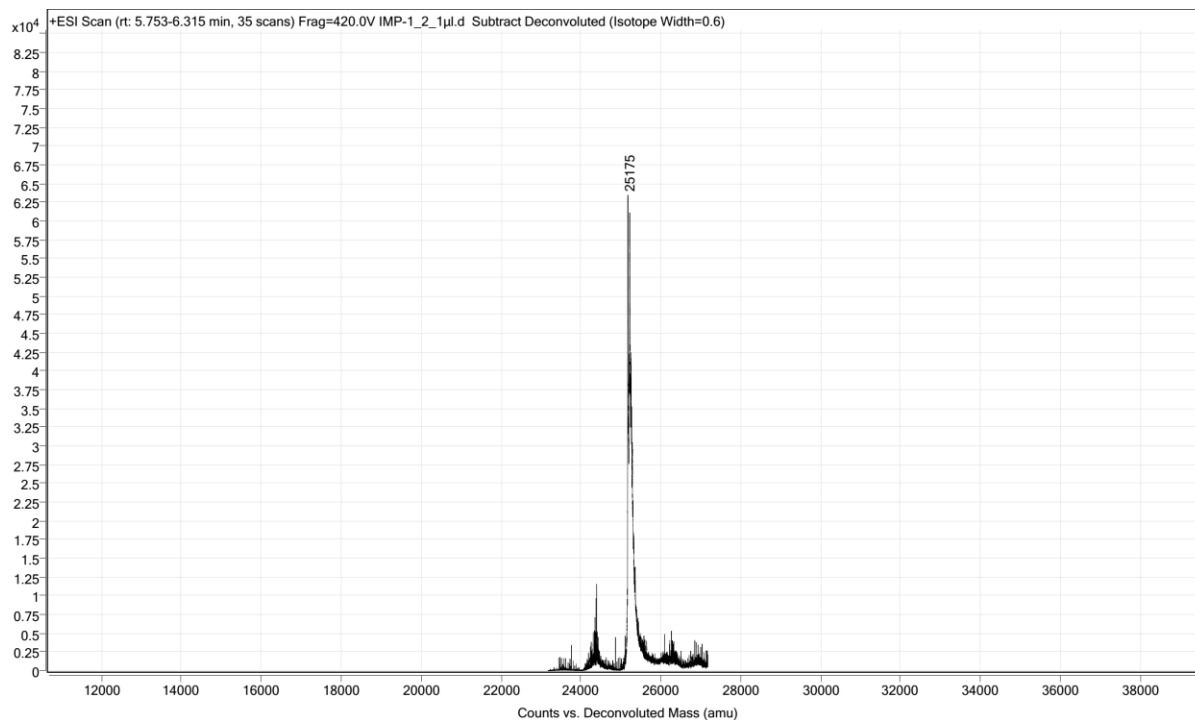
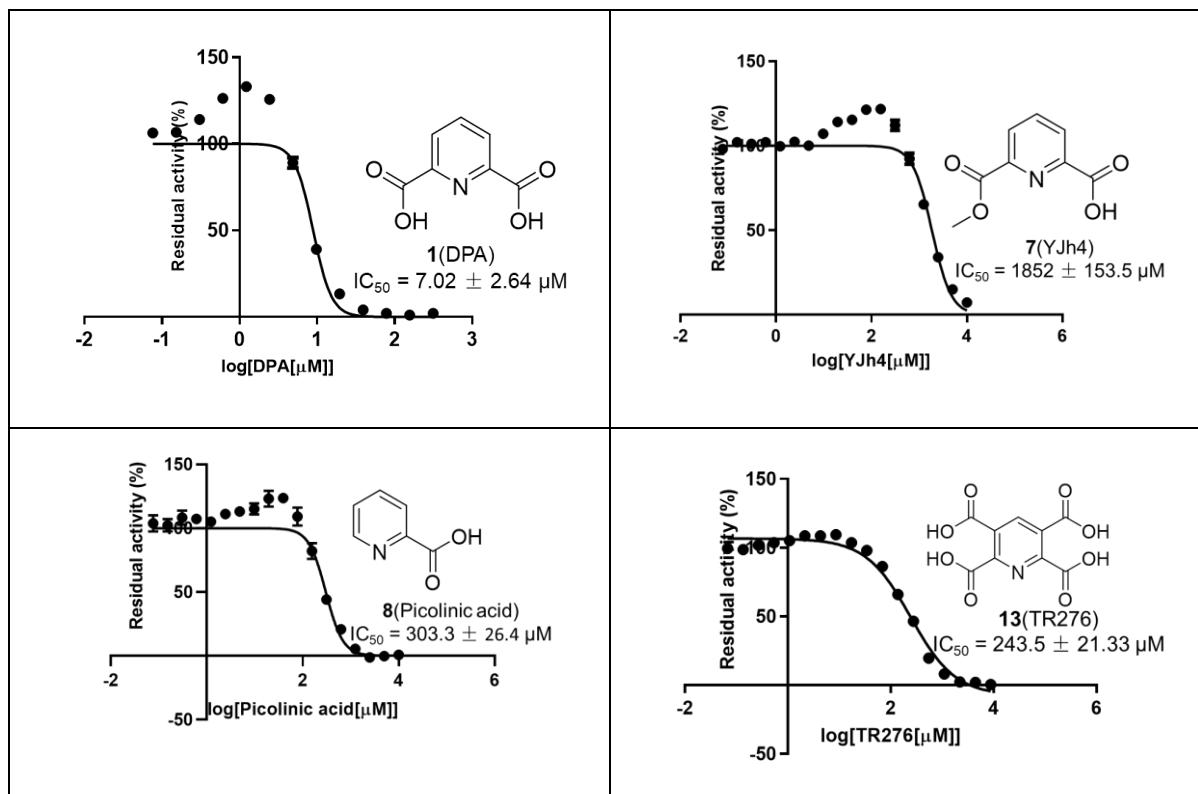
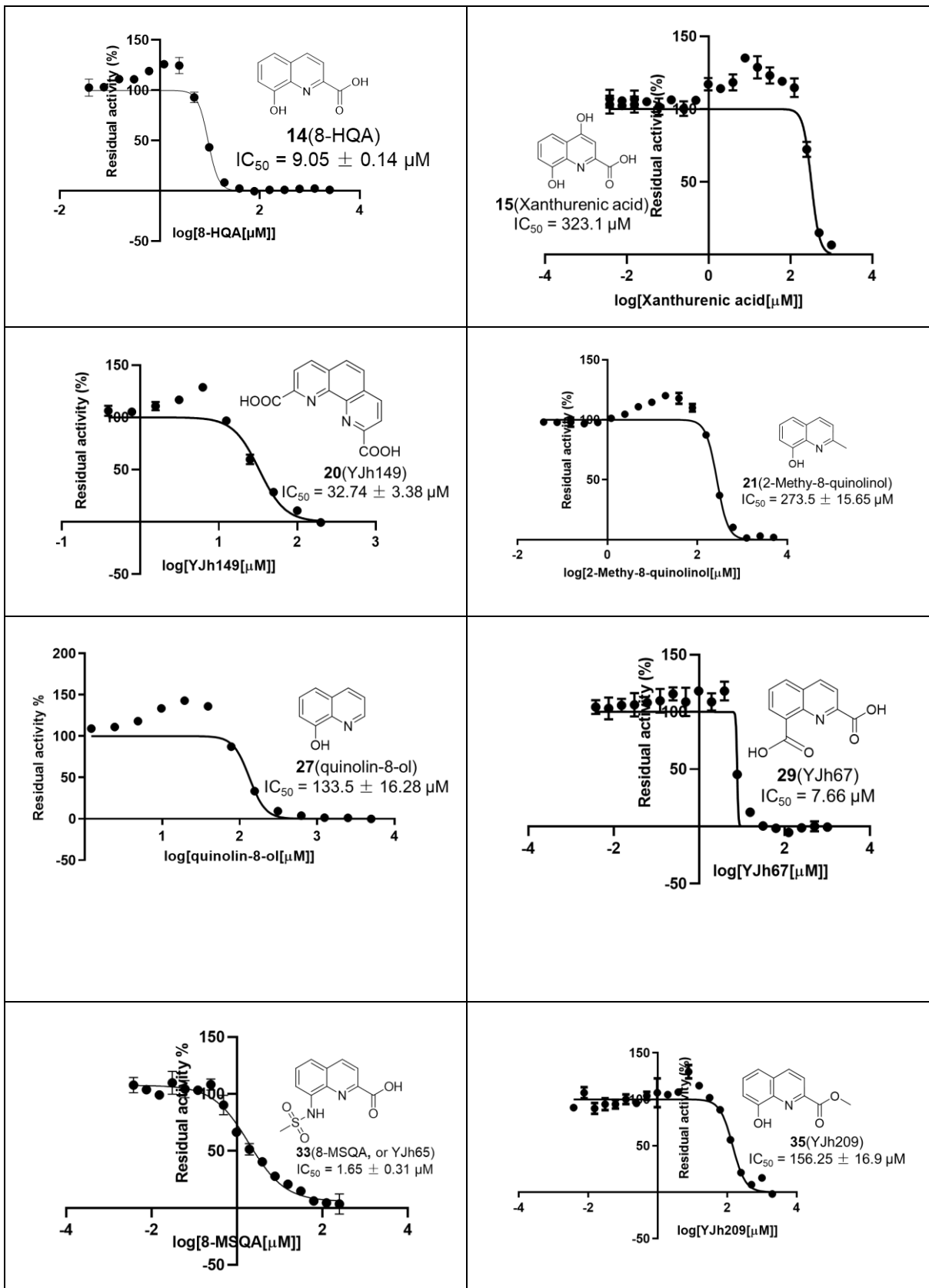


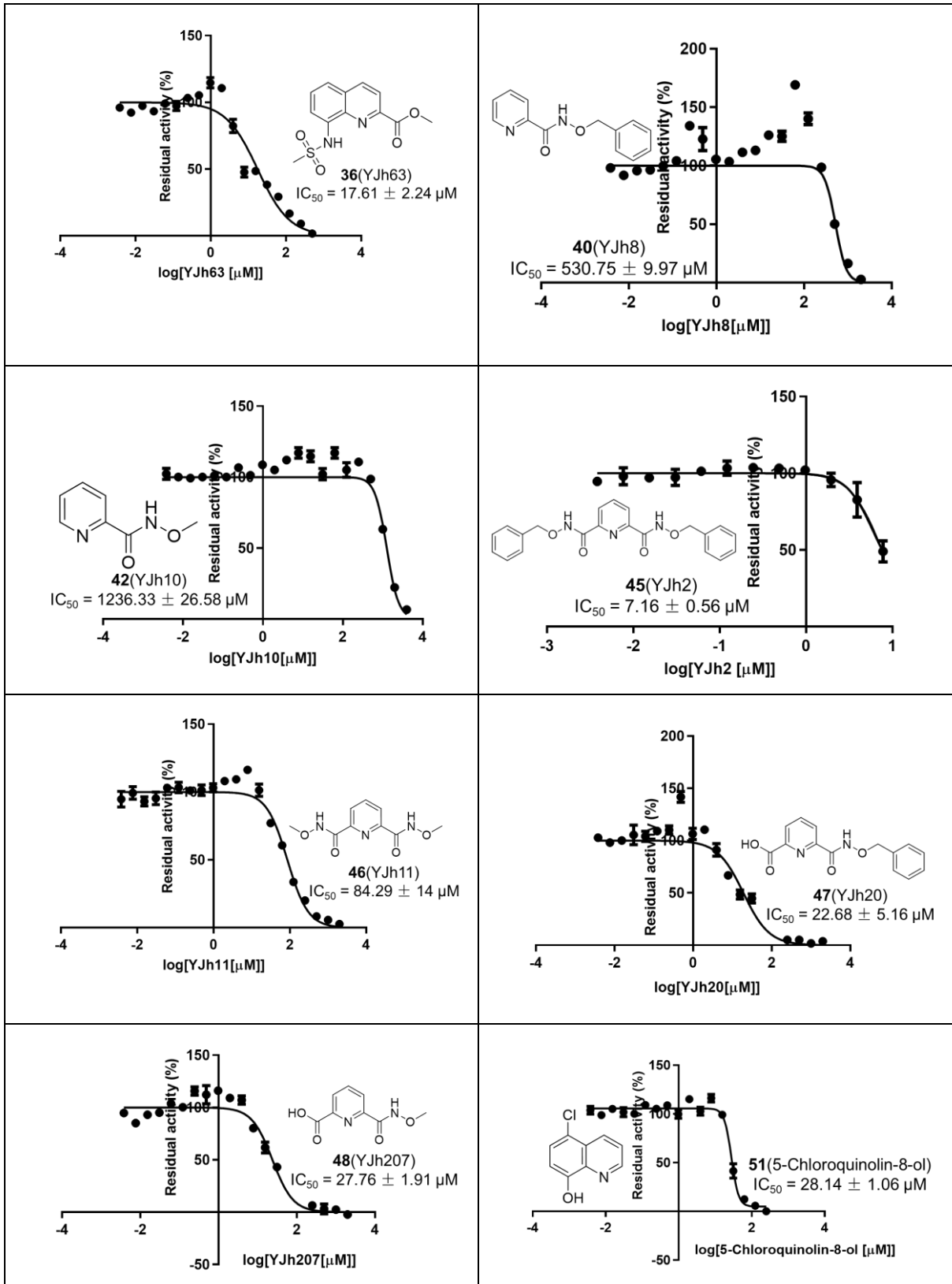
Figure S6 Mass spectrum for wild-type IMP-1 obtained under denaturing condition ^{f11}

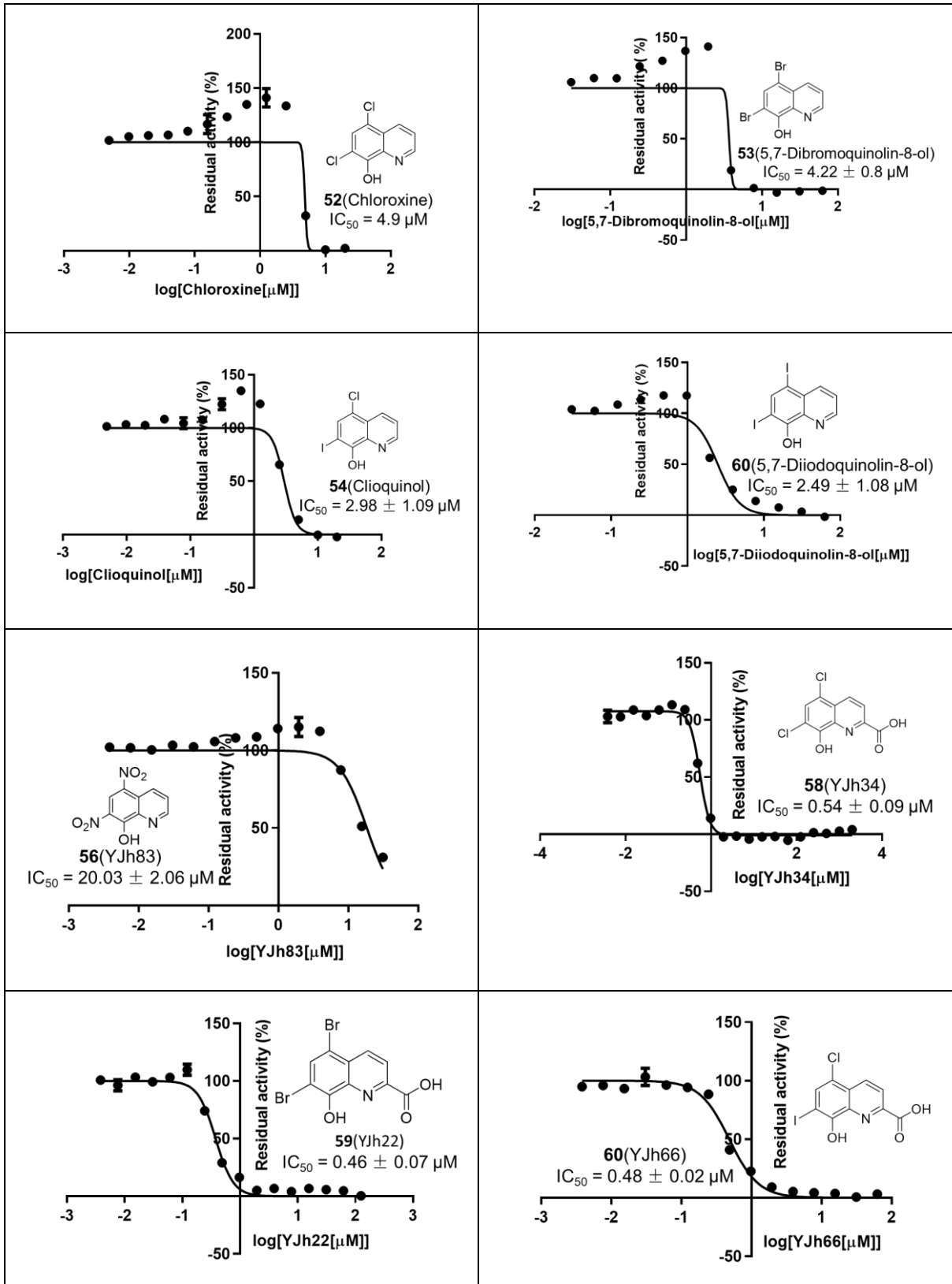
Table S2a IC₅₀ Curves of the Developed Inhibitors for NDM-1

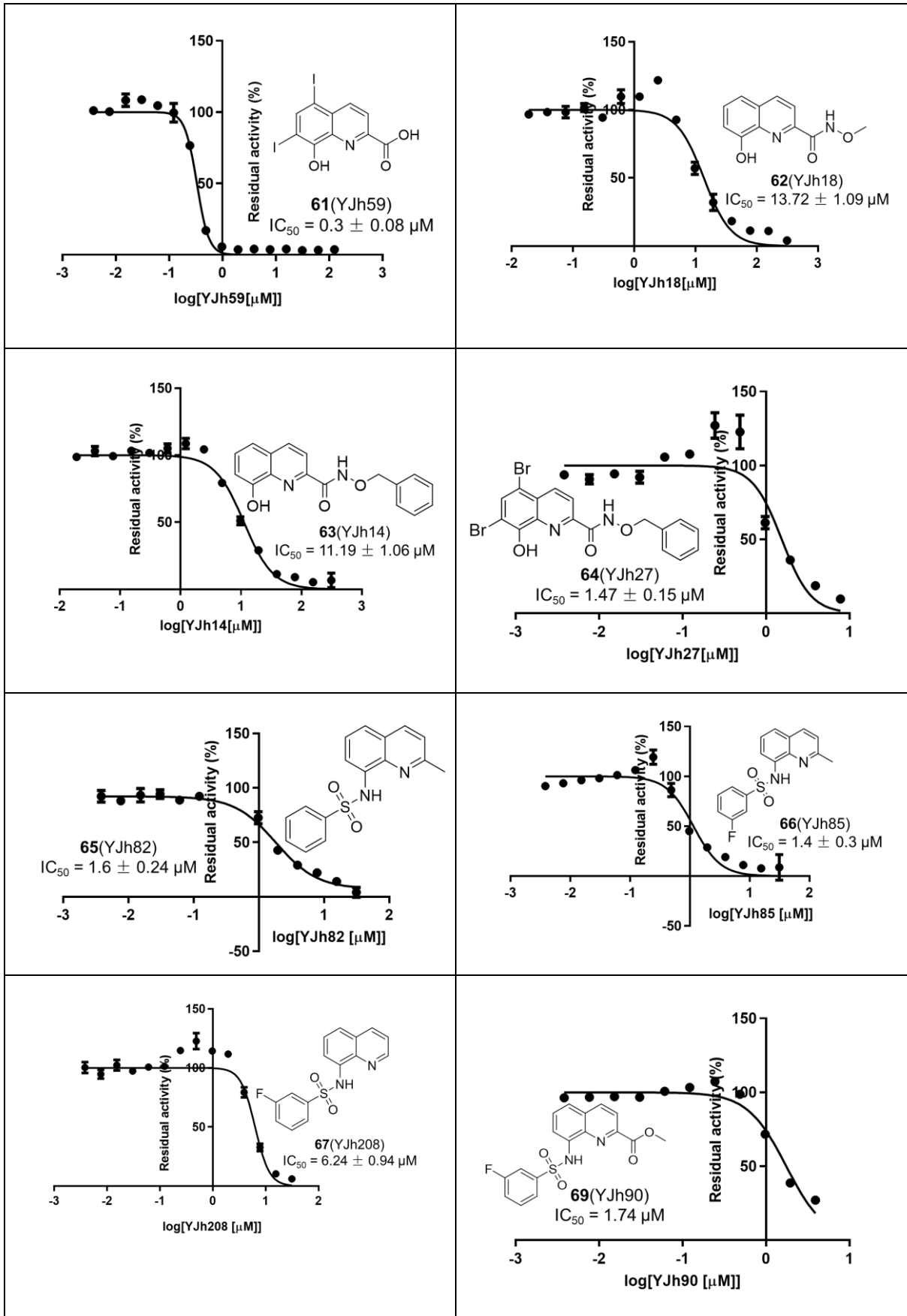


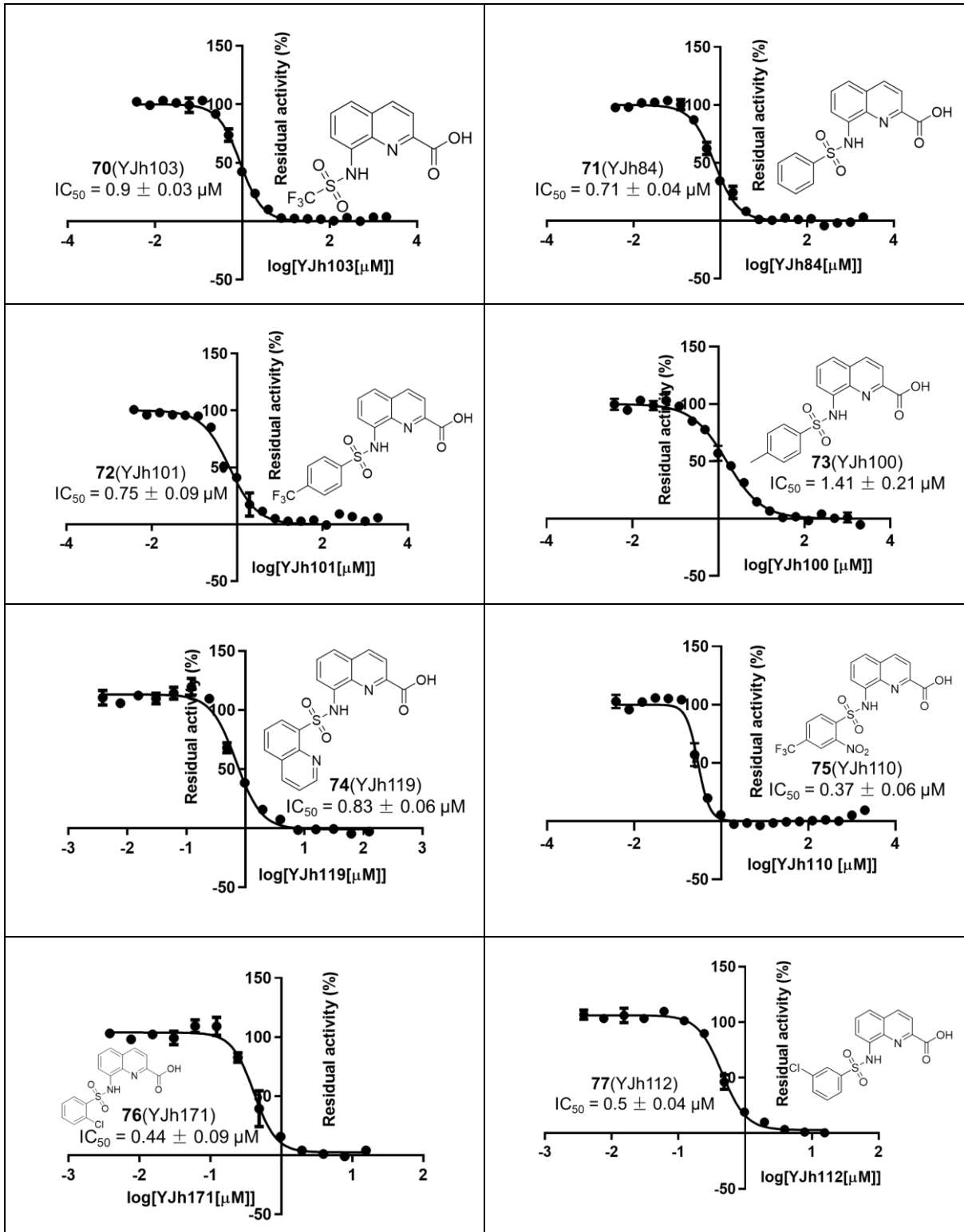
^{f11} Eleonore Christmann helped to measure the mass spectrum of the prepared sample for IMP-1.

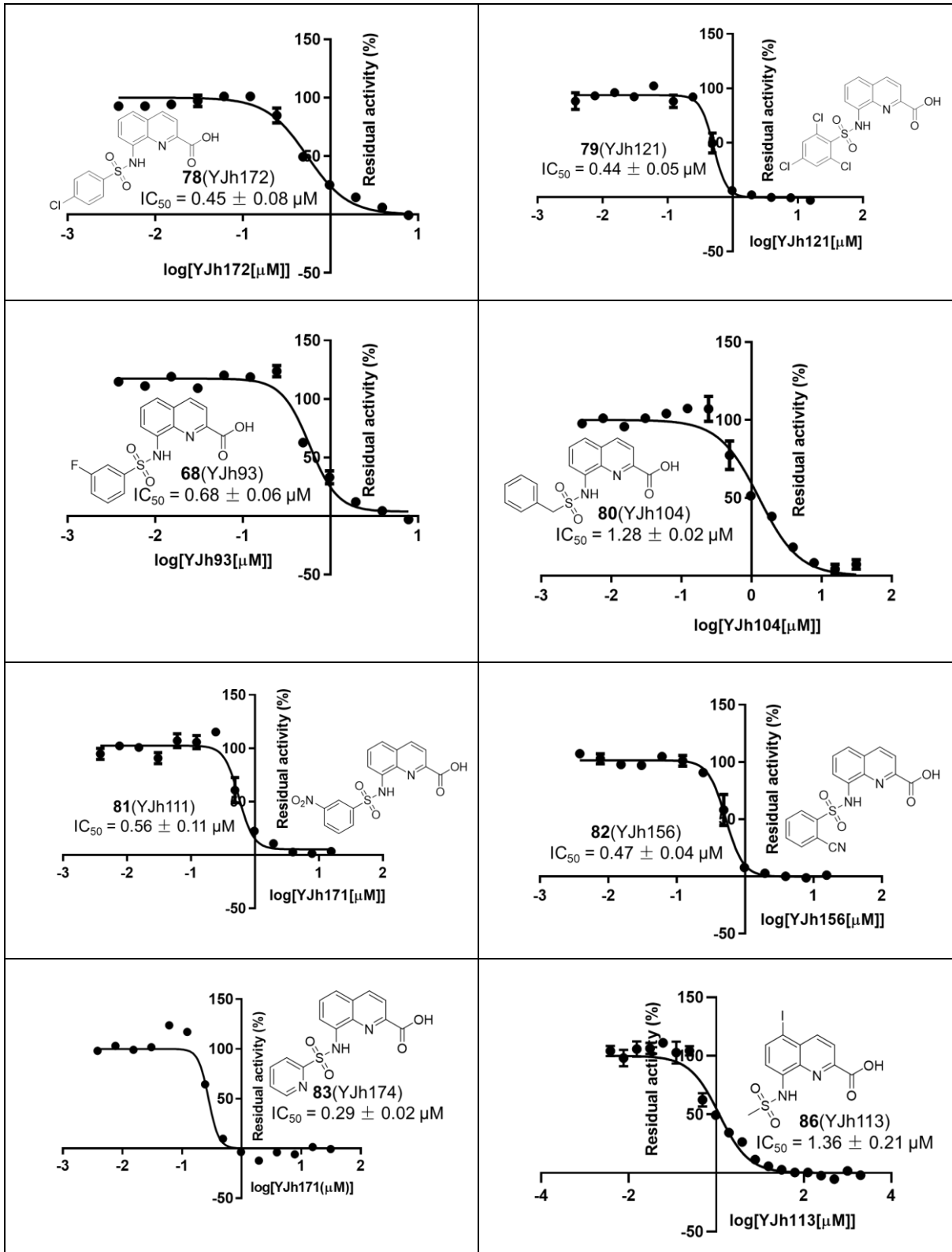


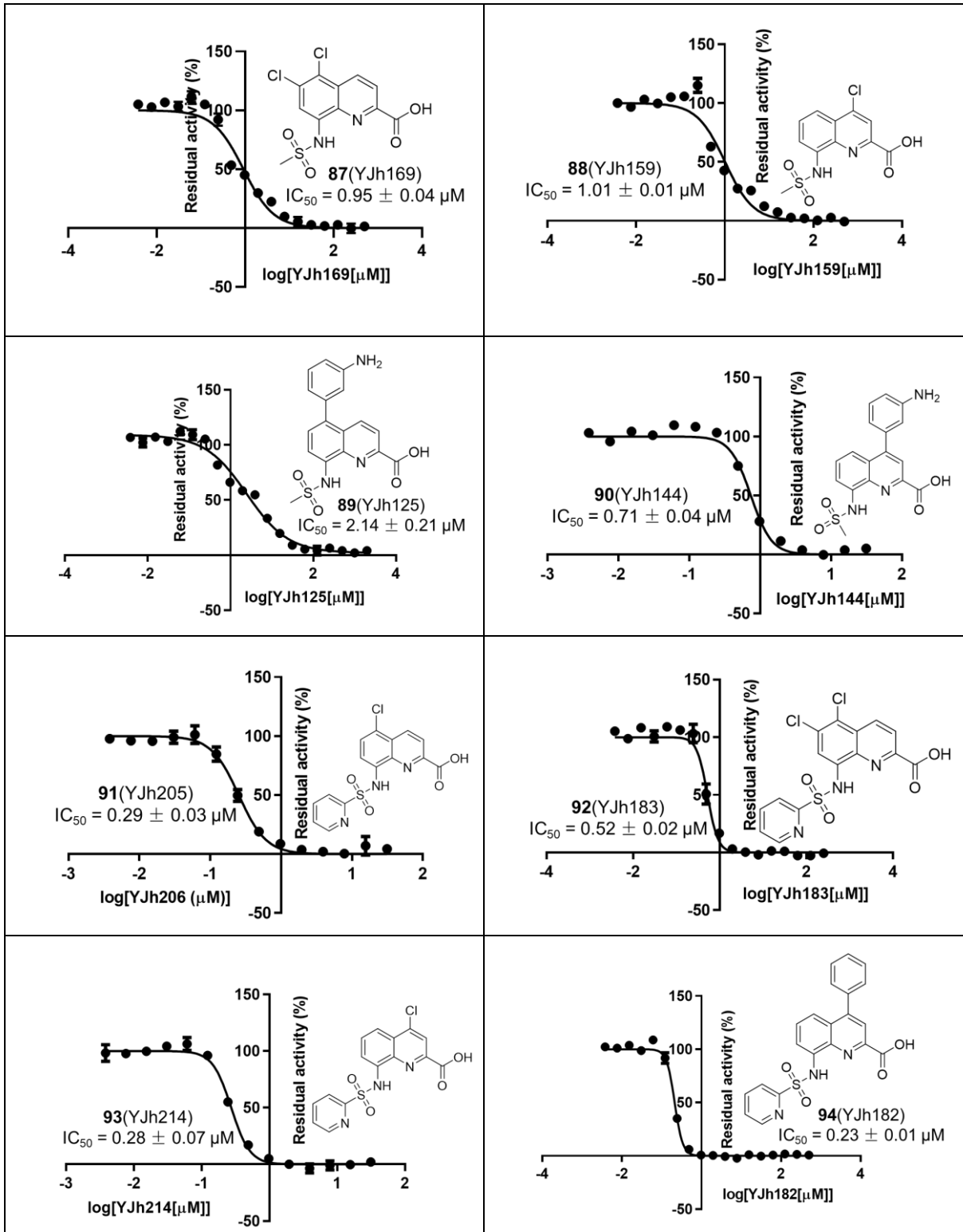












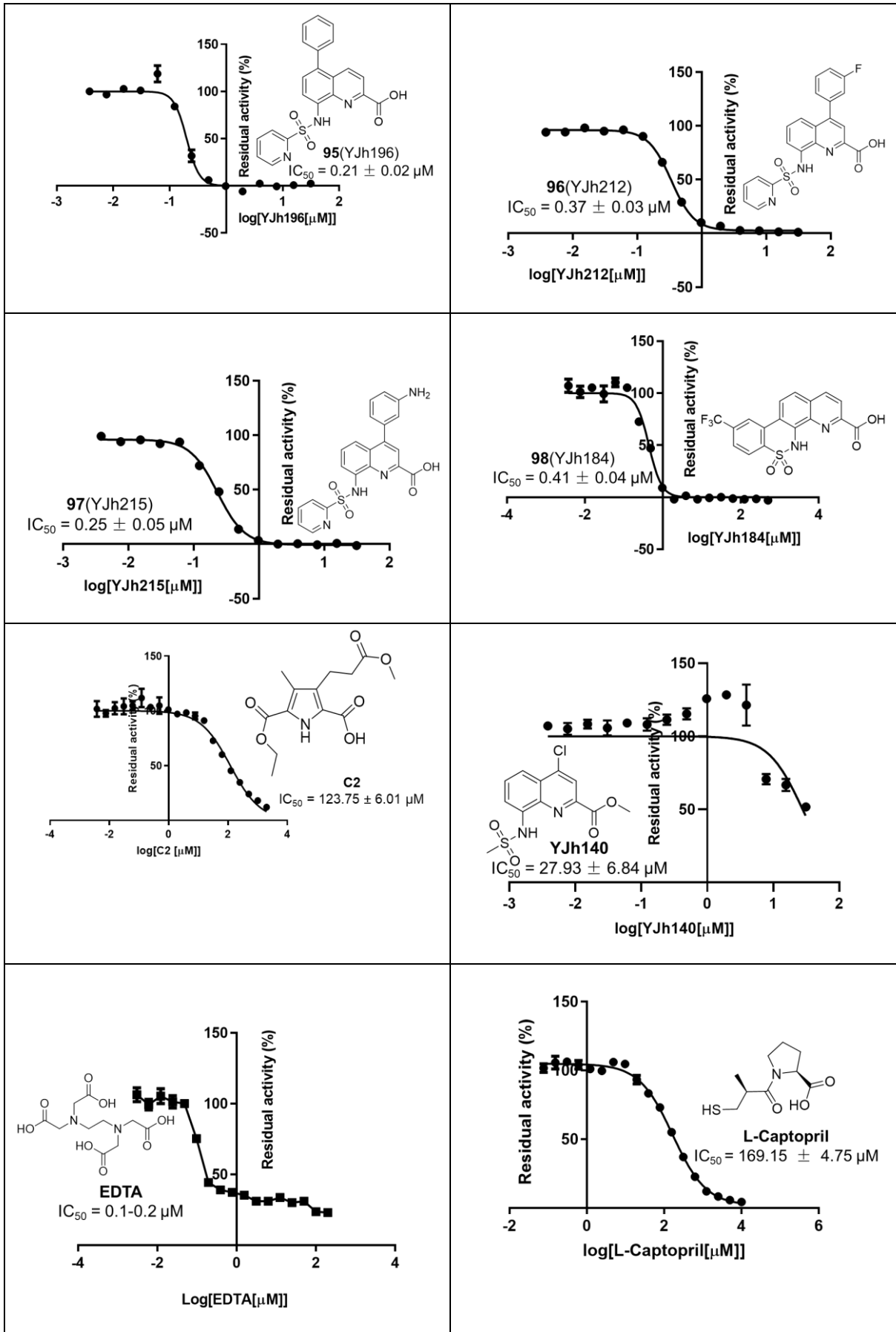
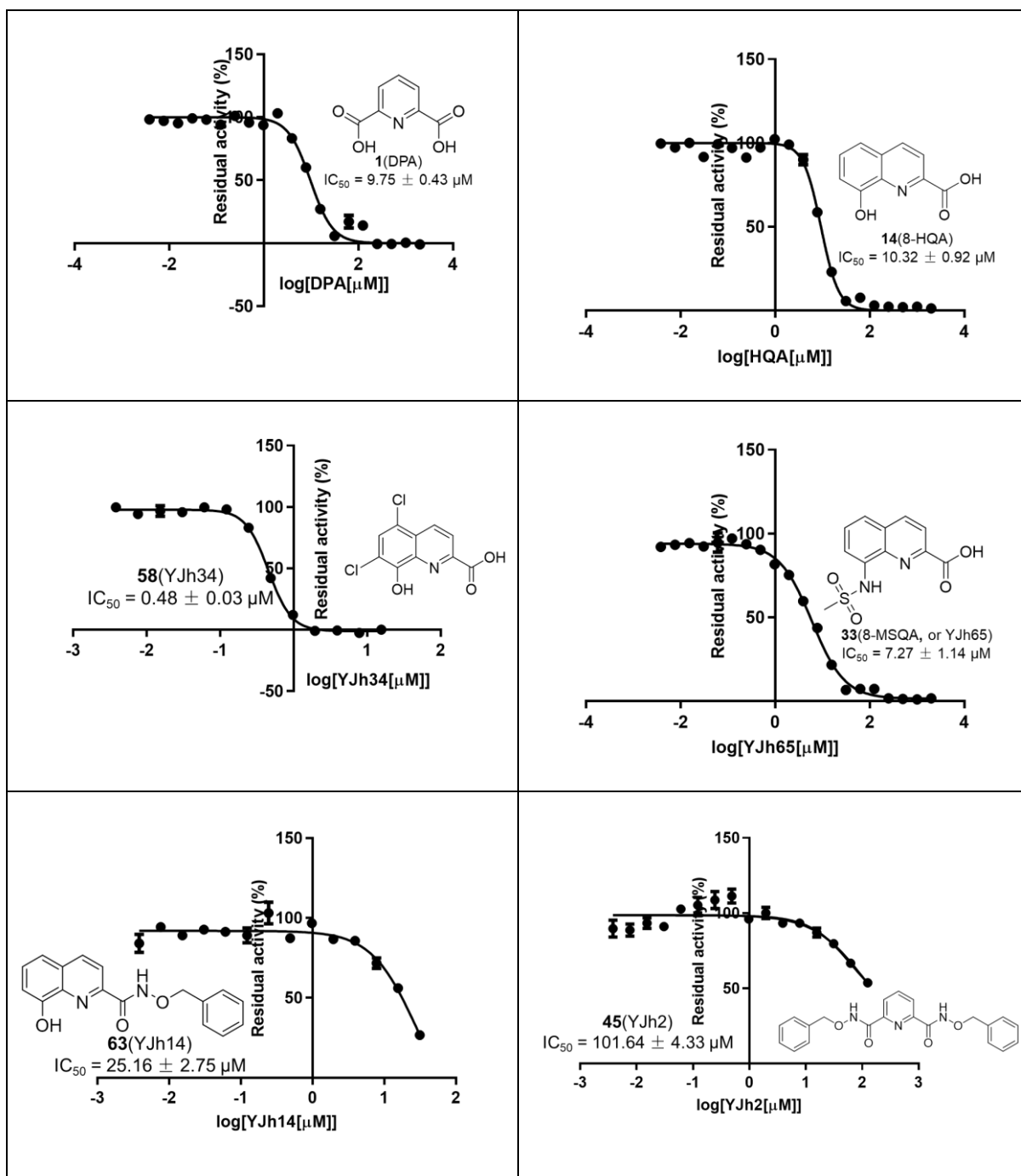


Table S2b IC₅₀ Curves of the Selected Inhibitors for IMP-1



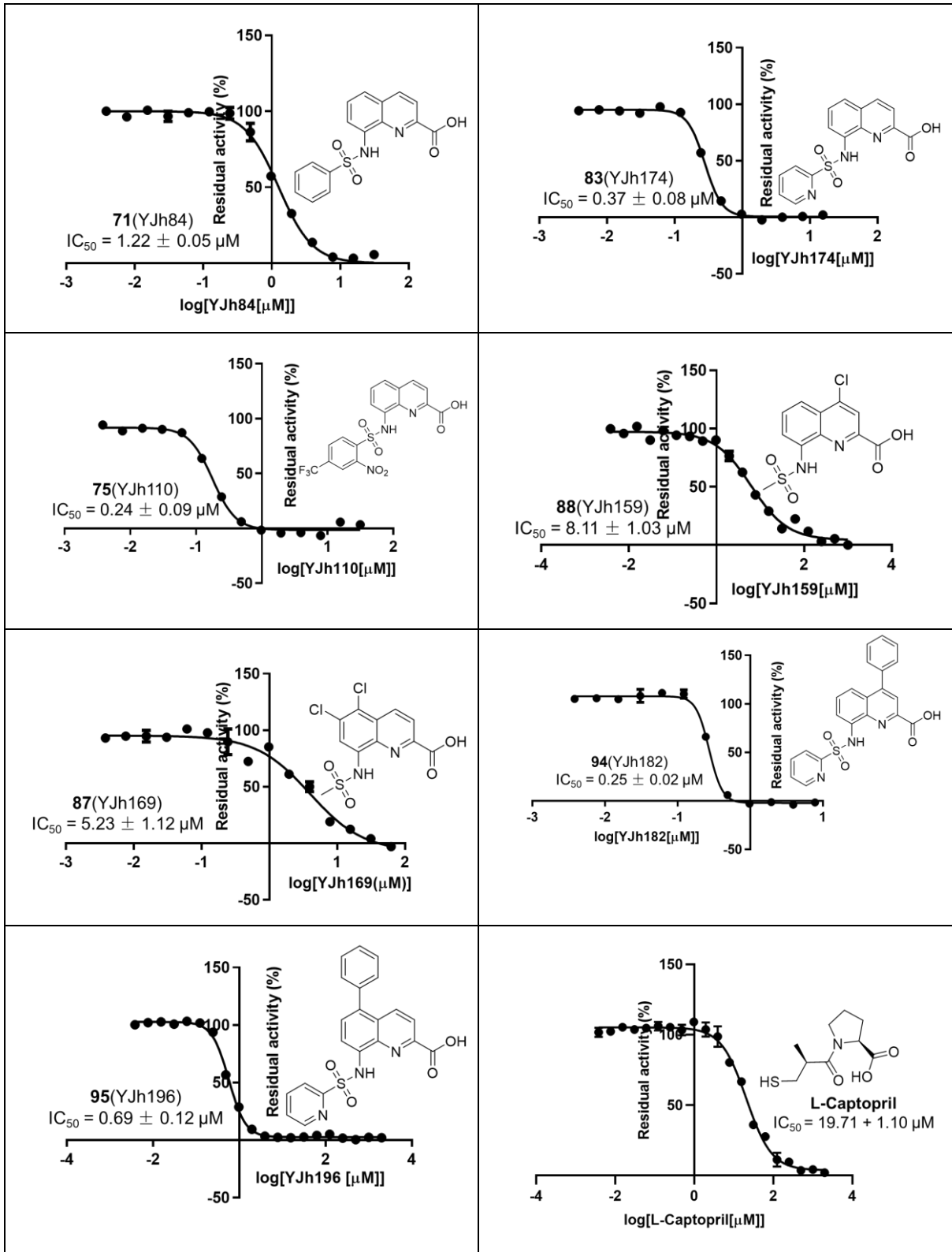
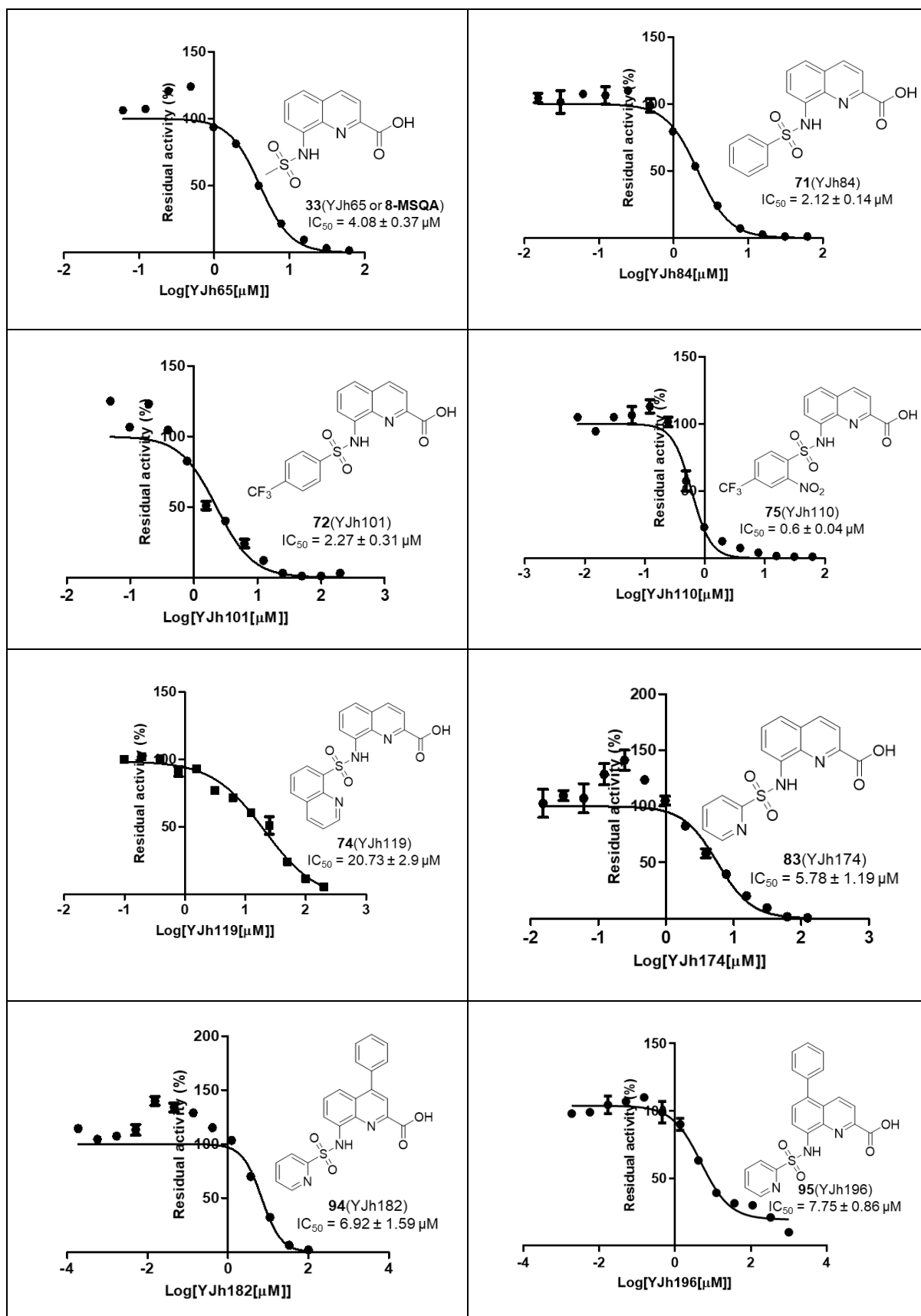
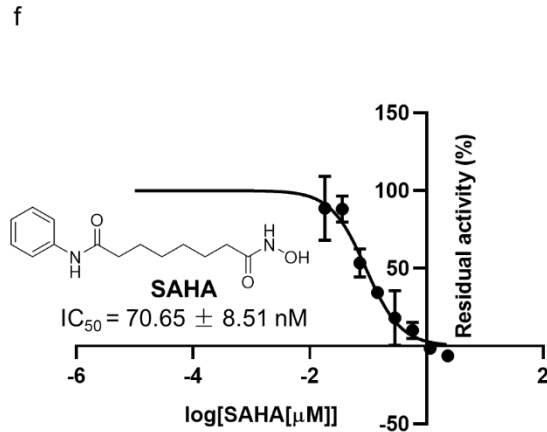
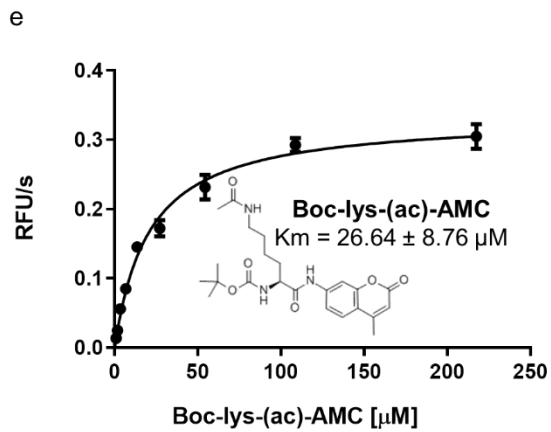
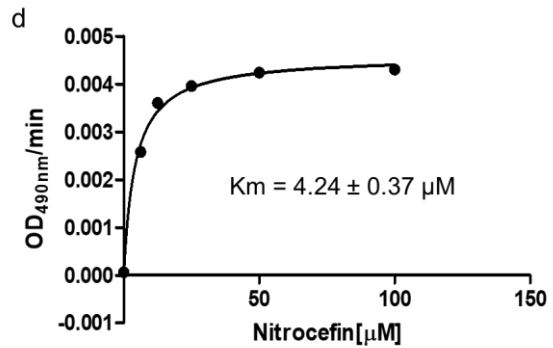
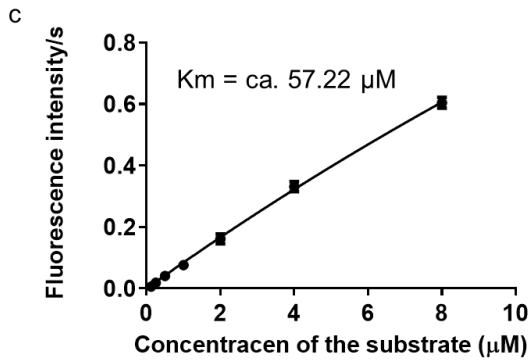
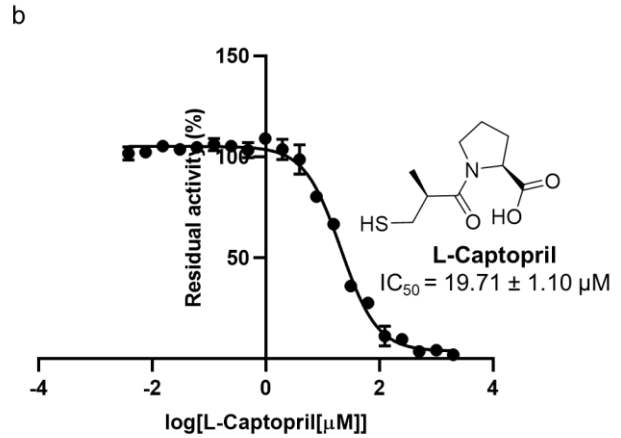
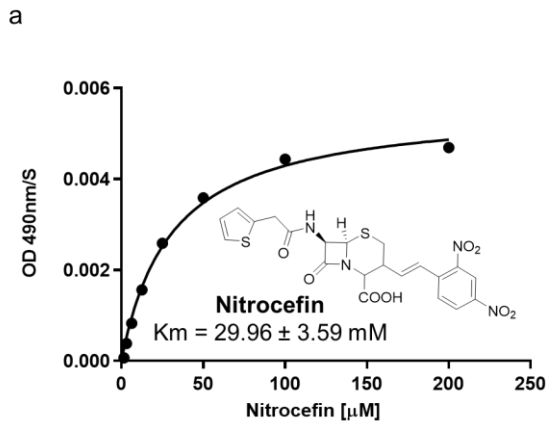
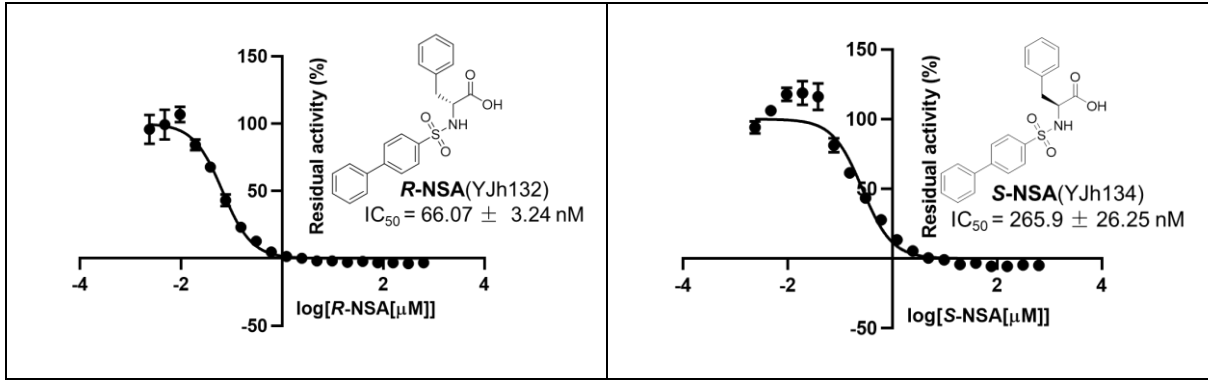


Table S2c IC₅₀ Curves of the Selected Inhibitors for MMP-2





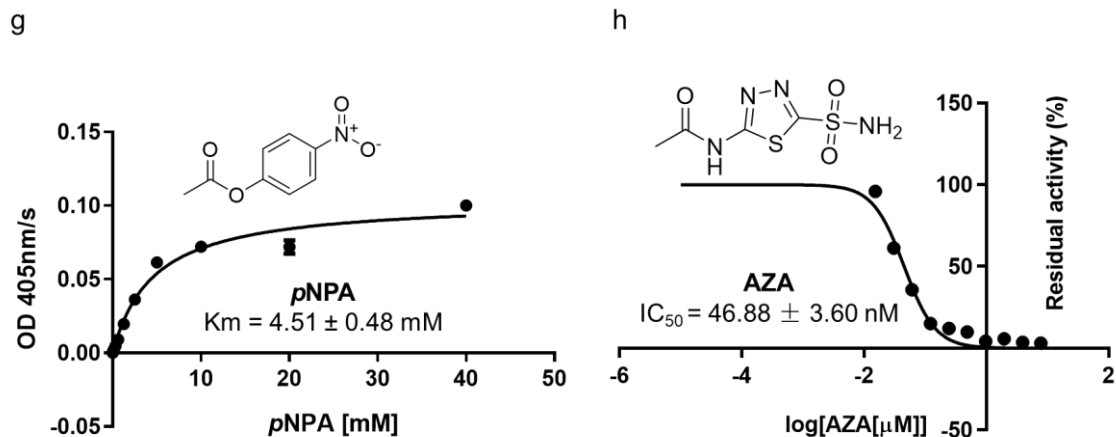
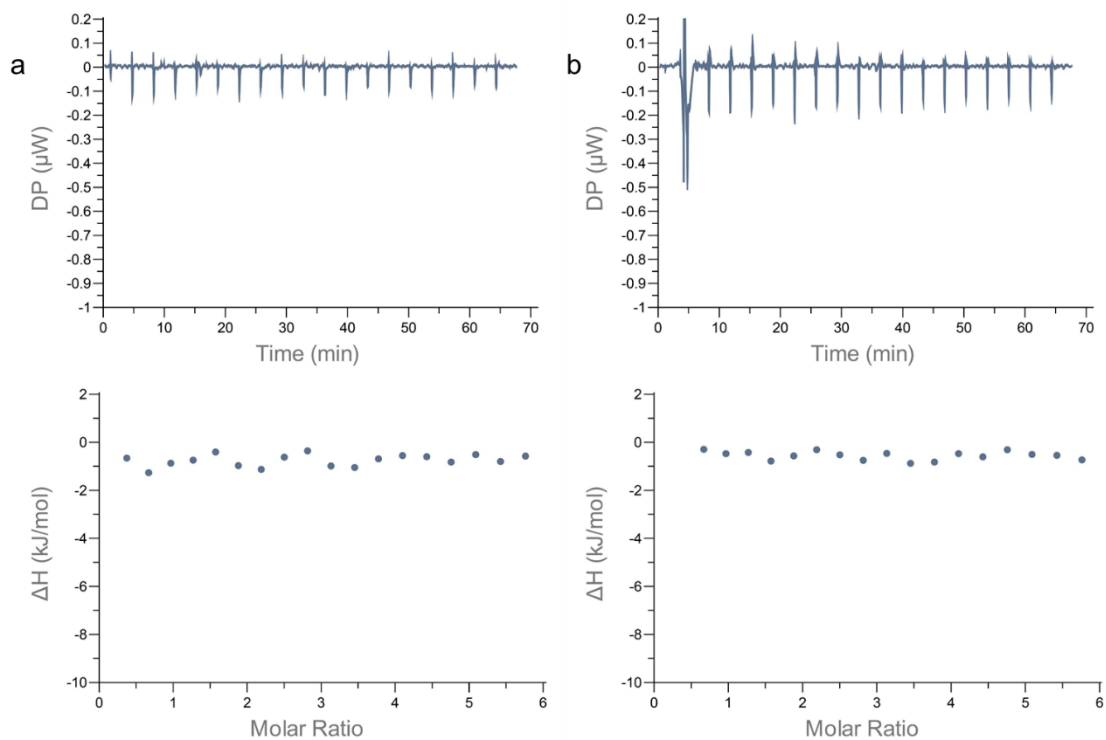


Figure S7 *In vitro* enzyme-based assays of the selected metalloenzymes. a. The K_m of nitrocefin for IMP-1; b. The IC_{50} curve of L-captopril for IMP-1; c. The K_m of the OMNIMMP® fluorogenic substrate for MMP-2; d. The K_m of nitrocefin for NDM-1 without zinc ions in the assay buffer; e. The K_m of the BOC-lys-(ac)-AMC for HDAC-1; f. The IC_{50} curve of SAHA for HDAC-1; g. The K_m of pNPA for hCAII; h. The IC_{50} curve of AZA for hCAII. All the measurements were performed in triplicate, and the obtained values were averaged.



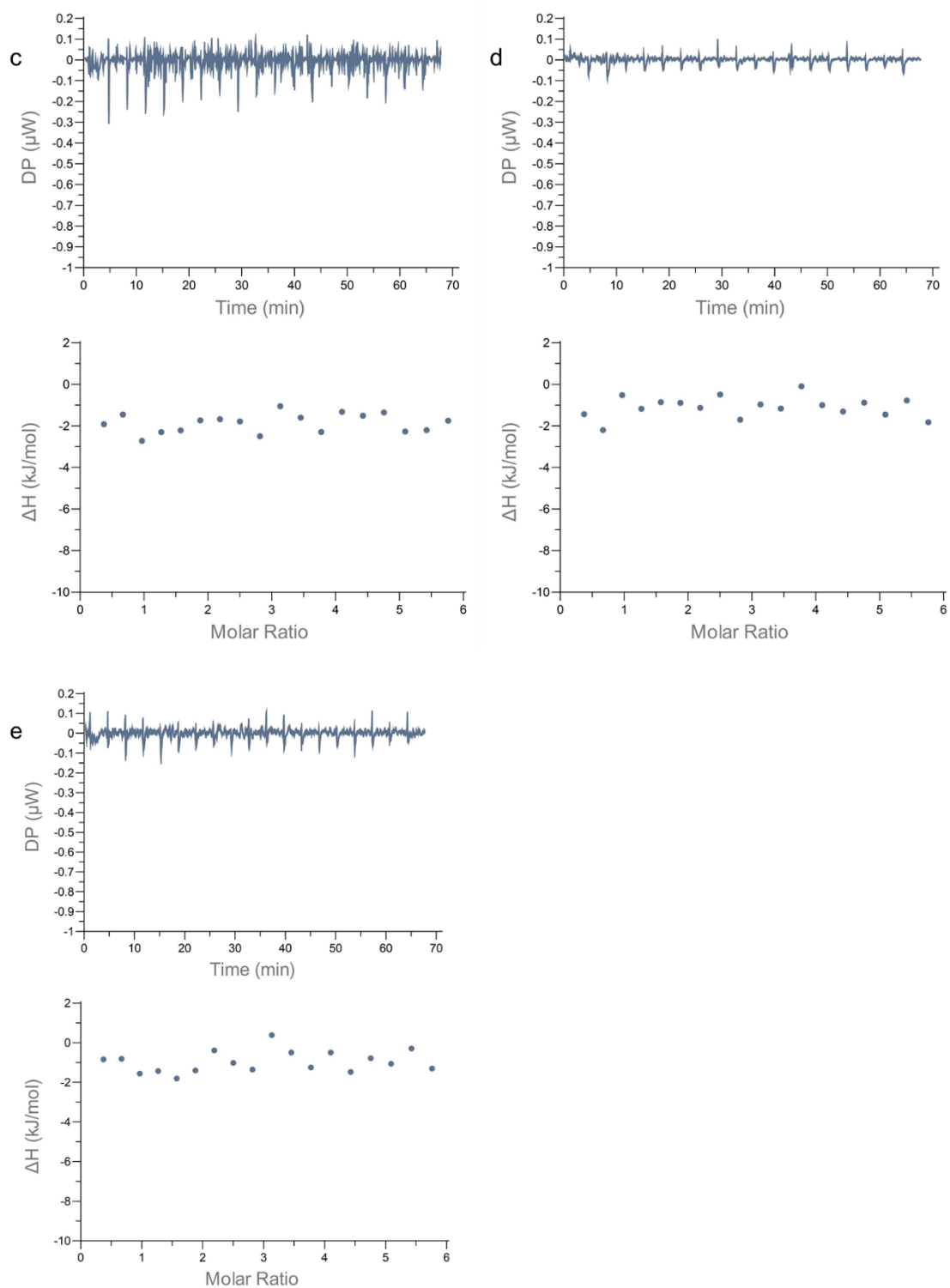
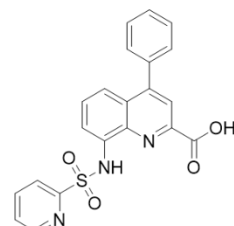
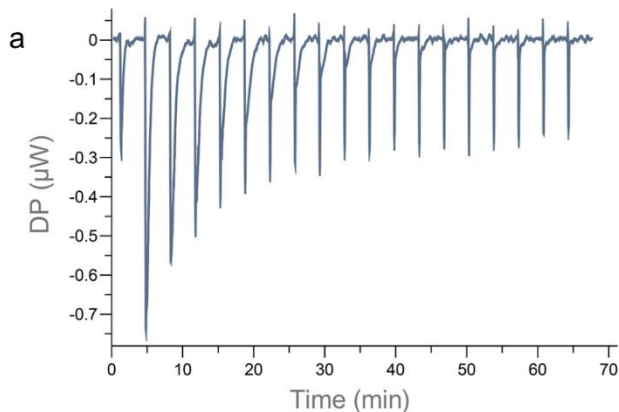


Figure S8 Thermograms of ITC assays for relevant control groups (Inhibitor titrating NDM-1 using truncated NDM-1). a. Assay buffer to assay buffer; b. Assay buffer to NDM-1; c. Compound **94**(YJh182) to assay buffer; d. Compound **95** (YJh196) to assay buffer; e. Compound **83**(YJh174) to assay buffer.

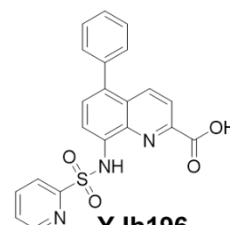
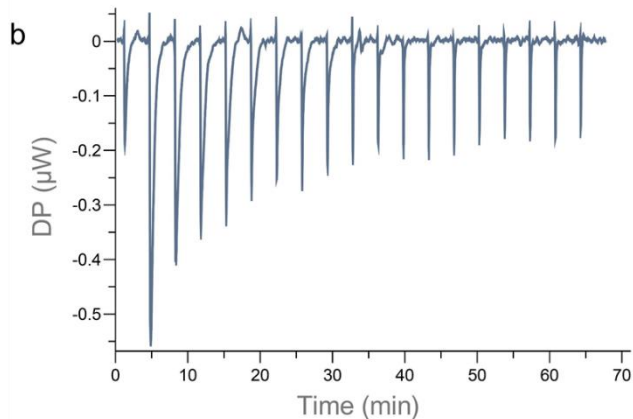
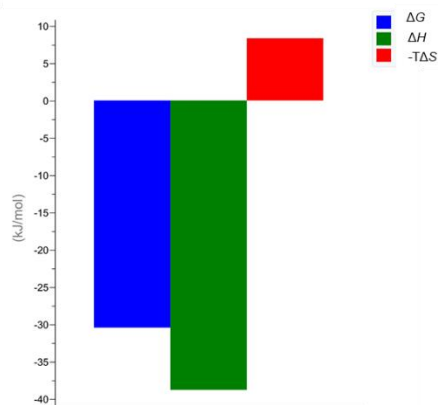
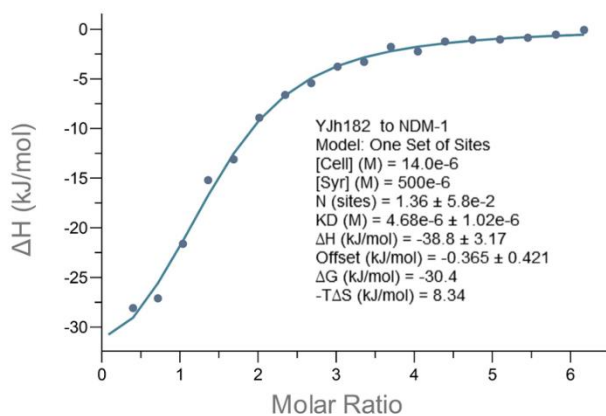


YJh182

$\text{IC}_{50} = 0.23 \pm 0.01 \mu\text{M}$

$\text{KD} = 4.68 \pm 1.02 \mu\text{M}$

$\text{N (sites)} = 1.36 \pm 0.058$

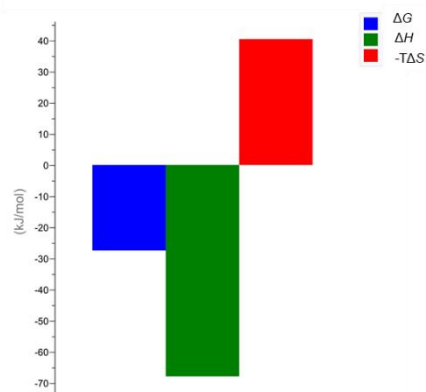
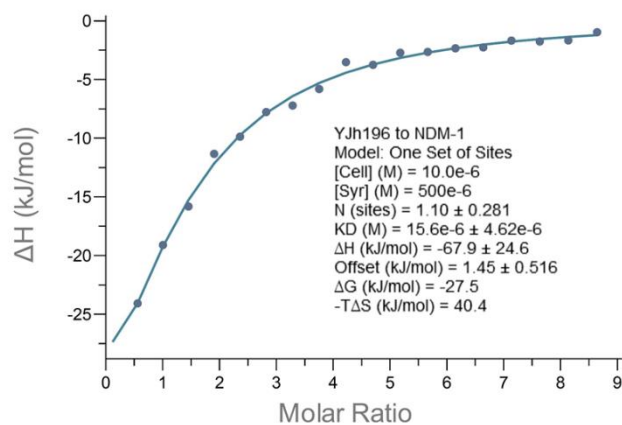


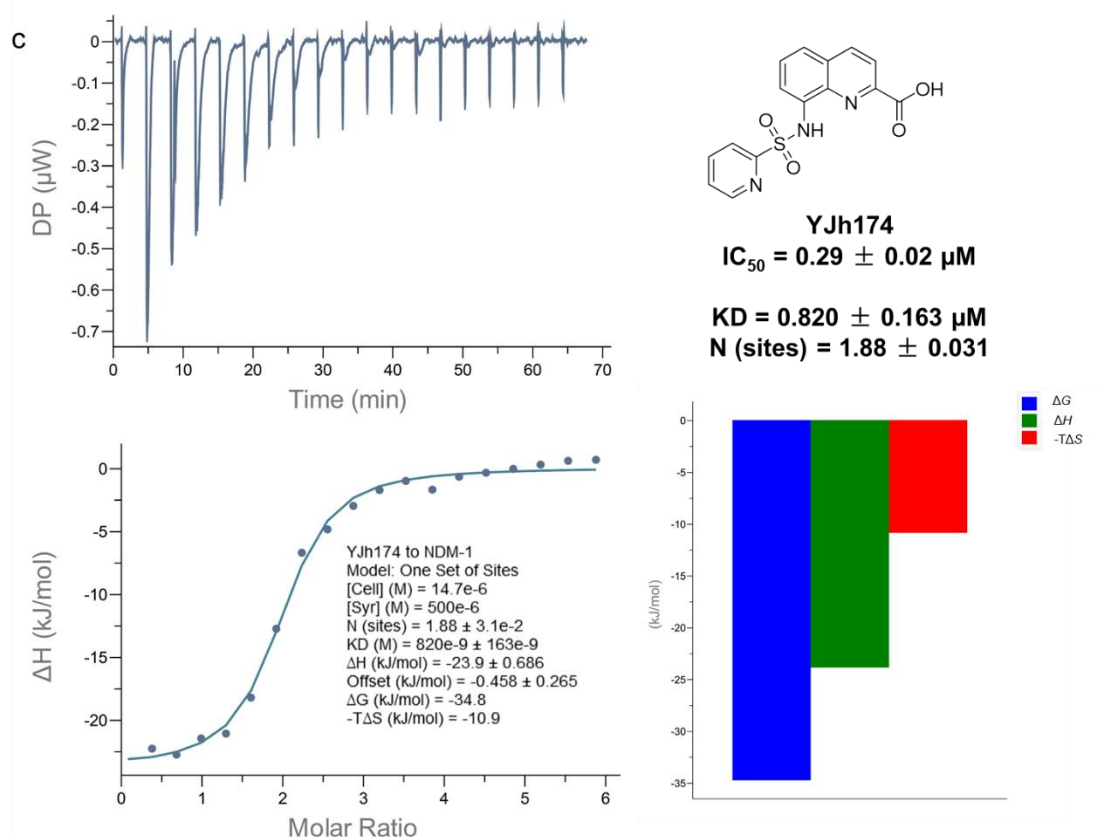
YJh196

$\text{IC}_{50} = 0.21 \pm 0.02 \mu\text{M}$

$\text{KD} = 15.6 \pm 4.62 \mu\text{M}$

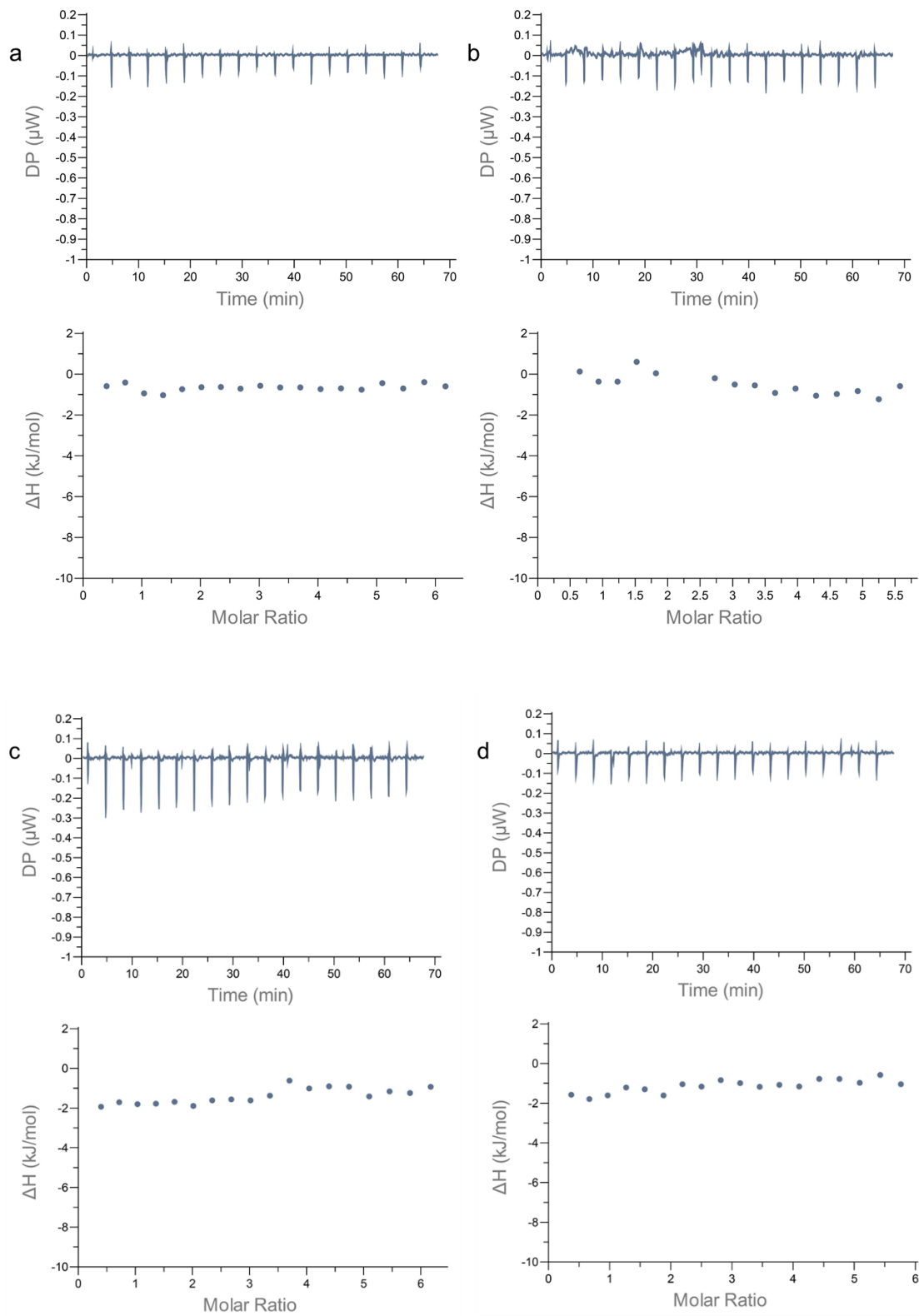
$\text{N (sites)} = 1.10 \pm 0.281$





^{a1} The K_d values obtained using the truncated NDM-1 were near to the K_i values calculated from the IC_{50} values than using the full-length NDM-1, the reason might come from the different stability of the truncated and the full-length NDM-1 at high concentrations. Although the K_d values were better by using the truncated NDM-1, the activity trends were kept.

Figure S9 Thermograms of ITC assays (Inhibitor titrating NDM-1 using full-length NDM-1) a. Compound **94**(YJh182) to NDM-1; b. Compound **95**(YJh196) to NDM-1; c. Compound **83**(YJh174) to NDM-1.



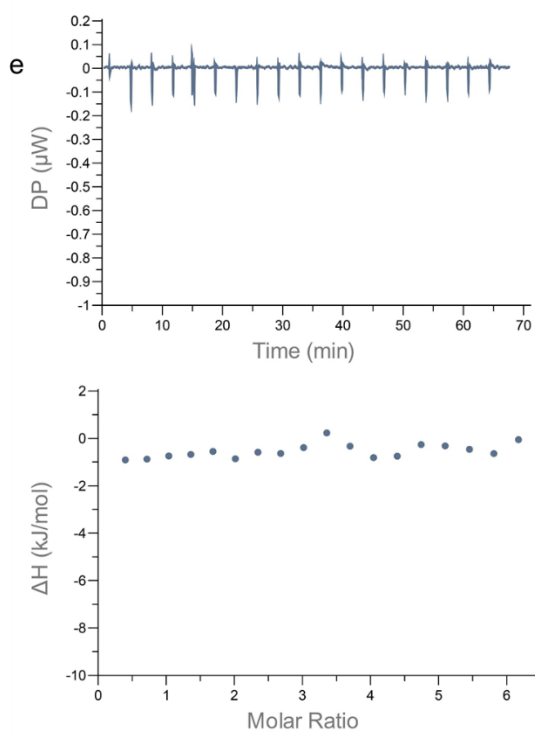
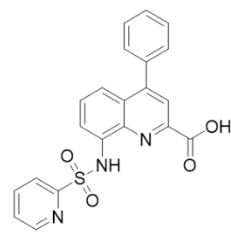
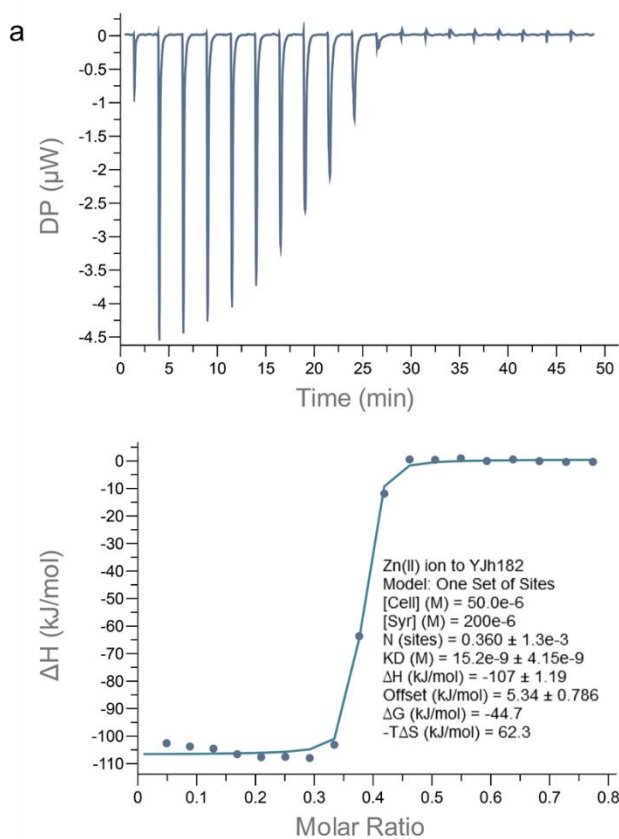
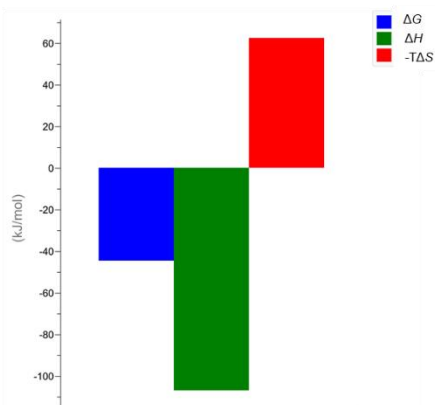
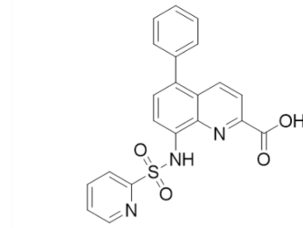
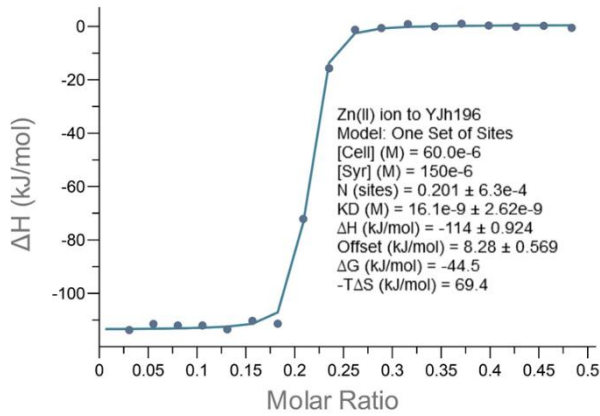
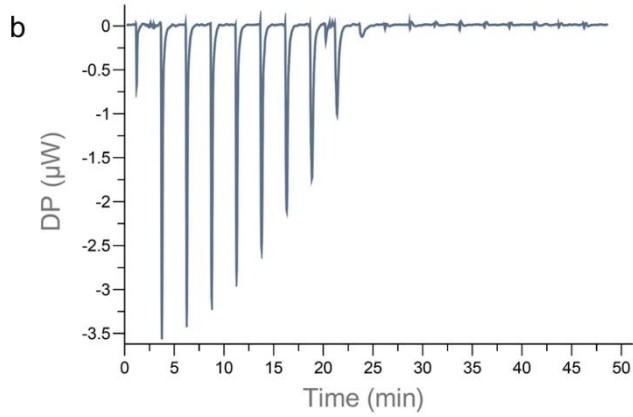


Figure S10 Thermograms of ITC assays for relevant control groups (Inhibitor titrating NDM-1 using full-length NDM-1). a. Assay buffer to assay buffer; b. Assay buffer to NDM-1; c. Compound **94(YJh182)** to assay buffer; d. Compound **95(YJh196)** to assay buffer; e. Compound **83(YJh174)** to assay buffer.

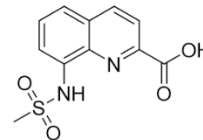
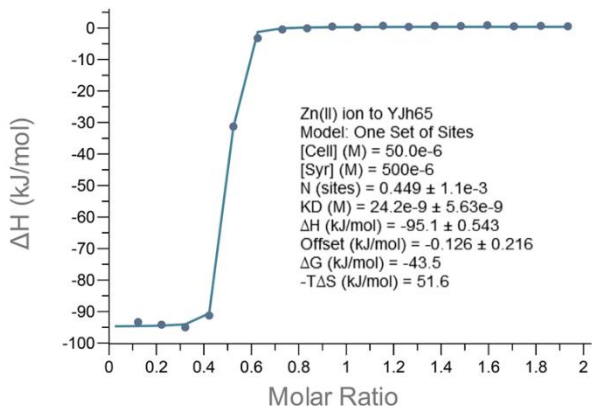
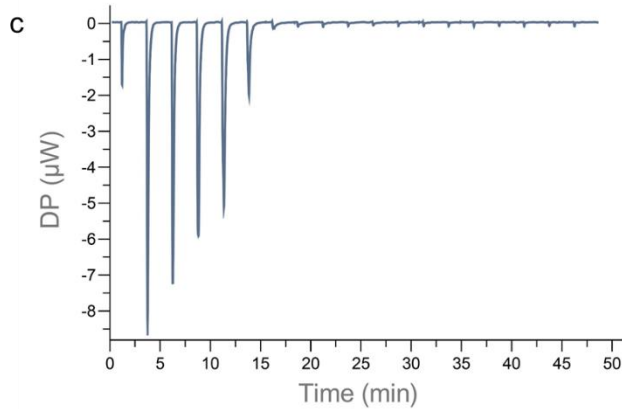
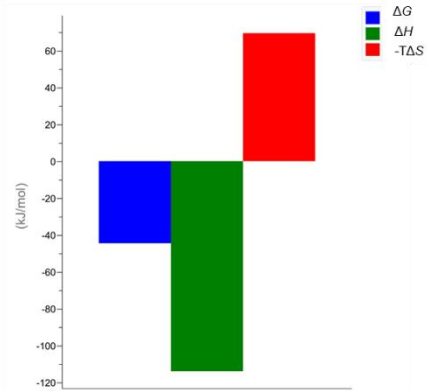


YJh182
 $K_d = 15.2 \pm 4.15 \text{ nM}$
 $N \text{ (sites)} = 0.360 \pm 0.001$

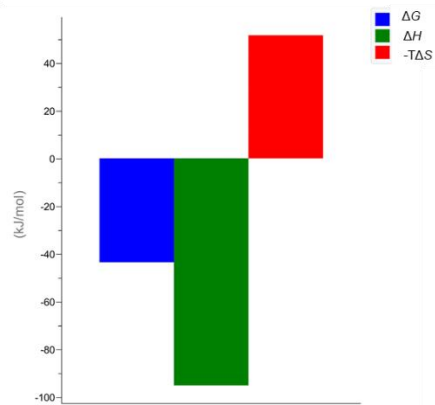


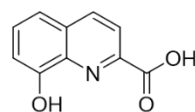
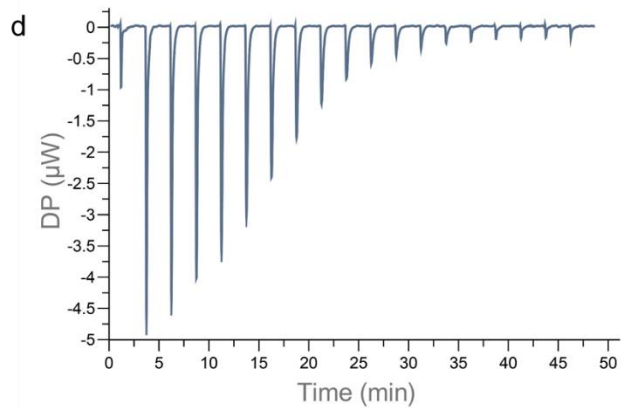


YJh196
 $K_d = 16.1 \pm 2.62 \text{ nM}$
 $N \text{ (sites)} = 0.201 \pm 0.001$

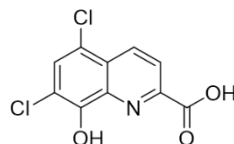
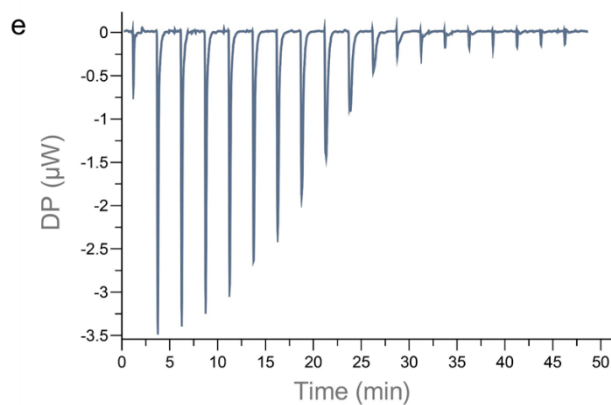
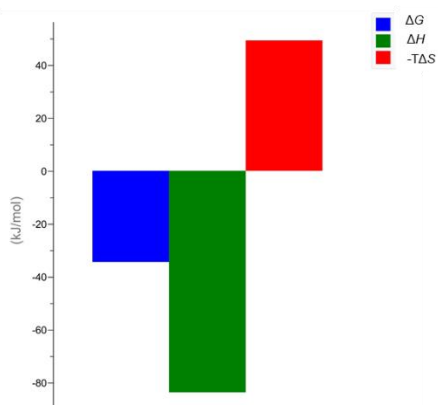
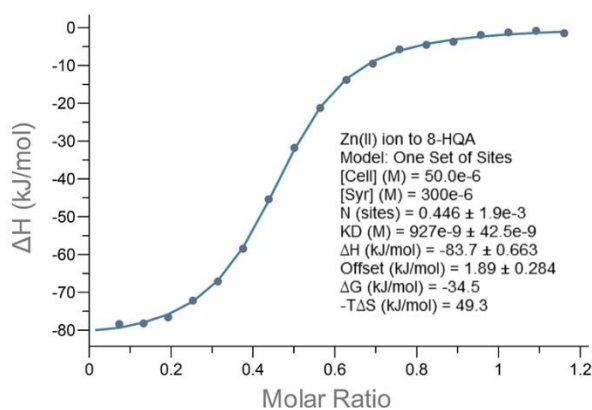


YJh65
 $K_d = 24.2 \pm 5.63 \text{ nM}$
 $N \text{ (sites)} = 0.449 \pm 0.001$

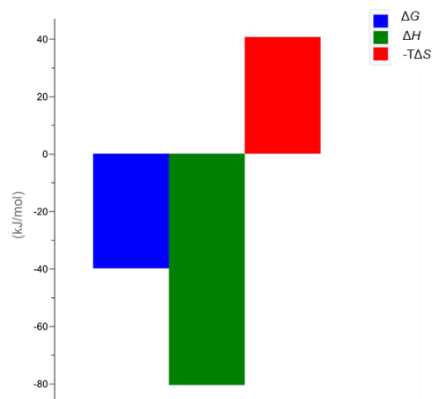
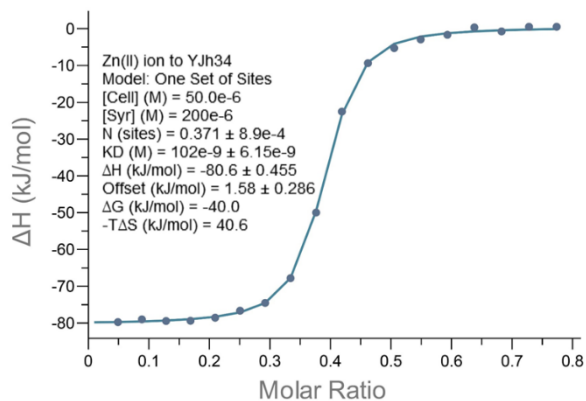




8-HQA
 $K_d = 927 \pm 42.5 \text{ nM}$
 $N (\text{sites}) = 0.446 \pm 0.002$



YJh34
 $K_d = 102 \pm 6.15 \text{ nM}$
 $N (\text{sites}) = 0.371 \pm 0.001$



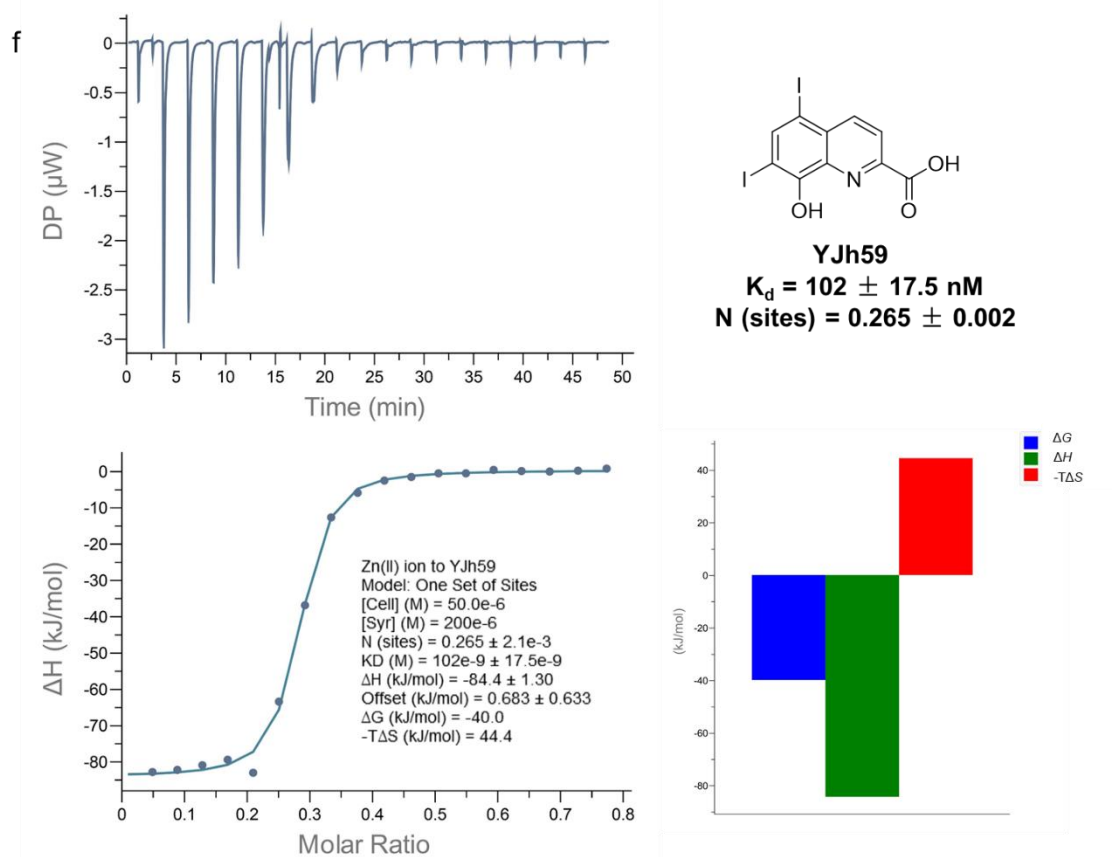
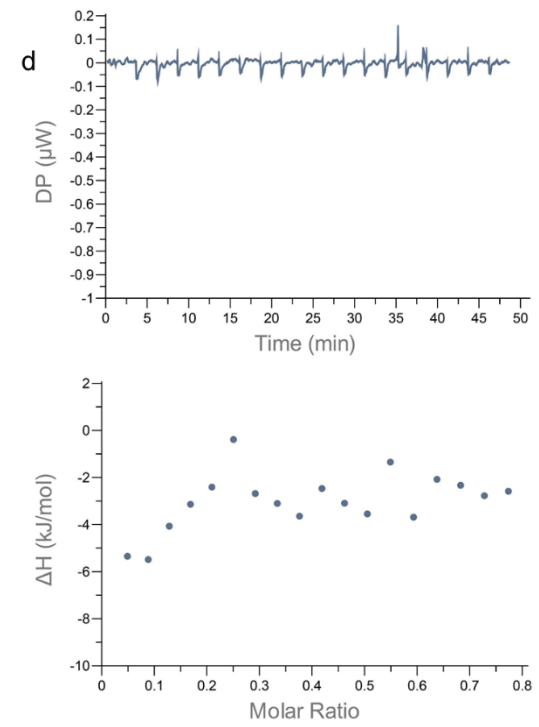
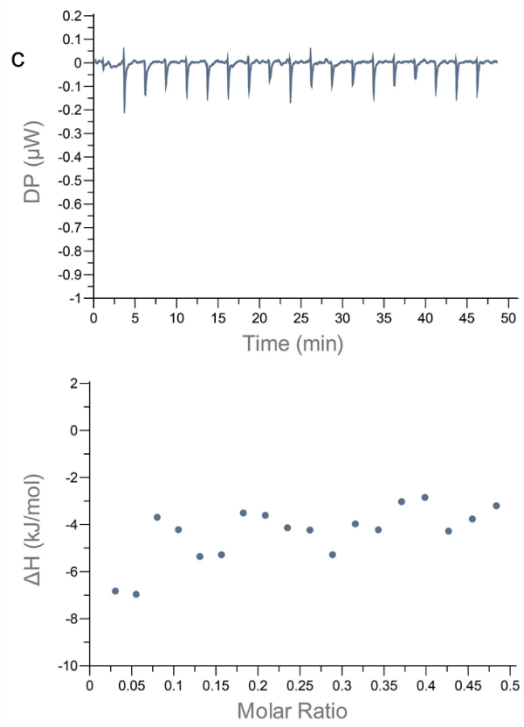
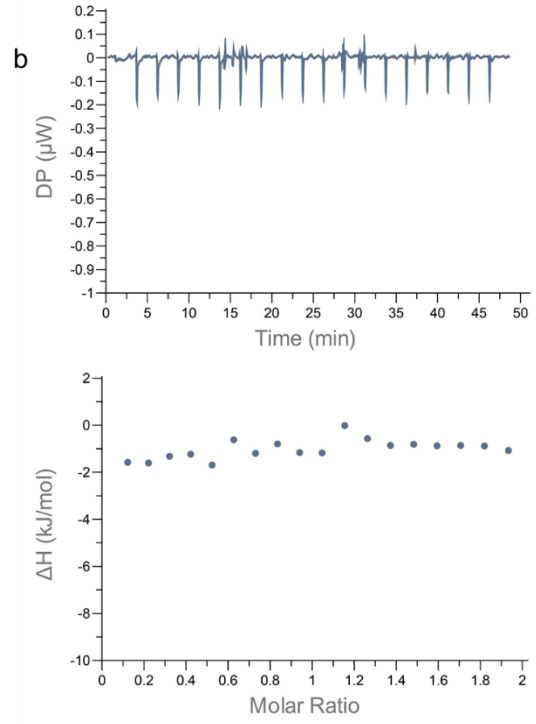
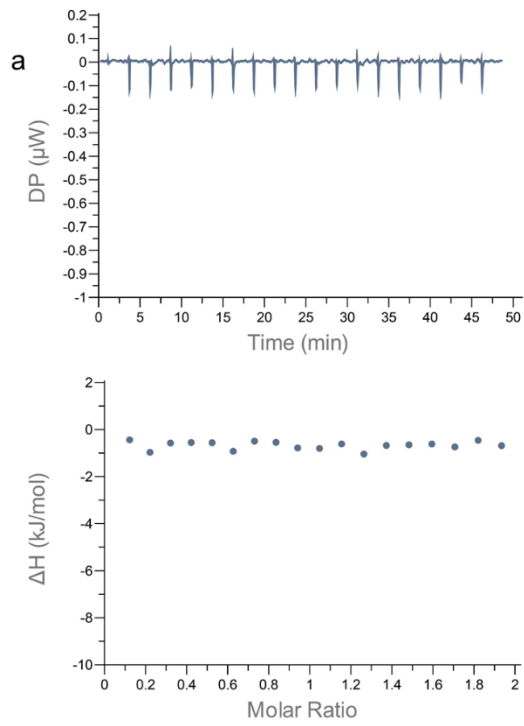
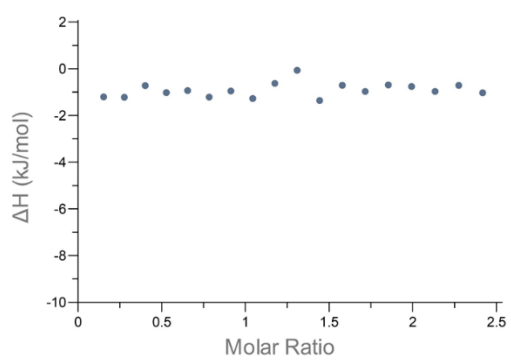
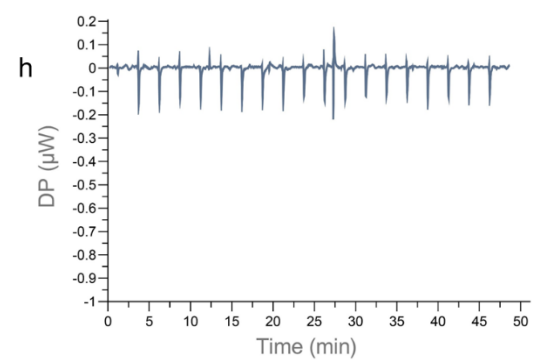
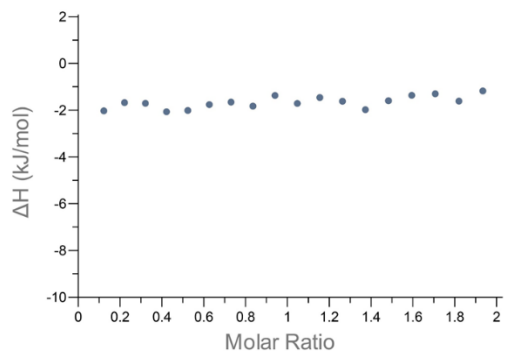
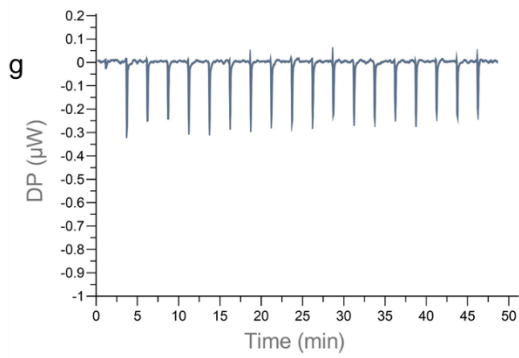
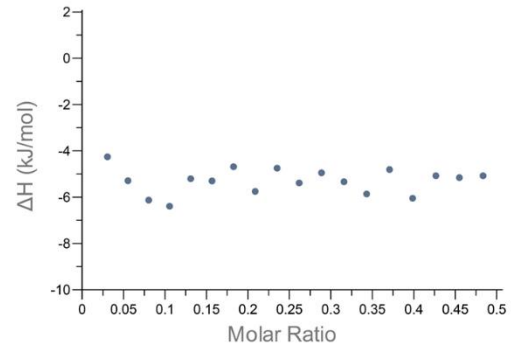
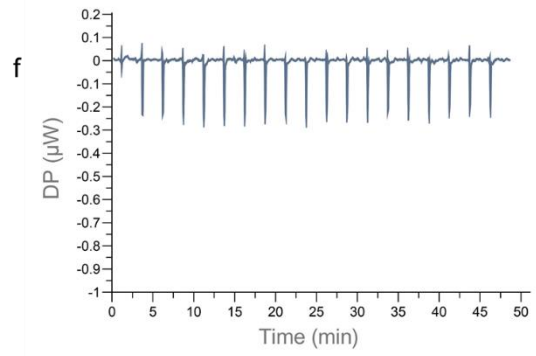
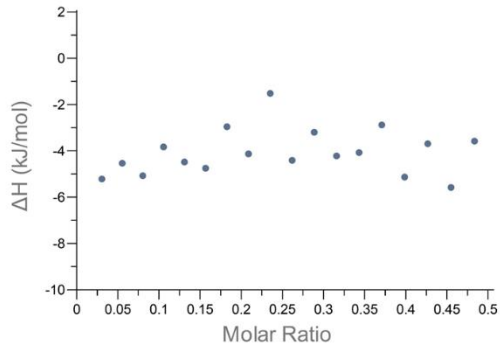
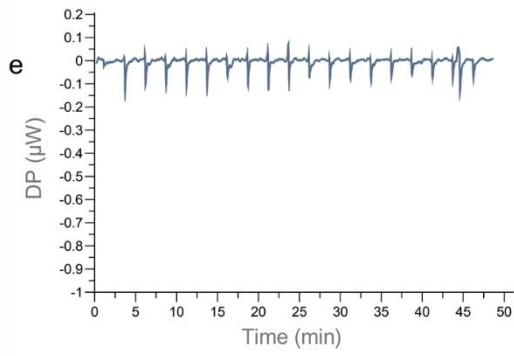
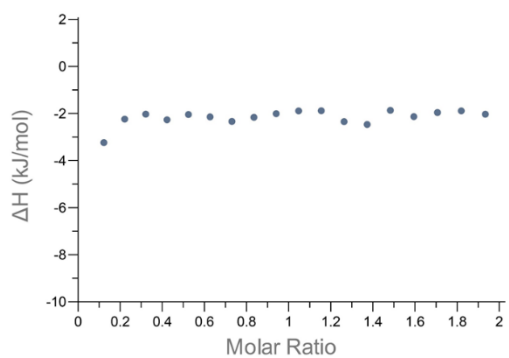
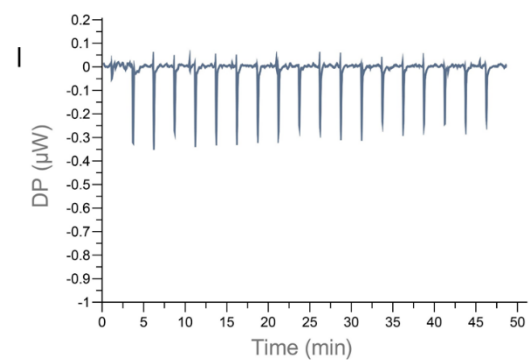
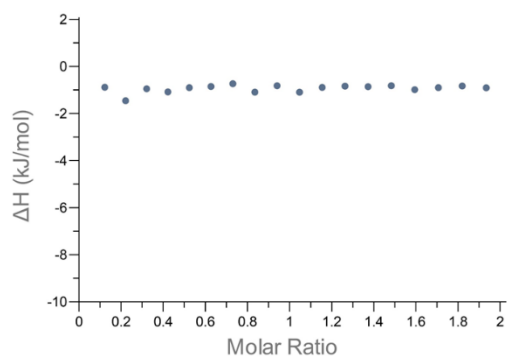
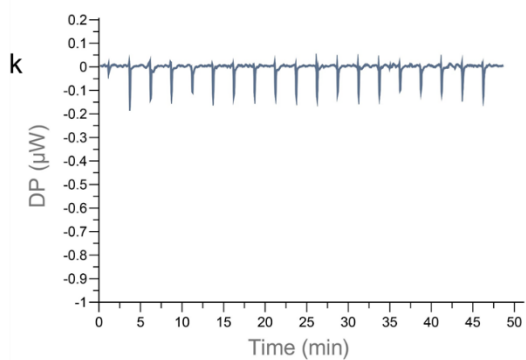
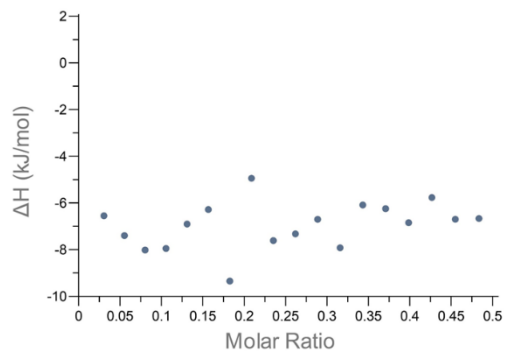
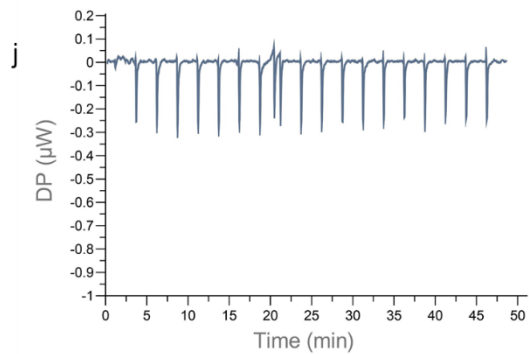
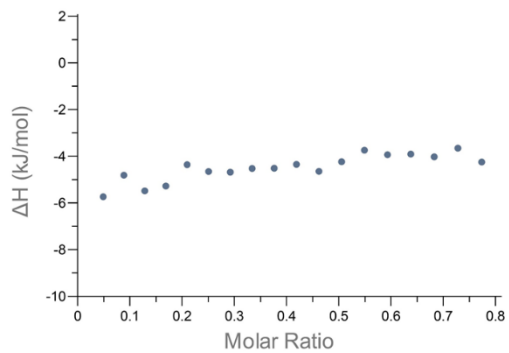
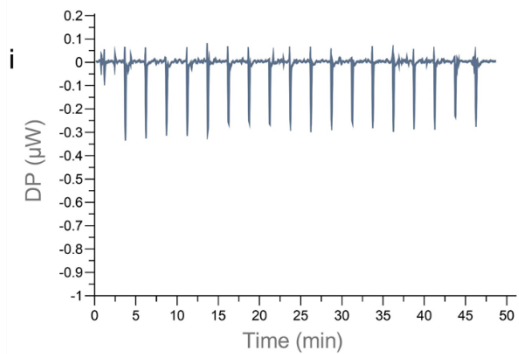


Figure S11 Thermograms of ITC assays (zinc ions titrating compounds). The corresponding controls were subtracted during data analysis and the thermograms of the controls are listed in **Figure S12**. a. Zinc ion (200 μM) titrating compound **94(YJh182)** (50 μM); b. Zinc ion (150 μM) titrating compound **95(YJh196)** (60 μM); c. Zinc ion (500 μM) titrating compound **8-MSQA(YJh65)** (50 μM); d. Zinc ion (300 μM) titrating compound **8-HQA** (50 μM); e. Zinc ion (200 μM) titrating compound **58(YJh34)** (50 μM); f. Zinc ion (200 μM) titrating compound **61(YJh59)** (50 μM).







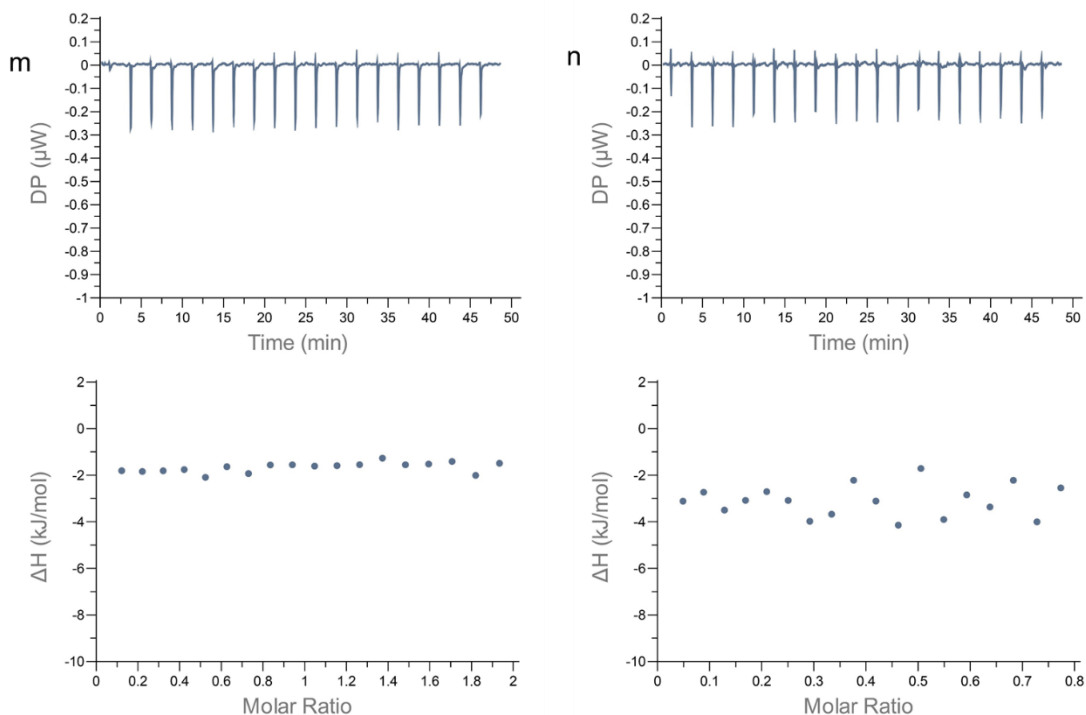
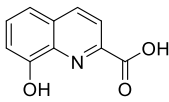
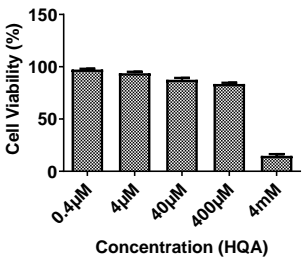
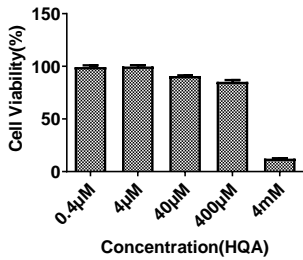
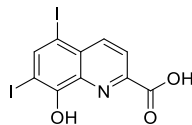
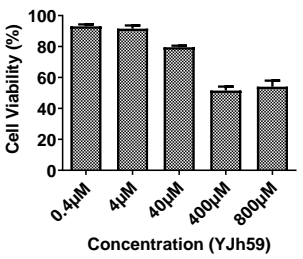
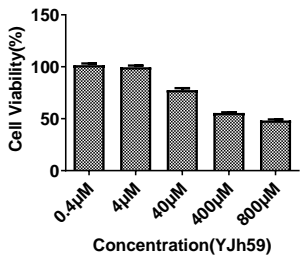
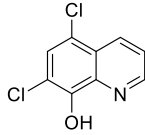
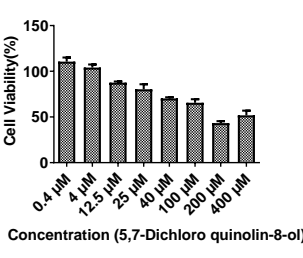
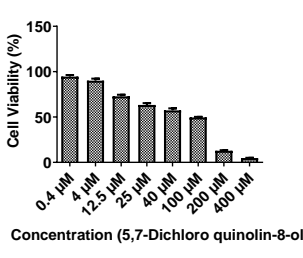
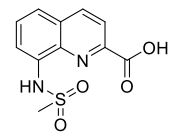
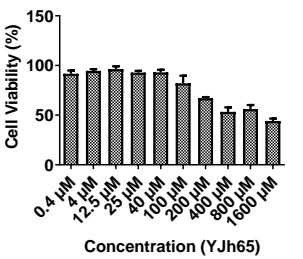
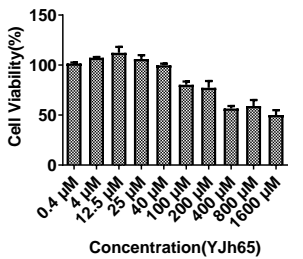
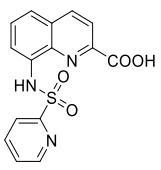
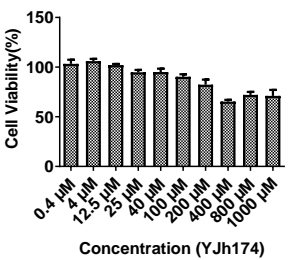
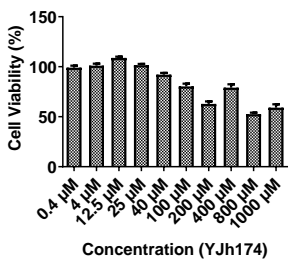
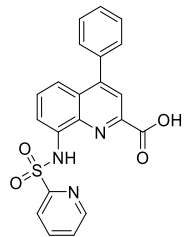
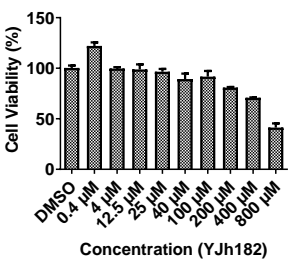
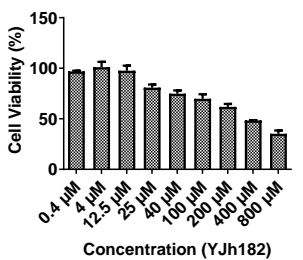
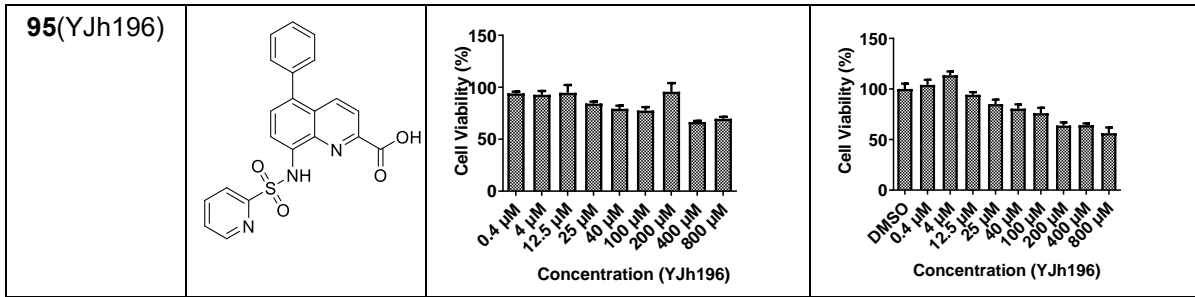


Figure S12 Thermograms of ITC assays for relevant control groups (zinc ion titrating compounds) a. Assay buffer to assay buffer; b. Zinc ions (500 μM) to assay buffer; c. Zinc ions (300 μM) to assay buffer; d. Zinc ions (200 μM) to assay buffer; e. Zinc ions (150 μM) to assay buffer; f. Assay buffer to compound **83(YJh174)** (60 μM); g. Assay buffer to EDTA (50 μM); h. Assay buffer to DPA (40 μM); i. Assay buffer to compound **94(YJh182)** (50 μM); j. Assay buffer to compound **95(YJh196)** (60 μM); k. Assay buffer to compound **8-MSQA (YJh65)** (50 μM); l. Assay buffer to compound **8-HQA** (50 μM); m. Assay buffer to compound **58(YJh34)** (50 μM); n. Assay buffer to compound **61(YJh59)** (50 μM).

Table S3 Alamar Blue Assays (HEK293 cell)

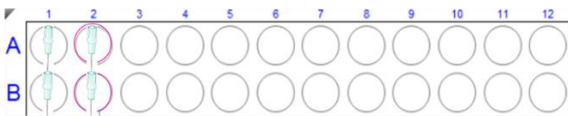
Cpd	Structure	12 h	24 h
DPA	<chem>O=C(O)c1ccn(c1)C(=O)O</chem>		
45(YJh2)	<chem>O=C(Oc1ccccc1)Nc2ccn(c2)C(=O)Nc3ccccc3</chem>		

<p>8-HQA</p>			
<p>61(YJh59)</p>			
<p>52 (Chloroxine or 5,7- dichloro quinolin-8- ol)</p>			
<p>8-MSQA (YJh65)</p>			
<p>83(YJh174)</p>			
<p>94(YJh182)</p>			



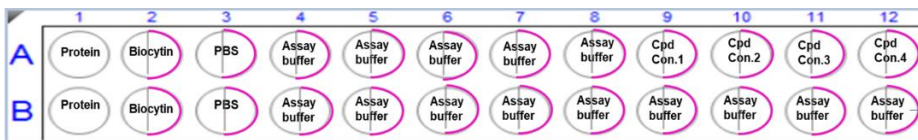
a

Sensor plate



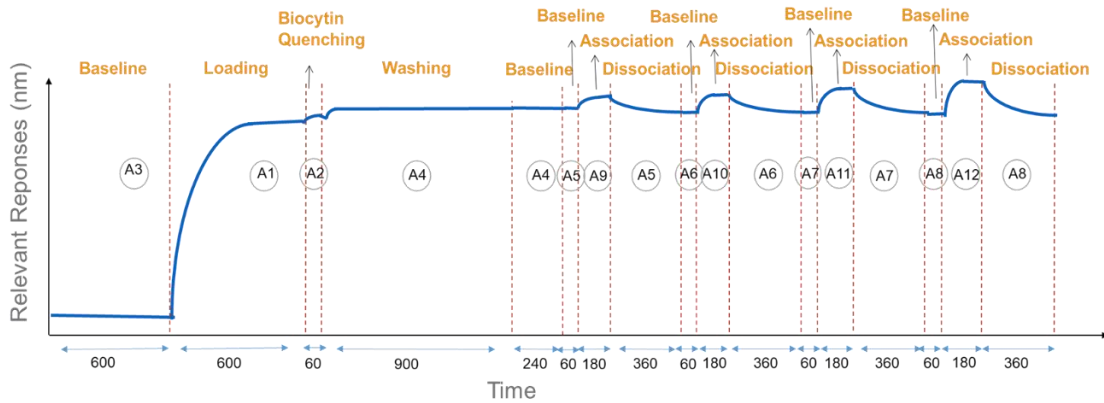
Reference sensors

Sample plate



Reference wells

Responses curve of sensor A1



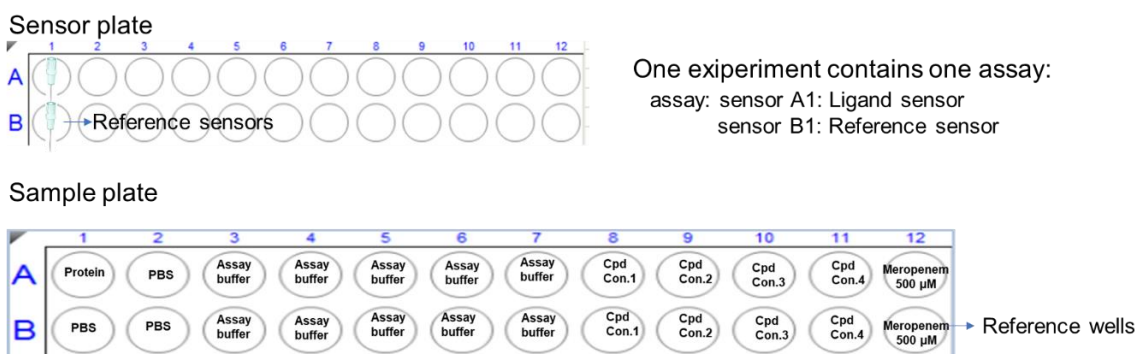
One experiment contains two assays:

1st assay: sensor A1: Ligand sensor
(use the A1 to A12 wells of the sample plate)
sensor B1: Ligand sensor
(use the B1 to B12 wells of the sample plate)

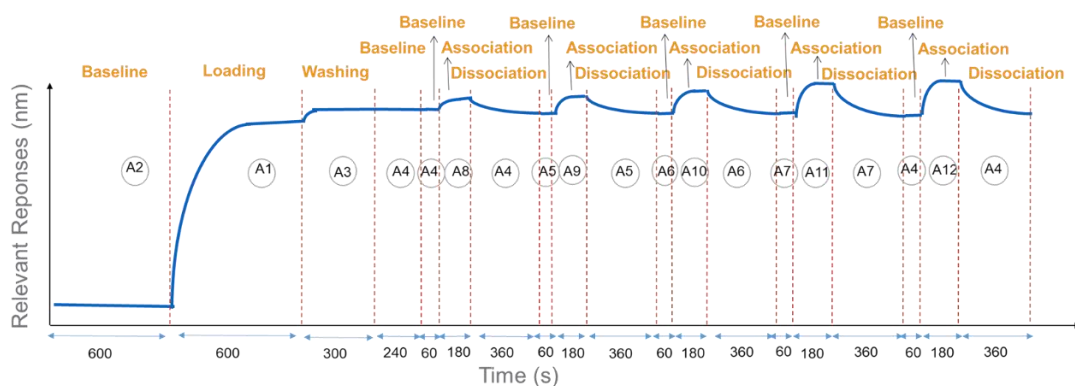
2nd assay: sensor A2: Reference sensor
(use the A2 to A12 wells of the sample plate)
sensor B2: Reference sensor
(use the B2 to B12 wells of the sample plate)

The program steps for sensor B1 were the same as those for sensor A1, except that a different row of the sample plate was used; The loading step of the sensors A2 and B2 was performed in A2 and B2 wells of the sample plate, respectively, and other steps were the same as those for sensors A1 and B1, respectively.

b



Responses curve of sensor A1



One experiment contains one assay:

1st assay: sensor A1: Ligand sensor (use the A1 to A12 wells of the sample plate)
 sensor B1: Reference sensor (use the B1 to B12 wells of the sample plate)

The program steps for sensor B1 were the same as those for sensor A1, except that a different row of the sample plate was used.

Figure S13 Description of the layouts for the plates and program settings of the BLI assays. a. The layouts for the plates and program settings of the Double Reference method; b. The layouts for the plates and program settings of the Reference Wells method.

Table S4 Fractional Abundance of Native MS Analysis at Ratio (P/L) 1 to 2 (%)

Num	Complex	NDM-1_buffer	NDM-1_0.05%DMSO	NDM-1_EDTA	NDM-1_L-Captopril	NDM-1_DPA	NDM-1_YJh34	NDM-1_YJh65	NDM-1_YJh174	NDM-1_YJh182	NDM-1_YJh196
1	apo-NDM-1 + 0 x Zn ²⁺			51.1		2.02		14.28	15.73	5.68	10.62
2	apo-NDM-1 + 1 x Zn ²⁺	7.54	5.3	8.47	2.93	13.57	12.69	9.13	10.39	4.74	3.82
3	apo-NDM-1 + 2 x Zn ²⁺	50.77	50.06	7.28	31.79	46.42	35.45	34.91	26.99	22.74	6.76
4	apo-NDM-1 + 3 x Zn ²⁺	9.04	11.74		7.22	5.97		4.2			
5	apo-NDM-1 + 0 x Zn ²⁺ + 1 x Cpd				1.38						
6	apo-NDM-1 + 1 x Zn ²⁺ + 1 x Cpd				1.1	5.85	9.78	5.85	8.42	6.96	6.03
7	apo-NDM-1 + 2 x Zn ²⁺ + 1 x Cpd				20.5	1.15	7.45	5.48	13.32	21.09	18.95
8	apo-NDM-1 + 3 x Zn ²⁺ + 1 x Cpd				9.35	4.84		3.03	5.8	14.46	2.62
9	apo-NDM-1 + 0 x Zn ²⁺ + 2 x Cpd					1.25					
10	apo-NDM-1 + 1 x Zn ²⁺ + 2 x Cpd							1.58			2.76
11	apo-NDM-1 + 2 x Zn ²⁺ + 2 x Cpd				1.72			1.52	4.92	19.86	5.29
12	apo-NDM-1 + 3 x Zn ²⁺ + 2 x Cpd				1.59				5.31		1.68
15	apo-NDM-1 + 2 x Zn ²⁺ + 3 x Cpd										1.47
16	apo-NDM-1 + 3 x Zn ²⁺ + 3 x Cpd										7.25

'Cpd' means 'compound'.

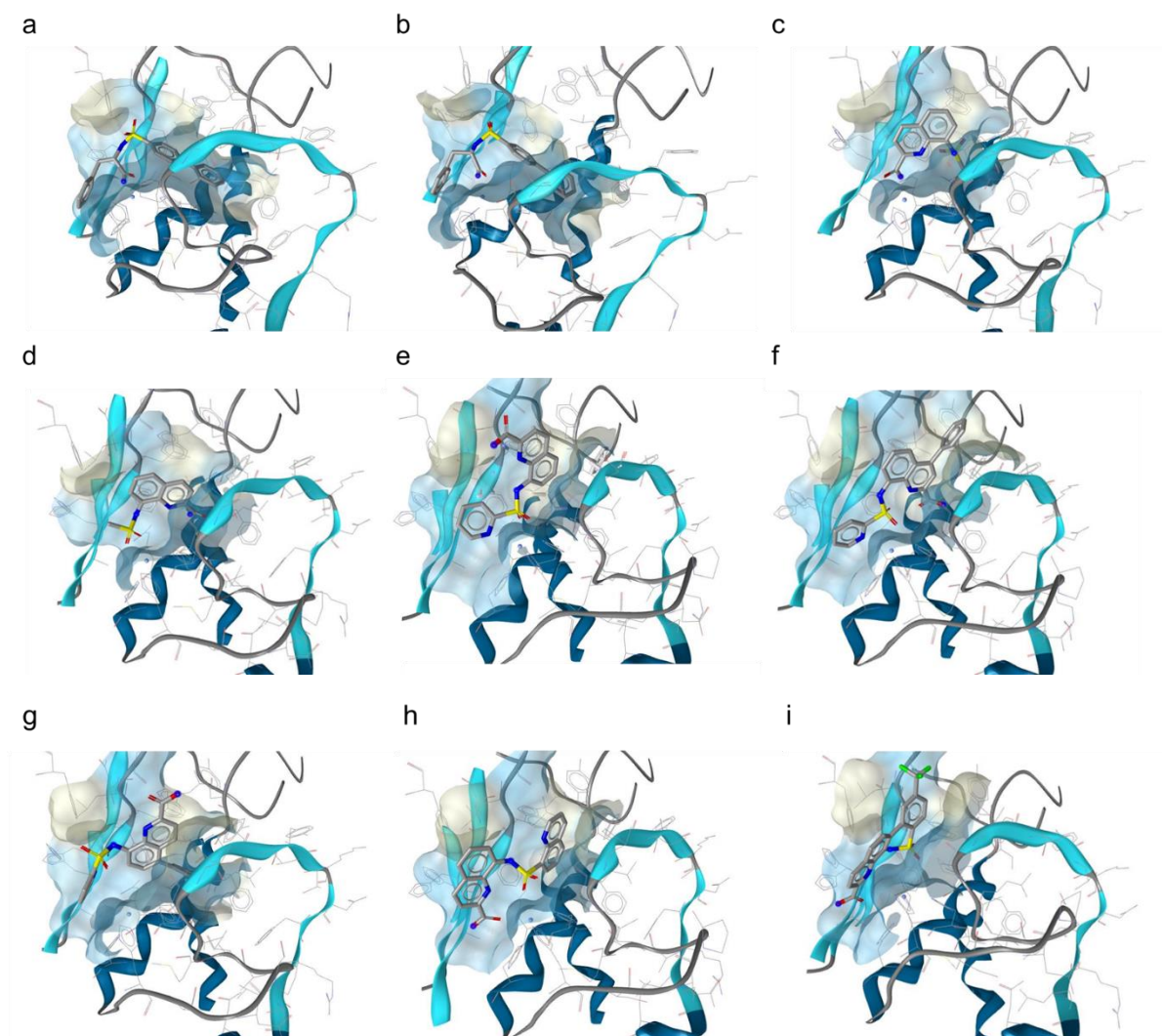
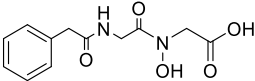
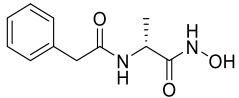
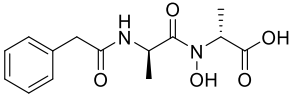
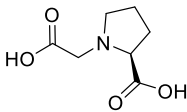
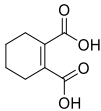
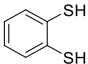
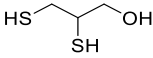
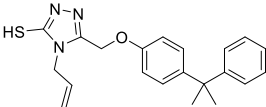
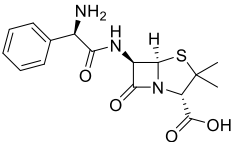
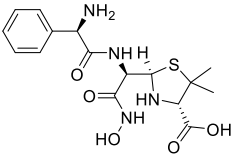
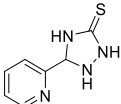


Figure S14 Proposed binding poses of **S-NSA** and **R-NSA** as well as some selected **8-MSQA** derivatives in the active site of the catalytic domain of MMP-2 (PDB ID: 1QIB). The docking studies were performed by Gold 5.8.1 and the results were analyzed by LigandScout 4.2. a. Proposed binding pose of **S-NSA** in the active site; b. Proposed binding pose of **R-NSA** in the binding pocket; c, d. Proposed binding poses of compound **8-MSQA(YJh65)** in the active site; e. One of the proposed binding poses of compound **83(YJh174)** in the active site; f. One of the proposed binding poses of compound **94(YJh182)** in the active site; g. One of the proposed binding poses of compound **95(YJh196)** in the active site; h. One of the proposed binding poses of compound **74(YJh119)** in the active site; i. One of the proposed binding poses of compound **98(YJh184)** in the active site.

Table S5 Some Other Structures

Compound	Structure	IC ₅₀ (μM)
YJa4		>1000 ^a
YJe4		-
YJd5		-
YJg4		>1000 ^a
YJh5		ca. 400-2000 ^a
Benzene-1,2-dithiol		83.76 ^{a2}
2,3-Dimercapto-1-propanol		50 ^{a2, a3}
U14		ca. 80-400
Ampicillin		700 ^{a2}
XW1		>1000 ^{a2}
MR327		≥1000 μM ^{a2}

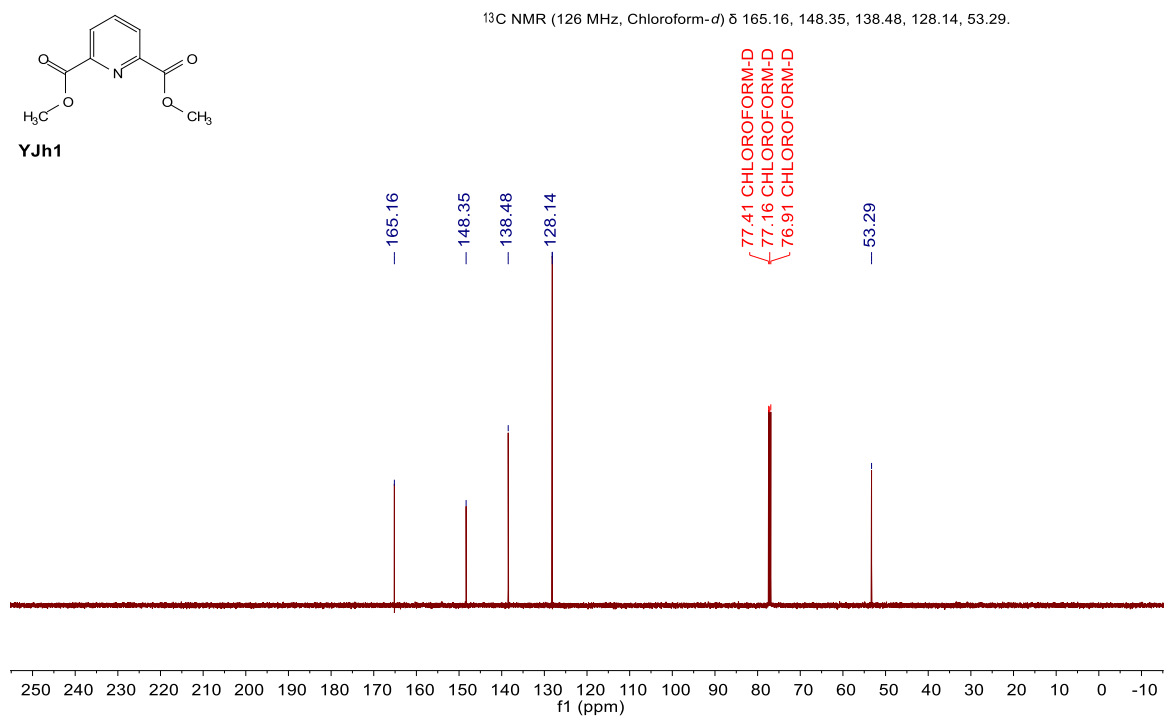
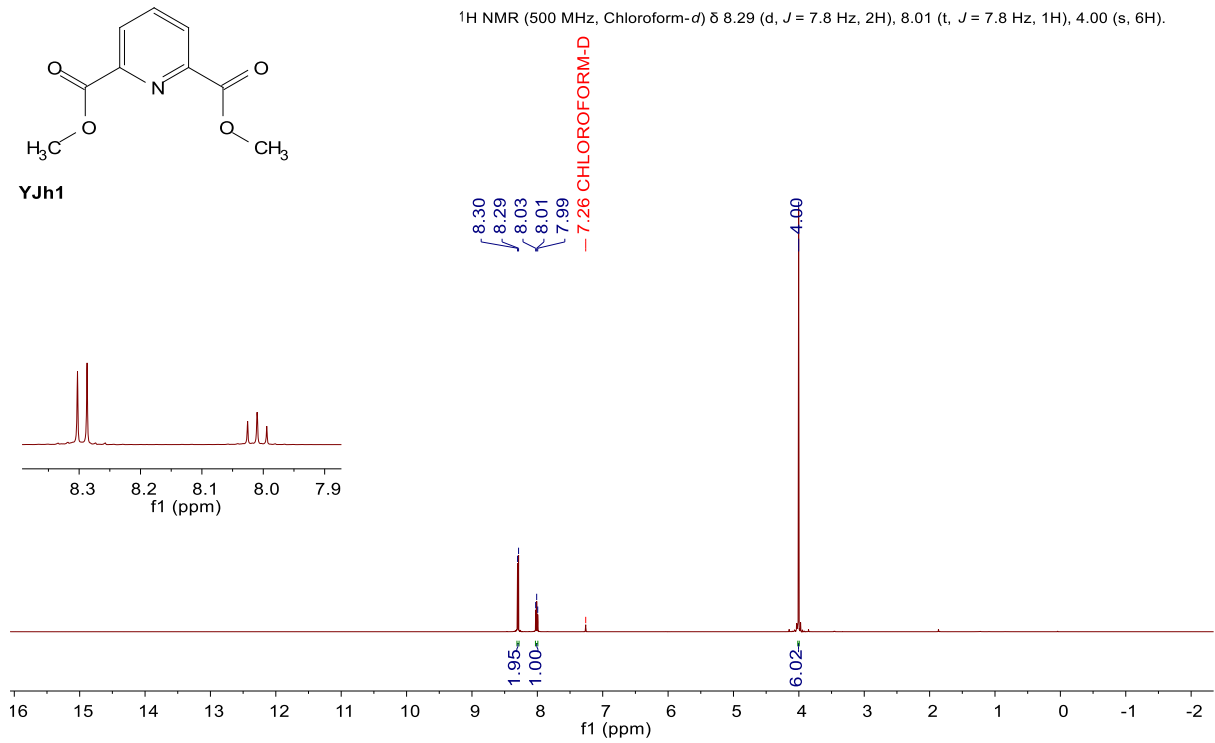
^aThe activity was tested using assay buffer containing 100 nM ZnSO₄.

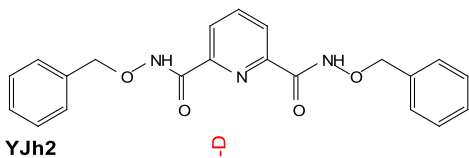
^{a2}The activity was tested using assay buffer containing 10 μM ZnSO₄.

^{a3}The activity was tested using imipenem as the substrate.

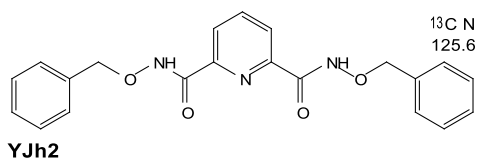
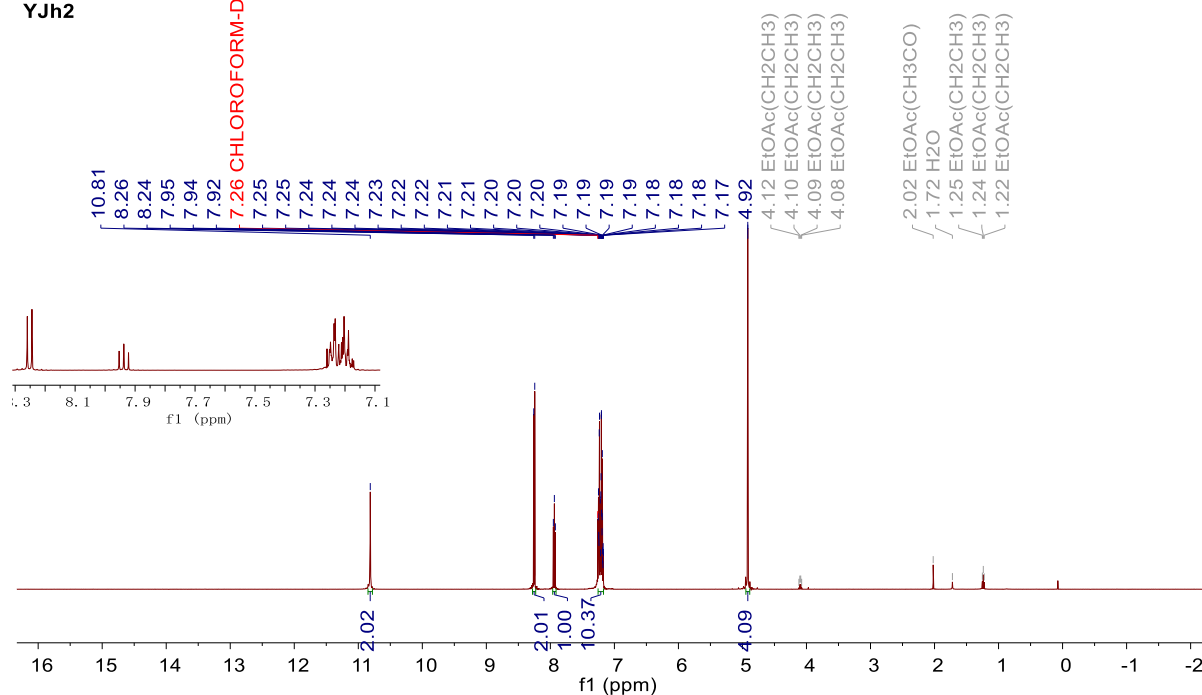
^{a4} '-' means 'did not test'.

6.2 NMR spectra

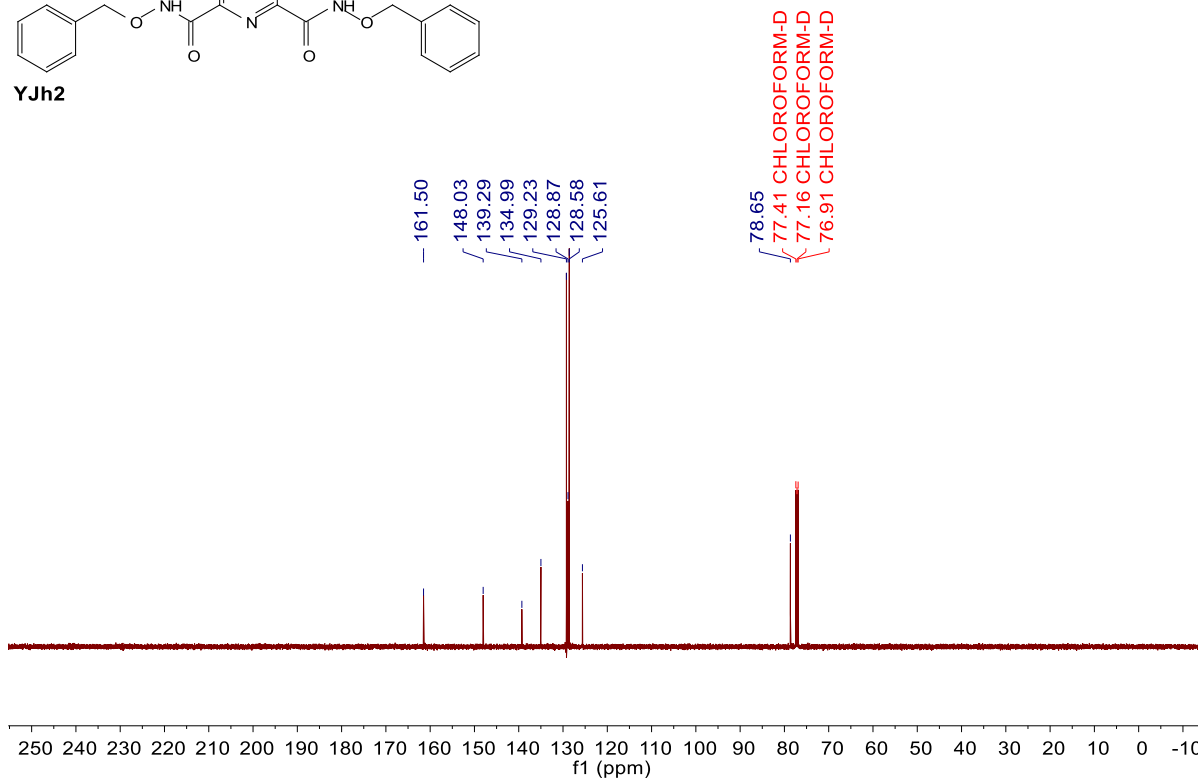


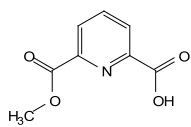


¹H NMR (500 MHz, Chloroform-*d*) δ 10.81 (s, 2H), 8.25 (d, *J* = 7.8 Hz, 2H), 7.94 (t, *J* = 8.1 Hz, 1H), 7.26 – 7.17 (m, 10H), 4.92 (s, 4H).



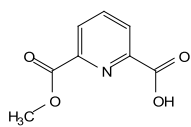
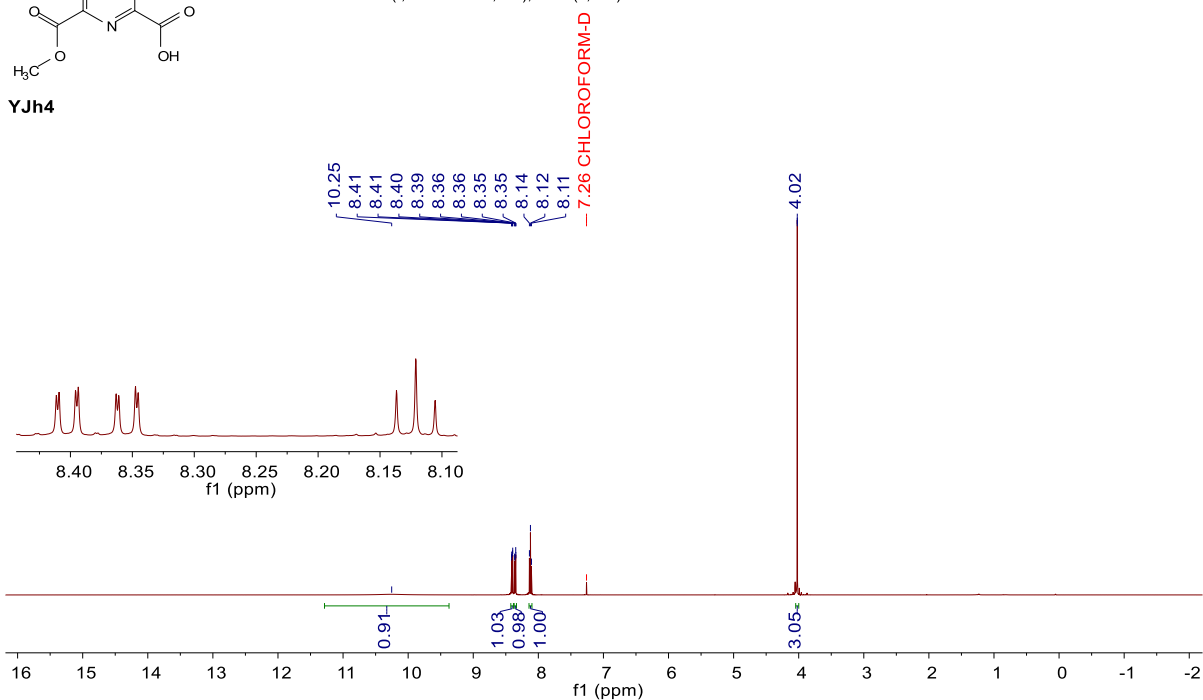
¹³C NMR (126 MHz, Chloroform-*d*) δ 161.50, 148.03, 139.29, 134.99, 129.23, 128.87, 128.58, 125.61, 78.65.





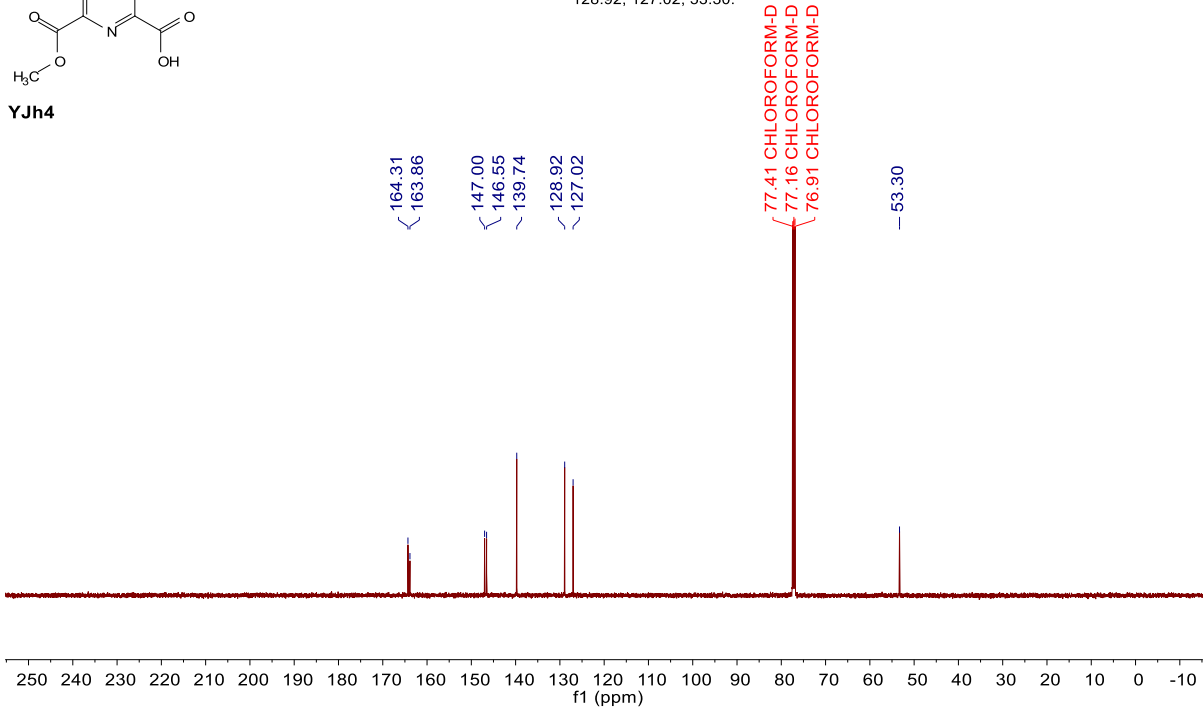
YJh4

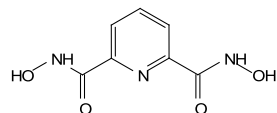
$^1\text{H NMR}$ (500 MHz, Chloroform- d) δ 10.25 (s, 1H), 8.40 (dd, J = 7.8, 1.1 Hz, 1H), 8.35 (dd, J = 7.9, 1.1 Hz, 1H), 8.12 (t, J = 7.8 Hz, 1H), 4.02 (s, 3H).



YJh4

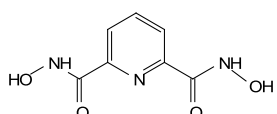
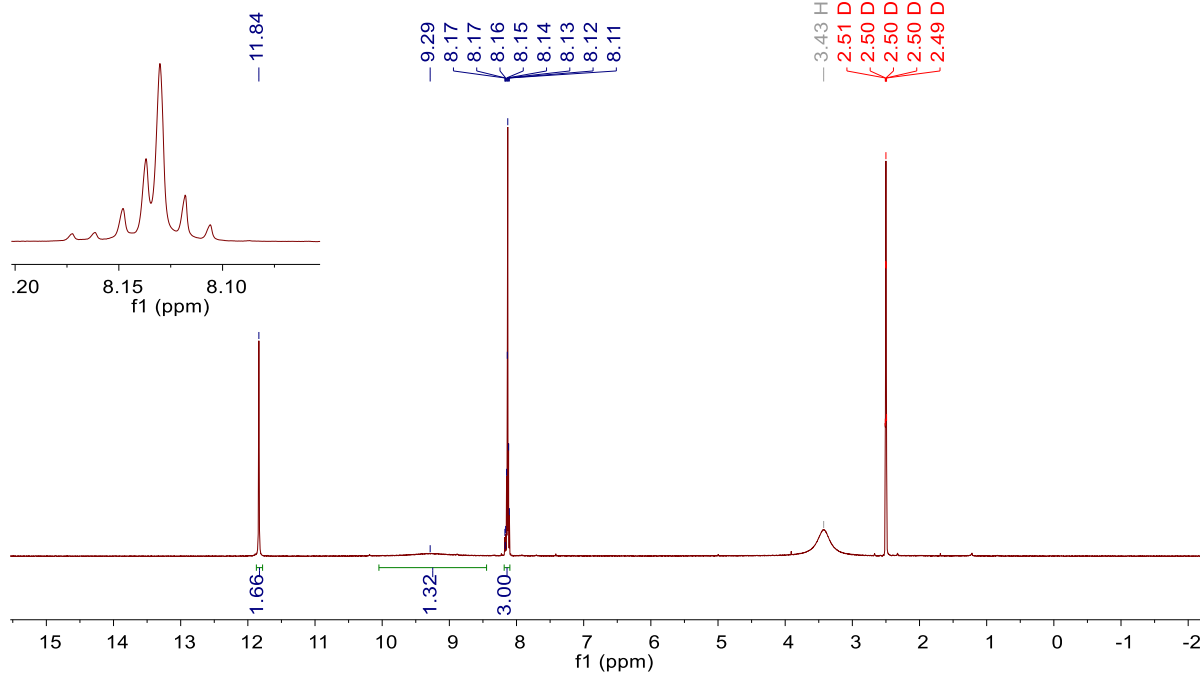
$^{13}\text{C NMR}$ (126 MHz, Chloroform- d) δ 164.31, 163.86, 147.00, 146.55, 139.74, 128.92, 127.02, 53.30.





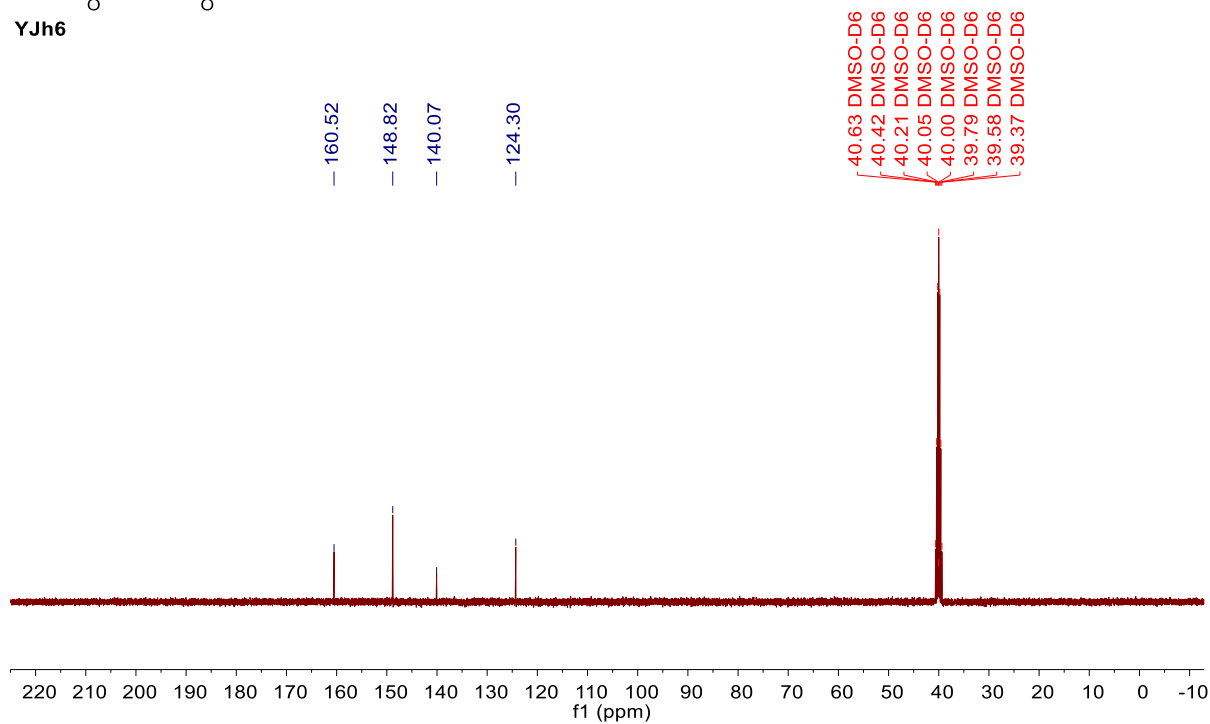
YJh6

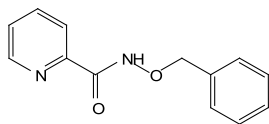
¹H NMR (400 MHz, DMSO-*d*₆) δ 11.84 (s, 2H), 9.29 (s, 2H), 8.45 – 7.79 (m, 3H).



YJh6

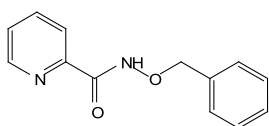
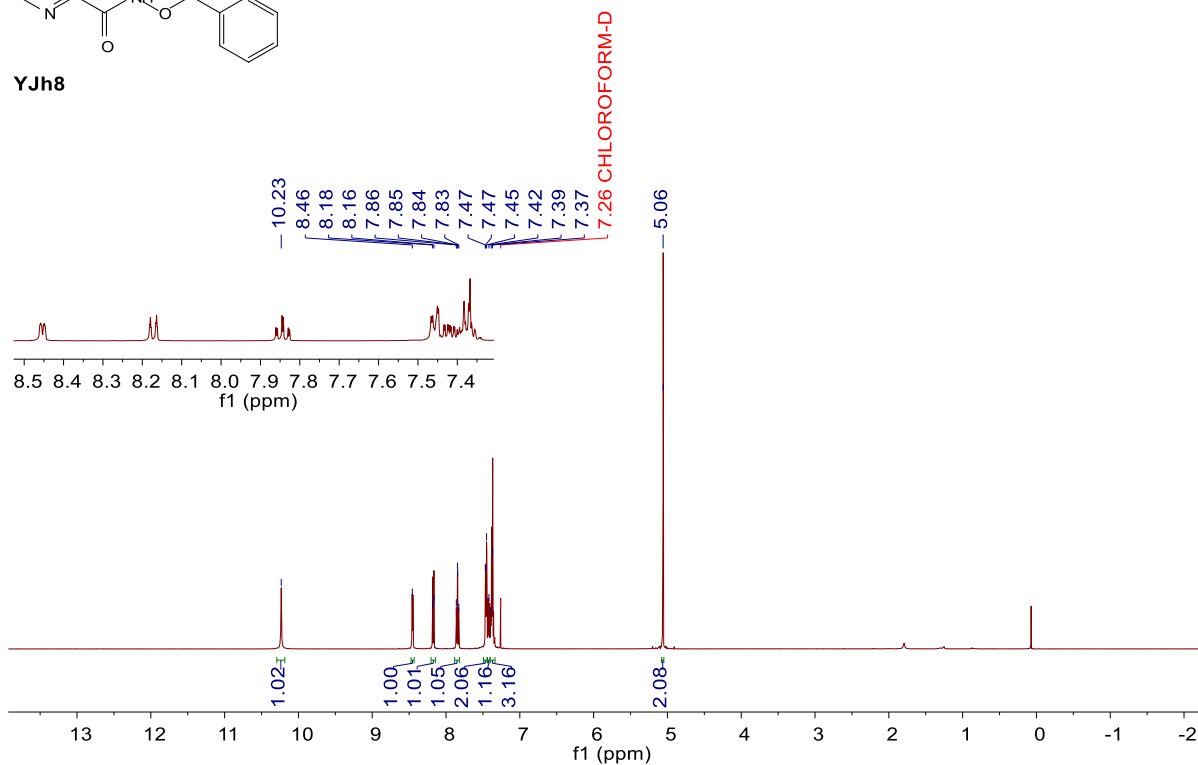
¹³C NMR (101 MHz, DMSO-*d*₆) δ 160.52, 148.82, 140.07, 124.30.





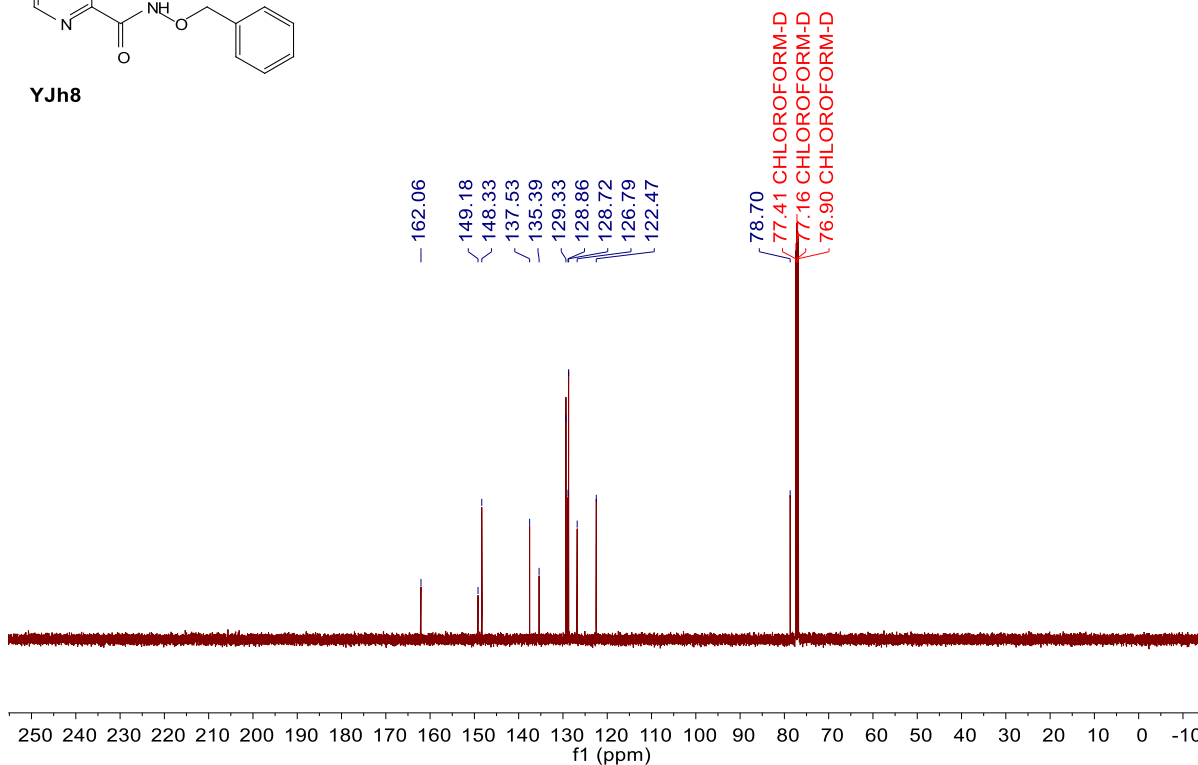
YJh8

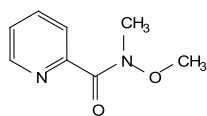
¹H NMR (500 MHz, Chloroform-*d*) δ 10.23 (s, 1H), 8.46 (s, 1H), 8.17 (d, *J* = 9.8 Hz, 1H), 7.96 – 7.77 (m, 1H), 7.53 – 7.31 (m, 6H), 5.06 (s, 2H).



YJh8

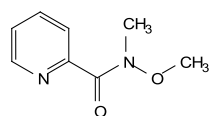
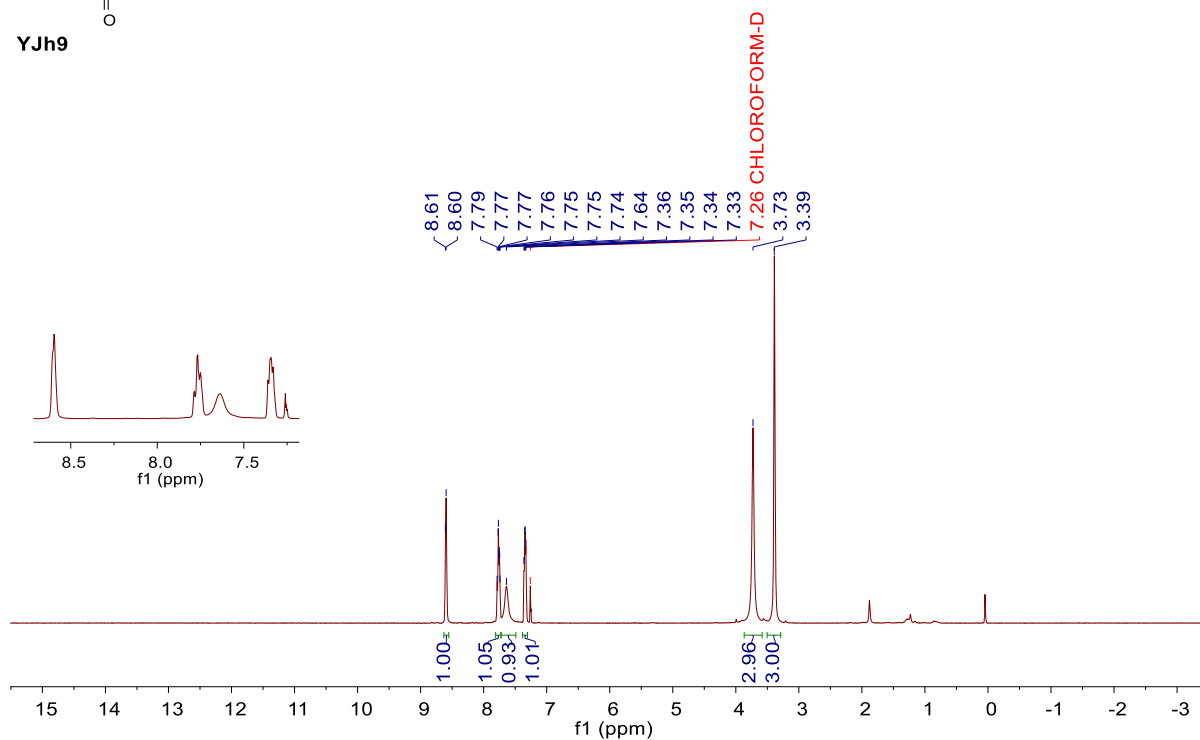
¹³C NMR (126 MHz, Chloroform-*d*) δ 162.06, 149.18, 148.33, 137.53, 135.39, 129.33, 128.86, 128.72, 126.79, 122.47, 78.70.





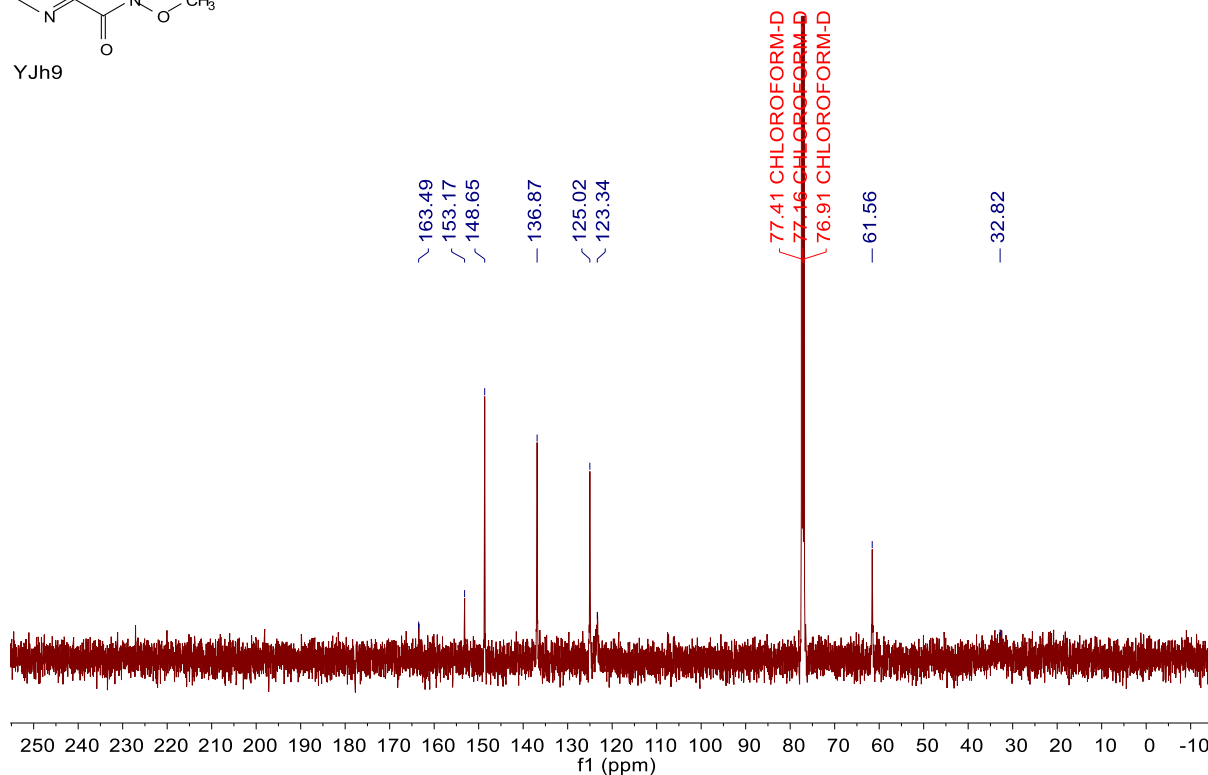
YJh9

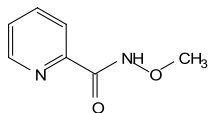
¹H NMR (400 MHz, Chloroform-*d*) δ 8.60 (d, *J* = 4.6 Hz, 1H), 7.95 – 7.70 (m, 1H), 7.64 (s, 1H), 7.35 (dd, *J* = 7.9, 4.5 Hz, 1H), 3.73 (s, 3H), 3.38 (s, 3H).



YJh9

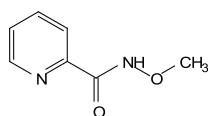
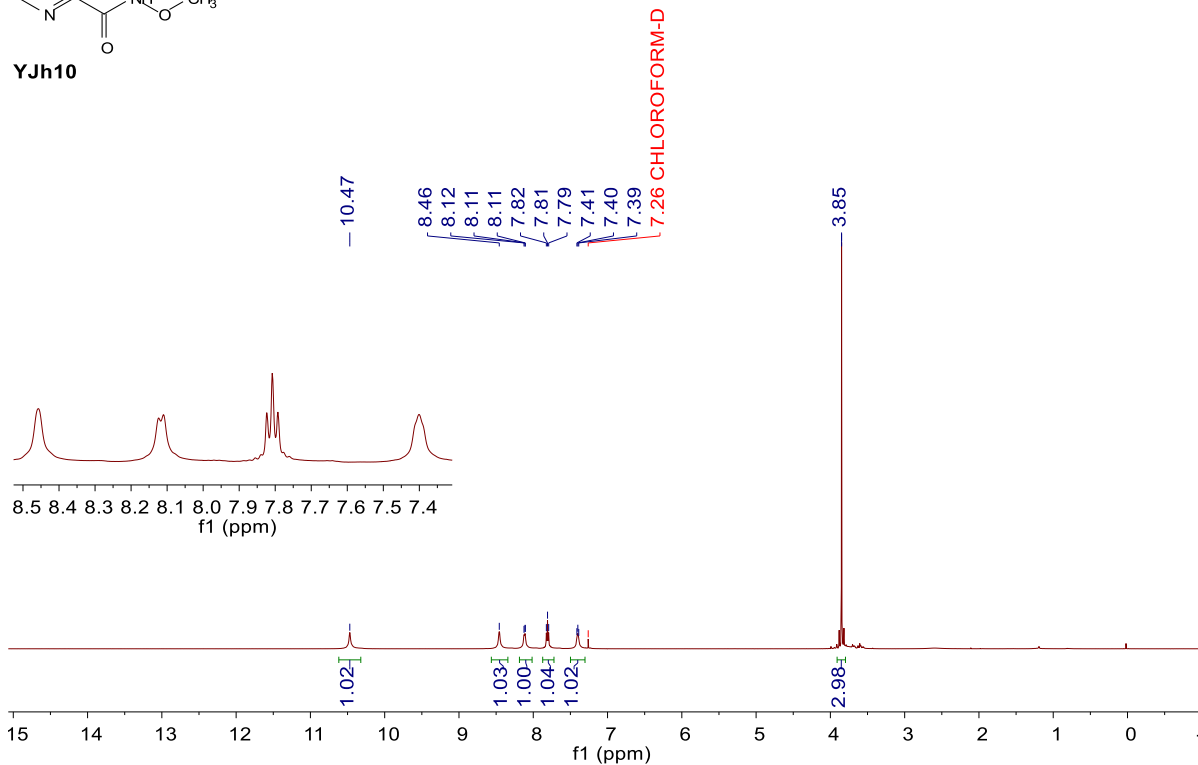
¹³C NMR (126 MHz, Chloroform-*d*) δ 163.49, 153.17, 148.65, 136.87, 125.02, 123.34, 61.56, 32.82.





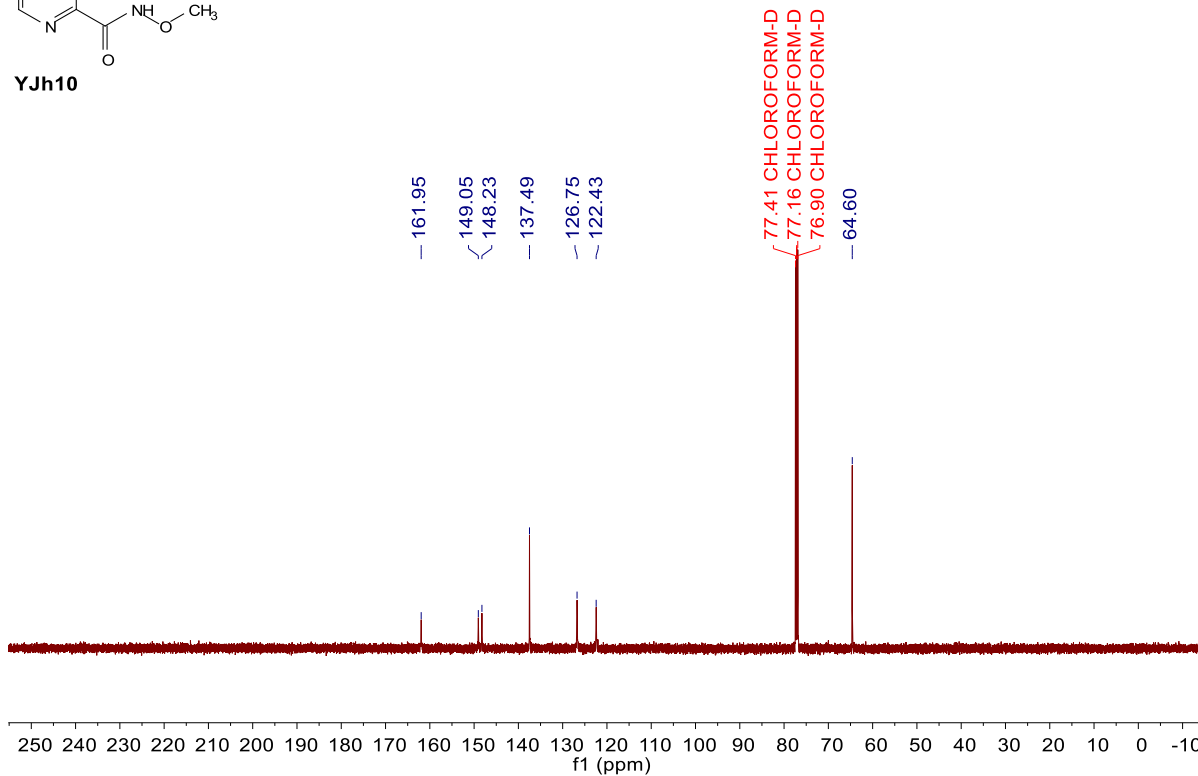
YJh10

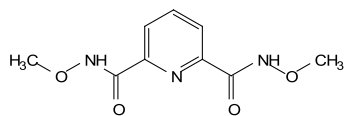
¹H NMR (500 MHz, Chloroform-*d*) δ 10.47 (s, 1H), 8.46 (s, 1H), 8.12 (d, *J* = 7.8 Hz, 1H), 7.81 (t, *J* = 7.8 Hz, 1H), 7.41 (d, *J* = 6.4 Hz, 1H), 3.85 (s, 3H).



YJh10

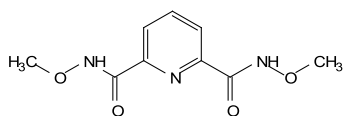
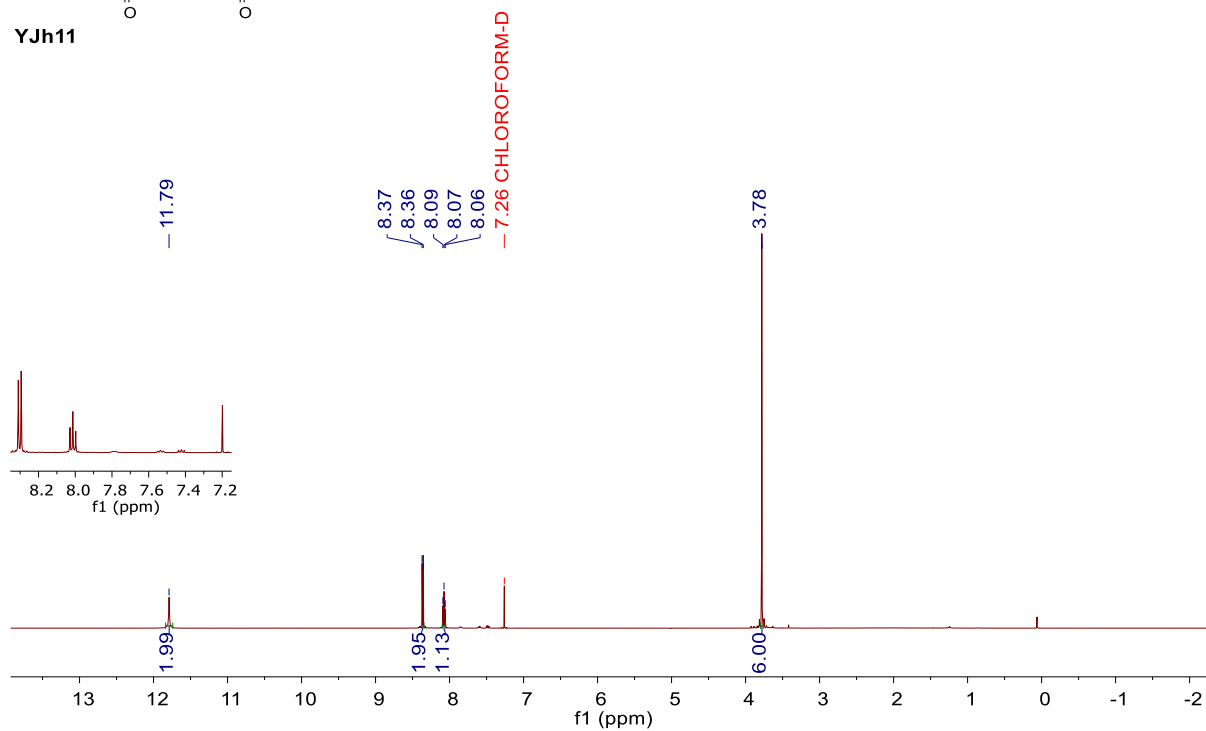
¹³C NMR (126 MHz, Chloroform-*d*) δ 161.95, 149.05, 148.23, 137.49, 126.75, 122.43, 77.41, 77.16, 76.90, 64.60.





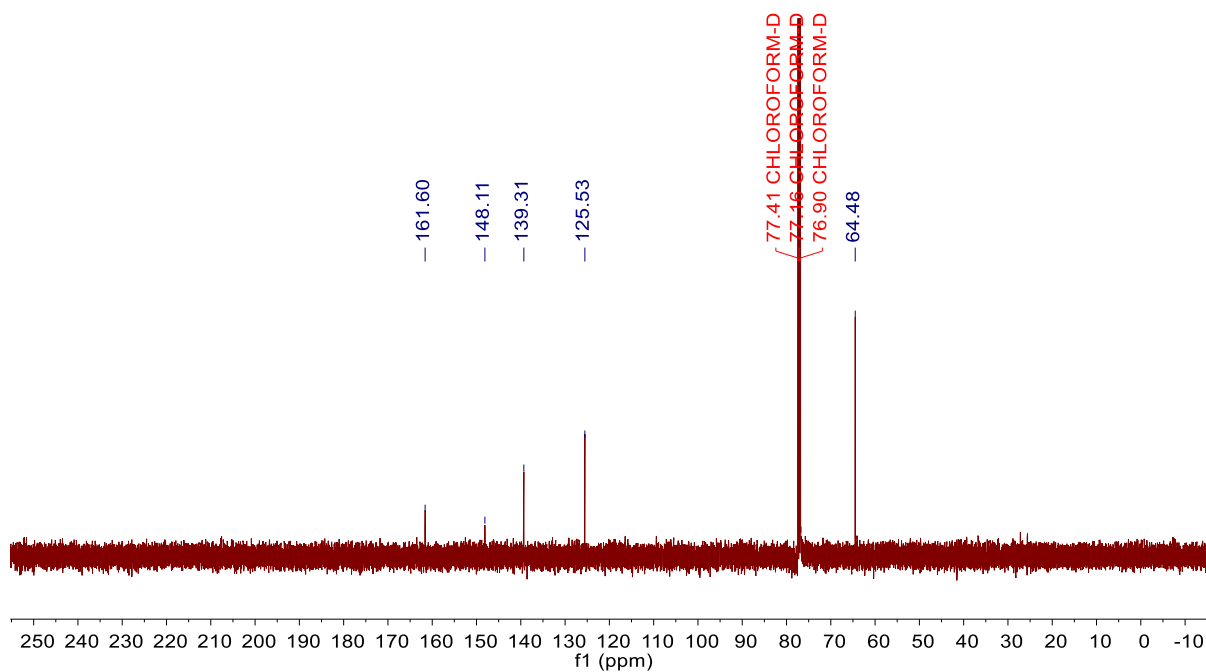
$^1\text{H NMR}$ (500 MHz, Chloroform- d) δ 11.79 (s, 2H), 8.36 (d, $J = 8.3$ Hz, 2H), 8.07 (t, $J = 7.7$ Hz, 1H), 3.78 (s, 6H).

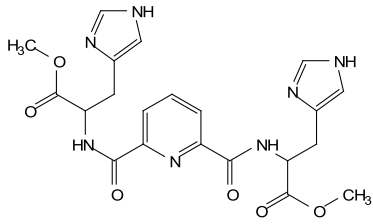
YJh11



$^{13}\text{C NMR}$ (126 MHz, Chloroform- d) δ 161.60, 148.11, 139.31, 125.53, 64.48.

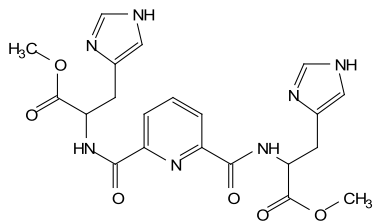
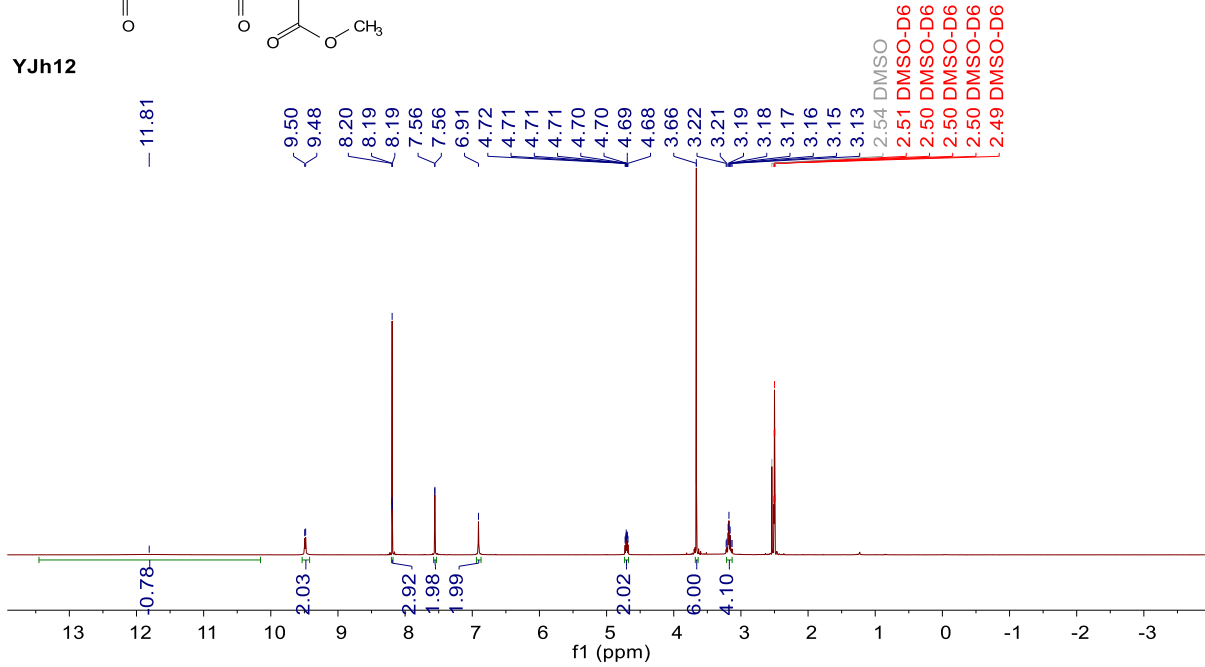
YJh11





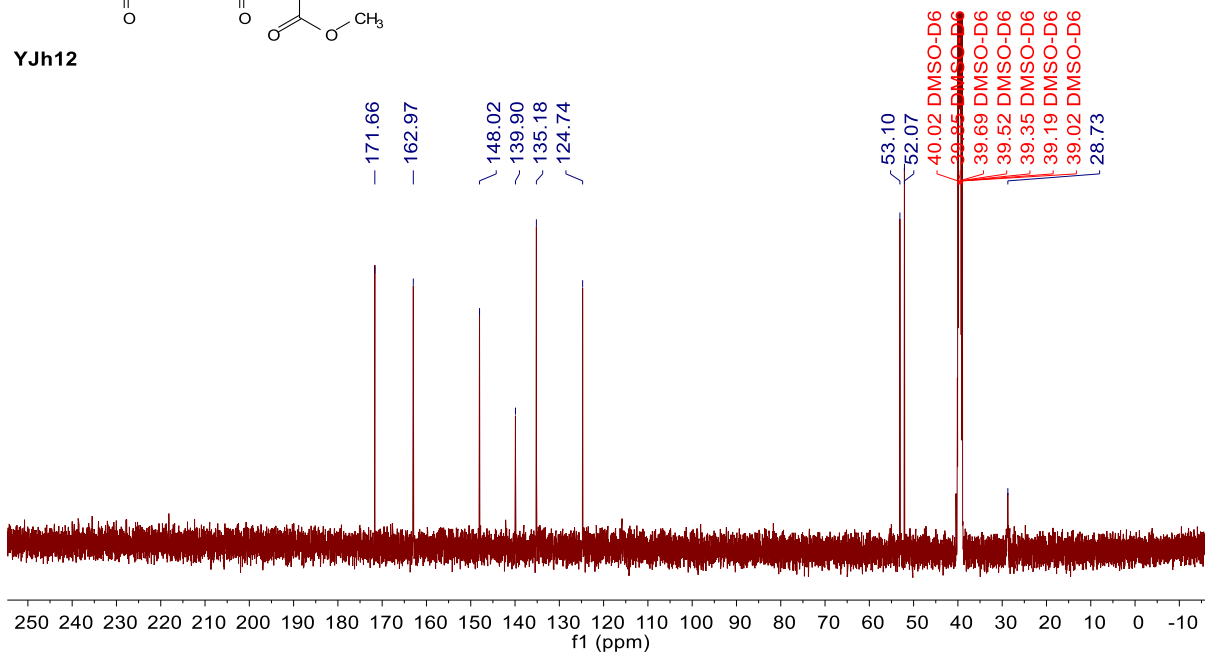
$^1\text{H NMR}$ (500 MHz, $\text{DMSO-}d_6$) δ 11.81 (s, 2H), 9.49 (d, $J = 7.2$ Hz, 2H), 9.03 – 7.89 (m, 3H), 7.56 (d, $J = 1.2$ Hz, 2H), 6.91 (s, 2H), 4.70 (ddd, $J = 8.4, 7.2, 5.5$ Hz, 2H), 3.66 (s, 6H), 3.31 – 2.97 (m, 4H).

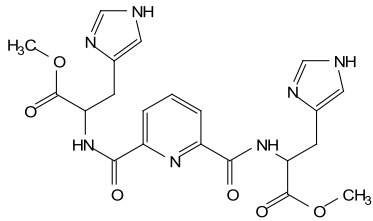
YJh12



$^{13}\text{C NMR}$ (126 MHz, $\text{DMSO-}d_6$) δ 171.66, 162.97, 148.02, 139.90, 135.18, 124.74, 53.10, 52.07, 28.73.

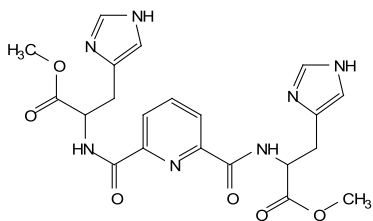
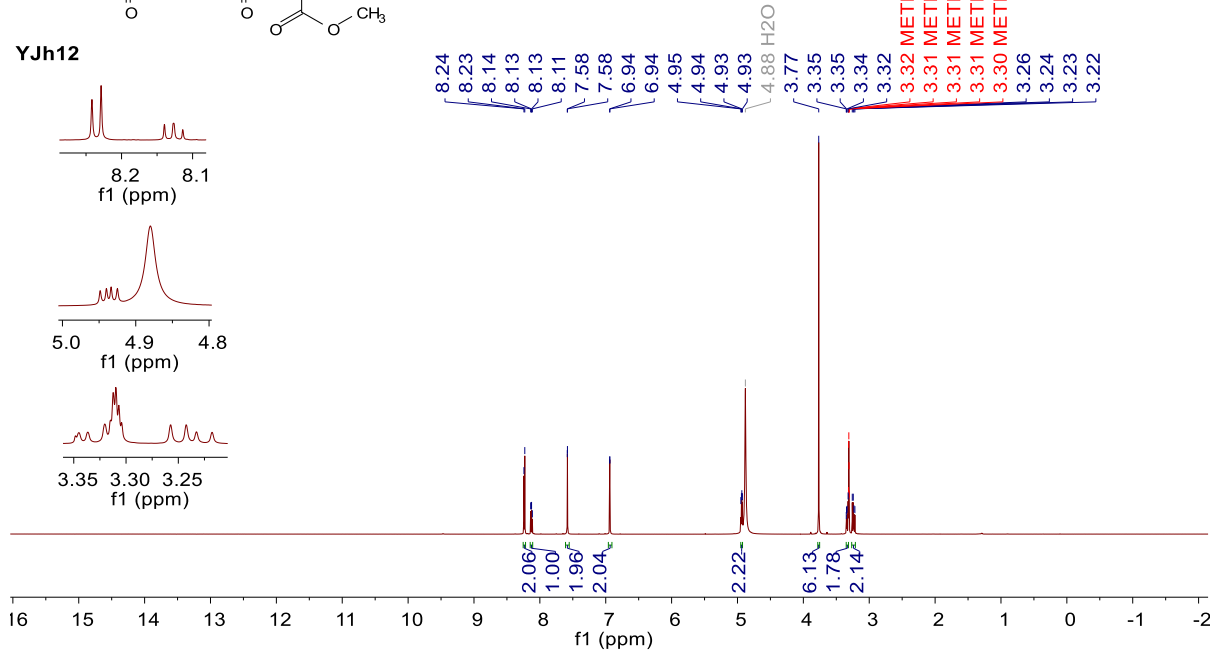
YJh12





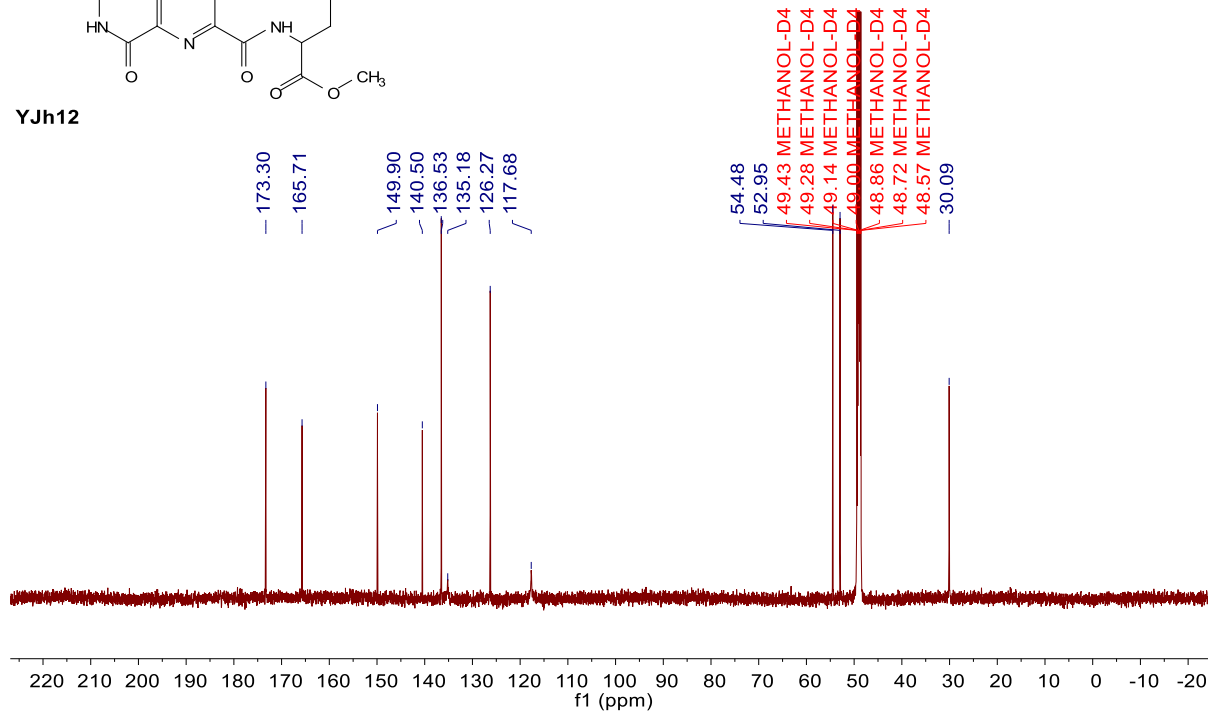
$^1\text{H NMR}$ (600 MHz, Methanol- d_4) δ 8.24 (d, $J = 7.7$ Hz, 2H), 8.13 (dd, $J = 8.2, 7.3$ Hz, 1H), 7.58 (d, $J = 1.2$ Hz, 2H), 6.94 (d, $J = 1.2$ Hz, 2H), 4.94 (dd, $J = 9.0, 5.1$ Hz, 2H), 3.77 (s, 6H), 3.37 – 3.20 (m, 4H).

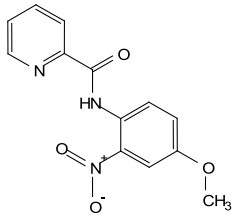
YJh12



$^{13}\text{C NMR}$ (151 MHz, Methanol- d_4) δ 173.30, 165.71, 149.90, 140.50, 136.53, 135.18, 126.27, 117.68, 54.48, 52.95, 30.09.

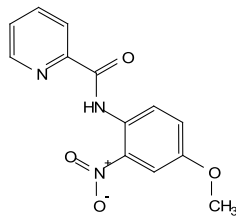
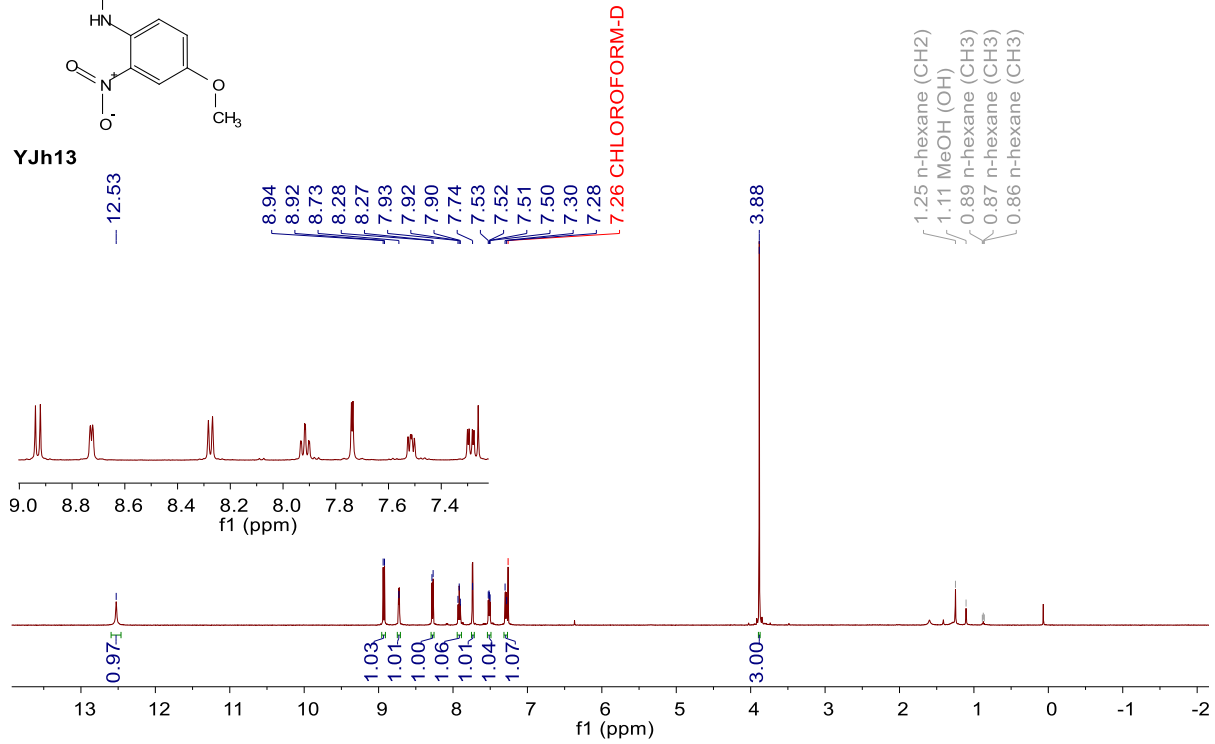
YJh12





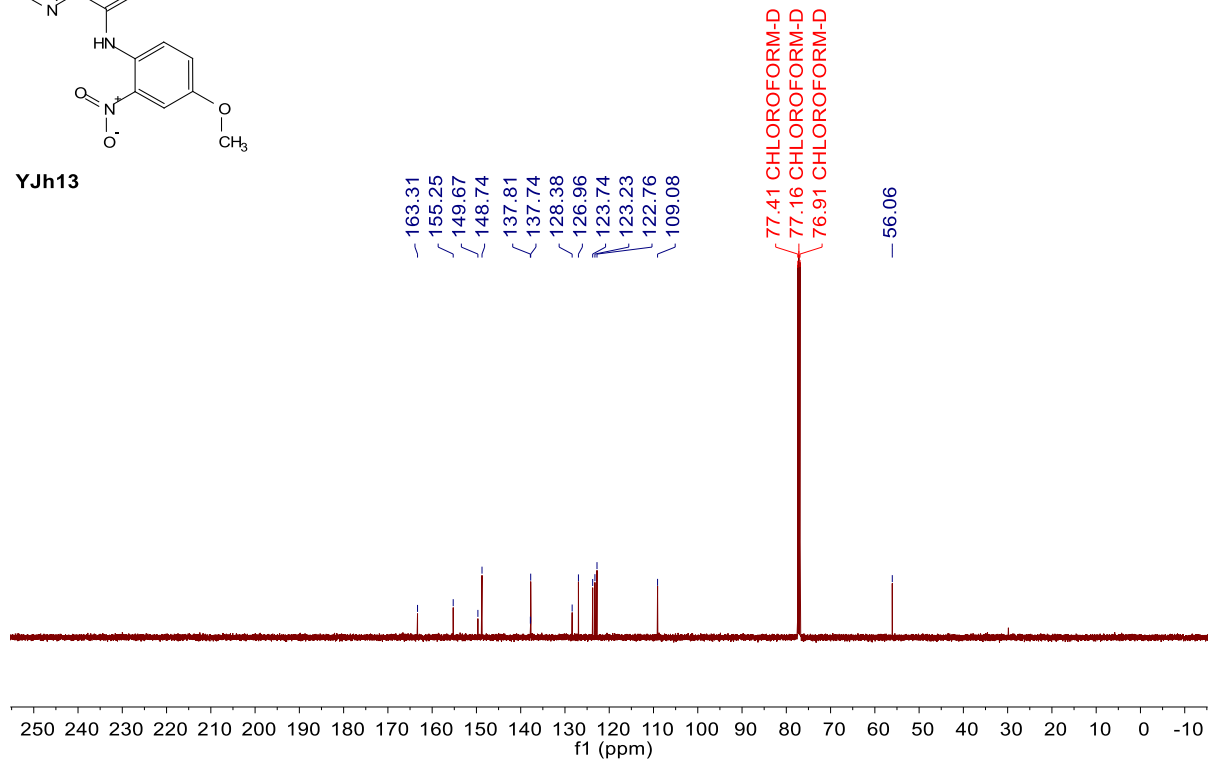
YJh13

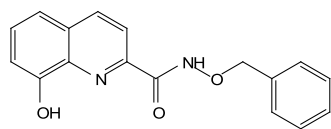
$^1\text{H NMR}$ (500 MHz, Chloroform- d) δ 12.53 (s, 1H), 8.93 (d, $J = 9.2$ Hz, 1H), 8.73 (s, 1H), 8.28 (d, $J = 7.8$ Hz, 1H), 7.92 (t, $J = 8.0$ Hz, 1H), 7.74 (s, 1H), 7.51 (dd, $J = 7.7, 4.9$ Hz, 1H), 7.29 (d, $J = 10.2$ Hz, 1H), 3.88 (s, 3H).



YJh13

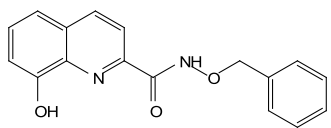
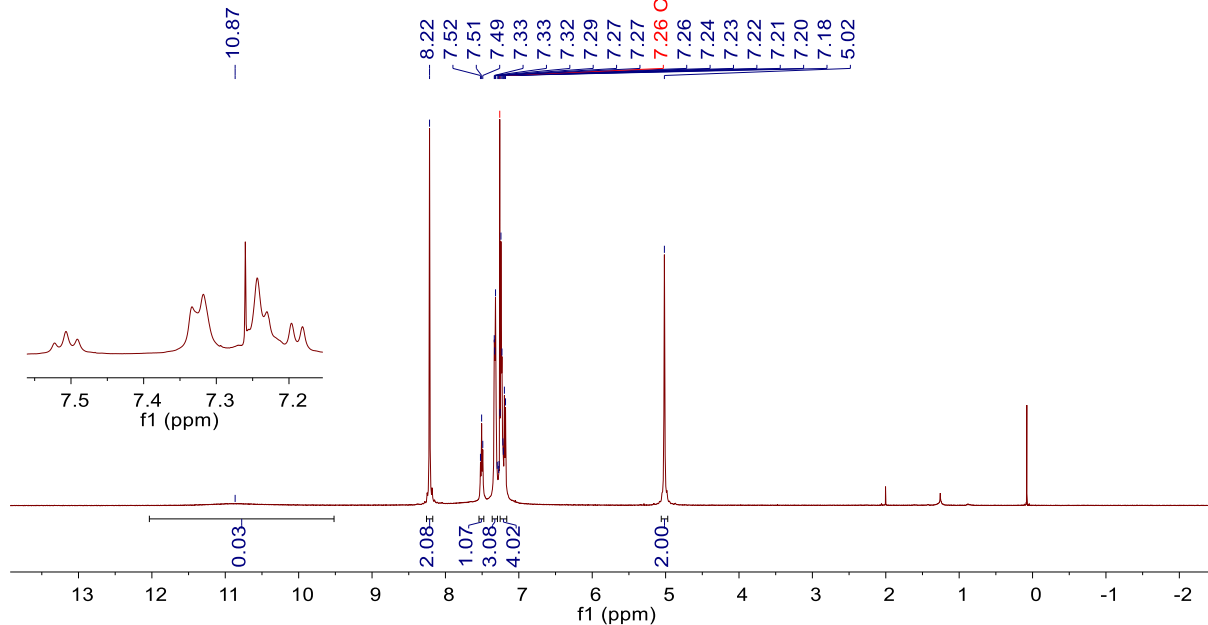
$^{13}\text{C NMR}$ (126 MHz, Chloroform- d) δ 163.31, 155.25, 149.67, 148.74, 137.81, 137.74, 128.38, 126.96, 123.74, 123.23, 122.76, 109.08, 56.06.





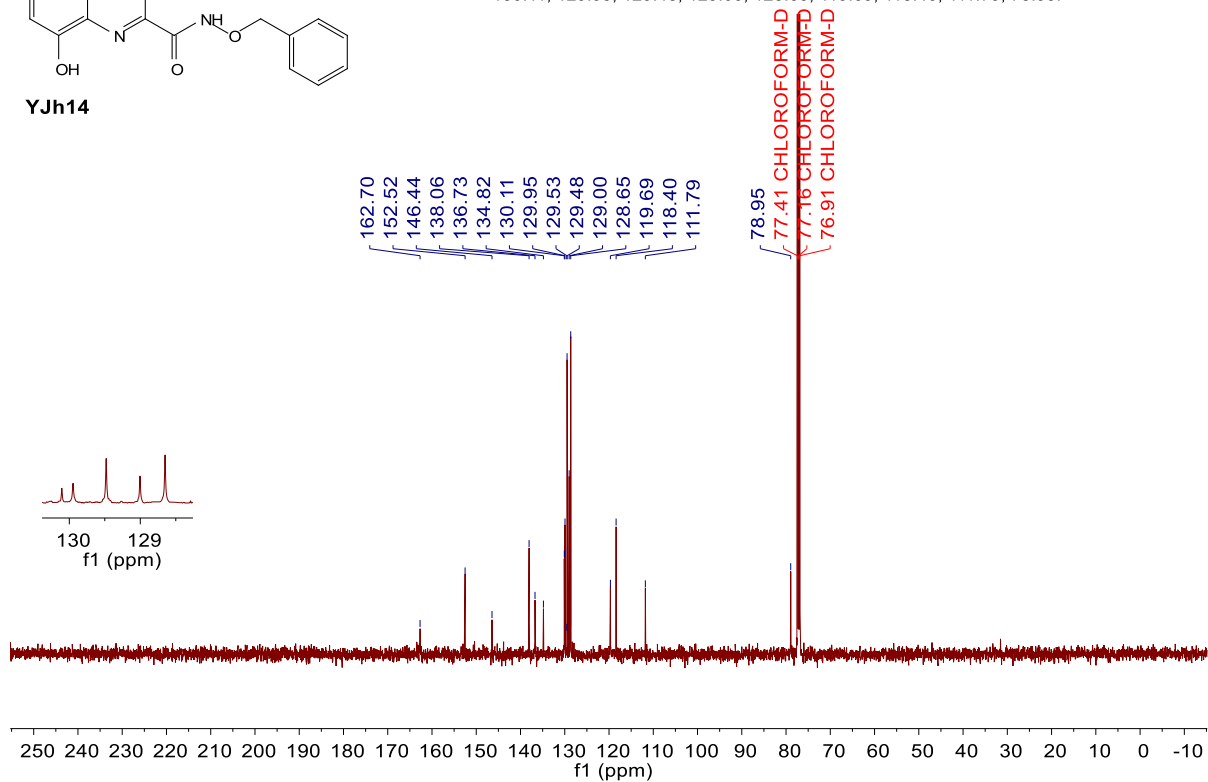
YJh14

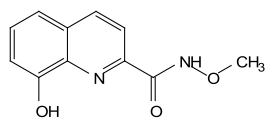
$^1\text{H NMR}$ (500 MHz, Chloroform- d) δ 8.22 (s, 2H), 7.51 (t, $J = 7.9$ Hz, 1H), 7.37 – 7.28 (m, 3H), 7.26 – 7.17 (m, 4H), 5.02 (s, 2H).



YJh14

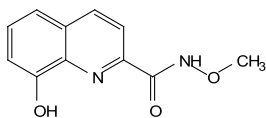
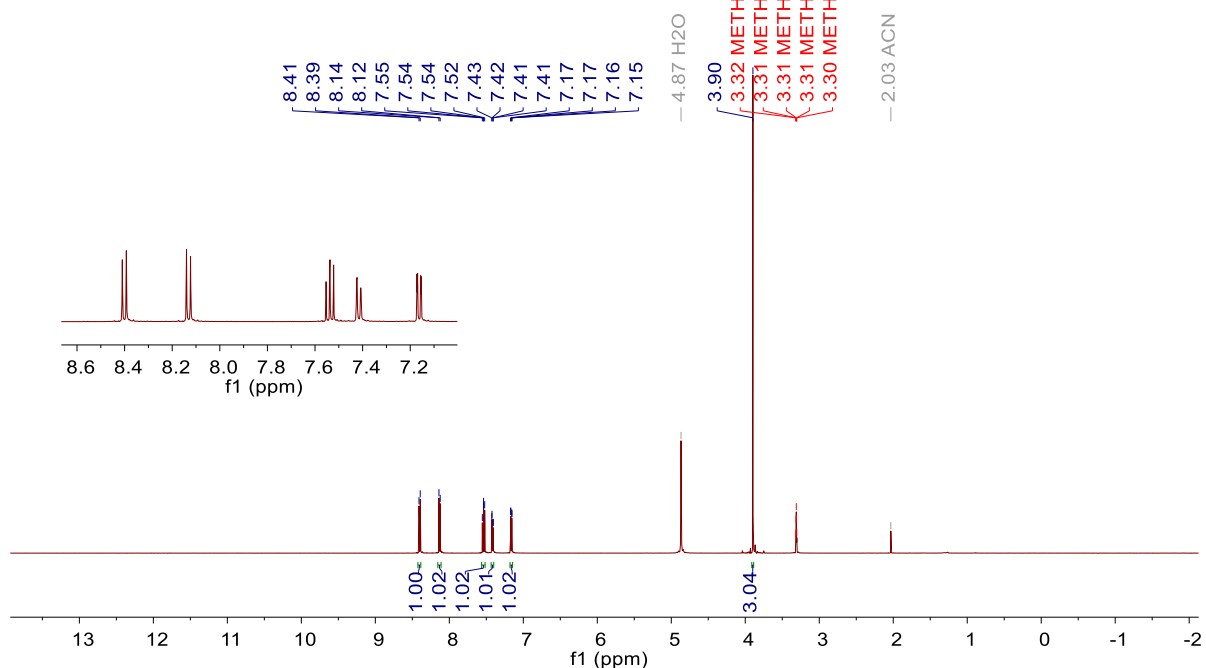
$^{13}\text{C NMR}$ (126 MHz, Chloroform- d) δ 162.70, 152.52, 146.44, 138.06, 136.73, 134.82, 130.11, 129.95, 129.48, 129.00, 128.65, 119.69, 118.40, 111.79, 78.95.





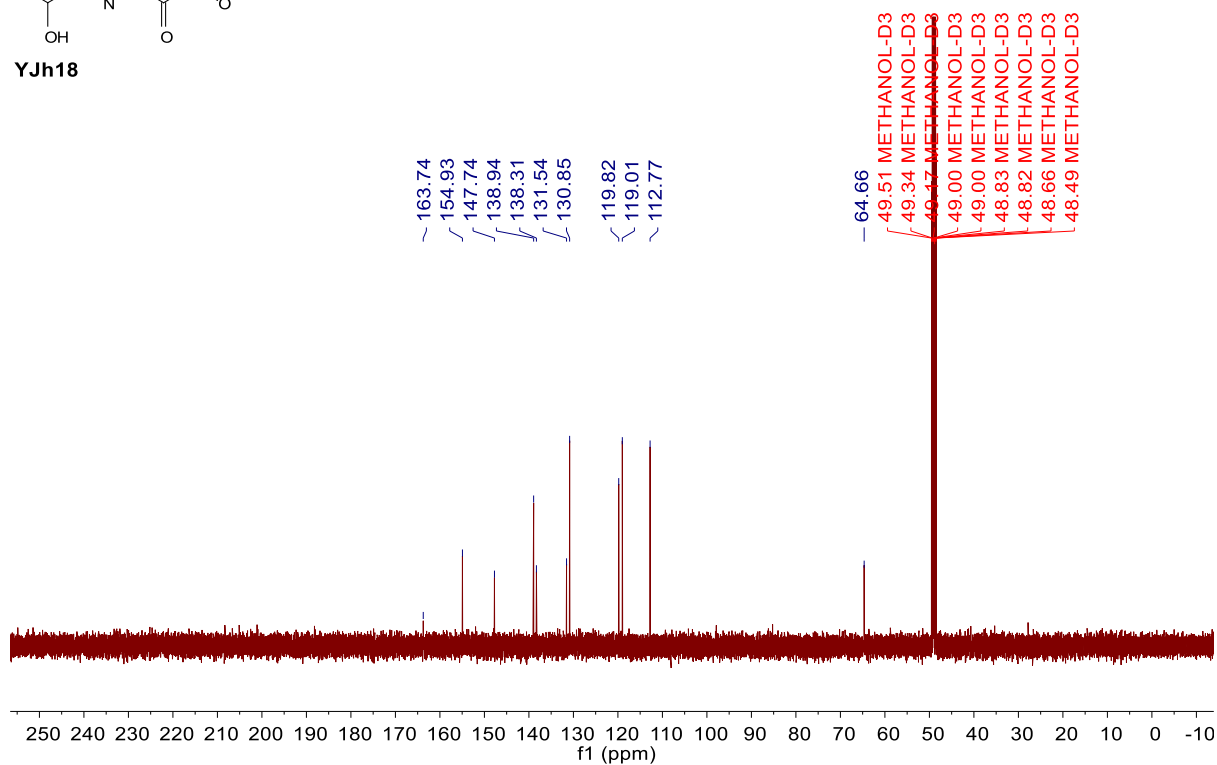
YJh18

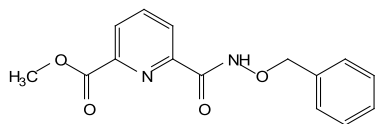
$^1\text{H NMR}$ (500 MHz, Methanol- d_4) δ 8.40 (d, $J = 8.5$ Hz, 1H), 8.13 (d, $J = 8.5$ Hz, 1H), 7.54 (dd, $J = 8.3, 7.6$ Hz, 1H), 7.42 (dd, $J = 8.3, 1.2$ Hz, 1H), 7.16 (dd, $J = 7.6, 1.2$ Hz, 1H), 3.90 (s, 3H).



YJh18

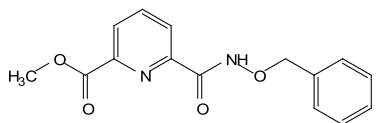
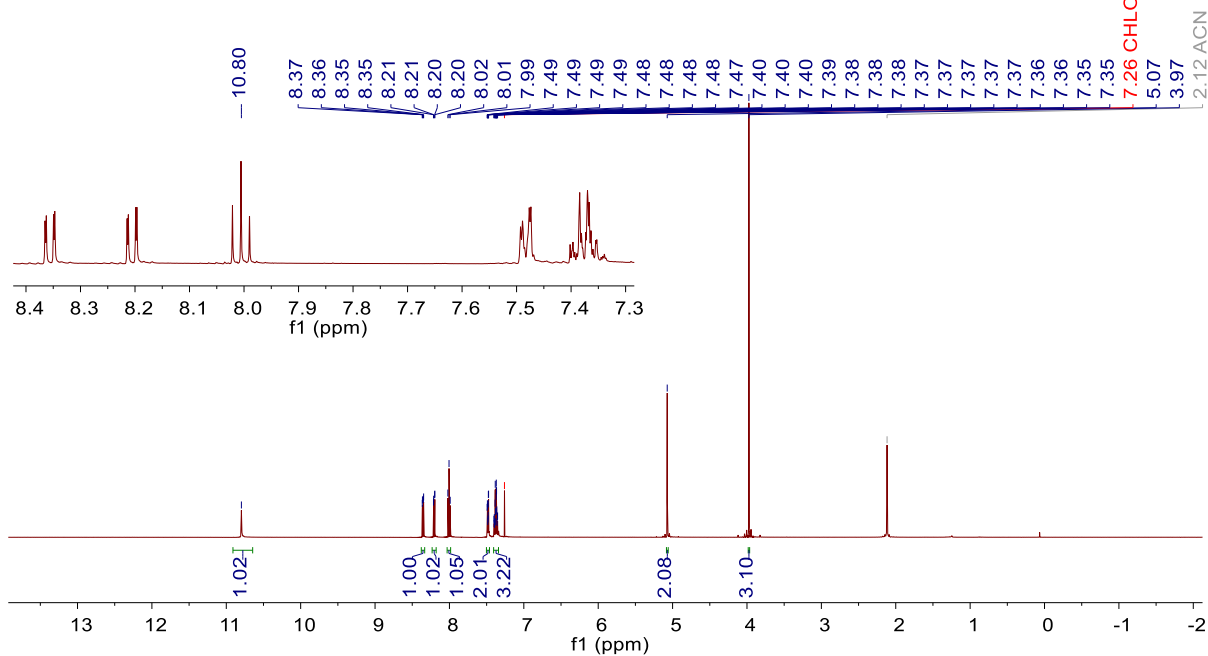
$^{13}\text{C NMR}$ (126 MHz, Methanol- d_4) δ 163.74, 154.93, 147.74, 138.94, 138.31, 131.54, 130.85, 119.82, 119.01, 112.77, 64.66.





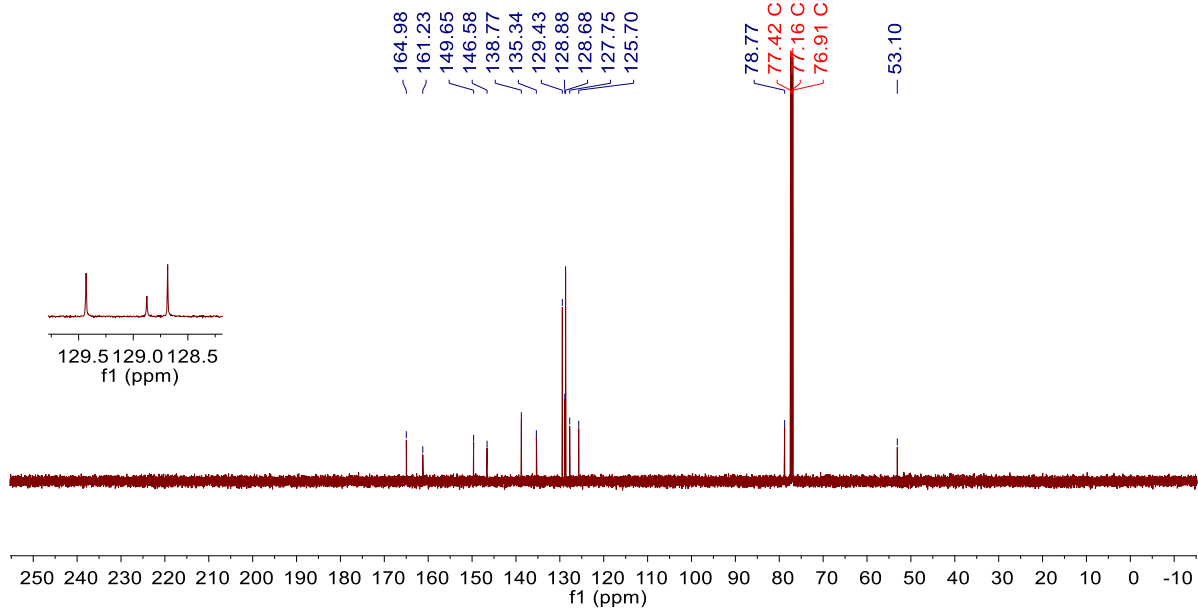
$^1\text{H NMR}$ (500 MHz, Chloroform-*d*) δ 10.80 (s, 1H), 8.36 (dd, $J = 7.8, 1.1$ Hz, 1H), 8.21 (dd, $J = 7.8, 1.1$ Hz, 1H), 8.01 (t, $J = 7.8$ Hz, 1H), 7.50 – 7.44 (m, 2H), 7.40 – 7.34 (m, 3H), 5.07 (s, 2H), 3.97 (s, 3H).

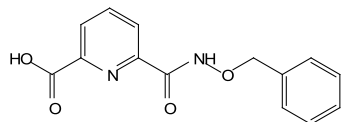
YJh19



$^{13}\text{C NMR}$ (126 MHz, Chloroform-*d*) δ 164.98, 161.23, 149.65, 146.58, 138.77, 135.34, 129.43, 128.88, 128.68, 127.75, 125.70, 78.77, 77.42, 77.16, 76.91, 53.10.

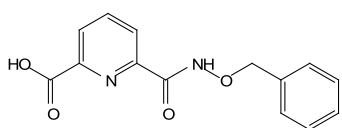
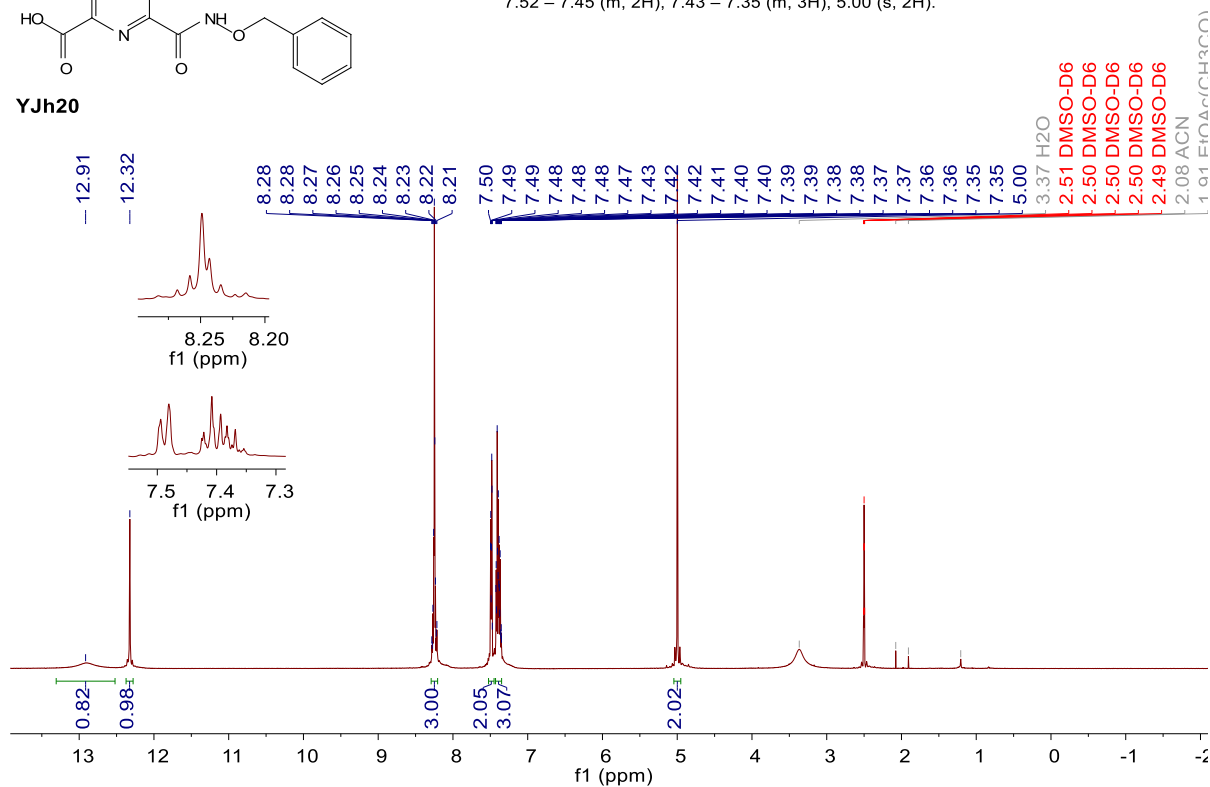
YJh19





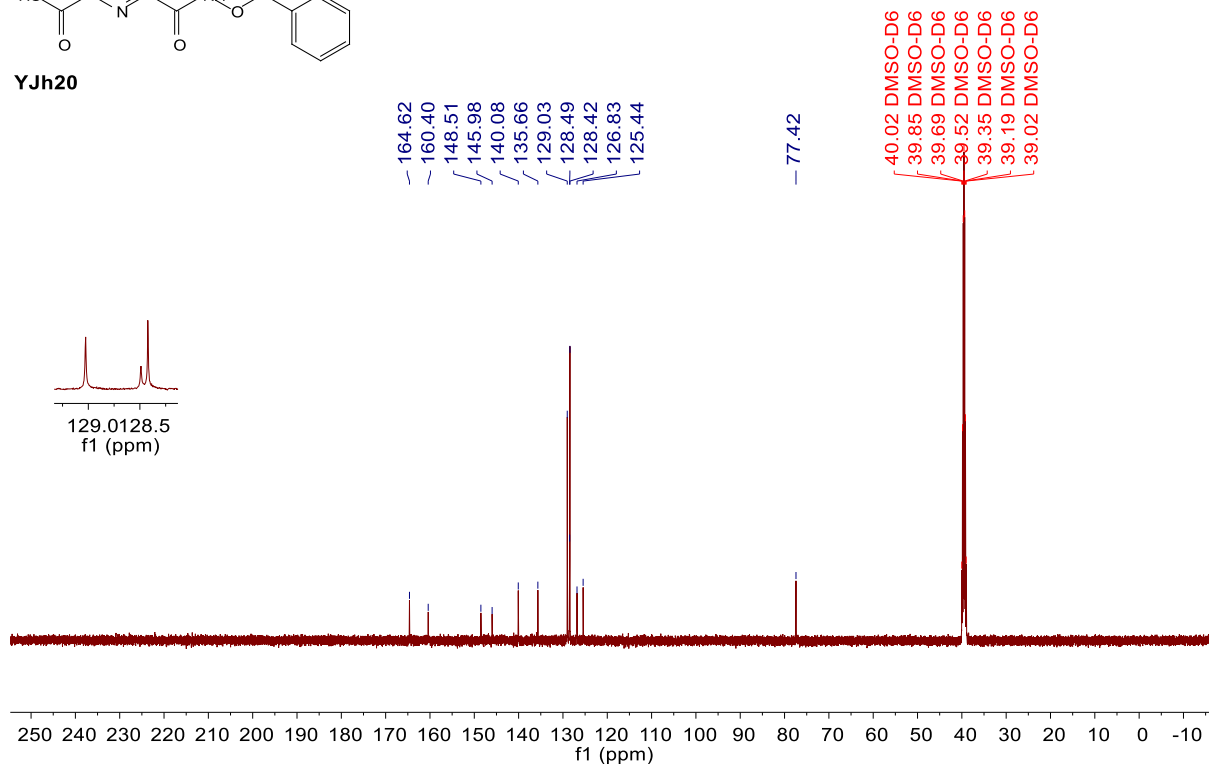
¹H NMR (500 MHz, DMSO-*d*₆) δ 12.91 (s, 1H), 12.32 (s, 1H), 8.29 – 8.21 (m, 3H), 7.52 – 7.45 (m, 2H), 7.43 – 7.35 (m, 3H), 5.00 (s, 2H).

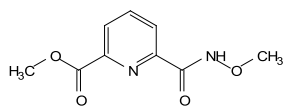
YJh20



¹³C NMR (126 MHz, DMSO-*d*₆) δ 164.62, 160.40, 148.51, 145.98, 140.08, 135.66, 129.03, 128.49, 128.42, 126.83, 125.44, 77.42.

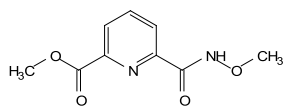
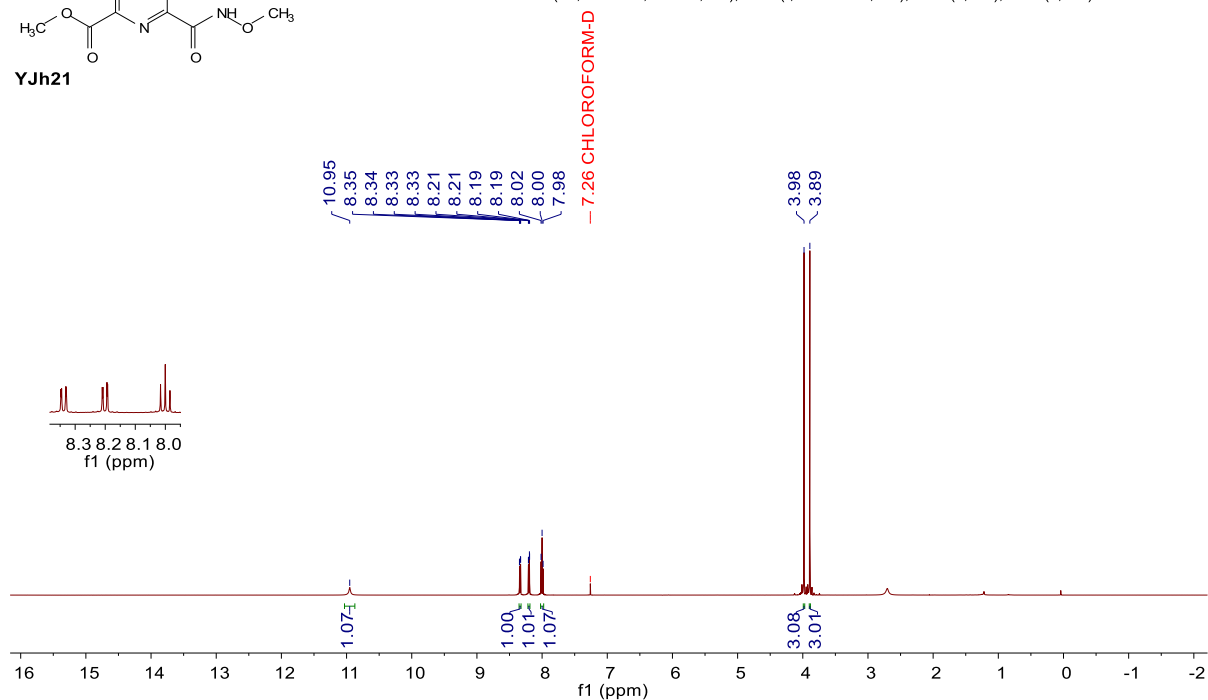
YJh20





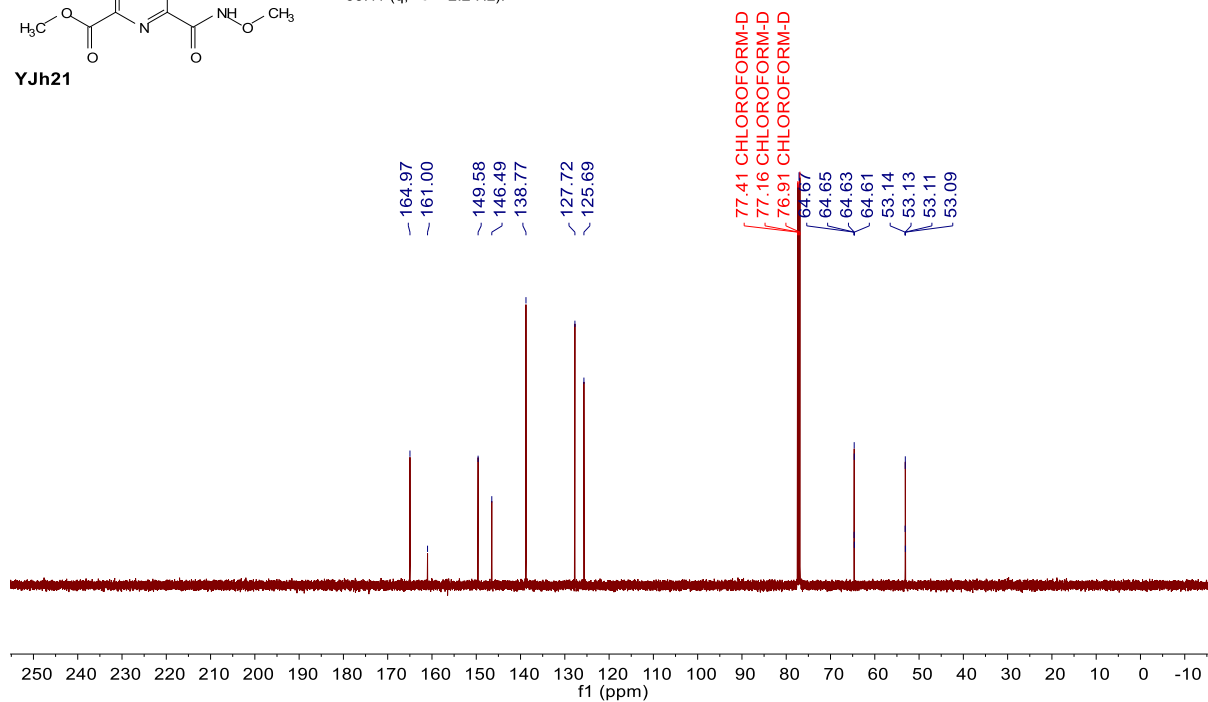
YJh21

¹H NMR (500 MHz, Chloroform-*d*) δ 10.95 (s, 1H), 8.34 (dd, *J* = 7.8, 1.1 Hz, 1H), 8.20 (dd, *J* = 7.8, 1.2 Hz, 1H), 8.00 (t, *J* = 7.8 Hz, 1H), 3.98 (s, 3H), 3.89 (s, 3H).

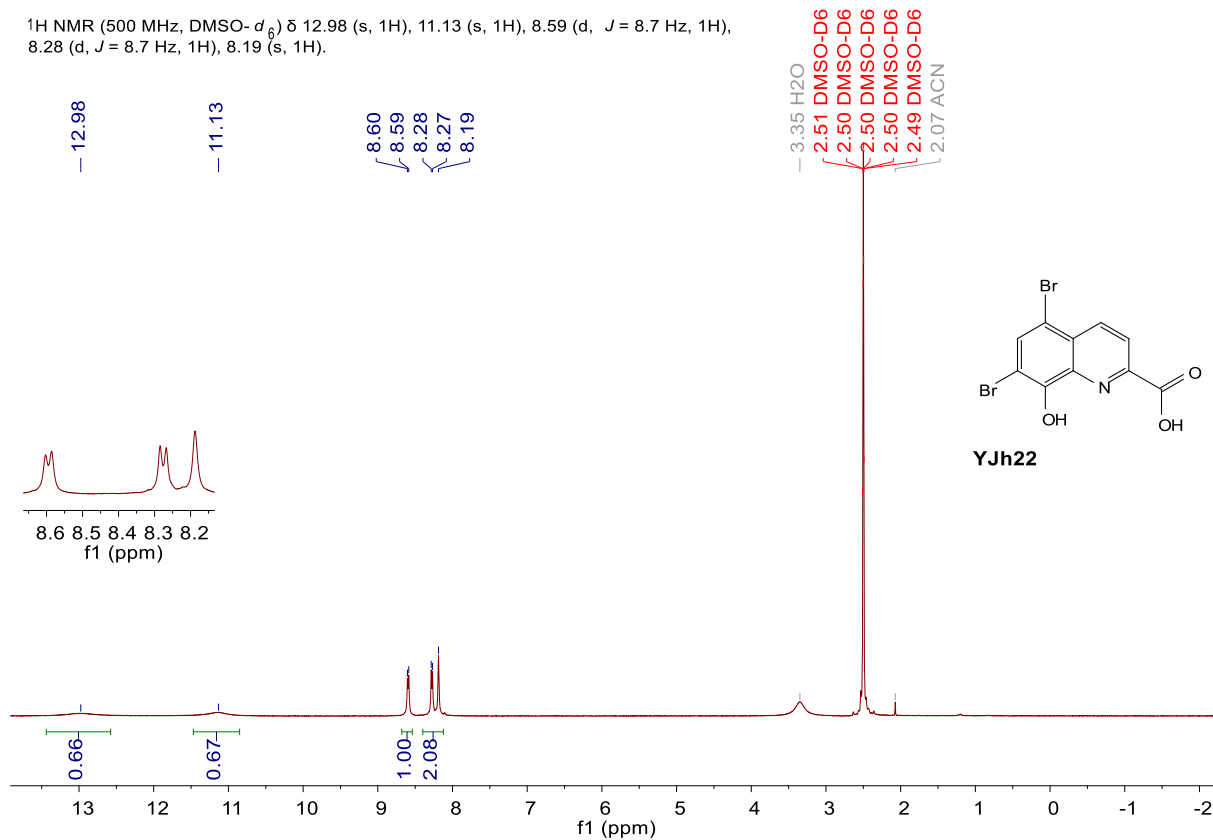


YJh21

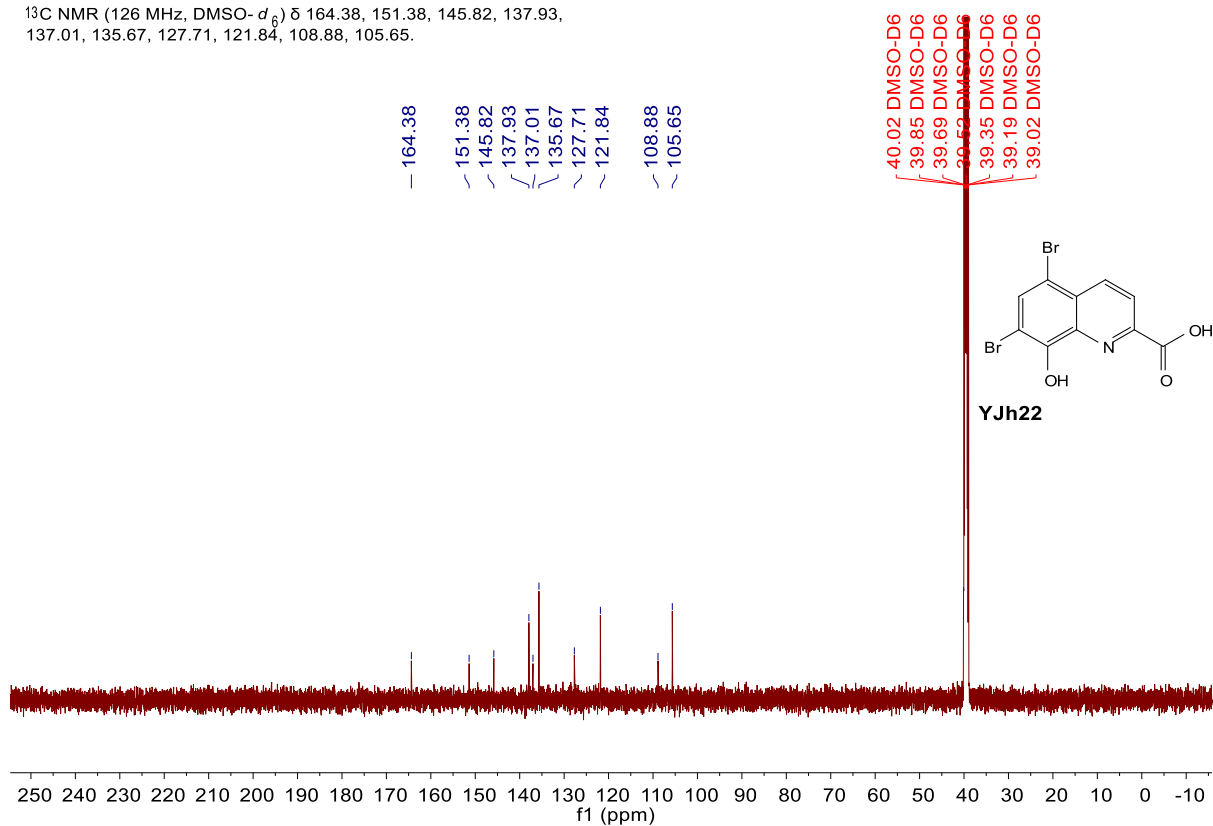
¹³C NMR (126 MHz, Chloroform-*d*) δ 164.97, 161.00, 149.58, 146.49, 138.77, 127.72, 125.69, 64.64 (q, *J* = 2.2 Hz), 53.11 (q, *J* = 2.2 Hz).

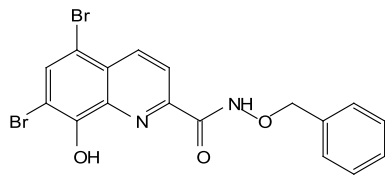


^1H NMR (500 MHz, $\text{DMSO}-d_6$) δ 12.98 (s, 1H), 11.13 (s, 1H), 8.59 (d, $J = 8.7$ Hz, 1H), 8.28 (d, $J = 8.7$ Hz, 1H), 8.19 (s, 1H).



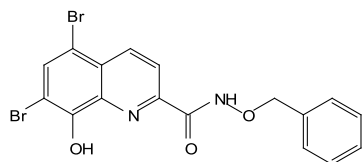
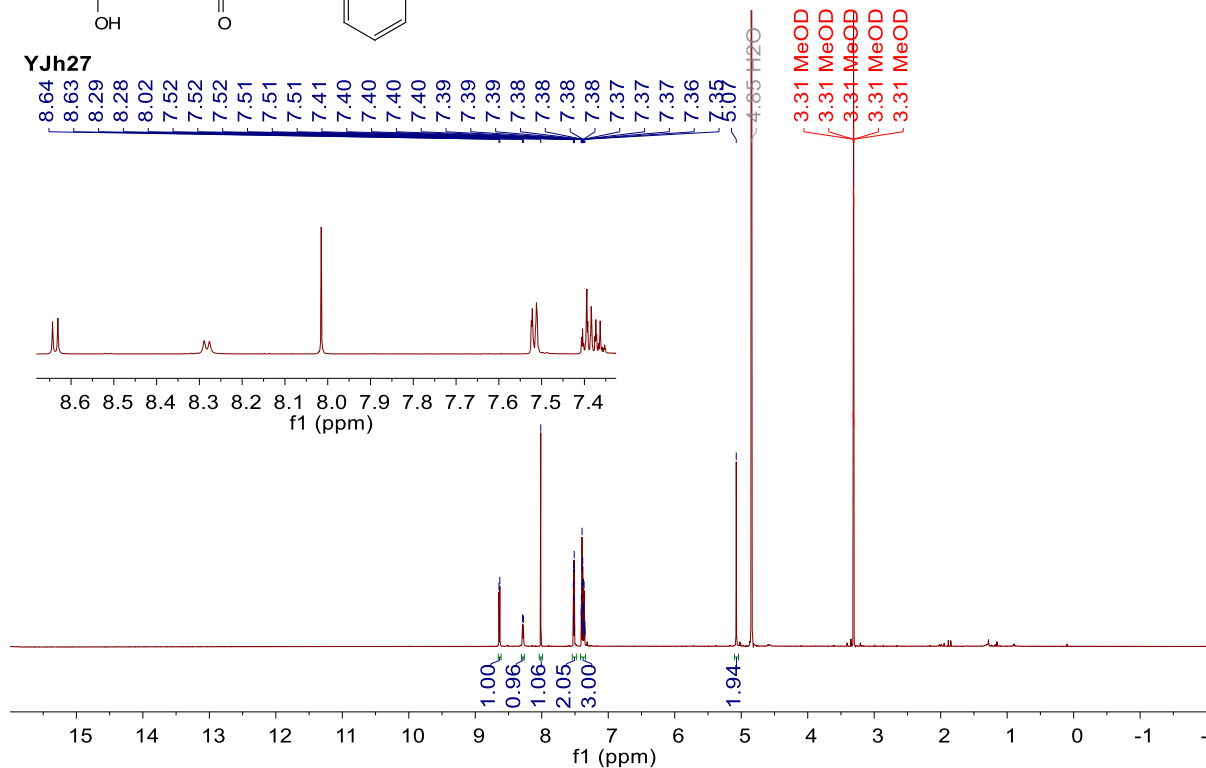
^{13}C NMR (126 MHz, $\text{DMSO}-d_6$) δ 164.38, 151.38, 145.82, 137.93, 137.01, 135.67, 127.71, 121.84, 108.88, 105.65.





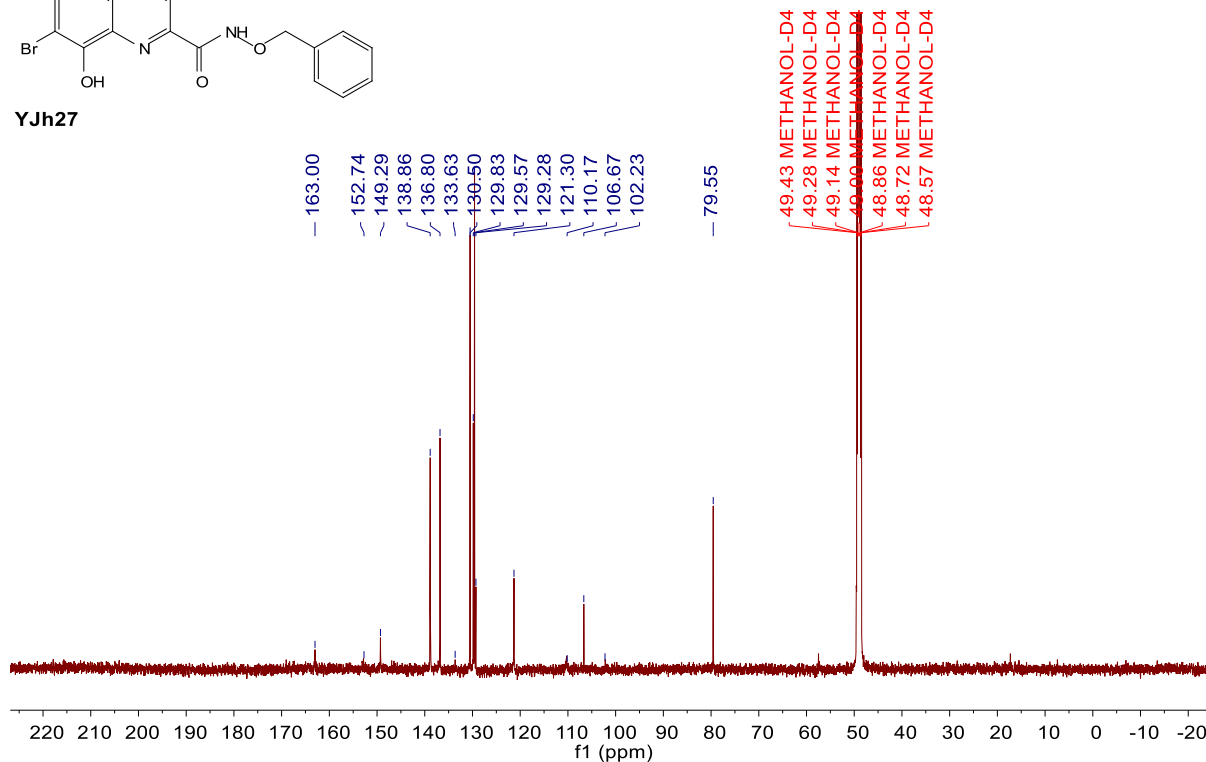
$^1\text{H NMR}$ (700 MHz, Methanol- d_4) δ 8.64 (d, $J = 8.7$ Hz, 1H), 8.28 (d, $J = 8.7$ Hz, 1H), 8.02 (s, 1H), 7.54 – 7.47 (m, 2H), 7.42 – 7.34 (m, 3H), 5.07 (s, 2H).

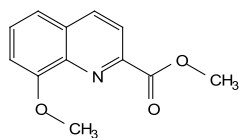
YJh27



$^{13}\text{C NMR}$ (151 MHz, Methanol- d_4) δ 163.00, 152.74, 149.29, 138.86, 136.80, 133.63, 130.50, 129.83, 129.57, 129.28, 121.30, 110.17, 106.67, 102.23, 79.55.

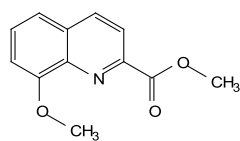
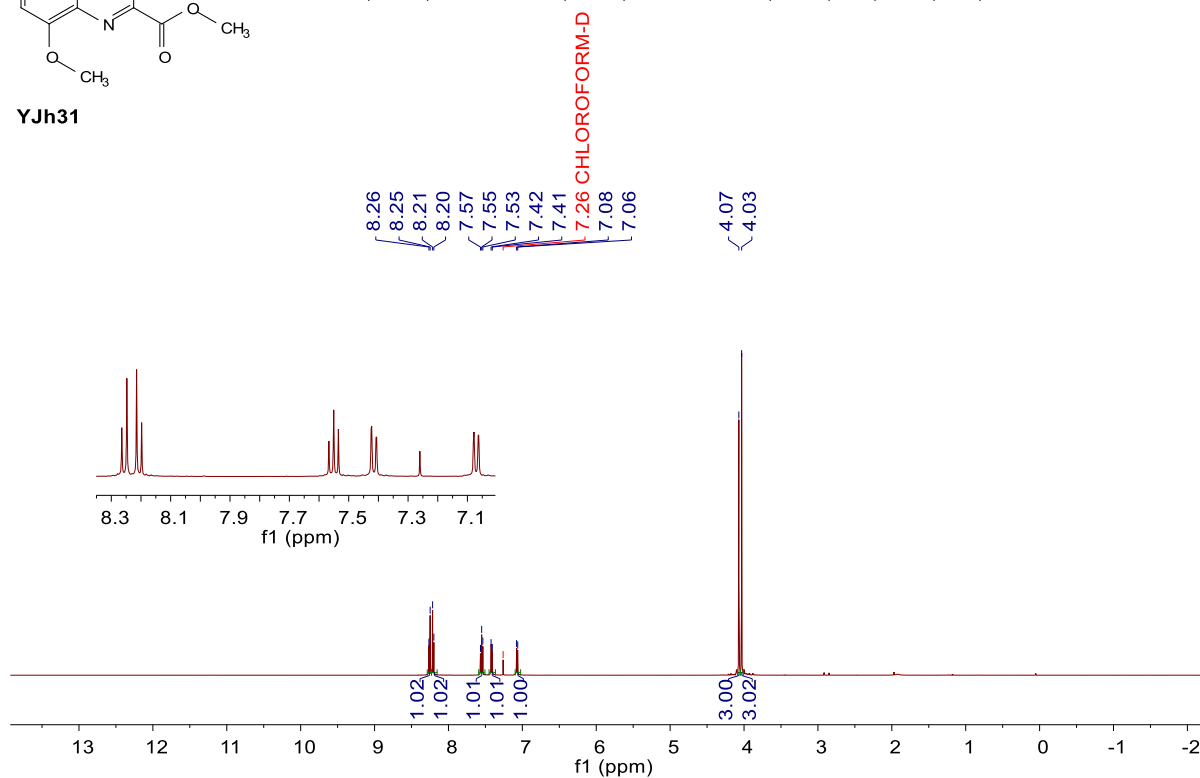
YJh27





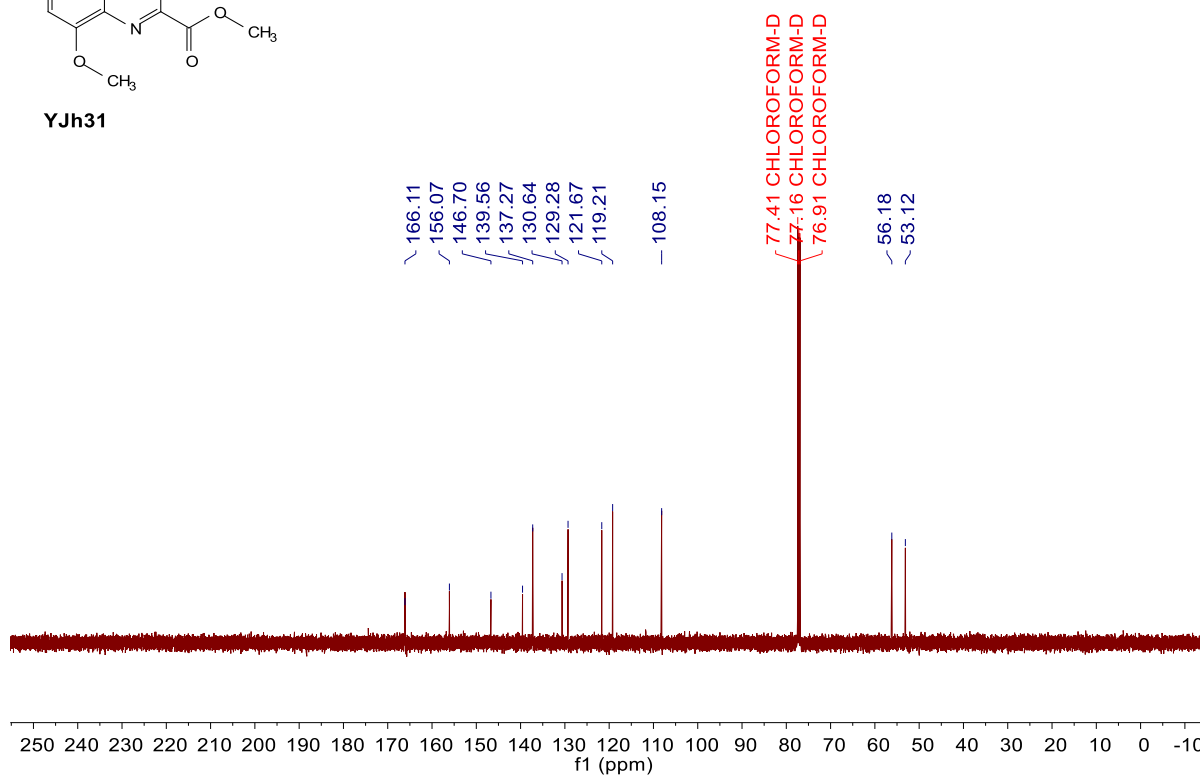
YJh31

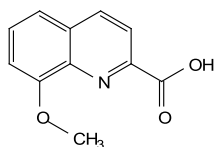
¹H NMR (500 MHz, Chloroform-*d*) δ 8.26 (d, *J* = 8.4 Hz, 1H), 8.21 (d, *J* = 8.5 Hz, 1H), 7.55 (t, *J* = 8.0 Hz, 2H), 7.41 (d, *J* = 8.5 Hz, 1H), 7.07 (d, *J* = 7.9 Hz, 1H), 4.07 (s, 5H), 4.03 (s, 5H).



YJh31

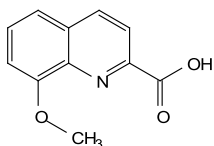
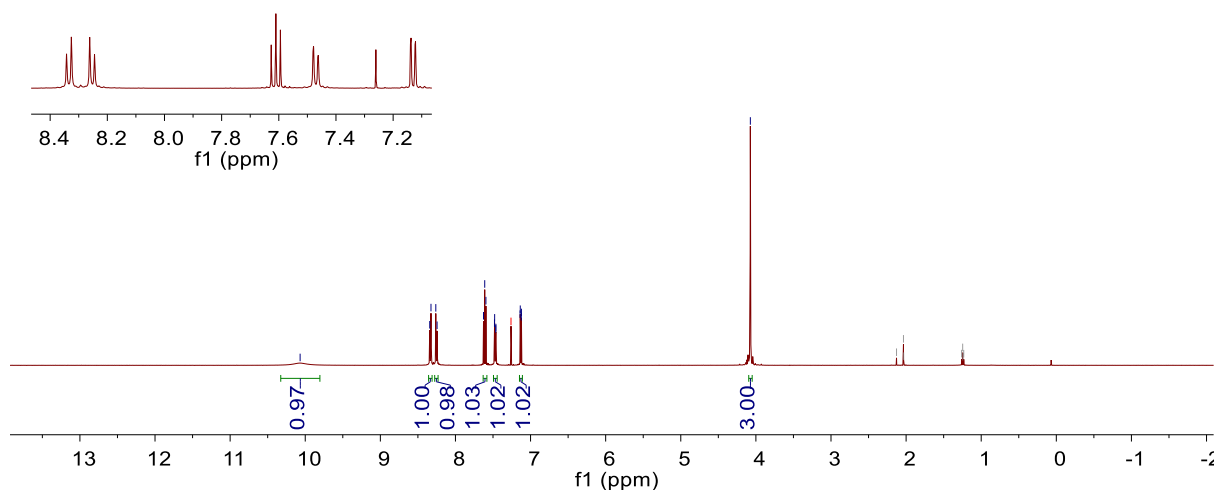
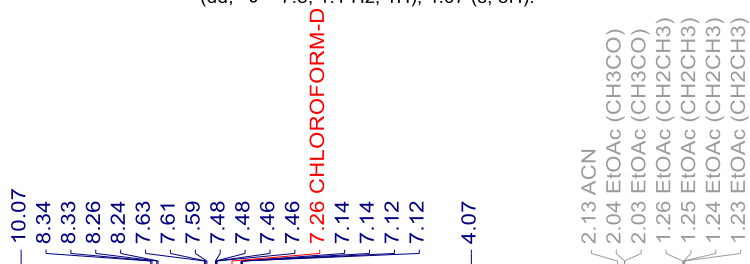
¹³C NMR (126 MHz, Chloroform-*d*) δ 166.11, 156.07, 146.70, 139.56, 137.27, 130.64, 129.28, 121.67, 119.21, 108.15, 56.18, 53.12.





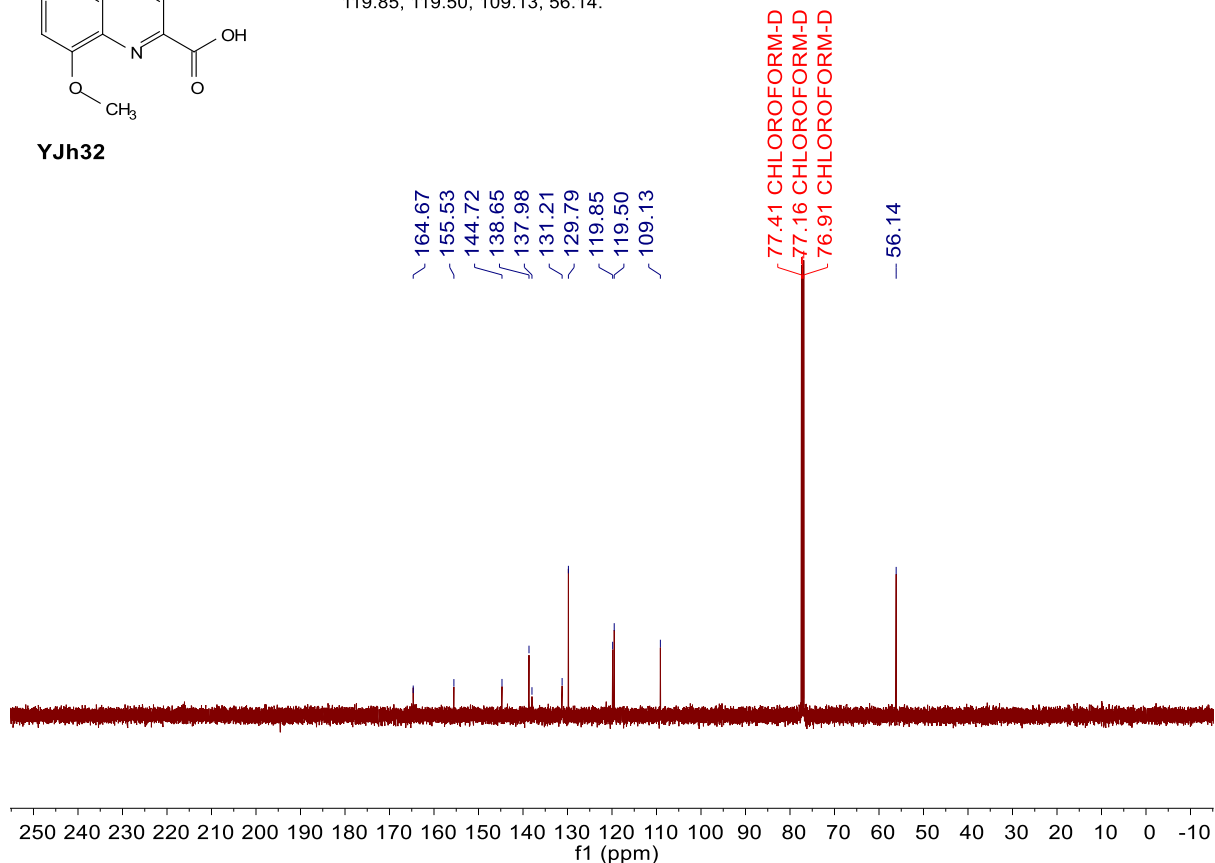
YJh32

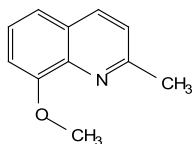
¹H NMR (500 MHz, Chloroform-*d*) δ 10.07 (s, 1H), 8.33 (d, *J* = 8.4 Hz, 1H), 8.25 (d, *J* = 8.4 Hz, 1H), 7.61 (t, *J* = 8.0 Hz, 1H), 7.47 (dd, *J* = 8.4, 1.2 Hz, 1H), 7.13 (dd, *J* = 7.8, 1.1 Hz, 1H), 4.07 (s, 3H).



YJh32

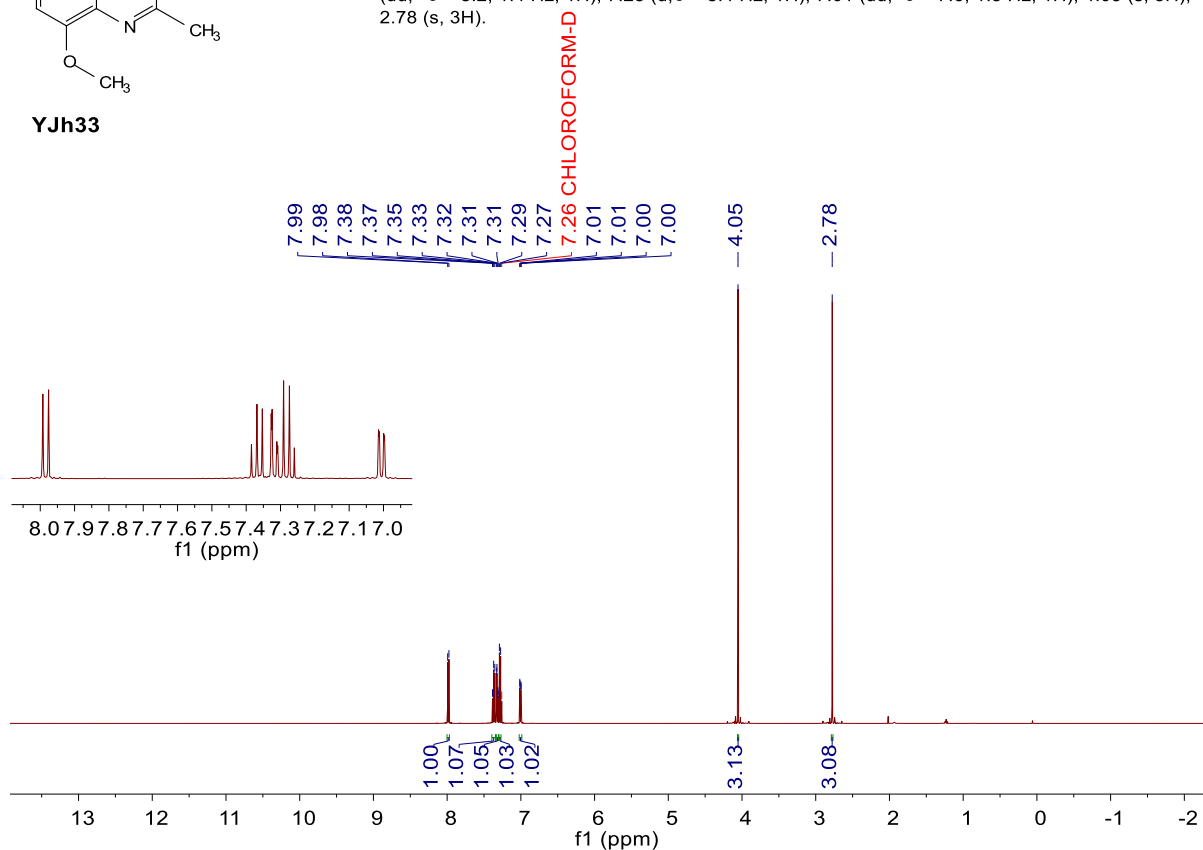
¹³C NMR (126 MHz, Chloroform-*d*) δ 164.67, 155.53, 144.72, 138.65, 137.98, 131.21, 129.79, 119.85, 119.50, 109.13, 56.14.



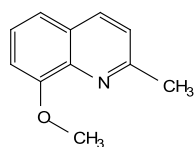
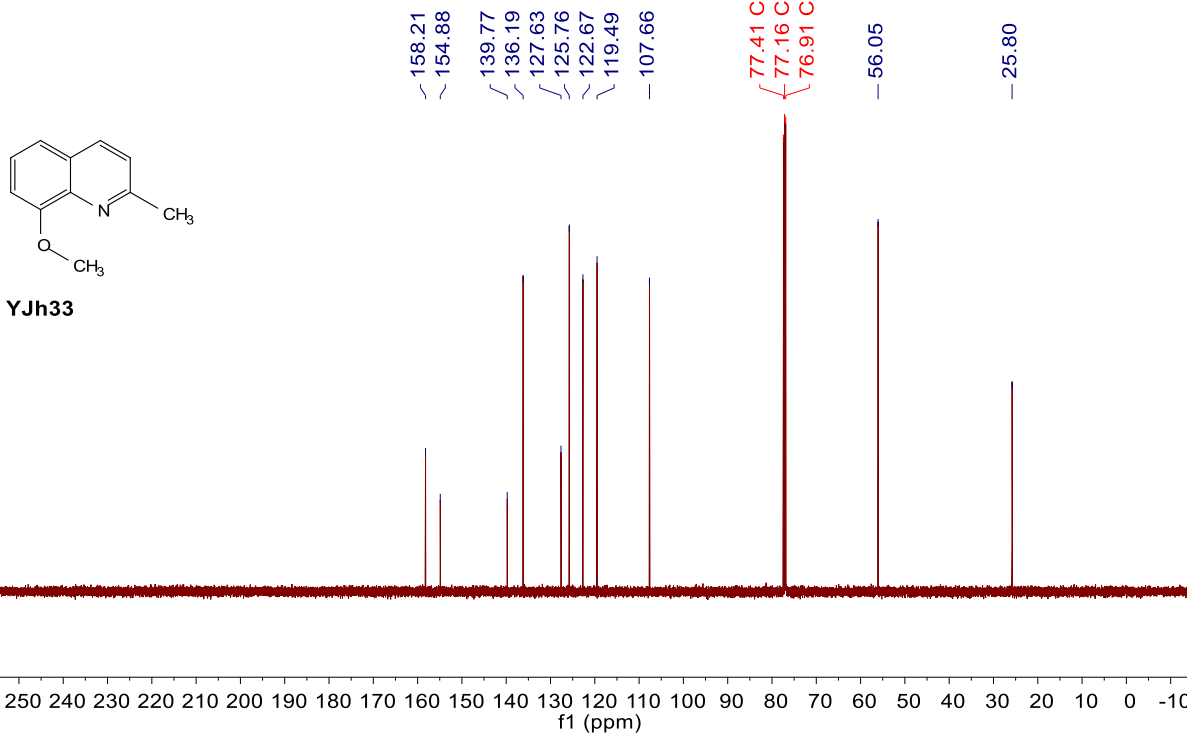


YJh33

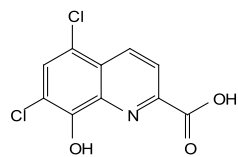
$^1\text{H NMR}$ (500 MHz, Chloroform-*d*) δ 7.98 (d, $J = 8.4$ Hz, 1H), 7.37 (t, $J = 8.1$ Hz, 1H), 7.32 (dd, $J = 8.2, 1.4$ Hz, 1H), 7.28 (d, $J = 8.4$ Hz, 1H), 7.01 (dd, $J = 7.6, 1.3$ Hz, 1H), 4.05 (s, 3H), 2.78 (s, 3H).



$^{13}\text{C NMR}$ (126 MHz, Chloroform-*d*) δ 158.21, 154.88, 139.77, 136.19, 127.63, 125.76, 122.67, 119.49, 107.66, 56.05, 25.80.

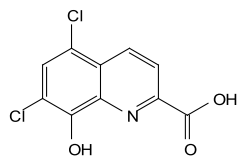
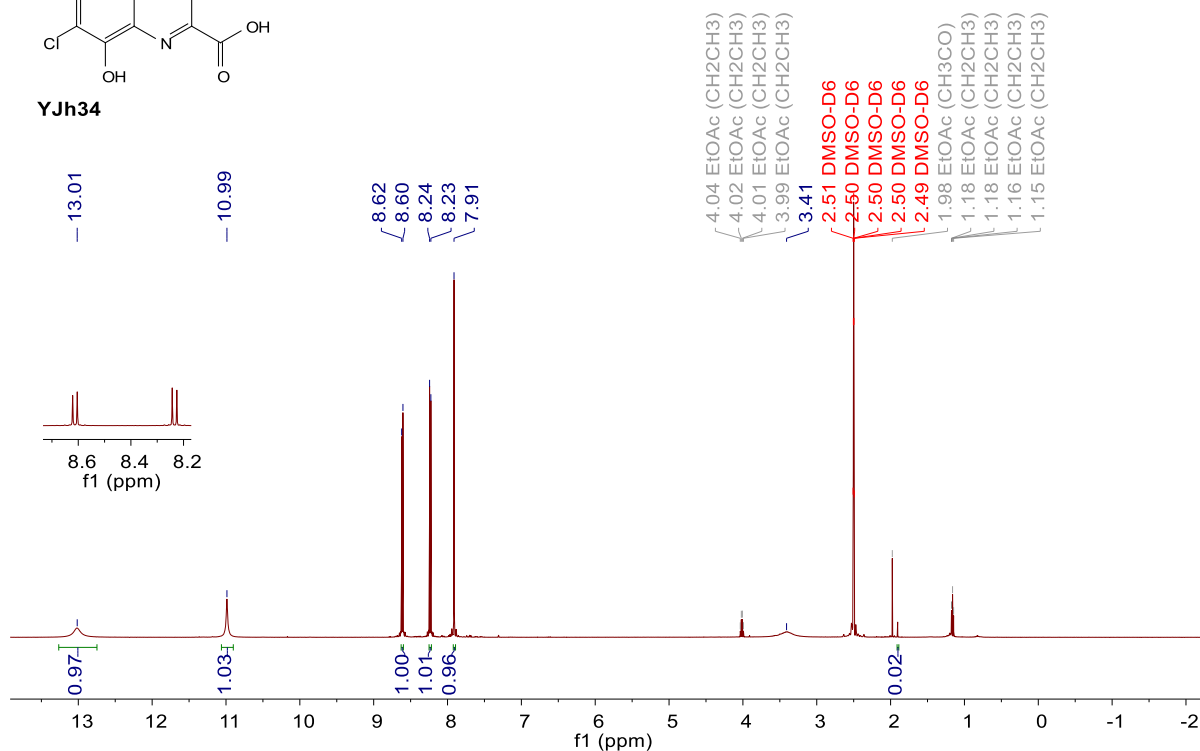


YJh33



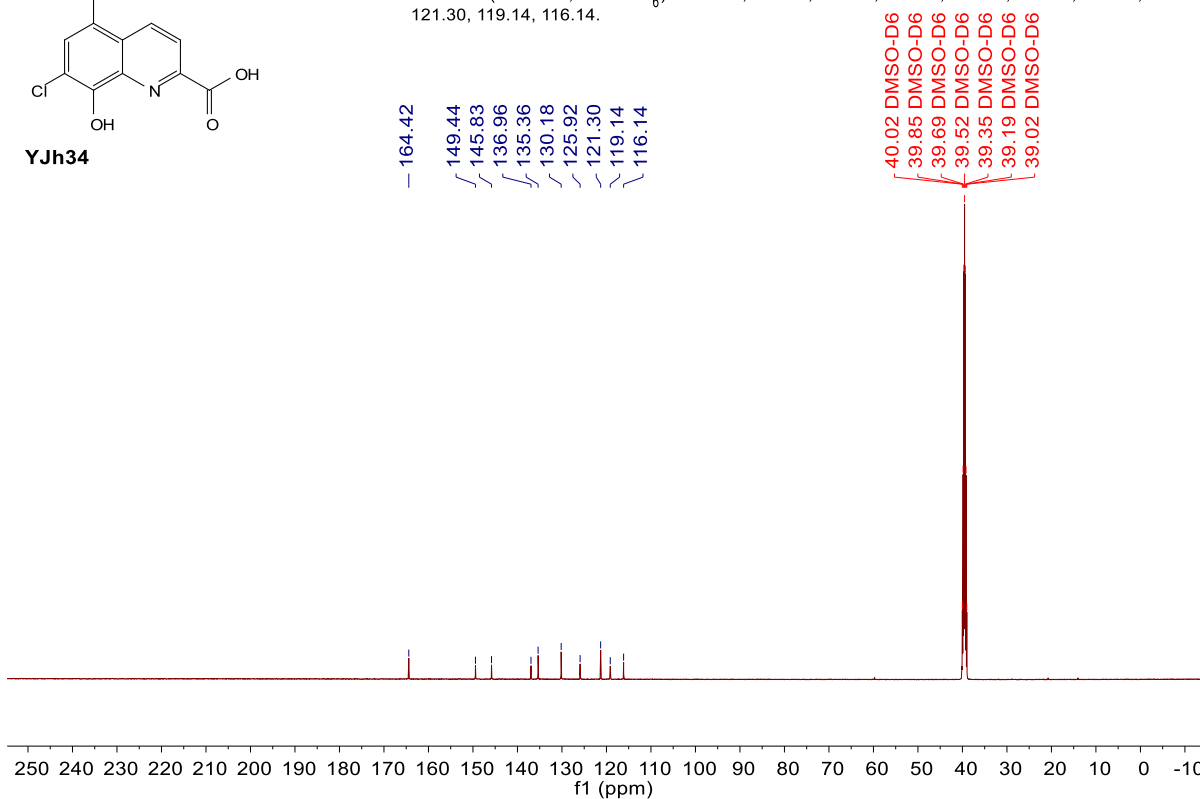
YJh34

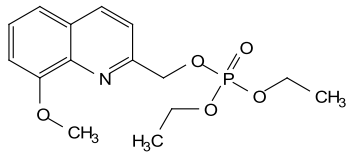
$^1\text{H NMR}$ (500 MHz, DMSO-d_6) δ 13.01 (s, 1H), 10.99 (s, 1H), 8.61 (d, $J = 8.7$ Hz, 1H), 8.23 (d, $J = 8.7$ Hz, 1H), 7.91 (s, 1H).



YJh34

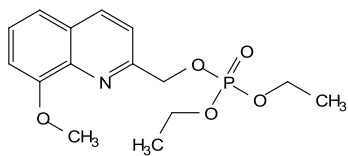
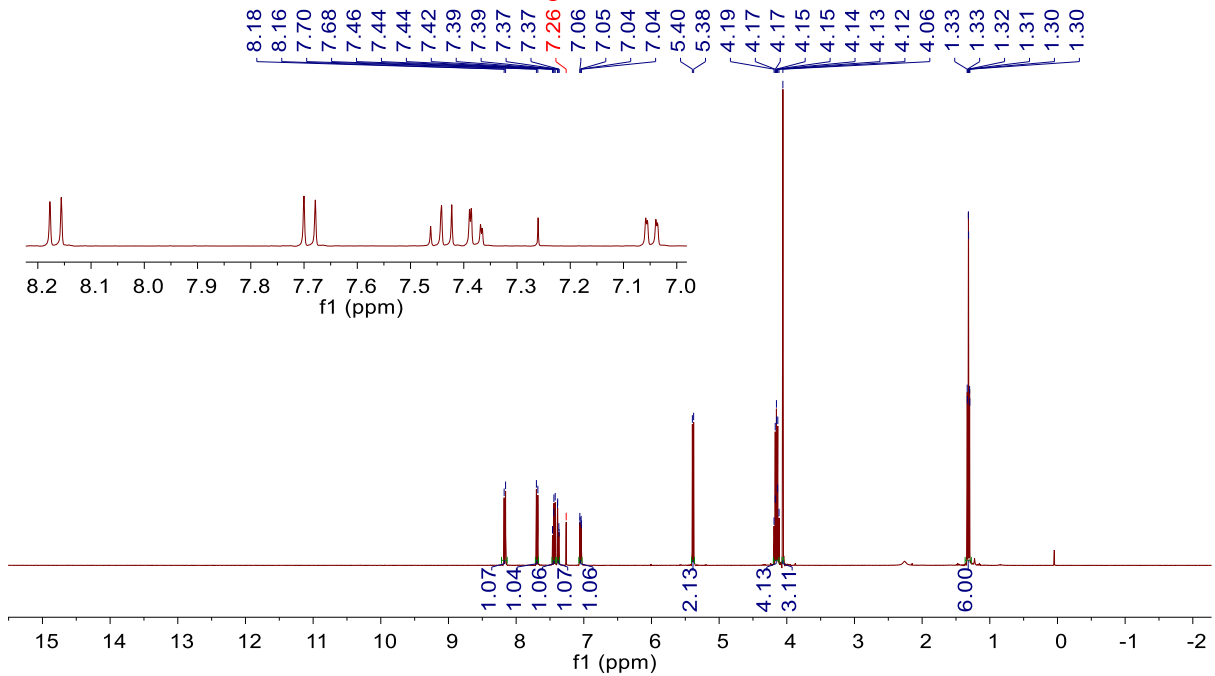
$^{13}\text{C NMR}$ (126 MHz, DMSO-d_6) δ 164.42, 149.44, 145.83, 136.96, 135.36, 130.18, 125.92, 121.30, 119.14, 116.14.





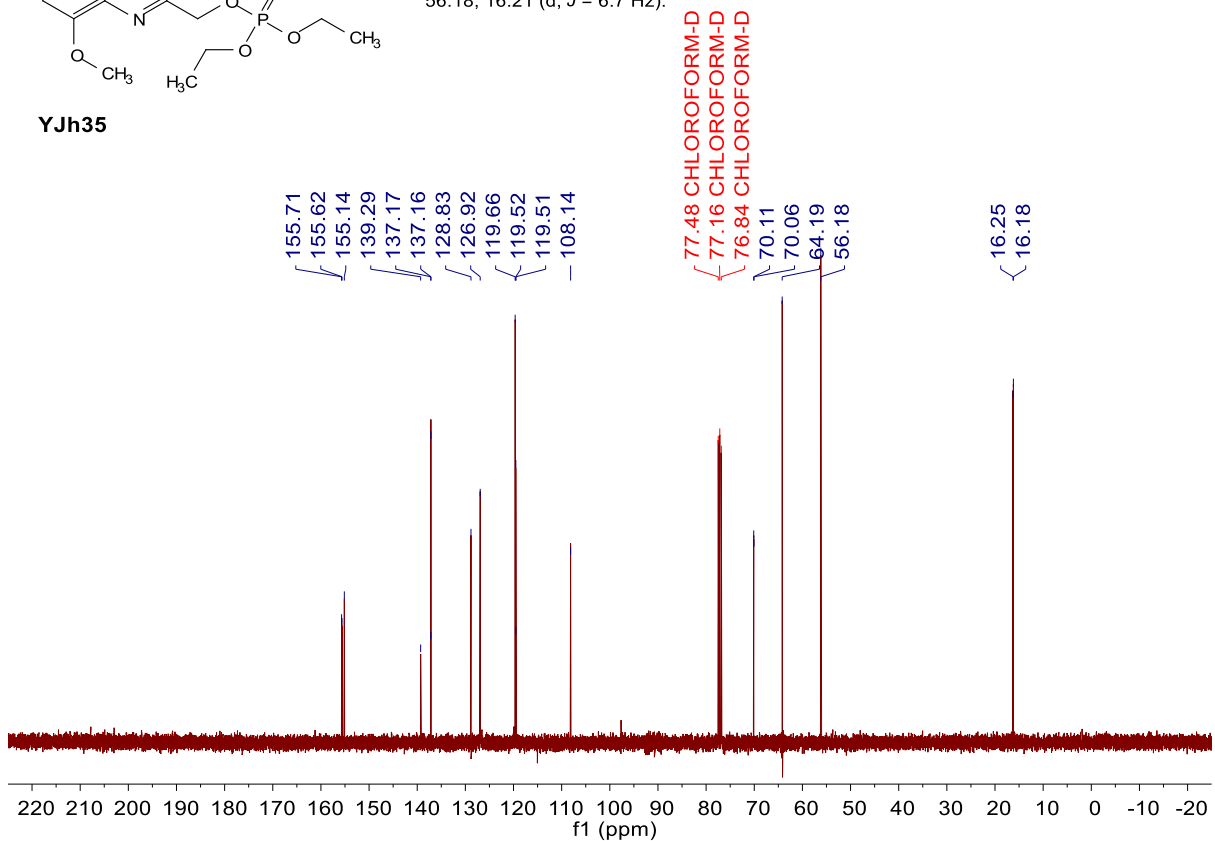
YJh35

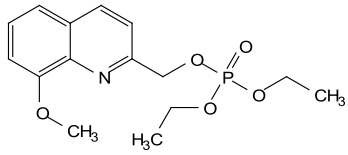
$^1\text{H NMR}$ (400 MHz, Chloroform- d) δ 8.17 (d, $J = 8.5$ Hz, 1H), 7.69 (d, $J = 8.5$ Hz, 1H), 7.44 (dd, $J = 8.2, 7.6$ Hz, 1H), 7.38 (dd, $J = 8.3, 1.4$ Hz, 1H), 7.05 (dd, $J = 7.6, 1.3$ Hz, 1H), 5.39 (d, $J = 7.5$ Hz, 2H), 4.20 – 4.12 (m, 4H), 4.06 (s, 3H), 1.32 (td, $J = 7.1, 1.0$ Hz, 6H).



YJh35

$^{13}\text{C NMR}$ (101 MHz, Chloroform- d) δ 155.67 (d, $J = 9.1$ Hz), 155.14, 139.29, 137.16, 128.83, 126.92, 119.66, 119.52 (d, $J = 1.0$ Hz), 108.14, 70.08 (d, $J = 5.7$ Hz), 64.19, 56.18, 16.21 (d, $J = 6.7$ Hz).

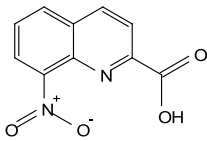
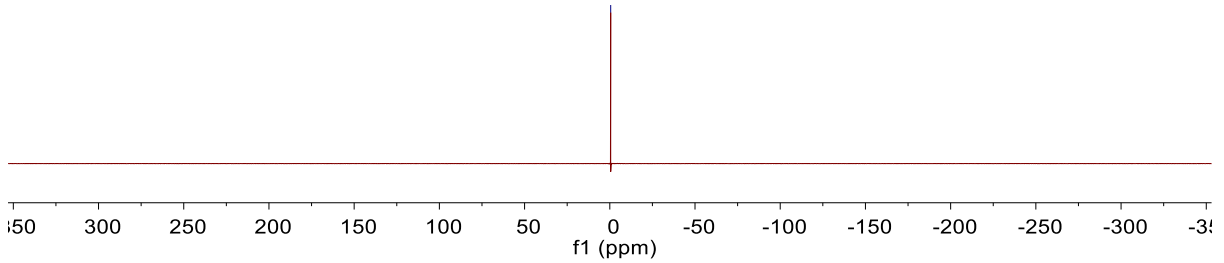




YJh35

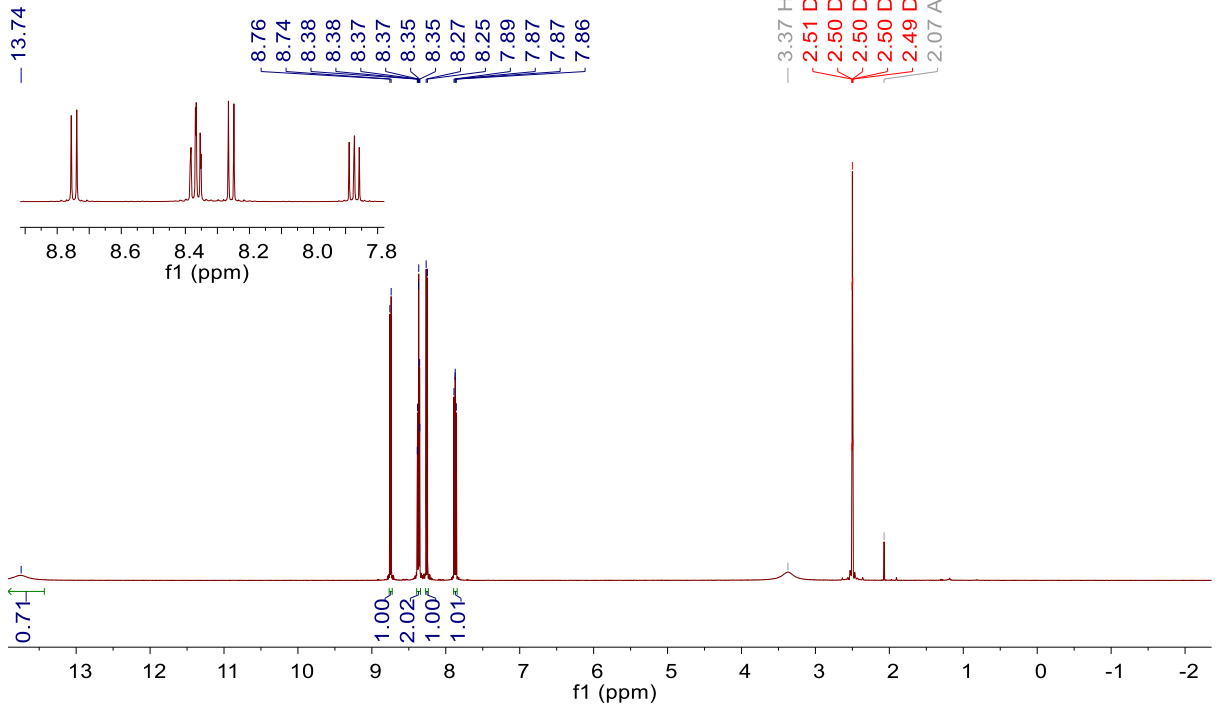
^{31}P NMR (162 MHz, Chloroform d) δ -0.53.

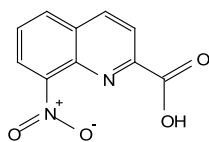
-0.53



YJh36

^1H NMR (500 MHz, DMSO- d_6) δ 13.74 (s, 1H), 8.75 (d, J = 8.6 Hz, 1H), 8.37 (td, J = 7.7, 1.3 Hz, 2H), 8.26 (d, J = 8.5 Hz, 1H), 7.87 (dd, J = 8.3, 7.5 Hz, 1H).



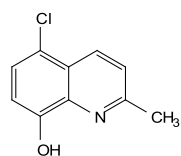
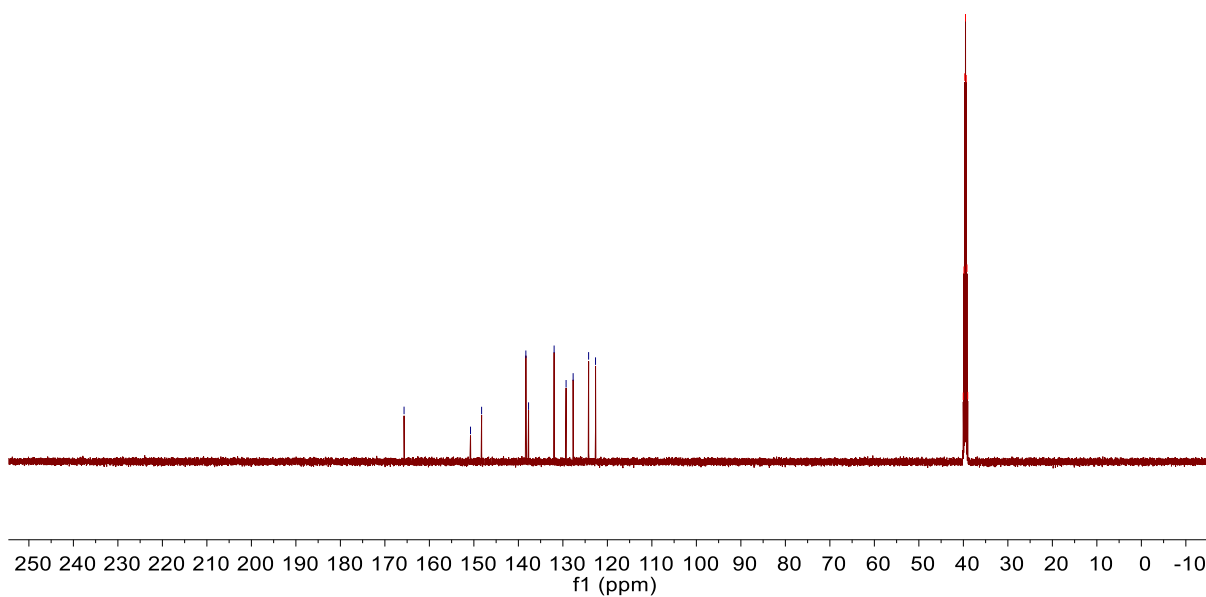


YJh36

^{13}C NMR (126 MHz, $\text{DMSO-}d_6$) δ 165.69, 150.76, 148.26, 138.32, 137.71, 131.97, 129.28, 127.69, 124.22, 122.66.

165.69
150.76
148.26
138.32
137.71
131.97
129.28
127.69
124.22
122.66

40.02 DMSO-D6
39.85 DMSO-D6
39.69 DMSO-D6
39.52 DMSO-D6
39.35 DMSO-D6
39.19 DMSO-D6
39.02 DMSO-D6



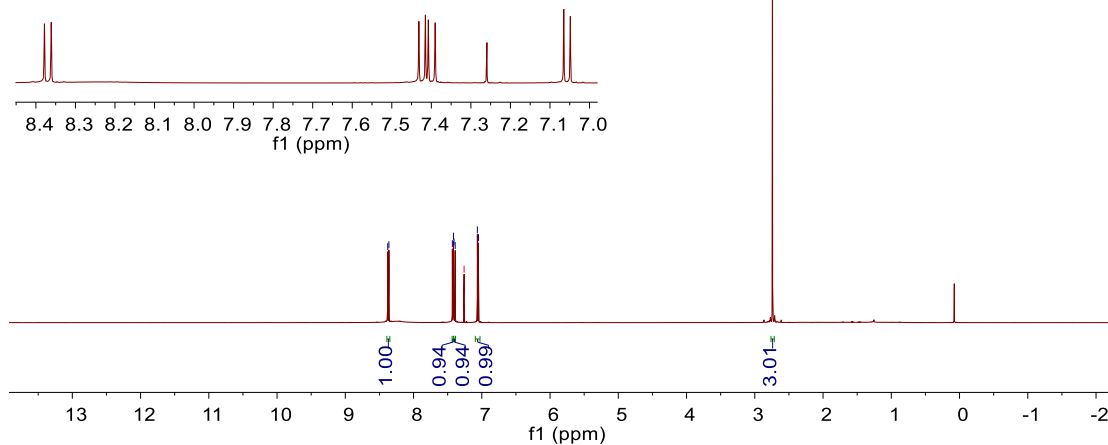
YJh37

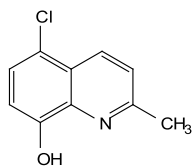
^1H NMR (500 MHz, Chloroform- d) δ 8.37 (d, $J = 8.6$ Hz, 1H), 7.42 (d, $J = 8.2$ Hz, 1H), 7.40 (d, $J = 8.6$ Hz, 1H), 7.06 (d, $J = 8.2$ Hz, 1H), 2.74 (s, 3H).

7.26 CHLOROFORM-D

8.38
8.36
7.43
7.42
7.41
7.39
7.26 CHLOROFORM-D
7.07
7.05

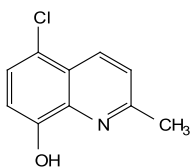
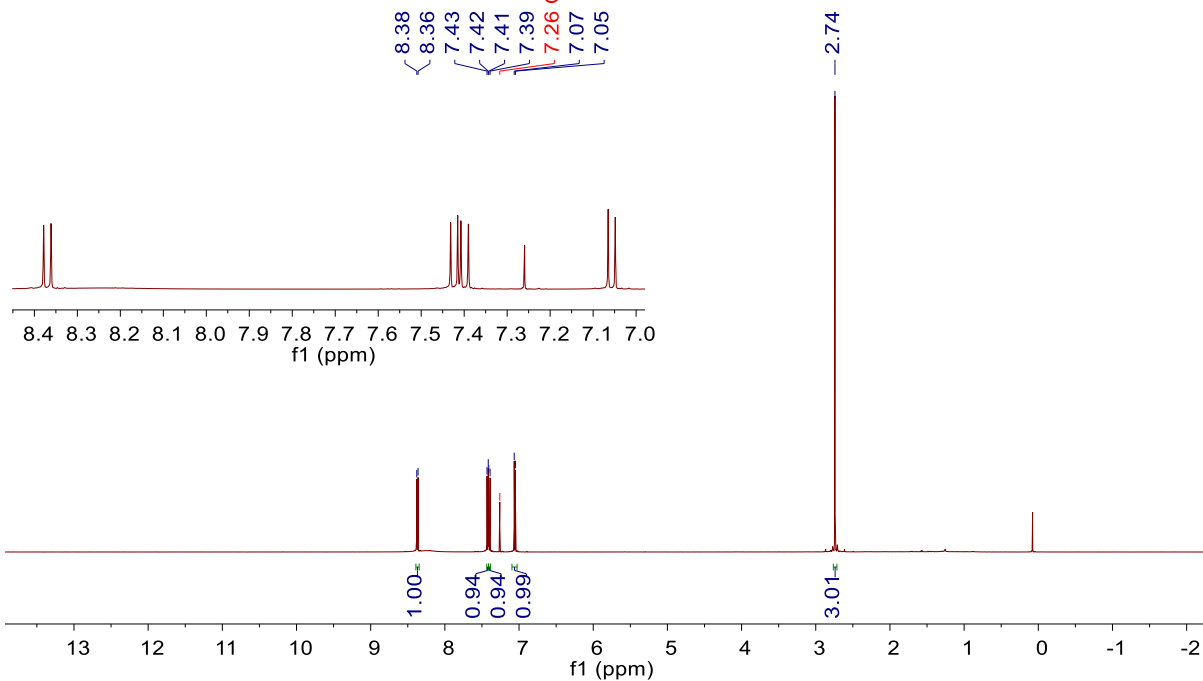
2.74





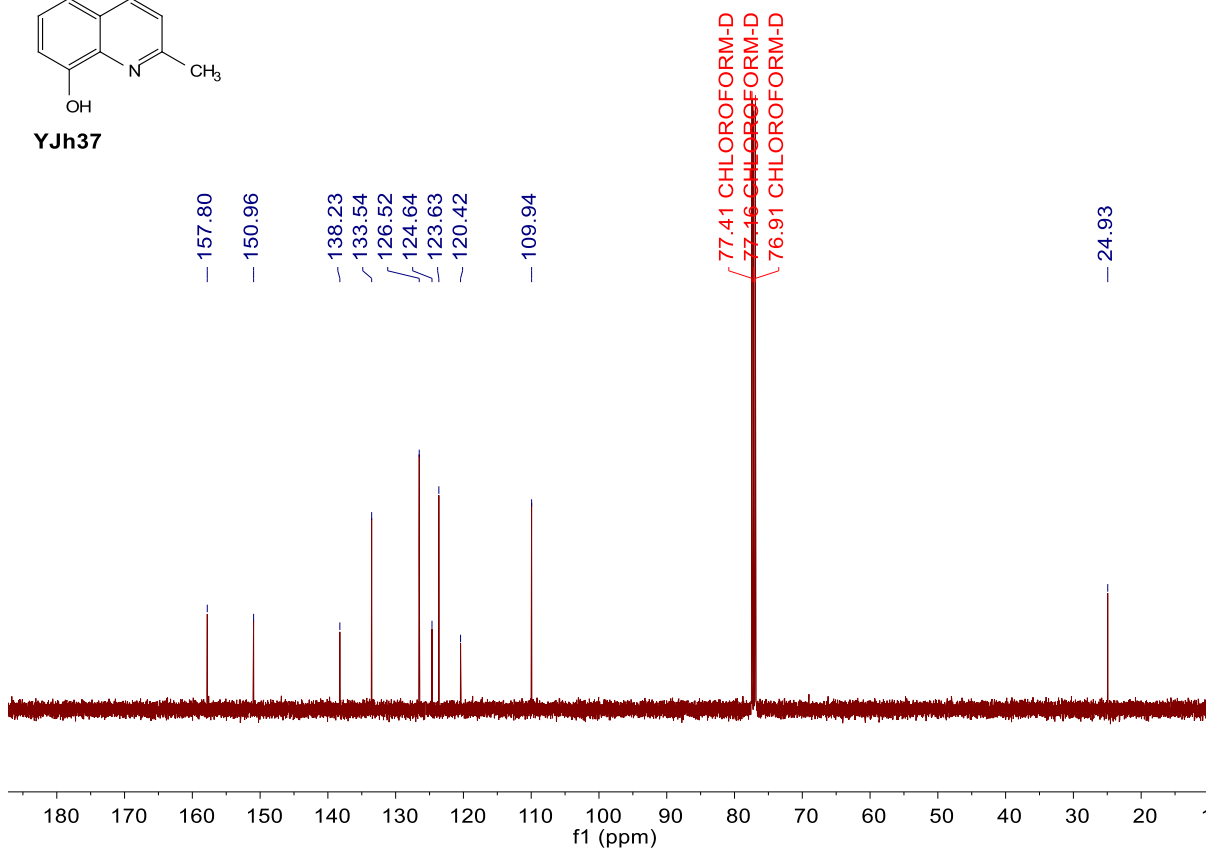
YJh37

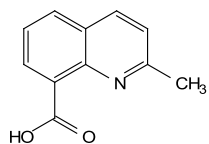
¹H NMR (500 MHz, Chloroform-*d*) δ 8.37 (d, *J* = 8.6 Hz, 1H), 7.42 (d, *J* = 8.2 Hz, 1H), 7.40 (d, *J* = 8.6 Hz, 1H), 7.06 (d, *J* = 8.2 Hz, 1H), 2.74 (s, 3H).



YJh37

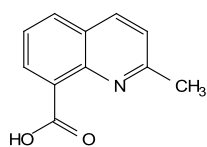
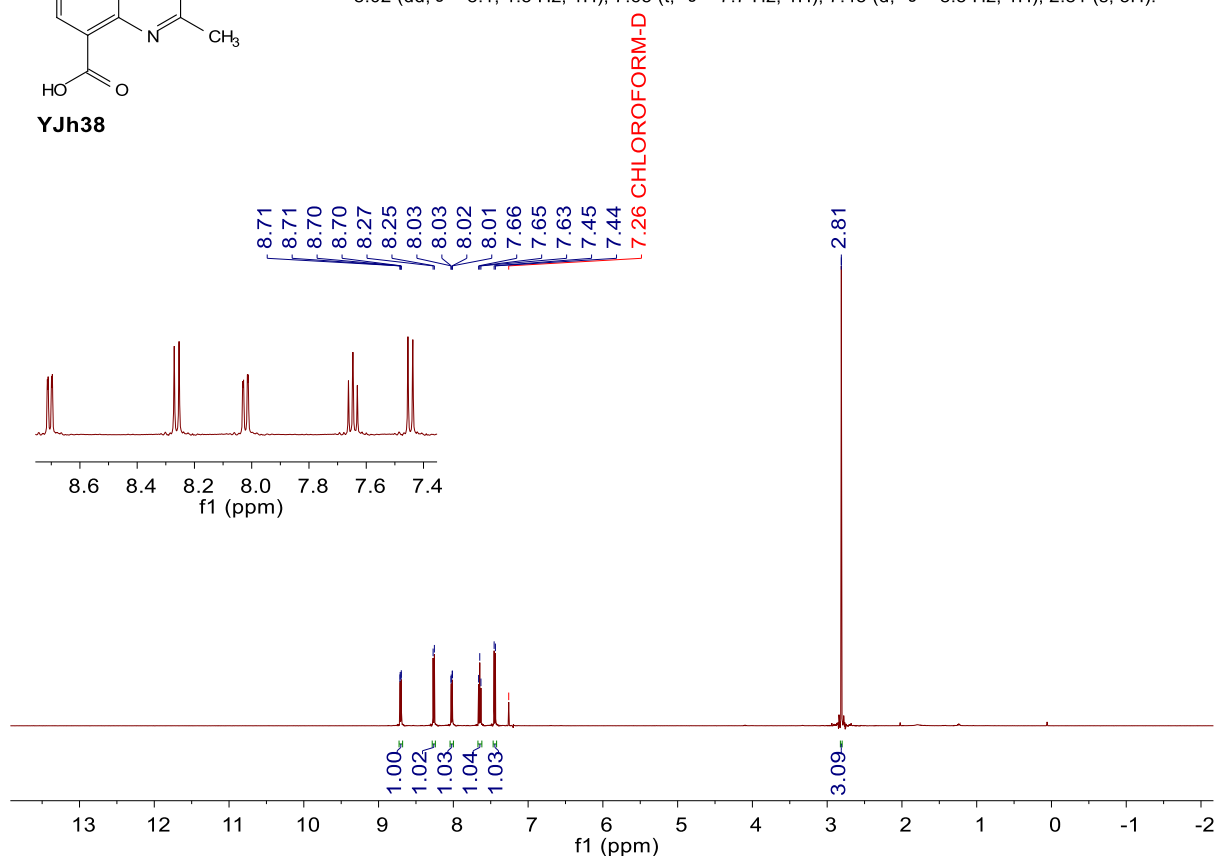
¹³C NMR (126 MHz, Chloroform-*d*) δ 157.80, 150.96, 138.23, 133.54, 126.52, 124.64, 123.63, 120.42, 109.94, 24.93.





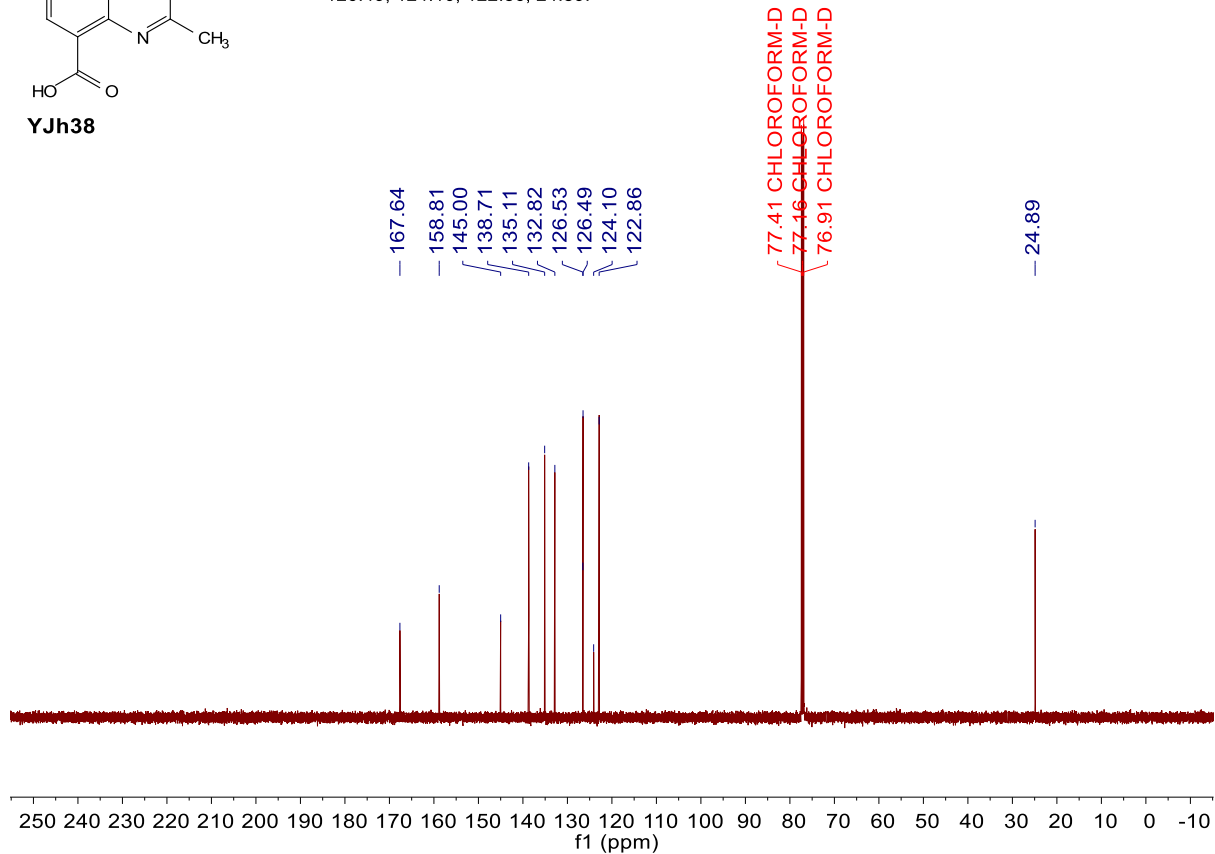
YJh38

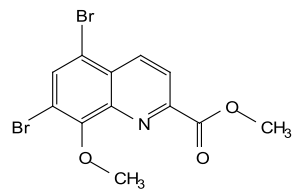
¹H NMR (500 MHz, Chloroform-*d*) δ 8.71 (dd, *J* = 7.3, 1.5 Hz, 1H), 8.26 (d, *J* = 8.5 Hz, 1H), 8.02 (dd, *J* = 8.1, 1.5 Hz, 1H), 7.65 (t, *J* = 7.7 Hz, 1H), 7.45 (d, *J* = 8.5 Hz, 1H), 2.81 (s, 3H).



YJh38

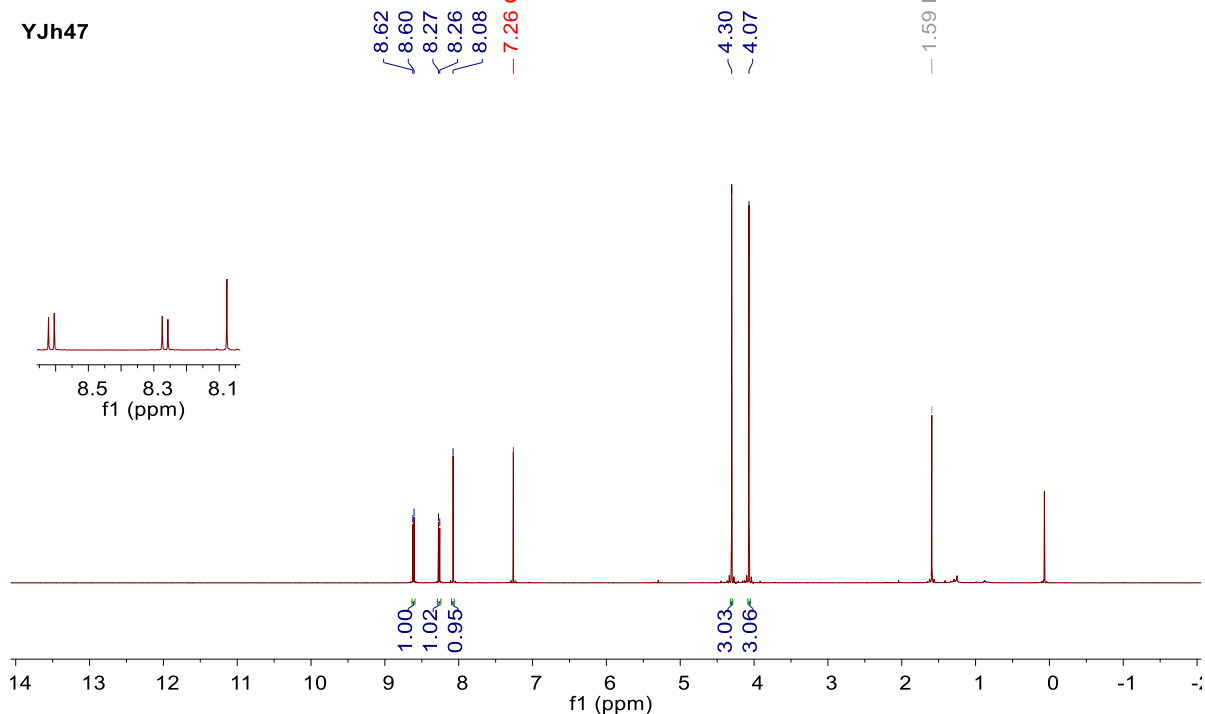
¹³C NMR (126 MHz, Chloroform-*d*) δ 167.64, 158.81, 145.00, 138.71, 135.11, 132.82, 126.53, 126.49, 124.10, 122.86, 24.89.



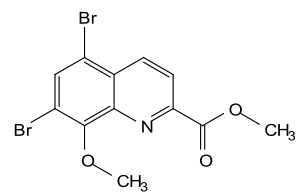
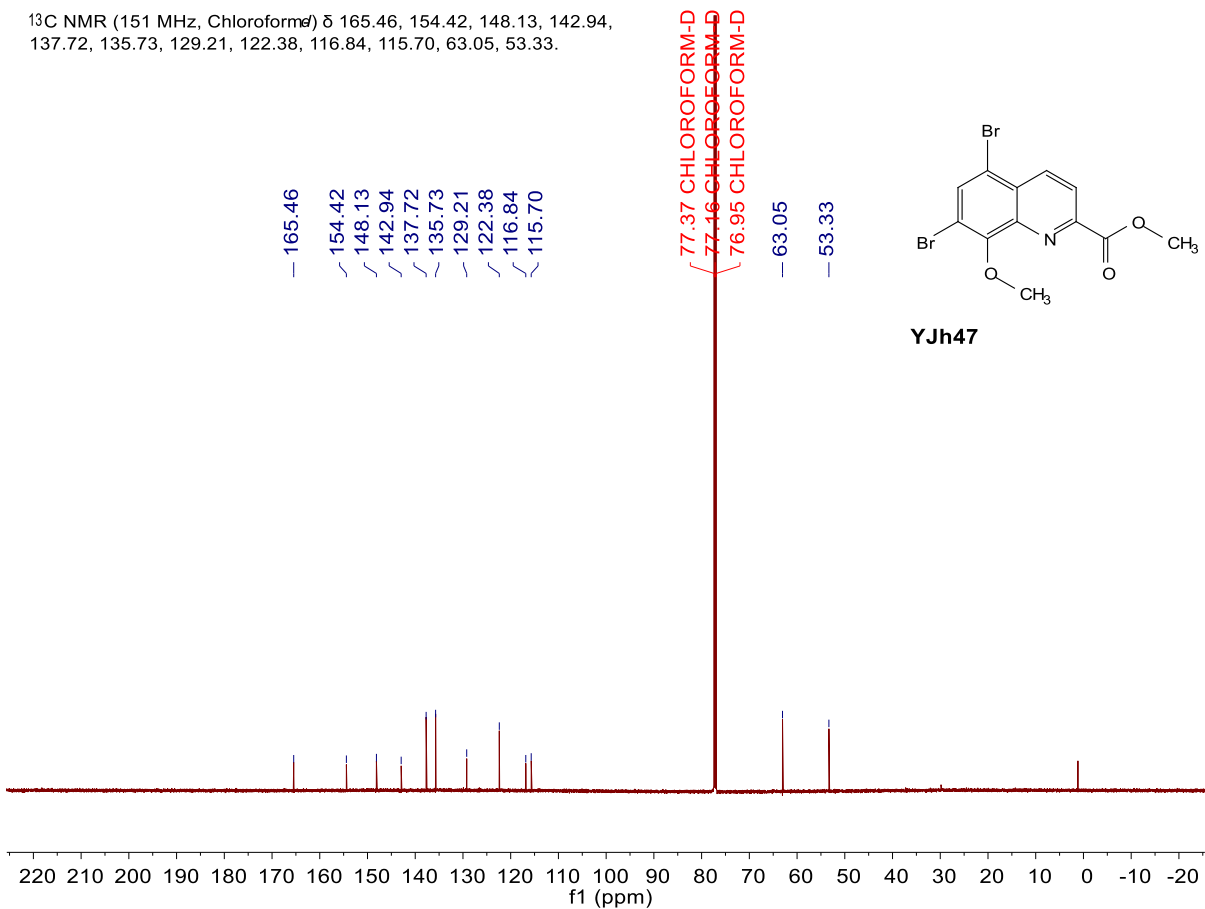


YJh47

¹H NMR (500 MHz, Chloroform-*d*) δ 8.61 (d, *J* = 8.8 Hz, 1H), 8.27 (d, *J* = 8.8 Hz, 1H), 8.08 (s, 1H), 4.30 (s, 3H), 4.07 (s, 3H).

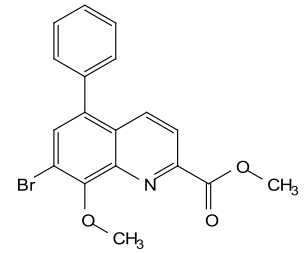


¹³C NMR (151 MHz, Chloroform) δ 165.46, 154.42, 148.13, 142.94, 137.72, 135.73, 129.21, 122.38, 116.84, 115.70, 63.05, 53.33.

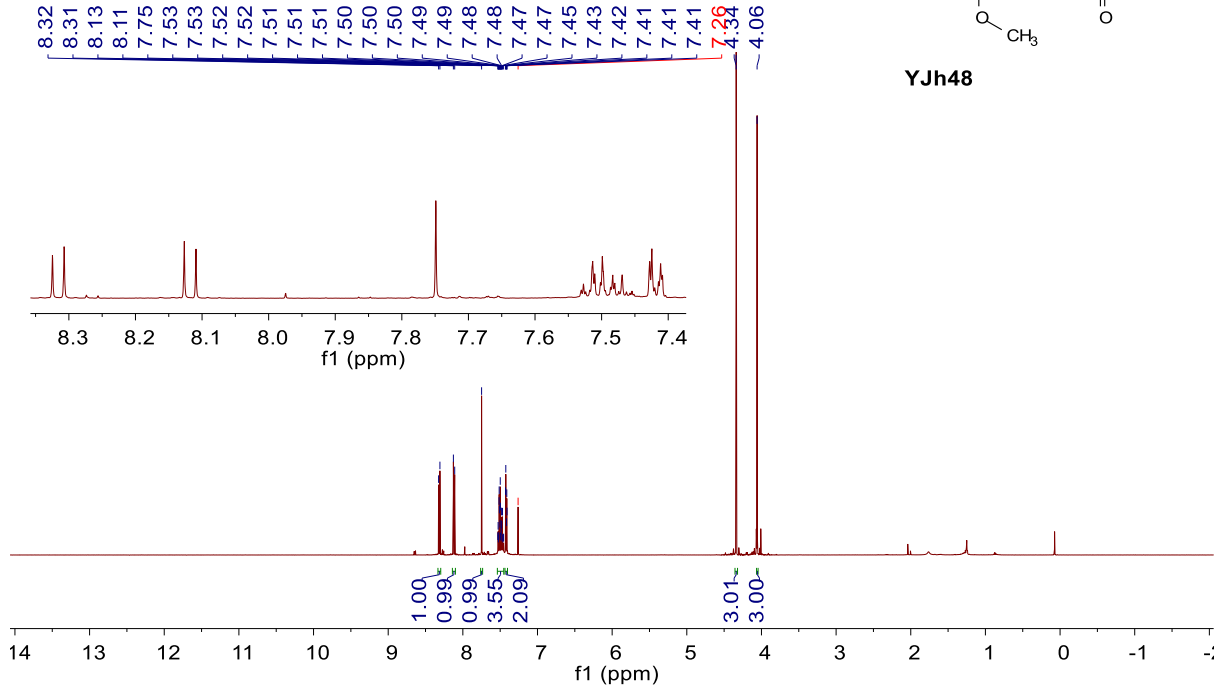


YJh47

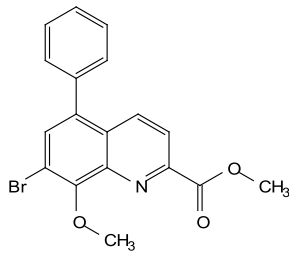
¹H NMR (500 MHz, Chloroform-*d*) δ 8.32 (d, *J* = 8.8 Hz, 1H), 8.12 (d, *J* = 8.8 Hz, 1H), 7.75 (s, 1H), 7.54 – 7.45 (m, 4H), 7.44 – 7.40 (m, 2H), 4.34 (s, 3H), 4.06 (s, 3H).



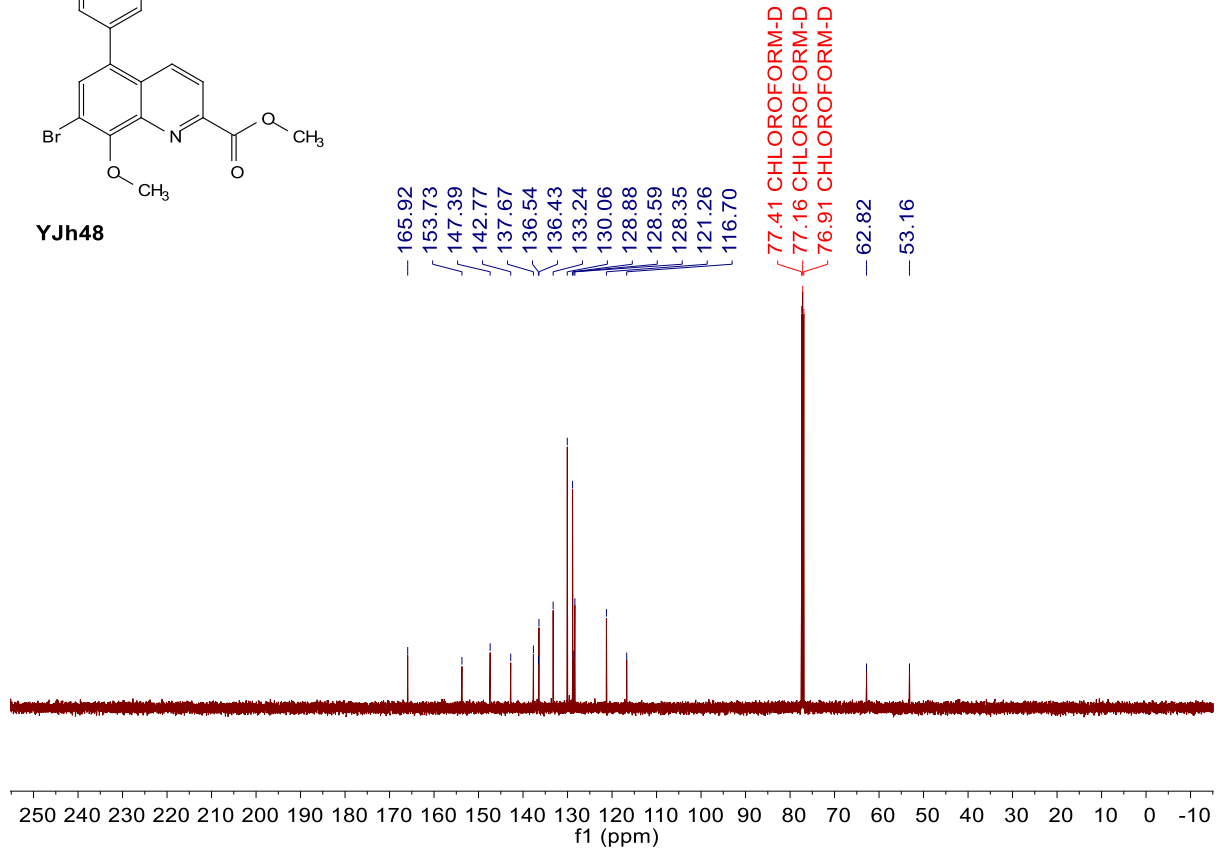
YJh48



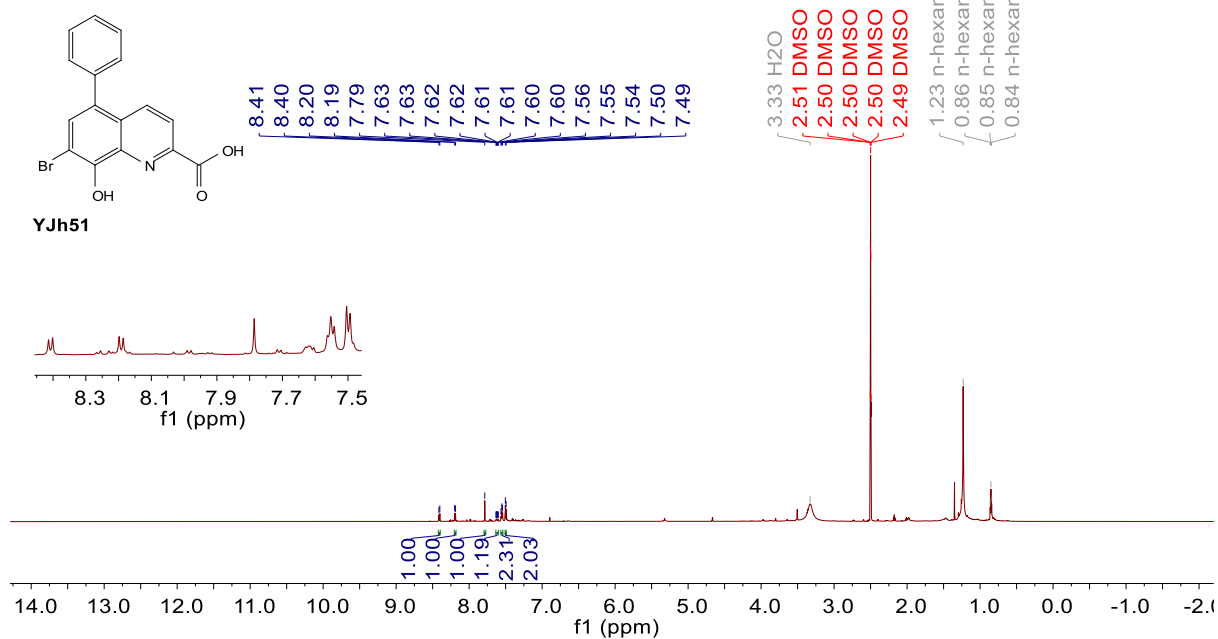
¹³C NMR (126 MHz, Chloroform) δ 165.92, 153.73, 147.39, 142.77, 137.67, 136.54, 136.43, 133.24, 130.06, 128.88, 128.59, 128.35, 121.26, 116.70, 62.82, 53.16.



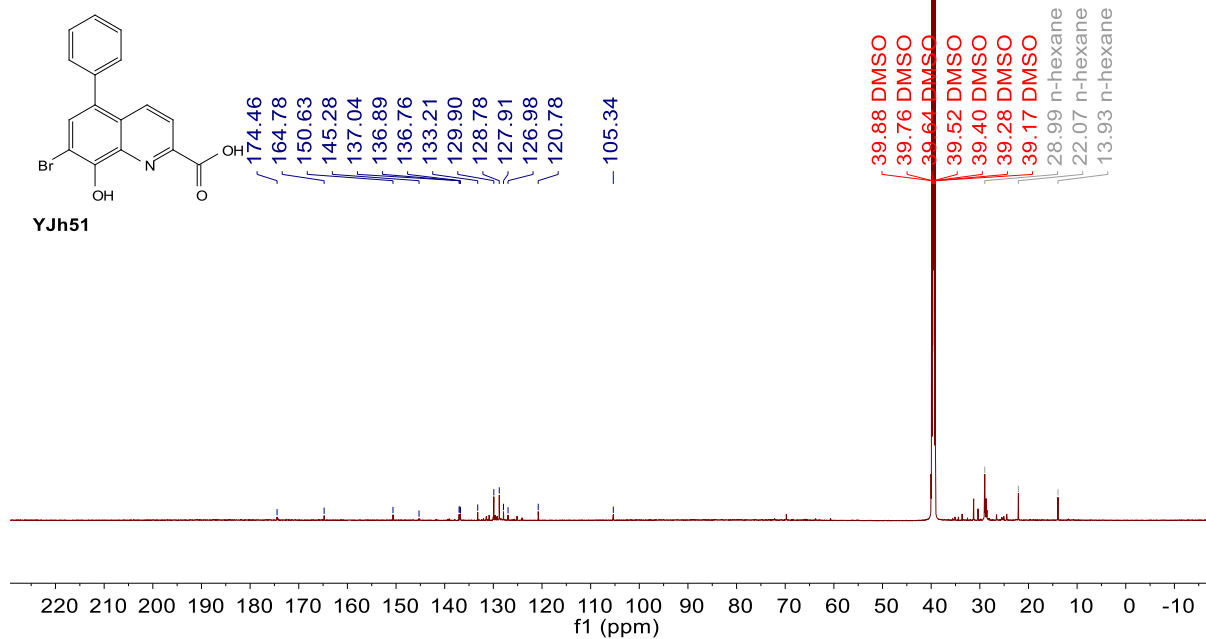
YJh48

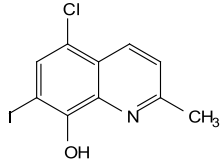


$^1\text{H NMR}$ (700 MHz, $\text{DMSO-}d_6$) δ 8.41 (d, $J = 8.7$ Hz, 1H), 8.19 (d, $J = 8.7$ Hz, 1H), 7.79 (s, 1H), 7.64 – 7.60 (m, 1H), 7.58 – 7.53 (m, 2H), 7.50 (d, $J = 7.2$ Hz, 2H).



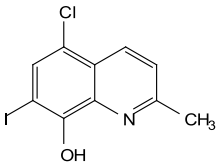
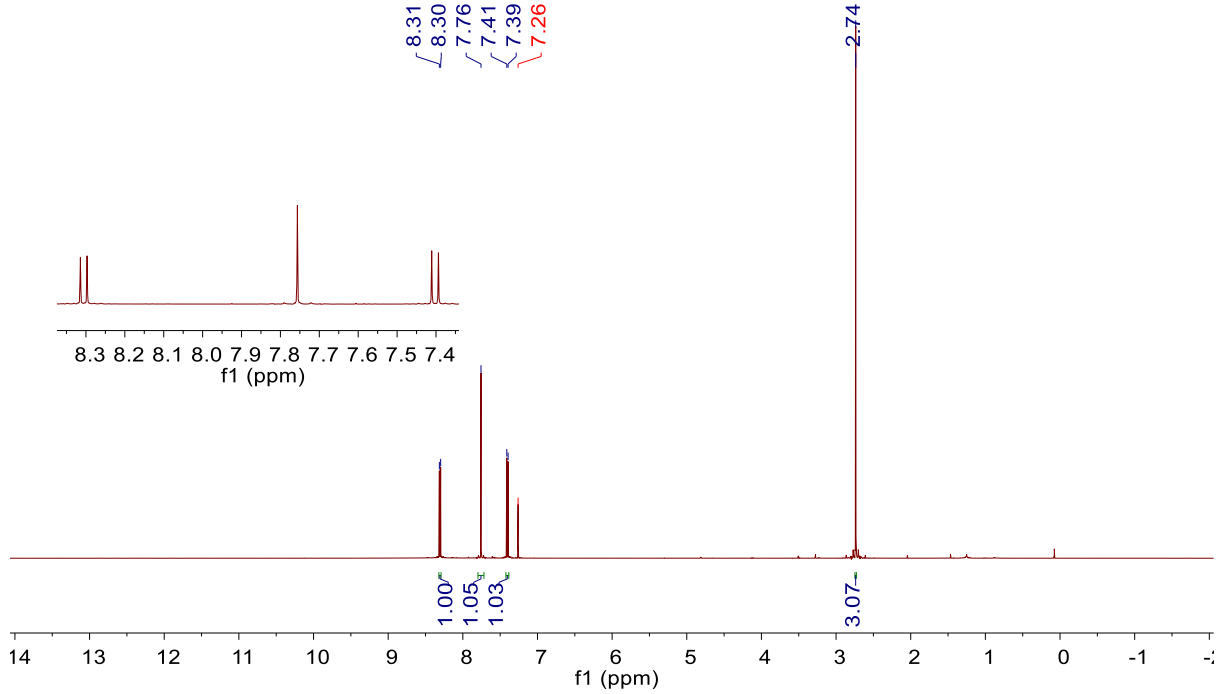
$^{13}\text{C NMR}$ (176 MHz, $\text{DMSO-}d_6$) δ 174.46, 164.78, 150.63, 145.28, 137.04, 136.89, 136.76, 133.21, 129.90, 128.78, 127.91, 126.98, 120.78, 105.34.





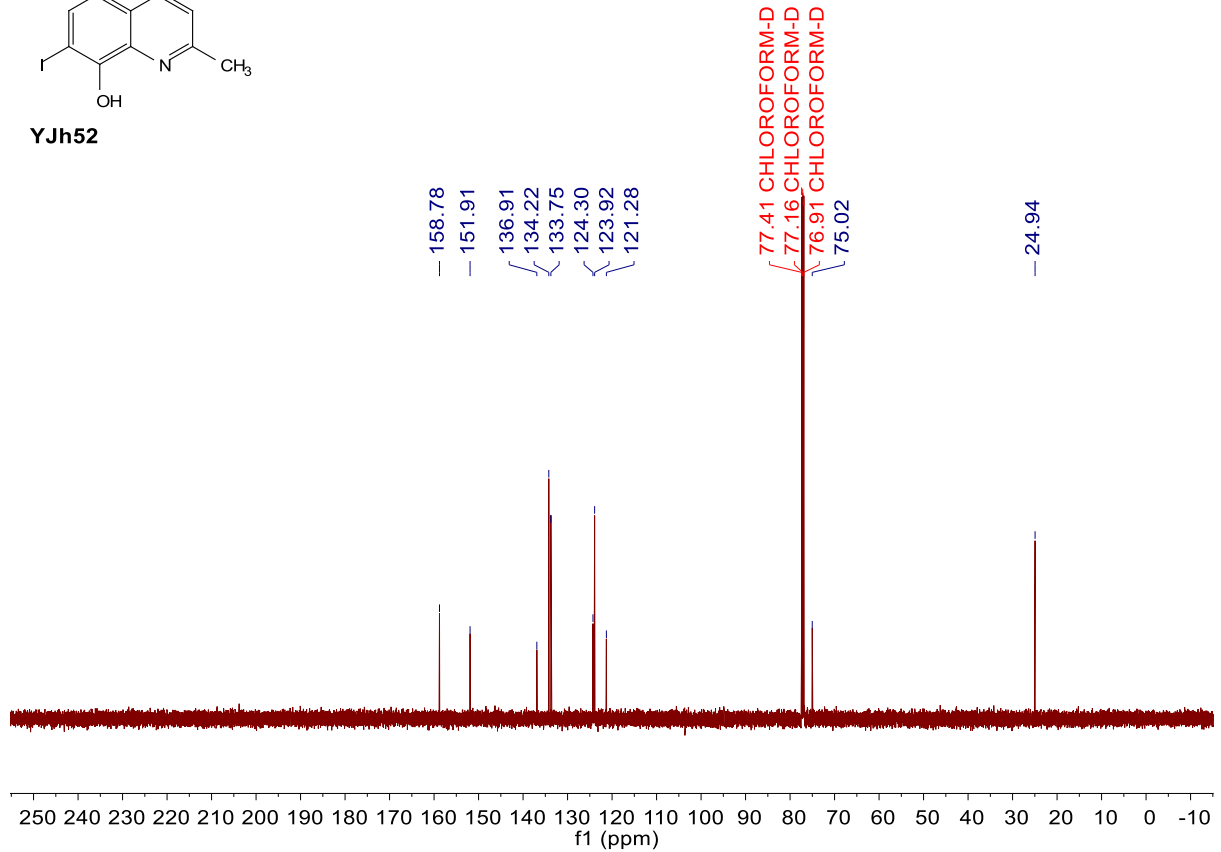
YJh52

¹H NMR (500 MHz, Chloroform-*d*) δ 8.31 (d, *J* = 8.6 Hz, 1H), 7.76 (s, 1H), 7.40 (d, *J* = 8.6 Hz, 1H), 2.74 (s, 3H).

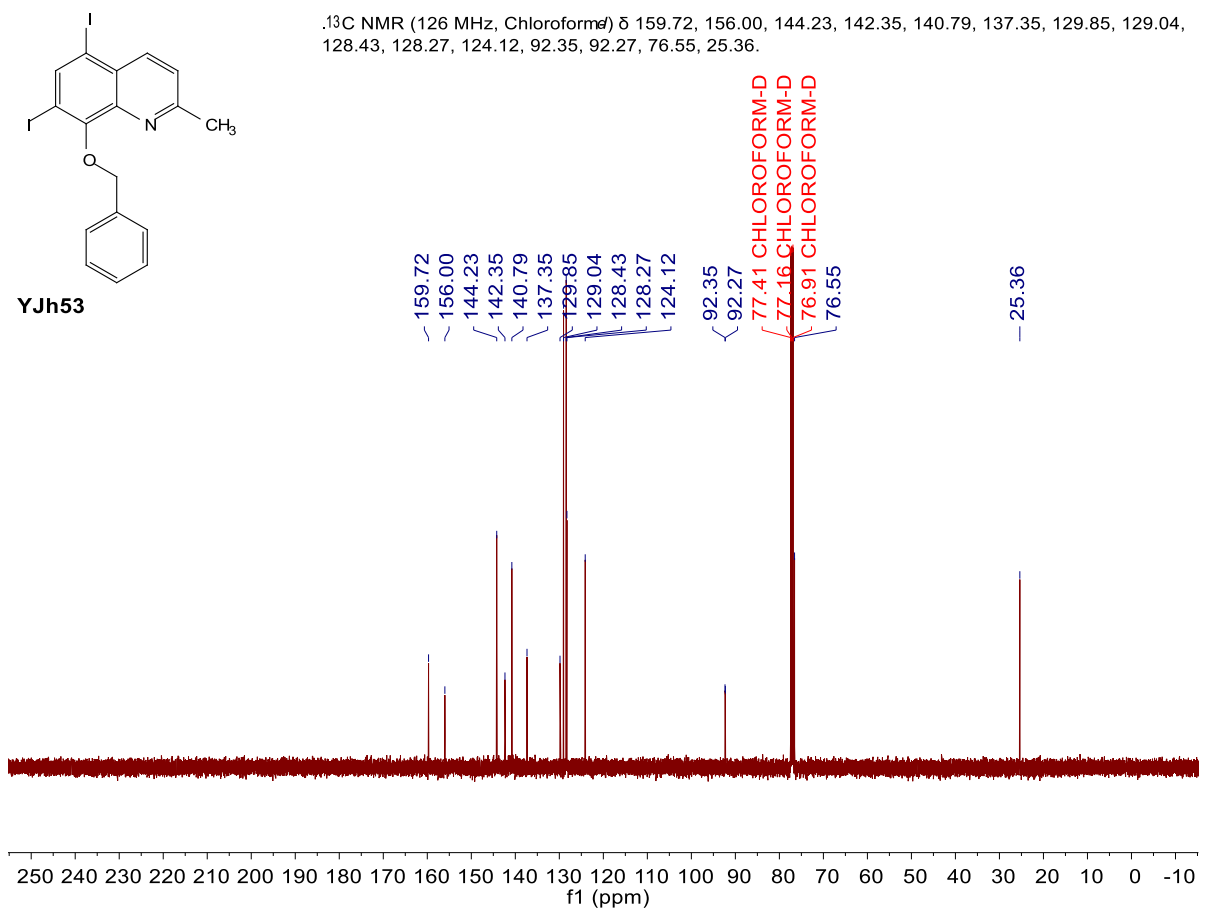
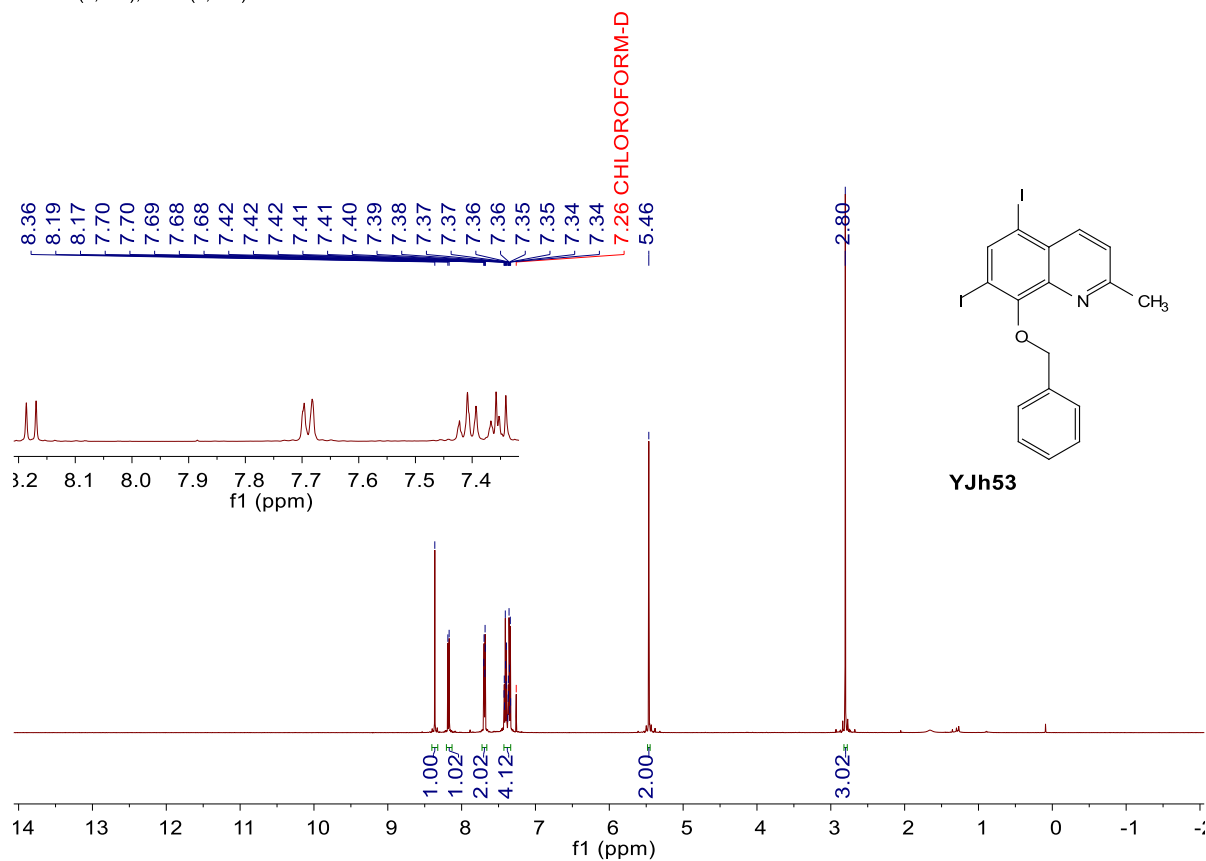


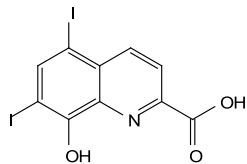
YJh52

¹³C NMR (126 MHz, Chloroform-*d*) δ 158.78, 151.91, 136.91, 134.22, 133.75, 124.30, 123.92, 121.28, 75.02, 24.94.



^1H NMR (500 MHz, Chloroform- d) δ 8.36 (s, 1H), 8.18 (d, J = 8.6 Hz, 1H), 7.73 – 7.62 (m, 2H), 7.46 – 7.32 (m, 4H), 5.46 (s, 2H), 2.80 (s, 3H).

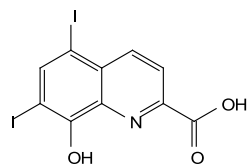
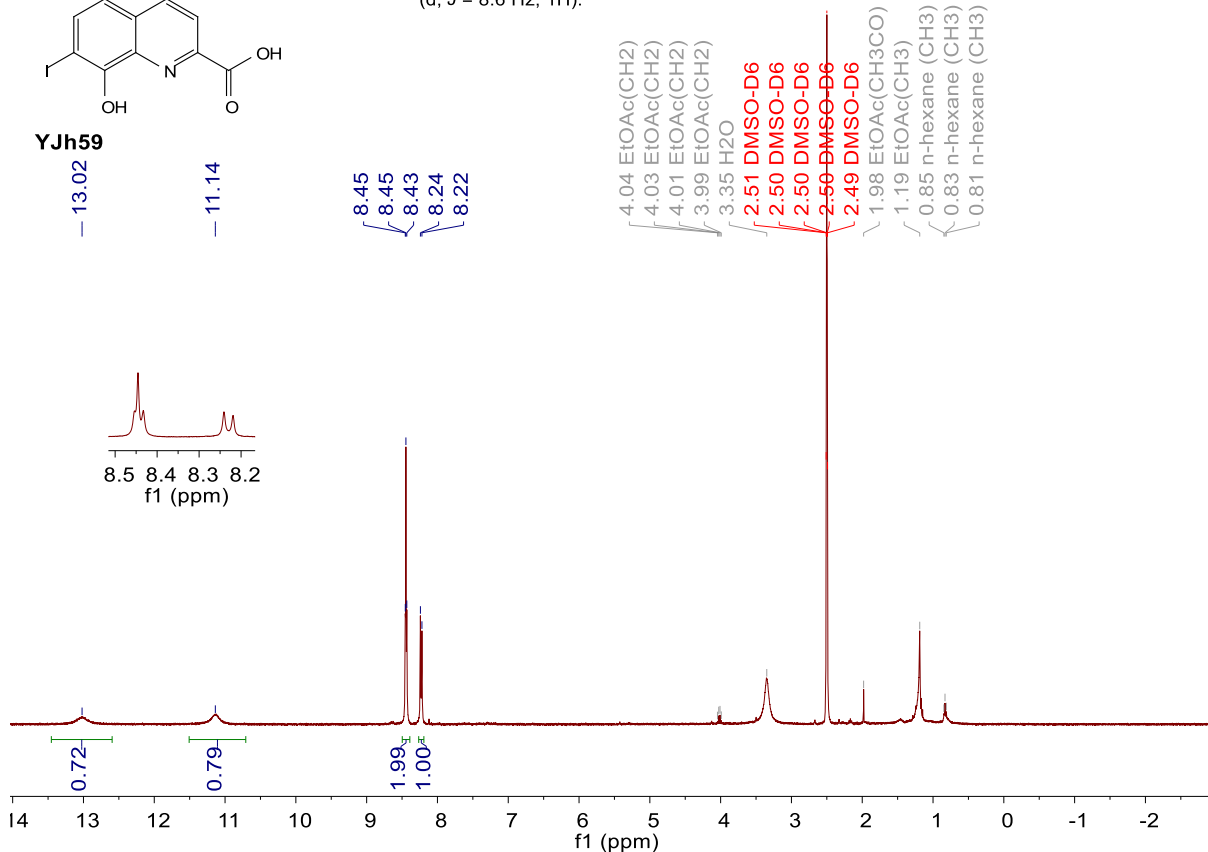




YJh59

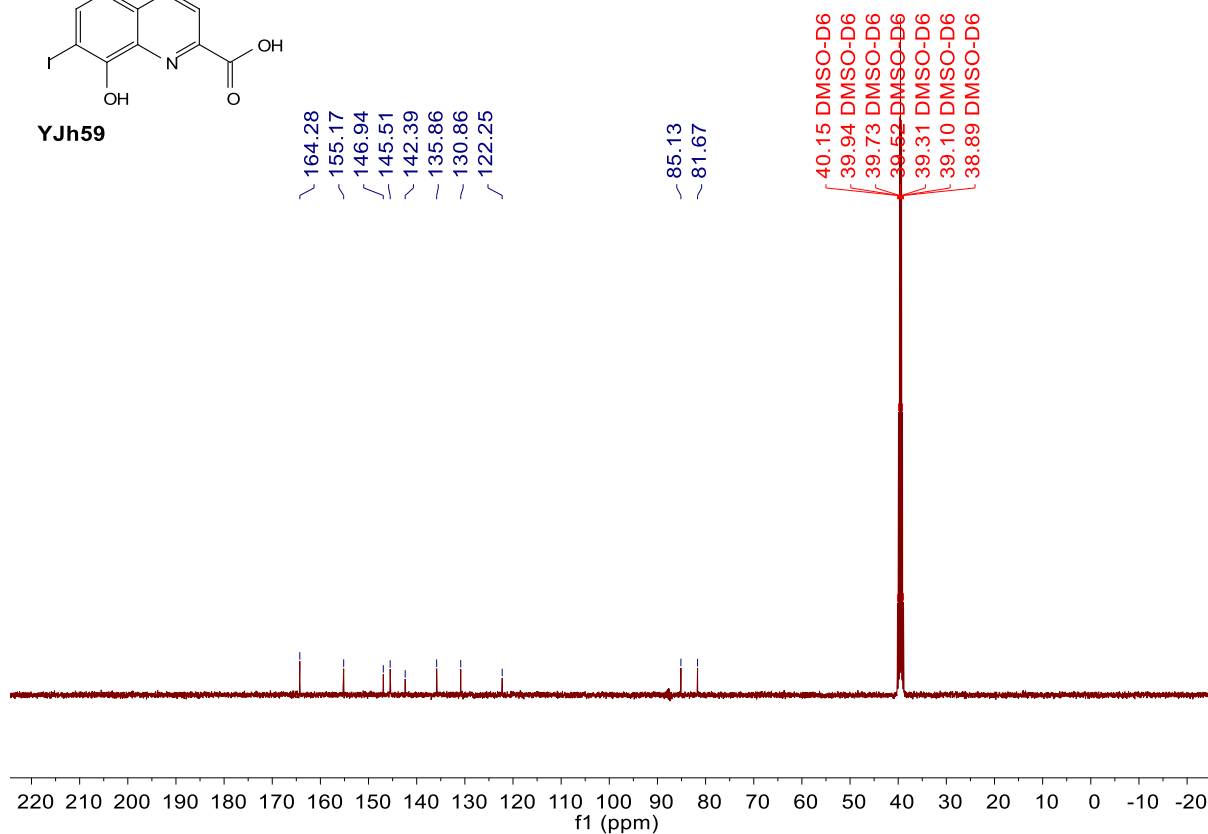
— 13.02
— 11.14

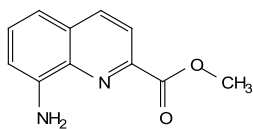
¹H NMR (400 MHz, DMSO-*d*₆) δ 13.02 (s, 1H), 11.14 (s, 1H), 8.50 – 8.39 (m, 2H), 8.23 (d, *J* = 8.6 Hz, 1H).



YJh59

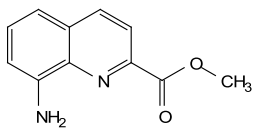
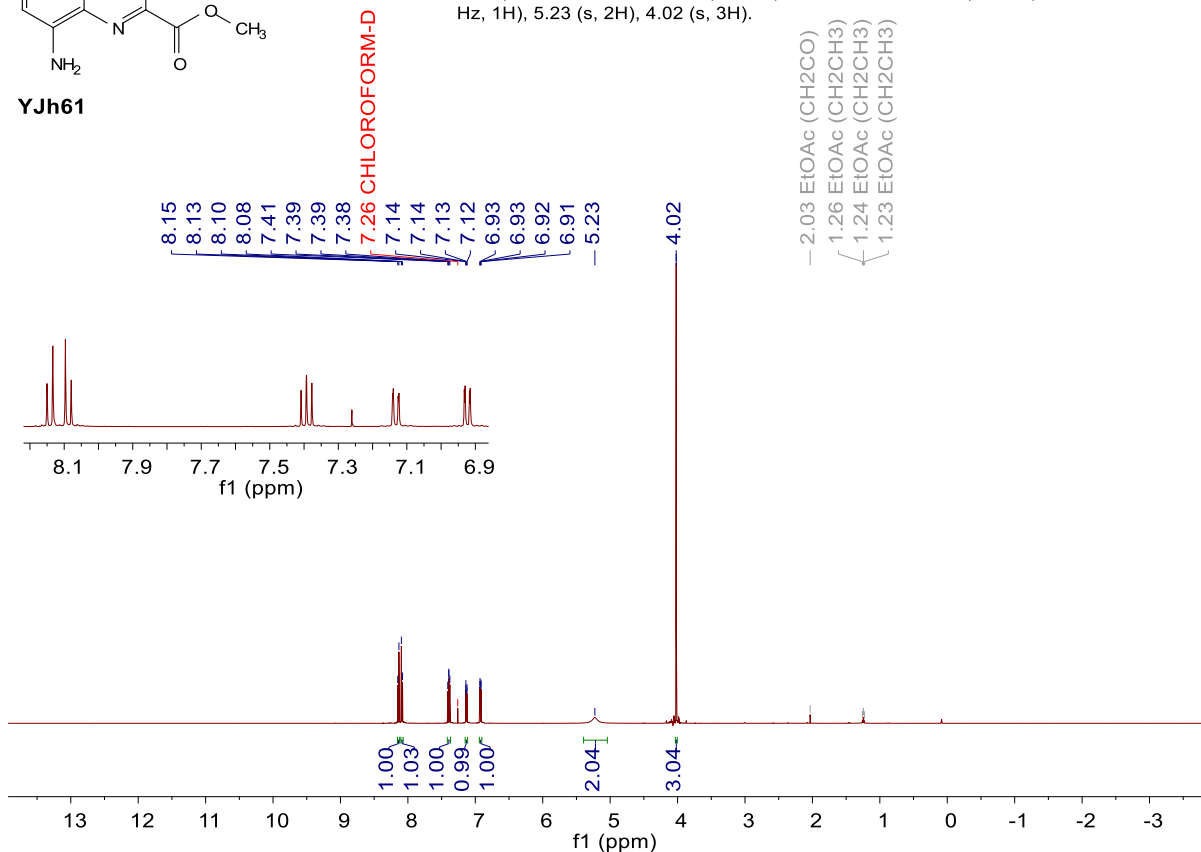
¹³C NMR (101 MHz, DMSO-*d*₆) δ 164.28, 155.17, 146.94, 145.51, 142.39, 135.86, 130.86, 122.25, 85.13, 81.67.





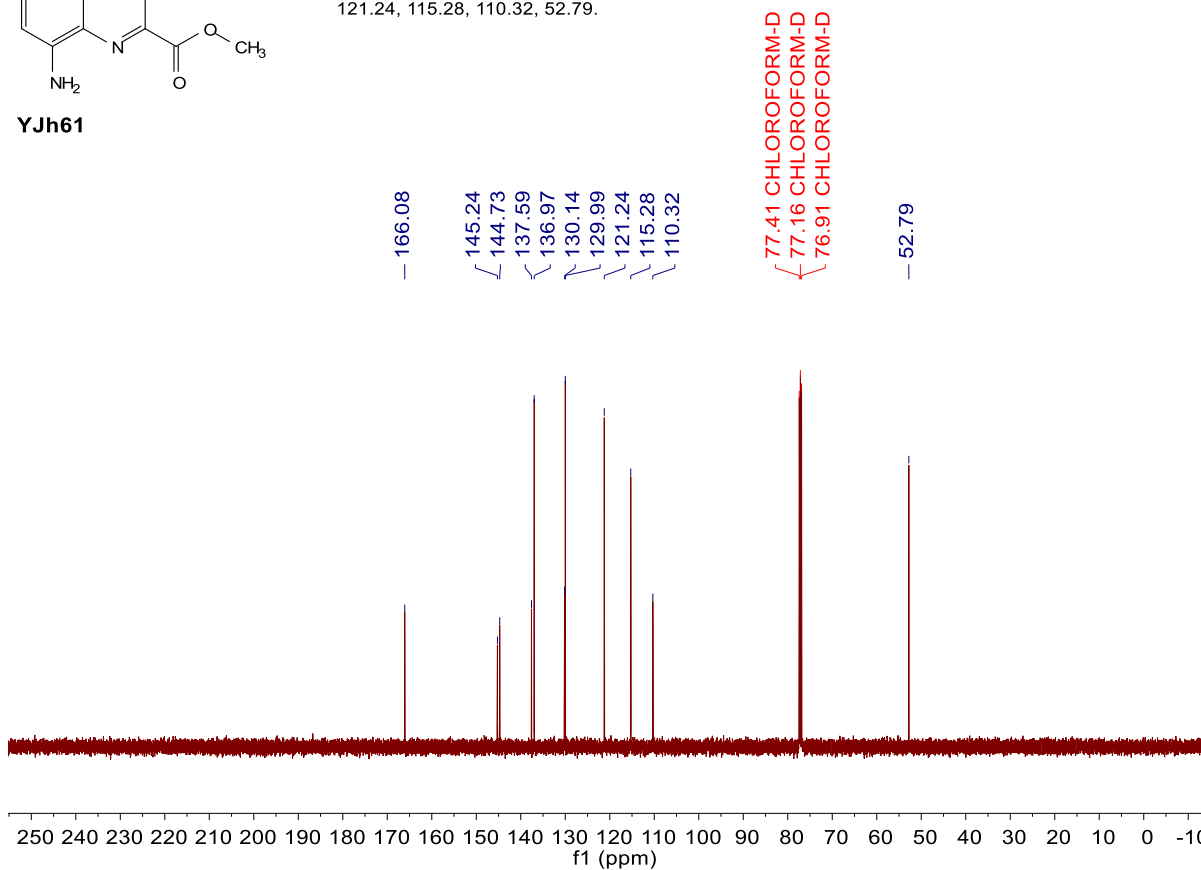
YJh61

$^1\text{H NMR}$ (500 MHz, Chloroform- d) δ 8.14 (d, $J = 8.6$ Hz, 1H), 8.09 (d, $J = 8.5$ Hz, 1H), 7.39 (dd, $J = 8.1, 7.6$ Hz, 1H), 7.13 (dd, $J = 8.2, 1.2$ Hz, 1H), 6.92 (dd, $J = 7.6, 1.2$ Hz, 1H), 5.23 (s, 2H), 4.02 (s, 3H).

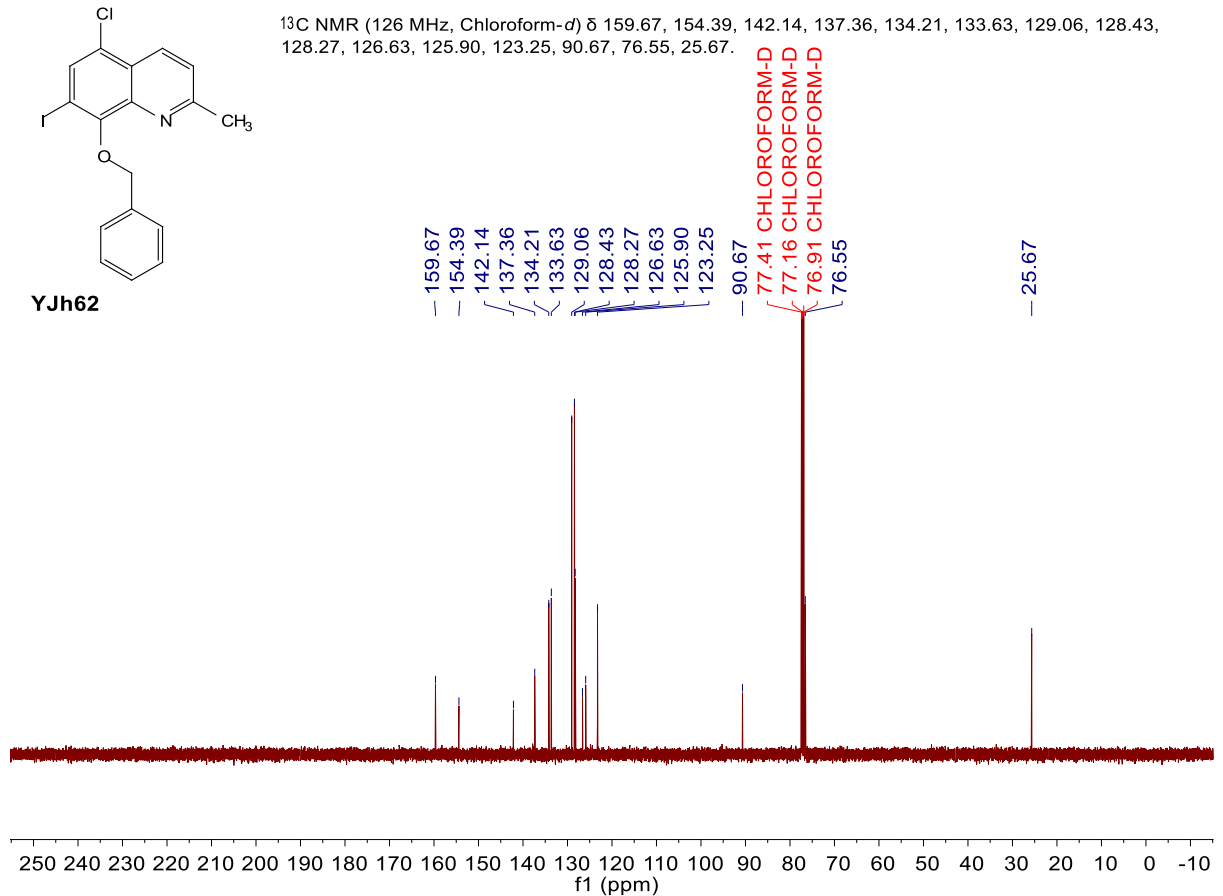
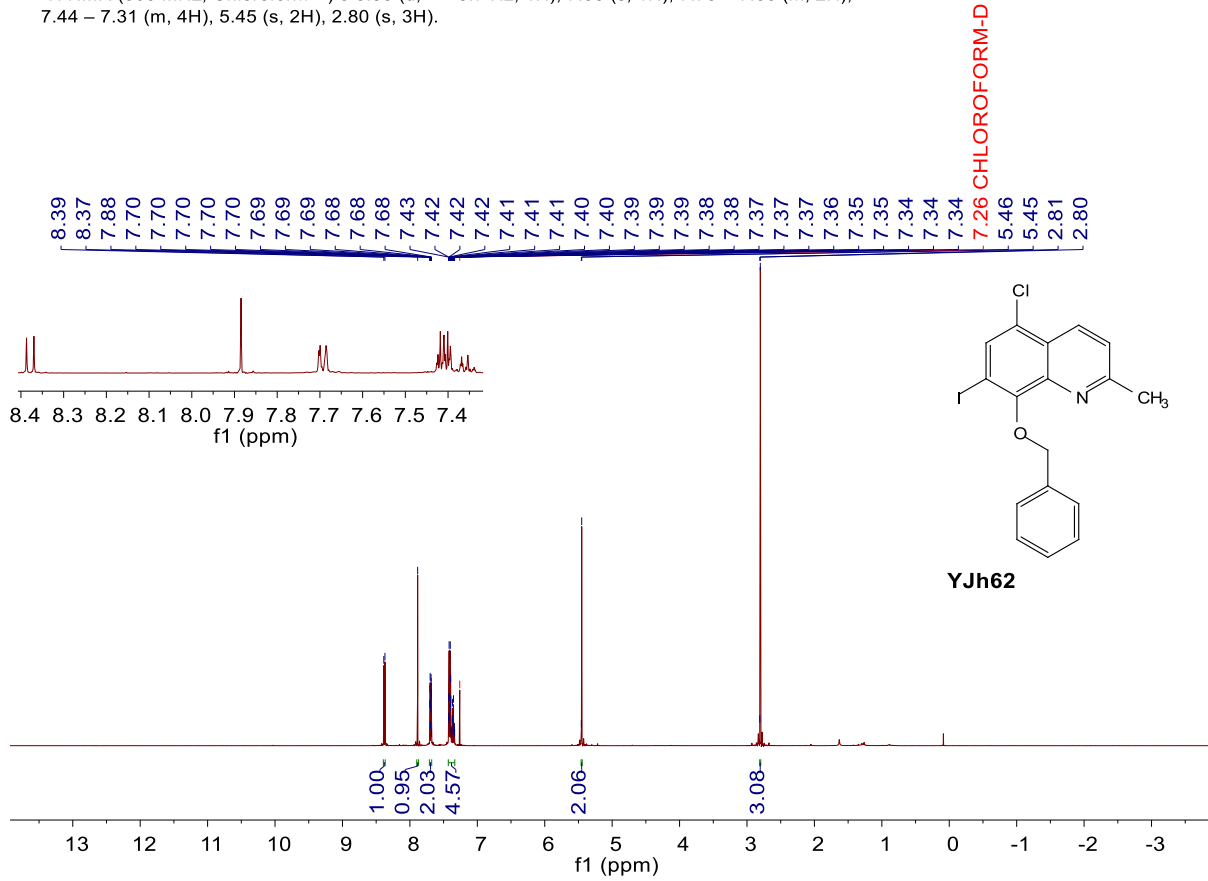


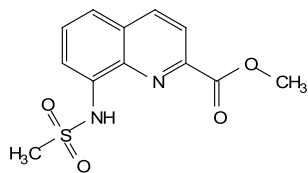
YJh61

$^{13}\text{C NMR}$ (126 MHz, Chloroform- d) δ 166.08, 145.24, 144.73, 137.59, 136.97, 130.14, 129.99, 121.24, 115.28, 110.32, 52.79.



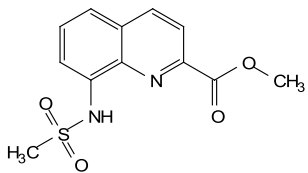
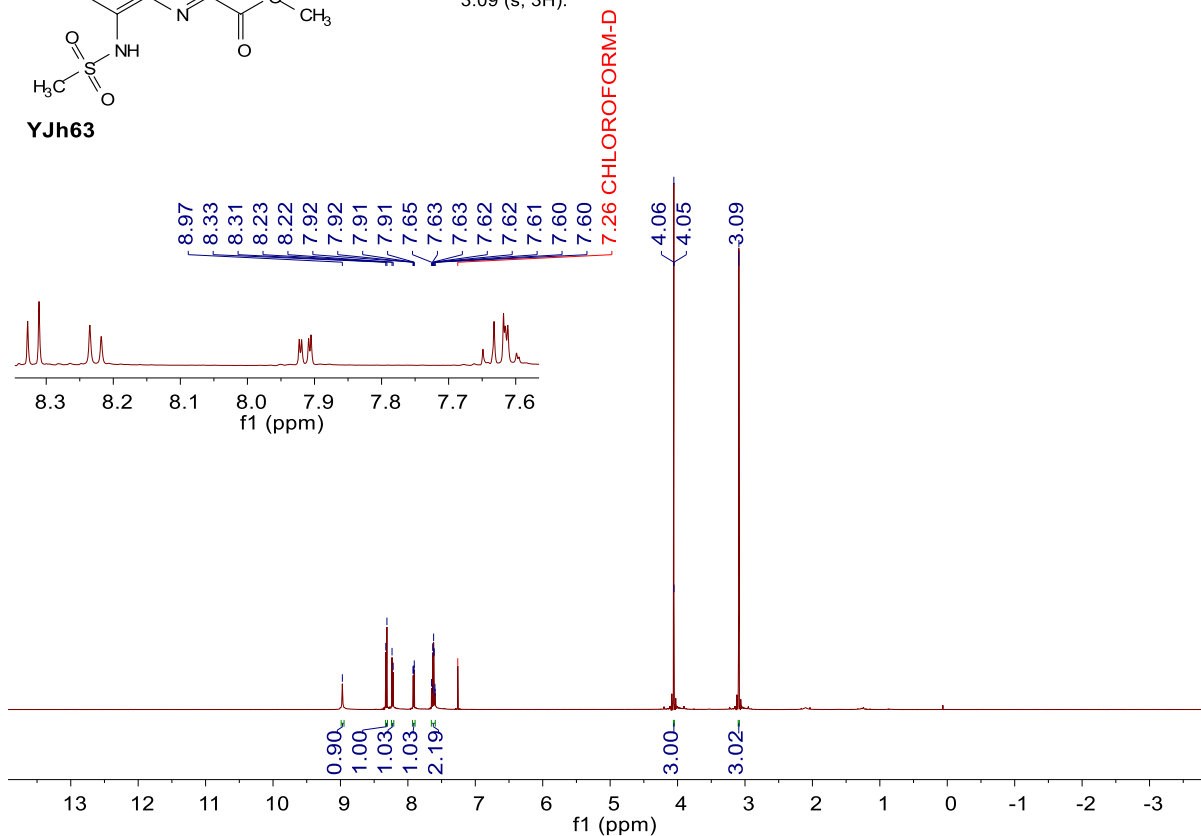
¹H NMR (500 MHz, Chloroform-*d*) δ 8.38 (d, *J* = 8.7 Hz, 1H), 7.88 (s, 1H), 7.75 – 7.66 (m, 2H), 7.44 – 7.31 (m, 4H), 5.45 (s, 2H), 2.80 (s, 3H).





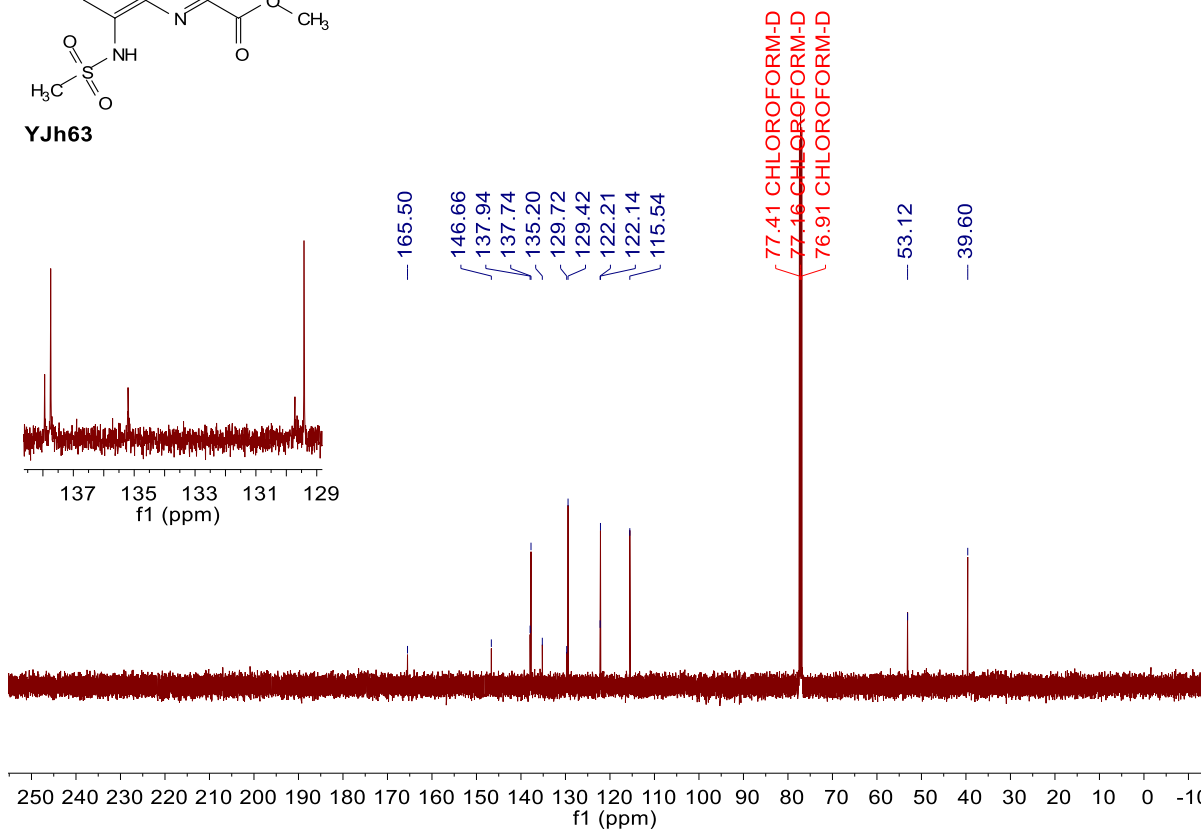
YJh63

¹H NMR (500 MHz, Chloroform-*d*) δ 8.97 (s, 1H), 8.32 (d, *J* = 8.5 Hz, 1H), 8.23 (d, *J* = 8.5 Hz, 1H), 7.91 (dd, *J* = 7.1, 1.8 Hz, 1H), 7.71 – 7.53 (m, 2H), 4.06 (s, 3H), 3.09 (s, 3H).

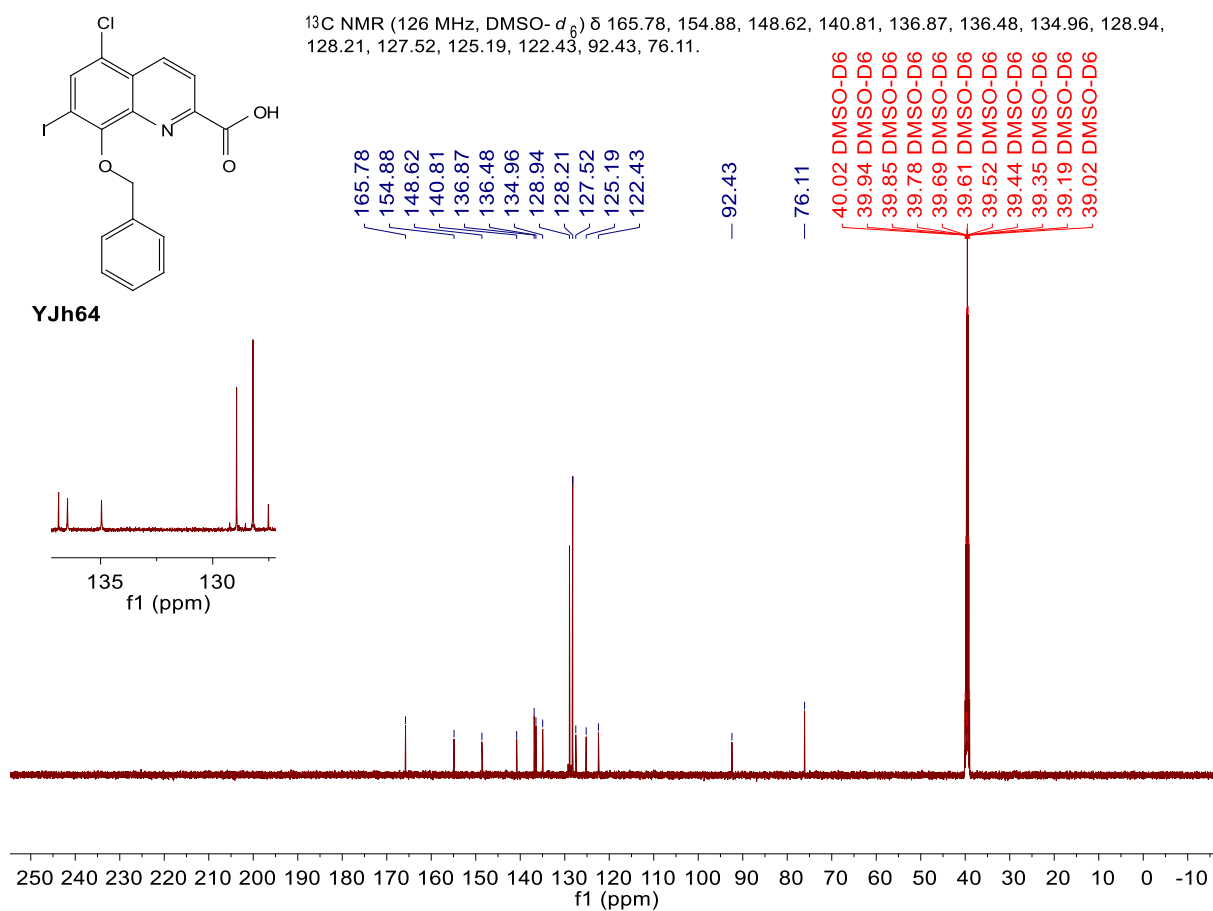
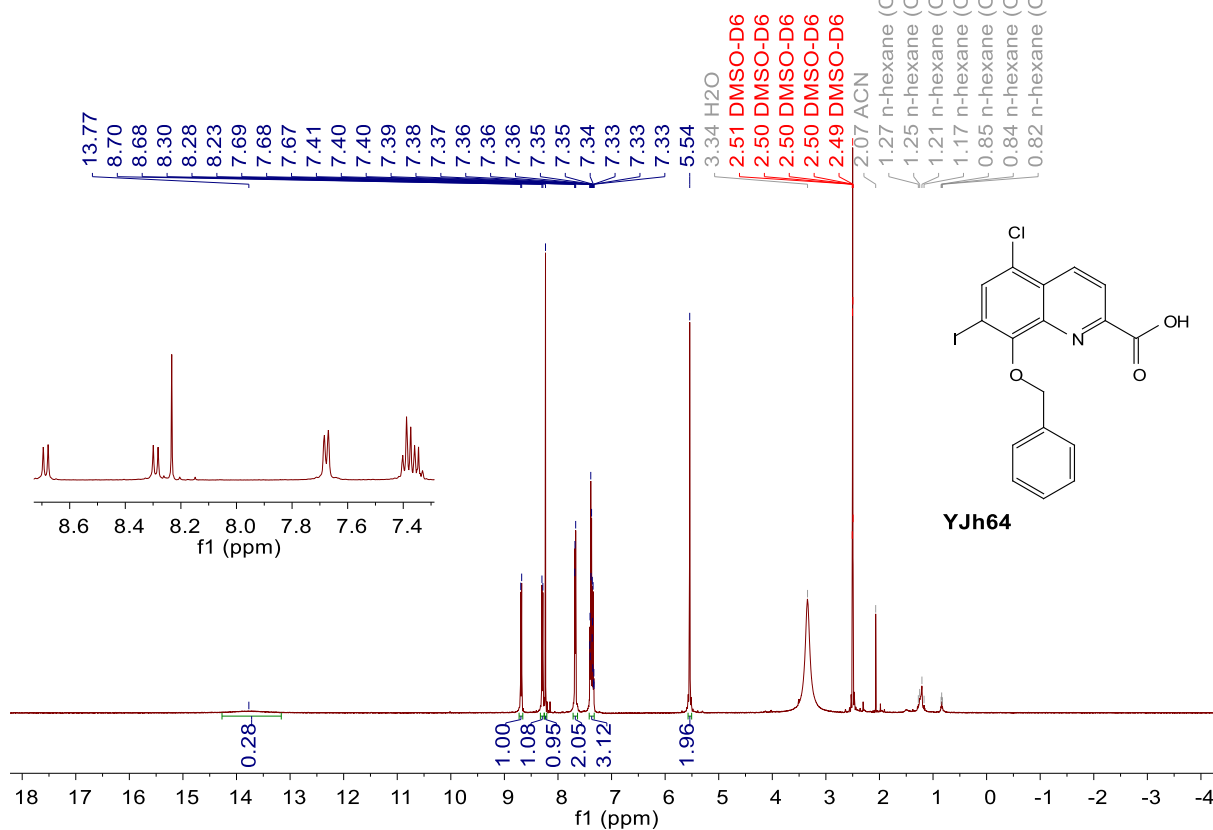


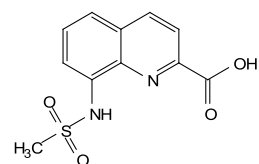
YJh63

¹³C NMR (126 MHz, Chloroform-*d*) δ 165.50, 146.66, 137.94, 137.74, 135.20, 129.72, 129.42, 122.21, 122.14, 115.54, 53.12, 39.60.



¹H NMR (500 MHz, DMSO-*d*₆) δ 13.77 (s, 1H), 8.69 (d, *J* = 8.7 Hz, 1H), 8.29 (d, *J* = 8.7 Hz, 1H), 8.23 (s, 1H), 7.72 – 7.64 (m, 2H), 7.42 – 7.32 (m, 3H), 5.54 (s, 2H).

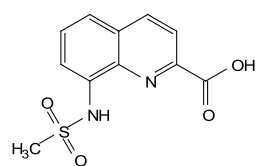
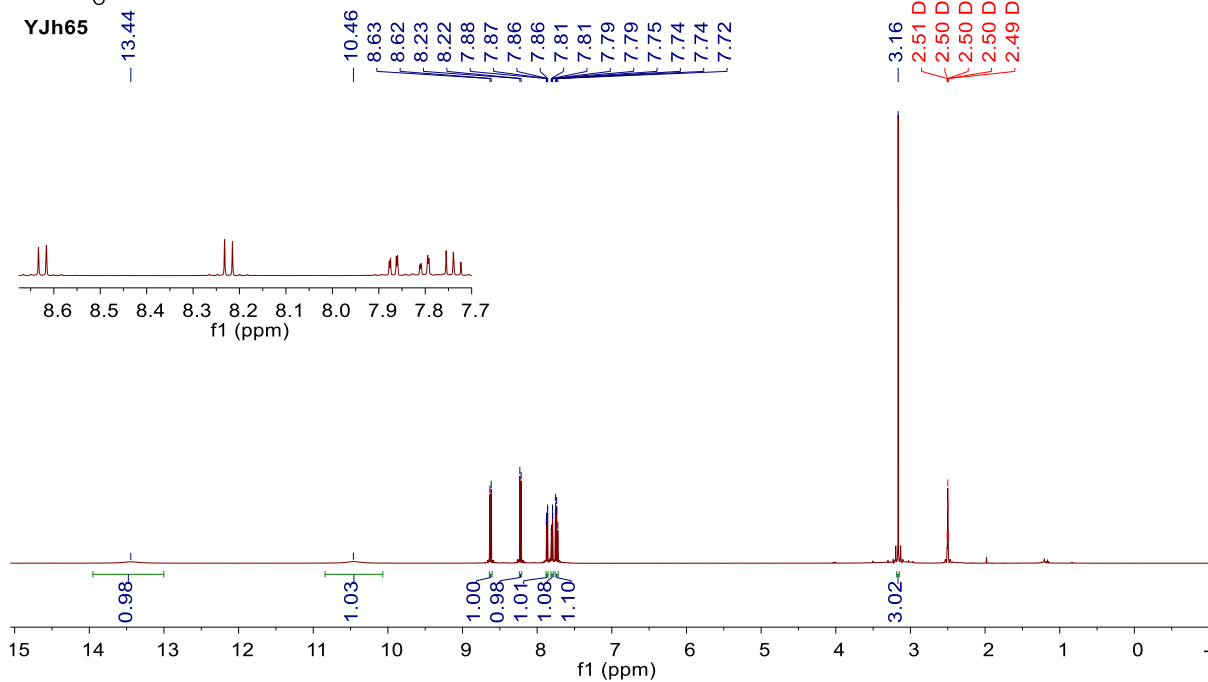




YJh65

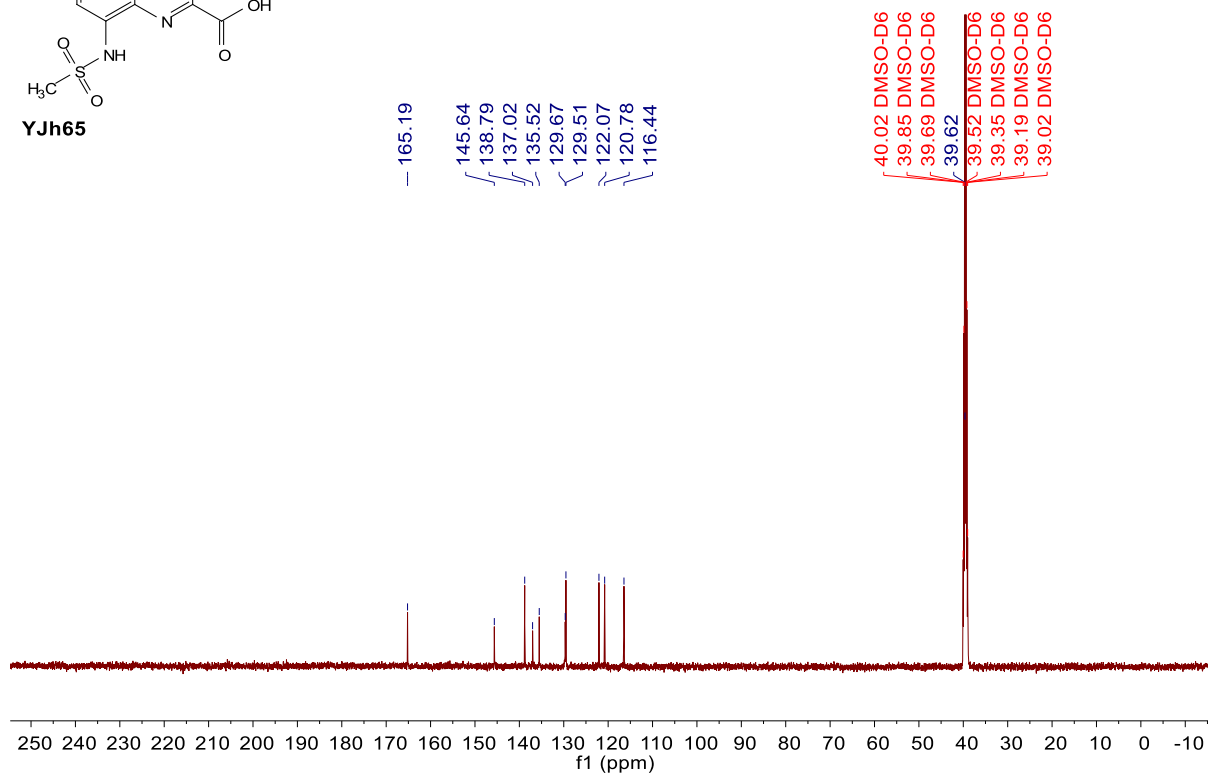
13.44

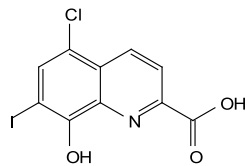
¹H NMR (500 MHz, DMSO-*d*₆) δ 13.44 (s, 1H), 10.46 (s, 1H), 8.62 (d, *J* = 8.5 Hz, 1H), 8.22 (d, *J* = 8.5 Hz, 1H), 7.87 (dd, *J* = 7.6, 1.3 Hz, 1H), 7.80 (dd, *J* = 8.3, 1.3 Hz, 1H), 7.74 (dd, *J* = 8.2, 7.6 Hz, 1H), 3.16 (s, 3H).



YJh65

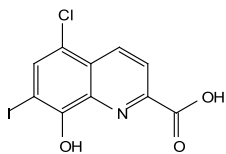
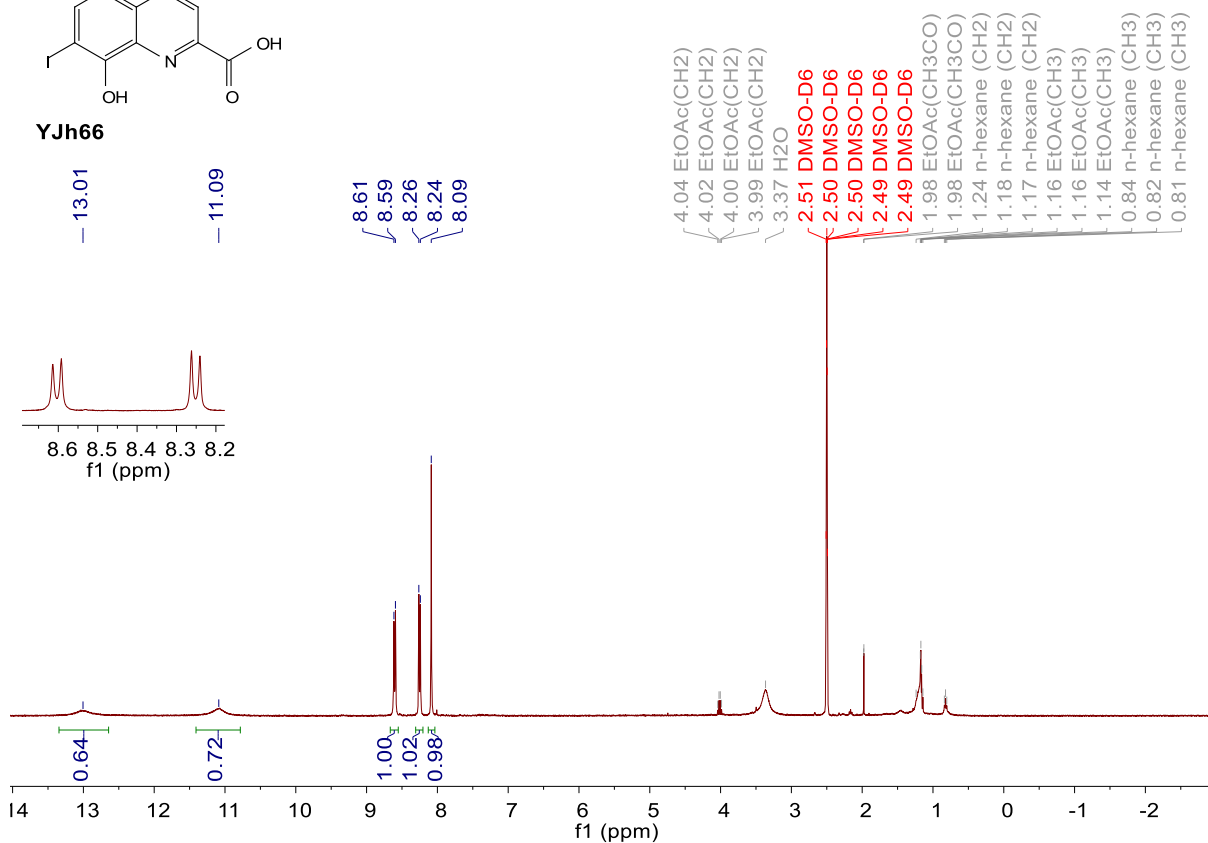
¹³C NMR (126 MHz, DMSO-*d*₆) δ 165.19, 145.64, 138.79, 137.02, 135.52, 129.67, 129.51, 122.07, 120.78, 116.44, 39.62.





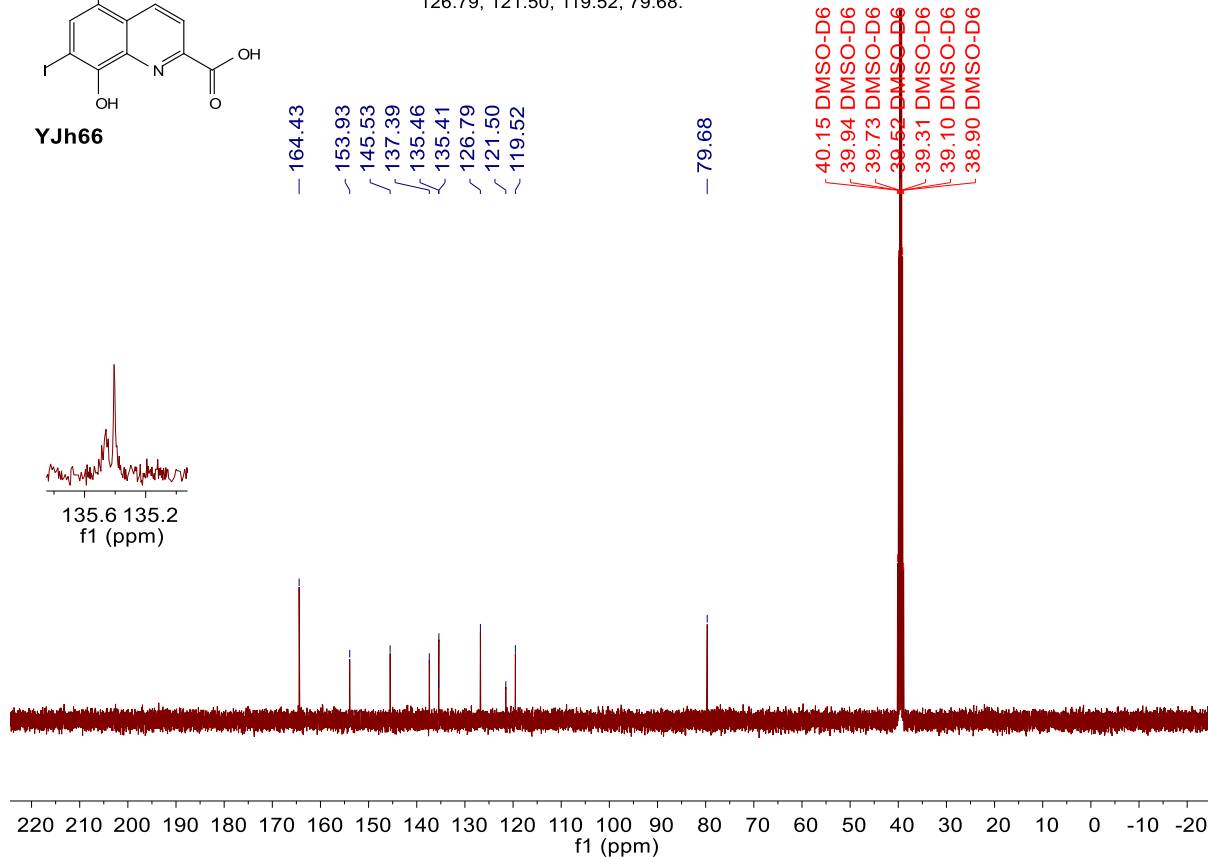
YJh66

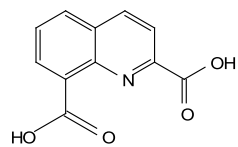
$^1\text{H NMR}$ (400 MHz, $\text{DMSO-}d_6$) δ 13.01 (s, 1H), 11.09 (s, 1H), 8.60 (d, $J = 8.6$ Hz, 1H), 8.25 (d, $J = 8.6$ Hz, 1H), 8.09 (s, 1H).



YJh66

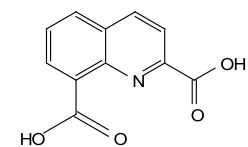
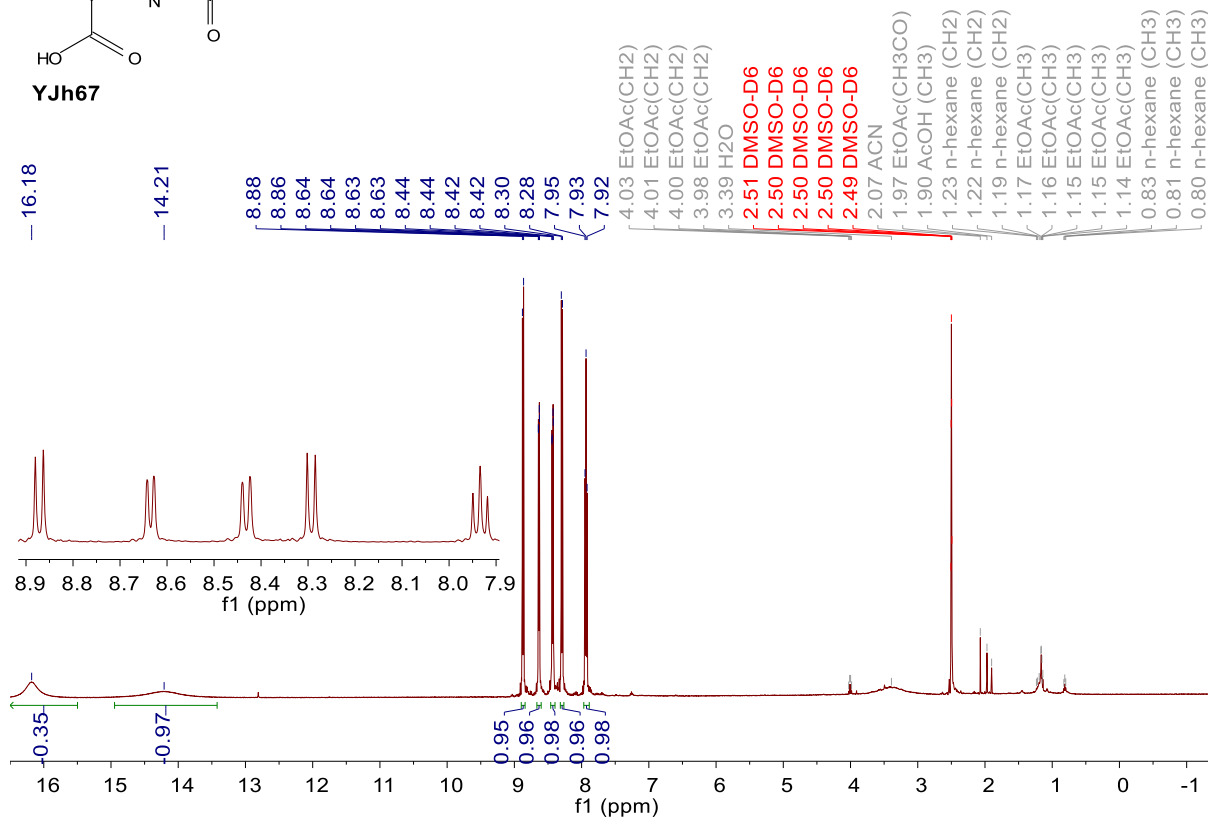
$^{13}\text{C NMR}$ (101 MHz, $\text{DMSO-}d_6$) δ 164.43, 153.93, 145.53, 137.39, 135.46, 135.41, 126.79, 121.50, 119.52, 79.68.





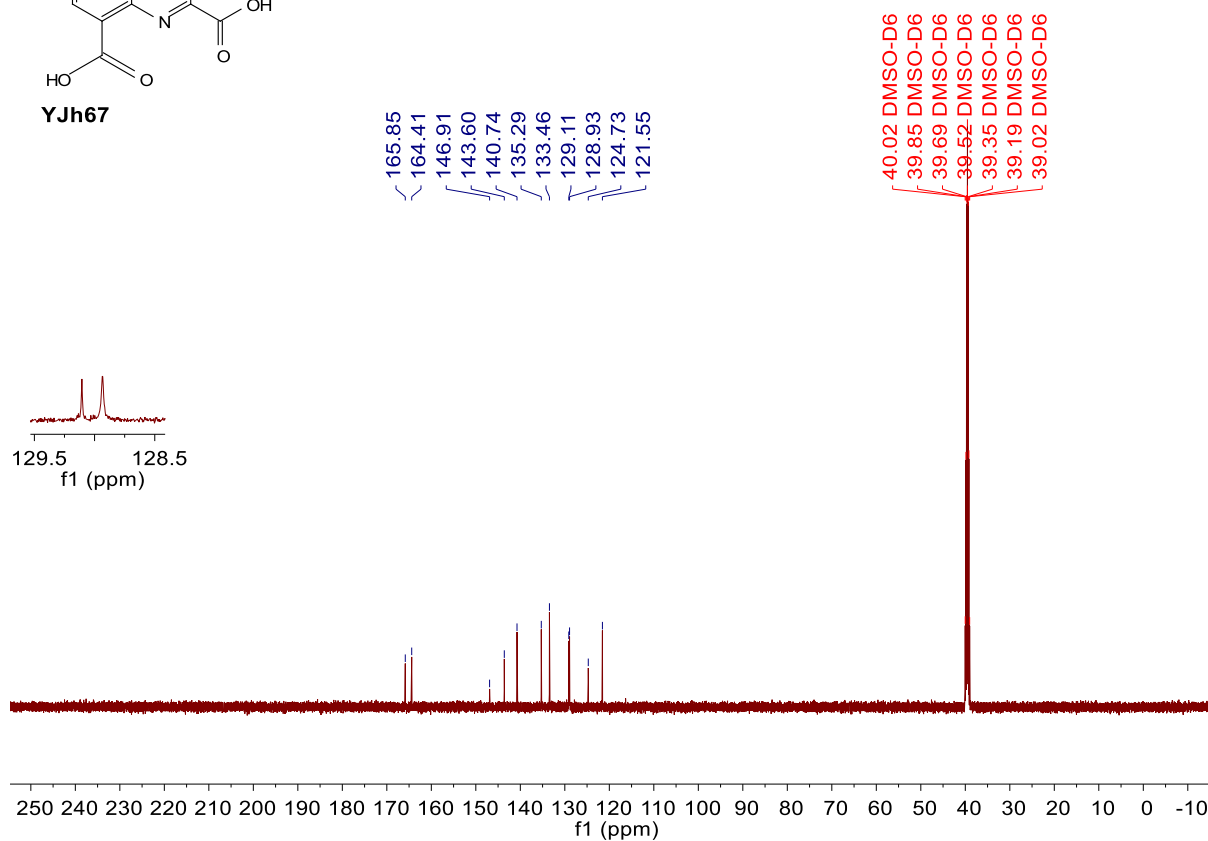
YJh67

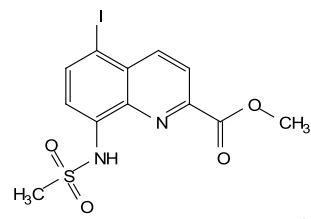
$^1\text{H NMR}$ (500 MHz, $\text{DMSO-}d_6$) δ 16.18 (s, 1H), 14.21 (s, 1H), 8.87 (d, $J = 8.6$ Hz, 1H), 8.63 (dd, $J = 7.2, 1.4$ Hz, 1H), 8.43 (dd, $J = 8.2, 1.5$ Hz, 1H), 8.29 (d, $J = 8.5$ Hz, 1H), 7.93 (t, $J = 7.7$ Hz, 1H).



YJh67

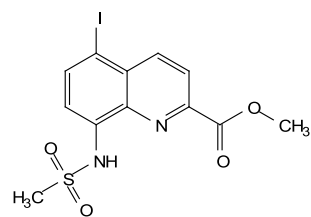
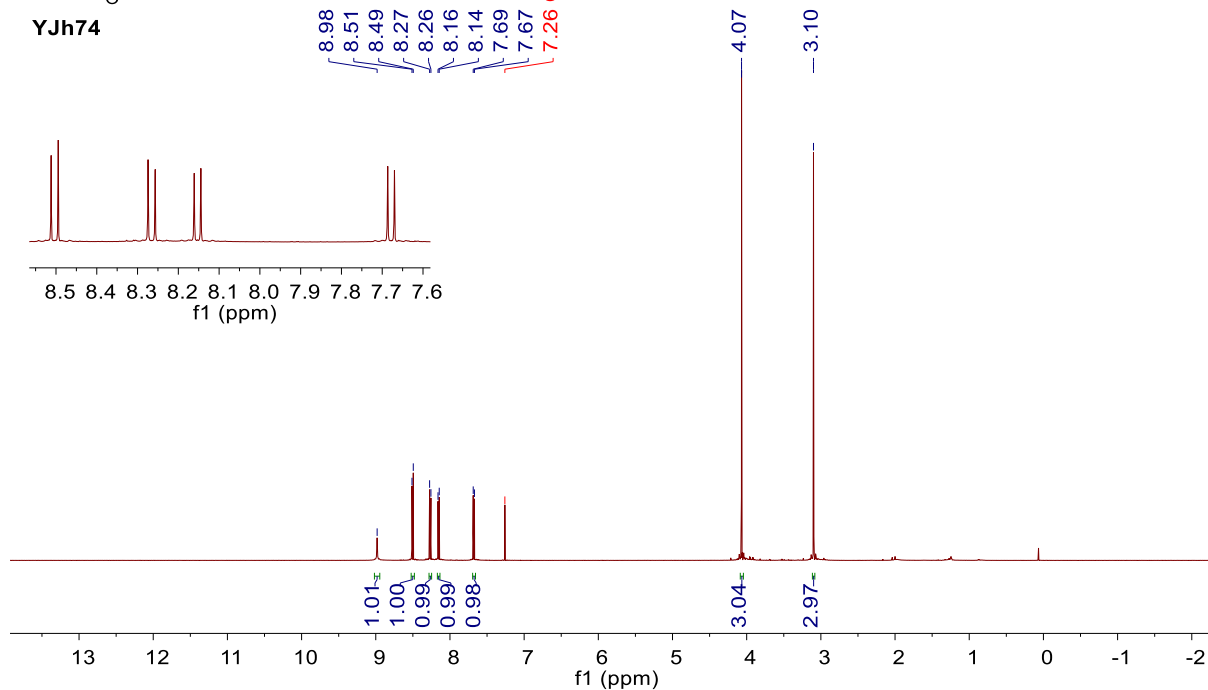
$^{13}\text{C NMR}$ (126 MHz, $\text{DMSO-}d_6$) δ 165.85, 164.41, 146.91, 143.60, 140.74, 135.29, 133.46, 129.11, 128.93, 124.73, 121.55.





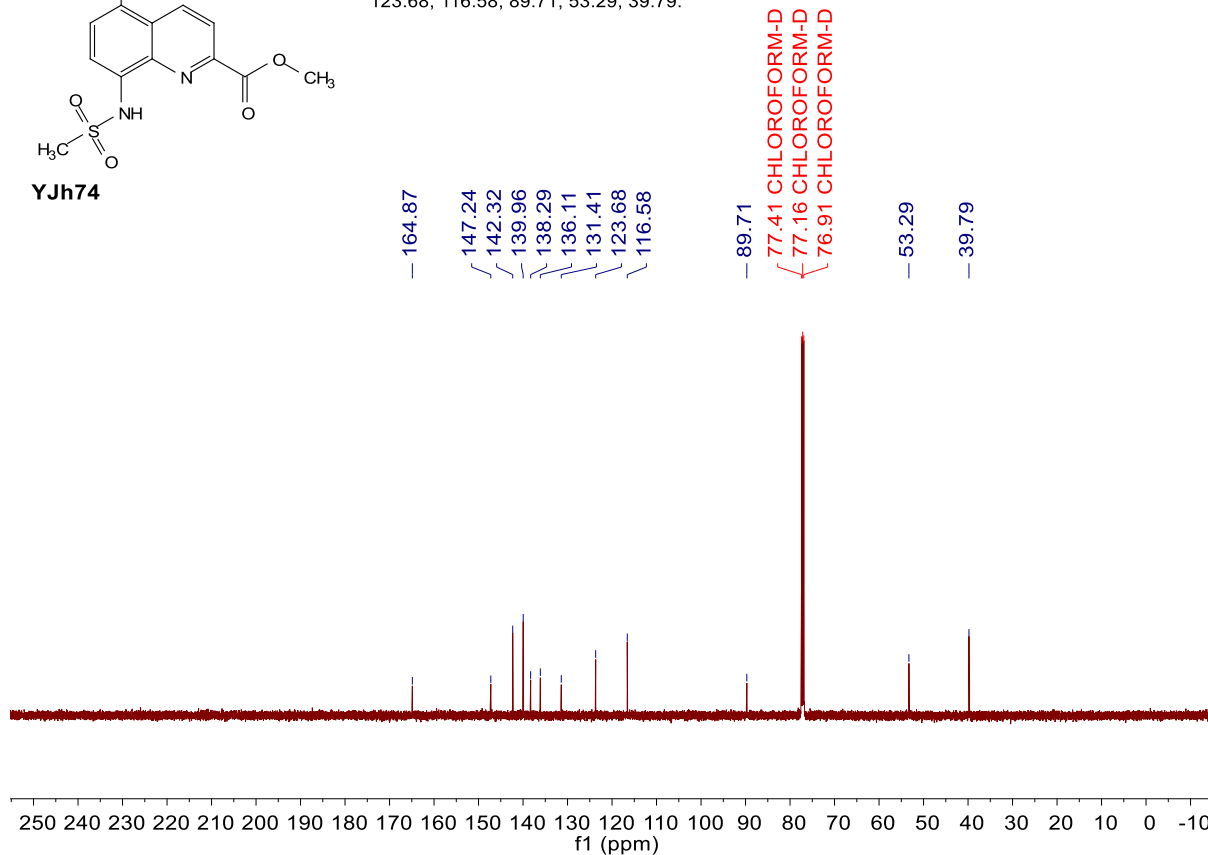
YJh74

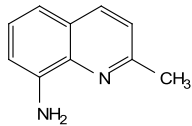
¹H NMR (500 MHz, Chloroform-*d*) δ 8.98 (s, 1H), 8.50 (d, *J* = 8.7 Hz, 1H), 8.27 (d, *J* = 8.7 Hz, 1H), 8.15 (d, *J* = 8.2 Hz, 1H), 7.68 (d, *J* = 8.2 Hz, 1H), 4.07 (s, 3H), 3.10 (s, 3H).



YJh74

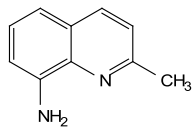
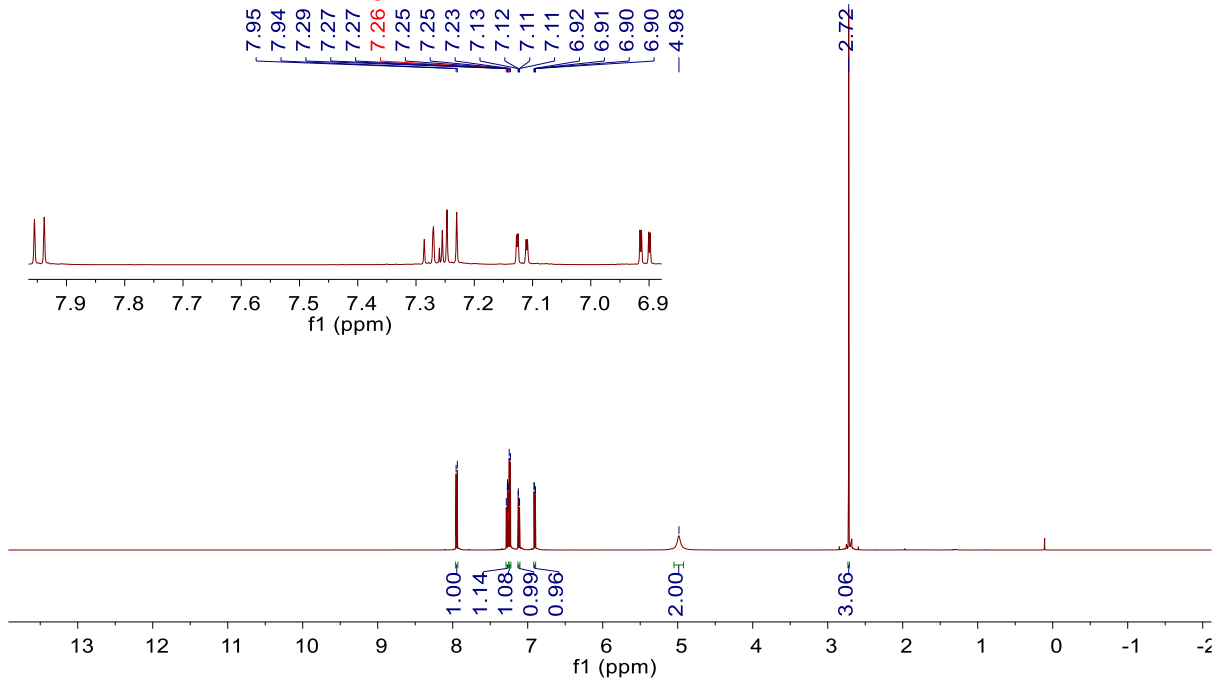
¹³C NMR (126 MHz, Chloroform-*d*) δ 164.87, 147.24, 142.32, 139.96, 138.29, 136.11, 131.41, 123.68, 116.58, 89.71, 53.29, 39.79.





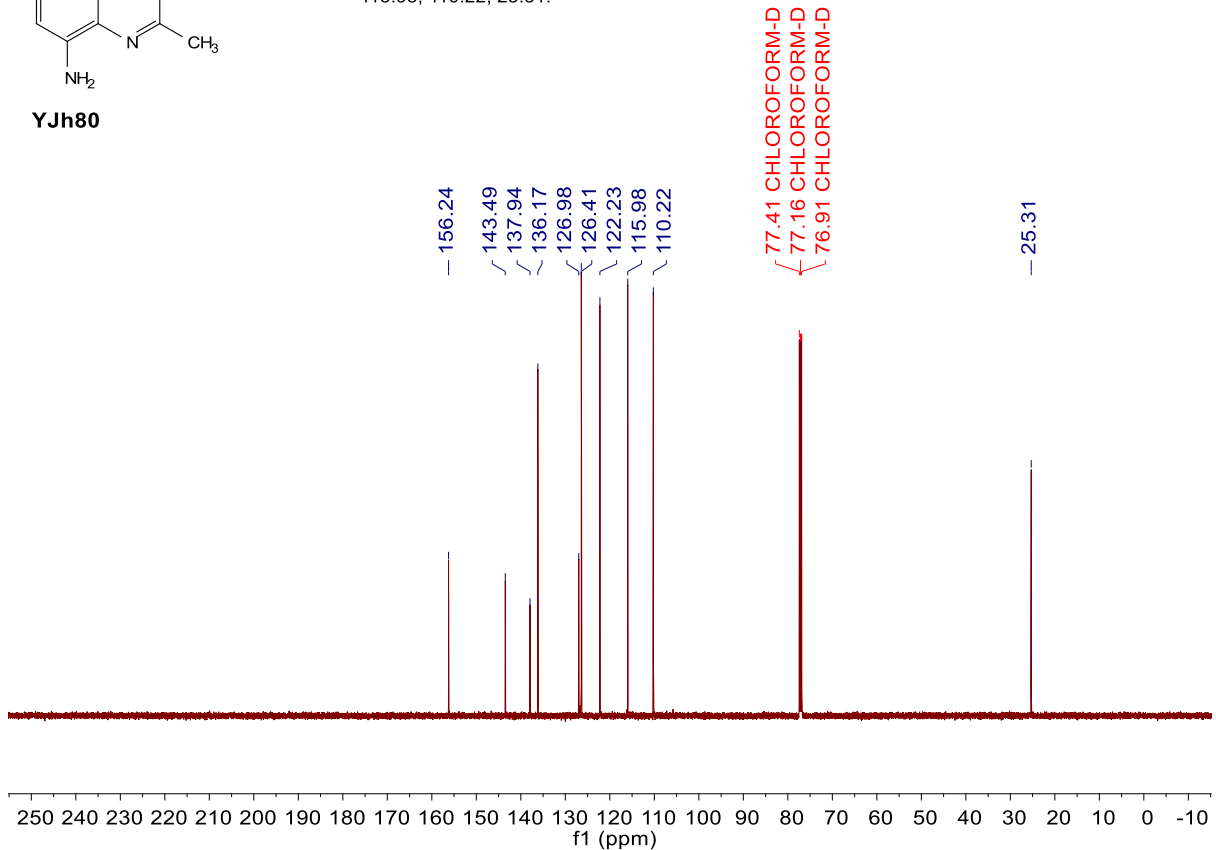
YJh80

¹H NMR (500 MHz, Chloroform-*d*) δ 7.95 (d, *J* = 8.4 Hz, 1H), 7.27 (dd, *J* = 8.1, 7.5 Hz, 1H), 7.24 (d, *J* = 8.4 Hz, 1H), 7.12 (dd, *J* = 8.1, 1.3 Hz, 1H), 6.91 (dd, *J* = 7.5, 1.3 Hz, 1H), 4.98 (s, 2H), 2.72 (s, 3H).

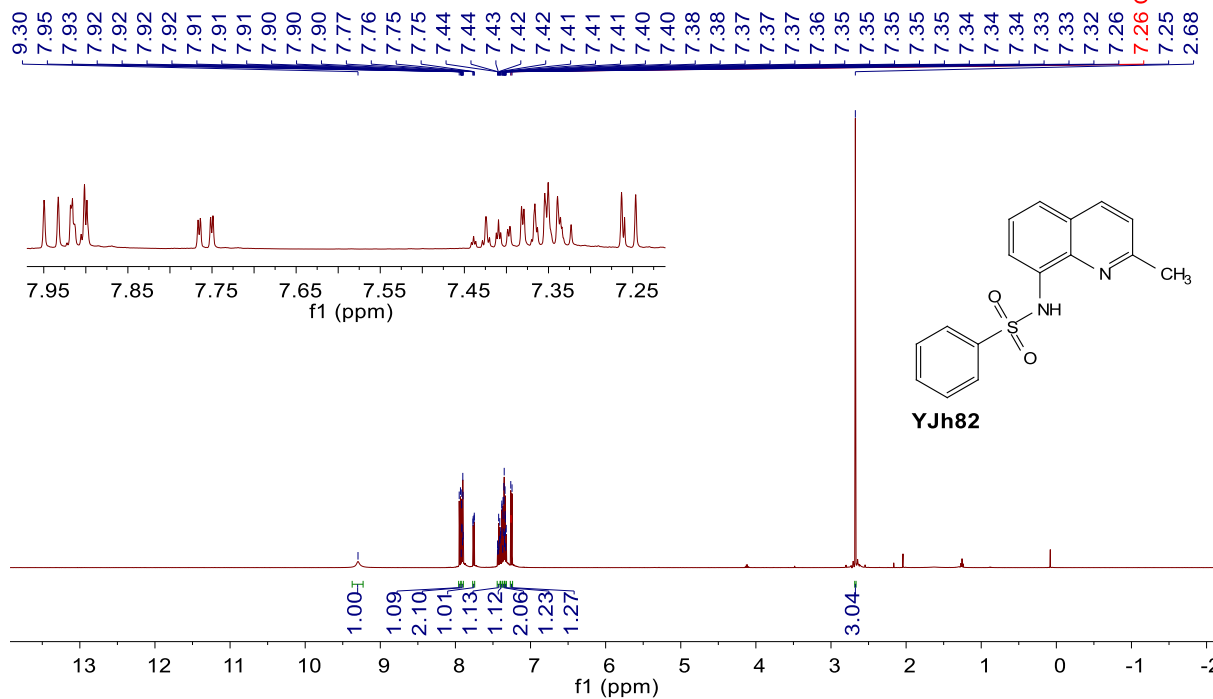


YJh80

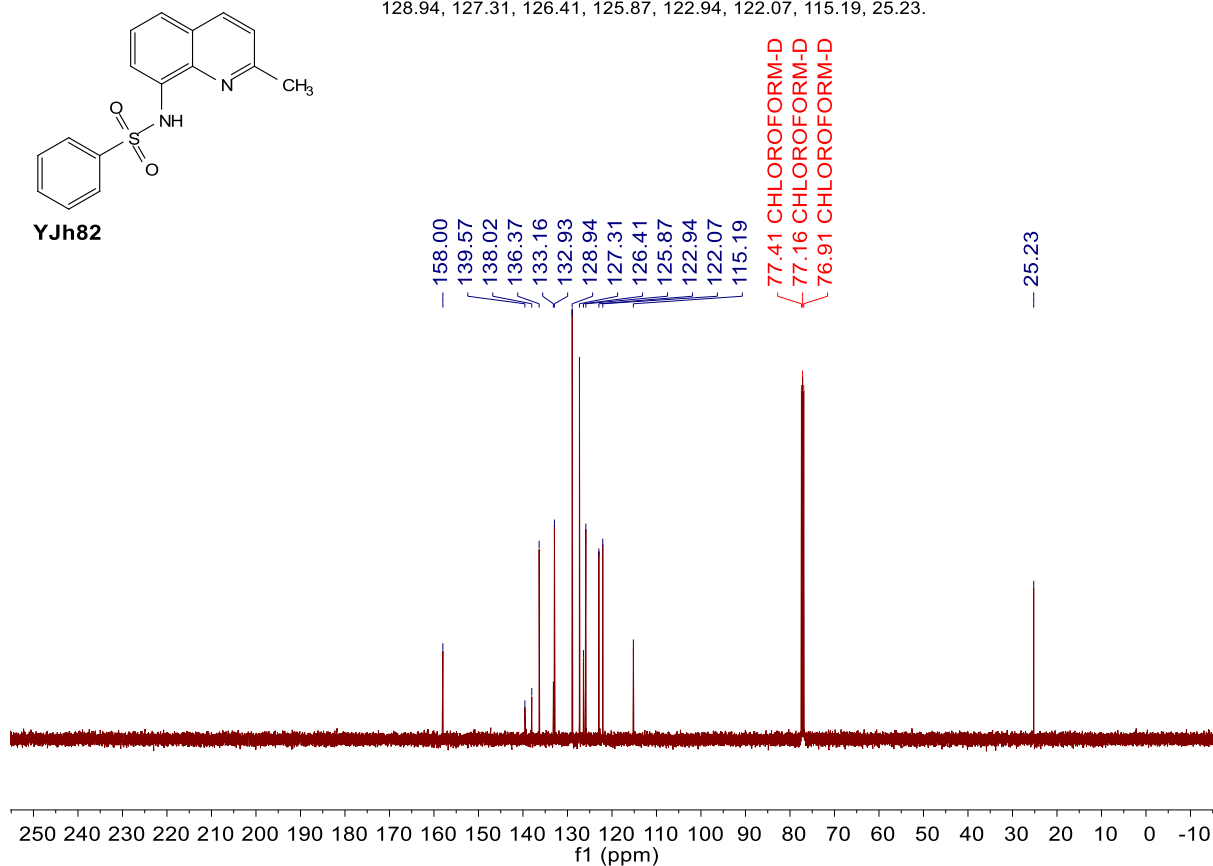
¹³C NMR (126 MHz, Chloroform-*d*) δ 156.24, 143.49, 137.94, 136.17, 126.98, 126.41, 122.23, 115.98, 110.22, 25.31.

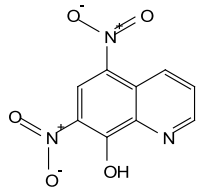


¹H NMR (500 MHz, Chloroform-*d*) δ 9.30 (s, 1H), 7.94 (d, *J* = 8.4 Hz, 1H), 7.95 – 7.87 (m, 2H), 7.76 (dd, *J* = 7.5, 1.4 Hz, 1H), 7.45 – 7.40 (m, 1H), 7.39 (dd, *J* = 8.2, 1.4 Hz, 1H), 7.37 – 7.31 (m, 3H), 7.25 (d, *J* = 8.4 Hz, 1H), 2.68 (s, 3H).



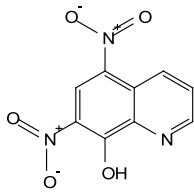
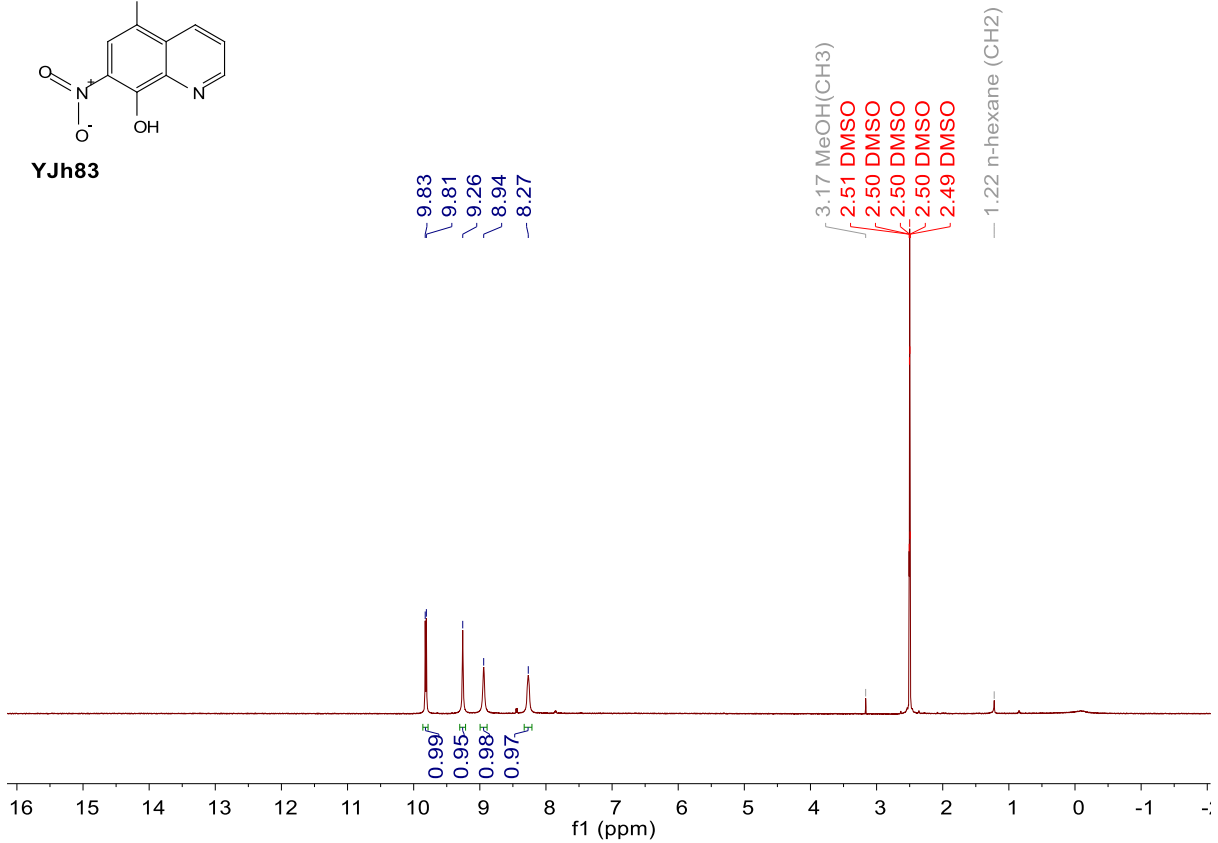
¹³C NMR (126 MHz, Chloroform-*d*) δ 158.00, 139.57, 138.02, 136.37, 133.16, 132.93, 128.94, 127.31, 126.41, 125.87, 122.94, 122.07, 115.19, 25.23.





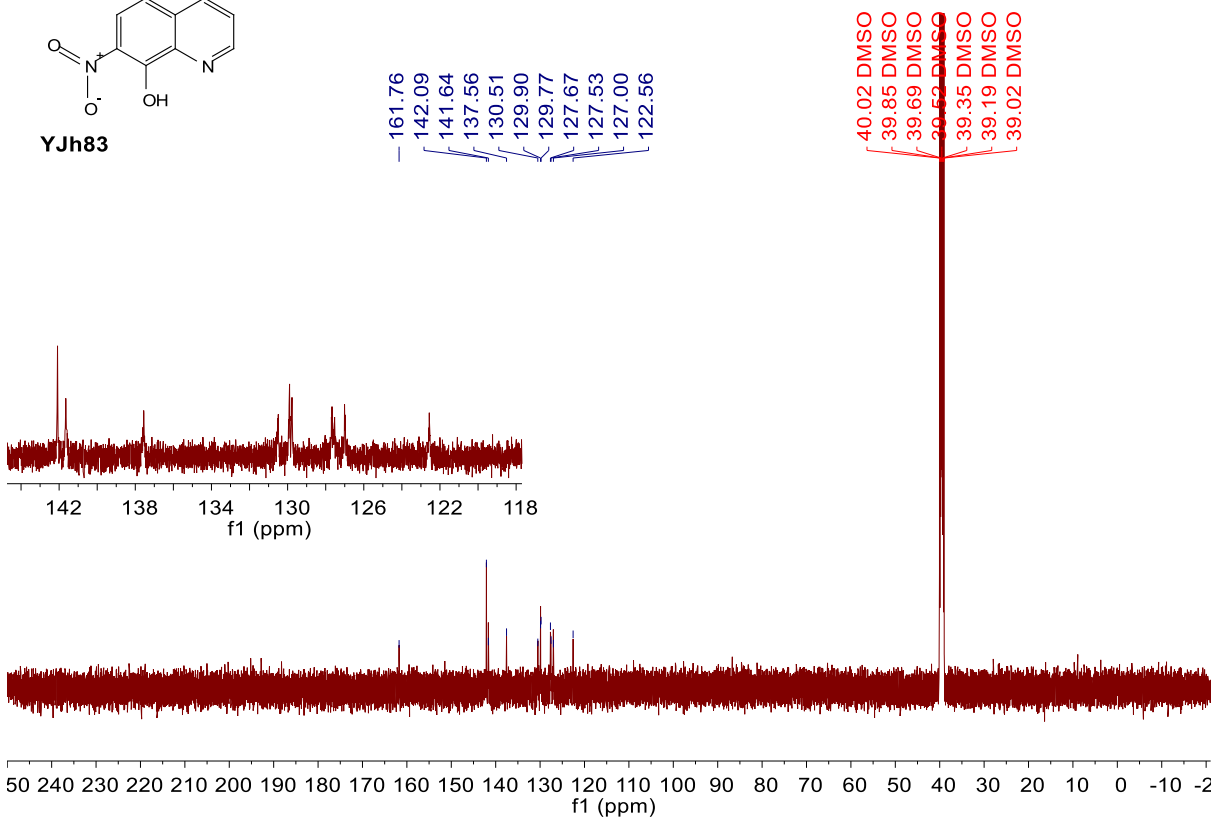
YJh83

¹H NMR (500 MHz, DMSO-*d*₆) δ 9.82 (d, *J* = 8.7 Hz, 1H), 9.26 (s, 1H), 8.94 (s, 1H), 8.27 (s, 1H).

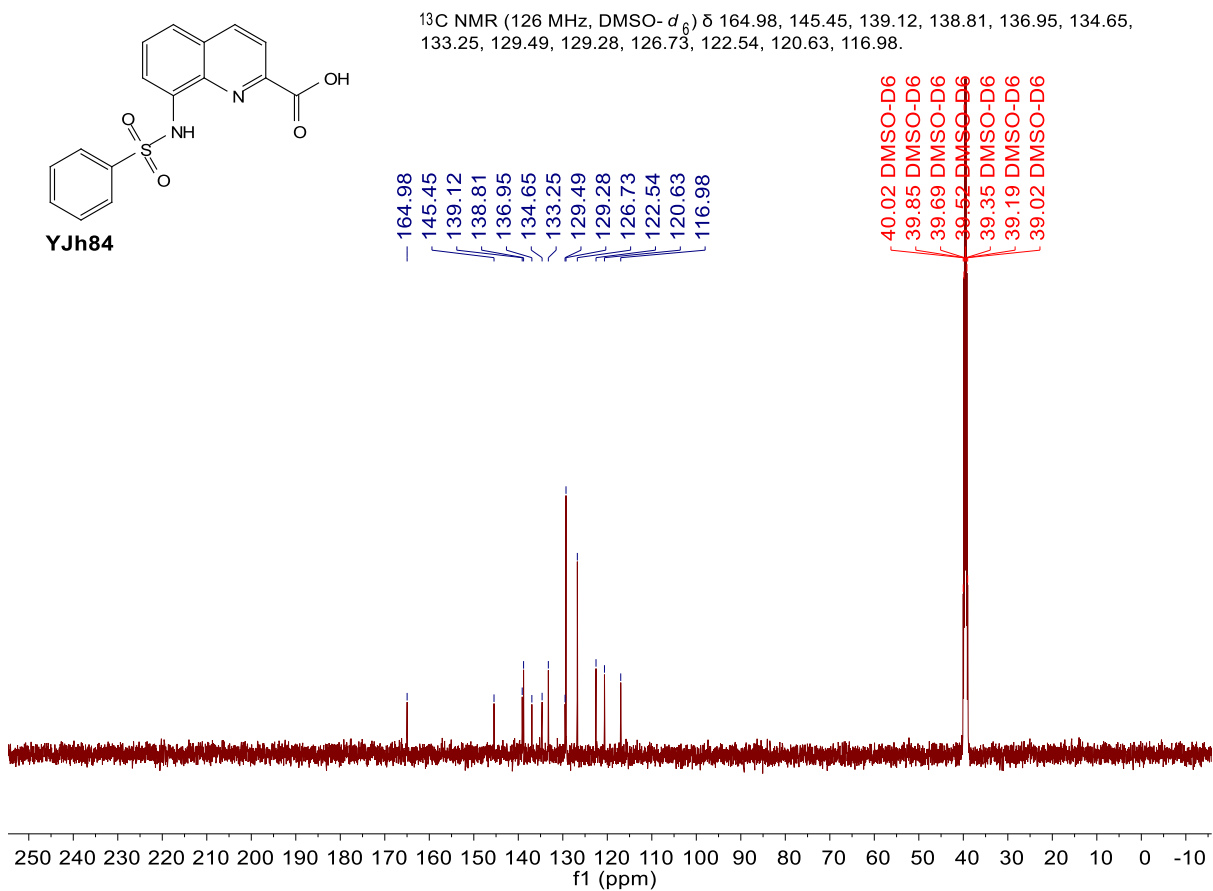
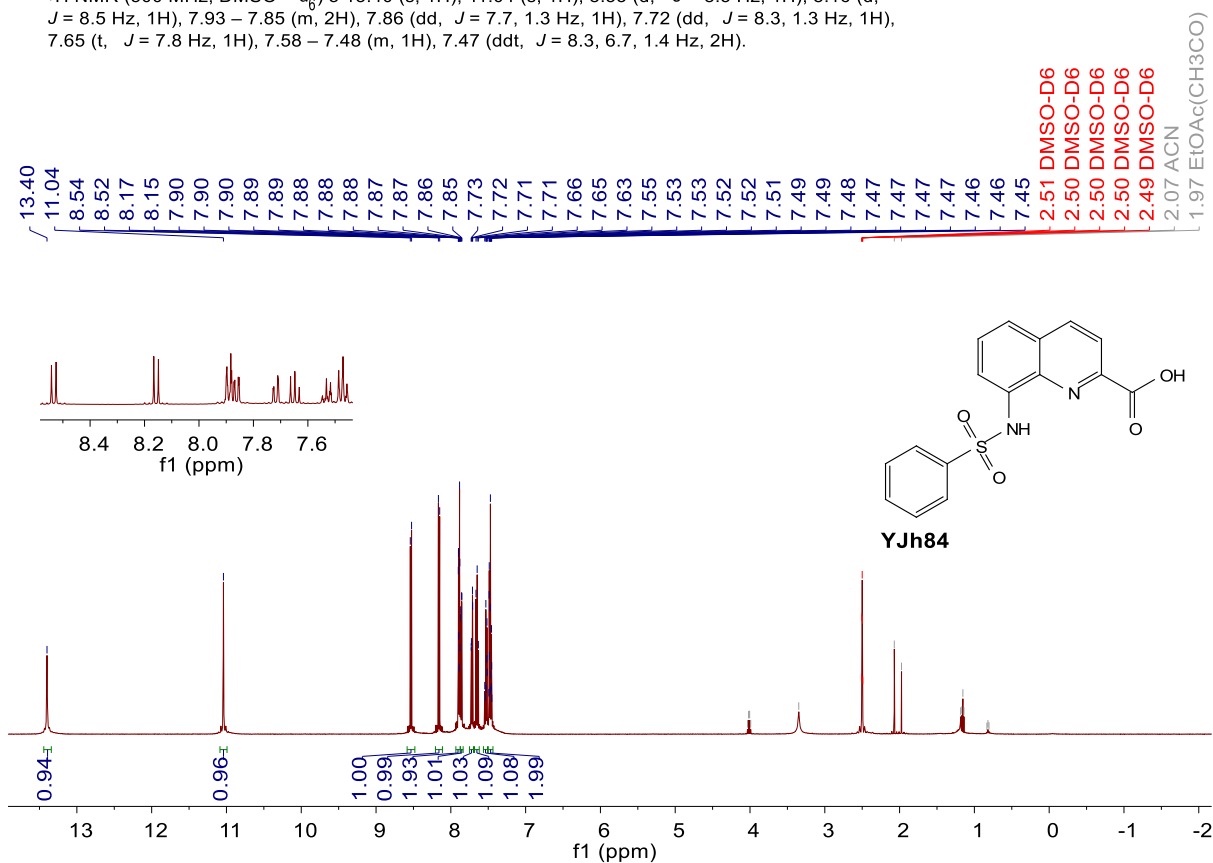


YJh83

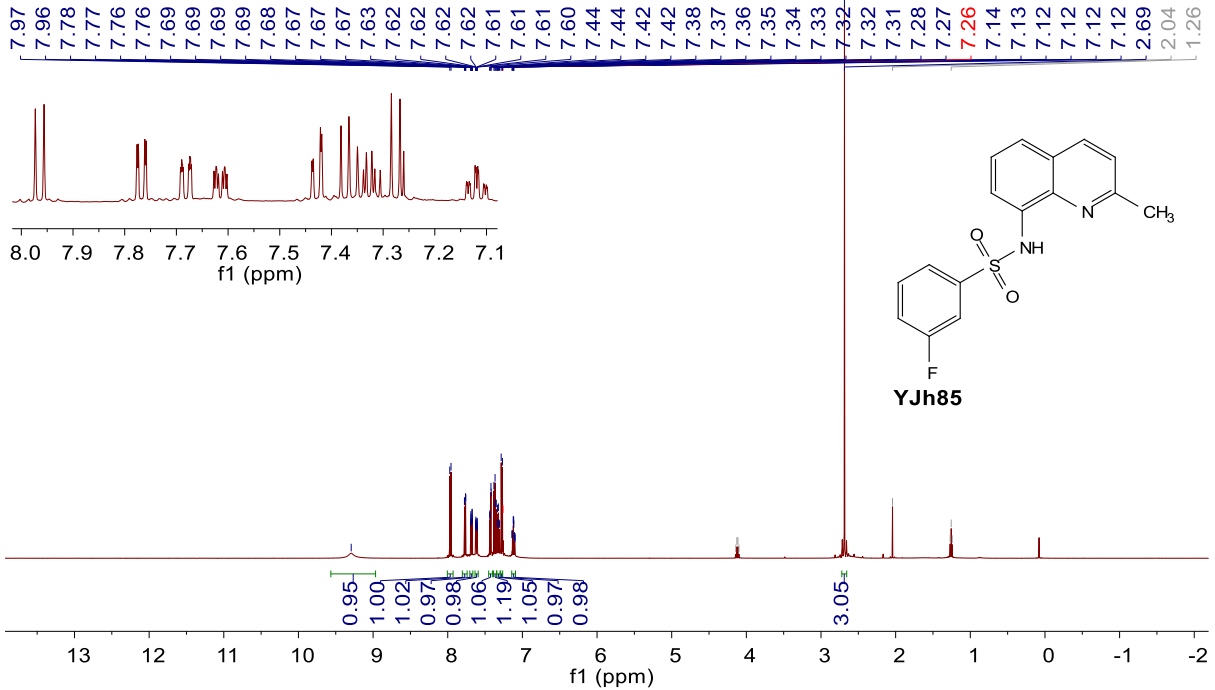
¹³C NMR (126 MHz, DMSO-*d*₆) δ 161.76, 142.09, 141.64, 137.56, 130.51, 129.84 (d, *J* = 16.0 Hz), 127.60 (d, *J* = 17.2 Hz), 127.00, 122.56.



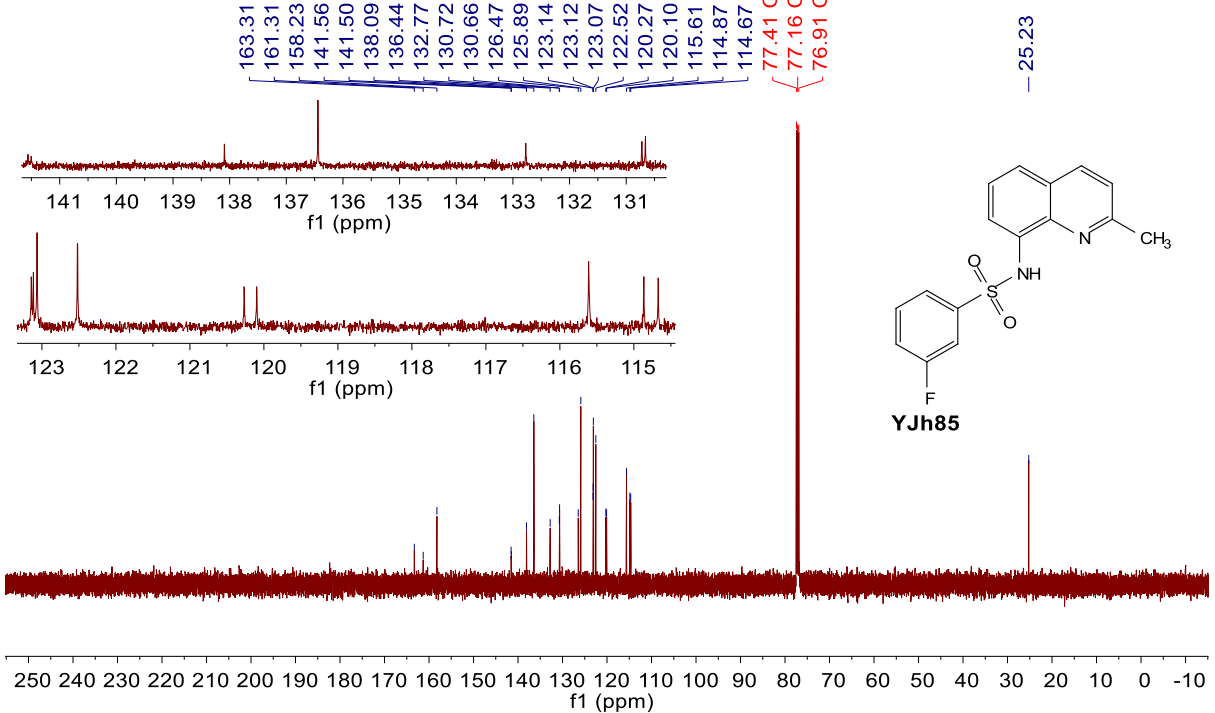
¹H NMR (500 MHz, DMSO-*d*₆) δ 13.40 (s, 1H), 11.04 (s, 1H), 8.53 (d, *J* = 8.5 Hz, 1H), 8.16 (d, *J* = 8.5 Hz, 1H), 7.93 – 7.85 (m, 2H), 7.86 (dd, *J* = 7.7, 1.3 Hz, 1H), 7.72 (dd, *J* = 8.3, 1.3 Hz, 1H), 7.65 (t, *J* = 7.8 Hz, 1H), 7.58 – 7.48 (m, 1H), 7.47 (ddt, *J* = 8.3, 6.7, 1.4 Hz, 2H).



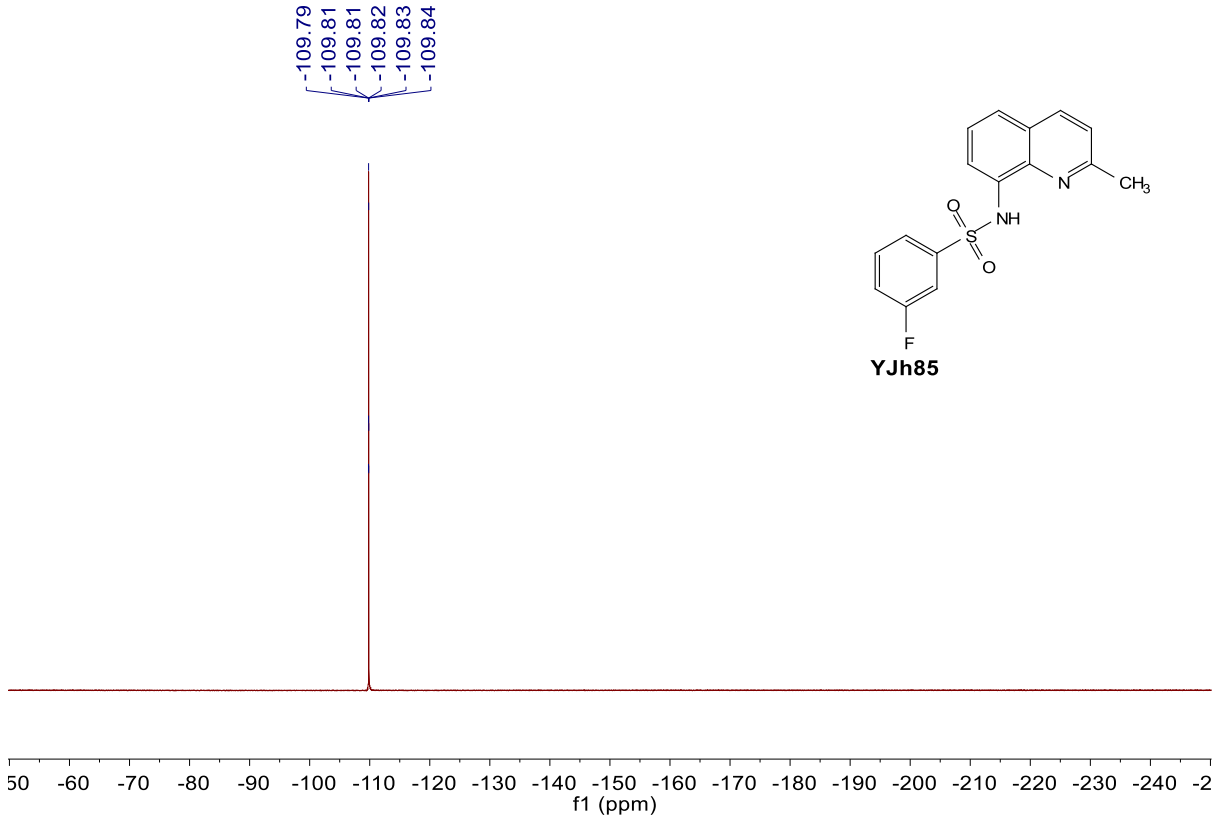
¹H NMR (500 MHz, Chloroform-*d*) δ 9.29 (s, 1H), 7.96 (d, *J* = 8.4 Hz, 1H), 7.77 (dd, *J* = 7.5, 1.3 Hz, 1H), 7.68 (ddd, *J* = 7.9, 1.7, 1.0 Hz, 1H), 7.63 – 7.59 (m, 1H), 7.43 (dd, *J* = 8.3, 1.3 Hz, 1H), 7.37 (dd, *J* = 8.3, 7.6 Hz, 1H), 7.34 – 7.30 (m, 1H), 7.28 (d, *J* = 8.4 Hz, 1H), 7.12 (tdd, *J* = 8.3, 2.6, 1.0 Hz, 1H), 2.69 (s, 3H).



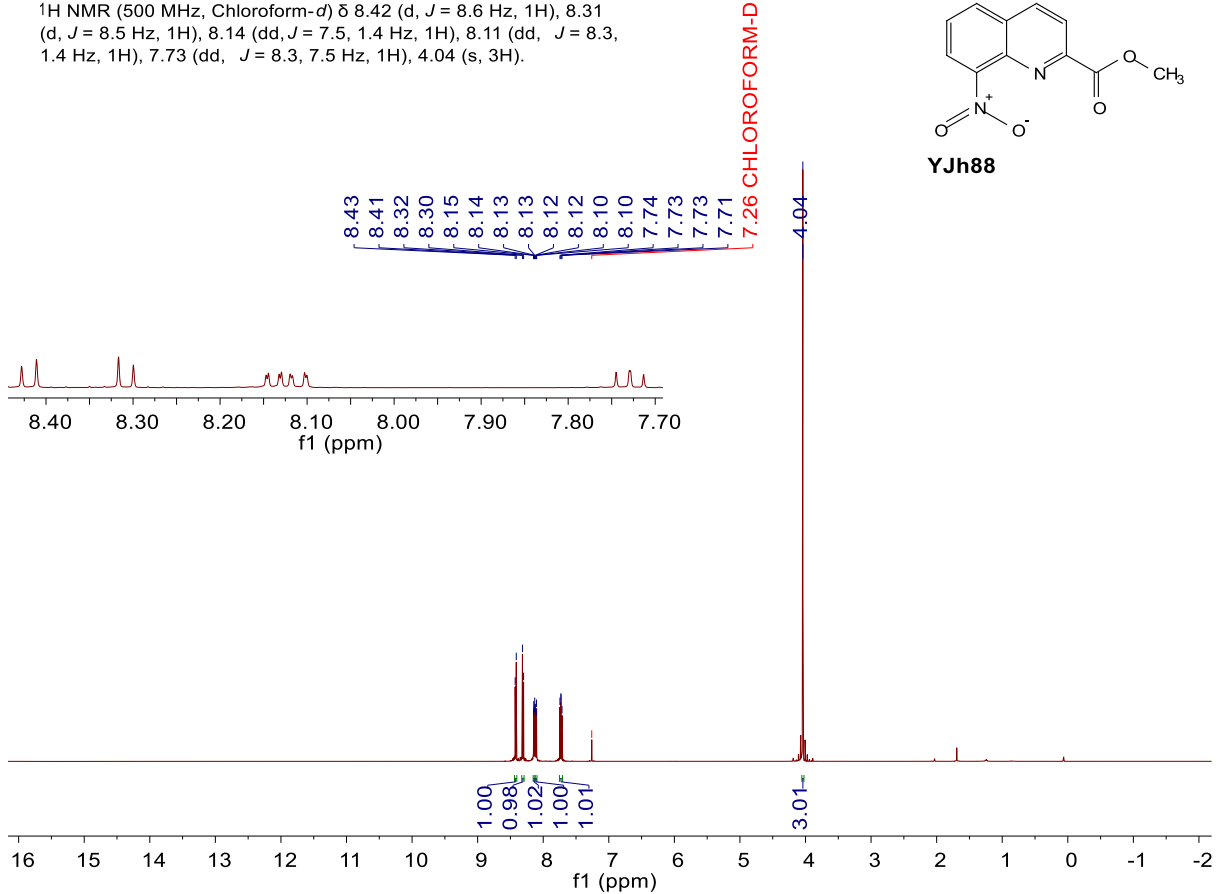
¹³C NMR (126 MHz, Chloroform-*d*) δ 162.31 (d, *J* = 251.5 Hz), 158.23, 141.53 (d, *J* = 7.2 Hz), 138.09, 136.44, 132.77, 130.69 (d, *J* = 7.8 Hz), 126.47, 125.89, 123.13 (d, *J* = 3.6 Hz), 123.07, 122.52, 120.18 (d, *J* = 21.4 Hz), 115.61, 114.77 (d, *J* = 24.4 Hz), 25.23.



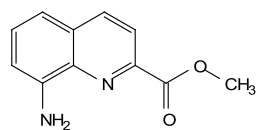
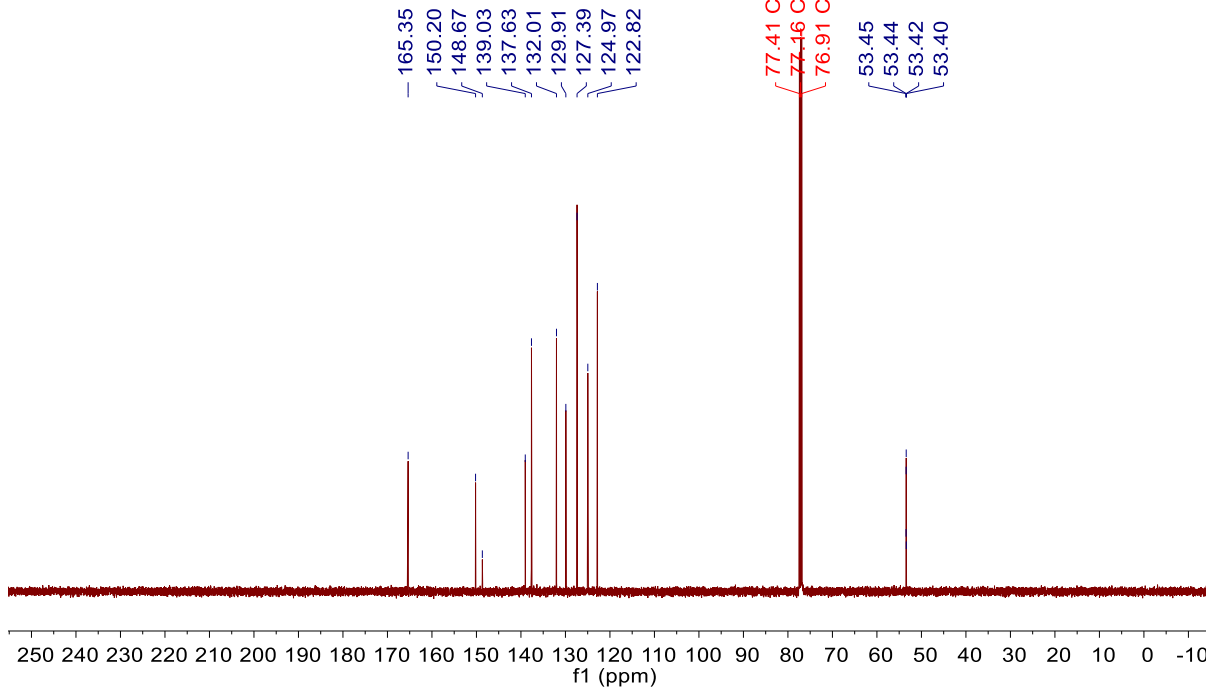
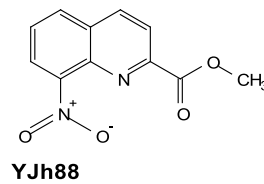
^{19}F NMR (471 MHz, Chloroform d) δ -109.82 (td, J = 8.6, 5.6 Hz).



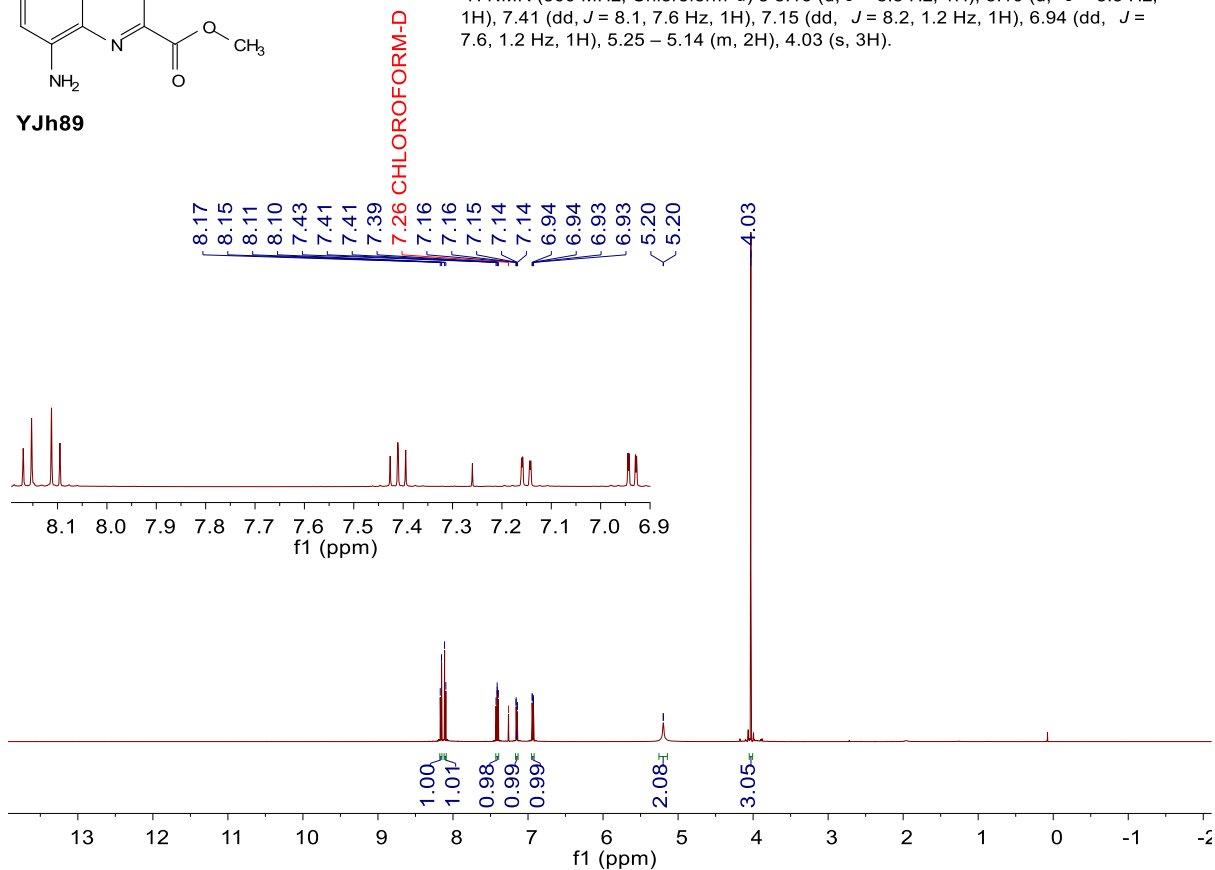
^1H NMR (500 MHz, Chloroform- d) δ 8.42 (d, J = 8.6 Hz, 1H), 8.31 (d, J = 8.5 Hz, 1H), 8.14 (dd, J = 7.5, 1.4 Hz, 1H), 8.11 (dd, J = 8.3, 1.4 Hz, 1H), 7.73 (dd, J = 8.3, 7.5 Hz, 1H), 4.04 (s, 3H).



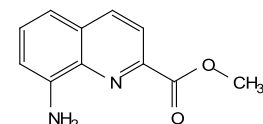
¹³C NMR (126 MHz, Chloroform-*d*) δ 165.35, 150.20, 148.67, 139.03, 137.63, 132.01, 129.91, 127.39, 124.97, 122.82, 53.43 (q, *J* = 2.2 Hz).



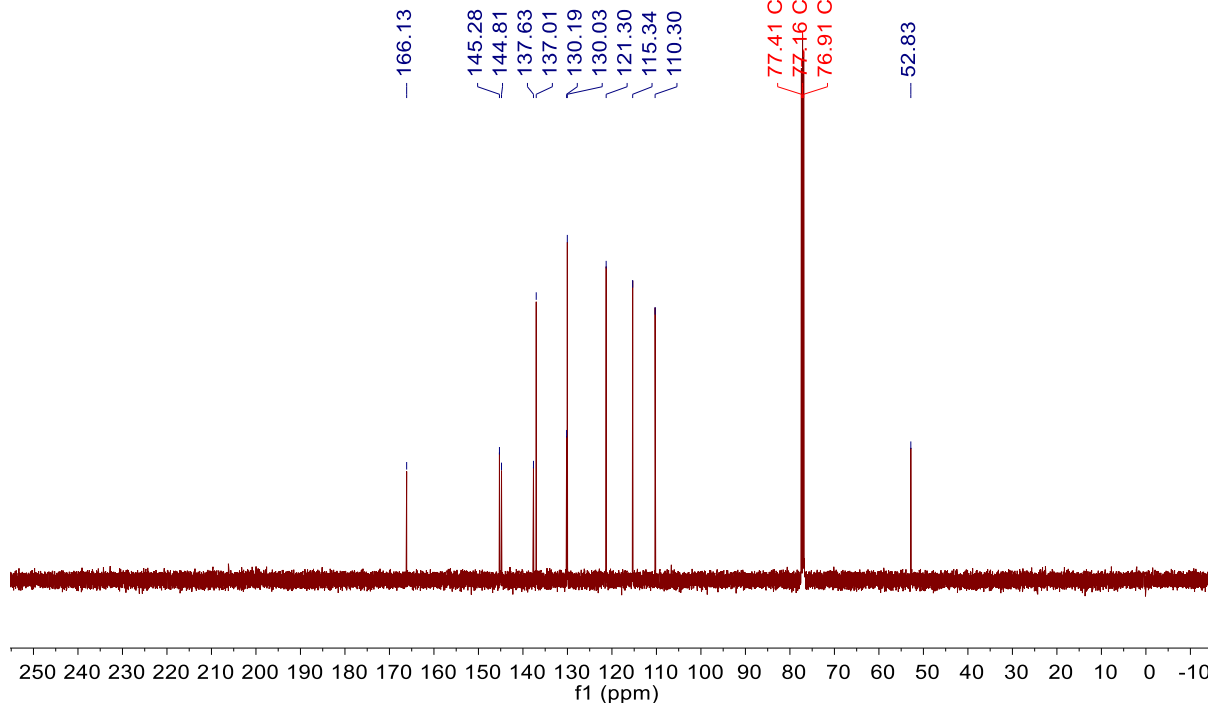
¹H NMR (500 MHz, Chloroform-*d*) δ 8.16 (d, *J* = 8.5 Hz, 1H), 8.10 (d, *J* = 8.5 Hz, 1H), 7.41 (dd, *J* = 8.1, 7.6 Hz, 1H), 7.15 (dd, *J* = 8.2, 1.2 Hz, 1H), 6.94 (dd, *J* = 7.6, 1.2 Hz, 1H), 5.25 – 5.14 (m, 2H), 4.03 (s, 3H).



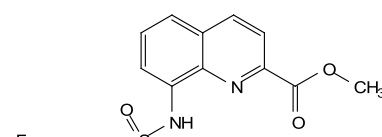
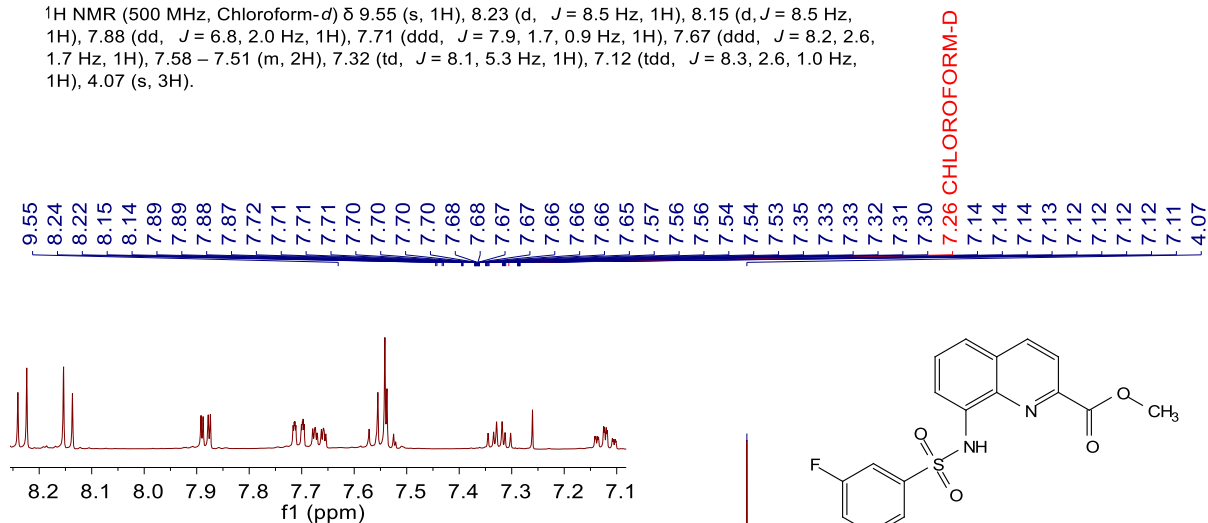
¹³C NMR (126 MHz, Chloroform-*d*) δ 166.13, 145.28, 144.81, 137.63, 137.01, 130.19, 130.03, 121.30, 115.34, 110.30, 52.83.



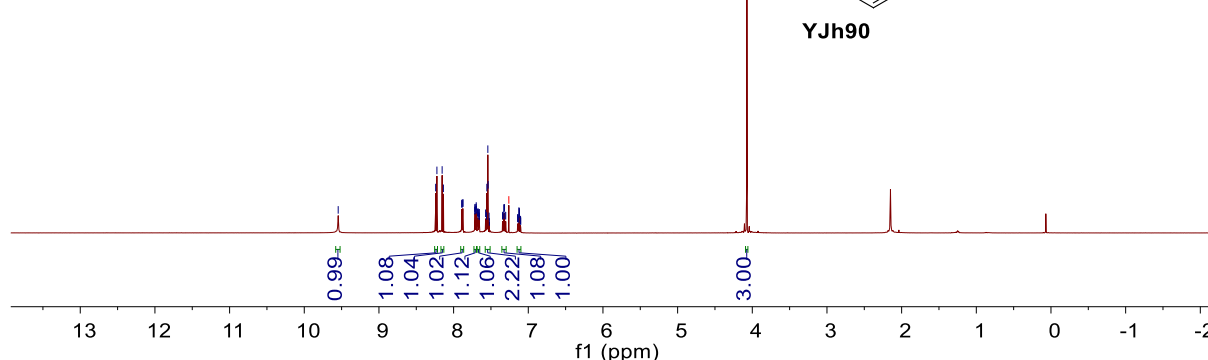
YJh89



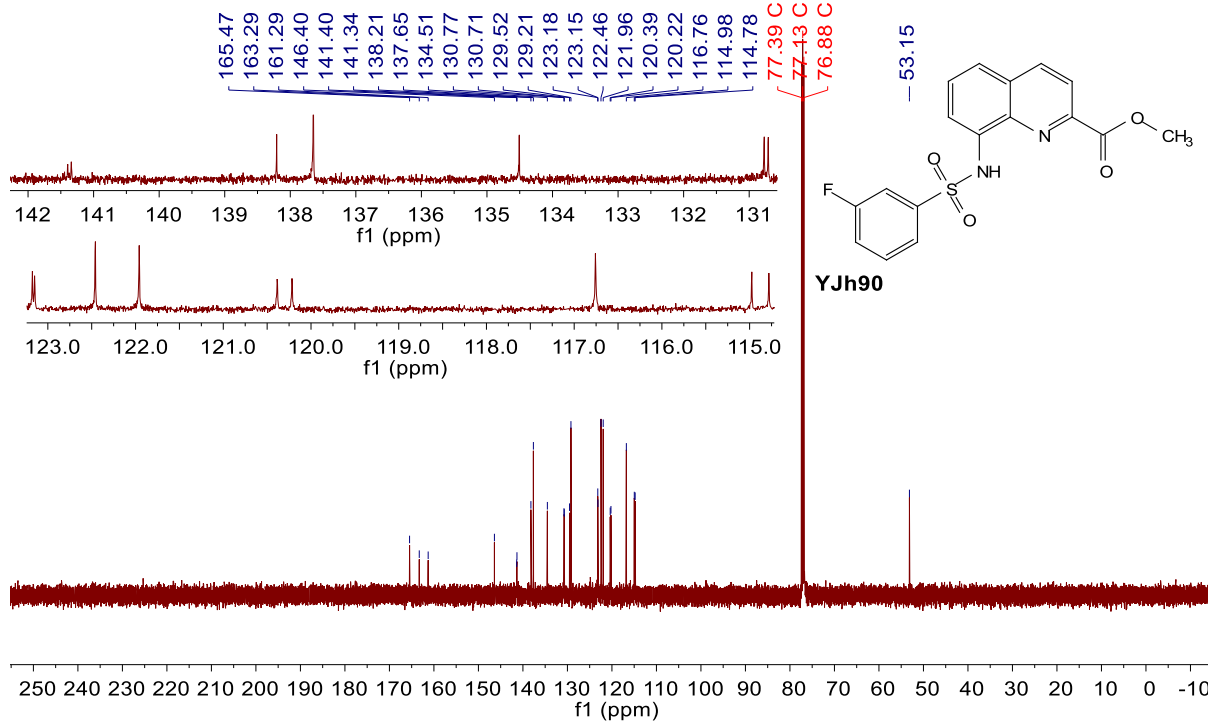
¹H NMR (500 MHz, Chloroform-*d*) δ 9.55 (s, 1H), 8.23 (d, *J* = 8.5 Hz, 1H), 8.15 (d, *J* = 8.5 Hz, 1H), 7.88 (dd, *J* = 6.8, 2.0 Hz, 1H), 7.71 (ddd, *J* = 7.9, 1.7, 0.9 Hz, 1H), 7.67 (ddd, *J* = 8.2, 2.6, 1.7 Hz, 1H), 7.58 – 7.51 (m, 2H), 7.32 (td, *J* = 8.1, 5.3 Hz, 1H), 7.12 (tdd, *J* = 8.3, 2.6, 1.0 Hz, 1H), 4.07 (s, 3H).



YJh90

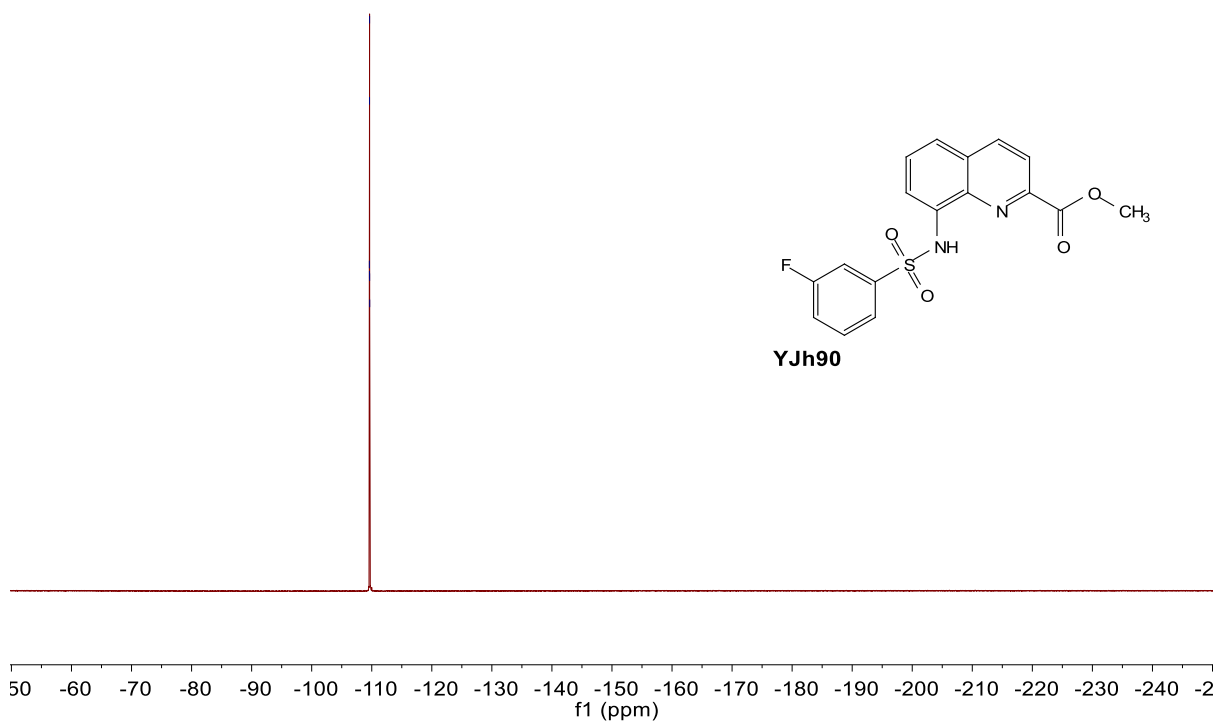


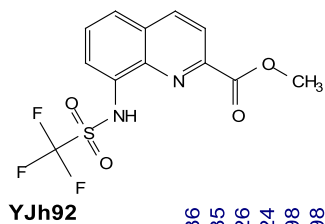
^{13}C NMR (126 MHz, Chloroform- d) δ 165.47, 162.29 (d, $J = 251.7$ Hz), 146.40, 141.37 (d, $J = 7.2$ Hz), 138.21, 137.65, 134.51, 130.74 (d, $J = 7.7$ Hz), 129.52, 129.21, 123.16 (d, $J = 3.2$ Hz), 122.46, 121.96, 120.30 (d, $J = 21.3$ Hz), 116.76, 114.88 (d, $J = 24.5$ Hz), 53.15.



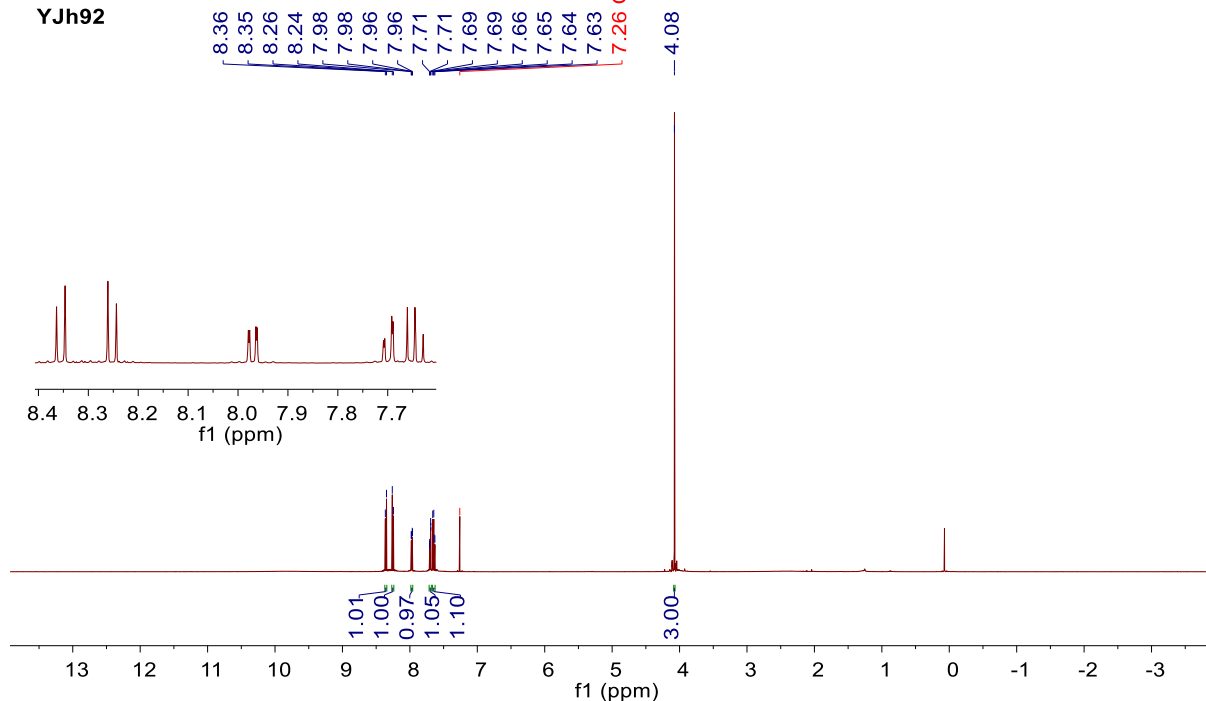
-109.61
-109.62
-109.63
-109.64
-109.64
-109.66

^{19}F NMR (471 MHz, Chloroform- d) δ -109.63 (td, $J = 8.1, 5.1$ Hz).

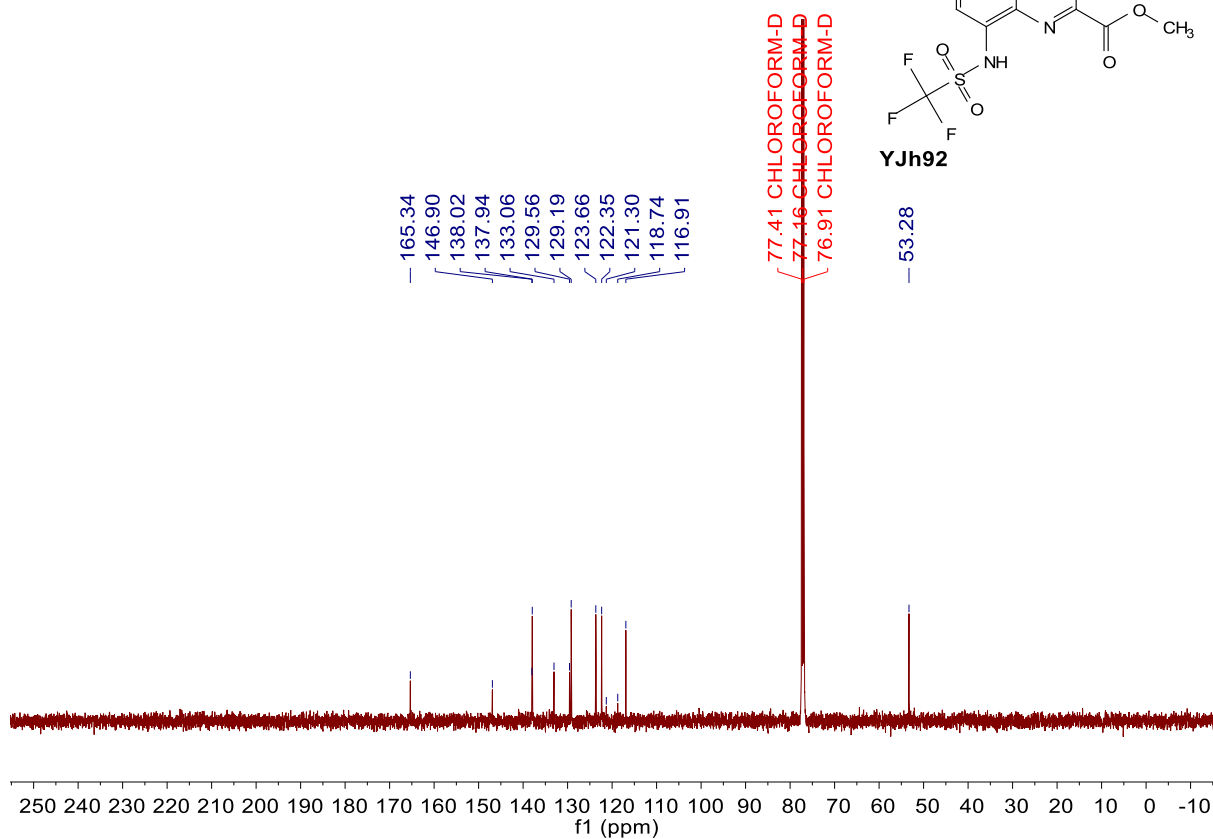
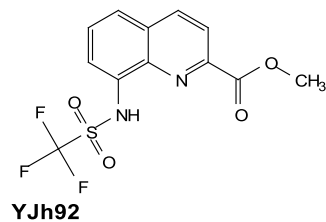




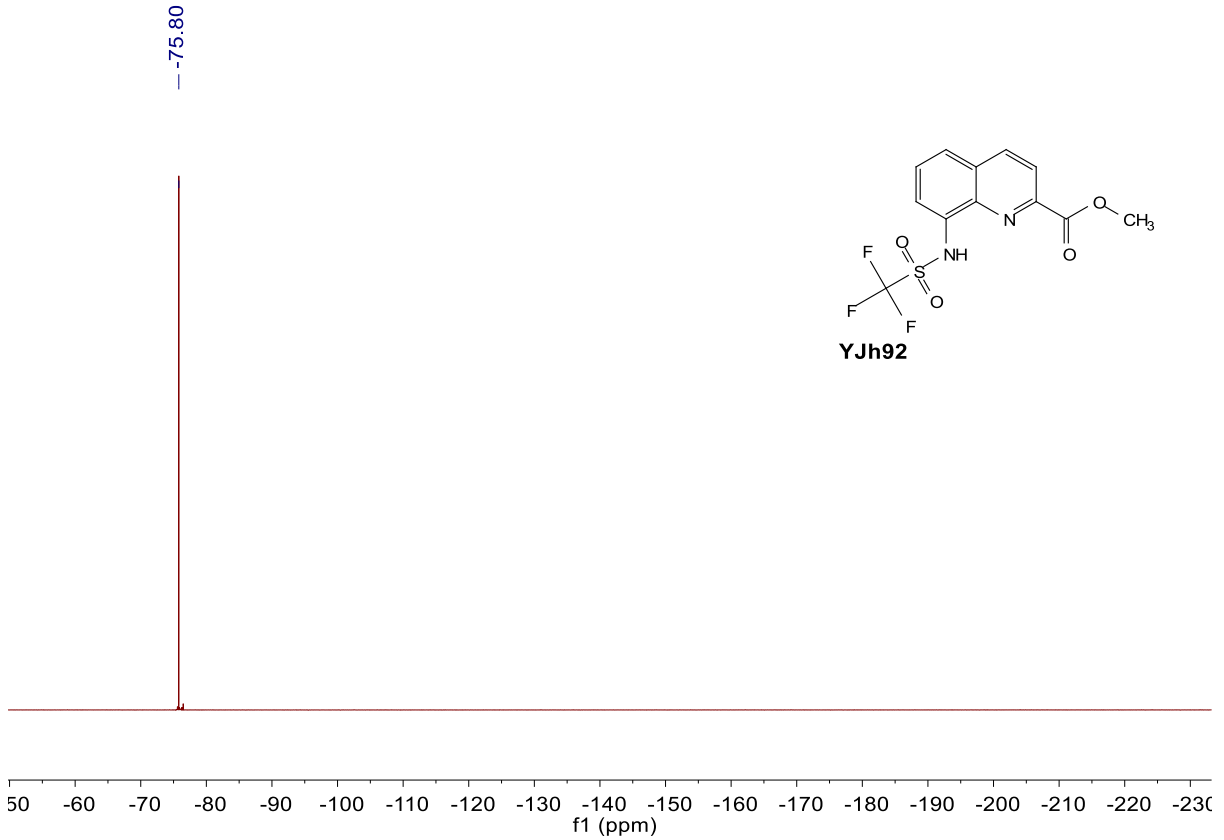
¹H NMR (500 MHz, Chloroform-*d*) δ 8.36 (d, *J* = 8.5 Hz, 1H), 8.25 (d, *J* = 8.5 Hz, 1H), 7.97 (dd, *J* = 7.6, 1.3 Hz, 1H), 7.70 (dd, *J* = 8.3, 1.3 Hz, 1H), 7.64 (dd, *J* = 8.4, 7.6 Hz, 1H), 4.08 (s, 3H).



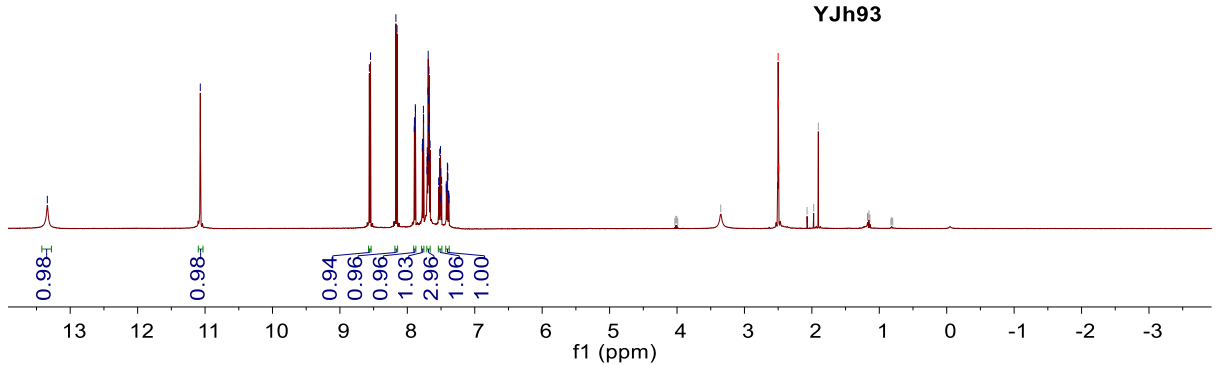
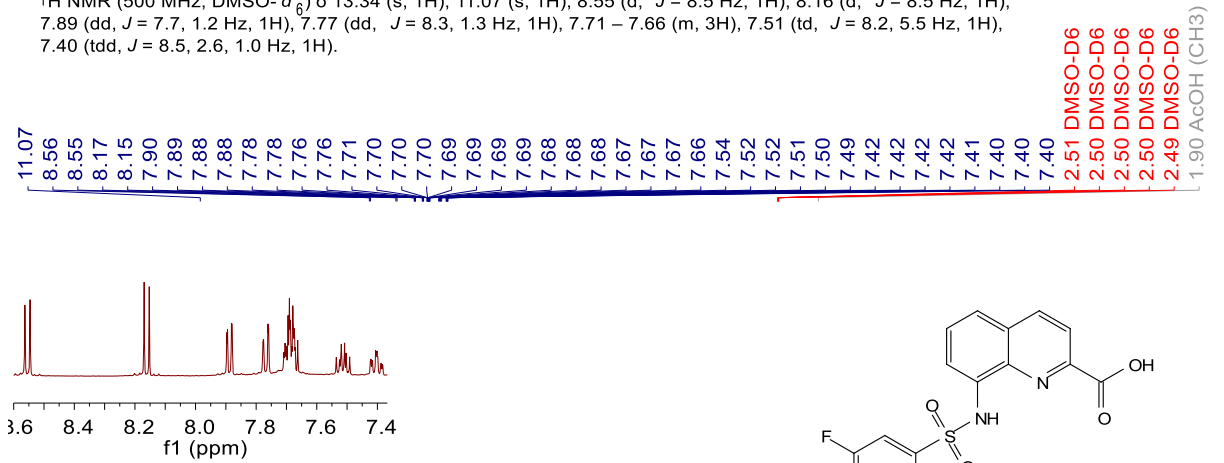
¹³C NMR (126 MHz, Chloroform-*d*) δ 165.34, 146.90, 138.02, 137.94, 133.06, 129.56, 129.19, 123.66, 122.35, 120.02 (q, *J* = 322.8 Hz), 116.91, 53.28.

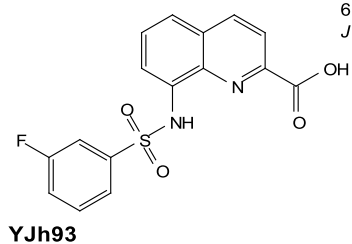


¹⁹F NMR (471 MHz, Chloroform-*d*) δ -75.80.

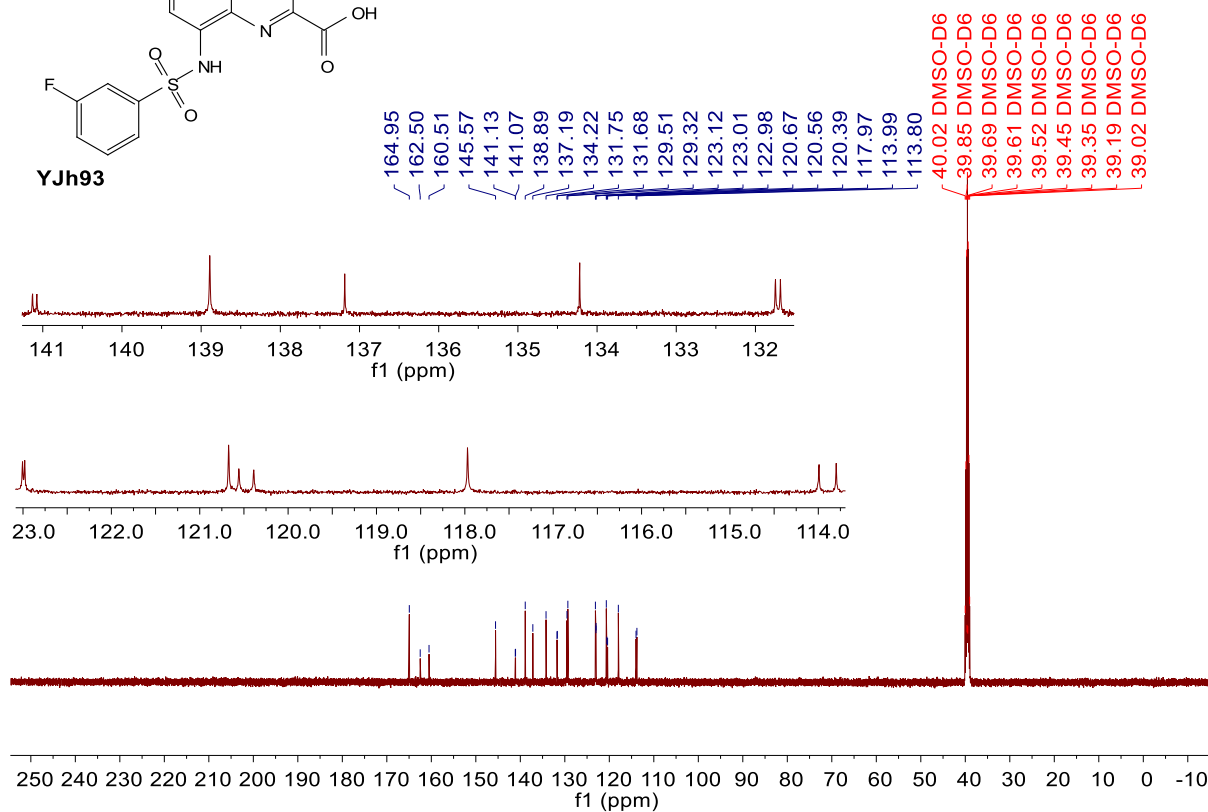


¹H NMR (500 MHz, DMSO-*d*₆) δ 13.34 (s, 1H), 11.07 (s, 1H), 8.55 (d, *J* = 8.5 Hz, 1H), 8.16 (d, *J* = 8.5 Hz, 1H), 7.89 (dd, *J* = 7.7, 1.2 Hz, 1H), 7.77 (dd, *J* = 8.3, 1.3 Hz, 1H), 7.71 – 7.66 (m, 3H), 7.51 (td, *J* = 8.2, 5.5 Hz, 1H), 7.40 (tdd, *J* = 8.5, 2.6, 1.0 Hz, 1H).



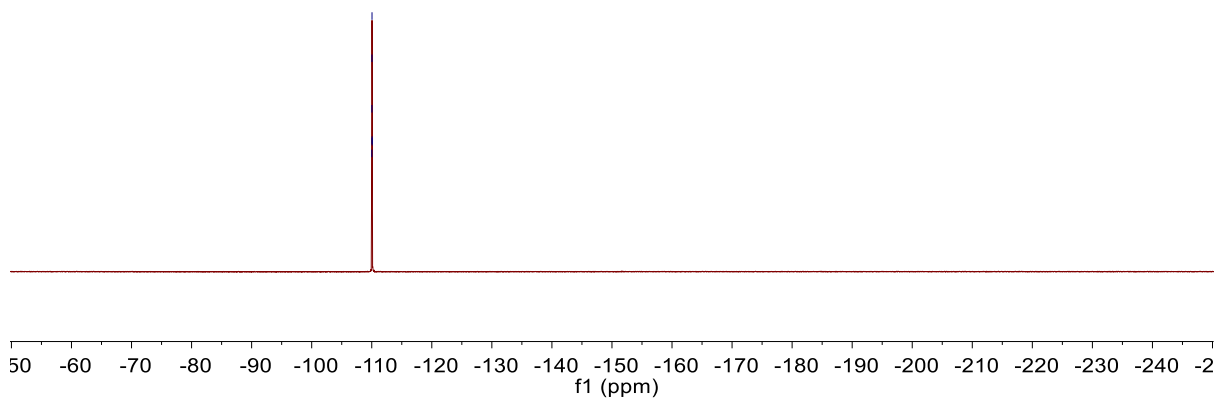
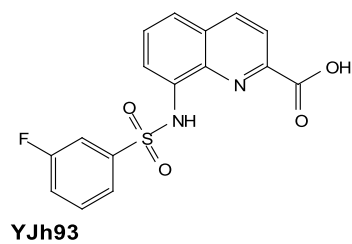


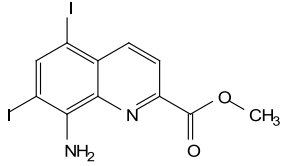
^{13}C NMR (126 MHz, $\text{DMSO}-d_6$) δ 164.95, 161.50 (d, $J = 249.1$ Hz), 145.57, 141.10 (d, $J = 6.9$ Hz), 138.89, 137.19, 134.22, 131.72 (d, $J = 7.9$ Hz), 129.51, 129.32, 123.12, 122.99 (d, $J = 3.1$ Hz), 120.67, 120.47 (d, $J = 21.2$ Hz), 117.97, 113.89 (d, $J = 24.5$ Hz).



^{19}F NMR (471 MHz, $\text{DMSO}-d_6$) δ -110.04 (td, $J = 8.6, 5.2$ Hz).

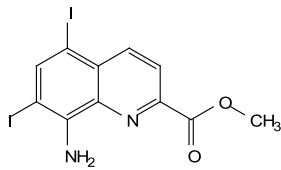
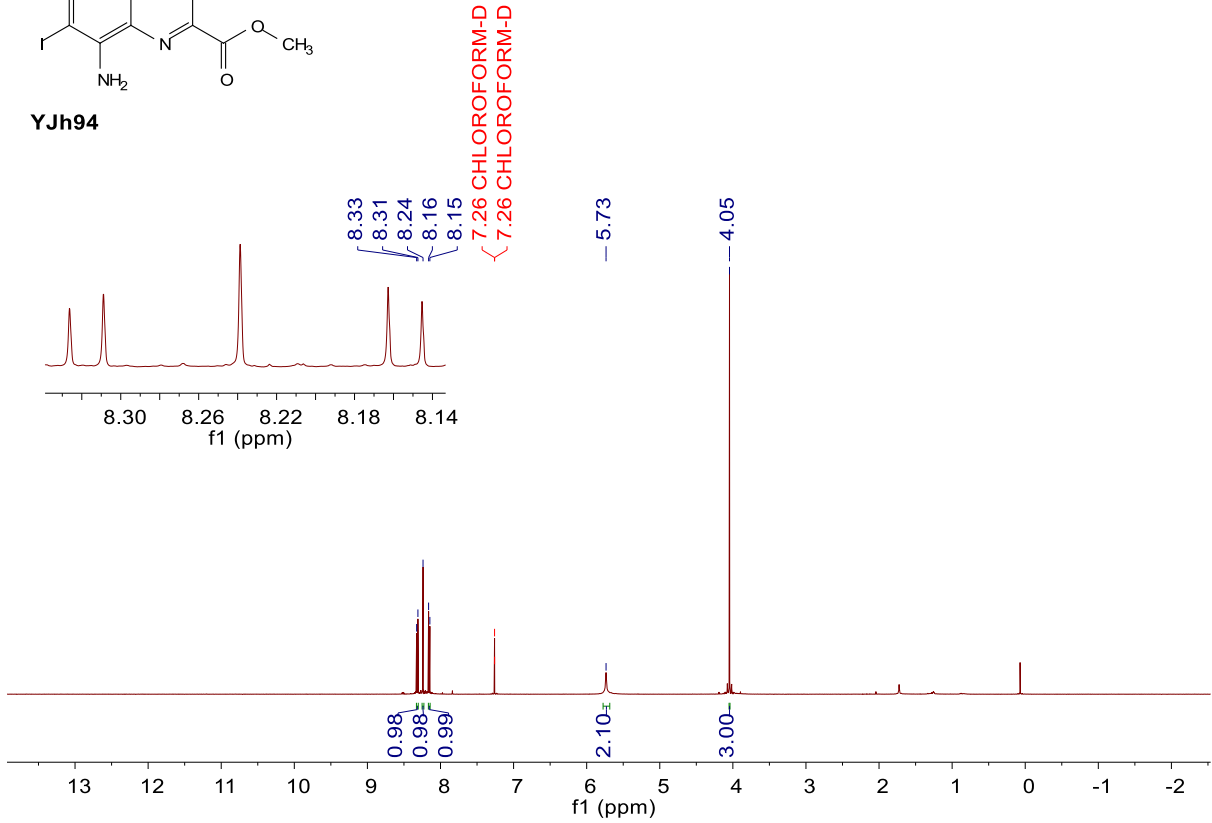
-110.02
-110.03
-110.03
-110.05
-110.05
-110.06





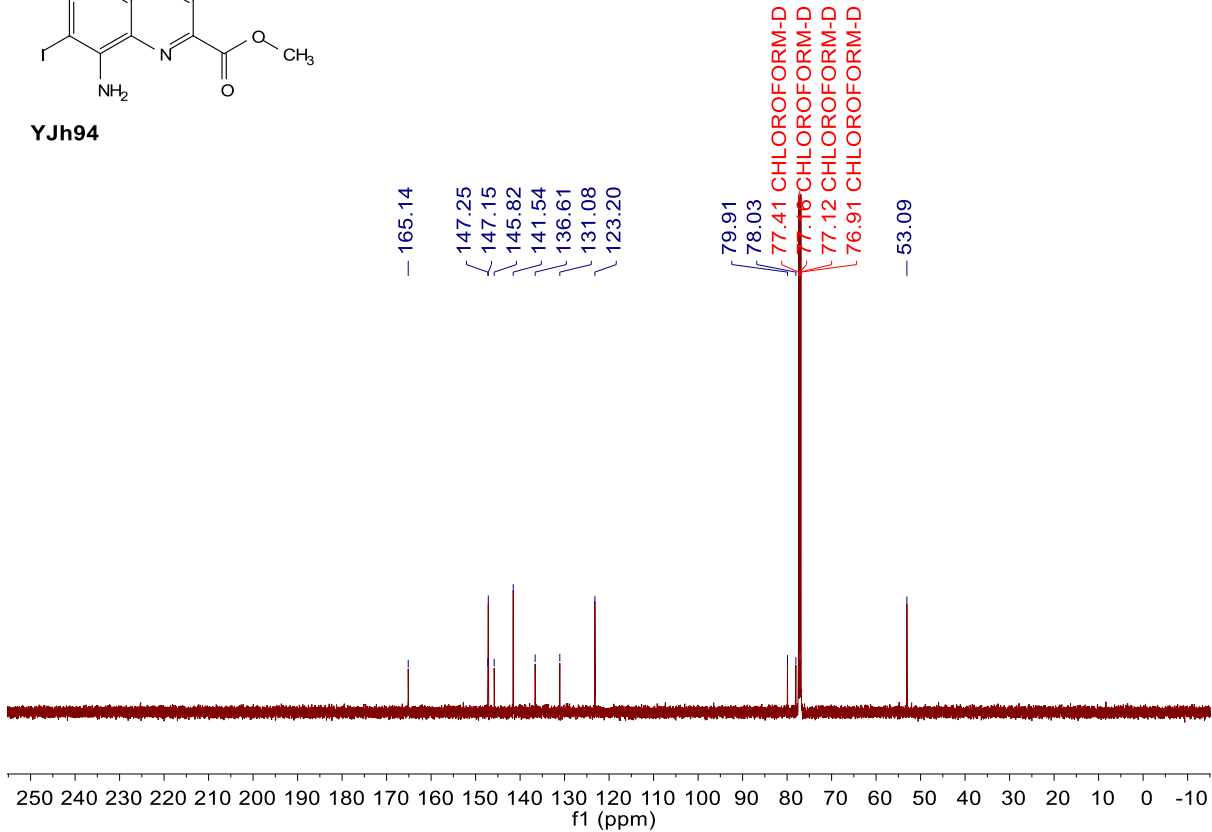
YJh94

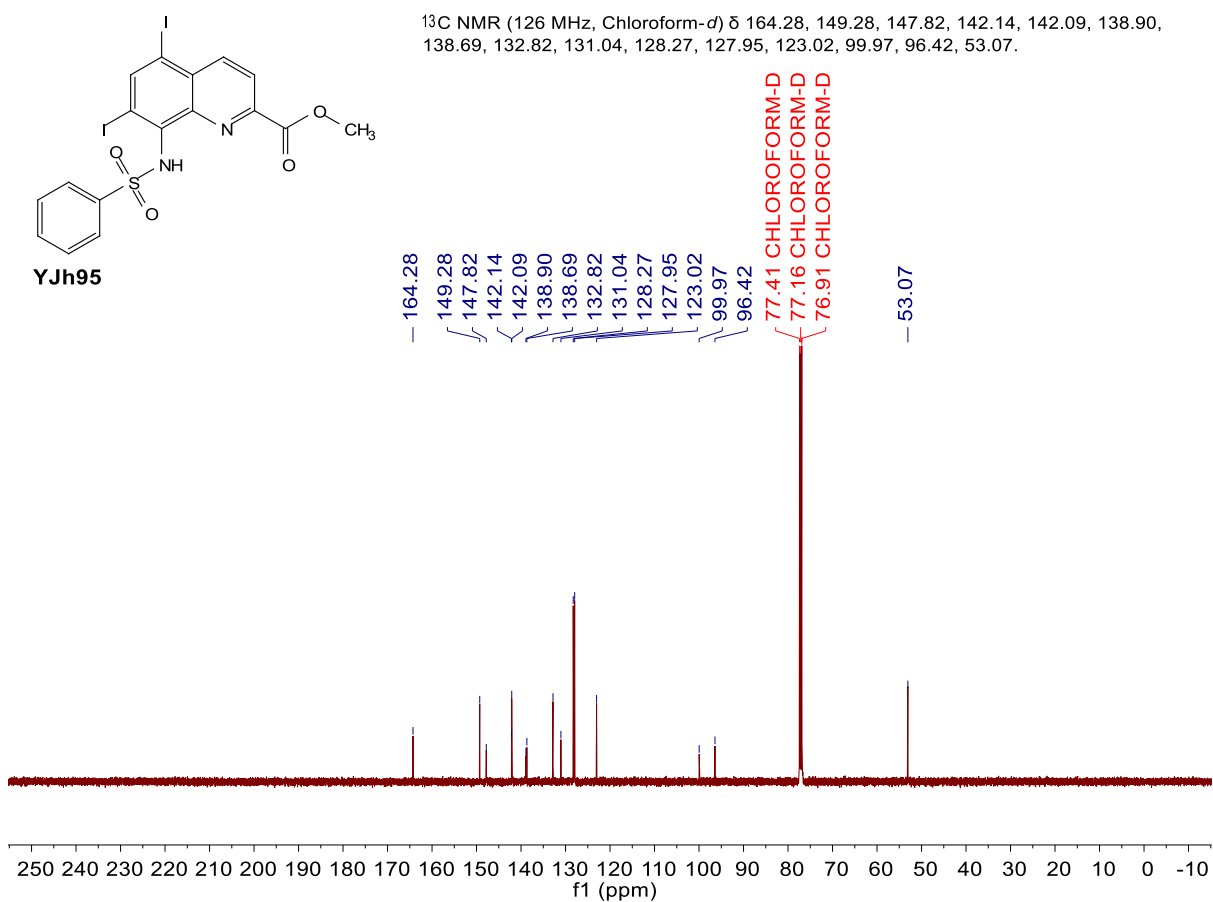
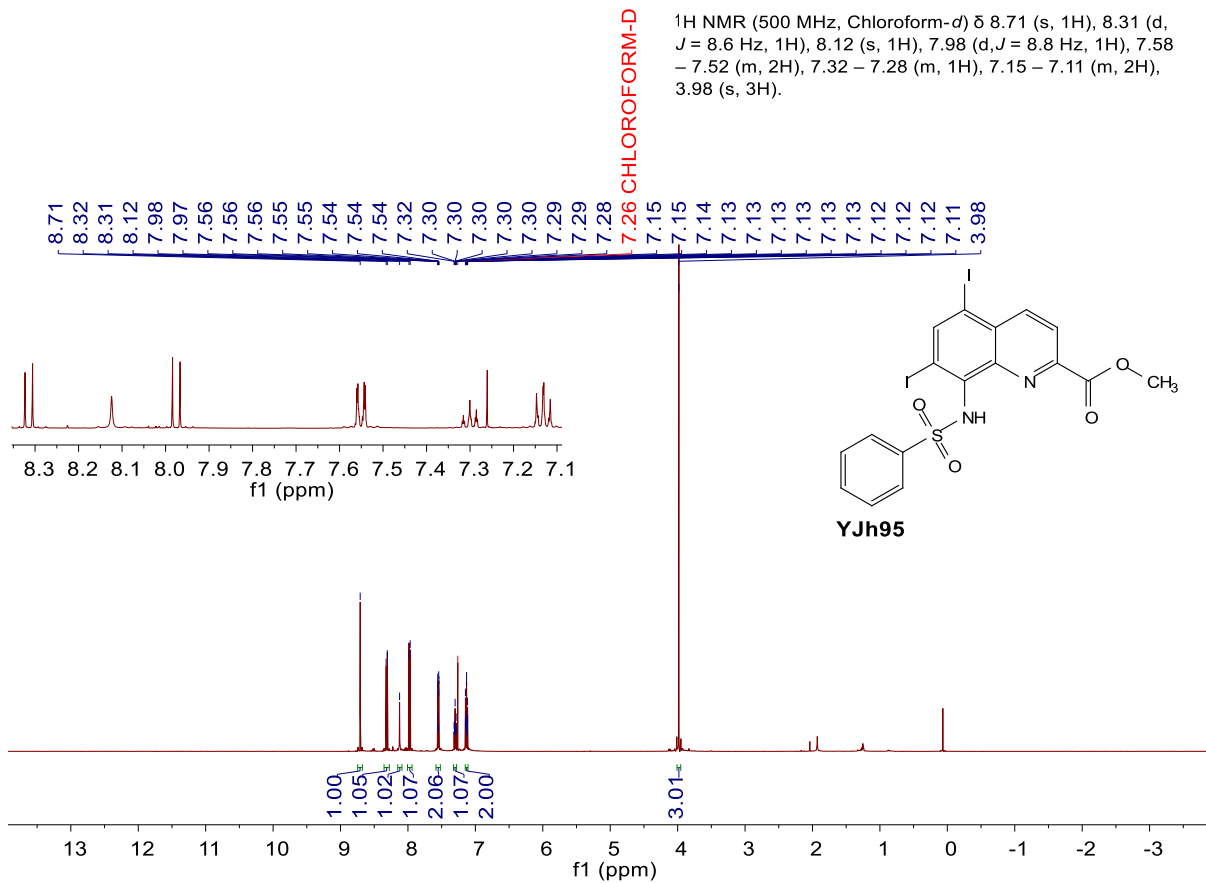
$^1\text{H NMR}$ (500 MHz, Chloroform- d) δ 8.32 (d, $J = 8.7$ Hz, 1H), 8.24 (s, 1H), 8.15 (d, $J = 8.7$ Hz, 1H), 5.73 (s, 2H), 4.05 (s, 3H).



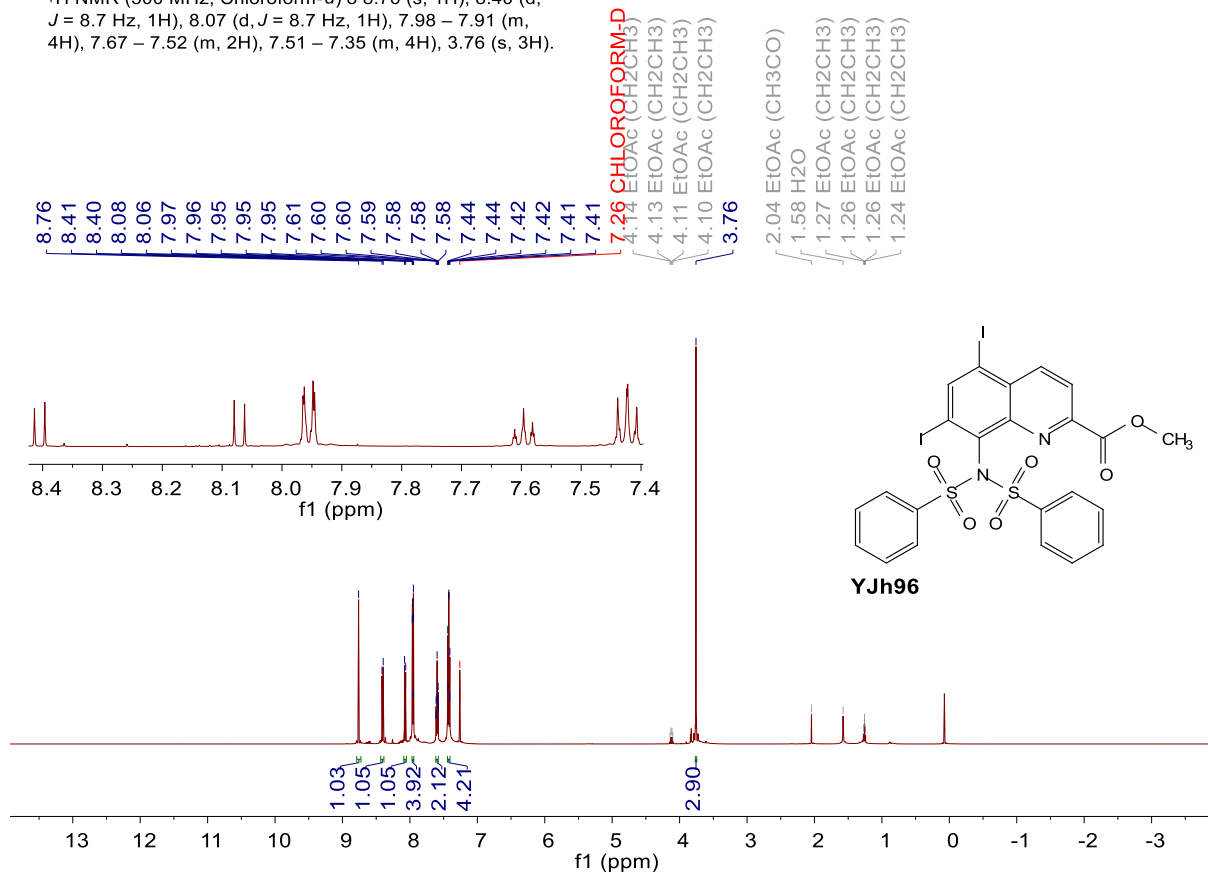
YJh94

$^{13}\text{C NMR}$ (126 MHz, Chloroform- d) δ 165.14, 147.25, 147.15, 145.82, 141.54, 136.61, 131.08, 123.20, 79.91, 78.03, 53.09.

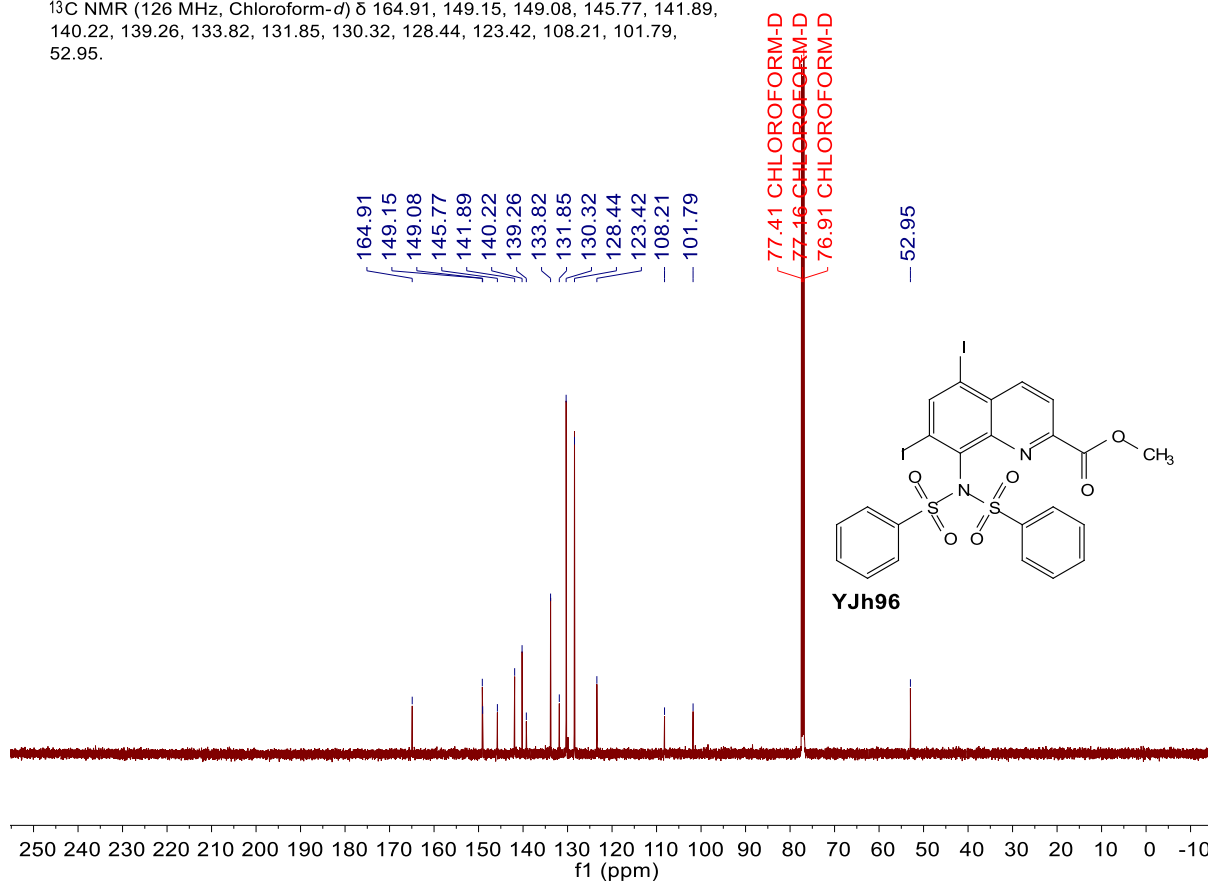


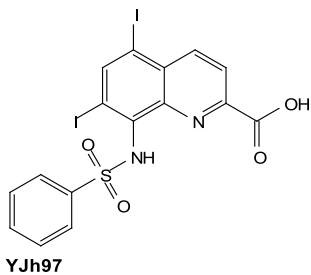


¹H NMR (500 MHz, Chloroform-*d*) δ 8.76 (s, 1H), 8.40 (d, *J* = 8.7 Hz, 1H), 8.07 (d, *J* = 8.7 Hz, 1H), 7.98 – 7.91 (m, 4H), 7.67 – 7.52 (m, 2H), 7.51 – 7.35 (m, 4H), 3.76 (s, 3H).

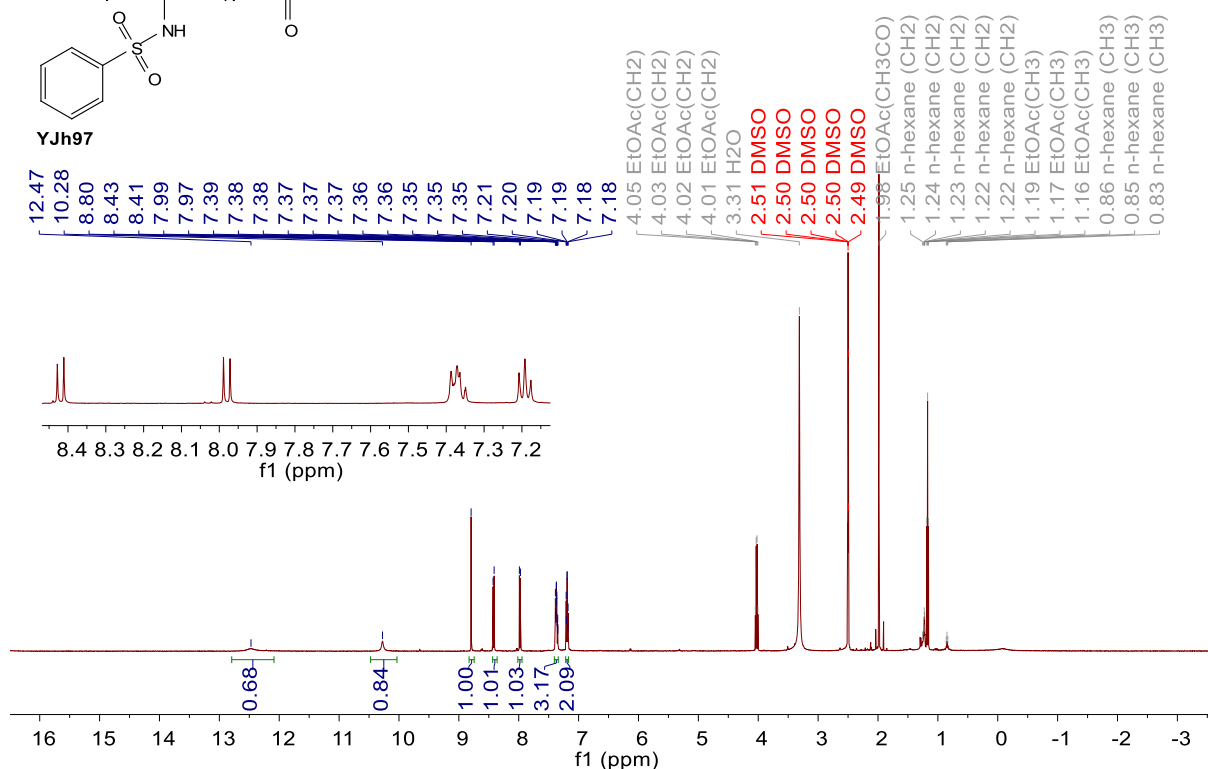


¹³C NMR (126 MHz, Chloroform-*d*) δ 164.91, 149.15, 149.08, 145.77, 141.89, 140.22, 139.26, 133.82, 131.85, 130.32, 128.44, 123.42, 108.21, 101.79, 52.95.

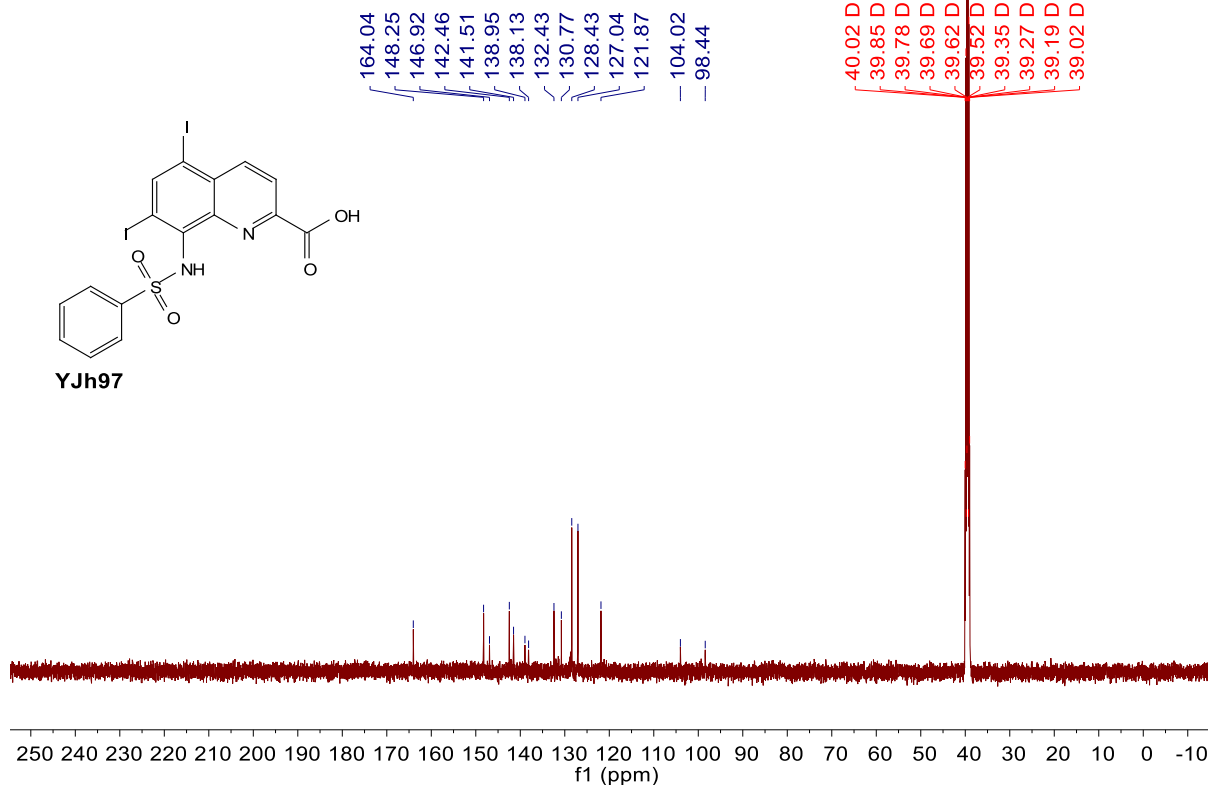




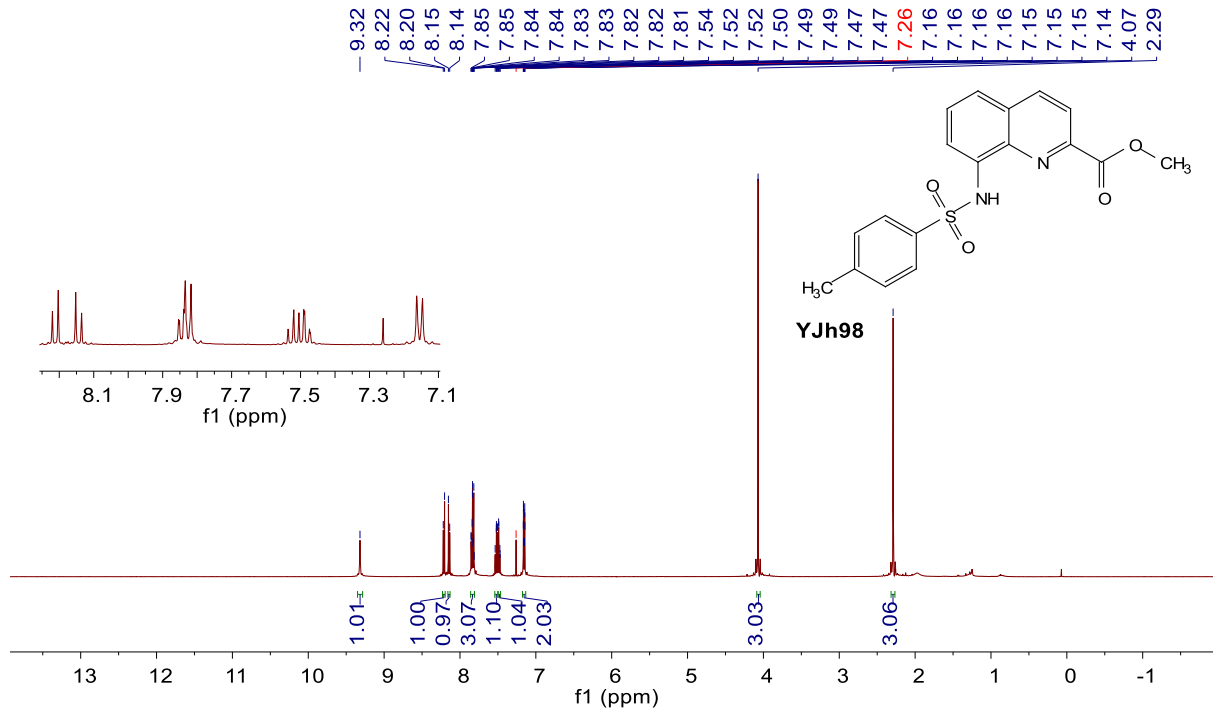
¹H NMR (500 MHz, DMSO-*d*₆) δ 12.47 (s, 1H), 10.28 (s, 1H), 8.80 (s, 1H), 8.42 (d, *J* = 8.6 Hz, 1H), 7.98 (d, *J* = 8.7 Hz, 1H), 7.41 – 7.34 (m, 3H), 7.22 – 7.17 (m, 2H).



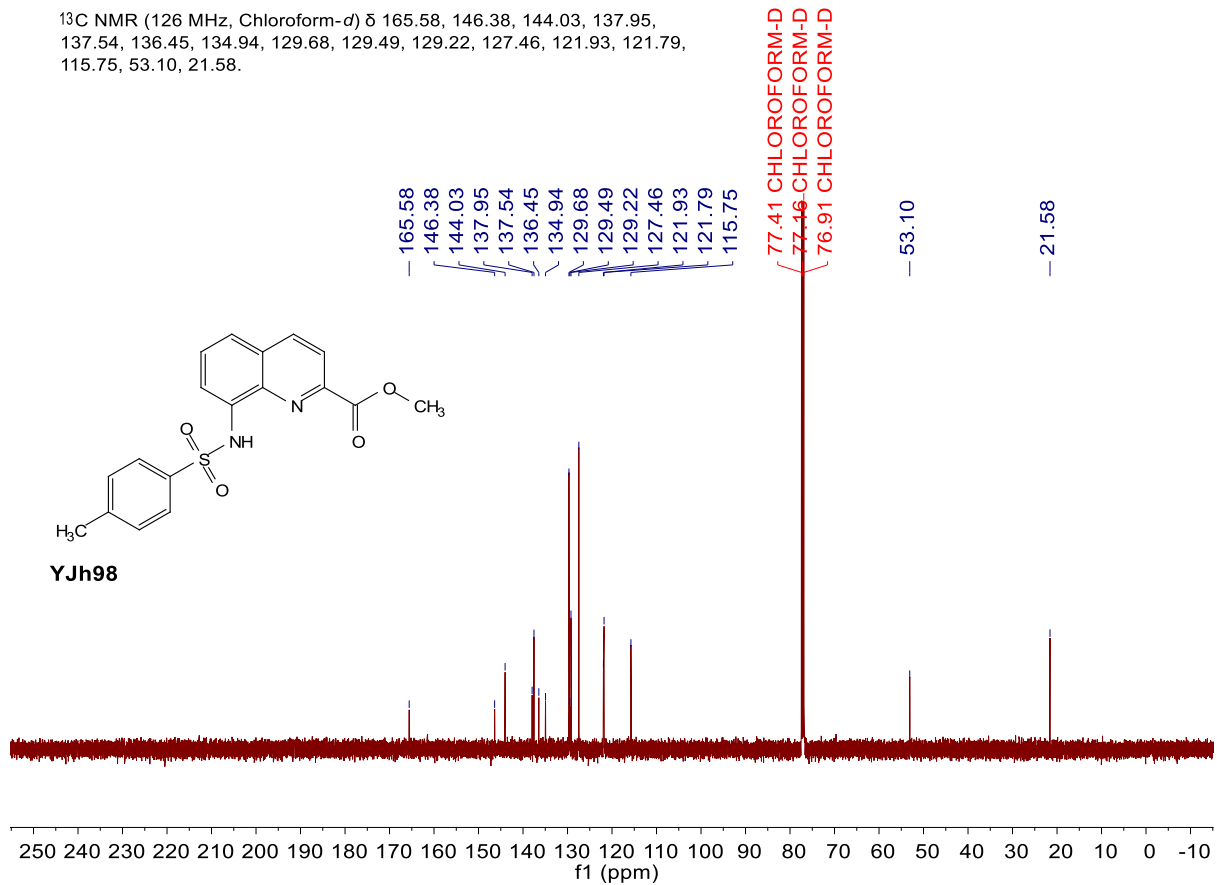
¹³C NMR (126 MHz, DMSO-*d*₆) δ 164.04, 148.25, 146.92, 142.46, 141.51, 138.95, 138.13, 132.43, 130.77, 128.43, 127.04, 121.87, 104.02, 98.44.



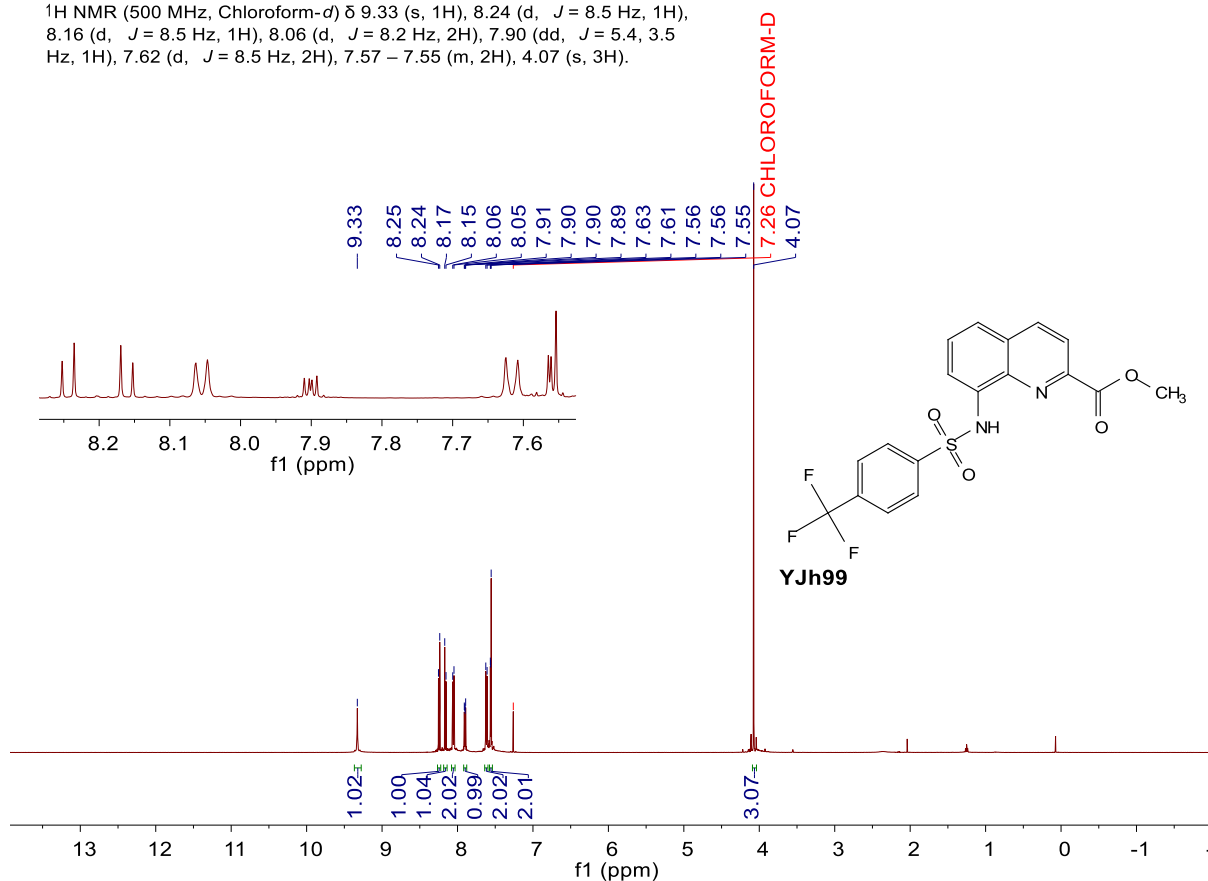
¹H NMR (500 MHz, Chloroform-*d*) δ 9.32 (s, 1H), 8.21 (d, *J* = 8.5 Hz, 1H), 8.14 (d, *J* = 8.5 Hz, 1H), 7.52 (dd, *J* = 8.2, 7.4 Hz, 1H), 7.48 (dd, *J* = 8.3, 1.5 Hz, 1H), 7.19 – 7.11 (m, 2H), 4.07 (s, 2H), 2.29 (s, 3H).



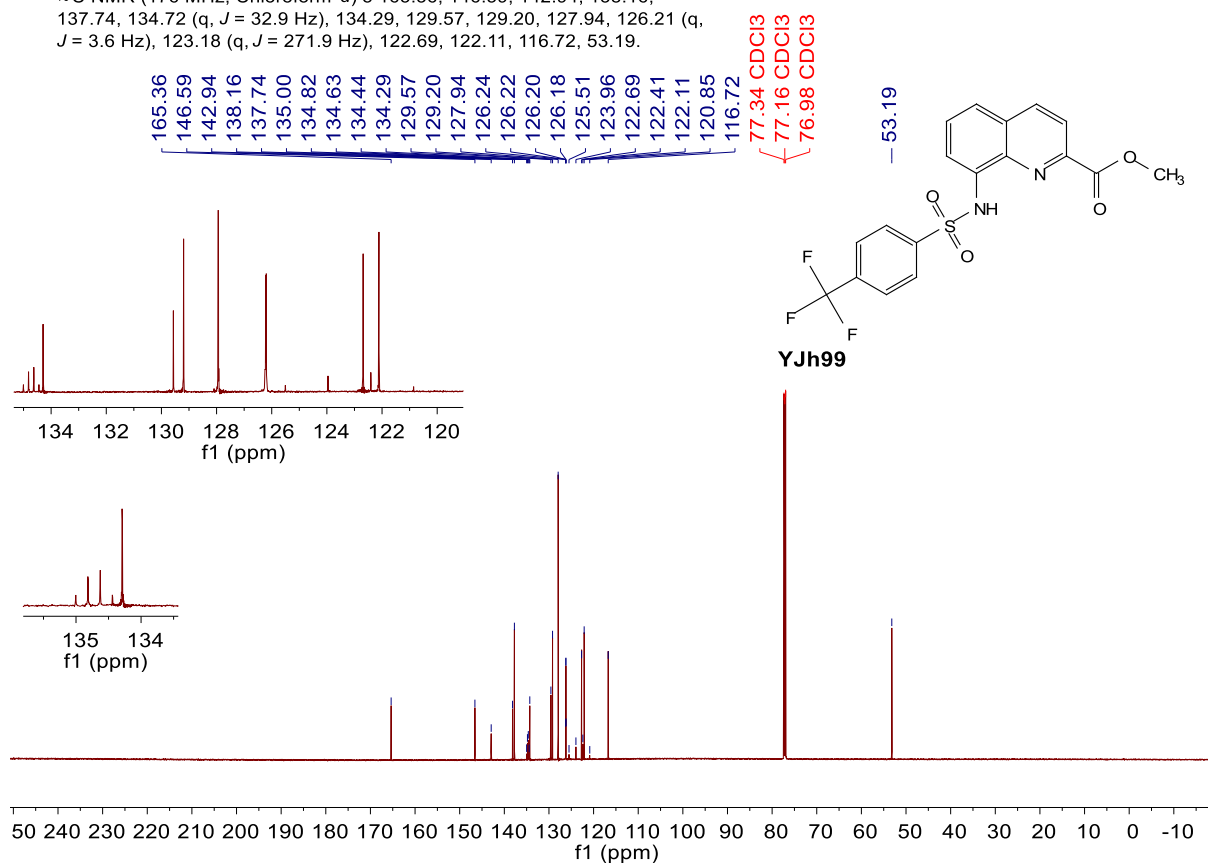
¹³C NMR (126 MHz, Chloroform-*d*) δ 165.58, 146.38, 144.03, 137.95, 137.54, 136.45, 134.94, 129.68, 129.49, 129.22, 127.46, 121.93, 121.79, 115.75, 53.10, 21.58.

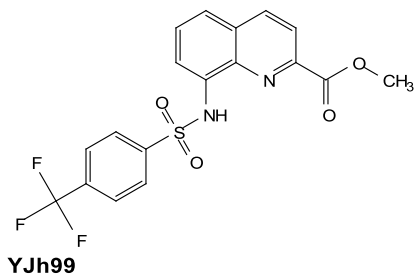


¹H NMR (500 MHz, Chloroform-*d*) δ 9.33 (s, 1H), 8.24 (d, *J* = 8.5 Hz, 1H), 8.16 (d, *J* = 8.5 Hz, 1H), 8.06 (d, *J* = 8.2 Hz, 2H), 7.90 (dd, *J* = 5.4, 3.5 Hz, 1H), 7.62 (d, *J* = 8.5 Hz, 2H), 7.57 – 7.55 (m, 2H), 4.07 (s, 3H).

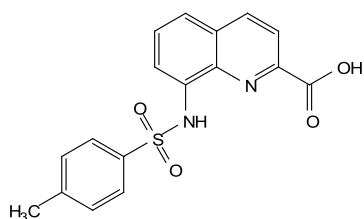
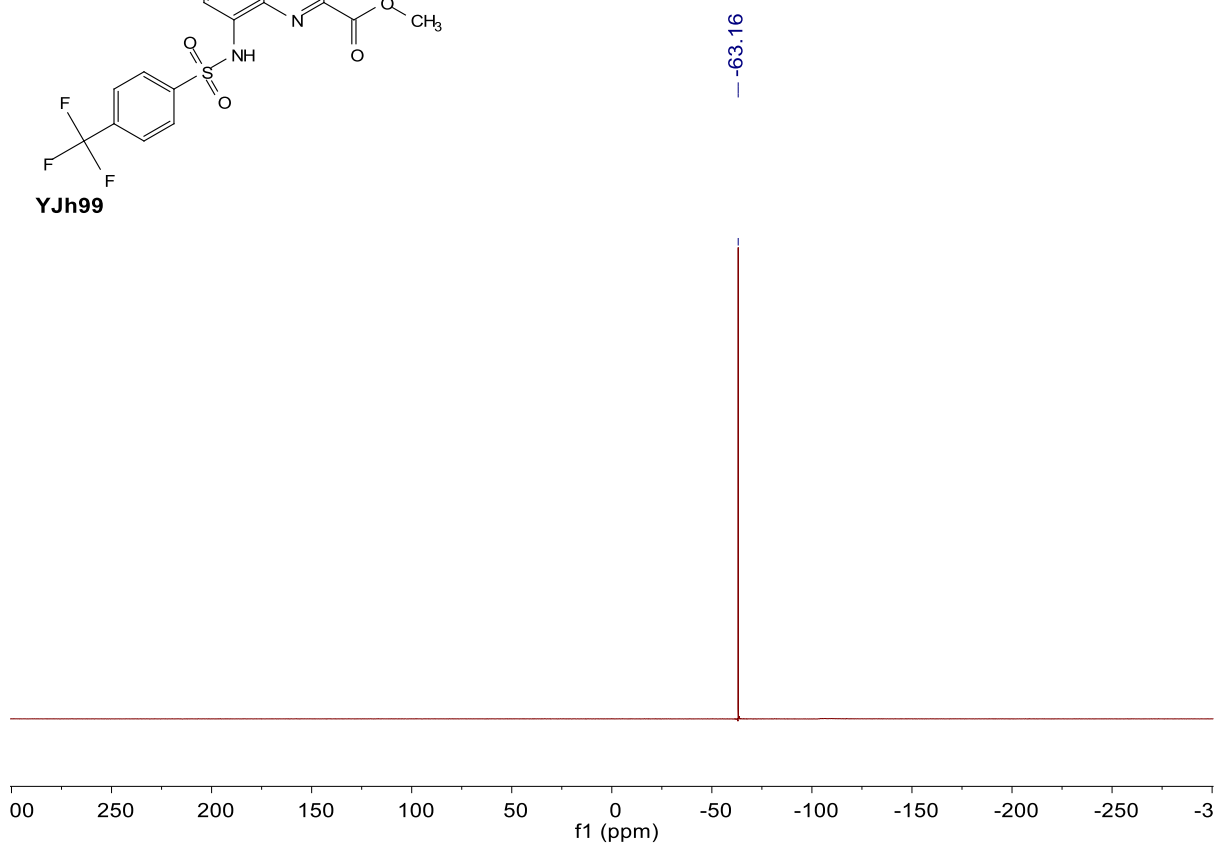


¹³C NMR (176 MHz, Chloroform-*d*) δ 165.36, 146.59, 142.94, 138.16, 137.74, 134.72 (q, *J* = 32.9 Hz), 134.29, 129.57, 129.20, 127.94, 126.21 (q, *J* = 3.6 Hz), 123.18 (q, *J* = 271.9 Hz), 122.69, 122.11, 116.72, 53.19.

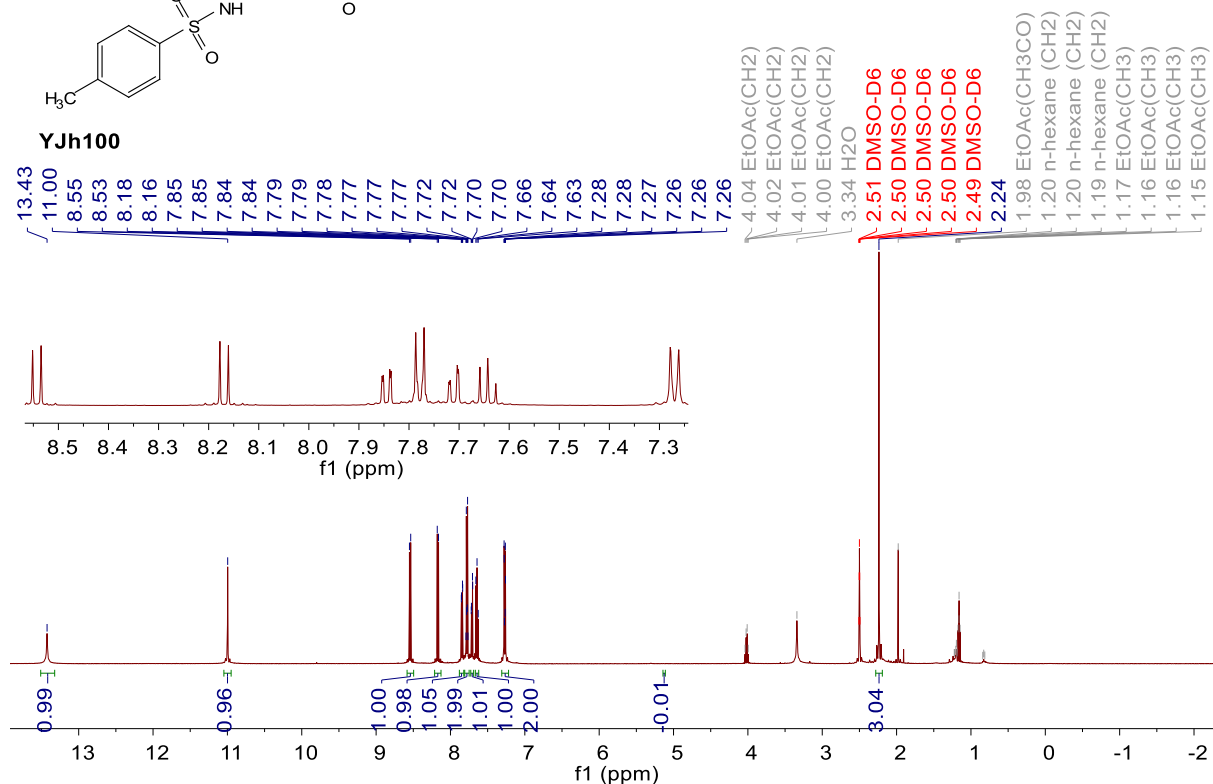




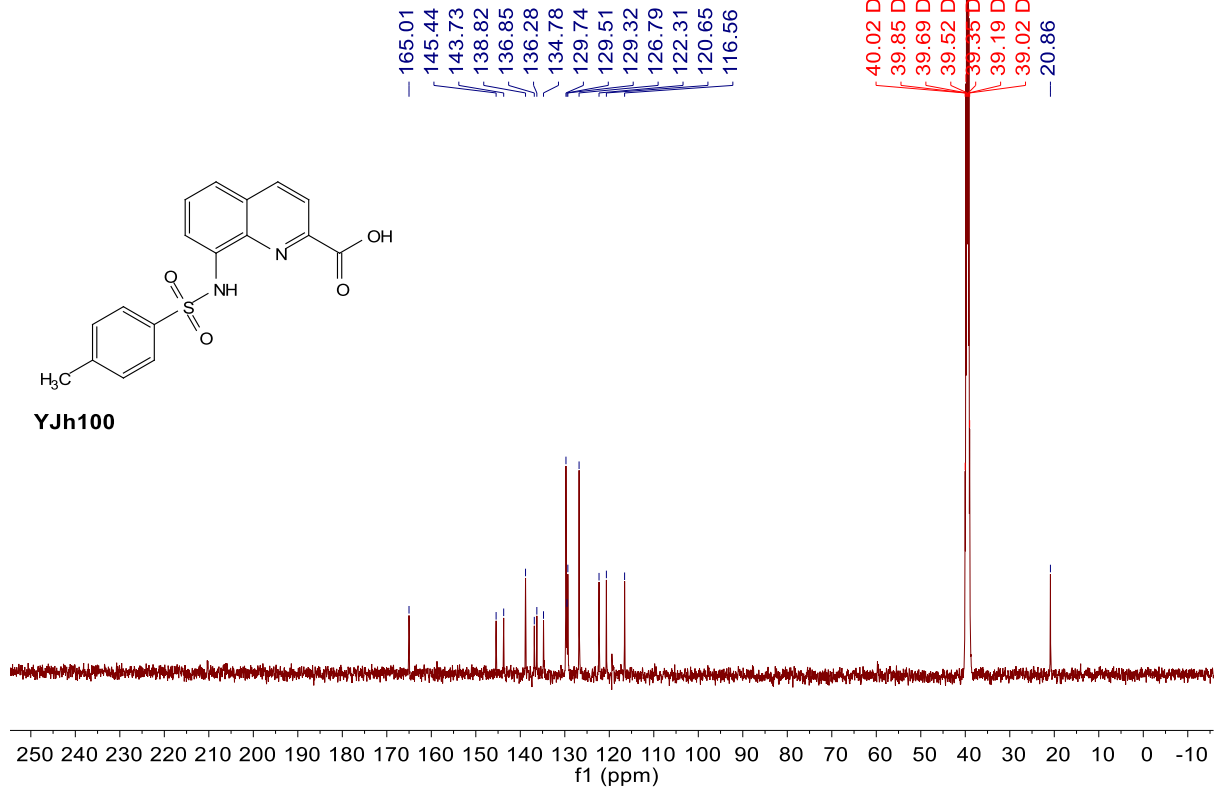
^{19}F NMR (376 MHz, Chloroform- d) δ -63.16.



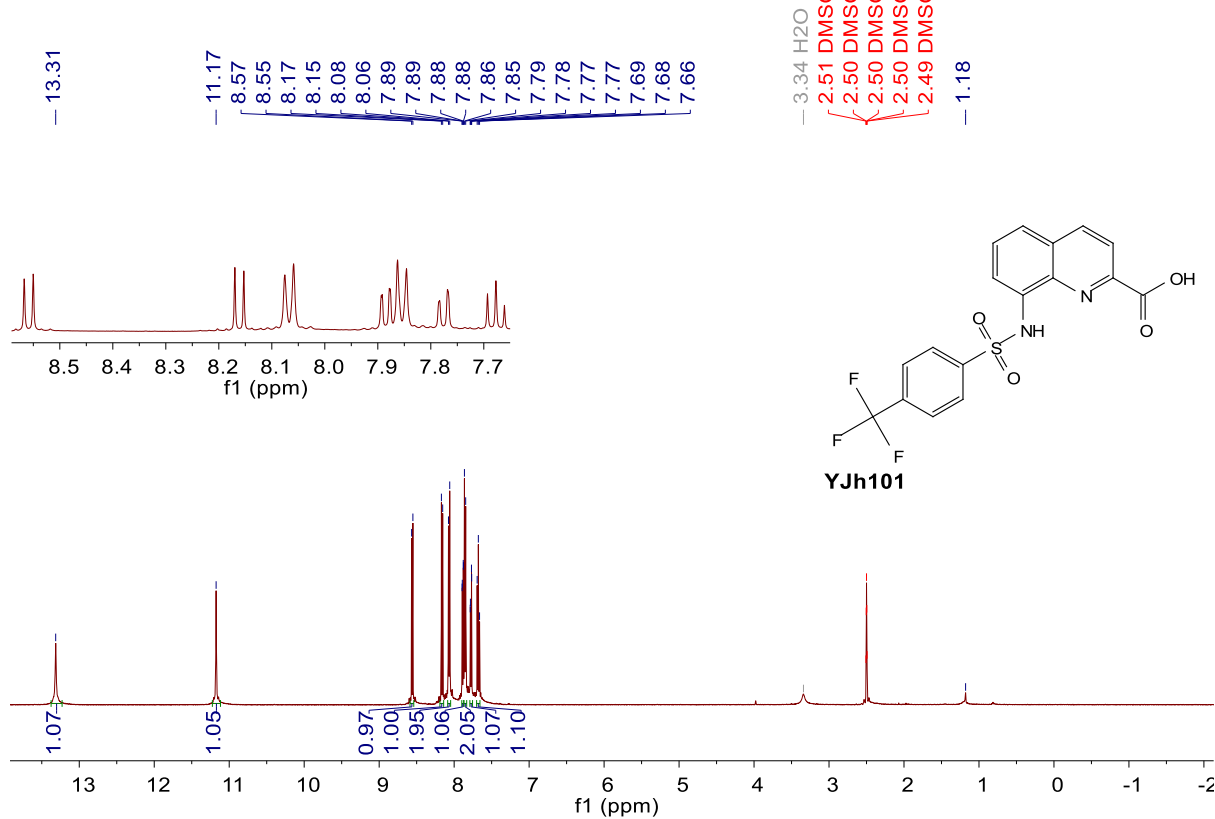
^1H NMR (500 MHz, DMSO- d_6) δ 13.43 (s, 1H), 11.00 (s, 1H), 8.54 (d, J = 8.5 Hz, 1H), 8.17 (d, J = 8.5 Hz, 1H), 7.84 (dd, J = 7.7, 1.3 Hz, 1H), 7.80 – 7.74 (m, 2H), 7.71 (dd, J = 8.3, 1.3 Hz, 1H), 7.64 (t, J = 8.0 Hz, 1H), 7.37 – 7.22 (m, 2H), 2.24 (s, 3H).

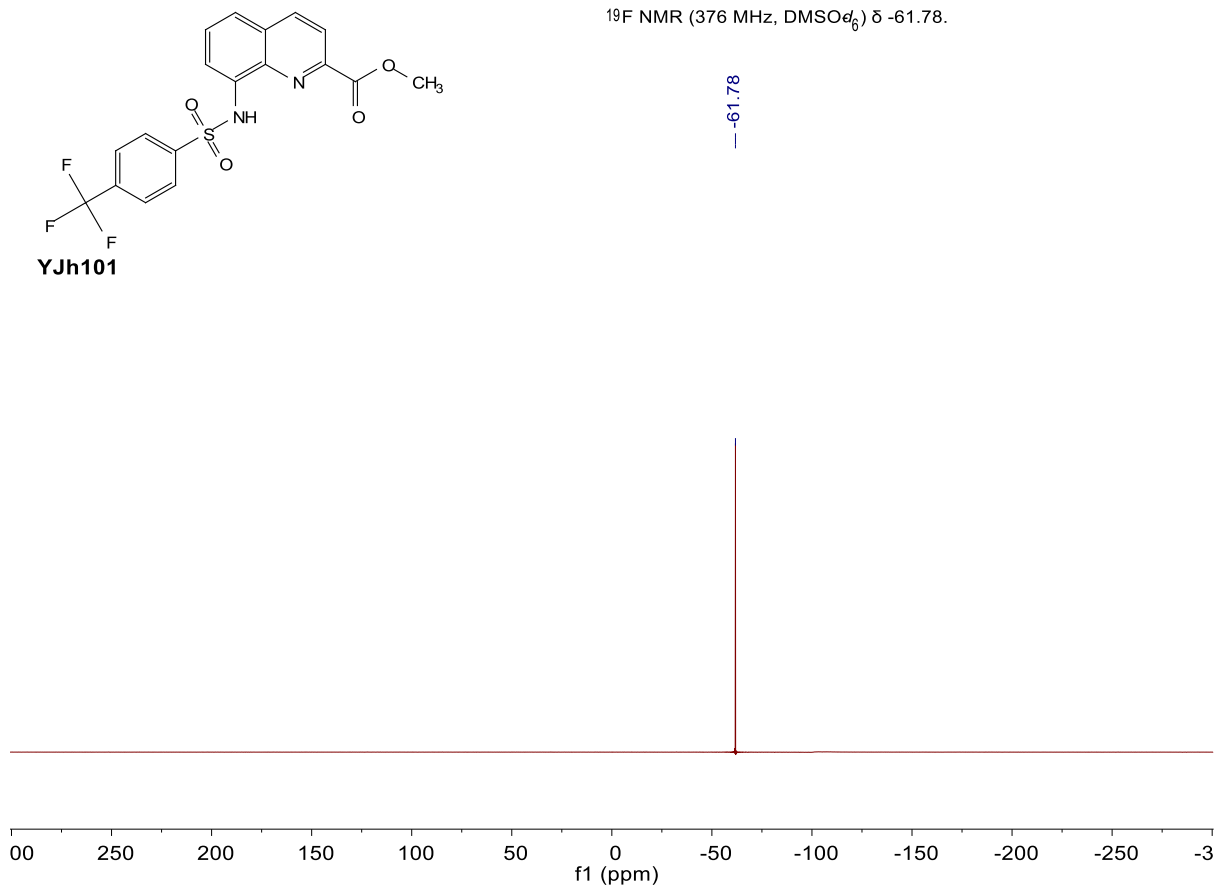
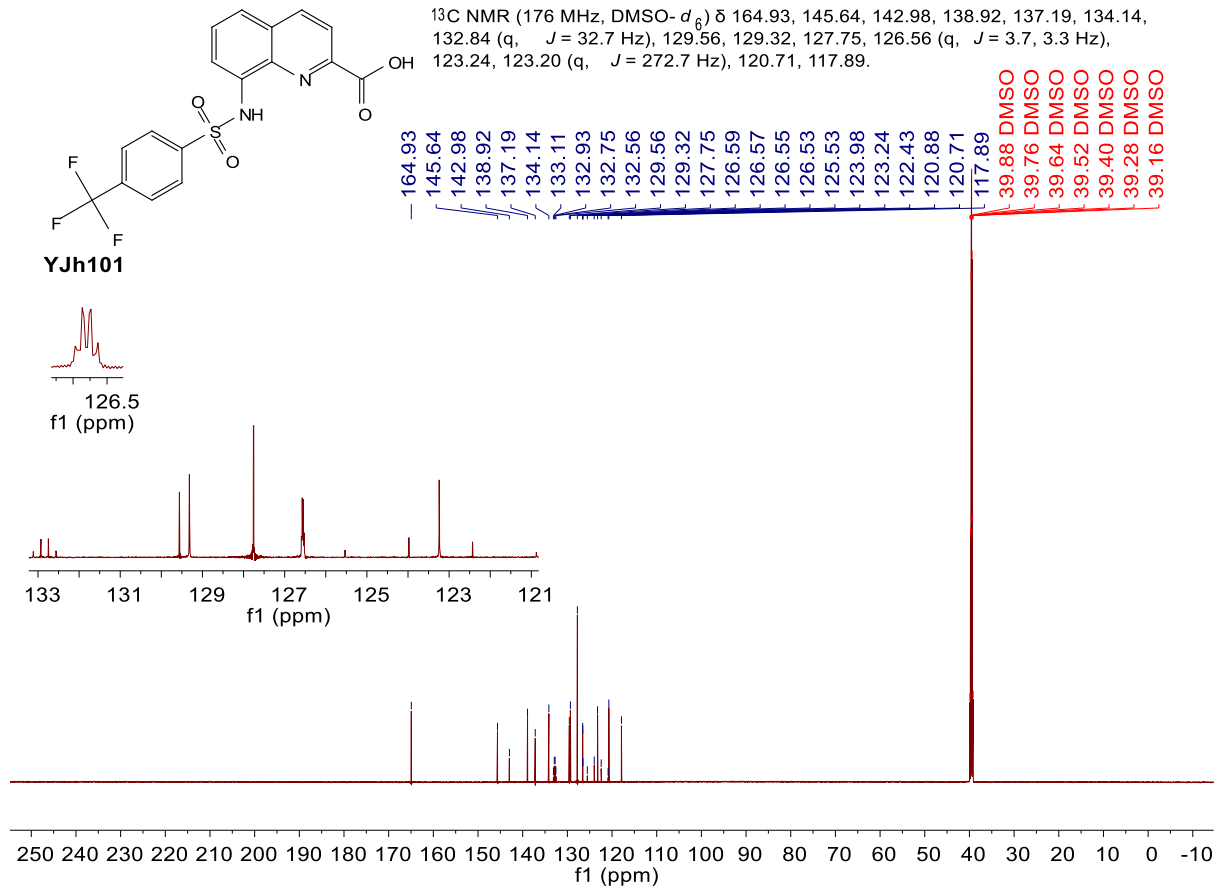


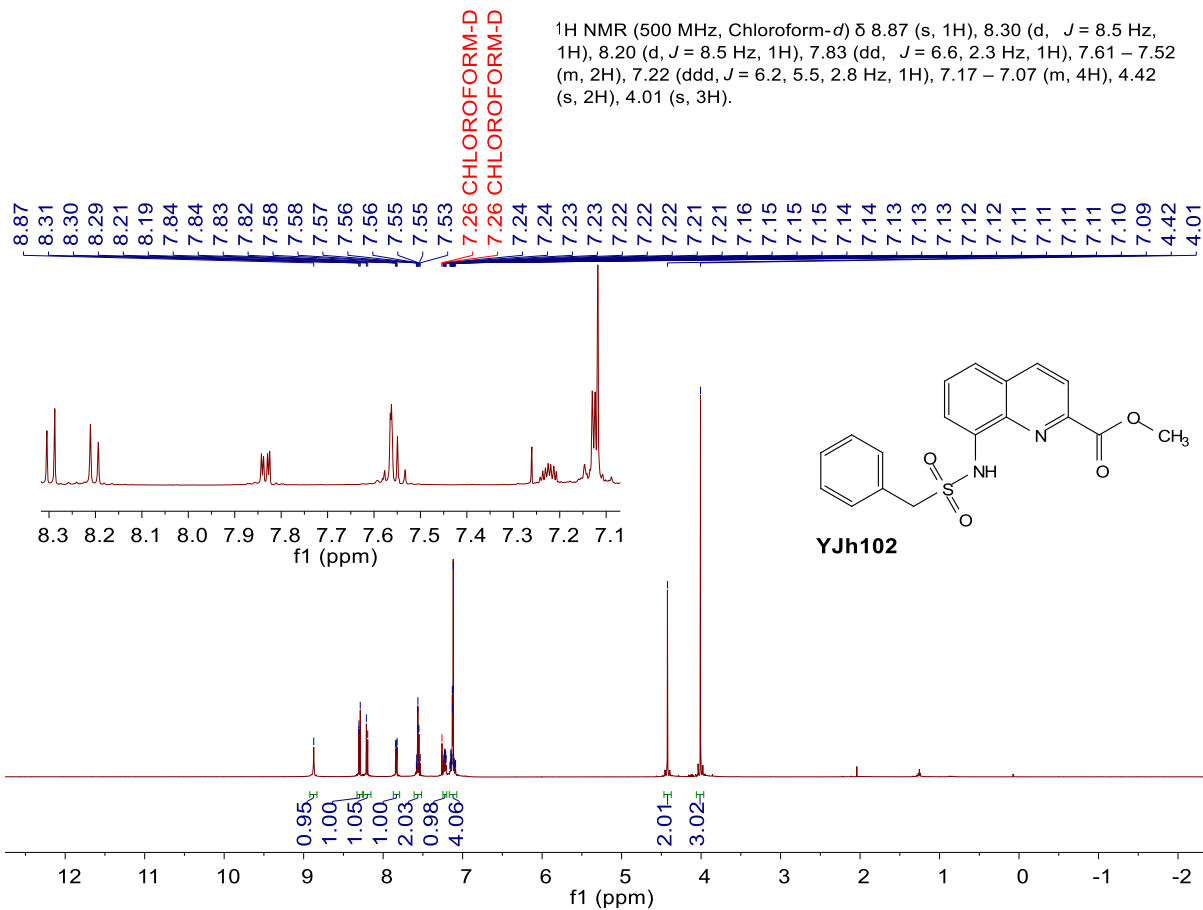
^{13}C NMR (126 MHz, $\text{DMSO}-d_6$) δ 165.01, 145.44, 143.73, 138.82, 136.85, 136.28, 134.78, 129.74, 129.51, 129.32, 126.79, 122.31, 120.65, 116.56, 20.86.



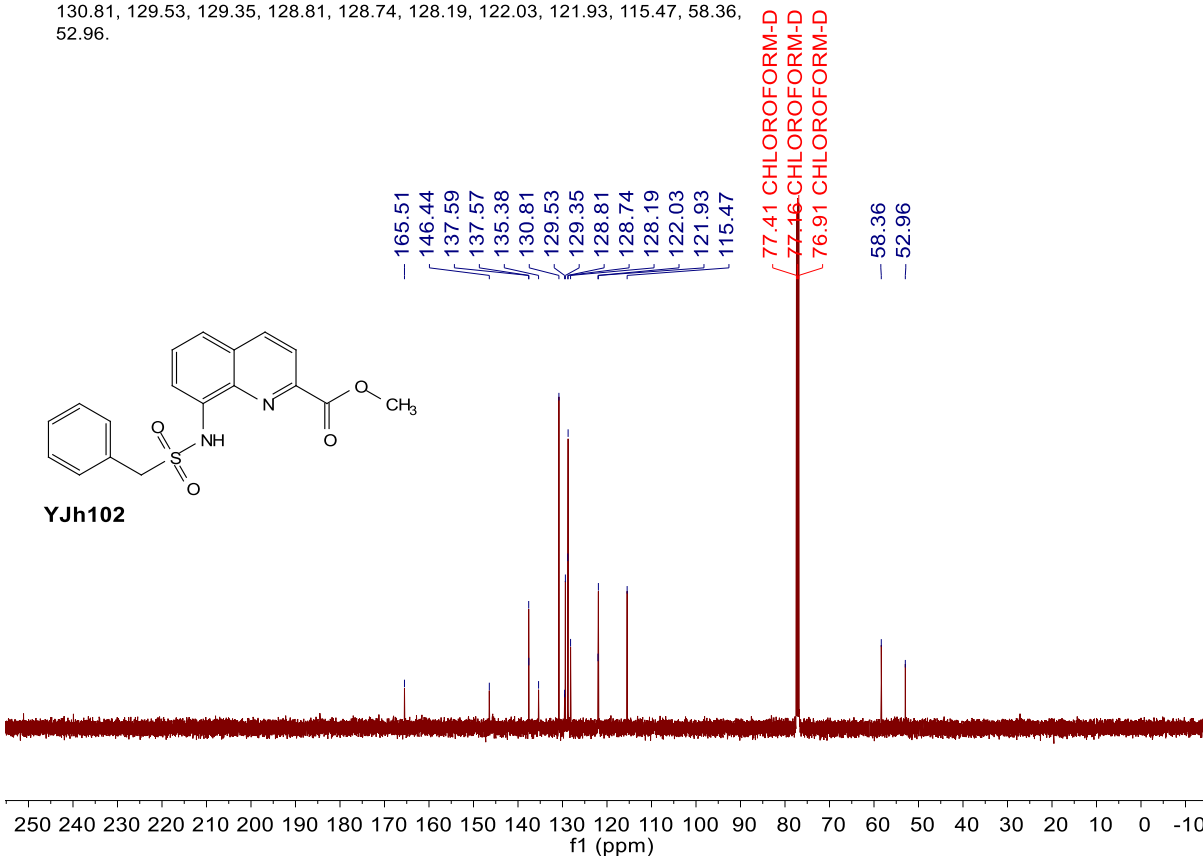
^1H NMR (500 MHz, $\text{DMSO}-d_6$) δ 13.31 (s, 1H), 11.17 (s, 1H), 8.56 (d, $J = 8.5$ Hz, 1H), 8.16 (d, $J = 8.5$ Hz, 1H), 8.07 (d, $J = 8.2$ Hz, 2H), 7.88 (dd, $J = 7.7, 1.2$ Hz, 1H), 7.85 (d, $J = 8.4$ Hz, 2H), 7.78 (dd, $J = 8.3, 1.3$ Hz, 1H), 7.68 (t, $J = 8.0$ Hz, 1H).







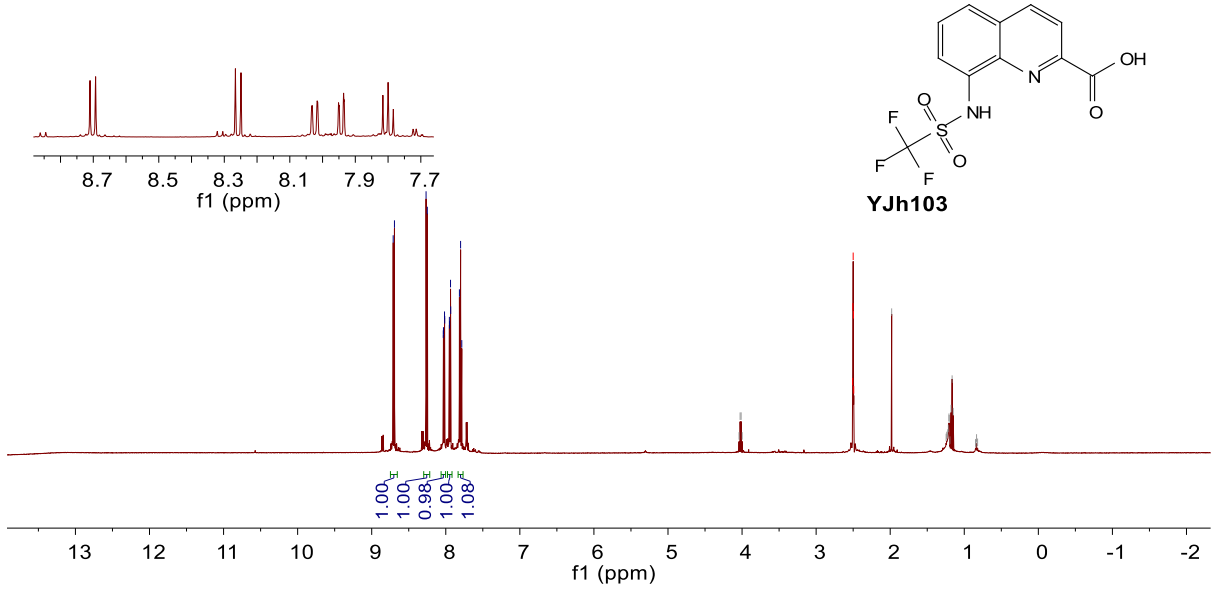
^{13}C NMR (126 MHz, Chloroform-*d*) δ 165.51, 146.44, 137.59, 137.57, 135.38, 130.81, 129.53, 129.35, 128.81, 128.74, 128.19, 122.03, 121.93, 115.47, 58.36, 52.96.



¹H NMR (500 MHz, DMSO-*d*₆) δ 8.70 (d, *J* = 8.5 Hz, 1H), 8.26 (d, *J* = 8.5 Hz, 1H), 8.02 (dd, *J* = 8.3, 1.2 Hz, 1H), 7.94 (dd, *J* = 7.7, 1.2 Hz, 1H), 7.80 (t, *J* = 8.0 Hz, 1H).

8.71
8.69
8.27
8.25
8.03
8.02
8.01
7.95
7.95
7.94
7.93
7.82
7.80
7.78

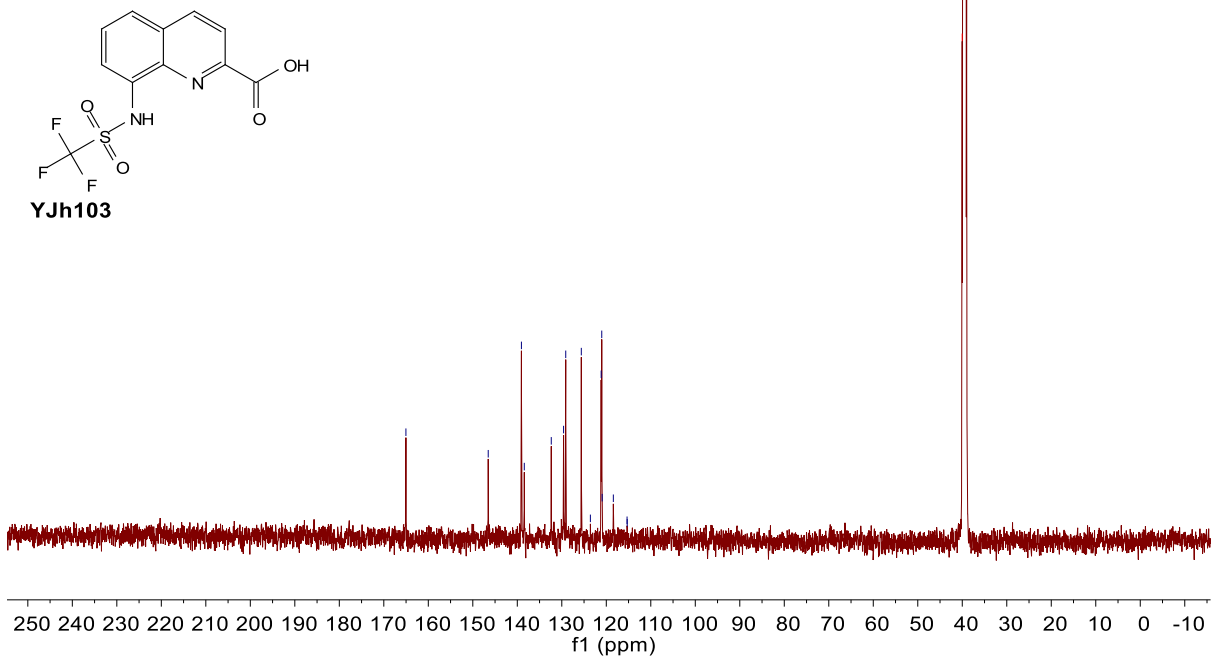
4.04 EtOAc(CH₂)
4.03 EtOAc(CH₂)
4.01 EtOAc(CH₂)
4.00 EtOAc(CH₂)
2.51 DMSO-D₆
2.50 DMSO-D₆
2.50 DMSO-D₆
2.49 DMSO-D₆
1.98 EtOAc(CH₃CO)
1.24 n-hexane (CH₂)
1.24 n-hexane (CH₂)
1.22 n-hexane (CH₂)
1.21 n-hexane (CH₂)
1.21 n-hexane (CH₂)
1.20 n-hexane (CH₂)
1.19 n-hexane (CH₂)
1.18 EtOAc(CH₃)
1.16 EtOAc(CH₃)
1.15 EtOAc(CH₃)
0.85 n-hexane (CH₃)
0.83 n-hexane (CH₃)
0.82 n-hexane (CH₃)

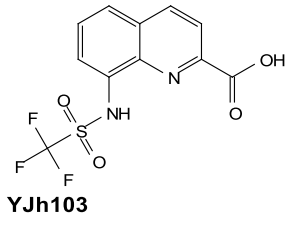


¹³C NMR (126 MHz, DMSO-*d*₆) δ 165.03, 146.53, 139.07, 138.43, 132.37, 129.60, 129.11, 125.61, 121.15, 121.02, 119.56 (q, *J* = 390.0 Hz).

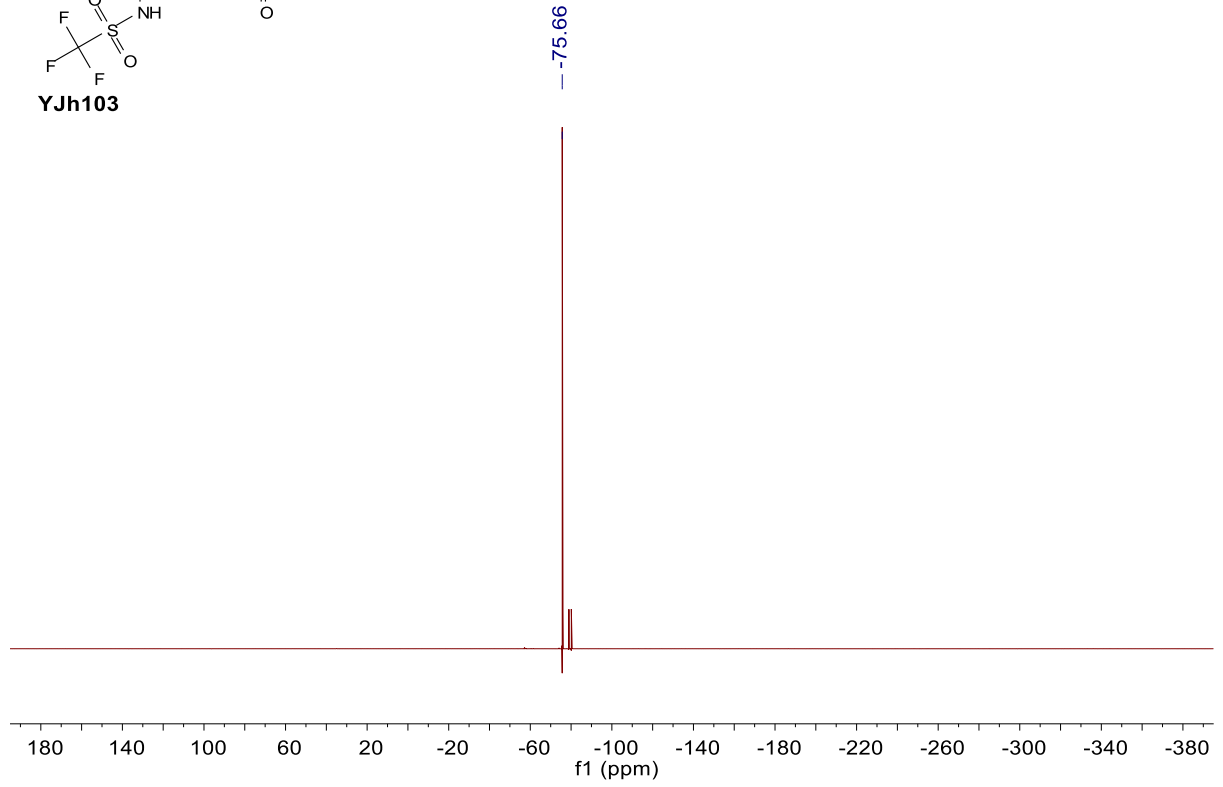
165.03
146.53
139.07
138.43
132.37
129.60
129.11
125.61
123.57
121.15
121.02
120.93
118.42
115.33
115.30

40.02 DMSO-D₆
39.85 DMSO-D₆
39.69 DMSO-D₆
39.52 DMSO-D₆
39.35 DMSO-D₆
39.19 DMSO-D₆
39.02 DMSO-D₆

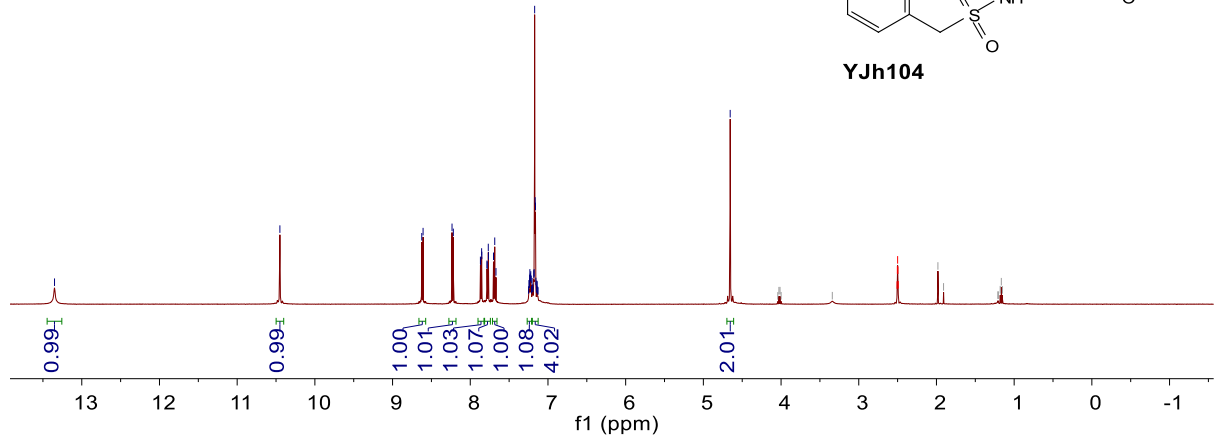
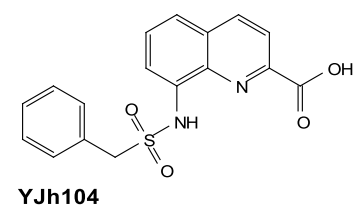
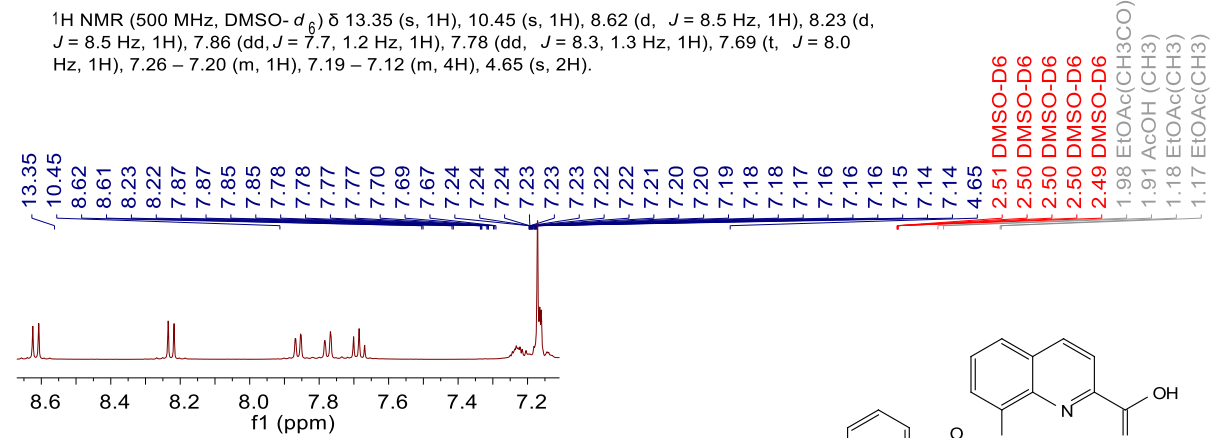




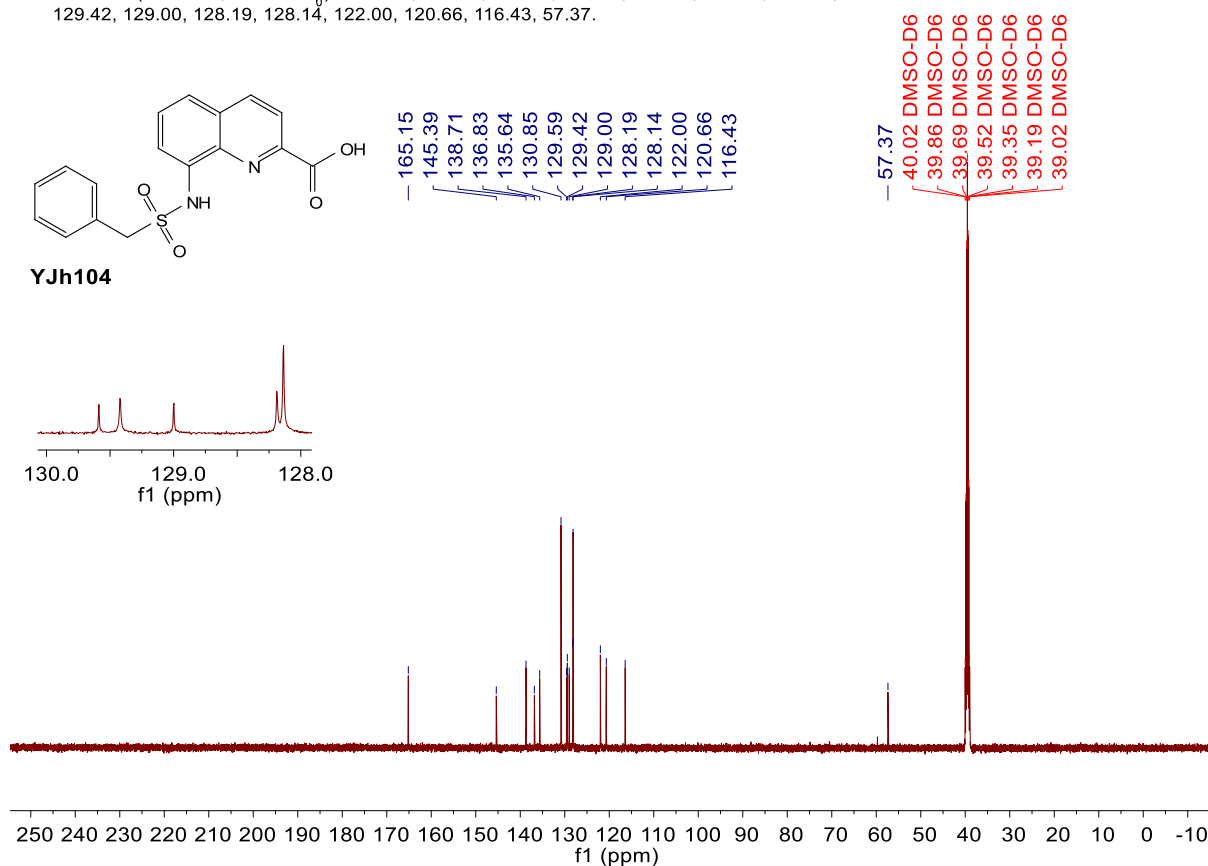
¹⁹F NMR (565 MHz, DMSO-*d*₆) δ -75.66.



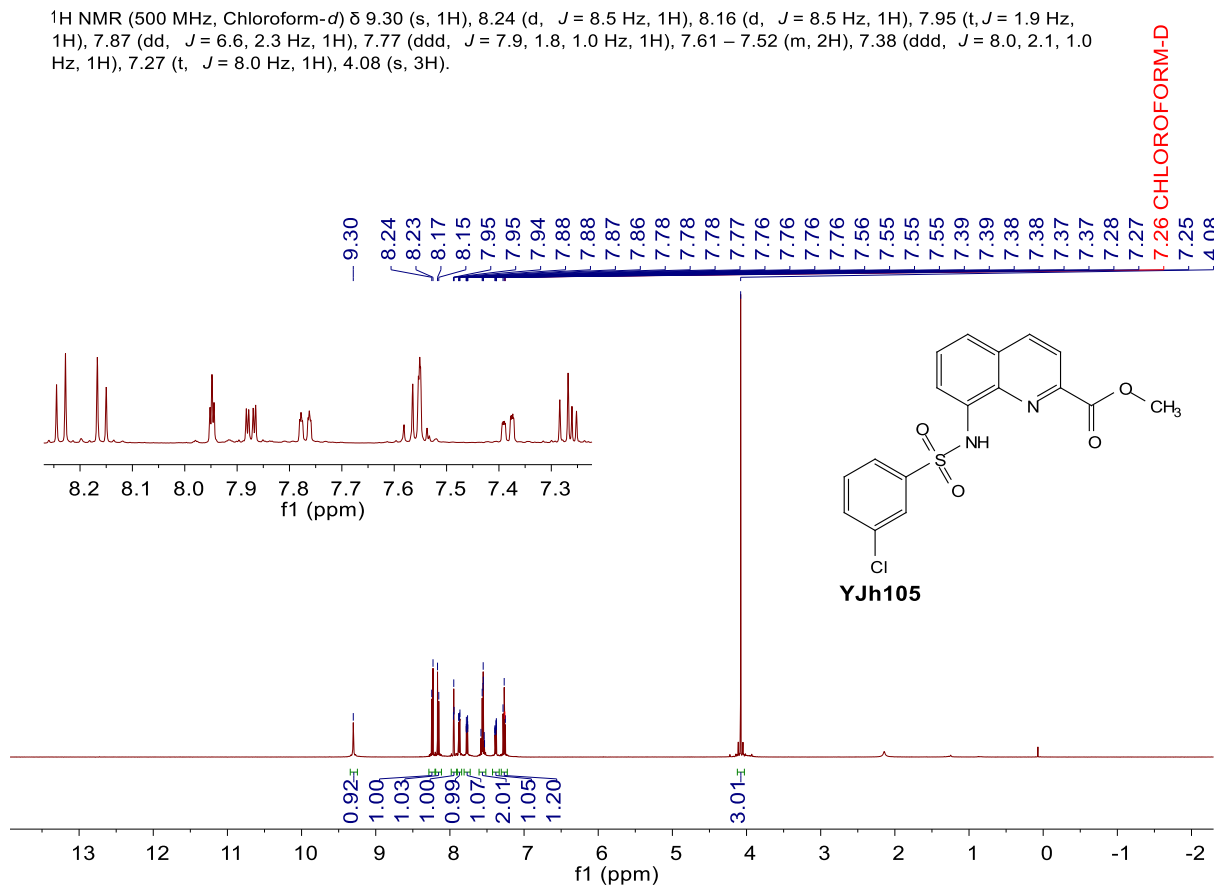
¹H NMR (500 MHz, DMSO-*d*₆) δ 13.35 (s, 1H), 10.45 (s, 1H), 8.62 (d, *J* = 8.5 Hz, 1H), 8.23 (d, *J* = 8.5 Hz, 1H), 7.86 (dd, *J* = 7.7, 1.2 Hz, 1H), 7.78 (dd, *J* = 8.3, 1.3 Hz, 1H), 7.69 (t, *J* = 8.0 Hz, 1H), 7.26 – 7.20 (m, 1H), 7.19 – 7.12 (m, 4H), 4.65 (s, 2H).



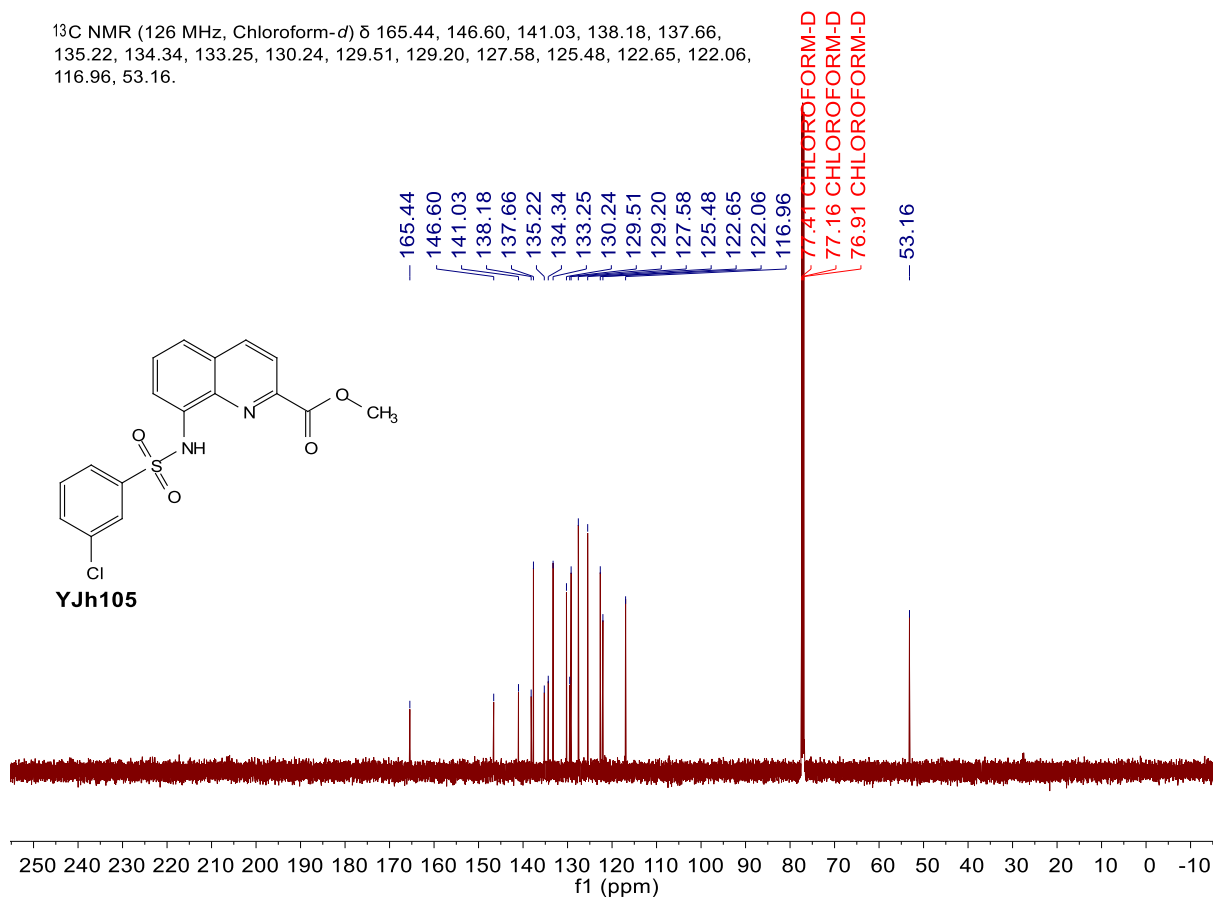
^{13}C NMR (126 MHz, DMSO- d_6) δ 165.15, 145.39, 138.71, 136.83, 135.64, 130.85, 129.59, 129.42, 129.00, 128.19, 128.14, 122.00, 120.66, 116.43, 57.37.



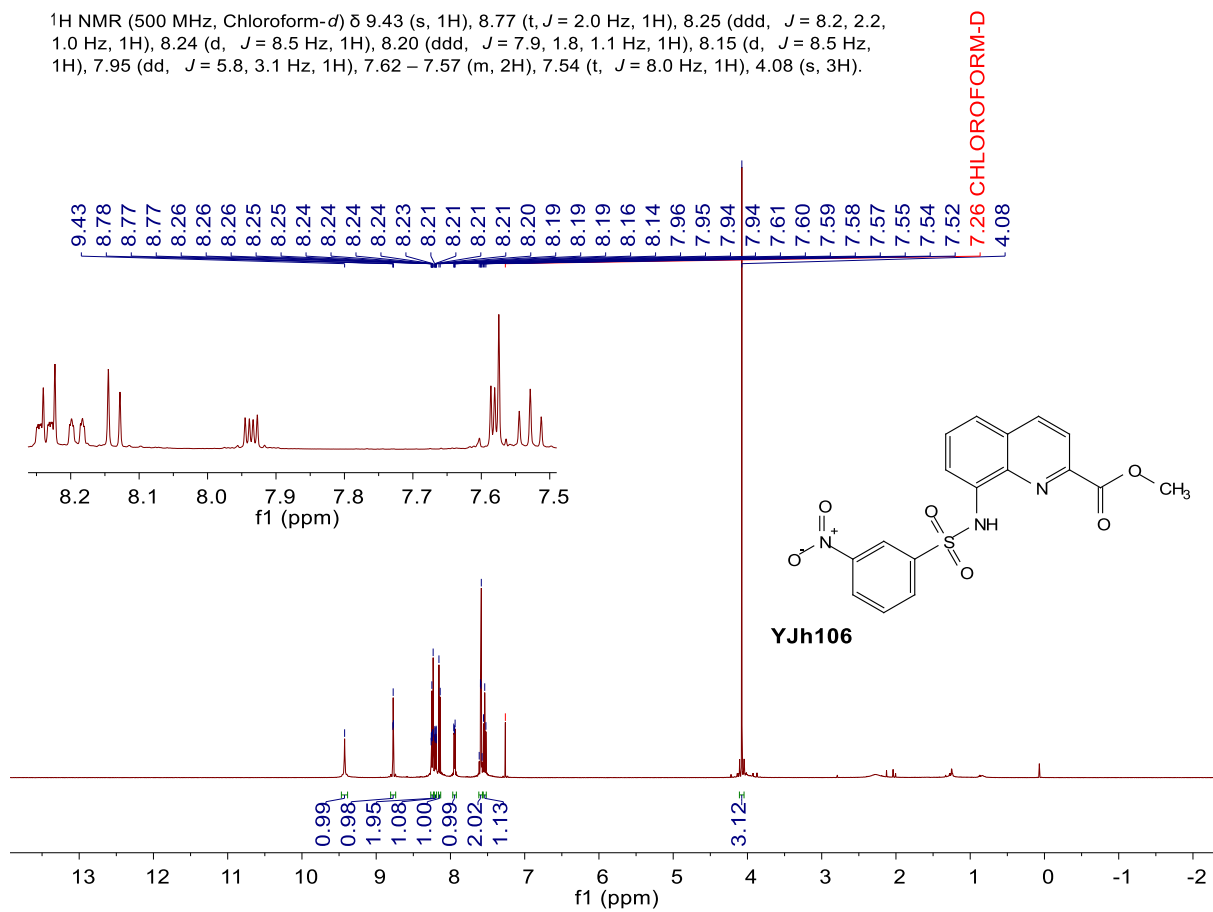
^1H NMR (500 MHz, Chloroform- d) δ 9.30 (s, 1H), 8.24 (d, J = 8.5 Hz, 1H), 8.16 (d, J = 8.5 Hz, 1H), 7.95 (t, J = 1.9 Hz, 1H), 7.87 (dd, J = 6.6, 2.3 Hz, 1H), 7.77 (ddd, J = 7.9, 1.8, 1.0 Hz, 1H), 7.61 – 7.52 (m, 2H), 7.38 (ddd, J = 8.0, 2.1, 1.0 Hz, 1H), 7.27 (t, J = 8.0 Hz, 1H), 4.08 (s, 3H).



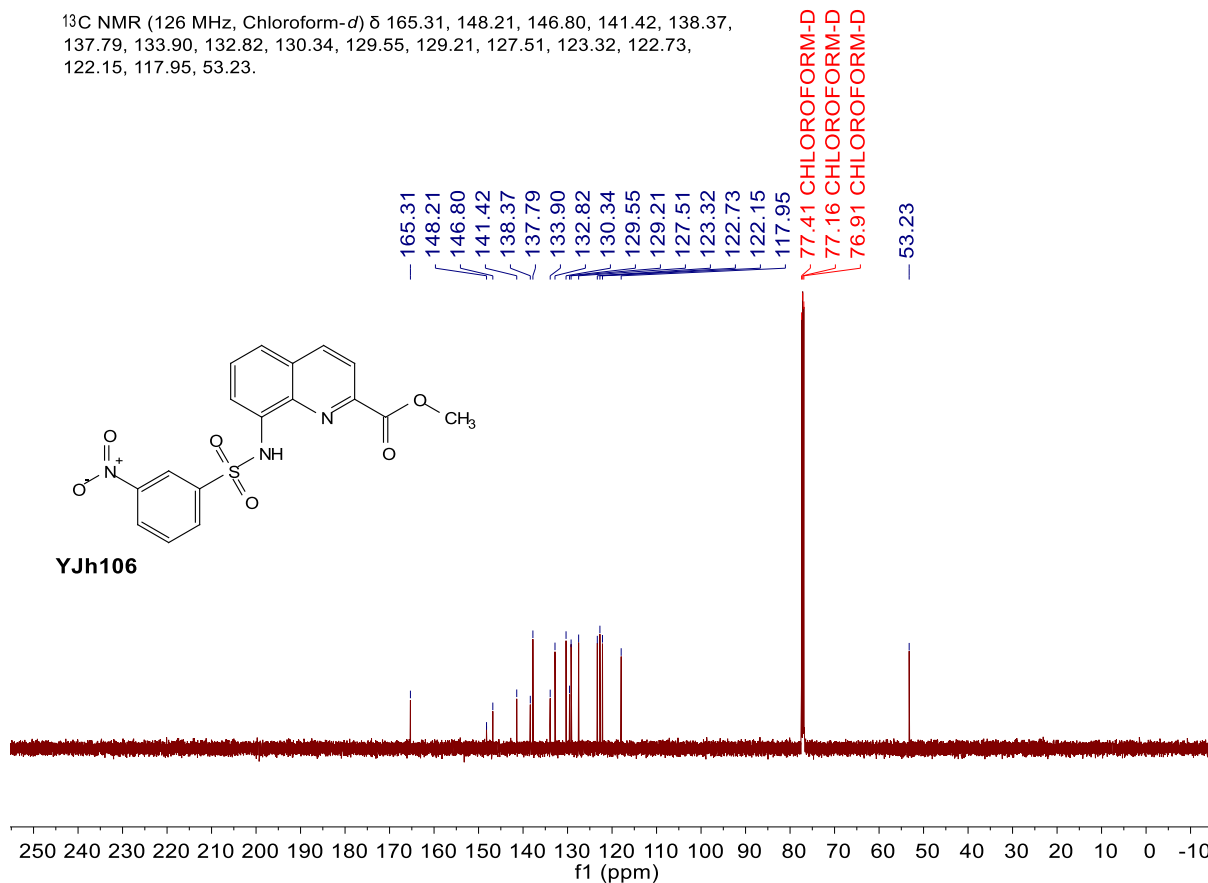
¹³C NMR (126 MHz, Chloroform-*d*) δ 165.44, 146.60, 141.03, 138.18, 137.66, 135.22, 134.34, 133.25, 130.24, 129.51, 129.20, 127.58, 125.48, 122.65, 122.06, 116.96, 53.16.



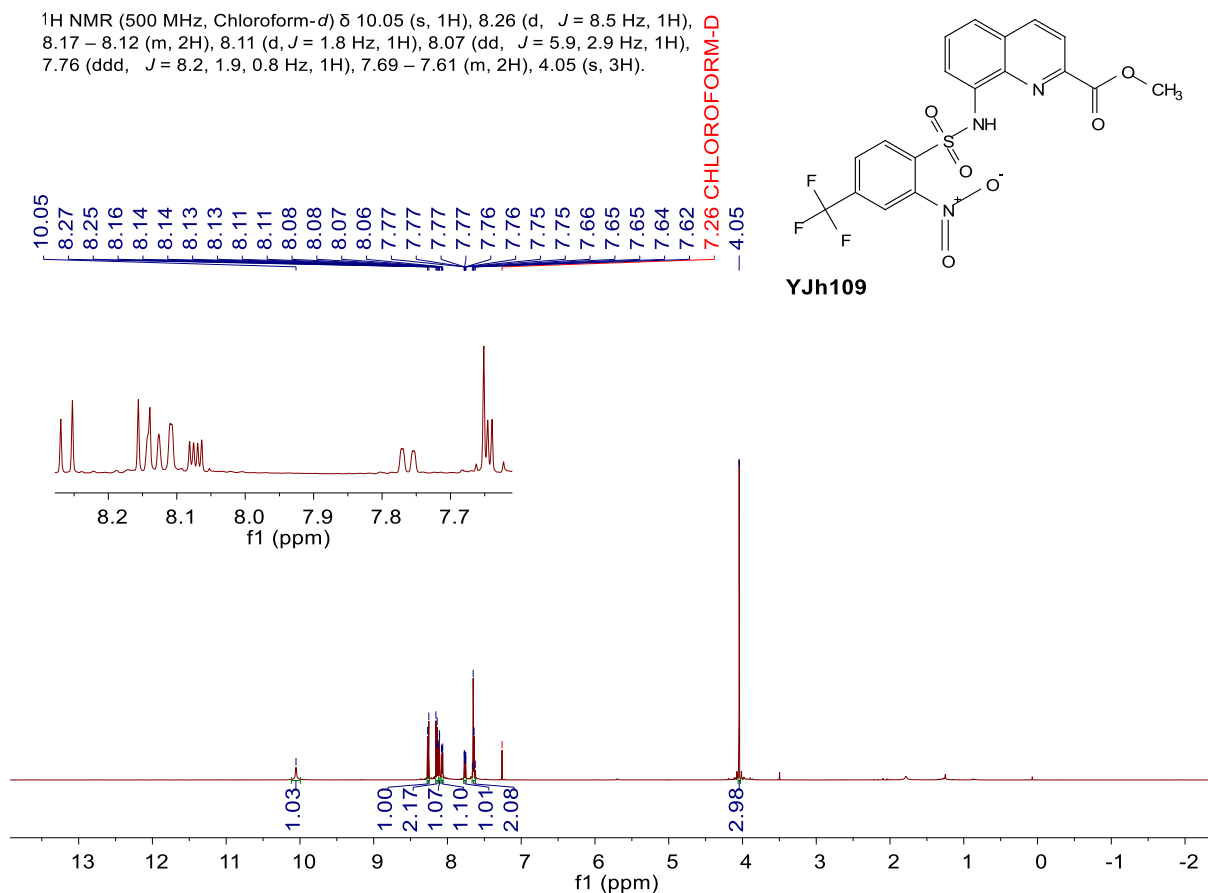
¹H NMR (500 MHz, Chloroform-*d*) δ 9.43 (s, 1H), 8.77 (t, *J* = 2.0 Hz, 1H), 8.25 (ddd, *J* = 8.2, 2.2, 1.0 Hz, 1H), 8.24 (d, *J* = 8.5 Hz, 1H), 8.20 (ddd, *J* = 7.9, 1.8, 1.1 Hz, 1H), 8.15 (d, *J* = 8.5 Hz, 1H), 7.95 (dd, *J* = 5.8, 3.1 Hz, 1H), 7.62 – 7.57 (m, 2H), 7.54 (t, *J* = 8.0 Hz, 1H), 4.08 (s, 3H).



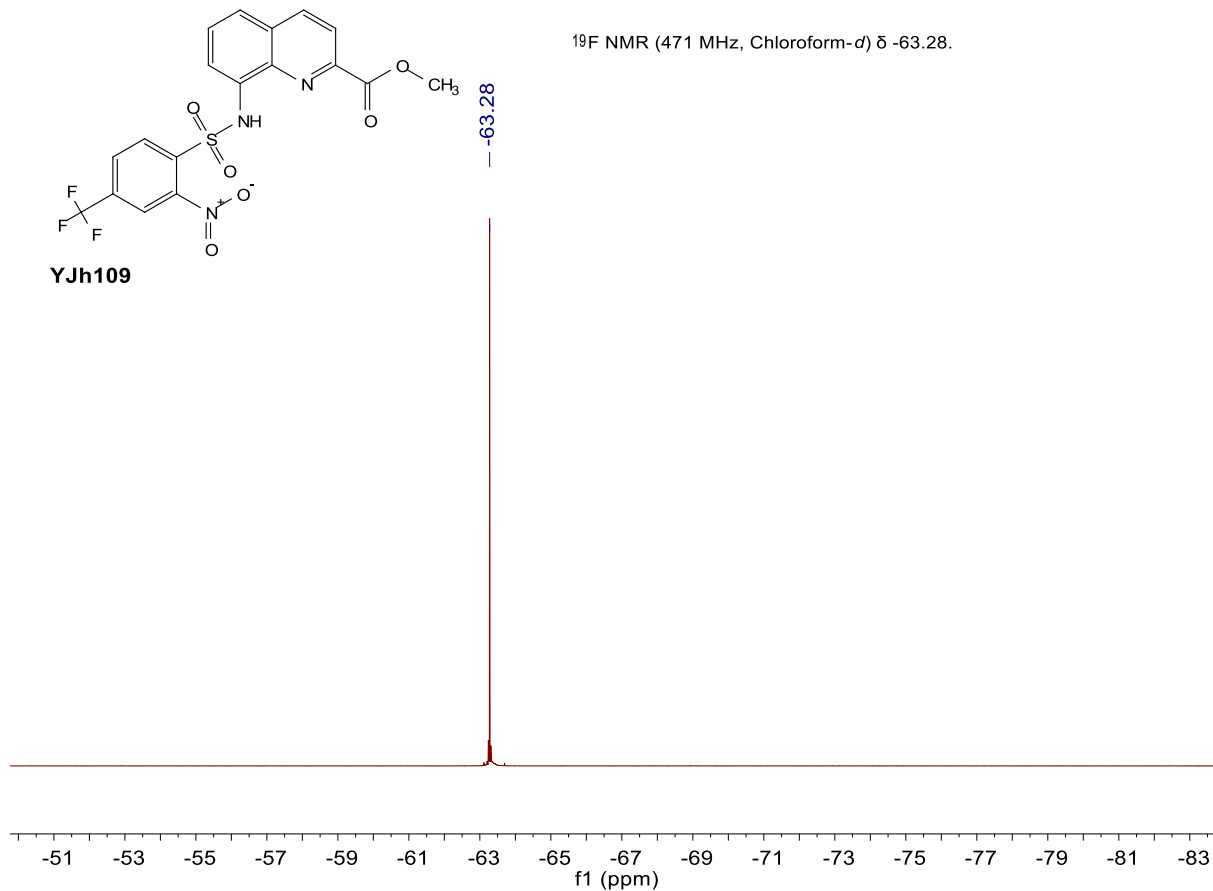
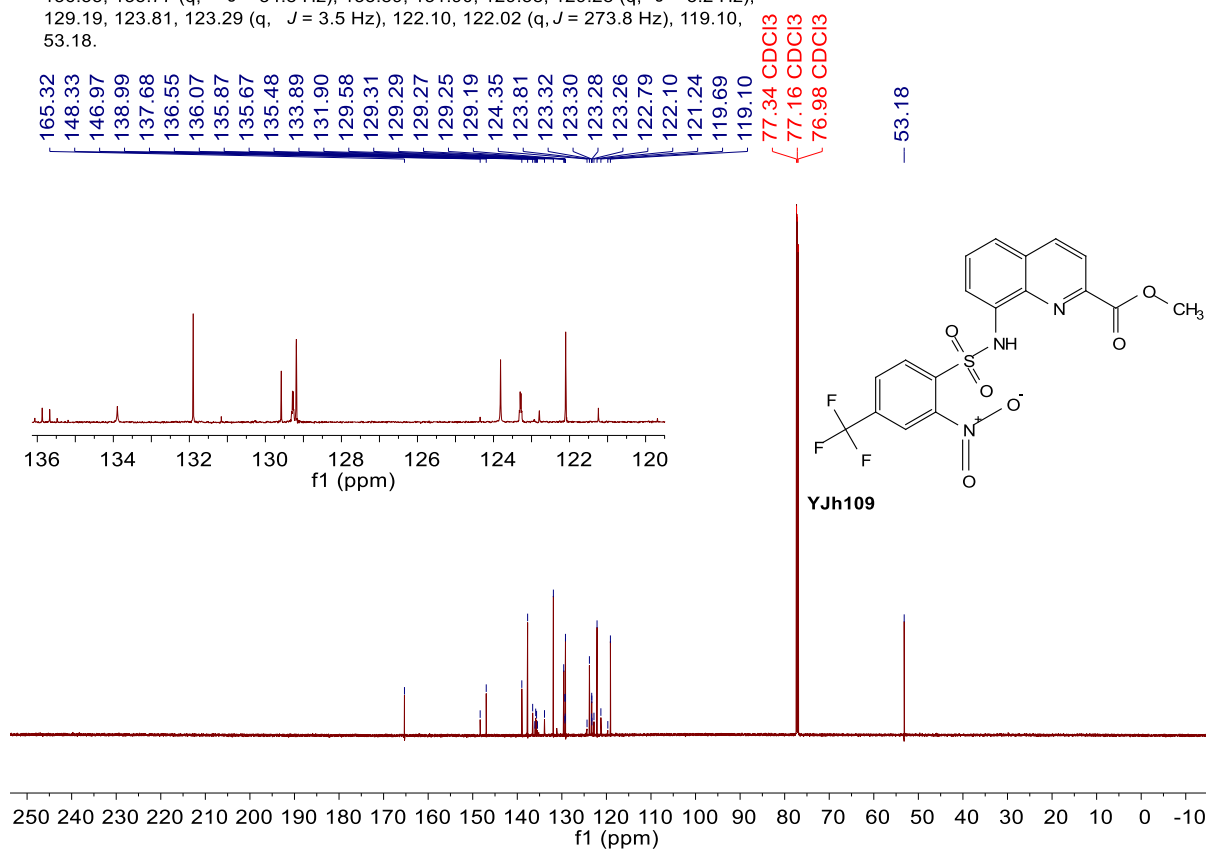
¹³C NMR (126 MHz, Chloroform-*d*) δ 165.31, 148.21, 146.80, 141.42, 138.37, 137.79, 133.90, 132.82, 130.34, 129.55, 129.21, 127.51, 123.32, 122.73, 122.15, 117.95, 53.23.



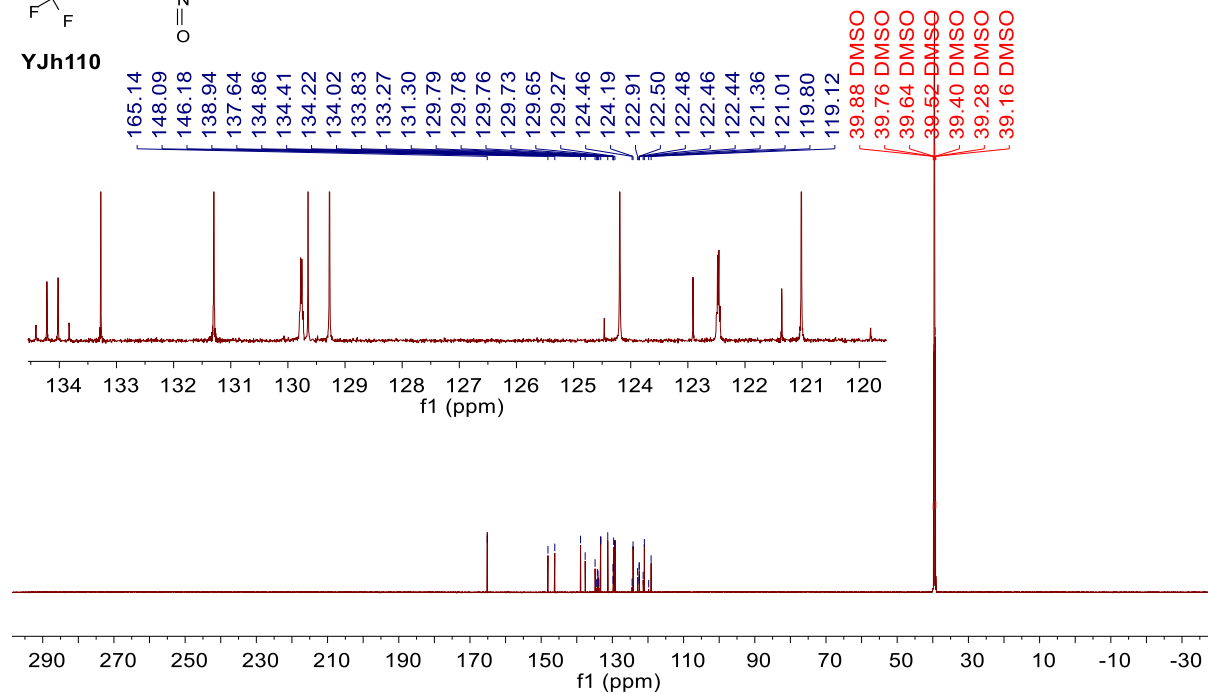
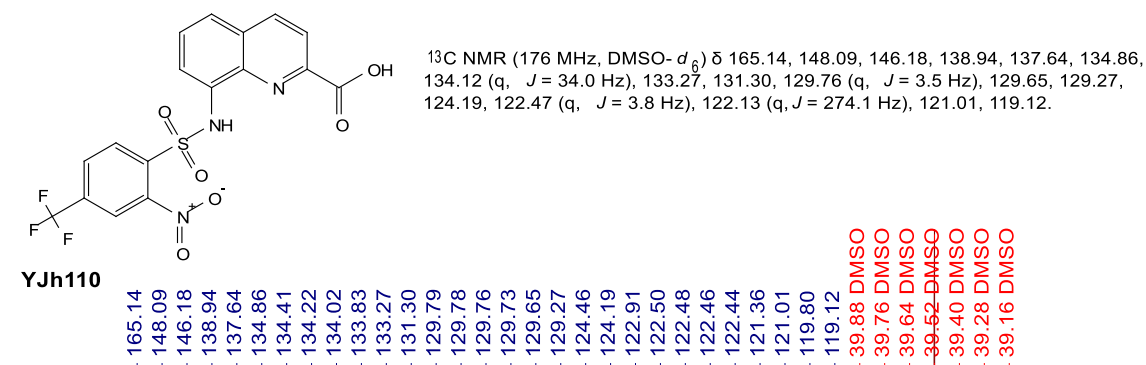
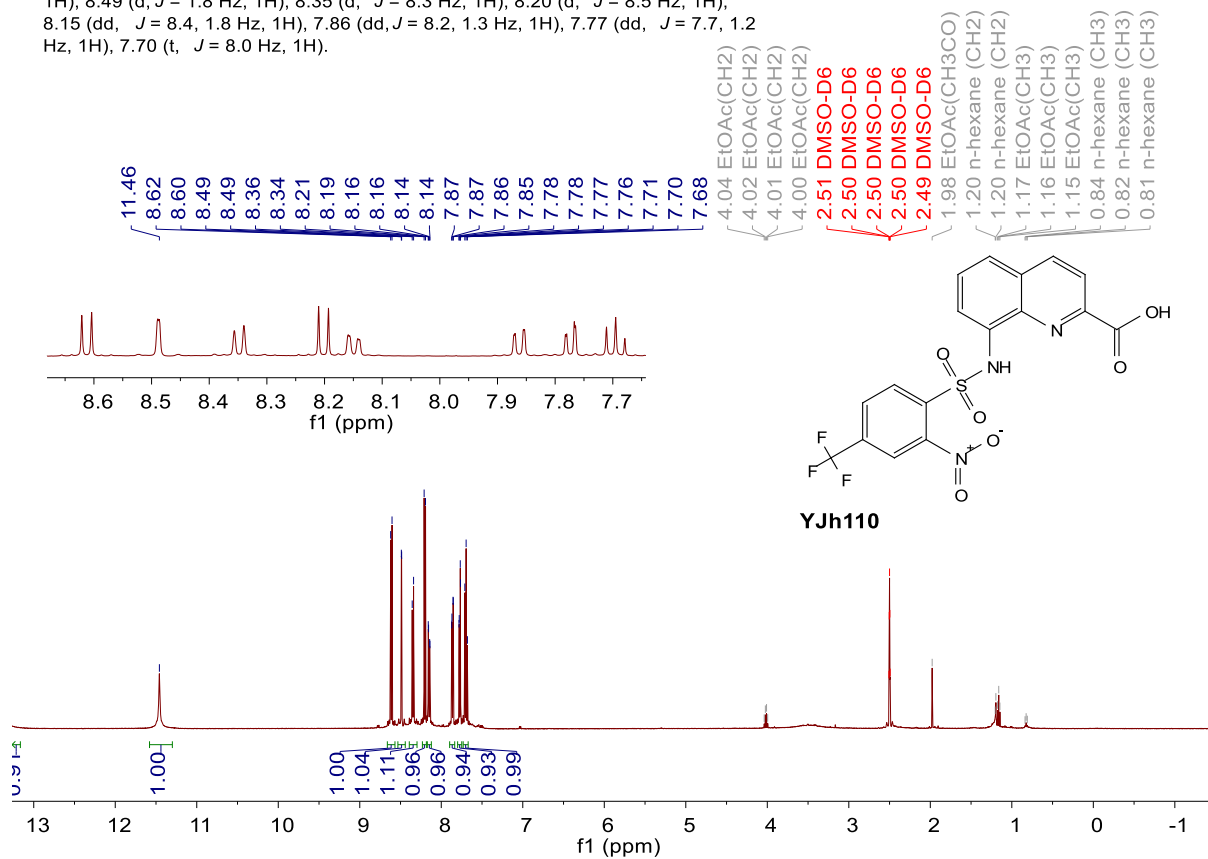
¹H NMR (500 MHz, Chloroform-*d*) δ 10.05 (s, 1H), 8.26 (d, *J* = 8.5 Hz, 1H), 8.17 – 8.12 (m, 2H), 8.11 (d, *J* = 1.8 Hz, 1H), 8.07 (dd, *J* = 5.9, 2.9 Hz, 1H), 7.76 (ddd, *J* = 8.2, 1.9, 0.8 Hz, 1H), 7.69 – 7.61 (m, 2H), 4.05 (s, 3H).

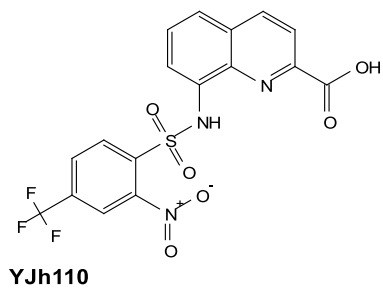


¹³C NMR (176 MHz, Chloroform-*d*) δ 165.32, 148.33, 146.97, 138.99, 137.68, 136.55, 135.77 (q, *J* = 34.8 Hz), 133.89, 131.90, 129.58, 129.28 (q, *J* = 3.2 Hz), 129.19, 123.81, 123.29 (q, *J* = 3.5 Hz), 122.10, 122.02 (q, *J* = 273.8 Hz), 119.10, 53.18.

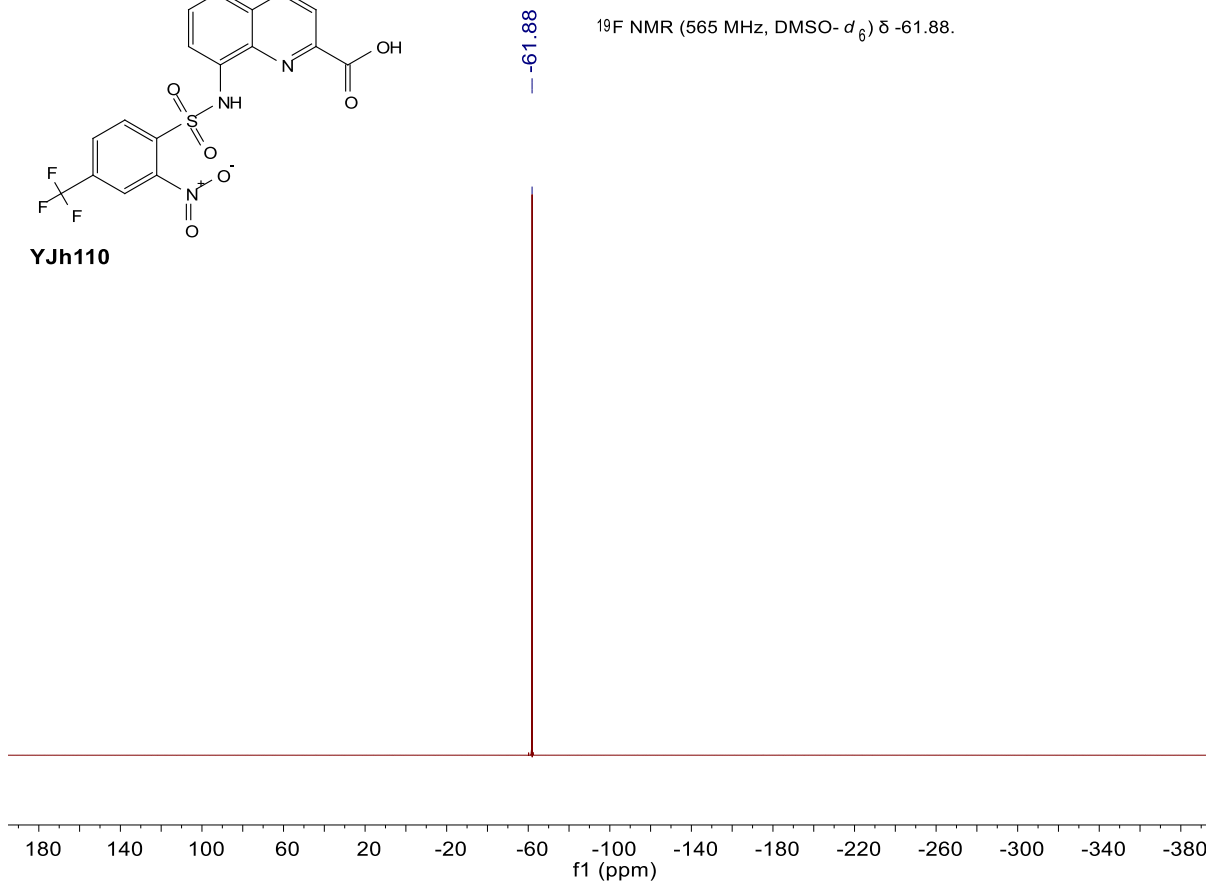


¹H NMR (500 MHz, DMSO-*d*₆) δ 13.37 (s, 1H), 11.46 (s, 1H), 8.61 (d, *J* = 8.5 Hz, 1H), 8.49 (d, *J* = 1.8 Hz, 1H), 8.35 (d, *J* = 8.3 Hz, 1H), 8.20 (d, *J* = 8.5 Hz, 1H), 8.15 (dd, *J* = 8.4, 1.8 Hz, 1H), 7.86 (dd, *J* = 8.2, 1.3 Hz, 1H), 7.77 (dd, *J* = 7.7, 1.2 Hz, 1H), 7.70 (t, *J* = 8.0 Hz, 1H).



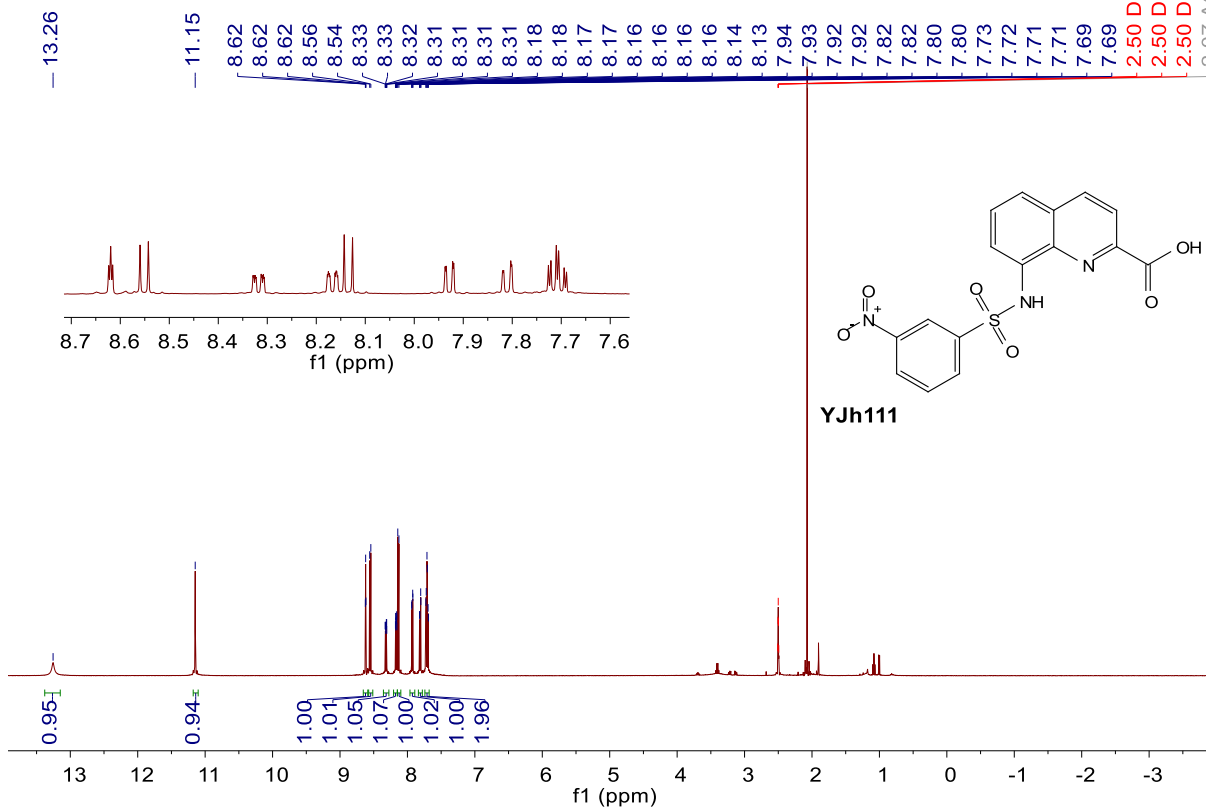
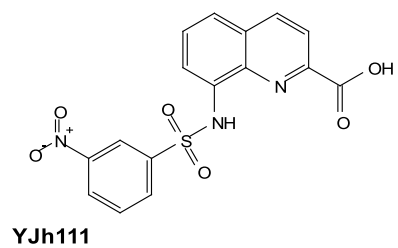
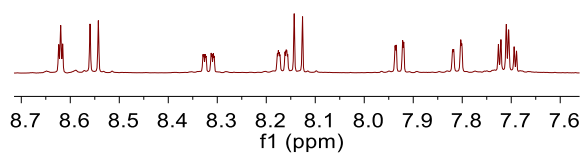


^{19}F NMR (565 MHz, $\text{DMSO}-d_6$) δ -61.88.

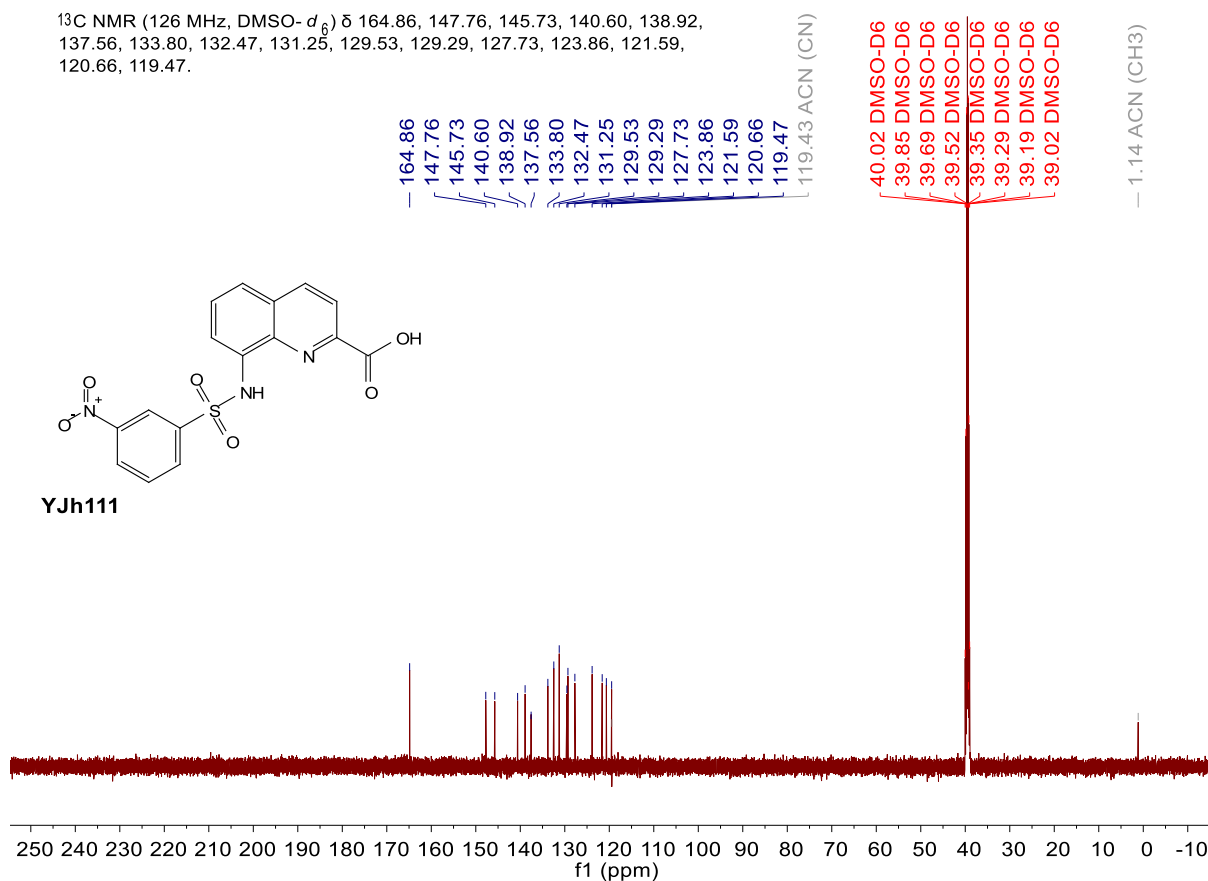


^1H NMR (500 MHz, $\text{DMSO}-d_6$) δ 13.26 (s, 1H), 11.15 (s, 1H), 8.62 (t, $J = 2.0$ Hz, 1H), 8.55 (d, $J = 8.5$ Hz, 1H), 8.32 (ddd, $J = 8.3, 2.3, 1.0$ Hz, 1H), 8.17 (ddd, $J = 7.9, 1.8, 1.0$ Hz, 1H), 8.13 (d, $J = 8.5$ Hz, 1H), 7.93 (dd, $J = 7.7, 1.2$ Hz, 1H), 7.81 (dd, $J = 8.3, 1.3$ Hz, 1H), 7.71 (td, $J = 8.0, 2.5$ Hz, 2H).

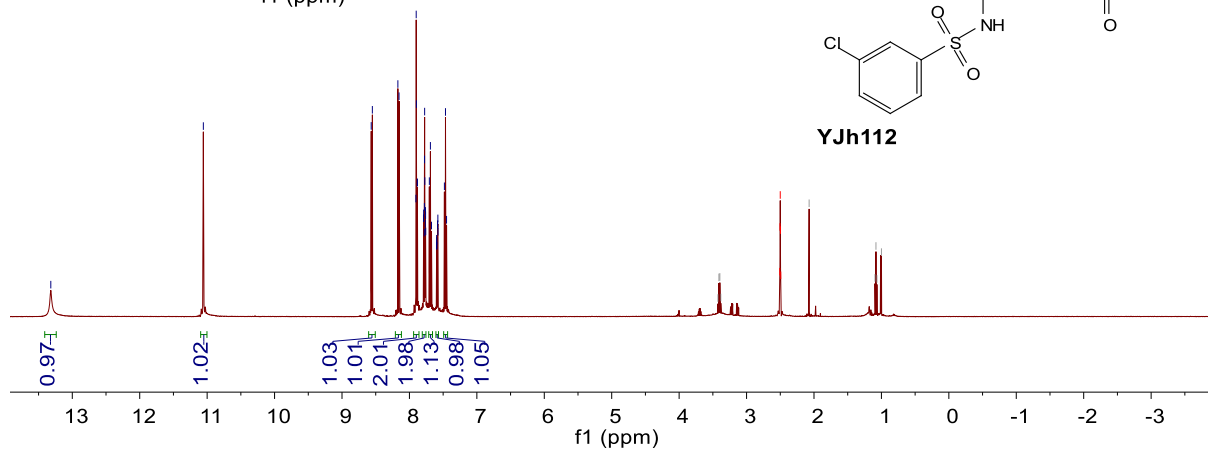
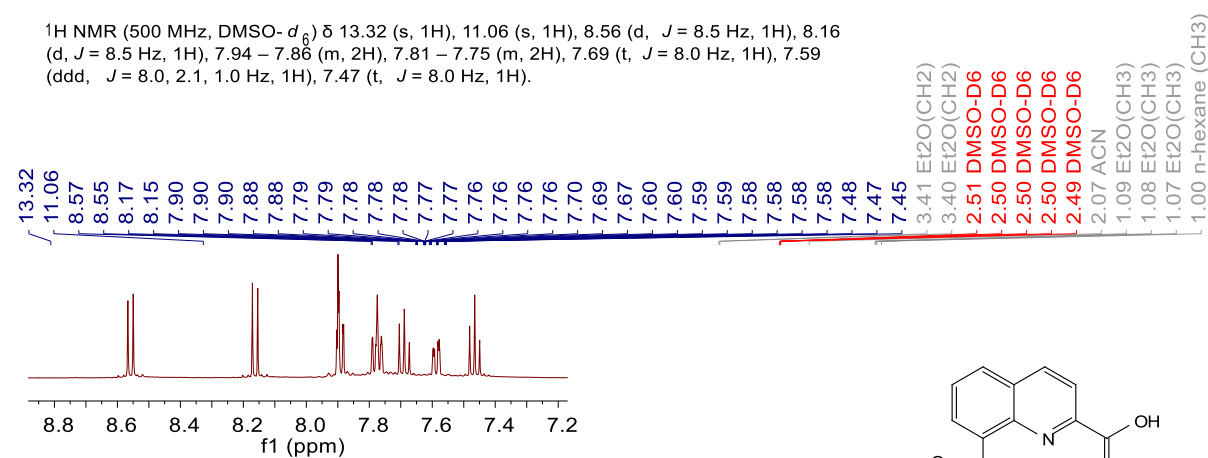
13.26
11.15
8.62
8.62
8.56
8.54
8.33
8.33
8.32
8.31
8.31
8.31
8.18
8.18
8.17
8.16
8.16
8.16
8.16
8.14
8.13
7.94
7.93
7.92
7.92
7.82
7.82
7.80
7.73
7.72
7.71
7.71
7.69
7.69
2.50 DMSO-D6
2.50 DMSO-D6
2.07 ACN



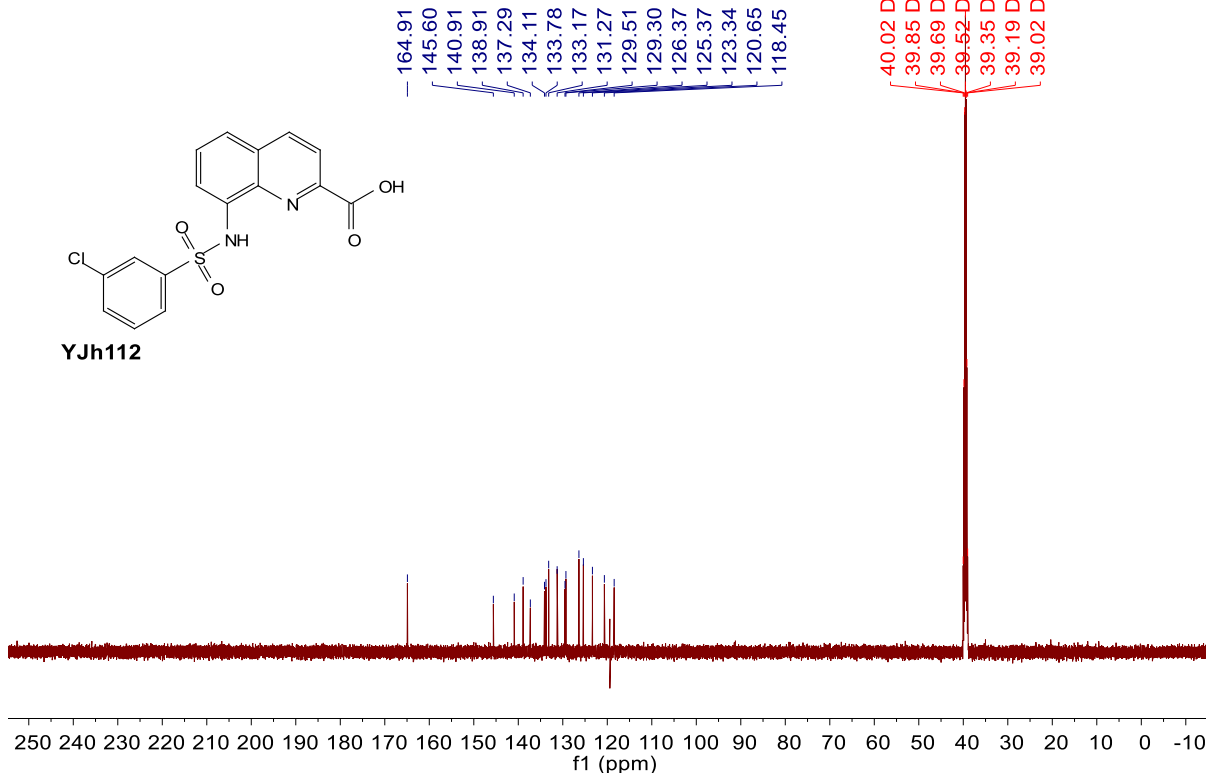
¹³C NMR (126 MHz, DMSO-*d*₆) δ 164.86, 147.76, 145.73, 140.60, 138.92, 137.56, 133.80, 132.47, 131.25, 129.53, 129.29, 127.73, 123.86, 121.59, 120.66, 119.47.



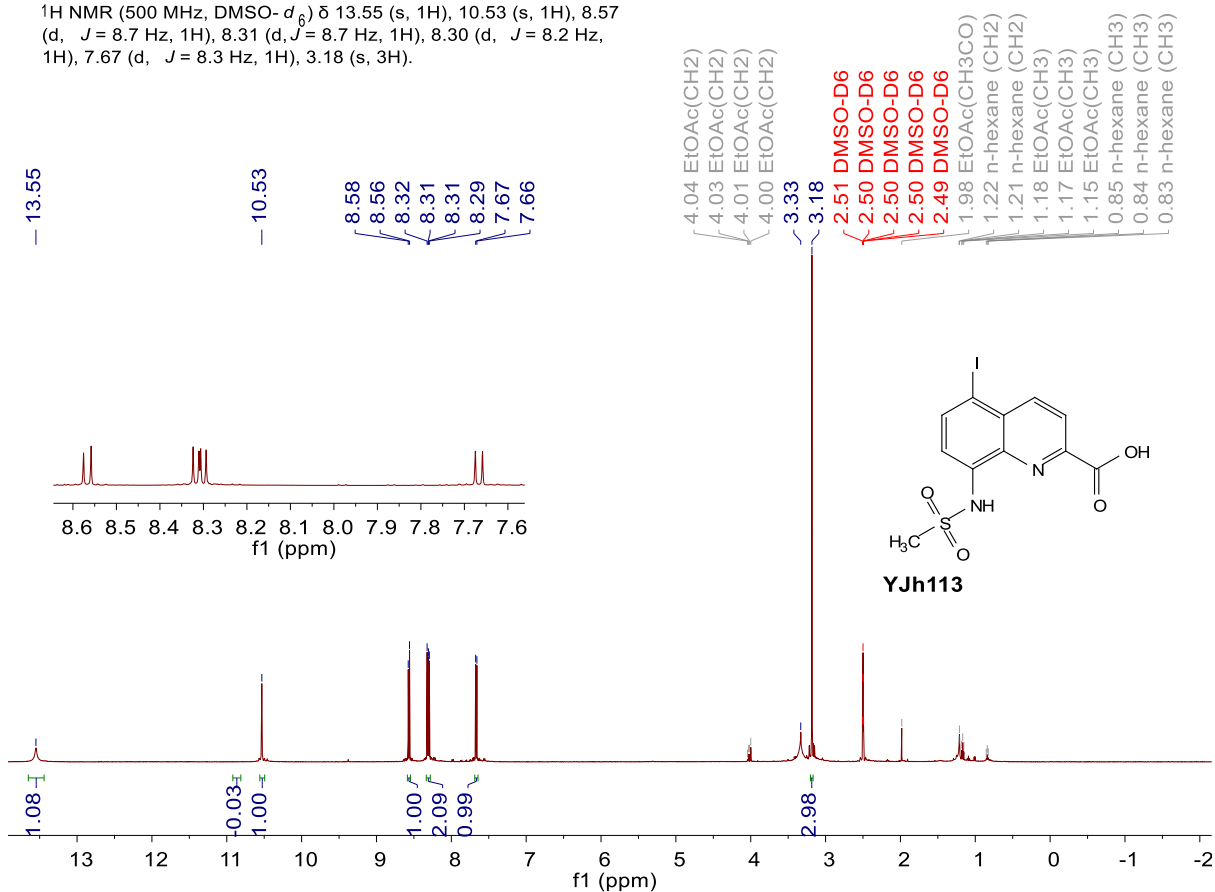
¹H NMR (500 MHz, DMSO-*d*₆) δ 13.32 (s, 1H), 11.06 (s, 1H), 8.56 (d, *J* = 8.5 Hz, 1H), 8.16 (d, *J* = 8.5 Hz, 1H), 7.94 – 7.86 (m, 2H), 7.81 – 7.75 (m, 2H), 7.69 (t, *J* = 8.0 Hz, 1H), 7.59 (ddd, *J* = 8.0, 2.1, 1.0 Hz, 1H), 7.47 (t, *J* = 8.0 Hz, 1H).

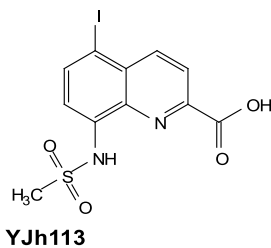


¹³C NMR (126 MHz, DMSO-*d*₆) δ 164.91, 145.60, 140.91, 138.91, 137.29, 134.11, 133.78, 133.17, 131.27, 129.51, 129.30, 126.37, 125.37, 123.34, 120.65, 118.45.

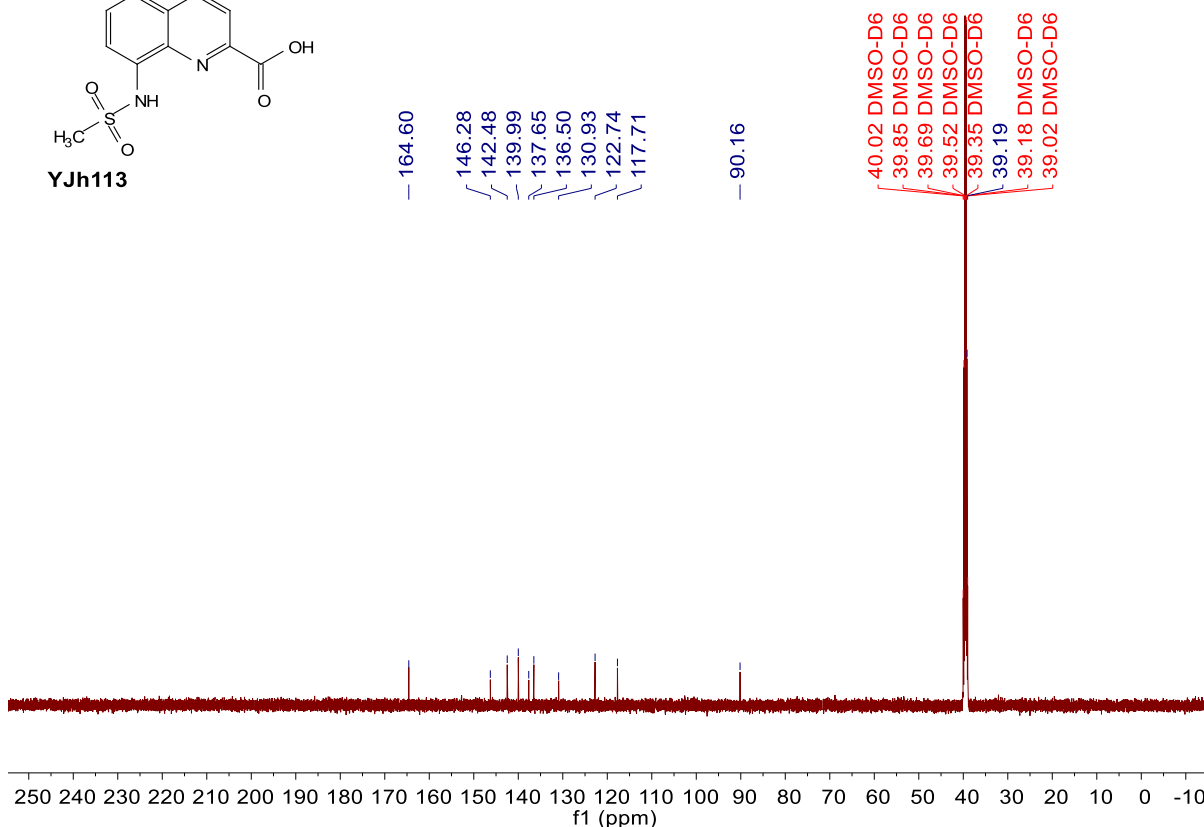


¹H NMR (500 MHz, DMSO-*d*₆) δ 13.55 (s, 1H), 10.53 (s, 1H), 8.57 (d, *J* = 8.7 Hz, 1H), 8.31 (d, *J* = 8.7 Hz, 1H), 8.30 (d, *J* = 8.2 Hz, 1H), 7.67 (d, *J* = 8.3 Hz, 1H), 3.18 (s, 3H).

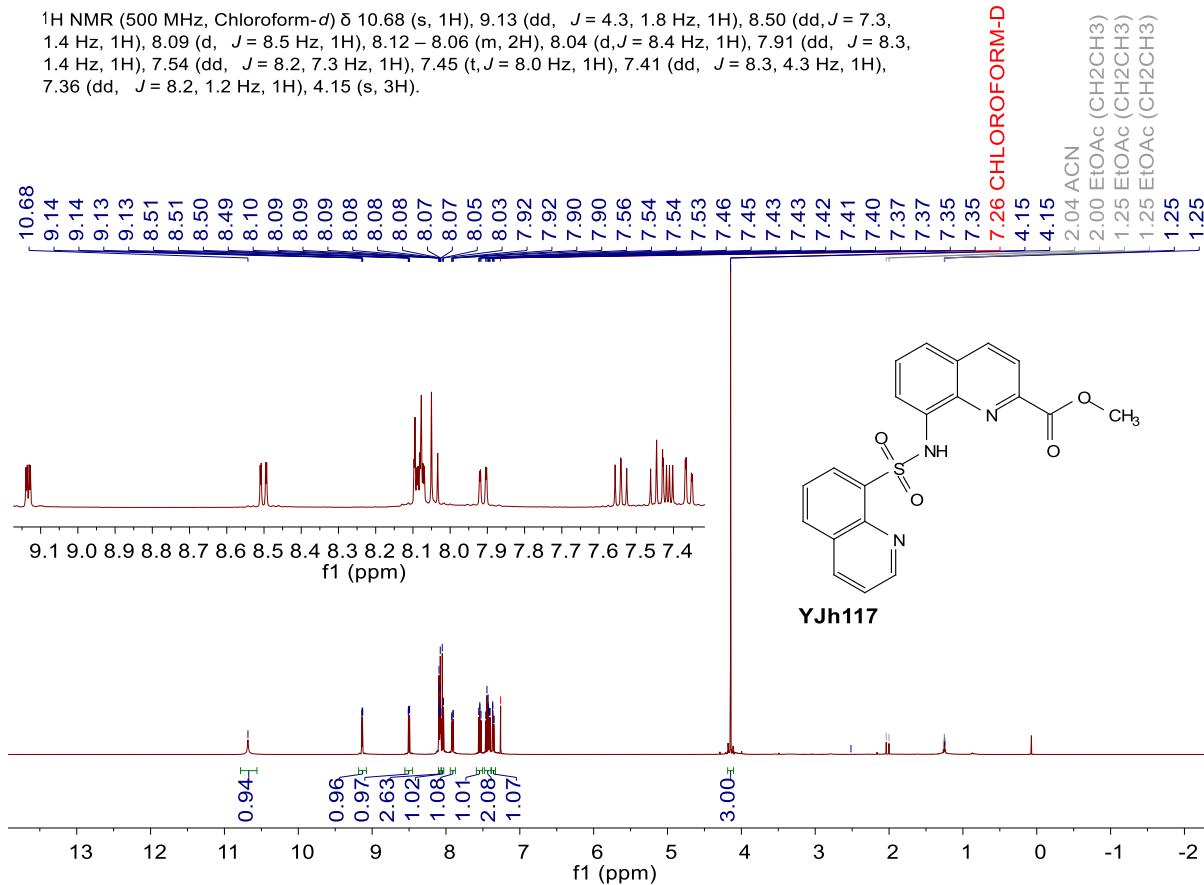




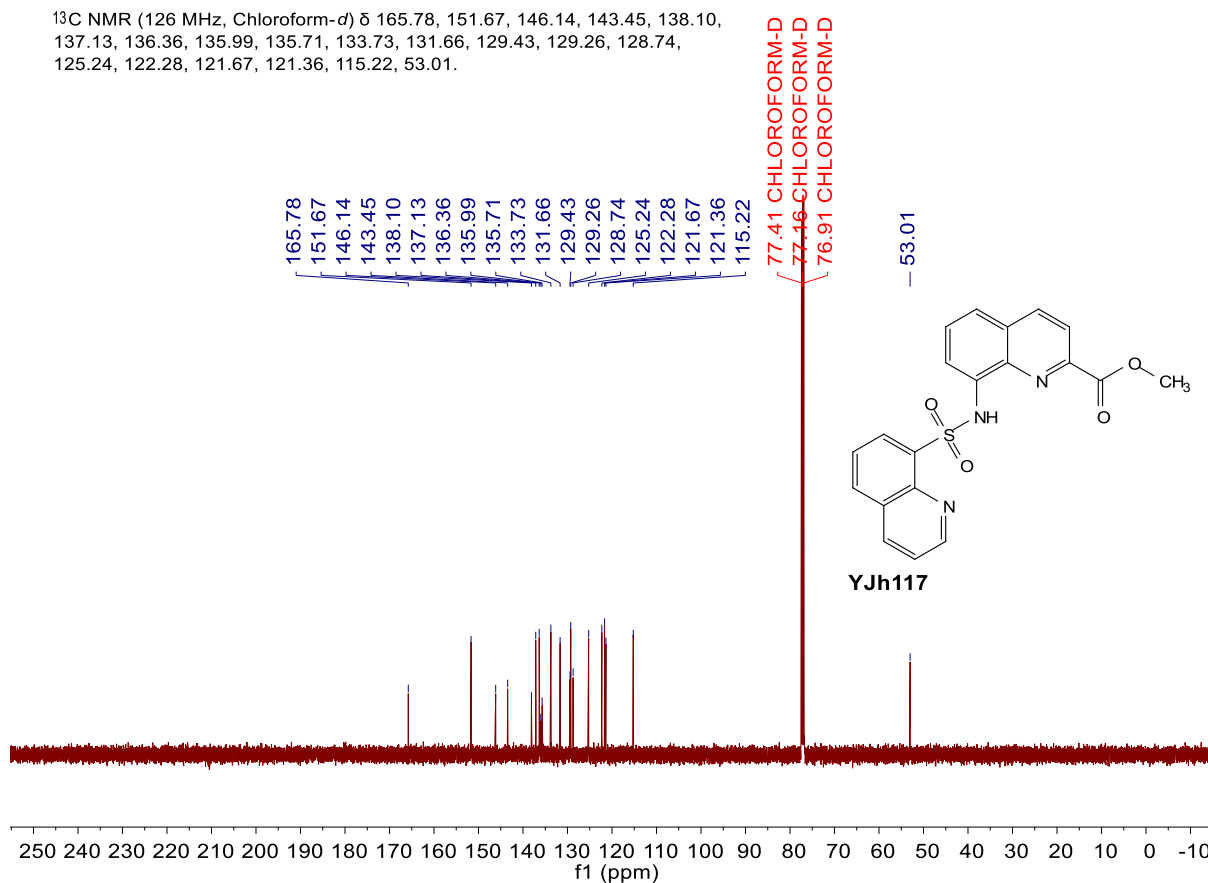
^{13}C NMR (126 MHz, $\text{DMSO-}d_6$) δ 164.60, 146.28, 142.48, 139.99, 137.65, 136.50, 130.93, 122.74, 117.71, 90.16, 39.19.



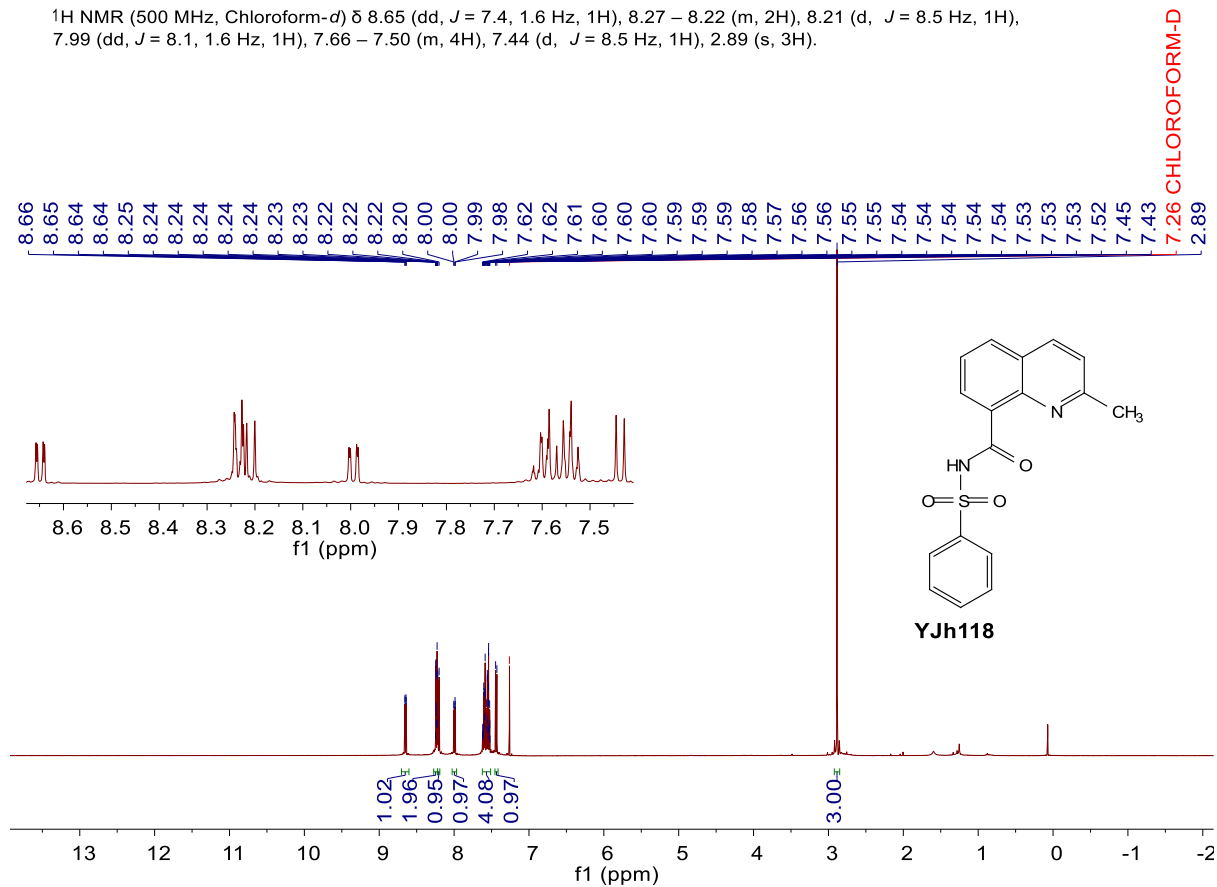
^1H NMR (500 MHz, Chloroform- d) δ 10.68 (s, 1H), 9.13 (dd, $J = 4.3, 1.8$ Hz, 1H), 8.50 (dd, $J = 7.3, 1.4$ Hz, 1H), 8.09 (d, $J = 8.5$ Hz, 1H), 8.12 – 8.06 (m, 2H), 8.04 (d, $J = 8.4$ Hz, 1H), 7.91 (dd, $J = 8.3, 1.4$ Hz, 1H), 7.54 (dd, $J = 8.2, 7.3$ Hz, 1H), 7.45 (t, $J = 8.0$ Hz, 1H), 7.41 (dd, $J = 8.3, 4.3$ Hz, 1H), 7.36 (dd, $J = 8.2, 1.2$ Hz, 1H), 4.15 (s, 3H).



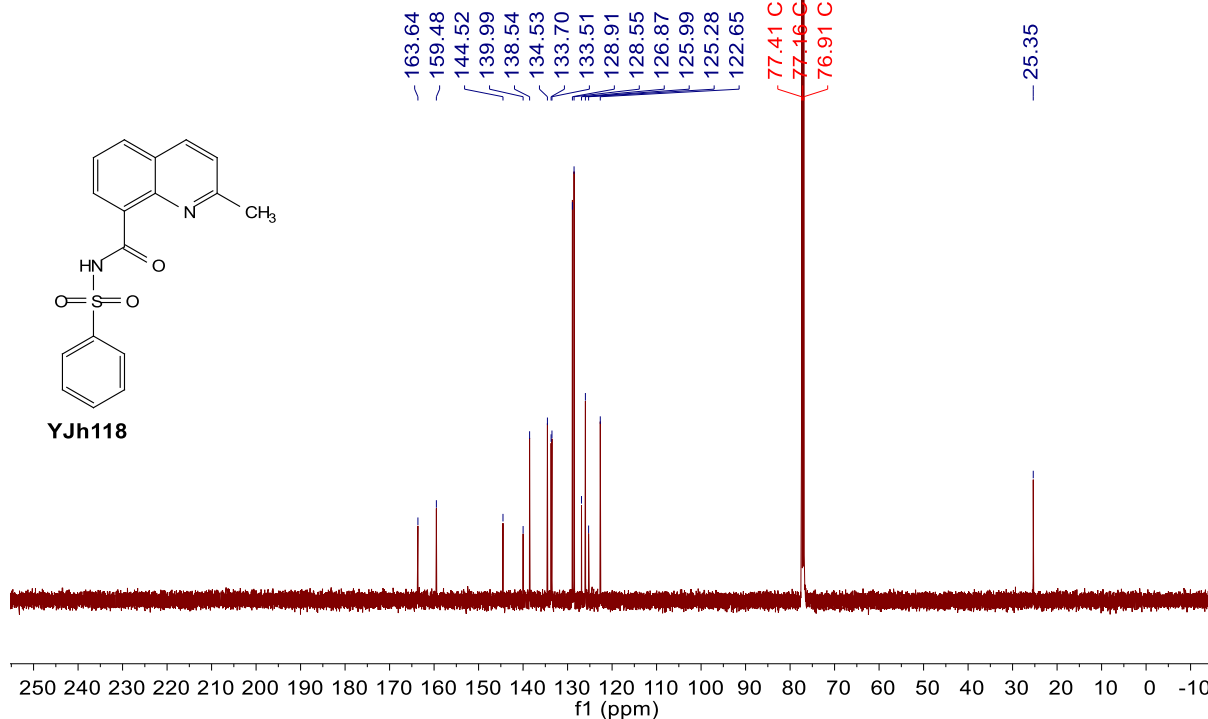
^{13}C NMR (126 MHz, Chloroform-*d*) δ 165.78, 151.67, 146.14, 143.45, 138.10, 137.13, 136.36, 135.99, 135.71, 133.73, 131.66, 129.43, 129.26, 128.74, 125.24, 122.28, 121.67, 121.36, 115.22, 53.01.



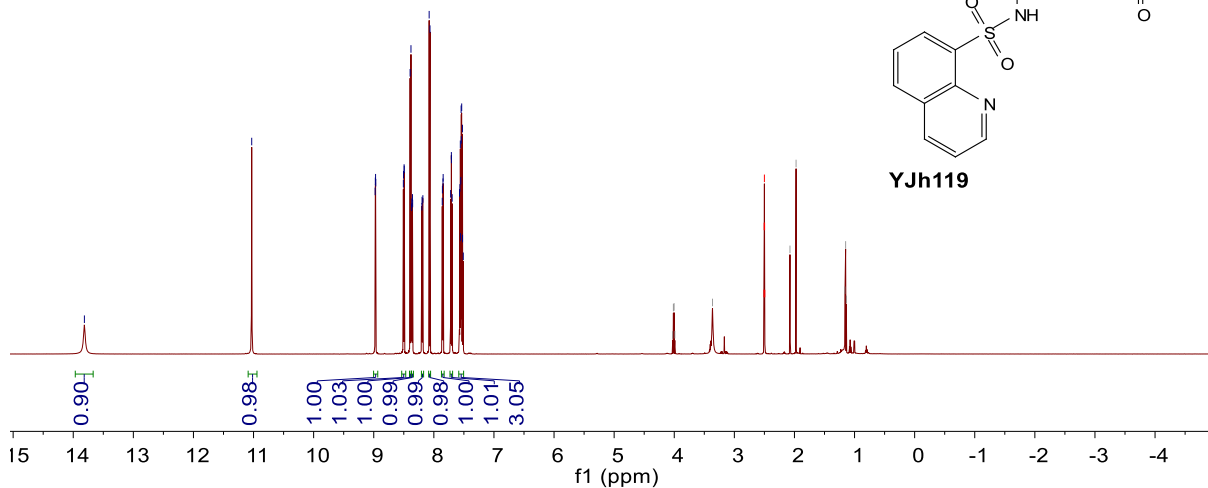
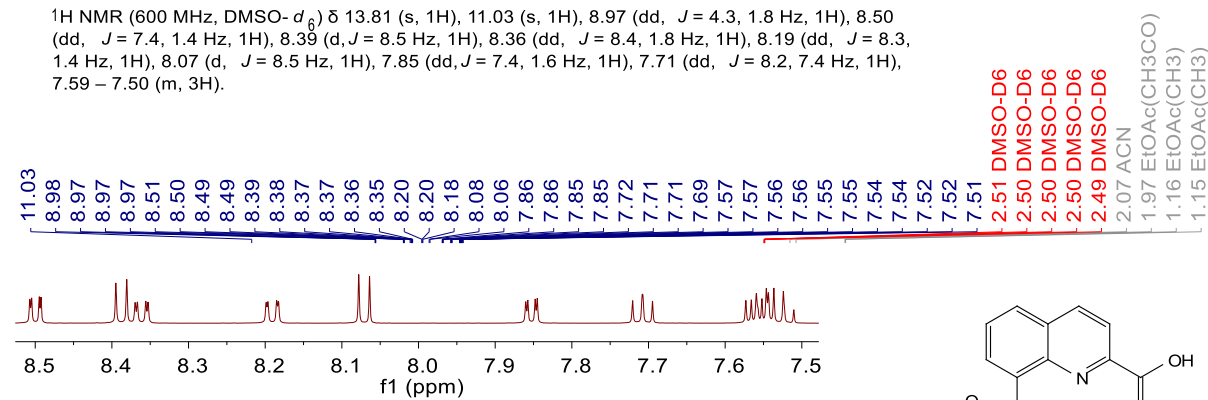
^1H NMR (500 MHz, Chloroform-*d*) δ 8.65 (dd, $J = 7.4, 1.6$ Hz, 1H), 8.27 – 8.22 (m, 2H), 8.21 (d, $J = 8.5$ Hz, 1H), 7.99 (dd, $J = 8.1, 1.6$ Hz, 1H), 7.66 – 7.50 (m, 4H), 7.44 (d, $J = 8.5$ Hz, 1H), 2.89 (s, 3H).



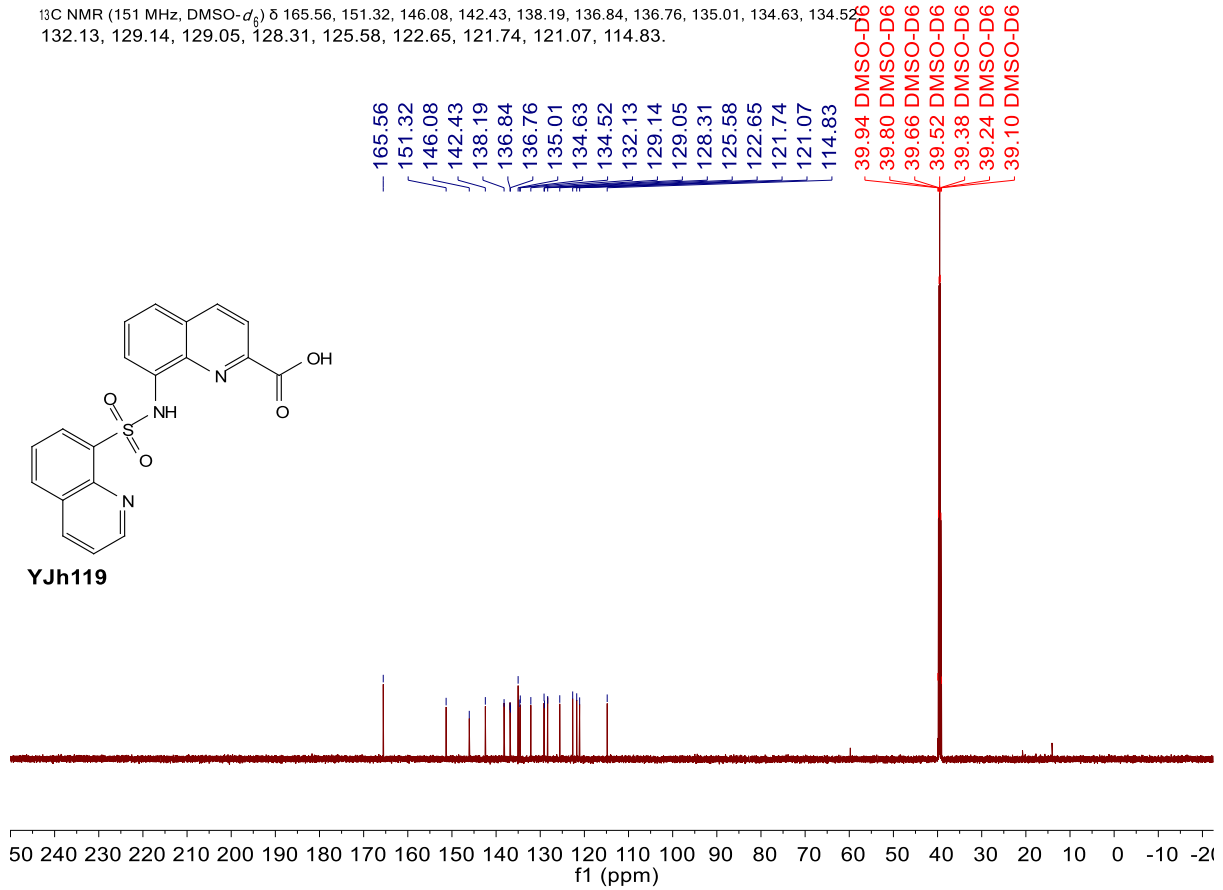
¹³C NMR (126 MHz, Chloroform-*d*) δ 163.59, 159.44, 144.48, 139.95, 138.50, 134.49, 133.66, 133.47, 128.87, 128.50, 126.83, 125.95, 125.24, 122.61, 25.31.



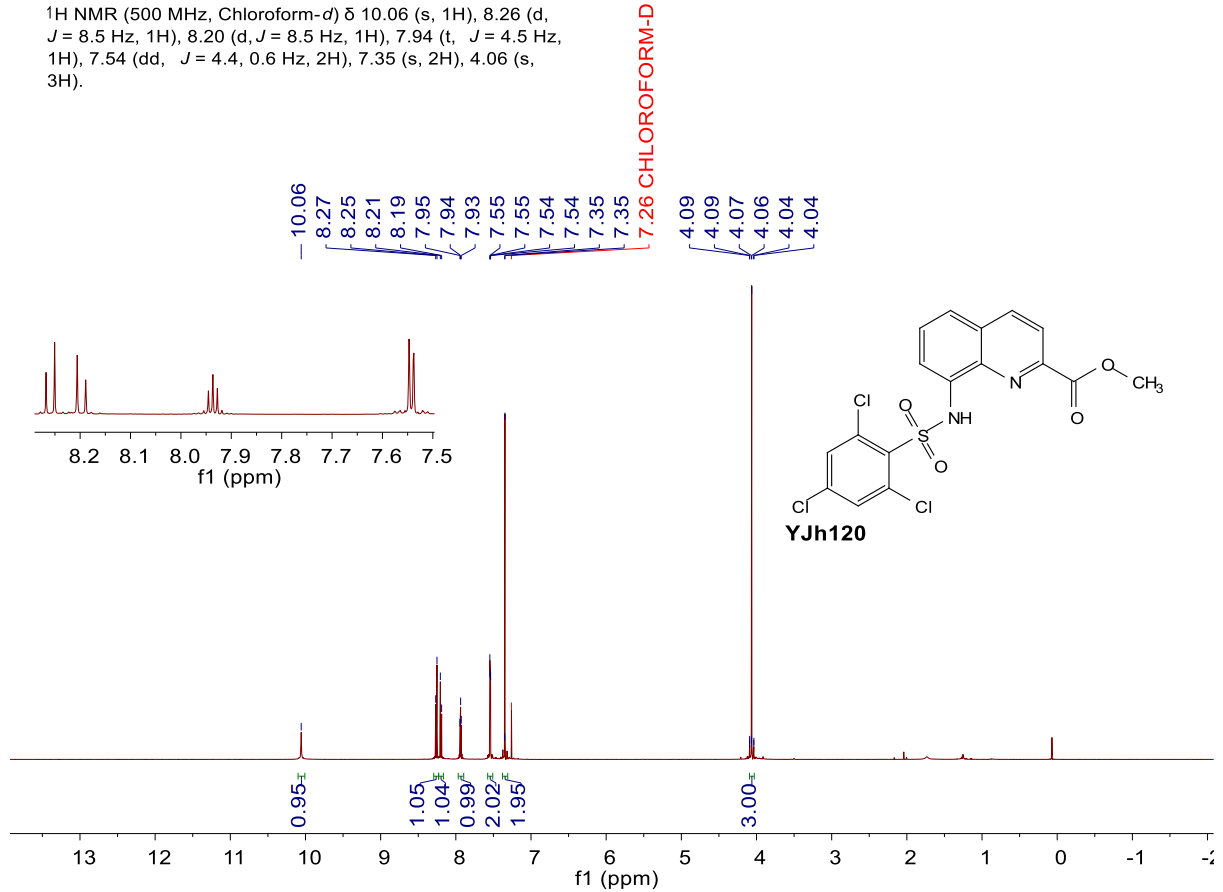
¹H NMR (600 MHz, DMSO-*d*₆) δ 13.81 (s, 1H), 11.03 (s, 1H), 8.97 (dd, *J* = 4.3, 1.8 Hz, 1H), 8.50 (dd, *J* = 7.4, 1.4 Hz, 1H), 8.39 (d, *J* = 8.5 Hz, 1H), 8.36 (dd, *J* = 8.4, 1.8 Hz, 1H), 8.19 (dd, *J* = 8.3, 1.4 Hz, 1H), 8.07 (d, *J* = 8.5 Hz, 1H), 7.85 (dd, *J* = 7.4, 1.6 Hz, 1H), 7.71 (dd, *J* = 8.2, 7.4 Hz, 1H), 7.59 – 7.50 (m, 3H).



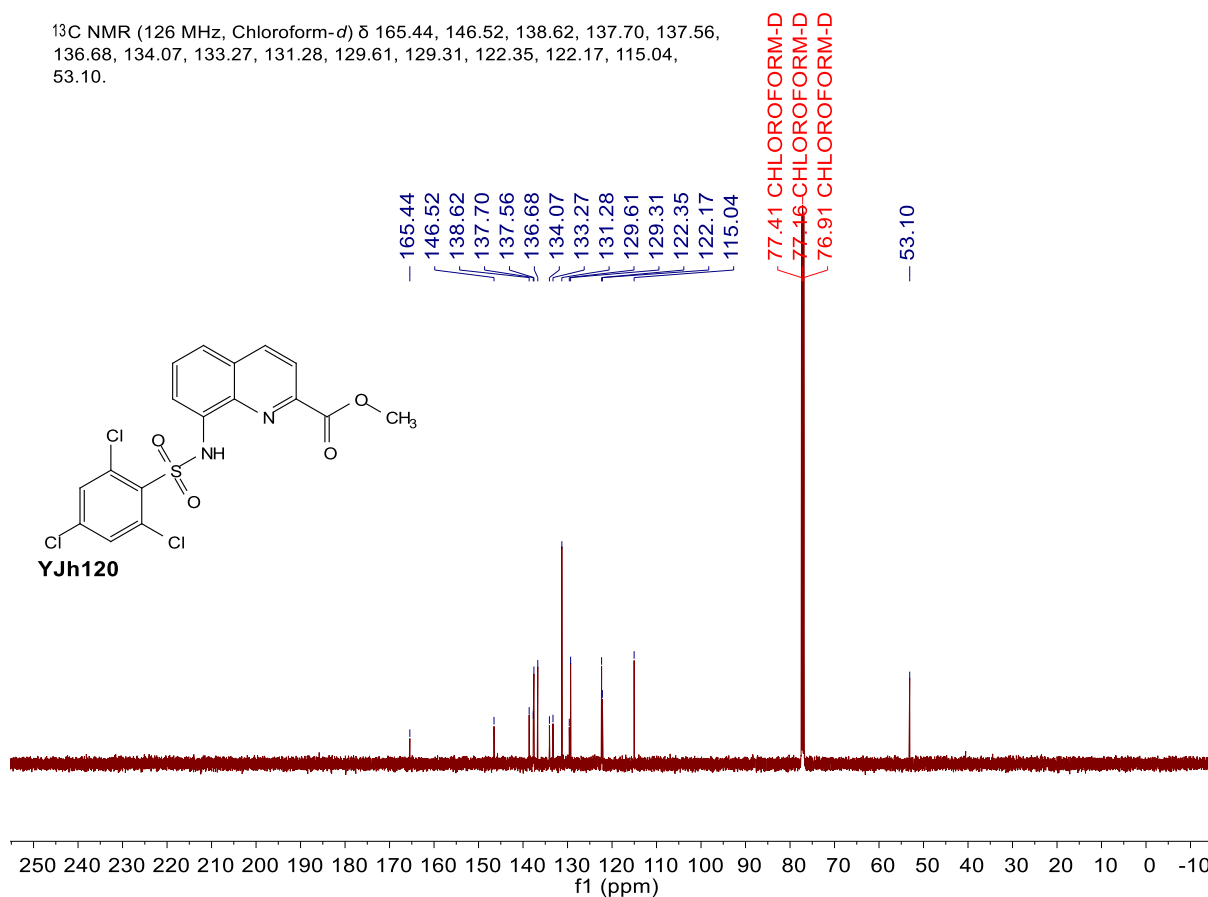
^{13}C NMR (151 MHz, $\text{DMSO-}d_6$) δ 165.56, 151.32, 146.08, 142.43, 138.19, 136.84, 136.76, 135.01, 134.63, 134.52, 132.13, 129.14, 129.05, 128.31, 125.58, 122.65, 121.74, 121.07, 114.83.



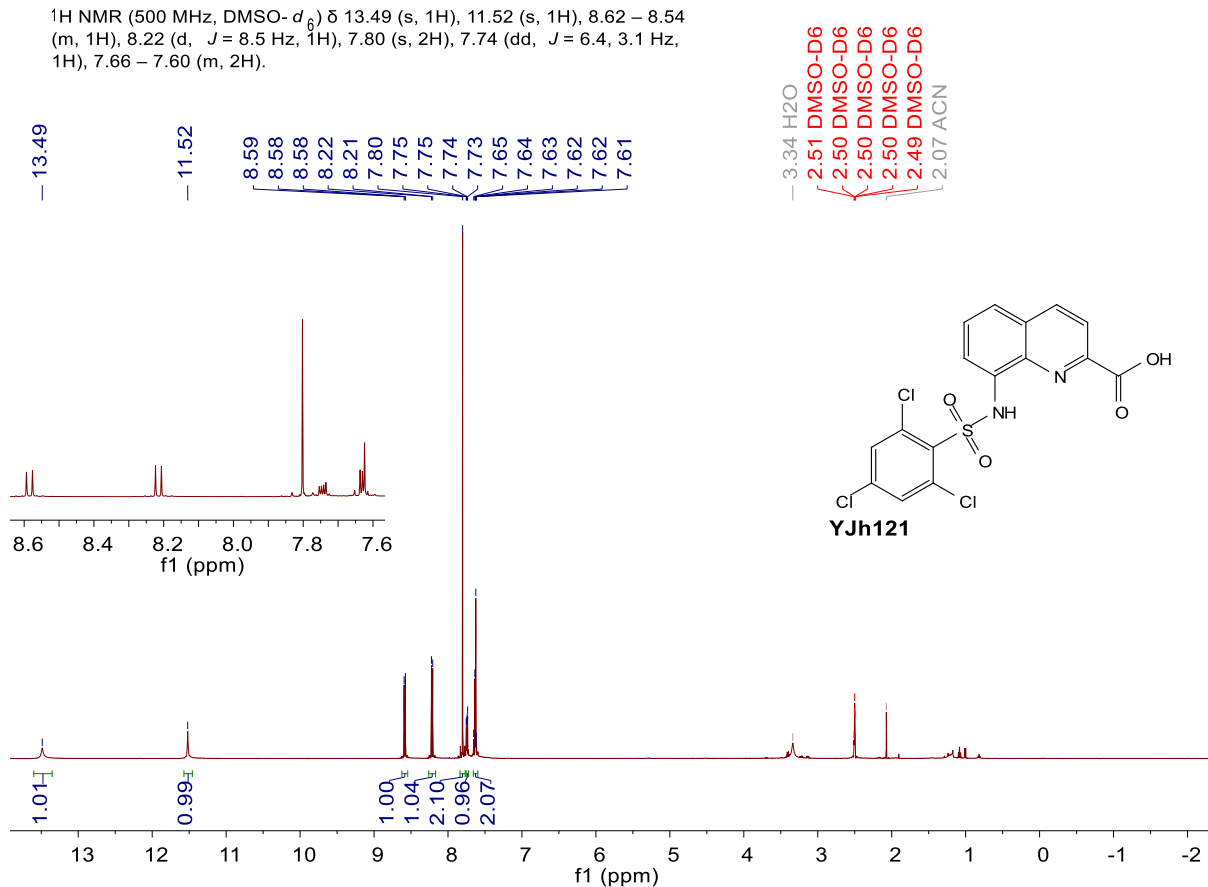
^1H NMR (500 MHz, $\text{Chloroform-}d$) δ 10.06 (s, 1H), 8.26 (d, $J = 8.5$ Hz, 1H), 8.20 (d, $J = 8.5$ Hz, 1H), 7.94 (t, $J = 4.5$ Hz, 1H), 7.54 (dd, $J = 4.4, 0.6$ Hz, 2H), 7.35 (s, 2H), 4.06 (s, 3H).

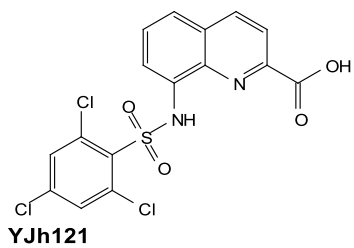


^{13}C NMR (126 MHz, Chloroform- d) δ 165.44, 146.52, 138.62, 137.70, 137.56, 136.68, 134.07, 133.27, 131.28, 129.61, 129.31, 122.35, 122.17, 115.04, 53.10.

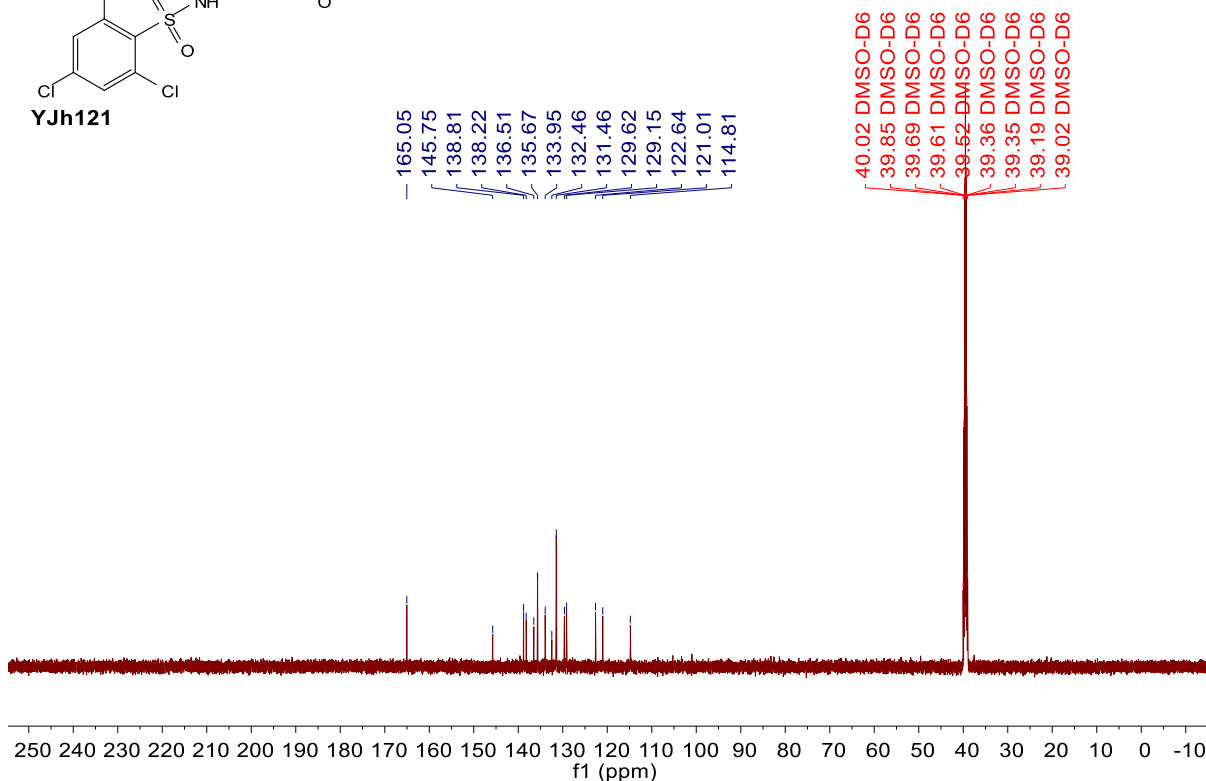


^1H NMR (500 MHz, DMSO- d_6) δ 13.49 (s, 1H), 11.52 (s, 1H), 8.62 – 8.54 (m, 1H), 8.22 (d, J = 8.5 Hz, 1H), 7.80 (s, 2H), 7.74 (dd, J = 6.4, 3.1 Hz, 1H), 7.66 – 7.60 (m, 2H).

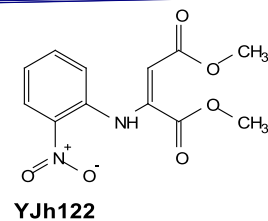
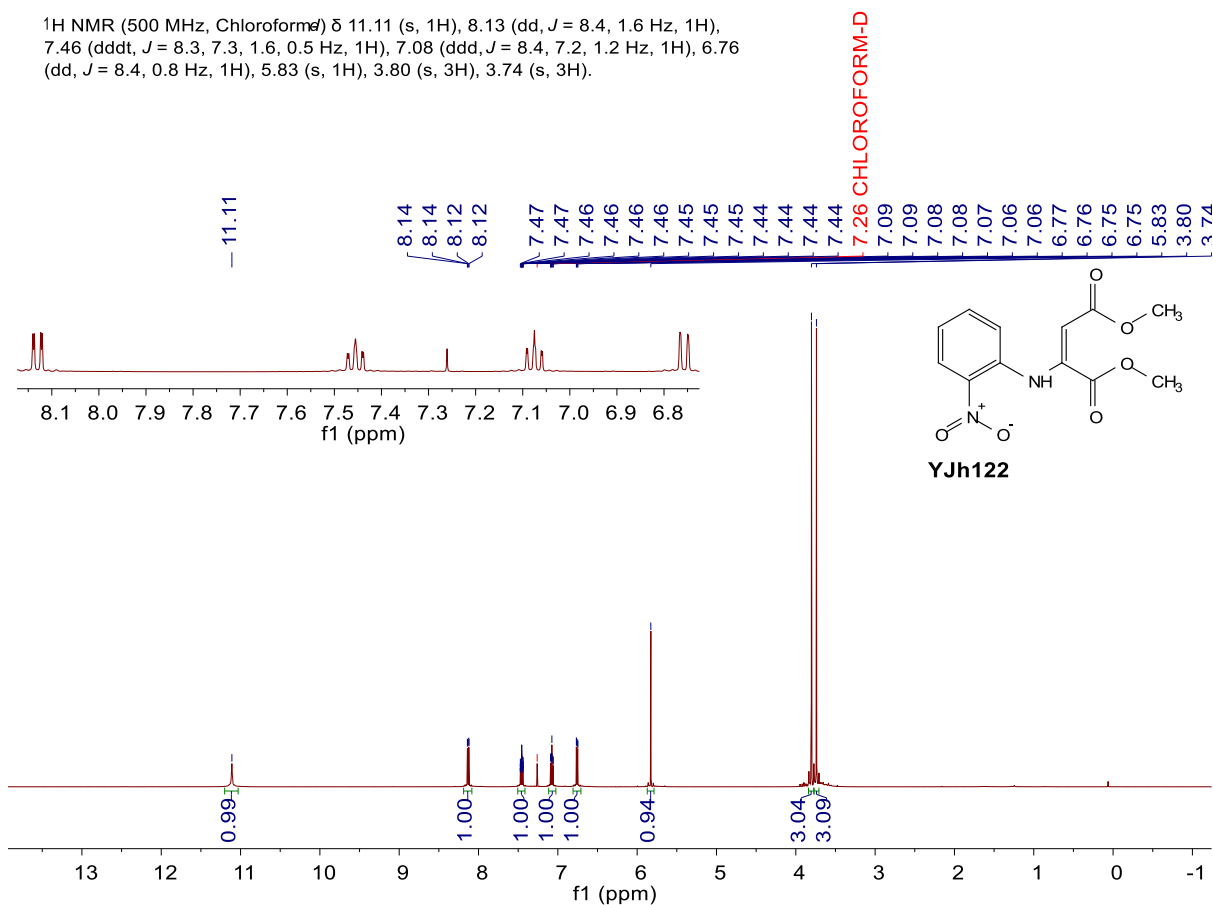




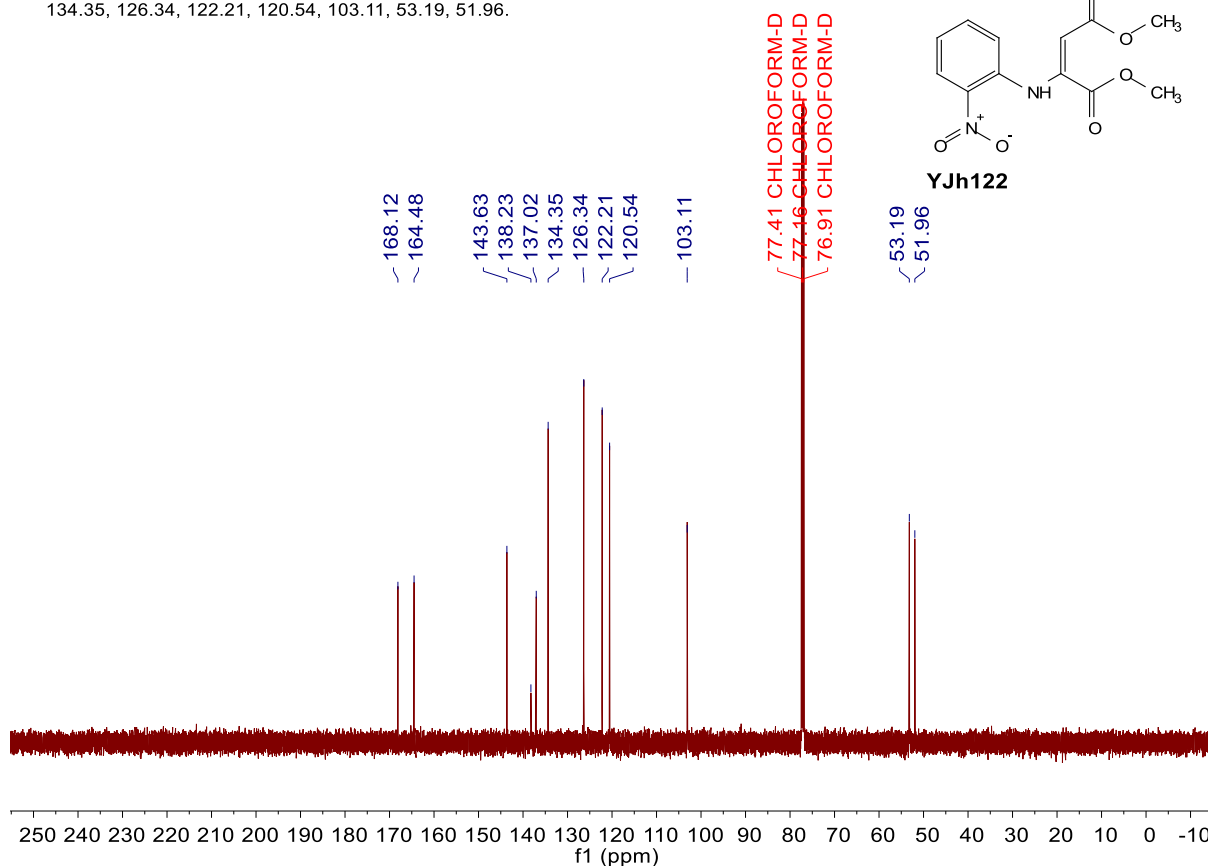
^{13}C NMR (126 MHz, $\text{DMSO-}d_6$) δ 165.05, 145.75, 138.81, 138.22, 136.51, 135.67, 133.95, 132.46, 131.46, 129.62, 129.15, 122.64, 121.01, 114.81.



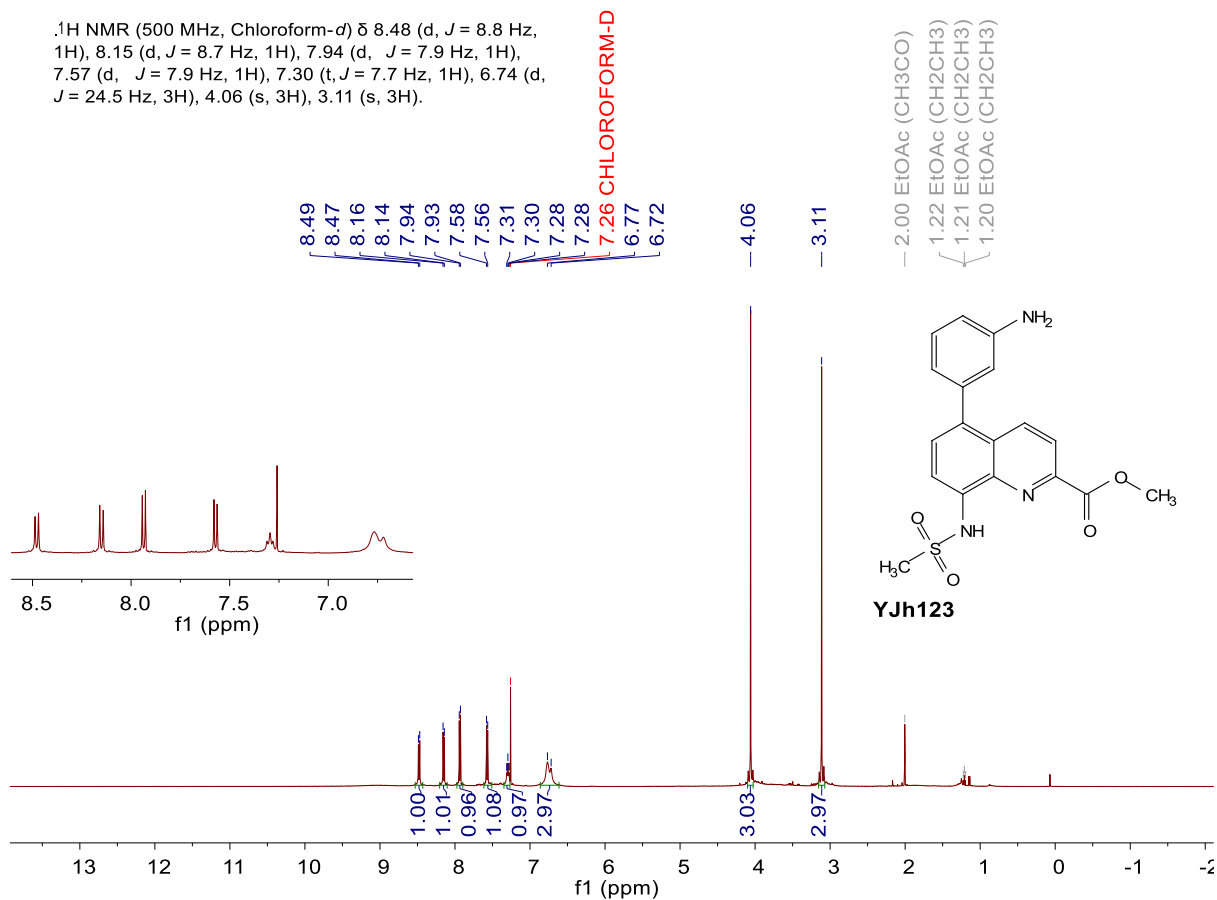
^1H NMR (500 MHz, Chloroform- d) δ 11.11 (s, 1H), 8.13 (dd, $J = 8.4, 1.6$ Hz, 1H), 7.46 (ddd, $J = 8.3, 7.3, 1.6, 0.5$ Hz, 1H), 7.08 (ddd, $J = 8.4, 7.2, 1.2$ Hz, 1H), 6.76 (dd, $J = 8.4, 0.8$ Hz, 1H), 5.83 (s, 1H), 3.80 (s, 3H), 3.74 (s, 3H).



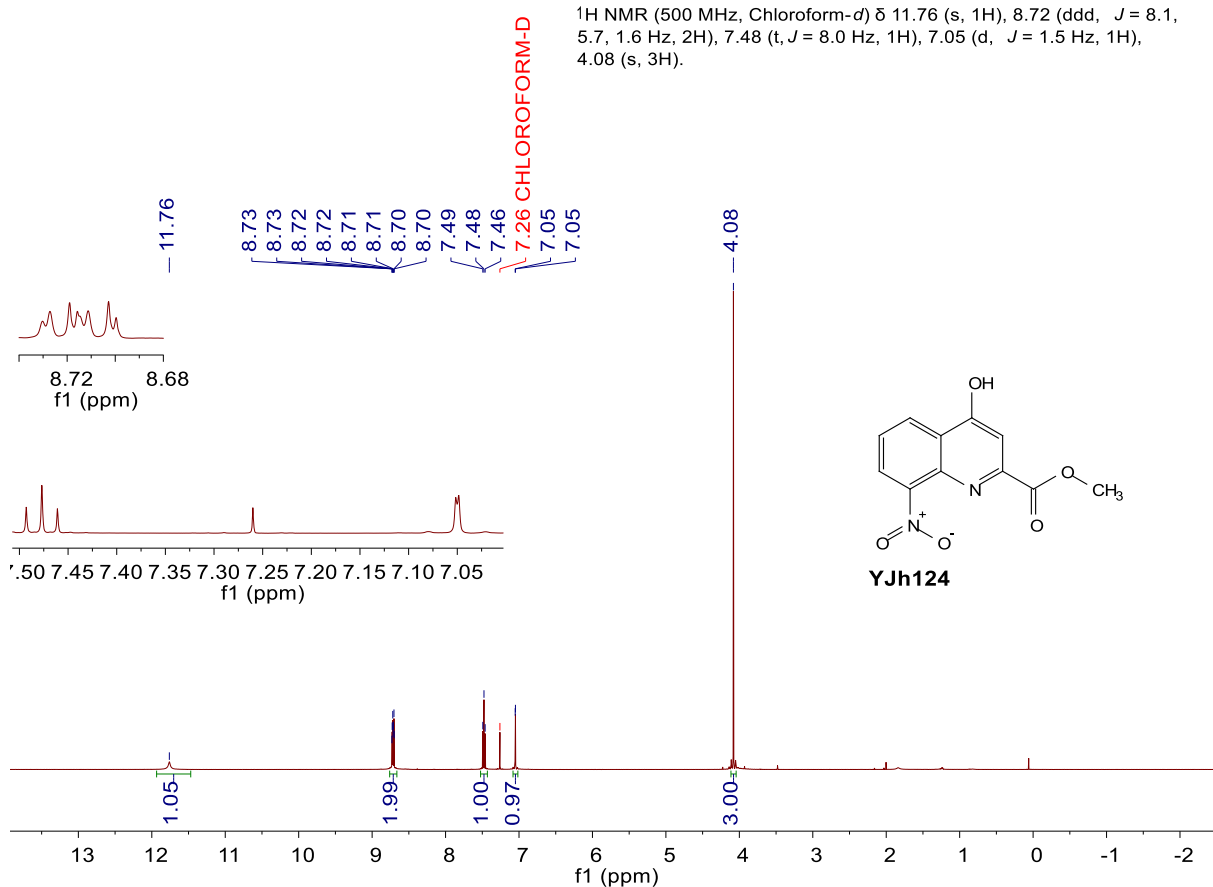
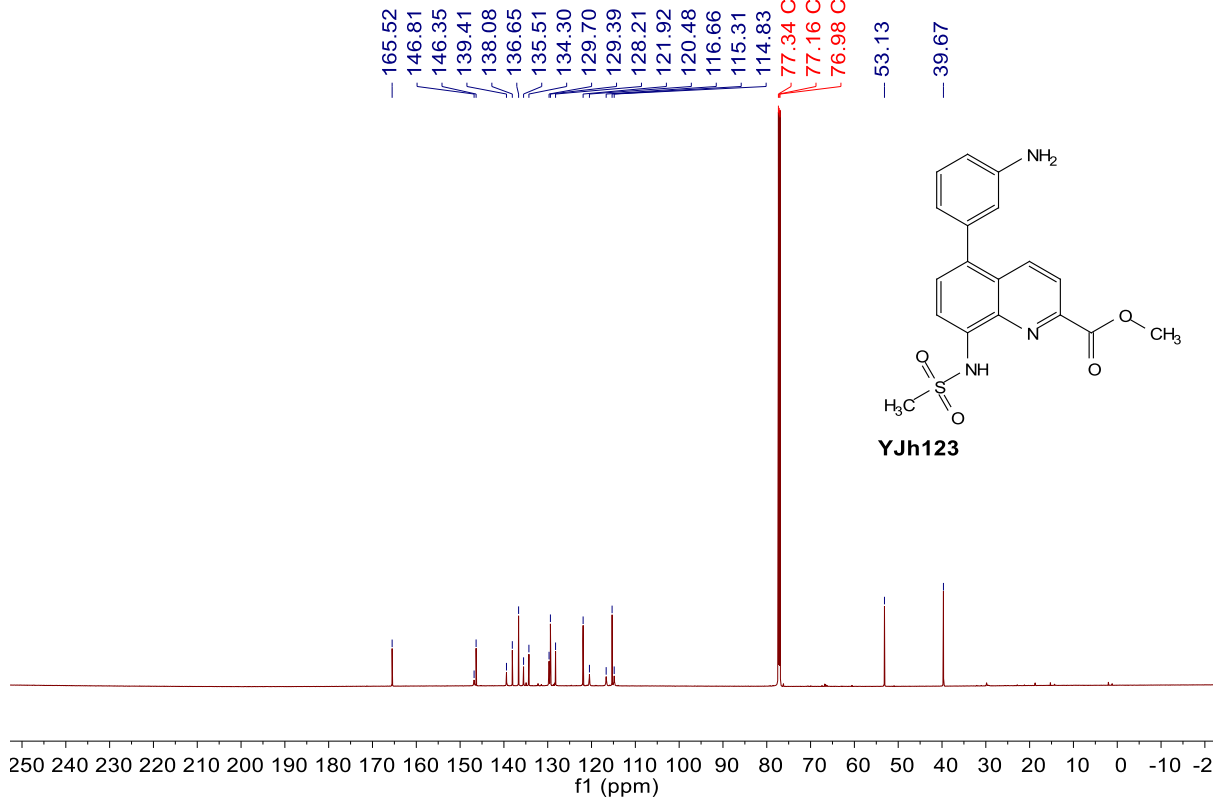
^{13}C NMR (126 MHz, Chloroform- d) δ 168.12, 164.48, 143.63, 138.23, 137.02, 134.35, 126.34, 122.21, 120.54, 103.11, 53.19, 51.96.



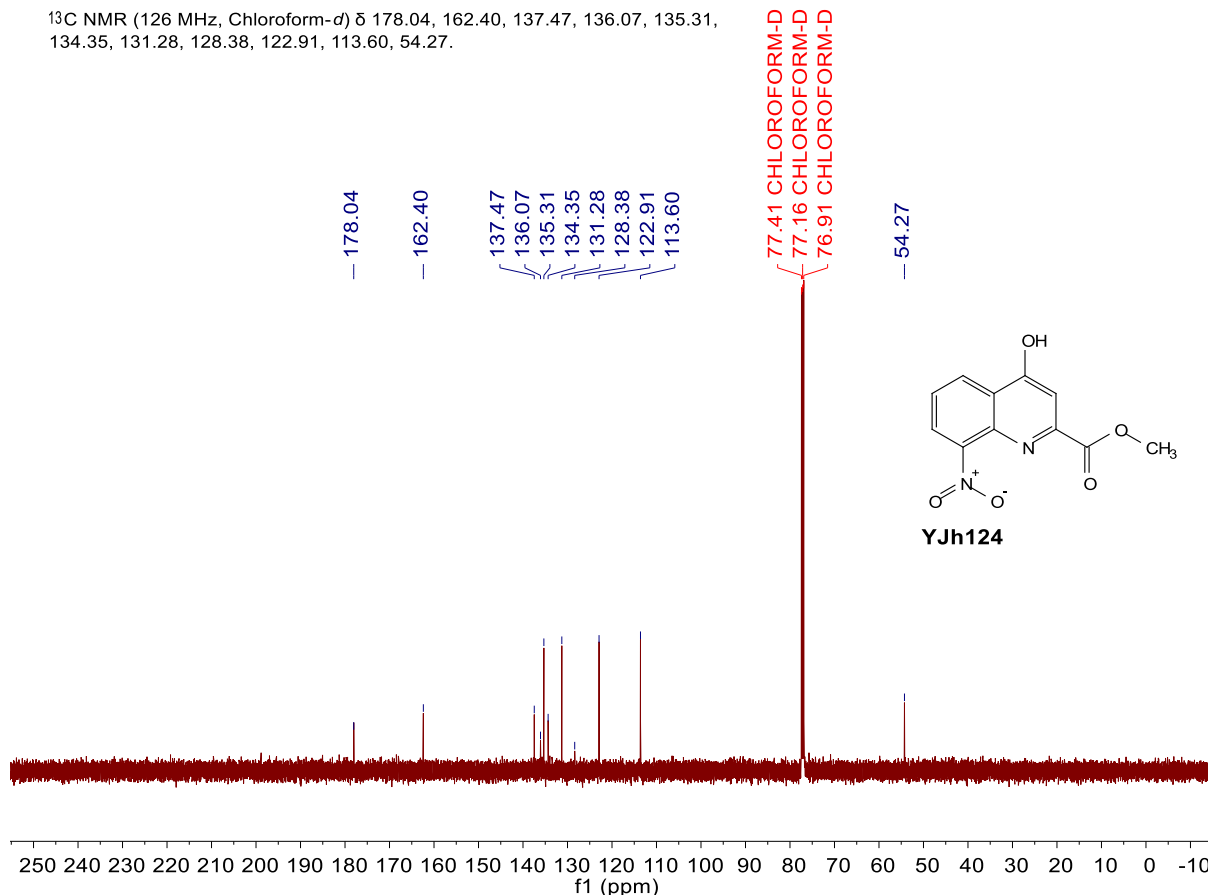
^1H NMR (500 MHz, Chloroform- d) δ 8.48 (d, J = 8.8 Hz, 1H), 8.15 (d, J = 8.7 Hz, 1H), 7.94 (d, J = 7.9 Hz, 1H), 7.57 (d, J = 7.9 Hz, 1H), 7.30 (t, J = 7.7 Hz, 1H), 6.74 (d, J = 24.5 Hz, 3H), 4.06 (s, 3H), 3.11 (s, 3H).



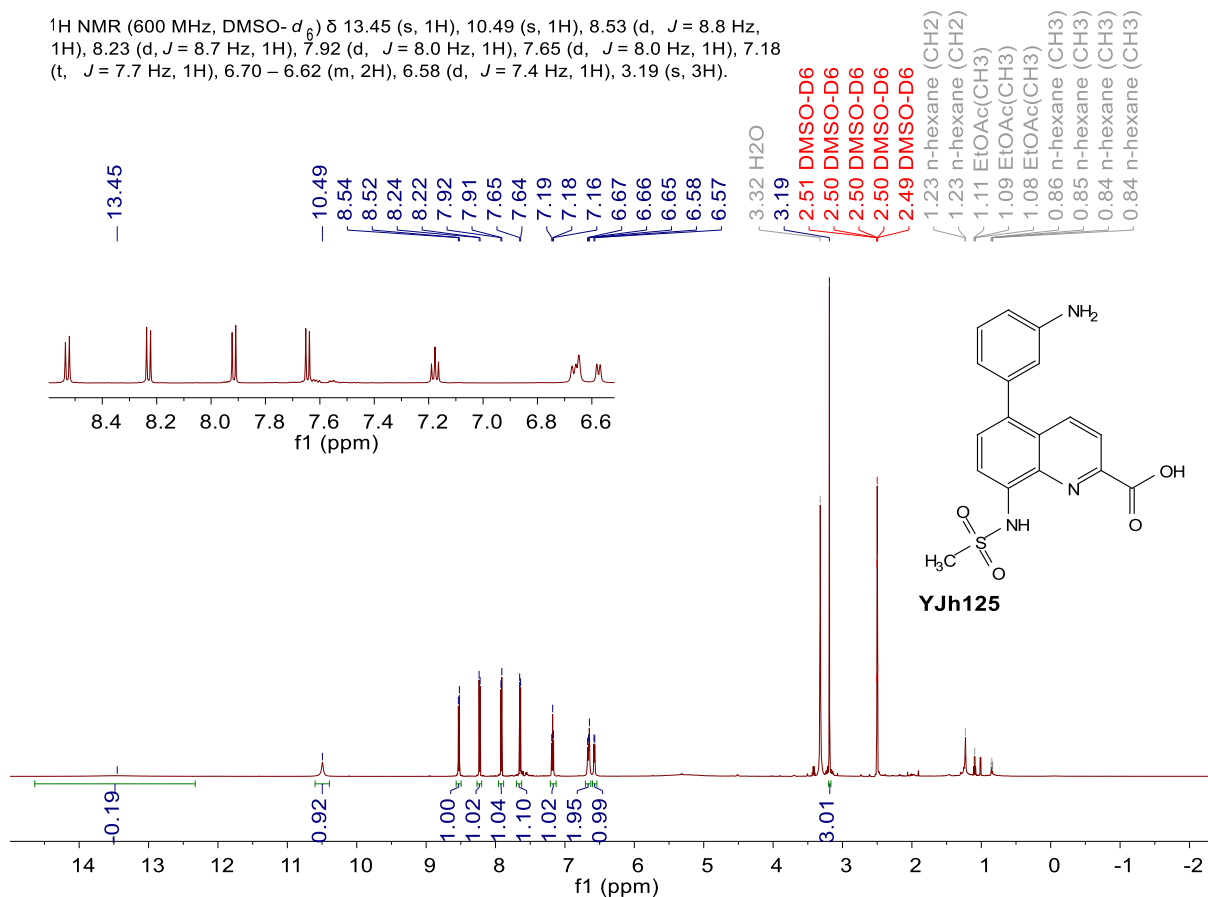
^{13}C NMR (176 MHz, Chloroform- d) δ 165.52, 146.81, 146.35, 139.41, 138.08, 136.65, 135.51, 134.30, 129.70, 129.39, 128.21, 121.92, 120.48, 116.66, 115.31, 114.83, 53.13, 39.67.



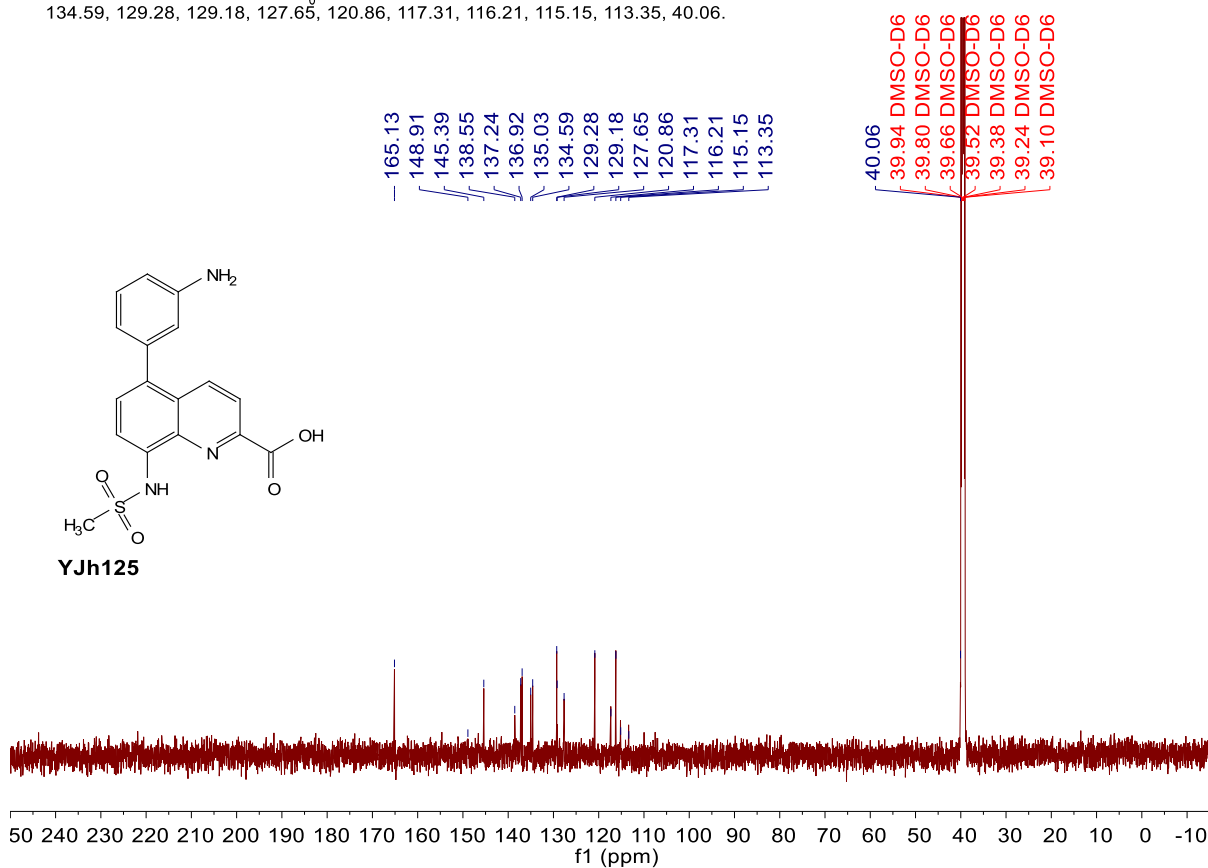
^{13}C NMR (126 MHz, Chloroform- d) δ 178.04, 162.40, 137.47, 136.07, 135.31, 134.35, 131.28, 128.38, 122.91, 113.60, 54.27.



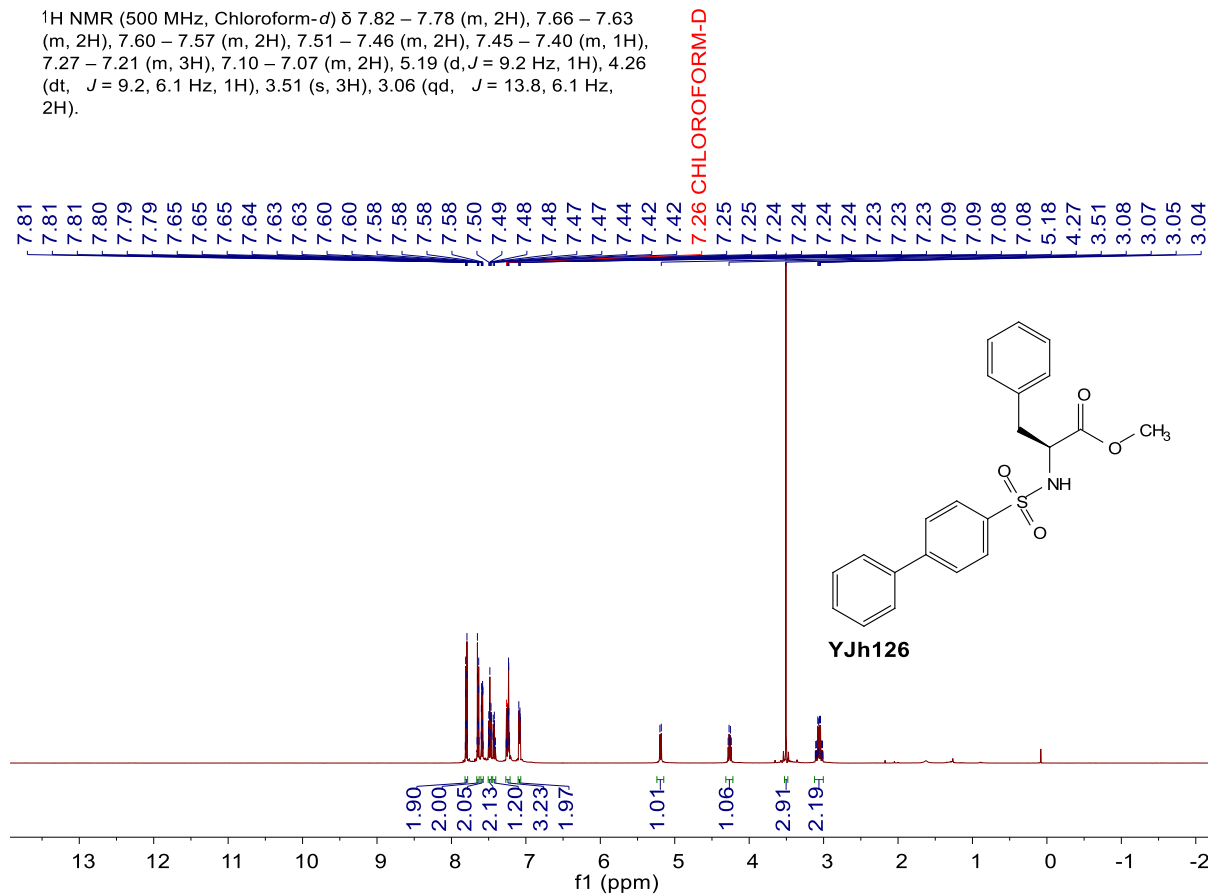
^1H NMR (600 MHz, DMSO- d_6) δ 13.45 (s, 1H), 10.49 (s, 1H), 8.53 (d, $J = 8.8$ Hz, 1H), 8.23 (d, $J = 8.7$ Hz, 1H), 7.92 (d, $J = 8.0$ Hz, 1H), 7.65 (d, $J = 8.0$ Hz, 1H), 7.18 (t, $J = 7.7$ Hz, 1H), 6.70 – 6.62 (m, 2H), 6.58 (d, $J = 7.4$ Hz, 1H), 3.19 (s, 3H).



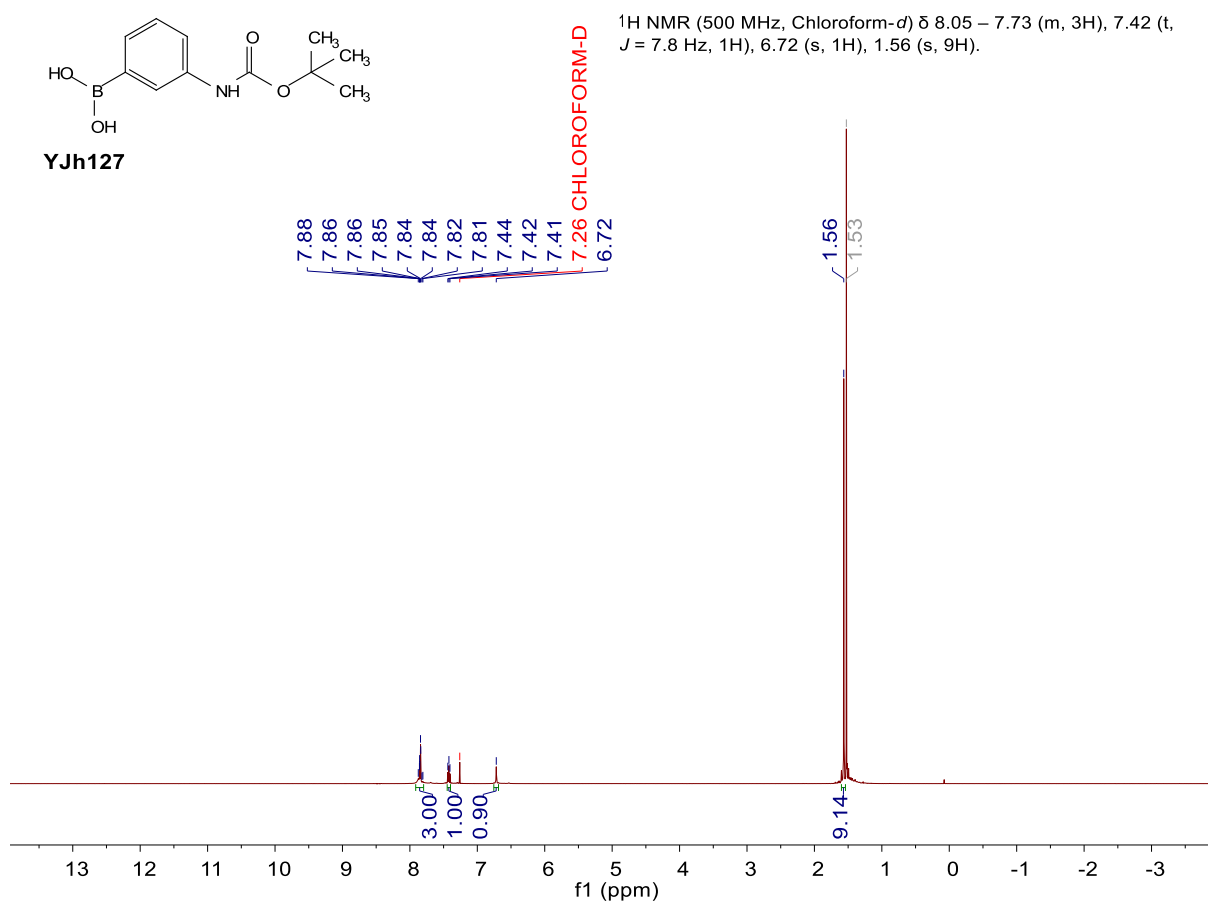
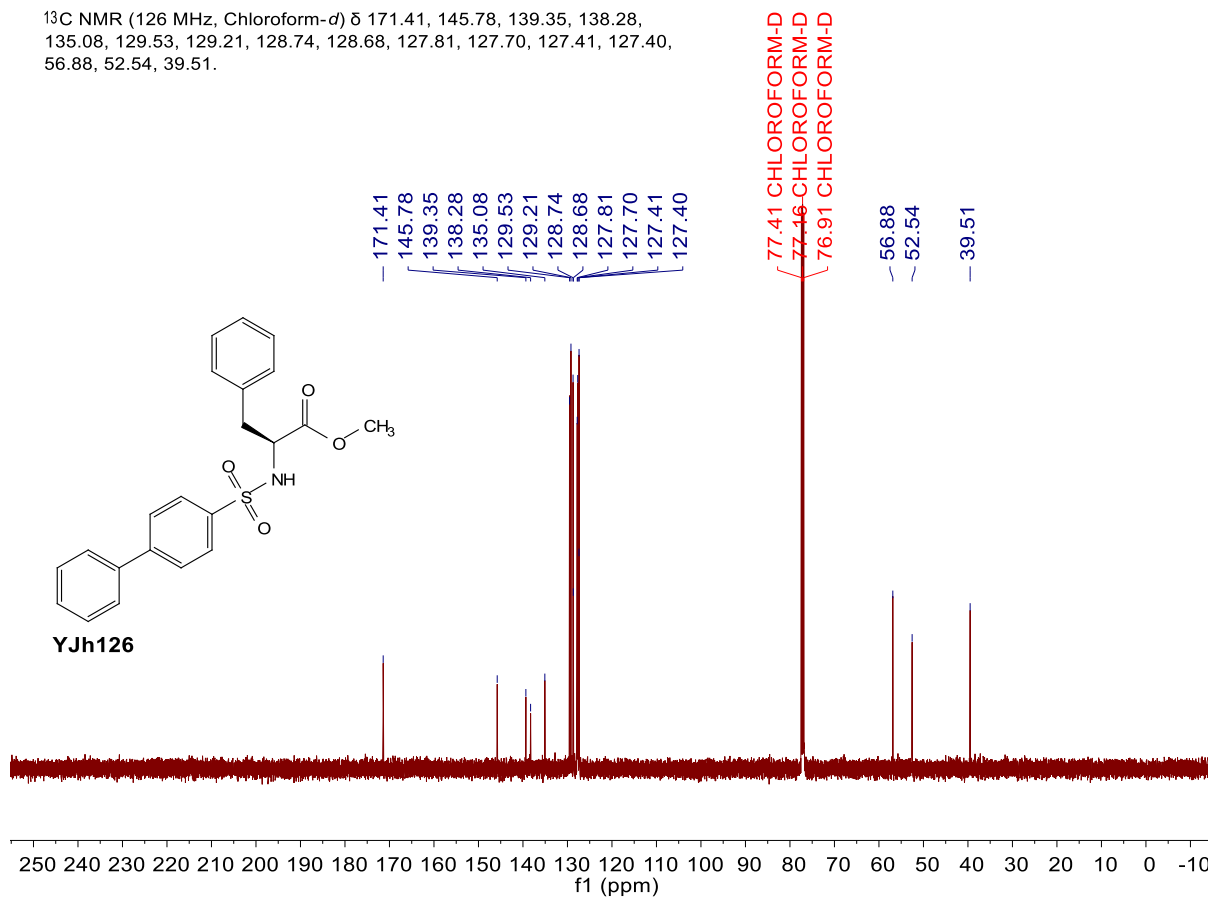
^{13}C NMR (151 MHz, $\text{DMSO-}d_6$) δ 165.13, 148.91, 145.39, 138.55, 137.24, 136.92, 135.03, 134.59, 129.28, 129.18, 127.65, 120.86, 117.31, 116.21, 115.15, 113.35, 40.06.



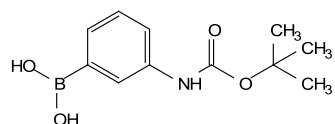
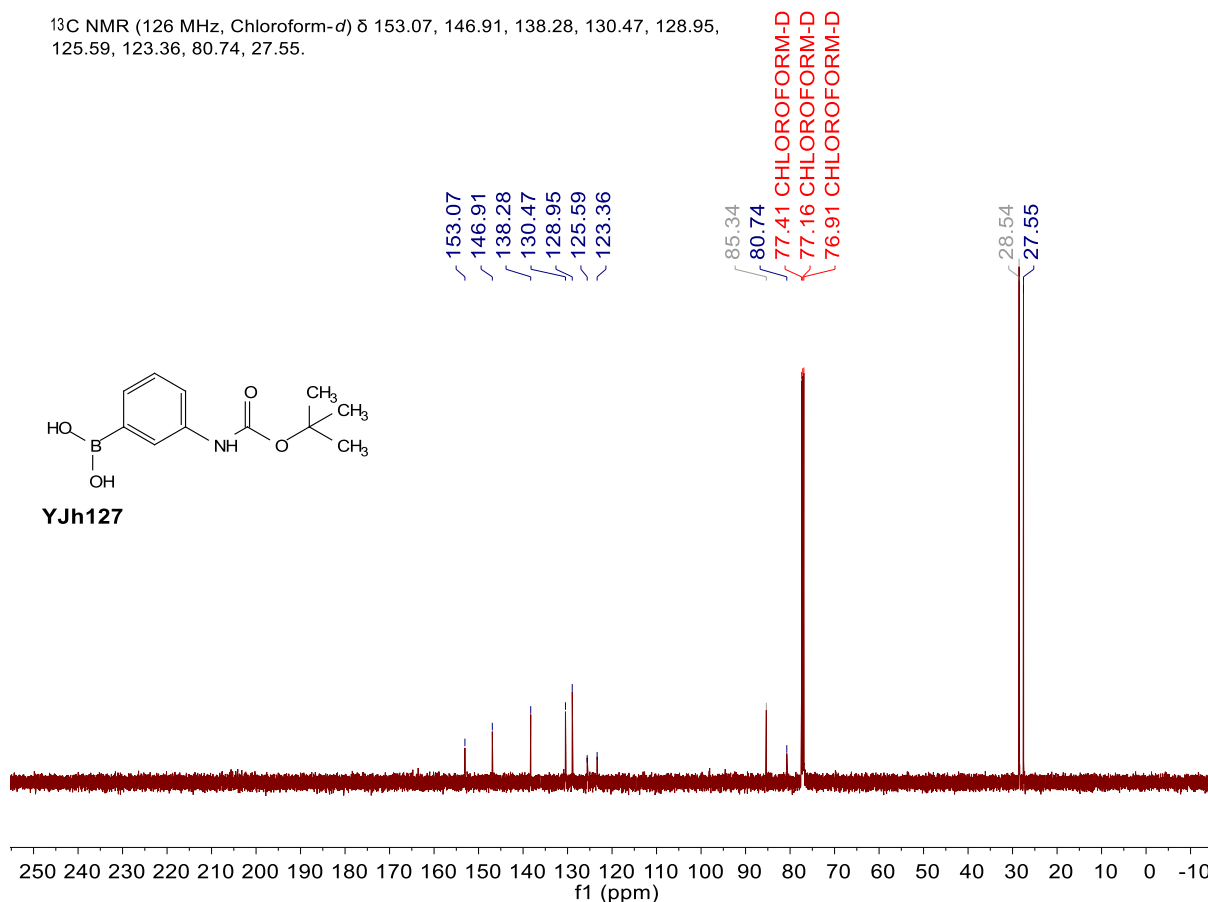
^1H NMR (500 MHz, $\text{Chloroform-}d$) δ 7.82 – 7.78 (m, 2H), 7.66 – 7.63 (m, 2H), 7.60 – 7.57 (m, 2H), 7.51 – 7.46 (m, 2H), 7.45 – 7.40 (m, 1H), 7.27 – 7.21 (m, 3H), 7.10 – 7.07 (m, 2H), 5.19 (d, $J = 9.2$ Hz, 1H), 4.26 (dt, $J = 9.2, 6.1$ Hz, 1H), 3.51 (s, 3H), 3.06 (qd, $J = 13.8, 6.1$ Hz, 2H).



^{13}C NMR (126 MHz, Chloroform-*d*) δ 171.41, 145.78, 139.35, 138.28, 135.08, 129.53, 129.21, 128.74, 128.68, 127.81, 127.70, 127.41, 127.40, 56.88, 52.54, 39.51.

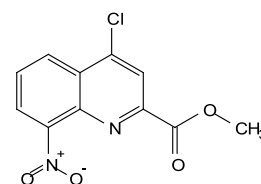
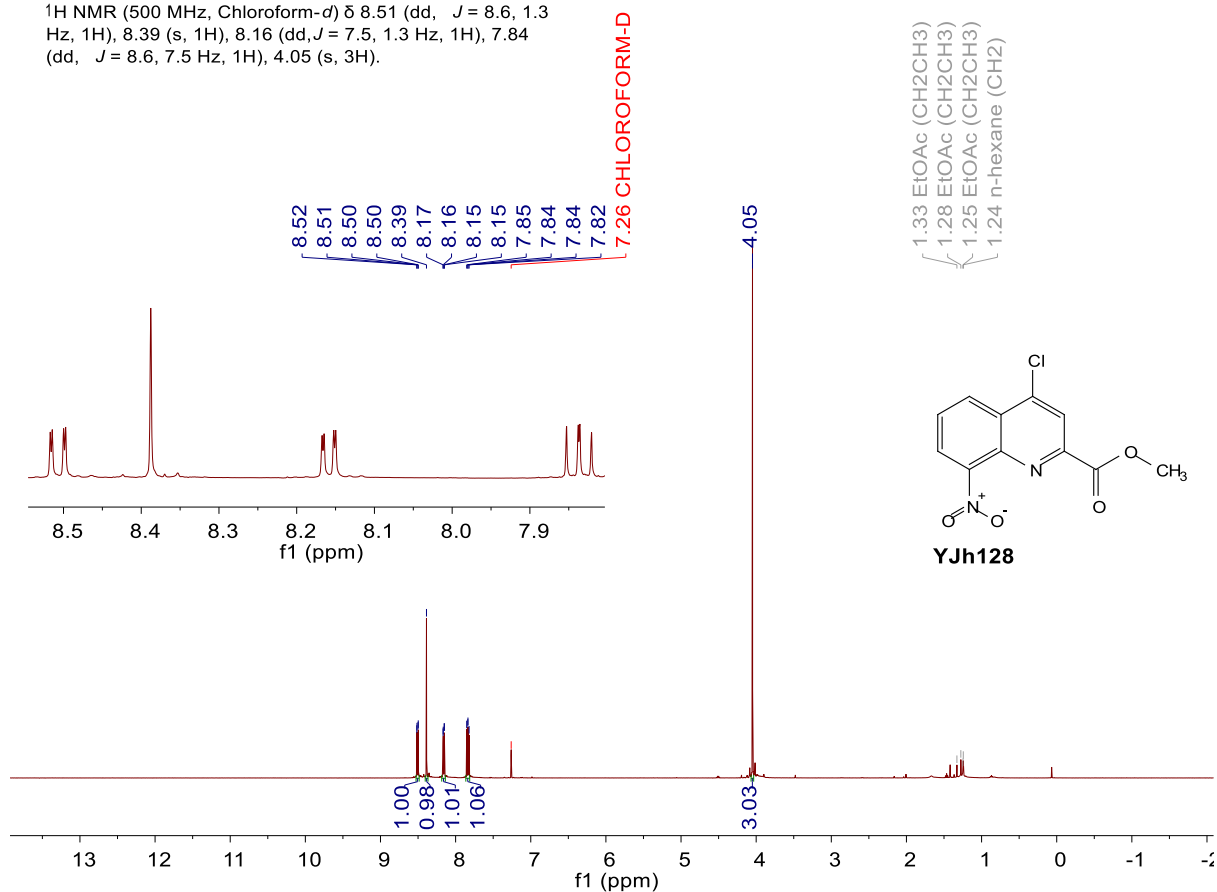


¹³C NMR (126 MHz, Chloroform-*d*) δ 153.07, 146.91, 138.28, 130.47, 128.95, 125.59, 123.36, 80.74, 27.55.



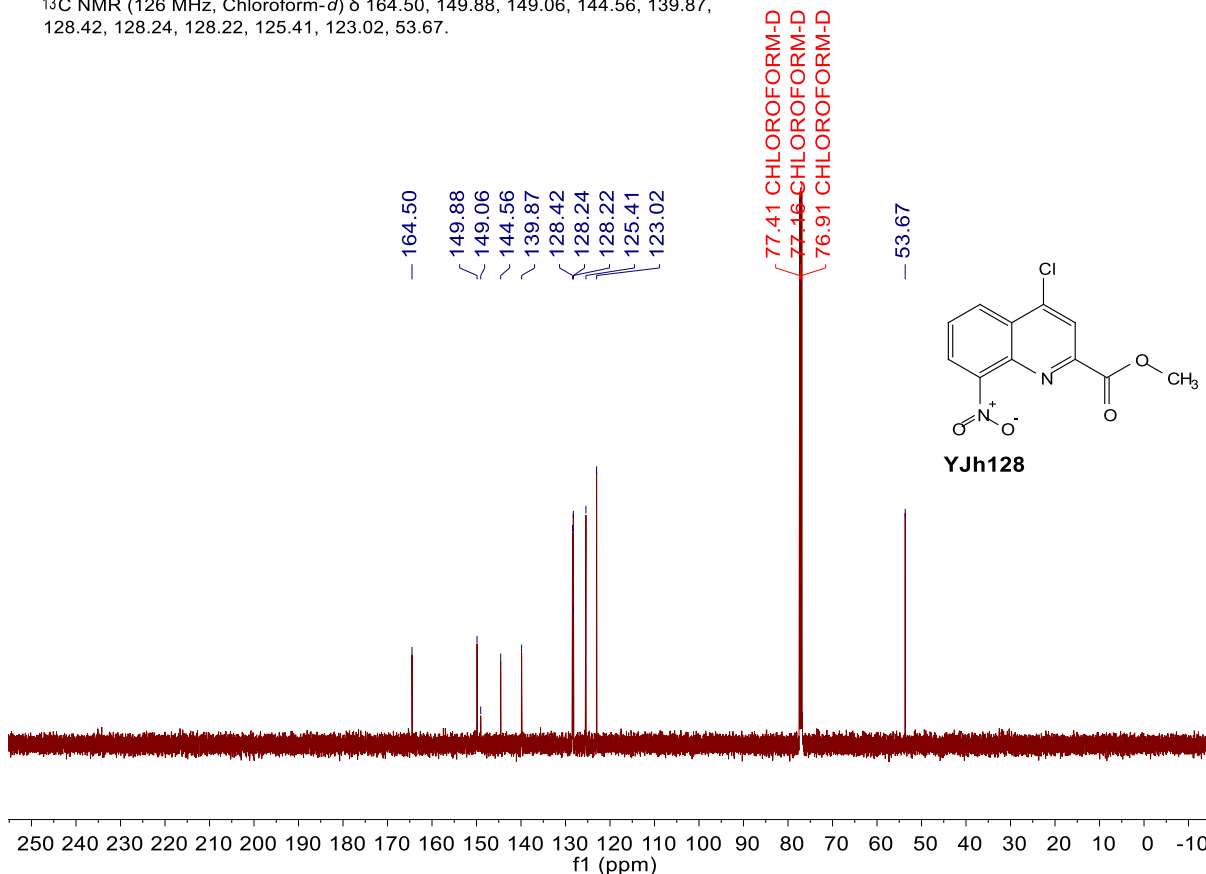
YJh127

¹H NMR (500 MHz, Chloroform-*d*) δ 8.51 (dd, *J* = 8.6, 1.3 Hz, 1H), 8.39 (s, 1H), 8.16 (dd, *J* = 7.5, 1.3 Hz, 1H), 7.84 (dd, *J* = 8.6, 7.5 Hz, 1H), 4.05 (s, 3H).

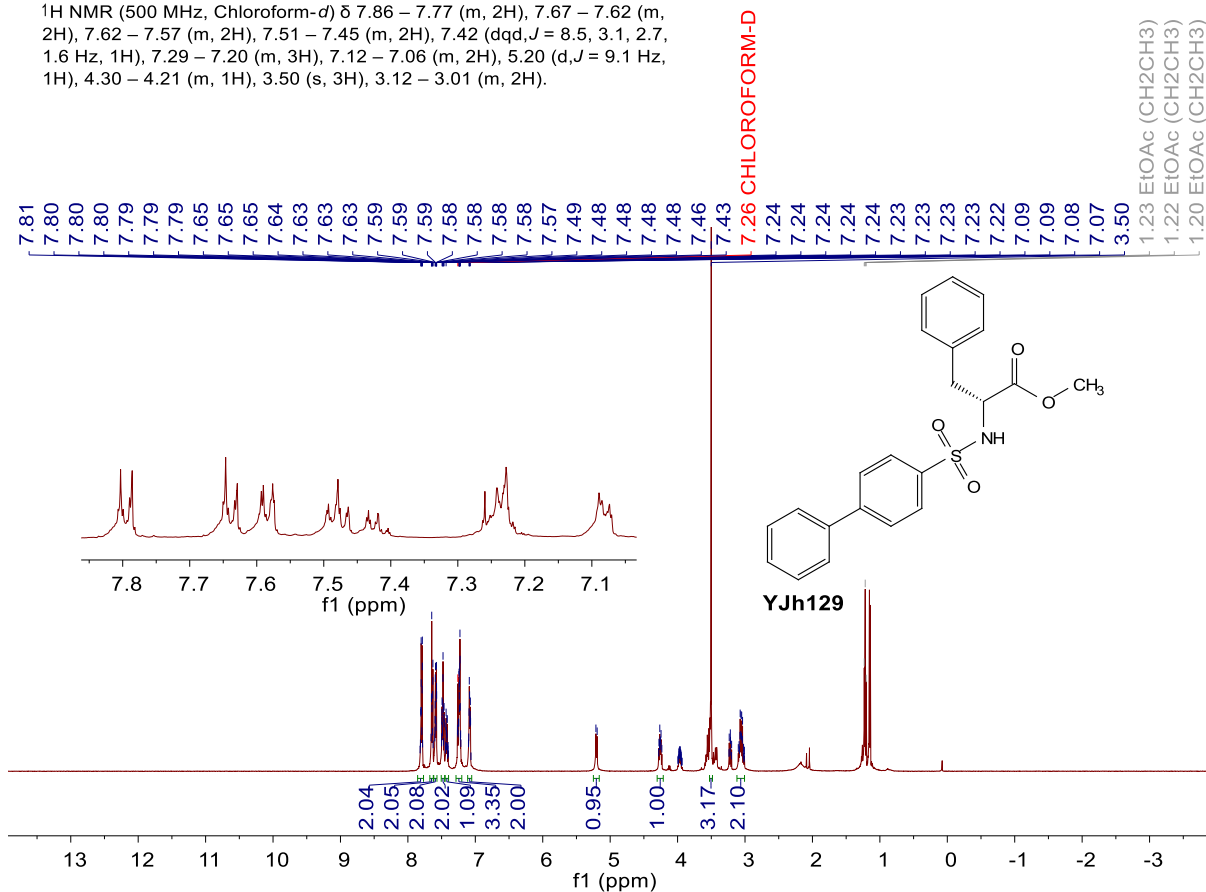


YJh128

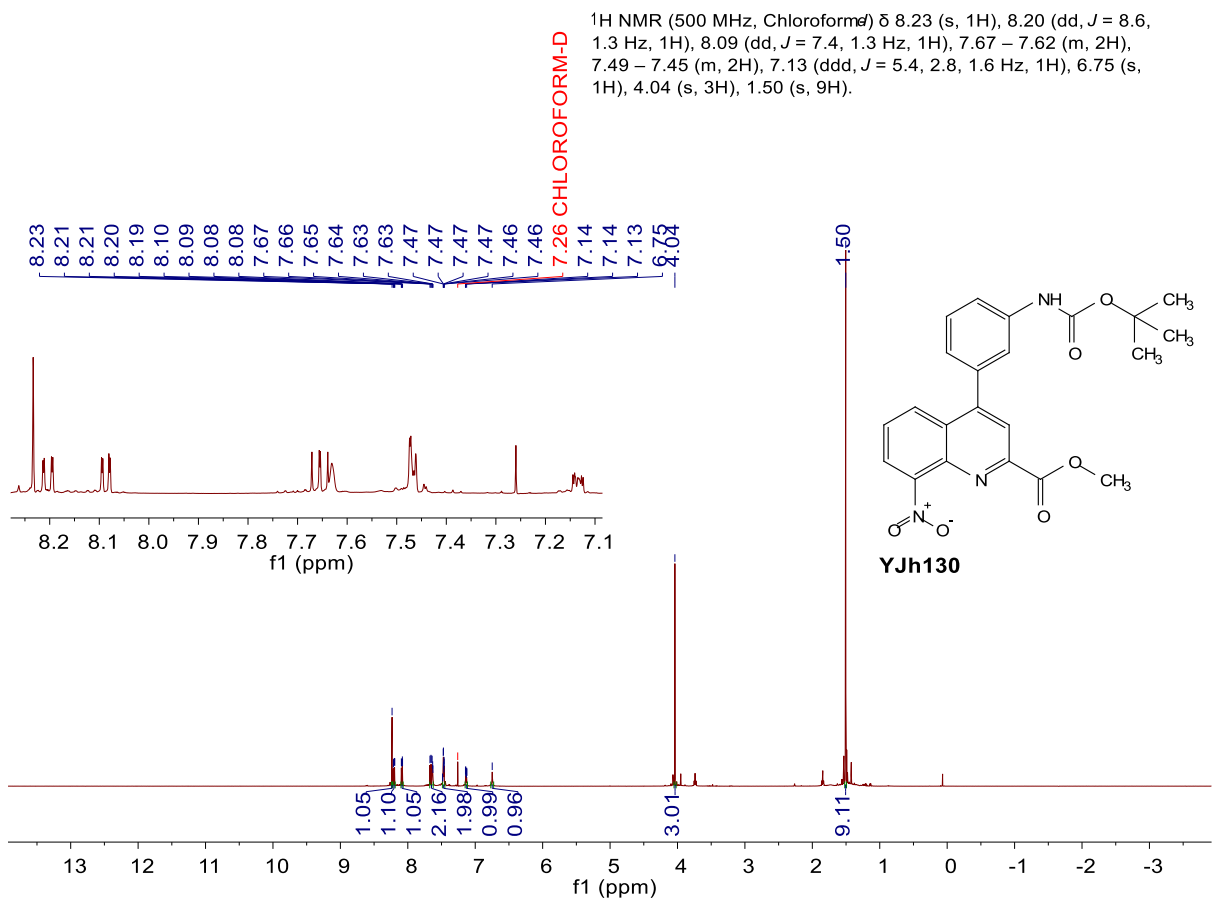
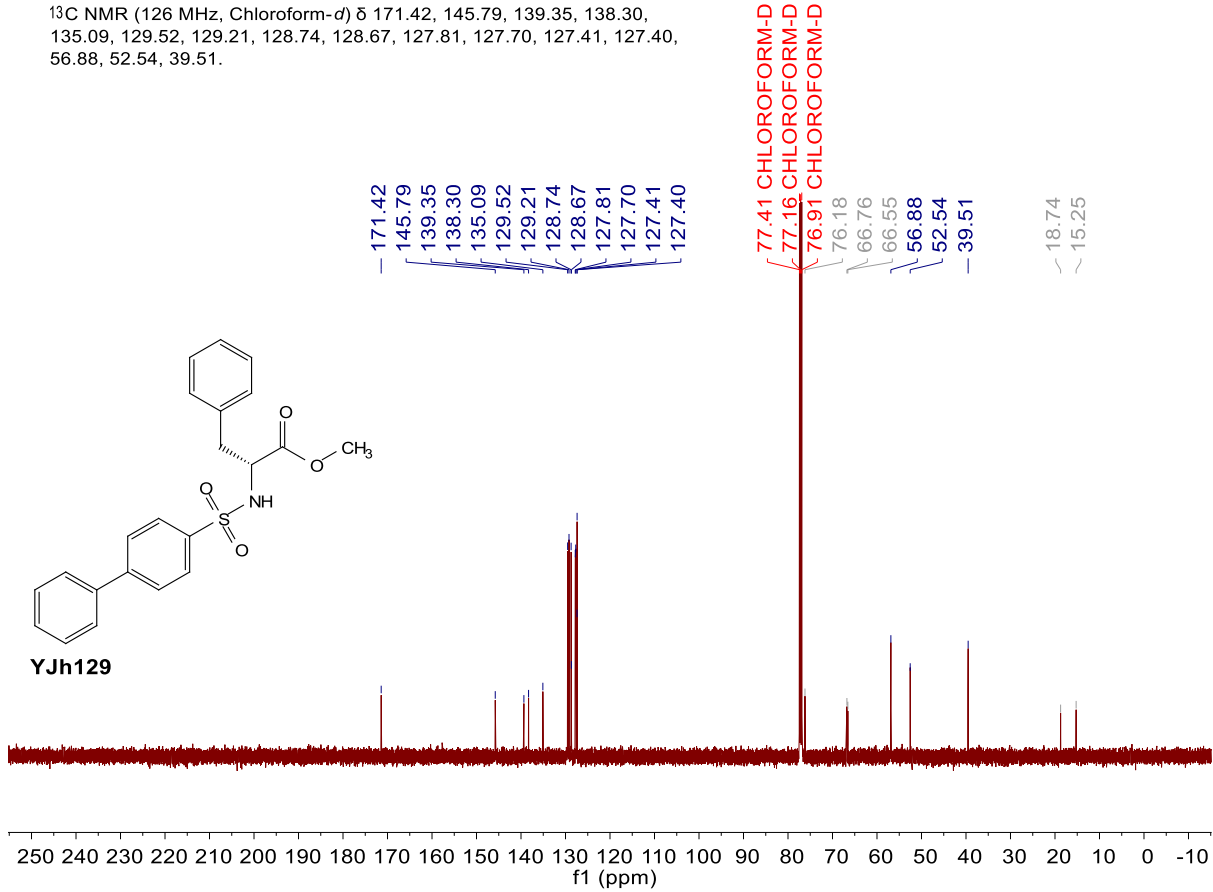
¹³C NMR (126 MHz, Chloroform-*d*) δ 164.50, 149.88, 149.06, 144.56, 139.87, 128.42, 128.24, 128.22, 125.41, 123.02, 53.67.



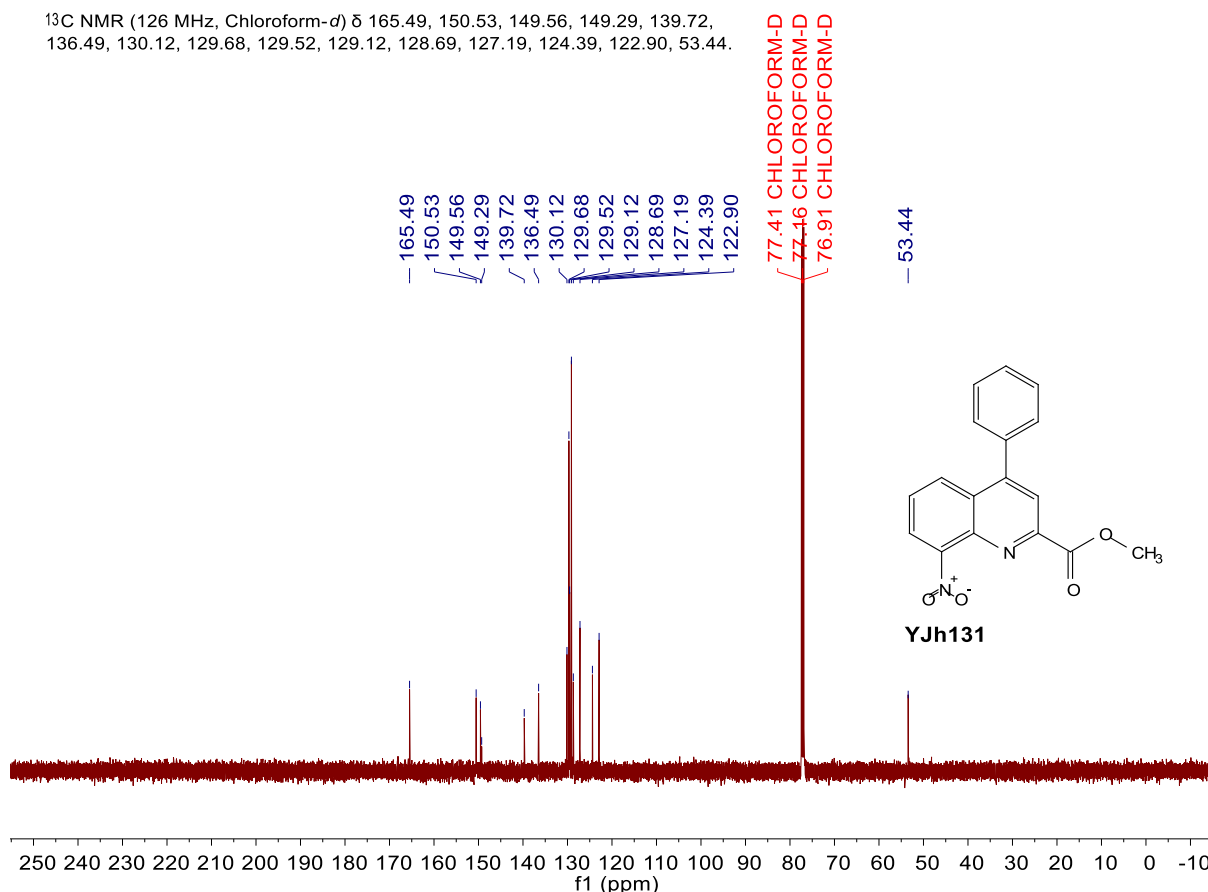
¹H NMR (500 MHz, Chloroform-*d*) δ 7.86 – 7.77 (m, 2H), 7.67 – 7.62 (m, 2H), 7.62 – 7.57 (m, 2H), 7.51 – 7.45 (m, 2H), 7.42 (dq, *J* = 8.5, 3.1, 2.7, 1.6 Hz, 1H), 7.29 – 7.20 (m, 3H), 7.12 – 7.06 (m, 2H), 5.20 (d, *J* = 9.1 Hz, 1H), 4.30 – 4.21 (m, 1H), 3.50 (s, 3H), 3.12 – 3.01 (m, 2H).



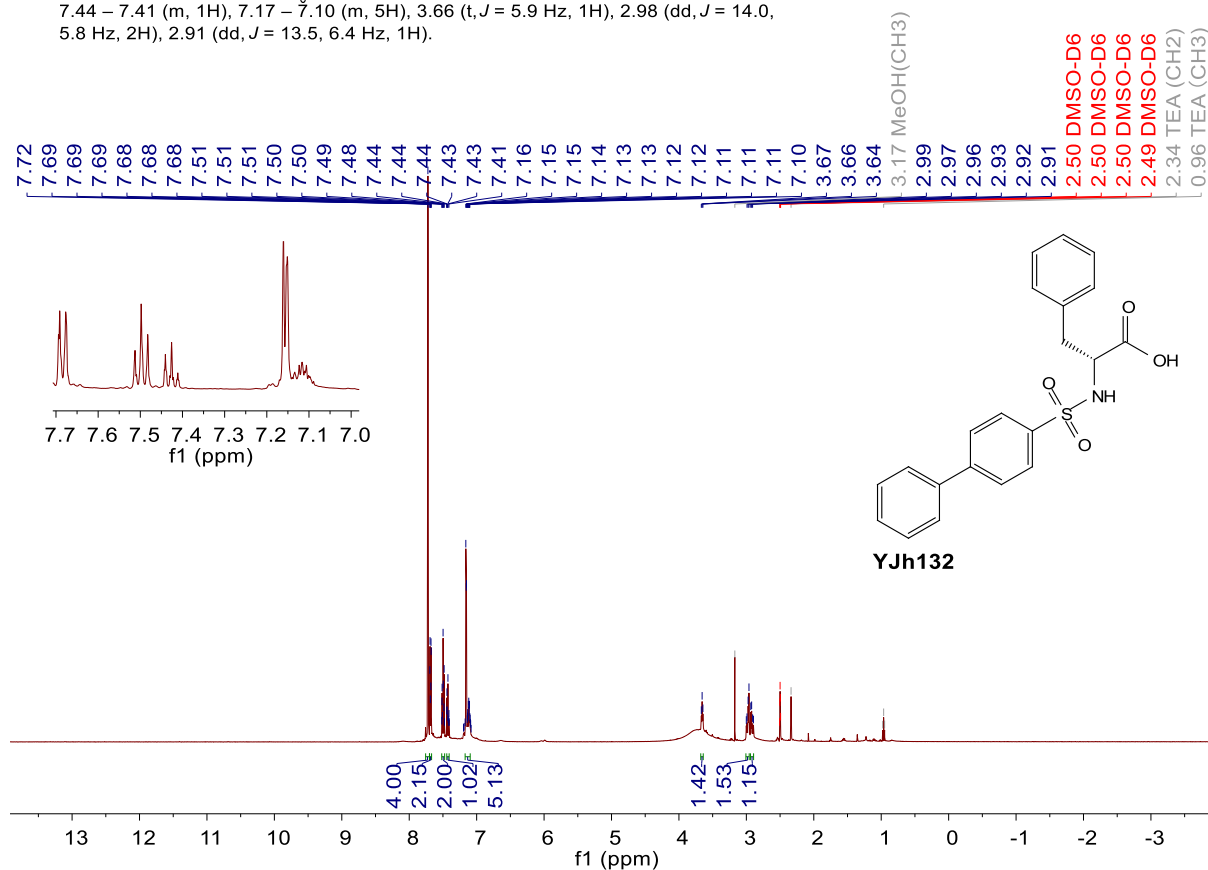
¹³C NMR (126 MHz, Chloroform-*d*) δ 171.42, 145.79, 139.35, 138.30, 135.09, 129.52, 129.21, 128.74, 128.67, 127.81, 127.70, 127.41, 127.40, 56.88, 52.54, 39.51.



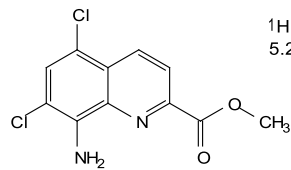
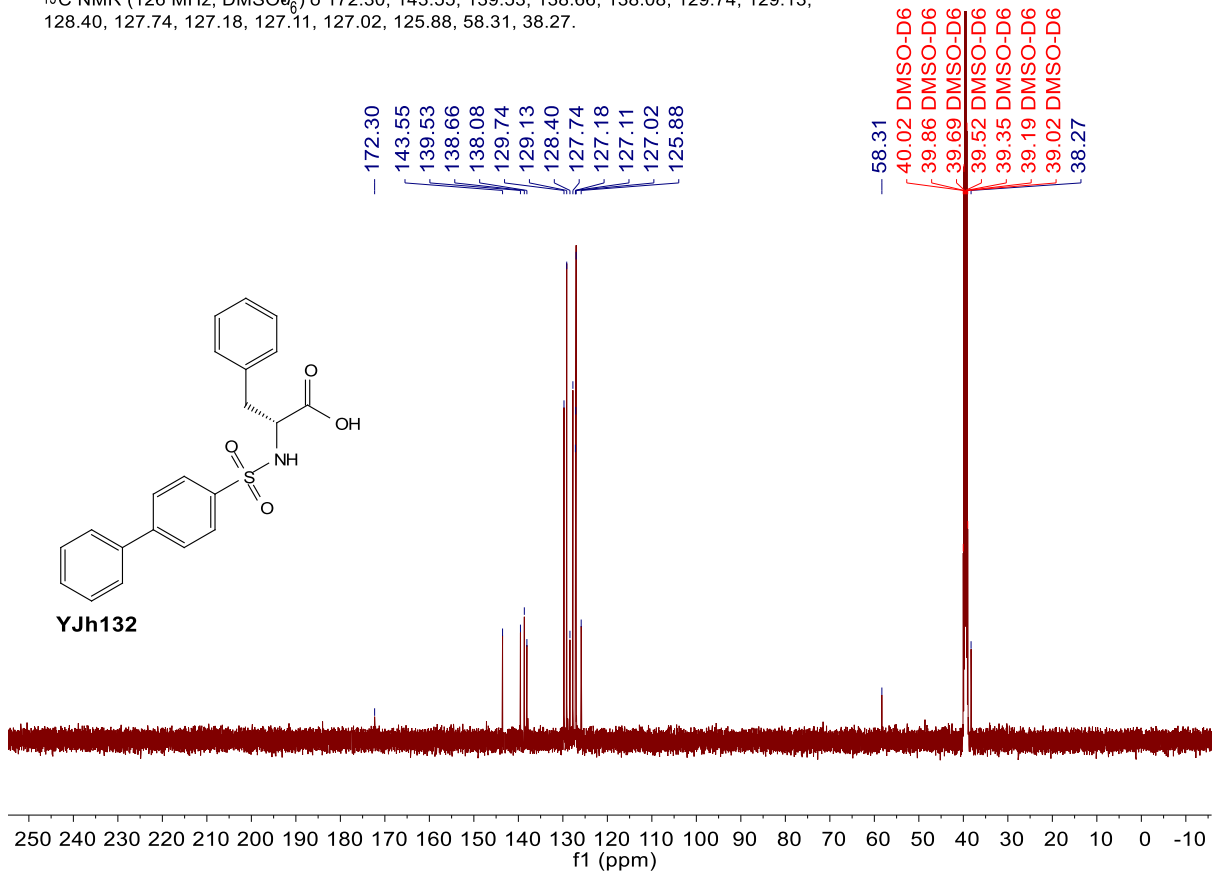
¹³C NMR (126 MHz, Chloroform-*d*) δ 165.49, 150.53, 149.56, 149.29, 139.72, 136.49, 130.12, 129.68, 129.52, 129.12, 128.69, 127.19, 124.39, 122.90.



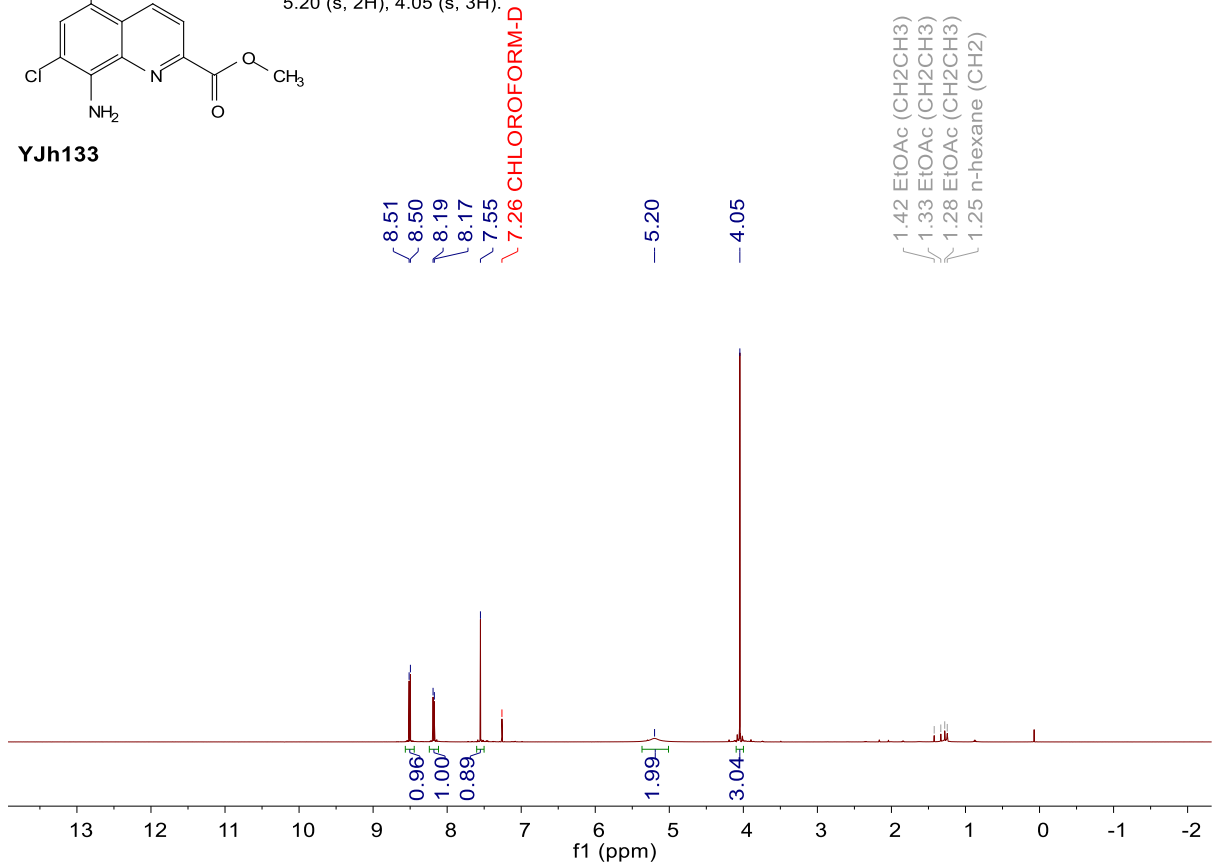
¹H NMR (500 MHz, DMSO-*d*₆) δ 7.72 (s, 4H), 7.70 – 7.67 (m, 2H), 7.52 – 7.47 (m, 2H), 7.44 – 7.41 (m, 1H), 7.17 – 7.10 (m, 5H), 3.66 (t, *J* = 5.9 Hz, 1H), 2.98 (dd, *J* = 14.0, 5.8 Hz, 2H), 2.91 (dd, *J* = 13.5, 6.4 Hz, 1H).



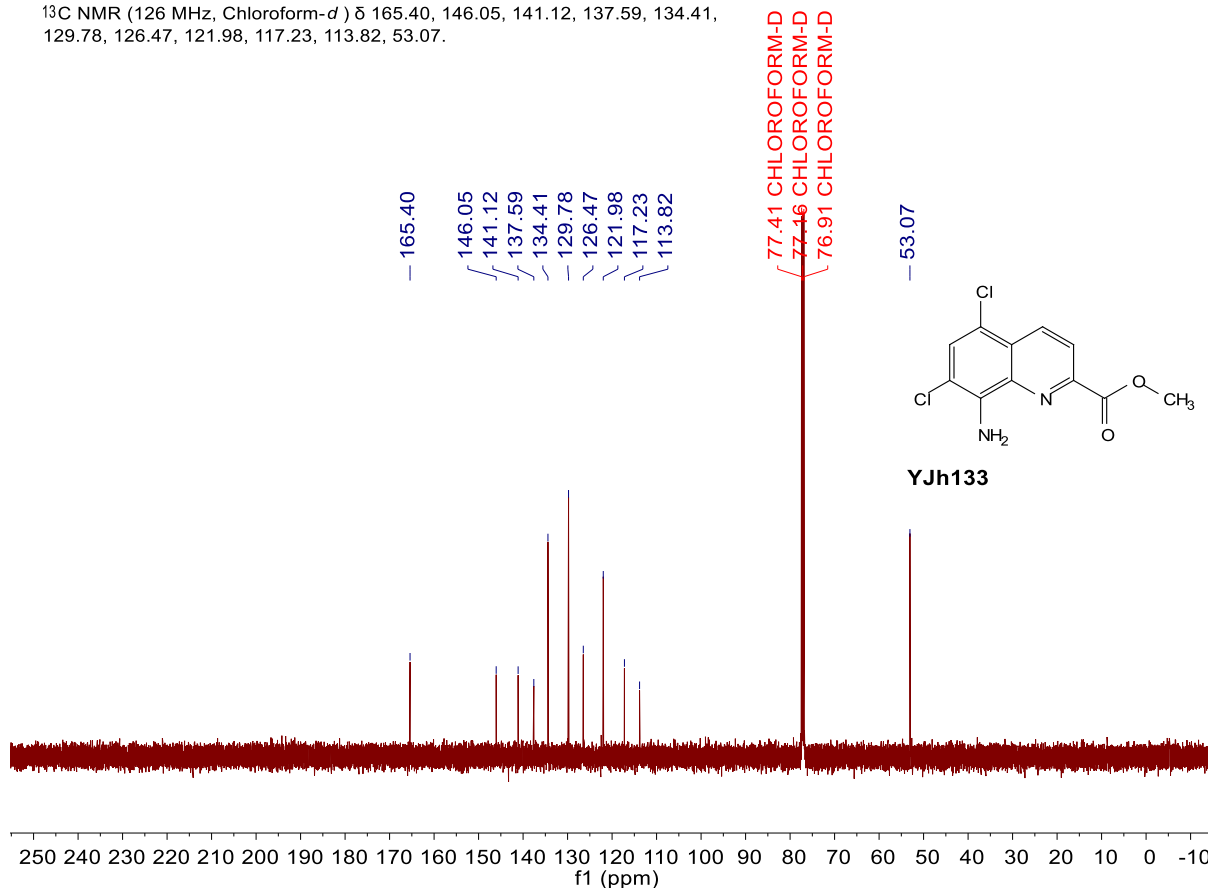
¹³C NMR (126 MHz, DMSO-d₆) δ 172.30, 143.55, 139.53, 138.66, 138.08, 129.74, 129.13, 128.40, 127.74, 127.18, 127.11, 127.02, 125.88.



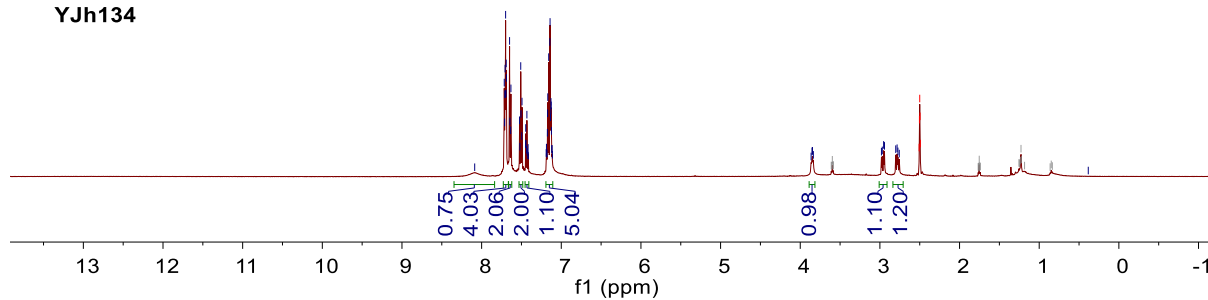
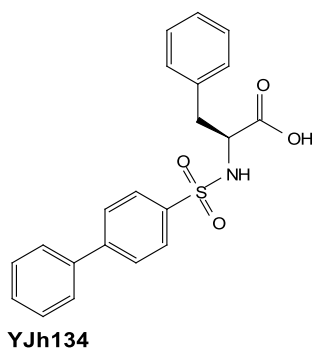
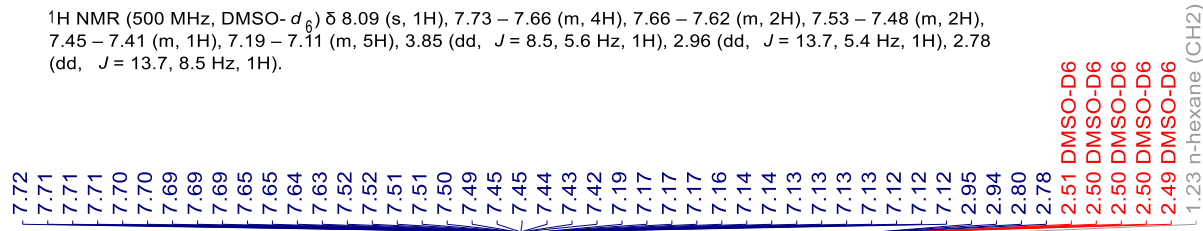
¹H NMR (500 MHz, Chloroform-d) δ 8.50 (d, *J* = 8.7 Hz, 1H), 8.18 (d, *J* = 8.7 Hz, 1H), 7.55 (s, 1H), 5.20 (s, 2H), 4.05 (s, 3H).



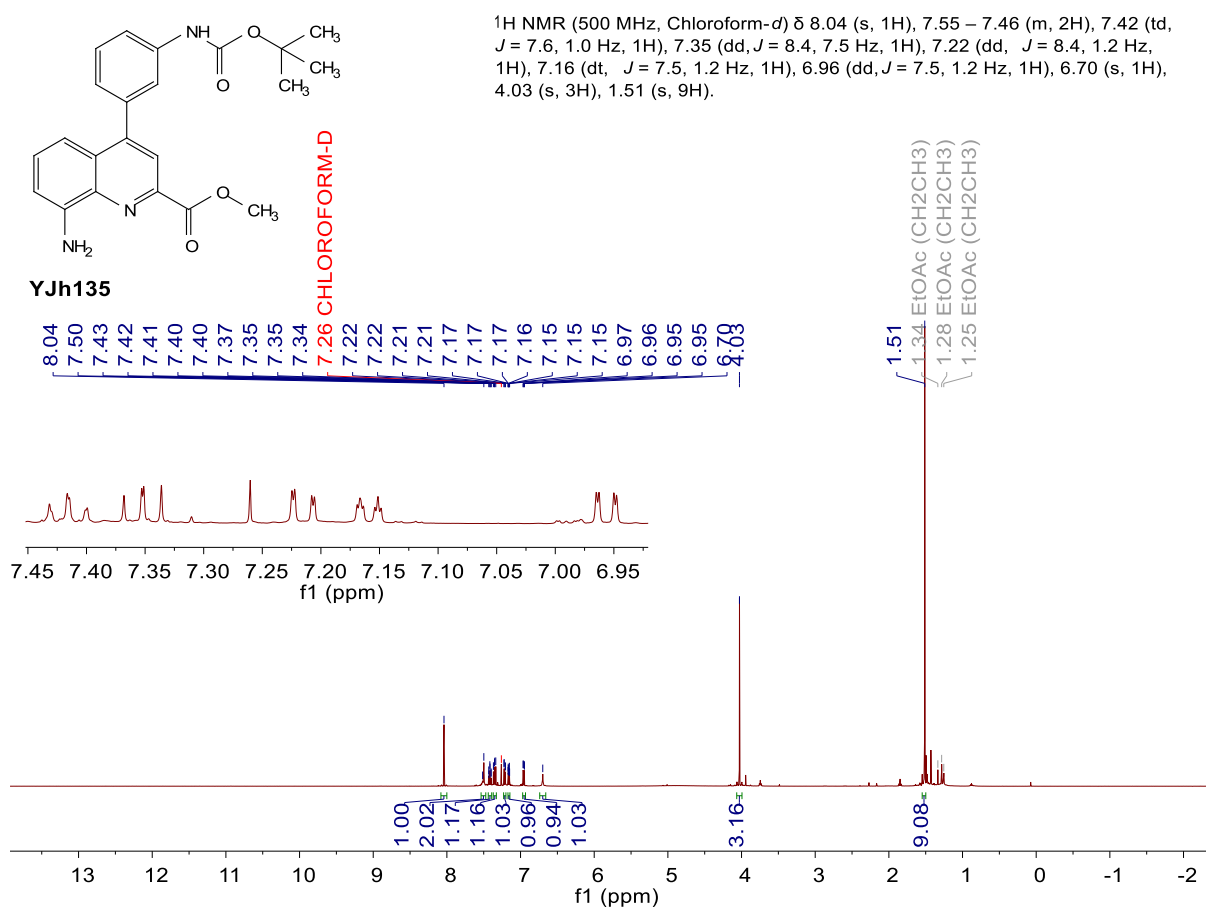
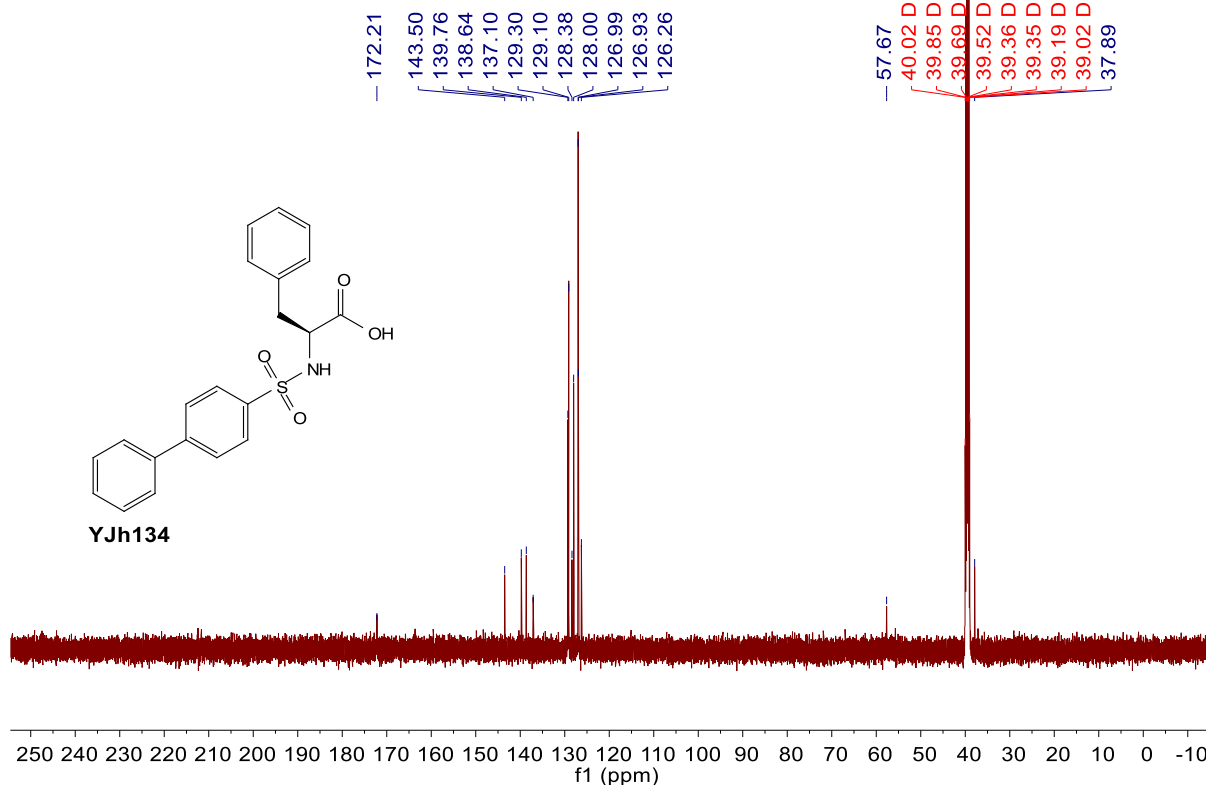
^{13}C NMR (126 MHz, Chloroform- d) δ 165.40, 146.05, 141.12, 137.59, 134.41, 129.78, 126.47, 121.98, 117.23, 113.82, 53.07.



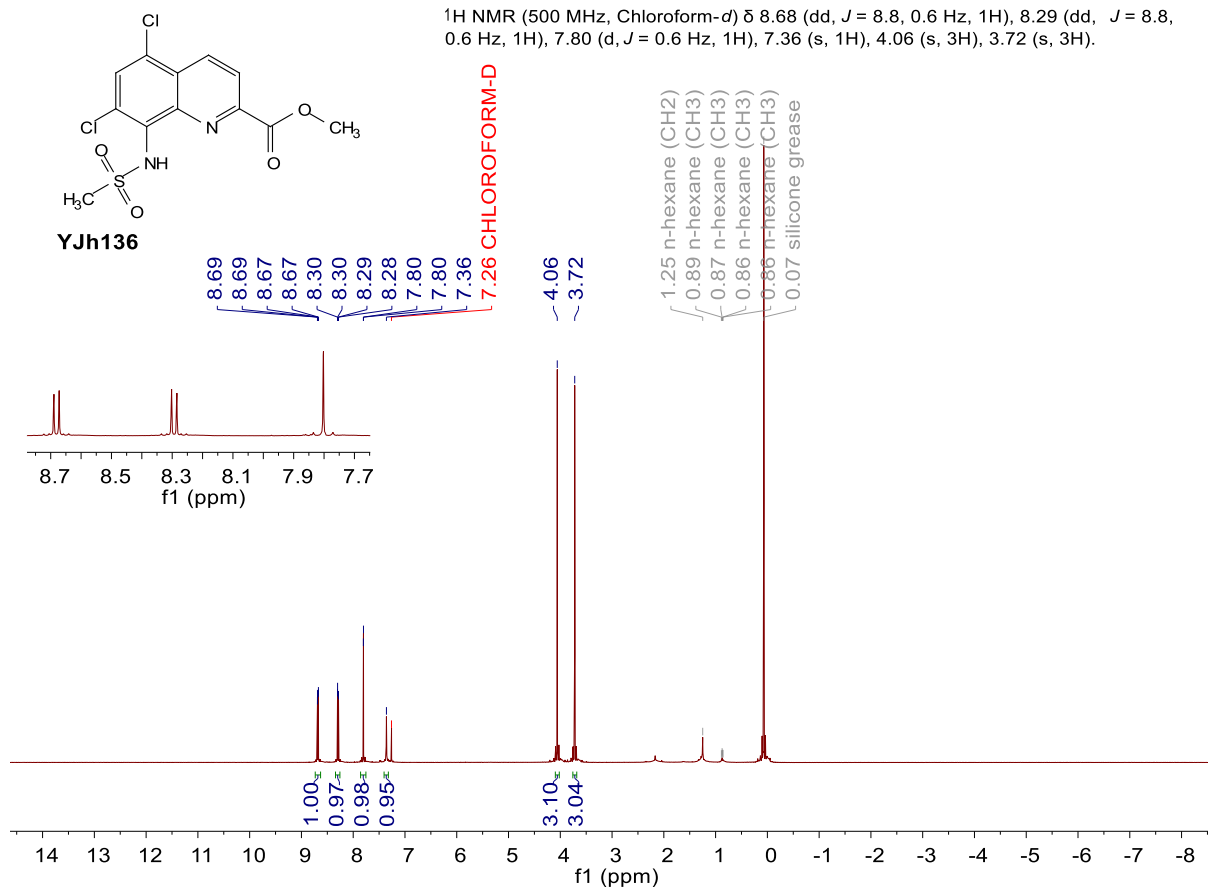
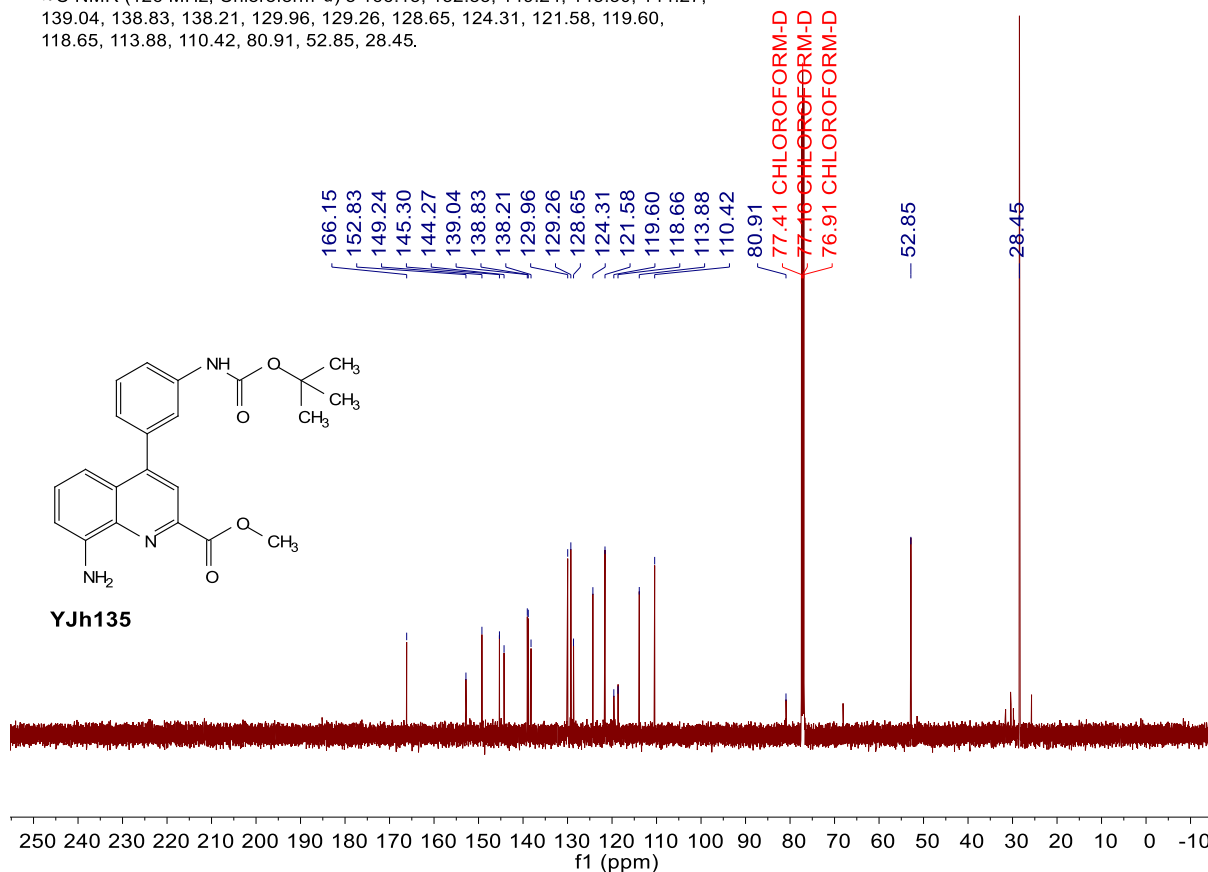
^1H NMR (500 MHz, DMSO- d_6) δ 8.09 (s, 1H), 7.73 – 7.66 (m, 4H), 7.66 – 7.62 (m, 2H), 7.53 – 7.48 (m, 2H), 7.45 – 7.41 (m, 1H), 7.19 – 7.11 (m, 5H), 3.85 (dd, J = 8.5, 5.6 Hz, 1H), 2.96 (dd, J = 13.7, 5.4 Hz, 1H), 2.78 (dd, J = 13.7, 8.5 Hz, 1H).



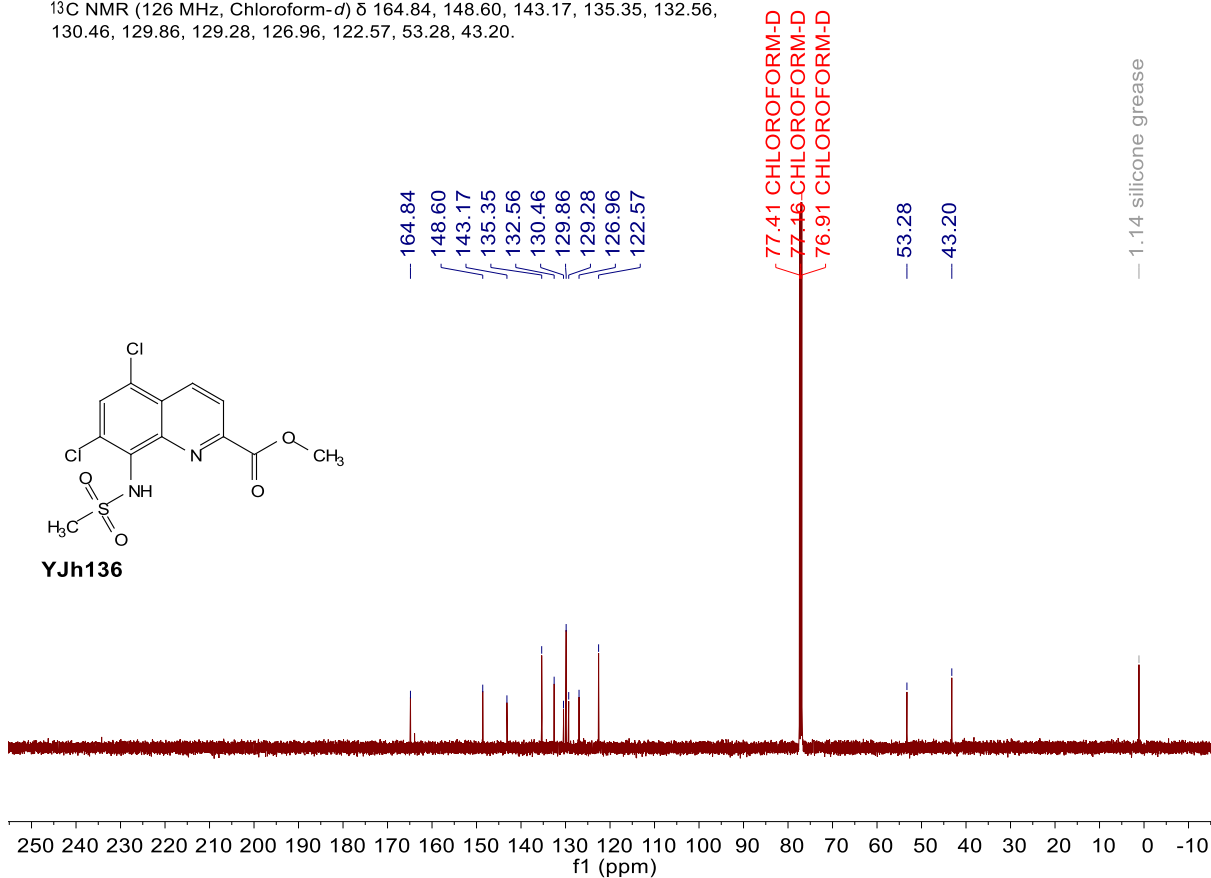
¹³C NMR (126 MHz, DMSO-*d*₆) δ 172.21, 143.50, 139.76, 138.64, 137.10, 129.30, 129.10, 128.38, 128.00, 126.99, 126.93, 126.26, 57.67, 37.89.



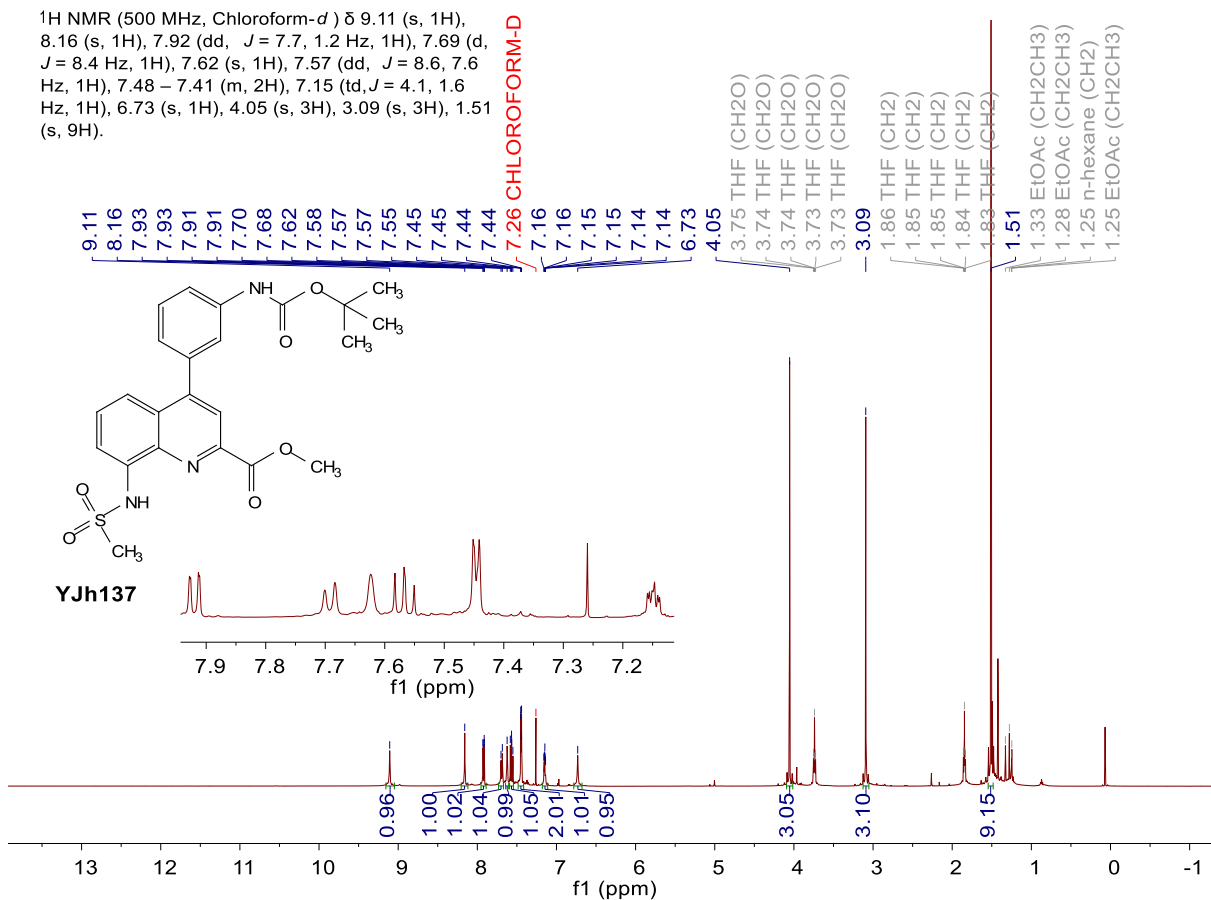
¹³C NMR (126 MHz, Chloroform-*d*) δ 166.15, 152.83, 149.24, 145.30, 144.27, 139.04, 138.83, 138.21, 129.96, 129.26, 128.65, 124.31, 121.58, 119.60, 118.66, 113.88, 110.42, 80.91, 52.85, 28.45.



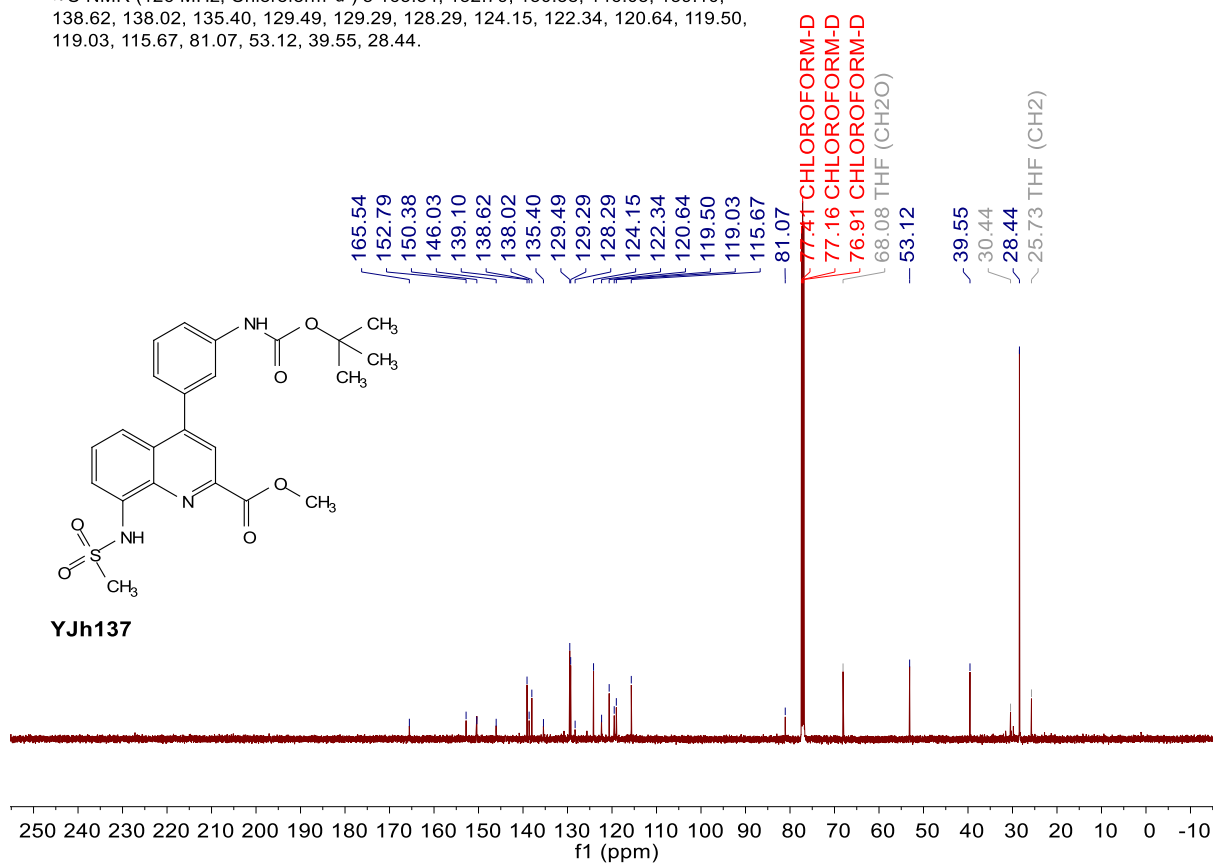
¹³C NMR (126 MHz, Chloroform-*d*) δ 164.84, 148.60, 143.17, 135.35, 132.56, 130.46, 129.86, 129.28, 126.96, 122.57, 53.28, 43.20.



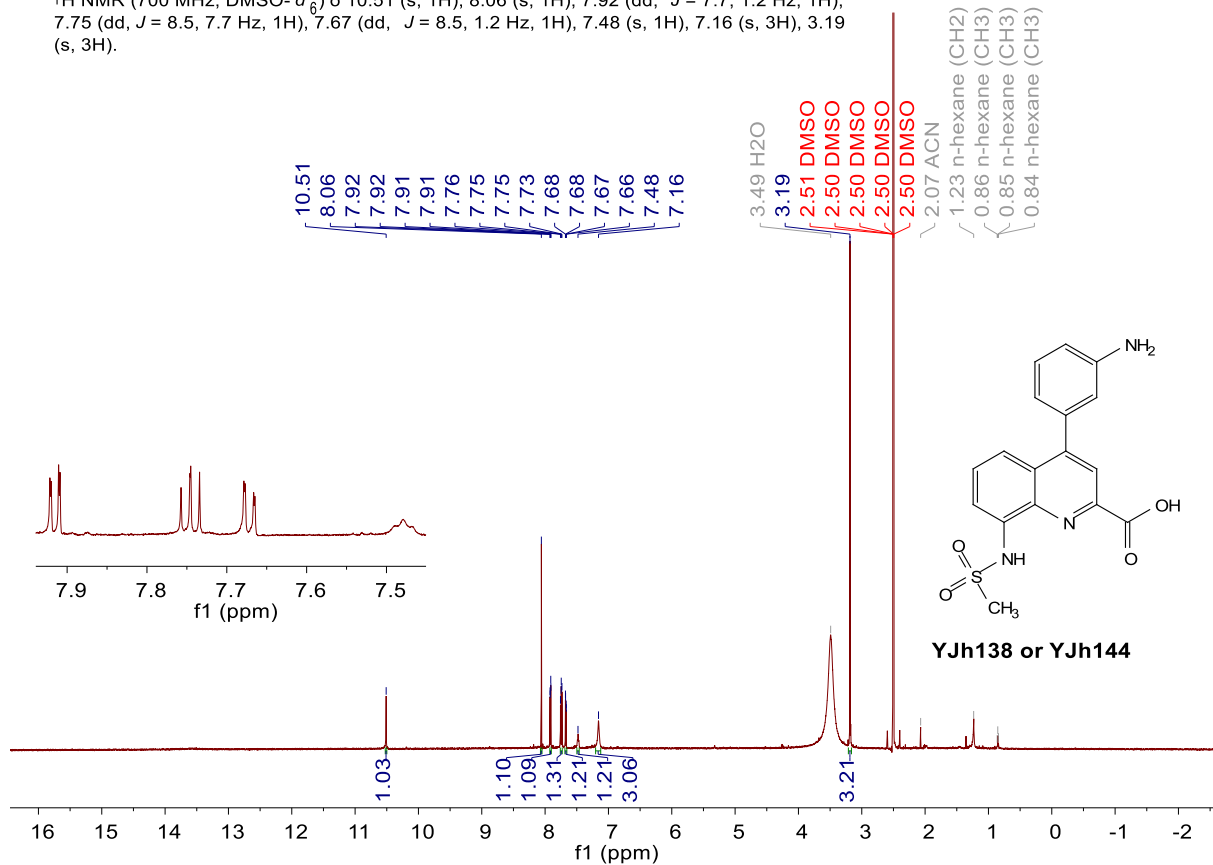
¹H NMR (500 MHz, Chloroform-*d*) δ 9.11 (s, 1H), 8.16 (s, 1H), 7.92 (dd, *J* = 7.7, 1.2 Hz, 1H), 7.69 (d, *J* = 8.4 Hz, 1H), 7.62 (s, 1H), 7.57 (dd, *J* = 8.6, 7.6 Hz, 1H), 7.48 – 7.41 (m, 2H), 7.15 (td, *J* = 4.1, 1.6 Hz, 1H), 6.73 (s, 1H), 4.05 (s, 3H), 3.09 (s, 3H), 1.51 (s, 9H).



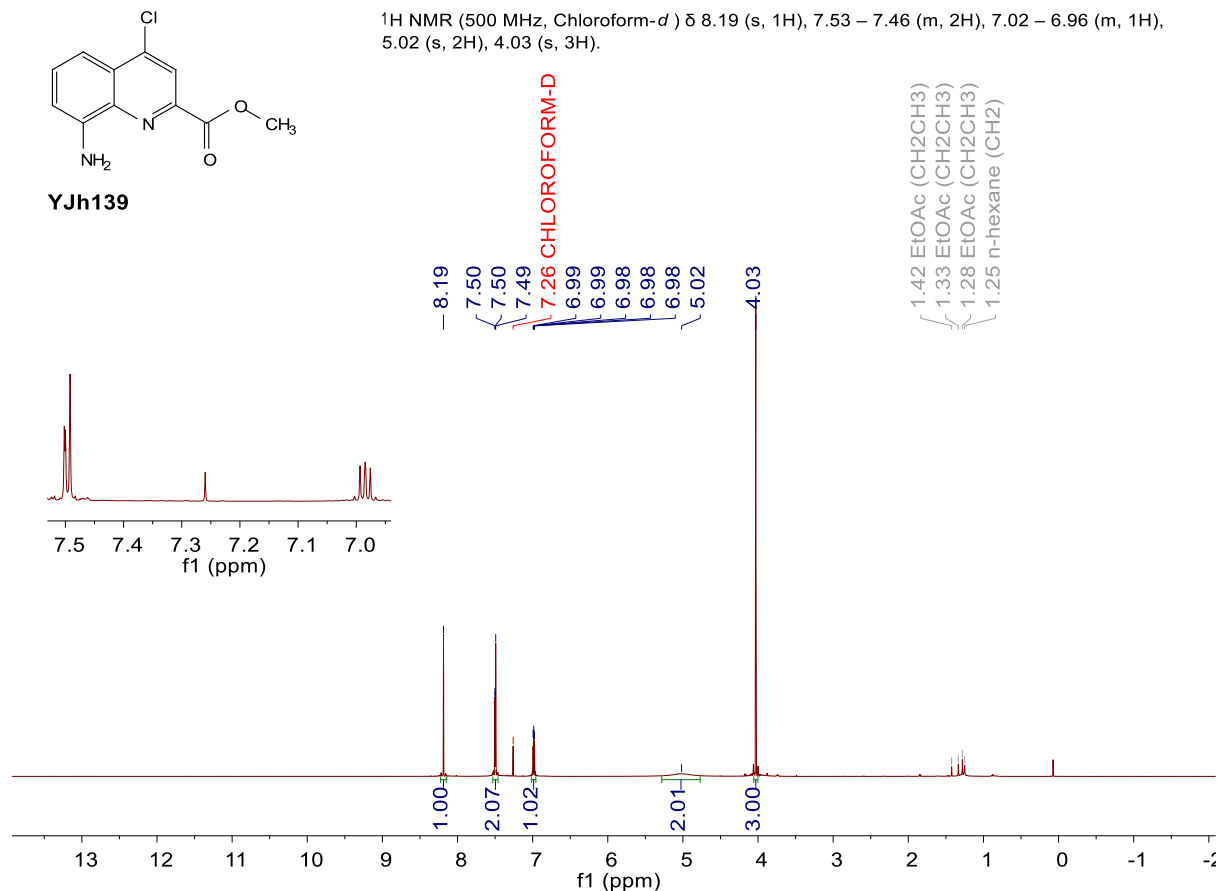
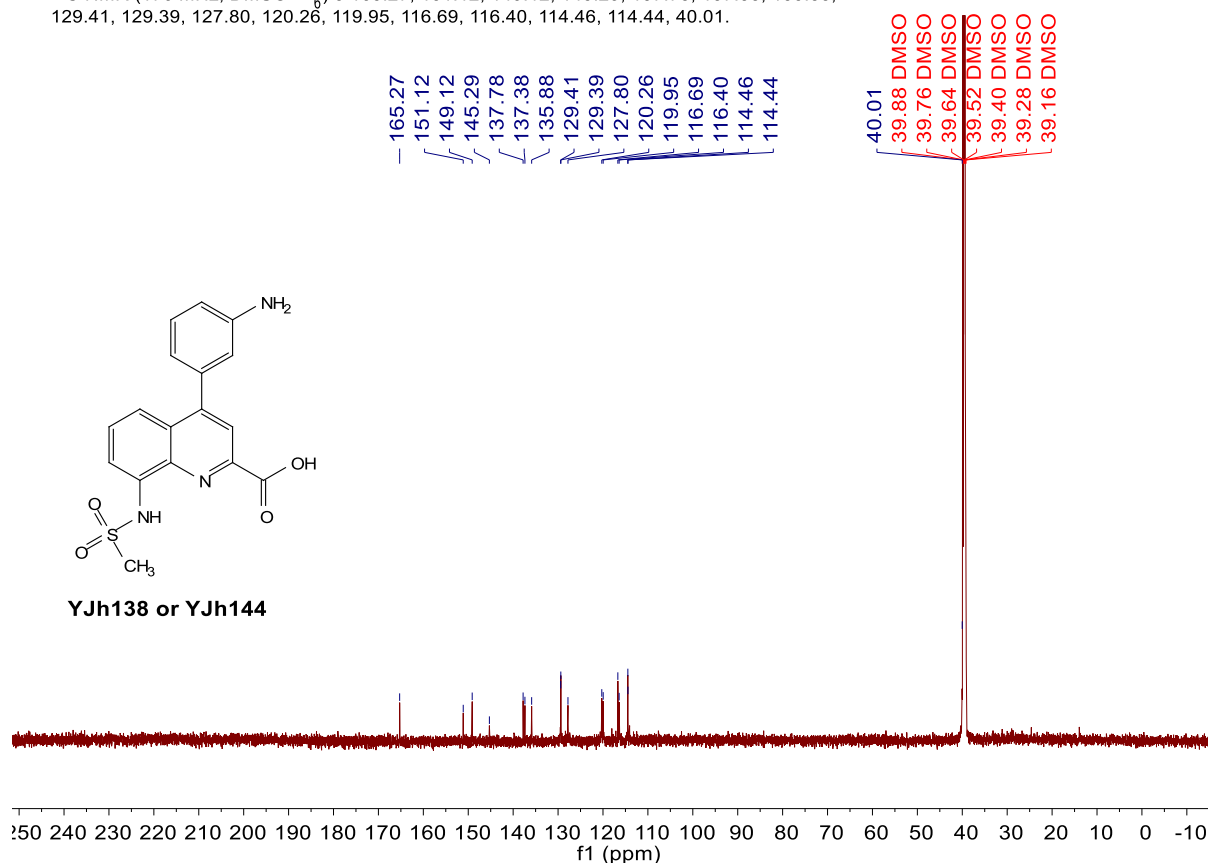
¹³C NMR (126 MHz, Chloroform-*d*) δ 165.54, 152.79, 150.38, 146.03, 139.10, 138.62, 138.02, 135.40, 129.49, 129.29, 128.29, 124.15, 122.34, 120.64, 119.50, 119.03, 115.67, 81.07, 53.12, 39.55, 28.44.



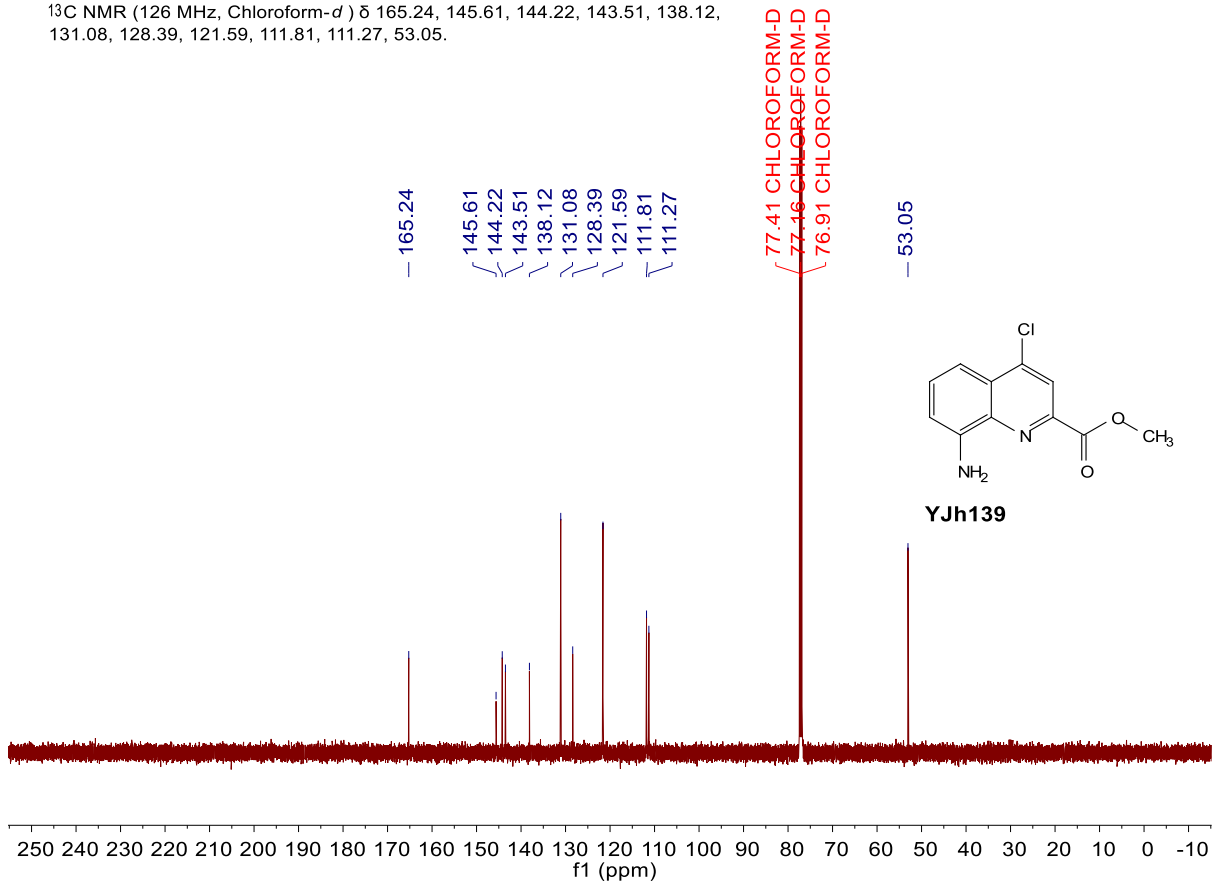
¹H NMR (700 MHz, DMSO-*d*₆) δ 10.51 (s, 1H), 8.06 (s, 1H), 7.92 (dd, *J* = 7.7, 1.2 Hz, 1H), 7.75 (dd, *J* = 8.5, 7.7 Hz, 1H), 7.67 (dd, *J* = 8.5, 1.2 Hz, 1H), 7.48 (s, 1H), 7.16 (s, 3H), 3.19 (s, 3H).



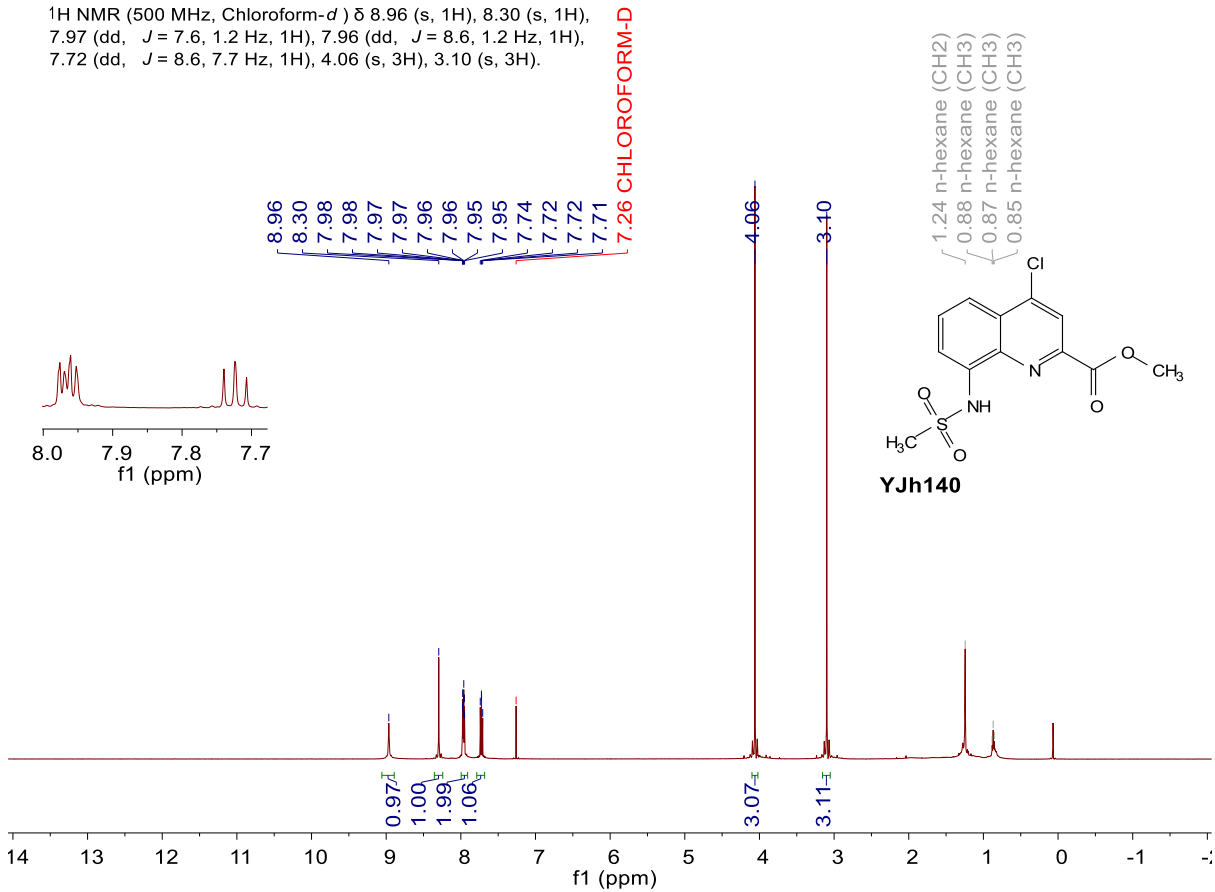
^{13}C NMR (176 MHz, $\text{DMSO-}d_6$) δ 165.27, 151.12, 149.12, 145.29, 137.78, 137.38, 135.88, 129.41, 129.39, 127.80, 120.26, 119.95, 116.69, 116.40, 114.46, 114.44, 40.01.



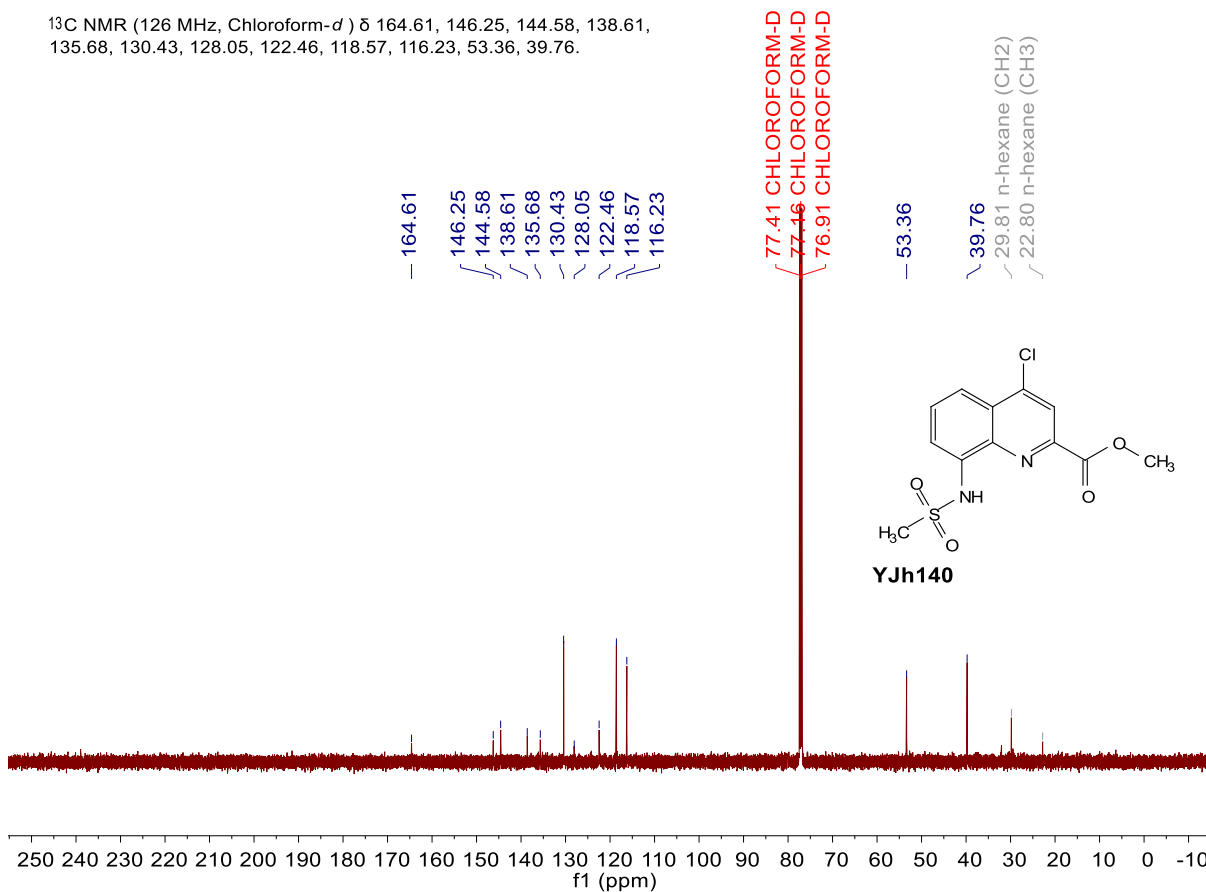
¹³C NMR (126 MHz, Chloroform-*d*) δ 165.24, 145.61, 144.22, 143.51, 138.12, 131.08, 128.39, 121.59, 111.81, 111.27, 53.05.



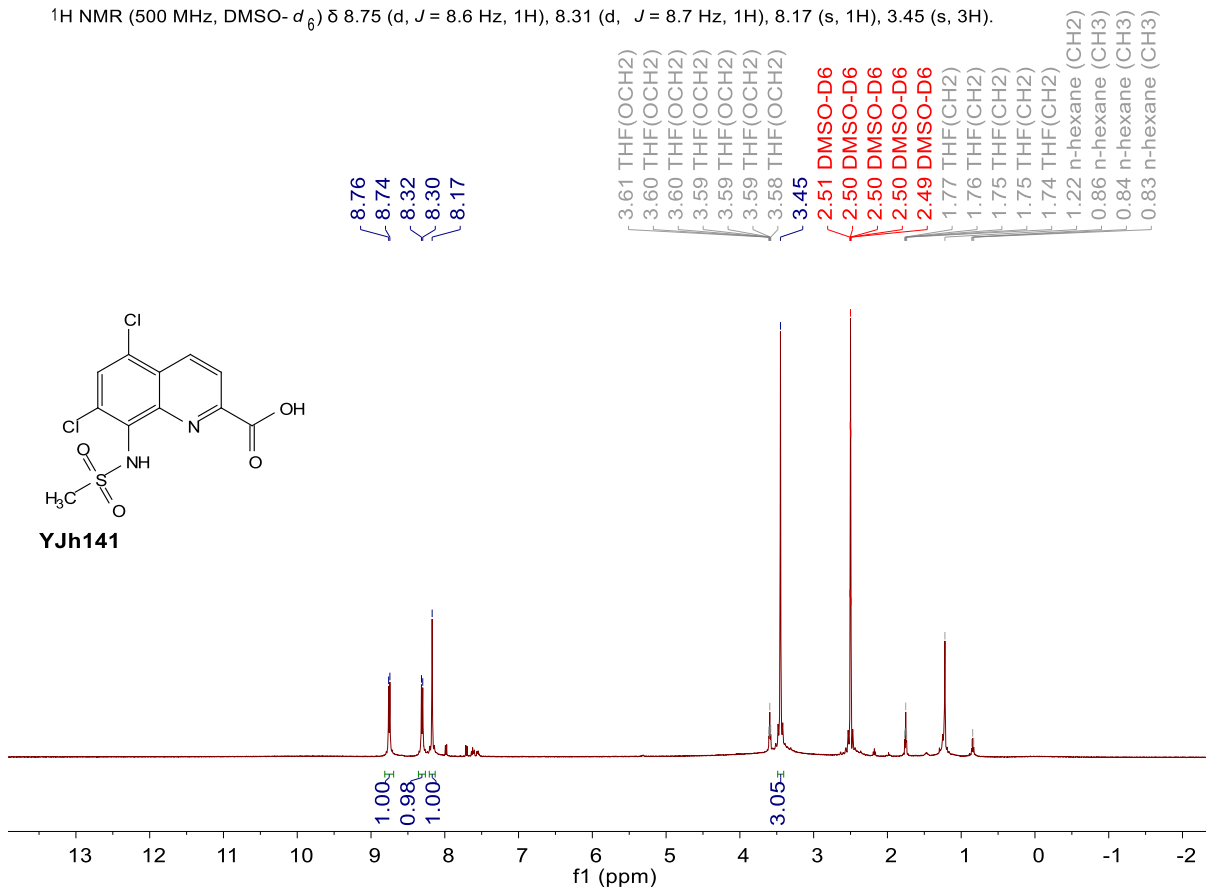
¹H NMR (500 MHz, Chloroform-*d*) δ 8.96 (s, 1H), 8.30 (s, 1H), 7.97 (dd, *J* = 7.6, 1.2 Hz, 1H), 7.96 (dd, *J* = 8.6, 1.2 Hz, 1H), 7.72 (dd, *J* = 8.6, 7.7 Hz, 1H), 4.06 (s, 3H), 3.10 (s, 3H).



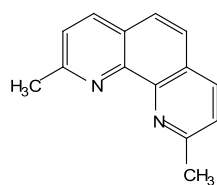
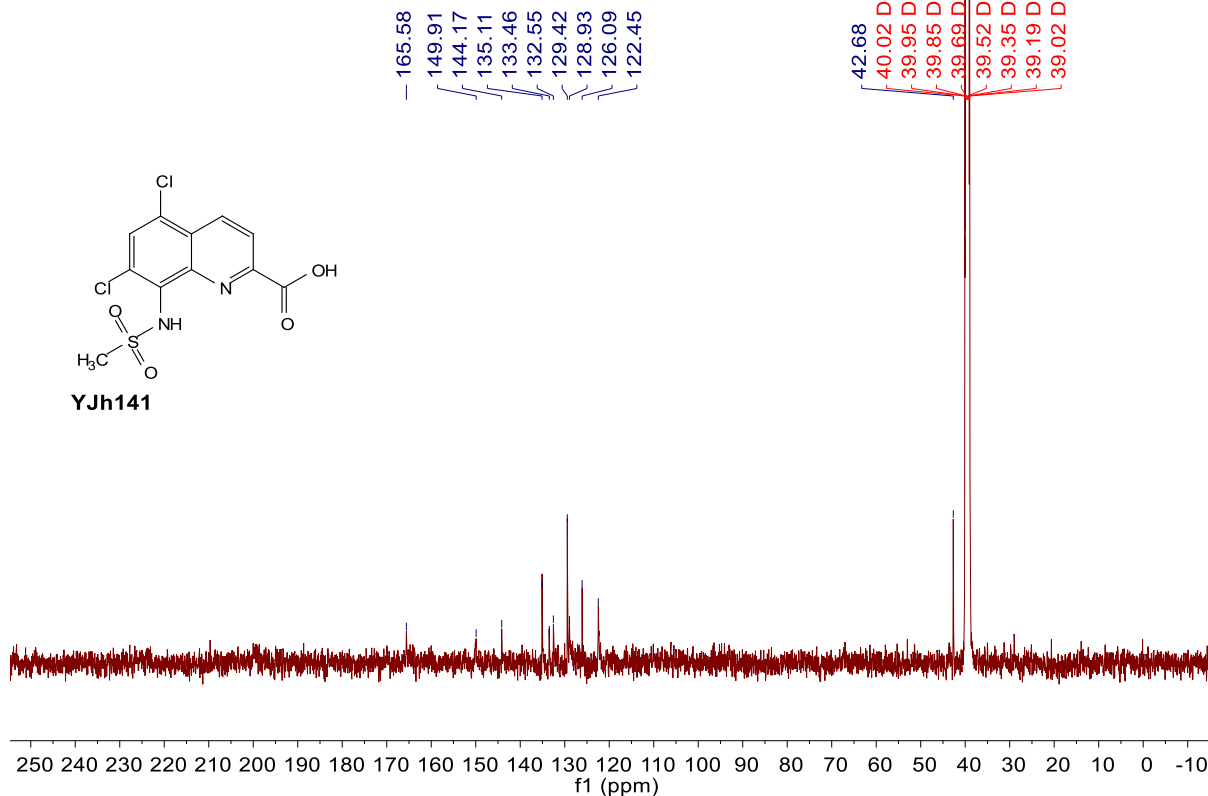
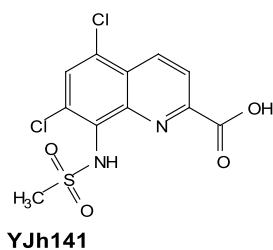
¹³C NMR (126 MHz, Chloroform-*d*) δ 164.61, 146.25, 144.58, 138.61, 135.68, 130.43, 128.05, 122.46, 118.57, 116.23, 53.36, 39.76, 29.81 n-hexane (CH₂), 22.80 n-hexane (CH₃)



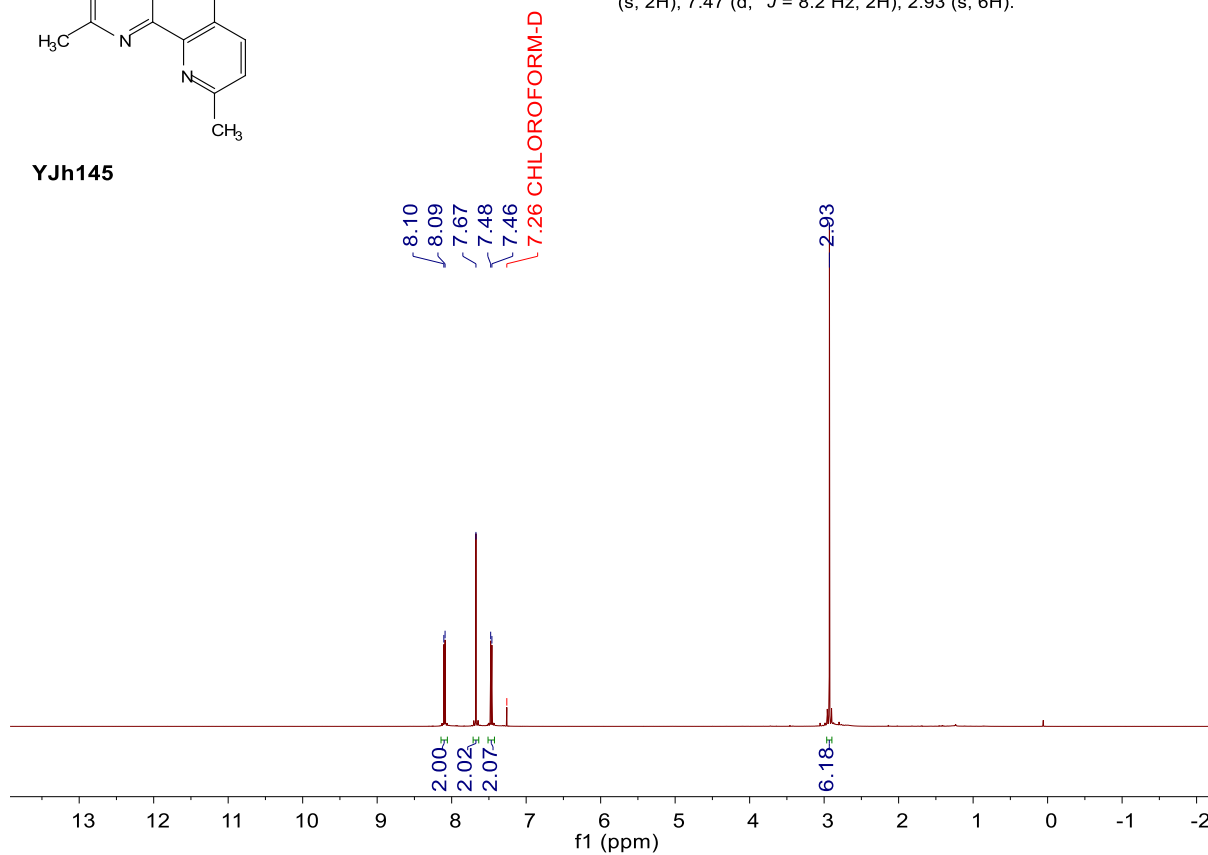
¹H NMR (500 MHz, DMSO-*d*₆) δ 8.75 (d, *J* = 8.6 Hz, 1H), 8.31 (d, *J* = 8.7 Hz, 1H), 8.17 (s, 1H), 3.45 (s, 3H).



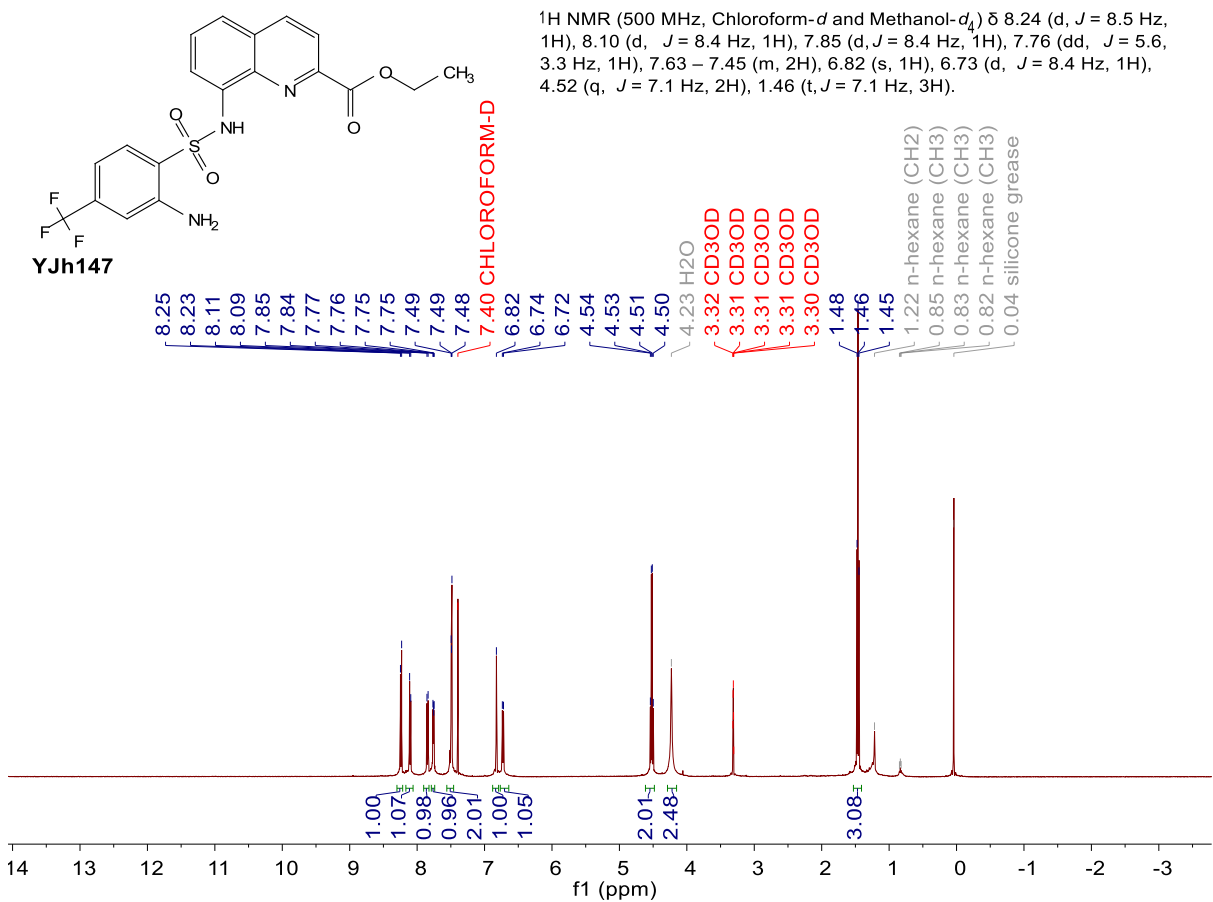
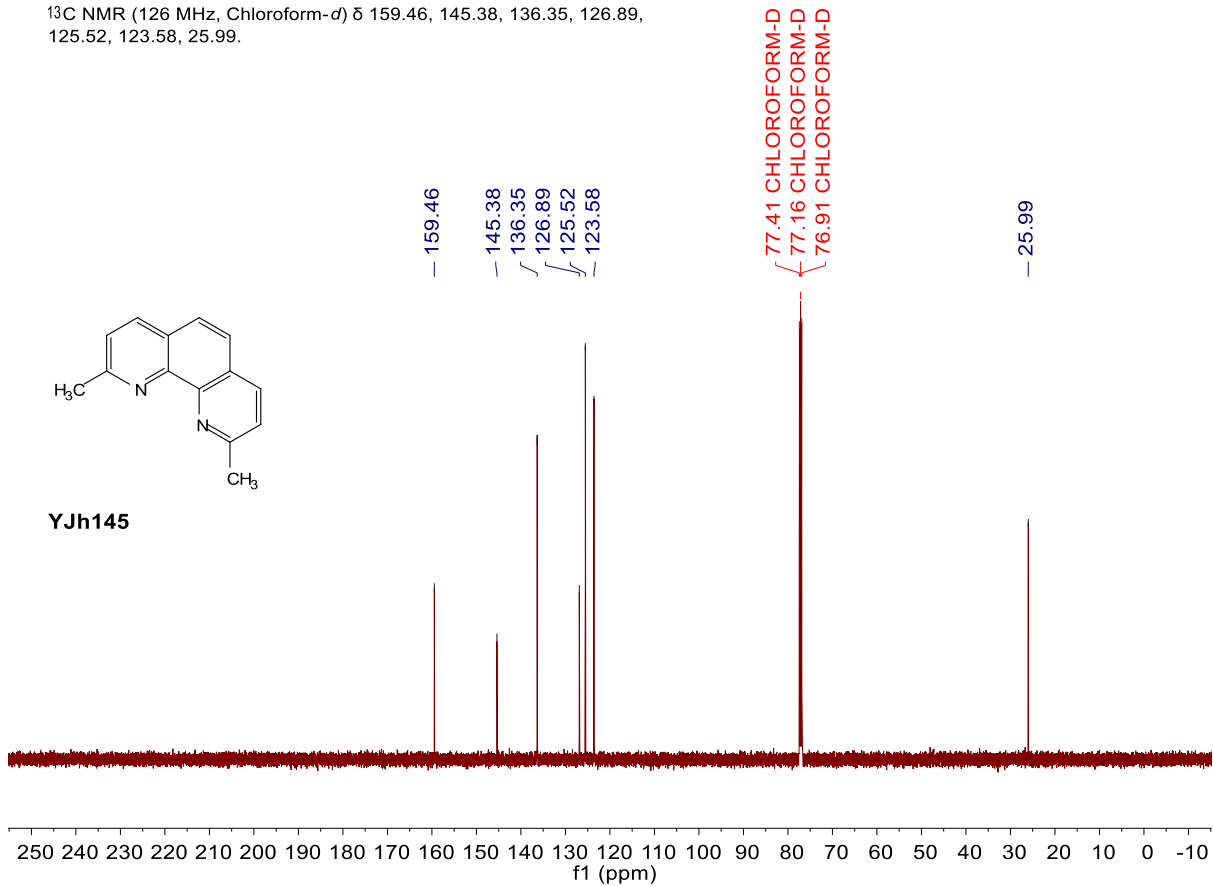
¹³C NMR (126 MHz, DMSO-*d*₆) δ 165.58, 149.91, 144.17, 135.11, 133.46, 132.55, 129.42, 128.93, 126.09, 122.45, 42.68.



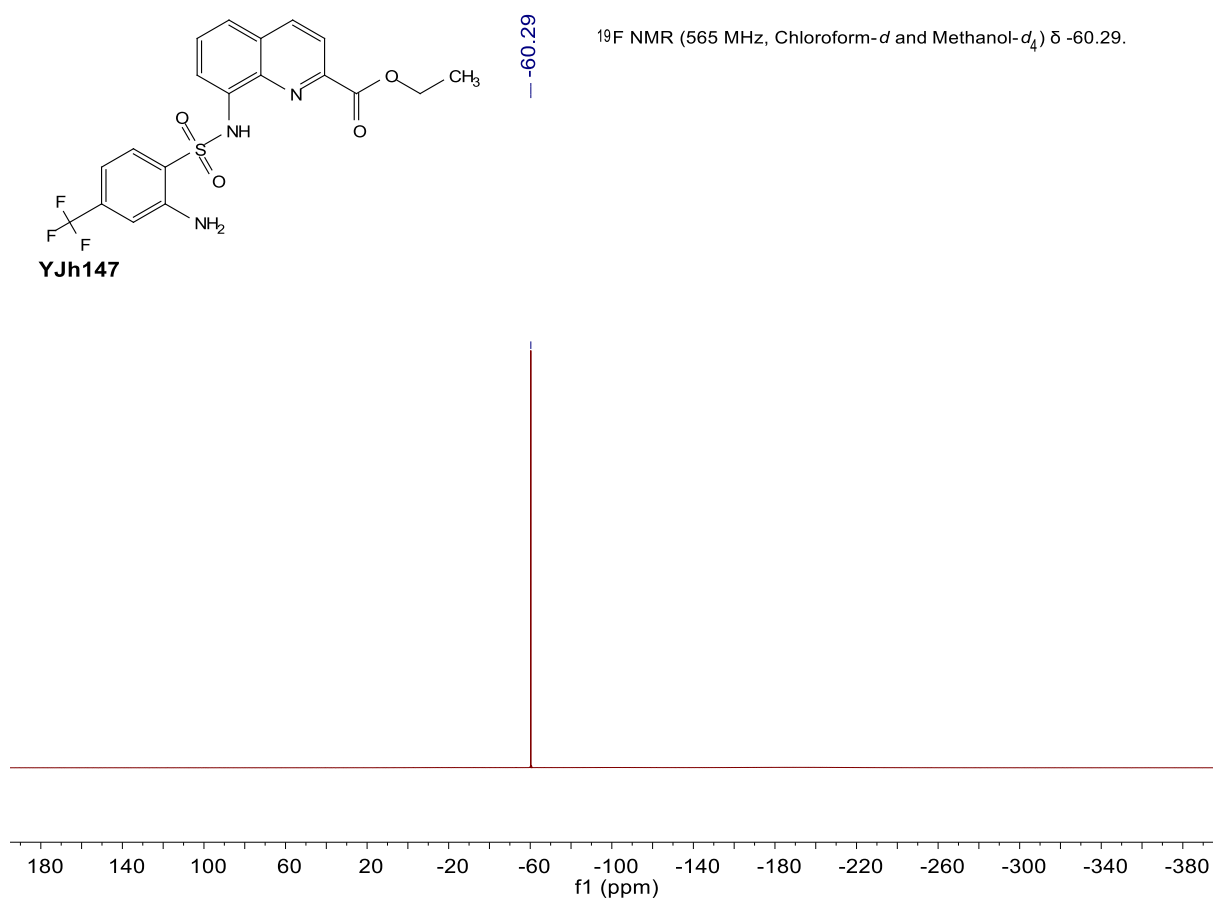
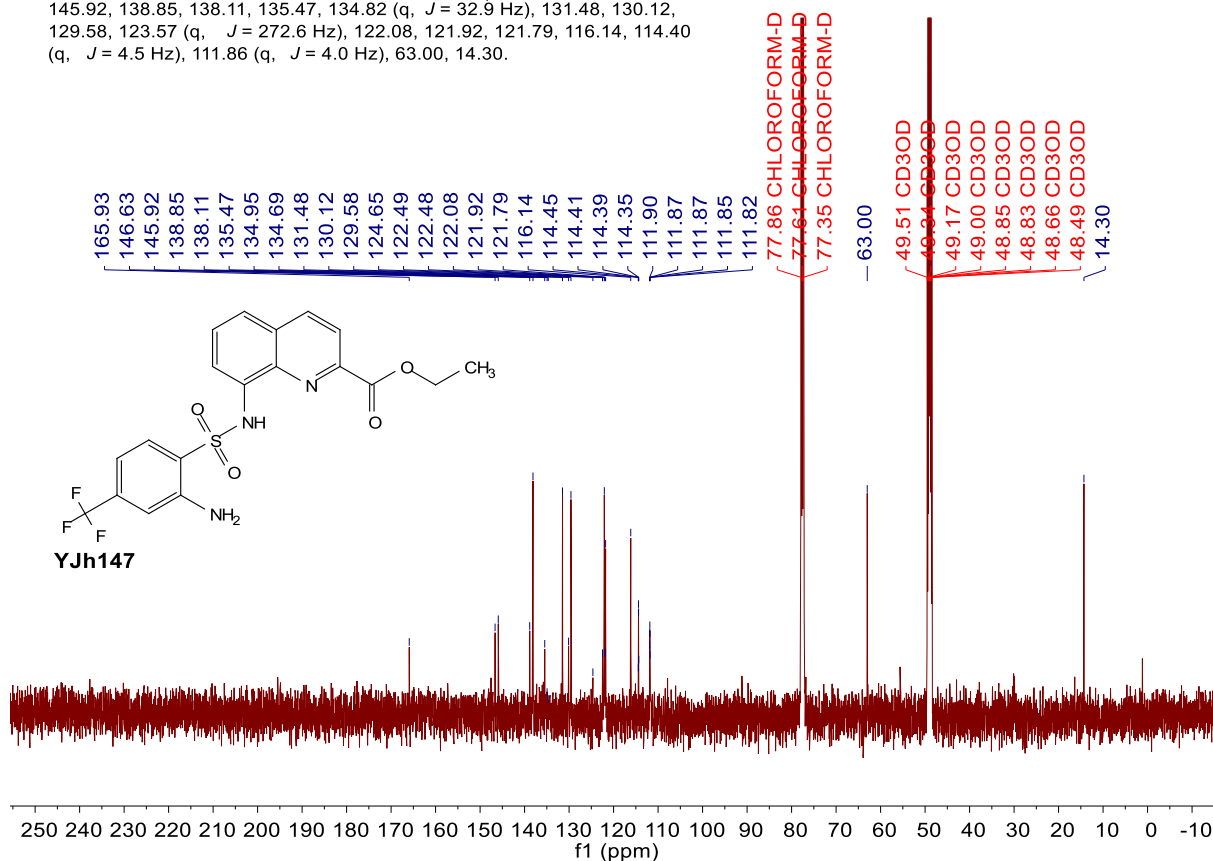
¹H NMR (500 MHz, Chloroform-*d*) δ 8.10 (d, *J* = 8.2 Hz, 2H), 7.67 (s, 2H), 7.47 (d, *J* = 8.2 Hz, 2H), 2.93 (s, 6H).



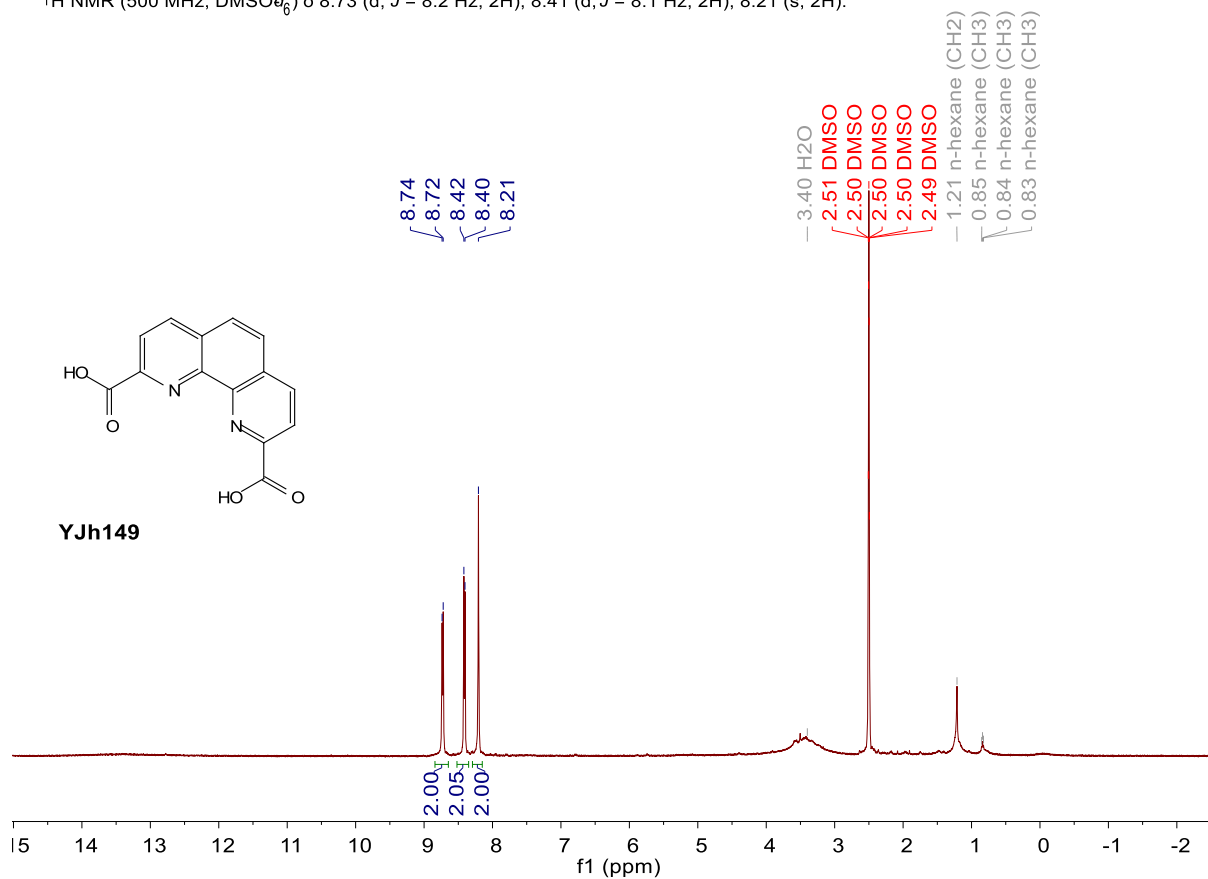
¹³C NMR (126 MHz, Chloroform-*d*) δ 159.46, 145.38, 136.35, 126.89, 125.52, 123.58, 25.99.



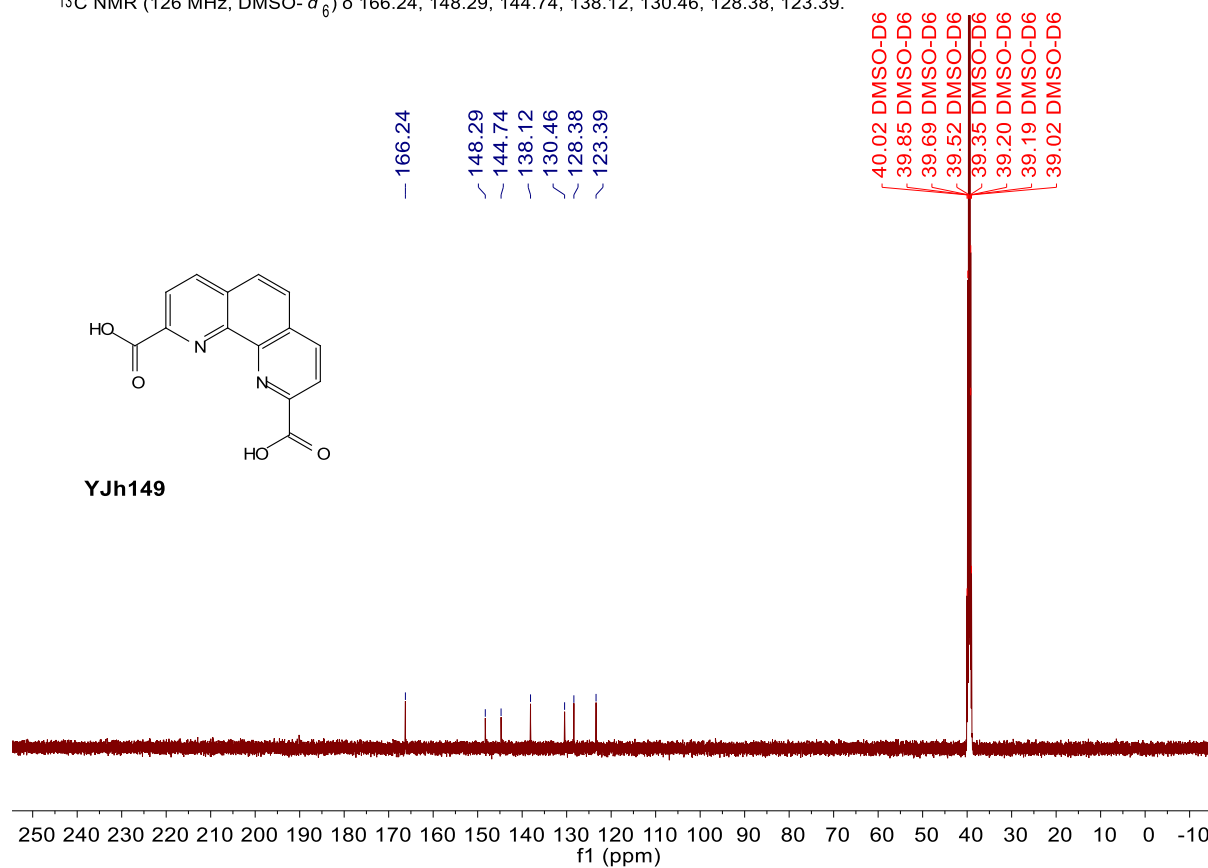
¹³C NMR (126 MHz, Chloroform-*d* and Methanol-*d*₄) δ 165.93, 146.63, 145.92, 138.85, 138.11, 135.47, 134.82 (q, *J* = 32.9 Hz), 131.48, 130.12, 129.58, 123.57 (q, *J* = 272.6 Hz), 122.08, 121.92, 121.79, 116.14, 114.40 (q, *J* = 4.5 Hz), 111.86 (q, *J* = 4.0 Hz), 63.00, 14.30.



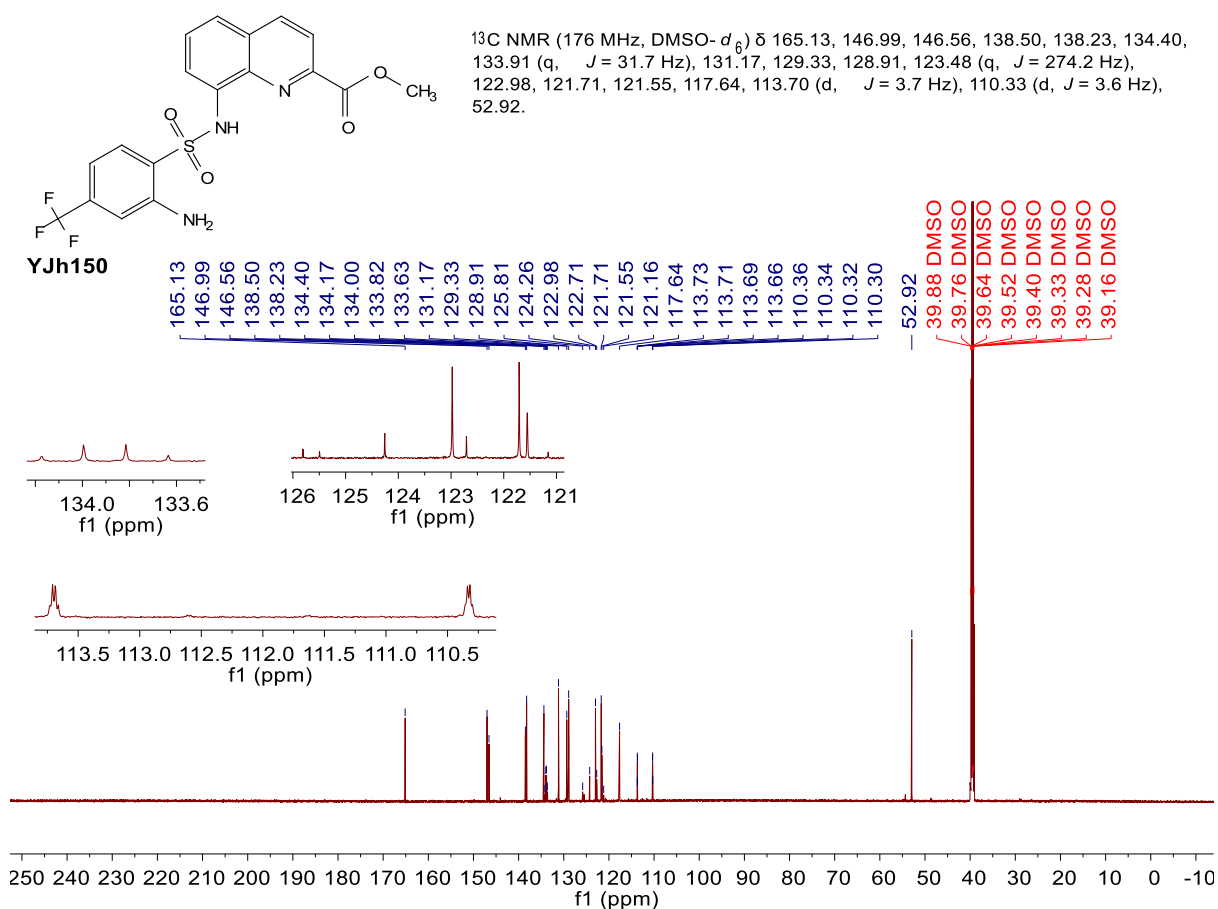
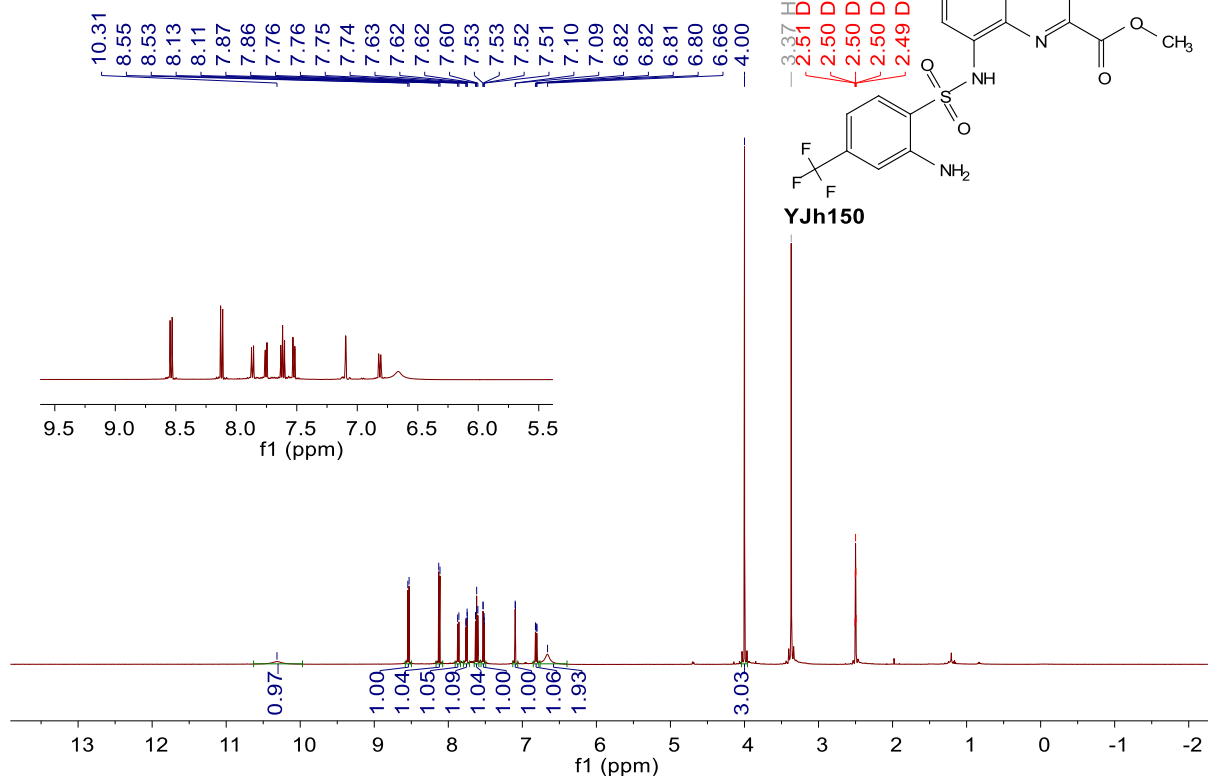
¹H NMR (500 MHz, DMSO-*d*₆) δ 8.73 (d, *J* = 8.2 Hz, 2H), 8.41 (d, *J* = 8.1 Hz, 2H), 8.21 (s, 2H).

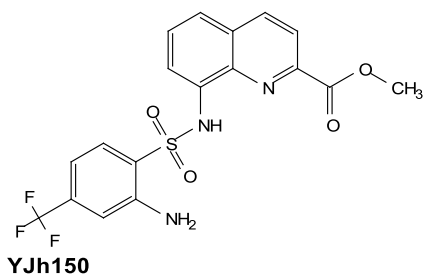


¹³C NMR (126 MHz, DMSO-*d*₆) δ 166.24, 148.29, 144.74, 138.12, 130.46, 128.38, 123.39.



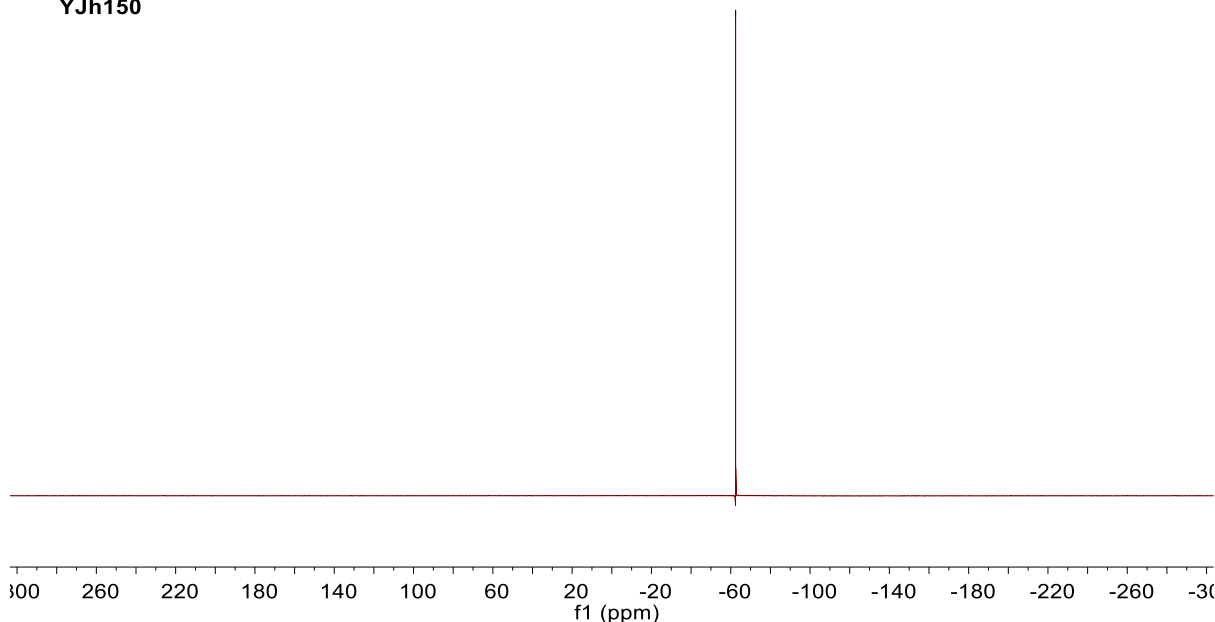
¹H NMR (500 MHz, DMSO-*d*₆) δ 10.31 (s, 1H), 8.54 (d, *J* = 8.6 Hz, 1H), 8.12 (d, *J* = 8.5 Hz, 1H), 7.87 (d, *J* = 8.4 Hz, 1H), 7.75 (dd, *J* = 8.3, 1.3 Hz, 1H), 7.62 (dd, *J* = 8.2, 7.7 Hz, 1H), 7.52 (dd, *J* = 7.7, 1.3 Hz, 1H), 7.10 (d, *J* = 1.8 Hz, 1H), 6.81 (dd, *J* = 8.5, 1.7 Hz, 1H), 6.66 (s, 2H), 4.00 (s, 3H).



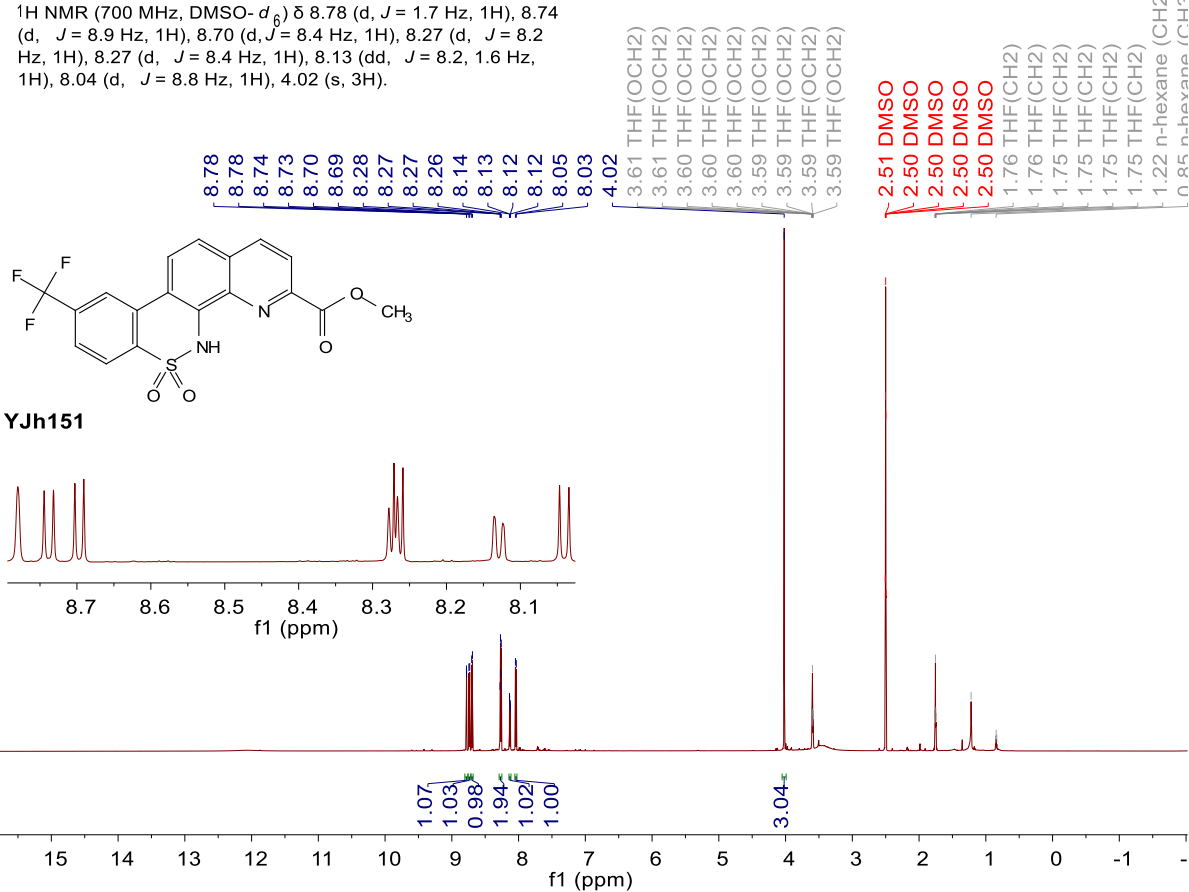


^{19}F NMR (471 MHz, $\text{DMSO}-d_6$) δ -62.43.

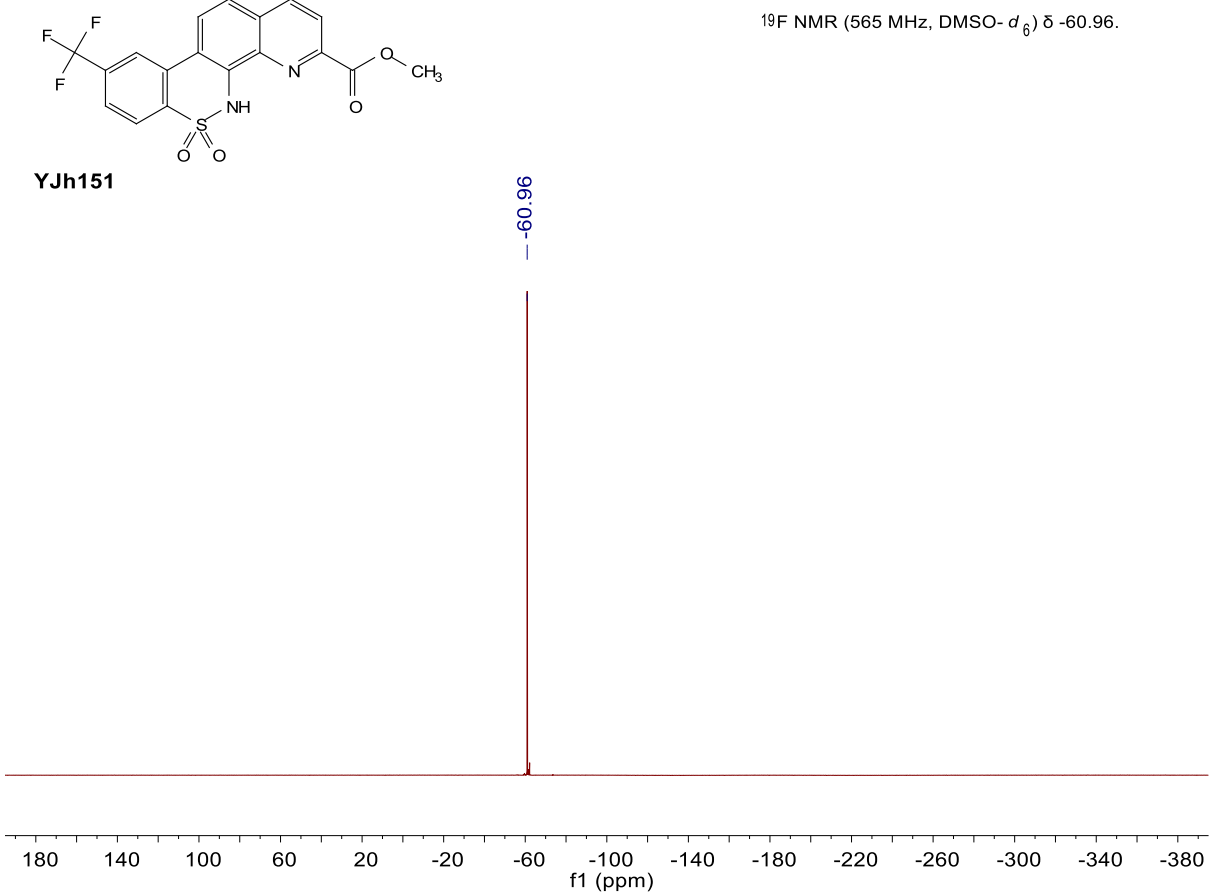
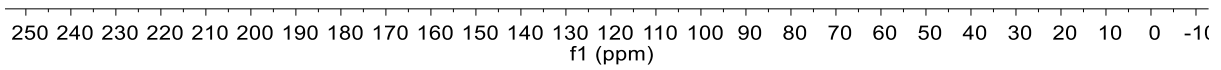
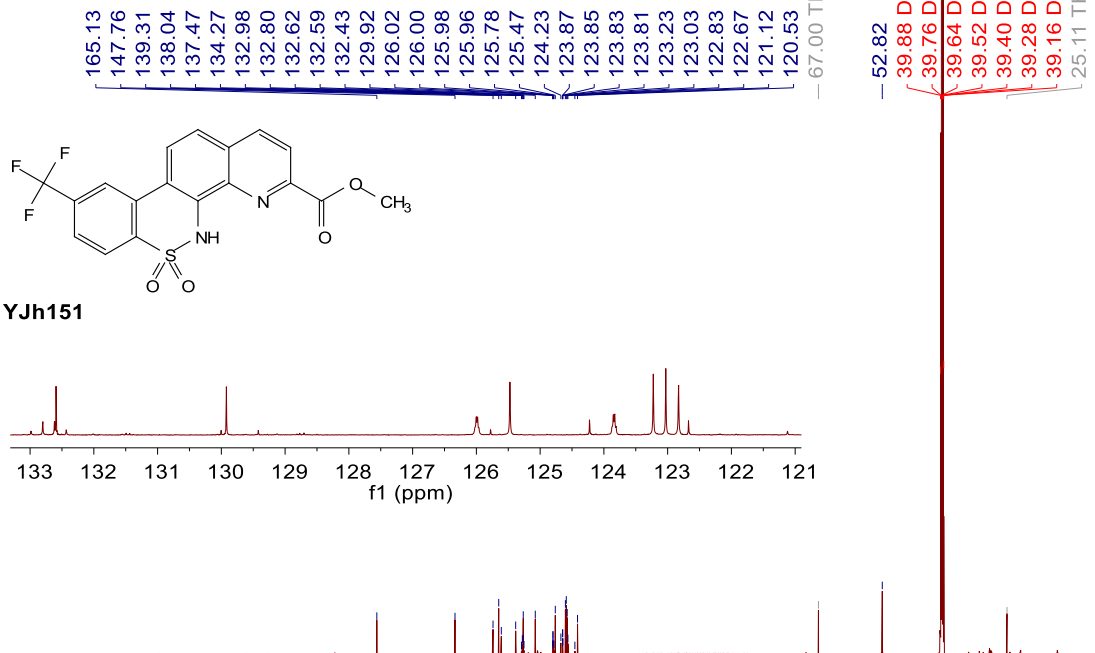
-62.43

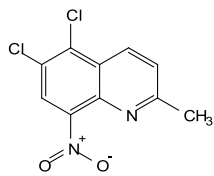


^1H NMR (700 MHz, $\text{DMSO}-d_6$) δ 8.78 (d, $J = 1.7$ Hz, 1H), 8.74 (d, $J = 8.9$ Hz, 1H), 8.70 (d, $J = 8.4$ Hz, 1H), 8.27 (d, $J = 8.2$ Hz, 1H), 8.27 (d, $J = 8.4$ Hz, 1H), 8.13 (dd, $J = 8.2, 1.6$ Hz, 1H), 8.04 (d, $J = 8.8$ Hz, 1H), 4.02 (s, 3H).



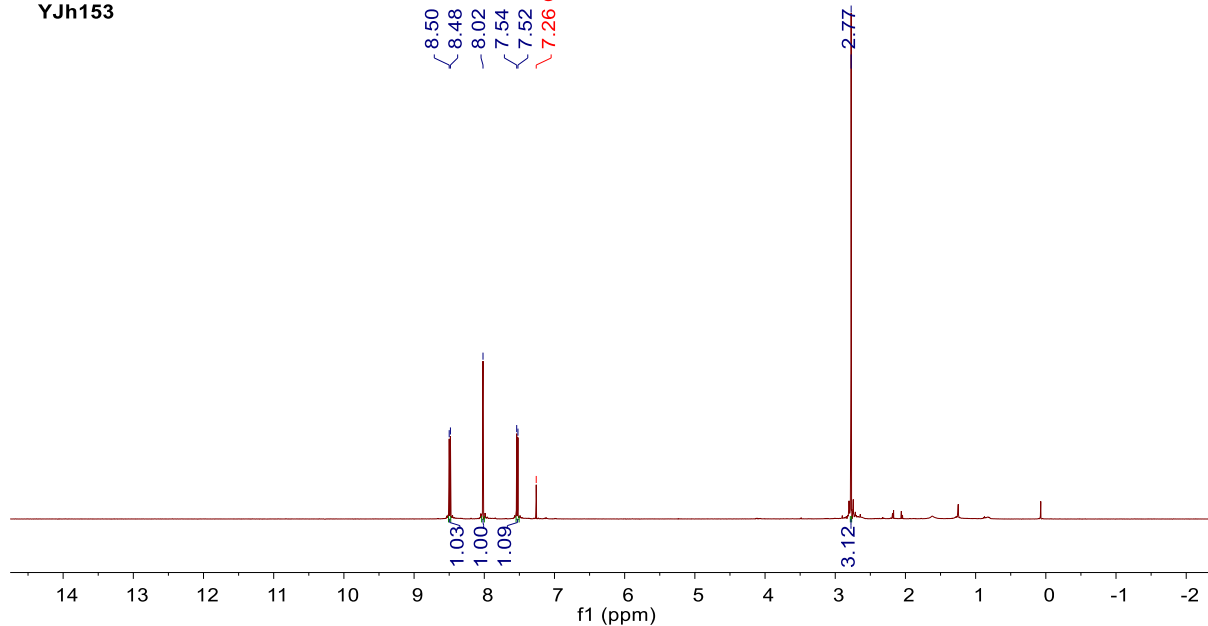
¹³C NMR (176 MHz, DMSO-*d*₆) δ 165.13, 147.76, 139.31, 138.04, 137.47, 134.27, 132.71 (q, *J* = 32.6 Hz), 132.59, 129.92, 125.99 (q, *J* = 3.8 Hz), 125.47, 123.84 (q, *J* = 3.9 Hz), 123.45 (q, *J* = 273.3 Hz), 123.23, 123.03, 122.83, 120.53, 52.82.



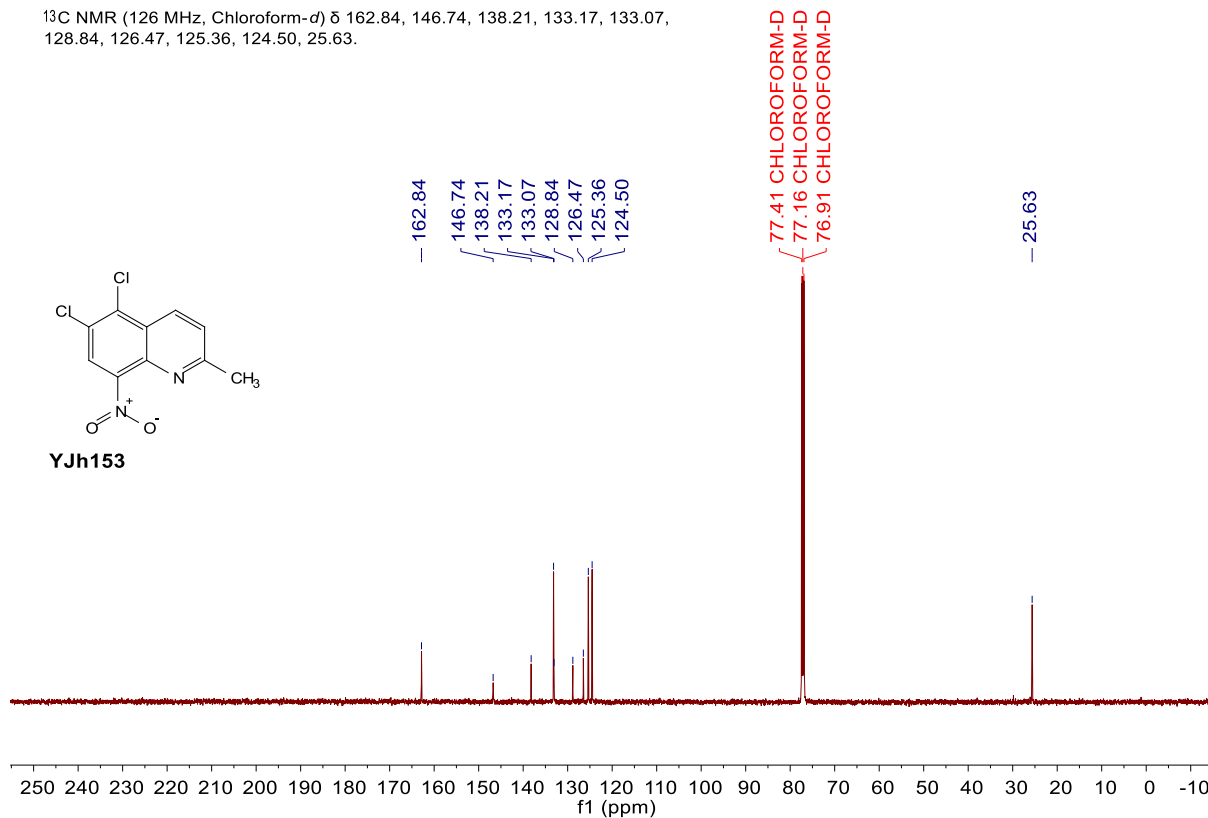


YJh153

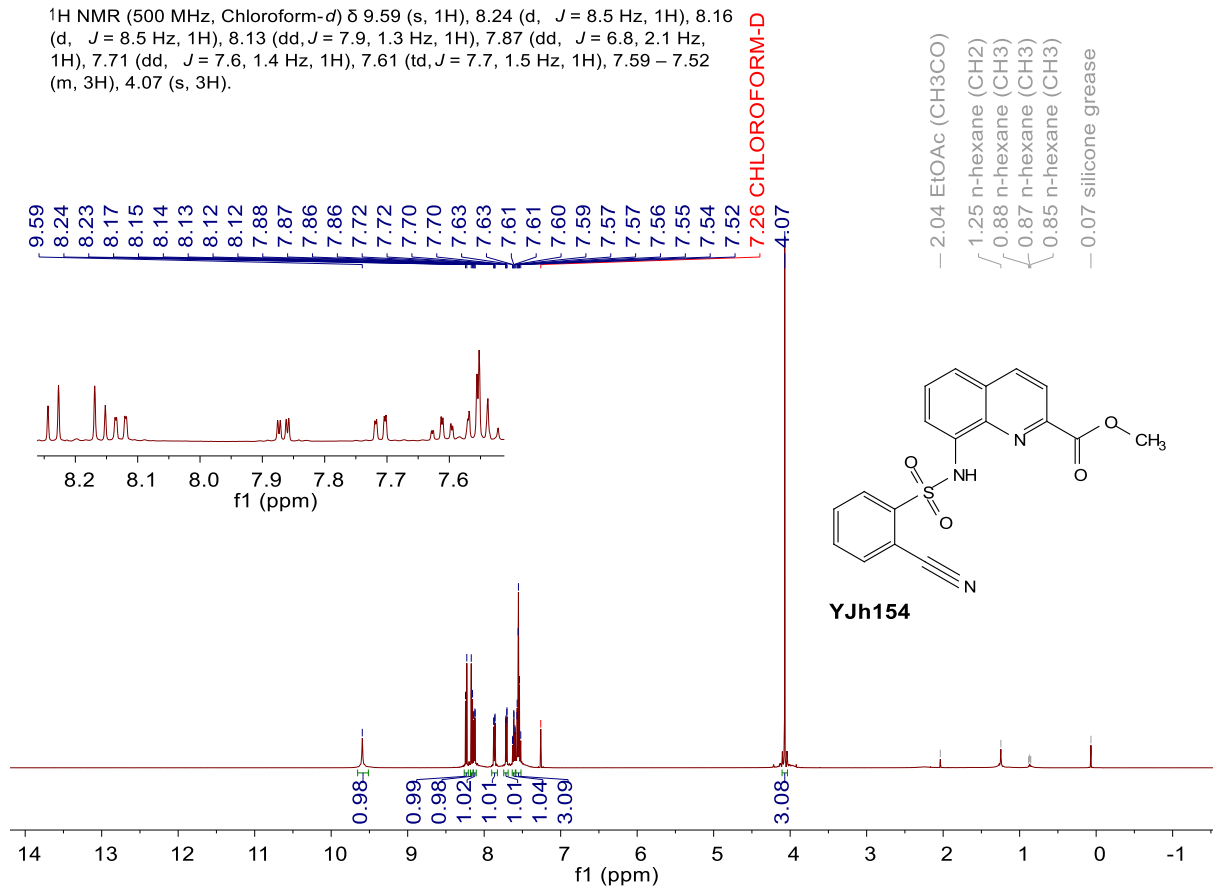
¹H NMR (500 MHz, Chloroform-*d*) δ 8.49 (d, *J* = 8.8 Hz, 1H), 8.02 (s, 1H), 7.53 (d, *J* = 8.8 Hz, 1H), 2.77 (s, 3H).



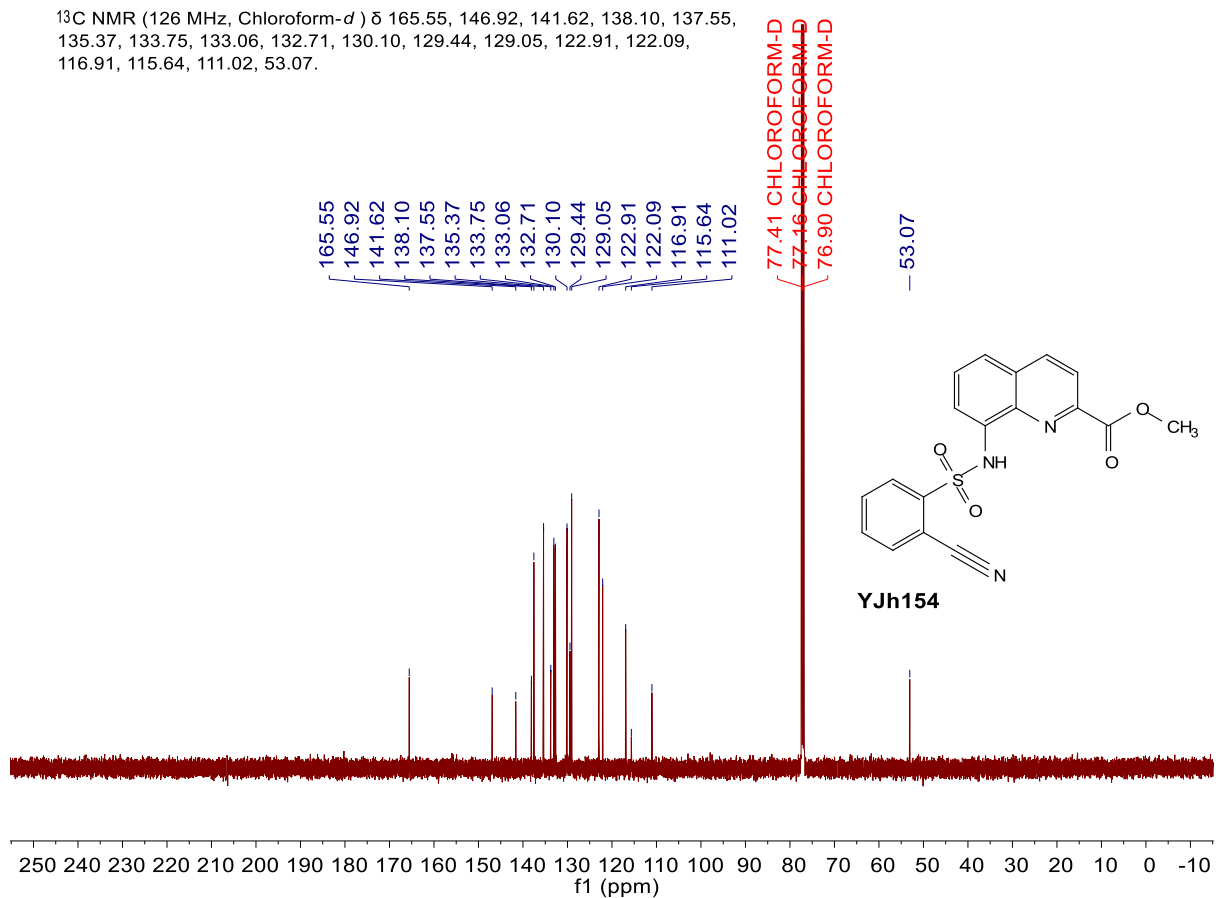
¹³C NMR (126 MHz, Chloroform-*d*) δ 162.84, 146.74, 138.21, 133.17, 133.07, 128.84, 126.47, 125.36, 124.50, 25.63.



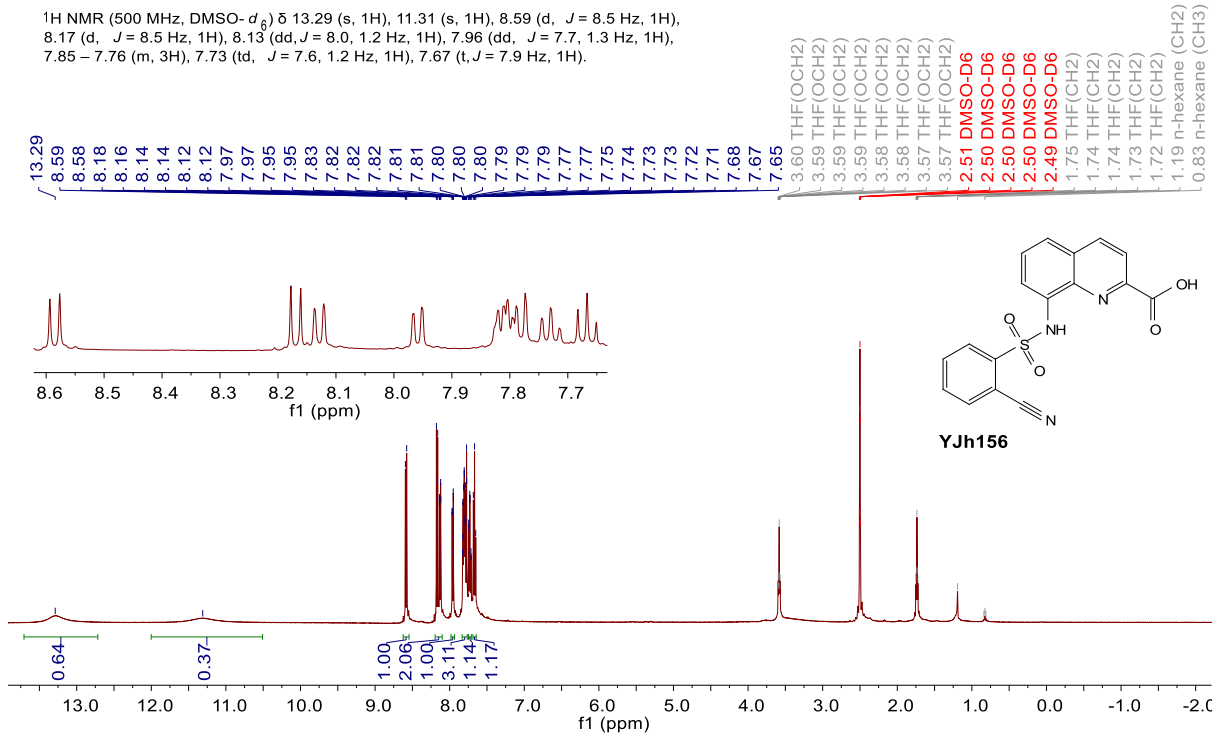
¹H NMR (500 MHz, Chloroform-*d*) δ 9.59 (s, 1H), 8.24 (d, *J* = 8.5 Hz, 1H), 8.16 (d, *J* = 8.5 Hz, 1H), 8.13 (dd, *J* = 7.9, 1.3 Hz, 1H), 7.87 (dd, *J* = 6.8, 2.1 Hz, 1H), 7.71 (dd, *J* = 7.6, 1.4 Hz, 1H), 7.61 (td, *J* = 7.7, 1.5 Hz, 1H), 7.59 – 7.52 (m, 3H), 4.07 (s, 3H).



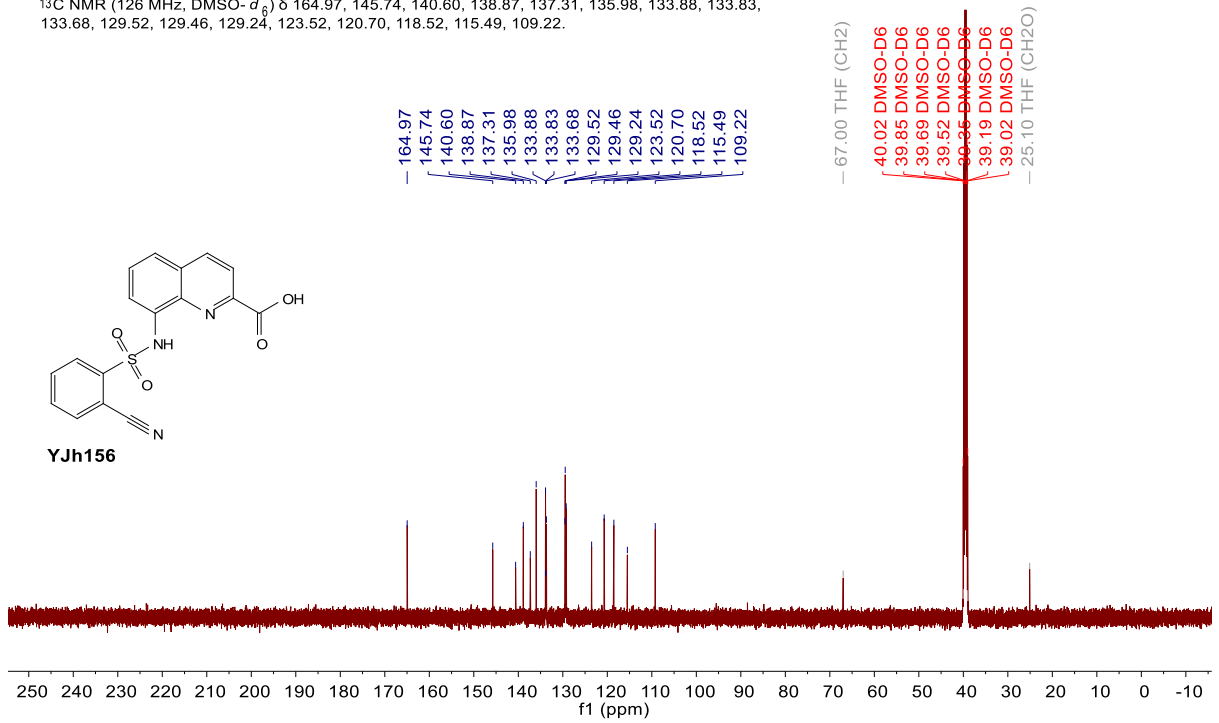
¹³C NMR (126 MHz, Chloroform-*d*) δ 165.55, 146.92, 141.62, 138.10, 137.55, 135.37, 133.75, 133.06, 132.71, 130.10, 129.44, 129.05, 122.91, 122.09, 116.91, 115.64, 111.02, 53.07.



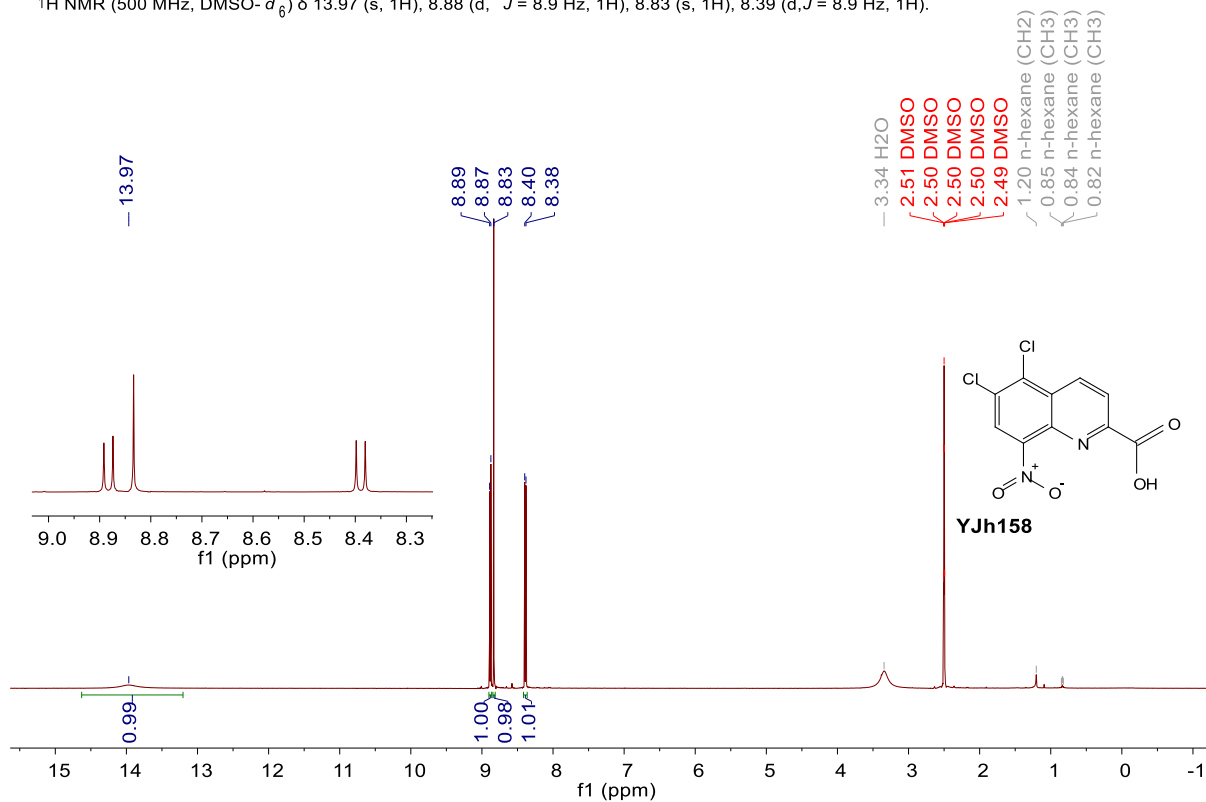
¹H NMR (500 MHz, DMSO-*d*₆) δ 13.29 (s, 1H), 11.31 (s, 1H), 8.59 (d, *J* = 8.5 Hz, 1H), 8.17 (d, *J* = 8.5 Hz, 1H), 8.13 (dd, *J* = 8.0, 1.2 Hz, 1H), 7.96 (dd, *J* = 7.7, 1.3 Hz, 1H), 7.85 – 7.76 (m, 3H), 7.73 (td, *J* = 7.6, 1.2 Hz, 1H), 7.67 (t, *J* = 7.9 Hz, 1H).



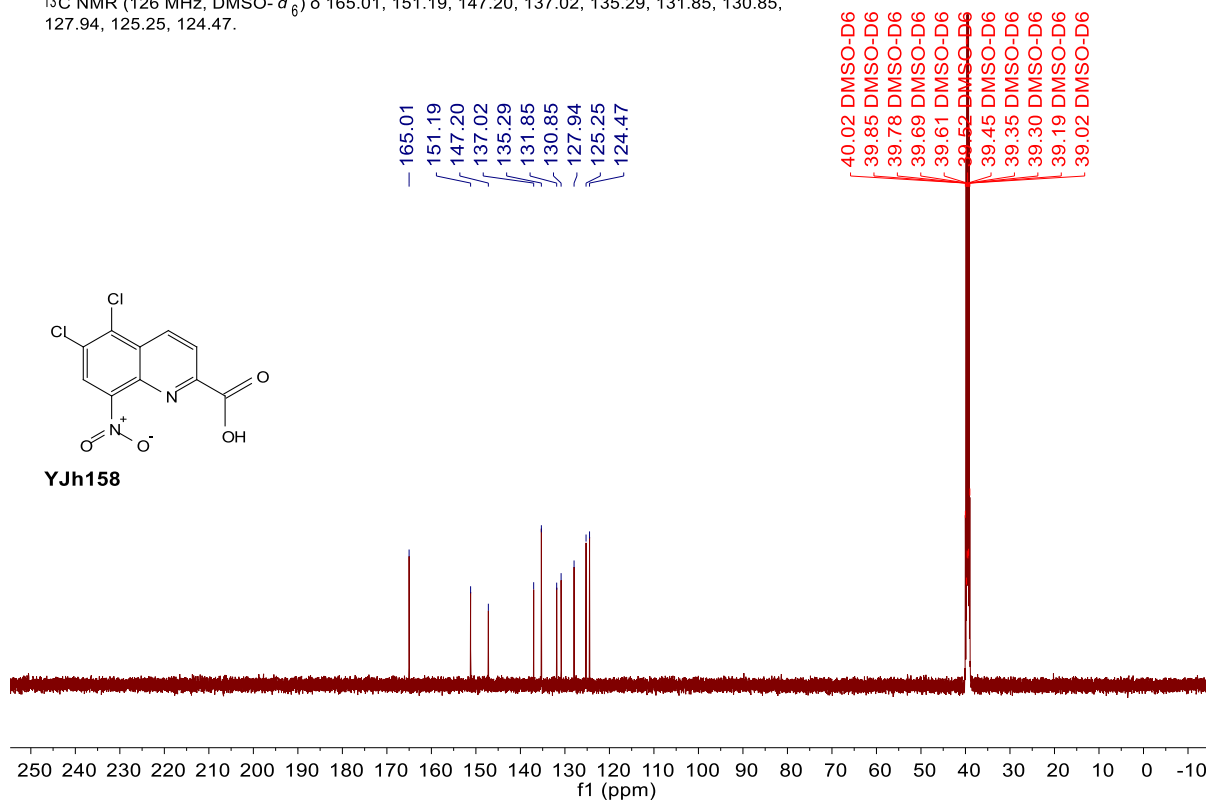
¹³C NMR (126 MHz, DMSO-*d*₆) δ 164.97, 145.74, 140.60, 138.87, 137.31, 135.98, 133.88, 133.83, 133.68, 129.52, 129.46, 129.24, 123.52, 120.70, 118.52, 115.49, 109.22.



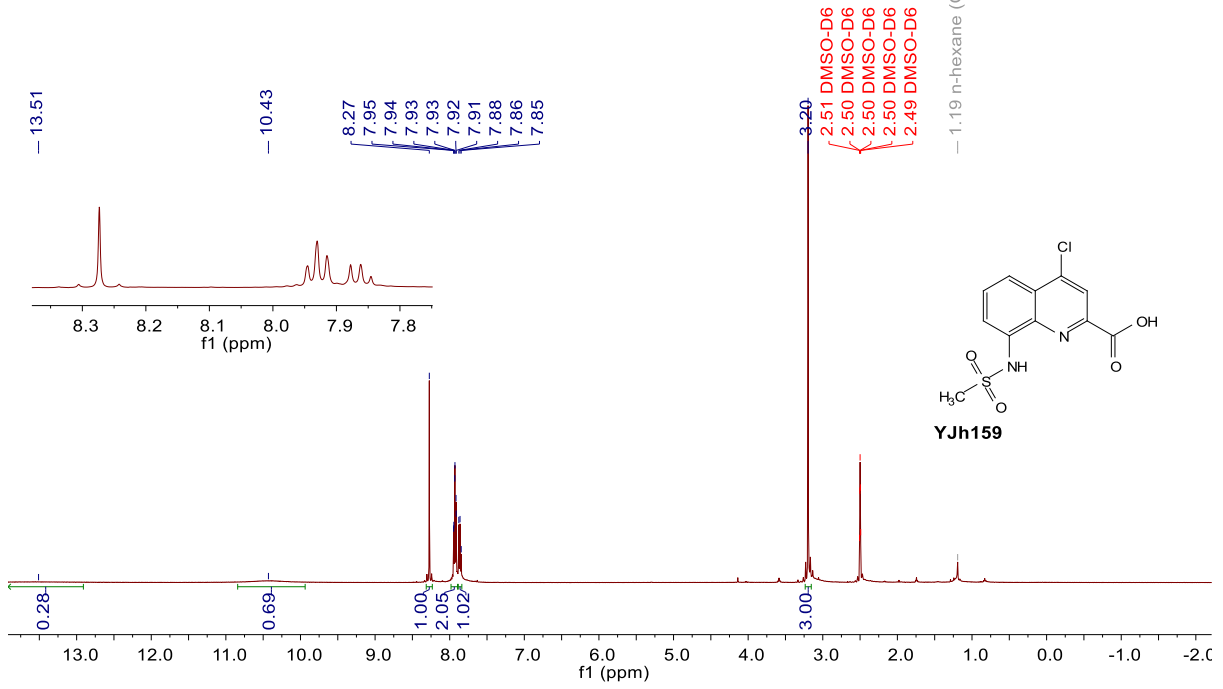
$^1\text{H NMR}$ (500 MHz, $\text{DMSO-}d_6$) δ 13.97 (s, 1H), 8.88 (d, $J = 8.9$ Hz, 1H), 8.83 (s, 1H), 8.39 (d, $J = 8.9$ Hz, 1H).



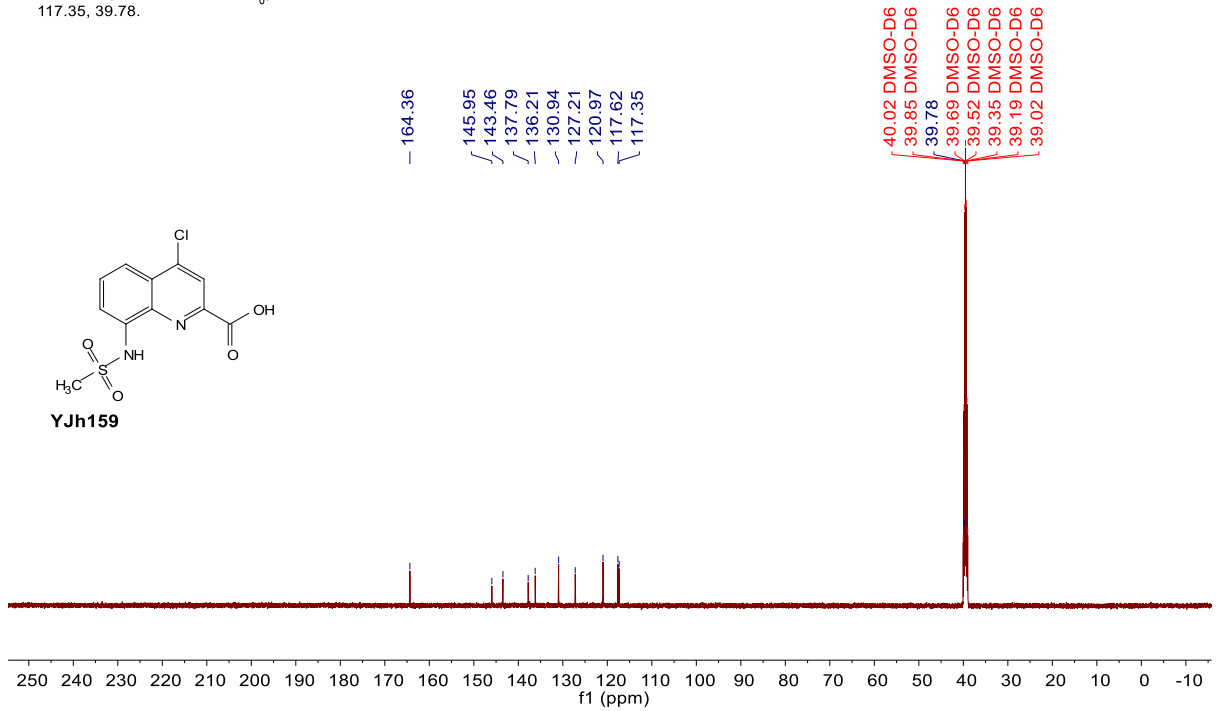
$^{13}\text{C NMR}$ (126 MHz, $\text{DMSO-}d_6$) δ 165.01, 151.19, 147.20, 137.02, 135.29, 131.85, 130.85, 127.94, 125.25, 124.47.



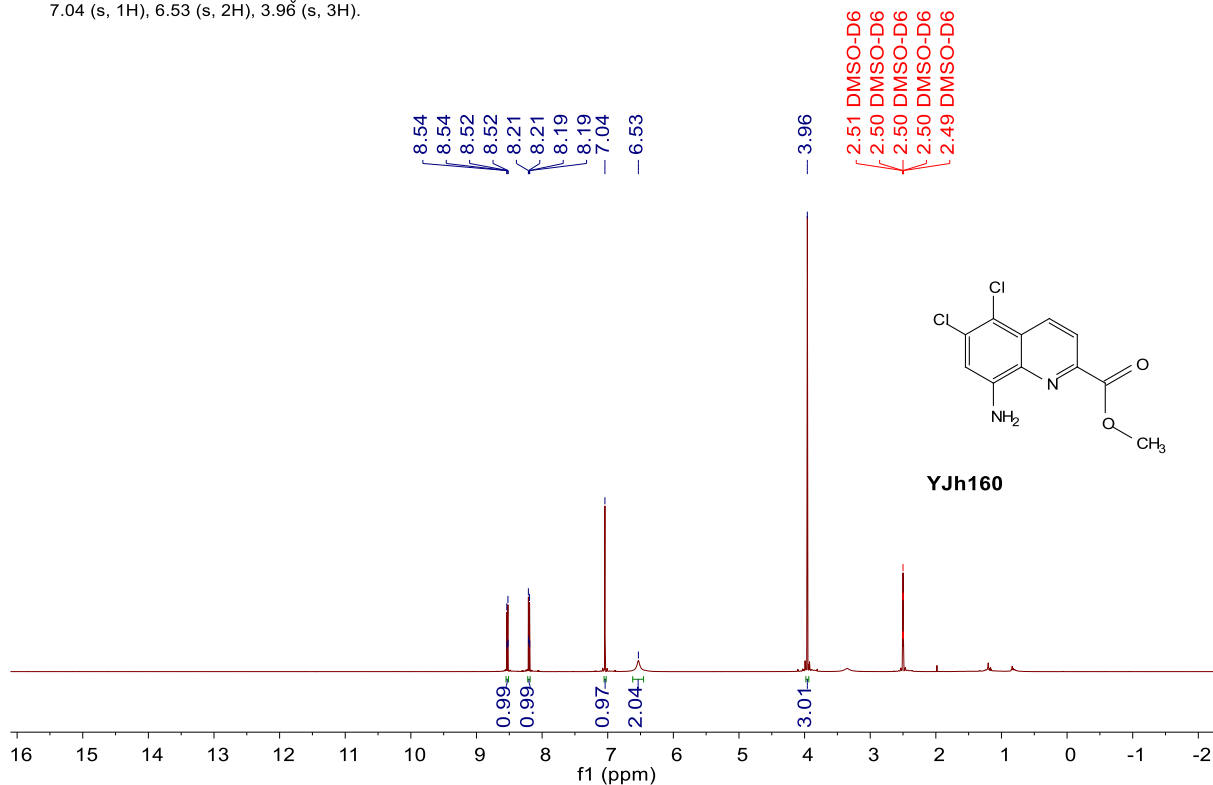
^1H NMR (500 MHz, $\text{DMSO-}d_6$) δ 13.51 (s, 1H), 10.43 (s, 1H), 8.27 (s, 1H), 7.96 – 7.90 (m, 2H), 7.86 (t, $J = 8.2$ Hz, 1H), 3.20 (s, 3H).



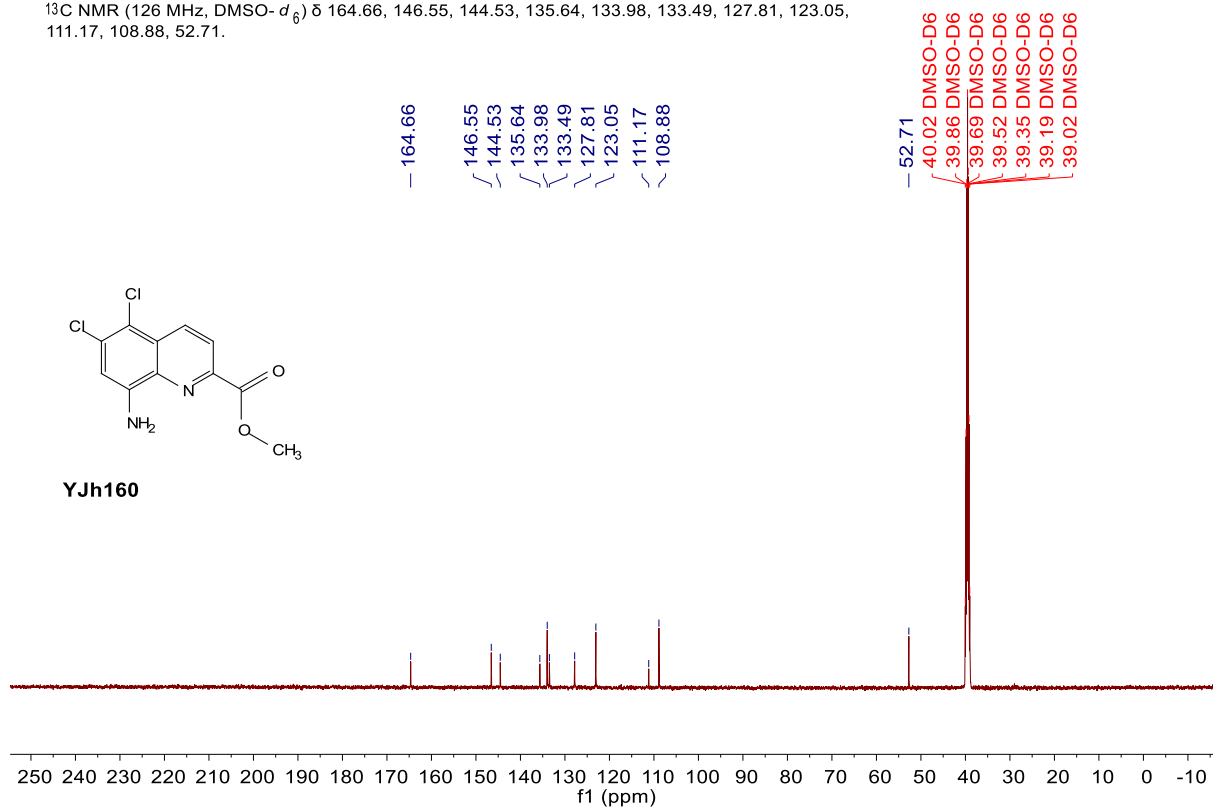
^{13}C NMR (126 MHz, $\text{DMSO-}d_6$) δ 164.36, 145.95, 143.46, 137.79, 136.21, 130.94, 127.21, 120.97, 117.62, 117.35, 39.78.



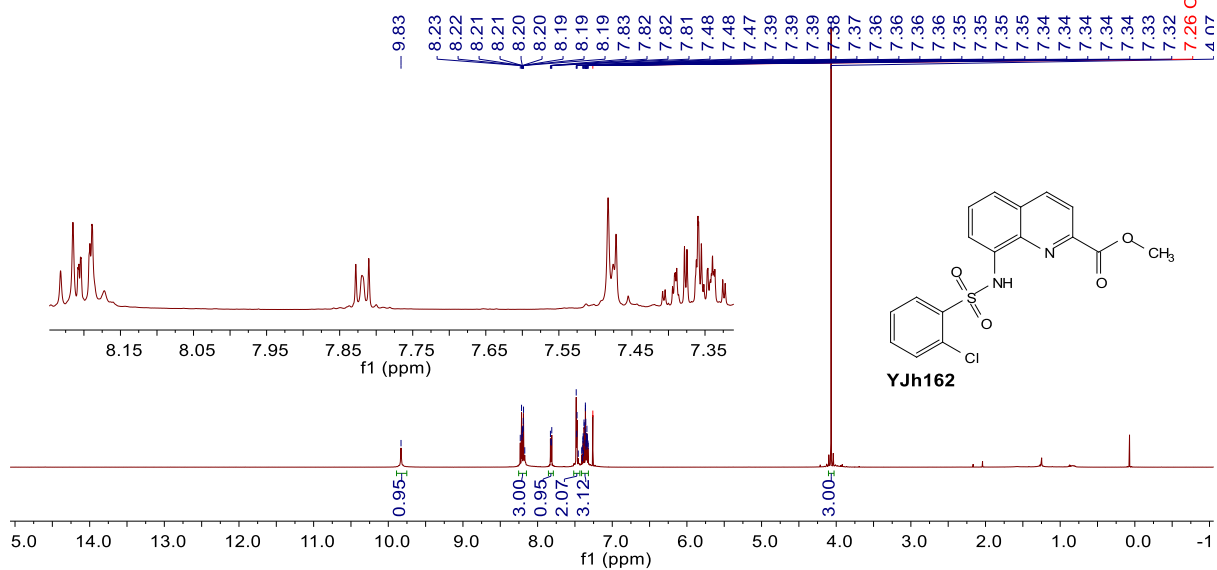
$^1\text{H NMR}$ (500 MHz, $\text{DMSO-}d_6$) δ 8.53 (dd, $J = 8.8, 1.3$ Hz, 1H), 8.20 (dd, $J = 8.8, 1.0$ Hz, 1H), 7.04 (s, 1H), 6.53 (s, 2H), 3.96 (s, 3H).



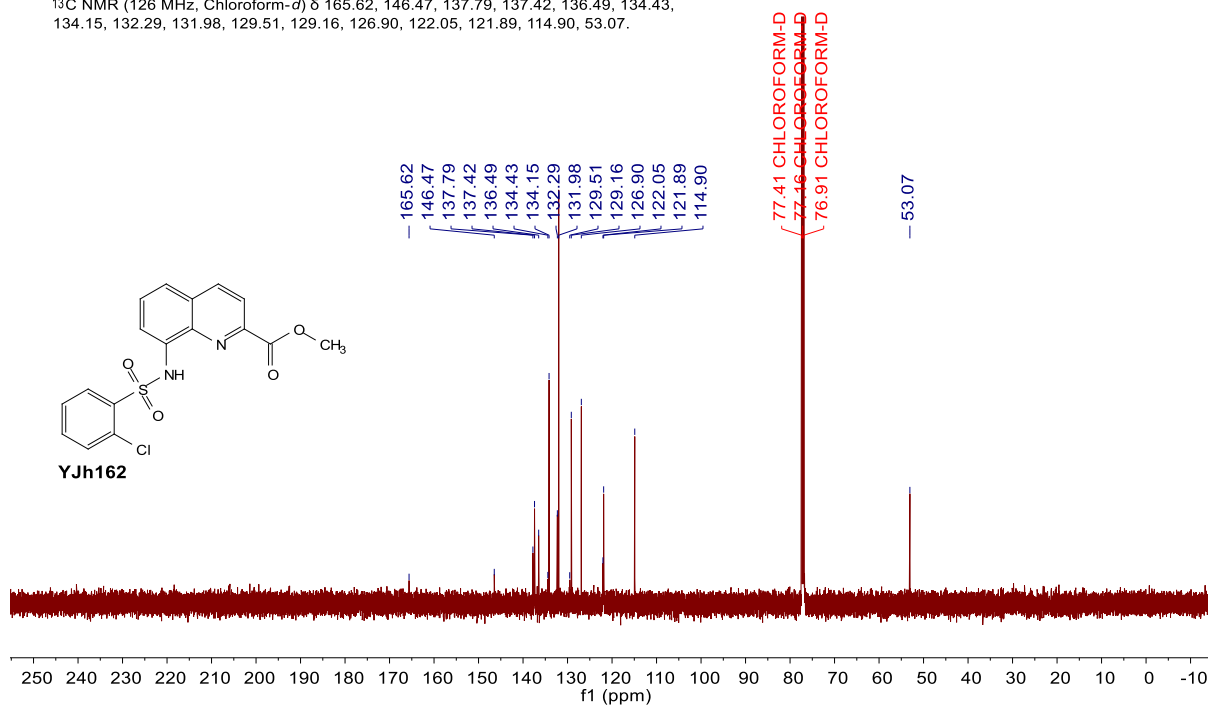
$^{13}\text{C NMR}$ (126 MHz, $\text{DMSO-}d_6$) δ 164.66, 146.55, 144.53, 135.64, 133.98, 133.49, 127.81, 123.05, 111.17, 108.88, 52.71.



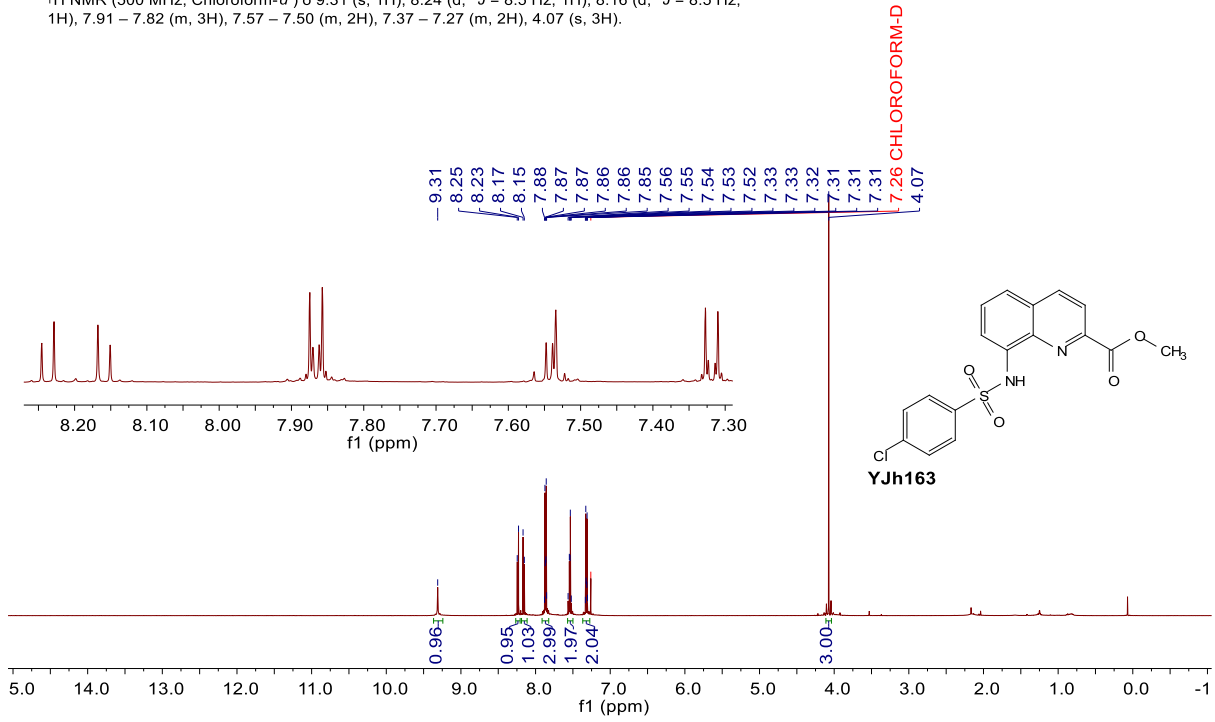
^1H NMR (500 MHz, Chloroform-*d*) δ 9.83 (s, 1H), 8.25 – 8.15 (m, 3H), 7.85 – 7.79 (m, 1H), 7.52 – 7.43 (m, 2H), 7.41 – 7.32 (m, 3H), 4.07 (s, 3H).



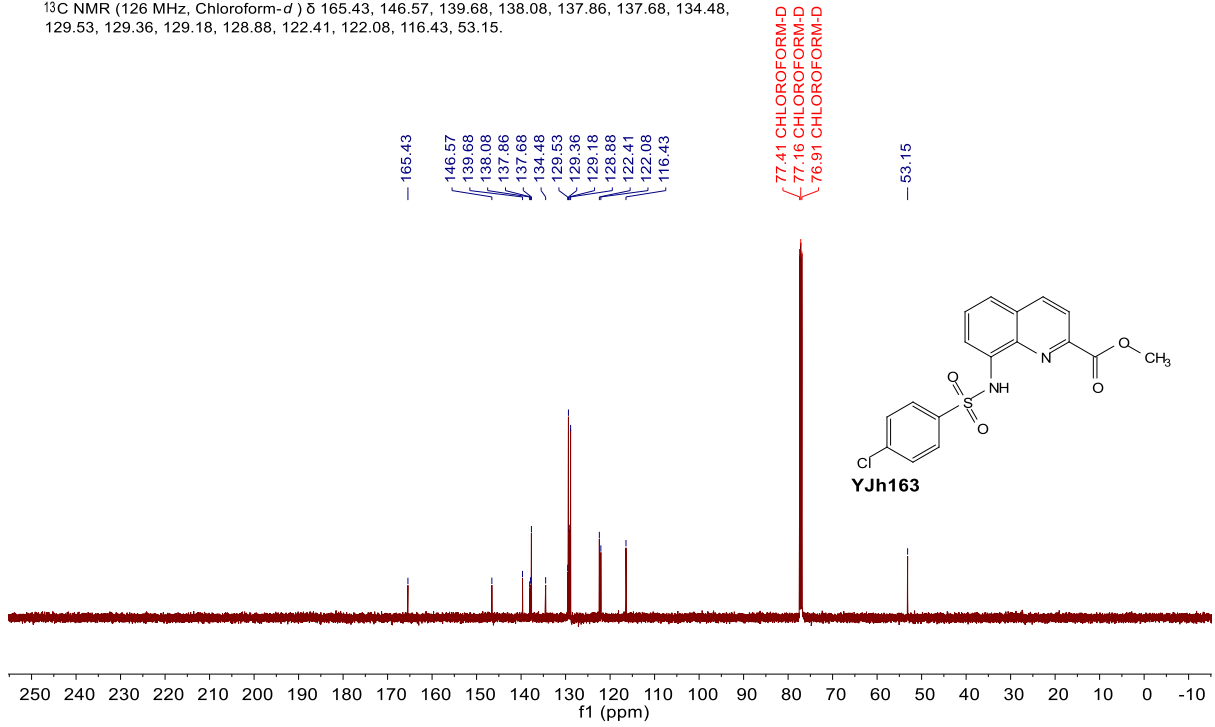
^{13}C NMR (126 MHz, Chloroform-*d*) δ 165.62, 146.47, 137.79, 137.42, 136.49, 134.43, 134.15, 132.29, 131.98, 129.51, 129.16, 126.90, 122.05, 121.89, 114.90, 53.07.



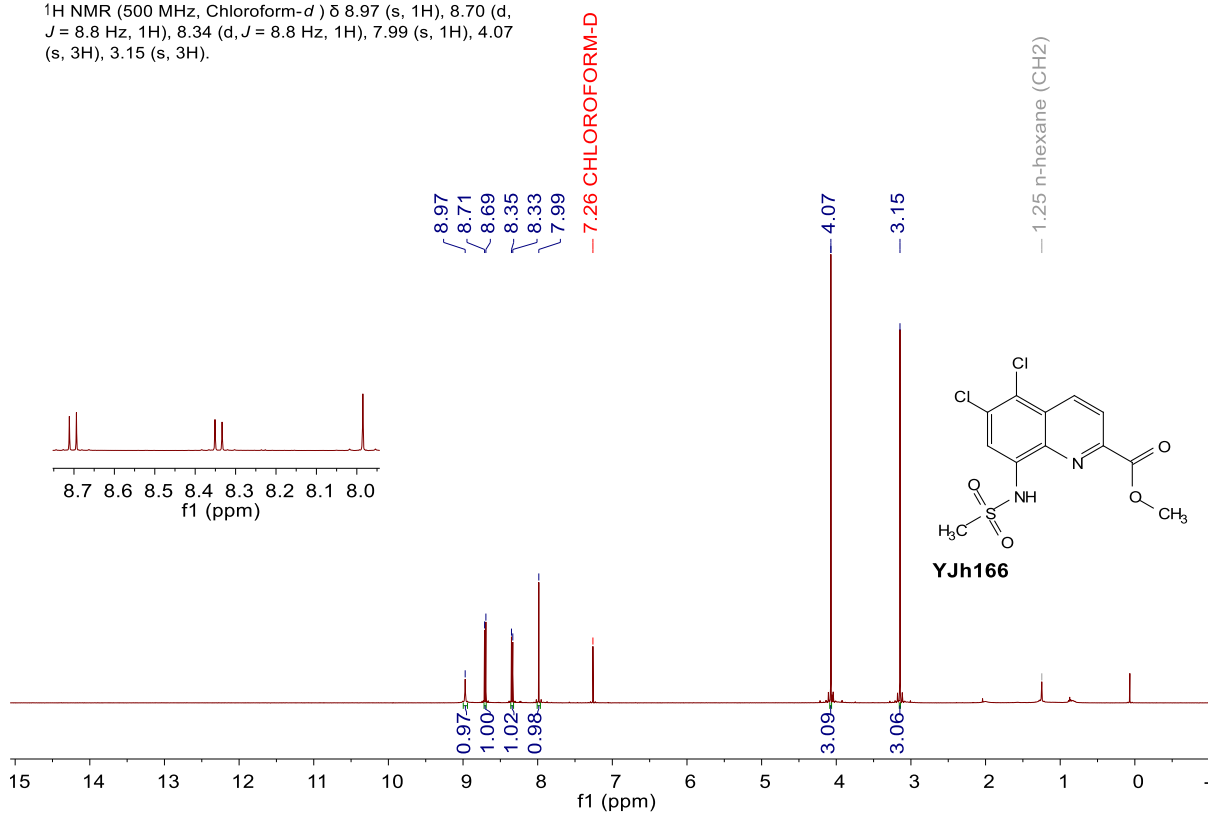
¹H NMR (500 MHz, Chloroform-*d*) δ 9.31 (s, 1H), 8.24 (d, *J* = 8.5 Hz, 1H), 8.16 (d, *J* = 8.5 Hz, 1H), 7.91 – 7.82 (m, 3H), 7.57 – 7.50 (m, 2H), 7.37 – 7.27 (m, 2H), 4.07 (s, 3H).



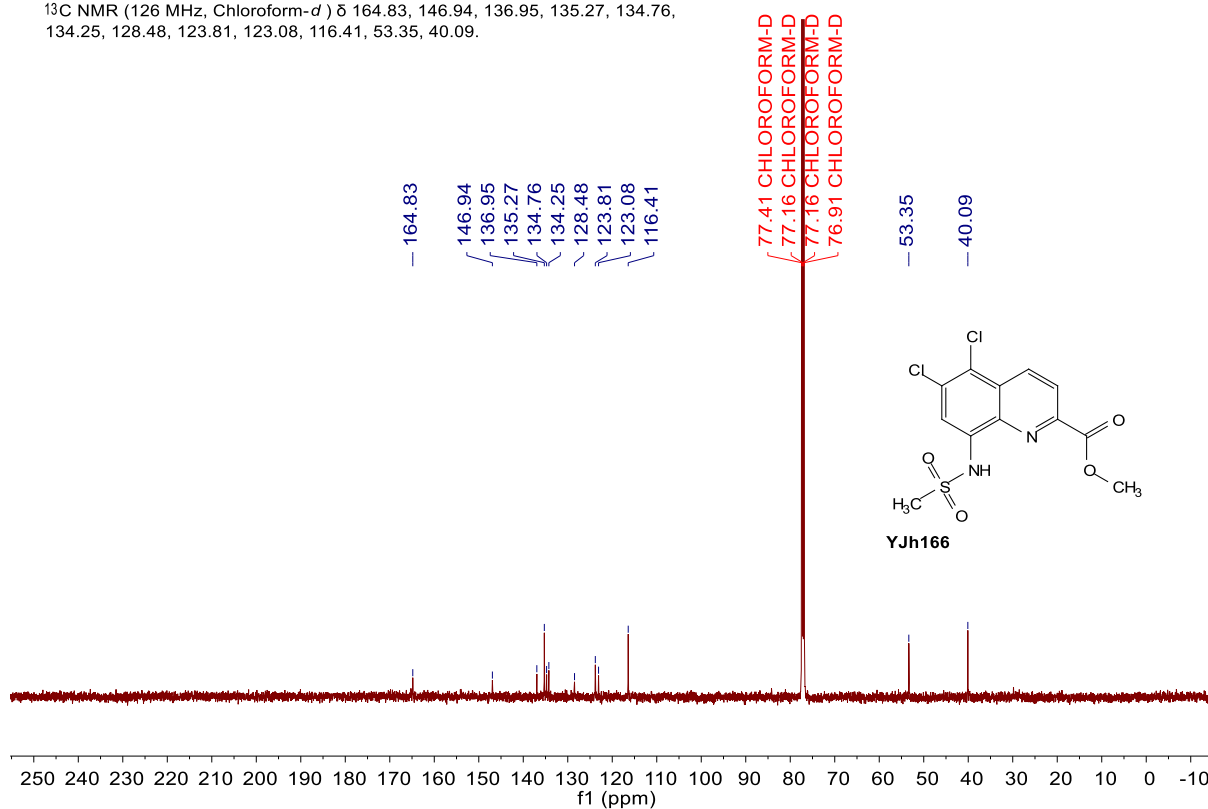
¹³C NMR (126 MHz, Chloroform-*d*) δ 165.43, 146.57, 139.68, 138.08, 137.86, 137.68, 134.48, 129.53, 129.36, 129.18, 128.88, 122.41, 122.08, 116.43, 53.15.



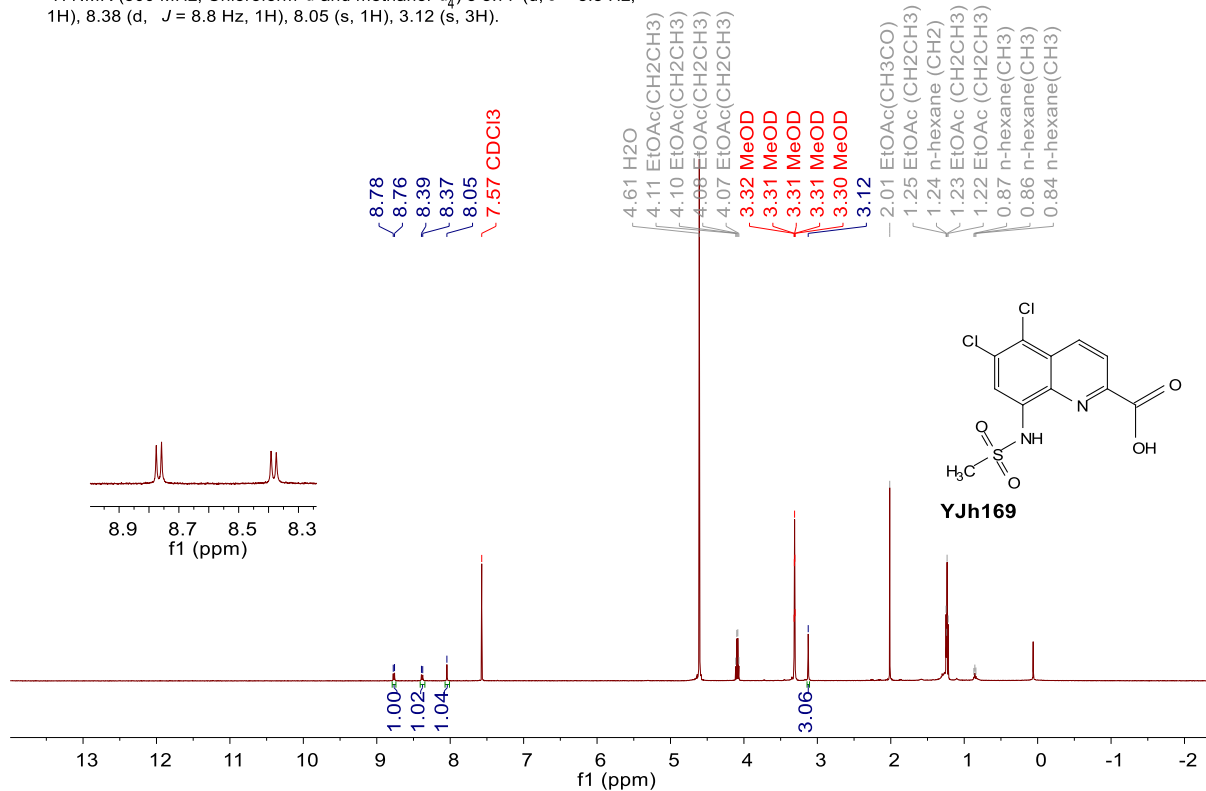
¹H NMR (500 MHz, Chloroform-*d*) δ 8.97 (s, 1H), 8.70 (d, *J* = 8.8 Hz, 1H), 8.34 (d, *J* = 8.8 Hz, 1H), 7.99 (s, 1H), 4.07 (s, 3H), 3.15 (s, 3H).



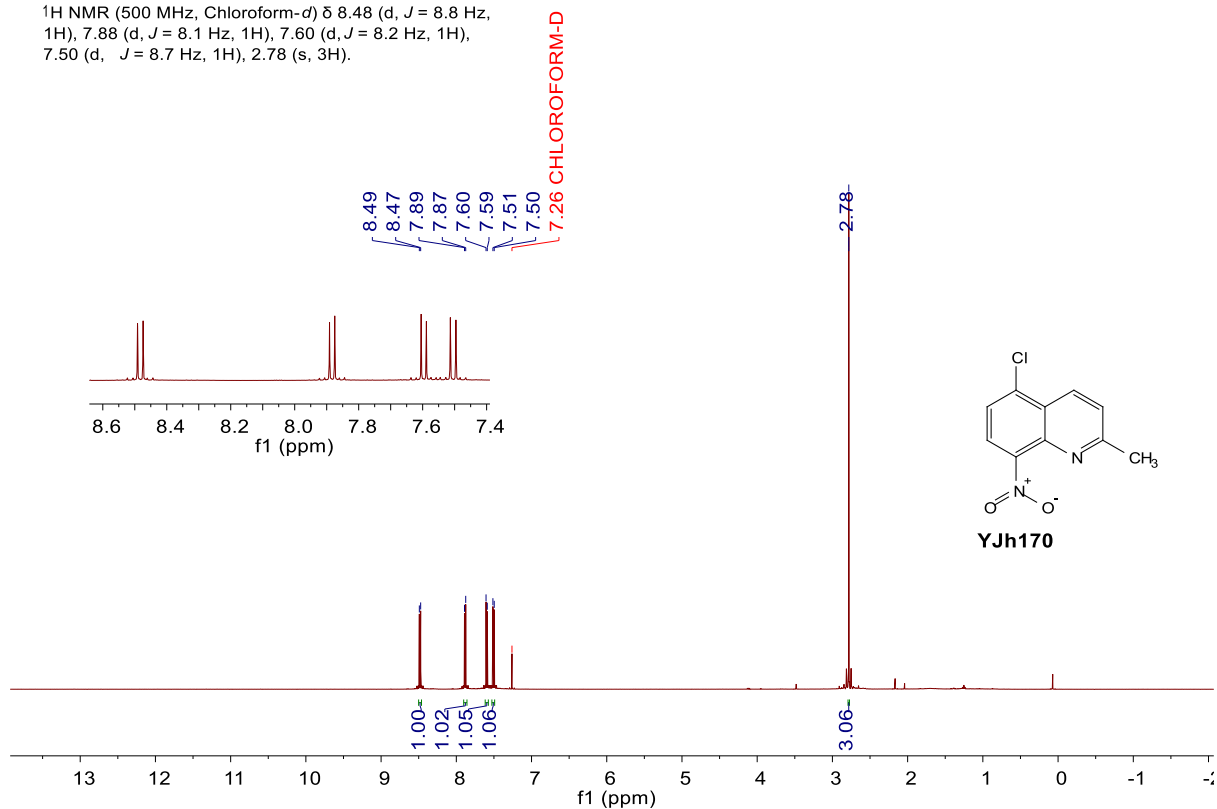
¹³C NMR (126 MHz, Chloroform-*d*) δ 164.83, 146.94, 136.95, 135.27, 134.76, 134.25, 128.48, 123.81, 123.08, 116.41, 53.35, 40.09.



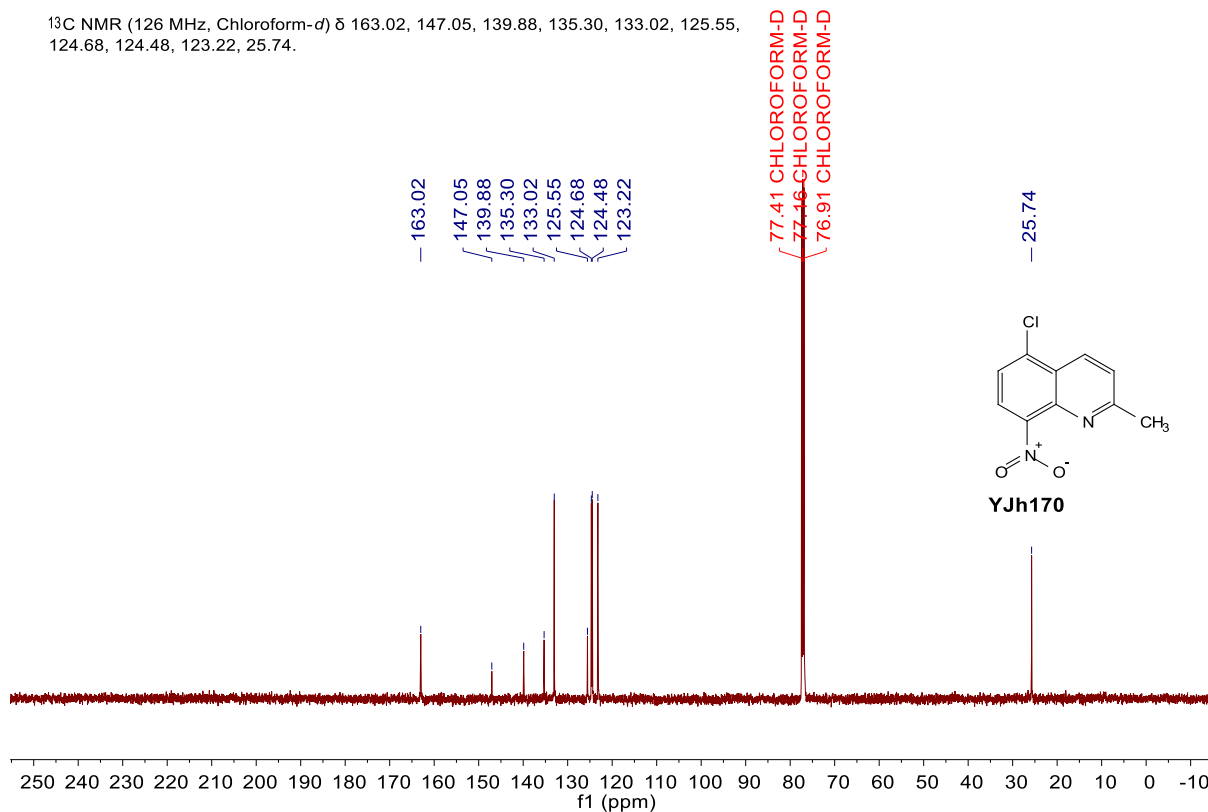
¹H NMR (500 MHz, Chloroform-*d* and methanol-*d*₄) δ 8.77 (d, *J* = 8.8 Hz, 1H), 8.38 (d, *J* = 8.8 Hz, 1H), 8.05 (s, 1H), 3.12 (s, 3H).



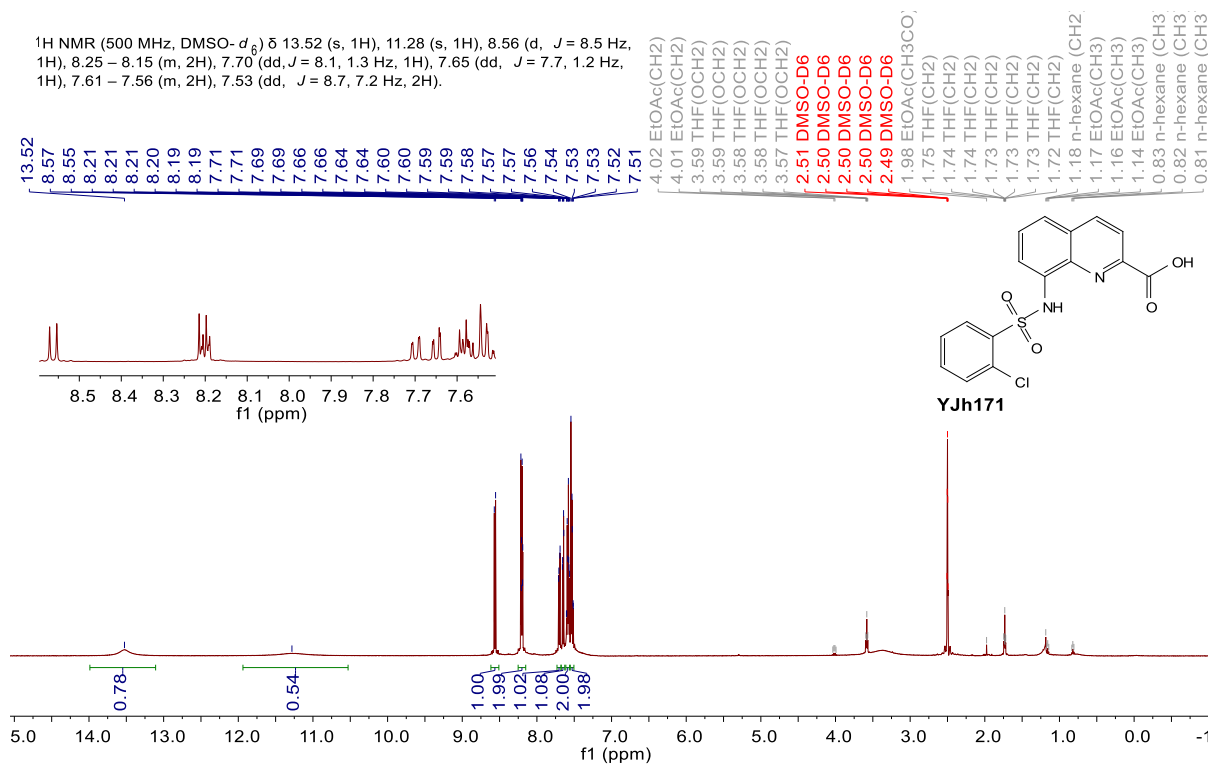
¹H NMR (500 MHz, Chloroform-*d*) δ 8.48 (d, *J* = 8.8 Hz, 1H), 7.88 (d, *J* = 8.1 Hz, 1H), 7.60 (d, *J* = 8.2 Hz, 1H), 7.50 (d, *J* = 8.7 Hz, 1H), 2.78 (s, 3H).



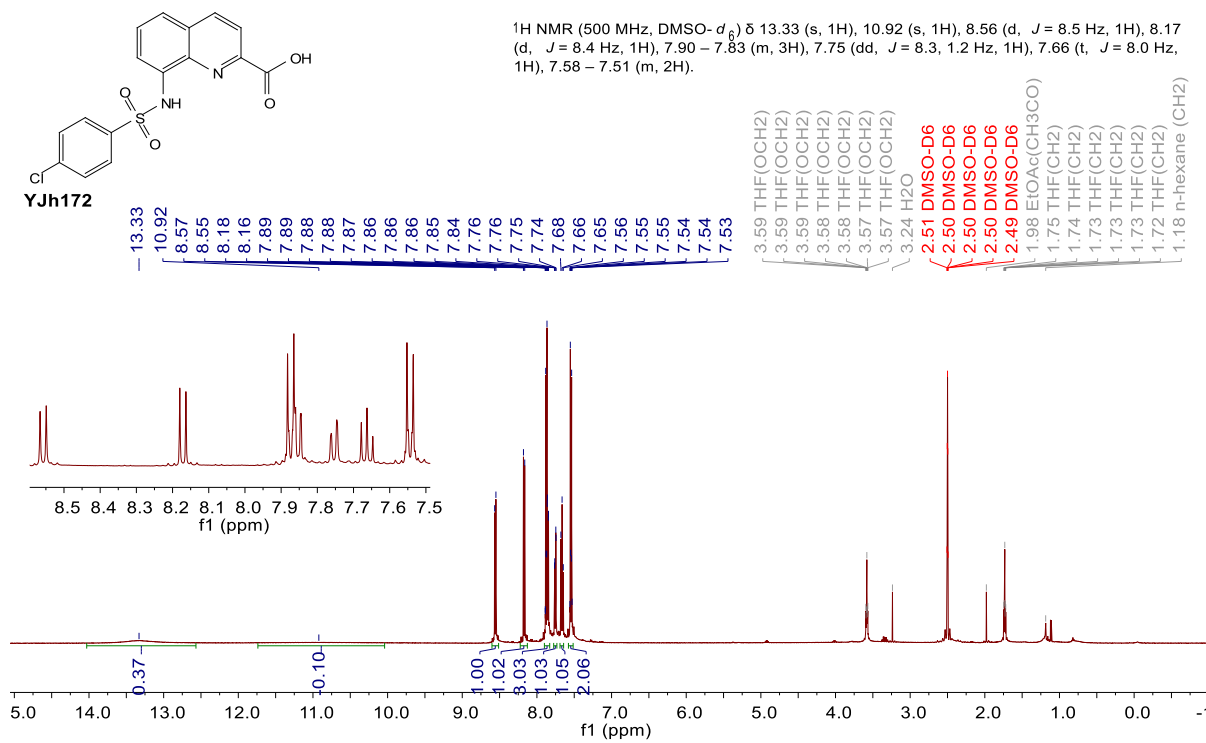
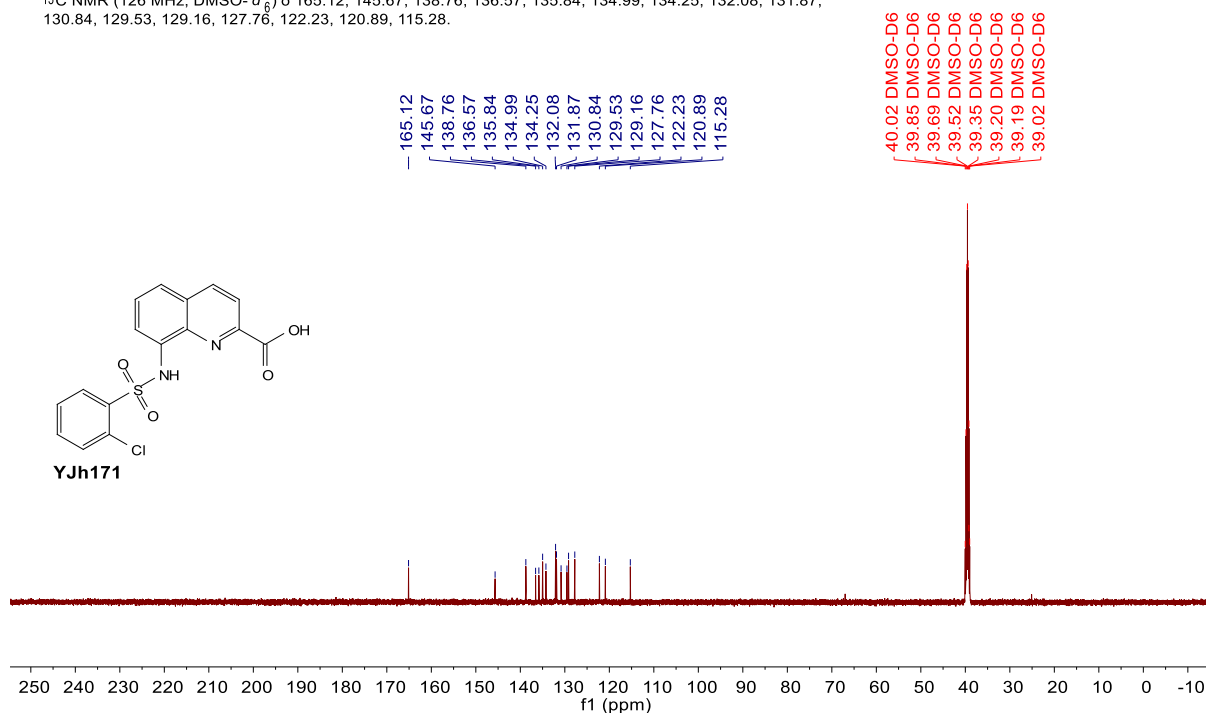
^{13}C NMR (126 MHz, Chloroform- d) δ 163.02, 147.05, 139.88, 135.30, 133.02, 125.55, 124.68, 124.48, 123.22, 25.74.



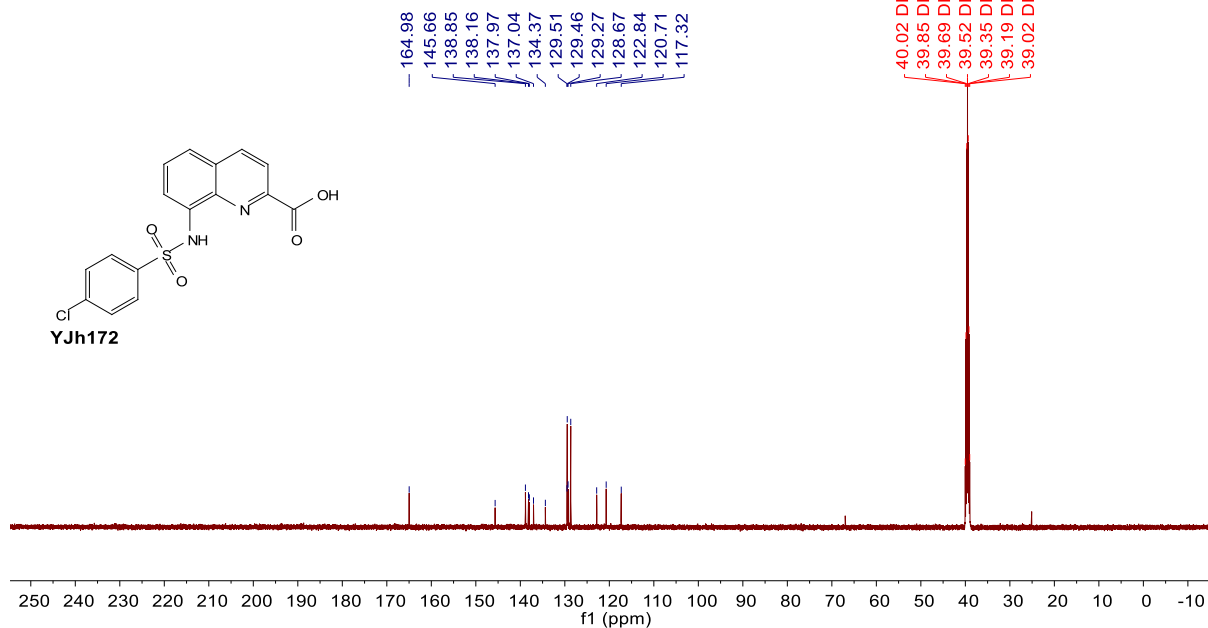
^1H NMR (500 MHz, DMSO- d_6) δ 13.52 (s, 1H), 11.28 (s, 1H), 8.56 (d, $J = 8.5$ Hz, 1H), 8.25 – 8.15 (m, 2H), 7.70 (dd, $J = 8.1, 1.3$ Hz, 1H), 7.65 (dd, $J = 7.7, 1.2$ Hz, 1H), 7.61 – 7.56 (m, 2H), 7.53 (dd, $J = 8.7, 7.2$ Hz, 2H).



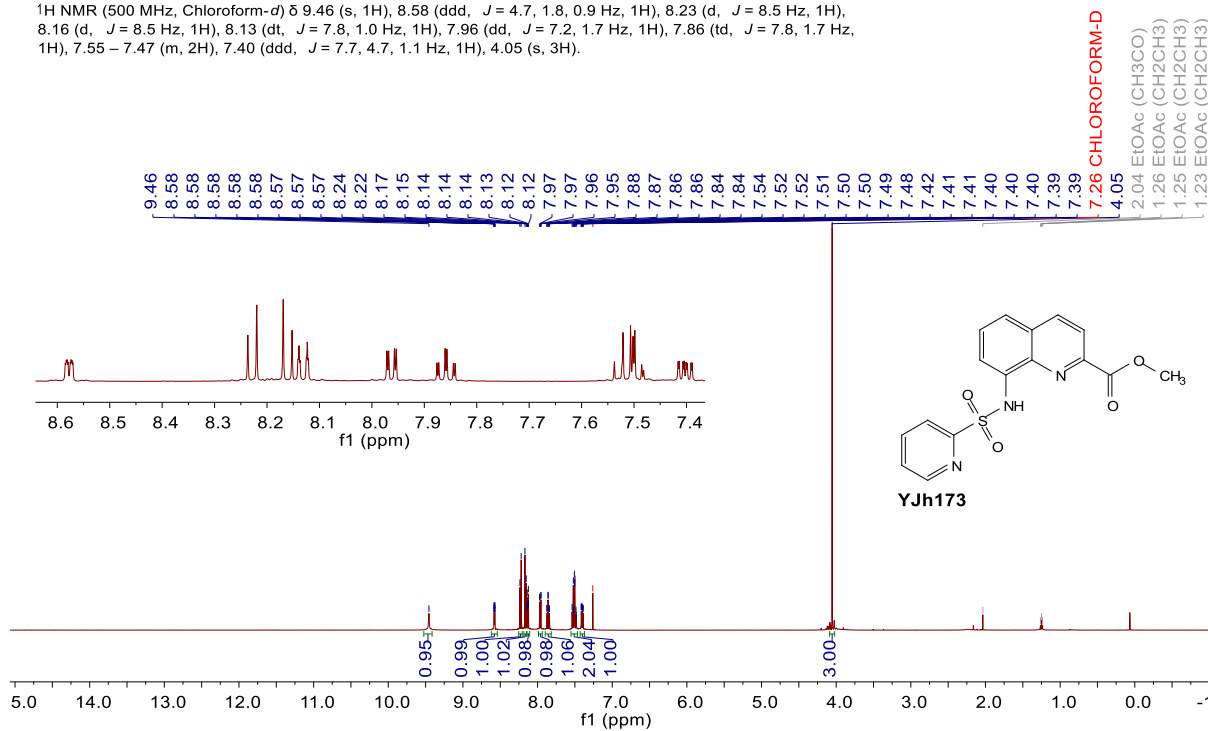
^{13}C NMR (126 MHz, $\text{DMSO}-d_6$) δ 165.12, 145.67, 138.76, 136.57, 135.84, 134.99, 134.25, 132.08, 131.87, 130.84, 129.53, 129.16, 127.76, 122.23, 120.89, 115.28.



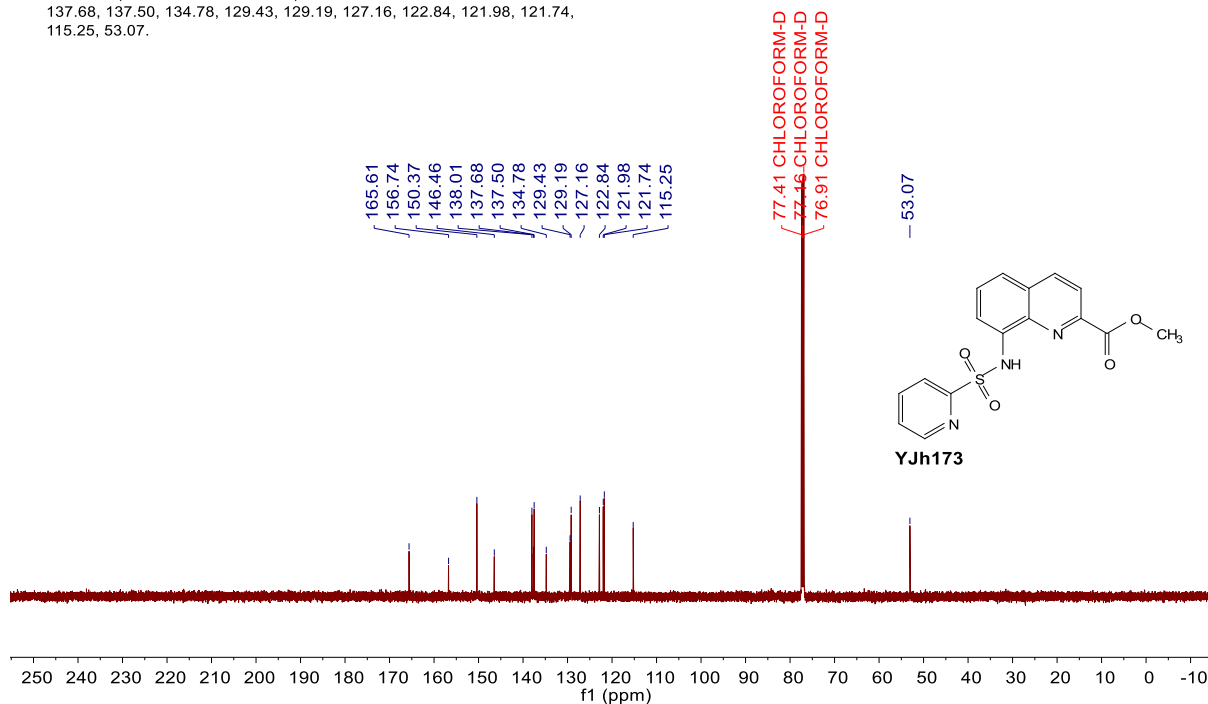
¹³C NMR (126 MHz, DMSO-*d*₆) δ 164.98, 145.66, 138.85, 138.16, 137.97, 137.04, 134.37, 129.51, 129.46, 129.27, 128.67, 122.84, 120.71, 117.32.



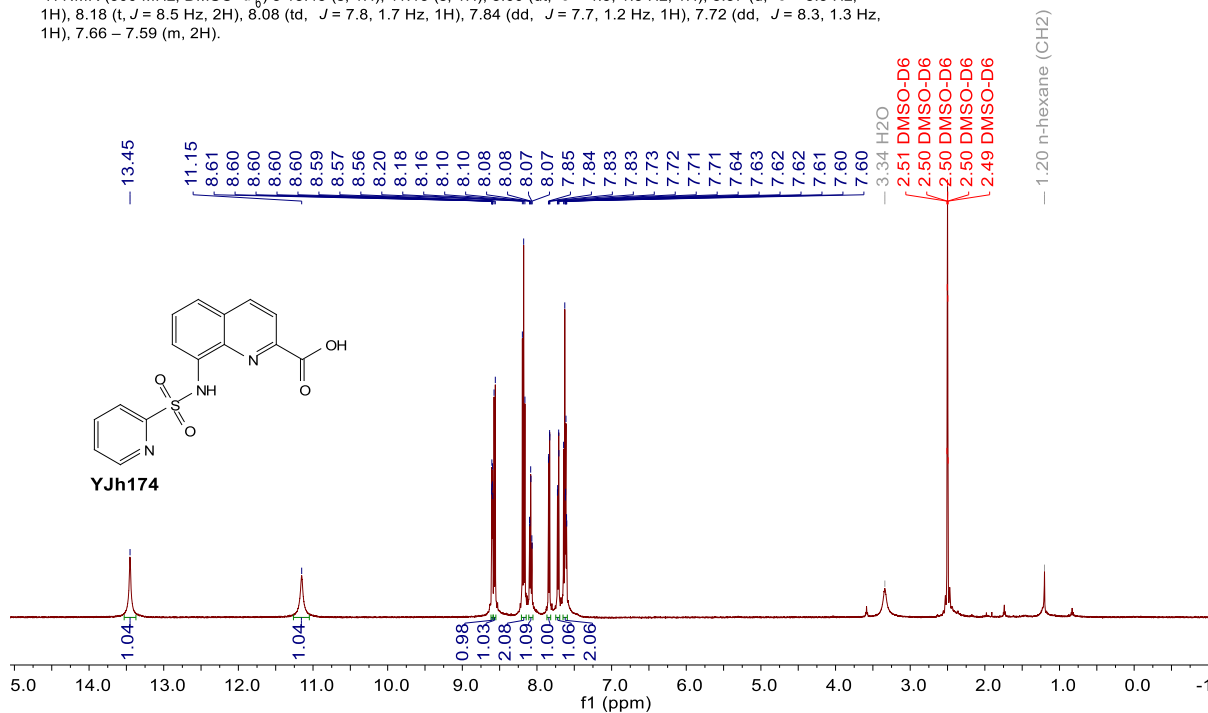
¹H NMR (500 MHz, Chloroform-*d*) δ 9.46 (s, 1H), 8.58 (ddd, *J* = 4.7, 1.8, 0.9 Hz, 1H), 8.23 (d, *J* = 8.5 Hz, 1H), 8.16 (d, *J* = 8.5 Hz, 1H), 8.13 (dt, *J* = 7.8, 1.0 Hz, 1H), 7.96 (dd, *J* = 7.2, 1.7 Hz, 1H), 7.86 (td, *J* = 7.8, 1.7 Hz, 1H), 7.55 – 7.47 (m, 2H), 7.40 (ddd, *J* = 7.7, 4.7, 1.1 Hz, 1H), 4.05 (s, 3H).



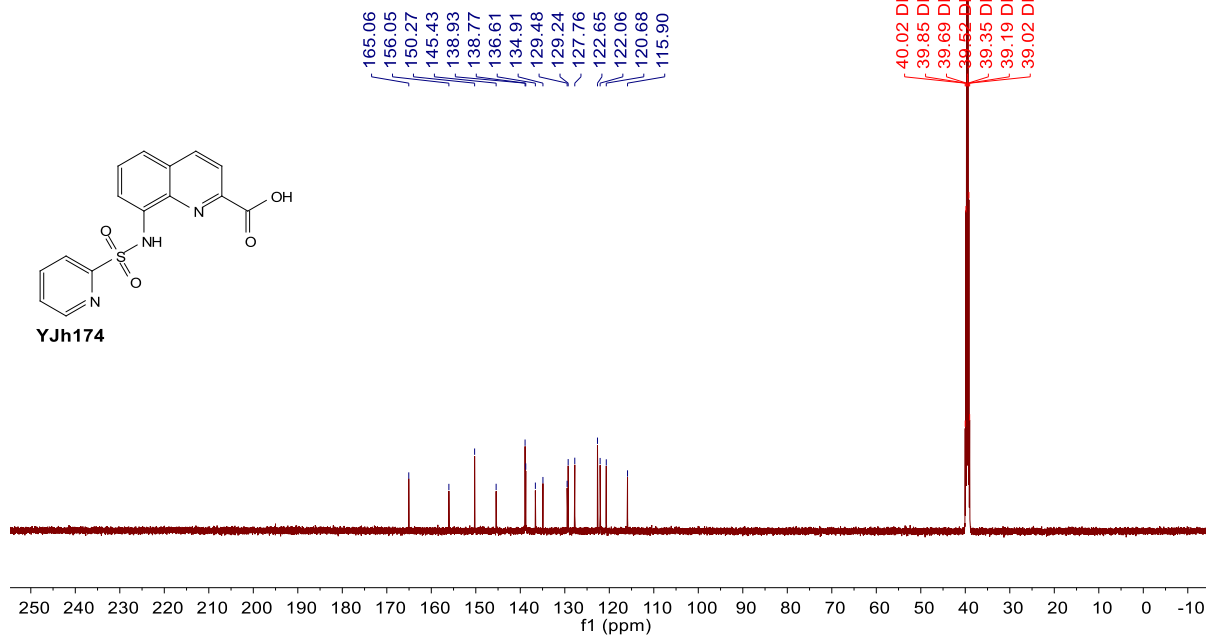
^{13}C NMR (126 MHz, Chloroform- d) δ 165.61, 156.74, 150.37, 146.46, 138.01, 137.68, 137.50, 134.78, 129.43, 129.19, 127.16, 122.84, 121.98, 121.74, 115.25, 53.07.



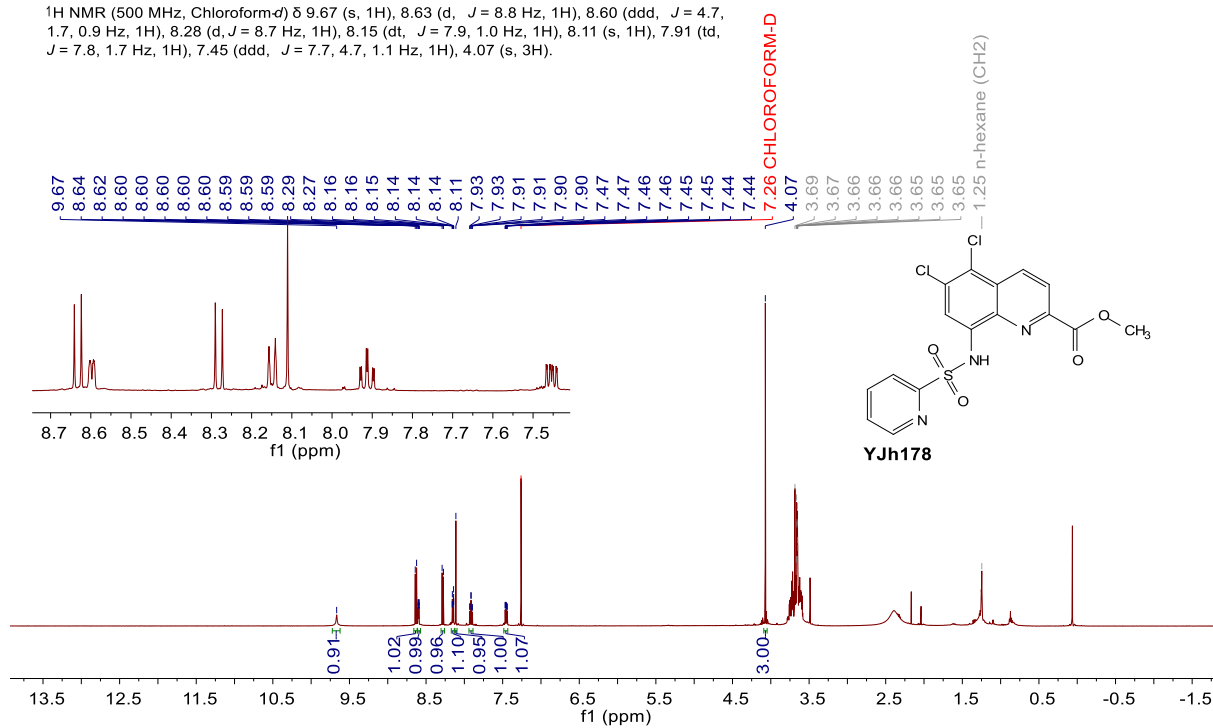
^1H NMR (500 MHz, DMSO- d_6) δ 13.45 (s, 1H), 11.15 (s, 1H), 8.60 (dt, $J = 4.5, 1.3$ Hz, 1H), 8.57 (d, $J = 8.5$ Hz, 1H), 8.18 (t, $J = 8.5$ Hz, 2H), 8.08 (td, $J = 7.8, 1.7$ Hz, 1H), 7.84 (dd, $J = 7.7, 1.2$ Hz, 1H), 7.72 (dd, $J = 8.3, 1.3$ Hz, 1H), 7.66 – 7.59 (m, 2H).



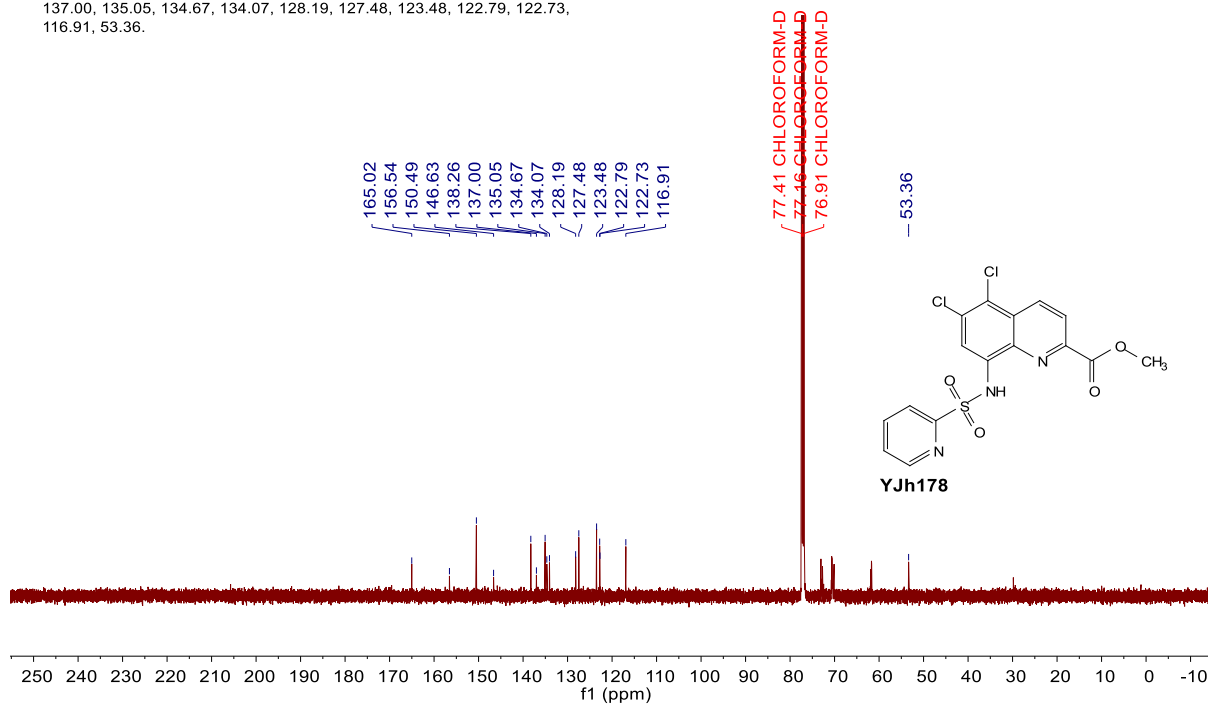
¹³C NMR (126 MHz, DMSO-*d*₆) δ 165.06, 156.05, 150.27, 145.43, 138.93, 138.77, 136.61, 134.91, 129.48, 129.24, 127.76, 122.65, 122.06, 120.68, 115.90.



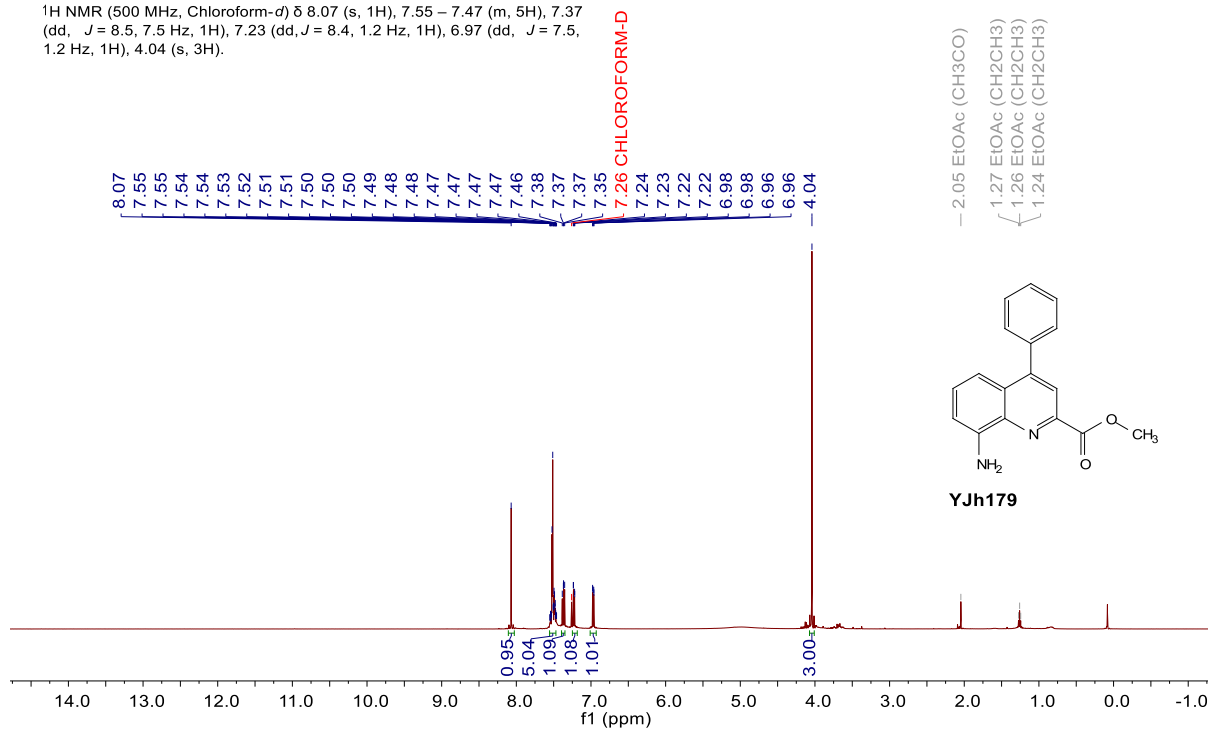
¹H NMR (500 MHz, Chloroform-*d*) δ 9.67 (s, 1H), 8.63 (d, *J* = 8.8 Hz, 1H), 8.60 (ddd, *J* = 4.7, 1.7, 0.9 Hz, 1H), 8.28 (d, *J* = 8.7 Hz, 1H), 8.15 (dt, *J* = 7.9, 1.0 Hz, 1H), 8.11 (s, 1H), 7.91 (td, *J* = 7.8, 1.7 Hz, 1H), 7.45 (ddd, *J* = 7.7, 4.7, 1.1 Hz, 1H), 4.07 (s, 3H).



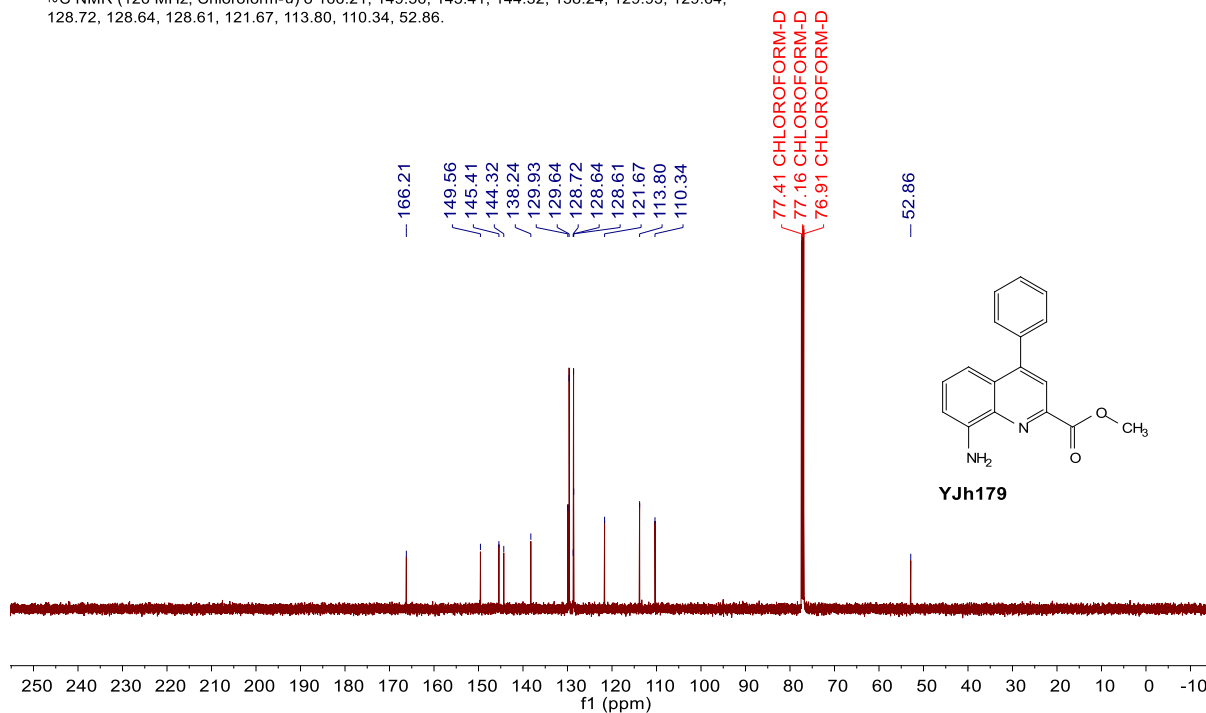
¹³C NMR (126 MHz, Chloroform-*d*) δ 165.02, 156.54, 150.49, 146.63, 138.26, 137.00, 135.05, 134.67, 134.07, 128.19, 127.48, 123.48, 122.79, 122.73, 116.91, 53.36.



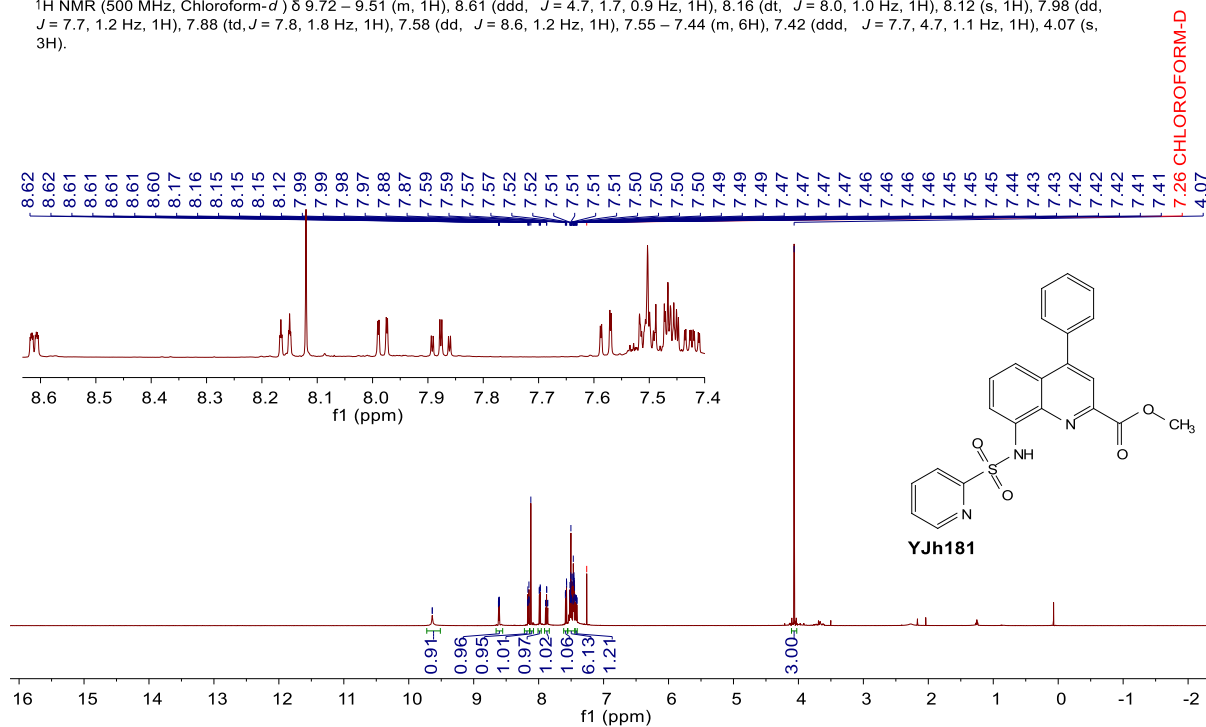
¹H NMR (500 MHz, Chloroform-*d*) δ 8.07 (s, 1H), 7.55 – 7.47 (m, 5H), 7.37 (dd, *J* = 8.5, 7.5 Hz, 1H), 7.23 (dd, *J* = 8.4, 1.2 Hz, 1H), 6.97 (dd, *J* = 7.5, 1.2 Hz, 1H), 4.04 (s, 3H).



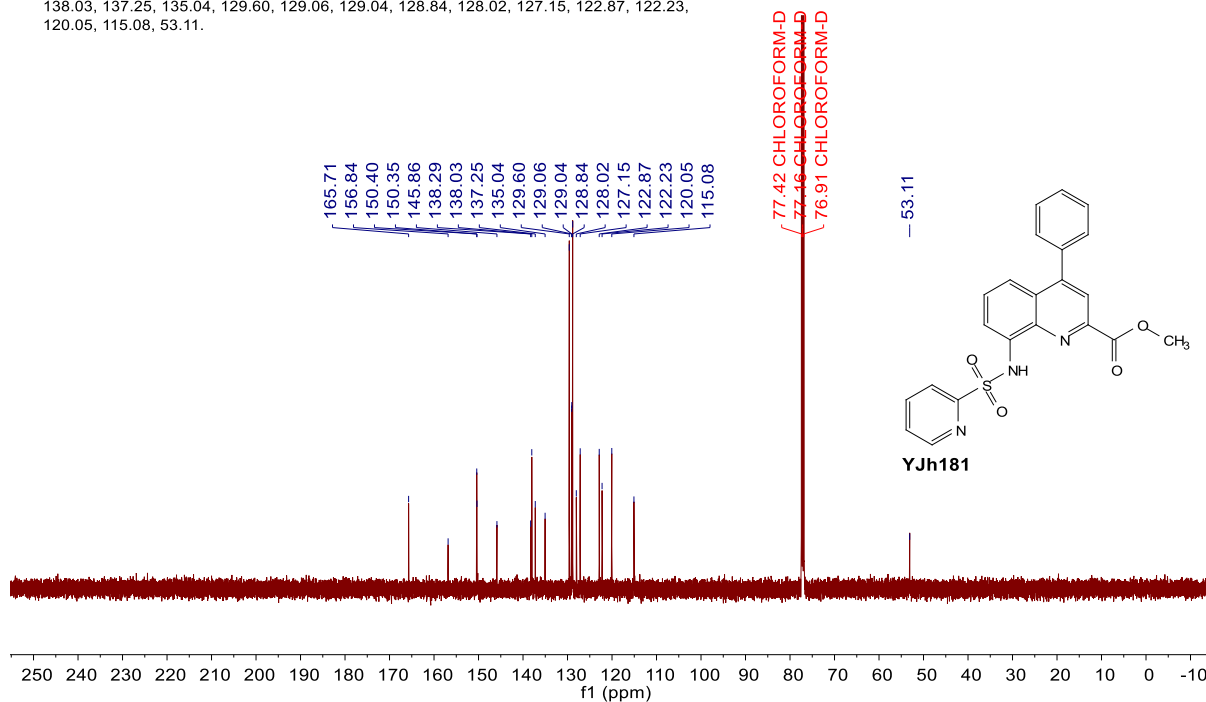
¹³C NMR (126 MHz, Chloroform-*d*) δ 166.21, 149.56, 145.41, 144.32, 138.24, 129.93, 129.64, 128.72, 128.64, 128.61, 121.67, 113.80, 110.34, 52.86.



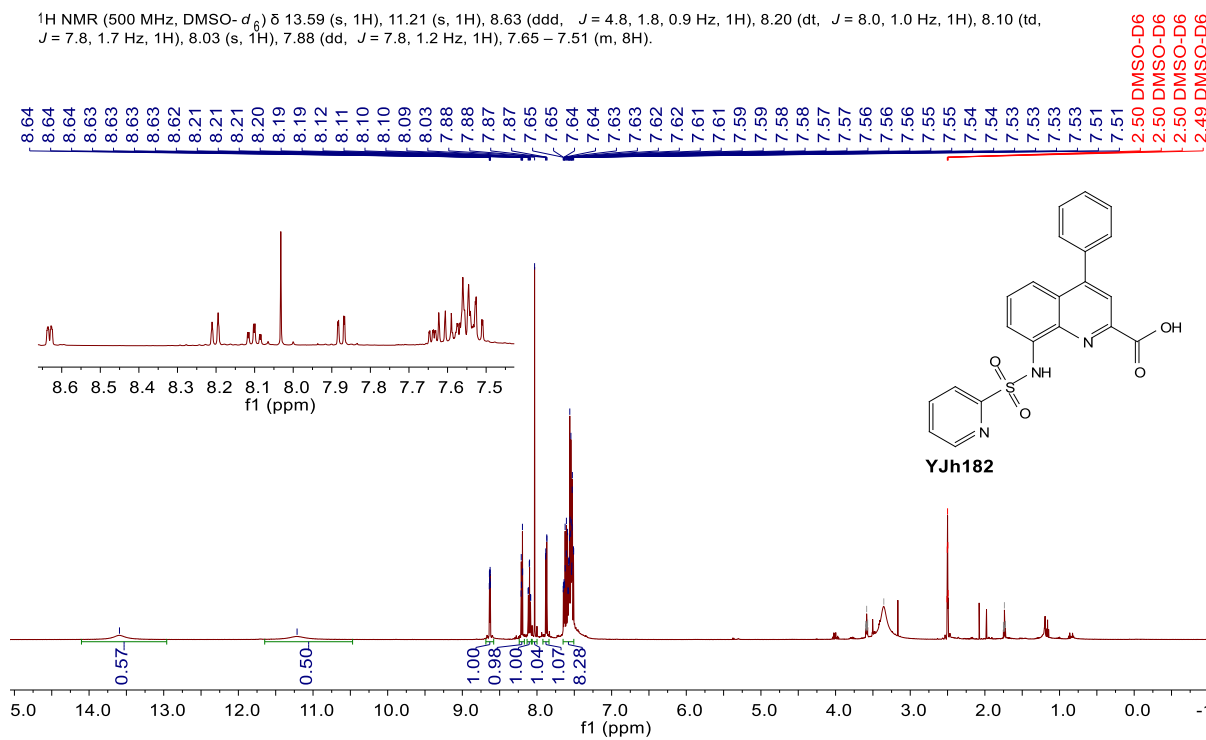
¹H NMR (500 MHz, Chloroform-*d*) δ 9.72 – 9.51 (m, 1H), 8.61 (ddd, *J* = 4.7, 1.7, 0.9 Hz, 1H), 8.16 (dt, *J* = 8.0, 1.0 Hz, 1H), 8.12 (s, 1H), 7.98 (dd, *J* = 7.7, 1.2 Hz, 1H), 7.88 (td, *J* = 7.8, 1.8 Hz, 1H), 7.58 (dd, *J* = 8.6, 1.2 Hz, 1H), 7.55 – 7.44 (m, 6H), 7.42 (ddd, *J* = 7.7, 4.7, 1.1 Hz, 1H), 4.07 (s, 3H).



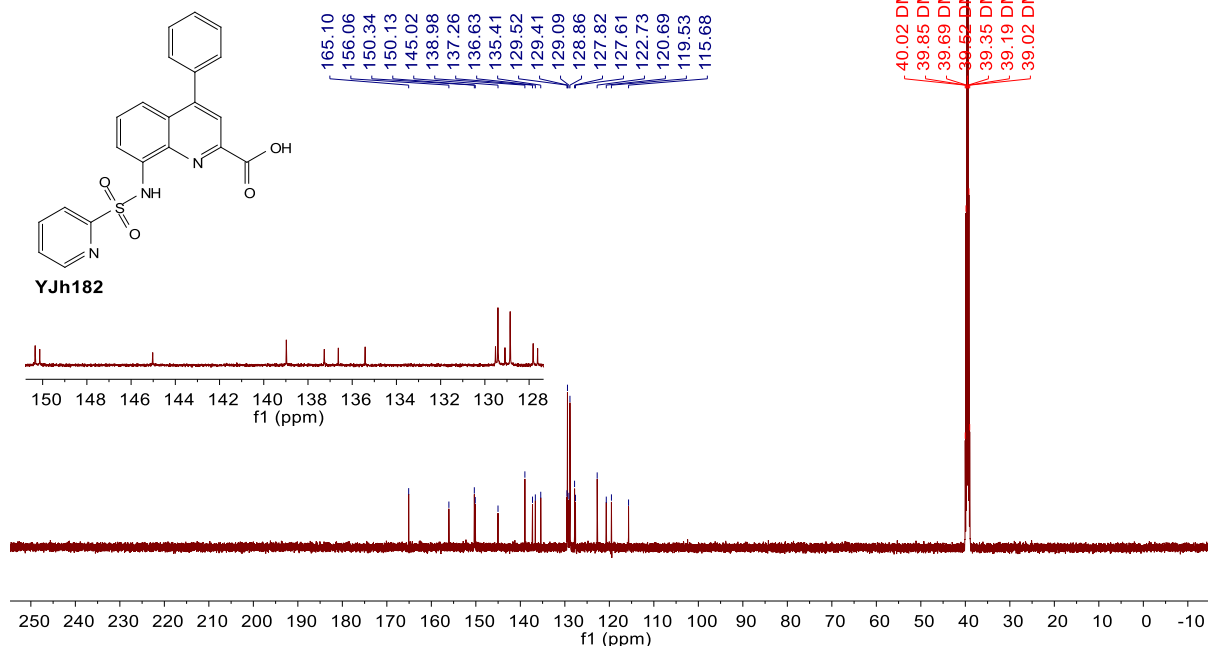
¹³C NMR (126 MHz, Chloroform-*d*) δ 165.71, 156.84, 150.40, 150.35, 145.86, 138.29, 138.03, 137.25, 135.04, 129.60, 129.06, 129.04, 128.84, 128.02, 127.15, 122.87, 122.23, 120.05, 115.08, 53.11.



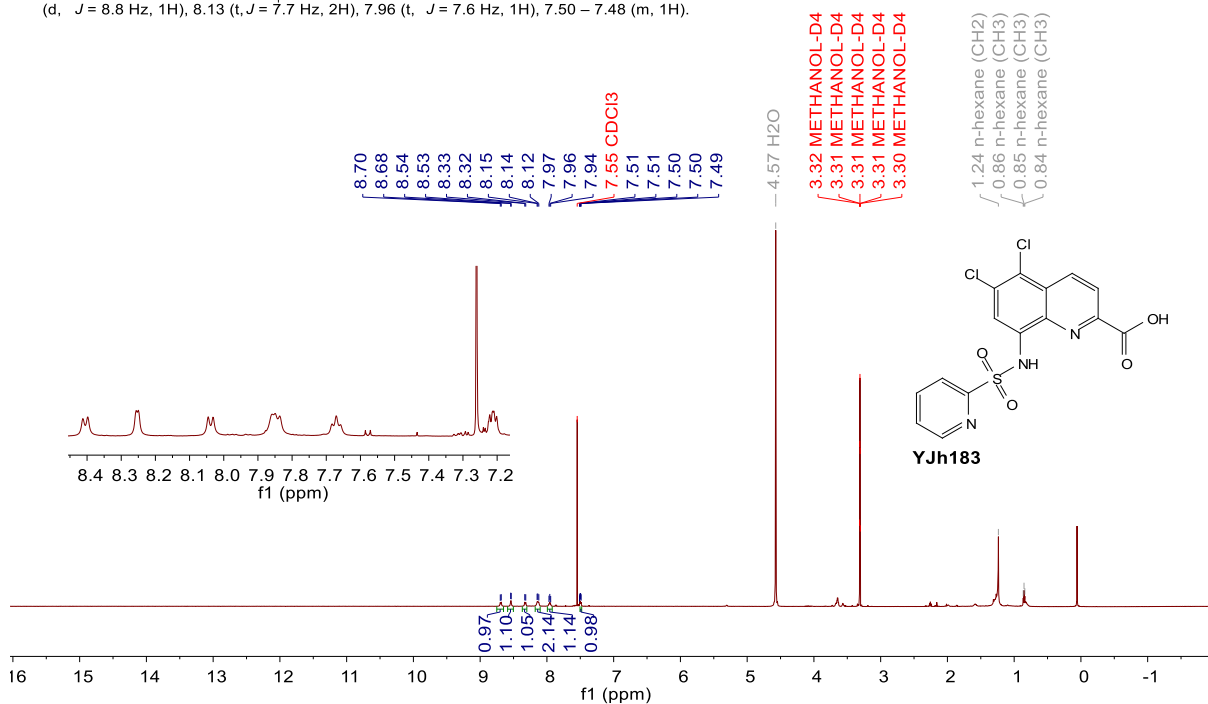
¹H NMR (500 MHz, DMSO-*d*₆) δ 13.59 (s, 1H), 11.21 (s, 1H), 8.63 (ddd, *J* = 4.8, 1.8, 0.9 Hz, 1H), 8.20 (dt, *J* = 8.0, 1.0 Hz, 1H), 8.10 (td, *J* = 7.8, 1.7 Hz, 1H), 8.03 (s, 1H), 7.88 (dd, *J* = 7.8, 1.2 Hz, 1H), 7.65 – 7.51 (m, 8H).



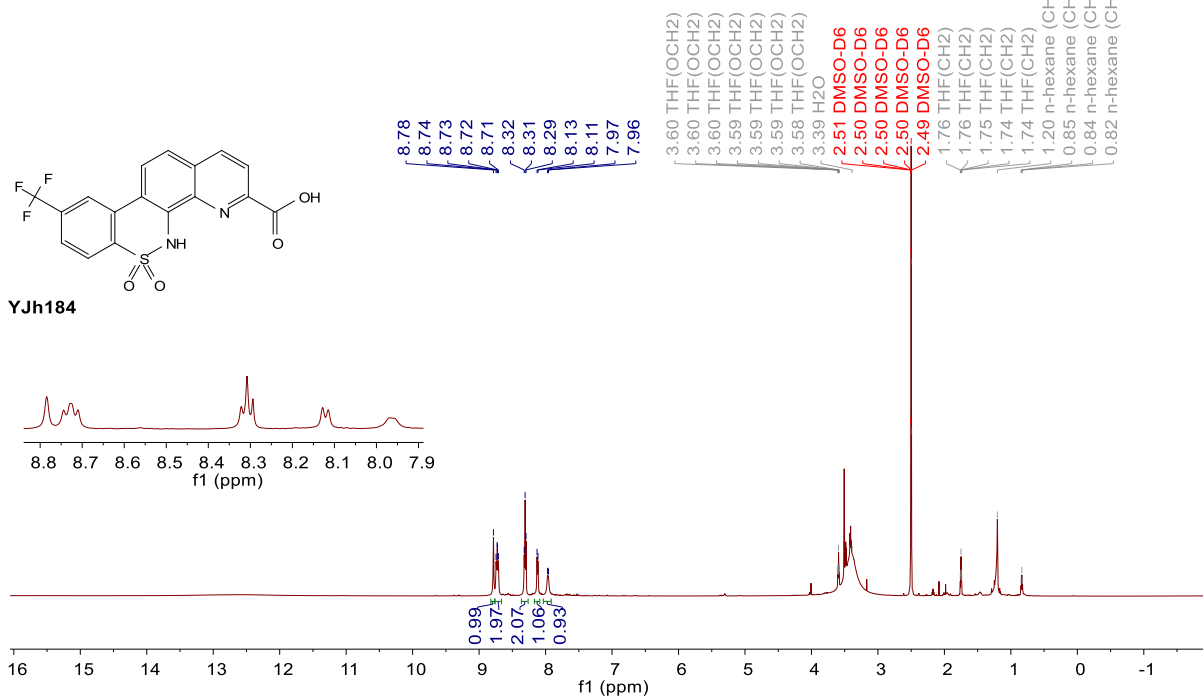
¹³C NMR (126 MHz, DMSO-*d*₆) δ 165.10, 156.06, 150.34, 150.13, 145.02, 138.98, 137.26, 136.63, 135.41, 129.52, 129.41, 129.09, 128.86, 127.82, 127.61, 122.73, 120.69, 119.53, 115.68.



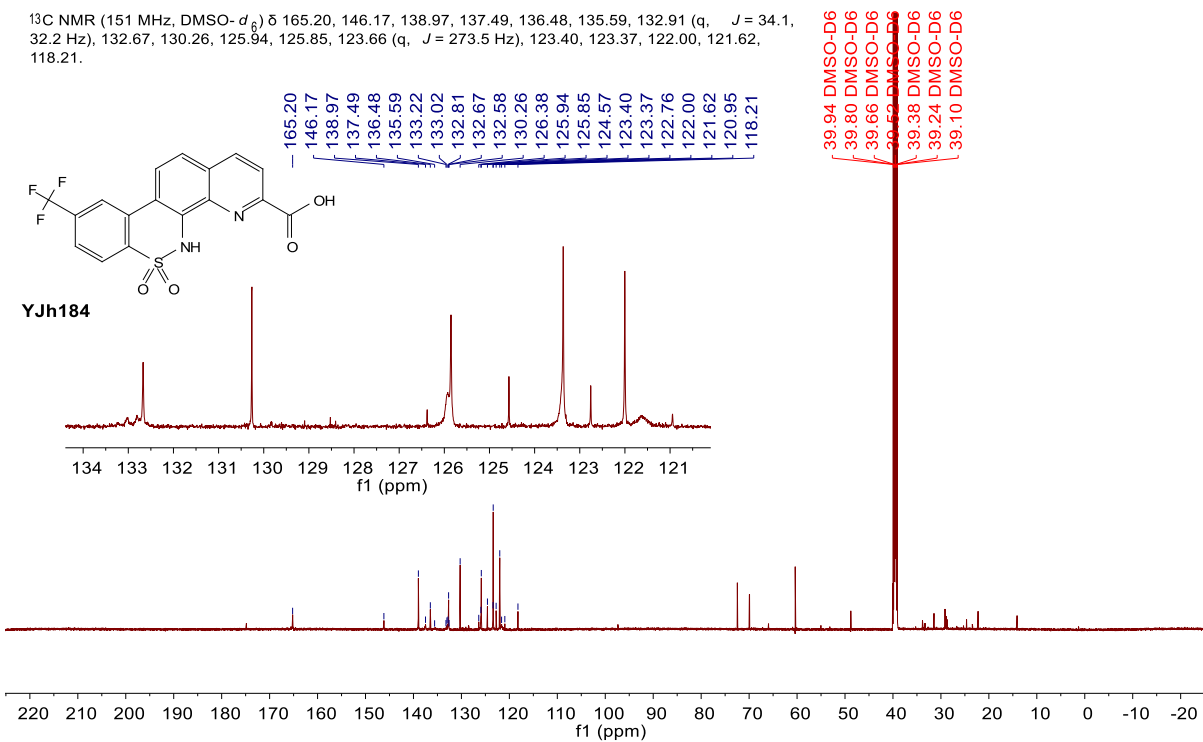
¹H NMR (600 MHz, Methanol-*d*₄) δ 8.69 (d, *J* = 8.7 Hz, 1H), 8.54 (d, *J* = 4.6 Hz, 1H), 8.32 (d, *J* = 8.8 Hz, 1H), 8.13 (t, *J* = 7.7 Hz, 2H), 7.96 (t, *J* = 7.6 Hz, 1H), 7.50 – 7.48 (m, 1H).

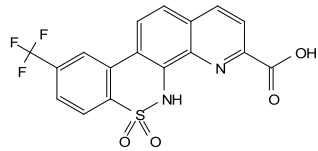


¹H NMR (600 MHz, DMSO-*d*₆) δ 8.83 – 8.67 (m, 3H), 8.31 (t, *J* = 8.3 Hz, 2H), 8.12 (d, *J* = 8.2 Hz, 1H), 7.96 (d, *J* = 8.7 Hz, 1H).



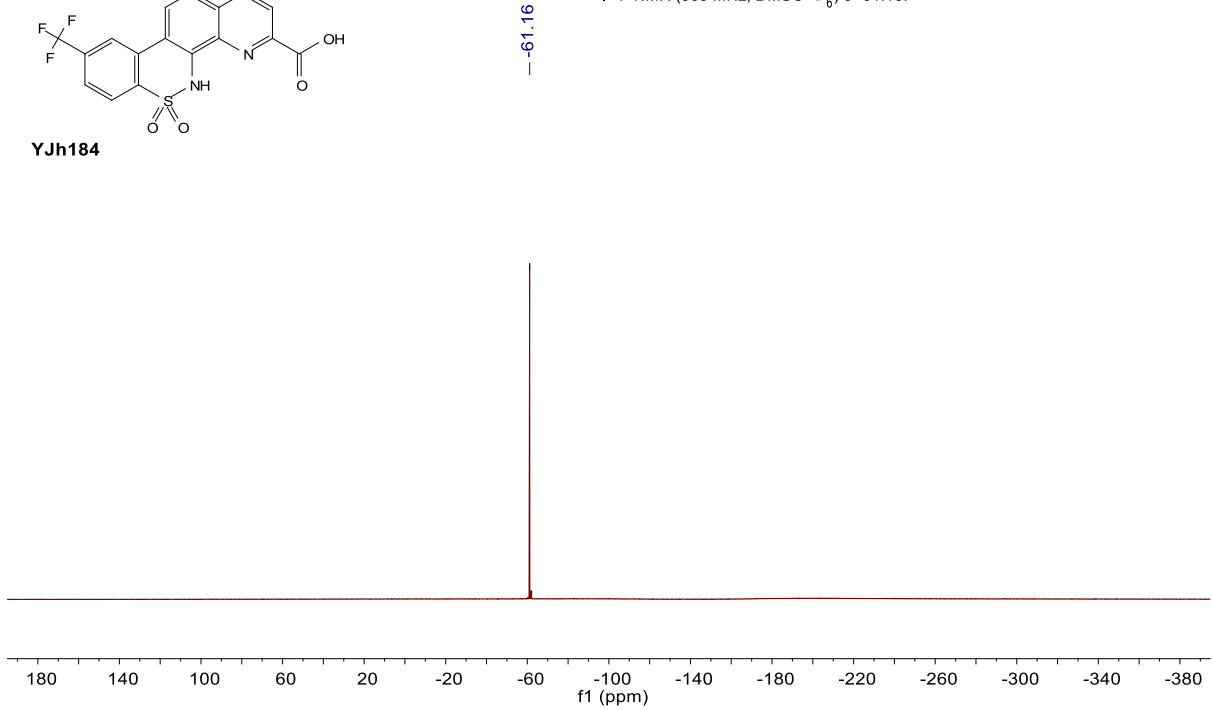
¹³C NMR (151 MHz, DMSO-*d*₆) δ 165.20, 146.17, 138.97, 137.49, 136.48, 135.59, 132.91 (q, *J* = 34.1, 32.2 Hz), 132.67, 130.26, 125.94, 125.85, 123.66 (q, *J* = 273.5 Hz), 123.40, 123.37, 122.00, 121.62, 118.21.



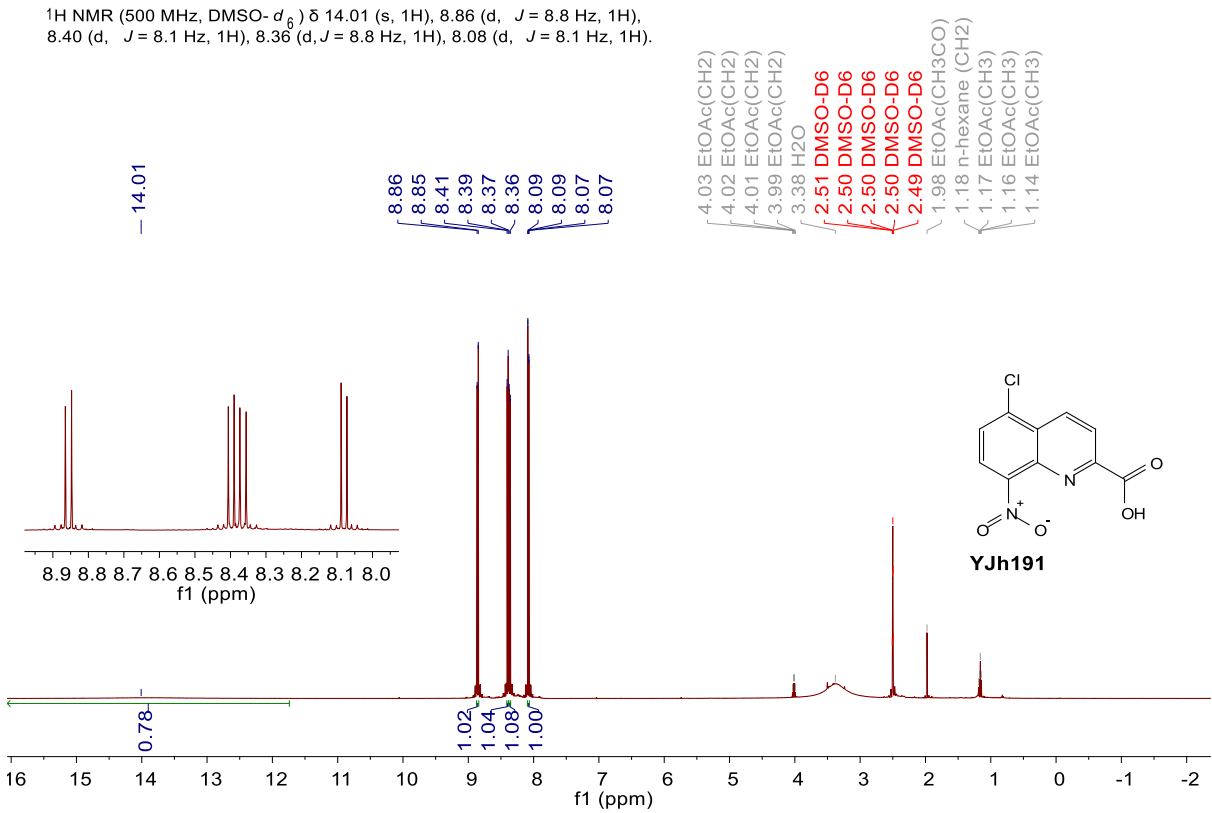


YJh184

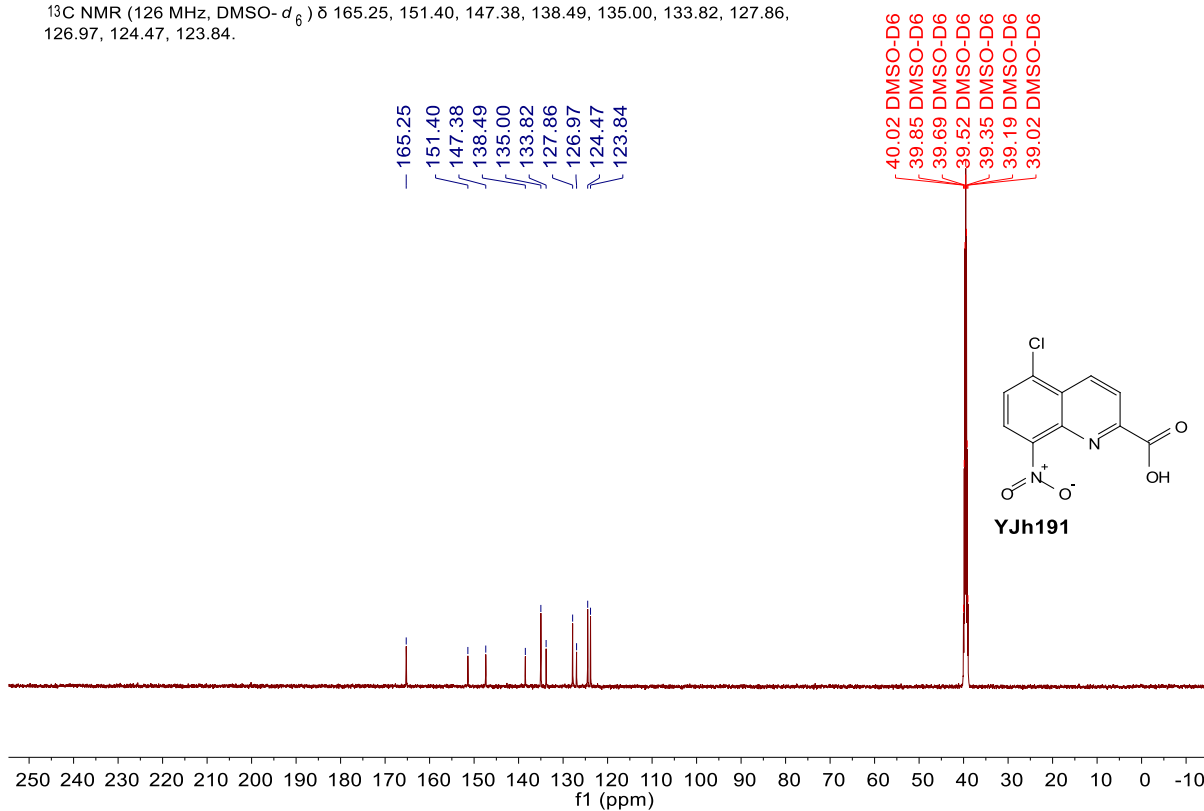
^{19}F NMR (565 MHz, $\text{DMSO}-d_6$) δ -61.16.



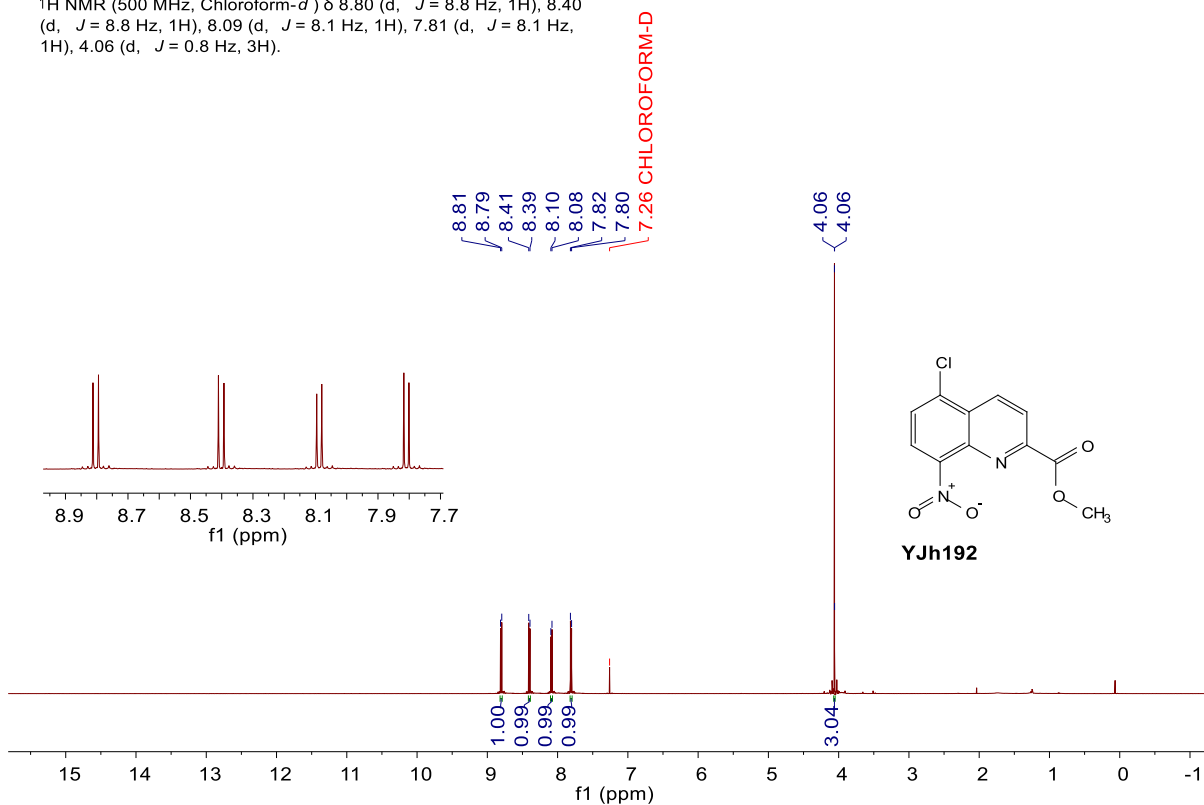
^1H NMR (500 MHz, $\text{DMSO}-d_6$) δ 14.01 (s, 1H), 8.86 (d, $J = 8.8$ Hz, 1H), 8.40 (d, $J = 8.1$ Hz, 1H), 8.36 (d, $J = 8.8$ Hz, 1H), 8.08 (d, $J = 8.1$ Hz, 1H).



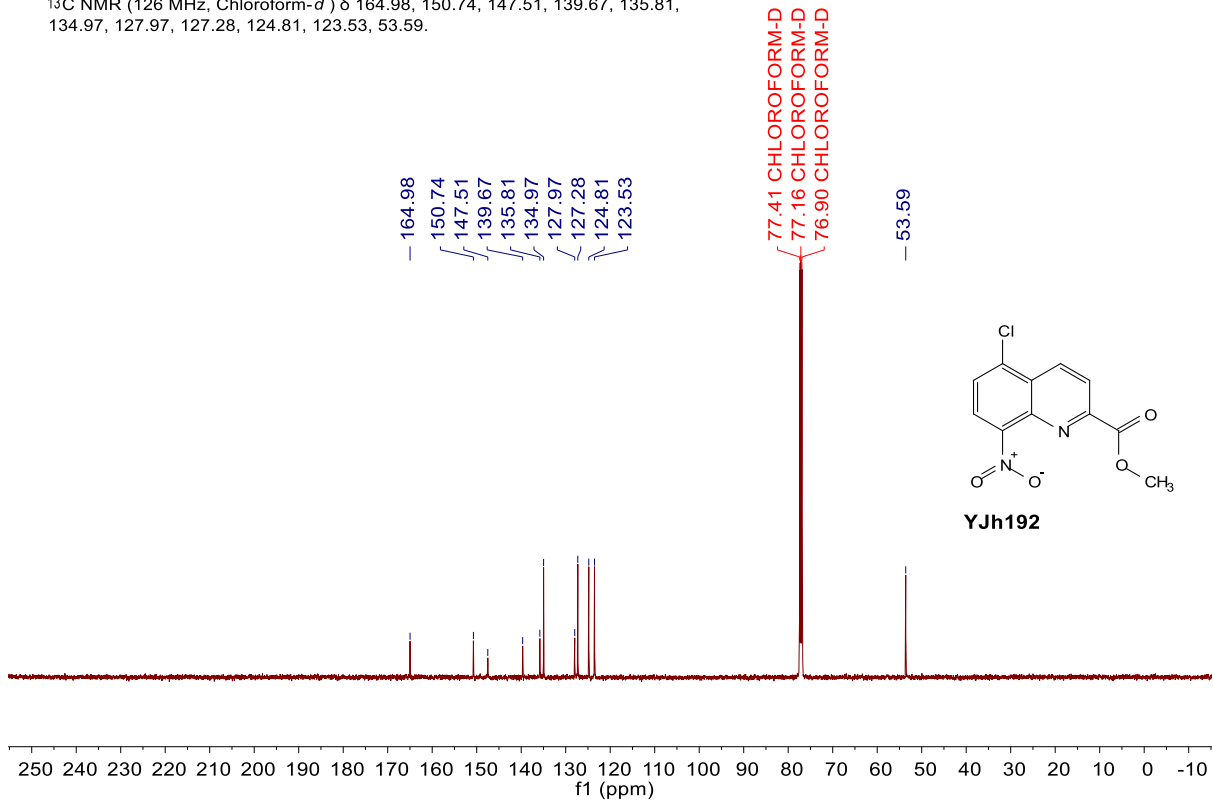
^{13}C NMR (126 MHz, $\text{DMSO-}d_6$) δ 165.25, 151.40, 147.38, 138.49, 135.00, 133.82, 127.86, 126.97, 124.47, 123.84.



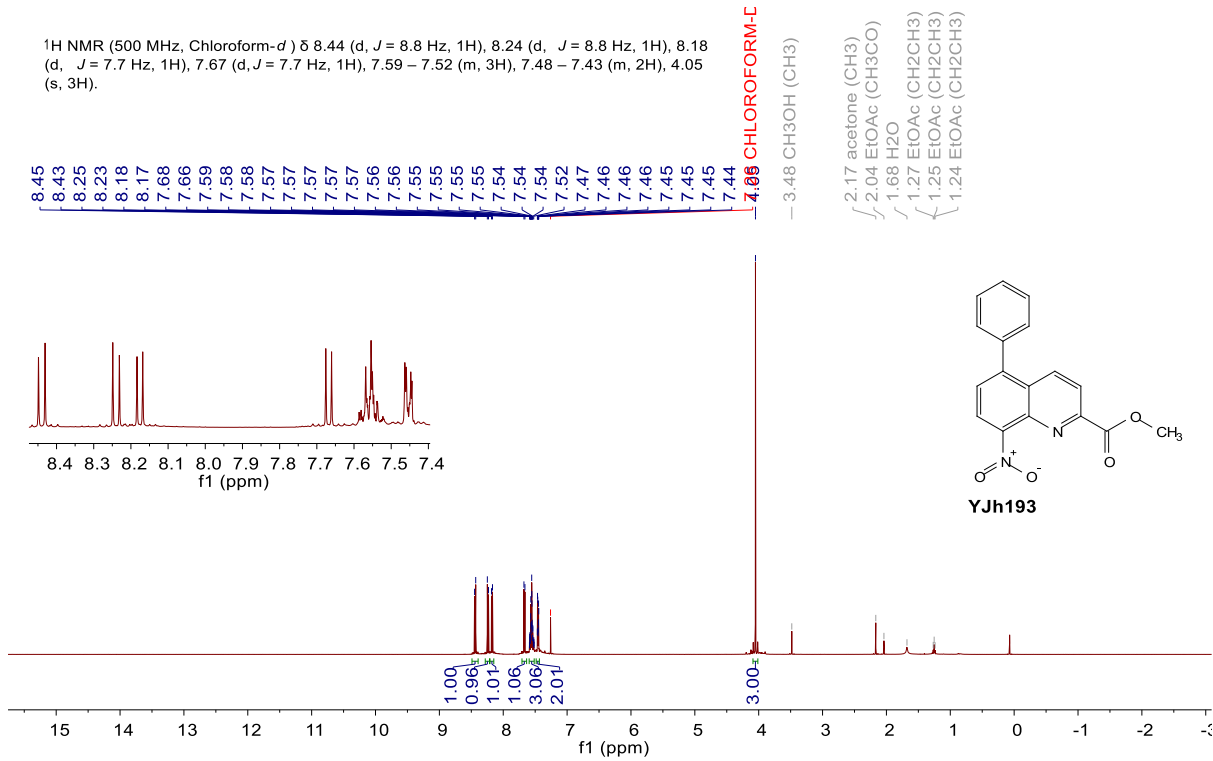
^1H NMR (500 MHz, Chloroform- d) δ 8.80 (d, $J = 8.8$ Hz, 1H), 8.40 (d, $J = 8.8$ Hz, 1H), 8.09 (d, $J = 8.1$ Hz, 1H), 7.81 (d, $J = 8.1$ Hz, 1H), 4.06 (d, $J = 0.8$ Hz, 3H).



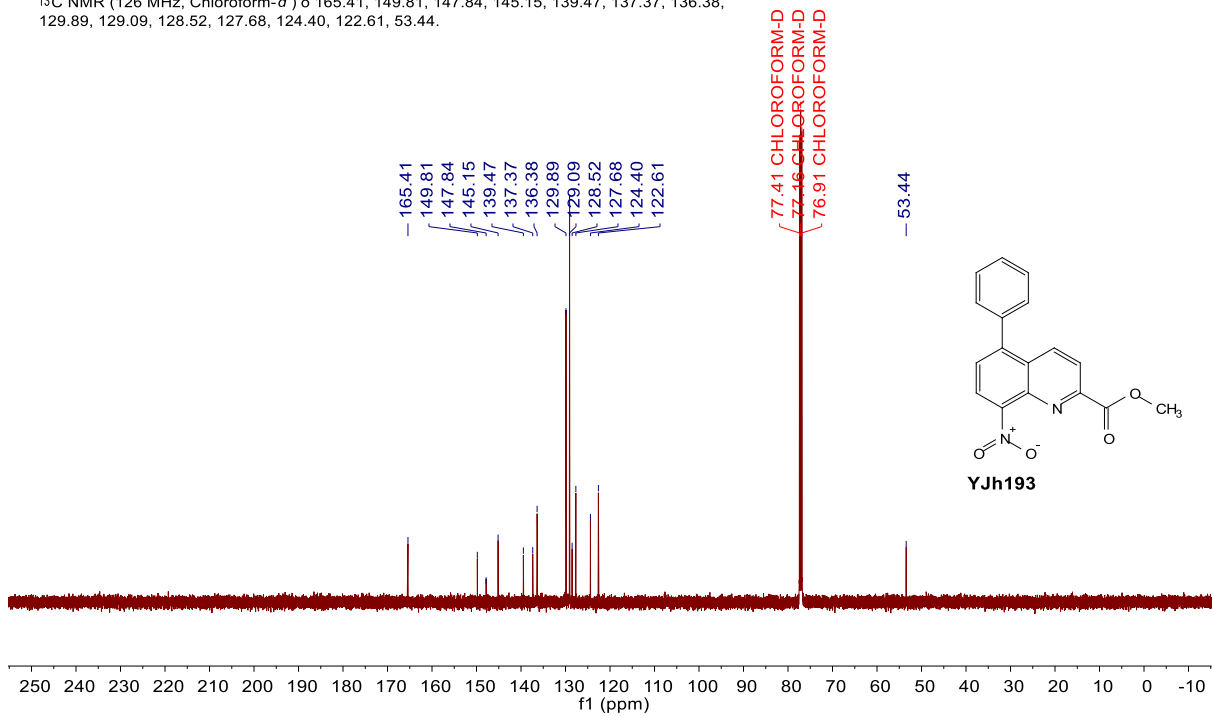
¹³C NMR (126 MHz, Chloroform-*d*) δ 164.98, 150.74, 147.51, 139.67, 135.81, 134.97, 127.97, 127.28, 124.81, 123.53, 53.59.



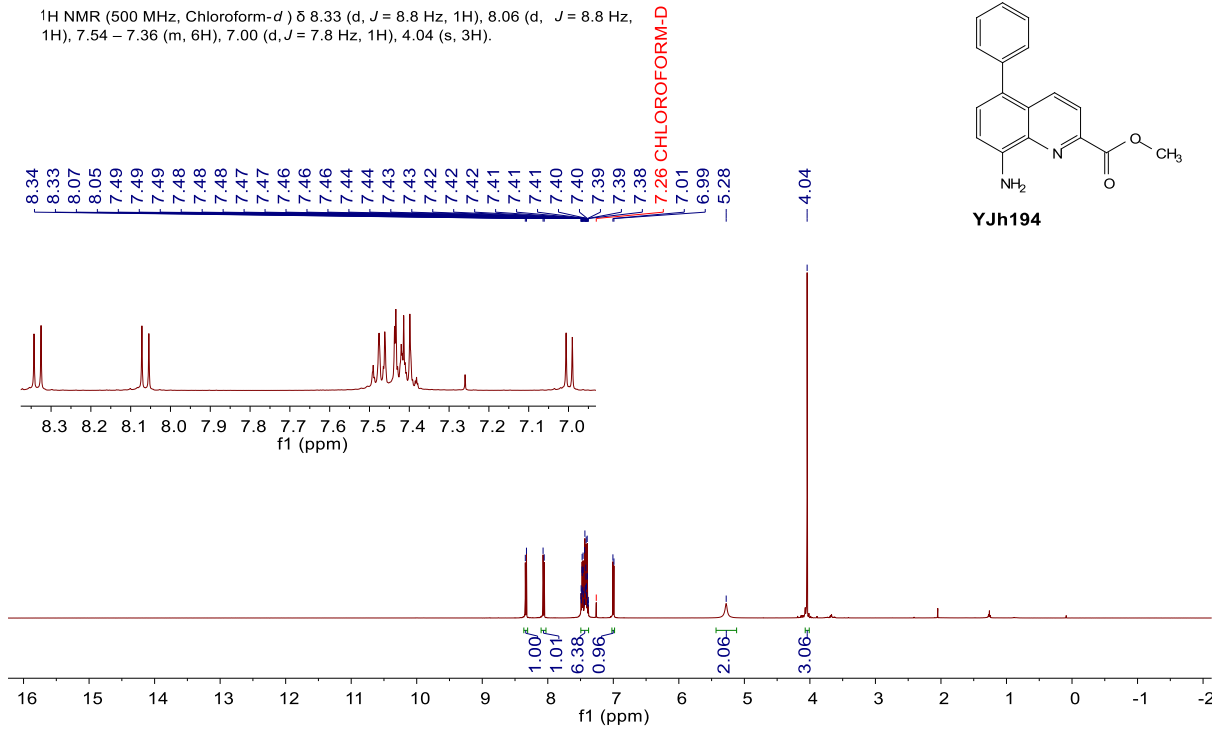
¹H NMR (500 MHz, Chloroform-*d*) δ 8.44 (d, *J* = 8.8 Hz, 1H), 8.24 (d, *J* = 8.8 Hz, 1H), 8.18 (d, *J* = 7.7 Hz, 1H), 7.67 (d, *J* = 7.7 Hz, 1H), 7.59 – 7.52 (m, 3H), 7.48 – 7.43 (m, 2H), 4.05 (s, 3H).



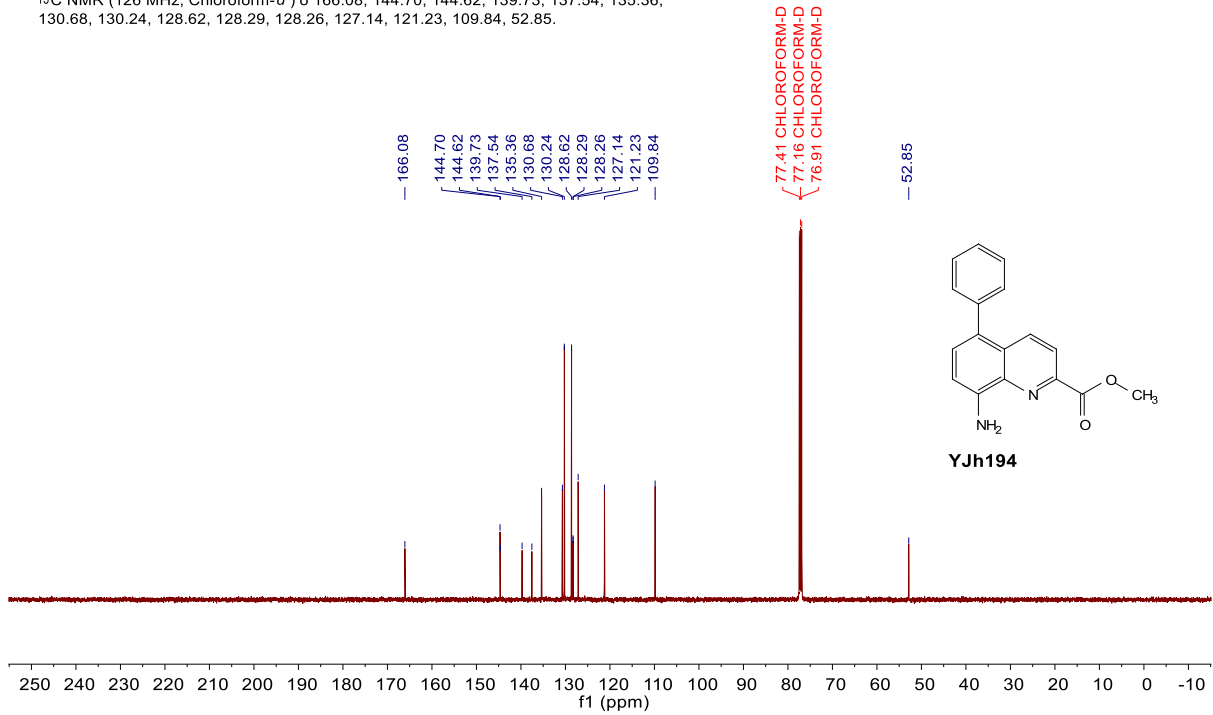
¹³C NMR (126 MHz, Chloroform-*d*) δ 165.41, 149.81, 147.84, 145.15, 139.47, 137.37, 136.38, 129.89, 129.09, 128.52, 127.68, 124.40, 122.61, 53.44.



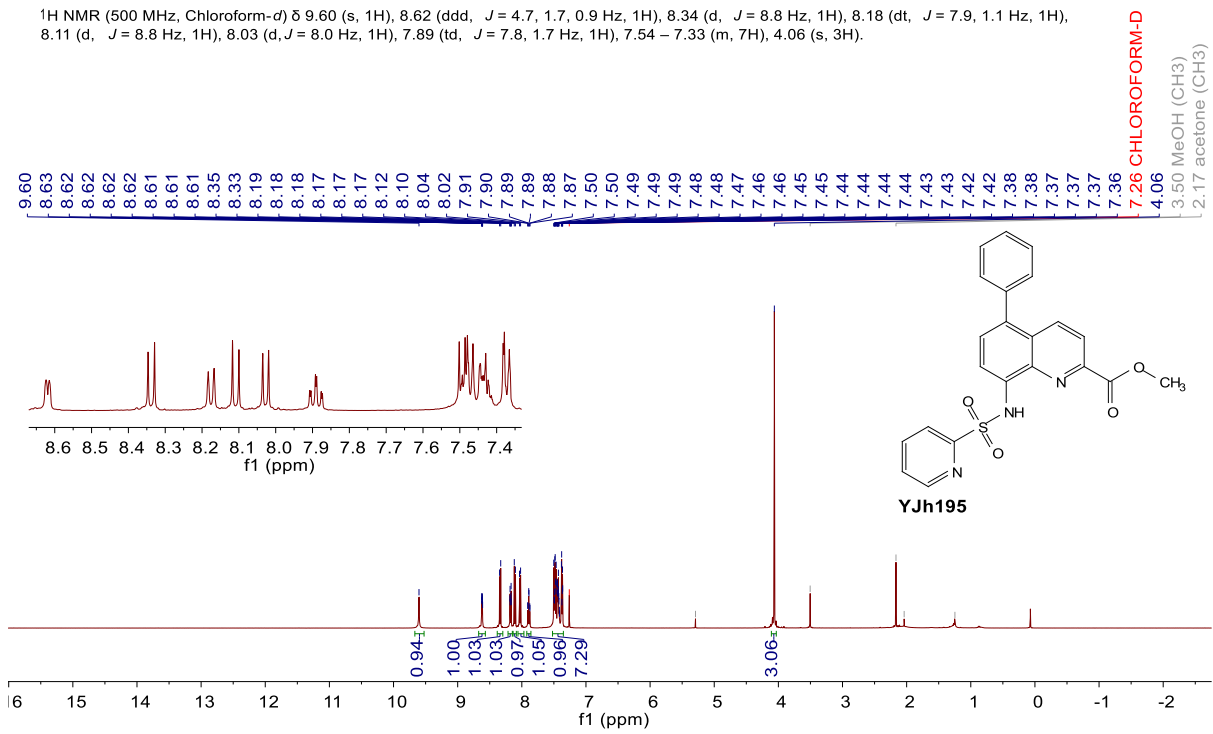
¹H NMR (500 MHz, Chloroform-*d*) δ 8.33 (d, *J* = 8.8 Hz, 1H), 8.06 (d, *J* = 8.8 Hz, 1H), 7.54 – 7.36 (m, 6H), 7.00 (d, *J* = 7.8 Hz, 1H), 4.04 (s, 3H).



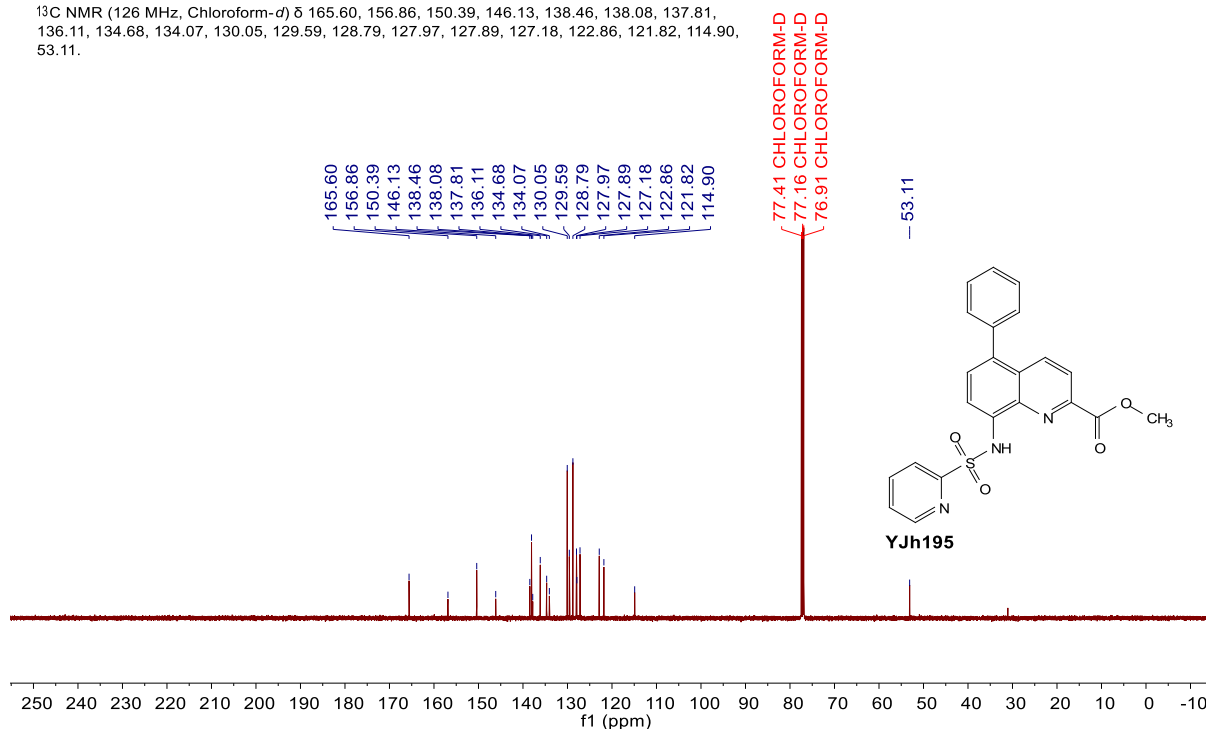
¹³C NMR (126 MHz, Chloroform-*d*) δ 166.08, 144.70, 144.62, 139.73, 137.54, 135.36, 130.68, 130.24, 128.62, 128.29, 128.26, 127.14, 121.23, 109.84, 52.85.



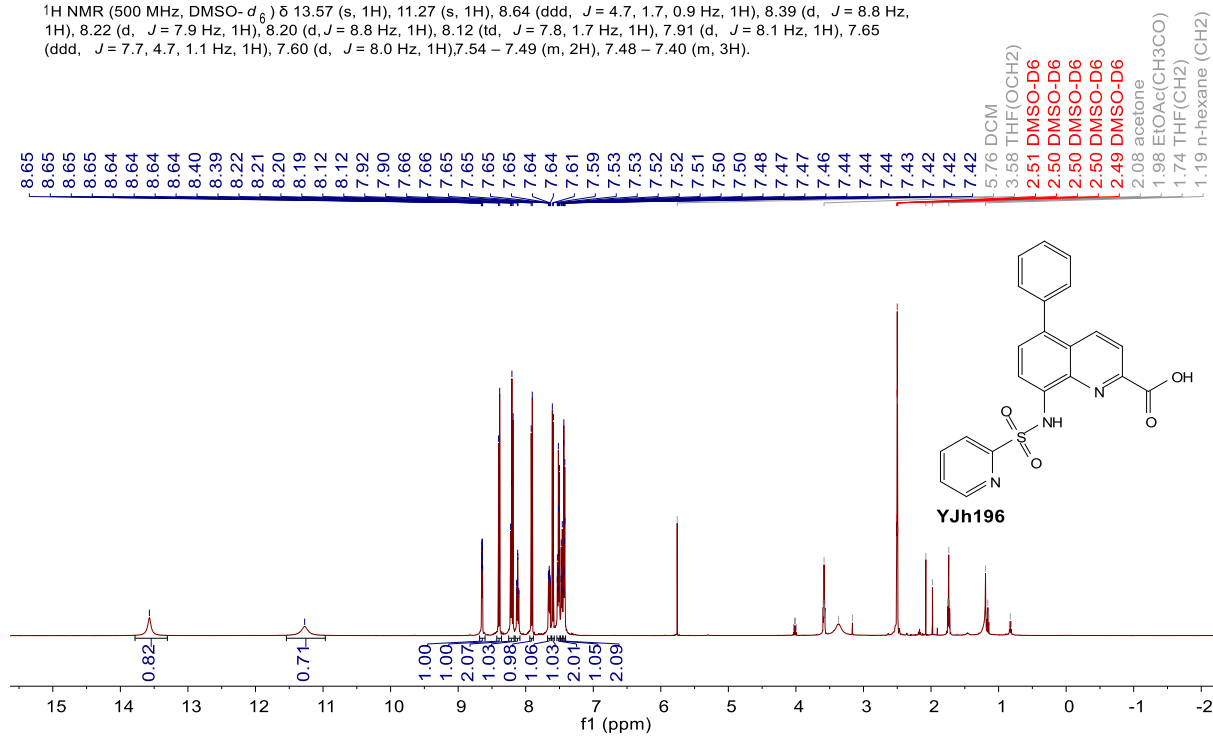
¹H NMR (500 MHz, Chloroform-*d*) δ 9.60 (s, 1H), 8.62 (ddd, *J* = 4.7, 1.7, 0.9 Hz, 1H), 8.34 (d, *J* = 8.8 Hz, 1H), 8.18 (dt, *J* = 7.9, 1.1 Hz, 1H), 8.11 (d, *J* = 8.8 Hz, 1H), 8.03 (d, *J* = 8.0 Hz, 1H), 7.89 (td, *J* = 7.8, 1.7 Hz, 1H), 7.54 – 7.33 (m, 7H), 4.06 (s, 3H).



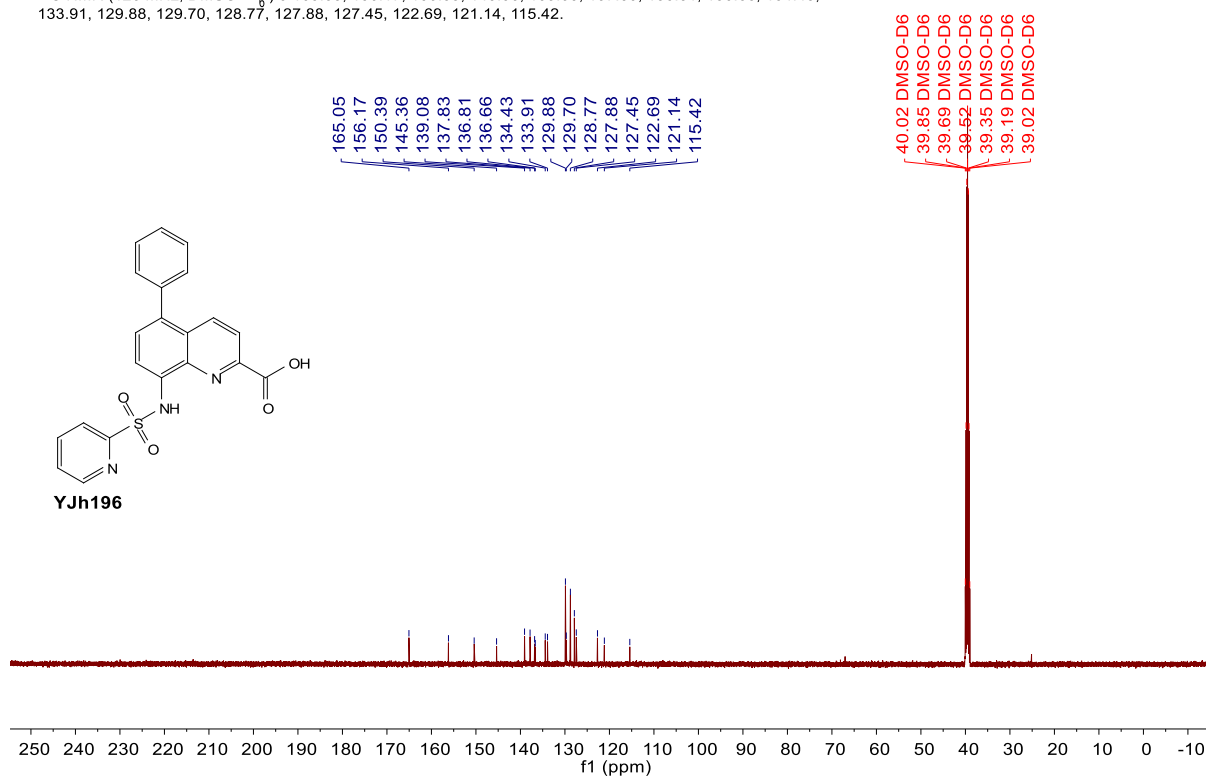
¹³C NMR (126 MHz, Chloroform-*d*) δ 165.60, 156.86, 150.39, 146.13, 138.46, 138.08, 137.81, 136.11, 134.68, 134.07, 130.05, 129.59, 128.79, 127.97, 127.89, 127.18, 122.86, 121.82, 114.90, 53.11.



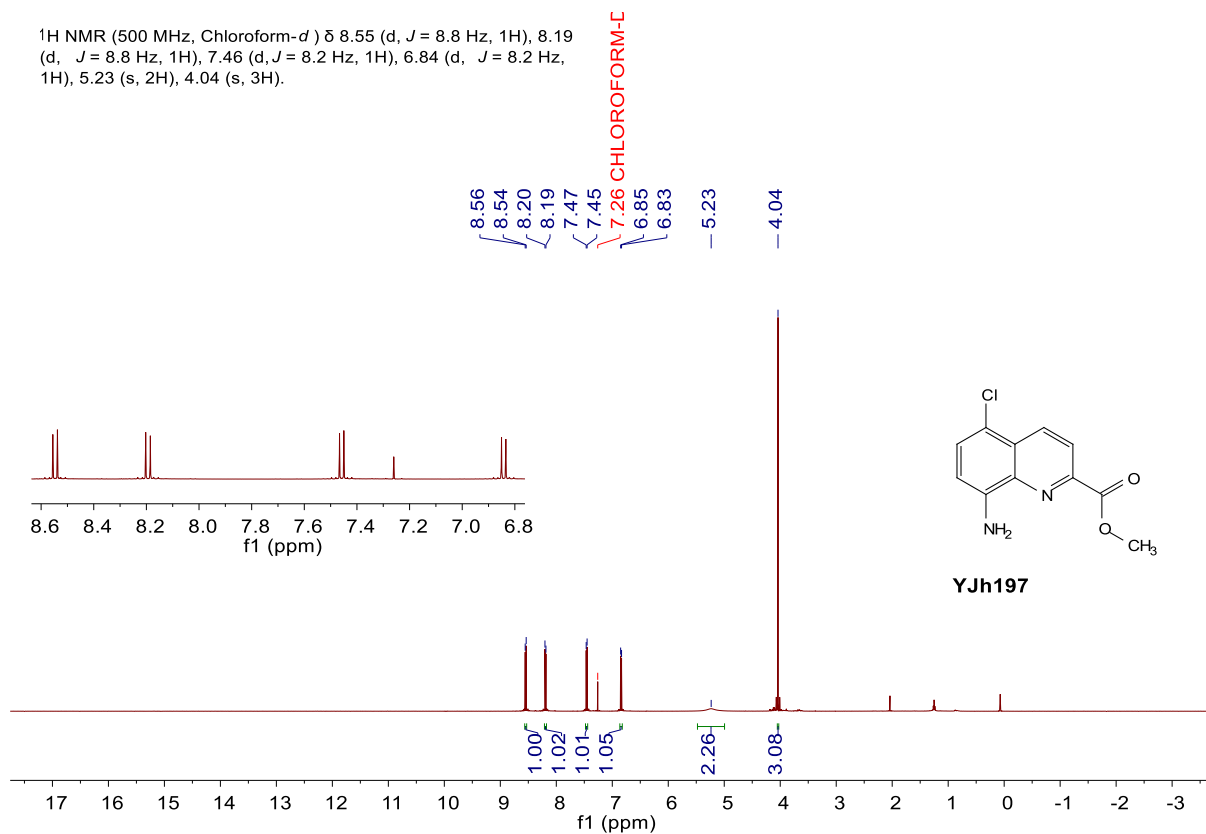
¹H NMR (500 MHz, DMSO-*d*₆) δ 13.57 (s, 1H), 11.27 (s, 1H), 8.64 (ddd, *J* = 4.7, 1.7, 0.9 Hz, 1H), 8.39 (d, *J* = 8.8 Hz, 1H), 8.22 (d, *J* = 7.9 Hz, 1H), 8.20 (d, *J* = 8.8 Hz, 1H), 8.12 (td, *J* = 7.8, 1.7 Hz, 1H), 7.91 (d, *J* = 8.1 Hz, 1H), 7.65 (ddd, *J* = 7.7, 4.7, 1.1 Hz, 1H), 7.60 (d, *J* = 8.0 Hz, 1H), 7.54 – 7.49 (m, 2H), 7.48 – 7.40 (m, 3H).



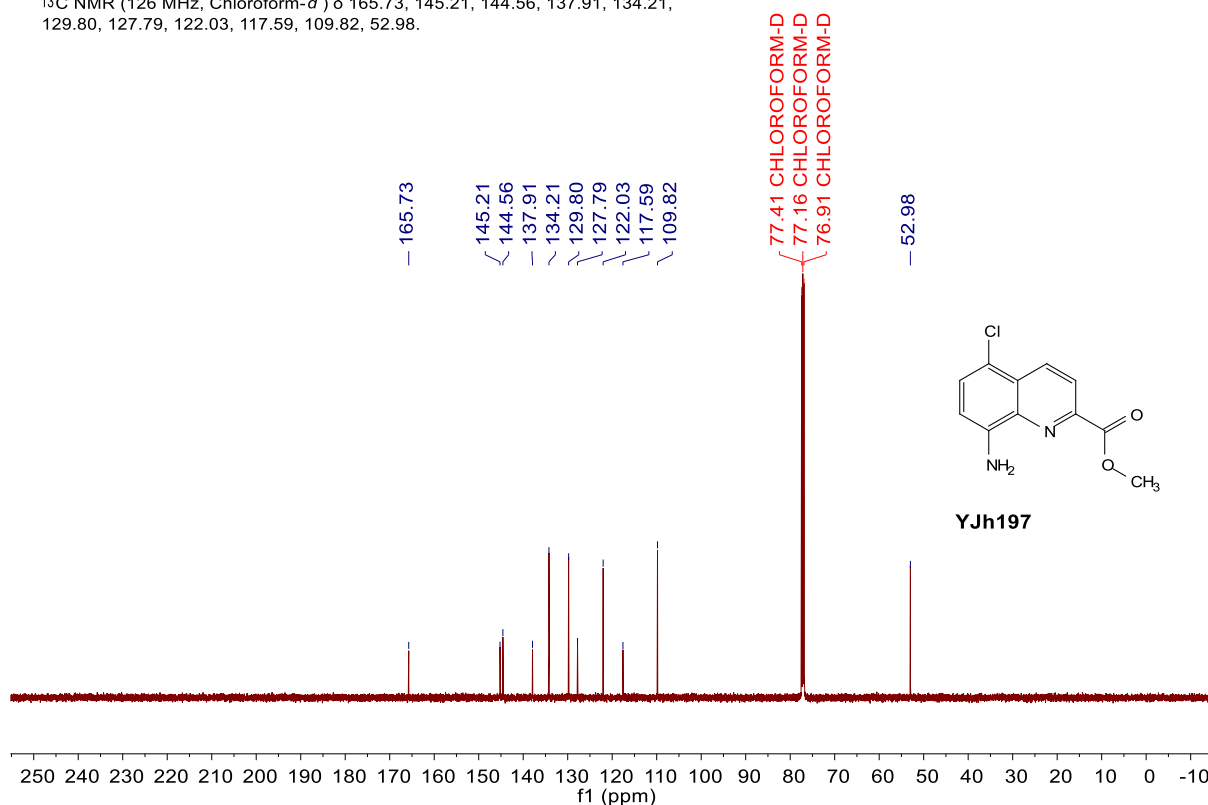
^{13}C NMR (126 MHz, $\text{DMSO}-d_6$) δ 165.05, 156.17, 150.39, 145.36, 139.08, 137.83, 136.81, 136.66, 134.43, 133.91, 129.88, 129.70, 128.77, 127.88, 127.45, 122.69, 121.14, 115.42.



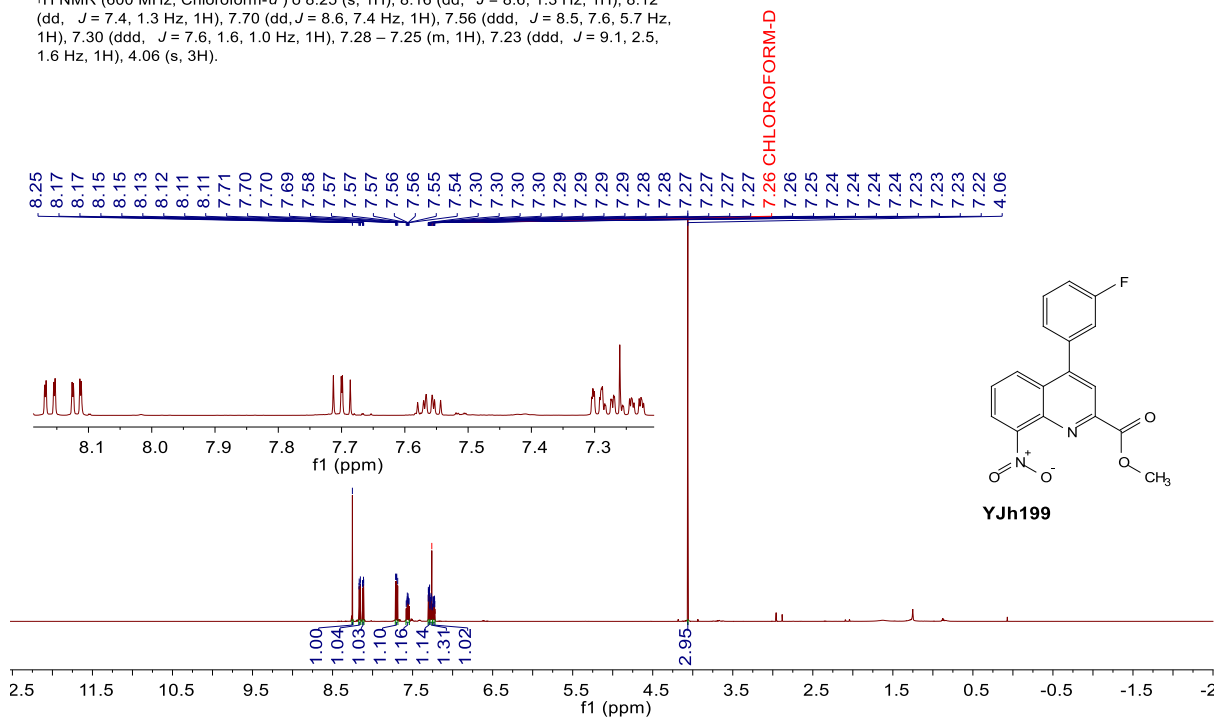
^1H NMR (500 MHz, $\text{Chloroform}-d$) δ 8.55 (d, $J = 8.8$ Hz, 1H), 8.19 (d, $J = 8.8$ Hz, 1H), 7.46 (d, $J = 8.2$ Hz, 1H), 6.84 (d, $J = 8.2$ Hz, 1H), 5.23 (s, 2H), 4.04 (s, 3H).



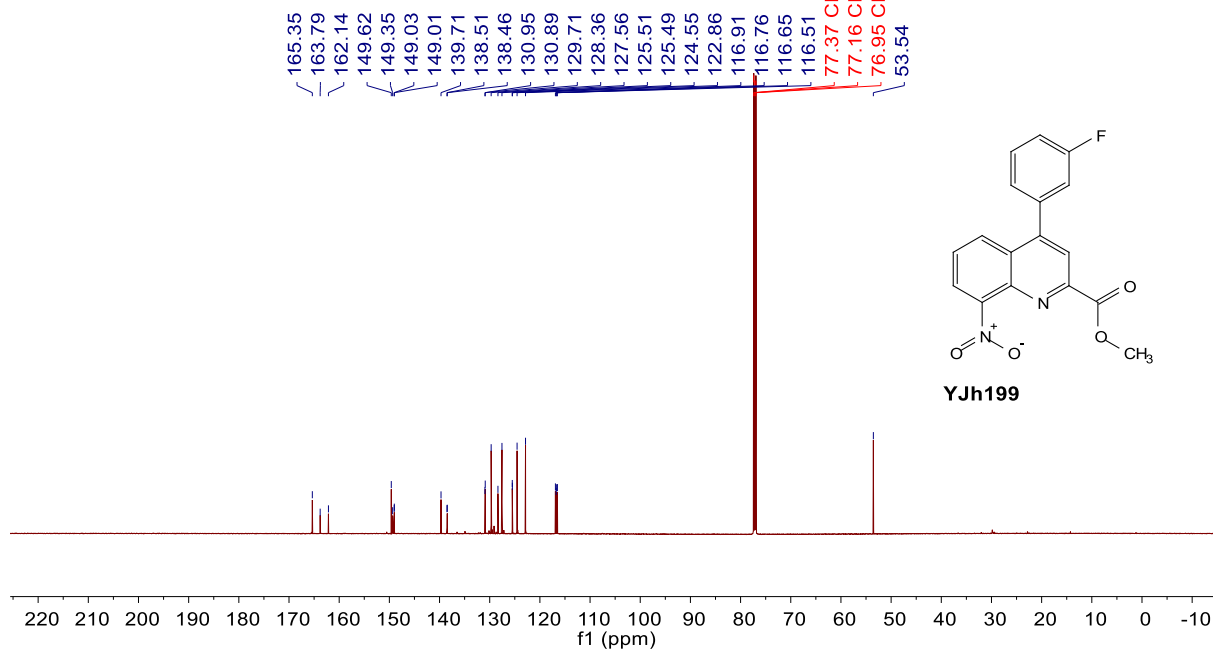
^{13}C NMR (126 MHz, Chloroform-*d*) δ 165.73, 145.21, 144.56, 137.91, 134.21, 129.80, 127.79, 122.03, 117.59, 109.82.



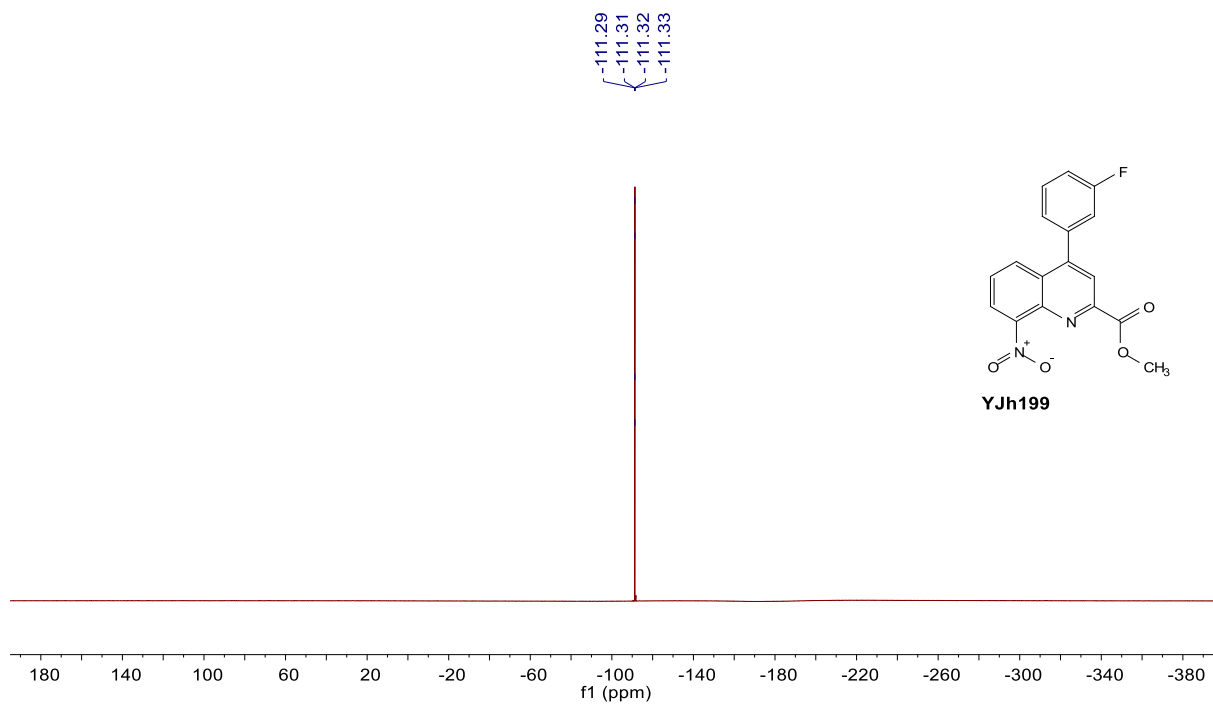
^1H NMR (600 MHz, Chloroform-*d*) δ 8.25 (s, 1H), 8.16 (dd, J = 8.6, 1.3 Hz, 1H), 8.12 (dd, J = 7.4, 1.3 Hz, 1H), 7.70 (dd, J = 8.6, 7.4 Hz, 1H), 7.56 (ddd, J = 8.5, 7.6, 5.7 Hz, 1H), 7.30 (ddd, J = 7.6, 1.6, 1.0 Hz, 1H), 7.28 – 7.25 (m, 1H), 7.23 (ddd, J = 9.1, 2.5, 1.6 Hz, 1H), 4.06 (s, 3H).



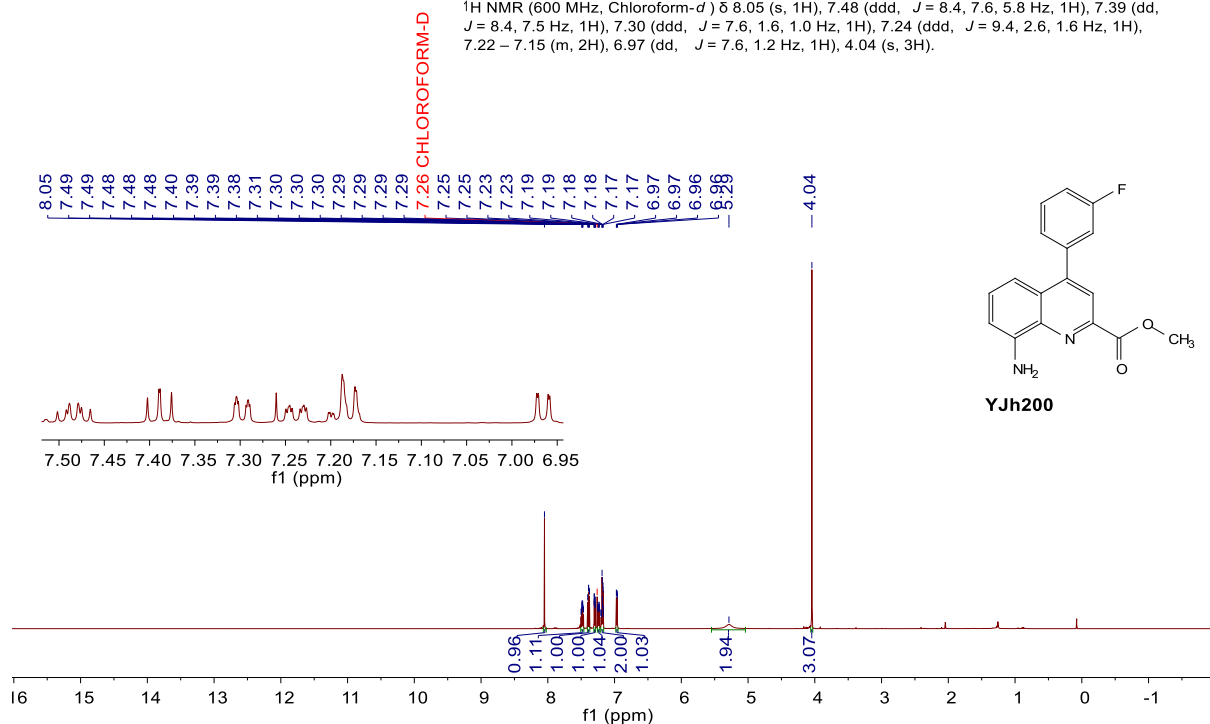
^{13}C NMR (151 MHz, Chloroform-*d*) δ 165.35, 162.97 (d, $J = 248.9$ Hz), 149.62, 149.35, 149.02 (d, $J = 2.1$ Hz), 139.71, 138.49 (d, $J = 7.9$ Hz), 130.92 (d, $J = 8.6$ Hz), 129.71, 128.36, 127.56, 125.50 (d, $J = 3.0$ Hz), 124.55, 122.86, 116.83 (d, $J = 22.6$ Hz), 116.58 (d, $J = 21.0$ Hz), 53.54.



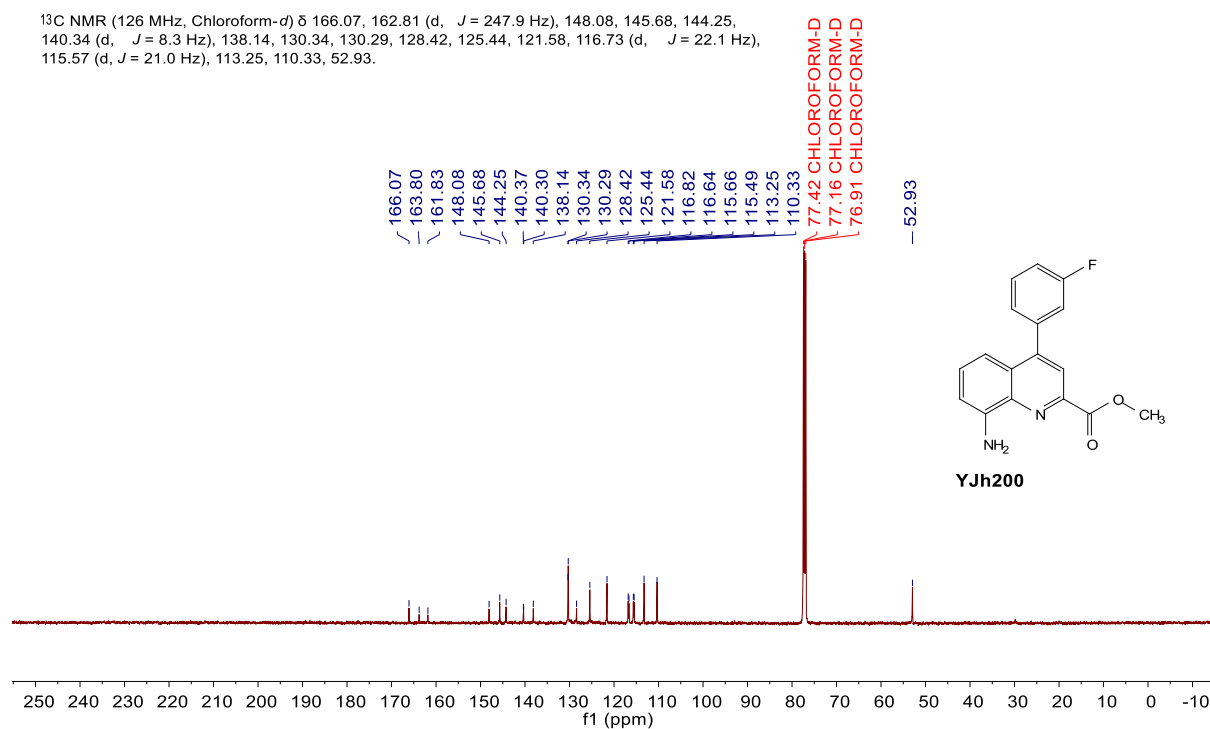
^{19}F NMR (565 MHz, Chloroform-*d*) δ -111.31 (q, $J = 8.2$ Hz).

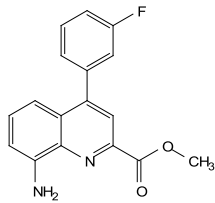


¹H NMR (600 MHz, Chloroform-*d*) δ 8.05 (s, 1H), 7.48 (ddd, *J* = 8.4, 7.6, 5.8 Hz, 1H), 7.39 (dd, *J* = 8.4, 7.5 Hz, 1H), 7.30 (ddd, *J* = 7.6, 1.6, 1.0 Hz, 1H), 7.24 (ddd, *J* = 9.4, 2.6, 1.6 Hz, 1H), 7.22 – 7.15 (m, 2H), 6.97 (dd, *J* = 7.6, 1.2 Hz, 1H), 4.04 (s, 3H).



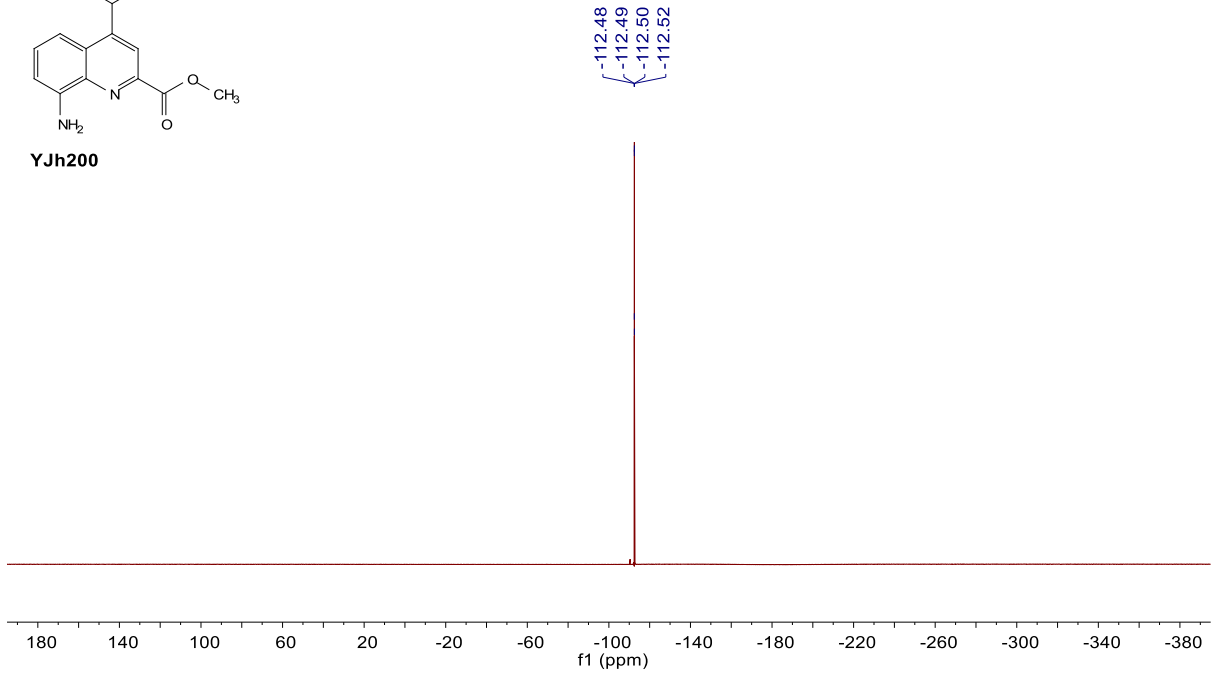
¹³C NMR (126 MHz, Chloroform-*d*) δ 166.07, 162.81 (d, *J* = 247.9 Hz), 148.08, 145.68, 144.25, 140.34 (d, *J* = 8.3 Hz), 138.14, 130.34, 130.29, 128.42, 125.44, 121.58, 116.73 (d, *J* = 22.1 Hz), 115.57 (d, *J* = 21.0 Hz), 113.25, 110.33, 52.93.



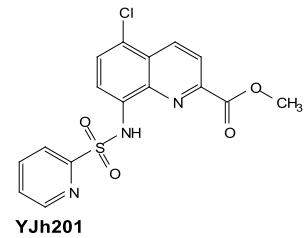
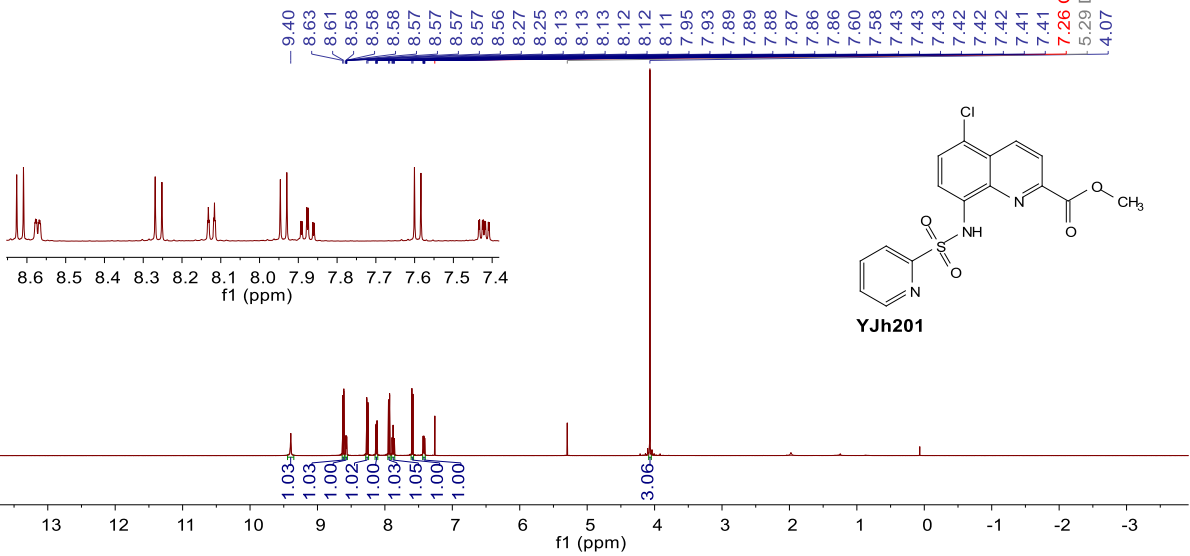


YJh200

¹⁹F NMR (565 MHz, Chloroform-*d*) δ -100.69 -- -147.25 (m).



¹H NMR (500 MHz, Chloroform-*d*) δ 9.40 (s, 1H), 8.62 (d, *J* = 8.7 Hz, 1H), 8.57 (ddd, *J* = 4.7, 1.8, 0.9 Hz, 1H), 8.26 (d, *J* = 8.7 Hz, 1H), 8.12 (dt, *J* = 7.9, 1.0 Hz, 1H), 7.94 (d, *J* = 8.4 Hz, 1H), 7.88 (td, *J* = 7.8, 1.7 Hz, 1H), 7.59 (d, *J* = 8.3 Hz, 1H), 7.42 (ddd, *J* = 7.7, 4.7, 1.1 Hz, 1H), 4.07 (s, 3H).

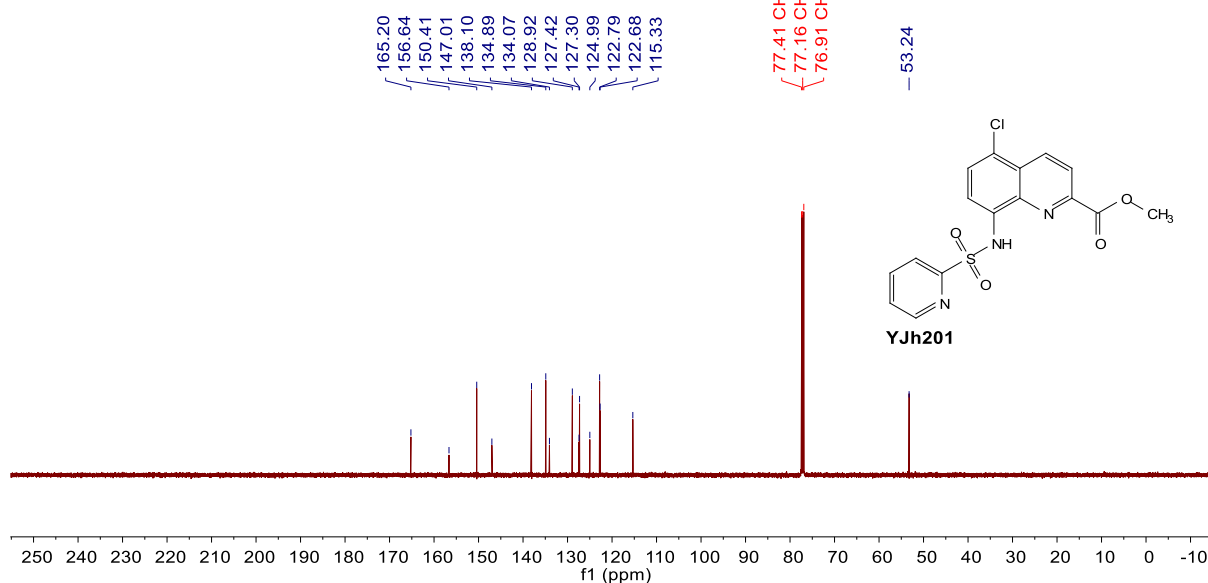


YJh201

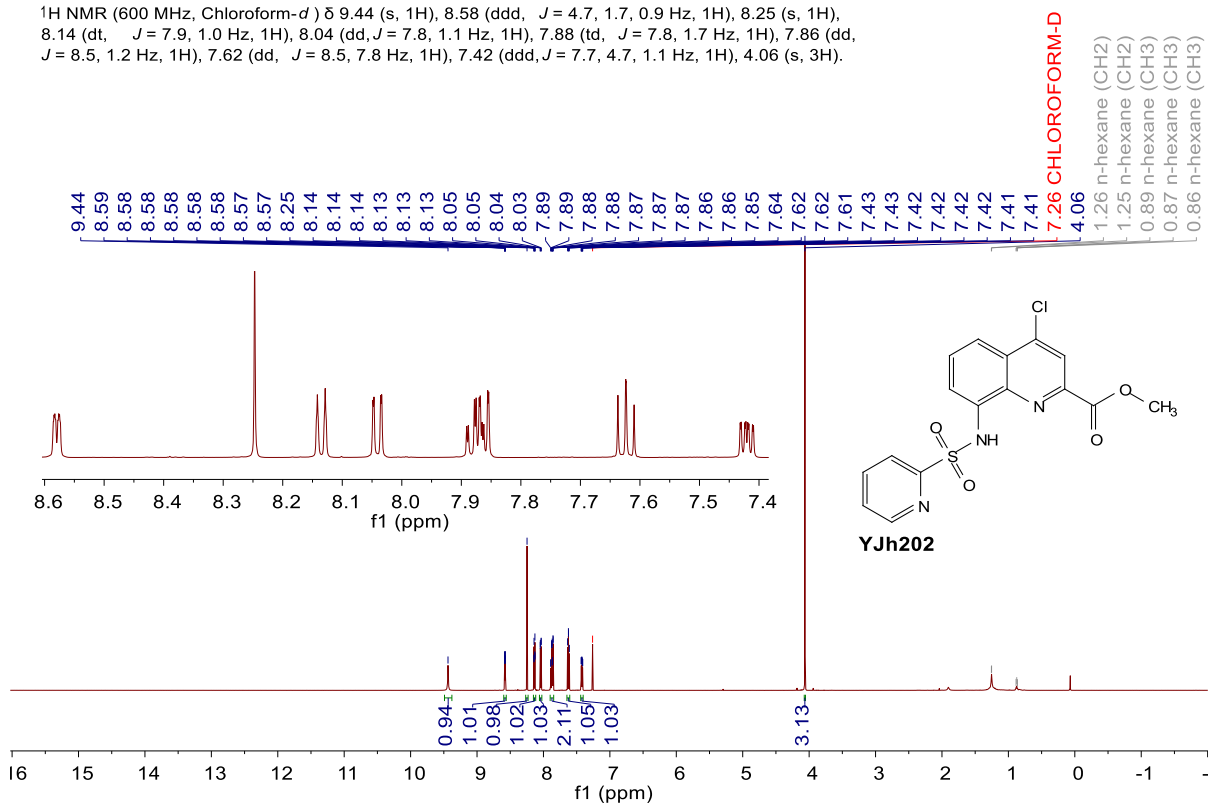
7.26 CHLOROFORM-D

5.29 DCM(CH2)

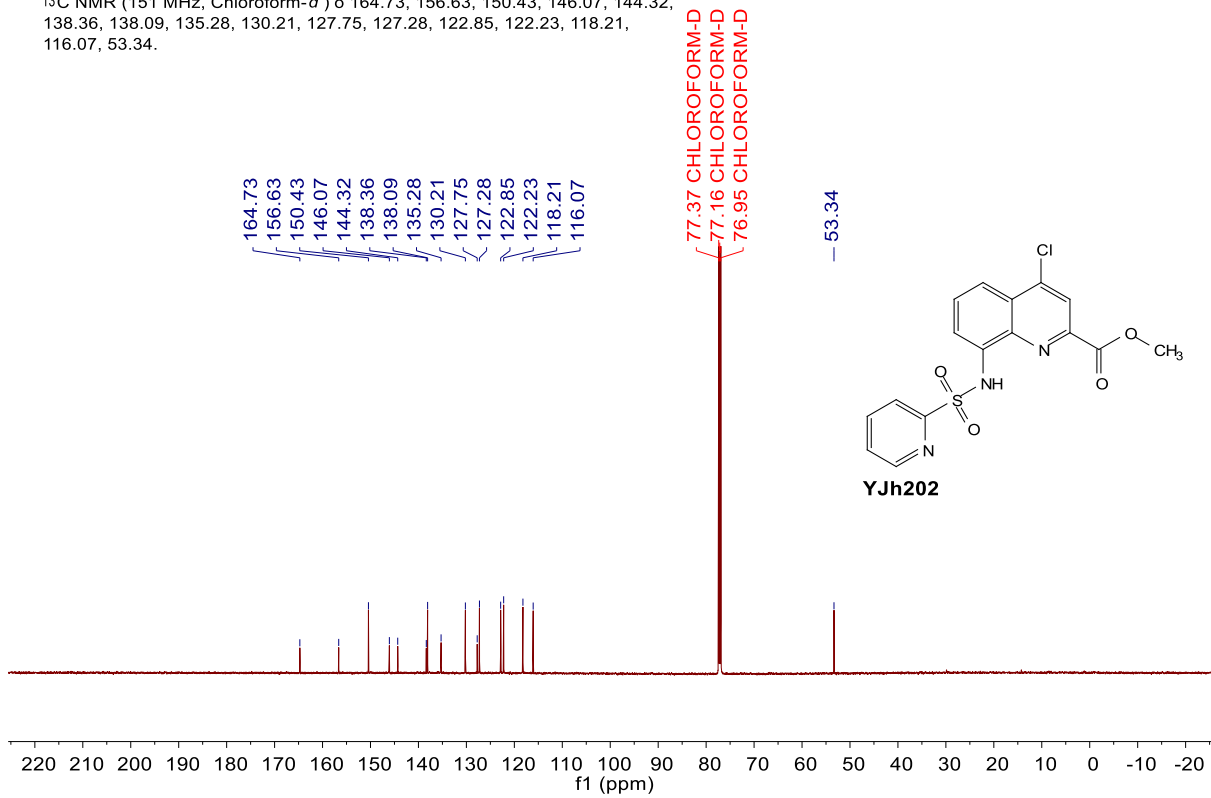
¹³C NMR (126 MHz, Chloroform-*d*) δ 165.20, 156.64, 150.41, 147.01, 147.00, 138.22, 138.10, 134.89, 134.07, 128.92, 127.42, 127.30, 124.99, 122.79, 122.68, 115.33, 53.24.



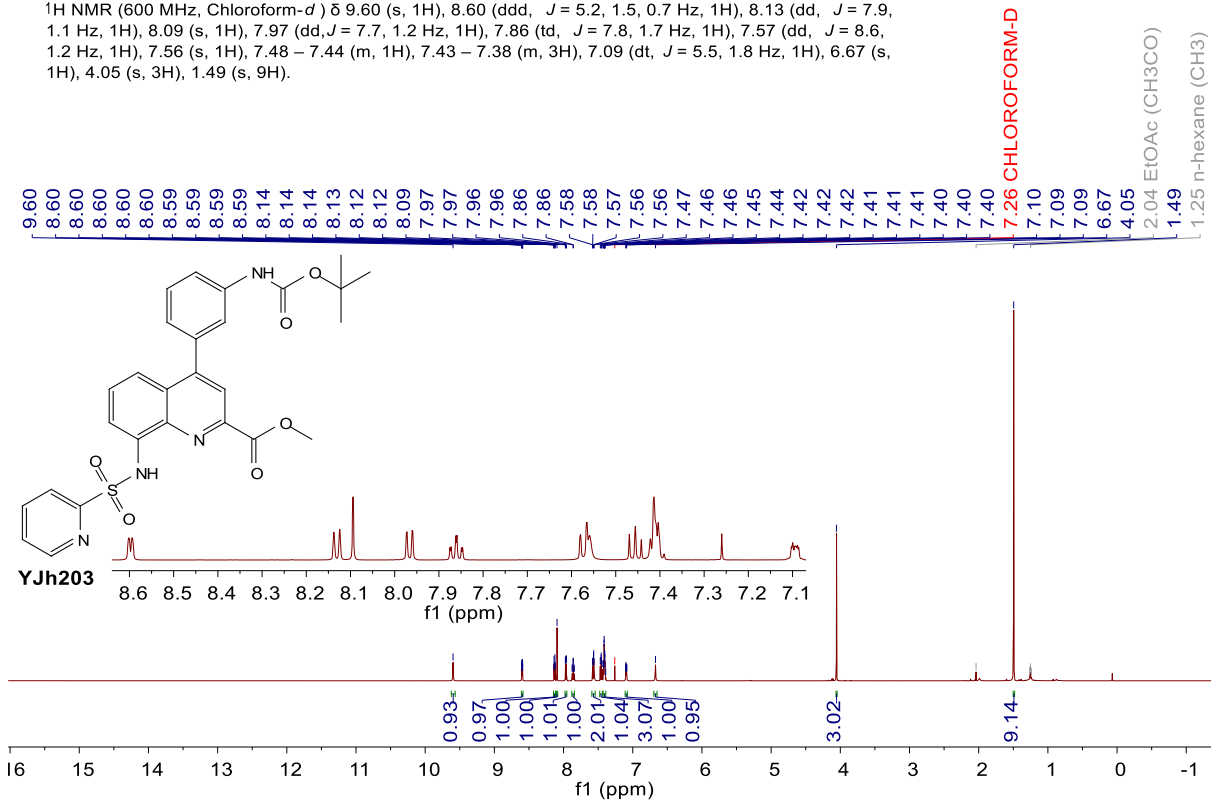
¹H NMR (600 MHz, Chloroform-*d*) δ 9.44 (s, 1H), 8.58 (ddd, *J* = 4.7, 1.7, 0.9 Hz, 1H), 8.25 (s, 1H), 8.14 (dt, *J* = 7.9, 1.0 Hz, 1H), 8.04 (dd, *J* = 7.8, 1.1 Hz, 1H), 7.88 (td, *J* = 7.8, 1.7 Hz, 1H), 7.86 (dd, *J* = 8.5, 1.2 Hz, 1H), 7.62 (dd, *J* = 8.5, 7.8 Hz, 1H), 7.42 (ddd, *J* = 7.7, 4.7, 1.1 Hz, 1H), 4.06 (s, 3H).



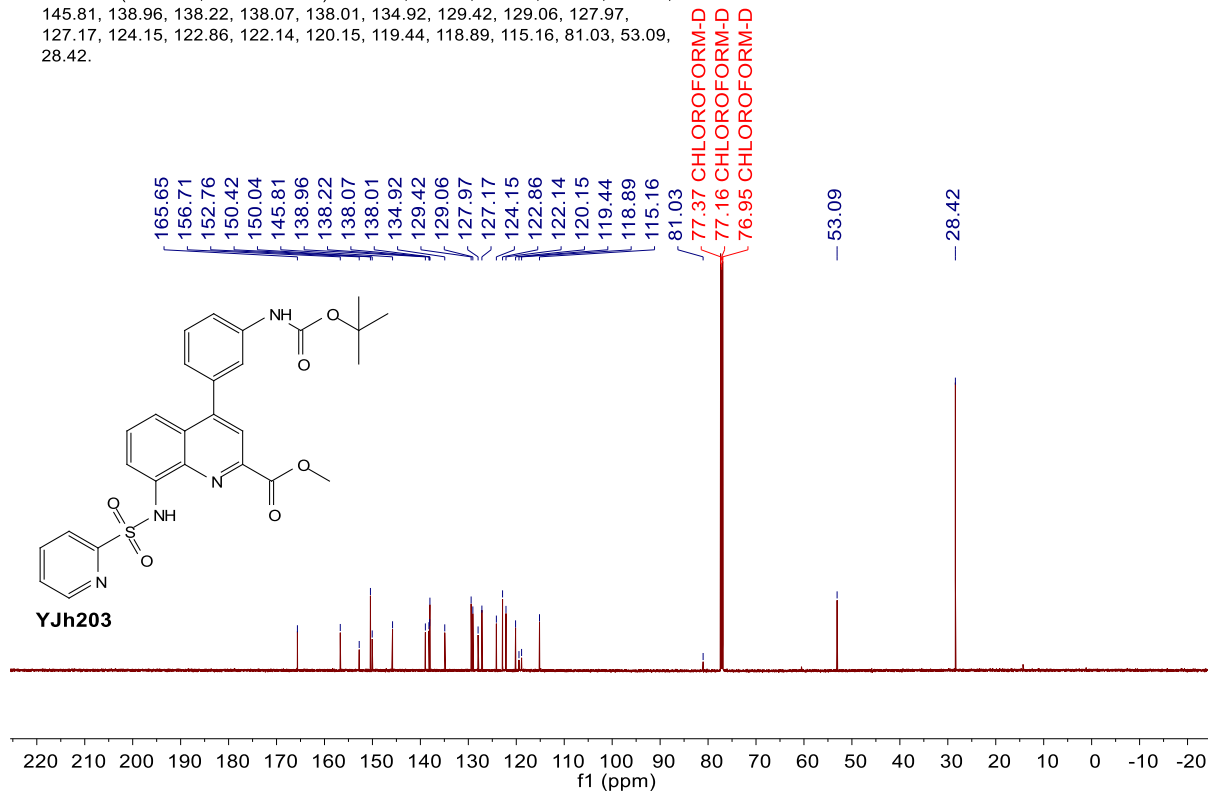
^{13}C NMR (151 MHz, Chloroform-*d*) δ 164.73, 156.63, 150.43, 146.07, 144.32, 138.36, 138.09, 135.28, 130.21, 127.75, 127.28, 122.85, 122.23, 118.21, 116.07, 53.34.



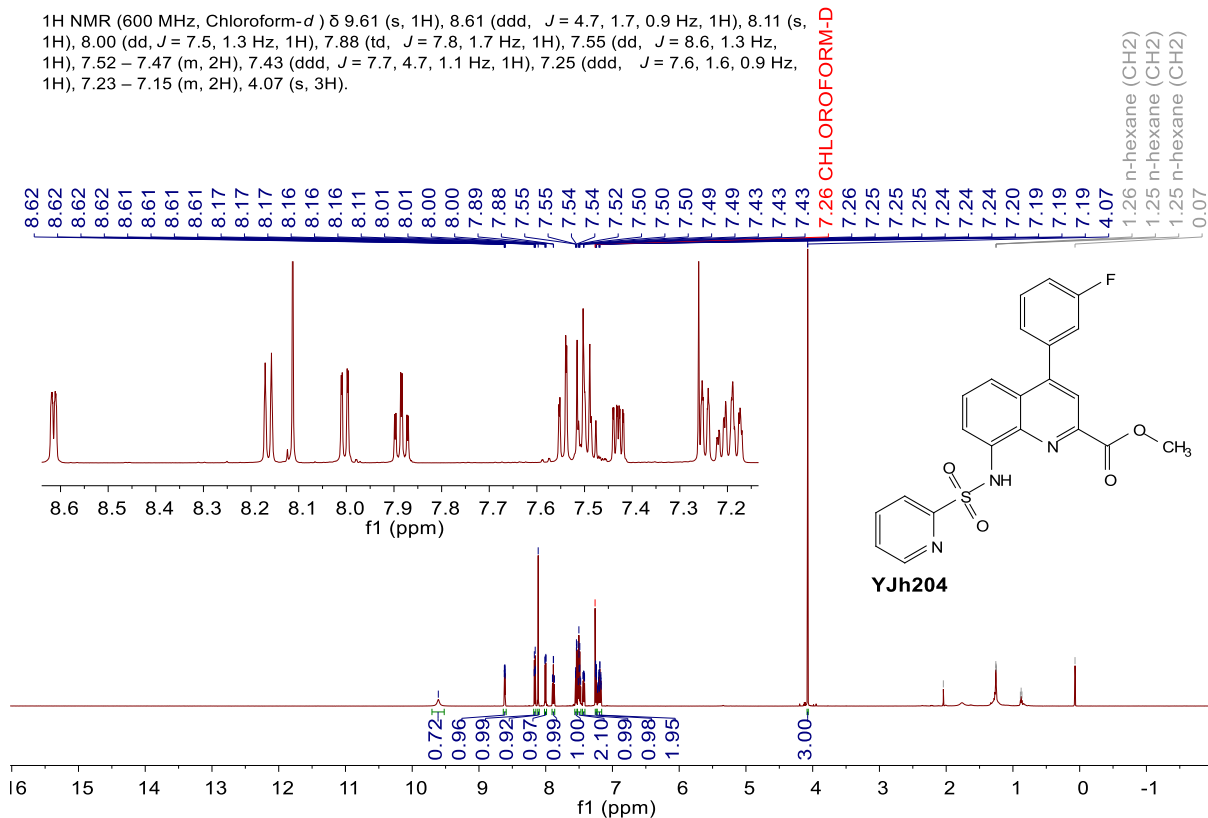
^1H NMR (600 MHz, Chloroform-*d*) δ 9.60 (s, 1H), 8.60 (ddd, $J = 5.2, 1.5, 0.7$ Hz, 1H), 8.13 (dd, $J = 7.9, 1.1$ Hz, 1H), 8.09 (s, 1H), 7.97 (dd, $J = 7.7, 1.2$ Hz, 1H), 7.86 (td, $J = 7.8, 1.7$ Hz, 1H), 7.57 (dd, $J = 8.6, 1.2$ Hz, 1H), 7.56 (s, 1H), 7.48 – 7.44 (m, 1H), 7.43 – 7.38 (m, 3H), 7.09 (dt, $J = 5.5, 1.8$ Hz, 1H), 6.67 (s, 1H), 4.05 (s, 3H), 1.49 (s, 9H).



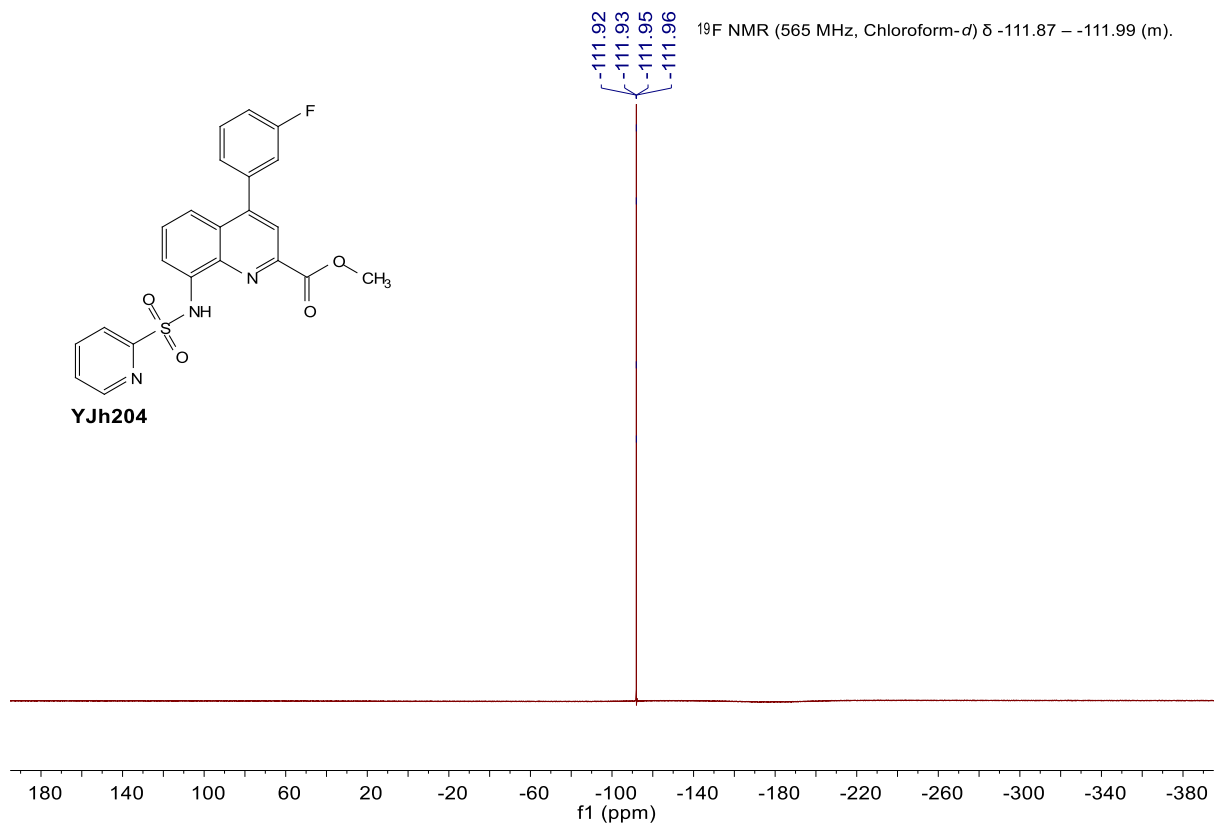
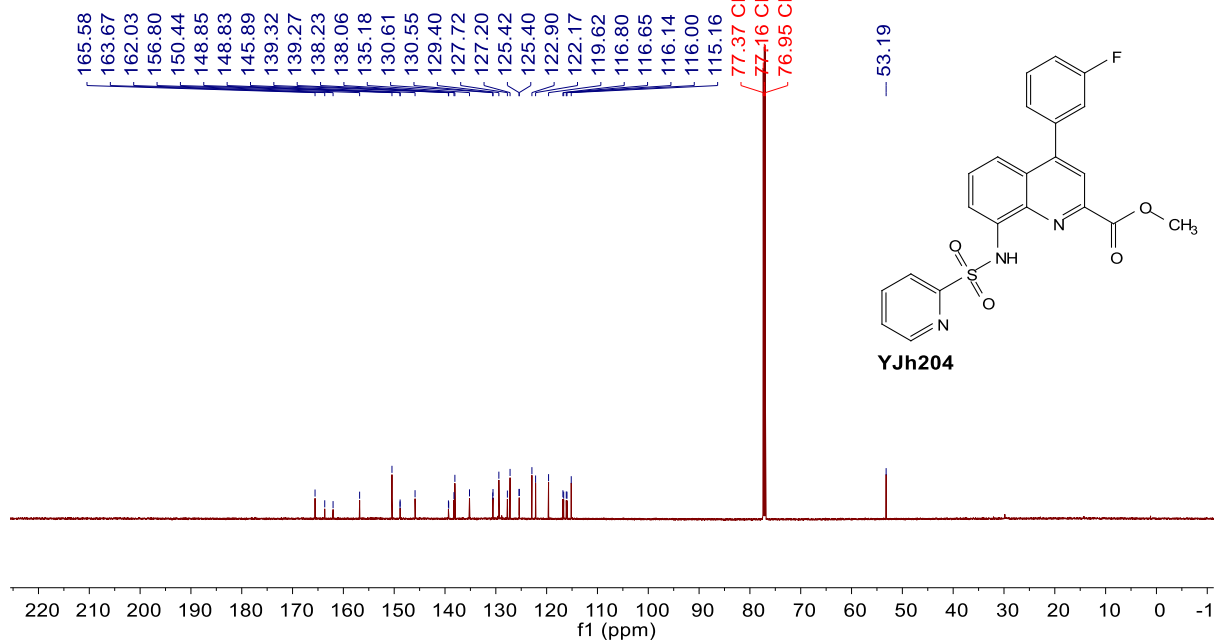
¹³C NMR (151 MHz, Chloroform-*d*) δ 165.65, 156.71, 152.76, 150.42, 150.04, 145.81, 138.96, 138.22, 138.07, 138.01, 134.92, 129.42, 129.06, 127.97, 127.17, 124.15, 122.86, 122.14, 120.15, 119.44, 118.89, 115.16, 81.03, 53.09, 28.42.

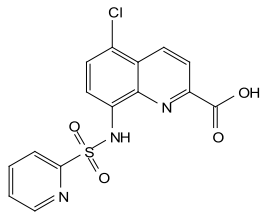


¹H NMR (600 MHz, Chloroform-*d*) δ 9.61 (s, 1H), 8.61 (ddd, *J* = 4.7, 1.7, 0.9 Hz, 1H), 8.11 (s, 1H), 8.00 (dd, *J* = 7.5, 1.3 Hz, 1H), 7.88 (td, *J* = 7.8, 1.7 Hz, 1H), 7.55 (dd, *J* = 8.6, 1.3 Hz, 1H), 7.52 – 7.47 (m, 2H), 7.43 (ddd, *J* = 7.7, 4.7, 1.1 Hz, 1H), 7.25 (ddd, *J* = 7.6, 1.6, 0.9 Hz, 1H), 7.23 – 7.15 (m, 2H), 4.07 (s, 3H).



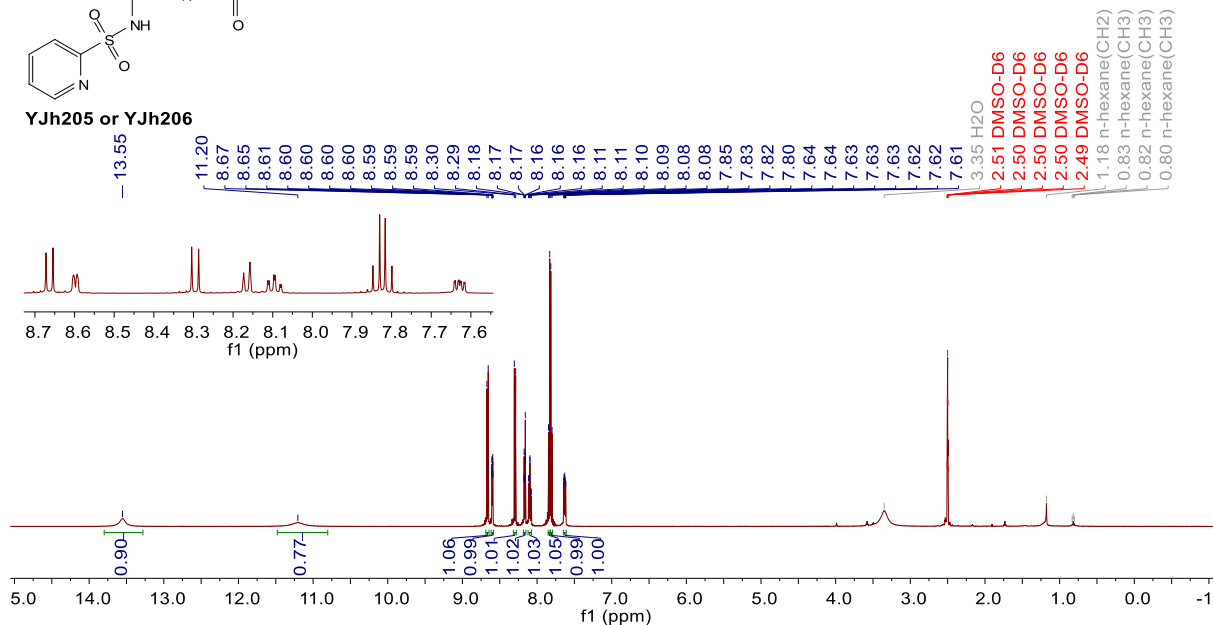
¹³C NMR (151 MHz, Chloroform-*d*) δ 165.58, 162.85 (d, *J* = 247.9 Hz), 156.80, 150.44, 148.84 (d, *J* = 2.1 Hz), 145.89, 139.30 (d, *J* = 7.5 Hz), 138.23, 138.06, 135.18, 130.58 (d, *J* = 8.3 Hz), 129.40, 127.72, 127.20, 125.41 (d, *J* = 2.9 Hz), 122.90, 122.17, 119.62, 116.72 (d, *J* = 22.6 Hz), 116.07 (d, *J* = 21.0 Hz), 115.16, 53.19.



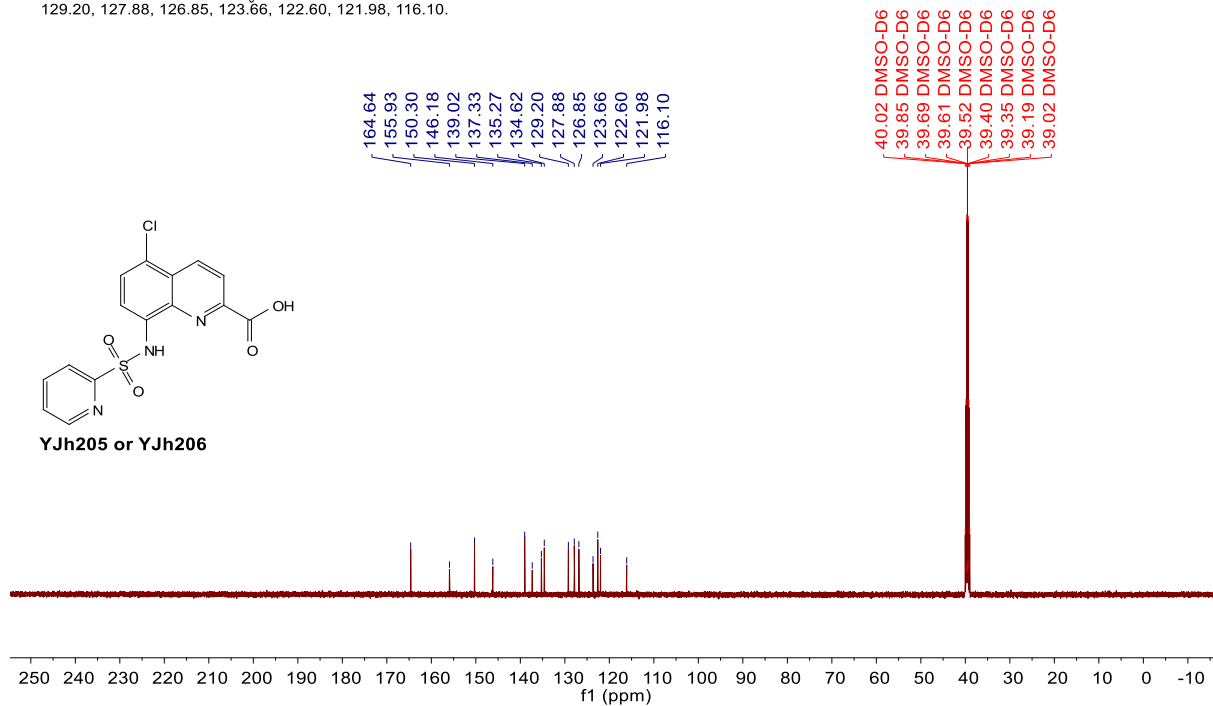


¹H NMR (500 MHz, DMSO-d₆) δ 13.55 (s, 1H), 11.20 (s, 1H), 8.66 (d, J = 8.7 Hz, 1H), 8.60 (ddd, J = 4.7, 1.7, 0.9 Hz, 1H), 8.30 (d, J = 8.7 Hz, 1H), 8.17 (dt, J = 7.9, 1.0 Hz, 1H), 8.10 (td, J = 7.8, 1.7 Hz, 1H), 7.84 (d, J = 8.5 Hz, 1H), 7.81 (d, J = 8.6 Hz, 1H), 7.63 (ddd, J = 7.6, 4.7, 1.2 Hz, 1H).

YJh205 or YJh206

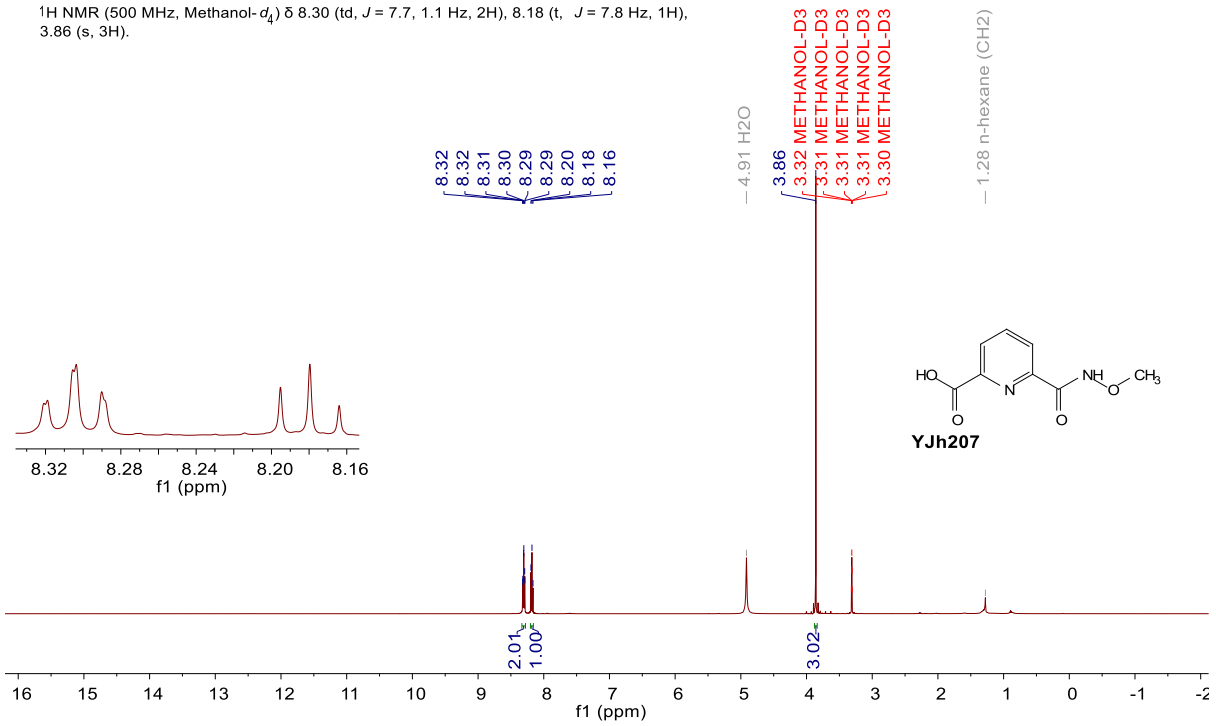


¹³C NMR (126 MHz, DMSO-d₆) δ 164.64, 155.93, 150.30, 146.18, 139.02, 137.33, 135.27, 134.62, 129.20, 127.88, 126.85, 123.66, 122.60, 121.98, 116.10.

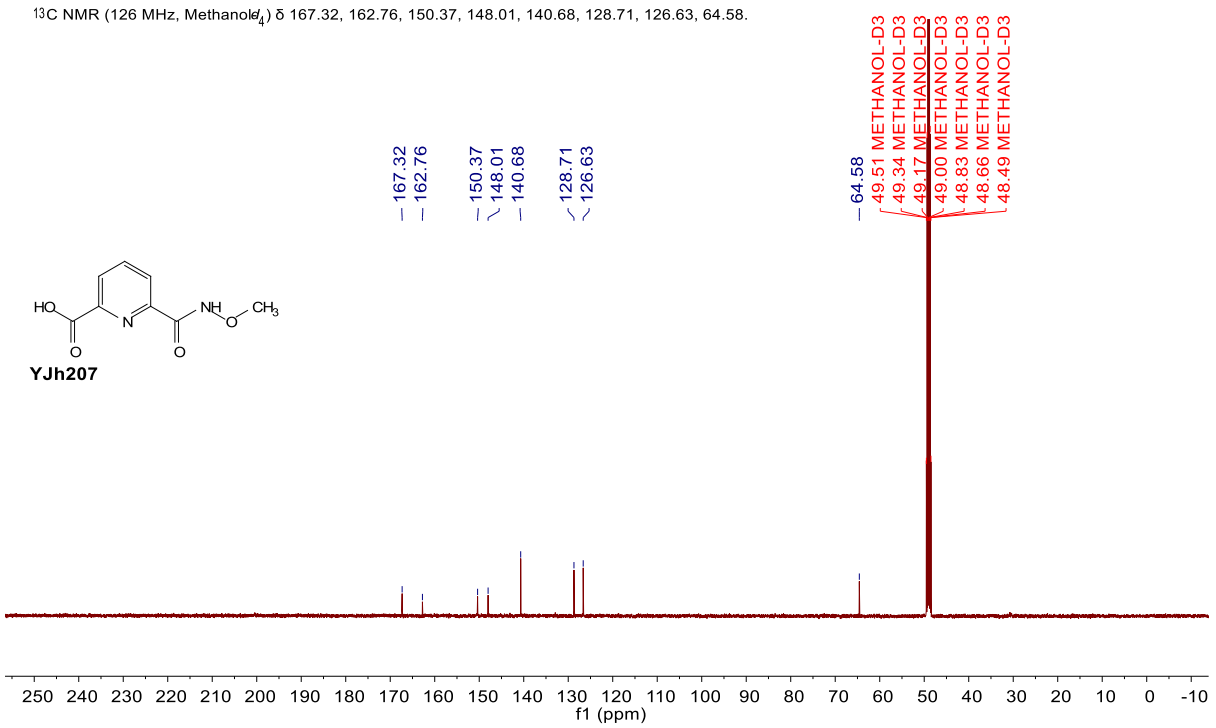


YJh205 or YJh206

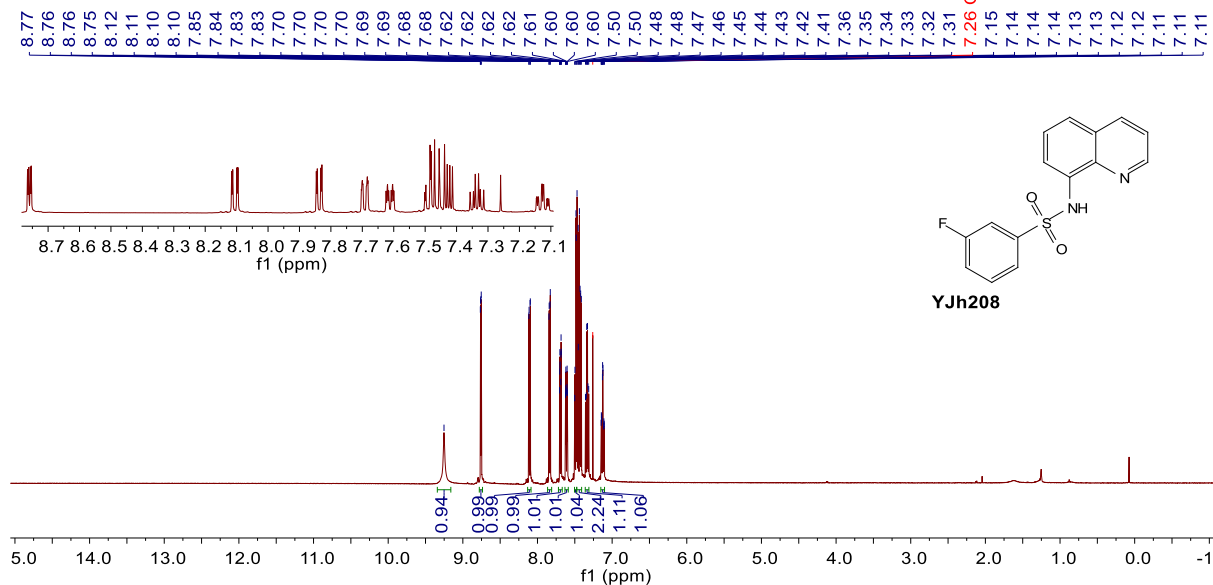
¹H NMR (500 MHz, Methanol-*d*₄) δ 8.30 (td, *J* = 7.7, 1.1 Hz, 2H), 8.18 (t, *J* = 7.8 Hz, 1H), 3.86 (s, 3H).



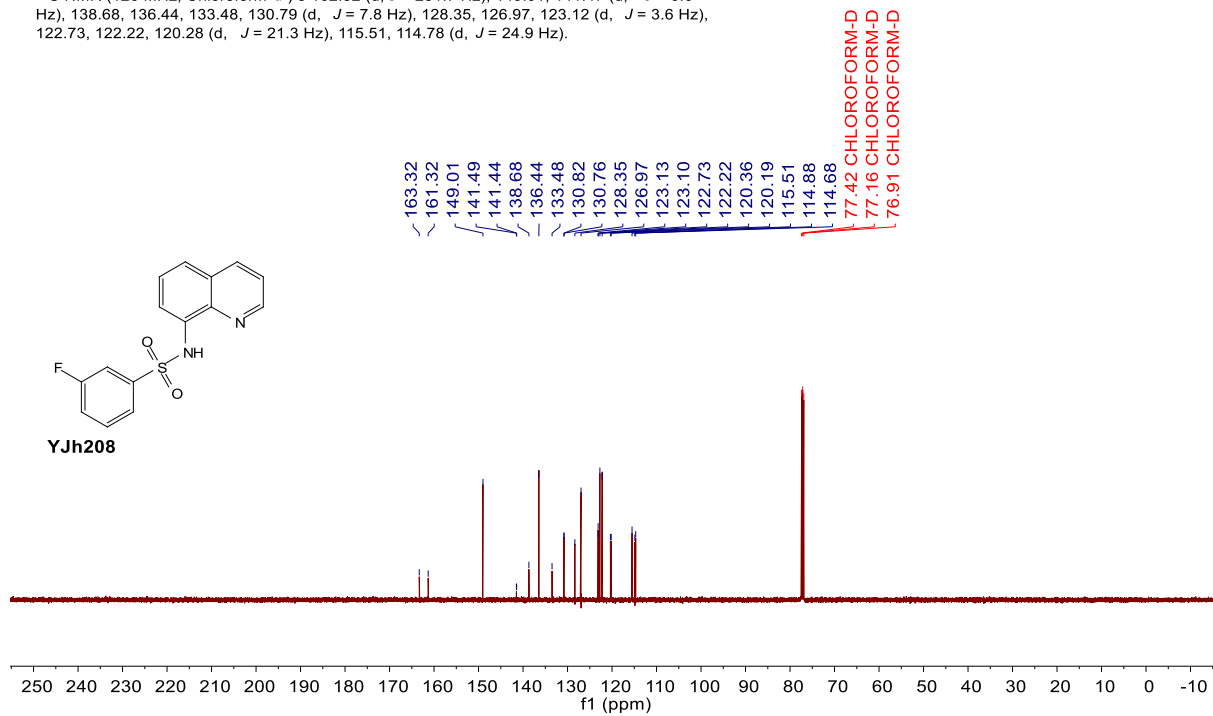
¹³C NMR (126 MHz, Methanol-*d*₄) δ 167.32, 162.76, 150.37, 148.01, 140.68, 128.71, 126.63, 64.58.



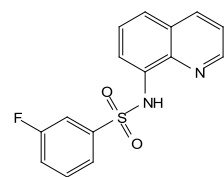
¹H NMR (500 MHz, Chloroform-*d*) δ 9.25 (s, 1H), 8.76 (dd, *J* = 4.2, 1.6 Hz, 1H), 8.11 (dd, *J* = 8.3, 1.7 Hz, 1H), 7.84 (dd, *J* = 7.3, 1.6 Hz, 1H), 7.69 (ddd, *J* = 7.8, 1.7, 0.9 Hz, 1H), 7.61 (ddd, *J* = 8.2, 2.6, 1.7 Hz, 1H), 7.49 (dd, *J* = 8.3, 1.6 Hz, 1H), 7.47 – 7.41 (m, 2H), 7.34 (td, *J* = 8.1, 5.3 Hz, 1H), 7.13 (tdd, *J* = 8.3, 2.6, 0.9 Hz, 1H).



¹³C NMR (126 MHz, Chloroform-*d*) δ 162.32 (d, *J* = 251.7 Hz), 149.01, 141.47 (d, *J* = 6.6 Hz), 138.68, 136.44, 133.48, 130.79 (d, *J* = 7.8 Hz), 128.35, 126.97, 123.12 (d, *J* = 3.6 Hz), 122.73, 122.22, 120.28 (d, *J* = 21.3 Hz), 115.51, 114.78 (d, *J* = 24.9 Hz).

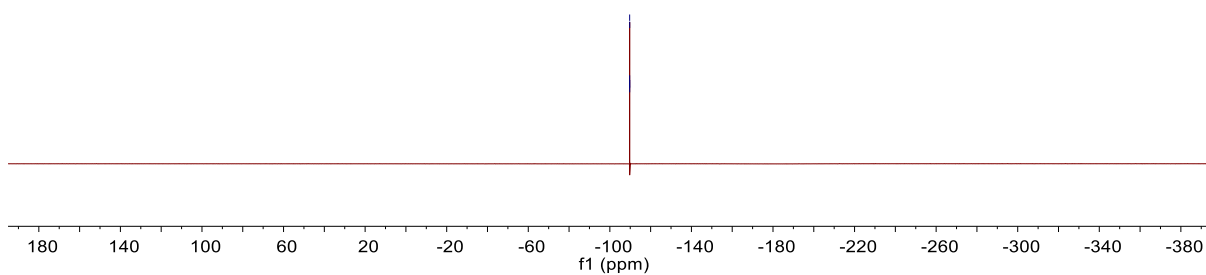


^{19}F NMR (565 MHz, Chloroform-*d*) δ -109.72 (td, $J = 7.9, 5.5$ Hz).

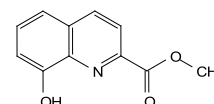
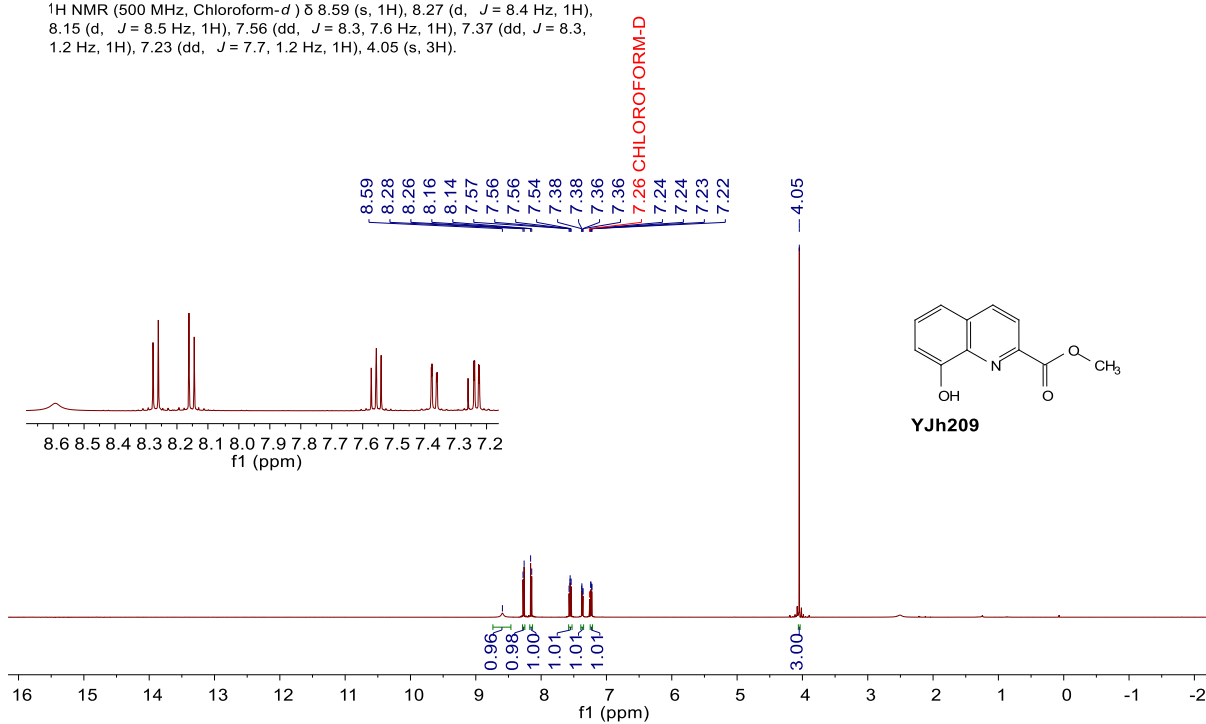


YJh208

-109.70
-109.71
-109.72
-109.73
-109.74

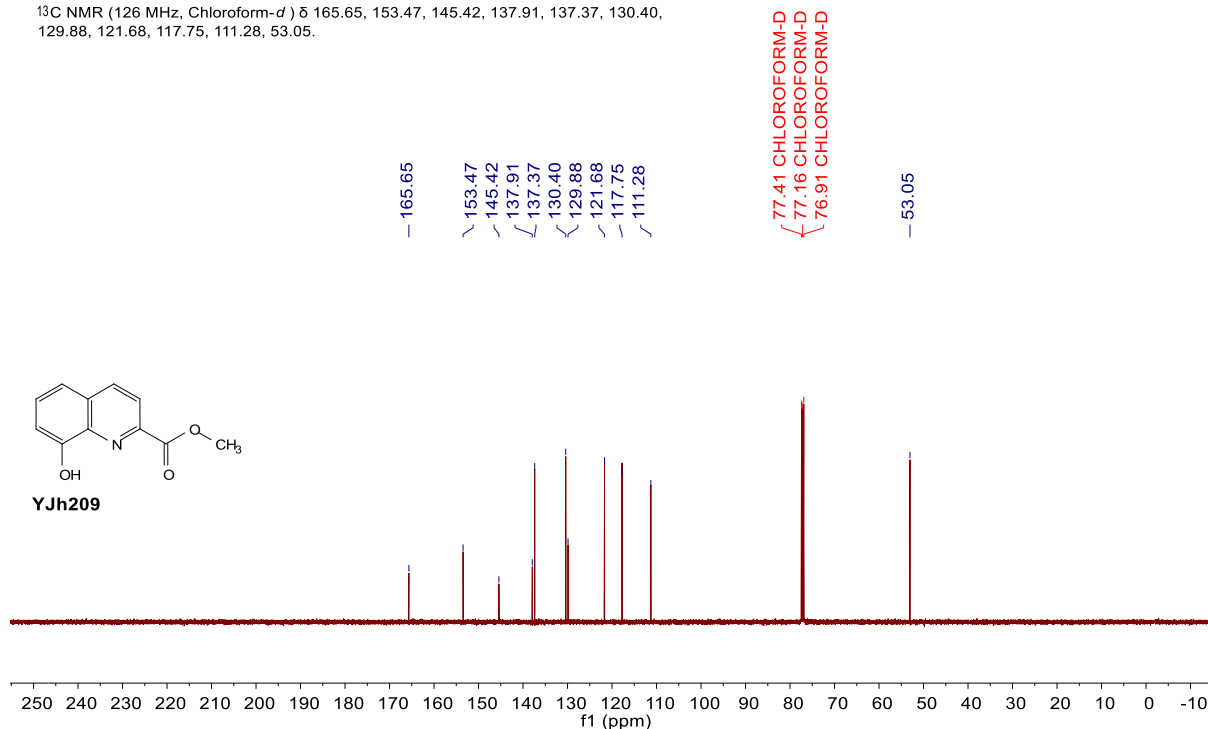


^1H NMR (500 MHz, Chloroform-*d*) δ 8.59 (s, 1H), 8.27 (d, $J = 8.4$ Hz, 1H), 8.15 (d, $J = 8.5$ Hz, 1H), 7.56 (dd, $J = 8.3, 7.6$ Hz, 1H), 7.37 (dd, $J = 8.3, 1.2$ Hz, 1H), 7.23 (dd, $J = 7.7, 1.2$ Hz, 1H), 4.05 (s, 3H).

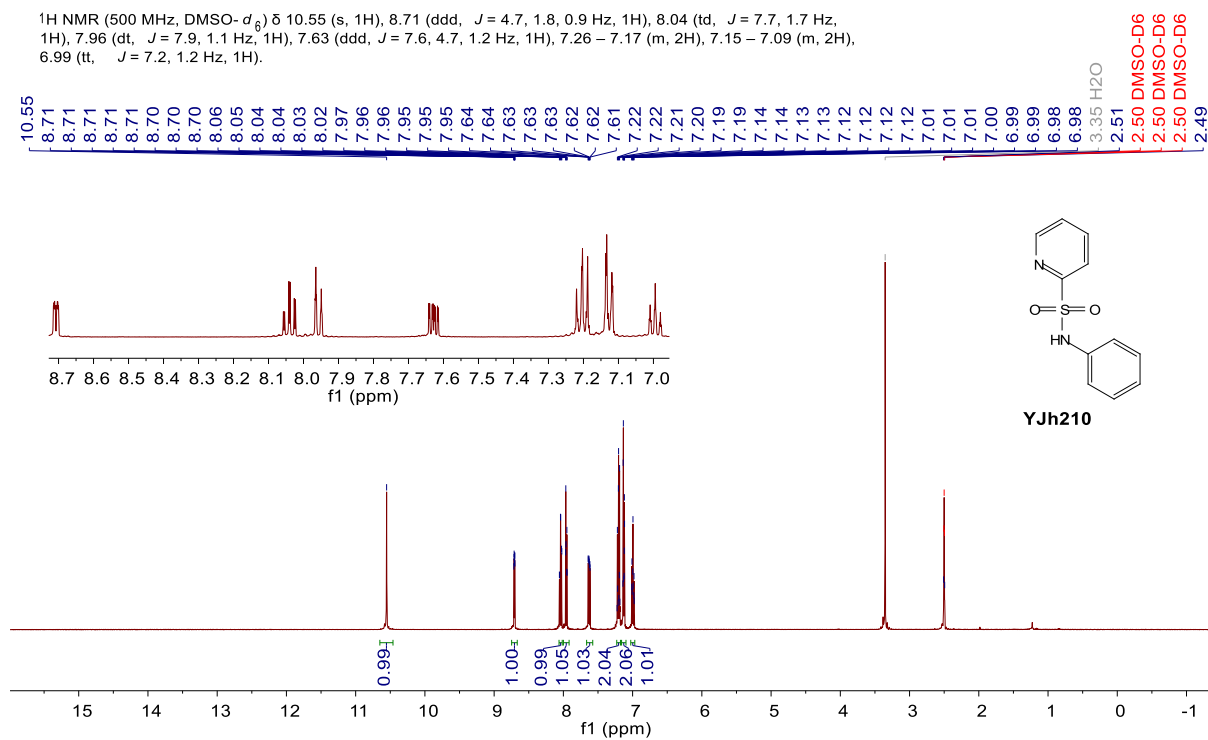


YJh209

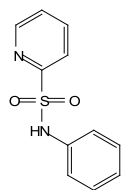
¹³C NMR (126 MHz, Chloroform-*d*) δ 165.65, 153.47, 145.42, 137.91, 137.37, 130.40, 129.88, 121.68, 117.75, 111.28, 53.05.



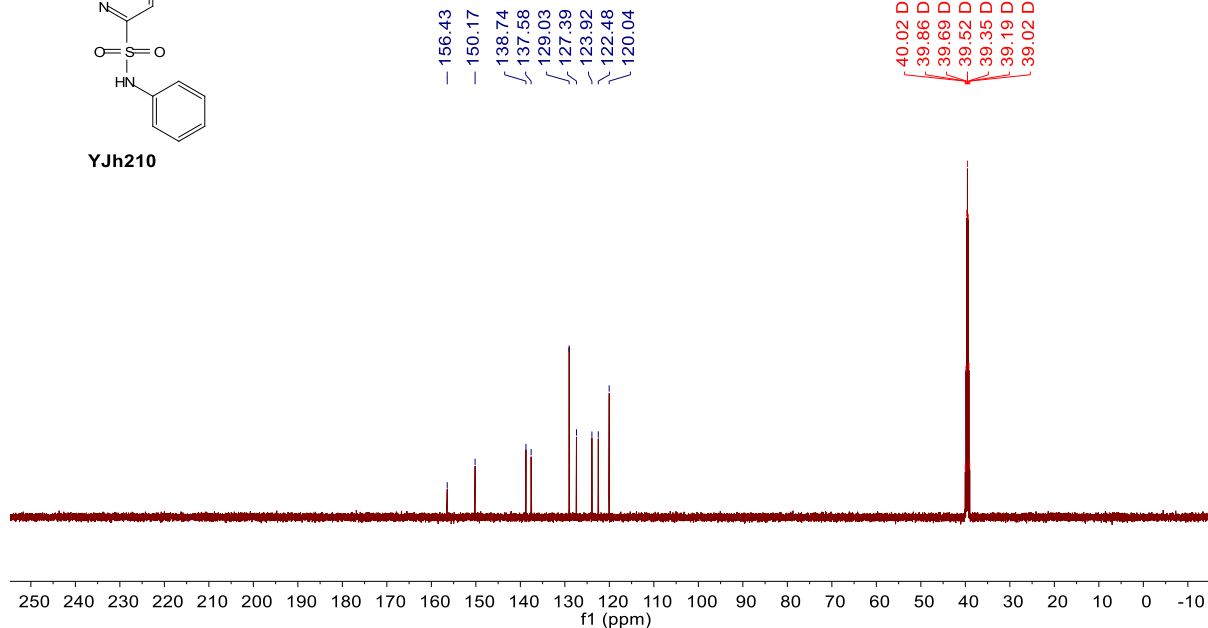
¹H NMR (500 MHz, DMSO-*d*₆) δ 10.55 (s, 1H), 8.71 (ddd, *J* = 4.7, 1.8, 0.9 Hz, 1H), 8.04 (td, *J* = 7.7, 1.7 Hz, 1H), 7.96 (dt, *J* = 7.9, 1.1 Hz, 1H), 7.63 (ddd, *J* = 7.6, 4.7, 1.2 Hz, 1H), 7.26 – 7.17 (m, 2H), 7.15 – 7.09 (m, 2H), 6.99 (tt, *J* = 7.2, 1.2 Hz, 1H).



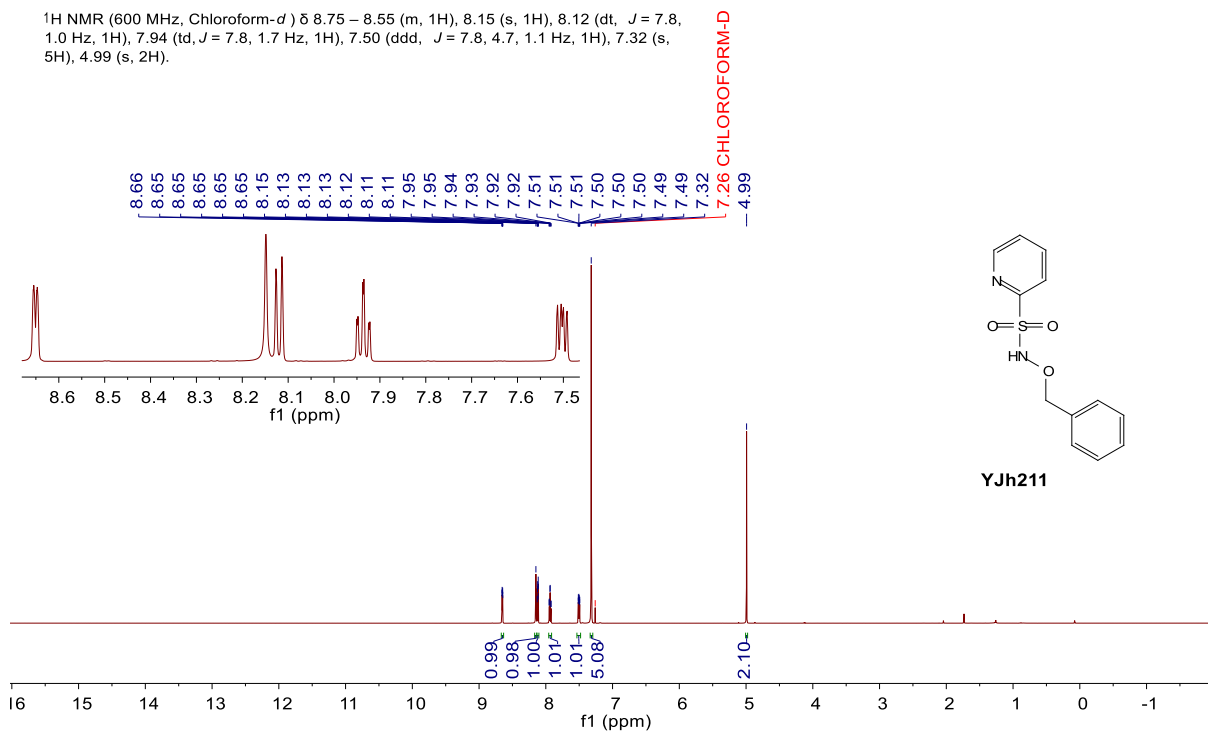
^{13}C NMR (126 MHz, $\text{DMSO}-d_6$) δ 156.43, 150.17, 138.74, 137.58, 129.03, 127.39, 123.92, 122.48, 120.04.



YJh210

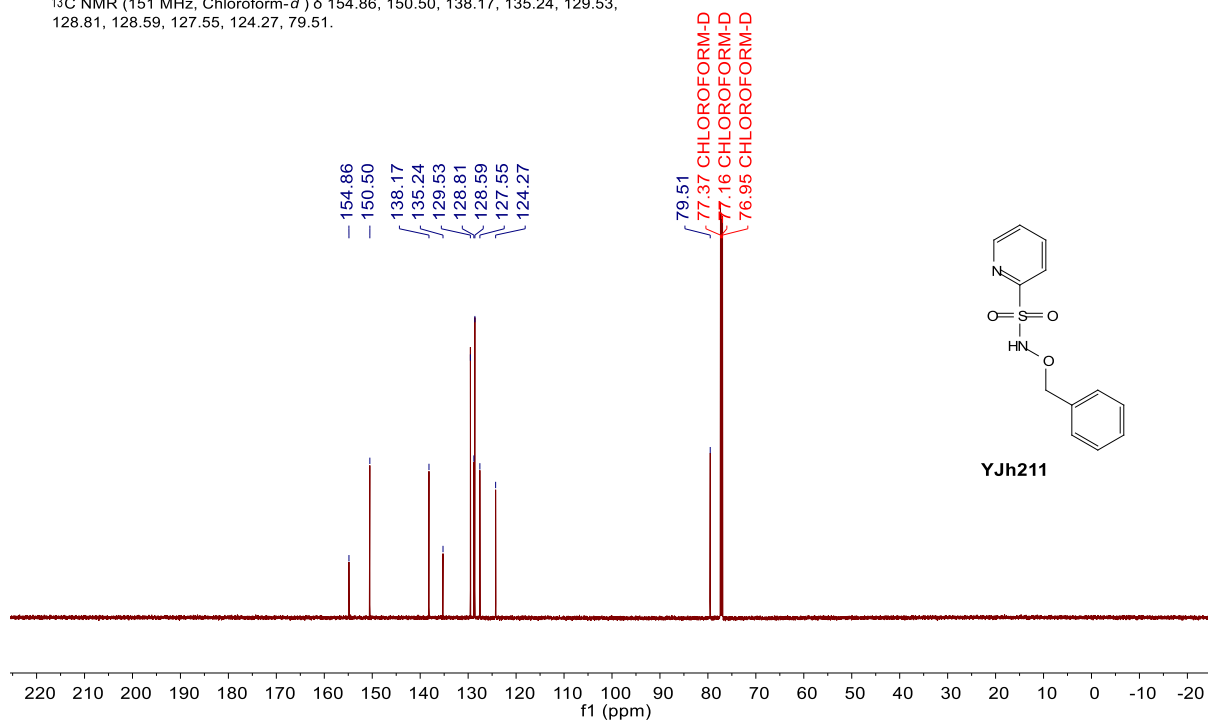


^1H NMR (600 MHz, $\text{Chloroform}-d$) δ 8.75 – 8.55 (m, 1H), 8.15 (s, 1H), 8.12 (dt, $J = 7.8, 1.0$ Hz, 1H), 7.94 (td, $J = 7.8, 1.7$ Hz, 1H), 7.50 (ddd, $J = 7.8, 4.7, 1.1$ Hz, 1H), 7.32 (s, 5H), 4.99 (s, 2H).

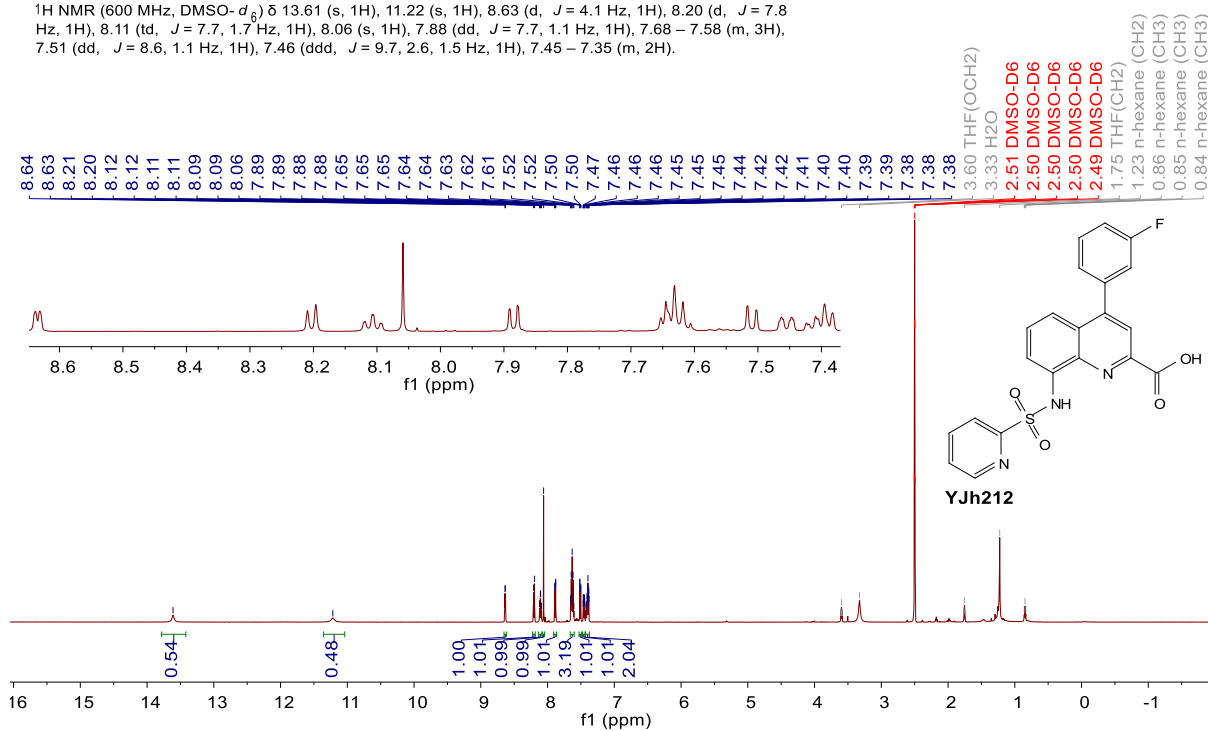


YJh211

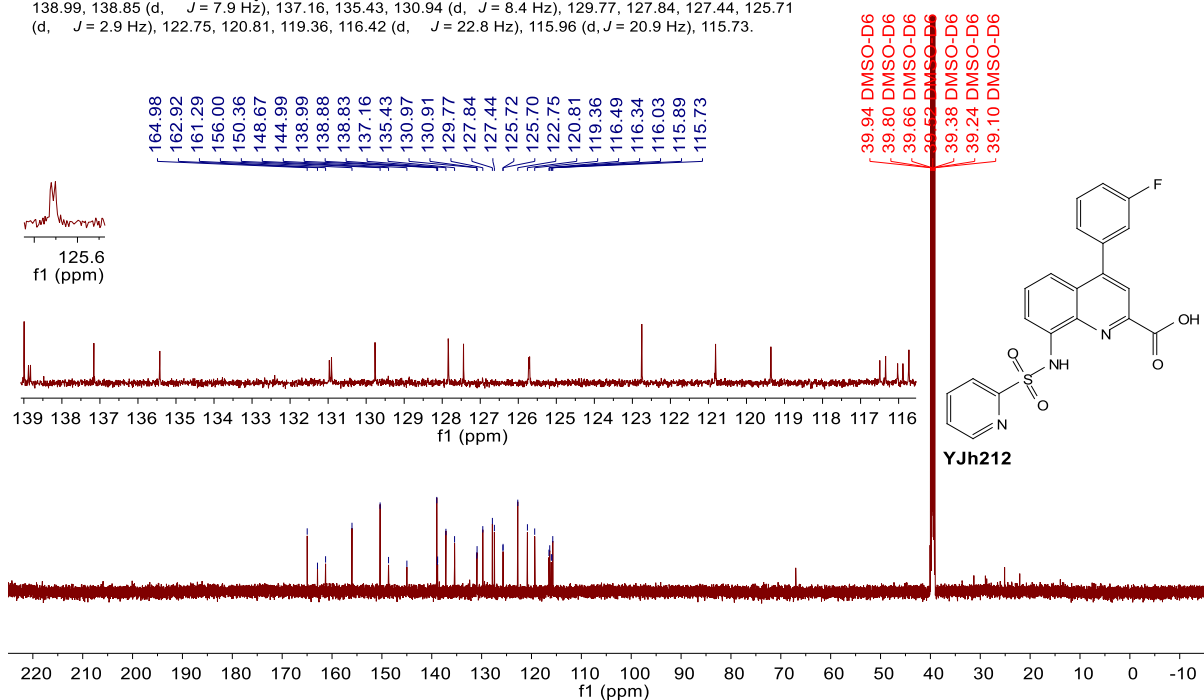
¹³C NMR (151 MHz, Chloroform-*d*) δ 154.86, 150.50, 138.17, 135.24, 129.53, 128.81, 128.59, 127.55, 124.27, 79.51.



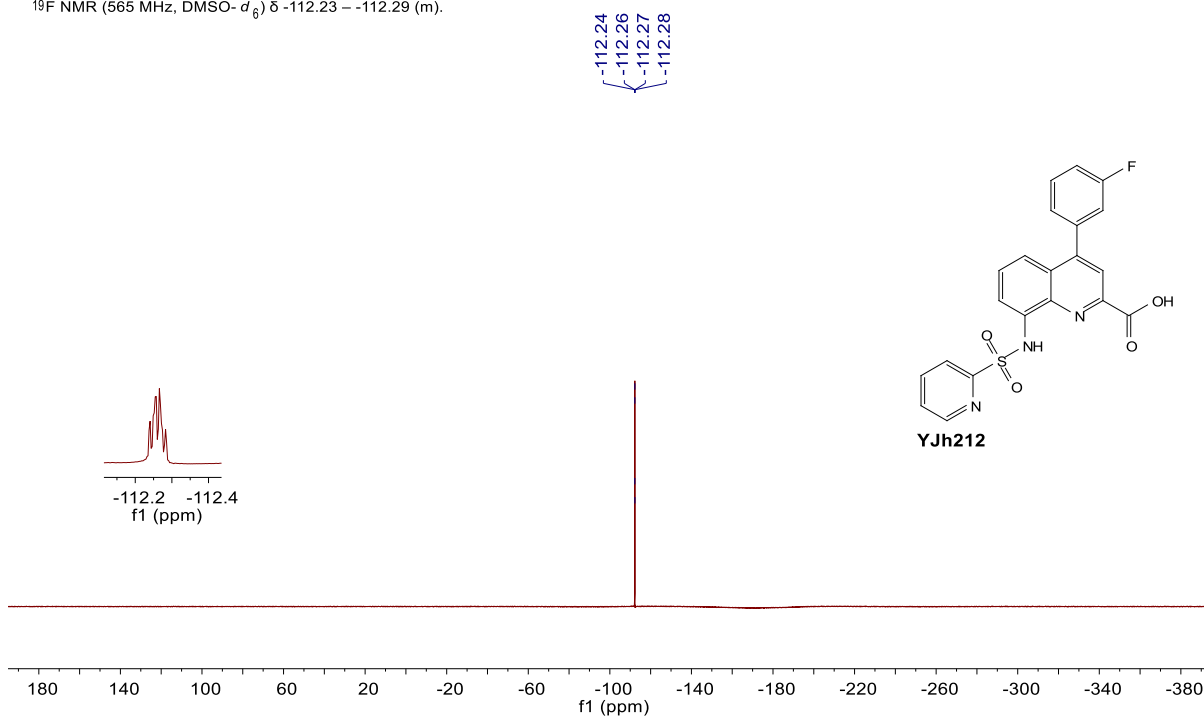
¹H NMR (600 MHz, DMSO-*d*₆) δ 13.61 (s, 1H), 11.22 (s, 1H), 8.63 (d, *J* = 4.1 Hz, 1H), 8.20 (d, *J* = 7.8 Hz, 1H), 8.11 (td, *J* = 7.7, 1.7 Hz, 1H), 8.06 (s, 1H), 7.88 (dd, *J* = 7.7, 1.1 Hz, 1H), 7.68 – 7.58 (m, 3H), 7.51 (dd, *J* = 8.6, 1.1 Hz, 1H), 7.46 (ddd, *J* = 9.7, 2.6, 1.5 Hz, 1H), 7.45 – 7.35 (m, 2H).



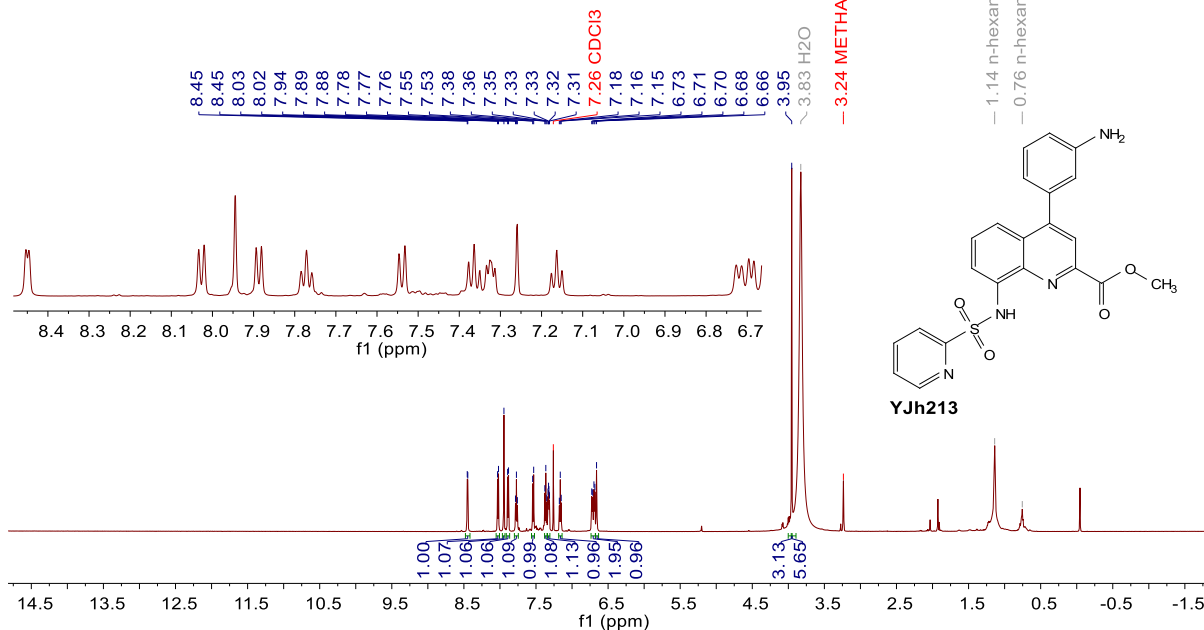
^{13}C NMR (151 MHz, $\text{DMSO}-d_6$) δ 164.98, 162.11 (d, $J = 245.0$ Hz), 156.00, 150.36, 148.67, 144.99, 138.99, 138.85 (d, $J = 7.9$ Hz), 137.16, 135.43, 130.94 (d, $J = 8.4$ Hz), 129.77, 127.84, 127.44, 125.71 (d, $J = 2.9$ Hz), 122.75, 120.81, 119.36, 116.42 (d, $J = 22.8$ Hz), 115.96 (d, $J = 20.9$ Hz), 115.73.



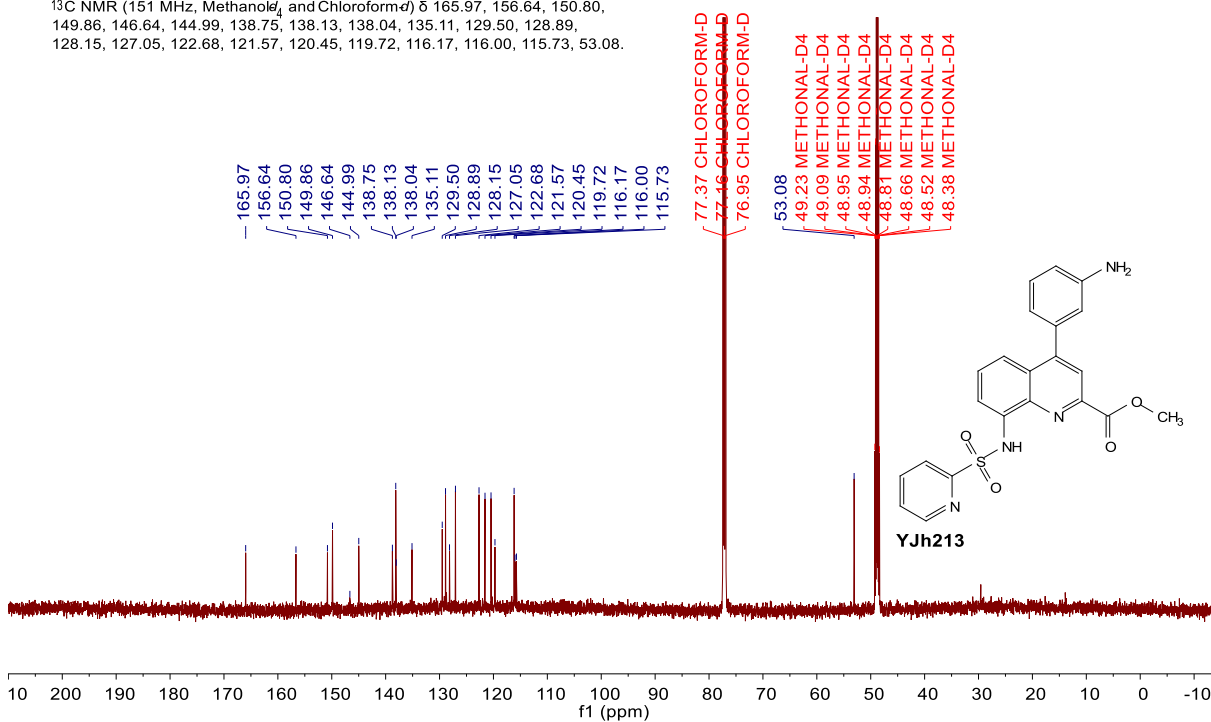
^{19}F NMR (565 MHz, $\text{DMSO}-d_6$) δ -112.23 – -112.29 (m).



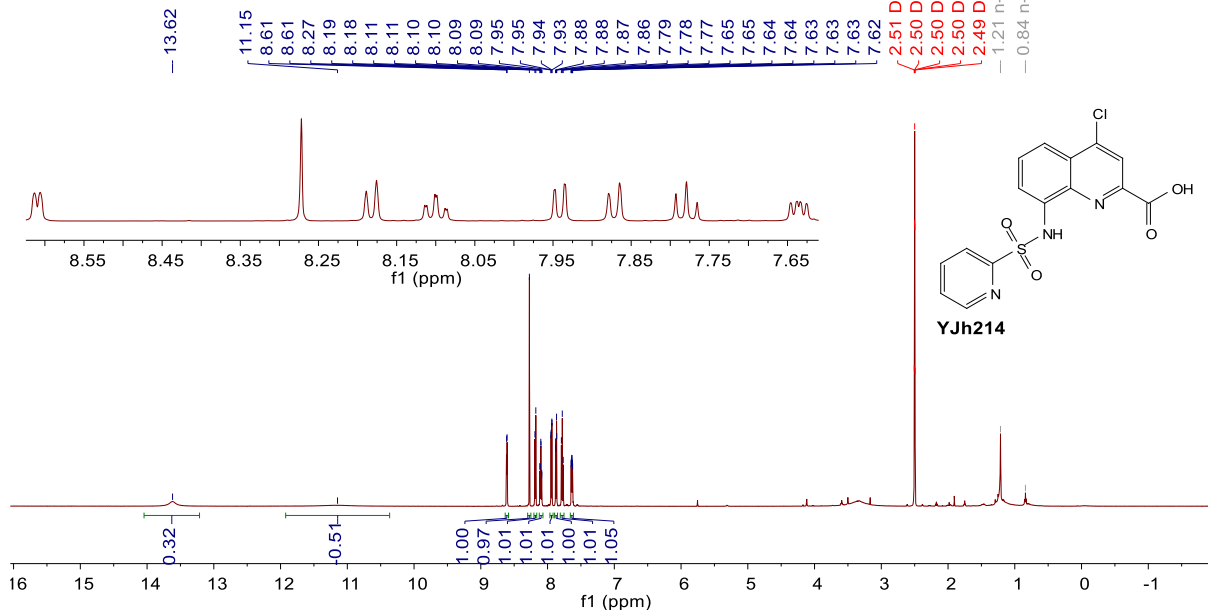
¹H NMR (600 MHz, Methanol-d₄ and Chloroform-d) δ 8.45 (d, J = 4.7 Hz, 1H), 8.03 (d, J = 7.9 Hz, 1H), 7.94 (s, 1H), 7.89 (d, J = 7.7 Hz, 1H), 7.77 (t, J = 7.8 Hz, 1H), 7.54 (d, J = 8.5 Hz, 1H), 7.36 (t, J = 8.2 Hz, 1H), 7.32 (dd, J = 7.6, 4.8 Hz, 1H), 7.16 (t, J = 7.8 Hz, 1H), 6.72 (d, J = 8.0 Hz, 1H), 6.69 (d, J = 7.6 Hz, 1H), 6.66 (s, 1H), 3.95 (s, 3H).



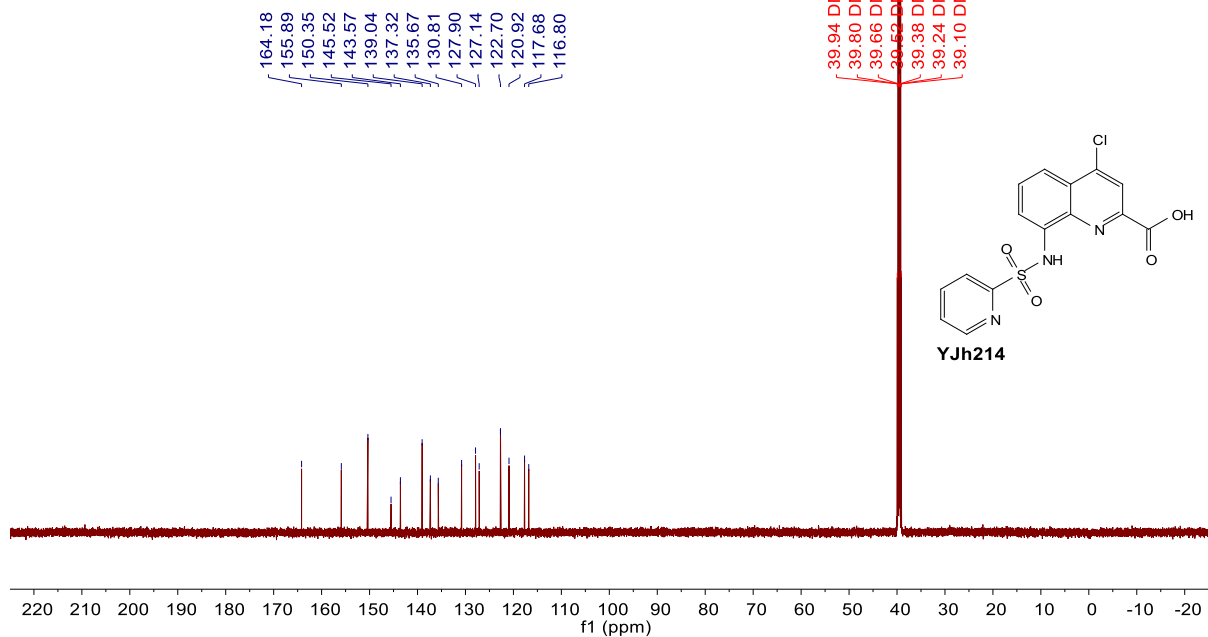
¹³C NMR (151 MHz, Methanol-d₄ and Chloroform-d) δ 165.97, 156.64, 150.80, 149.86, 146.64, 144.99, 138.75, 138.13, 138.04, 135.11, 129.50, 128.89, 128.15, 127.05, 122.68, 121.57, 120.45, 119.72, 116.17, 116.00, 115.73, 53.08.

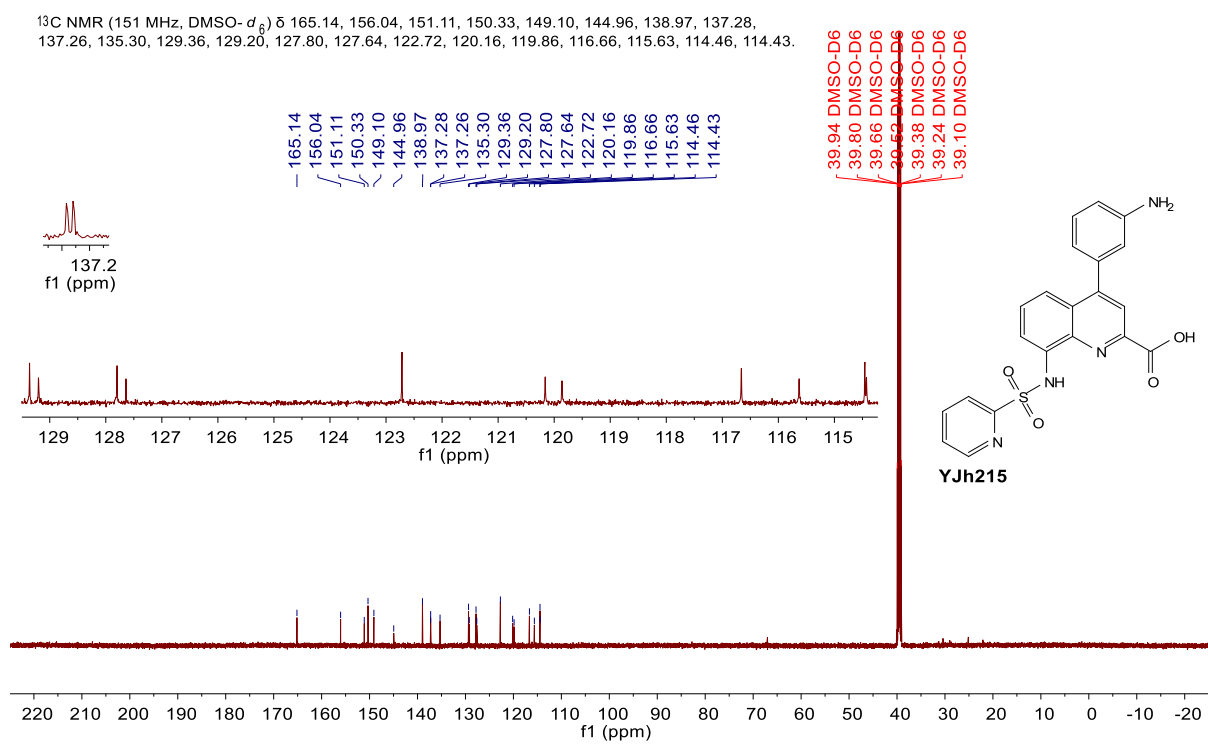
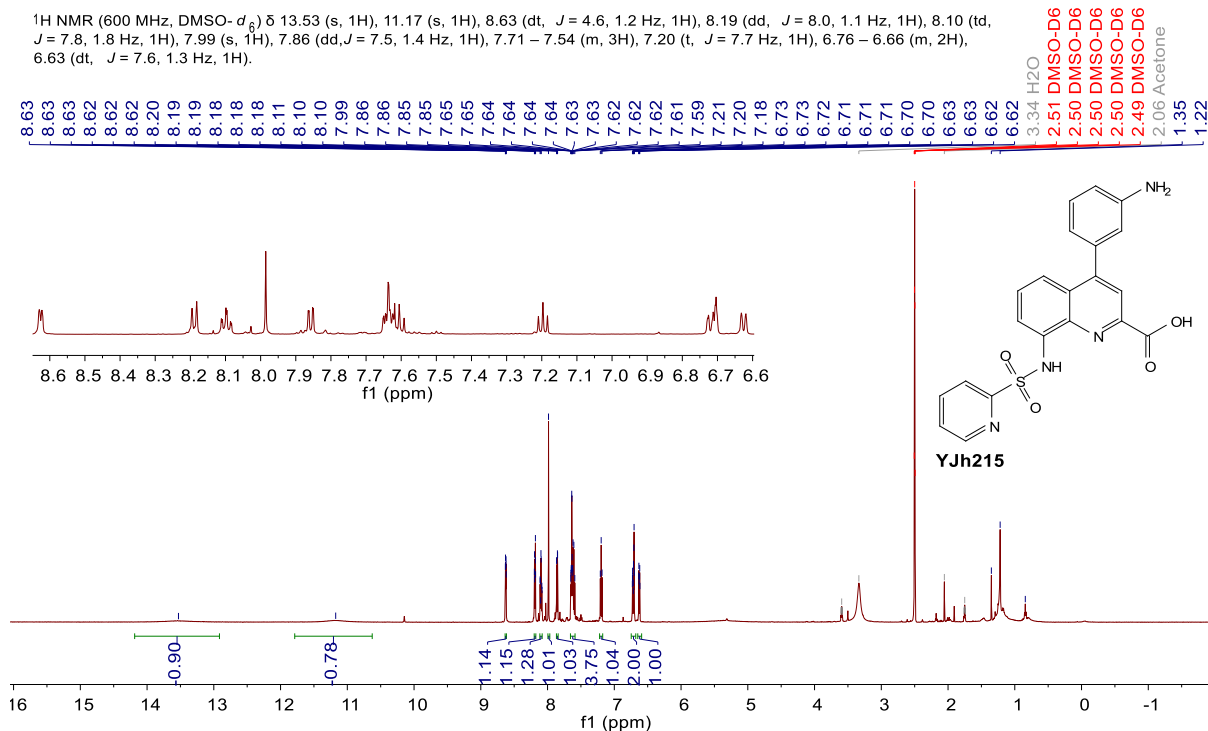


^1H NMR (600 MHz, $\text{DMSO}-d_6$) δ 13.62 (s, 1H), 11.15 (s, 1H), 8.61 (d, $J = 4.3$ Hz, 1H), 8.27 (s, 1H), 8.18 (d, $J = 7.9$ Hz, 1H), 8.10 (td, $J = 7.8, 1.7$ Hz, 1H), 7.94 (dd, $J = 7.8, 1.2$ Hz, 1H), 7.87 (dd, $J = 8.5, 1.2$ Hz, 1H), 7.78 (t, $J = 8.1$ Hz, 1H), 7.64 (ddd, $J = 7.7, 4.7, 1.1$ Hz, 1H).



^{13}C NMR (151 MHz, $\text{DMSO}-d_6$) δ 164.18, 155.89, 150.35, 145.52, 143.57, 139.04, 137.32, 135.67, 130.81, 127.90, 127.14, 122.70, 120.92, 117.68, 116.80.





7 References

1. Hutchings, M. I.; Truman, A. W.; Wilkinson, B. Antibiotics: Past, Present and Future. *Curr. Opin. Microbiol.* **2019**, *51*, 72-80.
2. Fair, R. J.; Tor, Y. Antibiotics and Bacterial Resistance in the 21st Century. *Perspect. Medicin. Chem.* **2014**, *6*, 25-64.
3. Livermore, D. M. Bacterial Resistance: Origins, Epidemiology, and Impact. *Clin. Infect. Dis.* **2003**, *36*, 11–23.
4. Kumar, S; Varela, M. F. Molecular Mechanisms of Bacterial Resistance to Antimicrobial Agents. *Chemotherapy* 2013, *14*, 522-534.
5. Elshamy, A. A.; Aboshanab, K. M. A Review on Bacterial Resistance to Carbapenems Epidemiology, Detection and Treatment Options. *Future Sci. O. A.* **2020**, *6*(3).
6. Penesyanyan, A.; Gillings, M.; Paulsen, I. T. Antibiotic Discovery: Combatting Bacterial Resistance in Cells and in Biofilm Communities. *Molecules* **2015**, *20*(4), 5286-5298.
7. Kumar, A.; Schweizer, H. P. Bacterial Resistance to Antibiotics: Active Efflux and Reduced Uptake. *Adv. Drug Deliv. Rev.* **2005**, *57*(10), 1486-1513.
8. Zgurskaya, H. I.; Lopez, C. A.; Gnanakaran, S. Permeability Barrier of Gram-Negative Cell Envelopes and Approaches to Bypass It. *A. C. S. Infect. Dis.* **2015**, *1*(11), 512-522.
9. Fernandez, L.; Hancock, R. E. Adaptive and Mutational Resistance: Role of Porins and Efflux Pumps in Drug Resistance. *Clin. Microbiol. Rev.* **2012**, *25*(4), 661-681.
10. Choi, U.; Lee, C. R. Distinct Roles of Outer Membrane Porins in Antibiotic Resistance and Membrane Integrity in *Escherichia coli*. *Front. Microbiol.* **2019**, *10*, 953.
11. Wright, G. D. Bacterial Resistance to Antibiotics: Enzymatic Degradation and Modification. *Adv. Drug Deliv. Rev.* **2005**, *57*(10), 1451-1470.
12. Lambert, P. A. Bacterial Resistance to Antibiotics: Modified Target Sites. *Adv. Drug Deliv. Rev.* **2005**, *57*(10), 1471-1485.
13. Dorr, T.; Moynihan, P. J.; Mayer, C. Editorial: Bacterial Cell Wall Structure and Dynamics. *Front. Microbiol.* **2019**, *10*, 2051.
14. Murray, P. R.; Rosenthal, K. S.; Pfaller, M. A. Medical Microbiology (Elsevier) **2021**.
15. Epanand, R. M.; Walker, C.; Epanand, R. F.; Magarvey, N. A. Molecular Mechanisms of Membrane Targeting Antibiotics. *Biochim. Biophys. Acta.* **2016**, *1858*(5), 980-987.
16. Llarrull, L. I.; Testero, S. A.; Fisher, J. F.; Mobashery, S. The Future of the β -Lactams. *Curr. Opin. Microbiol.* **2010**, *13*(5), 551-557.
17. Egan, A. J. F.; Errington, J.; Vollmer, W. Regulation of Peptidoglycan Synthesis and Remodelling. *Nat. Rev. Microbiol.* **2020**, *18*(8), 446-460.
18. Nicholas, R. A.; Davies, C. Structural Mechanisms of β -Lactam Antibiotic Resistance in Penicillin-binding Proteins. In *Antibiotic Discovery and Development* (Dougherty, T. J. and Pucci, M. J., Ed), Springer, Boston, MA, **2012**, 397–425.
19. A. Fleming, On the Antibacterial Action of Cultures of a Penicillium, with Special Reference to Their Use in the Isolation of *B. Influenzae*. *Brit. J. exp. Path.* **1929**, *10*, 226-236.
20. Chain, E.; Florey, H.; Gardner, A.; Heatley, N. G.; Jennings, M. A.; Orr-Ewing, J.; Sanders, A. G. Penicillin as a Chemotherapeutic Agent. *Lancet* **1940**, *236*, 226–228.
21. Brotzu, G. Research on a New Antibiotic. *Publications of the Cagliari Institute of Hygiene.* **1948**, 5-19.

22. Lima, L. M.; Silva, B. N. M.; Barbosa, G.; Barreiro, E. J. β -Lactam Antibiotics: An Overview from a Medicinal Chemistry Perspective. *Eur. J. Med. Chem.* **2020**, *208*, 112829.
23. Finberg, R. W.; Guharoy, R. Cephalosporins. In: *Clinical Use of Anti-infective Agents*. Springer, Cham. **2021**, 39-46.
24. Tamma, P. D.; Hsu, A. J. Defining the Role of Novel β -Lactam Agents That Target Carbapenem-Resistant Gram-Negative Organisms. *J. Pediatric. Infect. Dis. Soc.* **2019**, *8*(3), 251-260.
25. Codjoe, F. S.; Donkor, E. S. Carbapenem Resistance: A Review. *Med. Sci. (Basel)* **2017**, *6*(1).
26. Wilke, M. S.; Lovering, A. L.; Strynadka, N. C. β -Lactam Antibiotic Resistance: A Current Structural Perspective. *Curr. Opin. Microbiol.* **2005**, *8*(5), 525-533.
27. Behzadi, P.; Garcia-Perdomo, H. A.; Karpinski, T. M.; Issakhanian, L. Metallo- β -lactamases: A Review. *Mol. Biol. Rep.* **2020**, *47*(8), 6281–6294.
28. Bush, K. The ABCD's of β -Lactamase Nomenclature. *J. Infect. Chemother.* **2013**, *19*(4), 549-559.
29. Palzkill, T. Metallo- β -lactamase Structure and Function. *Ann. N. Y. Acad. Sci.* **2013**, *1277*, 91-104.
30. Ghafourian, S.; Sadeghifard, N.; Soheili, S.; Sekawi, Z. Extended Spectrum β -Lactamases: Definition, Classification and Epidemiology. *Curr. Issues Mol. Biol.* **2015**, *17*, 11-22.
31. Bush, K.; Bradford, P. A. Interplay between β -Lactamases and New β -Lactamase Inhibitors. *Nat. Rev. Microbiol.* **2019**, *17*(5), 295-306.
32. Naas, T.; Oueslati, S.; Bonnin, R. A.; Dabos, M. L.; Zavala, A.; Dortet, L.; Retailliau, P.; Iorga, B. I. Beta-Lactamase DataBase (BLDB) – Structure and Function. *J. Enzyme Inhib. Med. Chem.* **2017**, *32*, 917-919.
33. De Angelis, G.; Del Giacomo, P.; Posteraro, B.; Sanguinetti, M.; Tumbarello, M. Molecular Mechanisms, Epidemiology, and Clinical Importance of β -Lactam Resistance in *Enterobacteriaceae*. *Int. J. Mol. Sci.* **2020**, *21*, 5090.
34. Bradford, P. A. Extended-spectrum β -Lactamases in the 21st Century: Characterization, Epidemiology, and Detection of this Important Resistance Threat. *Clin. Microbiol. Rev.* **2001**, *14*(4), 933-951.
35. Peirano, G.; Pitout, J. D. D. Extended-spectrum β -Lactamase-producing *Enterobacteriaceae*: Update on Molecular Epidemiology and Treatment Options. *Drugs* **2019**, *79*(14), 1529-1541.
36. Theuretzbacher, U.; Carrara, E.; Conti, M.; Tacconelli, E. Role of New Antibiotics for KPC-producing *Klebsiella pneumoniae*. *J. Antimicrob. Chemother.* **2021**, *76*(Suppl 1), i47-i54.
37. Castanheira, M.; Simner, P. J.; Bradford, P. A. Extended-spectrum β -Lactamases: An Update on their Characteristics, Epidemiology and Detection. *J. A. C. Antimicrob. Resist.* **2021**, *3*(3), dlab092.
38. Ur Rahman, S.; Ali, T.; Ali, I.; Khan, N. A.; Han, B.; Gao, J. The Growing Genetic and Functional Diversity of Extended Spectrum β -Lactamases. *Biomed. Res. Int.* **2018**, *2018*, 9519718.
39. Potron, A.; Poirel, L.; Nordmann, P. Emerging Broad-spectrum Resistance in *Pseudomonas aeruginosa* and *Acinetobacter baumannii*: Mechanisms and Epidemiology. *Int. J. Antimicrob. Agents.* **2015**, *45*(6), 568-585.
40. Sheu, C. C.; Lin, S. Y.; Chang, Y. T.; Lee, C. Y.; Chen, Y. H.; Hsueh, P. R. Management of Infections Caused by Extended-spectrum β -Lactamase-producing *Enterobacteriaceae*: Current Evidence and Future Prospects. *Expert. Rev. Anti. Infect. Ther.* **2018**, *16*(3), 205-218.
41. Boyd, S. E.; Livermore, D. M.; Hooper, D. C.; Hope, W. W. Metallo- β -lactamases: Structure, Function, Epidemiology, Treatment Options, and the Development Pipeline. *Antimicrob. Agents. Chemother.* **2020**, *64*(10).

42. Jones, R. N.; Biedenbach, D. J.; Sader, H. S.; Fritsche, T. R.; Toleman, M. A.; Walsh, T. R. Emerging Epidemic of Metallo- β -lactamase-mediated Resistances. *Diagn. Microbiol. Infect. Dis.* **2005**, *51*(2), 77-84.
43. Bush, K. Past and Present Perspectives on β -Lactamases. *Antimicrob. Agents. Chemother.* **2018**, *62*(10).
44. Ju, L. C.; Cheng, Z.; Fast, W.; Bonomo, R. A.; Crowder, M. W. The Continuing Challenge of Metallo- β -lactamase Inhibition: Mechanism Matters. *Trends Pharmacol. Sci.* **2018**, *39*(7), 635-647.
45. Tamma, P. D.; Doi, Y.; Bonomo, R. A.; Johnson, J. K.; Simner, P. J.; Antibacterial Resistance Leadership Group. A Primer on AmpC β -Lactamases: Necessary Knowledge for an Increasingly Multidrug-resistant World. *Clin. Infect. Dis.* **2019**, *69*(8), 1446-1455.
46. Böhm, M.-E.; Razavi, M.; Flach, C.-F.; Larsson, D.G.J. A Novel, Integron-Regulated, Class C β -Lactamase. *Antibiotics* **2020**, *9*, 123.
47. Jeon, J. H.; Hong, M. K.; Lee, J. H.; Lee, J. J.; Park, K. S.; Karim, A. M.; Jo, J. Y.; Kim, J. H.; Ko, K. S.; Kang, L. W.; Lee, S. H. Structure of ADC-68, a Novel Carbapenem-hydrolyzing Class C Extended-spectrum β -Lactamase Isolated from *Acinetobacter baumannii*. *Acta. Crystallogr. D. Biol. Crystallogr.* **2014**, *70*(Pt 11), 2924-2936.
48. Tooke, C. L.; Hinchliffe, P.; Bragginton, E. C.; Colenso, C. K.; Hirvonen, V. H. A.; Takebayashi, Y.; Spencer, J. β -Lactamases and β -Lactamase Inhibitors in the 21st Century. *J. Mol. Biol.* **2019**, *431*(18), 3472-3500.
49. Powers, R. A. Structural and Functional Aspects of Extended-Spectrum AmpC Cephalosporinases. *Curr. Drug Targets* **2016**, *17*(9), 1051-1060.
50. Antunes, N. T.; Fisher, J. F. Acquired Class D β -Lactamases. *Antibiotics* **2014**, *3*, 398-434.
51. Poirel, L.; Naas, T.; Nordmann, P. Diversity, Epidemiology, and Genetics of Class D β -Lactamases. *Antimicrob. Agents Chemother.* **2010**, *54*(1), 24-38.
52. Crowder, M. W.; Spencer, J.; Vila, A. J. Metallo- β -lactamases: Novel Weaponry for Antibiotic Resistance in Bacteria. *Acc. Chem. Res.* **2006**, *39*(10), 721-728.
53. Bahr, G.; Gonzalez, L. J.; Vila, A. J. Metallo- β -lactamases in the Age of Multidrug Resistance: From Structure and Mechanism to Evolution, Dissemination, and Inhibitor Design. *Chem. Rev.* **2021**, *121*(13), 7957-8094.
54. Frohlich, C.; Chen, J. Z.; Gholipour, S.; Erdogan, A. N.; Tokuriki, N. Evolution of β -Lactamases and Enzyme Promiscuity. *Protein Eng. Des. Sel.* **2021**, *34*.
55. Palacios, A. R.; Rossi, M. -A.; Mahler, G. S.; Vila, A. J. Metallo- β -lactamase Inhibitors Inspired on Snapshots from the Catalytic Mechanism. *Biomolecules* **2020**, *10*, 854.
56. Wu, W.; Feng, Y.; Tang, G.; Qiao, F.; McNally, A.; Zong, Z. NDM Metallo- β -lactamases and their Bacterial Producers in Health Care Settings. **2019**, *Clin. Microbiol. Rev.* *32*(2), e00115-18.
57. Poirel, L.; Bonnin, R. A.; Boulanger, A.; Schrenzel, J.; Kaase, M.; Nordmann, P. Tn125-related Acquisition of blaNDM-like Genes in *Acinetobacter baumannii*. *Antimicrob. Agents Chemother.* **2012**, *56*(2), 1087-1089.
58. Joshi, P. R.; Acharya, M.; Kakshapati, T.; Leungtongkam, U.; Thummeepak, R.; Sitthisak, S. Co-existence of blaOXA-23 and blaNDM-1 Genes of *Acinetobacter baumannii* Isolated from Nepal: Antimicrobial Resistance and Clinical Significance. *Antimicrob. Resist. Infect. Control* **2017**, *6*, 21.
59. Carruthers, T. J.; Carr, P. D.; Loh, C. T.; Jackson, C. J.; Otting, G. Iron(III) Located in the Dinuclear Metallo- β -lactamase IMP-1 by Pseudocontact Shifts. *Angew. Chem. Int. Ed. Engl.* **2014**, *53*(51), 14269-14272.

60. Wang, J.; Chou, K. Metallo- β -Lactamases: Structural Features, Antibiotic Recognition, Inhibition, and Inhibitor Design. *Curr. Top. Med. Chem.* **2013**, *13*, 1242-1253.
61. Yan, Y. H.; Li, G.; Li, G. B. Principles and Current Strategies Targeting Metallo- β -lactamase Mediated Antibacterial Resistance. *Med. Res. Rev.* **2020**, *40*(5), 1558-1592.
62. González-Bello, C.; Rodríguez, D.; Pernas, M.; Rodríguez, Á.; Colchón, E. β -Lactamase Inhibitors to Restore the Efficacy of Antibiotics against Superbugs. *J. Med. Chem.* **2019**, *63*(5), 1859-188.
63. Tan, X.; Kim, H. S.; Baugh, K.; Huang, Y.; Kadiyala, N.; Wences, M.; Singh, N.; Wenzler, E.; Bulman, Z. P. Therapeutic Options for Metallo- β -lactamase-producing Enterobacterales. *Infect. Drug Resist.* **2021**, *14*, 125.
64. El-Sayed Ahmed, M. A. E.; Zhong, L. L.; Shen, C.; Yang, Y.; Doi, Y.; Tian, G. B. Colistin and its Role in the Era of Antibiotic Resistance: An Extended Review (2000-2019). *Emerg. Microbes. Infect.* **2020**, *9*(1), 868-885.
65. Castanheira, M.; Sader, H. S.; Deshpande, L. M.; Fritsche, T. R.; Jones, R. N. Antimicrobial Activities of Tigecycline and Other Broad-spectrum Antimicrobials Tested against Serine Carbapenemase- and Metallo- β -lactamase-producing Enterobacteriaceae: Report from the SENTRY Antimicrobial Surveillance Program. *Antimicrob. Agents Chemother.* **2008**, *52*(2), 570-573.
66. Sader, H. S.; Flamm, R. K.; Jones, R. N. Tigecycline Activity Tested against Antimicrobial Resistant Surveillance Subsets of Clinical Bacteria Collected Worldwide (2011). *Diagn. Microbiol. Infect. Dis.* **2013**, *76*(2), 217-221.
67. Livermore, D. M.; Mushtaq, S.; Warner, M.; Zhang, J.; Maharjan, S.; Doumith, M.; Woodford, N. Activities of NXL104 Combinations with Ceftazidime and Aztreonam against Carbapenemase-Producing Enterobacteriaceae. *Antimicrob. Agents Chemother.* **2011**, *55*(1), 390-394.
68. Papp-Wallace, K. M. The Latest Advances in β -Lactam/ β -lactamase Inhibitor Combinations for the Treatment of Gram-negative Bacterial Infections. *Expert Opin. Pharmacother.* **2019**, *20*(17), 2169-2184.
69. Samonis, G.; Maraki, S.; Karageorgopoulos, D. E.; Vouloumanou, E. K.; Falagas, M. E. Synergy of Fosfomicin with Carbapenems, Colistin, Netilmicin, and Tigecycline against Multidrug-resistant *Klebsiella pneumoniae*, *Escherichia coli*, and *Pseudomonas aeruginosa* Clinical Isolates. *Eur. J. Clin. Microbiol. Infect. Dis.* **2012**, *31*(5), 695-701.
70. Falagas, M. E.; Kanellopoulou, M. D.; Karageorgopoulos, D. E.; Dimopoulos, G.; Rafailidis, P. I.; Skarmoutsou, N. D.; Papafrangas, E. A. Antimicrobial Susceptibility of Multidrug-resistant Gram-negative Bacteria to Fosfomicin. *Eur. J. Clin. Microbiol. Infect. Dis.* **2008**, *27*(6), 439-443.
71. Falcone, M.; Menichetti, F.; Cattaneo, D.; Tiseo, G.; Baldelli, S.; Galfo, V.; Leonildi, A.; Tagliaferri, E.; Di Paolo, A.; Pai, M. P. Pragmatic Options for Dose Optimization of Ceftazidime/avibactam with Aztreonam in Complex Patients. *J. Antimicrob. Chemother.* **2021**, *76*(4), 1025-1031.
72. Jean, S. S.; Hsueh, S. C.; Lee, W. S.; Hsueh, P. R. Cefiderocol: A Promising Antibiotic against Multidrug-resistant Gram-negative Bacteria. *Expert Rev. Anti-Infect. Ther.* **2019**, *17*(5), 307-309.
73. Isler, B.; Harris, P.; Stewart, A. G.; Paterson, D. L. An Update on Cefepime and its Future Role in Combination with Novel β -Lactamase Inhibitors for MDR *Enterobacterales* and *Pseudomonas aeruginosa*. *J. Antimicrob. Chemother.* **2021**, *76*(3), 550-560.
74. Lohans, C. T.; van Groesen, E.; Kumar, K.; Tooke, C. L.; Spencer, J.; Paton, R. S.; Brem, J.; Schofield, C. J. A New Mechanism for β -Lactamases: Class D Enzymes Degrade 1 β -Methyl Carbapenems through Lactone Formation. *Angew. Chem. Int. Ed. Engl.* **2018**, *57*(5), 1282-1285.

75. Page, M. I.; Badarau, A. The Mechanisms of Catalysis by Metallo- β -lactamases. *Bioinorg. Chem. Appl.* **2008**, 576297.
76. Yong, D.; Toleman, M. A.; Giske, C. G.; Cho, H. S.; Sundman, K.; Lee, K.; Walsh, T. R. Characterization of a New Metallo- β -lactamase Gene, *bla*_{NDM-1}, and a Novel Erythromycin Esterase Gene Carried on a Unique Genetic Structure in *Klebsiella pneumoniae* Sequence Type 14 from India. *Antimicrob. Agents Chemother.* **2009**, 53(12), 5046-5054.
77. Melgarejo, J. L.; Cardoso, M. H.; Pinto, I. B.; Faria-Junior, C.; Mendo, S.; de Oliveira, C. E.; Franco, O. L. Identification, Molecular Characterization, and Structural Analysis of the *bla*_{NDM-1} Gene/enzyme from NDM-1-producing *Klebsiella pneumoniae* Isolates. *J. Antibiot. (Tokyo)* **2019**, 72(3), 155-163.
78. Abbas, F. M. Metallo- β -Lactamases: A Review. *Annals of R. S. C. B.* **2021**, 1308-1316.
79. Liang, Z.; Li, L.; Wang, Y.; Chen, L.; Kong, X.; Hong, Y.; Lan, L.; Zheng, M.; Guang-Yang, C.; Liu, H.; Shen, X.; Luo, C.; Li, K. K.; Chen, K.; Jiang, H. Molecular Basis of NDM-1, a New Antibiotic Resistance Determinant. *PLoS One* **2011**, 6(8), e23606.
80. Green, V. L.; Verma, A.; Owens, R. J.; Phillips, S. E.; Carr, S. B. Structure of New Delhi Metallo- β -lactamase 1 (NDM-1). *Acta Cryst.* **2011**, F67, 1160-1164.
81. Wei, W. J.; Yang, H. F.; Ye, Y.; Li, J. B. New Delhi Metallo- β -lactamase-mediated Carbapenem Resistance: Origin, Diagnosis, Treatment and Public Health Concern. *Chin. Med. J. (Engl)* **2015**, 128(14), 1969-1976.
82. Saini, A.; Bansal, R. Insights on the Structural Characteristics of NDM-1: The Journey so Far. *Advances in Biological Chemistry* **2012**, 2(4), 323-334.
83. Lohans, C. T.; Brem, J.; Schofield, C. J. New Delhi Metallo- β -lactamase 1 Catalyzes Avibactam and Aztreonam Hydrolysis. *Antimicrob. Agents Chemother.* **2017**, 61(12), e01224-17.
84. Kim, Y.; Tesar, C.; Mire, J.; Jedrzejczak, R.; Binkowski, A.; Babnigg, G.; Sacchetti, J.; Joachimiak, A. Structure of Apo- and Monometalated Forms of NDM-1—A Highly Potent Carbapenem-Hydrolyzing Metallo- β -Lactamase. *PLoS One* **2011**, 6(9), e24621.
85. Cheng, Z.; Thomas, P. W.; Ju, L.; Bergstrom, A.; Mason, K.; Clayton, D.; Miller, C.; Bethel, C. R.; VanPelt, J.; Tierney, D. L.; Page, R. C.; Bonomo, R. A.; Fast, W.; Crowder, M. W. Evolution of New Delhi Metallo- β -lactamase (NDM) in the Clinic: Effects of NDM Mutations on Stability, Zinc Affinity, and Mono-zinc Activity. *J. Biol. Chem.* **2018**, 293(32), 12606-12618.
86. Guo, Y.; Wang, J.; Niu, G.; Shui, W.; Sun, Y.; Zhou, H.; Zhang, Y.; Yang, C.; Lou, Z.; Rao, Z. A Structural View of the Antibiotic Degradation Enzyme NDM-1 from a Superbug. *Protein Cell* **2011**, 2(5), 384-394.
87. Gonzalez, L. J.; Bahr, G.; Nakashige, T. G.; Nolan, E. M.; Bonomo, R. A.; Vila, A. J. Membrane Anchoring Stabilizes and Favors Secretion of New Delhi Metallo- β -lactamase. *Nat. Chem. Biol.* **2016**, 12(7), 516-522.
88. Lopez, C.; Ayala, J. A.; Bonomo, R. A.; Gonzalez, L. J.; Vila, A. J. Protein Determinants of Dissemination and Host Specificity of Metallo- β -lactamases. *Nat. Commun.* **2019**, 10(1), 3617.
89. A, K.; Gupta, R.; R, S.; Vv, V.; S, G.; Goyal, P. New Delhi Metallo Beta Lactamase: Menace and its Challenges. *Journal of Molecular and Genetic Medicine* **2017**, 11(4).
90. Groundwater, P. W.; Xu, S.; Lai, F.; Váradi, L.; Tan, J.; Perry, J. D.; Hibbs, D. E. New Delhi Metallo- β -lactamase-1: Structure, Inhibitors and Detection of Producers. *Future Med. Chem.* **2016**, 8(9), 993-1012.

91. Thomas, P. W.; Zheng, M.; Wu, S.; Guo, H.; Liu, D.; Xu, D.; Fast, W. Characterization of Purified New Delhi Metallo- β -lactamase-1. *Biochemistry* **2011**, *50*(46), 10102-13.
92. Kim, Y.; Cunningham, M. A.; Mire, J.; Tesar, C.; Sacchettini, J.; Joachimiak, A. NDM-1, the Ultimate Promiscuous Enzyme: Substrate Recognition and Catalytic Mechanism. *FASEB J.* **2013**, *27*(5), 1917-1927.
93. Linciano, P.; Cendron, L.; Gianquinto, E.; Spyrakis, F.; Tondi, D. Ten Years with New Delhi Metallo- β -lactamase-1 (NDM-1): From Structural Insights to Inhibitor Design. *A. C. S. Infect. Dis.* **2019**, *5*(1), 9-34.
94. Sun, Z.; Hu, L.; Sankaran, B.; Prasad, B. V. V.; Palzkill, T. Differential Active Site Requirements for NDM-1 β -Lactamase Hydrolysis of Carbapenem Versus Penicillin and Cephalosporin Antibiotics. *Nat. Commun.* **2018**, *9*(1), 4524.
95. Feng, H.; Ding, J.; Zhu, D.; Liu, X.; Xu, X.; Zhang, Y.; Zang, S.; Wang, D. C.; Liu, W. Structural and Mechanistic Insights into NDM-1 Catalyzed Hydrolysis of Cephalosporins. *J. Am. Chem. Soc.* **2014**, *136*(42), 14694-14697.
96. Sharma, S.; Sharma, S.; Singh, P. P.; Khan, I. A. Potential Inhibitors Against NDM-1 Type Metallo- β -lactamases: An Overview. *Microb. Drug. Resist.* **2020**, *26*(12), 1568-1588.
97. Zheng, M.; Xu, D. New Delhi Metallo- β -lactamase I: Substrate Binding and Catalytic Mechanism. *J. Phys. Chem. B* **2013**, *117*(39), 11596-11607.
98. Li, X.; Zhao, D.; Li, W.; Sun, J.; Zhang, X. Enzyme Inhibitors: The Best Strategy to Tackle Superbug NDM-1 and Its Variants. *Int. J. Mol. Sci.* **2021**, *23*(1), 197.
99. Levina, E. O.; Khrenova, M. G. Metallo- β -Lactamases: Influence of the Active Site Structure on the Mechanisms of Antibiotic Resistance and Inhibition. *Biochem. (Mosc.)* **2021**, *86*(1), S24-S37.
100. Yang, H.; Aitha, M.; Marts, A. R.; Hetrick, A.; Bennett, B.; Crowder, M. W.; Tierney, D. L. Spectroscopic and Mechanistic Studies of Heterodimetallic Forms of Metallo- β -lactamase NDM-1. *J. Am. Chem. Soc.* **2014**, *136*(20), 7273-7285.
101. Feng, H.; Liu, X.; Wang, S.; Fleming, J.; Wang, D. C.; Liu, W. The Mechanism of NDM-1-catalyzed Carbapenem Hydrolysis is Distinct from that of Penicillin or Cephalosporin Hydrolysis. *Nat. Commun.* **2017**, *8*(1), 2242.
102. Xue, J.; Wang, P.; Kuang, J.; Zhu, Y. Computational Design of New Enzymes for Hydrolysis and Synthesis of Third-generation Cephalosporin Antibiotics. *Enzyme Microb. Technol.* **2020**, *140*, 109649.
103. Egorov, A. M.; Ulyashova, M. M.; Rubtsova, M. Y. Inhibitors of β -Lactamases. New Life of β -Lactam Antibiotics. *Biochem. (Mosc.)*, **2020**, *85*(11), 1292-1309.
104. Prunotto, A.; Bahr, G.; González, L. J.; Vila, A. J.; Peraro, M. D. Molecular Bases of the Membrane Association Mechanism Potentiating Antibiotic Resistance by New Delhi Metallo- β -lactamase 1. *A. C. S. Infect. Dis.* **2020**, *6*(10), 2719-2731.
105. Ali, A.; Gupta, D.; Khan, A. U. Role of Non-active Site Residues in Maintaining New Delhi Metallo- β -lactamase-1(NDM-1) Function: An Approach of Site Directed Mutagenesis and Docking. *FEMS Microbiol. Lett.* **2021**. *368*(4), fnz003.
106. King, D.; Strynadka, N. Crystal Structure of New Delhi Metallo- β -lactamase Reveals Molecular Basis for Antibiotic Resistance. *Protein Sci.* **2011**, *20*(9), 1484-1491.
107. Zhang, H.; Hao, Q. Crystal Structure of NDM-1 Reveals a Common β -Lactam Hydrolysis Mechanism. *FASEB J.* **2011**, *25*(8), 2574-2582.

108. Brem, J.; van Berkel, S. S.; Zollman, D.; Lee, S. Y.; Gileadi, O.; McHugh, P. J.; Walsh, T. R.; McDonough, M. A.; Schofield, C. J. Structural Basis of Metallo- β -lactamase Inhibition by Captopril Stereoisomers. *Antimicrob. Agents Chemother.* **2016**, *60*(1), 142-150.
109. King, D. T.; Worrall, L. J.; Gruninger, R.; Strynadka, N. C. New Delhi Metallo- β -lactamase: Structural Insights into β -Lactam Recognition and Inhibition. *J. Am. Chem. Soc.* **2012**, *134*(28), 11362-11365.
110. Rydzik, A. M.; Brem, J.; van Berkel, S. S.; Pfeffer, I.; Makena, A.; Claridge, T. D.; Schofield, C. J. Monitoring Conformational Changes in the NDM-1 Metallo- β -lactamase by ^{19}F NMR Spectroscopy. *Angew. Chem. Int. Ed. Engl.* **2014**, *53*(12), 3129-3133.
111. Fullington, S.; Cheng, Z.; Thomas, C.; Miller, C.; Yang, K.; Ju, L. C.; Bergstrom, A.; Shurina, B. A.; Bretz, S. L.; Page, R. C.; Tierney, D. L.; Crowder, M. W. An Integrated Biophysical Approach to Discovering Mechanisms of NDM-1 Inhibition for Several Thiol-containing Drugs. *J. Biol. Inorg. Chem.* **2020**, *25*(5), 717-727.
112. Brem, J.; van Berkel, S. S.; Aik, W.; Rydzik, A. M.; Avison, M. B.; Pettinati, I.; Umland, K. D.; Kawamura, A.; Spencer, J.; Claridge, T. D.; McDonough, M. A.; Schofield, C. J. Rhodanine Hydrolysis Leads to Potent Thioenolate Mediated Metallo- β -lactamase Inhibition. *Nat. Chem.* **2014**, *6*(12), 1084-1090.
113. Yusof, Y.; Tan, D. T. C.; Arjomandi, O. K.; Schenk, G.; McGeary, R. P. Captopril Analogues as Metallo- β -lactamase Inhibitors. *Bioorg. Med. Chem. Lett.* **2016**, *26*(6), 1589-1593.
114. Liu, S.; Jing, L.; Yu, Z. J.; Wu, C.; Zheng, Y.; Zhang, E.; Chen, Q.; Yu, Y.; Guo, L.; Wu, Y.; Li, G. B. ((S)-3-Mercapto-2-methylpropanamido)acetic Acid Derivatives as Metallo- β -lactamase Inhibitors: Synthesis, Kinetic and Crystallographic Studies. *Eur. J. Med. Chem.* **2018**, *145*, 649-660.
115. Duan, H.; Liu, X.; Zhuo, W.; Meng, J.; Gu, J.; Sun, X.; Zuo, K.; Luo, Q.; Luo, Y.; Tang, D.; Shi, H.; Cao, S.; Hu, J. 3D-QSAR and Molecular Recognition of *Klebsiella pneumoniae* NDM-1 Inhibitors. *Molecular Simulation* **2019**, *45*(9), 694-705.
116. Li, N.; Xu, Y.; Xia, Q.; Bai, C.; Wang, T.; Wang, L.; He, D.; Xie, N.; Li, L.; Wang, J.; Zhou, H.; Xu, F.; Yang, C.; Zhang, Q.; Yin, Z.; Guo, Y.; Chen, Y. Simplified Captopril Analogues as NDM-1 Inhibitors. *Bioorg. Med. Chem. Lett.* **2014**, *24*(1), 386-389.
117. Meng, Z.; Tang, M.; Yu, L.; Liang, Y.; Han, J.; Zhang, C.; Hu, F.; Yu, J. M.; Sun, X. Novel Mercapto Propionamide Derivatives with Potent New Delhi Metallo- β -lactamase-1 Inhibitory Activity and Low Toxicity. *A. C. S. Infect. Dis.* **2019**, *5*(6), 903-916.
118. Ma, G.; Wang, S.; Wu, K.; Zhang, W.; Ahmad, A.; Hao, Q.; Lei, X.; Zhang, H. Structure-guided Optimization of *D*-captopril for Discovery of Potent NDM-1 Inhibitors. *Bioorg. Med. Chem.* **2021**, *29*, 115902.
119. Buttner, D.; Kramer, J. S.; Klingler, F. M.; Wittmann, S. K.; Hartmann, M. R.; Kurz, C. G.; Kohnhauser, D.; Weizel, L.; Bruggerhoff, A.; Frank, D.; Steinhilber, D.; Wichelhaus, T. A.; Pogoryelov, D.; Proschak, E.; Challenges in the Development of a Thiol-Based Broad-Spectrum Inhibitor for Metallo- β -lactamases. *A. C. S. Infect. Dis.* **2018**, *4*(3), 360-372.

120. Klingler, F. M.; Wichelhaus, T. A.; Frank, D.; Cuesta-Bernal, J.; El-Delik, J.; Müller, H. F.; Sjuts, H.; Göttig, S.; Koenigs, A.; Pos, K. M.; Pogoryelov, D.; Proschak, E. Approved Drugs Containing Thiols as Inhibitors of Metallo- β -lactamases: Strategy to Combat Multidrug-Resistant Bacteria. *J. Med. Chem.* **2015**, *58*(8), 3626-3630.
121. Skagseth, S.; Akhter, S.; Paulsen, M. H.; Muhammad, Z.; Lauksund, S.; Samuelsen, O.; Leiros, H. S.; Bayer, A. Metallo- β -lactamase Inhibitors by Bioisosteric Replacement: Preparation, Activity and Binding. *Eur. J. Med. Chem.* **2017**, *135*, 159-173.
122. Gonzalez, M. M.; Kosmopoulou, M.; Mojica, M. F.; Castillo, V.; Hinchliffe, P.; Pettinati, I.; Brem, J.; Schofield, C. J.; Mahler, G.; Bonomo, R. A.; Llarrull, L. I.; Spencer, J.; Vila, A. J. Bisthiazolidines: A Substrate-Mimicking Scaffold as an Inhibitor of the NDM-1 Carbapenemase. *A. C. S. Infect. Dis.* **2015**, *1*(11), 544-554.
123. Rossi, M. A.; Martinez, V.; Hinchliffe, P.; Mojica, M. F.; Castillo, V.; Moreno, D. M.; Smith, R.; Spellberg, B.; Drusano, G. L.; Banchio, C.; Bonomo, R. A.; Spencer, J.; Vila, A. J.; Mahler, G. 2-Mercaptomethyl-thiazolidines Use Conserved Aromatic-S Interactions to Achieve Broad-range Inhibition of Metallo- β -lactamases. *Chem. Sci.* **2021**, *12*(8), 2898-2908.
124. Krajnc, A.; Brem, J.; Hinchliffe, P.; Calvopina, K.; Panduwawala, T. D.; Lang, P. A.; Kamps, J.; Tyrrell, J. M.; Widlake, E.; Saward, B. G.; Walsh, T. R.; Spencer, J.; Schofield, C. J. Bicyclic Boronate VNRX-5133 Inhibits Metallo- and Serine- β -lactamases. *J. Med. Chem.* **2019**, *62*(18), 8544-8556.
125. Brem, J.; Cain, R.; Cahill, S.; McDonough, M. A.; Clifton, I. J.; Jimenez-Castellanos, J. C.; Avison, M. B.; Spencer, J.; Fishwick, C. W.; Schofield, C. J. Structural Basis of Metallo- β -lactamase, Serine- β -lactamase and Penicillin-binding Protein Inhibition by Cyclic Boronates. *Nat. Commun.* **2016**, *7*, 12406.
126. Tsivkovski, R.; Totrov, M.; Lomovskaya, O. Biochemical Characterization of QPX7728, a New Ultrabroad-Spectrum β -Lactamase Inhibitor of Serine and Metallo- β -lactamases. *Antimicrob. Agents Chemother.* **2020**, *64*(6), e00130-20.
127. King, A. M.; Reid-Yu, S. A.; Wang, W.; King, D. T.; De Pascale, G.; Strynadka, N. C.; Walsh, T. R.; Coombes, B. K.; Wright, G. D. Aspergillomarasmine A Overcomes Metallo- β -lactamase Antibiotic Resistance. *Nature*, **2014**, *510*(7506), 503-506.
128. Albu, S. A.; Koteva, K.; King, A. M.; Al-Karmi, S.; Wright, G. D.; Capretta, A. Total Synthesis of Aspergillomarasmine A and Related Compounds: A Sulfamidate Approach Enables Exploration of Structure-Activity Relationships. *Angew. Chem. Int. Ed. Engl.* **2016**, *55*(42), 13259-13262.
129. Bergstrom, A.; Katko, A.; Adkins, Z.; Hill, J.; Cheng, Z.; Burnett, M.; Yang, H.; Aitha, M.; Mehaffey, M. R.; Brodbelt, J. S.; Tehrani, K. H. M. E.; Martin, N. I.; Bonomo, R. A.; Page, R. C.; Tierney, D. L.; Fast, W.; Wright, G. D.; Crowder, M. W. Probing the Interaction of Aspergillomarasmine A with Metallo- β -lactamases NDM-1, VIM-2, and IMP-7. *A. C. S. Infect. Dis.* **2018**, *4*(2), 135-145.
130. Zhang, J.; Wang, S.; Wei, Q.; Guo, Q.; Bai, Y.; Yang, S.; Song, F.; Zhang, L.; Lei, X. Synthesis and Biological Evaluation of Aspergillomarasmine a Derivatives as Novel NDM-1 Inhibitor to Overcome Antibiotics Resistance. *Bioorg. Med. Chem.* **2017**, *25*(19), 5133-5141.

131. Tehrani, K. H. M. E.; Fu, H.; Bruchle, N. C.; Mashayekhi, V.; Prats Lujan, A.; van Haren, M. J.; Poelarends, G. J.; Martin, N. I., Aminocarboxylic Acids Related to Aspergillomarasmine A (AMA) and Ethylenediamine-*N,N'*-disuccinic Acid (EDDS) are Strong Zinc-binders and Inhibitors of the Metallo- β -lactamase NDM-1. *Chem. Commun.* **2020**, 56(20), 3047-3049.
132. Chen, A. Y.; Thomas, C. A.; Thomas, P. W.; Yang, K.; Cheng, Z.; Fast, W.; Crowder, M. W.; Cohen, S. M. Iminodiacetic Acid as a Novel Metal-Binding Pharmacophore for New Delhi Metallo- β -lactamase Inhibitor Development. *Chem. Med. Chem.* **2020**, 15(14), 1272-1282.
133. Chen, A. Y.; Thomas, P. W.; Stewart, A. C.; Bergstrom, A.; Cheng, Z.; Miller, C.; Bethel, C. R.; Marshall, S. H.; Credille, C. V.; Riley, C. L.; Page, R. C.; Bonomo, R. A.; Crowder, M. W.; Tierney, D. L.; Fast, W.; Cohen, S. M. Dipicolinic Acid Derivatives as Inhibitors of New Delhi Metallo- β -lactamase-1. *J. Med. Chem.* **2017**, 60(17), 7267-7283.
134. Falconer, S. B.; Reid-Yu, S. A.; King, A. M.; Gehrke, S. S.; Wang, W.; Britten, J. F.; Coombes, B. K.; Wright, G. D.; Brown, E. D. Zinc Chelation by a Small-Molecule Adjuvant Potentiates Meropenem Activity *in Vivo* against NDM-1-Producing *Klebsiella Pneumoniae*. *A. C. S. Infect. Dis.* **2015**, 1(11), 533-543.
135. Zhai, L.; Zhang, Y. L.; Kang, J. S.; Oelschlaeger, P.; Xiao, L.; Nie, S. S.; Yang, K. W. Triazolylthioacetamide: A Valid Scaffold for the Development of New Delhi Metallo- β -lactmase-1 (NDM-1) Inhibitors. *A. C. S. Med. Chem. Lett.* **2016**, 7(4), 413-417.
136. Song, G. Q., Wang, W. M., Li, Z. S., Wang, Y., Wang, J. G. First Identification of Isatin- β -thiosemicarbazones as Novel Inhibitors of New Delhi Metallo- β -lactamase-1: Chemical Synthesis, Biological Evaluation and Molecular Simulation, *Chin. Chem. Lett.* **2018**, 29(6), 899-902.
137. Ning, N. Z.; Liu, X.; Chen, F.; Zhou, P.; Hu, L.; Huang, J.; Li, Z.; Huang, J.; Li, T.; Wang, H. Embelin Restores Carbapenem Efficacy against NDM-1-Positive Pathogens. *Front. Microbiol.* **2018**, 9, 71.
138. Liu, S.; Zhou, Y.; Niu, X.; Wang, T.; Li, J.; Liu, Z.; Wang, J.; Tang, S.; Wang, Y.; Deng, X. Magnolol Restores the Activity of Meropenem against NDM-1-producing *Escherichia coli* by Inhibiting the Activity of Metallo- β -lactamase. *Cell Death Discov.* **2018**, 4, 28.
139. Shi, C.; Chen, J.; Xiao, B.; Kang, X.; Lao, X.; Zheng, H. Discovery of NDM-1 Inhibitors from Natural Products. *J. Glob. Antimicrob. Resist.* **2019**, 18, 80-87.
140. Ge, Y.; Xu, L. W.; Liu, Y.; Sun, L. Y.; Gao, H.; Li, J. Q.; Yang, K. Dithiocarbamate as a Valuable Scaffold for the Inhibition of Metallo- β -lactmases. *Biomolecules*, **2019**, 9(11), 699.
141. Farley, A. J. M.; Ermolovich, Y.; Calvopina, K.; Rabe, P.; Panduwawala, T.; Brem, J.; Bjorkling, F.; Schofield, C. J. Structural Basis of Metallo- β -lactamase Inhibition by N-Sulfamoylpyrrole-2-carboxylates. *A. C. S. Infect. Dis.* **2021**, 7(6), 1809-1817.
142. Jackson, A. C.; Pinter, T. B. J.; Talley, D. C.; Baker-Agha, A.; Patel, D.; Smith, P. J.; Franz, K. J. Benzimidazole and Benzoxazole Zinc Chelators as Inhibitors of Metallo- β -lactamase NDM-1. *Chem. Med. Chem.* **2021**, 16(4), 654-661.
143. Zervosen, A.; Lu, W. P.; Chen, Z.; White, R. E.; Demuth, T. P., Jr.; Frere, J. M. Interactions between Penicillin-binding Proteins (PBPs) and Two Novel Classes of PBP Inhibitors, Arylalkylidene

- Rhodanines and Arylalkylidene Iminothiazolidin-4-ones. *Antimicrob. Agents. Chemother.* **2004**, 48(3), 961-969.
144. Grant, E. B.; Guiadeen, D.; Baum, E. Z.; Foleno, B. D.; Jin, H.; Montenegro, D. A.; Nelson, E. A.; Bush, K.; Hlasta, D. J. The Synthesis and SAR of Rhodanines as Novel Class C β -Lactamase Inhibitors. *Bioorg. Med. Chem. Lett.* **2000**, 10, 2179–2182.
145. Spicer, T.; Minond, D.; Enogieru, I.; Saldanha, S. A.; Mercer, B. A.; Allais, C.; Liu, Q.; Roush, W. R. ML302: A Novel Beta-lactamase (BLA) Inhibitor. *In Probe Reports from the NIH Molecular Libraries Program*; NCBI, **2012**.
146. Xiang, Y.; Chen, C.; Wang, W. M.; Xu, L. W.; Yang, K. W.; Oelschlaeger, P.; He, Y. Rhodanine as a Potent Scaffold for the Development of Broad-Spectrum Metallo- β -lactamase Inhibitors. *A. C. S. Med. Chem. Lett.* **2018**, 9(4), 359-364.
147. Chiou, J.; Wan, S.; Chan, K. F.; So, P. K.; He, D.; Chan, E. W.; Chan, T. H.; Wong, K. Y.; Tao, J.; Chen, S. Ebselen as a Potent Covalent Inhibitor of New Delhi Metallo- β -lactamase (NDM-1). *Chem. Commun.* **2015**, 51(46), 9543-9546.
148. Jin, W. B.; Xu, C.; Cheng, Q.; Qi, X. L.; Gao, W.; Zheng, Z.; Chan, E. W. C.; Leung, Y. C.; Chan, T. H.; Wong, K. Y.; Chen, S.; Chan, K. F. Investigation of Synergistic Antimicrobial Effects of the Drug Combinations of Meropenem and 1,2-Benzisoxenazol-3(2H)-one Derivatives on Carbapenem-resistant Enterobacteriaceae Producing NDM-1. *Eur. J. Med. Chem.* **2018**, 155, 285-302.
149. Su, J.; Liu, J.; Chen, C.; Zhang, Y.; Yang, K. Ebsulfur as a Potent Scaffold for Inhibition and Labelling of New Delhi Metallo- β -lactamase-1 *in Vitro* and *in Vivo*. *Bioorg. Chem.* **2019**, 84, 192-201.
150. Chen, C.; Liu, Y.; Zhang, Y. J.; Ge, Y.; Lei, J. E. Yang, K. W. The Assemblage of Covalent and Metal Binding Dual Functional Scaffold for Cross-class Metallo- β -lactamases Inhibition. *Future Med. Chem.* **2019**, 11(18), 2381–2394.
151. Kang, P. W.; Su, J. P.; Sun, L. Y.; Gao, H.; Yang, K. W. 3-Bromopyruvate as a Potent Covalently Reversible Inhibitor of New Delhi Metallo- β -lactamase-1 (NDM-1). *Eur. J. Pharm. Sci.* **2020**, 142, 105161.
152. Chen, C.; Yang, K. W.; Wu, L. Y.; Li, J. Q.; Sun, L. Y. Disulfiram as a Potent Metallo- β -lactamase Inhibitor with Dual Functional Mechanisms. *Chem. Commun.* **2020**, 56(18), 2755-2758.
153. Thomas, P. W.; Cammarata, M.; Brodbelt, J. S.; Monzingo, A. F.; Pratt, R. F.; Fast, W. A Lysine-targeted Affinity Label for Serine- β -lactamase Also Covalently Modifies New Delhi Metallo- β -lactamase-1 (NDM-1). *Biochemistry*, **2019**, 58(25), 2834-2843.
154. Christopheit, T.; Albert, A.; Leiros, H. S. Discovery of a Novel Covalent Non- β -lactam Inhibitor of the Metallo- β -lactamase NDM-1. *Bioorg. Med. Chem.* **2016**, 24(13), 2947-2953.
155. Thomas, P. W.; Cammarata, M.; Brodbelt, J. S.; Fast, W. Covalent Inhibition of New Delhi Metallo- β -lactamase-1 (NDM-1) by Cefaclor. *Chembiochem.* **2014**, 15(17), 2541-2548.

156. Wang, R.; Lai, T. P.; Gao, P.; Zhang, H.; Ho, P. L.; Woo, P. C.; Ma, G.; Kao, R. Y.; Li, H.; Sun, H. Bismuth Antimicrobial Drugs Serve as Broad-spectrum Metallo- β -lactamase Inhibitors. *Nat. Commun.* **2018**, *9*(1), 439.
157. Chen, C.; Sun, L. Y.; Gao, H.; Kang, P. W.; Li, J. Q.; Zhen, J. B.; Yang, K. W. Identification of Cisplatin and Palladium(II) Complexes as Potent Metallo- β -lactamase Inhibitors for Targeting Carbapenem-Resistant Enterobacteriaceae. *A. C. S. Infect. Dis.* **2020**, *6*(5), 975-985.
158. Thomas, P. W.; Spicer, T.; Cammarata, M.; Brodbelt, J. S.; Hodder, P.; Fast, W. An Altered Zinc-Binding Site Confers Resistance to a Covalent Inactivator of New Delhi Metallo- β -lactamase-1 (NDM-1) Discovered by High-throughput Screening. *Bioorg. Med. Chem.* **2013**, *21*(11), 3138-3146.
159. Khan, A. U.; Ali, A.; Danishuddin; Srivastava, G.; Sharma, A. Potential Inhibitors Designed Against NDM-1 Type Metallo- β -lactamases: An Attempt to Enhance Efficacies of Antibiotics Against Multi-drug-resistant Bacteria. *Sci. Rep.* **2017**, *7*(1), 9207.
160. Christopeit, T.; Leiros, H. K. Fragment-based Discovery of Inhibitor Scaffolds Targeting the Metallo- β -lactamases NDM-1 and VIM-2. *Bioorg. Med. Chem. Lett.* **2016**, *26*(8), 1973-1977.
161. Murray, C. W.; Rees, D. C. Opportunity Knocks: Organic Chemistry for Fragment-Based Drug Discovery (FBDD). *Angew. Chem. Int. Ed. Engl.* **2016**, *55*(2), 488-492.
162. Murray, C. W.; Rees, D. C. The Rise of Fragment-based Drug Discovery. *Nat. Chem.* **2009**, *1*(3), 187-192.
163. Erlanson, D. A.; McDowell, R. S.; O'Brien, T. Fragment-based Drug Discovery. *J. Med. Chem.* **2004**, *47*(14), 3463-3482.
164. Macalino, S. J.; Gosu, V.; Hong, S.; Choi, S. Role of Computer-aided Drug Design in Modern Drug Discovery. *Arch. Pharm. Res.* **2015**, *38*(9), 1686-1701.
165. Hassan Baig, M.; Ahmad, K.; Roy, S.; Mohammad Ashraf, J.; Adil, M.; Haris Siddiqui, M.; Khan, S.; Amjad Kamal, M.; Provazník, I.; Choi, I. Computer Aided Drug Design: Success and Limitations. *Curr. Pharm. Des.* **2016**, *22*(5), 572-581.
166. Viswanatha, T.; Marrone, L.; Goodfellow, V.; Dmitrienko, G. I. Assays for β -Lactamase Activity and Inhibition, In *New Antibiotic Targets*, Humana Press, **2008**, 239-260.
167. O'Callaghan, C. H.; Morris, A.; Kirby, S. M.; Shingler, A. H. Novel Method for Detection of β -Lactamases by Using a Chromogenic Cephalosporin Substrate. *Antimicrob. Agents Chemother.* **1972**, *1*(4), 283-288.
168. Ghavami, A.; Labbe, G.; Brem, J.; Goodfellow, V. J.; Marrone, L.; Tanner, C. A.; King, D. T.; Lam, M.; Strynadka, N. C.; Pillai, D. R.; Siemann, S.; Spencer, J.; Schofield, C. J.; Dmitrienko, G. I. Assay for Drug Discovery: Synthesis and Testing of Nitrocefins Analogues for Use as β -Lactamase Substrates. *Anal. Biochem.* **2015**, *486*, 75-77.
169. van Berkel, S. S.; Brem, J.; Rydzik, A. M.; Salimraj, R.; Cain, R.; Verma, A.; Owens, R. J.; Fishwick, C. W.; Spencer, J.; Schofield, C. J. Assay Platform for Clinically Relevant Metallo- β -lactamases. *J. Med. Chem.* **2013**, *56*(17), 6945-6953.

170. He, Y.; Zhou, S.; Sun, W.; Li, Q.; Wang, J.; Zhang, J. Emerione A, a Novel Fungal Metabolite as an Inhibitor of New Delhi Metallo- β -lactamase 1, Restores Carbapenem Susceptibility in Carbapenem-resistant Isolates. *J. Glob. Antimicrob. Resist.* **2022**, *28*, 216-222.
171. Makena, A.; Brem, J.; Pfeffer, I.; Geffen, R. E.; Wilkins, S. E.; Tarhonskaya, H.; Flashman, E.; Phee, L. M.; Wareham, D. W.; Schofield, C. J. Biochemical Characterization of New Delhi Metallo- β -lactamase Variants Reveals Differences in Protein Stability. *J. Antimicrob. Chemother.* **2015**, *70*(2), 463-469.
172. Shen, B.; Yu, Y.; Chen, H.; Cao, X.; Lao, X.; Fang, Y.; Shi, Y.; Chen, J.; Zheng, H. Inhibitor Discovery of Full-length New Delhi Metallo- β -lactamase-1 (NDM-1). *PLoS One* **2013**, *8*(5), e62955.
173. Li, G. B.; Brem, J.; Lesniak, R.; Abboud, M. I.; Lohans, C. T.; Clifton, I. J.; Yang, S. Y.; Jimenez-Castellanos, J. C.; Avison, M. B.; Spencer, J.; McDonough, M. A.; Schofield, C. J. Crystallographic Analyses of Isoquinoline Complexes Reveal a New Mode of Metallo- β -lactamase Inhibition. *Chem. Commun.* **2017**, *53*(43), 5806-5809.
174. Wang, Q.; He, Y.; Lu, R.; Wang, W. M.; Yang, K. W.; Fan, H. M.; Jin, Y.; Blackburn, G. M. Thermokinetic Profile of NDM-1 and its Inhibition by Small Carboxylic Acids. *Biosci. Rep.* **2018**, *38*(2).
175. Kimura, S.; Ishii, Y.; Yamaguchi, K. Evaluation of Dipicolinic Acid for Detection of IMP- or VIM-type Metallo- β -lactamase-producing *Pseudomonas aeruginosa* Clinical Isolates. *Diagn. Microbiol. Infect. Dis.* **2005**, *53*(3), 241-244.
176. Liu, Y.; Lotero, E.; Goodwin, J. G. Effect of Water on Sulfuric Acid Catalyzed Esterification. *J. Mol. Catal. Chem.* **2006**, *245*(1-2), 132-140.
177. Matsugi, M.; Tabusa, F.; Minamikawa, J. I. Doebner–Miller Synthesis in a Two-phase System: Practical Preparation of Quinolines. *Tetrahedron Lett.* **2000**, *41*(44), 8523-8525.
178. Polanski, J.; Zouhiri, F.; Jeanson, L.; Desmaële, D.; d'Angelo, J.; Mouscadet, J. F.; Gieleciak, R.; Gasteiger, J.; Le Bret, M. Use of the Kohonen Neural Network for Rapid Screening of Ex Vivo Anti-HIV Activity of Styrylquinolines. *J. Med. Chem.* **2002**, *45*(21), 4647-4654.
179. Ramann, G. A.; Cowen, B. J. Recent Advances in Metal-free Quinoline Synthesis. *Molecules*, **2016**, *21*(8), 986.
180. Kumari, L.; Salahuddin; Mazumder, A.; Pandey, D.; Yar, M. S.; Kumar, R.; Mazumder, R.; Sarafroz, M.; Ahsan, M. J.; Kumar, V.; Gupta, S. Synthesis and Biological Potentials of Quinoline Analogues: A Review of Literature. *Mini. Rev. Org. Chem.* **2019**, *16*(7), 653-688.
181. Weyesa, A.; Mulugeta, E. Recent Advances in the Synthesis of Biologically and Pharmaceutically Active Quinoline and Its Analogues: A Review. *R. S. C. Adv.* **2020**, *10*(35), 20784-20793.
182. Szala, M.; Nycz, J. E.; Malecki, G. J. New Approaches to the Synthesis of Selected Hydroxyquinolines and Their Hydroxyquinoline Carboxylic Acid Analogues. *J. Mol. Struct.* **2014**, *1071*, 34-40.
183. Chang, P. T.; Kung, F. L.; Talekar, R. S.; Chen, C. S.; Lai, S. Y.; Lee, H. Y.; Chern, J. W. An Improved Screening Model to Identify Inhibitors Targeting Zinc-enhanced Amyloid Aggregation. *Anal. Chem.* **2009**, *81*(16), 6944-6951.

184. Nycz, J. E.; Malecki, G. J. Synthesis, Spectroscopy and Computational Studies of Selected Hydroxyquinoline Carboxylic Acids and Their Selected Fluoro-, Thio-, and Dithioanalogues. *J. Mol. Struct.* **2013**, *1032*, 159-168.
185. Deraeve, C.; Boldron, C.; Maraval, A.; Mazarguil, H.; Gornitzka, H.; Vendier, L.; Pitie, M.; Meunier, B. Preparation and Study of New Poly-8-hydroxyquinoline Chelators for an Anti-Alzheimer Strategy. *Chem. Eur. J.* **2008**, *14*(2), 682-696.
186. Nuti, E.; Cuffaro, D.; Bernardini, E.; Camodeca, C.; Panelli, L.; Chaves, S.; Ciccone, L.; Tepshi, L.; Vera, L.; Orlandini, E.; Nencetti, S.; Stura, E. A.; Santos, M. A.; Dive, V.; Rossello, A. Development of Thioaryl-Based Matrix Metalloproteinase-12 Inhibitors with Alternative Zinc-Binding Groups: Synthesis, Potentiometric, NMR, and Crystallographic Studies. *J. Med. Chem.* **2018**, *61*(10), 4421-4435.
187. Vu, C. B.; Disch, J. S.; Springer, S. K.; Blum, C. A.; Perni, R. B. GlaxoSmithKline LLC, *Quinolines and Related Analogs as Sirtuin Modulators*. U.S. Patent 8685970, **2014**.
188. Di Fiore, A.; Maresca, A.; Supuran, C. T.; De Simone, G. Hydroxamate Represents a Versatile Zinc Binding Group for the Development of New Carbonic Anhydrase Inhibitors. *Chem. Commun.* **2012**, *48*(70), 8838-8840.
189. Porter, N. J.; Osko, J. D.; Diedrich, D.; Kurz, T.; Hooker, J. M.; Hansen, F. K.; Christianson, D. W. Histone Deacetylase 6-Selective Inhibitors and the Influence of Capping Groups on Hydroxamate-Zinc Denticity. *J. Med. Chem.* **2018**, *61*(17), 8054-8060.
190. Rowsell, S.; Hawtin, P.; Minshull, C. A.; Jepson, H.; Brockbank, S. M. V.; Barratt, D. G.; Slater, A. M.; McPheat, W. L.; Waterson, D.; Henney, A. M.; Pauptit, R. A. Crystal Structure of Human MMP9 in Complex with a Reverse Hydroxamate Inhibitor. *J. Mol. Biol.* **2002**, *319*(1), 173-181.
191. Adiguzel, E.; Yilmaz, F.; Emirik, M.; Ozil, M. Synthesis and Characterization of Two New Hydroxamic Acids Derivatives and Their Metal Complexes. An Investigation on the Keto/enol, E/Z and Hydroxamate/hydroximate Forms. *J. Mol. Struct.* **2017**, *1127*, 403-412.
192. Marmion, C. J.; Griffith, D.; Nolan, K. B. Hydroxamic Acids– An Intriguing Family of Enzyme Inhibitors and Biomedical Ligands. *Eur. J. Inorg. Chem.* **2004**, *2004*(15), 3003-3016.
193. Kurosaki, H.; Sharma, R. K.; Aoki, S.; Inoue, T.; Okamoto, Y.; Sugiura, Y.; Doi, M.; Ishida, T.; Otsuka, M.; Goto, M. Synthesis, Characterization, and Spectroscopic Properties of Three Novel Pentadentate Copper(II) Complexes Related to the Metal-chelating Inhibitors against DNA Binding with HIV-EP1. *J. Chem. Soc., Dalton Trans.* **2001**, *4*, 441-447.
194. Vieira De Almeida, M.; Vinicius de Nora Souza, M.; Rezende Barbosa, N.; Pittella Silva, F.; Wilson Amarante, G.; Helena Cardoso, S. Synthesis and Antimicrobial Activity of Pyridine Derivatives Substituted at C-2 and C-6 Positions. *Lett. Drug Des. Discov.* **2007**, *4*, 149-153.
195. Huang, Z.; Zhang, M.; Burton, S. D.; Katsakhyan, L. N.; Ji, H. Targeting the Tcf4 G¹³ANDE¹⁷ Binding Site to Selectively Disrupt β -catenin/T-cell Factor Protein-protein Interactions. *A. C. S. Chem. Biol.* **2014**, *9*(1), 193-201.

196. Mannino, C.; Nievo, M.; Machetti, F.; Papakyriakou, A.; Calderone, V.; Fragai, M.; Guarna, A. Synthesis of Bicyclic Molecular Scaffolds (BTAa): An Investigation Towards New Selective MMP-12 Inhibitors. *Bioorg. Med. Chem.* **2006**, *14*(22), 7392-7403.
197. Abouelhassan, Y.; Garrison, A. T.; Burch, G. M.; Wong, W.; Norwood IV, V. M.; Huigens III, R. W. Discovery of Quinoline Small Molecules with Potent Dispersal Activity against Methicillin-resistant *Staphylococcus aureus* and *Staphylococcus epidermidis* Biofilms Using a Scaffold Hopping Strategy. *Bioorg. Med. Chem. Lett.* **2014**, *24*(21), 5076-5080.
198. Basak, A.; Abouelhassan, Y.; Norwood IV, V. M.; Bai, F.; Nguyen, M. T.; Jin, S.; Huigens III, R. W. Synthetically Tuning the 2-Position of Halogenated Quinolines: Optimizing Antibacterial and Biofilm Eradication Activities via Alkylation and Reductive Amination Pathways. *Chem. Eur. J.* **2016**, *22*(27), 9181-9189.
199. Talekar, R. S.; Chen, G. S.; Lai, S. Y.; Chern, J. W. Nonreductive Deiodination of *ortho*-Iodo-Hydroxylated Arenes Using Tertiary Amines. *J. Org. Chem.* **2005**, *70*(21), 8590-8593.
200. Sakee, U.; Grigg, R. First Synthesis of 5-Chloro-7-[1,3]oxazolo[4,5-b]pyridin-2-ylquinolin-8-ol by Pd-Catalyzed Arylation. *Synth. Commun.* **2009**, *39*(17), 3031-3037.
201. Guillou, S.; Janin, Y. L. Optimized Palladium-based Approaches to Analogues of PK 11195. *J. Heterocycl. Chem.* **2008**, *45*(5), 1377-1384.
202. Radchatawedchakoon, W.; Promthong, N.; Sakee, U. First Synthesis of 5-and 7-Phenylethynyl-8-hydroxyquinolines by Sonogashira Reaction. *Lett. Org. Chem.* **2013**, *10*(9), 640-644.
203. Chen, A. Y.; Thomas, P. W.; Cheng, Z.; Xu, N. Y.; Tierney, D. L.; Crowder, M. W.; Fast, W.; Cohen, S. M. Investigation of Dipicolinic Acid Isosteres for the Inhibition of Metallo- β -lactamases. *ChemMedChem* **2019**, *14*(13), 1271-1282.
204. Hinchliffe, P.; Tanner, C. A.; Krismanich, A. P.; Labbe, G.; Goodfellow, V. J.; Marrone, L.; Desoky, A. Y.; Calvopina, K.; Whittle, E. E.; Zeng, F.; Avison, M. B.; Bols, N. C.; Siemann, S.; Spencer, J.; Dmitrienko, G. I. Structural and Kinetic Studies of the Potent Inhibition of Metallo- β -lactamases by 6-Phosphonomethylpyridine-2-carboxylates. *Biochemistry* **2018**, *57*(12), 1880-1892.
205. Clasby, M. C.; Chackalamannil, S.; Czarniecki, M.; Doller, D.; Eagen, K.; Greenlee, W. J.; Lin, Y.; Tsai, H.; Xia, Y.; Ahn, H. S.; Agans-Fantuzzi, J.; Boykow, G.; Chintala, M.; Foster, C.; Bryant, M.; Lau, J. Discovery and Synthesis of a Novel Series of Quinoline-based Thrombin Receptor (PAR-1) Antagonists. *Bioorg. Med. Chem. Lett.* **2006**, *16*(6), 1544-1548.
206. Desmaele, D.; Sliman, F. Synthesis of 5-Aryl- and 5-Heteroaryl-7-carboxyl-8-hydroxyquinolines through Suzuki Cross-Coupling Reaction with Potassium Organotrifluoroborates. *Synthesis* **2010**, *2010*(04), 619-630.
207. Musiol, R.; Jampilek, J.; Kralova, K.; Richardson, D. R.; Kalinowski, D.; Podeszwa, B.; Finster, J.; Niedbala, H.; Palka, A.; Polanski, J. Investigating Biological Activity Spectrum for Novel Quinoline Analogues. *Bioorg. Med. Chem.* **2007**, *15*(3), 1280-1288.
208. Karpińska, G.; Mazurek, A. P.; Dobrowolski, J. C. On Tautomerism and Substituent Effect in 8-Hydroxyquinoline-derived Medicine Molecules. *J. Mol. Struct.* **2010**, *961*(1-3), 101-106.

209. Venning, A. R.; Bohan, P. T.; Alexanian, E. J. Palladium-catalyzed, Ring-forming Aromatic C-H Alkylations with Unactivated Alkyl Halides. *J. Am. Chem. Soc.* **2015**, *137*(11), 3731-3734.
210. Nakamura, H.; Yoshida, T.; Todoko, M.; Ueno, K.; Takagi, M. Syntheses and Chelating Properties of Sulfonamidoquinolines. *Bull. Chem. Soc. Jpn.* **1984**, *57*(10), 2839-2846.
211. Peet, N. P.; Baugh, L. E.; Sunder, S.; Lewis, J. E. Synthesis and Antiallergic Activity of Some Quinolinones and Imidazoquinolinones. *J. Med. Chem.* **1985**, *28*(3), 298-302.
212. Qi, T.; Deschrijver, T.; Huc, I. Large-scale and Chromatography-free Synthesis of an Octameric Quinoline-based Aromatic Amide Helical Foldamer. *Nat. Protoc.* **2013**, *8*(4), 693-708.
213. Ong, C. W.; Liu, M.-C.; Lee, K.-D.; Chang, K. W.; Yang, Y.-T.; Tung, H.-W.; Fox, K. R. Synthesis of Bisquinoline-pyrrole Oligoamide as G-quadruplex Binding Ligand. *Tetrahedron* **2012**, *68*(27-28), 5453-5457.
214. Eswaran, S.; Adhikari, A. V.; Chowdhury, I. H.; Pal, N. K.; Thomas, K. D. New Quinoline Derivatives: Synthesis and Investigation of Antibacterial and Antituberculosis Properties. *Eur. J. Med. Chem.* **2010**, *45*(8), 3374-3383.
215. Deora, G. S.; Kantham, S.; Chan, S.; Dighe, S. N.; Veliyath, S. K.; McColl, G.; Parat, M. O.; McGeary, R. P.; Ross, B. P. Multifunctional Analogs of Kynurenic Acid for the Treatment of Alzheimer's Disease: Synthesis, Pharmacology, and Molecular Modeling Studies. *A. C. S. Chem. Neurosci.* **2017**, *8*(12), 2667-2675.
216. Zhang, W.; Huang, D.; Huang, M.; Huang, J.; Wang, D.; Liu, X.; Nguyen, M.; Vendier, L.; Mazeres, S.; Robert, A.; Liu, Y.; Meunier, B. Preparation of Tetradentate Copper Chelators as Potential Anti-Alzheimer Agents. *ChemMedChem* **2018**, *13*(7), 684-704.
217. Ashoka Sahadevan, S.; Cadoni, E.; Monni, N.; Saenz de Pipaon, C.; Galan Mascaros, J.-R.; Abhervé, A.; Avarvari, N.; Marchio, L.; Arca, M.; Mercuri, M. L. Structural Diversity in a New Series of Halogenated Quinolyl Salicylaldimides-Based Fe^{III} Complexes Showing Solid-State Halogen-Bonding/Halogen...Halogen Interactions. *Cryst. Growth Des.* **2018**, *18*(7), 4187-4199.
218. Koh, E. J.; El-Gamal, M. I.; Oh, C. H.; Lee, S. H.; Sim, T.; Kim, G.; Choi, H. S.; Hong, J. H.; Lee, S. G.; Yoo, K. H. New Diarylamides and Diarylureas Possessing 8-Amino(acetamido)quinoline Scaffold: Synthesis, Antiproliferative Activities against Melanoma Cell Lines, Kinase Inhibition, and in Silico Studies. *Eur. J. Med. Chem.* **2013**, *70*, 10-21.
219. Juchum, M.; Gunther, M.; Doring, E.; Sievers-Engler, A.; Lammerhofer, M.; Laufer, S. Trisubstituted Imidazoles with a Rigidized Hinge Binding Motif Act as Single Digit nM Inhibitors of Clinically Relevant EGFR L858R/T790M and L858R/T790M/C797S Mutants: An Example of Target Hopping. *J. Med. Chem.* **2017**, *60*(11), 4636-4656.
220. Moreno, S. N.; Docampo, R. Mechanism of Toxicity of Nitro Compounds Used in the Chemotherapy of Trichomoniasis. *Environ. Health Perspect.* **1985**, *64*, 199-208.
221. Concepcion, J.; Witte, K.; Wartchow, C.; Choo, S.; Yao, D.; Persson, H.; Wei, J.; Li, P.; Heidecker, B.; Ma, W.; Varma, R. Label-free Detection of Biomolecular Interactions Using BioLayer Interferometry for Kinetic Characterization. *Comb. Chem. High Throughput Screen.* **2009**, *12*(8), 791-800.

222. Han, B.; Zhang, M.; Sun, P.; Hou, S. Capturing the Interaction Kinetics of an Ion Channel Protein with Small Molecules by the Bio-layer Interferometry Assay. *J. Vis. Exp.* **2018**, (133), e56846.
223. Christopeit, T.; Carlsen, T. J.; Helland, R.; Leiros, H. K. Discovery of Novel Inhibitor Scaffolds against the Metallo- β -lactamase VIM-2 by Surface Plasmon Resonance (SPR) Based Fragment Screening. *J. Med. Chem.* **2015**, *58*(21), 8671-82.
224. Freyer, M. W.; Lewis, E. A. Isothermal Titration Calorimetry: Experimental Design, Data Analysis, and Probing Macromolecule/Ligand Binding and Kinetic Interactions. *Methods Cell Biol.* **2008**, *84*, 79-113.
225. Holdgate, G. A.; Ward, W. H. J. Measurements of Binding Thermodynamics in Drug Discovery. *Drug Discov. Today* **2005**, *10*(22), 1543-1550.
226. Korytowski, A. MicroCal PEAQ-ITC Training course, Malvern Panalytical, **2018**.
227. Guo, H.; Cheng, K.; Gao, Y.; Bai, W.; Wu, C.; He, W.; Li, C.; Li, Z. A Novel Potent Metal-binding NDM-1 Inhibitor was Identified by Fragment Virtual, SPR and NMR Screening. *Bioorg. Med. Chem.* **2020**, *28*(9), 115437.
228. Zheng, B.; Tan, S.; Gao, J.; Han, H.; Liu, J.; Lu, G.; Liu, D.; Yi, Y.; Zhu, B.; Gao, G. F. An Unexpected Similarity between Antibiotic-resistant NDM-1 and β -Lactamase II from *Erythrobacter litoralis*. *Protein & cell* **2011**, *2*(3), 250-258.
229. Boeri Erba, E.; Petosa, C. The Emerging Role of Native Mass Spectrometry in Characterizing the Structure and Dynamics of Macromolecular Complexes. *Protein Sci.* **2015**, *24*(8), 1176-1192.
230. Takano, K.; Arai, S.; Sakamoto, S.; Ushijima, H.; Ikegami, T.; Saikusa, K.; Konuma, T.; Hamachi, I.; Akashi, S. Screening of Protein-ligand Interactions under Crude Conditions by Native Mass Spectrometry. *Anal. Bioanal. Chem.* **2020**, *412*(17), 4037-4043.
231. Tauber, C.; Wamser, R.; Arkona, C.; Tugend, M.; Abdul Aziz, U. B.; Pach, S.; Schulz, R.; Jochmans, D.; Wolber, G.; Neyts, J.; Rademann, J. Chemical Evolution of Antivirals Against Enterovirus D68 through Protein-Templated Knoevenagel Reactions. *Angew. Chem. Int. Ed. Engl.* **2021**, *60*(24), 13294-13301.
232. Nguyen, G. T. H.; Tran, T. N.; Podgorski, M. N.; Bell, S. G.; Supuran, C. T.; Donald, W. A. Nanoscale Ion Emitters in Native Mass Spectrometry for Measuring Ligand-Protein Binding Affinities. *A. C. S. Cent. Sci.* **2019**, *5*(2), 308-318.
233. Chen, X.; Li, L.; Chen, S.; Xu, Y.; Xia, Q.; Guo, Y.; Liu, X.; Tang, Y.; Zhang, T.; Chen, Y.; Yang, C.; Shui, W. Identification of Inhibitors of the Antibiotic-resistance Target New Delhi Metallo- β -lactamase 1 by both Nanoelectrospray Ionization Mass Spectrometry and Ultrafiltration Liquid Chromatography/mass Spectrometry Approaches. *Anal. Chem.* **2013**, *85*(16), 7957-7965.
234. Niesen, F. H.; Berglund, H.; Vedadi, M. The Use of Differential Scanning Fluorimetry to Detect Ligand Interactions that Promote Protein Stability. *Nat. Protoc.* **2007**, *2*(9), 2212-21.
235. Wong, E. L.; Nawrotzky, E.; Arkona, C.; Kim, B. G.; Beligny, S.; Wang, X.; Wagner, S.; Lisurek, M.; Carstanjen, D.; Rademann, J. The Transcription Factor STAT5 Catalyzes Mannich Ligation Reactions Yielding Inhibitors of Leukemic Cell Proliferation. *Nat. Commun.* **2019**, *10*(1), 66.

236. Gao, K.; Oerlemans, R.; Groves, M. R. Theory and Applications of Differential Scanning Fluorimetry in Early-stage Drug Discovery. *Biophys. Rev.* **2020**, *12*(1), 85-104.
237. Wu, T.; Yoon, H.; Xiong, Y.; Dixon-Clarke, S. E.; Nowak, R. P.; Fischer, E. S. Targeted Protein Degradation as a Powerful Research Tool in Basic Biology and Drug Target Discovery. *Nat. Struct. Mol. Biol.* **2020**, *27*(7), 605-614.
238. Cimperman, P.; Baranauskiene, L.; Jachimoviciute, S.; Jachno, J.; Torresan, J.; Michailoviene, V.; Matuliene, J.; Sereikaite, J.; Bumelis, V.; Matulis, D. A Quantitative Model of Thermal Stabilization and Destabilization of Proteins by Ligands. *Biophys. J.* **2008**, *95*(7), 3222-3231.
239. Kabir, A.; Honda, R. P.; Kamatari, Y. O.; Endo, S.; Fukuoka, M.; Kuwata, K. Effects of Ligand Binding on the Stability of Aldo-keto Reductases: Implications for Stabilizer or Destabilizer Chaperones. *Protein Sci.* **2016**, *25*(12), 2132-2141.
240. Chen, J.; Wang, J.; Zhu, W. Zinc Ion-induced Conformational Changes in New Delhi Metallo- β -lactamase 1 Probed by Molecular Dynamics Simulations and Umbrella Sampling. *Phys. Chem. Chem. Phys.* **2017**, *19*(4), 3067-3075.
241. Stewart, A. C.; Bethel, C. R.; VanPelt, J.; Bergstrom, A.; Cheng, Z.; Miller, C. G.; Williams, C.; Poth, R.; Morris, M.; Lahey, O.; Nix, J. C.; Tierney, D. L.; Page, R. C.; Crowder, M. W.; Bonomo, R. A.; Fast, W. Clinical Variants of New Delhi Metallo- β -lactamase are Evolving to Overcome Zinc Scarcity. *A. C. S. Infect. Dis.* **2017**, *3*(12), 927-940.
242. Piccirilli, A.; Criscuolo, E.; Brisdelli, F.; Mercuri, P. S.; Cherubini, S.; De Sciscio, M. L.; Maccarrone, M.; Galleni, M.; Amicosante, G.; Perilli, M. Exploring the Role of L10 Loop in New Delhi Metallo- β -lactamase (NDM-1): Kinetic and Dynamic Studies. *Molecules*, **2021**, *26*(18), 5489.
243. Yao, C.; Wu, Q.; Xu, G.; Li, C. NMR Backbone Resonance Assignment of New Delhi Metallo- β -lactamase. *Biomol. NMR Assign.* **2017**, *11*(2), 239-242.
244. Riviere, G.; Oueslati, S.; Gayral, M.; Crechet, J. B.; Nhiri, N.; Jacquet, E.; Cintrat, J. C.; Giraud, F.; van Heijenoort, C.; Lescop, E.; Pethe, S.; Iorga, B. I.; Naas, T.; Guittet, E.; Morellet, N. NMR Characterization of the Influence of Zinc(II) Ions on the Structural and Dynamic Behavior of the New Delhi Metallo- β -lactamase-1 and on the Binding with Flavonols as Inhibitors. *A. C. S. Omega* **2020**, *5*(18), 10466-10480.
245. Golovanov, A. P.; Hautbergue, G. M.; Wilson, S. A.; Lian, L. Y. A Simple Method for Improving Protein Solubility and Long-term Stability. *J. Am. Chem. Soc.* **2004**, *126*(29), 8933-8939.
246. Trevino, S. R.; Scholtz, J. M.; Pace, C. N. Measuring and Increasing Protein Solubility. *J. Pharm. Sci.* **2008**, *97*(10), 4155-4166.
247. Ericsson, U. B.; Hallberg, B. M.; Detitta, G. T.; Dekker, N.; Nordlund, P. Thermofluor-based High-throughput Stability Optimization of Proteins for Structural Studies. *Anal. Biochem.* **2006**, *357*(2), 289-298.
248. Wu, S. J.; Gilliland, G. L.; Feng, Y. Solubility and Early Assessment of Stability for Protein Therapeutics. *Biophysical Methods for Biotherapeutics: Discovery and Development Applications*, **2014**, 65-91.
249. Malhotra, A. Tagging for Protein Expression. *Methods Enzymol.* **2009**, *463*, 239-258.

250. Greenfield, N. J. Using Circular Dichroism Spectra to Estimate Protein Secondary Structure. *Nat. Protoc.* **2006**, 1(6), 2876-2890.
251. Marcoccia, F.; Bottoni, C.; Sabatini, A.; Colapietro, M.; Mercuri, P. S.; Galleni, M.; Kerff, F.; Matagne, A.; Celenza, G.; Amicosante, G.; Perilli, M. Kinetic Study of Laboratory Mutants of NDM-1 Metallo- β -lactamase and the Importance of an Isoleucine at Position 35. *Antimicrob. Agents Chemother.* **2016**, 60(4), 2366-2372.
252. Kelly, S. M.; Price, N. C. The Application of Circular Dichroism to Studies of Protein Folding and Unfolding. *Biochim. Biophys. Acta.* **1997**, 1338, 161-185.
253. Khan, A. U.; Rehman, M. T. Role of Non-Active-Site Residue Trp-93 in the Function and Stability of New Delhi Metallo-beta-Lactamase 1. *Antimicrob. Agents Chemother.* **2016**, 60(1), 356-360.
254. Ali, A.; Gupta, D.; Srivastava, G.; Sharma, A.; Khan, A. U. Molecular and Computational Approaches to Understand Resistance of New Delhi metallo β -lactamase variants (NDM-1, NDM-4, NDM-5, NDM-6, NDM-7)-producing Strains against Carbapenems. *J. Biomol. Struct. Dyn.* **2019**, 37(8), 2061-2071.
255. Maryam, L.; Khalid, S.; Ali, A.; Khan, A. U. Synergistic Effect of Doripenem in Combination with Cefoxitin and Tetracycline in Inhibiting NDM-1 Producing Bacteria. *Future Microbiol.* **2019**, 14(8), 671-689.
256. Whitmore, L.; Wallace, B. A. Protein Secondary Structure Analyses from Circular Dichroism Spectroscopy: Methods and Reference Databases. *Biopolymers* **2008**, 89(5), 392-400.
257. Whitmore, L.; Wallace, B. A. DICHROWEB, an Online Server for Protein Secondary Structure Analyses from Circular Dichroism Spectroscopic Data. *Nucleic Acids Res.* **2004**, 32, 668-673.
258. Sreerama, N.; Venyaminov, S. Y.; Woody, R. W. Estimation of the Number of α -Helical and β -Strand Segments in Proteins Using Circular Dichroism Spectroscopy. *Protein Sci.* **1999**, 8(2), 370-380.
259. Sreerama, N.; Woody, R. W. A Self-consistent Method for the Analysis of Protein Secondary Structure from Circular Dichroism. *Anal. Biochem.* **1993**, 209(1), 32-44.
260. Van Stokkum, I. H. M.; Spoelder, H. J. W.; Bloemendal, M.; Van Grondelle, R.; Groen, F. C. A. Estimation of Protein Secondary Structure and Error Analysis from Circular Dichroism Spectra. *Anal. Biochem.* **1990**, 191(1), 110-118.
261. Provencher, S. W.; Gloeckner, J. Estimation of Globular Protein Secondary Structure from Circular Dichroism. *Biochemistry* **1981**, 20(1), 33-37.
262. Sreerama, N.; Woody, R. W. Estimation of Protein Secondary Structure from Circular Dichroism Spectra: Comparison of CONTIN, SELCON, and CDSSTR Methods with an Expanded Reference Set. *Anal. Biochem.* **2000**, 287(2), 252-260.
263. Manavalan, P.; Johnson Jr, W. C. Variable Selection Method Improves the Prediction of Protein Secondary Structure from Circular Dichroism Spectra. *Anal. Biochem.* **1987**, 167(1), 76-85.
264. Serra, P.; Bruczko, M.; Zapico, J. M.; Puckowska, A.; Garcia, M. A.; Martin-Santamaria, S.; Ramos, A.; de Pascual-Teresa, B. MMP-2 Selectivity in Hydroxamate-type Inhibitors. *Curr. Med. Chem.* **2012**, 19(7), 1036-1064.

265. Rosenblum, G.; Meroueh, S. O.; Kleifeld, O.; Brown, S.; Singson, S. P.; Fridman, R.; Mobashery, S.; Sagi, I. Structural Basis for Potent Slow Binding Inhibition of Human Matrix Metalloproteinase-2 (MMP-2). *J. Biol. Chem.* **2003**, *278*(29), 27009-27015.
266. Díaz, N.; Suárez, D.; Valdés, H. From the X-ray Compact Structure to the Elongated Form of the Full-length MMP-2 Enzyme in Solution: A Molecular Dynamics Study. *J. Am. Chem. Soc.* **2008**, *130*(43), 14070-14071.
267. Di Pizio, A.; Laghezza, A.; Tortorella, P.; Agamennone, M. Probing the S1' Site for the Identification of Non-zinc-binding MMP-2 Inhibitors. *ChemMedChem* **2013**, *8*(9), 1475-1482.
268. West, A. C.; Johnstone, R. W. New and Emerging HDAC Inhibitors for Cancer Treatment. *J. Clin. Invest.* **2014**, *124*(1), 30-39.
269. Sixto-Lopez, Y.; Bello, M.; Correa-Basurto, J. Insights into Structural Features of HDAC1 and its Selectivity Inhibition Elucidated by Molecular Dynamic Simulation and Molecular Docking. *J. Biomol. Struct. Dyn.* **2019**, *37*(3), 584-610.
270. Willis-Martinez, D.; Richards, H. W.; Timchenko, N. A.; Medrano, E. E. Role of HDAC1 in Senescence, Aging, and Cancer. *Exp. Gerontol.* **2010**, *45*(4), 279-285.
271. Finnin, M. S.; Donigian, J. R.; Cohen, A.; Richon, V. M.; Rifkind, R. A.; Marks, P. A.; Breslow, R.; Pavletich, N. P. Structures of a Histone Deacetylase Homologue Bound to the TSA and SAHA Inhibitors. *Nature* **1999**, *401*(6749), 188-193.
272. Lombardi, P. M.; Cole, K. E.; Dowling, D. P.; Christianson, D. W. Structure, Mechanism, and Inhibition of Histone Deacetylases and Related Metalloenzymes. *Curr. Opin. Struct. Biol.* **2011**, *21*(6), 735-743.
273. Wagner, F. F.; Weiwer, M.; Steinbacher, S.; Schomburg, A.; Reinemer, P.; Gale, J. P.; Campbell, A. J.; Fisher, S. L.; Zhao, W. N.; Reis, S. A.; Hennig, K. M.; Thomas, M.; Muller, P.; Jefson, M. R.; Fass, D. M.; Haggarty, S. J.; Zhang, Y. L.; Holson, E. B. Kinetic and Structural Insights into the Binding of Histone Deacetylase 1 and 2 (HDAC1, 2) Inhibitors. *Bioorg. Med. Chem.* **2016**, *24*(18), 4008-4015.
274. Lavoie, R.; Bouchain, G.; Frechette, S.; Woo, S. H.; Abou Khalil, E.; Leit, S.; Fournel, M.; Yan, P. T.; Trachy-Bourget, M. C.; Beaulieu, C.; Li, Z. Design and Synthesis of a Novel Class of Histone Deacetylase Inhibitors. *Bioorg. Med. Chem. Lett.* **2001**, *11*(21), 2847-2850.
275. Grozinger, C. M.; Schreiber, S. L. Deacetylase Enzymes: Biological Functions and the Use of Small-molecule Inhibitors. *Chem. Biol.* **2002**, *9*(1), 3-16.
276. Imtaiyaz Hassan, M.; Shajee, B.; Waheed, A.; Ahmad, F.; Sly, W. S. Structure, Function and Applications of Carbonic Anhydrase Isozymes. *Bioorg. Med. Chem.* **2013**, *21*(6), 1570-1582.
277. Supuran, C. T.; Scozzafava, A. Carbonic Anhydrase Inhibitors and Their Therapeutic Potential. *Expert Opin. Ther. Pat.* **2005**, *10*(5), 575-600.
278. Supuran, C. T. Carbonic Anhydrase Inhibitors. *Bioorg. Med. Chem. Lett.* **2010**, *20*(12), 3467-3474.
279. Supuran, C. T. Carbonic Anhydrase Inhibitors and Their Potential in a Range of Therapeutic Areas. *Expert Opin. Ther. Pat.* **2018**, *28*(10), 709-712.

280. Supuran, C. T.; Scozzafava, A.; Casini, A. Carbonic anhydrase inhibitors. *Med. Res. Rev.* **2003**, *23*(2), 146-89.
281. Kanth, B. K.; Lee, J.; Pack, S. P. Carbonic Anhydrase: its Biocatalytic Mechanisms and Functional Properties for Efficient CO₂ Capture Process Development. *Eng. Life Sci.* **2013**, *13*(5), 422-431.
282. Day, J. A.; Cohen, S. M. Investigating the Selectivity of Metalloenzyme Inhibitors. *J. Med. Chem.* **2013**, *56*(20), 7997-8007.
283. Cardinale, S. C.; Butler, M. M.; Ruthel, G.; Nuss, J. E.; Wanner, L. M.; Li, B.; Pai, R. P.; Peet, N. P.; Bavari, S.; Bowlin, T. L. Novel Benzimidazole Inhibitors of Botulinum Neurotoxin/A Display Enzyme and Cell-based Potency. *Botulinum J.* **2011**, *2*(1), 16-29.
284. Gupta, P. K.; Reid, R. C.; Liu, L.; Lucke, A. J.; Broomfield, S. A.; Andrews, M. R.; Sweet, M. J.; Fairlie, D. P. Inhibitors Selective for HDAC6 in Enzymes and Cells. *Bioorg. Med. Chem. Lett.* **2010**, *20*(23), 7067-7070.
285. Rajak, H.; Agarawal, A.; Parmar, P.; Thakur, B. S.; Veerasamy, R.; Sharma, P. C.; Kharya, M. D. 2,5-Disubstituted-1,3,4-oxadiazoles/thiadiazole as Surface Recognition Moiety: Design and Synthesis of Novel Hydroxamic Acid Based Histone Deacetylase Inhibitors. *Bioorg. Med. Chem. Lett.* **2011**, *21*(19), 5735-5738.
286. Dick, B. L.; Cohen, S. M. Metal-Binding Isosteres as New Scaffolds for Metalloenzyme Inhibitors. *Inorg. Chem.* **2018**, *57*(15), 9538-9543.
287. Bulut, N.; Kocyigit, U. M.; Gecibesler, I. H.; Dastan, T.; Karci, H.; Taslimi, P.; Durna Dastan, S.; Gulcin, I.; Cetin, A. Synthesis of Some Novel Pyridine Compounds Containing Bis-1,2,4-triazole/thiosemicarbazide Moiety and Investigation of Their Antioxidant Properties, Carbonic Anhydrase, and Acetylcholinesterase Enzymes Inhibition Profiles. *J. Biochem. Mol. Toxicol.* **2018**, *32*(1), e22006.
288. Gokcen, T.; Al, M.; Topal, M.; Gulcin, I.; Ozturk, T.; Goren, A. C. Synthesis of Some Natural Sulphonamide Derivatives as Carbonic Anhydrase Inhibitors. *Org. Commun.* **2017**, *10*(1), 15-23.
289. Kumar, R.; Sharma, V.; Bua, S.; Supuran, C. T.; Sharma, P. K. Synthesis and Biological Evaluation of Benzenesulphonamide-bearing 1,4,5-trisubstituted-1,2,3-triazoles Possessing Human Carbonic Anhydrase I, II, IV, and IX Inhibitory Activity. *J. Enzyme Inhib. Med. Chem.* **2017**, *32*(1), 1187-1194.
290. Scozzafava, A.; Briganti, F.; Ilies, M. A.; Supuran, C. T. Carbonic Anhydrase Inhibitors: Synthesis of Membrane-impermeant Low Molecular Weight Sulfonamides Possessing *in Vivo* Selectivity for the Membrane-bound versus Cytosolic Isozymes. *J. med. Chem.* **2000**, *43*(2), 292-300.
291. Supuran, C. T.; Scozzafava, A. Carbonic Anhydrase Inhibitors-Part 94. 1, 3, 4-Thiadiazole-2-sulfonamide Derivatives as Antitumor Agents. *Eur. J. Med. Chem.* **2000**, *35*(9), 867-874.
292. Martin, D. P.; Blachly, P. G.; Marts, A. R.; Woodruff, T. M.; de Oliveira, C. A.; McCammon, J. A.; Tierney, D. L.; Cohen, S. M. 'Unconventional' Coordination Chemistry by Metal Chelating Fragments in a Metalloprotein Active Site. *J. Am. Chem. Soc.* **2014**, *136*(14), 5400-5406.
293. Aygul, I.; Yaylaci Karahalil, F.; Supuran, C. T. Investigation of the Inhibitory Properties of Some Phenolic Standards and Bee Products against Human Carbonic Anhydrase I and II. *J. Enzyme Inhib. Med. Chem.* **2016**, *31*(s4), 119-124.

294. Chen, Y.; Cohen, S. M. Investigating the Selectivity of Metalloenzyme Inhibitors in the Presence of Competing Metalloproteins. *ChemMedChem* **2015**, *10*(10), 1733-8.
295. Hamid, R.; Rotshteyn, Y.; Rabadi, L.; Parikh, R.; Bullock, P. Comparison of Alamar Blue and MTT Assays for High Through-put Screening. *Toxicol. In Vitro* **2004**, *18*(5), 703-710.
296. O'brien, J.; Wilson, I.; Orton, T.; Pognan, F. Investigation of the Alamar Blue (resazurin) Fluorescent Dye for the Assessment of Mammalian Cell Cytotoxicity. *Eur. J. Biochem.* **2000**, *267*(17), 5421-5426.